ADVANCES IN THE TECHNOLOGY OF STAINLESS STEELS AND RELATED ALLOYS

Published by the
AMERICAN SOCIETY FOR TESTING AND MATERIALS
1916 Race St., Philadelphia 3, Pa.

ASTM Special Technical Publication No. 369

ADVANCES IN THE TECHNOLOGY OF STAINLESS STEELS AND RELATED ALLOYS

A compilation of papers presented at four symposiums: "Advances in the Technology of Stainless Steels and Related Alloys," sponsored by the American Society for Testing and Materials, Atlantic City, N.J., June, 1963; "Recent Advances in the Metallurgy of Stainless Steels," sponsored by the Metallurgical Society of the American Institute of Mining, Metallurgical, and Petroleum Engineers, Cleveland, Ohio, October, 1963; and "Stress Corrosion Cracking" and "Evaluation Tests for Stainless Steels," sponsored by the National Association of Corrosion Engineers in collaboration with The Electrochemical Society, New York, N.Y., March, 1963.

Reg. U.S. Pat. Off.

ASTM Special Technical Publication No. 369

Price $21.50; to ASTM, NACE, AIME, and ECS members $15.00

Published by the
AMERICAN SOCIETY FOR TESTING AND MATERIALS
1916 Race St., Philadelphia 3, Pa.

© BY AMERICAN SOCIETY FOR TESTING AND MATERIALS 1965
Library of Congress Catalog Card Number: 65-19685

Printed in Baltimore, Md.
April, 1965

FOREWORD

During 1963 the American Society for Testing and Materials; the Metallurgical Society of the American Institute of Mining, Metallurgical, and Petroleum Engineers; and The Electrochemical Society and the National Association of Corrosion Engineers, organized symposia dealing with several aspects of the technology of stainless steels. Members of these organizations who were concerned with these activities decided that it would be advantageous to those interested in stainless steels if the papers presented at these meetings could be combined in a single publication for convenient future reference. They formed an Intersociety Co-ordinating Committee to accomplish this.

With the collaboration of the authors of the several papers, the participating societies, and particularly the American Society for Testing and Materials which undertook publication of the papers in this volume, the desired consolidation of papers from the several societies has been achieved.

The symposia in which the several papers originated were as follows: (1) symposium on *Advances in the Technology of Stainless Steels and Related Alloys*, Atlantic City, N. J., June, 1963, Sponsored by ASTM Committee A-10, M. A. Cordovi, chairman; (2) symposium on *Stress Corrosion Cracking*, H. L. Logan, E. H. Phelps, and H. R. Copson, co-chairmen, and symposium on *Evaluation Tests for Stainless Steels*, R. B. Mears, chairman, Second International Congress on Metallic Corrosion Sponsored by NACE in collaboration with The Electrochemical Soc., New York, N. Y., March, 1963; and (3) symposium on *Recent Advances in the Metallurgy of Stainless Steels*, Cleveland, Ohio, October, 1963, sponsored by the Metallurgical Society of AIME, E. J. Dulis and L. R. Scharfstein, co-chairmen.

The task force concerned with this activity wishes to express its thanks to all who have co-operated in this venture. It is hoped that the results of this effort will be well received by those in whose interests it was undertaken and that its success will prompt similar future action in consolidating information from several sources in single publications for more convenient reference.

The Intersociety Co-ordinating Committee consisted of M. A. Cordovi, ASTM; E. J. Dulis, AIME; R. B. Mears, NACE; and E. H. Phelps, ECS, with F. L. LaQue, chairman.

NOTE—The Society is not responsible, as a body, for the statements and opinions advanced in this publication.

CONTENTS

Advances in the Technology of Stainless Steels and Related Alloys

PAGE

Effects of Vacuum Melting and Vacuum Annealing on the Properties of Austenitic Stainless Steels—D. B. Roach, W. B. Leffingwell, and A. M. Hall 1
Effects of Austrolling on the Properties of Crucible 422 Stainless Steel—R. C. Westgren and E. J. Dulis 8
Discussion 16
High-Strength Stainless Steel by Deformation and Low Temperatures—S. Floreen and J. R. Mihalisin 17
The Mechanisms of Deformation and Work Hardening in AISI Type 301 Stainless Steel—W. F. Barclay 26
Practical Aspects of Production Bright Annealing of Stainless Steel—R. C. Boyer and R. J. Perrine 30
Advancements in Extrusion and Cold Finishing of Stainless Steel and Irregular Shapes—J. J. Barrett 36
New Martensitic Age Hardening Stainless Steels—G. N. Aggen, C. M. Hammond, and R. A. Lula 40
Discussion 46
The Development of New High-Strength Stainless Steels—C. M. Hammond 47
Mechanical Properties and Corrosion Resistance of a High-Strength Chromium-Manganese-Nitrogen Stainless Steel—J. J. Heger 54
Discussion 61
Metallurgy of a Columbium-Hardened Nickel-Chromium-Iron Alloy—H. L. Eiselstein 62
Discussion 78
Properties of 12 Per Cent Chromium Alloys Modified with Small Columbium Additions—H. Tanczyn 80
Discussion 87
A High-Strength Weldable Stainless Steel for Elevated-Temperature Service—F. C. Hull 88
Discussion 98
Creep-Rupture Properties of Stainless Steels at 1600, 1800, and 2000 F—K. G. Brickner, G. A. Ratz, and R. F. Domagal 99
The Effects of Neutron Exposure and Reactor Environments on Stainless Steels—S. H. Bush and J. C. Tobin 112
Evaluation and Application of Stainless Steels in Cryogenic Environments—A. Hurlich and W. G. Scheck 127
Experience with Stainless Steels in Utility Power Plants—G. E. Lien 136
Discussion 142
Modified Type 316 Stainless Steel with Low Tendency to Form Sigma—C. E. Spaeder and K. G. Brickner 143
Effect of Composition and Section Size on Mechanical Properties of Some Precipitation Hardening Stainless Steels—W. C. Clarke, Jr. and H. W. Garvin 151
New Cast High-Strength Alloy Grades by Structure Control—F. H. Beck, E. A. Schoefer, J. W. Flowers, and M. G. Fontana 159
The Effect of Small Columbium Additions to Type 304 Stainless Steel—R. B. G. Yeo and T. E. Scott 175
Discussion 179

Stress Corrosion and Evaluation Tests for Stainless Steels

Effect of Heat Treatment and Welding on Corrosion Resistance of Austenitic Stainless Steels—J. Robert Auld 183
An Appraisal of Evaluation Tests for Stainless Steel Automotive Trim—E. H. Phelps and J. F. Bates 200
Accelerated Tests as a Method of Predicting Service Corrosion of Exterior Automotive Trim—G. F. Bush, W. J. Garwood, B. E. Tiffany 209
A Laboratory Test for Determining Susceptibility of Nickel-Molybdenum and Nickel-Molybdenum-Chromium Alloys to Intercrystalline Corrosion and Its Use in the Development of Resistant Alloys—H. Grafen 223
An Evaluation of Accelerated Strauss Testing—L. R. Scharfstein and C. M. Eisenbrown 235
The Relationship of Heat Treatment and Microstructure to Corrosion Resistance in Ni-Cr-Mo Alloys—M. A. Streicher 240
A Testing System for Detecting Susceptibility to Rapid Intergranular Attack in Various Grades of Austenitic Stainless Steels—M. A. Streicher 255
Effect of Heat Treatment, Composition, and Microstructure on Corrosion of 18 Cr-8 Ni-Ti Stainless Steels in Acids—M. A. Streicher 257

Recent Advances in the Metallurgy of Stainless Steels

Time-Temperature-Sensitization (TTS) Diagrams for Types 347, 304L, and 316L Stainless Steels—H. F. Ebling and M. A. Scheil 275
Discussion 283

PAGE

Alloying Precipitation Hardening Stainless Steels for Strength and Stability—D. C. Perry and M. W. Marshall 285
Discussion 290
Fine Structure and Properties of a 12-Cr MoWv Martensitic Stainless Steel—B. R. Banerjee, J. J. Hauser, and J. M. Capenos 291
Further Studies on the Formation of Sigma in 12 to 16 Per Cent Chromium Steels—D. C. Ludwigson and H. S. Link 299
Discussion 311
Development of a Modified Alloy 20 Stainless Steel—H. L. Black and L. W. Lherbier 312
Discussion 318
Relationship Between Metallurgical Structure and Properties of a Precipitation Hardening Stainless Steel—G. N. Aggen and R. H. Kaltenhauser 319
Aging Mechanisms in Precipitation-Hardening Stainless Steels—J. C. Wilkins, R. E. Pence, and D. C. Perry 331
Discussion 341
A Study of Internal-Friction Peaks in Type 304 Stainless Steel Containing Nitrogen—J. F. Eckel and C. R. Manning, Jr. 342
Discussion 347
Roping and Intergranular Corrosion of 430 Stainless Steel—E. A. Parker 348

RELATED ASTM PUBLICATIONS

Stress-Corrosion Cracking of Austenitic Chromium-Nickel Stainless Steels, STP 264 (1960)
Comparison of the Properties of Basic Oxygen and Open Hearth Steels, STP 364 (1963)
Trends in the Metallurgy of Low-Alloy, High-Yield-Strength Steels, Gillette Lecture (1963)

Advances in the Technology of Stainless Steels and Related Alloys

EFFECTS OF VACUUM MELTING AND VACUUM ANNEALING ON THE PROPERTIES OF AUSTENITIC STAINLESS STEELS

By D. B. Roach;[1] W. B. Leffingwell;[2] and A. M. Hall,[3]
Personal Member, ASTM

Synopsis

Two applications of vacuum technology to metallurgy are discussed. One concerns the consumable-electrode vacuum-arc remelting of AISI 316 stainless steel. An air-melted and a vacuum-arc remelted heat are compared with respect to composition, processing and welding, room- and high-temperature mechanical properties, magnetic permeability, inclusion count, and behavior in the Huey corrosion test. The vacuum heat was lower in carbon, oxygen, and hydrogen than the air-melted heat. The low oxygen and hydrogen were attributed to the melting process, while the low carbon was not. Both heats were similar in processing and welding behavior as well as in mechanical and physical properties. In Huey corrosion tests of sensitized material, the air-melted steel was attacked much faster than the vacuum-melted material. However, this difference was ascribed to the difference in carbon content between the two steels. Thus, in this study, no differences attributable to the consumable-electrode vacuum-arc remelting process were observed.

The other application was the vacuum annealing of AISI 301 strip. This material was compared with air-annealed and hydrogen-annealed stock. The air-annealed and vacuum-annealed steels had similar mechanical properties. However, the hydrogen-annealed steel had half of the ductility, 80 per cent of the formability and 75 per cent of the strength of the other materials. The increase in hydrogen content of the steel, when annealed in hydrogen, is considered responsible for these differences.

Vacuum technology has been put to work at a number of points in the consolidation, refining, working, fabrication, and heat treatment of a considerable variety of metals and alloys. The use of a vacuum in melting operations has come in for a particularly large share of attention. Such processes as vacuum-induction melting and consumable-electrode vacuum-arc remelting have been developed and applied to numerous metallic materials. The various vacuum melting processes have found principal application in the consolidation and refining of the reactive metals, the refractory metals, numerous superalloys, certain specialty steels, and a variety of ultrahigh-strength steels. Since World War II a copious literature has come into being on these subjects.

On the other hand, little information is to be found in the literature regarding the influence of vacuum melting on the properties of the stainless steels. Some data have been reported which showed that the ductile-to-brittle transition temperatures of vacuum - induction-melted AISI Types 430 and 446 stainless steels were well below room temperature, while the corresponding air-melted steels went through the ductile-to-brittle transition considerably above room temperature (1).[4] Data on AISI Types 403, 410, 422, and 446 steels show that the room-temperature impact strength, as measured by the Izod or the Charpy test, was markedly greater for vacuum-induction-melted alloys than for their air-melted counterparts (2). In other research, some of the properties of air-melted and vacuum-induction-melted chromium-nickel and chromium-nickel-molybdenum stainless steels were compared at room temperature and at 1300 F (3). The data indicate that the vacuum-melted material had slightly greater room-temperature tensile ductility and considerably greater rupture strength at 1300 F. The steels were of the 16 per cent chromium, 16 per cent nickel type containing 0.04 to 0.08 per cent carbon and 0.51 to 0.87 per cent columbium. In addition, comparative data have been reported on air-melted and on consumable-electrode vacuum-arc-remelted AM 355 (4). These data indicate that the vacuum-melted material was somewhat stronger and considerably more ductile than the corresponding air-melted material processed according to the same schedule. The gains in properties were attributed to the homogenizing action which may occur in consumable-electrode vacuum-arc remelting.

One of the programs described in this paper was directed at casting additional light on the influence of vacuum melting on the properties of austenitic stainless steel. Specifically, material from a commercial heat of consumable-electrode, vacuum-arc remelted AISI 316 was compared with material from a commercial heat of air-melted AISI 316. The criteria for the comparison were composition, processing behavior, corrosion resistance, microstructure, mechanical properties, and weldability.

The other program discussed here was a brief study of the influence on the tensile properties and cold-forming capability of chromium-nickel stainless steel strip produced by the environment used in annealing. Vacuum annealing was emphasized, and the material under study was commercially produced AISI 301.

Consumable-Electrode Vacuum-Arc Remelting

Materials and Procedures:

The two heats used in this investigation were made in the regular production facilities of the Sharon Steel Corp. The air-melted heat was produced in a direct-arc furnace, and the vacuum-melted steel was made by the consumable-electrode method, the electrodes having been made from a standard arc-melted heat. The heat analyses are given in Table 1. Except for carbon content, the differences in the heat analyses of the two steels were not considered particularly significant.

A 9- by 2- by 60-in. hot-rolled slab

[1] Research associate, Battelle Memorial Inst., Columbus, Ohio.

[2] Assistant chief metallurgist, Sharon Steel Corp., Sharon, Pa.

[3] Division chief, Battelle Memorial Inst., Columbus, Ohio.

[4] The boldface numbers in parentheses refer to the list of references appended to this paper.

Copyright© 1965 by ASTM International

from each heat was furnished as starting material for the experimental work. Transverse sections of the slabs, 2 by 2 by 9 in., were heated at 2150 F and forged to $\frac{7}{8}$-in. square bars which, in turn, were reheated to the same temperature and rolled to $\frac{5}{8}$-in. round bars to provide material for freezing-cycle hot tension tests. Sections 22 in. long were cut from the slabs, heated to 2150 F, and rolled to $\frac{1}{2}$-in. plate. Part of the plate was reserved for impact and magnetic permeability tests, and the remainder was reheated to 2000 F and rolled to 0.10-in.-thick strip. This strip was annealed 15 min at 1950 F, water quenched, and pickled in hot 5 per cent hydrofluoric acid-20 per cent nitric acid. Part of it was saved for weldability tests; part was cold rolled to 0.060-in. thickness, degreased, annealed and pickled, and machined into tensile, creep and stress-rupture specimens; part was cold rolled to 0.060-in. thickness, degreased, annealed, pickled and rerolled to 0.045-in. thickness to provide half-hard stock for tension tests; finally, some of the 0.045-in. strip was annealed and pickled for tension tests and corrosion tests.

TABLE 1—HEAT ANALYSES OF THE EXPERIMENTAL MATERIALS.

Heat No.	Composition, per cent								
	C	Mn	P	S	Si	Ni	Cr	Mo	Cu
1-E.....	0.054	1.84	0.019	0.012	0.35	13.04	16.70	2.26	0.11
5-V[a].....	0.029	1.76	0.018	0.012	0.65	12.53	17.87	2.32	0.10
5-V[b].....	0.020	1.59	0.016	0.014	0.59	12.34	17.63	2.05	...

[a] Before vacuum melting.
[b] After vacuum melting.

TABLE 2—ANALYSIS OF THE EXPERIMENTAL MATERIALS FOR GASEOUS ELEMENTS.

Heat No.	Thickness, in.	Analysis, ppm		
		O_2	H_2	N_2
1-E.....	2	60	2.8	300
1-E.....	0.045	55	1.2	370
5-V.....	2	14	0.5	290
5-V.....	0.045	33	0.5	320

The experimental materials were analyzed for oxygen, hydrogen, and nitrogen when in the form of 2-in.-thick slabs and 0.045-in.-thick strip. The results are shown in Table 2. In the form of 2-in.-thick slabs the vacuum melt showed much lower oxygen and hydrogen than the air melt and about the same nitrogen content. The 0.045-in.-thick material from the air melt was noticeably lower in hydrogen and somewhat higher in nitrogen than the corresponding 2-in.-thick stock. The vacuum-melted 0.045-in.-thick material showed lower oxygen and hydrogen contents and about the same nitrogen content as the air-melted material, but noticeably higher oxygen than the corresponding 2-in.-thick material.

The differences in the gas contents of the material in the two different thicknesses appeared to be caused either by pickup or loss of the various gases during processing. The air-melted steels appeared to lose hydrogen but to pick up nitrogen during hot working and annealing. The vacuum-melted steel appeared to pick up both oxygen and nitrogen.

Tensile properties were obtained for 0.060-in.- and 0.045-in.-thick material using standard sheet tension specimens. A strain rate of 0.02 min^{-1} was used to the yield point, after which a crosshead speed of 0.2 in. per min was employed. Charpy impact tests were made with the keyhole type of specimen. The material investigated was annealed. The holes for the notches were drilled perpendicular to the surface of the plates.

Magnetic permeability tests were made on three specimens $\frac{1}{4}$ in. in diameter by 1 in. in length cut from different areas of $\frac{1}{2}$-in.-thick annealed plate of each of the two steels. The permeability measurements were made with a direct-reading permeameter. Inclusion counts were made on sections of the 2-in.-thick slab and the 0.045-in. strip from the air melt and the 0.045-in.-thick strip from the vacuum melt. ASTM Recommended Practice E 45, Method A, for inclusion ratings was used in this work.[5]

The corrosion evaluation consisted in determining the performance of the materials in the Huey 65 per cent boiling nitric acid test, as carried out according to ASTM Recommended Practice A 262.[6] Briefly, the test consisted of completely immersing triplicate 2- by $\frac{1}{2}$- by 0.045-in. specimens in the boiling acid solution. A 1000-ml Erlenmeyer flask and condenser apparatus, heated by an electric hot plate, were used for each group of three specimens. A comparable surface finish for each specimen was obtained by hand polishing with 120-grit abrasive paper. The test consisted of five periods each of 48-hr duration. Weight loss was determined after each test period.

The rate of corrosion was calculated from $R = KW/AST$
where:
R = rate of corrosion in mils penetration per month,
K = 43,900,
W = weight loss,
A = total surface area, sq in.,
S = density of the material, g per cu cm, and
T = duration of the test period, hr.

Specimens were tested as annealed at 1950 F for 15 min and air cooled and as sensitized by heating at 1200 F for 1 hr followed by furnace cooling.

Three rupture tests and three creep tests were made at 1200 F on each of the materials in the form of 0.060-in.-thick strip. Creep as well as stress-rupture data were obtained from the rupture tests, but only creep data were obtained from the creep tests. Stresses for the rupture tests were chosen to produce failure in less than 1000 hr, and all creep tests were discontinued after about 1000 hr.

Welding quality was investigated by preparing welded joints in annealed 0.10-in.-thick strip produced from the two heats of steel and testing them for bend ductility, tensile strength, and elongation. In addition, to determine if a difference in crack sensitivity existed between weld deposits made in these steels, the high-temperature ductility of bar stock was obtained over the temperature range from 2550 to 2000 F the range in which cracking generally occurs. These data were obtained during a freezing and cooling cycle designed to simulate the conditions that exist during the cooling of a weld deposit.

In studying the bend ductility of welded joints, the guided bend test was used with two types of joint and two types of specimen per joint. In one type of specimen the weld was transverse to the rolling direction, and in the other it was parallel to the rolling direction. In one type of joint no filler wire was used, while in the other a small amount of filler wire was used to insure a cross section in the weld metal at least equal to that of the base material. A commercial Type 316 filler

[5] Recommended Practice for Determining the Inclusion Content of Steel, *1964 Book of ASTM Standards*, Part 31.

[6] Recommended Practice for Boiling Nitric Acid Test for Corrosion-Resisting Steels, *1964 Book of ASTM Standards*, Part 3.

wire was deposited with the tungsten-arc process for this purpose. The weld reinforcement was left on all of the bend specimens. Tests were made with the root of the weld in tension and also with the face of the weld in tension. In the longitudinal bend specimen, the weld metal, heat-affected zones, and base metal were deformed together, while the ductility of the weld metal only was determined from the transverse bend specimen. The guided bend tests were made using dies of various radii. The specimens were first bent 180 deg over the die with the largest radius, and if no failure occurred, they were deformed over successively smaller dies until they failed. The bend ductility of the welded joints was calculated from the smallest radius over which they could be bent 180 deg before failure occurred.

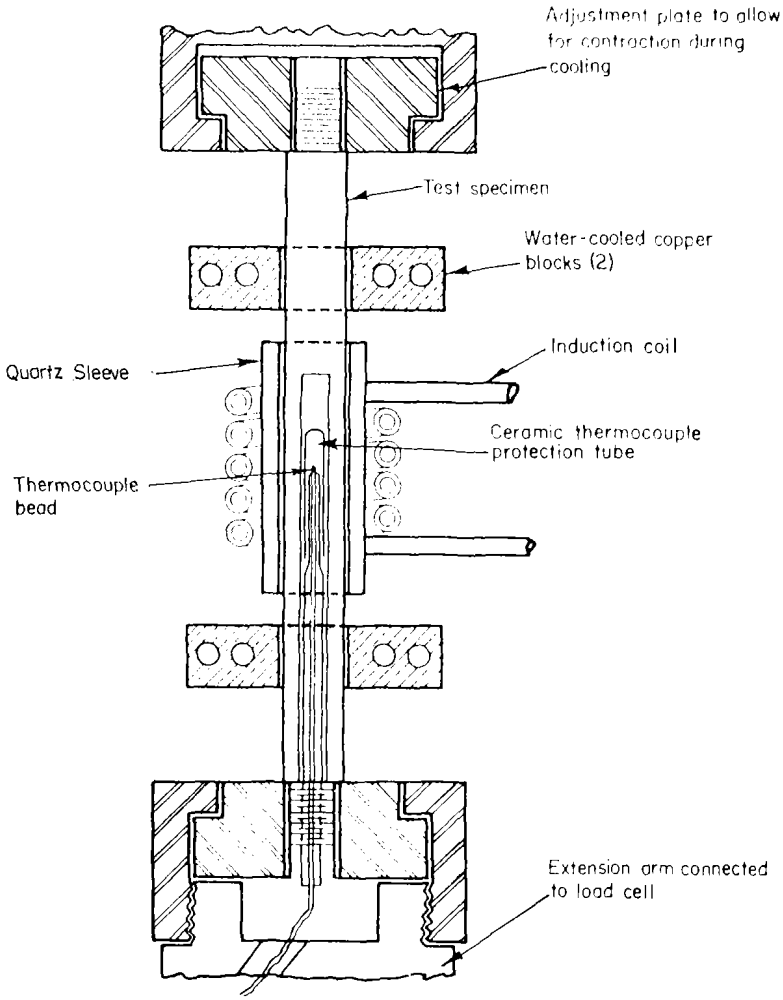


FIG. 1—Cross Section of Test Specimen Showing Method of Attachment to Testing Machine.

TABLE 3—AVERAGE TENSILE PROPERTIES OF 0.060- AND 0.045-GAGE STRIP.[a]

Heat No.	Thickness, in.	Condition	Direction	Tensile Strength, 1000 psi	Yield Strength, 1000 psi	Elongation in 2 in., per cent
1-E.....	0.060	annealed[b]	longitudinal	78.0	29.5	61.5
5-V.....	0.060	annealed	longitudinal	79.0	30.5	59.5
1-E.....	0.045	annealed[b]	longitudinal	80.5	31.0	62.5
5-V.....	0.045	annealed	longitudinal	80.0	31.0	63.5
1-E.....	0.045	half hard[c]	longitudinal	121	110	16.5
5-V.....	0.045	half hard	longitudinal	120	111	18.5
1-E.....	0.045	annealed	transverse	79.0	29.5	59.0
5-V.....	0.045	annealed	transverse	79.5	31.0	61.5
1-E.....	0.045	half hard	transverse	123	104	14.5
5-V.....	0.045	half hard	transverse	118	101	16.5

[a] Averaged from quadruplicate tests.
[b] 1950 F for 15 min and air cooled.
[c] 25 per cent cold reduction.

The freezing cycle tension test was developed at Battelle during the course of a study to determine the cause of weld metal cracking in low and high alloy steel (5). The test specimen and the method of heating and loading it are shown in Fig. 1. The apparatus was designed so that the strength and ductility of the material could be obtained over the temperature range from the solidus to room temperature. Air pressure was used to activate an air cylinder which was connected by an extension arm and holder to the specimen being tested. The load applied to the test specimen was recorded on a high-speed recorder from strain gages attached to a load cell connected to the lower extension arm. A 30-kw spark-gap induction unit was used to heat the specimens to the liquid range. The specimens were heated to a temperature of 2900 F in approximately 20 sec. They were then allowed to cool to various predetermined temperatures and rapidly loaded to failure on reaching the desired temperature. The temperature of the specimens was measured by placing a platinum-platinum-10 per cent rhodium thermocouple in the molten zone as shown in Fig. 1. The couple was protected from the molten alloy by a thin-walled ceramic tube. A quartz sleeve was used to retain the molten metal while above the solidus temperature. After a few tests were made and cooling curves were obtained for each, it was apparent that the heating and cooling cycles were the same for both materials. As a result, subsequent heating and cooling times were selected from these curves rather than from thermocouples placed in each specimen.

To maintain a low temperature gradient across the diameter of the specimen, water-cooled copper blocks were clamped adjacent to the melt zone on each end of the specimen. By recording the temperature at the center and the outside edge of the specimen, it was found that the temperature gradient across the specimen during cooling never exceeded 25 F.

From the results of the freezing cycle tension test, it has been possible to determine the effects of relatively small changes in chemical composition on cracking susceptibility. If the material exhibited low ductility at elevated temperatures, the cracking resistance also was poor.

Results:

Forging and Rolling—Although no

quantitative measure of forgeability was used, it can be said that the bars forged well and no difference in forgeability between the two heats was observed. Likewise, the materials negotiated hot and cold rolling successfully; the surfaces of stock rolled from each heat were good and no edge cracking occurred.

TABLE 4—AVERAGE CHARPY IMPACT PROPERTIES OF ½-IN.-THICK PLATE AT ROOM AND SUBZERO TEMPERATURES.[a]

Heat No.	Average Charpy Values,[b] ft-lb		
	Room Temperature	−100 F	−320 F
1-E	83.0	83.0	73.0
5-V	88.5	75.0	80.0

[a] Averaged from triplicate tests.
[b] Keyhole-type specimens.

TABLE 5—INCLUSION COUNTS FOR THE STAINLESS STEELS UNDER INVESTIGATION.

Heat No.	Specimen No.	Specimen Thickness, in.	Inclusion Count by ASTM Method A[a]
1-E	1	0.045	A-1 thin + D-2 thin
1-E	2	0.045	D-1 heavy
5-V	1	0.045	D-2 thin
5-V	2	0.045	D-1 thin
1-E	1	2	A-2 thin + D-1 thin
1-E	2	2	A-2 heavy + D-3 thin
1-E	3	2	A-2 thin + D-2 thin

[a] A—Sulfide inclusions; D—Oxide inclusions.

TABLE 6—AVERAGE RESULTS OF CORROSION TESTS IN 65 PER CENT BOILING NITRIC ACID FOR FIVE 48-HR TEST PERIODS.

Condition	Corrosion Rate in Mils Penetration per Month	
	Heat 1-E	Heat 5-V
Annealed[a]	0.87	0.86
Sensitized[b]	14.5	1.54

[a] Annealed at 1950 F for 15 min and air cooled.
[b] Sensitized at 1200 F for 1 hr and furnace cooled.

Tensile and Impact Properties—From Table 3 it is seen that both heats had essentially the same tensile properties. Likewise, both had high impact resistance at all test temperatures, including −320 F, as shown in Table 4. This behavior is characteristic of AISI 316.

Magnetic Permeability and Inclusion Count—The results of the magnetic permeability tests showed that all of the specimens had the same permeability of 1.005, which indicated that all were fully austenitic. As to nonmetallic inclusions, those in the vacuum-melted steel tended to be thinner; otherwise, there was little to choose between the two materials. The results obtained from the inclusion counts are listed in Table 5.

Performance in the Huey Corrosion Test—Table 6 gives the average corrosion rates obtained for the two materials, as annealed and as sensitized. Each value shown in the table is the average of the results obtained from three specimens; the individual results were in good agreement with each other. In addition, each value in the table is the average of the results from five 48-hr immersion periods. As annealed, the two materials behaved alike. However, when sensitized, the vacuum-melted

TABLE 7—RUPTURE AND CREEP DATA FOR 0.060-GAGE STRIP AT 1200 F.

Heat No.	Specimen No.	Stress, psi	Rupture Time, hr	Total Elongation, per cent	Minimum Creep Rate, per cent per hour
1-E	1	35 000	5.3	33.7	2.3
1-E	2	27 500	65.6	38.9	0.22
1-E	3	20 000	861.7	42.1	0.020
1-E	4	13 000	1028.0[a]	2.50[b]	0.0015
1-E	5	9 000	1003.5[a]	0.414[b]	0.00026
1-E	6	6 000	1006.6[a]	0.108[b]	0.00006
5-V	2	35 000	2.7	38.8	5.0
5-V	1	27 500	59.0	35.0	0.16
5-V	3	20 000	509.4	30.4	0.026
5-V	4	13 000	1013.0[a]	4.01[b]	0.0032
5-V	6	9 000	1170.6[a]	0.48[b]	0.0002
5-V	7	6 000	1005.9[a]	0.088[b]	0.000035

[a] Test discontinued at this time.
[b] Total strain at the time the creep test was discontinued.

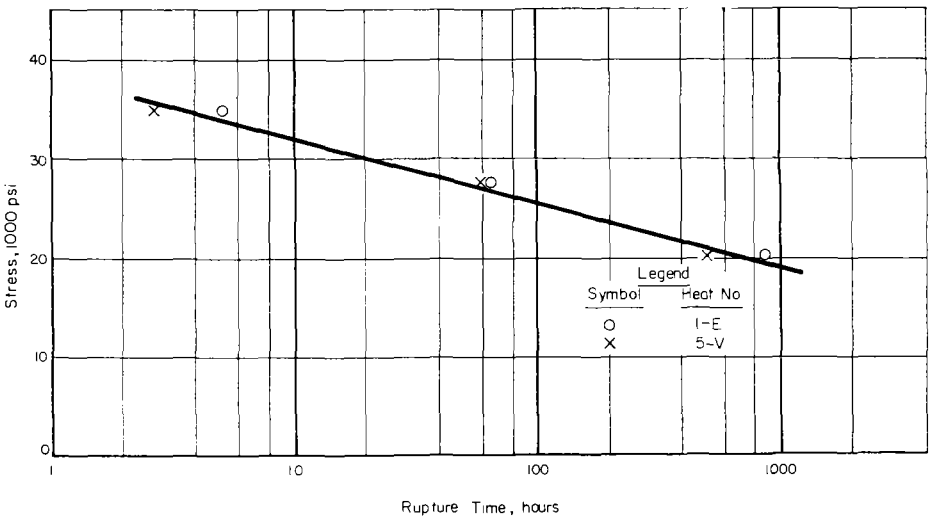


FIG. 2—Stress Versus Rupture Time for 0.060-Gage Strip at 1200 F.

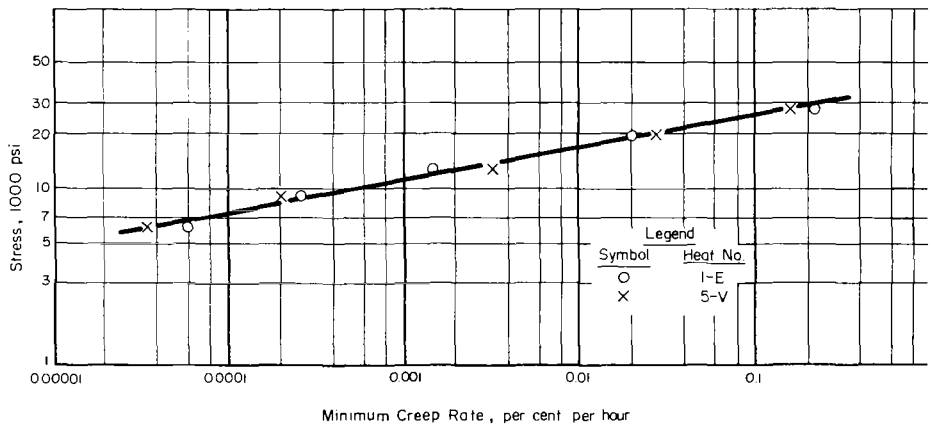


FIG. 3—Stress Versus Minimum Creep Rate for 0.060-Gage Strip at 1200 F.

steel displayed nearly ten times the resistance of the air-melted material. This difference is attributed to the extra low carbon content of the former.

Creep and Stress-Rupture Data—The rupture and creep data obtained are listed in Table 7. Rupture time versus stress is plotted in Fig. 2, while minimum creep rate is shown in Fig. 3 as a function of stress. In each figure, a single curve has been used to represent the behavior of both heats. It is considered that deviations of the individual data points from the curves are well within the normally expected scatter band. The ductility at rupture of the two materials was strikingly similar for equivalent stresses and times.

Weldability Results—Sixteen bend specimens were prepared from each of the steels. All of the different types of bend specimens could be formed around a radius less than the thickness of the sheet material without failing. This amount of deformation represents approximately 33 per cent elongation in the outer fibers of the bend specimen. The data indicated that there was no difference in the bend ductility of welded joints made in the two materials.

Duplicate transverse and longitudinal tension specimens were machined from samples of each heat in which the welds were made without filler wire. The weld reinforcement was removed. The results of the tension tests are listed in Table 8. The joint efficiency of the specimens was good. In most cases, the tensile strength was equal to that of the unwelded base material. In all but one of the specimens, failure occurred in the base metal.

Tension test data also were obtained on transverse welded joints prepared with Type 316 filler wire. The test results are shown in Table 9. Again, the weld-joint properties were about equal to those of the base material, and no appreciable difference was found in the mechanical properties of the two different heats of steel.

TABLE 8—TENSILE PROPERTIES OF 0.100-GAGE SPECIMENS WELDED WITHOUT THE USE OF FILLER WIRE.

Heat No.	Specimen No.	Relationship of Weld to Direction of Rolling of Base Plate	Elongation in 2 in., per cent	Tensile Strength, psi	Location of Fracture
1-E.....	1	transverse	56.0	77 600	base metal
	2	transverse	47.5	76 200	base metal
	3	parallel	44.5	75 800	heat-affected zone
	4	parallel	44.0	76 200	heat-affected zone
5-V.....	1	transverse	52.5	71 700	base metal
	2	transverse	57.5	72 200	base metal
	3	parallel	43.0	68 900	fusion zone
	4	parallel	50.5	72 100	base metal

TABLE 9—TENSION TEST DATA FOR 0.100-GAGE SHEET SPECIMENS WELDED WITH TYPE 316 STAINLESS STEEL FILLER WIRE.

Heat No.	Specimen No.	Relationship of Weld to Direction of Rolling of Base Plate	Elongation in 2 in., per cent	Tensile Strength, psi	Location of Fracture
1-E.....	1	transverse	49.5	74 600	base metal
	2	transverse	48.0	74 200	base metal
5-V.....	1	transverse	48.0	68 000	base metal
	2	transverse	53.5	73 900	base metal

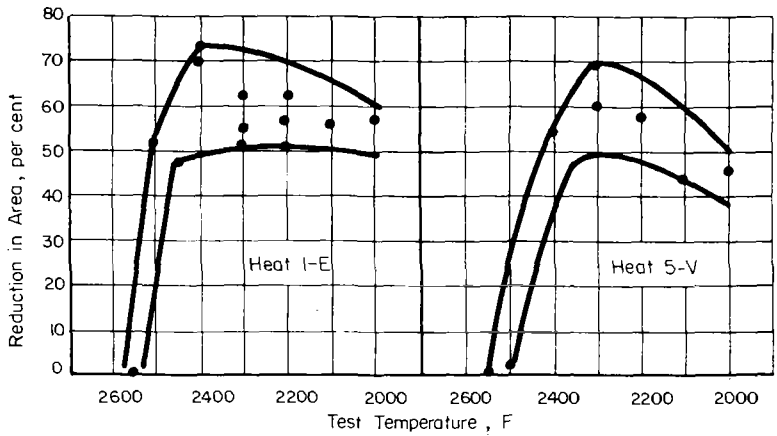


FIG. 4—High-Temperature Ductility of Air-Melted Heat 1-E and Vacuum-Melted Heat 5-V.

The data obtained from the freezing cycle tension test are plotted in Fig. 4. The actual reduction of area values obtained at each temperature are shown along with curves depicting the maximum and minimum limits of ductility. As can be noted, neither steel exhibited any appreciable ductility at 2550 F. This was as expected because this temperature is only slightly lower than the solidus temperature. As the test temperature was lowered, the ductility increased rapidly to quite high values. The ductility was highest over the range from approximately 2300 to 2400 F. Below 2300 F, the ductility decreased, which is characteristic of steels tested in this temperature range. From these data, it appeared that neither steel was susceptible to weld metal hot cracking, which occurs in some materials because of low ductility at temperatures just below the nominal solidus.

Discussion:

Direct-arc air melted AISI 316 has been compared with consumable-electrode vacuum-arc remelted AISI 316 in a variety of respects. The properties involved in the comparison have been composition, workability, tensile properties, impact values, creep, stress-rupture, inclusion content, behavior in the Huey corrosion test, and weldability. In almost all respects, both materials behaved the same and were of equal quality. The principal difference in behavior was the performance of sensitized specimens in the Huey boiling 65 per cent nitric acid corrosion test. And this difference can be ascribed entirely to the difference in carbon content between the two heats of steel.

From the results obtained, the only clearly discernible difference between the two heats of stainless steel was in composition. The vacuum-melted steel was lower in carbon, oxygen, and hydrogen. Here, it can be said that the low oxygen and low hydrogen were a particular consequence of the melting method. However, no performance or quality effect, as measured in terms of the parameters used in this investigation, could be attributed to low oxygen or low hydrogen or to any other factor specific to the method of melting. In

sum, since only minor differences were found between the air-melted and the consumable-electrode vacuum-arc remelted material, and these differences were not found to influence quality and performance, no technical basis has emerged for melting AISI 316 stainless steel by practices other than standard air-melting procedures.

TABLE 10—COMPOSITION OF MATERIALS USED IN ANNEALING STUDIES.

Material Designation	Composition, per cent					Remarks
	C	Mn	Si	Ni	Cr	
A	0.108	0.70	0.49	6.88	16.89	low ductility
B	0.088	0.68	0.43	6.95	16.82	low ductility
C	0.130	0.61	0.41	7.23	16.84	normal ductility

TABLE 11—RESULTS OF HYDROGEN ANALYSES.

Material	Annealing Medium	Hydrogen Content, ppm
A	air	1.7
B	air	1.2
C	air	1.2
A	vacuum	0.5
B	vacuum	0.5
C	vacuum	0.5
A	hydrogen	8.1
B	hydrogen	8.1
C	hydrogen	8.4

TABLE 12—RESULTS OF TENSION TESTS ON STRIP ANNEALED IN VARIOUS ENVIRONMENTS.[a]

Material	Annealing Medium	Yield Strength, 0.2 Per Cent Offset, psi	Tensile Strength, psi	Elongation in 2 in., per cent
C	air	39 300	125 900	85
B	air	33 000	142 500	47.5
C	hydrogen	35 000	92 700	36
B	hydrogen	29 500	96 200	24
C	vacuum	35 500	124 500	81
B	vacuum	30 600	143 500	42.5

[a] Averaged from quadruplicate tests.

TABLE 13—RESULTS OF OLSEN CUP TESTS.[a]

Material	Annealing Medium	Load at Failure, lb	Depth of Penetration, in.
C	air	4600	0.493
A	air	4800	0.478
C	hydrogen	3100	0.384
A	hydrogen	3400	0.397
C	vacuum	5000	0.526
A	vacuum	4850	0.470

[a] Averaged from quadruplicate tests.

VACUUM ANNEALING

Materials and Procedures:

The experimental materials comprised cold rolled and annealed 0.020-in.-thick by 3-in.-wide stock from three different heats of AISI 301 stainless steel. The composition of the steels is given in Table 10; the first two were reported as having low tensile ductility, while the third was said to have normal ductility.

From Material A, 12 specimens, 3 by $2\frac{1}{2}$ in., were sheared for Olsen cup testing. Twelve longitudinal strip tension specimens with reduced-section dimensions of $\frac{1}{2}$ by $2\frac{1}{2}$ in. were machined from Material B. From Material C, 12 cup and 12 tension specimens were prepared.

Four cup specimens from Materials A and C and four tension specimens from Materials B and C were annealed under each of the following conditions:

1. in air at 1900 F for 30 min
2. in vacuum at 1900 F for 30 min
3. in hydrogen at 1900 F for 30 min

The specimens annealed in air were cooled in air. For annealing in hydrogen, a horizontal furnace with an Inconel muffle and a hydrogen flow rate of 8 to 10 cu ft per hr was employed. This muffle was so constructed that one end of it extended outside the furnace and was water cooled. Annealing was accomplished by placing the specimens in the cold zone of the muffle, purging the muffle with hydrogen, and then moving the specimens into the hot zone of the muffle. After annealing for 30 min, the specimens were moved to the cold zone where they cooled in hydrogen.

For vacuum annealing, a vertical furnace was used. This furnace was constructed with a "bell" section at the top which operated in the vacuum, yet was maintained at about room temperature. Annealing was accomplished by inserting the specimens, held in a specially constructed rack, in the bell section. A vacuum was then drawn and the specimens were lowered into the hot zone. Upon annealing for 30 min, the specimens were returned to the bell section where they cooled in the vacuum. The equipment used developed a vacuum of 5×10^{-4} mm of mercury; however, upon placing the specimens in the hot zone, the vacuum dropped to 0.25 mm. About 15 min was required to regain the high vacuum of 5×10^{-4} mm. It was noted that, during vacuum annealing, a white powdery deposit had formed on the inside of the furnace. This deposit may possibly have been chromium which had vaporized from the specimens and condensed on the furnace parts during annealing.

Strip specimens for hydrogen determinations were annealed with the cup and tension specimens under the three conditions.

Results:

The results of hydrogen determinations on material annealed in the three different environments are given in Table 11. After each annealing treatment, all three materials had very similar hydrogen contents. Those annealed in air had about 1.2 ppm, those annealed in vacuum had about 0.5 ppm, and those annealed in hydrogen contained about 8 ppm hydrogen.

The results of the tension tests are given in Table 12. For Material C of normal ductility, annealing in air and in vacuum resulted in average tensile elongations of 85 and 81 per cent, respectively, while annealing in hydrogen produced a ductility of 36 per cent. For Material B with low ductility, the corresponding elongation values were 47.5, 42.5, and 24 per cent. Annealing in air, in hydrogen, or in vacuum had little effect on the yield strength of either material. However, annealing in hydrogen resulted in a noticeable decrease in the ultimate tensile strength of both.

The results of the Olsen cup tests are given in Table 13. For Material C of normal ductility, depths of penetration at failure of 0.493, 0.526, and 0.384 in. after annealing in air, in vacuum, and in hydrogen, respectively, were obtained. For the low-ductility stock, Material A, the corresponding values were 0.478, 0.470, and 0.397 in. For Material C, loads of 4600 and 5000 lb were required to produce failure of the material air annealed and vacuum annealed, while a load of only 3100 lb was observed for the specimens annealed in hydrogen. For Material A, no significant difference in the load at failure (4800 lb) was noted for specimens vacuum annealed or air annealed. For material hydrogen annealed, the load at failure was only 3400 lb.

Ends of the cup and tension specimens which had been annealed in hydrogen and in vacuum were examined metallographically. A slight amount of grain-boundary carbide precipitation was

observed by use of the electrolytic oxalic acid etch. The amount of carbide precipitation was of the same order for specimens annealed in hydrogen as it was for those annealed in vacuum. Material C appeared to show somewhat more carbide precipitation than the others, possibly because of its somewhat higher carbon content. The specimens annealed in hydrogen had a somewhat larger grain size than those annealed in vacuum.

Discussion of Results:

The results of this study indicate that vacuum annealing at 1900 F for 30 min can result in a low hydrogen content (0.5 ppm) in Type 301 stainless steel strip. However, annealing in air also can result in a low hydrogen content (1.2 ppm). Annealing in hydrogen, on the other hand, can produce a considerable increase in the hydrogen content of the steel.

No significant differences in yield strength, tensile strength, or cup or tensile ductility were found in specimens annealed in vacuum and in air. Annealing in hydrogen, however, resulted in (1) a drop in tensile ductility of about 50 per cent, (2) a reduction in cup ductility of about 20 per cent, (3) a reduction in tensile strength of about 25 per cent, but no significant change in yield strength. It is inferred that the increase in hydrogen content which occurred on annealing in hydrogen was responsible for these changes. Similar effects have been observed in the commercial bright annealing of AISI Type 301 strip in hydrogen-containing atmospheres. However, the magnitude of such effects has been much smaller because the time at temperature in commercial bright annealing is much shorter.

Acknowledgment:

The authors wish to express their appreciation to the Sharon Steel Corp. for sponsoring the programs upon which this paper is based. At the same time, the authors wish to thank the company for granting permission to publish the results reported here.

REFERENCES

(1) J. H. Moore, "Promises and Problems Posed by Vacuum Melting," *Journal of Metals*, Vol. 6, 1954, pp. 1368–1369.

(2) J. H. Moore, "Vacuum-Induction Melting," *National Symposium on Vacuum Technology Transactions*, Edited by E. A. Perry and J. H. Durant, Pergamon Press, New York, N. Y., 1956, pp. 202–208.,

(3) K. Bungardt and H. Sychrovsky, "Properties of Steels Melted Under Reduced Pressure," *Stahl und Eisen*, Vol. 76, No. 16, 1956, pp. 1040–1049.

(4) W. W. Dyrkacz, "Quality Improvements in Stainless Steels and Superalloys by Vacuum Melting," *Metal Progress*, Vol. 75, 1959, pp. 138, 140–142, 144.

(5) R. P. Sopher, A. J. Jacobs, and P. J. Rieppel, "Investigation of Weld-Metal Cracking in High-Strength Steel," *The Welding Journal*, Vol. 34, No. 11, 1955, Research Supplement, pp. 544S–552S.

EFFECTS OF AUSTROLLING ON THE PROPERTIES OF CRUCIBLE 422 STAINLESS STEEL

By R. C. Westgren[1] and E. J. Dulis[1]

Synopsis

Austrolling Crucible 422 stainless steel increased yield strength by as much as 45 per cent and tensile strength by 30 per cent. The fracture toughness characteristics, as indicated by net fracture strength and K_c values, were significantly superior after austrolling. The net fracture strength of conventionally heat-treated steel was 122,000 psi and of austrolled steel was as high as 212,000 psi.

The increased resistance to cracking under stress in a salt solution and in a cathodically hydrogen-charged environment (hydrogen cracking) was significantly improved after austrolling.

A relationship was shown between mechanical fatigue notch crack propagation and stress corrosion and hydrogen cracking. The microstructural changes imparted by austrolling influenced fracture characteristics that were reflected in mechanical and electrochemical properties of the steel.

Metastable austenite deformation is a strengthening technique for hardenable steel that involves plastic deformation below the recrystallization temperature as well as in a temperature range where no decomposition of austenite occurs. On subsequent cooling, the deformed austenite transforms to martensite or bainite or both. Metastable austenite deformation has also been described as ausworking, ausforming, and austrolling.

The early reports (1,2)[2] on this process prompted several investigations (3,4,5). Although some research has been conducted on the effect of metastable austenite deformation on the properties of 12 per cent chromium stainless steels (6–10), only limited data are available on the high-strength modified 12 per cent chromium steels, that is, those with secondary hardening characteristics. The present work was undertaken to provide a better understanding of the mechanism of austrolling and to evaluate the effect of this process on directionality of tensile properties, notched tensile properties, tempering characteristics, and stress-corrosion and hydrogen-cracking characteristics of such a steel.

Materials

Crucible 422—a 12 per cent chromium, hardenable stainless steel—was ideally suited for austrolling since an extremely long incubation period exists in the bay area of the time-temperature-transformation curve, and no bainite reaction takes place (Fig. 1). Air-melted material from a commercial heat (30-ton) and vacuum-induction-melted material from a laboratory heat (50-lb) were used in this investigation. The air-melted steel was in the form of 0.090-in.-thick sheet, and the vacuum-melted steel in the form of 0.75-in.-thick plate. The composition of the air-melted heat conformed with the nominal composition of Type 422; however, the carbon and nitrogen contents of the vacuum-melted heat were lower than those normally found (Table 1).

Procedure

Austrolling:

To secure adequate reductions by rolling as well as to minimize heat losses, sandwich composites (4 by 6 in.) of three or four of the 0.090-in.-thick sheets of the air-melted steel were prepared by welding all four edges. To achieve higher reductions in thickness than were possible with sandwich composites, 2-in.-long, 3-in.-wide samples of the vacuum-melted 0.75-in.-thick plate were used.

Rolling was done on a two-high laboratory mill. The sandwich composites and the plate samples were austenitized at 1900 F for 30 min and 1 hr, respectively, air-cooled to approximately 100 F above the desired rolling temperature, charged into a furnace held at the rolling temperature, soaked for 10 to 15 min, and rolled. Two temperatures, 1000 and 1150 F, were chosen for deformation temperatures, and reductions in thickness up to 90 per cent were achieved. The sandwich composites were reheated between every two passes, and the plates were reheated after each pass. Through the use of Tempilsticks, the estimated lowest temperatures encountered during rolling at 1000 and 1150 F were approximately 900 and 1000 F, respectively. After being rolled to the desired thickness reductions, the sandwich composites were air-cooled, and the plate samples were oil-quenched to room temperature.

For comparison purposes, 0.090-in.-thick samples of the air-melted steel and 0.080-in.-thick samples (hot-rolled from the 0.75-in.-thick plate) of the vacuum-melted steel were conventionally hardened by austenitizing at 1900 F for $\frac{1}{2}$ and 1 hr, respectively, and oil-quenched.

With the exception of the material used in tempering studies, all samples were tempered at 980 F for 1 hr. Only the center one or two sheets were taken from the sandwich composites for testing purposes. To eliminate the effects of oxidation and decarburization, all samples were surface ground.

Tension Tests:

Unnotched tension-test specimens in both the longitudinal and transverse directions were prepared from the conventionally heat-treated and the austrolled samples. Two types of longitudinal notched test specimens, edge-notched and center-notched (Fig. 2), were also prepared. For the edge-notched specimens, the root radii were ground so that the theoretical stress concentration factor (K_t) was 6.3. The center-notched specimens were prepared in accordance with ASTM recommendations (11); the notches were made by electrical discharge machining followed by cracking in a tension-tension fatigue machine. Both types of notched specimens were tested at a crosshead travel speed of 0.05 in./min.

[1] Former staff metallurgist and director of product research and development, respectively, Crucible Steel Company of America, Pittsburgh, Pa.

[2] The boldface numbers in parentheses refer to the list of references appended to this paper.

Copyright© 1965 by ASTM International

www.astm.org

Except for the testing on unnotched longitudinal specimens of the vacuum-melted steel at 1000 F, all tension tests were conducted at room temperature.

Tempering Studies:

To study the effect of austrolling on the tempering characteristics of Type 422, conventionally hardened and austrolled samples of the vacuum-melted steel were tempered for 1 hr at selected temperatures in the range of 800 to 1200 F. Hardnesses (DPH) were determined by taking an average of seven readings on transverse sections of samples with a Tukon testing machine and subsequently converting DPH numbers to those on the Rockwell C scale.

Stress-Corrosion and Hydrogen-Cracking Tests:

Test specimens (0.50 in. wide and 5.00 in. long) were prepared from both conventionally heat-treated and austrolled samples of the vacuum-melted steel. All specimens were stressed to 150,000 psi by bending (2-point loading) in test fixtures and then finished with No. 360 grit paper. The specimens were coated with acrylic resin—except for the area of maximum stress—to eliminate any secondary galvanic effects.

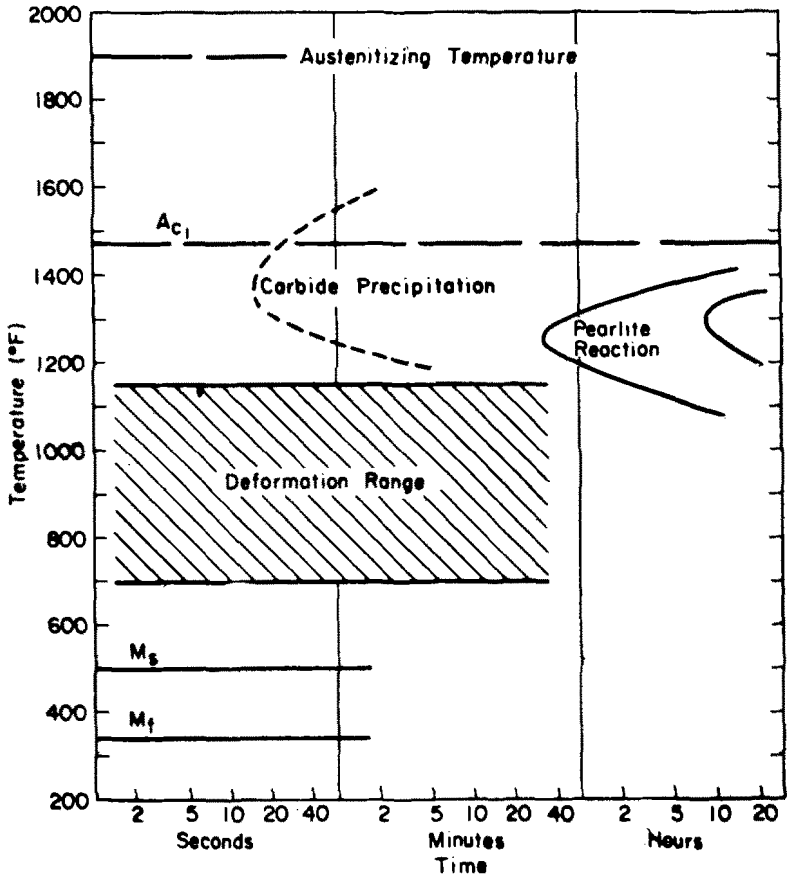


FIG. 1—Time-Temperature-Transformation Diagram for Crucible 422 Stainless Steel.

TABLE 1—CHEMICAL COMPOSITIONS OF CRUCIBLE 422 STAINLESS STEEL, PER CENT.

Heat	C	Mn	P	S	Si	Ni	Cr	V	W	Mo	N
142761[a]	0.23	0.68	0.019	0.018	0.36	0.69	11.71	0.26	0.93	0.94	0.034
090285[b]	0.20	0.70	0.002	0.007	0.05	0.74	11.54	0.24	1.12	1.13	0.002

[a] 30-ton air-melted heat.
[b] 50-lb vacuum-induction-melted heat.

One series of tests was performed in a constant-humidity cabinet (100 F, 98 per cent relative humidity). A 5 per cent NaCl solution was applied, twice a day, to the specimens which were removed from the cabinet once every day and examined macroscopically. The criterion for failure was the existence of cracks when the surfaces were viewed at 40× magnification.

Cathodic hydrogen-cracking tests were performed at a current density of 0.6 amp/in.^{2} in a 0.1N sulfuric acid solution containing 3 mg arsenic per liter. The specimens were removed from the solution and examined at 10× magnification after a 2-min exposure; these 2-min exposures were repeated until failure occurred.

RESULTS AND DISCUSSION

Tension Tests:

The results of the room-temperature tension tests on the air-melted steel (Table 2 and Fig. 3) showed that the difference in austrolling temperatures (1150 and 1000 F) had little effect on tensile properties.

The longitudinal tensile strength increased continually with increasing deformation up to a thickness reduction of 75 per cent; higher reductions could not be achieved because of limitations posed by sample size and rolling equipment. However, the yield strength was not significantly increased until thickness reductions in excess of 60 per cent had been obtained. Comparison of edge-notched and unnotched tensile strength values showed that austrolling decreased the notch sensitivity of Type 422. In general, the elongation tended to decrease with increasing deformation.

The transverse yield and tensile strengths of the air-melted steel increased more rapidly than the longitudinal strengths with increasing deformation, and, at 75 per cent reduction in thickness, the directionality of strength properties was marked. Although the transverse elongation values decreased with increasing deformation, the decrease was not as great as for the longitudinal elongation.

The results of room-temperature tension tests on the vacuum-melted steel (Table 3) showed that sizable increases in both the longitudinal and transverse yield and tensile strengths were effected by austrolling to thickness reductions of 85 to 90 per cent. Although the elongation decreased as a result of deformation in the metastable austenite temperature range, the resultant ductility was still quite reasonable—transverse and longitudinal elongations were decreased the same amount. There was no indication of notch sensitivity at a K_t of 6.3. The magnitude of the change in the longitudinal room-temperature strength properties imparted by austrolling may be summarized as follows:

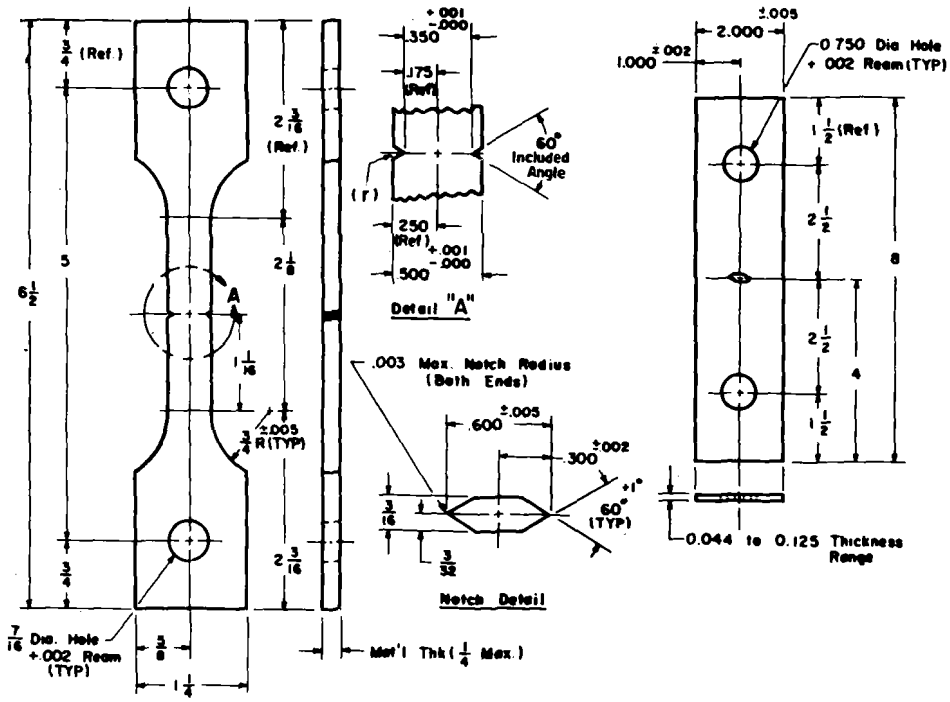


FIG. 2—Notched Tension-Test Specimens.

TABLE 2—ROOM-TEMPERATURE TENSILE PROPERTIES OF THE AIR-MELTED STEEL.

Hardening Treatment[a]	Thickness Reduction, per cent	Direction of Test	0.2 Per Cent Offset Yield Strength, 1000 psi	Tensile Strength, 1000 psi		Elongation in 2 in., per cent
				Unnotched	Notched[b]	
Conventional	0	long.	...	238	201	10.0
	0	long.	174	238	189	11.0
	0	trans.	176	233	...	5.5
Austrolled at 1150 F	35	long.	174	276	241	9.0
	35	long.	178	276	242	9.0
	50	long.	190	279	260	7.0
	50	long.	188	279	258	7.0
	50	trans.	212	292	...	6.0
	50	trans.	208	292	...	6.5
	60	long.	186	279	279	6.0
	60	long.	192	277	266	7.0
	65	long.	189	279	277	5.0
	65	long.	192	282	...	5.0
	65	trans.	217	297	...	3.5
	65	trans.	221	300	...	6.0
	75	long	235	289	286	8.5
	75	long.	237	281	295	6.0
	75	trans.	275	316	...	3.0
	75	trans.	277	315	...	3.5
Austrolled at 1000 F	30	long.	173	269	269	7.5
	30	long.	173	271	259	8.0
	55	long.	180	272	263	6.5
	55	long.	181	274	274	7.0
	60	long.	182	280	252	7.5
	60	long.	185	282	272	6.0
	70	trans.	212	299	...	5.5
	70	trans.	212	288	...	5.0
	75	long.	...	277	297	4.0
	75	long.	229	294	300	4.0
	75	trans.	264	309	...	...
	75	trans.	268	314	...	4.0

[a] All samples were austenitized at 1900 F for ½ hr, hardened as indicated, and then tempered at 980 F for 1 hr.
[b] K_t = 6.3.

	Change Due to Austrolling, per cent	
	85 per cent at 1000 F	90 per cent at 1150 F
Yield strength	+45	+41
Tensile strength	+30	+26
Elongation	−32	−45

These results indicate that, for a given deformation, higher strength is obtained at lower austrolling temperatures.

The results of longitudinal tension tests conducted at 1000 F (Table 3) showed that austrolling also improved the elevated-temperature strength of the vacuum-melted steel. This improvement was most pronounced for the material austrolled 85 per cent at 1000 F for which increases of 20 and 14 per cent in yield and tensile strengths, respectively, were obtained.

It should be noted that the hardness and hence the tensile strength of the conventionally hardened and tempered vacuum-melted steel were considerably lower than the hardness and tensile strength of the conventionally hardened and tempered air-melted steel. This discrepancy is probably due to the difference in the carbon and nitrogen contents of the two heats (Table 1). The as-quenched and quenched and tempered hardness values for the two heats differed by as much as 4 points Rockwell C.

The results of center-notched tension tests (Table 4) showed that the fracture toughness of the vacuum-melted steel was considerably improved by austrolling. On the basis of net fracture strength, a greater improvement in fracture toughness was effected by austrolling at 1000 F than at 1150 F; the average net fracture strength values for the conventionally hardened and the 1000 F austrolled materials were 122,000 and 212,000 psi, respectively. Although the average ratios of net fracture to yield strength of the conventionally hardened and 1150 F austrolled materials were similar (0.72 and 0.68), this ratio was considerably higher (0.86) for the 1000 F austrolled material. When the three materials are compared on the basis of K_c, another fracture toughness parameter, no differences exist between the materials austrolled at 1000 and 1150 F; however, the austrolled materials were superior to the conventionally heat-treated material. The agreement between the K_{c1} values (based on critical crack length measured by 24-frames/sec moving pictures) and the K_{c3} values (based on

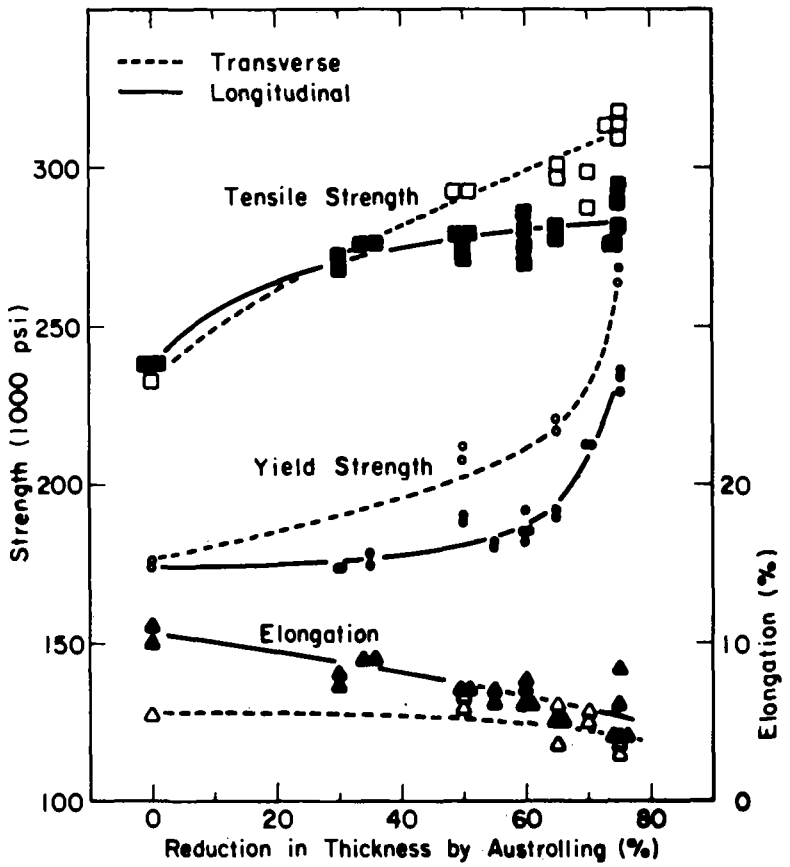


FIG. 3—Effect of Austrolling at 1000 and 1150 F on the Room-Temperature Tensile Properties of the Air-Melted Steel.

TABLE 3—TENSILE PROPERTIES OF THE VACUUM-MELTED STEEL.

Hardening Treatment[a]	Test Temperature, deg F	Direction of Test	0.2 Per Cent Offset Yield Strength, 1000 psi	Tensile Strength, 1000 psi		Elongation in 2 in., per cent
				Unnotched	Notched[b]	
Conventional	75	long.	167	221	209	12.0
	75	long.	170	223	249	11.5
	75	trans.	168	215	...	10.0[c]
	75	trans.	168	216	...	12.0[c]
Austrolled 90 per cent at 1150 F	75	long.	238	276	295	6.0
	75	long.	234	279	273	7.0
	75	long.	242	283	...	6.5
	75	long.	237	279	...	6.5
	75	trans.	279	308	...	7.0[c]
	75	trans.	280	308	...	5.0[c]
Austrolled 85 per cent at 1000 F	75	long.	248	292	312	14.0
	75	long.	245	287	312	7.0
	75	long.	240	288	...	9.0
	75	long.	245	286	...	8.0
	75	trans.	273	309	...	7.0[c]
	75	trans.	278	311	...	7.0[c]
Conventional	1000	long.	121	164	...	8.0
	1000	long.	122	171	...	8.0
Austrolled 90 per cent at 1150 F	1000	long.	127	173	...	10.0
	1000	long.	132	178	...	7.5
Austrolled 85 per cent at 1000 F	1000	long.	140	191	...	6.0
	1000	long.	150	193	...	5.5

[a] All samples were austenitized at 1900 F for 1 hr, hardened as indicated, and then tempered at 980 F for 1 hr.
[b] K_t = 6.3.
[c] Elongation in 1-in. gage length.

measurements of percentage shear) was very good; unfortunately, K_{c1} values could not be determined for the 1000 F austrolled material because the scope of the available plot would not permit the graphical solution of the essential q_c values.

The difference in fracture appearance of the austrolled and conventionally hardened center-notch test specimens was quite striking (Fig. 4). The average percentage shear values (measured at 10×) for 1150 F austrolled, 1000 F austrolled, and conventionally hardened test specimens were 77, 75, and 23 per cent, respectively.

Metallographic examination of the fracture regions of the specimens showed a difference in fracture mode. The conventionally heat-treated specimen primarily exhibited both the large angular contour and the small grain deformation typical of brittle-type fracture, whereas the austrolled specimens exhibited both a smooth contour and grain elongation typical of ductile-type fracture.

Electron microfractographs[3] (Fig. 5) of the center portions of the fractured center-notched specimens (Fig. 4) clearly distinguish between the modes of fracture. The conventionally heat-treated steel fractures (Fig. 5 (*top*)) show the characteristics of brittle fracture such as large cleavage facets containing "river" marks (*A*) and cleavage "tongues" (*B*). The austrolled steel fracture (Fig. 5 (*bottom*)) shows the randomly oriented "dimpled" structure characteristic of flat transverse portions of ductile fracture.

The increased fracture ductility of the austrolled steel is believed to be attributable to the decrease in size and more uniform distribution of both precipitate and dislocation substructure in the austrolled steel; these are factors that would reduce dislocation pileups and, hence, would reduce the probability of fracture. Distortion of the martensite during the austenite-to-martensite transformation occurs due to the martensitic growth process in the deformed (austrolled) austenite, wherein barriers of deformation bands in the austenite have to be overcome (13). Upon tempering at 980 F for 1 hr, the following processes take place in an interrelated manner:

[3] An electron microfractograph technique involving a stripped cellulose acetate replica was used. The replicas stripped from the fracture surface were metal shadowed by a rotary technique and carbon coated. The carbon replica was separated from the primary acetate replica by dissolving the acetate film in warm acetone (see Ref. **12**).

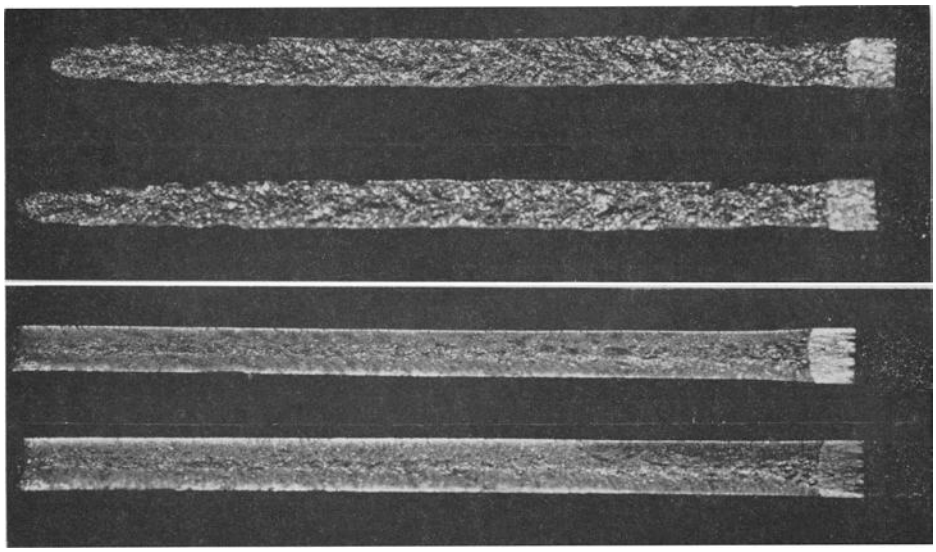
(1) carbide precipitation, (2) polygonization in the martensite, and (3) partial relief of residual stresses. In contrast, conventionally heat-treated steel contains well-defined undistorted martensite needles developed during the austenite-to-martensite transformation. Upon tempering, carbide precipitation and some stress relief occur. Thus, the increase in fracture toughness of the austrolled imparted by austrolling is directly associated with higher strengths at elevated temperatures, and this behavior is shown by the increase in yield and tensile strength of the austrolled steel at 1000 F.

Representative quenched and quenched-and-tempered microstructures of the conventionally hardened and the austrolled materials (Fig. 7) show that a

TABLE 4—ROOM-TEMPERATURE FRACTURE TOUGHNESS CHARACTERISTICS OF THE VACUUM-MELTED STEEL.[a]

Hardening Treatment[b]	Net Fracture Strength, 1000 psi	K_{c1}, 1000 psi $\sqrt{\text{in.}}$	K_{c3}, 1000 psi $\sqrt{\text{in.}}$	0.2 Per Cent Offset Yield Strength, 1000 psi	Ratio of Net Fracture to Yield Strength
Conventional	115	101	117	168	0.68
	130	126	128	168	0.77
Austrolled 90% at 1150 F	157	152	148	238	0.66
	170	188	189	238	0.71
Austrolled 85% at 1000 F	206	...	143	246	0.84
	219	...	182	246	0.89

[a] 0.045-in.-thick longitudinal specimens.
[b] All samples were austenitized at 1900 F for 1 hr, hardened as indicated, and then tempered at 980 F for 1 hr.



(*top*) Conventionally hardened
(*bottom*) Austrolled at 1150 F

FIG. 4—Fracture appearance of Center-Notched Tension-Test Specimens.

steel may be associated with the significantly smaller fracture facets in steel given this prior treatment as compared with conventionally heat-treated steel.

Tempering Studies:

The results of the tempering tests on the vacuum-melted steel showed that, compared to conventionally heat-treated material, the hardness increase resulting from austrolling was not only maintained but increased after tempering (Table 5 and Fig. 6). The retarded tempering highly distorted martensitic microstructure was inherited from the heavily deformed austenite. A detailed explanation of the mechanisms involved in the tempering of this steel after austrolling has been included in another publication (13).

Stress-Corrosion and Hydrogen-Cracking Tests:

For martensitic 12 per cent chromium steels (including the Type 422 of the present investigation), the usual form of cracking is hydrogen cracking. The more common form of stress-corrosion cracking associates (1) crack formation at anodic reaction sites and (2) crack propagation by either a continuous electrochemical mechanism or a periodic electrochemical-mechanical mechanism (14). Hydrogen cracking is not initiated at anodic reaction sites.

The results of the stress-corrosion tests performed in the 5 per cent NaCl solution under a stress of 150,000 psi (Table 6) showed that austrolling significantly increased time to failure. Also, in the cathodic hydrogen cracking tests, similar results were found. As shown in Figs. 8 and 9 for the hydrogen crack test specimens, the cracks that formed in the austrolled materials were short and discontinuous, whereas those that formed in the conventionally hardened material were longer with more continuous paths. The explanation previously given in relation to fracture toughness in tensile stressing also applied to fracture mode in stress corrosion and hydrogen cracking. The shorter fracture paths of austrolled steel are associated with increased resistance to crack propagation.

The results of these tests show that the significant strength increases imparted by austrolling do not affect the crack propagation characteristics adversely in 12 per cent chromium martensitic steels. This finding is in agreement with the results of the center-notched tensile fracture toughness properties previously discussed.

CONCLUSIONS

1. The tensile strength of Type 422 stainless steel increased continually with increasing deformation by austrolling; significant increases in yield strength were not obtained until reductions in thickness in excess of 60 per cent were obtained.

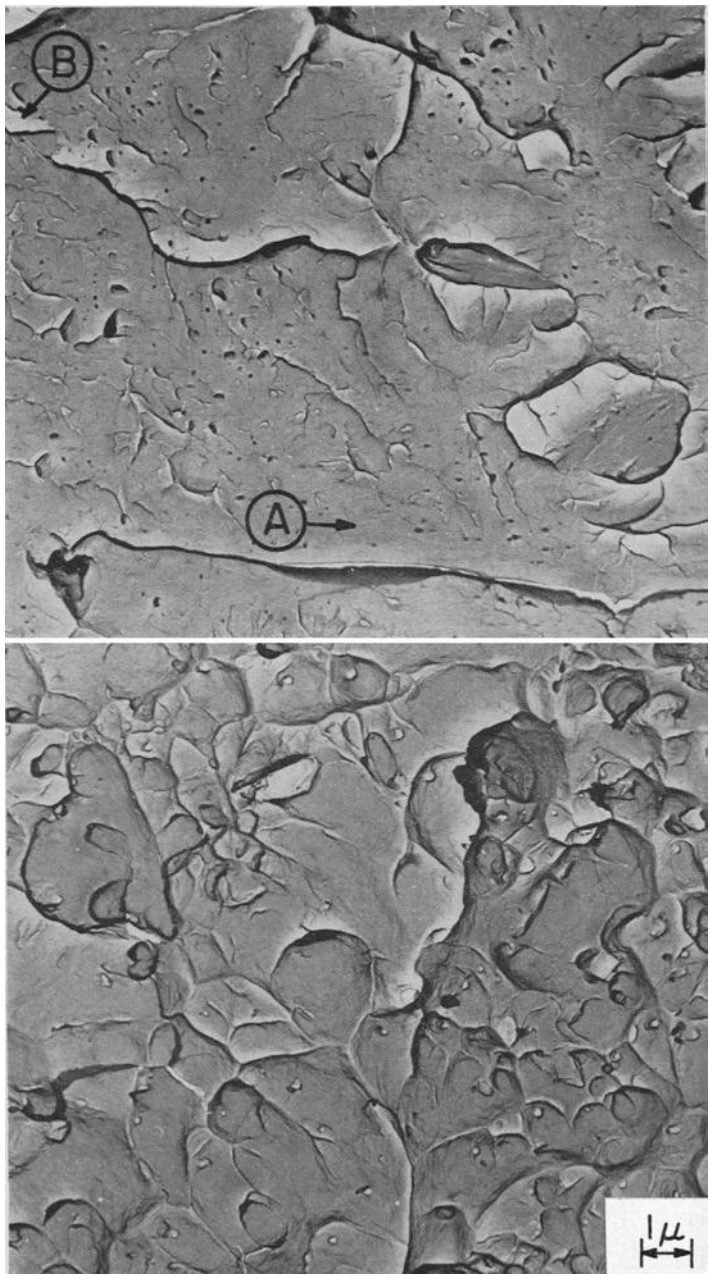
2. Austrolling resulted in directionality of strength properties; the transverse yield and tensile strengths were higher than the longitudinal yield and tensile strengths.

3. Tensile ductility (elongation) decreased with increasing deformation.

4. Ratios of notched (K_t = 6.3) to unnotched tensile strengths were, in general, increased by austrolling.

5. Fracture toughness characteristics, reflected by net fracture strengths and K_c values, were significantly superior after austrolling.

6. For a given large amount of de-



(*top*) Conventionally hardened
(*bottom*) Austrolled at 1150 F

FIG. 5—Electron Microfractographs of Fractured Center-Notched Tension-Test Specimens.

TABLE 5—TEMPERING CHARACTERISTICS OF THE VACUUM-MELTED STEEL.

Tempering Treatment	Rockwell Hardness[a], C Scale		
	Conventionally Hardened	Austrolled 90% at 1150 F	Austrolled 85% at 1000 F
As-quenched.....	50	56	57
800 F for 1 hr.....	46	56	56
900 F for 1 hr.....	47	55	56
980 F for 1 hr.....	47	54	55
1050 F for 1 hr.....	41	49	49
1100 F for 1 hr.....	33	41	43
1200 F for 1 hr.....	29	39	39

[a] Converted from DPH numbers (10-kg load).

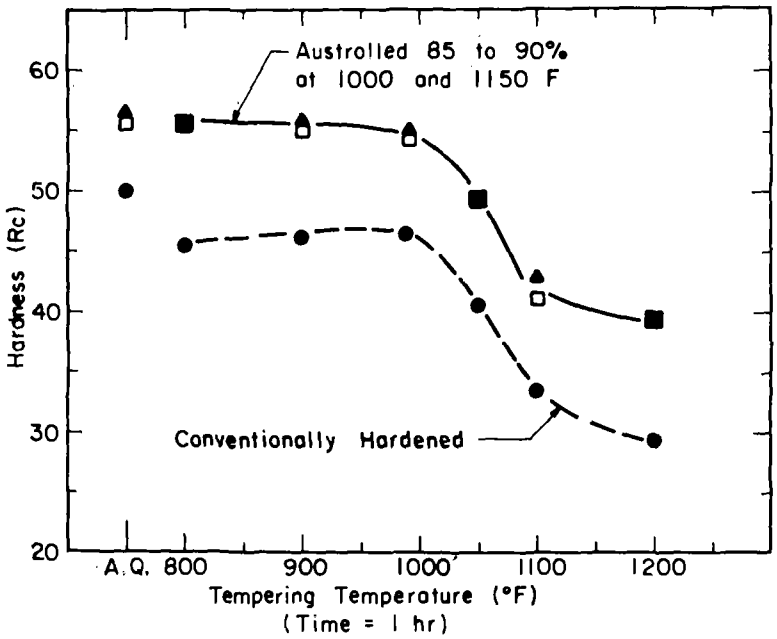
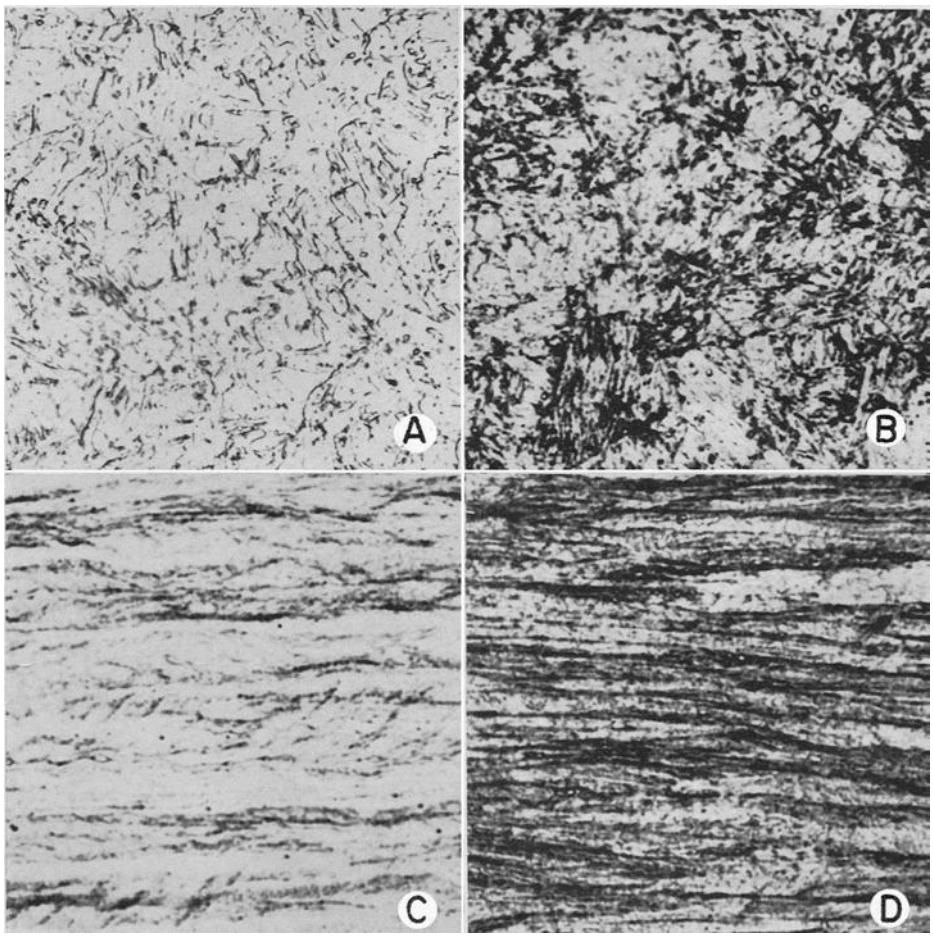


FIG. 6—Variation of Hardness with Tempering Temperature for the Vacuum-Melted Steel.



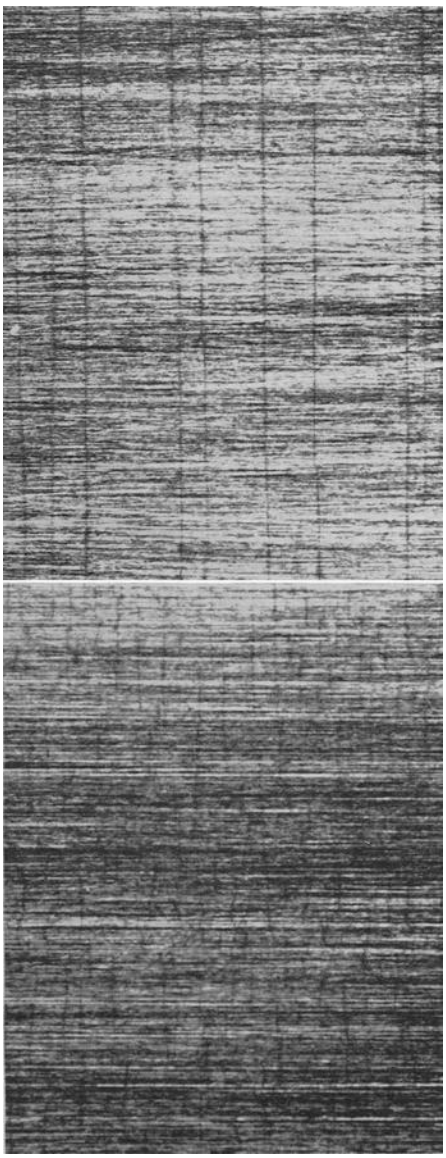
(*a*) Conventionally hardened; as-quenched
(*b*) Conventionally hardened; tempered at 980 F
(*c*) Austrolled at 1150 F; as-quenched
(*d*) Austrolled at 1150 F; tempered at 980 F

FIG. 7—Representative Microstructures of As-Quenched and Quenched-and-Tempered Vacuum-Melted Steel. Etched in Picral-HCl (×1000).

TABLE 6—RESULTS OF STRESS-CORROSION AND HYDROGEN-CRACKING TESTS ON THE VACUUM-MELTED STEEL.

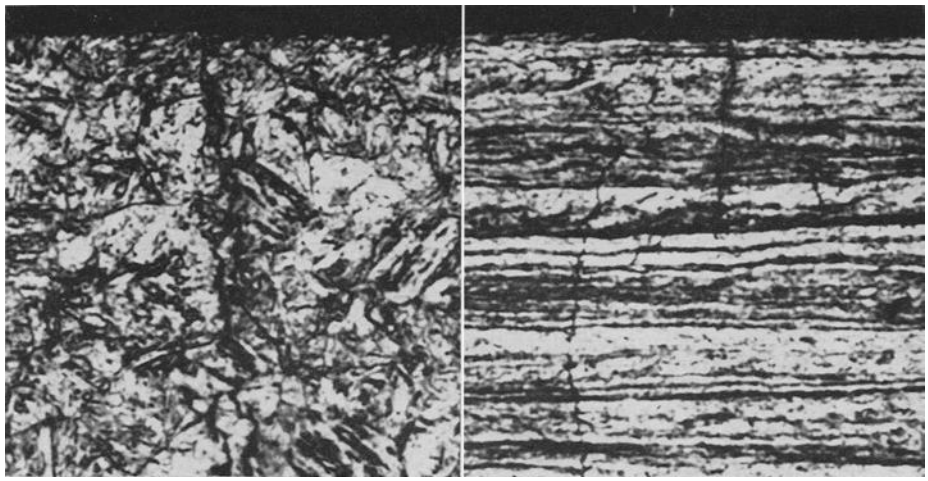
Hardening Treatment[a]	Stress, 1000 psi	Failure Time in 5 % NaCl Solution, days	Failure Time in 0.1N H_2SO_4 + 3 mg As per liter, 0.6 amp per sq. in., min
Conventional	150	2	6
	150	14	6
Austrolled 90 per cent at 1150 F	150	>36	16
	150	>36	18
Austrolled 85 per cent at 1000 F	150	>36	16
	150	>36	16

[a] All samples were austenitized at 1900 F for 1 hr, hardened as indicated, and then tempered at 980 F for 1 hr.



(*top*) Conventionally hardened
(*bottom*) Austrolled at 1150 F

FIG. 8—Typical Appearance of Specimens That Failed in the Hydrogen-Cracking Test.



(*left*) Conventionally hardened
(*right*) Austrolled at 1150 F

FIG. 9—Difference in Modes of Cracking in Hydrogen-Cracking Test Specimens. Etched in Picral-HCl (×1000).

formation, better strength and toughness were obtained by austrolling at 1000 F rather than 1150 F.

7. In addition to substantially increasing hardness, austrolling to reductions of thickness of 85 to 90 per cent in the temperature range of 1000 to 1150 F resulted in a significant retardation of tempering in the temperature range of 800 to 1200 F.

8. Austrolling increased the resistance to cracking under stress in a salt solution and in a cathodically charged environment.

Acknowledgment:

The authors gratefully acknowledge the assistance of J. M. Capenos, L. Redmerski, and W. Getchell of the Crucible research staff for their valuable assistance in the various experimental phases of this investigation. Also, the helpful discussions with J. P. Hirth, Ohio State University, are acknowledged.

REFERENCES

(1) R. F. Harvey, "Step Quenching, Hot Peening, Improve Lean Alloys," *Iron Age*, Dec. 27, 1951, Vol. 168, pp. 70–71.

(2) E. M. H. Lips and H. van Zuilen, "Improved Hardening Technique," *Metal Progress*, August, 1954, Vol. 66, pp. 103–104.

(3) C. W. Marschall, "Hot-Cold Working of Steel to Improve Strength," *Report No. 192*, Defense Metals Information Center, Oct. 11, 1963.

(4) V. F. Zackay, M. W. Justusson, and D. J. Schmatz, "Strengthening by Martensitic Transformations," *Strengthening Mechanism in Solids*, Am. Soc. Metals, 1962, pp. 179–216.

(5) M. W. Justusson and V. F. Zackay, "Engineering Properties of Ausformed Steels," *Metal Progress*, December, 1962, Vol. 82, pp. 111–114.

(6) F. A. Malagari, "Discussion to Paper by J. C. Shyne, V. F. Zackay, and D. J. Schmatz," *Transactions*, Am. Soc. Metals, Vol. 52, 1960, pp. 367–370.

(7) J. E. Srawley and T. C. Lupton, "Ausworked 12% Cr Steel with High Yield Strength and Fracture Resistance," *NRL Progress Report PB 161278*, U.S. Naval Research Laboratory, February, 1960, pp. 7–10.

(8) K. J. Irvine, F. B. Pickering, and J. Garstone, "The Effect of Composition on the Structure and Properties of Martensite," *Journal Iron and Steel Inst.*, Vol. 196, September, 1960, pp. 66–81.

(9) Y. Hosoi and K. Pinnow, "The Tensile Properties of Type 410 Stainless Deformed Before and After Martensite Transformation," *Transactions*, Am. Soc. Metals, Vol. 53, 1961, pp. 591–602.

(10) R. A. Grange and J. B. Mitchell, "Strengthening Low-Alloy Steels by Deforming Austenite," *Metals Engineering Quarterly*, Vol. 1, February, 1961, pp. 41–53.

(11) Special ASTM Committee Report, "Fracture Testing of High Strength Sheet Materials," *ASTM Bulletin*, January, 1960, pp. 29–40.

(12) B. R. Banerjee, J. J. Hauser, and J. M. Capenos, "Etch-Shadow Extraction Replica in Fracture Studies," *Review Scientific Instruments*, Vol. 34, May, 1963, pp. 477–479.

(13) B. R. Banerjee, R. C. Westgren, J. M. Capenos, and E. J. Dulis, "Ausworking Type 422 Stainless Steel," *Transactions*, Am. Soc. Metals, Vol. 56, 1963, pp. 629–642.

(14) S. Barnartt, "General Concepts of Stress-Corrosion Cracking," *Corrosion*, Vol. 18, September, 1962, pp. 322t–331t.

DISCUSSION

J. J. HEGER[1]—The austrolled steels and conventionally heat-treated steels were tested in stress corrosion at the same stress level. What would be the results if the stress were a given fraction of the yield strength? Does austrolling increase the fatigue and corrosion fatigue strength to the same proportion that it increases the tensile and yield strength?

R. C. WESTGREN AND E. J. DULIS *(authors)*—The points raised by Mr. Heger are pertinent for a fuller understanding of the effects of austrolling on the properties of 12 per cent chromium martensitic steels. Unfortunately, our tests were limited to those reported in the paper, so we are unable to shed further light on the questions raised. Additional work will be required to more fully resolve such aspects as fatigue, corrosion fatigue, and fracture time under different stresses.

[1] Chief research engineer, stainless steel, U. S. Steel Corp., Pittsburgh, Pa.

HIGH-STRENGTH STAINLESS STEEL BY DEFORMATION AT LOW TEMPERATURES

By S. Floreen[1] and J. R. Mihalisin[2]

Synopsis

A series of nickel-chromium stainless alloys made by air and vacuum melting were rolled 20 or 40 per cent at temperatures ranging from −320 to 400 F. Smooth and sharp-notched sheet-tensile properties were measured after heat treating the cold-rolled pieces for 24 hr at 800 F. Yield strengths up to 260 ksi were obtained. Hardening resulted primarily from martensite formation, and also from work hardening of the austenite prior to transformation. The yield strengths were correlated in terms of composition.

Lowering the silicon content to 0.1 per cent significantly raised the toughness. Over the ranges studied none of the remaining elements had effects comparable to silicon. The toughness at a given strength level also depended upon the rolling conditions, but not upon the per cent martensite.

Tests at −320 F with a low-silicon alloy showed a notch-tensile ratio of 1.0 at 297 ksi ultimate tensile strength. The results suggest that a low-silicon 301-type composition would have good cryogenic properties.

Several investigations have shown that very high strengths can be obtained by cold or sub-zero rolling Type 18-8 stainless steels (1–11).[3] To date, however, there has been little systematic study of the effects of composition on the mechanical properties of stainless steels treated this way. It is recognized that lower alloy content grades are more easily hardened by cold rolling or sub-zero rolling, but information on the influence of rolling conditions and composition on strength properties is lacking. One of the objects of the present program was to survey the influence of composition and rolling conditions on strength.

A more serious problem is that of toughness. The general results have indicated that when the yield strengths of cold-rolled stainless steels are on the order of 250,000 psi, toughness is poor. There is some evidence that lower carbon and nitrogen contents improve toughness (**4, 5, 10**). There apparently has been no consistent study, however, of the influence of alloying elements on toughness. A study of toughness versus composition was the second object of this investigation.

[1] Supervisor, Iron-Nickel Alloys Section, Research Laboratory, The International Nickel Co., Inc., Bayonne, N.J.

[2] Metal Physics Section, Research Laboratory, The International Nickel Co., Inc., Bayonne, N.J.

[3] The boldface numbers in parentheses refer to the list of references appended to this paper.

Experimental Procedure

Only variations in the principal alloying elements, nickel, chromium, manganese, silicon, carbon and nitrogen, common to stainless steels, were made in this study. No attempt was made to evaluate the effects of subversive elements, or other alloying elements such as titanium or columbium which are used in some grades of stainless steel. The carbon contents in this study were in the 0.04 to 0.08 weight per cent range, and the nitrogen contents varied from 0.01 to 0.05 per cent. The remaining elements varied approximately as follows: 5 to 10 per cent nickel, 17 to 20 per cent chromium, 0.01 to 1.0 per cent manganese, and 0.01 to 0.5 per cent silicon.

Thirty-pound heats were prepared using electrolytic metal charges. Heats were made by either air induction melting or vacuum induction melting. The air-melted heats containing less than 0.14 per cent silicon were deoxidized by adding 0.1 per cent aluminum. The final aluminum contents in these heats were on the order of 0.05 per cent. The compositions of all the heats are given in Table 1.

The 4 by 4 in. ingots from each heat were soaked one hour at 2100 F, rough forged, cropped, and then forged to 1-in. thick plate. The plates were soaked 1 hr at 1900 F and hot rolled to $\frac{1}{4}$-in. thicknesses. They were then cold rolled, annealed for 1 hr at 1950 F, and air cooled. The sheets were then given a final light machining to remove scale and to obtain the desired thickness prior to the final rolling.

Sub-zero rolling was done primarily at −106 F to a total reduction of thickness of 40 per cent. A number of additional specimens were also rolled 20 per cent at −106 F, and 20 or 40 per cent at −320 F. Also some specimens were rolled 20 or 40 per cent at +70 F, +200 F, and +400 F. These latter tests were made primarily to evaluate some of the effects of rolling temperature on the strength.

Rolling was done using a two-high Stanat mill with 8-in. diameter rolls. The reductions per pass were on the order of 0.005 to 0.008 in. except for the final pass, which was generally lighter. All of the sheets were rolled to a final thickness of 0.060 in.

Baths of solid CO_2 plus isopentane (−106 F), and liquid nitrogen (−320 F) were used for the sub-zero rolling. Strips were cooled in the bath, removed, and given one pass through the rolling mill, and then returned to the bath and allowed to come to the bath temperature again before making another pass.

A water bath was used for the +70 F rolling, and a small electric oven for rolling at +200 F and +400 F. The general procedure was the same as that used for sub-zero rolling.

Although the strips before rolling were initially at some known temperature, the actual temperature during deformation may have been considerably different from this initial value. Brown and coworkers (**9**) have attempted to estimate the sheet temperature during rolling by measuring the temperature immediately before and immediately after rolling. In the present work, the initial temperature prior to rolling is designated as the rolling temperature, without attempting to estimate the exact temperature during rolling. This simplification is reasonable for the present comparative type of tests.

Copyright© 1965 by ASTM International

www.astm.org

After rolling, the specimens were heat treated for 24 hr at 800 F. Heat treatments of this type raise the strength of sub-zero rolled 18-8 alloys (1–3, 6). The reasons for the resultant benefits are not certain. This particular heat treatment is not necessarily the optimum one, but it was beyond the scope of this work to study this variable in detail. A few specimens, however, were tested in the as-rolled condition without any heat treatment.

TABLE 1—CHEMICAL COMPOSITION OF NICKEL-CHROMIUM STAINLESS ALLOYS, WEIGHT PER CENT.

Alloy	Ni	Cr	Mn	Si	C	N
VACUUM-MELTED HEATS						
1	7.6	18.0	0.95	0.09	0.05	0.05
2	10.1	19.8	0.45	0.10	0.04	0.01
3	10.3	18.3	0.72	0.11	0.04	0.01
4	6.7	18.8	0.67	0.12	0.04	0.01
5	5.3	17.0	0.48	0.07	0.05	0.01
6	7.7	18.9	0.78	0.11	0.05	0.01
7	8.6	18.8	0.75	0.10	0.06	0.01
8	8.2	18.4	0.01	0.10	0.05	0.01
9	8.8	18.6	0.47	0.57	0.05	0.01
AIR-MELTED HEATS						
10	7.4	18.7	0.05	0.13	0.07	0.02
11	9.0	18.4	0.92	0.50	0.05	0.02
12	9.0	18.4	1.01	0.01	0.04	0.03
13	7.7	18.5	0.81	0.44	0.04	0.05
14	8.1	18.5	0.82	0.46	0.05	0.03
15	8.1	18.7	0.13	0.13	0.06	0.05
16	6.0	17.7	0.25	0.05	0.08	0.04
17	5.5	17.7	0.21	0.08	0.08	0.03

TABLE 2—ROOM-TEMPERATURE TENSION-TEST RESULTS. SPECIMENS HEAT TREATED 24 HR AT 800 F AFTER ROLLING.

Alloy	0.2% Offset Yield Strength, ksi	Ultimate Tensile Strength (UTS), ksi	Elongation in 2 in., %	Notch Tensile Strength (NTS), ksi	Net Fracture Stress, ksi	NTS/UTS
ROLLED 20% AT −320 F						
1	265	265	4	...	...	...
2	185	193	14	...	...	...
3	175	190	9	...	...	...
4	215	253	6	...	...	...
5	199	200	11	...	...	...
6	250	252	3	247	272	0.98
7	247	250	4	236	270	0.94
8	260	262	4	262	281	1.00
9	275	278	4	261	303	0.94
10	257	259	3	239	256	0.92
11	172	198	10	199	245	1.00
12	203	214	6	218	230	1.02
13	217	225	5	246	288	1.09
14	212	221	5	232	276	1.05
15	239	243	4	235	288	0.97
17	235	238	2	240	281	1.01
ROLLED 40% AT −320 F						
2	254	259	3	229	251	0.88
3	254	257	9	...	...	...
4	249	251	3	223	241	0.89
5	214	215	8	...	...	...
ROLLED 20% AT −106 F						
1	252	252	11	...	...	...
2	101	139	33	...	...	...
5	191	191	11	...	...	...
6	221	223	4	241	272	1.08
7	133	174	10	206	245	1.18
8	200	237	16	...	...	...
9	121	174	11	191	242	1.10
10	222	227	4	226	263	1.00
12	174	188	5	199	233	1.05
17	220	225	5	...	...	...

The strips were then machined to NASA-type smooth and edge-notched tension specimens (4). The notched tensile specimens had a stress concentration factor, K_t, of 18 or larger.

The majority of the tension tests were conducted at room temperature. Ink staining was used to estimate the net fracture stress (12). Several specimens were tested at −320 F using a liquid nitrogen bath around the specimens.

Only longitudinal specimens were tested, because the experimental rolling mill did not have sufficient capacity to roll transverse specimens. For reductions up to 40 per cent, however, the mechanical anisotropy of cold-rolled stainless steel is not severe (3,8,9), and thus longitudinal specimens were considered to be satisfactory for screening tests.

A number of specimens were examined by X-ray diffraction to determine the phases present and the amounts of martensite formed. Many specimens were also examined by optical and electron microscopy. The resistance of two sub-zero rolled alloys to atmospheric stress corrosion was also evaluated. The results of these latter studies will also be described.

RESULTS AND DISCUSSION

Effects of Rolling Conditions on Yield Strength:

Table 2 summarizes the room-temperature tensile properties of the specimens heat treated 24 hr at 800 F after rolling. The results show that yield strengths between 68,000 and 275,000 psi were obtained with changes in rolling temperature, reduction, and composition.

Figure 1 shows the yield strength of three of the alloys versus rolling temperature after 20 per cent reduction. The least stable alloy, containing 5.3 per cent nickel, had an essentially constant yield strength of 195,000 psi over the entire range of rolling temperatures. The most stable alloy, containing 10.1 per cent nickel, had relatively low strengths over this range. The intermediate alloy, containing 7.6 per cent nickel, had low yield strengths after warm rolling, but showed a marked increase in strength with sub-zero rolling.

Figure 2 compares the effects of 20 and 40 per cent reduction on the yield strengths of two of these alloys. The 5.3 per cent nickel alloy showed an increase in yield strength of only about 10,000 psi with 40 per cent reduction compared to 20 per cent reduction.

Conversely, much larger gains in yield strength were obtained with the 10.1 per cent nickel alloy using 40 per cent reduction.

The strengthening of 18-8 stainless steel by cold work results primarily from the transformation of metastable austenite to martensite during deformation.

TABLE 2—*Concluded.*

Alloy	0.2% Offset Yield Strength, ksi	Ultimate Tensile Strength (UTS), ksi	Elongation in 2 in., %	Notch Tensile Strength (NTS), ksi	Net Fracture Stress, ksi	NTS/UTS
			ROLLED 40% AT −106 F			
1	263	264	8	252	284	0.96
2	222	232	4	241	253	1.04
4	251	251	3	247	265	0.98
5	203	209	8	229	249	1.09
6	262	263	3	261	303	0.99
7	249	250	3	262	294	1.05
8	257	259	4	271	310	1.05
9	254	264	3	246	264	0.93
10	274	274	2	277	298	1.01
11	246	254	3	222	265	0.88
12	236	240	3	238	265	0.99
13	261	261	3	236	272	0.90
14	254	255	4	238	274	0.93
15	237	239	3	249	273	1.04
16	249	251	3	252	290	1.00
17	232	235	3	234	259	1.00
			ROLLED 20% AT +70 F			
1	144	165	22	...	...	...
2	90	118	39	...	...	...
4	210	212	8	...	...	...
5	186	186	8	...	...	...
6	135	173	24	...	...	...
7	109	148	29	...	...	...
8	131	164	24	...	...	...
9	70	106	45	...	...	...
10	84	165	29	...	...	...
11	108	132	28	...	...	...
			ROLLED 40% AT +70 F			
2	136	148	10	...	...	...
3	101	116	34	...	...	...
4	195	195	9	...	...	...
6	191	207	5	217	234	1.05
7	159	183	7	189	219	1.03
8	191	208	6	223	257	1.08
9	156	163	8	192	222	1.18
10	198	209	6	216	250	1.03
11	156	175	11	...	...	...
12	174	194	9	...	...	...
16	222	223	4	230	244	1.03
17	215	216	6	200	240	0.94
			ROLLED 20% AT +200 F			
1	74	141	26	...	...	...
2	73	96	34	...	...	...
5	195	195	33	...	...	...
			ROLLED 40% AT +200 F			
2	113	126	57	...	...	...
5	207	207	36	...	...	...
			ROLLED 20% AT +400 F			
1	69	131	28	...	...	...
2	68	94	49	...	...	...
3	76	99	10	...	...	...
4	106	161	20	...	...	...
5	199	200	51	...	...	...
			ROLLED 40% AT +400 F			
2	96	111	14	...	...	...
3	102	116	22	...	...	...
5	213	213	20	...	...	...

X-ray examination of the present cold-rolled alloys supported this conclusion. Specimens with yield strengths of 200,000 psi or higher generally contained 70 to 100 per cent martensite. Figure 3 illustrates the relation between yield strength and martensite content as measured by X-ray diffraction for the 10.1 per cent nickel alloy. Figure 4 is an optical microscopic study of the microstructure of this 10.1 per cent nickel alloy after the two reductions (20 and 40 per cent) at various temperatures. There is a marked difference between the structures obtained upon rolling at sub-zero and elevated temperatures. The structures obtained upon rolling at elevated temperatures appear to bear only slip traces from deformation whereas the structures formed at sub-zero temperatures are darkly etching and reveal orientation relationships between the martensite and parent austenite lattice.

No microstructural difference could be observed here to account for the different strength levels at a given martensite content as shown in Fig. 3. For instance, rolling 20 per cent at −320 F results in the same amount of martensite formation as rolling 40 per cent at −106 F. Any difference in microstructure is not obvious.

Electron micrographs of these same structures delineate the martensite with more clarity. This is shown in Fig. 5, micrographs of shadowed negative replicas after rolling 20 and 40 per cent at −106 F and −320 F. The structures are similar to those shown by Reed (13). It appears that the martensite needles are parallel to (111) austenite planes. Again the effect of degree of rolling on strength as shown in Fig. 3 is not obvious from these higher magnification studies.

The epsilon (hexagonal close-packed) transition phase observed by many workers in studies of metastable stainless steels was observed in this work only under special conditions. The (10.1) epsilon peak was clearly observed in X-ray diffraction patterns of alloys which transformed partially to martensite on cooling to room temperature. No epsilon phase was observed after cold rolling and heat treating. This result is in accord with previous work in which the epsilon phase disappears with large amounts of deformation or heat treatments on the order of 800 F (13–16).

The main reason for achieving higher

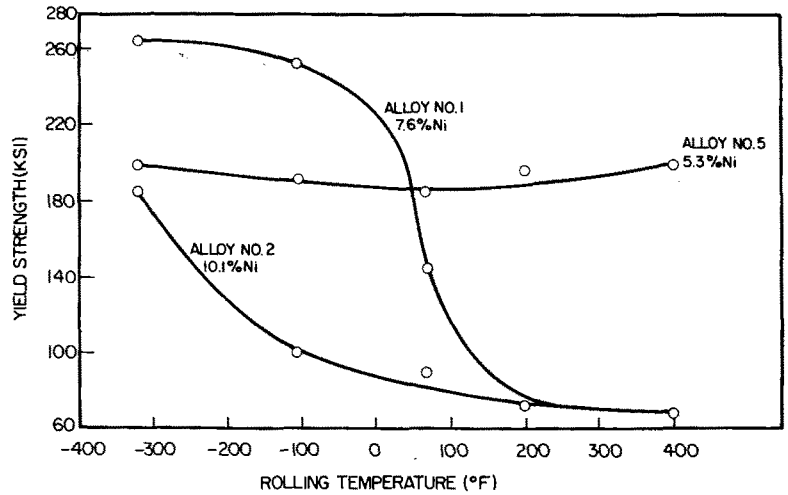


FIG. 1—Yield Strength Versus Rolling Temperature for Three Alloys. All Specimens Rolled 20 Per Cent and Heat Treated at 800 F for 24 hr After Rolling.

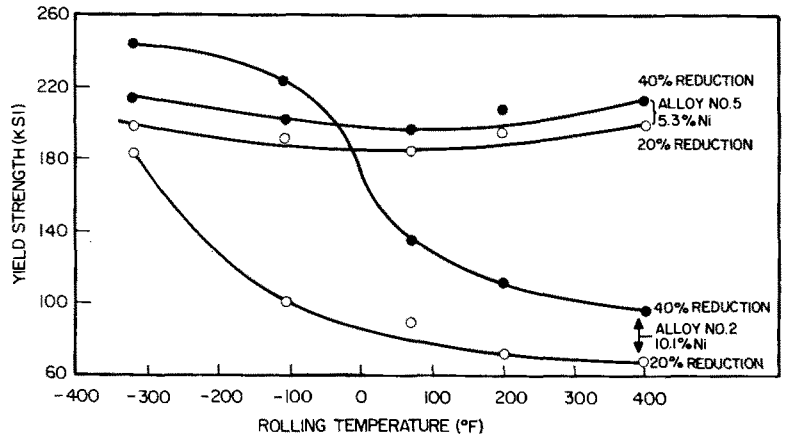


FIG. 2—Yield Strength Versus Rolling Temperature for Two Alloys. Specimens Rolled 20 and 40 Per Cent and Heat Treated at 800 F for 24 hr After Rolling.

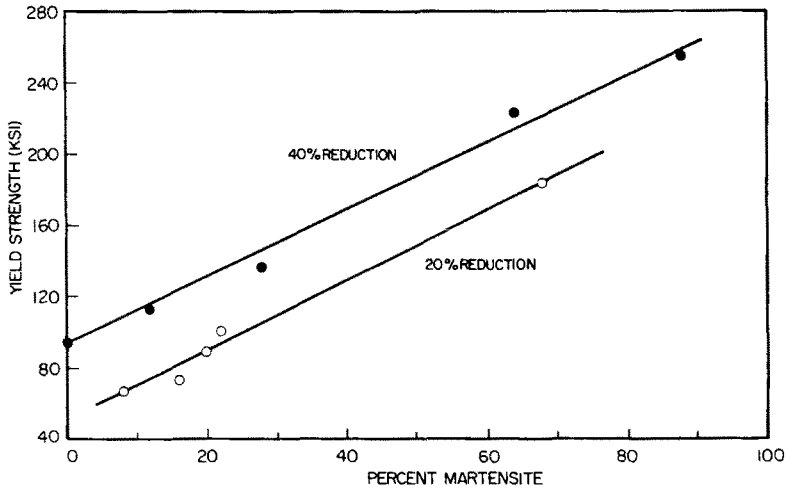


FIG. 3—Yield Strength Versus Per Cent Martensite for Alloy No. 2 (10% Ni) Cold Rolled 20 and 40 Per Cent at Various Temperatures. Heat Treated at 800 F for 24 hr After Rolling.

strengths exemplified by Figs. 1 and 2 is the formation of martensite by rolling. With lower rolling temperatures and larger reductions increasing amounts of martensite are formed, and the strength increases accordingly. The data for the 7.6 per cent nickel alloy in Fig. 1, and the 10.1 per cent nickel alloy in Fig. 2 suggest that most of the strength change is produced within a relatively small change in rolling conditions.

There appear to be other factors influencing strength in addition to martensite formation. Figure 3, for example, shows that for a given martensite content, the specimens rolled 40 per cent were significantly stronger than those rolled 20 per cent. Thus the amount of cold work also is important. Presumably this effect is due to work hardening of the austenite prior to transformation, or work hardening of the martensite after transformation, or both. The results with the 5.3 per cent nickel alloy illustrated in Fig. 2 indicate that there is little work hardening of the martensite. With this alloy, approximately 99 per cent martensite was formed after only 20 per cent reduction over the entire range of rolling temperatures. As noted previously, the 40 per cent reduction increased the strength about only 10,000 psi, indicating very little strengthening from cold rolling of martensite.

One must conclude, therefore, that work hardening of the austenite prior to transformation produces a significant amount of strengthening which is incorporated in some unknown fashion into the final strength of the martensite (14). This same effect has also been noted in the related method of strengthening by ausforming (17,18).

Effects of Composition on Yield Strength:

Assuming martensite formation to be mainly responsible for strength, it should be possible to correlate the effects of composition in terms of the M_d temperature. Since the M_d temperature is proportional to the more easily estimated M_s temperature (19,20), the correlations made here will be in terms of M_s.

The effects of the individual alloying elements on the M_s temperature have been estimated by Eichelman and Hull (21). Based on their findings, the relative stability, S, of an alloy may be defined as:

$$S = \text{Ni} + 0.68(\text{Cr}) + 0.55(\text{Mn}) + 0.45(\text{Si}) + 27(\text{C} + \text{N}) \quad (1)$$

Higher values of S indicate an alloy that would be more resistant to transformation to martensite.

Plots of yield strength versus S for several different rolling conditions are shown in Figs. 6 and 7. The data may be represented with reasonable accuracy by a smooth curve for each rolling condition. Thus, empirically, the correlation of strength with S appears useful. It should be noted, however, that such a correlation may only be useful within

certain composition limits. In particular, larger amounts of carbon and nitrogen may strengthen the martensite to an extent that overweighs the change in S (5).

The curves in Figs. 6 and 7 indicate that for a given rolling condition there is an optimum value of S which will have the highest strength. Similar results have been shown by Carlsen and Thomas using a different composition correlation (11). The value of S producing the highest strength varies somewhat with the rolling conditions. With lighter reductions and higher temperatures, this maximum occurs at lower values of S. This would be expected, since more stable alloys will not transform as readily to martensite at higher temperatures and lighter reductions.

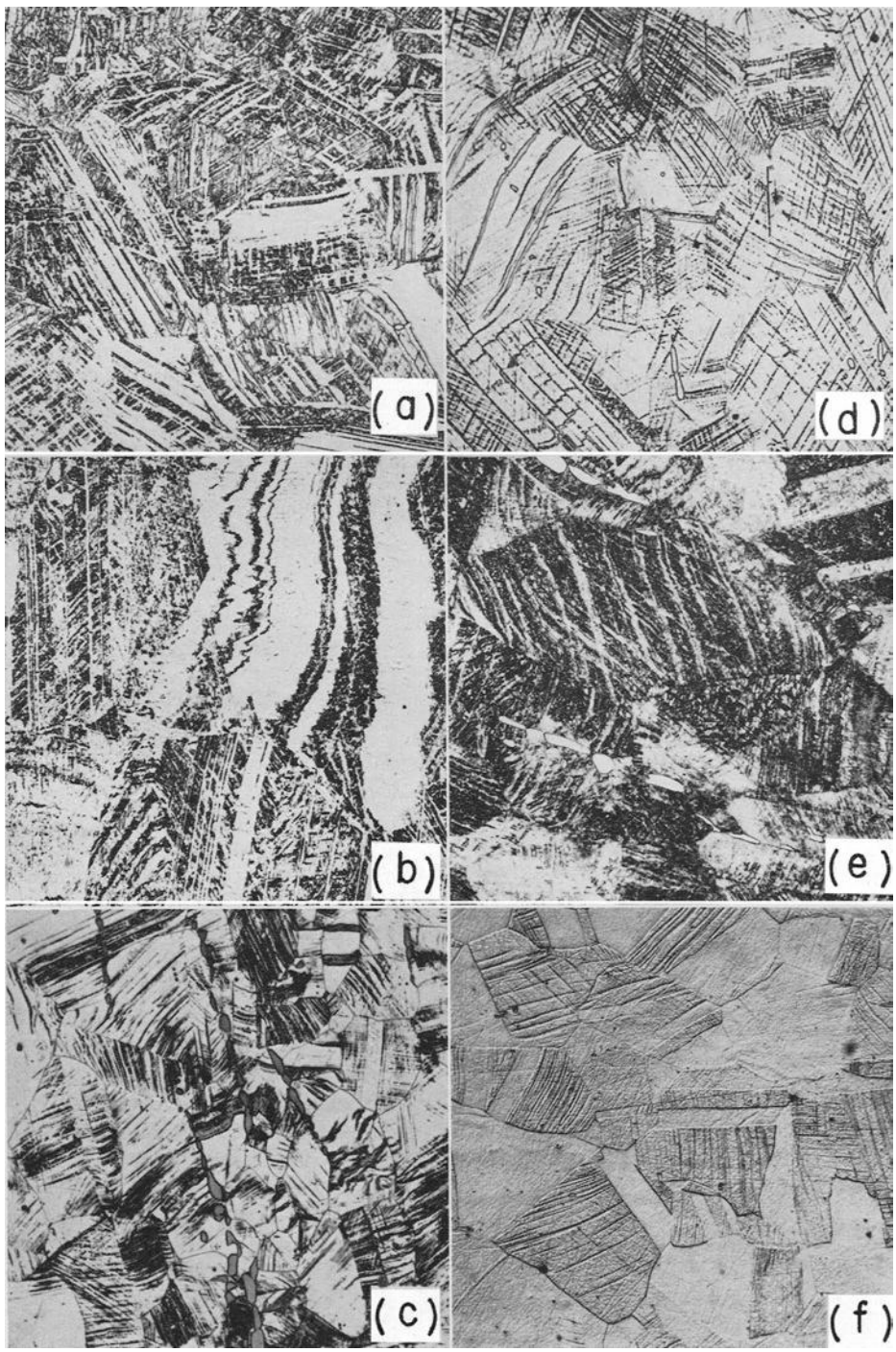
For a given rolling condition, the drop in strength with increasing S above the maximum value is due to decreasing amounts of martensite formation. This conclusion is supported by the X-ray diffraction results.

The drop in strength below the maximum with decreasing values of S is puzzling. Originally it was believed that as the austenite became less stable martensite would form either on cooling to the rolling temperature, or during the initial stages of rolling. In either case, there would be little work hardening of the austenite, and this strengthening contribution would not be included in the final strength. However, two tests in which the heat treatment after rolling was omitted indicate that S was a function of heat treatment also. The results in Figs. 6 and 7 are based on heat treatments of 24 hr at 800 F after rolling. Two of the less stable alloys were rolled 40 per cent at −106 F and tested without heat treatment. The results are given in Table 3. It is seen that when the heat treatment was omitted the yield strengths were much higher.

This result is surprising, and contrary to the usual increase in strength produced by heat treatment. Figure 8 exemplifies the more normal gain in strength with the 800 F heat treatment for another alloy having a higher stability. These results show a marked increase in strength with heat treatment after sub-zero rolling.

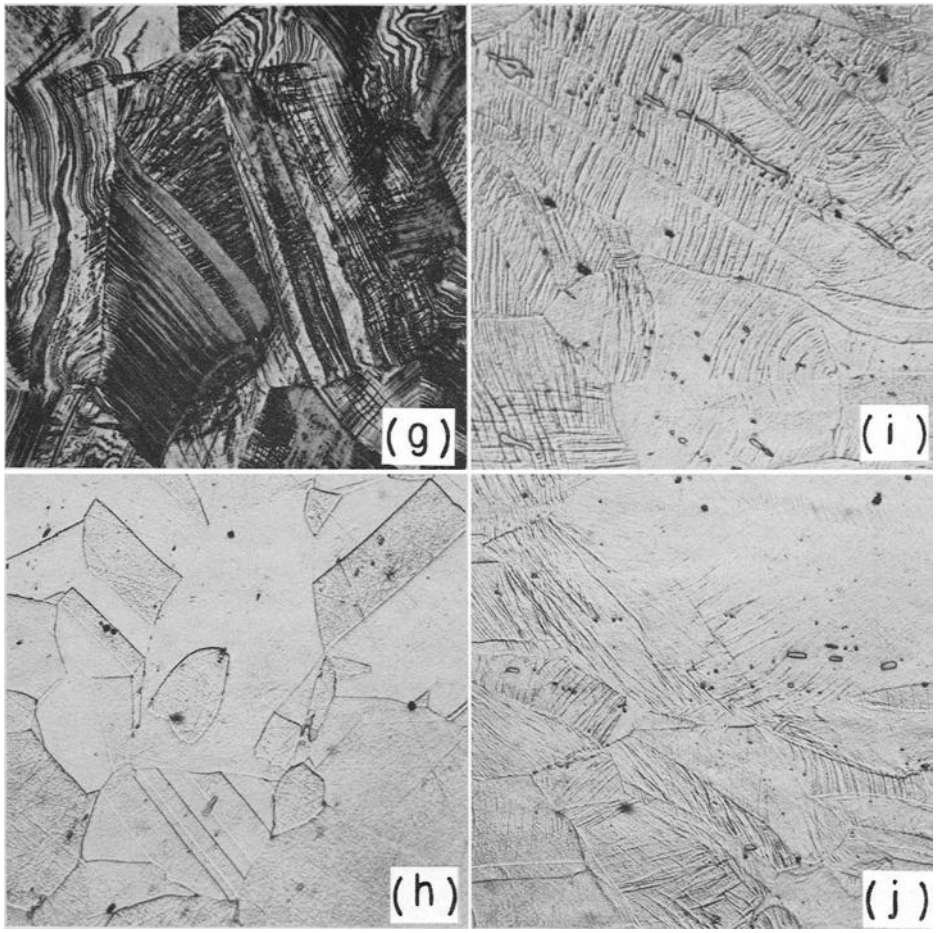
X-ray diffraction studies of the less-stable alloys showed amounts of martensite on the order of 100 per cent after rolling, whereas the specimens around the peaks of the yield strength versus S curves had martensite contents on the order of 85 to 95 per cent. It thus appears that some minimum amount of austenite may be necessary to obtain strengthening by heat treatment after rolling. Bastien and Dedieu (22) have also noted that when a stainless steel was completely transformed to martensite by cold working there was a loss in strength with subsequent heat treatment. Alloys containing some residual austenite, however, showed an increase in strength after heat treating (22).

Examination of specimens before and



(*a*) Rolled 20% at −320 F, 185 ksi yield strength.
(*b*) Rolled 40% at −320 F, 254 ksi yield strength.
(*c*) Rolled 20% at 70 F, 90 ksi yield strength.
(*d*) Rolled 20% at −106 F, 101 ksi yield strength.
(*e*) Rolled 40% at −106 F, 222 ksi yield strength.
(*f*) Rolled 20% at 200 F, 73 ksi yield strength.

FIG. 4—Microstructures of Alloy No. 2 (10.1% Ni After Cold Rolling and Heat Treating 24 hr at 800 F. Picric-Hydrochloric Etch (× 250).



(*g*) Rolled 40% at 70 F, 136 ksi yield strength.
(*h*) Rolled 20% at 400 F, 68 ksi yield strength.
(*i*) Rolled 40% at 200 F, 113 ksi yield strength.
(*j*) Rolled 40% at 400 F, 96 ksi yield strength.

FIG. 4.—(*Concluded*).

after heat treatment using X-ray diffraction and electron microscopy revealed only a change in etching response; no changes in microstructure of phase content could be detected. Thus the influence of heat treatment on structure has not been defined. In view of the effect of austenite it would seem, however, that more than stress-relief is involved. One might postulate that austenite serves as a sink for atoms diffusing from martensite during heat treatment.

In view of these effects of heat treatment it is clear that the strength versus S curves in Figs. 6 and 7 are not fundamental in nature. Such curves might be of empirical value in allowing the prediction of strength produced by a given rolling condition and heat treatment.

Effects of Composition and Rolling Conditions on Toughness:

In the majority of the tensile results in Table 2 the net fracture stress measured by the ink stain technique was well above the yield strength, and accurate estimates of G_c and K_c were not possible. These results indicate that at yield strengths of 250,000 psi the values of G_c were in excess of 1000 in.-lb/in.^{2}, and the values of K_c were in excess of 180 ksi $\sqrt{\text{in.}}$

A much more distinct, and perhaps more meaningful, evaluation of toughness can be made in terms of the ratios of notch to tensile strength. At lower strengths the specimens almost invariably had a ratio of 1.0 or higher. With yield strengths above 230,000 psi, however, the distinct composition effect of silicon becomes evident.

Figure 9 summarizes the yield strengths and notch-tensile ratios at two silicon levels of specimens rolled 40 per cent at −106 F. The alloys containing 0.44 to 0.57 per cent silicon had notch-tensile ratios ranging from 0.88 to 0.93, and an average ratio of 0.91. At the same strength level the specimens containing 0.01 to 0.13 per cent silicon had notch-tensile ratios ranging from 0.96 to 1.05, and an average ratio of 1.01. Thus lowering the silicon content significantly improved toughness.

The effect of silicon appeared to be about the same in both air- and vacuum-melted alloys. Statistical analysis of the data indicated that none of the remaining elements affected toughness to the extent that silicon did. The effect of silicon in the specimens rolled at −320 F is not certain, because only one of the higher silicon content alloys had a yield strength above 225 ksi. Therefore it is not possible to make a good comparison of the properties at the two silicon levels.

Another general result is that, although many of the specimens rolled 20 per cent at −320 F had yield strengths comparable to those rolled 40 per cent at −106 F, the notch-tensile ratios of the specimens rolled 20 per cent at −320 F were lower. Comparing low silicon heats with yield strengths over 230 ksi, the average notch-tensile ratio of the specimens rolled 20 per cent at −320 F was 0.96, while the average ratio for the specimens rolled 40 per cent at −106 F was 1.01. This result is somewhat surprising, because earlier studies of sub-zero rolling indicated that better ductility resulted from lighter reductions at lower temperatures (2). This earlier conclusion was based on elongation values, however, which do not always correlate with notch-tensile results. Thus, in some cases, better toughness may result from rolling to larger reductions at higher temperatures.

There was no correlation of toughness with per cent martensite. In particular, specimens containing 100 per cent martensite had toughness after the 800 F heat treatment comparable to those containing residual austenite. This result is shown in Table 3. Thus retained austenite is not a requirement for good toughness in these alloys.

The marked influence of heat treatment on toughness is also illustrated in Table 3. A detailed study of the effect of heat treatment on toughness has been conducted by Brown and co-workers (3). As already indicated, the reasons for the changes in properties with heat treatment are not clear.

−320 F Tension Tests:

As a further evaluation of the effect of silicon on toughness, specimens from a high- and a low-silicon heat were sub-

zero rolled, heat treated, and then tested at −320 F. The results of these tests are given in Table 4. The marked increase in toughness of the low-silicon heat is clearly evident. In particular, the notch ratio of 1.01 for the low-silicon sample rolled 40 per cent at −106 F indicates that this alloy may be useful in cryogenic applications.

The reason for the effect of silicon on toughness is unknown at this time. Metallographic and X-ray diffraction comparisons of alloys with high and low silicon content showed no significant differences in structure. No evidence of the epsilon phase was detected, and thus the effect of silicon does not seem to be related to the presence of this phase during testing.

Corrosion Resistance:

No thorough study of the corrosion resistance of sub-zero rolled stainless steels has been made. From scattered tests, however, the corrosion resistance appeared satisfactory when the steels contained large amounts of martensite (1,3,23).

A preliminary evaluation of the resistance to atmospheric stress corrosion of two of the present alloys was made. Small samples of Heats 2 and 5 (10.1 and 5.3 per cent nickel) were cold rolled 40 per cent at −320 F and heat treated at 800 F. Strips 3.0 by 0.062 by 0.1875 in. were ground from the sheets and loaded in 3-point bending to an outer-fiber stress of 200,000 psi. After over one year exposure to the Bayonne atmosphere there was no evidence of cracking or rusting in these samples.

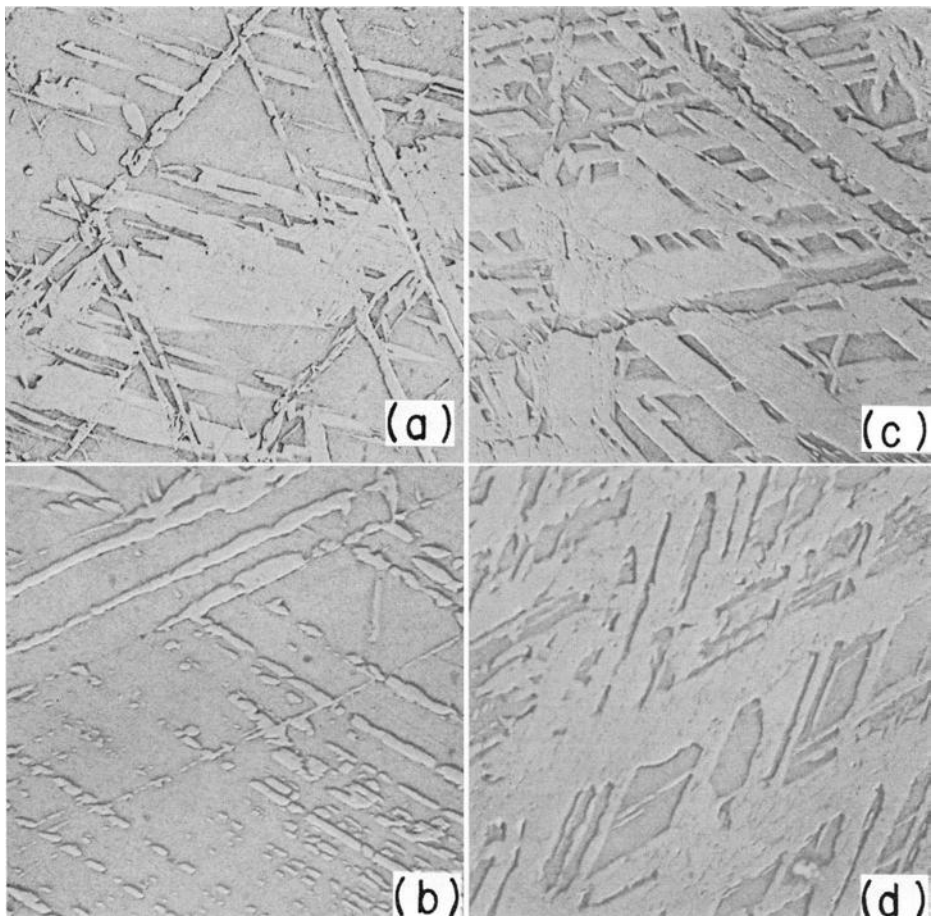
These results again support the general conclusion that sub-zero rolled stainless steels have at least satisfactory corrosion resistance. A more comprehensive study of the corrosion behavior of these materials would be very useful, however.

GENERAL COMMENTS

The general results indicate that good strength and toughness qualities can be obtained in sub-zero rolled stainless steel by use of a suitable composition and rolling procedure. In itself this finding is significant, because in the past the toughness qualities have been poor at high strength levels.

The best strength and toughness properties were obtained by rolling low-silicon alloys 40 per cent at −106 F, and heat treating 24 hr at 800 F. The curves in Fig. 6 indicate that for this particular case the optimum value of S is about 22.5. Assuming 0.10 per cent silicon, 0.10 per cent carbon plus nitrogen, 0.5 per cent manganese, and 17.5 per cent chromium, the nickel content on the basis of Eq (1) should then be approximately 7.7 per cent. The optimum composition is thus essentially a low-silicon, low-carbon-and-nitrogen, Type 301 stainless steel.

It is worth noting in this regard that the nominal composition ranges for nickel, chromium, and manganese in



(*a*) Rolled 20% at −320 F, 185 ksi yield strength.
(*b*) Rolled 20% at −106 F, 101 ksi yield strength.
(*c*) Rolled 40% at −320 F, 254 ksi yield strength.
(*d*) Rolled 40% at −106 F, 222 ksi yield strength.

FIG. 5—Electron Micrographs of Specimens of Alloy No. 2 (10.1% Ni) Showing Structures Produced by Rolling and Heat Treating 24 hr at 800 F (×8000).

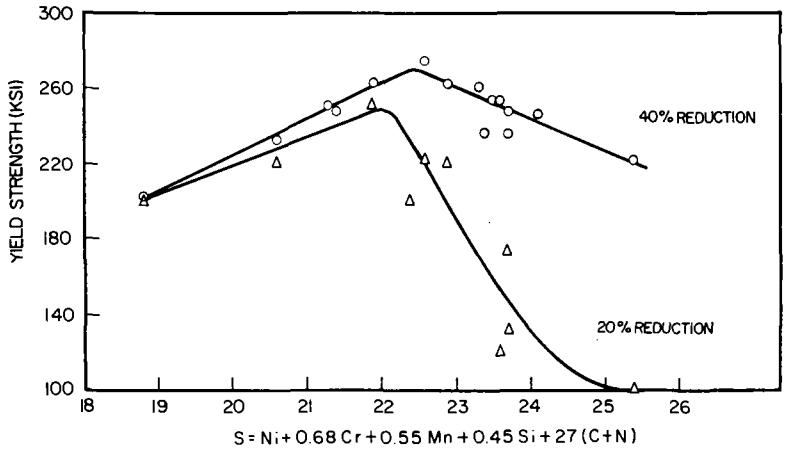


FIG. 6—Yield Versus Stability, S, for Specimens Rolled at −106 F. Heat Treated 24 hr at 800 F After Rolling.

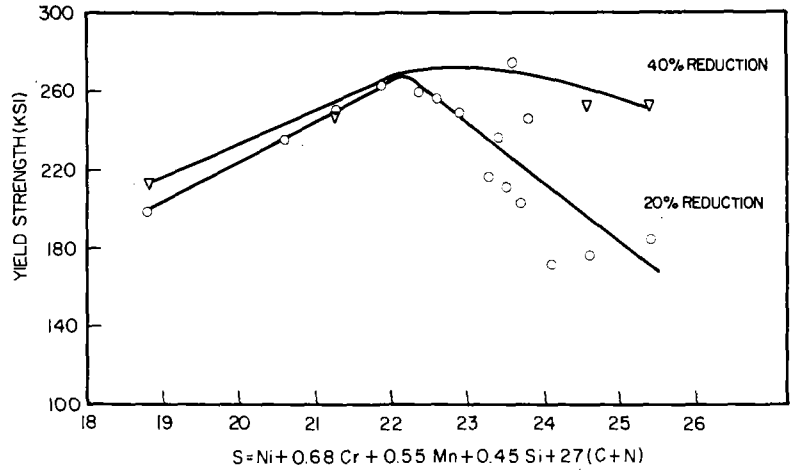


FIG. 7—Yield Strength Versus Stability, S, for Specimens Rolled at −320 F. Heat Treated 24 hr at 800 F After Rolling.

TABLE 3—TENSION TEST RESULTS FOR ALLOYS ROLLED 40% AT −106 F TESTED WITH AND WITHOUT HEAT TREATMENT OF 24 HR AT 800 F AFTER ROLLING.

Alloy	Condition	0.2% Offset Yield Strength, ksi	Ultimate Tensile Strength (UTS), ksi	Elongation in 2 in., %	Notch Tensile Strength (NTS), ksi	Net Fracture Stress, ksi	NTS/UTS
16.....	as cold rolled	272	273	0.4	176	208	0.64
16.....	800 F, 24 hr	249	251	3	252	290	1.00
17.....	as cold rolled,	[a]	273	0.1	[b]	[b]	[b]
17.....	800 F, 24 hr	232	235	3	234	259	1.00

[a] Broke before 0.2% offset.
[b] Not measured.

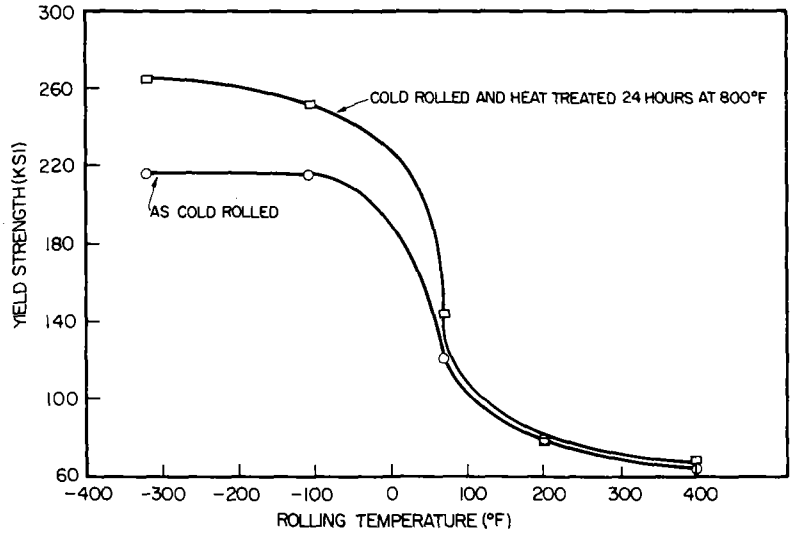


FIG. 8—Yield Strength Versus Rolling Temperature for Alloy No. 1 (7.6% Ni) Rolled 20 Per Cent and Tested As-Rolled and After Heat Treating 24 hr at 800 F.

Type 301 stainless steel are broad. A composition on the low side in these elements would have a yield strength of about only 200,000 psi, instead of about 250,000 psi. Thus the total composition should be controlled to somewhat narrower limits than the present commercial ranges if reproducible properties are to be insured. Fortunately, the shapes of the curves in Figs. 6 and 7 are fairly flat, and thus the composition specifications may not need to be so narrow as to preclude commercial control.

The reasons for the effects of heat treatment, silicon content, and rolling procedure on properties are not clear at this time. In this respect the present work has raised more questions than it has answered. More thorough study of some of these problems should be very rewarding. More potent tools than conventional replica electron microscopy and X-ray diffraction will be required to investigate these questions. In particular, the observation of the fine structure of martensite by transmission electron microscopy would be a likely approach.

CONCLUSIONS

A study has been made of the effects of composition and rolling practice on the strength properties of Type 18-8 stainless steels. The results have shown:

1. Lowering the silicon content to the 0.01 to 0.13 weight per cent range significantly improved the toughness qualities of sub-zero rolled 18-8 stainless steels. At these silicon levels notch-tensile ratios of 1.0 were obtained at yield strengths up to 274,000 psi.

2. For the best combination of strength and toughness a suitable composition appears to be approximately 7 to 8.5 nickel, 18 to 19 chromium, 0.1 to 1 manganese, 0.01 to 0.15 silicon, 0.04 to 0.08 carbon, and 0.01 to 0.04 nitrogen.

3. Preliminary tests at −320 F indicated that notch-tensile ratios of 1.0 at yield strengths on the order 300,000 psi could be obtained with lower-silicon alloys.

4. The toughness is to some extent dependent upon the rolling conditions. Reductions of 40 per cent at −106 F gave comparable yield strengths but better toughness than 20 per cent reduction at −320 F. Residual austenite is not required for good toughness.

5. The effect of composition on yield strength properties after cold rolling and heat treating 24 hr at 800 F could be correlated in terms of the influence of the alloying elements on the M_s temperature.

6. The 800 F heat treatment after rolling apparently raised the yield strength of sub-zero rolled alloys when they contained some minimum amount of austenite. With no austenite, this heat treatment lowered the strength.

7. Hardening by sub-zero rolling results primarily from martensite formation. A significant amount of hardening also may result from the work hardening of the austenite prior to transformation to martensite.

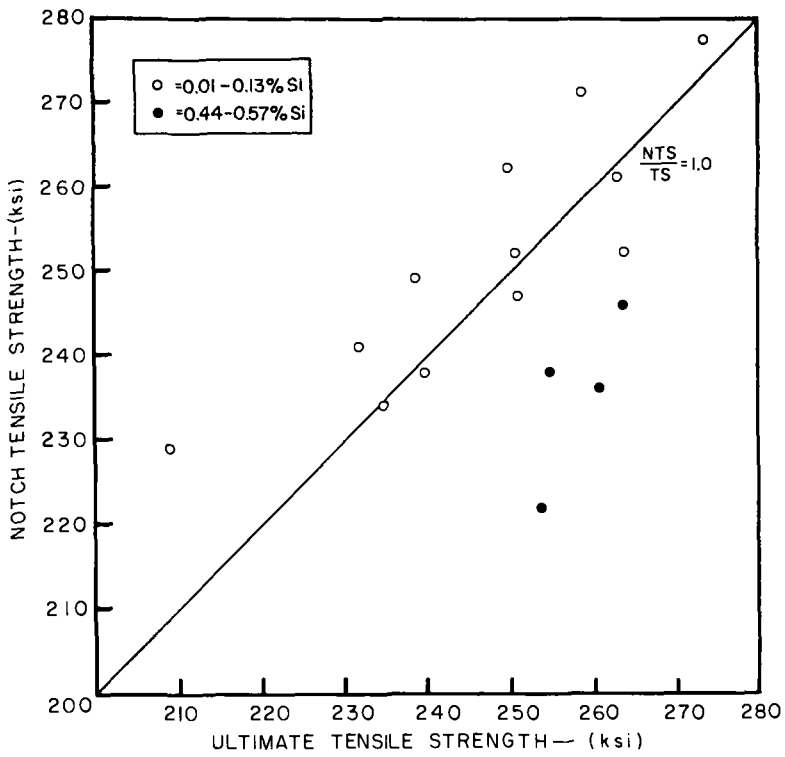


FIG. 9—Tensile Properties of Specimens Rolled 40% at −106 F and Heat Treated 24 hr at 800 F, Showing Effect of Silicon Content.

TABLE 4—RESULTS OF TENSION TESTS AT −320 F.

Alloy	% Si	Condition	0.2% Offset Yield Strength, ksi	Ultimate Tensile Strength (UTS), ksi	Elongation in 2 in., %	Notch Tensile Strength (NTS), ksi	Net Fracture Stress, ksi	NTS/UTS
14.....	0.46	A[a]	273	286	21	180	316	0.63
15.....	0.13	A	275	287	6[c]	270	327	0.94
14.....	0.46	B[b]	312	313	2	223	307	0.71
15.....	0.13	B	296	297	1[c]	300	369	1.01

[a] A = 20% reduction at −320 F plus 800 F for 24 hr.
[b] B = 40% reduction at −106 F plus 800 F for 24 hr.
[c] Broke at knife edge.

REFERENCES

(1) N. A. Ziegler and P. H. Brace, "Hardening of Austenitic Stainless Steels by Mechanical Working at Sub-zero Temperatures," *Proceedings*, Am. Soc. Testing Mats., Vol. 50, 1950, p. 861.

(2) V. N. Krivobok and A. M. Talbot, "Effect of Temperature on the Mechanical Properties, Characteristics, and Processing of Austenitic Stainless Steel," *Proceedings*, Am. Soc. Testing Mats., Vol. 50, 1950), p. 895.

(3) G. B. Espey, A. J. Rapko, and W. F. Brown "Effect of Cold Rolling and Stress Relief on the Sharp Edge Notch Tensile Characteristics of Austenitic Stainless Steel Sheet Alloys," *Proceedings*, Am. Soc. Testing Mats., Vol. 59, 1959, p. 816.

(4) G. B. Espey, M. H. Jones, and W. F. Brown, "The Sharp Edge Notch Tensile Strength of Several High Strength Steel Sheet Alloys," *Proceedings*, Am. Soc. Testing Mats., Vol. 59, 1959, p. 837.

(5) J. F. Watson and J. L. Christian, "Low Temperature Properties of Cold Rolled AISI Types 301, 304 ELC, and 310 Stainless Sheet Steel," *ASTM STP No. 287*, Am. Soc. Testing Mats., 1960, p. 170.

(6) C. R. Mayne, "Effect of Zerolling on the Properties of Modified Type 347 Stainless Steel," *ASTM STP No. 287*, Am. Soc. Testing Mats., 1960, p. 150.

(7) D. W. McDowell and J. R. Mihalisin, "Zerolling Boosts Strength of Stainless Steel," *Materials in Design Engineering*, Vol. 53, May, 1961, p. 10.

(8) M. P. Hansen, "Smooth and Sharp Notch Tensile Properties of Cold Reduced AISI 301 and 304L Stainless Steel at 75, −320, and −423°F," *NASA Technical Note D-592*, 1961.

(9) G. B. Espey, M. H. Jones, and W. F. Brown, "Some Factors Influencing the Fracture Toughness of Sheet Alloys for Use in Lightweight Cryogenic Tankage," *ASTM STP No. 302*, Am. Soc. Testing Mats., 1961.

(10) J. F. Watson and J. L. Christian, "A Study of Austenite Decomposition at Cryogenic Temperatures," *Transactions*, Met. Soc. of AIME, Vol. 224, 1962, p. 998.

(11) K. M. Carlsen and K. C. Thomas, "Effect of Composition, Heat Treatment and Cold Rolling of Mechanical Properties of Cr-Ni Stainless Steels," *Transactions Quarterly*, Am. Soc. Metals, Vol. 55, 1962, p. 462.

(12) "Fracture Testing of High-Strength Sheet Materials," *ASTM Bulletin*, January, 1960, p. 29.

(13) R. P. Reed, "The Spontaneous Martensitic Transformation in 18% Cr, 8% Ni Steels," *Acta Metallurgica*, Vol. 10, 1962, p. 865.

(14) B. Cina, "Effect of Cold Work on the γ-α Transformation in Some Fe-Ni-Cr Alloys," *Journal of the Iron Steel Inst.*, Vol. 177, 1954, p. 406.

(15) H. Otte, "The Formation of Stacking Faults in Austenite and Its Relation to Martensite," *Acta Metallurgica*, Vol. 10, 1957, p. 614.

(16) J. F. Breedis and W. D. Robertson, "The Martensitic Transformation in Single Crystals of Iron-Chromium-Nickel Alloys," *Acta Metallurgica*, Vol. 10, 1962, p. 1077.

(17) V. F. Zackay, W. M. Justusson, and J. D. Schmatz, "Deformation of Metastable Austenite—An Interim Progress Report," *Metals Progress*, Vol. 80, September, 1961, p. 68.

(18) W. M. Justusson and D. J. Schmatz, "Some Observations on the Strength of Martensite Formed from Cold-Worked Austenite," *Transactions Quarterly*, Am. Soc. Metals, Vol. 55, 1962, p. 640.

(19) T. Angel, "Formation of Martensite in Metastable Austenite," *Journal of the Iron Steel Inst.*, Vol. 177, 1954, p. 165.

(20) H. C. Fielder, B. L. Averbach, and M. Cohen. "The Effect of Deformation on the Martensitic Transformation in Austenitic Stainless Steels," *Transactions*, Am. Soc. Metals, Vol. 47, 1955, p. 267.

(21) H. C. Eichelman and F. C. Hull, "The Effect of Composition on the Temperature of Spontaneous Transformation of Austenite to Martensite in 18-8 Type Stainless Steel," *Transactions*, Am. Soc. Metals, Vol. 45, 1953, p. 77.

(22) P. G. Bastien and J. M. B. Dedieu, "Formation and Tempering of Martensite in 18-8 Steels," *Journal of the Iron Steel Inst.*, Vol. 183, 1956, p. 254.

(23) N. N. Lyulicheva and N. V. Pisareva, "Corrosion Resistance of Austenitic Steels Worked at Sub-zero Temperatures," *Izvest Chem. Met.*, February, 1960, p. 78.

THE MECHANISMS OF DEFORMATION AND WORK HARDENING IN AISI TYPE 301 STAINLESS STEEL

By W. F. Barclay[1]

Synopsis

The mechanical properties of austenitic and martensitic stainless steels have been the subject of numerous research papers. The most complex types of materials, however, are the semiaustenitic steels which transform from austenite to martensite during plastic deformation. The most common commercial material which makes use of this characteristic is AISI Type 301. The research reported here had as its goal the determination of the mechanisms which control strain hardening and plastic deformation in commercially produced Type 301. The primary research tools used to reveal the mechanisms of deformation were the measurement of martensite forming during plastic deformation and the examination, by electron transmission and electron diffraction, of tension specimens deformed to various increments of plastic strain.

The work of Angel (1)[2] and Powell et al (2) revealed that the transformation from austenite to martensite during plastic deformation varied with the mode of deformation and was a maximum for uniaxial tension. It is usually a good approximation to describe plastic flow by the equation:

$$S = ae^n \quad \ldots\ldots\ldots\ldots (1)$$

where:

S = true stress,
e = true strain,
n = work-hardening coefficient, and
a = material constant evaluated from test data.

The rate of work hardening is then described by n and determined as the slope of a ln S versus ln e curve.

Angel directly related a change in n with strain in 18Cr-8Ni alloys to the fraction of martensite formed. The alloy stability could be predicted successfully by consideration of chemical composition as indicated by Angel (1), and Eichelman and Hull (3). The less stable the austenite at room temperature, the quicker it transformed with strain, and the higher the n value.

Early research, as reported in the literature, considered only three mechanisms of deformation to be operative in semiaustenitic stainless steels: (1) dislocation motion (slip) in austenite, (2) martensite formation, and (3) dislocation motion (slip) in martensite. This was later modified by Cina (4) who added the formation of a hexagonal close-packed phase which accompanied martensite formation but which disappeared with complete transformation to martensite. This hexagonal close-packed phase has more recently been reported by Dash and Otte (5) in a pure 18Cr-12Ni alloy where transformation occurred by cooling below the martensite start temperature. Other recent research has also revealed the structure of stacking faults (6) and of martensite (7,8) as revealed by electron transmission microscopy. Although martensite formation due to deformation has been studied by electron transmission microscopy of unstable iron nickel alloys,[3] there has been no correlation of observed work hardening during tensile straining with structure on a fine scale as was done in the research reported here.

Experimental Procedures

All testing of mechanical properties was performed at room temperature on specimens of recommended ASTM dimensions made from 0.020-in. thick strip products produced commercially. Mechanical properties reported here were determined on an Instron tension testing machine at a constant crosshead rate of 0.05 in./min. The true strain was obtained by measuring the minimum cross section dimensions every 5 per cent longitudinal strain as measured by a Baldwin extensometer over a 2-in. gage length. The extensometer remained on the gage length until fracture occurred.

The martensite content of the tension specimens was determined using a technique similar to that of Chapman and Jominy (9), and Form and Baldwin (10). In this technique, a magnetic coil induced a magnetic field in the specimen, while a secondary coil was used to measure the induced magnetization which in turn was proportional to the martensite content of the tension specimen. A tension specimen of Type 301 was used for a standard of 100 per cent martensite, after it had been destabilized and cold rolled to 100 per cent martensite as indicated by X-ray measurements. This specimen was used to establish a full-scale deflection range of 10 mv on a 0.1-sec full-scale response recorder which measured induced magnetization (martensite content) as a function of time. The correct strain intervals were marked on the curve manually. The effect of changing specimen geometry during tension tests was taken into consideration by measuring the full-scale deflection of various geometry 100 per cent martensite tension specimens which simulated the geometry of strained test specimens. In this manner, corrections were made which allowed calculation of the per cent martensite by volume for dynamically strained tension specimens. This method of martensite determination, as checked on identical specimens by X-ray measurements and the volume change within the gage length, was found to agree within ± 5 per cent.

All studies of the microstructures were done on an RCA EMU 3-100 kv electron microscope. Specimens were prepared from within the gage length of bulk tension specimens. The foil preparation was performed in two stages. First, chemical thinning was achieved using a 30 per cent HNO_3, 15 per cent HCl, 10 per cent HF, 45 per cent H_2O solution as recommended by Keown and Pickering (11). This reduced the metal thickness

[1] Supervisor, High-Temperature Alloy and Stainless Steel Research, Republic Steel Corp., Research Center, Metallurgical Div., Cleveland, Ohio.

[2] The boldface numbers in parentheses refer to the list of references appended to this paper.

[3] L. Leonard, private communication.

Copyright© 1965 by ASTM International

TABLE 1—CHEMICAL COMPOSITION OF ALLOYS, WEIGHT PER CENT.

Alloy	C	Mn	Si	Cr	Ni	Mo	P	S
A	0.10	1.18	0.57	17.04	7.10	0.26	0.029	0.009
D	0.09	1.25	0.48	16.98	7.70	0.32	0.023	0.010

TABLE 2—MECHANICAL PROPERTIES OF ALLOYS.

Alloy	Yield Strength, 0.2% Offset, psi	Tensile Strength, psi	Elongation in 2 in., %	n
A	38 600	134 000	78.0	0.752
D	40 500	130 000	67.0	0.710

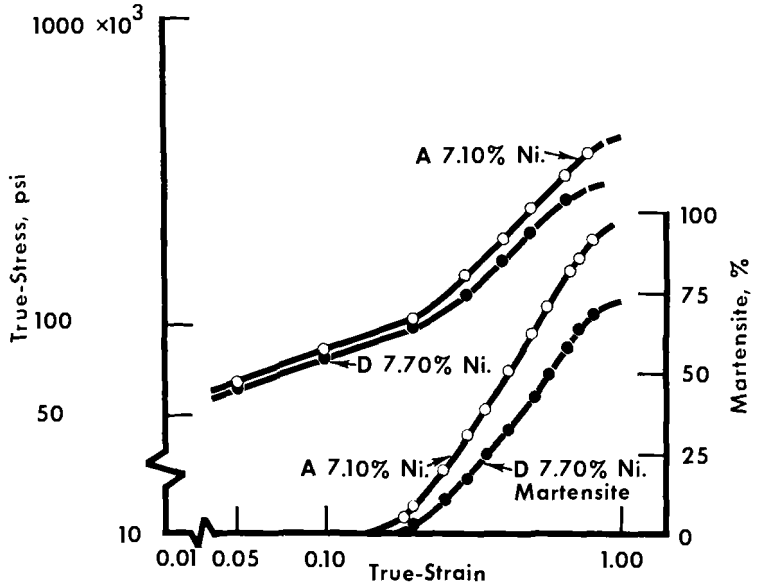


FIG. 1—True Stress-True Strain Plot Showing the Relation of Alloy Stability to Strain Hardening and Martensite Formation.

from 0.020 in. to 0.003 to 0.006 in. Electropolishing followed using the "window method" (12) with an electrolyte mixture of one part perchloric acid to 20 parts glacial acetic acid.

EXPERIMENTAL RESULTS AND DISCUSSION

The chemical composition and mechanical properties of the two analyses investigated are given in Tables 1 and 2, respectively. Note that the alloy compositions are very similar with the exception of nickel content. The alloys represent a low- and high-stability commercial Type 301 as controlled by nickel content. The log true stress-log true strain curves are plotted in Fig. 1 for both alloys. Note that the less stable alloy A has the higher rate of work hardening as well as the greater amount of martensite formed with strain as would be expected. The stability of the alloys is also reflected by the strain at which a change in slope occurs which coincides with the onset of martensite transformation. In a broader range of chemistries than those reported here, it was found that the onset

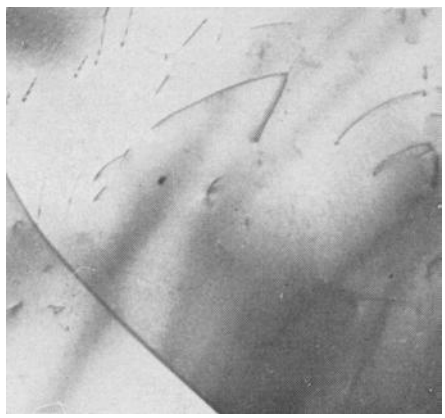


FIG. 2—Low Dislocation Density in an Austenite Grain of Annealed Type 301 Stainless Steel (×66,000).

of instability occurred between a true strain of 0.18 and 0.30 and accompanied the gross transformation to martensite.

The structure of the alloys is clearly defined by the series of electron transmission micrographs shown in Figs. 2–8. The annealed initial structure of very low dislocation density is seen in Fig. 2. Annealing twins were often present but are not seen here. With plastic strain, the dislocation density increased until, at about 0.08 to 0.10 strain, dislocation tangles were forming into fairly dense cells. The appearance of cells coincided with the appearance of stacking faults as shown in Fig. 3. These structures are classified as stacking faults, for they did not give twin diffraction patterns when studied by selected area electron diffraction. Further straining results in an increase in stacking fault density. By the

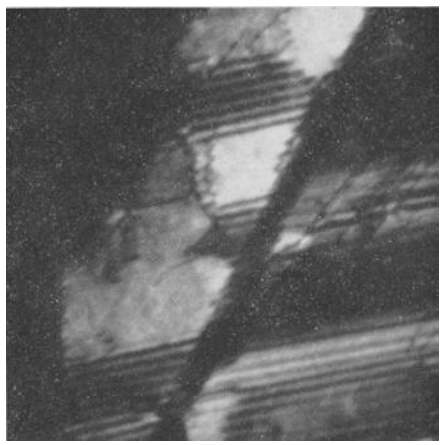


FIG. 3—Dislocation Tangles, Cell Formation, Stacking Faults, and Deformation Twins in Austenite Strained 0.10 (×66,000).

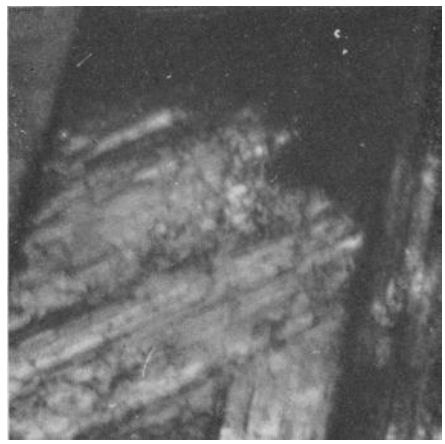


FIG. 4—Heavy Dislocation Density with an Increased Amount of Twinning, 0.20 Strain (×39,250).

time a strain of 0.20 has been reached, the dislocation density in the austenite is becoming very heavy, and deformation twins of lenticular shape have formed (Fig. 4). The twins have been differentiated from the stacking faults by the selected area diffraction patterns which showed a twin orientation superimposed on that of the face-centered cubic matrix grain. The twins could be identified in electron transmission by their lenticular shape, greater thickness, and more uniform contrast density than

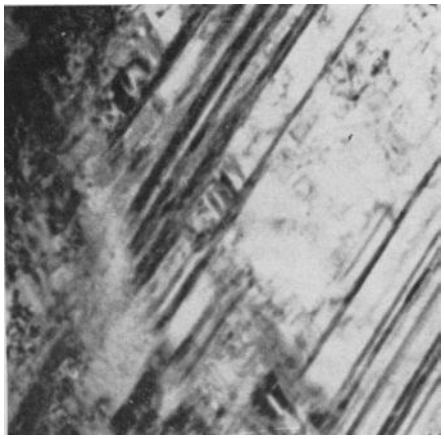
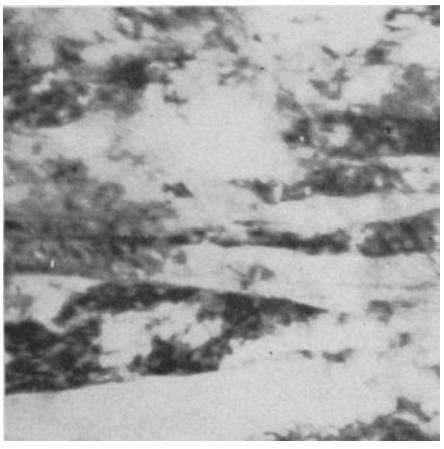


FIG. 5—An Example of Stacking Faults and Deformation Twins Formed During 0.30 Strain (×65,450).



FIG. 6—Deformation Martensite in a Matrix Strained 0.50 (×39,250).



NOTE—Increase in dislcoation density within the martensite.

FIG. 7—Deformation Martensite in a Matrix Strained 0.60 (×67,000).

the stacking faults. It was also between 0.20 and 0.30 strain that the first martensite plates were observed. These plates contained a very heavy dislocation density which appeared to be slightly less than that in the surrounding austenite. The increase in strain from 0.30 to 0.60, represented by Figs. 5, 6, and 7, resulted in a greater quantity of martensite, more twinned austenite, and a dislocation density in the austenite which was so heavy that it prevented detailed study. In this region of increased strain, an increase in the dislocation density of the martensite was apparent. Strain above 0.60 resulted in an extremely heavy dislocation density accompanied by a twin-like structure in the martensite. This is best illustrated by Fig. 8. The twinning is on a very fine scale and cannot be positively identified by electron diffraction. The twin-like structure had an appearance similar to that of twinned martensite observed in



NOTE—Sample taken near the fracture area at 0.72 strain.

FIG. 8—An Extremely Heavy Dislocation Density in Deformation Martensite Which Also Exhibits Twinned Martensite (×65,450).

iron-30.9 Ni alloys by Warlimont (13) and Richman (14). The twins were, however, much smaller than those reported by either author. The twins in the martensite may be due either to the high dislocation density in the austenite before martensite formation, or they may occur with strain subsequent to martensite formation.

CONCLUSIONS

The microstructure of Type 301, as it changes with plastic deformation, is both complex and unique in the types of phases which appear. The change of work hardening coefficient with strain has been definitely related to the formation of deformation martensite. A less stable alloy undergoes transformation sooner, has more martensite formation at a given strain, and reaches a higher tensile strength and more uniform elongation than a more stable alloy. There is, of course, an optimum austenite stability below which alloys transform to martensite too quickly with strain, and have a comparable tensile strength with lower elongations.

The deformation of Type 301 has been observed to occur by at least six mechanisms: (1) dislocation motion in austenite; (2) dislocation tangles, cell formation, and formation of stacking faults; (3) deformation twins in austenite; (4) martensite formation; (5) dislocation motion in martensite; and (6) deformation twins in martensite. The mechanisms are listed in order of appearance with increasing strain. It must be remembered that several mechanisms are operative simultaneously.

The structures observed indicate that one volume of austenite may be expected to proceed through Stages 1 to 6, consecutively, with increasing strain. The structures suggest that most of the plastic deformation occurs via deformation mechanisms in the austenite Stages 1 through 3, plus martensite formation in Stage 4. In unbalanced alloys which are less stable than Type 301, more martensite forms at low plastic strains, and the total strain to fracture may be 0.40 as compared to 0.68 to 0.80 for commercial Type 301. Lean, 7.0 Ni, Type 301 analyses are observed to have extremely good elongation since they have an optimum combination of strain in the austenite, with complete transformation to martensite before fracture and deformation in the martensite. If the alloy composition is too rich (high Ni content), the increased alloy stability results in excessive dislocation generation and twinning in the austenite, causing fracture before complete transformation to martensite can occur.

REFERENCES

(1) T. Angel, "Martensite in Austenitic Stainless Steels," *Journal*, Iron and Steel Inst., Vol. 177, No. 1, 1954, p. 169.

(2) G. W. Powell, E. R. Marshall, and W. A. Backofen, "Strain Hardening of Austenitic Stainless Steel," *Transactions*, Am. Soc. Metals, Vol. 50, 1958, pp. 478–497.

(3) G. H. Eichelman, Jr. and F. C. Hull, "The Effect of Composition on the Transformation of Austenite to Martensite in 18-8 Type Stainless Steel," *Transactions*, Am. Soc. Metals, Vol. 45, 1953, pp. 77–95.

(4) B. Cina, "Effect of Cold Work on the $\gamma \rightarrow \alpha$ Transformation in Some Fe-Ni-Cr Alloys," *Journal*, Iron and Steel Inst., Vol. 177, No. 1, 1954, pp. 406–422.

(5) J. Dash and H. Otte, "Thin Film Transmission Observations of Athermal Transformations in Stainless Steel," 5th International Congress for Electron Microscopy,

Vol. I, Academic Press, New York and London, 1962, p. HH-3.

(6) J. A. Venables, "The Observation of Mechanical Twins in Face-Centered Cubic Material," European Regional Conference on Electron Microscopy, Delft, 1961, pp. 443–446.

(7) J. F. Breedis, "On the Nucleation of Martensite in Thin Foils of Fe-16 Wt.% Cr-12 Wt.% Ni," *Electron Microscopy*, 5th International Congress for Electron Microscopy, Vol. 1, Academic Press, New York and London, 1962, p. HH-5.

(8) P. M. Kelly, "The Formation of Martensite and Bainite in Steels," *Electron Microscopy*, 5th International Congress for Electron Microscopy, Vol. 1, Academic Press, New York and London, 1962, p. HH-5.

(9) R. D. Chapman and W. E. Jominy, "A Method for Determining the Continuous Cooling Transformation in Steel," *Transactions*, Am. Soc. Metals, Vol. 47, 1955, p. 869.

(10) G. W. Form and W. M. Baldwin, Jr., "The Influence of Strain Rate and Temperature on the Ductility of Austenitic Stainless Steels," *Transaction*, Am. Soc. Metals, Vol. 48, 1956, pp. 474–485.

(11) S. R. Keown and F. B. Pickering, "A Chemical Technique for the Preparation of Thin Metal Foils for Transmission Electron Microscopy," *Journal*, Iron and Steel Inst., Vol. 200, 1962, p. 757.

(12) H. M. Tomlinson, "An Electropolishing Technique for the Preparation of Metal Specimens for Transmission Electron Microscopy," *Philosophical Magazine*, Vol. 3, 1958, p. 367.

(13) H. Warlimont, "On the Martensitic Structure of Iron-30.9% Nickel Alloy," *Electron Microscopy*, 5th International Congress for Electron Microscopy, Vol. 1, Academic Press, New York and London, 1962, p. HH-6.

(14) R. H. Richman, "Plastic Deformation Modes in Fe-Ni-C Martensite," *Transactions*, Am. Institute of Mining and Metallurgical Engrs., Vol. 227, 1963, pp. 159–166.

PRACTICAL ASPECTS OF PRODUCTION BRIGHT ANNEALING OF STAINLESS STEEL

By R. C. Boyer[1] and R. J. Perrine[2]

Synopsis

Bright annealing is the annealing of stainless steel sheet and strip continuously in a controlled-atmosphere furnace (depicted). The furnace atmosphere system includes an ammonia storage tank, a dissociator, and an adsorption dryer. Furnace capacity depends upon its specific size, source, temperature, and cooling rate, as well as the emissivity of the material processed. Atmosphere problems are purity and nitrogen pickup. Purity of the dissociated ammonia gas depends upon initial raw ammonia contaminants and dissociator performance. Nitrogen pickup can be prevented by annealing in purified hydrogen atmospheres. Production problems include atmosphere system leakage, maintenance of a temperature head, strip cleaning problems, and crystallized surface. Fabrication problems have included soldering and drawing. The advantages of bright annealed strip are improved surface finish, reduced buffing costs, and improved corrosion resistance.

Bright annealing, as referred to in this paper, is the annealing of stainless steel sheet and strip continuously in a controlled-atmosphere furnace. This protective furnace atmosphere protects the steel from oxidation, thereby eliminating the usual pickling operations associated with conventional annealing. The surface finish, after bright annealing, is the same as it was in the "as cold rolled" condition. The furnace atmospheres are usually dry hydrogen or dry dissociated ammonia which is composed of 75 per cent hydrogen and 25 per cent nitrogen.

To produce the stainless steel required by the automotive industry, it was necessary to do considerable polishing and buffing to impart a satisfactory corrosion resistance, but competitive and economic conditions in the industry demanded corrosion resistance with minimum buffing. Various investigators found that conventionally annealed and bright pickled Type 430 stainless steel resulted in a chromium-depleted surface with reduced corrosion resistance. In addition, it was found that annealing in an inert atmosphere, such as dry dissociated ammonia or hydrogen, did not result in a chrome-depleted surface.

The joint efforts of the stainless producers and the builders of industrial furnaces resulted in bright annealing furnaces that would provide a product which would be competitive with conventional annealed and pickled material in regard to operating costs, to meeting annealed properties, and so on, and yet would not change the surface, thus solving the corrosion (chrome-depletion) problem.

Bright Annealing Unit

The bright annealing unit is composed of the following major components (Fig. 1):

A Payoff reel or uncoiler.

D Shear—for preparation of the ends of the coils for welding.

K Welding unit—for welding of the coils for continuous operation.

F Strip or sheet cleaning unit—usually alkaline cleaner or trichlorethylene.

G Accumulators:

Entrance accumulator—main purpose to allow for time to weld the coils together.

Exit accumulator—main purpose to allow time for the removal of the coil from the take-up reel.

3 Annealing zone—containing inert atmosphere of dry dissociated ammonia or hydrogen. May be of muffle type or high purity refractory brick lined furnace type.

4 Cooling zone—containing inert atmosphere of dry dissociated ammonia or hydrogen.

J Take-up reel or recoiler.

In addition to the above, located at strategic positions are tension and speed control bridles, together with edge guides and steering rolls to ensure centering of the strip along the line.

Atmosphere Producing System

The major components of the furnace atmosphere (dissociated ammonia) system are an ammonia storage tank, a dissociator for the cracking of ammonia to hydrogen and nitrogen, and an adsorbing dryer of the molecular sieve type with fully automatic controls for the further reduction of the dew point of the dissociated ammonia.

The ammonia dissociator consists essentially of one or more retorts filled with a catalyst, which is heated externally and through which gaseous ammonia is passed. The ammonia dissociates according to the reaction $2NH_3 \rightarrow 3H_2 + N_2$. For any given conditions, the per cent of dissociation will depend upon the temperature, the rate of flow, and the condition of the catalyst. Brief descriptions of various parts of the dissociator follow:

1. *Pressure Reducing Valve*—The ammonia vapor supply enters the dissociator through a constant-pressure reducing valve. This reducing valve is set for the minimum inlet pressure to the retorts (not to exceed 30 psi max) necessary to obtain the rated capacity of the dissociator with a back pressure of 5 psi at the throttling valve. A pressure relief valve located downstream from the pressure reducing valve will open if the pressure at this point exceeds the maximum of 30 psi. A pressure gage indicates the pressure at the above point.

2. *Dissociator Retort*—After passing through the pressure reducing valve, the ammonia enters the dissociator retorts which are filled with a catalyst. The dissociator retorts are located in a refractory-lined heating chamber, and heat is supplied for the dissociating process by means of nozzle mix burners which operate on "high-low" control. From the dissociator retorts, the disso-

[1] Metallurgist, Republic Steel Corp., Massillon, Ohio.

[2] Director of research, The Electric Furnace Co., Salem, Ohio.

Copyright© 1965 by ASTM International

www.astm.org

ciated ammonia goes to a water-cooled surface cooler and then passes through the flow meter and into the service line.

3. *Safety Alarm System*—In order for the ammonia dissociator to operate efficiently, the temperature of the dissociator retorts must be at the proper value. Too low an operating temperature will leave a high percentage of residual ammonia in the dissociator; on the other hand, too high an operating temperature will decrease the life of the alloy retorts and the catalyst. Temperature control equipment is provided to hold the temperature of the dissociator at the desired operating value. The alarm system will operate if the temperature of the dissociator varies more than the permissible preset values. An ammonia pressure gage with high- and low-pressure contacts is provided with related alarm system. An air-operated alarm horn is provided in case the burner gas pressure fails or is shut off.

Operational and Controlling Factors

Furnace Performance:

The capacity of a given furnace depends upon the specific size, source temperature, and equally important, its ability to cool the work below a certain minimum temperature to prevent oxidation. Another factor which has a significant bearing on the production capacity is brightness. This inherent factor, known as absorptivity or emissivity, varies from 0.12 for mirror bright to 0.3 for dull stainless steels and may sometimes be outside of this range.

Annealing to obtain certain physical properties requires that the steel be heated above the recrystallization temperature or slightly higher, followed by a short soak and cool, or a cool immediately. To obtain maximum production, the furnace is operated at the maximum strip speed which will permit the strip to reach the desired temperature. Actual time to reach temperature sets the strip speed, and this time depends upon the source temperature. Furthermore, the time is directly proportional to the density, specific heat, and thickness of the strip, and is inversely proportional to the emissivity.

The time to heat a given strip to some temperature can be expressed by a mathematical expression derived from the following equations:

$$q = V \times D \times S\,(T_i - T_o)$$

where:

q = heat content of the metal, Btu,
V = volume, ft^3,
D = density, lb/ft^3,
S = specific heat,
T_i = final temperature, and
T_o = original temperature.

$$Q = 0.172 \times A \times e\left[\left(\frac{T_2}{100}\right)^4 - \left(\frac{T_1}{100}\right)^4\right]$$

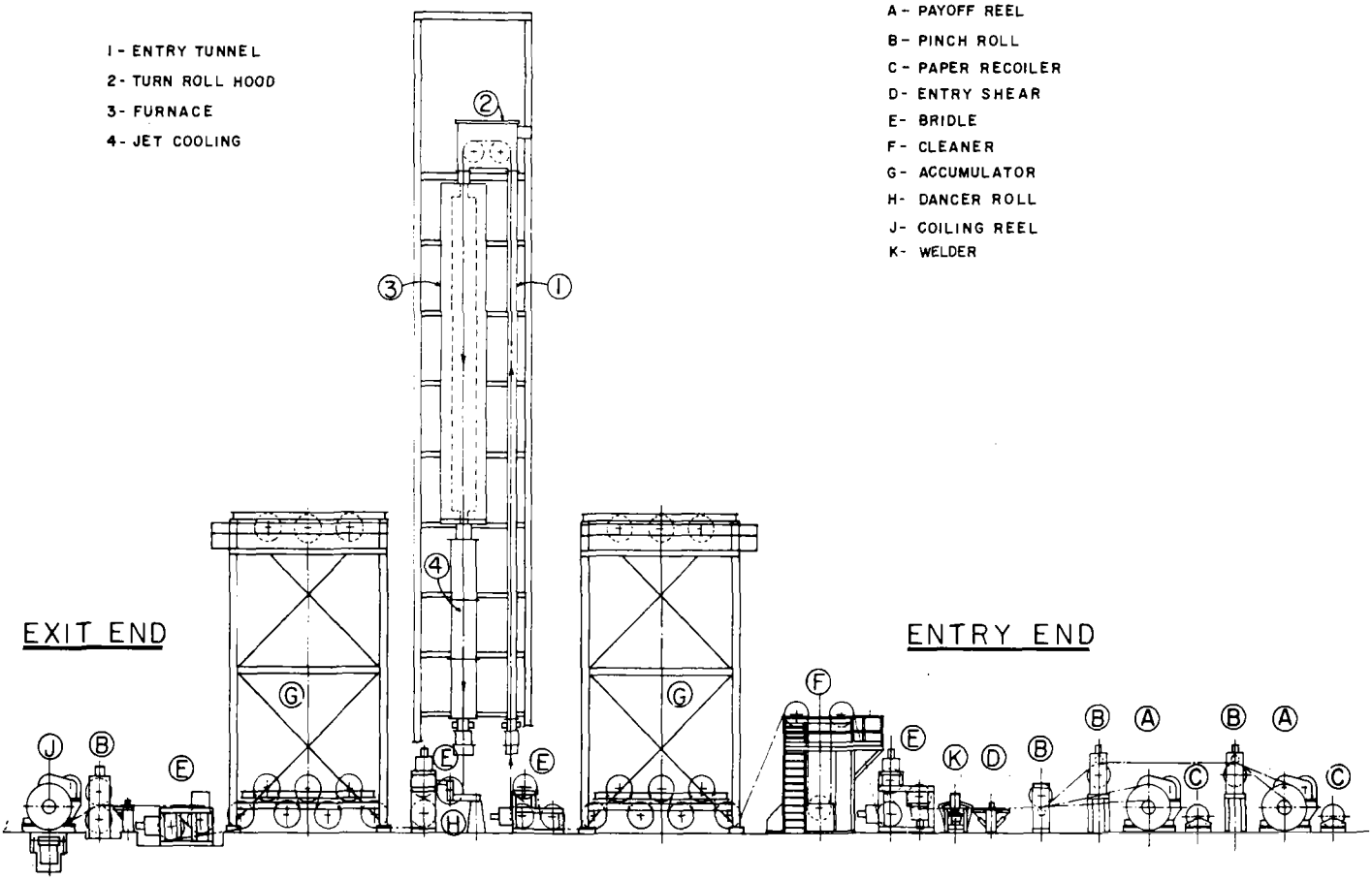


FIG. 1—Schematic Arrangement of Bright Annealing Line.

where:

Q = Btu/hr/ft^2, rate of radiation transfer,
A = area, ft^2,
e = emissivity,
T_2 = absolute temperature of surroundings, and
T_1 = absolute temperature of work.

By working with a square foot of metal 1 in. thick and expressing time in seconds, we can obtain new values for q and Q represented by q^1 and Q^1 respectively.

$$\theta = \frac{q^1}{Q^1}$$

where θ is the required time in seconds to heat metal 1 in. thick to temperature.

$$\theta = \frac{q^1 \times t}{Q^1 \times e}$$

where:
θ = required actual time, seconds,
t = thickness of metal, and
e = emissivity.

The heat-up time can be calculated from the ideal heating curve, Fig. 2. 4920 sec/in. of thickness. By increasing the source temperature to 1600 and 1800 F, the time to reach 1500 F can be reduced to 2950 and 1680 sec, respectively. These figures would indicate that the strip speed could be increased by factors of 1.7 and 2.9 with the above temperature heads. Unfortunately, these heating rates will never be obtained in a production furnace since the source temperature is dragged down at the

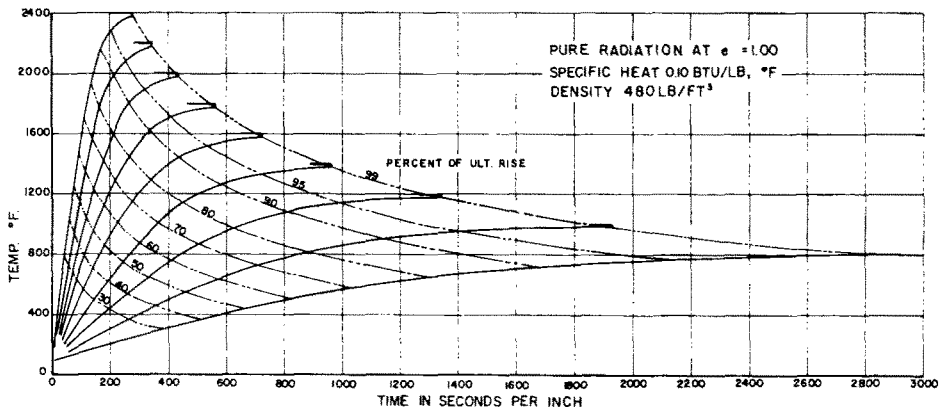


FIG. 2—Ideal Heating Curves.

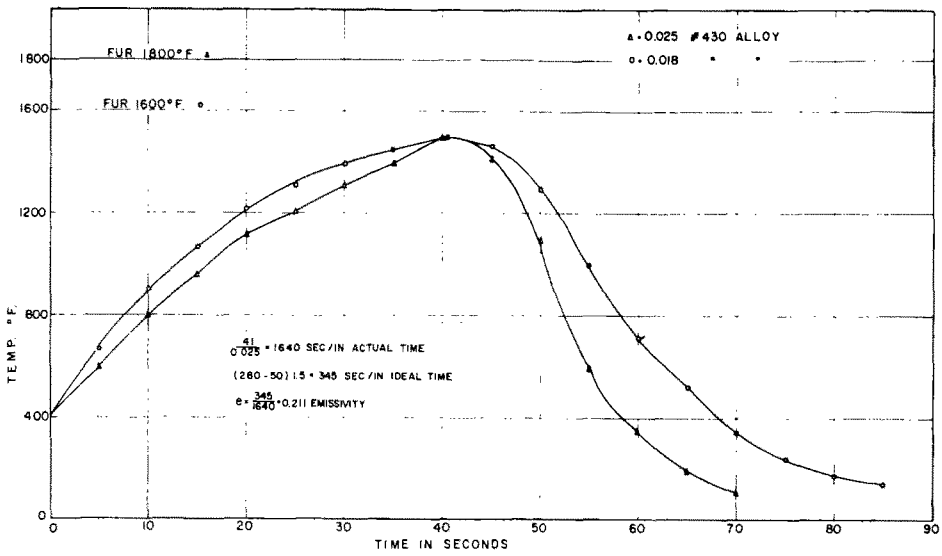


FIG. 3—Actual Heating and Cooling Curves.

Although these ideal conditions never exist in practice, the curves are very useful in estimating furnace strip speeds or furnace capacities. Reference to the curve indicates a time of 820 sec/in. of black body thickness is required to reach a work temperature equal to 99 per cent of the source temperature, 1500 F. For the curves to be applicable to stainless steel, it is necessary to correct for specific heat and emissivity factor. Assuming a specific heat factor of 1.5 and emissivity of 0.25, the heating time now becomes 820 × 1.5/0.25, or entrance end by the cold strip. Another intangible factor which affects the heating time is the emissivity. Values can be obtained readily from published data but require judicious interpretation and use. For example, the terms used to designate the surface finish do not enable one always to select the proper values. Laboratory tests indicate that there is considerable variation in the emissivity due to surface finish, even for a designated classification, such as bright, mirror bright, and so on. The apparent emissivity values obtained from tests correlated with various surface finishes would enable one to judge better more representative values. Attention should be called to the fact that heating in a highly reducing atmosphere often increases the brightness resulting in lower emissivity values as the surface oxide is reduced or other surface contaminates are removed.

The apparent emissivity can be obtained by running a time-temperature curve on a representative specimen, or on the strip itself under actual operating conditions. From these curves, Fig. 3, and the ideal curve, the time for corresponding temperature increment can be read. The time read from the ideal curve must be multiplied by 1.5 to correct for the difference in specific heat for the chart and stainless alloy Type 430. The ratio of the ideal time to the actual time is the apparent emissivity.

Reference to the time-temperature curves, Fig. 3, shows that the two steels, 0.018 and 0.025 in. thick and having approximately the same emissivity coefficient, can be heated to the annealing temperature in the same time or strip speed. Further examination of the time-temperature curves shows that the heavier-gage metal was cooled at a faster rate by increasing the mass velocity. The cooling rate for a given gas temperature is proportional to the mass velocity of the circulating atmosphere raised to the 0.78 power. Calculations indicate the heat transfer capacity for the 0.025-in. thick strip is in the neighborhood of 30 Btu/ft²/hr deg F. The lighter-gage strip cooled 50 per cent slower, representing a transfer capacity of approximately 16 Btu/ft²/hr deg F.

The cooling rate of bright strip depends upon several factors, such as the emissivity, mass velocity of the impinging atmosphere, and gas temperature. For a given mass velocity and gas temperature, the cooling rate is inversely proportional to the emissivity. Thus, the emissivity has a direct bearing on the ability to cool as well as heat in a given furnace. The importance of knowing the apparent emissivity of the stainless strip cannot be overemphasized.

The present-day practice is to operate with a temperature head. If the apparent emissivity is something different from the value used in setting up production speeds, a change in the line speed will be necessary if the steel is to be annealed at the same temperature. When the emissivity is a higher value, the strip will heat to the annealing temperature

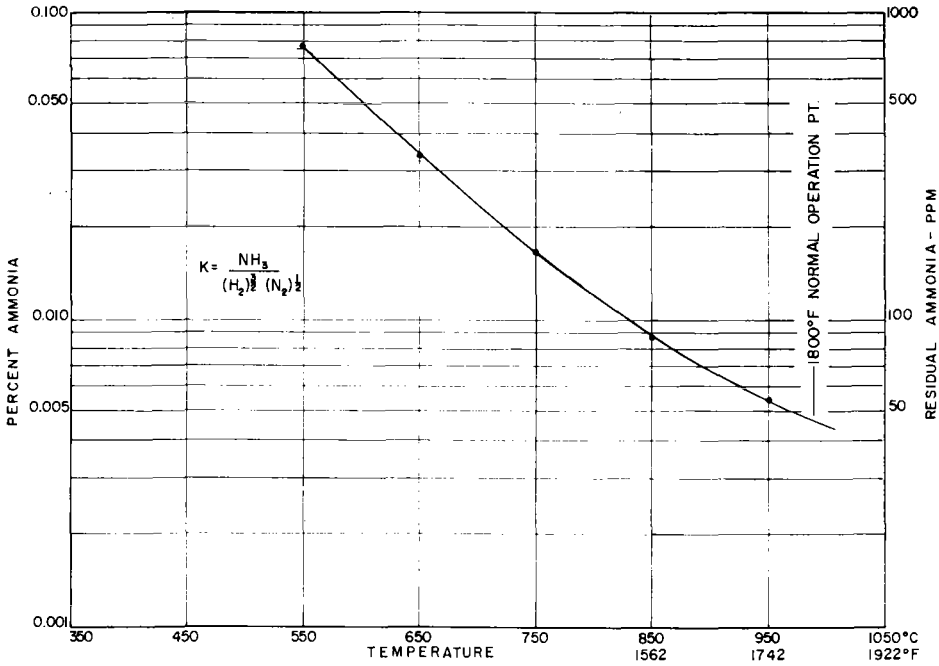


FIG. 4—Residual NH_3 at Equilibrium Versus Temperature at One Atmosphere.

TABLE 1—DEW-POINT VALUES RESULTING FROM DIFFERENT INLET LOCATIONS.[a]

Position	Static Cool, 2400 ft³/hr			Cooling Hood, 2400 ft³/hr		
	Max	Min	Avg	Max	Min	Avg
1S[b]	43	56	50	50	63	53
1F[c]	53	66	57	54	65	58
2S[d]	44	60	52	52	65	55
2F[e]	55	64	60	56	72	60
Charge[f]	45	62	53	52	65	55
Discharge[g]	62	74	66	75	85	82

[a] All readings are negative and deg F.
[b] 1S = first zone between shell and refractory.
[c] 1F = first zone furnace.
[d] 2S = second zone between shell and refractory.
[e] 2F = second zone furnace.
[f] Charge = entrance vestibule.
[g] Discharge = cooling hood.

TABLE 2—DEW-POINT VALUES AFFECTED BY FLOW.[a]

Position	Cooling Hood					
	2400 ft³/hr			3400 ft³/hr		
	Max	Min	Avg	Max	Min	Avg
1S[b]	50	63	53	50	57	53
1F[c]	54	65	58	55	62	58
2S[d]	52	65	55	57	71	64
2F[e]	56	72	60	64	75	67
Charge[f]	52	65	55	50	60	56
Discharge[g]	75	85	82	82	90	85

[a] All readings are negative and deg F.
[b] 1S = first zone between shell and refractory.
[c] 1F = first zone furnace.
[d] 2S = second zone between shell and refractory.
[e] 2F = second zone furnace.
[f] Charge = entrance vestibule.
[g] Discharge = cooling hood.

in less time. In the aforementioned example, a time of 2950 sec/in. was required to heat stainless steel with an emissivity coefficient of 0.25 to 1500 F in a 1600 F source temperature. If the emissivity was 0.3 instead of 0.25 the time would have been only 2450 sec/in. thickness. Conversely, a lower value of 0.2 would have resulted in a longer time or 3650 sec/in. of thickness. Thus, compensation in strip speed is required if the material is not to be under or over the desired annealing temperature. Either condition may result in higher hardness values. It is doubtful if the emissivity for a specific metal finish will vary to this degree, but cognizance of this factor on annealing is of vital importance.

Atmosphere Requirements:

Two other problems associated with the bright annealing of stainless alloys are the extreme quality of the atmosphere required and nitrogen pickup. The atmosphere most commonly used is dissociated ammonia gas. However, purified hydrogen atmospheres may be employed where nitrogen pickup becomes a problem.

The quality of the dissociated ammonia gas depends upon the grade of raw ammonia used and dissociator performance. Dew-point reading and residual-ammonia determinations on the generated atmosphere are an indirect measure of the bright-annealing quality. When the best grade ammonia, (metal treating), is dissociated, dew-point values in the range of −70 to −80 F can be expected. Metal treating ammonia can be supplied to the following specifications: NH_3 content minimum 99.999 per cent, moisture 0.001 per cent, oil 3 ppm.

Residual ammonia in the dissociated gas atmosphere ranges from 60 to 100 ppm for good dissociator performance, and in some cases may be higher. Reference to the curve, Fig. 4, gives theoretical residual ammonia values for equilibrium conditions at various temperatures. For example, the charts show a value of −48 to −50 ppm for a temperature of 1800 F. Since ideal conditions are never obtained in actual practice, we can expect somewhat higher values from a dissociator. The pressure at which the dissociator operates also has a direct bearing on the residual. It increases in direct proportion to the absolute pressure. At 15 psig the residual would double, increasing to 100 ppm.

By passing the atmosphere through a molecular sieve dryer, both the dew-point and residual-ammonia values can be further reduced. Good dryer performance should lower the dew point to a value of −90 to −100 F, and the residual is usually reduced to less than 10 ppm. An atmosphere of this quality should present no problem in obtaining a bright metal surface unless adversely affected after being introduced into the furnace.

Some deterioration in quality is expected and does take place in the furnace. The degree depends upon several factors such as: (1) volume flow (ft³/hr), (2) location of the atmosphere inlet ports,

(3) venting of atmosphere, and (4) contaminates carried in with the strip, among others. A brief discussion of these factors is essential to understand how they influence bright annealing.

carried into the furnace which results in some degree of atmosphere poisoning. Aside from the above potential, a reaction of hydrogen with small traces of oxygen or oxides raises the dew point in

TABLE 3—DEW-POINT VALUES AFFECTED BY PRESSURE.[a]

Position	Static Cooling, 2400 ft³/hr								
	0.1 to 0.4-in.-Water Column			0.5 to 0.9-in.-Water Column			1.0 to 1.8-in.-Water Column		
	Max	Min	Avg	Max	Min	Avg	Max	Min	Avg
1S[b]	45	56	50	45	54	51	46	54	55
1F[c]	52	62	58	54	62	58	52	63	57
2S[d]	44	58	49	47	60	52	49	60	54
2F[e]	55	63	60	52	70	61	56	65	60
Charge[f]	50	65	55	46	55	50	48	60	53
Discharge[g]	60	74	66	62	76	69	60	74	67

[a] All readings are negative and deg F.
[b] 1S = first zone between shell and refractory.
[c] 1F = first zone furnace.
[d] 2S = second zone between shell and refractory.
[e] 2F = second zone furnace.
[f] Charge = entrance vestibule.
[g] Discharge = cooling hood.

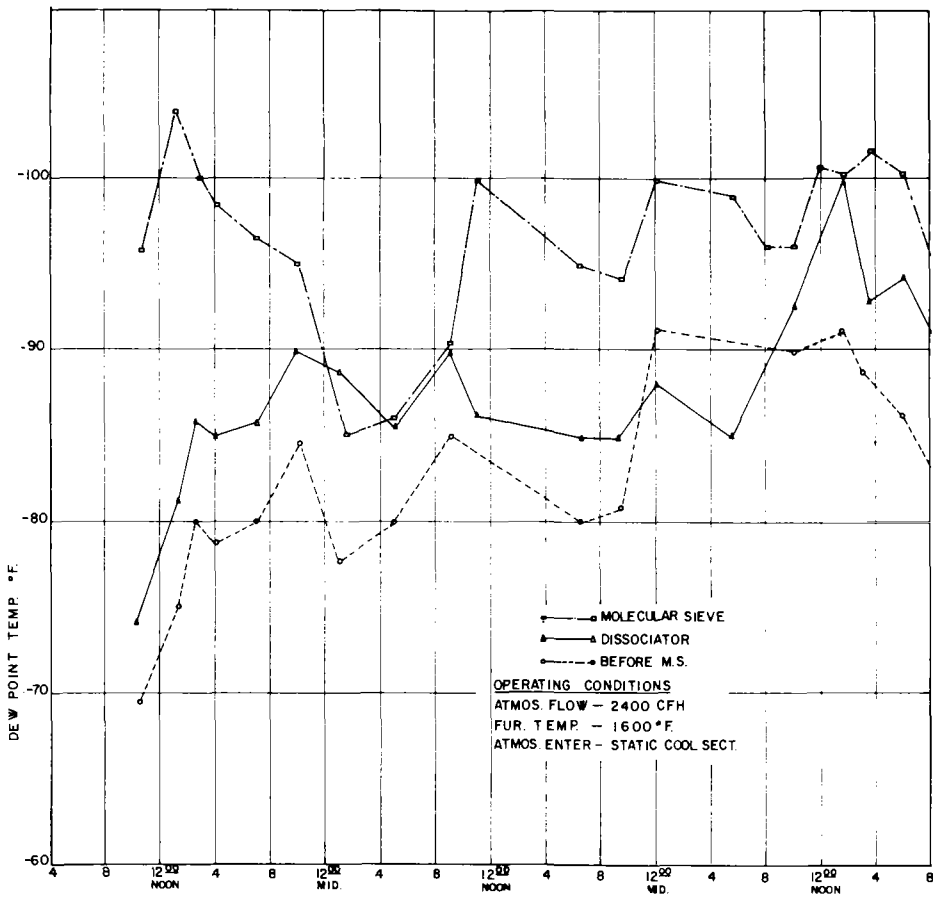


FIG. 5—Dew-Point Values of Dissociated NH_3 Gas to Furnace Versus Time.

An adequate flow of atmosphere is required to maintain a positive pressure inside the furnace and reduce to a minimum the backward diffusion of the atmosphere from the heating zone into the cooling hood. Even though the most stringent cleaning conditions are imposed on the strip, some contaminate is

the heating zone as compared to the atmosphere introduced. This reaction further impairs the bright annealing quality of the atmosphere. For these reasons it is desirable to introduce the atmosphere into the cooling hood. Atmosphere introduced at this location and vented at the charging end will ensure the best possible atmosphere environment during the critical stage of cooling.

A study of Table 1 shows dew-point readings under actual production annealing of 430 alloy. The results compiled in the table represent conditions of operation over a long period of time at two different locations (static-cool and between two jet-cool sections). Dew-point readings were taken at six different locations along the length of the furnace. There was no significant difference in dew-point readings taken at the first five locations. Readings taken at the discharge location showed a marked improvement. The dew point changed from −66 to −82 F when the atmosphere was introduced into the cooling hood.

Flow was increased from 2400 to 3400 ft³/hr to see if this would have any effect on the dew point. Increasing the flow did not effect any significant improvement, as indicated in Table 2. Although the dew point in the second furnace zone and cooling hood was slightly lower, it is doubtful if this small change improved the bright annealing quality of the atmosphere.

The results of a study of the dew-point values operating at various furnace atmosphere pressures are recorded in Table 3. Over the pressure range studied, 0.1 to 1.8-in.-water column, there was little, if any, difference. It can be concluded that operating under the conditions of this study, pressure had no effect on the dew point at any of the various locations. Even though there was no obvious improvement in dew point, there were some operating advantages at the higher pressure levels.

Daily dew-point readings, as indicated in Figs. 5 and 6, compare day-to-day operation.

Increasing the flow did show a marked improvement when annealing the 200 series alloys. The metal surface was bright with no sign of a grayish cast. When the rate of flow was changed, the grayish cast would appear at the low flow and disappear in 15 min at the higher rate of flow. This would lead one to believe that flow was also a contributing factor in the bright annealing of these alloys.

The test was repeated with purified hydrogen. Dew-point readings for all practical purposes were the same as those for the dissociated ammonia gas atmosphere. At the low flow, a grayish cast was observed on the metal. When the flow was increased the metal came

from the furnace bright. This performance substantiates, at least to some degree, the findings obtained with dissociated ammonia gas atmosphere.

Stainless alloys can be annealed successfully in protective atmospheres of dissociated ammonia gas and purified hydrogen. The former cannot be used when nitriding is a factor. Nitrogen pickup impairs the physical properties and lowers the resistance to corrosion.

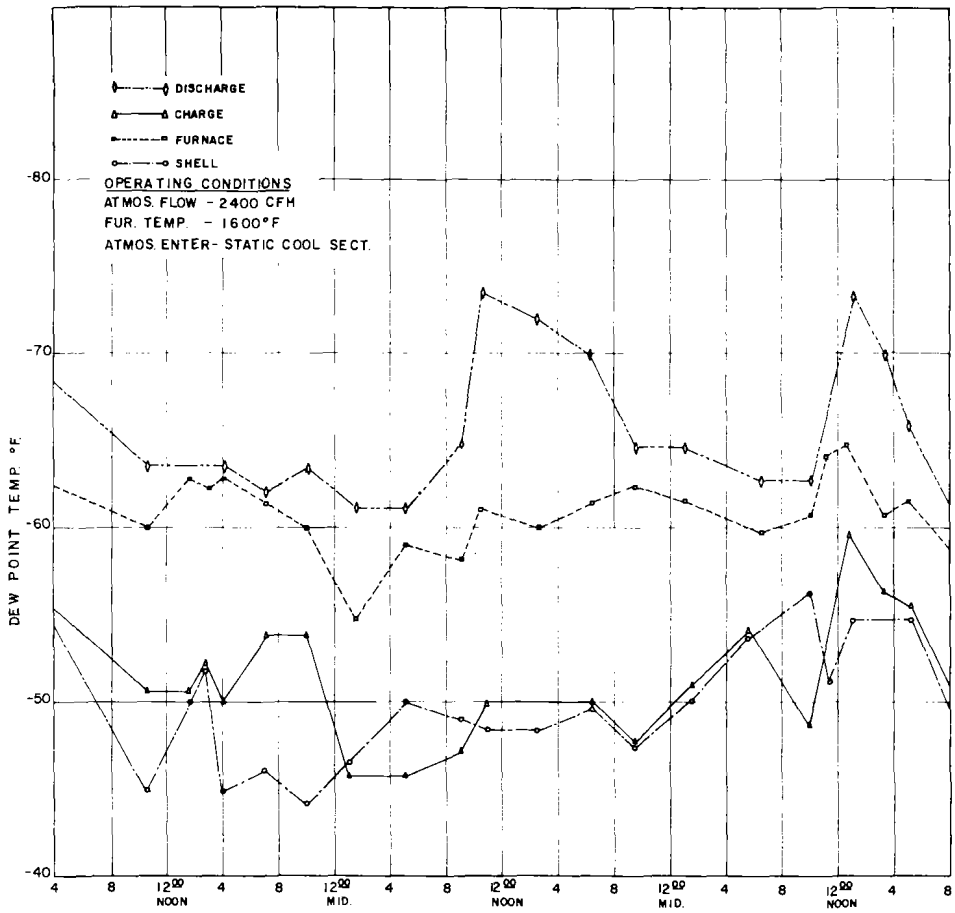


FIG. 6—Dew-Point Values of Atmosphere in Furnace Versus Time.

This is true especially where very thin strip (foil) is annealed.

Tests run on very thin coupons in dissociated ammonia gas atmospheres nitrided regardless of the residual concentration. Nitriding was experienced even when all the residual ammonia was scrubbed from the atmosphere. Nitrogen pickup can be prevented by annealing in purified hydrogen atmospheres. However, some precautions must be observed since nitriding has occurred in hydrogen atmospheres. It has been associated with inadequate purging or the lack of proper conditioning of the furnace when changing from dissociated ammonia gas to purified hydrogen.

PRODUCTION PROBLEMS

Leaks in Protective Atmosphere System:

If a bright, oxide-free surface is to be maintained, any leaks in the ammonia and dissociated ammonia system must be detected and isolated as quickly as possible. Some methods of detecting leaks are by means of sulfur tapers, dew-point analyzer, and visual testers at the various critical sections of the system.

Practice of Maintaining a Furnace Temperature Head:

Setting the furnace at a higher temperature than normally required for annealing is referred to as a temperature head. This is done to increase production capacity by allowing faster line speeds. However, stoppages or slowing down of the line speed can cause high hardness in the straight chromium types and grain growth in chromium nickel types of stainless steel.

Cleaning Unit Problems:

(*a*) Trichlorethylene type—Since this type of unit basically removes oil, it is prone to leaving a dirty residue or smut on the surface.

(*b*) Alkaline cleaner type—This type of unit will remove the dirty residue or smut on the surface by a scrubbing action. However, if proper precautions are not taken, spots of the cleaning solution or minerals from the water may mark the surface after annealing.

Crystallized Surface:

Since the surface of the bright annealed product is not oxidized and pickled as in a conventional furnace, the finish should not be in a "finely divided state" (for example, result of grinding or coarse roll pattern), or it can result in a crystallized surface in the end product.

FABRICATOR PROBLEMS

Soldering:

Since the nature of the bright-annealed finish is such as to have less wetability for the flux, there is currently a soldering problem which requires some special production techniques and requires some development work.

Drawing:

The retention of the lubricant has been reported as more difficult by some fabricators, which has required some modification of lubricants and methods.

ADVANTAGES OF BRIGHT-ANNEALED PRODUCT

In summary, some of the advantages of a bright-annealed product are: (1) improved surface finish over a conventional annealed and pickled product, (2) reduced buffing costs, and (3) improved corrosion resistance.

In conclusion, bright annealing has made its place in the advancement of the art of producing stainless steel.

ADVANCEMENTS IN EXTRUSION AND COLD FINISHING OF STAINLESS STEEL IRREGULAR SHAPES

By J. J. Barrett[1]

Synopsis

Since the beginning of commercial stainless steel extrusion in the United States in 1951, advancements in the technique of extrusion die design, improved extrusion die materials, and improved methods of extrusion die production have broadened the market for extruded steel products, and, more recently, cold finishing of stainless steel irregular shape extrusions has further broadened the market. Multiple orifice die designs, research in the hot work die steel area, electric discharge machine process for finishing of extrusion die orifices, use of EDM for cold draw die production, and correlation of extruded product design to make possible further finishing by cold drawing are refinements in the metal processing industry which have made possible the production of more intricate configurations with closer dimensional control.

In the short period of slightly more than a decade the commercial extrusion of stainless steel in this country has risen from infancy to reliable production maturity.

In the early 1950's, successful extrusion practices were developed around the Ugine-Sejournet process, which introduced the use of glass as a lubricant. With this advancement in the art of metal working, a new industry was born in the United States, and, as might well be predicted, the ingenuity and resourcefulness of production and technical people took this basic idea through many developmental steps and have now built it into an important industrial production tool.

In the segment of the industry concerned with irregular stainless steel shapes, the advances have been based on increased knowledge of glass technology, new techniques of extrusion die design, improved die materials, and better methods of die production. In addition, some of the techniques developed for extrusion die making have been carried over into cold-draw die making so that the commercial production of irregular shapes cold-drawn from extrusions has been developed into a commercial reality.

Use of Glass in Extrusion

The use of glass is extremely important to the stainless steel extruder because not only does it insulate the tools of the extrusion press from billet heat, which is on the order of 2100 to 2200 F, but it also permits the extrusion of austenitic stainless steels without danger of contamination from carbon, which is present in other conventional hot-working lubricants.

A great body of information has been accumulated on the chemical and physical properties of a variety of glasses. Also, the method of applying glass to the operation has been much improved, progressing from woven fiber glass and glass wool, to powdered or granular glass, or to pads made from granular glass. Today all these methods are available to the extruder.

TABLE 1—NOMINAL COMPOSITIONS OF SOME CAST HOT-WORK STEELS INVESTIGATED FOR EXTRUSION DIES, WEIGHT PER CENT.

	C	Mn	Si	Cr	Mo	V	Ni	W
Cr-Ni	0.27	...	0.45	2.00	0.25	...	2.50	...
H-11	0.40	0.40	1.05	5.00	1.35	0.50	...	...
H-12	0.35	0.35	1.00	5.00	1.50	0.40	...	1.50
H-13	0.35	0.35	1.00	5.00	1.50	1.00	...	...
H-14	0.40	0.35	1.50	5.00	...	...	...	5.00
H-21	0.30	0.30	0.30	3.35	...	0.25	...	9.00
M-2	0.80	...	...	4.00	5.00	2.00	...	6.00
M-2 (Mod.)	0.50	...	...	4.00	5.00	2.00	...	6.00

Extrusion Die Making

Concurrent with the work on glass lubricants, extrusion die making also went through a series of developments. Originally, dies for extruding steel were machined from wrought, hot-work die steels. As production rates increased, the slow and tedious machining of each die was out of the question, so the next step was to machine a pattern and cast the extrusion die.

In order to further expedite die production, an electronically controlled milling machine was adapted to follow a line drawing of the extrusion die orifice and automatically mill this orifice shape in an aluminum blank, which then became the pattern for the cast-die process. By the use of shell-mold casting techniques, it now became possible to produce large quantities of extrusion dies at a reasonable cost.

Die Finishing

The economical production of extrusion dies having been achieved, the next effort was to improve the product made from these dies by more closely controlling the die orifice dimensions. One solution to this problem was the introduction of electrodischarge machine (EDM) abilities to the finishing of cast dies. With this speedy and extremely accurate method of die finishing, two things were accomplished: (1) the attainment of highly irregular orifice shapes was made possible in less time and (2) close dimensional control of orifices from die to die became feasible on a production scale. All orifices can now be produced with identical configurations—something that is virtually impossible with manual finishing operations.

The more intricate configurations made possible with EDM-finished dies then called for an improvement in die materials. Intensive efforts were made to produce and test extrusion dies made from a variety of tool steels in order to improve the hot strength of the extrusion die to permit full utilization of the

[1] Manager, Extrusion Sales, The Babcock & Wilcox Co., Tubular Products Div., Beaver Falls, Pa.

Copyright© 1965 by ASTM International

capabilities developed in the production of die orifices. Table 1 shows a list of hot-work tool steels which have been investigated, many of which are available for production runs. With a variety of die steels from which to choose, the extruder can now select the grade best suited for any particular job requirement.

Another development in extrusion die practice was the introduction of the multiport die to steel extrusion practice. The development of this technique, in which two, three, or possibly four orifices are made in an individual die (Fig. 1), permits the extrusion of more tons per hour of relatively small shapes through the use of larger billets, still maintaining a reasonable ratio of billet cross-sectional area to extruded product cross-sectional area. The application of this technique to the extrusion of stainless steel has been a great step forward in the commercial production of this product.

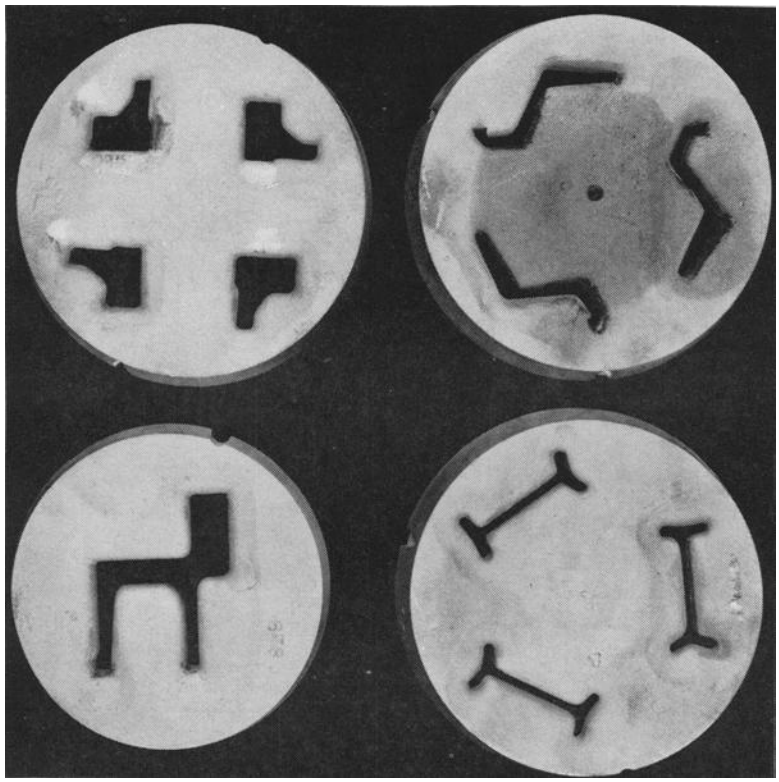


FIG. 1—Multiport Dies.

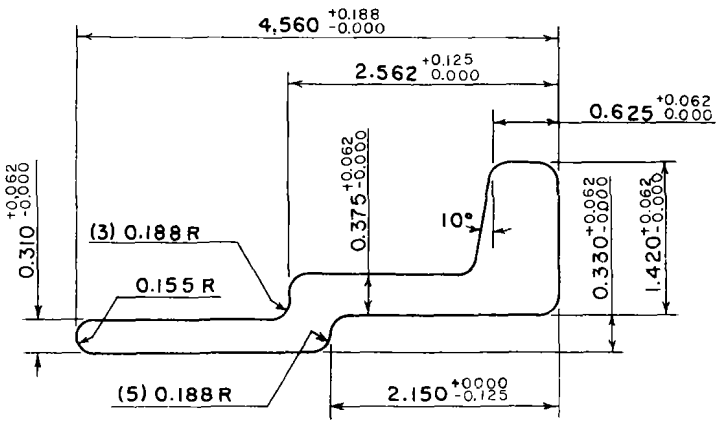


FIG. 2—A Typical Shape Extruded in the Early 1950's.

COLD-DRAWN PROCESS

The more closely defined shapes available with EDM-finished extrusion dies, made it possible to successfully cold draw the product of the extrusion press. By cold drawing, of course, a finishing step was provided which could improve the surface finish of the extrusion and also give much closer dimensional control, so that finish machining of the extrusion could be reduced to a bare minimum.

With the addition of cold drawing, the need immediately arose for accurate and inexpensive ways to produce cold-drawing dies. Many of the techniques learned in the production of extrusion dies are now used in cold-drawing die production, particularly the use of EDM equipment for finishing these dies. Instead of sectional dies for relatively thin sections, it is now possible to produce these as one-piece dies, securing a better die at much less cost.

It is interesting to note the improvement in the quality of extruded stainless product now available to industry. An example of a typical shape produced

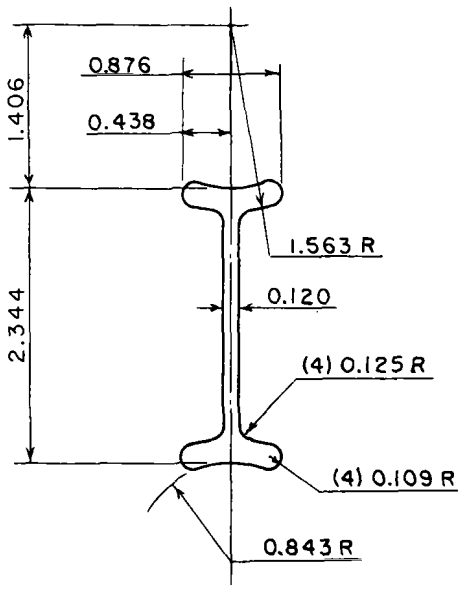


FIG. 3—A Typical Shape Extruded Today.

ten years ago is shown in Fig. 2. Here the limitations dictated by the knowledge of the art at that time prohibited any further refinement than is shown in the drawing. Note the generous corner and fillet radii and the relatively heavy section. Figure 3 shows a typical section that is producible today on a commercial basis as a hot-finished, as-extruded product. Figure 4 is another example of an intricate shape which can be produced in large volume at reasonable cost by today's methods.

Figures 5, 6, and 7 are examples of cold-drawn stainless steel irregular shapes, and a comparison of the tolerances shown on these shapes to those shown on the as-extruded shapes indicates the improvement in product obtainable by the addition of cold drawing.

Table 2 presents a comparison of

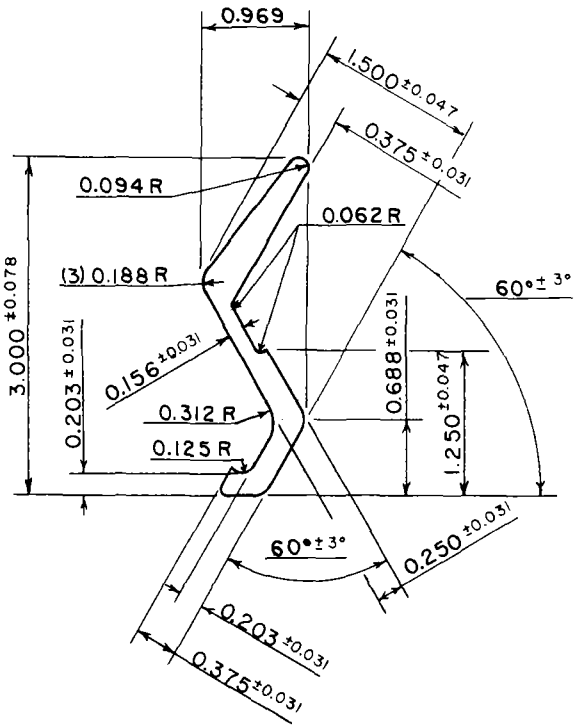


FIG. 4—Another Typical Shape Extruded Today.

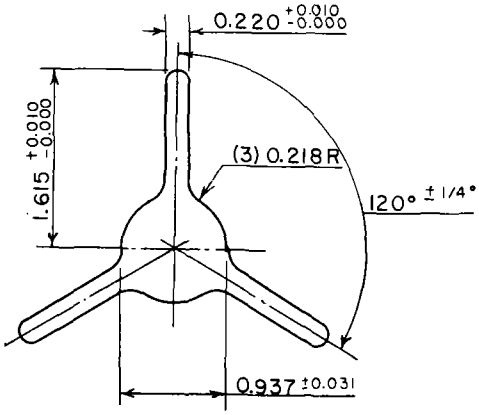


FIG. 5—Typical Cold-Drawn Extrusion Produced Today.

considerable improvement in dimensional control can be obtained by cold drawing; however, in addition a comparable improvement in surface finish can also be provided.

The advantages offered by the cold-drawn process can be used by the machiner of stainless sections by reducing or eliminating his machining operations, and by the fabricator who must polish some or all of the shape surfaces.

If designs of machined stainless parts are made with the capabilities of the extrusion-cold draw process in mind, sections can be obtained that will require little or no machining. To assist the designer, a few suggestions may be in order, so that maximum use can be made of the advantages of the process.

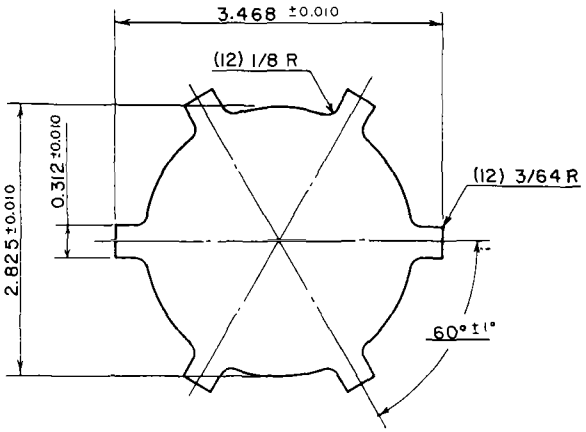


FIG. 6—Typical Cold-Drawn Extrusion Produced Today.

tolerances between hot-finished, as-extruded, stainless steel sections and cold-drawn sections. It is evident that

1. Consider the size range of the finished part. By referring to Table 3 it will be seen that cross-sectional area should be at least 0.5 sq. in. and that section thickness should be at least 0.125 in. Also, the part must be contained within a circumscribed circle of 6.500 in.

2. Consider dimensional tolerances. Generally speaking, tolerances of ±0.005

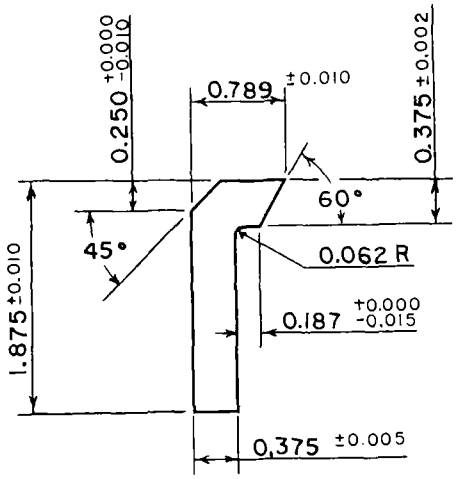


FIG. 7—Typical Cold-Drawn Extrusion Produced Today.

TABLE 2—DIMENSIONAL TOLERANCES OF EXTRUDED AND COLD-DRAWN IRREGULAR STAINLESS STEEL SHAPES.

Dimension	Total Tolerances, in.	
	Extruded	Cold Drawn
To 1 in.	0.040	0.010
1 to 3 in.	0.062	0.010
3 to 4 in.	0.093	0.010
Over 4 in.	0.125	0.010

TABLE 3—SIZE RANGE EXTRUDED AND COLD-DRAWN IRREGULAR STAINLESS STEEL SHAPES.

Dimension or Description	Extruded	Cold Drawn
Cross-sectional area, min, sq in.	¾	½
Over-all size	contained within a 6½ in. circumscribed circle	
Section thickness, min, in.	3/16	⅛
Length, max, ft	40	32
Weight, max, lb (approximate)	375	320

in. are possible; however, the length tolerances of long, thin appendages should be more generous, if possible. Also, in this product, as in any precision part, it is always wise to apply close tolerances only where needed, in order to keep costs to a minimum.

3. Consider corner and fillet radii. By the nature of the process, sharp corners or chamfers are not obtainable. Radii should be specified, instead.

4. Consider narrow, deep grooves. Because of extrusion and cold-draw die problems in forming such grooves, they are difficult and sometimes impossible to produce in long lengths.

5. Consider hollow sections. Because of extrusion limitations, holes can be located only in the center of symmetrical shapes. Also, in steel extrusions, only one hole can be made in a shape.

6. Consider the possibility of permitting the mill to vary the shape to conform to the limits imposed by the mill processes. If the section design can be flexible enough to permit negotiation between the user and the producer, a more practical and economical solution can often be obtained.

SUMMARY

In summary, then, it is now possible to obtain, in production quantities on a commercial basis, a greatly improved stainless steel extruded product in the hot-finished condition and a superior product in the cold-drawn condition. This improvement in product quality in a relatively short time has been accomplished by constant effort on the part of production and research men to improve the process, through such things as glass research, multiple orifice die designs, research in hot-work die steel, and die finishing by EDM methods. It is reasonable to assume that these advances will continue and that within another ten years the quality of stainless steel irregular extruded shapes will improve further and the user of extrusions in the 1970's will have available a still more highly refined product.

NEW MARTENSITIC AGE HARDENING STAINLESS STEELS

By G. N. Aggen,[1] Personal Member, ASTM; C. M. Hammond;[2] and R. A. Lula,[3] Personal Member, ASTM

Synopsis

The development of three new martensitic stainless steels is described. As annealed these alloys possess a relatively soft martensitic structure which is amenable to cold processing and forming operations. Two of these alloys may be strengthened from 150,000 to 200,000 psi ultimate tensile strength by means of low temperature precipitation-hardening treatments. Some physical, mechanical, and corrosion properties of these alloys are shown. The anticipated areas of application for the alloys are described.

The usefulness of stainless steels in industrial equipment is attributed not only to their resistance to corrosion but also to their engineering properties. In fact, a substantial proportion of the stainless steels produced today is used because of their combined mechanical and corrosion properties. This explains the continuous trend, over the years, to develop stainless steels with higher strengths.

Referring primarily to flat rolled products, the high-strength steels used in structural applications can be classified as follows:

1. The martensitic stainless steels such as AISI Type 410.
2. The metastable austenitic stainless steels, such as AISI Types 301 and 201.
3. The controlled transformation precipitation hardening stainless steels, such as 17-7 PH, 15-7 Mo, AM-350, and AM-355.

These steels find a large field of application in the missile and aircraft industries, the transportation industry for railroad and trucking equipment and the building industry. They are used to a lesser extent in a score of other applications.

There are certain limitations to the present high-strength stainless steels which will be discussed here in order to illustrate the advantages of the new martensitic age-hardening steels. The martensitic grades are relatively inexpensive and can be easily fabricated in the annealed condition. The hardening treatment consists in austenitizing at 1700 to 2000 F, followed by tempering. The treatments may create difficulties, especially for complex parts, because of scaling and distortion. Welding is feasible but involved, since preheating is sometimes required and postweld treatments are always necessary. The strength in the hardened condition is substantial, but the toughness is limited (1).[4]

The metastable austenitic stainless steels are by far the most widely used in structural applications. They cannot be hardened by heat treatment, but, having a high rate of work hardening, they can be cold rolled to various strength levels called "tempers." Since the rate of work hardening is strongly affected by small variations in composition and cold rolling temperatures, the strength range of any temper is larger than in heat treatable materials. The formability, which is restricted, can vary within one temper because of its relationship to strength level. As a result of unidirectional cold rolling, the mechanical properties are anisotropic. The modulus of elasticity, so important in designs controlled by elastic stability, decreases with increasing strength, thus detracting from the advantages of the higher strength attained by cold rolling. Special design procedures had to be devised for designing with anisotropic steels with decreasing moduli (2,3).

The controlled transformation precipitation hardening stainless steels have been developed specifically to overcome some of the limitations of the martensitic and austenitic steels. They possess an excellent combination of fabricating and engineering properties. They possess disadvantages, however, because of their delicate metallurgical balance and complicated heat treatments. These are reflected in high processing as well as fabricating costs, which generally limit their use to aircraft and missile applications.

The development of the new steels to be discussed here was partly based upon a certain metallurgical characteristic of the "maraging" steels recently developed by the International Nickel Co. (4). Though fully martensitic in the annealed condition, the martensite is relatively soft (Rc 28 to 32), has a very low work hardening rate, and is capable of severe deformation without cracking. This characteristic, which is extremely important to producers and fabricators, was exploited in the development of the new alloys.

The three grades discussed here, that is, AM-363, AM-362, and AM-367, have basically the same metallurgical characteristics. They are martensitic steels with practically identical properties in the annealed condition. The degree of hardening during aging varies considerably, however, as do their fields of application. AM-363 has the leanest conceivable composition and exhibits practically no age hardening (Rc 25 annealed or aged). The strength level is approximately the same as $\frac{1}{4}$ or $\frac{1}{2}$ hard Type 301 and only slightly higher than the low-alloy high-strength steels. The fields of application are also about the same. AM-362 is more highly alloyed and can be age hardened to about Rc 45. The alloy is primarily designed for applications requiring high strength and good corrosion resistance at a moderate cost. AM-367 is even more highly alloyed and can be hardened to very high strength levels (about Rc 50). It is designed for applications in the missile and air frame industries where material properties are of paramount importance and cost is of secondary importance. The physical and mechanical properties of these alloys were largely obtained from commercial heats, but because of their newness, some

[1] Research associate, Research Center, Allegheny Ludlum Steel Corp., Brackenridge, Pa.
[2] Research associate, Research Center, Allegheny Ludlum Steel Corp., Brackenridge, Pa.
[3] Chief research metallurgist, Research Center, Allegheny Ludlum Steel Corp., Brackenridge Pa.

[4] The boldface numbers in parentheses refer to the list of references appended to this paper.

Copyright© 1965 by ASTM International

www.astm.org

of the data were necessarily obtained from laboratory heats.

AM-363

The goal strived for in AM-363 was to produce a completely martensitic stainless steel as cheaply as possible. The residual elements (manganese, silicon, phosphorus, and sulfur) were restricted to the lowest possible level consistent with inexpensive melting practices and raw materials. A chromium level of about 11.5 per cent was selected as the least amount necessary to confer reasonably good corrosion resistance to the alloy. A carbon level of about 0.05 per cent max and possibly lower appeared feasible. In order to attain good formability, sufficient titanium was added to remove the carbon and nitrogen from solid solution in the martensite. Nickel was added in amounts sufficient to produce a completely austenitic structure at elevated temperatures, since a structure free of delta ferrite was desired to assure good hot workability thereby keeping production costs low.

The effect of nickel content on 12 per cent chromium, 0.25 per cent titanium, and 0.03 per cent carbon alloys was evaluated separately. The mechanical properties and formability, measured by transverse bends, were evaluated in the annealed condition and after a stress relieving operation at 1000 F. The results are shown in Fig. 1. The bend properties are measured by the minimum ratio of bend radius R to sheet thickness, t, which will produce no cracks upon bending a specimen through an angle of 135 deg. The increase in strength, between 2 and 3.25 per cent nickel, is caused by a reduction in delta ferrite content. The stress-relieving treatment increases the yield strength and elongation at all values of nickel. At all but the 9.75 per cent nickel level, the tensile strength decreases upon stress relieving. At 9.75 per cent nickel, the increase in properties is caused doubtlessly by age hardening. The best combination of bend properties, strength, and alloy cost is obtained at 3.25 per cent nickel. To assure freedom from delta ferrite at hot processing temperatures, however, a nickel content of 4 per cent was selected.

Silicon, a potent solid solution hardener of ferrite, also was evaluated separately in 12 per cent chromium, 0.25 per cent titanium alloys. The effect of silicon on transverse bend properties, of both as-annealed and stress-relieved sheet, is shown in Fig. 2. As the figure illustrates, low silicon is desirable because of its extremely potent effect upon formability as measured by transverse-bend properties. Manganese was found to have no apparent effect. The effect of titanium to carbon ratio on the tensile and transverse bend properties was also examined in 12 per cent chromium, 0.16 to 0.37 per cent titanium alloys. The results are shown in Fig. 3. A ratio of about eight is required to obtain good bend results and minimum martensite hardness. Based upon these laboratory results the following optimum composition aim was derived:

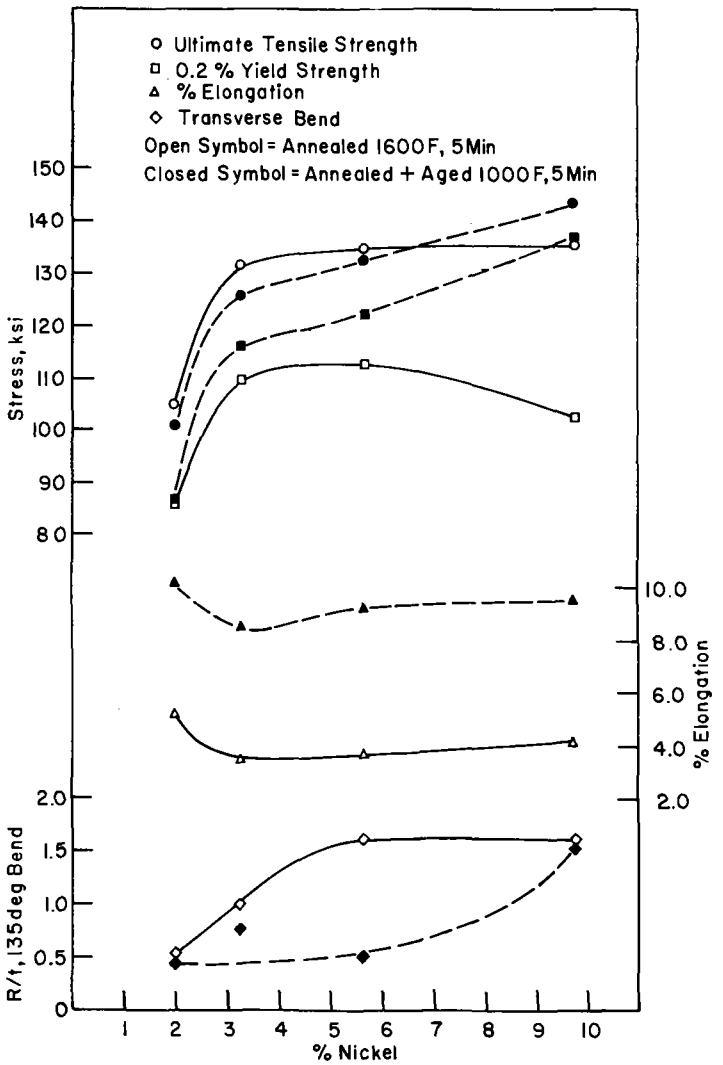


FIG. 1—AM-363 Mechanical Properties Versus Nickel Content.

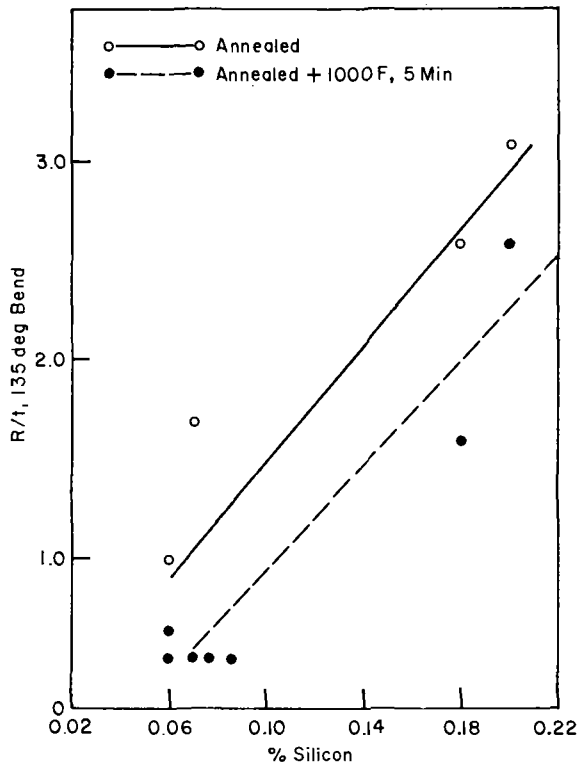


FIG. 2—AM-363 Transverse Bends, 0.030-In. Sheet, 0.25 Per Cen Titanium.

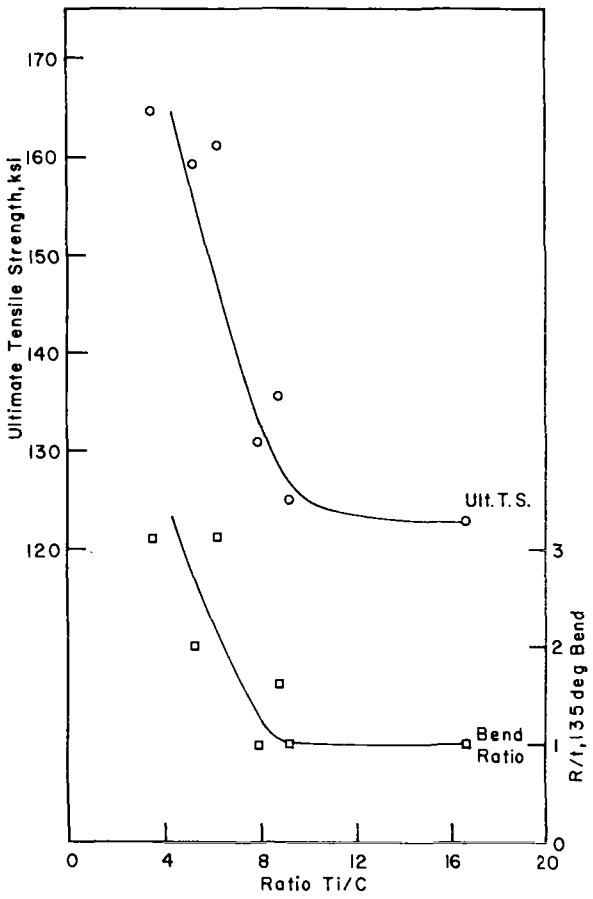


FIG. 3—Annealed Transverse Properties of AM-363 Versus Ti/C Ratios.

TABLE 1—TYPICAL TRANSVERSE PROPERTIES OF ANNEALED 0.060 IN. AM-363 SHEET.

Test Temperature, deg F	Yield Strength, 0.02%, ksi	Yield Strength, 0.2%, ksi	Ultimate Tensile Strength, ksi	Elongation in 2 in., %	Notched Tensile Strength, ksi[a]
−100	110.1	130.4	146.7	10.0	159.6
−50	100.1	123.8	134.3	11.5	150.8
70	89.7	112.3	125.3	11.5	141.7
200	89.1	108.5	118.2	9.5	134.1
300	79.3	103.9	113.5	6.5	...
400	77.6	101.3	108.4	6.0	121.5
500	73.3	97.0	105.5	4.5	...
600	79.5	96.4	102.8	3.0	108.6

[a] Edge-notched tension specimen, 0.0007 in. radius (Ref. 7).

TABLE 2—PROPERTIES OBTAINED ON AM-363 ALL-WELD METAL SPECIMENS

Heat Treatment	Yield Strength, 0.2% ksi	Ultimate Tensile Strength, ksi	Elongation in 4d, %	Reduction in Area, %	Notched Tensile Strength, ksi[a]	Charpy V-Notch Impact, ft-lb
None.....	113.9	133.2	14.0	67.0	189.2	120 and 92
900 F, 4 hr.....	114.9	116.9	21.4	57.6	190.3	98 and 81

[a] Round bar edge-notched tension specimen, K_t = 4.9.

TABLE 3—CORROSION RESISTANCE OF AM-363 AND TYPE 430.

Testing Medium	Time	AM-363	Type 430
25% boiling nitric acid.....	Five 48-hr periods	0.0124 IPM[a]	0.0007 IPM
60% boiling acetic acid.....	24 hr	0.0347 IPM	0.025 IPM
20% boiling phosphoric acid.....	24 hr	0.0009 IPM	0.015 IPM

[a] IPM = Inches per month.

C	Mn	Si	Cr	Ni	Ti	Fe
0.03	0.10	0.08	11.50	4	0.40	balance

The transformation temperatures, measured dilatometrically at heating and cooling rates of 250 F/hr are: Ac_1, 1250 F; Ac_3, 1375 F; Ms, 770 F; and Mf, 500 F. The alloy is annealed at about 1500 to 1700 F. An annealing temperature of about 1650 F appears to produce the best transverse-bend properties. The alloy exhibits little response to age hardening at the temperatures examined (800 to 1050 F). Reheating to these temperatures increases the proportional limit, yield strength, and ductility slightly.

Typical transverse properties of annealed 0.060-in. sheet from a production heat are shown in Table 1. Production heats consistently have passed 0.5 R/t bends (135 deg) in the transverse, or poorer, direction at room temperature. Like the maraging steels the tensile elongation of sheet is deceptively low owing to the low work-hardening rate of AM-363. Fractures are all 100 per cent shear type, and the reduction of area, though not ordinarily measured on sheet, is high. The tensile properties are relatively insensitive to temperature over the range of 70 to 600 F.

The alloy has outstanding weld properties. Tension tests on transversely welded sheet and plate consistently break in the base metal heat affected zone at values of stress in excess of the unwelded base-metal strength. Properties obtained on all weld-metal specimens are illustrated in Table 2. The welding techniques used were the same as those for austenitic stainless steels. No preheat nor postheat is required to obtain completely sound welds. The ductility values shown on the all-weld-metal tension tests are better illustrations of the inherent ductility of AM-363 than elongation values obtained on sheet. The corrosion resistance of AM-363 is illustrated by the data shown in Table 3. In 5 per cent salt spray AM-363 shows a few rust spots in 200 hr, whereas Type 430 appears about the same after 72 hr.

AM-362

In some respects similar aims were strived for in developing AM-362. Again a low cost alloy, free of delta ferrite, was desired. Manganese, phosphorus, sulfur, and silicon were again restricted to readily achievable limits to allow economical

cold fabrication of the alloy. In addition, a higher level of strength and corrosion resistance was desired. The latter was achieved by increasing the chromium content to 15 per cent.

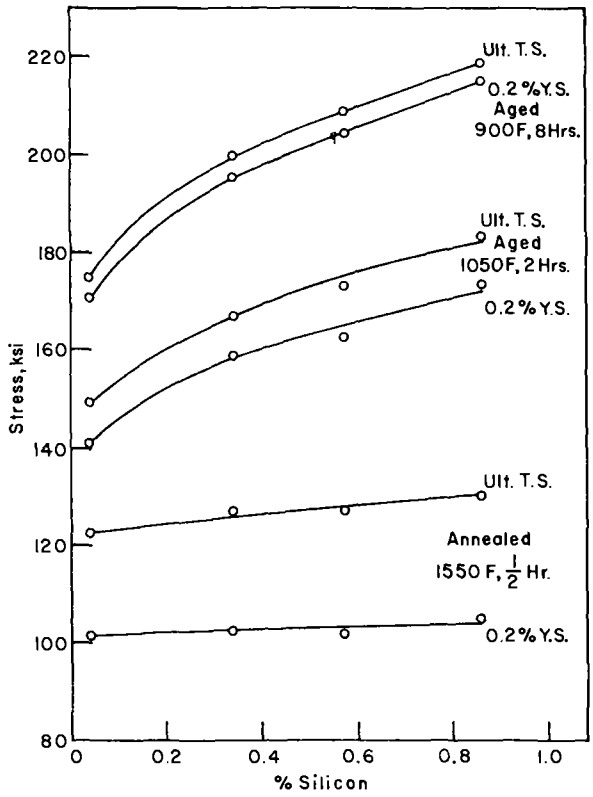


FIG. 4—Tensile Properties of AM-362 Bar Versus Silicon Content (0.75 Per Cent Ti).

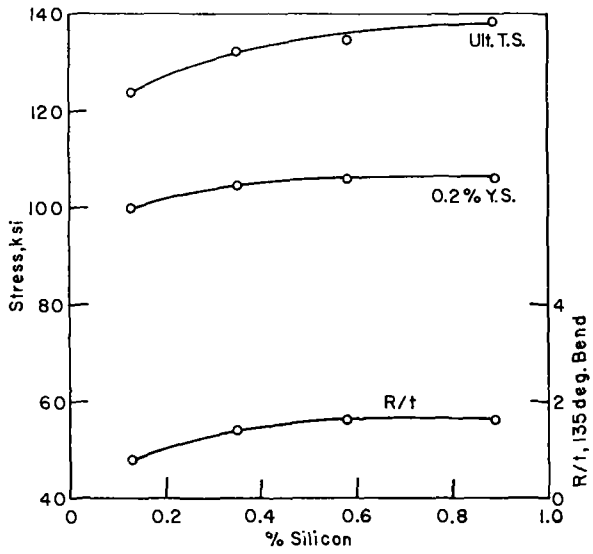


FIG. 5—Mechanical Properties of Annealed AM-362 Sheet Versus Silicon Content.

A high strength level appears readily attainable by utilizing a well-known age-hardening reaction that occurs in iron-nickel-titanium alloys. In 1931, Wasmuht (5) reported that the titanium content, necessary to produce age hardening in iron-titanium systems, was reduced markedly by additions of nickel and silicon. This information was later utilized by Smith et al (6) and led to the development of Stainless W. They found, contrary to the results by Wasmuht, that silicon up to 2 per cent exerted no appreciable effect upon the precipitation hardening reaction. Columbium was found to substitute successfully for titanium in producing age hardening. The optimum composition arrived at by Smith et al was 17 per cent chromium, 7 per cent nickel, 0.50 per cent silicon, 0.70 per cent titanium, and 0.20 per cent aluminum. The structure contains 5 to 25 per cent delta ferrite, about 5 per cent retained austenite, and the balance martensite.

Neither silicon nor delta ferrite was desired in AM-362, the former to improve cold fabricability in the annealed condition and the latter to improve hot workability and transverse ductility. Using a base composition of 15 per cent chromium and 6 per cent nickel (the latter to provide a structure free of delta ferrite) the effects of silicon, titanium, carbon, and manganese were evaluated. Figure 4 shows the effect of silicon, at a titanium level of 0.75 per cent on the annealed and annealed-and-aged properties of AM-362 bar. Silicon increased the annealed tensile strength about 10,000 psi per 1 per cent addition. Contrary to Smith et al (6), who found that silicon up to 2 per cent does not exert any discernible effect upon the precipitation hardening reaction in Stainless W, it is shown in Fig. 4 that silicon, in the range of 0.1 to 0.8 per cent, has a very strong effect upon the age hardening of AM-362. At higher values of silicon, the element has a lesser but still appreciable effect.

The effects of silicon upon the annealed transverse tensile and bend properties are shown in Fig. 5. Silicon reduces the bend properties, but the effect is not apparently as severe as on AM-363. Silicon, as in the case of bar, increases the annealed tensile strength of sheet. In this series, an increase of about 15,000 to 20,000 psi per 1 per cent silicon was observed.

Manganese in the range of 0.10 to 1.5 per cent has no apparent effect upon the annealed or aged tensile properties. The annealed transverse bend properties are not affected by manganese up to about 0.4 per cent but appear to decrease slightly at higher contents. Carbon from 0.015 to 0.05 per cent shows no apparent effect upon any of the properties measured. Titanium was evaluated between about 0.40 and 0.75 per cent. Over this range, the yield and tensile properties increase 30,000 psi.

The mechanical properties of AM-362 were further evaluated in the age-hardened condition. The primary purpose was to determine the effects of alloy additions upon the toughness of the alloy. Sheet was evaluated by sharp edge-notched tension specimens (7) prepared from transverse test coupons. Since the fracture toughness is highly dependent upon strength level, the aging

TABLE 4—RESULTS OBTAINED ON AM-362 TRAVERSE SHEET SPECIMENS.

Heat Number	Composition Variable	Aging Heat Treatment	Yield Strength, 0.2%, ksi	Ultimate Tensile Strength, ksi	Elongation in 2 in., %	Notched Tensile Strength, ksi[a]	Ratio NS/UTS
GL 58A	0.13 Si	900 F, 8 hr	172.0	183.5	5.0	202.7	1.10
GL 60A	0.35 Si	800 F, 3 hr	162.3	168.8	5.0	182.5	1.08
GL 60B	0.58 Si	800 F, 3 hr	163.4	173.5	6.0	174.2	1.00
GL 64	0.89 Si	800 F, 2 hr	163.5	174.8	5.2	173.3	0.99
GM 47	1.00 Mn	900 F, 8 hr	180.6	195.2	4.0	180.9	0.93
GM 50	1.44 Mn	900 F, 8 hr	...	187.0	4.0	174.6	0.93
GM 5	Stainless W	800 F, 1 hr	170.6	184.4	9.5	159.3	0.86

[a] Edge-notched tension specimen 0.0007 in. radius (Ref. 7).

TABLE 5—LONGITUDINAL NOTCHED TENSILE PROPERTIES OF AM-362 BARS.
(Heat Treatment: 1500 F, ½ hr, air cooled, plus 900 F, 8 hr, air cooled.)

Heat Number	Composition Variable	Hardness, Rc	Yield Strength, 0.2%, ksi	Ultimate Tensile Strength, ksi	Elongation in 4d, %	Reduction of Area, %	Notched Tensile Strength, ksi[a]	Ratio NS/UTS
GV 49	0.04 Si	39.5	170.9	174.9	18.0	59.9	283.2	1.62
GV 38	0.34 Si	45.0	195.7	199.9	17.0	56.1	272.0	1.36
GV 78	0.57 Si	47.0	204.3	208.4	15.0	52.9	191.8	0.92
GV 80	0.86 Si	47.0	215.0	218.8	13.0	42.3	208.0	0.95
GV 1	0.47 Mn	39.5	170.2	173.6	20.0	61.0	274.4	1.58
GV 96	0.37 Si	45.0	206.6	210.4	14.5	52.0	199.8	0.95

[a] Round bar edge-notched tension specimen, $K_t = 4.9$.

TABLE 6—TYPICAL PROPERTIES OF AM-362 BARS FROM A COMMERCIAL HEAT

Aging Treatment	Hardness, Rc	Yield Strength, 0.2 %, psi	Ultimate Tensile Strength, psi	Elongation in 4d, %	Reduction of Area, %
None	25	108 600	127 000	15.5	67.8
900 F, 2 hr	41	173 200	183 200	15.2	56.6
900 F, 8 hr	43	181 900	188 800	13.5	53.6
925 F, 2 hr	43	175 000	182 200	14.2	55.4
1000 F, 2 hr	40	169 200	174 000	16.0	59.1
1050 F, 2 hr	34	145 800	154 600	18.0	63.6

TABLE 7—IMPACT PROPERTIES OF ½ IN. AM-362 PLATE FROM A COMMERCIAL HEAT.

Aging Treatment	Test Direction	Hardness, Rc	Yield Strength, 0.2%, psi	Ultimate Tensile Strength, psi	Elongation 4d, %	Reduction of Area, %	Charpy V-Notch[a] ft-lb
900 F 4 hr	Longitudinal	40.5	184 100	189 000	13.5	51.1	5.5
900 F, 4 hr	Transverse	40.5	183 800	190 300	12.0	46.1	4.0
1050 F, 2 hr	Longitudinal	34	148 100	156 700	17.5	64.8	40.0
1050 F, 2 hr	Transverse	34	152 500	157 300	15.5	53.4	22.5

[a] Axes of notches perpendicular to plate surface. Test results are averages of three values.

TABLE 8—CORROSION RESISTANCE OF AGED AM-362 AND TYPE 430.

Testing Medium	Time	AM-362	Type 430
25% boiling nitric acid	Five 48-hr periods	0.0009	0.0007 IPM[a]
60% boiling acetic acid	24 hr	0.0002	0.025 IPM
20% boiling phosphoric acid	24 hr	0.0002	0.015 IPM

[a] IPM = Inches per month.

temperatures were adjusted for each heat in an attempt to evaluate this property at equivalent strength levels. This was done by underaging the higher silicon heats at selected times and temperatures, while aging the low silicon heats to maximum hardness. Similar effects could have been attained by overaging the high silicon heats, but this would necessitate aging above the austenite reversion temperature. The retained austenite, thus formed, would introduce an undesired variable.

Table 4 describes the results that were obtained on transverse sheet specimens. The significant analysis differences are included. The manganese content of the first group of heats is about 0.09 per cent, and the silicon content of the second group is about 0.15 per cent. The Stainless W heat contains 0.38 per cent manganese and 0.50 per cent silicon. Manganese and silicon, either individually or together, appear to reduce the notch toughness. GM 5, of Stainless W composition, has both higher manganese and silicon content and exhibits the lowest notch properties.

The longitudinal notched tensile properties of bars were also evaluated. In this case the notched tension tests were conducted on heats given the same aging heat treatments. This resulted in considerable variations in tensile properties as shown in Table 5.

Because of the variation in strength levels, it is more difficult to correlate the changes in notch strength with composition. The relatively small differences in strength level, however, do not appear to account for the large differences in notch strength that was observed. This is illustrated particularly well by the notch properties of heats GV 38 and GV 78. The effects of combined silicon and manganese additions appear to be particularly deleterious, but the effect of silicon alone appears to be significant.

The results of these experiments led to the following composition for AM-362.

C	Mn	Si	Cr	Ni	Ti
0.03	0.10	0.08	15	6	0.75

The strength of the alloy is largely controlled by titanium, an element which also is a strong ferrite former. Consequently, the nickel and chromium must be adjusted to maintain a composition free of delta ferrite at different strength levels. The transformation temperatures of AM-362, measured dilatometrically at heating and cooling rates of 250 F/hr, are: Ac_1, 1166 F; Ac_3, 1300 F; Ms, 510 F; and Mf, 350 F.

The alloy is annealed at 1500 to 1550 F and aged at 900 to 1050 F. Typical properties of bars from a commercial heat are shown in Table 6. The bar was annealed 1 hr at 1525 F and air cooled. The impact properties of ½ in. plate, from the same heat, are shown in Table 7.

AM-362, like AM-363, is readily weldable without preheat or postheat. The weld metal, however, is relatively sluggish, and care is required to obtain satisfactory appearing welds. The corrosion resistance of aged AM-362 is illustrated in Table 8.

After 1000 hr in a 5 per cent salt spray cabinet, AM-362 exhibited only a few scattered rust spots. The stress corrosion resistance of the alloy is also excellent in 5 per cent salt spray. Transverse sheet specimens from four laboratory heats

have been evaluated after aging at temperatures of 900, 1000, and 1050 F, at stresses equal to 70 per cent of the ultimate tensile strengths. No failures were observed over test periods of 1120 hr.

AM-367

The composition of AM-367 is: carbon, 0.03 per cent max; manganese and silicon, 0.15 per cent max; chromium, 14 per cent; nickel, 3.5 per cent; cobalt, 15.5 per cent; molybdenum, 2 per cent; and titanium, 0.4 per cent. This alloy can be strengthened to yield strengths in the range of 200,000 to 240,000 psi by aging in the temperature range of 800 to 850 F. At these strength levels, AM-367 has excellent toughness as measured by edge-notched tension tests (7). The details on the metallurgy and mechanical properties of AM-367 have been published elsewhere (8,9). See also p. 47.

PROCESSING OF COMMERCIAL-SIZE HEATS

Several commercial electric arc-furnace heats of AM-362 and AM-363, ranging in size from 10 to 70 tons, have been produced and evaluated. The hot-working and cold-rolling characteristics of these steels are excellent and very suitable for the present mill equipment. Both alloys have been cold rolled in strip form beyond 75 per cent without any difficulty. AM-362 seamless tubing has been cold drawn to 90 per cent reduction in wall thickness with similar success. AM-362 wire has been cold drawn 99 per cent without intermediate anneals. These cold reductions are in excess of those feasible with the other stainless-steel grades. They illustrate the good producibility of these steels and contribute to their favorable cost structure.

AM-363 is being produced primarily in sheet form with a strength level of 110 to 130 ksi. The potential of this steel lies primarily in cold-formed structural members in the transportation industry. AM-362 is produced mostly in bar form, as an all-purpose maraging stainless steel. Its machinability is superior to other similar martensitic grades even in the hardened state, thus making it possible to deliver it in the aged condition from the mill. Heat treatment by the user, therefore, can be eliminated. AM-362 sheet, plate, wire, and tubing have also been produced successfully. Aircraft quality material probably will require consumable electrode remelting in order to improve the surface quality.

SUMMARY

AM-363, 362, and 367 are three new maraging stainless steels recently developed at the Research Center of Allegheny Ludlum Steel Corp. These steels are age-hardenable martensitic steels with nearly identical properties in the annealed condition. The degree of hardening during aging varies considerably, however, as does the field of application.

AM-363 has the leanest composition and exhibits practically no hardening during aging treatments at temperatures over the range of 800 to 1050 F. The yield strength of this alloy is 110,000 psi at room temperature. The field of application is envisioned as the same for Types 301 and 201.

AM-362 is more highly alloyed and can be age hardened to a room-temperature yield strength of about 180,000 psi. The alloy is primarily designed for applications requiring high strength and good corrosion resistance.

AM-367 is highly alloyed and can be hardened to room-temperature yield strengths in the range of 200,000 to 240,000 psi. This alloy is designed for applications in the missile and airframe industries, where material properties are of paramount importance and cost is of secondary importance.

REFERENCES

(1) G. B. Espey, M. H. Jones, and W. F. Brown, Jr., "The Sharp Edge-Notch Tensile Strength of Several High-Strength Steel Sheet Alloys," *Proceedings*, Am. Soc. Testing Mats., Vol. 59, 1959, p. 837.

(2) M. Watter and R. A. Lincoln, "Strength of Stainless Steel Structural Members as Function of Design," Allegheny Ludlum Steel Corp., 1950.

(3) R. E. Peterson and A. O. Bergholm, "Effect of Forming and Welding on Stainless Steel Columns," *Aerospace Engineering*, Vol. 20, No. 4, April, 1961.

(4) R. E. Decker, J. T. Eash, and A. J. Goldman, "18% Nickel Maraging Steel," *Transaction Quarterly*, Am. Soc. Metals, Vol. 55, No. 2, March, 1962, p. 58.

(5) R. Wasmuht, "Über die Ausscheidungshärtung des Eisens durch Titan," *Archiv für das Eisenhuttenwesen*, Bd. 5, 1931, S. 45.

(6) R. Smith, E. H. Wyche, and W. W. Gorr, *Transactions*, Am. Institute Mining, Metallurgical, and Petroleum Engrs., Vol. 167, 1956, p. 313.

(7) "Fracture Testing of High-Strength Sheet Materials," Special ASTM Committee Report, *ASTM Bulletin*, February, 1960.

(8) C. M. Hammond, "AM-367—A New Precipitation Hardening Stainless Steel," *Metal Progress*, Vol. 82, No. 6, December, 1962, p. 92.

(9) C. M. Hammond, "AM-367—A Stainless Steel That Combines High Strength With Toughness," *Cobalt*, No. 18, March, 1963, p. 8.

DISCUSSION

ARTHUR COHEN[1]—Certain steels were described as having up to 25 per cent delta ferrite. Would you describe how these phases were identified since we have not had experience in this field? Presumably, it is a metallographic technique. Would the author kindly advise us as to etchants and the cycles? It is also our belief that considerable investigation in the use of columbium in stainless steels has been done by the Canadian Bureau of Mines and Technical Surveys, Physical Metallurgical Div. S. Gertsman, chief of the Division, could confirm this.

G. N. AGGEN, C. M. HAMMOND, AND R. A. LULA (*authors*)—Delta ferrite in these alloys can generally be recognized quite easily under a microscope by its characteristic smooth appearance and rounded contours. A specific etchant that we use on these alloys comprises the following: 10 cm^3 nitric acid, 10 cm^3 acetic acid, 15 cm^3 hydrochloric acid, and 2 or 3 drops of glycerol.

The etchant should be used as freshly mixed and is applied by swabbing for 5 to 15 sec at room temperature. The etchant should be free of water if it is to be effective. After initially etching the specimen, it should be lightly repolished and re-etched with a fresh mixture.

Under these conditions the martensite in these alloys is lightly attacked while the ferrite remains light and smooth. In a longitudinal section the ferrite will appear as stringers or irregular globules depending upon the working practice or thermal treatments imparted to the specimen.

G. D. GARDNER[2]—The very good corrosion resistance shown for these high-temperature materials should open up many applications, especially since they can be welded without seriously reducing the mechanical properties. Because of this combination of excellent characteristics, it would be interesting to know if this material has good fatigue strength at the high strength levels. Has any work been done on fatigue testing, particularly under conditions of triaxial stress?

MESSRS. AGGEN, HAMMOND, AND LULA—We have no fatigue properties on these alloys as yet. Smooth fatigue properties are presently being obtained on specimens of AM-362 bar. Both smooth and notched fatigue tests are also being conducted on AM-363 sheet specimens.

G. L. OLSON[3]—What annealing atmosphere is recommended for maraging Types 362, 363, and 367? Is it oxide, cracked ammonia, hydrogen, inert gases, or a vacuum? If oxide annealing is permissible, what methods are recommended to remove the resulting scale?

MESSRS. AGGEN, HAMMOND, AND LULA—During production of these materials all annealing operations have been conducted in air atmospheres. We feel certain that inert gas and vacuum annealing would be suitable also. Since these materials are martensitic, hydrogen-containing atmospheres probably should be avoided during annealing unless they are first evaluated and found suitable for these alloys.

Pickling procedures used on the conventional grades of stainless steel are satisfactory when removing annealing scales. A typical bath contains 10 to 15 per cent nitric acid and up to 3 per cent hydrofluoric acid operating at 120 to 140 F. In the case of AM-363 the hydrofluoric content should be limited to $\frac{1}{2}$ per cent to avoid some gage removal. The nitric-hydrofluoric bath may be preceded by a 7 to 10 per cent sulfuric bath at 140 to 160 F to hasten scale removal.

Aging at 850 to 1050 F can be conducted safely in any of the atmospheres cited. Oxide scales produced on AM-362 and AM-363 at these temperatures can be removed by the same procedures used to remove annealing scales. The corrosion resistance of AM-367 is impaired by aging so that special precautions must be observed to remove aging scales. For further information see paper "The Development of New High-Strength Stainless Steels" by C. M. Hammond, p. 47.

[1] Supervisor of metallurgy, Materials Engineering Dept., Carrier Air Conditioning Co., Syracuse, N. Y.

[2] U. S. Industrial Chemicals Co., Tuscola, Ill.

[3] Director, product development, Trent Tube Co., East Troy, Wis.

THE DEVELOPMENT OF NEW HIGH-STRENGTH STAINLESS STEELS

By C. M. Hammond[1]

Synopsis

Several maraging stainless steels have been developed from some basic information on the effect of certain alloying elements upon the martensite transformation (Ms) temperature, upon the suppression of delta ferrite, and upon the age-hardening response. This paper describes the research program which led to the development of these alloys.

High-strength stainless steels such as 17-7 PH, PH 15-7 Mo, AM-350, and AM-355 are used by the aircraft and missile industries. However, some of these steels are plagued by poor resistance to crack propagation at the higher strength levels. As a result, there is a definite need for a stainless steel that combines high strength and good resistance to crack propagation.

This paper will describe the research program which led to the development of several maraging stainless steels. However, only one of the alloys studied, AM-367, will be described in detail. At the outset of this developmental program, the following goals were outlined: (1) low strength and good formability in the annealed condition, (2) strengths approaching 250,000 psi after hardening, (3) good resistance to crack propagation at the higher strength levels, and (4) corrosion resistance equal to other high-strength stainless steels.

Two types of alloys appear to satisfy the formability and strength requirements stated: (1) semiaustenitic stainless steels strengthened by the martensite transformation, or by a combination of the martensite transformation and age hardening, and (2) low-carbon martensitic stainless steels strengthened by age hardening. The intermediate treatments to upset the stability of the austenite in semiaustenitic stainless steels generally precipitate grain boundary phases which can be deleterious to resistance to crack propagation. Therefore, this research concentrated on the use of low-carbon martensitic stainless steels strengthened by age hardening. This approach seemed reasonable based upon the early work of Aborn (1)[2] on low-carbon martensites and the more recent work by Bieber[3] and Decker et al (2) on iron-nickel martensites.

The Ms of the low-carbon martensitic stainless steels must be closely controlled in order to complete the transformation of austenite to martensite at room temperature or −100 F, since the precipitate will only age harden the martensite. In addition to controlling the Ms, no delta ferrite should be in the structure of the alloy in order to minimize mechanical property anisotropy. Titanium and molybdenum were the age-hardening elements that were studied, since these elements have been shown to significantly increase the hardness of martensitic alloys after aging. Cobalt was studied as a substitute for nickel to suppress delta ferrite formation.

The general approach in this study was to measure the effects of chromium, nickel, cobalt, titanium, and molybdenum upon the Ms, to determine the effects of cobalt and titanium on delta ferrite formation and to study the effects of cobalt, titanium, and molybdenum on the age-hardening response of stainless steels. For the most part, these measurements were made on specimens from 30-g heats. From these data, it was possible to calculate alloy compositions which were free of retained austenite and delta ferrite and which could be substantially age hardened. This type of approach to alloy development minimized the number of larger heats necessary for final development of the alloys.

Procedure

Thirty-gram heats were melted to study the effect of several of the elements of interest upon the Ms. Seventeen-pound ingots were melted and processed to evaluate the effects of cobalt and titanium upon the delta ferrite reaction and to evaluate mechanical properties of promising alloy compositions. The detailed experimental procedures follow. High-purity raw materials were used throughout this investigation.

Determination of Ms Factors:

The effects of chromium, nickel, cobalt, molybdenum, and titanium upon the Ms were determined on specimens from 30-g heats. The heats were induction melted in alumina crucibles under a purified argon atmosphere. The metal was solidified in the crucible, and the piped section of the ingot was cut off prior to processing. The cropped ingots were pressed at room temperature to $\frac{1}{4}$ in. square bars. A $\frac{1}{4}$ in. cube was cut from the bar for a specimen to determine the Ms by thermal analysis (3). The Ms specimens were homogenized at 2000 F for 16 hr prior to measuring the Ms. No segregation was found in the thermal analysis specimens before or after homogenization. No contamination of the specimens or thermocouple wires occurred during the determination of the Ms. A typical thermal analysis curve is shown in Fig. 1.

The effect of chromium upon the Ms was measured at 0.03 per cent carbon and 4 per cent nickel. The Ms depression factor for nickel was determined at 0.03 per cent carbon and 12 per cent chromium. Cobalt's effect upon the Ms was evaluated at 0.03 per cent carbon, 12 per cent chromium, and 4 per cent nickel. The effect of titanium and molybdenum upon the Ms was measured at 0.03 per cent carbon, 12 per cent chromium, 4 per cent nickel, and 15 per cent cobalt. These analyses were chosen for study to make the data useful for alloy development, if the effects of the above elements on the Ms were not additive.

The Effects of Cobalt and Titanium Upon Delta Ferrite:

Seventeen-pound heats were vacuum induction melted to study the effects of

[1] Research associate, Research Center, Allegheny Ludlum Steel Corp., Brackenridge, Pa.

[2] The boldface numbers in parentheses refer to the list of references appended to this paper.

[3] Clarence Bieber, private communication.

Copyright© 1965 by ASTM International

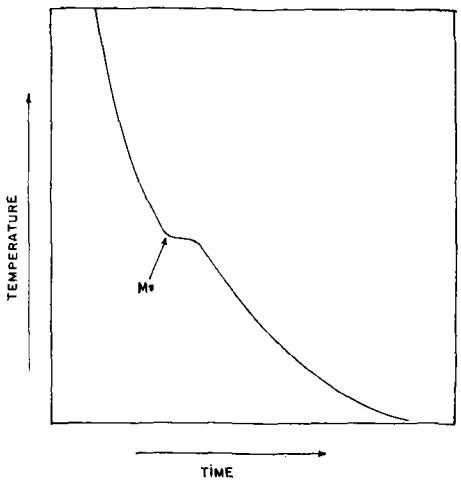


FIG. 1—A Typical Thermal Analysis Curve.

were sand blasted and cold rolled 50 per cent to about 0.060 in. thick. Small specimens were annealed, and the percentage of delta ferrite was measured by a calibrated Magne-Gage manufactured by the American Instrument Co. Inc., Silver Spring, Md.

Since the percentage of delta ferrite was measured magnetically, no martensite could be present in the specimens subjected to the Magne-Gage measurements. The analyses of these heats were designed from the Ms measurements so that no martensite would be present at room temperature. However, some heats contained martensite presumably because of partitioning of elements in the

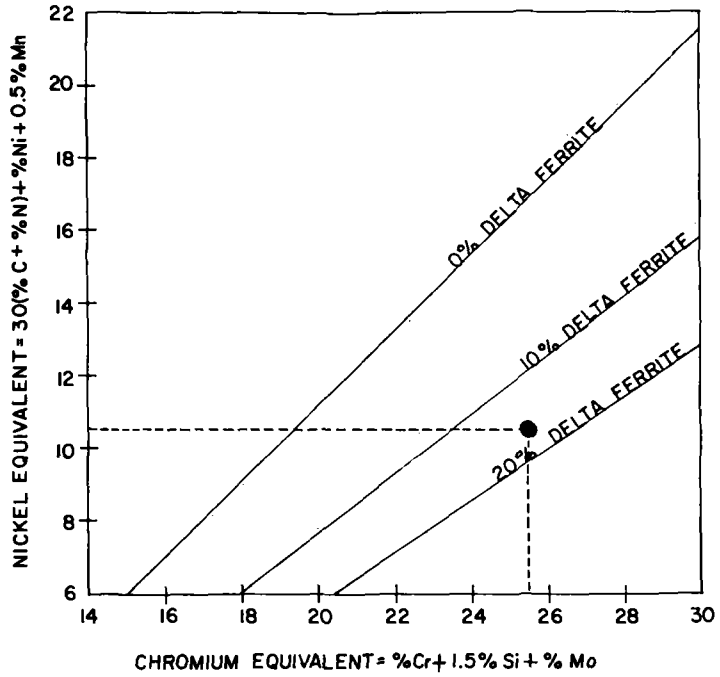


FIG. 2—Diagram for Predicting the Amount of Delta Ferrite in Wrought Stainless Steels (from Ferree).

cobalt and titanium upon delta ferrite formation in stainless steels. The heats used to determine the nickel equivalent of cobalt and the chromium equivalent of titanium contained only chromium and nickel as other major elements; cobalt and titanium were not simultaneously added to the same heat. A slice was cut from the hot top end of the ingot to determine the effects of cobalt and titanium in the as-cast condition. The remainder of the ingots was hot pressed to 1-in.-thick slabs from a furnace set at 2000 F. The slabs were ground and hot rolled to 0.250 in. thick from a 2000 F furnace. The sheet bars were ground and hot rolled to 0.120 in. thick from a 1700 F furnace; the finishing temperature was approximately 1550 F. The sheets

austenite and delta ferrite at elevated temperatures. The martensite-containing heats were not used to measure the percentage of delta ferrite.

The nickel equivalent factor for cobalt and the chromium equivalent factor for titanium were calculated using the delta ferrite diagrams of Schaeffler (4) and Ferree[4] for cast and wrought stainless steels, respectively. All the heats were designed to contain some delta ferrite by using assumed nickel and chromium equivalent factors for cobalt and titanium. The chromium equivalent of chromium and the nickel equivalent of nickel were assumed to be 1.0 in compliance with the diagrams of Schaeffler and Ferree. An example of calculating the nickel equivalent of cobalt is shown in Fig. 2. The skew lines denote the percentage of delta ferrite expected at various nickel and chromium equivalents. For a heat containing 0.008 per cent carbon, 0.0014 per cent nitrogen, 25.4 per cent chromium, 4.77 per cent nickel, and 8.08 per cent cobalt, the nickel equivalent excluding cobalt is 5.1; the chromium equivalent is 25.4. The measured percentage of delta ferrite was 16.5 per cent; therefore, the nickel equivalent must have been 10.3 for this percentage of delta ferrite. The following equation can be written:

$$Ni_e = 10.3 = 5.1 + 8.1x$$

where x is the nickel equivalent factor for cobalt. In this case, the nickel equivalent of cobalt is 0.64. The chromium equivalent of titanium was calculated in a similar manner. The only portion of the Ferree diagram which has any meaning for these alloys is the iso-delta ferrite lines. This technique of calculating the equivalents for cobalt- and titanium-bearing alloys assumes the validity of the Ferree and Schaeffler diagrams for these elements, and the actual values obtained are correction factors to modify the relationships to include cobalt and titanium.

Mechanical Properties:

Seventeen-pound heats of promising alloy compositions were vacuum induction melted and processed similar to the heats made to determine nickel and chromium equivalents. Smooth and notched tension specimens were prepared from the 0.060-in. sheet. The notched specimen was similar to that proposed by the ASTM Fracture Committee (5).

Small samples were used to determine heat treatments for optimum hardness. The heat treatment which resulted in the greatest hardness response for practically all the alloys investigated was: anneal or austenitize at 1600 F for 15 min and air cool, refrigerate at −100 F for 16 hr to insure complete transformation to martensite, and age at 950 F for 8 hr, and air cool. Therefore, this heat treatment was used for screening the experimental alloys that were investigated. All heat treatments were performed in air atmosphere furnaces.

One by two-inch specimens were annealed, refrigerated, and aged at 800, 900, 950, 1000, and 1050 F for various times, and prepared for corrosion testing. The corrosion test used was an exposure

[4] J. A. Ferree, unpublished information.

TABLE 1—AIM AND FINAL CHEMICAL ANALYSES OF 30-G HEATS FOR Ms TEMPERATURE MEASUREMENTS, WEIGHT PER CENT.

Heat No.	C	Cr	Ni	Co	Ti	Mo
1						
aim	0.03	...	4.0	...	...	...
final	0.035	...	3.86	...	...	...
2						
aim	0.03	4.0	4.0	...	...	...
final	0.035	3.96	3.93	...	...	...
3						
aim	0.03	8.0	4.0	...	...	...
final	...	...	...	...	...	...
4						
aim	0.03	12.0	4.0	...	...	...
final	0.03	11.90	3.97	...	...	...
5						
aim	0.03	12.0	4.0	5.0	...	...
final	0.035	11.89	3.95	4.80	...	...
6						
aim	0.03	12.0	4.0	10.0	...	...
final	...	...	...	...	...	...
7						
aim	0.035	12.0	4.0	15.0	...	...
final	0.033	11.94	3.59	14.60	...	...
9						
aim	0.03	12.0	4.0	15.0	...	2.0
final	...	...	...	...	...	...
10						
aim	0.03	12.0	4.0	15.0	...	4.0
final	0.037	12.00	4.04	15.00	...	4.00
11						
aim	0.03	12.0	4.0	15.0	...	6.0
final	0.037	12.00	3.98	15.00	...	5.90
20						
aim	0.035	12.0	4.0	15.0	0.5	...
final	0.040	12.00	3.92	15.00	0.38	...
21						
aim	0.035	12.0	4.0	15.0	1.0	...
final	0.039	12.00	4.02	15.00	0.87	...
22						
aim	0.035	12.0	4.0	15.0	1.25	...
final	0.041	12.00	3.96	15.00	1.11	...
24						
aim	0.035	12.0	4.0	...	...	...
final	0.037	12.00	4.00	...	...	...
25						
aim	0.035	12.0	8.0	...	...	...
final	...	...	...	...	...	...

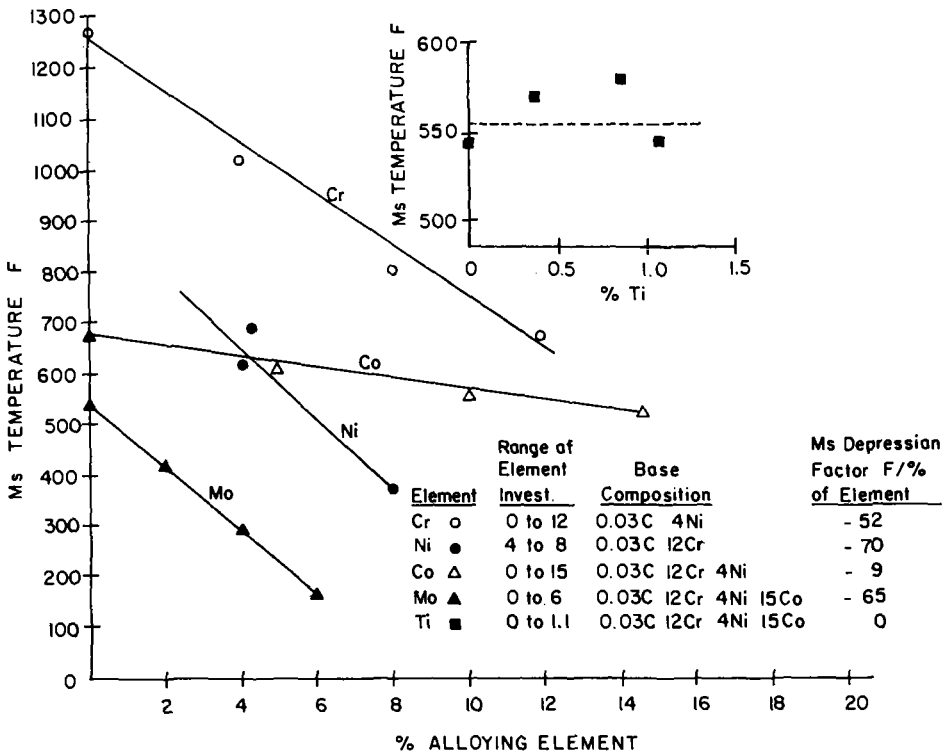


FIG. 3—Effect of Cr, Ni, Co, Mo, and Ti on the Ms Temperature.

of an unstressed specimen in 20 per cent salt spray for 100 hr.

RESULTS AND DISCUSSION

Determination of Ms Factors:

Table 1 contains the analyses of the 30-g heats prepared for the Ms studies. The excellent analytical control from the melting technique is evident for all elements except titanium. This was particularly important since the compositions contained several elements, only one of which was intentionally varied.

The effect of each element on the Ms is shown in Fig. 3. From these data, it is possible to derive the following two

TABLE 2—COMPARISON OF THE EFFECTS OF Ni, Cr, Co, Ti, AND Mo ON THE Ms TEMPERATURE OF LOW ALLOY STEELS, CONVENTIONAL STAINLESS STEELS, AND THE STAINLESS STEELS INVESTIGATED IN THIS RESEARCH, DEG F/PER CENT.

Element	Data for Low Alloy Steels (5-7)	Data for Stainless Steels (8,9)	This Research
Ni	−30 to −34	−110	−70
Cr	−27 to −50	−75	−52
Co	+22	−17	−9
Ti	...	...	0 to −100
Mo	0 to −50	...	−65

Ms equations for alloys containing 0.03 per cent carbon:

Ms = 1530 − 70 (per cent Ni) − 52 (per cent Cr) − 9 (per cent Co) − 0 (per cent Ti) [for alloys aged with Ti.] 1

Ms = 1530 − 70 (per cent Ni) − 52 (per cent Cr) − 9 (per cent Co) − 65 (per cent Mo) [for alloys aged with Mo.] 2

In order to use these equations, the alloy must be completely austenitic prior to quenching, and the cooling rate during quenching must be rapid enough to avoid austenite decomposition products other than martensite. These conditions were satisfied during this investigation. The Ms depression factors for the elements investigated in this research are significantly different from those proposed for low-alloy and conventional stainless steels (6–10). These data are compared in Table 2.

During the development of AM-367 and other maraging stainless steels, compositions were studied which were significantly different from the base compositions shown in Fig. 3. However, the measured Ms temperatures agreed within 25 F of the Ms calculated from the above equations. Therefore, the Ms factors for each alloying element appear to be addi-

tive and are of more general use than the comparison in Table 2 implies.

Two equations are shown above because the Ms depression factor for titanium is not zero when titanium is added to Fe-Ni-Cr-Co-Mo alloys; the factor is approximately −100 F for each 1 per cent of titanium. This interaction somewhat complicated the design of maraging steels containing both molybdenum and titanium.

The Effects of Co and Ti Upon Delta Ferrite:

The analyses of the 17 lb heats melted to study the effects of cobalt and titanium upon delta ferrite are shown in Table 3. The nickel equivalent of cobalt for cast and wrought specimens varied between 0.6 and 0.8. The chromium equivalent of titanium for cast and wrought specimens ranged from 1.4 to 1.6. Therefore, for the purpose of designing alloys, 0.7 was used as the nickel equivalent of cobalt, and 1.5 as the chromium equivalent of titanium.

Irvine et al (11) have shown that cobalt is approximately 0.6 as effective as nickel in suppressing delta ferrite in 0.1 C-17 Cr-4 Ni alloys. In addition, Coutsouradis (10) has shown that cobalt lowers the Ms temperature of 0.1 C-18 Cr alloys approximately 17 F/per cent of cobalt. These data are in fair agreement with the data presented in this research on the effect of cobalt on suppressing delta ferrite and lowering the Ms temperature.

Alloy Design:

These data can now be used to calculate compositions of stainless steels which will be free of delta ferrite and retained austenite. Experience indicates that the alloy should contain approximately 14 per cent chromium for good corrosion resistance. If other elements which stabilize delta ferrite are added for age hardening for a total chromium equivalent of 17, then a nickel equivalent of 8 will be necessary to eliminate delta ferrite, Fig. 2. The equation for calculating the nickel equivalent is: 30 (per cent C + per cent N) + 0.5 (per cent Mn + per cent Ni) + 0.7 (per cent Co). The carbon and nitrogen contents must be low in order to insure good formability of the martensite in the annealed condition. It has been shown in similar alloys that the manganese content must be about 0.15 per cent maximum for good notch ductility (2); therefore, only nickel and cobalt can be used to eliminate delta ferrite. The amounts of nickel and cobalt that can be used will depend upon the Ms temperature. According to recent data on iron-carbon alloys, the Ms temperature should be 280 F to limit retained austenite to 10 per cent after cooling to −100 F (12). In the case of alloys age hardened only with titanium, nickel alone can be used to eliminate delta ferrite since the Ms temperature of a 14 Cr-8 Ni alloy is 250 F from Ms (Eq 1), and titanium does not lower the Ms temperature. For alloys aged with molybdenum, both nickel and cobalt will be necessary to eliminate delta ferrite, since molybdenum additions will lower the Ms temperature from 250 F by 65 F/per cent molybdenum. If nickel alone is used to balance the composition, undesirable amounts of retained austenite will result.

This type of scheme was used to calculate compositions of larger heats to be used to evaluate tensile properties, notch tensile properties, and corrosion resistance. The use of the Ms and equivalent relationships greatly reduced the number of larger heats necessary to optimize the composition of AM-367 and the other stainless steels. Alloys aged principally with titanium and molybdenum, respectively, were prepared and evaluated.

TABLE 3—CHEMICAL ANALYSES OF HEATS USED FOR THE DETERMINATION OF THE Ni EQUIVALENT OF Co AND THE Cr EQUIVALENT OF Ti, WEIGHT PER CENT.

Heat No.	C	Mn	P	S	Si	Cr	Ni	Co	Ti	N
RV 326	0.017	0.007	0.015	0.009	0.024	23.98	6.76	9.75	...	0.0018
RV 327	0.024	0.008	0.007	0.012	0.028	25.40	4.77	8.08	...	0.0014
RV 329	0.024	0.007	0.006	0.008	0.028	18.25	9.78	...	1.48	0.0014
RV 330	0.018	0.008	0.006	0.009	0.028	17.19	11.69	...	1.51	0.0016
RV 331	0.019	0.007	0.007	0.009	0.028	14.09	12.65	...	2.07	0.0014

TABLE 4—THE EFFECT OF Mo, Co, AND Ti ON THE AGE HARDENING OF Fe-Ni-Cr-Co ALLOYS.

Heat No.[a]	Analysis, weight per cent					Annealed Hardness, Rc	Aged Hardness, max, Rc
	Cr	Ni	Co	Mo	Ti		
7	12	4	15	0	...	34	34
9	12	4	15	2	...	34	44
10	12	4	15	4	...	33	50
11	12	4	15	6	...	33	53
RV 369	15.5	3.5	7	2	0.5	28	41
RV 368	15.5	3.5	10	2	0.5	29	45
RV 367	15.5	3.5	15.5	2	0.5	34	52

[a] The detailed analyses of Heats 7 to 11 are in Table 1. The nominal analyses of the important elements of Heats RV 369, 368, and 367 are shown in this table; the remainder of the analyses are: C-0.03 per cent max, Mn and Si-0.10 per cent max, P and S-0.01 per cent max.

Mechanical Properties:

Alloys aged with titanium—Initially alloys containing titanium were investigated. The compositions studied were over the range of 12 to 15 per cent chromium, 6 to 8 per cent nickel, and 0.5 to 2.0 per cent titanium. Some interesting low-strength alloys were uncovered in this study, but the high-strength alloys (yield strength >210,000 psi) were brittle as measured by a notch tension test. Cobalt was added to some of these alloys in an attempt to lower the transition temperature. The alloys containing cobalt were also brittle, and as a result the emphasis was shifted to alloys age hardened with molybdenum.

Alloys aged with molybdenum—The 30 g heats, Nos. 7 through 11, were initially studied to determine the effect of molybdenum on age-hardening response. These data are shown in Table 4. The zero per cent molybdenum heat did not age harden; the heats containing 2, 4, and 6 per cent molybdenum hardened to 44, 50, and 53 Rc, respectively. However, the 4 and 6 per cent molybdenum heats, Nos. 10 and 11, contained large quantities of chi phase. It was thought that this phase would be harmful to corrosion resistance and notch properties; therefore, it was decided to limit the molybdenum to 2 per cent at a 15 per cent cobalt level. This means that the alloy would only age to a hardness of 44 Rc, which would not satisfy the strength goal outlined earlier.

Three 17-lb heats were made to study the effects of cobalt and titanium on the age hardening. For these heats the chromium content was increased from 12 to 15.5 per cent. A titanium addition of 0.5 per cent was made to these three heats in order to increase the age hardening

TABLE 5—TENSILE PROPERTIES FROM 0.060-IN. SHEET.

Heat Treatment	Yield Strength, 0.2%, ksi	Ultimate Tensile Strength, ksi	Elongation in 2 in., %	UTS/NTS Ratio
Annealed	100.9	145.5	8.5	...
Annealed and aged	218.5	226.4	8.0	1.07

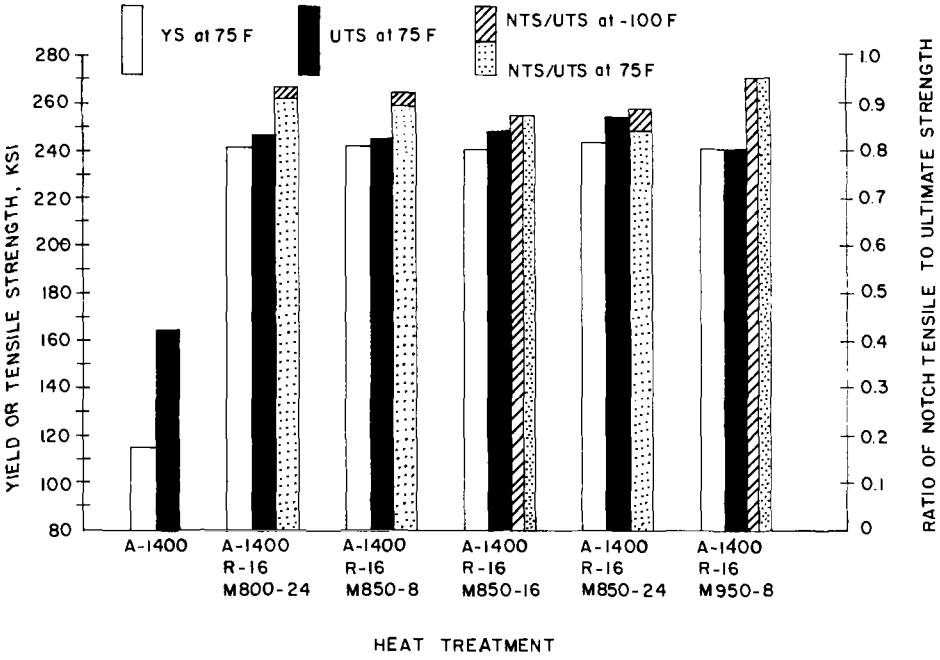


FIG. 4—Effect of Aging Treatment After a 1400 F Anneal Upon the Mechanical Properties of AM-367.

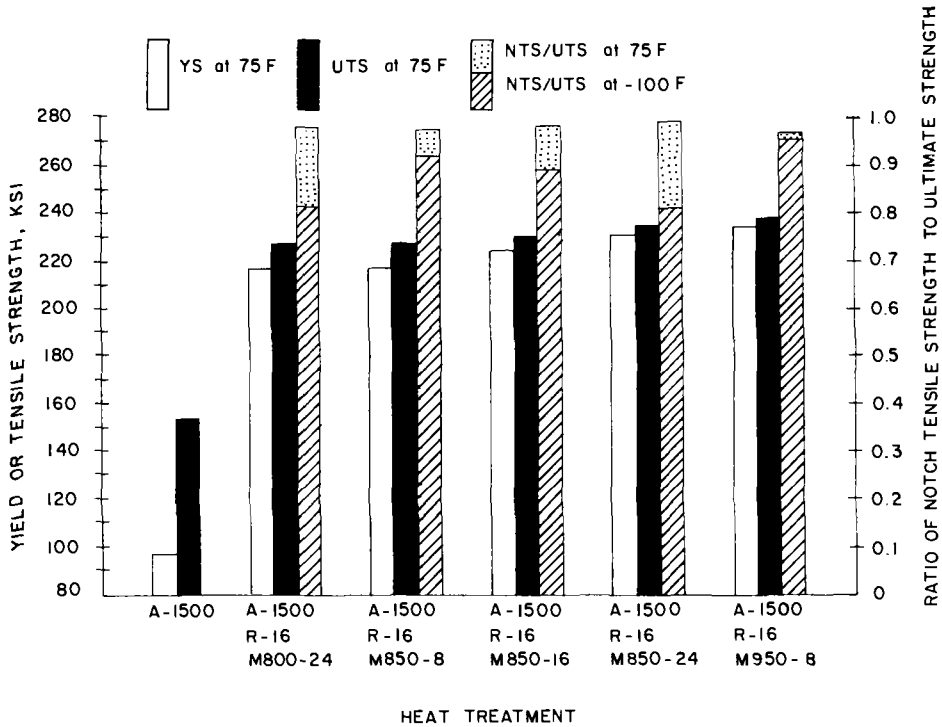


FIG. 5—Effect of Aging Treatment After a 1500 F Anneal Upon the Mechanical Properties of AM-367.

response. The total chromium equivalent of these alloys is 18.25. According to Fig. 2, a nickel equivalent of 9.25 will be necessary to eliminate delta ferrite. Since the nickel content was fixed at 3.5 per cent for the present, about 10 per cent cobalt will be needed to balance the composition. In this series of heats it was decided to study a composition containing delta ferrite so that the series contained heats with 7, 10, and 15 per cent cobalt. The calculated Ms temperature of the 15 per cent cobalt heat was approximately 65 F below 280 F, but this was sufficiently close for the purpose of these heats.

The data in Table 4 show that increasing the cobalt content from 7 to 15 per cent increased the aged hardness from 41 to 52 Rc. Also heat RV-367 age hardened to 52 Rc compared to heat No. 9 which aged to 44 Rc. Therefore, titanium apparently has a substantial effect upon the aging reaction. (It is also possible that the 3 per cent increase in chromium affects the aging response, but, since 0.5 per cent titanium age hardened the titanium alloys studied above, it is more reasonable that the titanium is responsible for the hardening boost.)

The composition of RV-367 was close to the desired alloy as far as age-hardening response was concerned, but the alloy was not completely martensitic at room temperature and had to be refrigerated at −100 F for 16 hr to complete the transformation. It was at this point that titanium was found to lower the Ms temperature approximately 100 F/per cent titanium. In order to compensate for this effect, the chromium was decreased to 14 per cent. This compositional change essentially completed the development of AM-367, although other compositions were evaluated to determine if any improvement in mechanical properties would result. None did, so that the composition of AM-367 is: carbon-0.03 per cent max, manganese-0.15 per cent max, silicon-0.15 per cent max, phosphorus and sulfur-0.01 per cent max, chromium-14 per cent, nickel-3.5 per cent, cobalt-15.5 per cent, molybdenum-2 per cent, and titanium-0.5 per cent. The tensile properties from 0.060-in. sheet produced in the laboratory are shown in Table 5. The annealed properties are low enough for adequate formability, and the properties after aging combine high yield and tensile strengths with excellent notch ductility.

On the basis of these laboratory data, a 5000-lb production heat has been successfully melted and processed into various product forms. The mechanical properties have been previously published (**13,14**). Figures 4 and 5 summarize the properties from 0.025-in. sheet. In Figs. 4 and 5 symbols have been used to designate heat treatments. For example, A-1500 means annealed at 1500 F,

R-16 means refrigerated 16 hr at −100 F, and M-800-24 means maraged at 800 F for 24 hr. These data show that AM-367 can be strengthened to a yield strength of 230,000 psi, a tensile strength of 236,000 psi, and maintain a notch ratio of 1.0, while other precipitation hardening stainless steels can only be strengthened to yield strengths between 175,000 and 180,000 psi, tensile strengths between 190,000 and 200,000 psi, and maintain notch toughness (15).

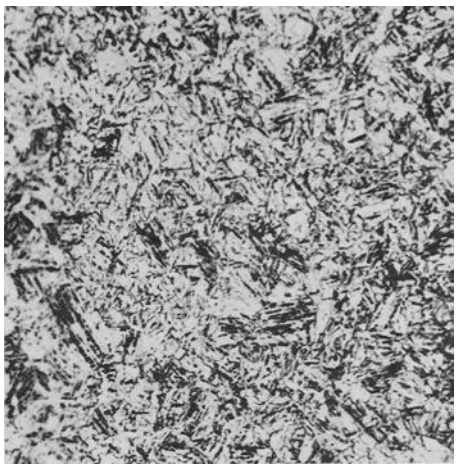


FIG. 6—Structure of 0.125-in. Sheet of AM-367 After Annealing at 1500 F (500× magnification).



FIG. 7—Structure of Thin Foil of AM-367 After Annealing at 1500 F (33,000× magnification).

For the best combination of mechanical properties and corrosion resistance, it is recommended that the following heat treatment be used for sheet; anneal at 1400 to 1500 F, refrigerate at −100 F for 16 hr, and age at 850 F for 8 hr. The best impact properties of bar were obtained after an anneal at 1400 F, followed by refrigeration at −100 F, and an age at 850 F for 8 hr. The surfaces of corrosion specimens were initially prepared by grinding or buffing. With this surface preparation, specimens heat treated as outlined above did not rust in 20 per cent salt spray in 100 hr. A pickled surface rusts severely in salt spray, and this method of surface preparation is not recommended. It is not known why the corrosion resistance of this alloy is so sensitive to surface preparation, but this phenomenon will undoubtedly limit the commercial applications of the alloy. The corrosion problem was subsequently solved by decreasing the cobalt content to 5 per cent and increasing the nickel content to 6.75 per cent to prevent delta ferrite.

Structure:

In the annealed condition, AM-367 is essentially completely martensitic. The structure is difficult to resolve by light microscopy as shown in Fig. 6. However, the fine martensitic structure is delineated by transmission electron microscopy of thin foils as shown in Fig. 7. The martensite appears to be in the form of plates similar to the martensitic structures reported by Kelley and Nutting (16). Most of the martensite plates contain a high density of dislocations. It is possible that the fine martensitic structure of AM-367 is responsible for the excellent toughness of this alloy.

As yet, the mechanism of strengthening of AM-367 has not been determined. It is believed that the alloy is hardened by a fine dispersion of second phase particles, nucleated at the many sites in the fine structure of the martensite.

CONCLUSIONS

The development of maraging stainless steels was greatly aided by the determinations of Ms temperature depression factors and nickel and chromium equivalent factors for elements of potential interest in the analyses. From these data, alloy compositions could be calculated so that the alloy structures would not contain retained austenite or delta ferrite.

One of the products of this alloy development program, AM-367, is an age-hardenable martensitic stainless steel, which possesses adequate formability in the annealed condition and can be hardened to room-temperature yield strengths of 220,000 to 240,000 psi by a simple aging treatment. At these strength levels, AM-367 is resistant to catastrophic crack propagation as measured by a notch tension test. The corrosion resistance of the alloy is greatly affected by surface preparation, and in order to achieve adequate corrosion resistance the surface must be prepared by mechanical means. Subsequent modifications in the cobalt and nickel contents have solved the corrosion problems.

ACKNOWLEDGMENTS

The author is indebted to R. K. Teorsky, P. O. Lange, G. N. Aggen, R. A. Lula, and D. L. Burk of the Research Center of Allegheny Ludlum for their assistance in various phases of this development.

REFERENCES

(1) R. A. Aborn, "Low Carbon Martensites," *Transactions*, Am. Soc. Metals, Vol. 48, 1956, p. 51.

(2) R. F. Decker, J. T. Eash, and A. J. Goldman, "18% Nickel Maraging Steel," *Transaction Quarterly*, Am. Soc. Metals, Vol. 55, No. 1, March, 1962, p. 58.

(3) C. M. Hammond and D. L. Burk, "A Simplified Thermal Analysis Technique For Measuring Transformation Temperatures of Steels," *Materials Research and Standards*, Vol. 4, No. 6, Am. Soc. Testing Mats., June, 1964, p. 275.

(4) W. T. DeLong, "Revised Section of Schaeffler Constitution Diagrams," *Metal Progress Data Sheet*, February, 1960, p. 100-B.

(5) "Fracture Testing of High Strength Sheet Materials," Special ASTM Committee Report, *ASTM Bulletin No. 243*, Am. Soc. Testing Mats., January, 1960, pp. 29–40, February, 1960, p. 18.

(6) P. Payson and R. A. Grange, "The Temperature Range of Martensite Formation in Steel," *Metals Handbook*, Am. Soc. Metals, 1948 Edition, p. 611.

(7) H. H. Chiswik and A. B. Greninger, "Influence of Ni, Mo, Co, and Si on the Kinetics and Ar Temperatures of the Austenite to Martensite Transformation in Steels," *Transactions*, Am. Soc. Metals, Vol. 32, 1944, p. 483.

(8) V. Zyuzin, V. Sadovski, and S. Branchuck, *Metallurg*, Vol. 14, Nos. 10–11, 1939, pp. 75–80.

(9) G. H. Eichelman and F. C. Hull, "The Effect of Composition on the Temperature of Spontaneous Transformation of Austenite to Martensite in 18-8 Type Stainless Steel," *Transactions*, Am. Soc. Metals Vol. 45, 1953, p. 77.

(10) D. Contsouradis, "Action du Cobalt dans les Aciers a Durcissement Structural," *Memoires Scientifiques Rev. Metallurg*, LVIII, No. 7, 1961.

(11) K. J. Irvine, D. T. Llewellyn, and F. B. Pickering, "Controlled Transformation Stainless Steels," *Journal Iron and Steel Inst.*, Vol. 192, Part 3, July, 1959, p. 218.

(12) D. P. Koistenin and R. E. Marburger, "A

General Equation Prescribing The Extent of the Austenite—Martensite Transformation in Pure Iron—Carbon Alloys and Plain Carbon Steels," *Acta Metallurgica*, Vol. 7, 1959, p. 59.

(13) C. M. Hammond, "AM-367—A New Precipitation Hardening Stainless Steel," *Metal Progress*, Vol. 82, No. 6, December, 1962, p. 92.

(14) C. M. Hammond, "AM-367—A Stainless Steel That Combines High Strength With Toughness," *Cobalt*, No. 18, March, 1963, p. 8.

(15) G. B. Espey, M. H. Jones, and W. F. Brown, "The Sharp-Edge Notch Tensile Strength of Several High Strength Steel Sheet Alloys," *Proceedings*, Am. Soc. Testing Mats., Vol. 59, 1959, p. 837.

(16) P. M. Kelley and J. Nutting, "The Morphology of Martensite," *Journal Iron and Steel Inst.*, Vol. 197, 1961, p. 199.

MECHANICAL PROPERTIES AND CORROSION RESISTANCE OF A HIGH-STRENGTH CHROMIUM-MANGANESE-NITROGEN-STAINLESS STEEL

By J. J. Heger,[1] Personal Member, ASTM

Synopsis

As a consequence of a nickel shortage in the early 1930's, German investigators undertook the development of austenitic chromium-manganese stainless steels. These investigators established the composition limits for the iron-chromium-manganese system, and their results are discussed. American investigators were able to obtain higher chromium contents in austenitic steels by the use of nitrogen. Using both nickel and nitrogen in combination with manganese, these investigators developed the steels that are accepted today as AISI Types 201 and 202. Further work in America indicated that fully austenitic steels containing over 18 per cent chromium, using manganese and nitrogen as austenite formers, were possible. In this paper the structural diagrams for the iron-chromium-manganese-nitrogen system are presented. These diagrams permit the establishment of composition limits for fully austenitic chromium-manganese-nitrogen stainless steel.

The melting, processing, mechanical properties, and corrosion resistance of one of the chromium-manganese-nitrogen austenitic stainless steels is described. This steel contains upward of 0.40 per cent nitrogen with the result that its room-temperature mechanical properties are twice those of the conventional chromium-nickel austenitic stainless steels. Data are presented showing the effect of cold rolling on the room- and elevated-temperature tensile strength and compressive strength. In addition, data are presented illustrating the fatigue strength of this material in the annealed and cold rolled condition. The results of laboratory and service corrosion tests indicate that the corrosion resistance of the chromium-manganese-nitrogen stainless steels is equivalent to that of 17 per cent chromium Type 430 stainless steel in all environments tested and is similar to Type 304 stainless steel in many of the environments tested. Although the stress corrosion resistance of the chromium-manganese-nitrogen stainless steel is erratic, it is always superior to that of the chromium-nickel austenitic stainless steels, such as Type 304. The possibility, therefore, exists that some slight modification in the chromium-manganese-nitrogen stainless steel will provide the long-wished-for austenitic stainless steel having immunity to transgranular stress corrosion cracking.

The possibility of developing non-nickel austenitic stainless steels was first given serious consideration in the early 1930's by German investigators. Because manganese and nickel are similar in their effect on the transformation of iron, the German investigations were devoted, almost entirely, to the use of manganese as a substitute for nickel. These investigations resulted in a series of 14 per cent chromium, nickel-free austenitic stainless steels that contained about 8 to 12 per cent manganese. Some of these steels had additions of titanium, copper, and molybdenum to enhance corrosion resistance and elevated-temperature strength. However, these endeavors were not entirely successful because a completely austenitic steel containing over 15 per cent chromium was never developed. Although chromium-manganese steels containing upwards of 18 per cent chromium are described in German literature, such steels have a duplex structure (austenite plus ferrite) and are extremely difficult to hot work. The situation can be best summarized by Fig. 1 taken from Kinzel and Franks[2] which illustrates sections of the iron-chromium-manganese diagram. As will be noted, the achievement of a completely austenitic structure in a steel containing over 14 per cent chromium is not possible even though the manganese content may be as high as 20 per cent. Indeed, as the manganese content increases from about 8 to about 20 per cent, the amount of chromium for a completely austenitic structure decreases from about 14 to about 12 per cent.

American Investigations

Because of government restrictions on the use of nickel, which were imposed during the early part of World War II and intensified during the Korean conflict, a nickel shortage became evident in the United States. As a consequence of this apparent nickel shortage, studies were initiated in this country to develop substitute steels for the austenitic chromium-nickel stainless steels. Ultimately, these studies resulted in the development of a series of steels in which nitrogen, as well as manganese, were substituted for part of the nickel in the chromium-nickel austenitic stainless steels.

The beneficial effects of nitrogen in a chromium-manganese-nickel stainless steel are illustrated in Figs. 2 and 3, taken from the work of Binder and his associates.[3] Note that the increase in the nitrogen content of a steel containing 18.5 per cent chromium and 6 per cent manganese lowers the nickel required for a completely austenitic structure from 11 to 7 per cent.

Figure 4 summarizes the work of Binder and his associates in the substitution of manganese and nitrogen for all or part of the nickel in austenitic stainless steels. Several things are evident from this figure.

Note that at 0 per cent nickel the maximum chromium content attainable in a completely austenitic structure is slightly above 15 per cent. Recall that the earlier German work indicated this maximum chromium content to be about 14 per cent, so the increase in nitrogen content from about 0.03 to 0.15 per cent has increased the chromium content from 14 to 15.5 per cent. Also note that the results of Binder's work confirm the German work illustrating that, as the manganese content of the steel is in-

[1] Chief research engineer, Stainless Steel Applied Research U. S. Steel Corp., Pittsburgh, Pa.

[2] A. B. Kinzel and R. Franks, *Alloys of Iron and Chromium*, Vol. II, McGraw Hill Book Co., Inc., New York, N. Y., 1940, p. 277.

[3] W. O. Binder,, R. Franks, and J. Thompson, "Austenitic Chromium-Manganese-Nickel Steels Containing Nitrogen," *Transactions*, Am. Soc. Metals, Vol. 47, 1955, pp. 231–266.

Copyright© 1965 by ASTM International

www.astm.org

creased above about 12 per cent, the area of the austenite field decreases. In other words, above about 12 per cent, manganese could be called a ferrite former. Another interesting feature of this diagram is that above about 12 per cent manganese the boundary between the austenite and austenite-ferrite fields

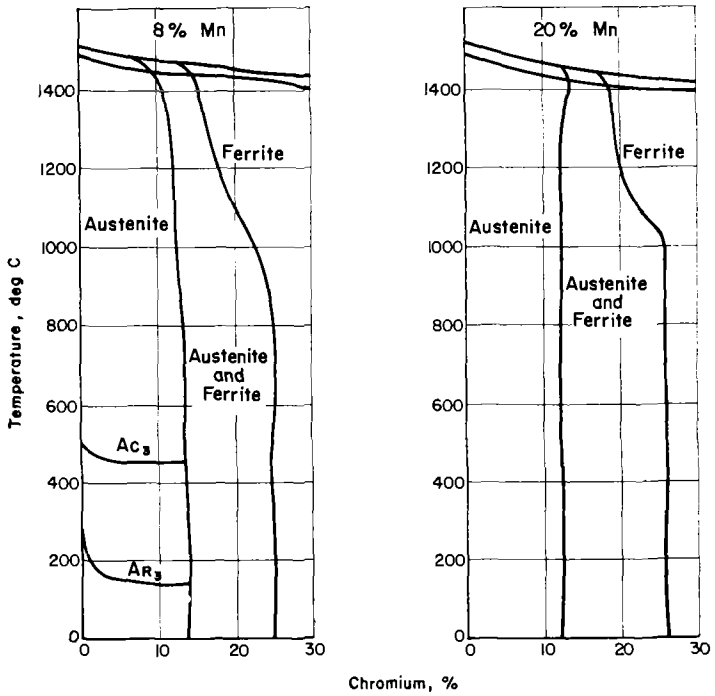


FIG. 1—Constant-Manganese Sections of the Iron-Chromium-Manganese Diagram (from Kinzel and Franks).

CHROMIUM-MANGANESE-NITROGEN STAINLESS STEEL

Although Binder's results and those of other investigators available during the early 1950's illustrated the beneficial effects of nitrogen on expanding the austenite field in the iron-chromium-manganese system, initial attempts to exploit this advantage of nitrogen were unsuccessful. When nitrogen contents in excess of about 0.25 per cent were added to the steels known at that time (steels containing normally 18 per cent chromium-6 per cent manganese-4 per cent nickel), the nitrogen solubility of the material was exceeded, and the phenomenon known as "bleeding" ingots was encountered. At about that period, D. J. Carney[4] of U. S. Steel Corp. reasoned that the effects of a combination of chromium and manganese on increasing nitrogen solubility might be greater than the effect of either element alone, and that the proper combinations of these elements should permit the addition of sufficient quantities of nitrogen to produce a completely austenitic microstructure in chromium-manganese steels containing as much as 18 per cent chromium. Carney's initial experiments demonstrated that nitrogen contents as high as 0.50 per cent could be attained by normal melting practices in steels containing 18 per cent chromium and 15 per cent manganese. These results prompted an investigation of the effects of high nitrogen contents on the phase relationships in the chromium-manganese system. The results of these studies are illustrated in Fig. 5, from Carney.[4] This figure shows that a minimum nitrogen content of 0.35 per cent produces a completely austenitic microstructure in steels containing 17.5 per cent chromium, 15 per cent manganese, and 0 per cent nickel. Similar structural composition diagrams were made for steels containing 1, 2, and 3 per cent nickel.

A useful steel that has been developed from the work of Carney has a composition shown in Table 1 and contains 0.10 per cent carbon, 15 per cent manganese, 17 per cent minimum chromium, 0.35 per cent minimum nitrogen, and no nickel. This steel was introduced by U. S. Steel in 1956 under the trademark, Tenelon. Because Tenelon stainless steel is unique in that it is a nonnickel austenitic steel containing over 17 per cent chromium, and has exceptionally high strength in the annealed condition, its characteristics should be of interest.

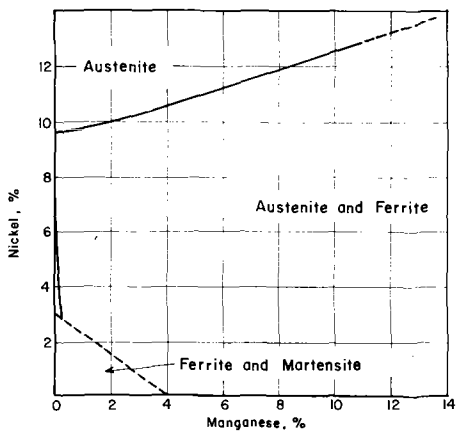


FIG. 2—Phases in 18.5 Per Cent Chromium Steels, 0.05 to 0.08 Per Cent Carbon, and 0.03 Per Cent Nitrogen Heated 15 min at 1075 C and Air Cooled (from Binder et al).

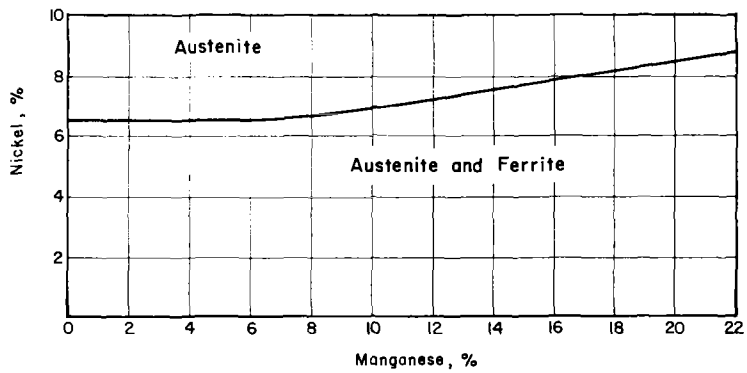


FIG. 3—Phases in 18.5 Per Cent Chromium Steels, 0.05 to 0.08 Per Cent Carbon, and 0.12 to 0.15 Per Cent Nitrogen Heated 15 min at 1075 C and Air Cooled (from Binder et al).

at low nickel contents is, for all intents and purposes, a straight line. Binder's important contribution served as the basis for the development of the chromium-manganese-nickel-nitrogen stainless steels that were adopted as standard Types 201 and 202 by the American Iron and Steel Inst. in 1955.

[4] D. J. Carney, "Nickel-Free and Low Nickel Austenitic Stainless Steels," *Regional Technical Meetings*, Am. Iron Steel Inst., 1955, pp. 103–113.

Melting:

The high nitrogen content of this chromium-manganese-nitrogen stainless steel is obtained during melting by the addition of nitrided ferrochromium pellets and nitrided electrolytic manganese. Because the high nitrogen solubility desired is a function of the chromium as well as the manganese content of the material, these nitrogen additions must be made at the latter part of the heat, that is, when almost all of the chromium and manganese is in the bath. In fact, normal melting practice for this grade of steel requires making these additions during the last 45 to 30 min of the heat.

Because of some concern regarding the segregation of nitrogen during ingot solidification, several studies have been made of the nitrogen distribution in slabs that have been rolled from chromium-manganese-nitrogen ingots. The results of one of these studies is shown in Fig. 6. Note that a slight increase in nitrogen content is to be found in the top cut of the slab. However, this segregation is not considered to be excessive or harmful for most applications. The macroetch quality of all of the slabs studied in this investigation was satisfactory, and metallographic examination revealed a completely austenitic structure in the as-rolled slab product.

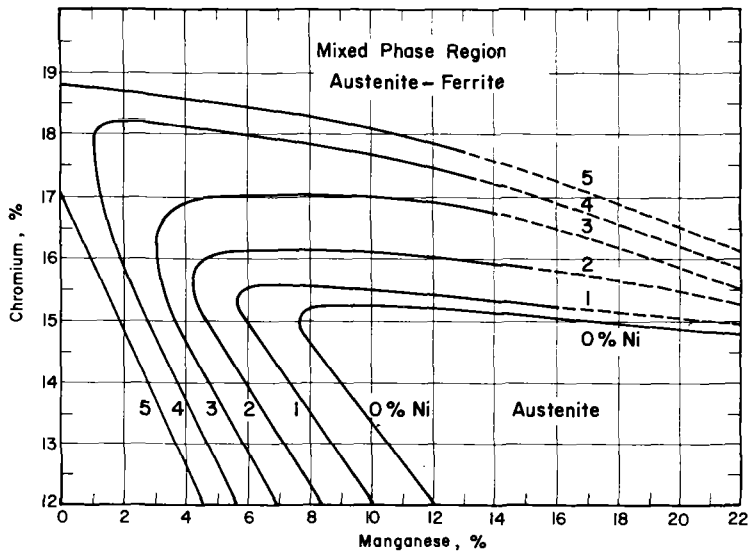


FIG. 4—Structure of 12 to 18 Per Cent Chromium, 0 to 22 Per Cent Manganese, 0 to 10 Per Cent Nickel Steels Containing 0.10 to 0.12 Per Cent Carbon and 0.08 to 0.15 Per Cent Nitrogen After Heating 15 min at 1075 C and Air Cooled (from Binder et al).

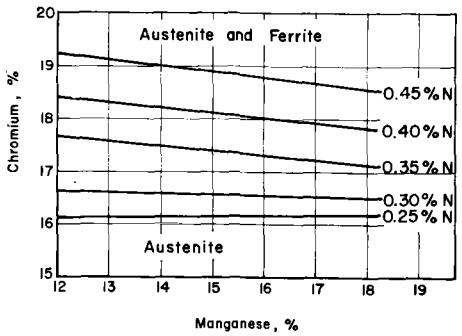


FIG. 5—Structure Diagram for 0.00 Per Cent Nickel, 0.25 to 0.45 Per Cent Nitrogen Steels After Heating for 1 hr at 2300 F and Water Quenching (from Carney).

Hot Working:

The hot working of this steel presents no unusual problems, provided its chemical composition is kept within the limits established by the structural diagrams illustrated previously. For example, the results summarized in Fig. 7 indicate that the hot workability of this steel, as measured by the hot twist test, is only slightly (and perhaps insignificantly) poorer than that of Type 304 stainless steel.

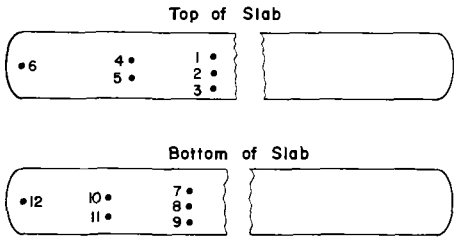
Cold Working:

On the other hand, cold working poses some problems. As indicated above, this steel has appreciably higher strength than the standard chromium-nickel-austenitic stainless steels. Furthermore, it work hardens at a somewhat higher rate than these steels. Consequently, after a given amount of cold reduction, the chromium-manganese-nitrogen steel will have a higher yield and tensile strength than other austenitic stainless steels, and thus it can be considered to be more difficult to cold work unless provisions are made for increased power. Not infrequently this steel will require more annealing treatments to obtain a given amount of cold reduction than will the standard chromium - nickel - austenitic stainless steels.

TABLE 1—CHEMICAL COMPOSITION OF Cr-Mn-N STAINLESS STEEL,[a] WEIGHT PER CENT.

C	Mn	P	S	Ni	Si	N	Cr
0.08 to 0.12	14.50 to 16.00	0.045 max	0.03 max	0.05 to 0.75	0.03 to 1.00	0.35 to 0.45	17.00 to 18.50

[a] U. S. Patent No. 2 778 731.



Specimen	C	Mn	Cr	N
1	0.12	15.45	...	0.50
2	0.11	15.55	...	0.55
3	0.09	15.25	...	0.46
4	0.11	15.35	...	0.49
5	0.11	15.25	18.01	0.51
6	0.11	15.25	...	0.48
7	0.10	15.05	...	0.49
8	0.10	15.05	...	0.46
9	0.08	14.95	...	0.43
10	0.08	14.95	...	0.43
11	0.09	14.85	18.01	0.46
12	0.09	15.15	...	0.48
Ladle	0.10	15.50	17.76	0.41

FIG. 6—Chemical Segregation in Slab Product of Cr-Mn-N Stainless Steel (from Carney).

Mechanical and Tensile Properties:

Perhaps the most unusual characteristic of this steel, and one of its more useful attributes, is its high mechanical strength and good ductility at room and elevated temperatures. The results of a large number of tests which have been made on bar, sheet, and plate product nitrogen steel are shown in Table 2, along with comparable typical properties for Types 302 and 301 chromium-nickel-austenitic stainless steels.

Impact Strength:

As shown in Table 3, excellent V-notch impact strength is obtained at room temperature, at −100 F, and even at −200 F. However, this property decreases to 13 ft-lb at −300 F. Current work being performed in U. S. Steel's Applied Research Laboratory is aimed at the development of a chromium-manganese-nitrogen stainless steel having a minimum impact strength of 15 ft-lb at −420 F.

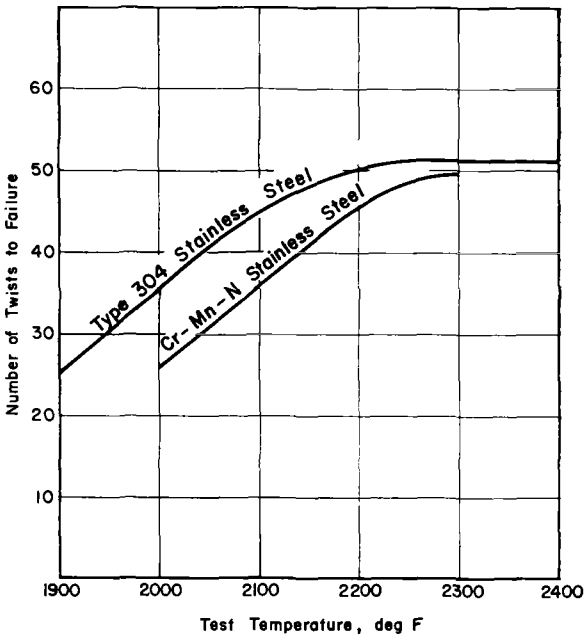


FIG. 7—Comparative Hot-Twist Results of Type 304 Stainless Steel and Cr-Mn-N Austenitic Stainless Steel.

TABLE 2—MINIMUM TENSILE PROPERTIES FOR Cr-Mn-N AUSTENITIC STAINLESS STEEL COMPARED WITH TYPICAL PROPERTIES FOR TYPES 302 AND 301.

	Cr-Mn-N	Type 302	Type 301
Yield strength, 0.2% offset, psi	70 000	40 000	40 000
Tensile strength, psi	120 000	90 000	110 000
Elongation in 2 in., per cent	45	50	60

TABLE 3—CHARPY V-NOTCH IMPACT STRENGTH OF Cr-Mn-N AUSTENITIC STAINLESS STEEL.

Test Temperature, deg F	Impact Strength, ft/lb
78	220[a]
−100	220[a]
−200	52
−300	13

[a] No break.

indicate that the typical room-temperature yield strength of this material is between 75,000 and 80,000 psi, the typical tensile strength is between 130,000 and 135,000 psi, with elongations ranging from 50 to 55 per cent. Current results indicate a yield strength of 70,000 psi, a tensile strength of 125,000 psi, and an elongation in 2 in. of 45 per cent may be conservative minimum values. Tentative minimum room-temperature tensile properties of the chromium-manganese-

Effect of Cold Work:

The higher rate of work hardening of the chromium-manganese-nitrogen steel and its higher initial strength at room temperature permits the development of high strength in this material with less cold work than is required for steels such as Type 301. An example of this is shown in Fig. 8. As will be noted in the figure, the tensile properties of the chromium-manganese-nitrogen stainless steel at a given amount of cold reduction are appreciably higher than those of Type 301. As an example, at only 5 per cent reduction the chromium-manganese stainless steel has a tensile strength that is equal to that of Type 301 which has been cold reduced 18 per cent.

Compressive Strength:

The high strength characteristics of this steel exhibited in tension tests are also evident from the results of compression tests as shown in Fig. 9. These results were obtained on sheet specimens that were initially 0.064 in. thick and which were cold reduced the indicated amount from this thickness. As will be noted, a compressive yield strength up to 200,000 psi can be obtained by cold

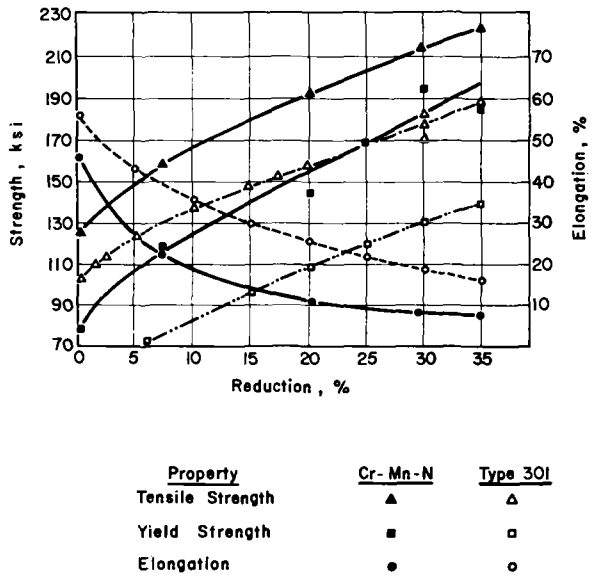


FIG. 8—Effect of Cold Rolling on the Room-Temperature Tensile Properties of Cr-Mn-N Austenitic Stainless Steel and Type 301 Stainless Steel.

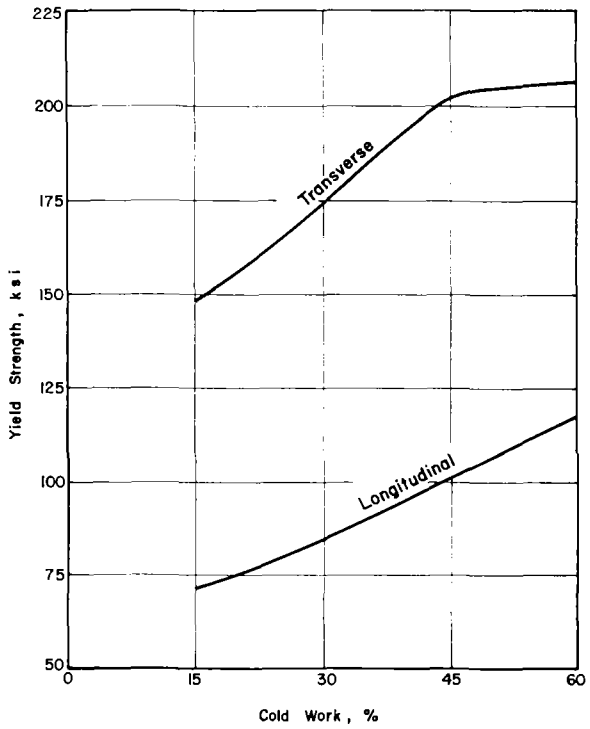


FIG. 9—Effect of Cold Work on the Room-Temperature Compressive Yield Strength of Cr-Mn-N Austenitic Stainless Steel.

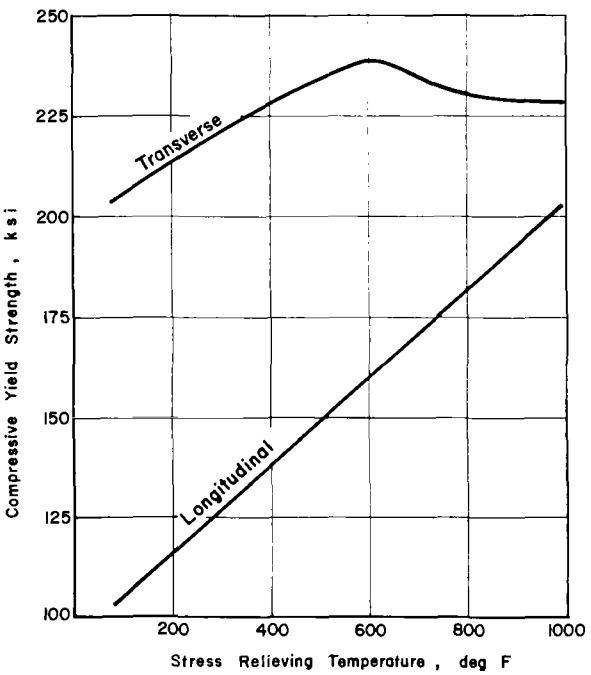


FIG. 10—Effect of Stress Relieving Temperature on the Room-Temperature Compressive Yield Strength of 0.039-in. Thick Cr-Mn-N Austenitic Stainless Steel Cold Reduced 45 Per Cent.

reduction. However, as is true for all cold-rolled austenitic stainless steels, the compressive yield strength in the longitudinal direction is disproportionately low. Fortunately, this discrepancy between longitudinal and transverse compressive yield strength can be minimized by the employment of stress relieving treatments. The data shown in Fig. 10 indicate that this discrepancy is at a minimum when a stress relieving temperature of 1000 F is employed.

Elevated-Temperature Properties:

As might be expected from its high room-temperature properties, the elevated-temperature tensile properties of the chromium-manganese-nitrogen stainless steel are superior to those of the normal chromium-nickel stainless steel. This comparison is shown in Fig. 11. As will be noted, the tensile strength of this material decreases from its initial room-temperature strength continuously with an increase in temperature. This is a typical behavior for austenitic stainless steels. The creep strength and the creep rupture strength of this material are also superior to those of the normal chromium-nickel stainless steels. The comparison for the rupture strength in 10,000 hr is shown in Fig. 12. These data would suggest that the use of the high nitrogen-chromium-manganese stainless steels could result in economies because the higher elevated-temperature strength of this material would permit the use of lighter wall thicknesses.

The elevated-temperature tensile and compressive properties of cold worked material are illustrated in Figs. 13 and 14, respectively. Because of previous results indicating the beneficial effects of stress relieving, the tests were made on specimens that had been stress relieved for 2 hr at 800 F. These data suggest that excellent properties of cold worked material are maintained up to temperatures of about 1000 F.

Fatigue Strength:

The fatigue strength of this steel is also excellent. Figure 15 illustrates the results of room-temperature, reverse bending fatigue tests on sheet product, which, in the annealed condition, had a thickness of 0.062 in., and which was cold reduced the indicated amounts from this thickness. The endurance limit of this material (53,000 psi for the annealed condition) is greater than that expected for the normal chromium-nickel-austenitic stainless steels.

Physical Properties:

Table 4 lists the physical constants for the chromium-manganese-nitrogen stainless steel. The density, electrical resistivity, magnetic permeability in the annealed condition, and coefficient of thermal expansion are practically the same as those of the chromium-nickel-austenitic stainless steels. However, of particular importance is the stability of the austenite in this material. Cold reductions as high as 60 per cent increase the magnetic permeability of this material only slightly—from a value of 1.002 in the annealed condition to 1.011 in the cold reduced condition. Thus, this material should find interesting applications where high strength and low magnetic permeability are required.

Welding:

Welding has been performed with Types 308, 309, and 310 electrodes. Type 310 electrodes give deposits that are nonmagnetic for those applications where low permeability is a requirement. Otherwise, Types 308 and 309 electrodes have been found to be satisfactory. The made from coated rods are shown in Table 5. This table also shows the chemical composition of the weld metal. In one instance the lime coating resulted in a nitrogen content of 0.30 per cent, which is 0.05 per cent under the desired minimum of 0.35 per cent. In the other instance, the electrode coating retained the

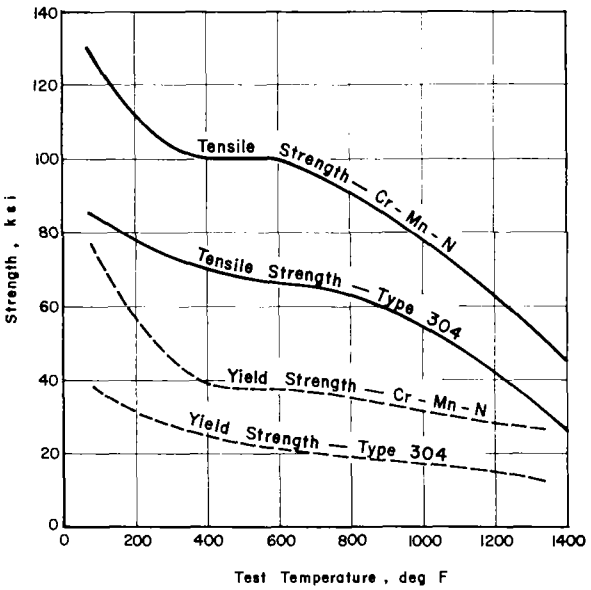


FIG. 11—Elevated-Temperature Tensile and Yield Strengths of Annealed Type 304 and Cr-Mn-N Austenitic Stainless Steels.

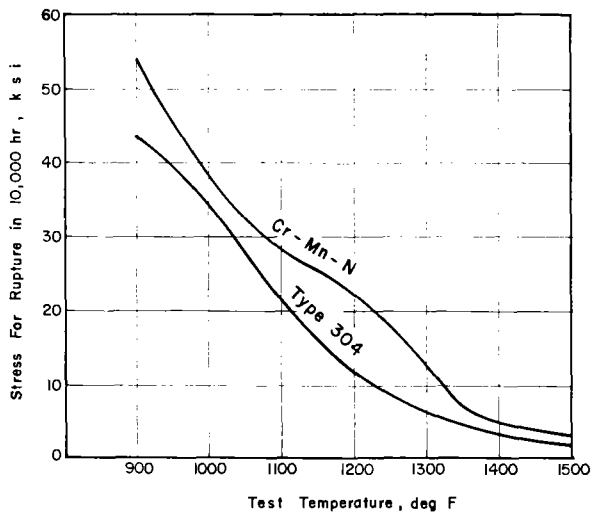


FIG. 12—Stress for Rupture in 10,000 hr for Type 304 and Cr-Mn-N Austenitic Stainless Steels.

joint efficiencies of deposits made with these electrodes are about 90 per cent (based on tensile strength), but the yield strength of the weld material is low compared to that of the original steel. Joint efficiences in excess of 100 per cent for both yield and tensile properties can be obtained by the use of welding wire of the same composition with coatings developed particularly for use with this composition. Some of the typical tension test results obtained from weld pads satisfactory nitrogen level of the parent metal. Both types of electrode coatings produced deposits that had yield and tensile strengths well in excess of the minimum desired for this material. The coating that did not permit the retention of the full nitrogen content of the material produced a sound but partially ferritic weld, whereas the coating which permitted the retention of the full nitrogen content of the material produced a sound and fully austenitic weld. Thus, for applications where low magnetic permeability is required, this second type of electrode coating should be used. Otherwise, the first type can be used satisfactorily.

Excellent results have been obtained in the resistance welding of the chromium-manganese-nitrogen stainless steel. Spot welds in 0.048-in.-thick sheet have exhibited greater tension-pullout strength than those in Type 301 stainless steel. Flash resistant welds are capable of extensive deformation without failure in the fusion zone. Where feasible, this technique produces the soundest welds of any joining method. The high strength of the chromium-manganese-nitrogen steel dictates greater holding times and welding forces than are used for the 18-8 grades. In 0.048-in.-thick sheet, for example, the spot welding force and hold time are $1\frac{1}{2}$ and 2 times greater, respectively, than those used for 18-8 stainless steel equally thick.

CORROSION RESISTANCE

During the past several years an extensive series of corrosion tests have been conducted on the chromium-manganese-nitrogen stainless steel. The results of these tests can be summarized as follows:

Atmospheric:

Observations of test panels after about four years' exposure to rural atmospheres, and to industrial atmospheres in which chloride contamination is quite low, indicate that the chromium-manganese-nitrogen stainless is comparable to chromium-nickel austenitic stainless steel in these environments. After about three years' exposure to marine atmosphere, tests show that the chromium-manganese-nitrogen stainless is comparable to AISI Type 430 stainless steel.

Oil Field:

Laboratory tests have indicated that chromium-manganese-nitrogen stainless has promise for use as oil-well sucker rods at substantially higher stress levels than possible with conventional sucker-rod materials. Field tests of chromium-manganese-nitrogen stainless sucker rods are in progress.

Chemical Process:

Tests in a benzene-toluene-xylene refining plant, a naphthalene fractionator, a crude oil fractionator, boiler flue gas, sulfur vapor, and molten sulfur have shown that this steel is generally comparable to Type 304 stainless steel in these

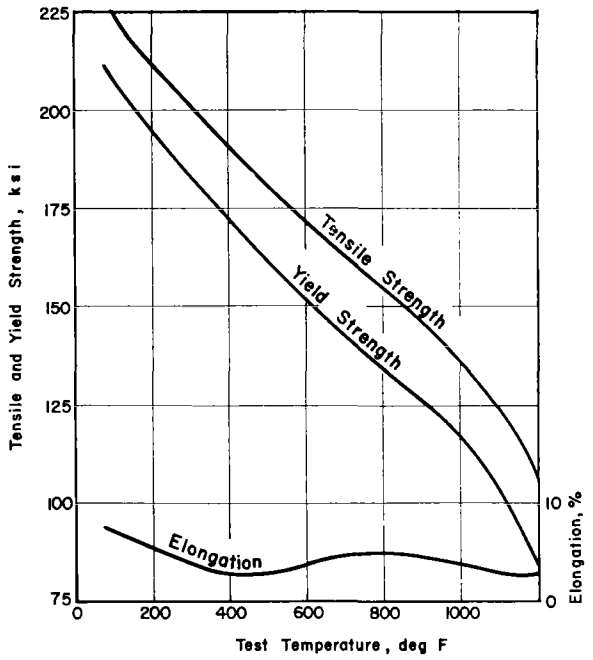


FIG. 13—Elevated-Temperature Tensile Properties of 0.035-in. Thick Cr-Mn-N Austenitic Stainless Steel Cold-Rolled 45 Per Cent and Stress Relieved 2 hr at 800 F.

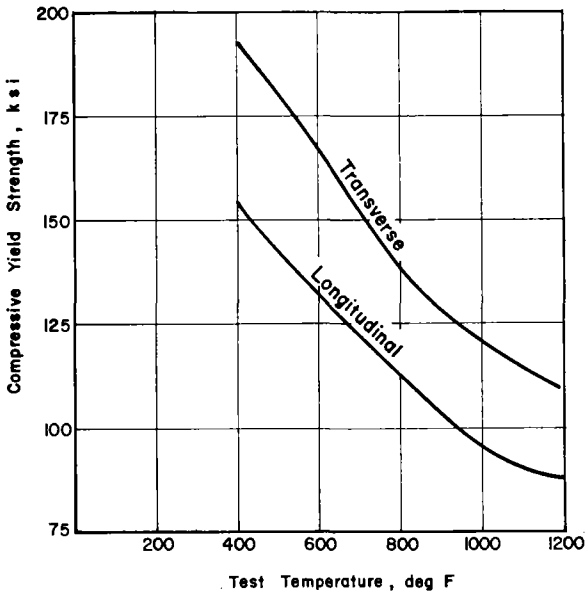


FIG. 14—Elevated-Temperature Compressive Yield Strength of 0.035-in. Thick Cr-Mn-N Austenitic Stainless Steel Cold-Rolled 45 Per Cent and Stress Relieved 2 hr at 800 F.

environments. In severely corrosive chemical-process environments, the corrosion resistance of the chromium-manganese-nitrogen stainless steel appears to be comparable to that of Type 430 stainless steel. Because of the specific corrosive nature of chemical-process environments, it is desirable to conduct tests under actual service conditions to establish the suitability of this steel or any other material for a particular chemical environment.

Dairy:

Tests in 32 different dairy cleaning and sanitizing solutions indicated that the chromium-manganese-nitrogen stainless is equivalent, from the corrosion resistance standpoint, to Type 302 stainless steel in these cleaners and sanitizers.

Antifreeze:

The corrosion resistance of the chromium-manganese-nitrogen stainless steel has been determined in uninhibited and commercial antifreeze solutions. It was found in these tests that this steel was fully as resistant as Type 302 stainless steel.

Laboratory Tests:

The results of laboratory tests on the chromium-manganese-nitrogen stainless in a number of acid solutions are shown in Table 6. It will be noted that in the

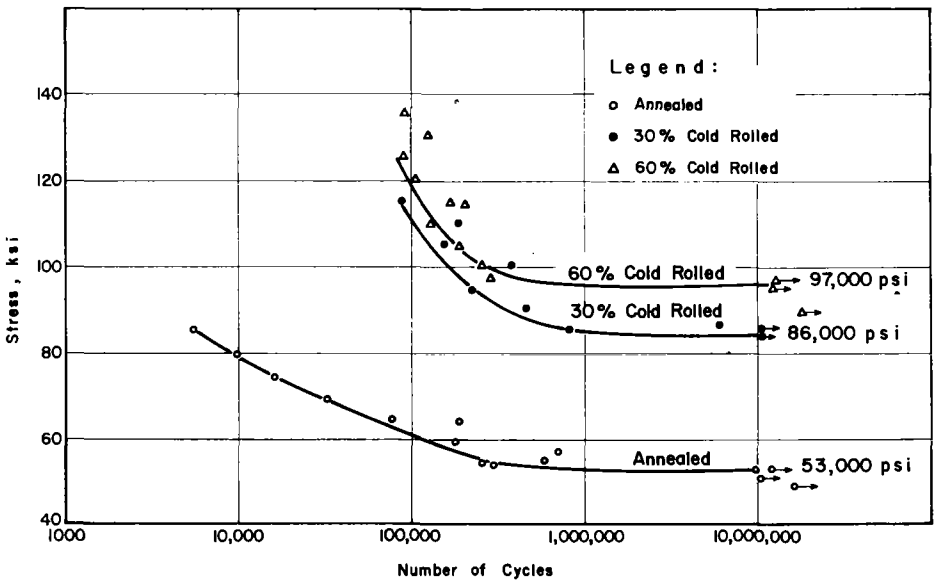


FIG. 15—Room-Temperature Fatigue Strength of Cr-Mn-N Austenitic Stainless Steel Sheet.

TABLE 4—PHYSICAL CONSTANTS OF CHROMIUM - MANGANESE - NITROGEN STAINLESS STEEL AND AISI TYPE 301 STAINLESS STEEL.

	Chromium-Manganese-Nitrogen	AISI Type 301
Melting range, deg F	...	2550 to 2590
Density, lb/in.^{3}	0.278	0.29
Electrical resistivity, microhm-cm:		
annealed	72.6	72
cold reduced 15%	73.8	...
cold reduced 30%	75.1	...
cold reduced 45%	77.0	...
cold reduced 60%	77.4	...
Magnetic permeability:		
annealed	1.002	1.003
cold reduced 10%	...	1.10
cold reduced 15%	1.002	...
cold reduced 30%	1.004	...
cold reduced 45%	1.007	...
cold reduced 60%	1.011	...
severely cold worked		10.0
Mean coefficient of thermal expansion, 10^{-6}/F:		
70 to 700 F	9.927	...
70 to 900 F	10.177	...
70 to 1100 F	10.719	...
70 to 1300 F	11.084	...
70 to 1500 F	11.206	...
70 to 1700 F	11.298	...
70 to 1900 F	11.697	...
32 to 212 F	...	9.4
32 to 572 F	...	9.5
32 to 932 F	...	10.1
32 to 1112 F	...	10.4

TABLE 5—RESULTS OF CHEMICAL ANALYSES AND TENSION TESTS OF WELD DEPOSITS OF Cr-Mn-N WELD METAL.

Specimen No.	Source of Chips	C	Mn	Si	S	P	Cr	Ni	N
		Chemical Composition, Weight Per Cent							
13896	pad	0.09	15.6	0.39	0.013	0.020	17.63	0.42	0.33
13896	tensile bar	0.08	16.4	0.53	0.012	0.019	17.70	0.41	0.30
13965	pad	0.08	15.0	0.38	...	...	18.02	0.12	0.41
13965	tensile bar	0.08	15.2	0.39	0.013	0.018	17.81	0.42	0.42

Specimen No.	Yield Strength, ksi	Tensile Strength, ksi	Elongation in 2 in., %	Radius of Arc, %	Comments
	Tension Test Results				
13896-1	96.6	126.8	34	40	sound, partially ferritic
13896-2	95.9	125.3	32	42	sound, partially ferritic
13965-1	99.6	122.7	37	54	sound, fully austenitic
13965-2	98.1	128.4	34	47	sound, fully austenitic

TABLE 6—CORROSION RESISTANCE OF Cr-Mn-N STAINLESS STEEL IN VARIOUS ACIDS.

Environment	Corrosion Rate After 96 hr Exposure, mils per month				
	Cr-Mn-N	Type 301	Type 302	Type 201	Type 430
5% Lactic acid, 86 F	0.01	0.01	0.01	0.01	0.01
10% Phosphoric acid, 86 F	0.01	0.01	0.01	0.01	0.01
60% Acetic acid, 158 F	0.01	0.01	0.01	0.01	0.017
5% Sulfuric acid, 86 F	390	1.0	1.0	13.0	390
5% Nitric acid, boiling	0.07	0.030	0.030	0.030	0.13

NOTE—In boiling 65% nitric acid the following comparative corrosion data were obtained. All specimens were annealed 30 min at 1950 F. All were subjected to five 48-hr boils, and the results are the average of five boils.

Type of Steel	Penetration Per Month, mils
AISI Type 430 stainless steel	4.0
AISI Type 301 stainless steel	1.0
Cr-Mn-N stainless steel	3.4

milder acids, the corrosion losses of this steel are about equal to that of Types 301, 302, and 201 stainless steels. In stronger acids, this steel is inferior to these grades but equal to or better than Type 430.

Stress Corrosion:

The stress corrosion resistance of the chromium-manganese-nitrogen stainless steel, although erratic, appears to be generally superior to that of the chromium-nickel stainless steels. In the boiling 42 per cent magnesium chloride test, some specimens have failed in 20 to 600 hr. The average life of the chromium-nickel steels in this test is 4 hr.

SUMMARY

In summary, the nickel-free chromium-manganese-nitrogen stainless steel represents a new addition to the stainless steel family. The high room- and elevated-temperature yield and tensile strength of this material combined with its good corrosion resistance broadens the already wide field of applications for the versatile stainless steel family. The retention of low magnetic permeability even after cold working to high tensile strength levels provides probably for the first time a high-strength, nonmagnetic stainless steel.

Because this steel has exceptionally high mechanical strength in the annealed condition, it should find ready acceptance by code writing bodies, particularly because the high strength can be obtained without heat treatment.

Continued work both in the laboratory and in actual applications should determine the adequacy of such steels for applications where resistance to stress corrosion is needed. Perhaps as this phenomenon becomes better understood, some slight modification in these steels will result in the long-hoped-for austenitic stainless steel having immunity to transgranular chloride stress corrosion cracking.

DISCUSSION

ARTHUR COHEN.[1]—Has any activity been directed toward getting ASME Boiler Code approval for the use of this alloy? If I also recall correctly, some rather strong feelings were expressed that this alloy, or some minor modification thereof, may be the long-sought-for austenitic stainless steel which is not sensitive to stress corrosion cracking. Would you comment on this?

J. J. HEGER (*author*)—Some activity has been directed toward getting ASME Boiler Code approval for the chromium-manganese-nitrogen stainless steel. The subject of the stress-corrosion resistance of this steel is tantalizing, because some heats have not failed even under the most rigorous test conditions, whereas other heats have failed—although in times greater than those encountered with the chromium-nickel austenitic stainless steel. These results suggest that some minor modification to the present steel may result in a steel that is immune to stress-corrosion cracking.

M. G. FONTANA[2]—Are comparable corrosion data available for stronger nitric acid such as the Huey test and fuming nitric acid?

MR. HEGER—Comparable data in 65 per cent nitric acid (Huey Test) are shown in Table 6. As will be noted, the chromium-manganese-nitrogen stainless steel has a corrosion resistance in this environment similar to Type 430 stainless steel. No data are available as yet for fuming nitric acid.

D. W. MCDOWELL[3]—How do the high strength chromium-manganese-nitrogen stainless steels compare in appearance with conventional austenitic stainless steels?

MR. HEGER—In appearance the chromium-manganese-nitrogen stainless steels compare more closely with the ferritic stainless steels, such as Type 430, in color and appearance.

[1] Supervisor of metallurgy, Materials Engineering Dept., Carrier Air Conditioning Co., Syracuse, N. Y.

[2] Ohio State University, Columbus, Ohio.

[3] Southwest Research Inst., San Antonio, Tex.

METALLURGY OF A COLUMBIUM-HARDENED NICKEL-CHROMIUM-IRON ALLOY

By H. L. Eiselstein[1]

Synopsis

Inconel alloy 718 is a relatively new high-strength, weldable alloy that is suitable for service at temperatures from −423 F up to 1300 F. The excellent properties of this alloy over this temperature range result from extensive research on the influences of various elements and heat treatments. This paper describes the metallurgical investigation relating the nature of the alloy to the development of optimum properties.

The constitution of Inconel[2] alloy 718 has been studied using air-melted and vacuum-melted material and most of the known techniques for determining the various phases. In the early development of this alloy (52.5 per cent nickel, 19 per cent chromium, 18 per cent iron, 5.0 per cent columbium, 3 per cent molybdenum, 0.15 per cent silicon, 0.10 per cent copper, 0.20 per cent manganese, 1.0 per cent titanium, 0.4 per cent aluminum, 0.04 per cent carbon, and 0.007 per cent sulfur), air melts were made in a 30-lb induction furnace; specimens were forged to $\frac{9}{16}$-in. squares. To determine the effects of the influencing elements, the specimens in most cases were annealed and aged to maximum values. The electron probe. electron microscope, X-ray diffraction, X-ray fluorescence, wet chemical analysis, and computer were all employed to study the structure, presence of various phases, chemical analyses of the particular phases, and analyses of mechanical property data.

Establishing Nickel and Columbium Contents:

Since it was believed that columbium would be the major element influencing the properties of a high nickel-chromium alloy, its effect in relation to per cent nickel was initially singled out. Figure 1 shows the effect of nickel and columbium plus tantalum content and heat treatment on room-temperature yield strength. The data are representative of specimens annealed for 1 hr at 1900 F and water quenched without aging, and of specimens annealed for 1-hr at 1900 F, water quenched plus aged at 1250 to 1350 F (as required for maximum strength) for 16 hr, and air cooled.

Note that for the range of nickel shown, columbium contents of 4.5 to 6.5 per cent have little effect on solid solution hardening of annealed materials. In contrast, the effect of such columbium contents in increasing yield strength of an aged high-nickel alloy is quite pronounced. Below about 30 per cent nickel, there is no appreciable effect. Maximum yield strength, depending upon columbium and tantalum content, appears to occur when nickel content is between 50 to 55 per cent. (Throughout this paper, tantalum content in combination with columbium may be considered to be approximately $\frac{1}{10}$ of the total columbium plus tantalum.)

This trend is the same for room-temperature tensile strength as shown in Fig. 2. The 0.2 per cent yield-strength curve differs slightly from that shown in Fig. 1 because of the difference in columbium content.

In the initial development of this alloy, the primary aim was for high-tensile properties; stability of the age-hardening constituent, as with all age-hardening type alloys, would be a factor in regard to high-temperature creep. However, an attempt was made to exploit high-temperature properties as well; therefore, creep rupture tests were conducted at 1200, 1300, and 1400 F.

At these temperatures, the 100-hr rupture strength of a nickel-iron—15 per cent chromium, 6 per cent columbium, 3 per cent molybdenum, 0.6 per cent aluminum, 0.6 per cent titanium, and 0.005 per cent B-alloy, as a function of nickel content, is shown in Fig. 2. At 1200 F, the optimum high-temperature strength is again obtained with about 50 to 55 per cent nickel. The optimum 100-hr rupture strength at 1300 and 1400 F is attained with approximately 73 per cent nickel (when the iron is reduced to zero). It is interesting to note the change in the curves as the mechanism for failure changes from that for tensile yield (slip) to that of creep rupture (dislocation climb).

After establishing the optimum nickel content, the hardening effect of columbium was further analyzed by varying its content in the alloy. Figure 1 had shown different yield strengths, for aged specimens of 50 to 55 per cent nickel, with change in columbium content. Figure 3 shows that with as little as 2 per cent columbium, there is some age-hardening effect and that yield strength increases almost linearly with columbium contents ranging from 2 to 6 per cent before the yield strength begins to taper off with higher columbium. For annealed material, an increase in columbium content does give some solid solution hardening. There is less effect of increase of columbium on tensile strength as compared to its effect on yield strength, but the same trend is evidenced.

Although Fig. 3 suggests the advantage of still higher strength with columbium content above 5 per cent, the reduction in ductility factors limits the columbium content.

Factors Limiting Aluminum Plus Titanium Content:

A reduction in elongation with increasing aluminum plus titanium content also tends to limit the amount of these elements. In addition, Fig. 4 shows that a maximum 100-hr rupture strength is attained with an aluminum plus titanium content of about 1.2 per cent (aluminum to titanium ratio of 1 to 1).

Strengthening Mechanism:

With the knowledge that age hardening of this alloy is dependent upon nickel and columbium and on how these elements combine with titanium and aluminum to affect the process, a study was made of the structure and phases to

[1] Section head, metallurgical services, Huntington Alloy Products Div., The International Nickel Co., Inc., Huntington, W. Va.

[2] Inconel is a trademark of The International Nickel Co., Inc.

Copyright© 1965 by ASTM International

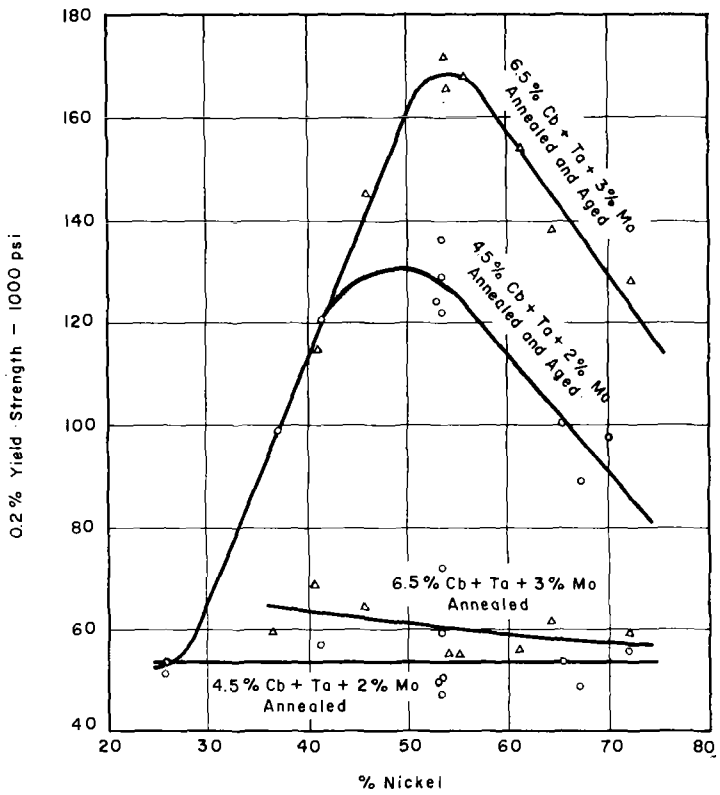


FIG. 1—Effect of Nickel and Columbium Plus Tantalum Content on the Room-Temperature Yield Strength of Ni, Cr, Cb, Mo, Al, Ti, and Fe Alloys: Annealed at 1900 F/1 Hr, Water Quenched Plus Aged at 1250 to 1350 F/16 Hr, Air Cooled; and Annealed at 1900 F/1 Hr, Water Quenched, No Aging Treatment.

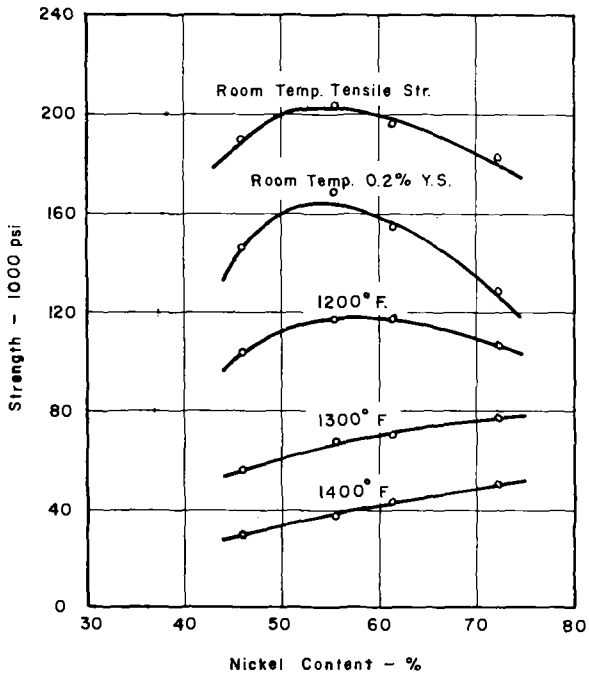


FIG. 2—Room-Temperature Strength and 100 Hr Rupture Strength of Ni, Fe, 15 per cent Cr 6 per cent Cb, 3 per cent Mo, 0.6 per cent Al, 0.6 per cent Ti, and 0.005 per cent B Forged Alloys. All Materials Were Solution Treated at 1900 to 2000 F/1 Hr, Water Quenched Plus Aged at 1300 to 1350 F/16 Hr, Air Cooled.

determine the actual strengthening phase.

Specimens were solution treated at the highest temperature that would not initiate melting (burning) of the alloy. After heating at 2200 F for 1 hr, the specimens were directly aged by quenching in furnaces at various lower temperatures, holding for 4 hr, and water quenching. Hardness tests were made to check age hardening, and these results are shown in Fig. 5. Note that highest hardnesses are achieved after aging at temperatures of about 1300 and 1400 F.

Age hardening constituents could not be detected with a light microscope, so detection by electron microscope[3] became necessary (Fig. 6).

By electrolytic dissolving of a specimen in 20 per cent phosphoric acid and centrifuging, the hardening precipitate was separated out of the solution. A study of the residue by X-ray diffraction and fluorescence, for indications of lattice parameter, revealed a face centered cubic crystal structure. To identify the composition of the age hardening precipitate, the separated residue was analyzed chemically. Table 1 shows that the precipitate was identified as columbium rich gamma prime $Ni_3(CbTiAl)$. An analysis for aluminum could not be made because of insufficient amount of residue. However, on the basis of approximately equivalent aluminum and titanium and using atomic per cent analysis as a guide, an approximate gamma prime analysis may be assumed as: 75 per cent nickel, 15 per cent columbium, 5 per cent titanium, and 5 per cent aluminum.

Grain Boundary Carbide:

In addition to the gamma prime precipitate, the electron microscope studies revealed the precipitation of a grain boundary carbide film (Fig. 6). Electron transmission studies of extracted films showed them to be of a dendritic and cellular nature.

The occurrence of film was determined through variation of solution temperatures and times and aging temperatures and times. The carbide film could be studied easily by using standard metallographic equipment and special etching techniques that cause the carbide to stand in relief in the grain boundary.

Carbide and Other Precipitates:

Solution temperatures, utilized in the study of grain boundary carbide, in some cases overlapped temperatures which affected precipitation of age hardening constituents; therefore, the occurrence of carbides and other precipitates became a simultaneous study.

Figure 7 is a photomicrograph of a sample solution heated for 1 hr at 2100 F, water quenched, and heated at 1500 F for 100 hr and air cooled. It revealed massive carbides (blocky or globular types) and a coarse gamma prime type

[3] Work conducted by J. F. Radavich, Purdue University, W. Lafayette, Ind.

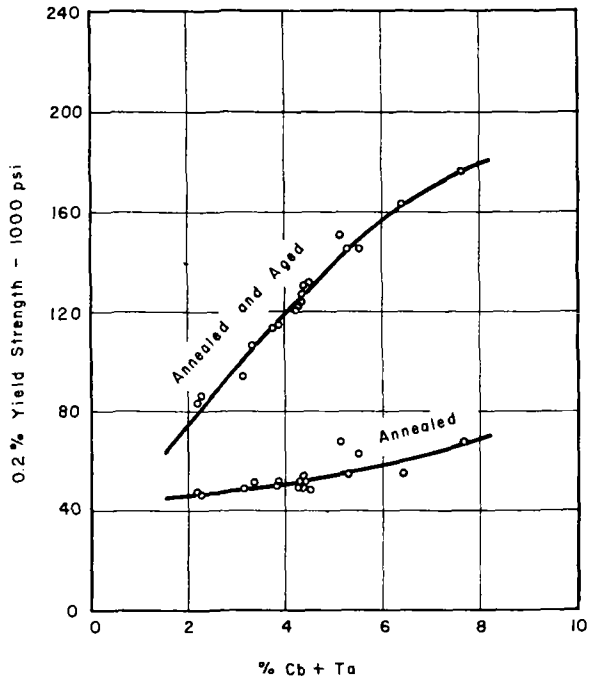


FIG. 3—Effect of Per Cent Cb Plus Ta on 0.2 per cent Yield Strength: Material Was Annealed at 1900 F/1 Hr, Water Quenched, Aged at 1250 to 1350 F/16 Hr, Air Cooled.

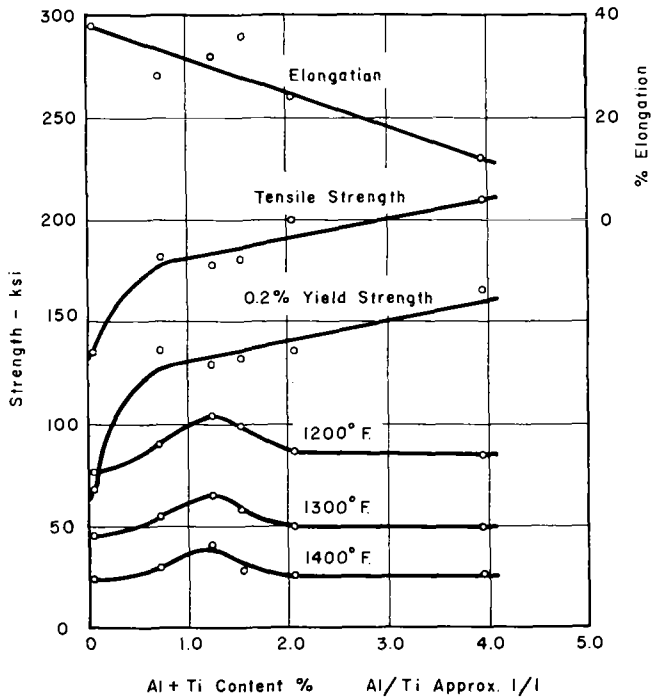


FIG. 4—Tensile Properties and 100 Hr Rupture Strength at Temperatures Indicated for 53 per cent Ni, 21 per cent Cr, Balance Fe, 4 per cent Cb, 2 per cent Mo Alloys. Material Was Annealed at 1900 F/1 Hr, Water Quenched Plus Aged for 16 Hr at Temperatures Which Produce Maximum Properties.

of precipitate. This same heat treatment, with the exception of 100 F increase in precipitation temperature, was the next step in the study of precipitates, and the result is shown in Fig. 8. For this aging treatment of 100 hr at 1600 F, the structure evidences a Widmänstatten pattern of precipitate or needle-like phase. A small background precipitate persists.

The needle-like phase was suspected to be eta phase, Ni_3Ti, because the latter transforms from gamma prime in similar systems. However, further study showed this needle phase to be orthorhombic Ni_3Cb.

Increasing the aging temperature to 1700 F (100 hr) after solution treating at 2100 F for 1 hr yielded another agglomerate-type phase in addition to needles (Fig. 9). Initially, this phase was thought to be agglomerated needles however, as studies progressed, thi phase was identified as Laves.

Effects of Initial Solution Temperature:

The relationship of solution annealin temperature and time and aging tem perature and time in regard to occur rence of grain boundary carbide an needles, is indicated in Figs. 10–12. Fo the occurrence of needles, when a solu tion temperature of 1900 F is employe as compared to 2100 F, longer agin times are necessary. Needles do occu after very short aging times, however when the solution temperature is 1700 F

As solution temperature decrease from 2100 to 1900 F, the aging-tempera ture range for grain boundary carbid precipitation decreases, and aging tim for the initiation of carbide film increases When the solution temperature is 1700 I (Fig. 12), there is no formation of grai boundary carbide film upon subsequen aging.

The bending back and downward o the carbide film curves at the top i possibly due to changes in the form o the carbide; therefore, the carbide phas may still be present at temperature about these curves but in a form n longer detectable by the test method o procedure that was employed.

Effect of Grain Boundary Carbide o Properties:

Some data (1)[4] show that intergranu lar carbides are not only beneficial bu necessary to achieve optimum stress rupture life. In some alloys, formatio of carbides at grain boundaries result in a chromium depleted zone adjacen to the carbides. There also is less gamm prime in the depleted zone. Thus, thi zone is weaker but more ductile tha adjacent areas.

To determine the effect of the carbid film on mechanical properties, specimen were heated to various solution tempera tures, held for 4 min or 1 hr ac or both and aged at 1325 F for 16 hr ac. Th results of creep rupture, tension test and film surveys showed no sudde changes with the presence or absence o carbide film.

Anomalies:

During the investigation, certai anomalies were observed in age-harden ing response. Up to 1350 F and for time longer than 2 min, the response an

[4] The boldface numbers in parentheses refe to the list of references appended to this pape

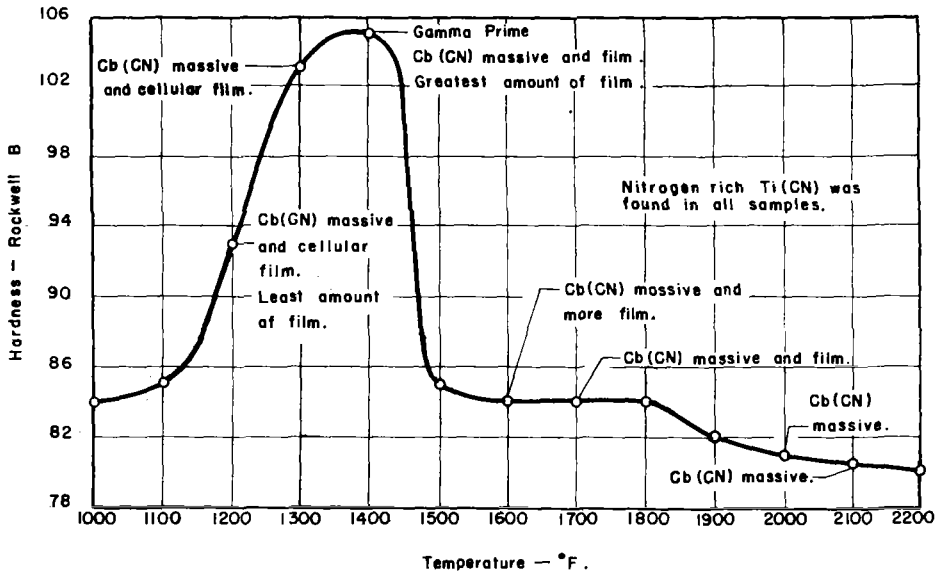


FIG. 5—Hardness Response and Phases Found After Heating at 2200 F/1 Hr, Isothermally Transferring Specimens to the Above Temperatures, Holding for 4 Hr and Water Quenching.

TABLE 1—RELATIVE AMOUNTS OF NICKEL, COLUMBIUM, AND TITANIUM IN GAMMA PRIME RESIDUE.[a]

Relative Weight Per Cent Analysis		
Ni	Cb	Ti
75.19	20.70	4.11
Relative Atomic Per Cent Analysis		
Ni	Cb	Ti
80.56	14.03	5.41

[a] Residue extracted from specimen heat treated at 2200 F for 1 hr, ITT 1400 F for 4 hr, and air cooled.

hardnesses of 38 and 39 Rc are typical of gamma prime hardened alloys (Fig. 13). Above about 1400 F, the upper portions of the curves do not bend back and, therefore, do not indicate overaging or softening. For example, aging at 1450 F for 10 hr gives an approximate hardness of 25 Rc and this same hardness is maintained after aging for 100 hr. Furthermore, note that the 20 Rc hardness curve rises (between 1500 and 1600 F and for aging times between 10 and 100 hr), indicating possibly another phase or effect retarding overaging.

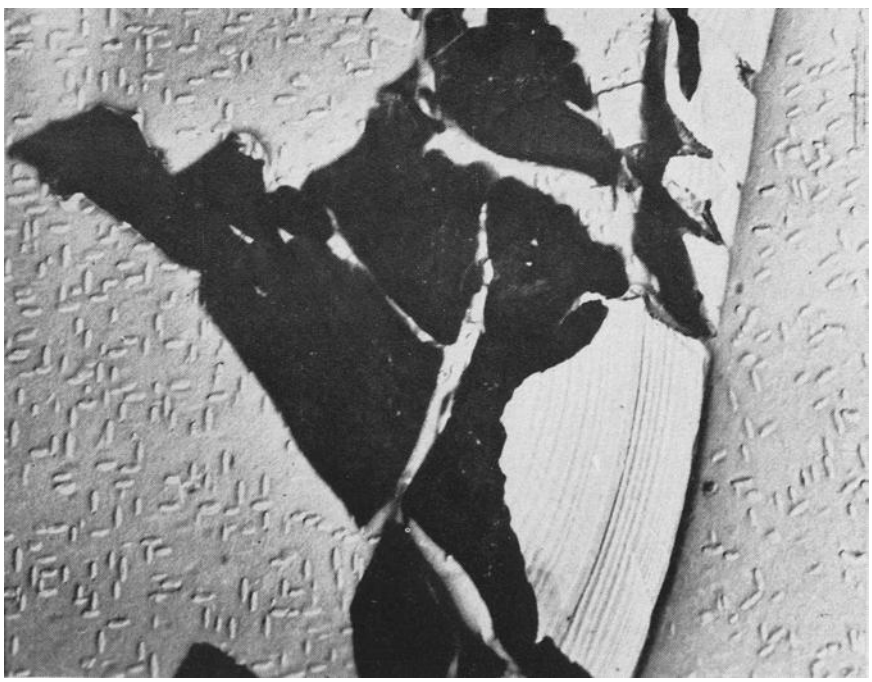


FIG. 6—Grain Boundary Carbide Film in Specimen Heated at 2200 F/1 Hr, Isothermally Transferred to 1400 F and Held for 4 Hr, Water Quenched (electron micrograph—×17,500).

Another unknown arising from this investigation and studied simultaneously with the additional age-hardening effect was the appearance of dark constituents, called freckles, on the etched cross section of large rounds. To establish the constitution of this alloy, it was necessary to determine the effects of these

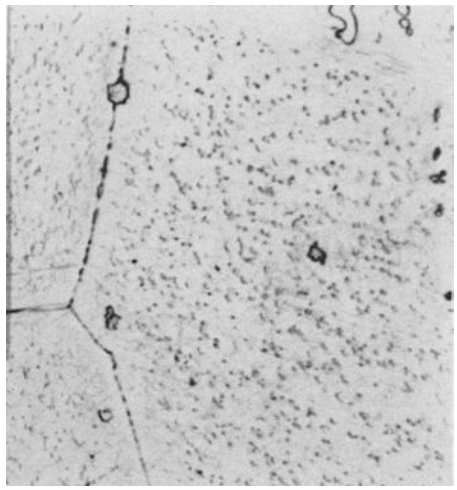


FIG. 7—Overaged Gamma Prime Type of Precipitate in Specimen Heated at 2100 F/1 Hr, Water Quenched Plus Aged at 1500 F/100 Hr. (Etchant—5 per cent chromic acid).

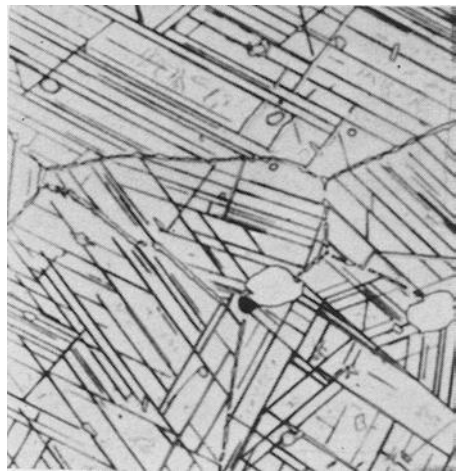


FIG. 8—Widmänstatten Pattern of Needles With a Small Background Precipitate in Specimen Heated at 2100 F/1 Hr, Water Quenched and Heated at 1600 F/100 Hr, Air Cooled. (Etchant—5 per cent chromic acid).

anomalies and identify the phase or phases involved.

Laves Phase:

In the annealed and aged condition, specimens containing the dark constituents had yield strengths of approximately 120,000 psi as compared to the normally expected value of 150,000 psi. Ductility of such specimens also was poor.

The constituent was isolated by dis-

solving a freckled region and analyzing the residue by X-ray fluorescence. The results of this analysis showed the residue to be high in columbium, molybdenum, and nickel with smaller quantities of iron, chromium, and titanium (Table 2). This analysis as well as X-ray diffraction patterns, identified the phase as Laves (isomorphous with Fe_2Ti and rich in columbium).

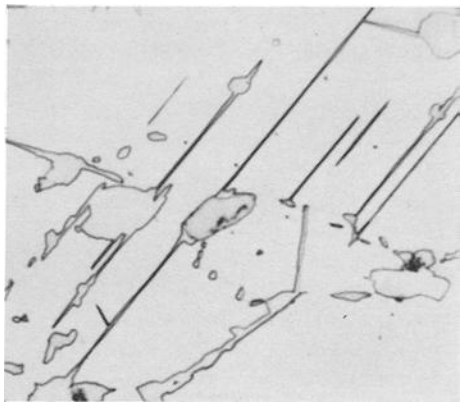


FIG. 9—Needle and Agglomerate Type Phases in Specimen Heated at 2100 F/1 Hr, Water Quenched and Heated at 1700 F/100 Hr, Air Cooled. (Etchant—5 per cent chromic acid).

Coring:

Large forged billets were etched electrolytically with chromic acid for metallographic study of Laves phase. It is shown as the small white particles in the dark areas of the photomicrographs in Fig. 14. The light areas are dendrites which are generally associated with coring effects. The shading in the dendrites indicates a variable composition, with the core generally purer than the exterior layers.

The properties of these structures were investigated, with a difference noted in elongation. A specimen with structure of Fig. 14(*a*) had zero elongation, while the structure with less coring and smaller amount of precipitate in the dark area had an elongation of 15 per cent.

An electron probe study was made at the Bayonne Research Laboratory of The International Nickel Co. to determine the chemistry of the light and dark structures. With both types of structures shown in Fig. 14, the light areas analyzed 2 per cent columbium; the dark areas, 3 per cent columbium; and the white precipitate (Laves phase) in the dark areas analyzed 50 per cent columbium. So the difference in elongation noted above is attributed to the amount of constituents rather than to differences in chemical composition.

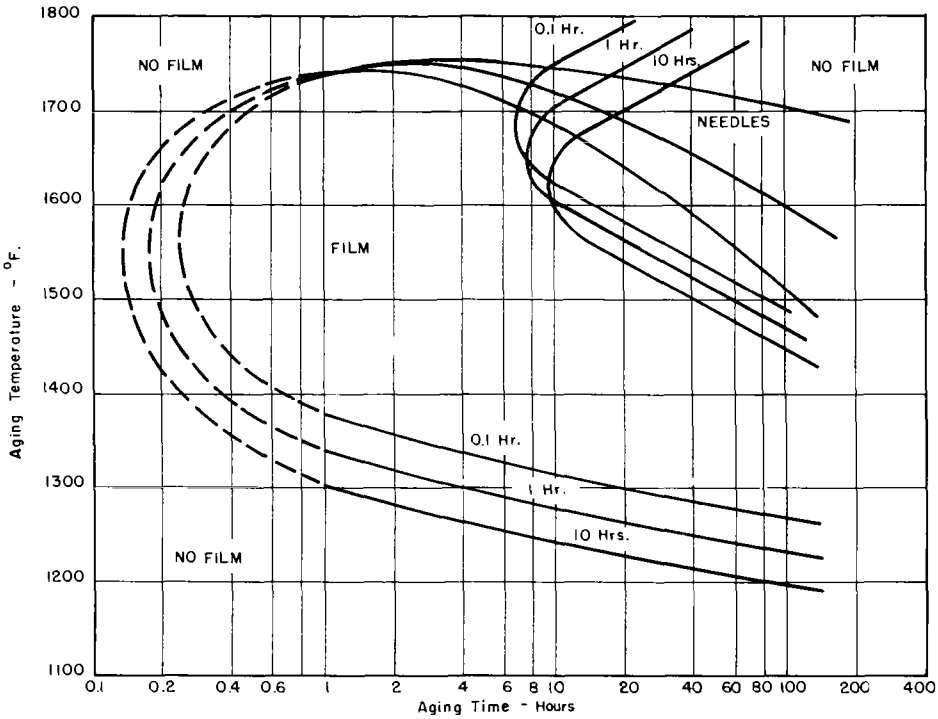


FIG. 10—Occurrence of Grain Boundary Carbide Film and Needles in Sheet (0.062 in. gage) After Annealing at 2100 F and Aging at Various Temperatures for the Times Indicated.

Diagrams of Precipitating Phases:

To establish the conditions for existence of Laves phase and for coring or segregation of columbium, additional specimens were studied. A number of specimens with varying amounts of columbium plus tantalum (3 to 9 per cent) were heated at 2100 F for 100 hr and for this same length of time at 100 deg intervals below 2100 F. These heat treated specimens were tested for hardness. Specimens also were digested electrolytically so that the insoluble precipitates could be identified by X-ray fluorescence analysis. The resultant data were plotted in the form of a phase diagram for a simple binary system with Inconel alloy 718 base, referring to all elements in the austenitic matrix and columbium plus tantalum as the solute.

Data for each phase in this diagram were plotted separately to establish individual curves for the particular phase. Phase diagrams for gamma prime, the orthorhombic stable phase, Ni_3Cb, and the Laves phase are illustrated in Fig. 15.

In Fig. 15, the curves for both gamma prime and Ni_3Cb overlap. Table 3 shows the chemical analysis of two vacuum-melted heats and the composition of residue extracted from specimens heat treated in the area of gamma prime plus Ni_3Cb. X-ray diffraction analyses of both residues reveal Ni_3Cb and gamma prime as about equal in the specimens; in the HV 257 residue, there also is a weak indication of M_6C.

Although some sensitivity is lost through use of X-ray diffraction as compared to the use of light microscope, in quantity of material detected, phase identification is more exact. Because of some loss in sensitivity, the boundary lines for the various phases probably extend beyond the curves shown.

For all specimens, X-ray diffraction was utilized to detect gamma prime—the most important constituent. With about 4 per cent columbium content, gamma prime begins to precipitate from solution at a temperature of about 1600 F.

X-ray diffraction studies of specimens identified the needle phase as Ni_3Cb. This orthorhombic phase was thus distinguished from eta phase, Ni_3Ti, and in this respect Inconel alloy 718 differs from other gamma prime type alloys.

For example, Duranickel[5] alloy 301, Monel[5] alloy K-500, Inconel[5] alloy 702, and Inconel[5] alloy 700 are all age hardened by gamma prime which is stable and does not transform into another phase.

Another class of gamma prime type alloys, A-286, Incoloy[5] alloy 901, Nimonic[5] 80, and Inconel[5] alloy X-750

[5] Duranickel, Monel, Inconel, Incoloy, and Nimonic are trademarks of The International Nickel Co., Inc.

transform from face center cubic to hexagonal—close pack eta phase. This transformation is similar to that of the gamma prime transformation in Inconel alloy 718 only in appearance; that is, change from a dot-type precipitate to a needle-like phase.

In the phase diagram for nickel columbides, Fig. 15, the curve bends over at the bottom because equilibrium is not obtained after 100 hr at the temperatures shown. Also, in Fig. 15 one additional point at 1050 F is plotted for gamma prime enabling the lower portion of that curve to be shown. This point was estimated for the beginning of hardening from Fig. 13.

The needle or orthorhombic phase is partially responsible for the slower aging response discussed previously in connection with Fig. 13. Laves phase is another constituent that affects aging response.

Figure 15 superimposes the curves for the three phases—gamma prime, orthorhombic or needle, and Laves—and also indicates Rc hardness. With 5 per cent columbium plus tantalum and 100 hr aging treatment at 1500 F, the microstructure consists essentially of gamma prime, with some orthorhombic or needle phase, Ni_3Cb, and Laves phase, A_2B. (Compare with photomicrograph in Fig. 7.) At 1600 F and 5 per cent columbium plus tantalum, gamma prime is absent (borderline), and this is shown by Fig. 8—a photomicrograph of predominantly needle phase with some Laves phase and small background gamma prime precipitate. Increasing the aging temperature to 1700 F, eliminates completely the gamma prime phase; the needle phase remains but apparently is borderline, and Laves phase is present (compare with photomicrograph in Fig. 9). Close examination of Fig. 9 reveals definite separations or boundary lines between some of the needles and other phases. The elongated medium sized particles are considered to be the Laves phase.

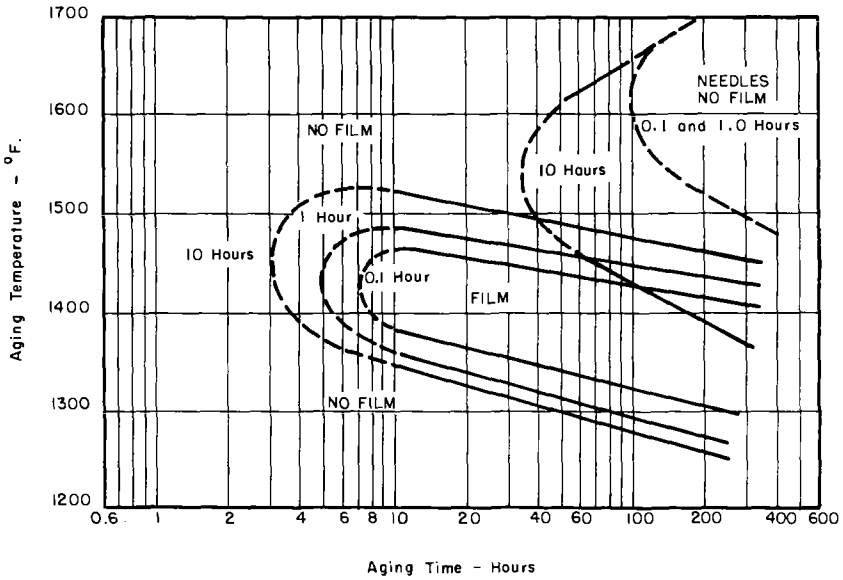


FIG. 11—Occurrence of Grain Boundary Carbide and Needles in Sheet (0.062 in. gage) After Annealing at 1900 F and Aging at Various Temperatures for the Times Indicated.

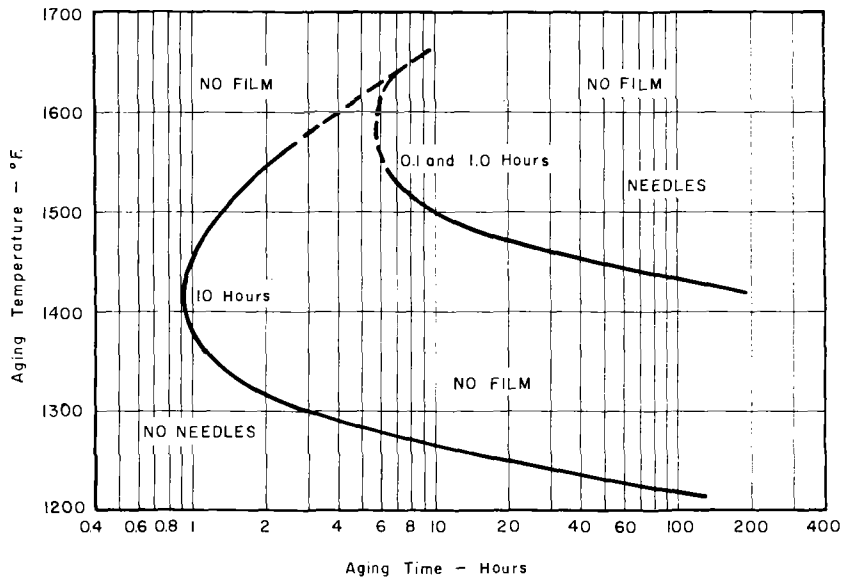


FIG. 12—Occurrence of Needles in Sheet (0.062 in. gage) After Annealing at 1700 F and Aging at Various Temperatures for the Times Indicated. (Note the absence of grain boundary film).

Diagram for Carbide Phases:

The influence of columbium plus tantalum on the development of carbide phases with different aging temperatures is shown by the carbide phase diagram in Fig. 16. Large quantities of MC-type carbide (where M denotes the metallic component), identified as columbium carbide with some titanium and titanium nitride dissolved in it or CbTi(CN), develop with all conditions of heat treatment (Figs. 5 and 16). Some of these carbides segregate during solidification and appear on etched cross sections as freckles (similar to freckles of Laves phase). However, the etchant employed reveals strongly Laves phase while masking the presence of the carbides. Because of this masking effect, some interdendritic segregation which initially appeared to be residual Laves phase actually was MC-type carbide. These insoluble segregates tend to reduce strength and ductility. Shape and distribution of these carbide particles are influenced by casting procedure.

Grain boundary carbide film MC, identified as CbC, goes in and out of solution and is present as indicated by the diagrams in Fig. 17 and by Fig. 5. The M_6C has only been identified in the X-ray extraction residues. No chromium carbide was detected.

Partial Phase Diagram of Inconel Alloy 718:

By identifying the high temperature phase as Laves, it could be utilized as the basis for construction of a partial phase diagram for this alloy. To reduce this alloy to a manageable phase diagram, 718 base was considered to be all elements in the austenitic matrix and columbium plus tantalum the solute (Fig. 18).

The precipitation of Laves phase, A_2B, is indicated by the curved line which is the same as the Laves curves

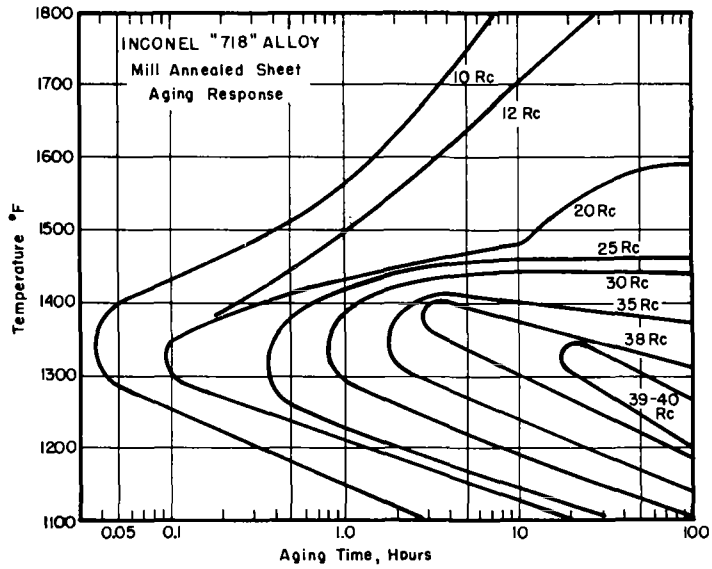


FIG. 13—Effect of Aging Temperature and Time on Rockwell "C" Hardness of Mill Annealed Sheet. (Initial hardness as annealed was R_c 4).

TABLE 2—X-RAY FLUORESCENT ANALYSIS OF LAVES RESIDUES.

Ingot Chemistry, Weight Per Cent											
C	Mn	Fe	S	Si	Cu	Ni	Cr	Al	Ti	Mo	Cb + Ta
0.06	0.33	18.13	0.007	0.35	0.04	55.30	18.55	0.34	0.77	3.05	5.05

Fluorescent Analyses of Residues[a]						
Heat Treatment	Ni	Fe	Cr	Ti	Cb	Mo
Forging	12	5	4	2	56	21
1900 F/1 hr, WQ + 1700 F/50 hr, WQ[b]	32.20	5.63	...	3.67	38.00	...
1900 F/1 hr, WQ + 1700 F/50 hr, WQ[b]	27	6	4	2	55	6
2250 F/1 hr, WQ + 1700 F/50 hr, WQ[b]	31	8	7	3	48	3

[a] These analyses are only approximate and assume 100 per cent of residue is made up of these elements.
[b] This is wet chemical analysis.

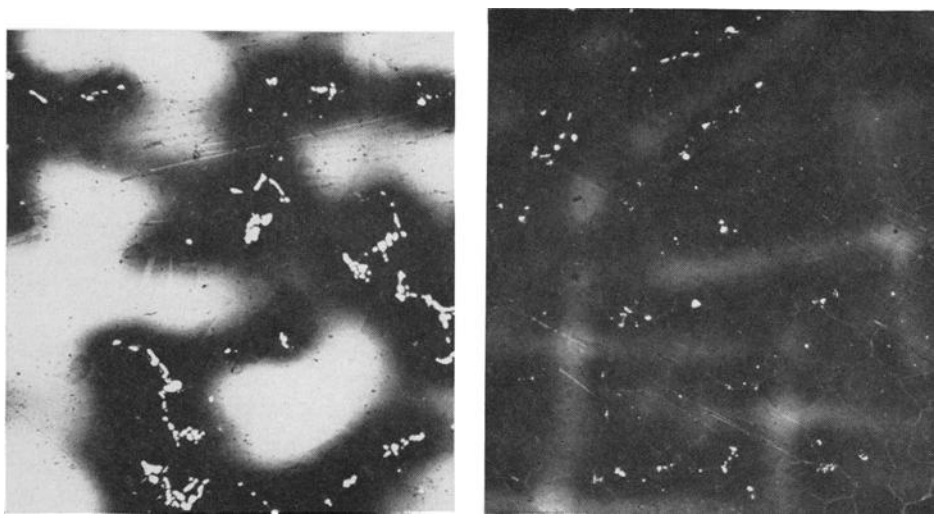


FIG. 14—Cast Structure of Large Forged Billet (small amount of work) Comprises Dendrites (the large light areas) Matrix (dark area) and Laves Phase (small white areas in matrix). (*a*) Such structure had 0 per cent elongation (over-etched with chromic acid). (*b*) Such structure had 15 per cent elongation (over-etched with chromic acid).

shown in Fig. 15. The solidus line, obtained from previous hot bend test data, is added on this plot, and its intersection with the curve at 2150 F and about 7 per cent columbium forms the terminal solid solution. At this eutectic temperature, the melt precipitates crystals of gamma plus crystals of Laves.

As-Cast Structure:

The effect of undercooling or supercooling, as is the case in solidification of commercial ingots, on the solidus line is shown in Fig. 18. Microprobe results from the specimens of Fig. 14 are superimposed on the equilibrium diagram, showing the effect of the nonequilibrium conditions.

This condition of undercooling is more readily explained by the similar, aluminum-copper phase diagram. The explanation by Brick (2) of the coring and divorced eutectic formation in the 4 per cent copper aluminum base casting alloy may be applied directly to Fig. 18. This suppression of equilibrium between the liquid metal and the solid primary crystals explains the dendritic or cored crystallites and divorced Laves eutectic shown in Figs. 14 and 19.

Fineness of structure or size of dendrites is a function of cooling rate as shown by Fig. 19. For the cast structure of Inconel alloy 718 containing 5.4 per cent columbium plus tantalum, the toe end develops a finer dispersion of Laves and smaller dendrites than the head end. Welds joining thin sheets and electron beam welds apparently solidify fast enough to suppress the Laves reaction entirely.

Effect of Aging Temperature and Time:

It has been shown that the formation of phases is strongly dependent upon solution annealing temperature; therefore, high temperatures involved in forming and fabricating also must be considered in processing this alloy.

Specimens were solution annealed at 2100 F and aged at various temperatures and times to establish the initiation of the various phases. The results are shown in the form of a time-temperature transformation diagram, Fig. 17.

Stability:

Figure 20 shows the effect of long time relaxation test at 1300 F/50,000 psi on a specimen solution treated at 1800, for 1 hr, water quenched and aged at 1325 F for 16 hr, and air cooled. The structures exhibit over-aged gamma prime in the background, carbides in grain boundaries (Laves phase cannot be detected), and an indication of the needle phase in agreement with the phase diagrams established. The yield strengths are decreased

from the pre-test level of about 150,000 psi.

Structure of a creep rupture specimen after testing for 5470.7 hr at 1350 F and 10,000 psi, as viewed by means of electron microscope, is shown in Fig. 21. The specimen had been heat treated initially at 1700 F for 1 hr, water quenched and aged at 1325 F for 16 hr, and air cooled. Phases present are gamma prime (dots), orthorhombic (needles), Laves (flat, irregular shapes), carbides (circular, irregular shapes), and areas depleted of age hardening constituent (gamma).

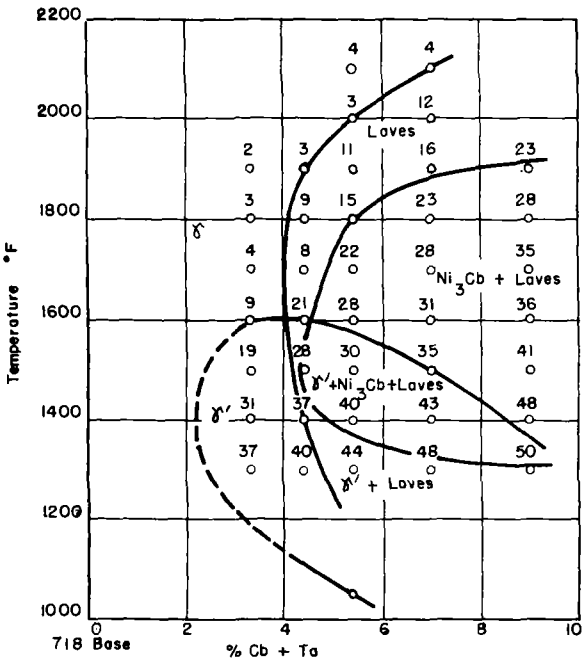


FIG. 15—Composite Phase Diagram Shows the Occurrence of Various Phases After Heating for 100 Hr at the Temperatures Indicated. (Rockwell "C" hardness also is shown for the heat treated specimens).

DEVELOPMENT OF PROPERTIES

Since the room-temperature properties as established in this study (3) were relatively high, further improvement of over-all properties appeared to necessitate working with the optimum treatment for creep-rupture strength. The stress-rupture requirement for notch ductility has limited most heat treatments to date.

Figure 22 shows that the maximum ratio of notch-rupture life to smooth-bar life, while still retaining useful ductility or elongation, is attained with a 1750 to 1800 F anneal. This temperature range is between the temperature for best smooth-bar elongation (1625 F) and that for best rupture life (1900 F). A treatment at 1625 F could precipitate Laves and orthorhombic Ni_3Cb. The 1900 F treatment results in almost complete solution treatment without growing coarse grains. Depending on prior thermal history, the 1750 to 1800 F anneal is likely to be a precipitation treatment or, at best, only a partial solution anneal.

The best age-hardening treatment had been previously established (3) on a melt containing the minimum columbium, titanium, and aluminum as 1325 F for 8 hr, furnace cooled 20 F/hr to 1150 F, and air cooled.

Modifications of Heat Treatment:

To improve creep rupture properties, in accordance with that predicted in Fig. 22, tests were made on 19 specimens representing different lots solution annealed at 1800 and 1900 F. The effect of the 100 deg higher solution annealing temperature was to double the rupture life and halve the elongation.

Notch ductility of such alloys as Inconel alloy X-750, Waspaloy, and Incoloy alloy 901 is improved with a three step heat treatment; therefore, similar type treatments (involving an intermediate aging step) were tried for Inconel alloy 718 to attain both increased rupture life and improved ductility in the 1200 to 1300 F temperature range.

The results of this study were negative. There is no apparent advantage in using an intermediate age or change in heat treatment; therefore, an attempt was made to modify chemistry to increase notch ductility and over-all properties.

Modifications in Composition:

Figure 4 has shown maximum rupture properties with 1.2 per cent aluminum plus titanium. Properties discussed to

TABLE 3—CHEMICAL AND X-RAY FLUORESCENT ANALYSES OF ORTHORHOMBIC RESIDUES.

CHEMICAL COMPOSITION OF VACUUM-MELTED HEATS

	C	Mn	Fe	S	Si	Cu	Ni	Cr	Al	Ti	Cb + Ta	Mo	B
HV 257	0.04	0.25	16.78	0.007	0.45	0.02	54.20	18.94	0.51	1.13	4.42	3.08	0.001
HV 269	0.04	0.21	15.82	0.006	0.42	0.02	54.22	18.97	0.50	1.14	5.44	3.15	0.001

ELEMENTS IN EXTRACTION RESIDUE,[a] WEIGHT PER CENT

	Ni	Fe	Cr	Ti	Al	Cb	Mo
HV 257	63	3	2	3	0.21	28	1
HV 269	59	2	1	2	0.48	34	2

ELEMENTS IN EXTRACTION RESIDUE, ATOMIC PER CENT

	Ni	Fe	Cr	Ti	Al	Cb	Mo
HV 257	69.4	3.5	2.5	4.1	0.52	19.5	1
HV 269	66.7	2.4	1.3	2.8	1.2	24	1.4

[a] Specimens obtained from extractions using 20 per cent H_3PO_4 solution in H_2O. Both HV 257 and HV 269 were given the following treatment: 2000 F/1 hr WQ + 1500 F/100 hr WQ.

this point have been based on approximately a 1 to 1 ratio of these elements; a logical step was to study the effects of varying this ratio.

In altering the ratio, it was desired to improve properties while retaining weldability and the sluggish age-hardening characteristic already established. Figure 23 shows how the percentage of aluminum and titanium, in combination, influences the rate of age hardening. Speed of aging response or aging is controlled by the amount of aluminum and titanium content with titanium apparently the more effective accelerator of age hardening. By maintaining low aluminum and titanium content, sluggish response can be maintained, and relatively thick sections can be readily welded in the annealed condition. Thinner sections can be welded in the aged condition. Waspaloy, René 41, and Inconel alloy 700 all age harden very rapidly; the rate for age hardening of Inconel alloy 718 is less than that for the other three alloys.

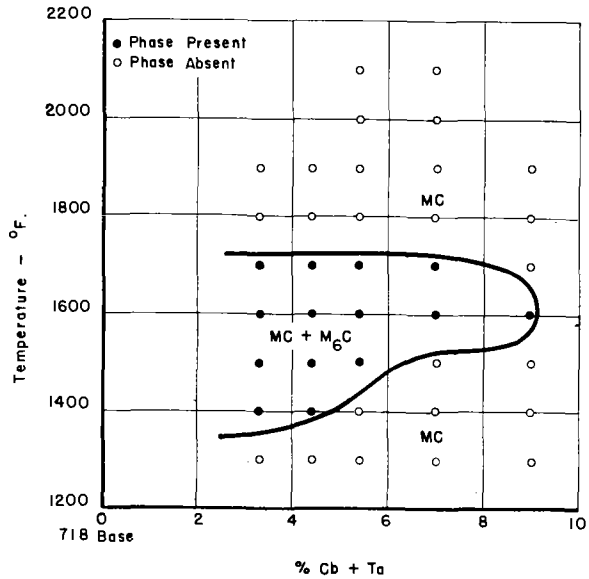


FIG. 16—Phase Diagram for M_6C Developed by Heating Specimens of Various Percentages of Cb Plus Ta for 100 Hr at the Temperatures Indicated.

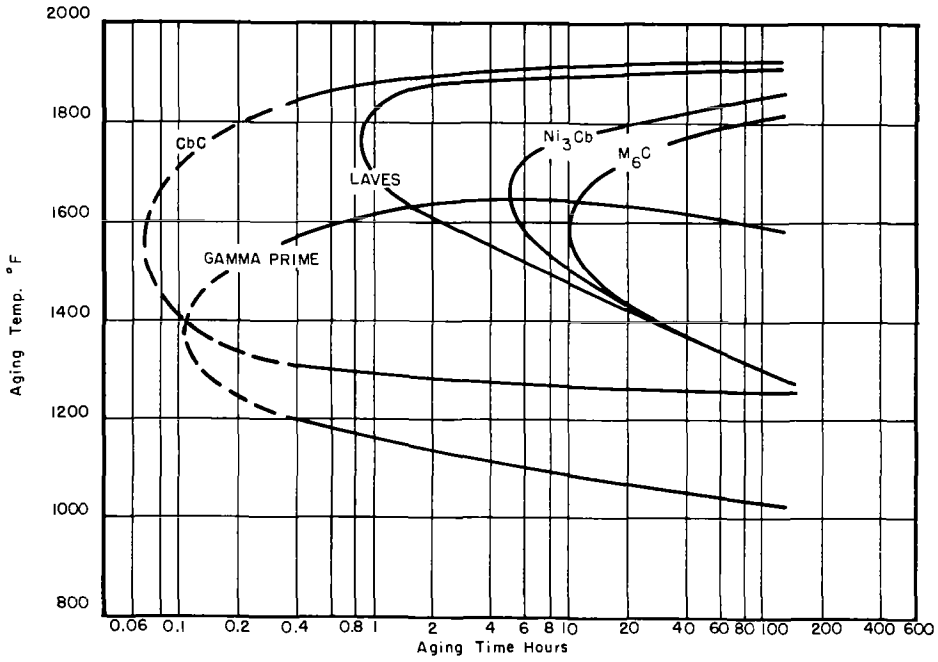


FIG. 17—Time-Temperature Transformation Diagram for Inconel Alloy 718 After Annealing at 2100 F/1 hr and Water Quenched.

To further study the effects of aluminum and titanium as well as boron and columbium, some 30 modified compositions of Inconel alloy 718 were made in the form of 30-lb ingots, by vacuum induction melting. The ingots were forged to $\frac{9}{16}$-in.-square bar stock. Tension specimens were tested at room temperature, 1200 and 1300 F, after the following heat treatment: 1750 and 1900 F for 1 hr, air cooled plus 1325 F for 8 hr, furnace cooled 20 F/hr to 1150 F, and air cooled. Stress-rupture tests of smooth and notched bars were conducted at 1300 and 1400 F after solution annealing at 1700, 1800, 1900, or 2000 F and standard aging treatment (as shown for the tension specimens). There was insufficient material to make all of these tests from any one melt, so the 1900 F solution anneal was singled out for the most exhaustive testing.

Both graphical correlation and regression analysis of data were made (4). The most interesting regression analysis made on an IBM 1410 computer are reported here.

Effect of Elements on Tensile Properties:

Trials for linear regression analysis of room-temperature yield strength of Inconel alloy 718 are shown in Table 4. Data for these trials were based on a 1900 F solution anneal (and standard aging treatment) to ensure that chemistry rather than work hardening effect would be the major influence on properties.

Thirty-two different equations were investigated, by means of the IBM 1410 computer, to establish the most significant variables and most appropriate equation for predicting yield-strength values. These equations were based on variations of the following polynomial:

$$Y = A_0 + A_1X_1 + A_2X_2 + A_3X_1X_2 + A_4X_1^2 + A_5X_2^2 + \cdots$$

where:

Y = dependent variables (yield strength or rupture life),
A_0 = constant,
X_i = independent variables (aluminum, titanium, boron, carbon), and
A_i = coefficients of independent variables.

Table 4 shows the significant variables for the various runs or possible equation factors and the corresponding per cent correlation (representing a figure of merit). Run 3 was selected for the regression equation because the significant variables appeared to be the most logical from a metallurgical standpoint, the per cent correlation was relatively high, the number of variables relatively few, and all were statistically significant.

The regression equation used is shown in Table 5 which compared predicted and observed values for room-temperature yield strength. Note that there is a close agreement of values.

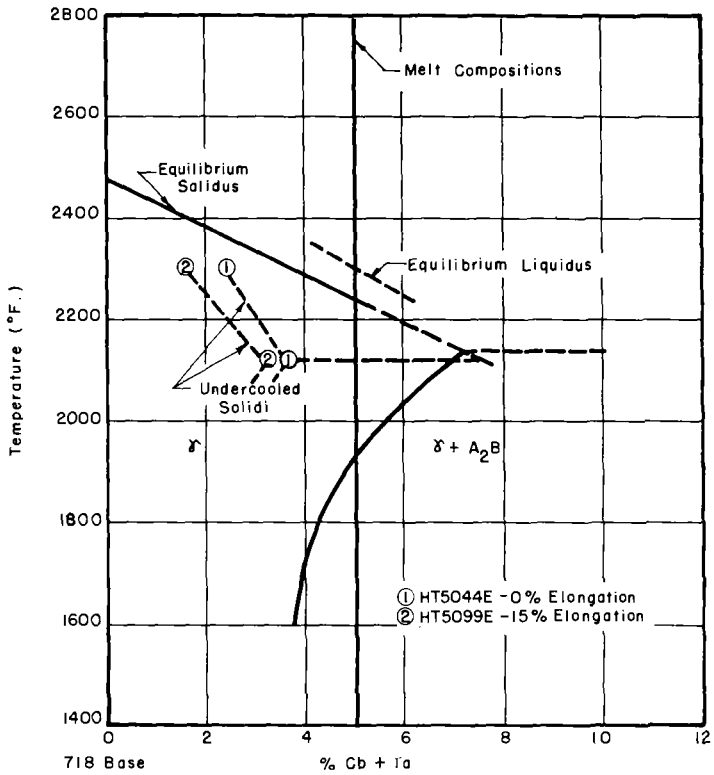


FIG. 18—Change of Solidus From Equilibrium Condition due to Undercooling Which Normally Occurs in Casting of Commercial Ingots.

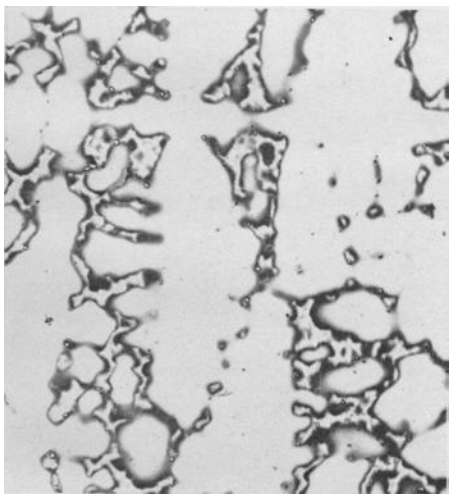


FIG. 19(*a*)—Cast Structure of Specimens (5.4 per cent Cb plus Ta) From Head End Shows Dendrites (large light areas), Matrix (dark area) and Laves Phase (light area) in Matrix (overetched in chromic acid—×100).

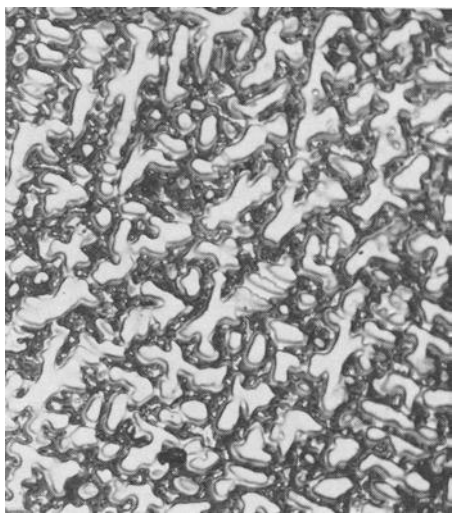


FIG. 19(*b*)—Cast Structure of Specimen (5.4 per cent Cb plus Ta) From Toe End Shows Finer Dispersion of Laves and Smaller Dendrite Size Than in Head End. (Overetched in chromic acid—×100).

Room-temperature yield strengths (predicted by regression equation) as functions of aluminum and titanium contents are shown in Table 6. It indicates the desirability of changing the aluminum-titanium ratio of approximately 1 to 1 (upper right range or corner of Table 6) to a slightly higher titanium and lower aluminum (lower left range or corner of Table 6). A common specification range is 0.4 to 0.8 per cent aluminum and 0.65 to 1.15 per cent titanium. It is possible to increase the present minimum probability values for room-temperature yield strength by reducing aluminum content, and still more so, by increasing the titanium. Therefore, for tension limited applications a recent specification range is 0.2 to 0.6 per cent aluminum and 0.7 to 1.4 per cent titanium.

Table 7 compares room-temperature tensile properties for specimens containing high and low levels of aluminum. The advantage of higher titanium and lower aluminum is evident.

Effect of Elements on Rupture Life:

For analysis of stress-rupture results, the effects of boron, aluminum, and titanium, as well as solution annealing temperature, were considered. Boron was expected to have a more pronounced

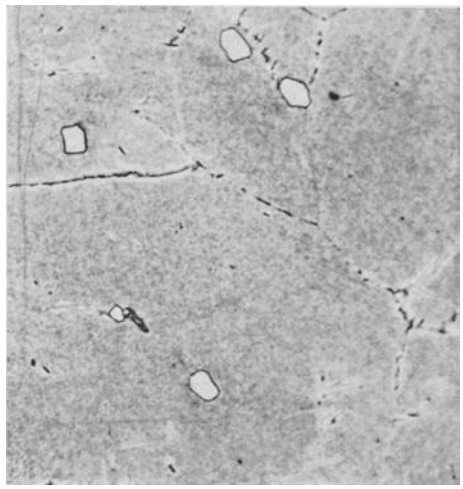


FIG. 20—Structure of Longitudinal Section (1800 F/1 hr, water quenched plus 1325 F/16 hr, air cooled) After Relaxation at 1300 F/50,000 Psi for 1272 Hr. (Etchant—chromic acid, × 1000). Room-Temperature Tensile Properties Are: Tensile Strength 170,500 Psi; 0.2 per cent Yield Strength 117,000 Psi Elongation 23 per cent; Reduction of Area 26 per cent; and Rockwell "C", 38.

effect on rupture life than on tensile properties. The data indicate that both 1800 and 1900 solution anneals, as mentioned previously, yield longer rupture life after aging than a lower solution annealing temperature of 1750 F. For solution annealing temperatures of 1750 and 1800 F, rupture life cannot be significantly improved by changes in chemistry. However, rupture life can be drastically altered by prior processing variables when employing these solution temperatures.

In regard to smooth bar life, compositional variations appear to be most effective for specimens solution annealed at 1900 F. Therefore, these data were selected for regression analysis on the computer.

Twenty-two trials for best regression

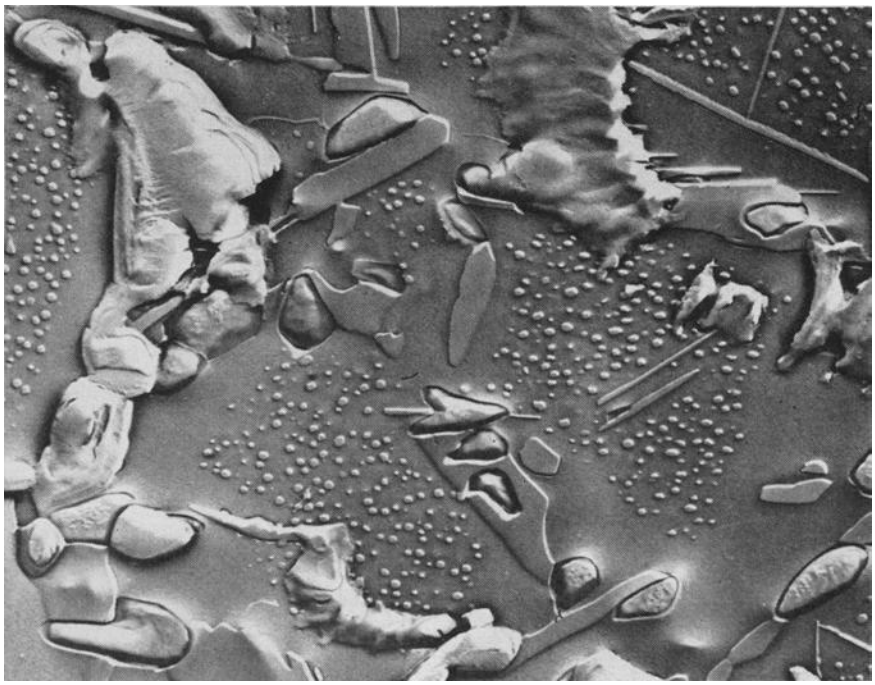


FIG. 21—Structure of Specimen (1700 F/1 hr, water quenched plus 1325 F/16 hr, air cooled) After Stress Rupture Testing for 5470.7 Hr at 1350 F and 10,000 Fsi. Phases Present Are Gamma Prime (dots), Orthorhombic (needles), Laves (flat, irregular shapes), Carbides (circular, irregular shapes), and Gamma (areas depleted of age hardening constituent).

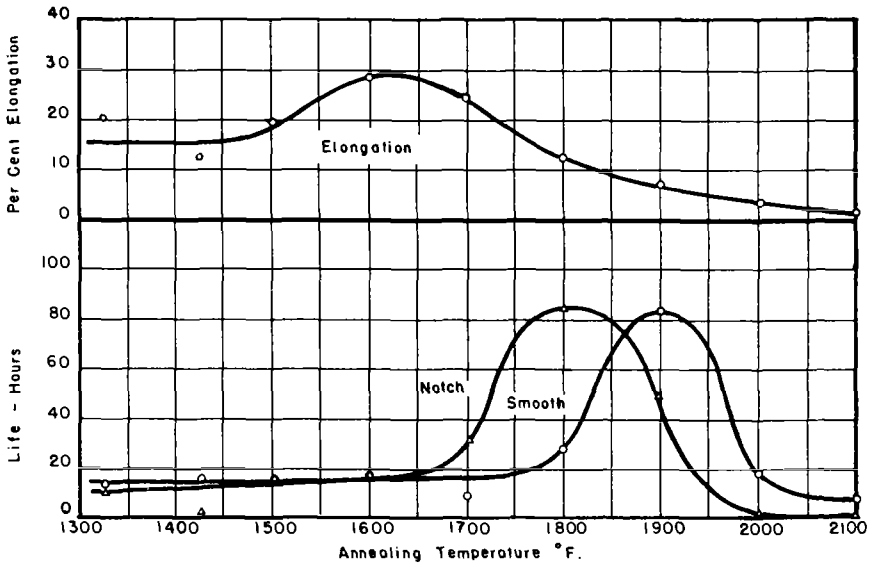


FIG. 22—Effect of Annealing Temperature on Stress Rupture Properties (1300 F/75,000 psi). Specimens Are From Hot Rolled Material ($\frac{1}{2}$ in. diameter) Annealed for 1 Hr, Water Quenched Plus Aged at 1325 F/16 Hr, Air Cooled (0.37 per cent Al, 0.72 per cent Ti, 4.94 per cent Cb + Ta, and 0.004 per cent B).

analysis of smooth-bar-rupture life of Inconel alloy 718, using a 1900 F for 1-hr anneal plus 1325 F for 8 hr, furnace cooled to 1150 F, and air cooled, were made. From these trials, Run 21 was selected for the regression equation. This equation is shown in Table 8 along with the best equation for notch-bar life.

Table 8 gives smooth and notched-bar life as predicted by regression analysis, showing the effect of variations in chemistry. From these data, the significant points appear to be:

1. If aluminum, titanium, and boron content are all at their lowest levels simultaneously, specimens will be notch brittle (as shown by zero in parentheses).

2. With a 1900 F anneal (and standard aging treatment) boron increases smooth- and notch-bar life when present in the range of 0.004 to 0.006 per cent. It seems to be most effective with low aluminum and high titanium.

3. Increasing carbon contents, with the presence of 0.004 to 0.006 per cent boron, result in lower smooth-bar life but higher notch-bar life. With 0.02 per cent carbon both smooth- and notch-bar life decrease with increasing quantities of aluminum.

4. Generally, low carbon, 0.004 to 0.006 per cent boron, high titanium, and low aluminum yield the longest smooth-bar life while retaining notch ductility.

Large forged products given a 1750 or 1800 F anneal may be expected to behave similarly to the 1900 F data presented here because of their higher finishing temperature ($\frac{9}{16}$-in.-square bars, finished cold). Properties of sheet products and small bars will be lower and in accord with the $\frac{9}{16}$-in.-square bar data, not shown, when annealed at 1750 or 1800 F.

Table 9 compares stress rupture data for specimens containing high and low levels of aluminum. The data show the advantage of employing higher annealing temperatures, lower aluminum, and higher titanium.

Strengthening Mechanism:

By changing to lower aluminum content, it is expected that tensile property improvement will be reflected at service temperatures of −423 F up to 1300 F. Higher properties are attributed to larger mismatch between the lattice and columbium rich gamma prime, $Ni_3(CbTiAl)$. With the amount of gamma prime constant, an increase in aluminum makes the gamma prime richer in aluminum and causes the lattice parameter to decrease (smaller mismatch) and approach that of ordinary gamma prime, Ni_3Al. No attempt has been made to confirm this theory by X-ray diffraction.

Commercial Heat Treatments:

Much of the above has been devoted to developing the optimum heat treatment and composition for the best combination of ductility, tensile strength, and smooth and notch stress-rupture properties—that is, make a general purpose material. The opportunity to develop this concept on a commercial scale has not occurred because the use of the alloy quickly segregated into separate and special requirements. The expense of developing a compromise at this stage has appealed to no one.

The conservative notch ductile anneal

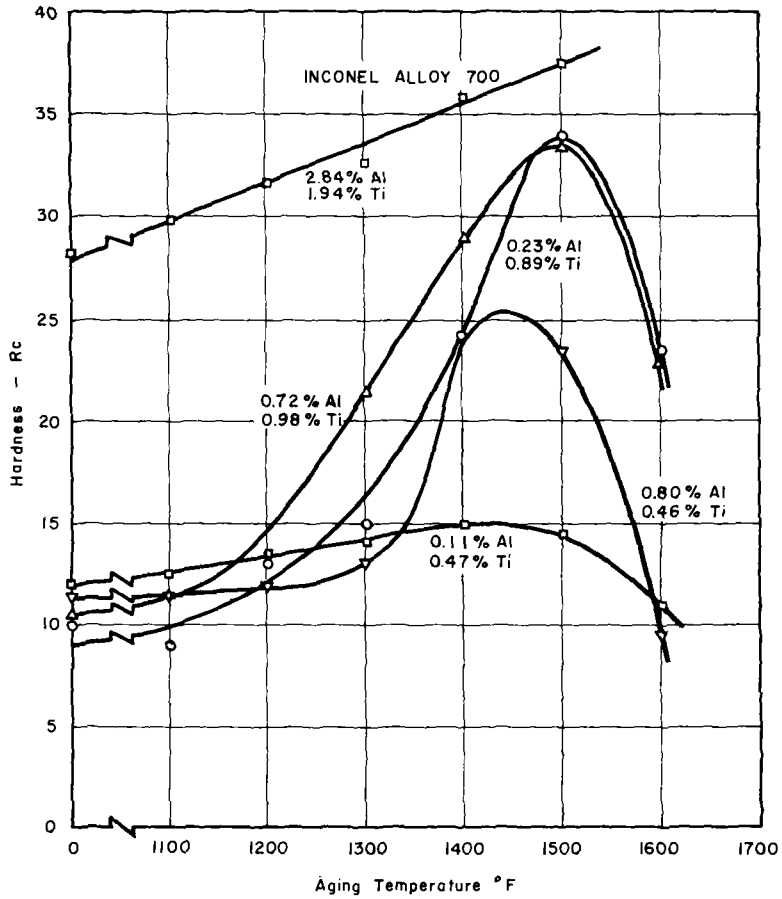


FIG. 23—Influence of Various Combinations of Al and Ti on Age Hardening Response. (Specimens were taken from forged $\frac{9}{16}$ in. square bars annealed at 2000 F/1 hr, water quenched plus aged for 6 min at temperatures indicated. Titanium apparently is the more effective element in speeding aging response and increasing hardness).

at 1750 F for 1 hr, followed by aging at 1325 F for 8 hr and furnace cooling to 1150 F, has prevailed for those uses requiring tensile and rupture strength. The 1750 F anneal is more of a stress relief anneal and does not fully soften the material. Material in this annealed condition is not suited for severe cold-forming operations. It just so happens that the uses requiring a soft ductile material for forming and better ductility in the annealed and aged state are now all tensile limited. A 1950 F anneal for 1 hr is specified for this service.

Associated with the 1950 F anneal are higher aging temperatures. Increases in the amount of gamma prime hardening elements, especially aluminum, require increased aging temperatures to produce optimum age hardening.

A one to one comparison of these two annealing treatments is made for 20 different commercial compositions for tensile properties at room temperature and 1200 F (Figs. 24 and 25). The 95 per cent confidence limits have been omitted from Fig. 25 for clarity. Stress-rupture test results are shown in Fig. 26 for the 1750 F annealed condition. All tests were notch ductile.

The source material for these tests was the 1 by 2 by 20-in. quality control test forging made to evaluate each melt.

TABLE 4—TRIALS FOR LINEAR REGRESSION ANALYSIS OF ROOM-TEMPERATURE YIELD STRENGTH OF INCONEL ALLOY 718 USING A 1900 F/1 HR ANNEAL PLUS 1325 F/8 HR F.C. TO 1150 F, NUMBER OF OBSERVATIONS = 30.

Run No.	Independent Variables	Degrees of Freedom	Significant Variables—Confidence Levels		Correlation, %
			1%	5%	
1	Ti,Ti^2,B,B^2, C × Al,Al × Ti,C × Ti	22	Al × Ti	Ti	89
2	Ti,Ti^2,Al,Al^2, Al × Ti, Cb	23	Al × Ti	Ti,Cb	92
3	Ti,Cb,Al,Al^2, Al × Ti	24	Ti,Al × Ti	Cb,Al,Al^2	91
4	Ti,Cb,Al,Al^2, Al × Ti,Al × B	23	Ti,Al × Ti	Cb,Al,Al^2	91
5	Ti,Cb,Al,Al^2, Al × Ti,Cb × Ti	23	Al × Ti	Al,Al^2	91
6	Ti,Cb,Al,Al,^{2} Al × Ti, C	23	Ti,Al × Ti	Cb	92
7	C,Al,Ti,Cb,Al × Ti	24	Ti,Cb,Al × Ti	...	90
8	C,Al,Ti,Cb,Al × Ti,C × Cb	23	Ti,Al × Ti	...	90
9	C,Al,Ti,Cb	25	Cb,Al	Ti	86
10	Cb,Al,Ti	26	Al,Ti	Cb	84
11	Cb,Al,Ti,Al × Ti	25	Ti,Al × Ti	Cb	88
12	Cb,Al,Ti,Al × Ti,Al × Cb	24	Ti,Al × Ti	Cb	89
13	Cb,Al,Ti,Al × Ti,Ti × Cb	24	...	Al × Ti	89
14	Ti,Ti^2, Al,Al^2,Al × Ti	24	Ti, Al × Ti	...	90
15	Ti,Cb,Al,Al × Ti	25	Ti, Al × Ti	Cb	89
16	Ti,Cb,Al^2, Al × Ti	25	Ti	Cb,Al × Ti	89
17	Ti,Cb,Al,Al^2,Al × Ti,Al^3	23	Ti,Al × Ti	Cb	92
18	Ti,Cb,exp(Al), Al × Ti	25	Ti	Cb,Al × Ti	89
19	Ti,Cb,Al,Al^2	25	Ti	Cb	86
20	Ti,Cb,Al,Al^2,Al × Ti, Al × Cb	23	Ti,Al × Ti	Al^2	91
21	Ti,Al^2, Al × Ti,Cb	25	Ti	Al × Ti,Cb	89
22	Ti,Al^2, Al × Ti,Cb,Al,C × Ti	23	Ti, Al × Ti	Al^2,Cb	91
23	Ti,Al^2, Al × Ti,Cb,Al,Al × C	23	Ti,Al × Ti	Al^2,Cb,Al	91
24	Ti,Al^2,Al × Ti,Cb,Al,C × Cb	23	Ti,Al × Ti	Cb	92
25	Al × Ti,Ti × Cb	27	Al × Ti,Ti × Cb	...	89
26	Al × Ti, Ti × Cb,Ti	26	Al × Ti	Ti × Cb	89
27	Al × Ti, Ti × Cb,Al	26	Al × Ti,Ti × Cb	...	89
28	Al × Ti,Ti × Cb,Al × Cb	26	Al × Ti,Ti × Cb	...	89
29	Al × Ti,Ti × Cb,C	26	Al × Ti,Ti × Cb	...	89
30	Al × Ti,Ti × Cb,C × Cb	26	Al × Ti,Ti × Cb	...	89
31	Al × Ti,Ti × Cb,Cb	26	Al × Ti,Ti × Cb	...	89
32	Al × Ti,Ti × Cb,Al^2	26	Al × Ti,Ti × Cb	...	89

Careful control of the hot working conditions is necessary to develop the structure to meet all of the test requirements.

TABLE 5—REGRESSION EQUATION PREDICTED VALUES COMPARED TO OBSERVED VALUES FOR ROOM-TEMPERATURE YIELD STRENGTH OF INCONEL ALLOY 718.

HEAT treatment: 1900 F/1 hr, air cooled plus 1325 F/8 hr, furnace cooled to 1150 F, air cooled

Regression equation used: Room-temperature yield strength (ksi) = 90.55 + 42.5% Ti + 9.54% Cb + 64.64% Al − 62.0 (% Al)² − 53.34 (% Al × % Ti)

Standard deviation = 6.97 ksi

Observation No.	Observed Value, 1000 psi	Predicted Value, 1000 psi	Difference Obs.-Pred., 1000 psi
1	157.0	159.6	−2.6
2	172.5	160.8	11.7
3	180.0	174.7	5.3
4	156.0	165.5	−9.5
5	144.8	150.2	−5.4
6	138.0	133.4	4.6
7	147.5	156.9	−9.4
8	156.0	160.0	−4.0
9	160.0	159.8	0.2
10	158.0	161.3	−3.3
11	149.5	157.5	−8.0
12	164.5	157.5	7.0
13	161.5	157.8	3.7
14	173.0	171.5	1.5
15	153.5	162.0	−8.5
16	154.5	159.3	−4.8
17	147.5	148.9	−1.4
18	154.0	153.1	0.9
19	156.5	154.8	1.7
20	173.5	174.3	−0.8
21	198.5	196.9	1.6
22	170.0	166.5	3.5
23	188.5	196.9	−8.4
24	152.0	152.5	−0.5
25	166.5	157.8	8.7
26	180.5	167.9	12.6
27	170.5	167.4	3.1
28	202.5	197.4	5.1
29	159.5	153.3	6.2
30	150.0	160.7	−10.7
Accumulated difference			0.0

In the making of many products, forgings, bars, sheet, plate, and so on, the manufacturing variables are under less precise control; consequently, the standard deviation for some of these products is greater than shown in Figs. 24–26.

Material with the 1750 F annealed condition is ordered to 0.4 to 0.8 per cent aluminum, 0.65 to 1.15 per cent titanium, and 5.0 to 5.5 per cent columbium + tantalum. On the other hand, material for the softer 1950 F anneal has a different set of gamma prime forming constituents specified, namely, 0.2 to 0.6 per cent aluminum, 0.7 to 1.4 per cent titanium, and 4.75 to 5.50 per cent columbium + tantalum. The data in Figs. 24–26 represent compositions within these two ranges, that is, 0.2 to 0.6 per cent aluminum, 0.8 to 1.0 per cent titanium, and 4.8 to 5.4 per cent columbium + tantalum.

Properties at Cryogenic Temperatures:

Room temperature and minus 320 F tensile data for Inconel alloy 718 are correlated in Fig. 27. The points in the graphs represent both cold rolled and

TABLE 6—ROOM-TEMPERATURE YIELD STRENGTHS (1000 PSI) PREDICTED BY REGRESSION EQUATION.

(1900 F/1 hr, ac + 1325 F/8 hr, fc To 1150 F Cb + Ta = 5.0%)

Titanium Content, %	0.1% Al	0.2% Al	0.4% Al	0.6% Al	0.8% Al
0.4	158.9	161.4	162.6	158.9	150.2
0.6	166.4	167.8	166.9	161.0	150.2
0.8	173.8	174.1	171.1	163.1	150.1
1.0	181.2	180.5	175.3	165.2	150.1
1.2	188.7	186.9	179.6	167.3	150.1
1.4	196.1	193.2	183.8	169.4	150.0
1.6	203.5	199.6	188.0	171.5	150.0

TABLE 7—EFFECT OF ALUMINUM AND TITANIUM ON ROOM-TEMPERATURE TENSILE PROPERTIES OF INCONEL ALLOY 718 SPECIMENS ANNEALED PLUS AGED 1325 F/8 HR, FURNACE COOLED TO 1150 F, AND AIR COOLED, (Cb + Ta = 5%; B = 0.004%).

Annealing Treatment		0.15% Al		0.75% Al	
		0.65% Ti	1.45% Ti	0.65% Ti	1.45% Ti
1750 F/1 hr, ac	yield strength, psi, 165 500	182 500		161 000	178 000
	tensile strength, psi, 203 000	220 000		210 000	218 000
	elongation, %, 18.0	14.0		20.0	7.0
	r.a., %, 39.0	24.0		27.0	9.5
1900 F/1 hr, ac	yield strength, psi, 170 000	188 500		152 000	166 500
	tensile strength, psi, 203 500	218 500		192 000	213 000
	elongation, %, 20.0	18.0		24.0	24.0
	r.a., %, 43.0	46.5		46.5	37.0

TABLE 8—SMOOTH AND NOTCH BAR LIFE (HR) OF INCONEL ALLOY 718 AS PREDICTED BY REGRESSION EQUATIONS.[a]

Test conditions: 1300 F/75,000 psi

Heat treatment: 1900 F/1 hr, air cooled plus 1325 F/8 hr, furnace cooled to 1150 F, air cooled

Regression equations: Smooth-bar life (hr) = −295.2 + 526.2% Ti − 169.1% Ti² + 62,890% B − 5.467 × 10⁶% B² − 1405% C × Ti + 1621% C × Al − 122.9% Al × Ti

Standard deviation = 17.2 hr

Notch-bar life (hr) = −544.9 + 292, 700% B − 27.11 × 10⁶% B + 171.0% Ti² − 225.2% Al × Ti + 596.2% C × Al

Standard deviation = 120.3 hr

		0.02% C			0.06% C			0.10% C		
		0.6% Ti	1.0% Ti	1.4% Ti	0.6% Ti	1.0% Ti	1.4% Ti	0.6% Ti	1.0% Ti	1.4% Ti
0.002% B	0.1% Al	43 (0)	129 (82)	161 (238)	15 (6)	79 (106)	89 (262)	0 (30)	29 (130)	16 (285)
	0.5% Al	26 (0)	93 (40)	105 (159)	25 (95)	69 (159)	59 (278)	24 (214)	45 (279)	12 (398)
	0.8% Al	14 (0)	65 (8)	63 (100)	32 (162)	61 (199)	36 (291)	50 (354)	57 (390)	9 (482)
0.004% B	0.1% Al	103 (242)	189 (347)	221 (498)	76 (266)	139 (366)	149 (522)	48 (290)	90 (390)	77 (545)
	0.5% Al	86 (236)	153 (300)	165 (419)	85 (355)	129 (419)	119 (539)	84 (474)	105 (539)	73 (658)
	0.8% Al	74 (231)	126 (268)	123 (361)	92 (422)	121 (459)	96 (551)	110 (613)	117 (650)	70 (742)
0.006% B	0.1% Al	119 (285)	205 (386)	237 (541)	92 (309)	156 (410)	165 (565)	65 (333)	106 (434)	93 (589)
	0.5% Al	103 (279)	169 (343)	182 (463)	101 (398)	145 (463)	135 (582)	100 (518)	122 (582)	89 (701)
	0.8% Al	90 (274)	142 (312)	140 (404)	108 (465)	138 (502)	113 (595)	127 (656)	133 (693)	86 (785)
0.008% B	0.1% Al	92 (112)	178 (212)	210 (367)	65 (136)	128 (236)	138 (391)	37 (159)	79 (260)	66 (415)
	0.5% Al	75 (105)	142 (170)	154 (209)	74 (225)	118 (289)	108 (408)	73 (344)	94 (408)	62 (527)
	0.8% Al	63 (101)	115 (138)	112 (230)	81 (291)	110 (329)	85 (421)	99 (482)	106 (519)	59 (612)

[a] Notch bar values shown in parentheses.

TABLE 9—EFFECT OF ALUMINUM AND TITANIUM ON STRESS RUPTURE LIFE (1300 F/75,000 psi) OF INCONEL ALLOY 718 SPECIMENS ANNEALED PLUS AGED AT 1325 F/8 HR, FURNACE COOLED TO 1150 F, AND AIR COOLED (Cb + Ta = 5.0%; B = 0.004%).

Annealing Treatment		0.15% Al		0.75% Al	
		0.65% Ti	1.45% Ti	0.65% Ti	1.45% Ti
1750 F/1 hr, ac	smooth-bar life, hr	14.5	18.9	22.4	16.9
	elongation, %	35.0	34.0	36.0	29.0
	notch-bar life, hr	78.2	53.5	96.9	60.0
1800 F/1 hr, ac	smooth-bar life, hr	32.9	33.1	77.4	40.5
	elongation, %	25.0	31.0	17.0	24.0
	notch-bar life, hr	308.4	189.1	258.3	156.7
1900 F/1 hr, ac	smooth-bar life, hr	98.4	206.3	113.3	152.4
	elongation, %	16.0	12.0	11.0	7.0
	notch-bar life, hr	568.6	582.4	299.6	432.4
2000 F/1 hr, ac	smooth-bar life, hr	255.0	296.1	91.2	215.6
	elongation, %	8.0	8.0	8.0	4.0
	notch-bar life, hr	247.4	385.2	129.4	20.4

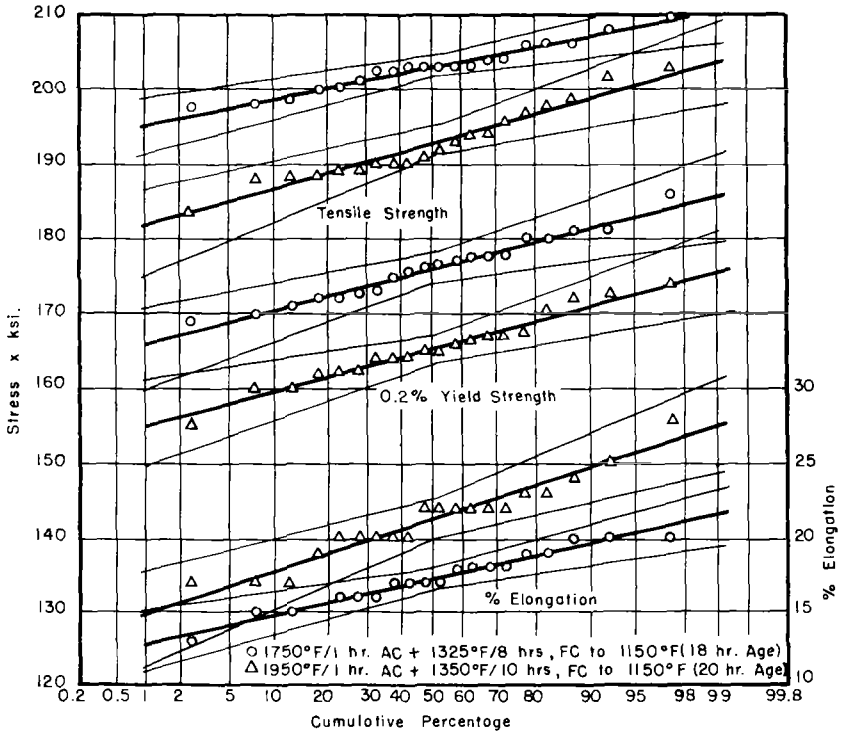


FIG. 24—Cumulative Frequency Plots for Room-Temperature Tensile Properties (1 by 2-in.-forged flats; 20 specimens each heat treatment).

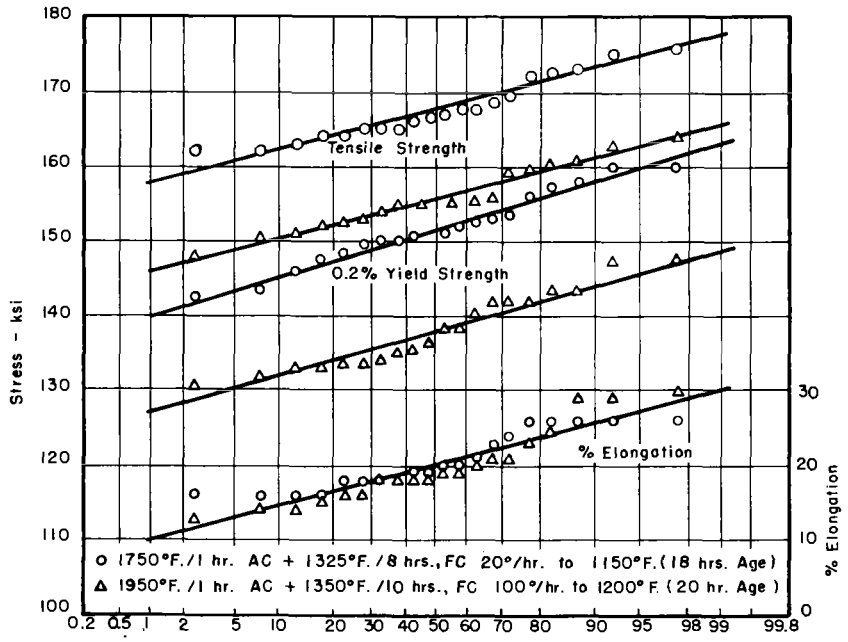


FIG. 25—Cumulative Frequency Plots for 1200 F Tensile Properties, (1 by 2-in.-forged flats; 20 specimens each heat treatment).

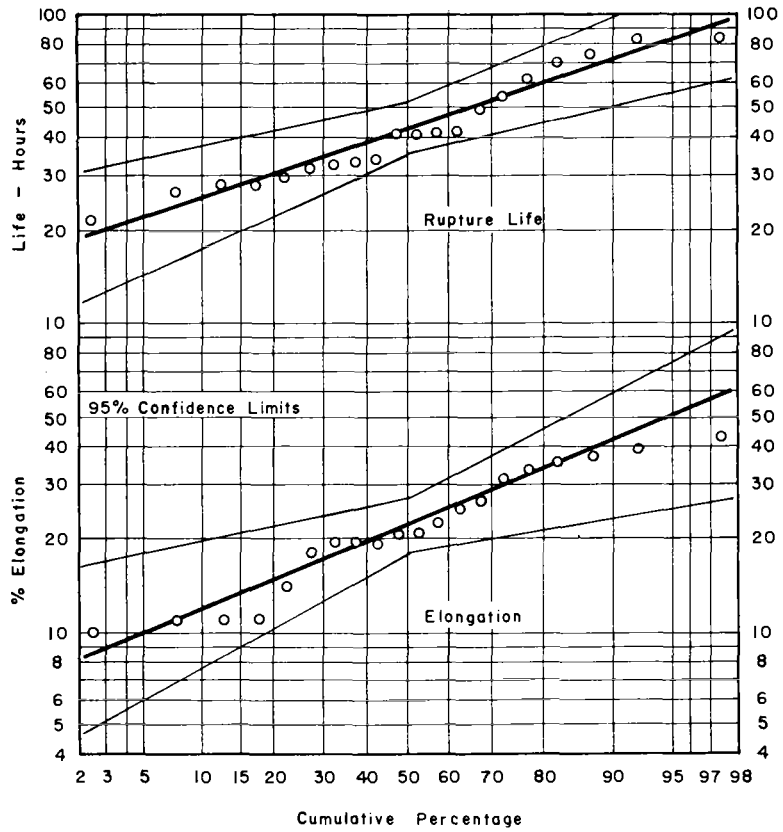


FIG. 26—Cumulative Frequency Plots for Stress-Rupture Properties at 1300 F/75,000 Psi, (20 specimens were heat treated at 1750 F/1 hr ac + 1325 F/8 hr fc 20 F/hr to 1150 F, total aging time 18 hr).

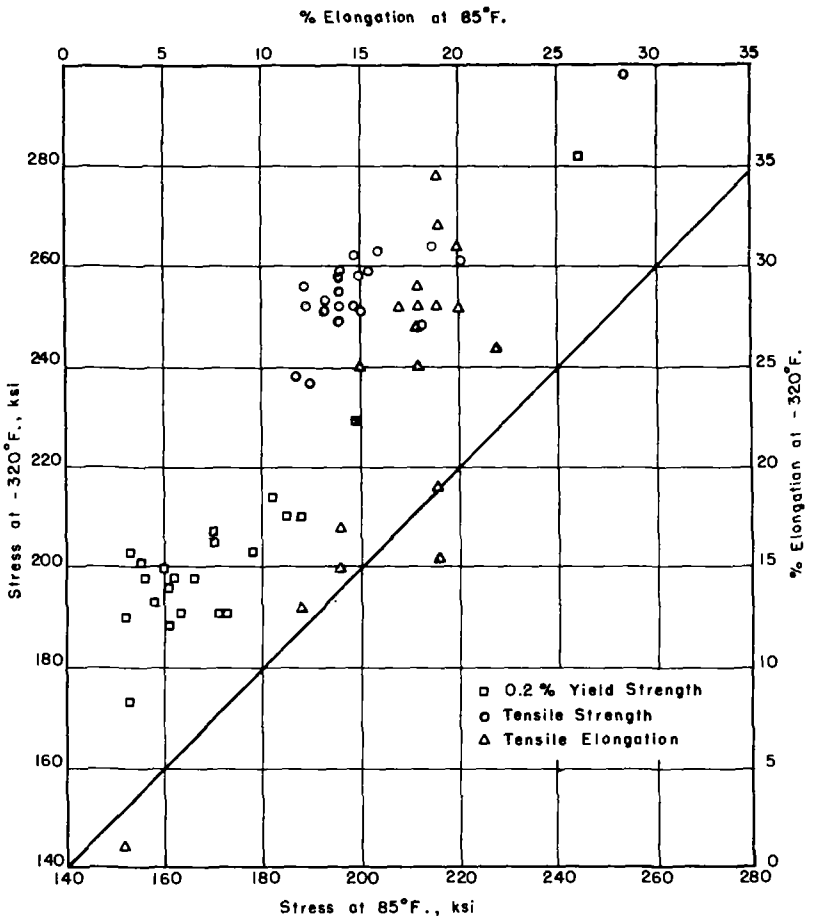


FIG. 27—Correlation of Tensile Data at Room Temperature and at −320 F. (Since the 45 deg line indicates equivalent properties at 85 F and at −320 F, the graphs show higher tensile and yield strengths at −320 F).

aged, and cold rolled, annealed and aged specimens. The broken line represents equivalent properties at 85 F and −320 F. The higher yield and tensile strengths at −320 F are clearly indicated. The same trend also is evidenced for elongation.

SUMMARY AND CONCLUSIONS

The nature of Inconel alloy 718 has been explained through the determination and identification of its various phases. These phases are summarized as follows:

1. Five minor phases were identified in this study. They are: CbTi(CN), M_6C; Laves, A_2B; Ni_3Cb; and gamma prime, Ni_3 (CbTiAl).

2. The M_6C phase was present at all columbium levels tested (3.32 to 8.98 per cent) and appeared to go into solution at approximately 1700 F. It is a nickel-columbium rich carbide.

3. The Laves phase is a nickel-columbium rich phase occurring at columbium levels of 4.42 per cent and above and at temperatures from 1300 to 1900 F. Two specimens, 5.44 and 7.01 per cent columbium, were also tested at 2000 and 2100 F; the Laves phase was not found with 5.44 per cent columbium but was found with 7.01 per cent columbium at both 2000 and 2100 F. These were the only two heats available for test above 1900 F.

4. The Ni_3Cb orthorhombic phase also appeared at columbium levels of 4.42 per cent and above, and went into solution at approximately 1800 F.

5. The gamma prime phase was the metastable face centered cubic form of Ni_3Cb. It was not found at temperatures above 1600 F.

6. The CbTi(CN) phase appeared in all specimens of this study.

7. As good a combination of mechanical properties can be obtained with a lower total of gamma prime forming elements if the aluminum content is maintained in the range 0.2 to 0.6 per cent rather than the usual 0.4 to 0.8 per cent.

8. Mechanical property statistics in accord with recent production practices and specifications have been presented representative of the alloys properties from −320 to 1300 F.

Acknowledgments:

The author wishes to express his appreciation to E. L. Raymond for conducting X-ray diffraction analysis and the identification of phases and to W. R. Shawver for handling computer programming and regression analysis of data.

REFERENCES

(1) W. Betteridge, *The Nimonic Alloys*, Chapter 6, Edward Arnold Ltd., London, 1959, pp. 66–67.

(2) R. M. Brick, "Fundamental Principles Involved in Segregation in Alloys," *Transactions*, Am. Institute Mining, Metallurgical, and Petroleum Engrs., Vol. 161, 1945, p. 67.

(3) *Current Data Report Inconel 718 Age Hardenable Nickel-Chromium Alloy*, Huntington Alloy Products Div., The International Nickel Co., Huntington, W. Va., May, 1961.

(4) M. Ezekiel and K. A. Fox, *Methods of Correlation and Regression Analysis—Linear and Curvilinear*, John Wiley and Sons, Inc., New York, N.Y., 3rd Edition.

SUPPLEMENTARY BIBLIOGRAPHY

(5) *Supplementary Data Report Inconel Age Hardenable Nickel-Chromium Alloy 718*, Huntington Alloy Products Div., The International Nickel Co., Huntington, W. Va., September, 1962.

(6) J. F. Barker, "A Superalloy for Medium Temperatures," *Metal Progress*, May, 1962, pp. 72–76.

(7) M. Kaufman and A. E. Palty, "The Phase Structure of Inconel 718 and 702 Alloys," *Transactions*, Am. Institute Mining, Metallurgical, and Petroleum Engrs., December, 1961, p. 1253.

(8) M. A. Tiner and J. E. Fischler, "A Study of Mechanical Behavior of Inconel 718 Alloy for Design of a Glide Vehicle," *Proceedings*, Am. Soc. Testing Mats., Vol. 60, 1960.

(9) J. Dubue and G. Welter, "Compression and Buckling Characteristics of Annealed and Aged Inconel 718 Nickel-Chromium Alloy at Temperatures up to 1400 F," *ASTM Preprint 8lb*, Am. Soc. Testing Mats., 1961.

(10) S. Weiss, W. P. Hughes, and H. J. Macke, "Welding Evaluation of High Temperature Sheet Materials by Restrained Patch Testing," *Welding Journal-Welding Research Supplement*, January, 1962, p. 17S.

DISCUSSION

R. C. HALL[1]—In addition to silicon, what is the effect of manganese on the hot workability and mechanical properties of Inconel 718?

H. L. EISELSTEIN (*author*)—The manganese contents of all compositions investigated have been kept below 1 per cent. No correlation of any property with manganese has been detected. Our experience with silicon was different. Our one and only attempt to make an alloy with 1 per cent silicion broke up during forging. We never tried this much silicon again and were more careful in forging those with somewhat lesser amounts. Besides having an adverse effect on hot malleability, silicon also reduces stress rupture properties. Shown in the following table are data at 1200 F and 100,000 psi on material aged at 1325 F/16 hr. The test material was $\frac{9}{16}$-in.-square forgings made from small laboratory air induction melts.

Annealing Treatment	Rupture Life at 1200 F/100,000 psi, hr[a]	
	0.2% Si	0.8% Si
1700 F/1 hr	22.4 to 23.2 (47.7 to 99.8)	15.4 to 18.1 (37.0 to 81.0)
1800 F/1 hr	86.8 to 103.1 (200.3 to 237.7)	30.8 to 33.2 (40.4 to 103.2)

[a] Notch bar values are shown in parentheses.

J. F. BARKER[2] (*presented in written form*)—The author is to be commended for his excellent paper describing the metallurgy of Inconel 718. We at General Electric feel that the development of Inconel 718 was one of the more significant advances in high temperature metallurgy made in the last 10 years. The good welding characteristics of Inconel 718 is enabling the design of engine structures heretofore impossible. As a user of Inconel 718, we are appreciative of the wealth of experimentation and testing that went into the development and release of the alloy. This minimizes part of the risk involved in using a new material.

Prior to using Inconel 718 at General Electric, we have put the alloy through some fairly rigorous tests. These tests primarily relate to the weldability of sheet. The data we have generated collaborates that reported by Mr. Eiselstein concerning aging response. We believe that the key to Inconel 718's resistance to strain age cracking after welding is its slow response to aging. The principal benefit is that weld restraint is kept at a minimum so that the stresses are never built up to a level to cause failure by cracking. The low restraint is attributed to the following:

1. *Low annealed yield strength*—Sluggish aging rate results in lower annealed yield strength. Residual welding stresses are limited by the yield strength.

2. *As-welded weld heat-affected zones ductile*—Slow aging rate prevents heat affected zone from aging due to the heat generated by welding.

3. *Welds capable of being stress relieved before aging occurs*—Data illustrating the sluggishness of Inconel 718 compared with other super alloys are shown in Fig. 28. Here, after the first 20 sec of aging at 1400 F, René 41 increases in hardness by 8 Rc points while Inconel 718 is unchanged. After 1 min, René 41 has aged 11 Rc points and Inconel 718 has still not changed. The spread in hardness between René 41 and Inconel 718 is 12 Rc points after 3 min. The gap between the two eventually closes after about 13 min of aging. The significance of this data is that restrained Inconel 718 weldments can be heated through the embrittling aging temperature range more slowly and safely than conventional precipitation hardening alloys such as René 41. Some of the more complex René 41 fabrications cannot be heated rapidly enough to avoid strain age cracking in the embrittling range because of differential heating rates caused by mass effects and self-shielding occurring in the part.

In regard to carbide films, Figs. 10–12 of the paper show that a grain boundary carbide film forms upon aging after solution treatments of 2100 and 1900 F but not after 1700 F. This is consistent with what has been observed in other alloys such as A-286, V57, and René 41. That is, high temperature solution treatments partially dissolve matrix and other globular carbides and these re-precipitate as thin films upon aging at lower temperatures.

In conclusion, I would like to congratulate Mr. Eiselstein and The International Nickel Co. on their fine development work, and I want to thank them for asking General Electric to comment on the work reported.

MR. EISELSTEIN—I wish to thank J. F. Barker for his comments on weldability. The paper treats this important problem all too briefly.

H. J. WAGNER[3] (*presented in written form*)—Mr. Eiselstein has made an important contribution to the understanding of the metallurgical factors that affect the strength of Inconel alloy 718. His referencing of the paper by Kaufman and Palty (Ref. 7) and the article by Barker (Ref. 6) invites comparison with these works, and differences appear between the current and this past work that raise serious questions.

For example, Kaufman stated that the major hardening phase is orthorhombic Ni_3Cb. The present paper calls γ', that is, FCC $Ni_3(CbAlTi)$ "the most important constituent." Barker went further, agreeing that columbium-containing γ' is the strengthening phase and stating that "the Ni_3Cb phase is noncoherent with the matrix [and therefore] contributes little to the strength of the alloy." One apparent answer to the differences is brought out, namely that the metastable FCC γ' transforms to the stable orthorhombic Ni_3Cb above about 1400 F. Since Kaufman's work involved aging times of 100 hr at 1300, 1400, and 1500 F (shorter times at higher temperatures), it might be reasoned that he examined the specimens in the "overaged" condition. This paper, however, regards as anamolous the observation that hardness is maintained even after 100 hr aging at 1450 F. Can we assume that strengthening in the overaged material is by orthorhombic Ni_3Cb, or is it by interaction of other phases?

Another question surrounds the existence and composition of the Laves A_2B phase. Kaufman refers to this phase as $Fe_2(TiCb)$ and says that it occurs in sheet

[1] Research and development, Universal-Cyclops Steel Corp., Bridgeville, Pa.

[2] Advanced alloy evaluation, General Electric Co., Flight Propulsion Div., Cincinnati, Ohio.

[3] Battelle Memorial Institute, Columbus, Ohio.

material after long exposures, or high solution temperatures. Barker refers to M_2(TiCbMo) Laves phase, but says that it occurs only in castings. This paper describes the phase as high in columbium, molybdenum, and nickel with smaller quantities of iron, chromium, and titanium, based on X-ray fluorescence analysis of the separated "freckled" regions. The phase was observed in large forged rounds where some cast substructure remained. Evidently it forms preferentially at interdendritic areas where the columbium concentration has increased during the solidification process. Mr. Eiselstein's pseudobinary diagram of Base 718 and Laves phase shows the relationship very clearly.

Finally, it is surprising that no chromium or molybdenum were detected in the $(NiCb)_6C$, and that evidently the formation of any chromium carbides was completely surpressed. Kaufman found Cr_7C_3, but suggested that a high solutioning temperature (2250 F) may have aided its formation. It appears that, at the low carbon level, columbium effectively ties up the available carbon as CbC (with dissolved titanium and nitrogen).

MR. EISELSTEIN—I suppose Kaufman and Palty missed the gamma prime particles because they were too fine for their filter or collection technique. We had that problem. I agree with Barker; the gamma prime is coherent with the matrix and the Ni_3Cb phase contributes little to the strength of the alloy. Recent studies by a combination of thin foil electron microscopy and X-ray diffraction have shown the gamma prime is actually body centered tetragonal and definitely coherent with the matrix. A possible explanation as to why the alloy does not show severe signs of overaging at 1450 F may be the precipitation of Laves particles at just the right rate to compensate for the gamma prime to Ni_3Cb transformation. At any rate all three phases are present at 145 F and 100 hr. Unfortunately I have been unable to measure their three separate effects in this alloy.

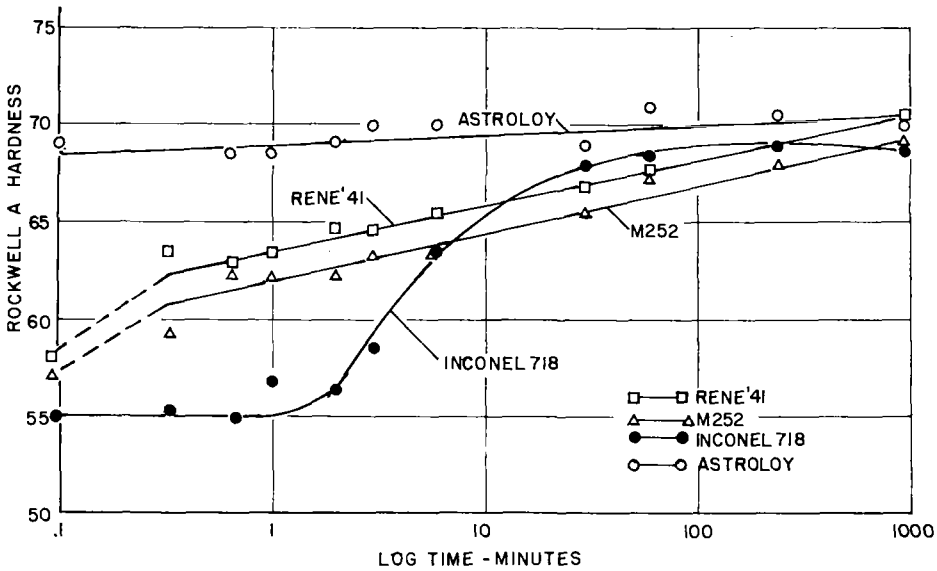


FIG. 28—Hardness Versus Aging Time at 1400 F for René 41, M252 and Inconel 718 Sheet.

The Laves phase does preferentially form in interdendritic areas. To prevent my agreement with this remark being misleading to others, I want to point out that Laves particles will also precipitate out from a homogenous solid solution with the appropriate heat treatment.

Presumably the molybdenum content of 3 per cent in Inconel alloy 718 is too low to make its presence noticed in the carbides. Inconel alloy 625 is similar in many respects to Inconel 718 but contains 9 per cent molybdenum, about 4 per cent columbium, and 22 per cent chromium. The carbides in Inconel alloy 625 are more to Wagner's (and my) expectations. The M_6C does contain molybdenum and when solution treated at 2200 F (close to Kaufman and Palty's 2250 F) can form $M_{23}C_6$ in minor quantities. Not enough $M_{23}C_6$ has been collected for chemical analysis of chromium and other elements.

MR. EISELSTEIN (*author's closure*)—I wish to thank the discussers for their comments and interest shown in the paper. Development work is still going on. Interesting results are being obtained in our efforts to produce notch ductility using high solution temperatures. Figure 22 shows notch ductility decreasing rapidly for solution treatments above 1800 F for 1 hr. New heat treatments show promise of producing notch ductility in material solution treated at 1950 F for 1 hr, thereby combining notch ductility with the superior tensile ductility shown in Fig. 24.

PROPERTIES OF 12 PER CENT CHROMIUM ALLOYS MODIFIED WITH SMALL COLUMBIUM ADDITIONS

By H. Tanczyn[1]

Synopsis

A nominal addition of 0.15 per cent columbium to a heat-hardenable 12 per cent chromium stainless steel (Type 410) is without effect on the general corrosion resistance and quenched hardness of this material. The columbium addition produces a refinement in grain size, a reduced susceptibility to temper embrittlement, a mild improvement in resistance to stress-corrosion cracking, a marked improvement in control of tempered hardness, and an increase in the elevated-temperature mechanical strength of the 12 per cent chromium stainless steel.

The commercial utility of the nominal 12 per cent chromium stainless steel received recognition about fifty years ago (1).[2] In the intervening years, numerous modifications of the 12 per cent chromium stainless steel have been tailored for specific applications with as many as twelve modifications listed in 1958 (2). The characteristics of these alloys as typified by AISI Type 410, have been utilized in a myriad of industrial applications. Among these characteristics are a broad range of attainable mechanical strength, good damping capacity, resistance to chemical, heat, and mechanical erosion, and fabricability by numerous practicable procedures. Briefly, the 12 per cent chromium stainless steel has weathered the tests of extensive commercial production and application (3).

In common with other materials, the useful characteristics of Type 410 stainless steel find company with certain drawbacks which are of commercial importance. These include susceptibility to temper embrittlement and lowered corrosion resistance with specific heat treatments, sensitivity to time-temperature variations on tempering in the range 950 to 1100 F, susceptibility to stress corrosion cracking, and a relatively high degree of air-hardenability in welding (4,5). Efforts aimed at overcoming these deficiencies without sacrifice of the desirable characteristics of this material have yielded limited success.

This paper presents results of a development program which disclosed that a minor addition of columbium to 12 per cent chromium stainless steel produced a desirable combination of properties without sacrifice of its basic characteristics (5,6).

Materials:

The materials tested in this program were obtained from commercial electric furnace heats of this alloy. The chemical compositions are listed in Tables 1–5. For comparison purposes, information on regular Type 410 stainless steel is included with that for the columbium-modified Type 410 material.

Hardening Characteristics:

Type 410 stainless steel is characterized by a capability of being hardened to a quenched hardness of about Brinell 390 to 430 (Rc 39 to 44). The quenched hardness varies directly with soluble carbon content (4). Information in Table 1 shows that the addition of 0.15 per cent columbium did not alter the normal quenched hardness of Type 410 stainless steel.

Temperability:

Heat-hardened stainless steels are reheated usually to obtain an acceptable compromise between hardness, toughness, stability, and other specific requirements. Reheating of the hardened Type 410 Cb within the temperature range 300 to 900 F yielded hardness values similar to those obtained with the regular Type 410. With reheating temperatures in the range 950 to 1400 F, however, Type 410 Cb material retained higher hardness levels than the counterpart straight chromium stainless steel. The master tempering curves, Fig. 1, interrelate the effects of time and temperature to permit the expression of both factors in a single tempering parameter (7). The master tempering curves indicate that the rate of change of hardness for Type 410, in tempering, is reduced by a minor addition of columbium. The tempering characteristics of the 12 per cent chromium stainless steels are illustrated in a second manner in Fig. 2. Type 410 Cb exhibits a graduated series of hardness plateaus on tempering in the range 950 to 1300 F. This condition is compared to a marked sensitivity of regular Type 410 to time-temperature effects, particularly in the range 1000 to 1150 F. The engineering aspects of the tempering characteristics shown for the 12 per cent chromium-columbium stainless steel can be found in these features:

1. In tempering, close control of hardness level and marked uniformity of hardness are developed.

2. For a specific hardness, within a broad range of Rc 24 to 38, the required tempering temperature for Type 410 Cb will be higher than that applicable for regular Type 410.

In regard to the first feature, commercial heat treating shops and in-plant heat treating departments have encountered difficulty in producing regular Type 410 items uniformly to specified hardness levels in the Rc 25 to 35 range by tempering treatments. The tempering characteristics of Type 410 Cb can be used to advantage in this situation to yield close control of hardness and to produce a uniformity of hardness.

The applicability of a comparatively high tempering temperature for hardness levels within the range of Rc 20 to 32 is useful from the standpoint of improved relief of internal mechanical stresses and for dimensional stability in Type 410 Cb products.

The tempering of martensitic alloy steels and stainless steels has received a great deal of study (8–14). Reheating of regular Type 410 in the as-hardened condition at temperatures up to 700 F produces a partial relief of internal stresses and induces the appearance of an M_3C-type carbide (M denotes the metallic component). Hardness measurements

[1] Senior research engineer, research and technology, Armco Steel Corp., Baltimore, Md.

[2] The boldface numbers in parentheses refer to the list of references appended to this paper.

Copyright© 1965 by ASTM International

www.astm.org

TABLE 1—QUENCHED HARDNESS DATA.

Material	Chemical Composition, per cent								Quenched Hardness Range, Rc[a] [b]
	C	Mn	P	S	Si	Cr	Ni	Cb	
410.....	0.11	0.40	0.013	0.017	0.29	11.89	0.21	<0.005	41 to 43
410.....	0.12	0.45	0.014	0.018	0.23	11.97	0.20	<0.005	42 to 44
410 Cb...	0.12	0.50	0.015	0.015	0.30	12.08	0.23	0.15	42 to 44
410 Cb...	0.12	0.58	0.013	0.014	0.33	11.79	0.26	0.19	42 to 44
410 Cb...	0.13	0.43	0.011	0.019	0.20	11.67	0.16	0.10	43 to 44

[a] Hardening treatment: 1800 F, oil quenched.
[b] Specimen sizes: 1 in. square by 6 in.; 2 in. square by 6 in.; 4 in. square by 6 in.

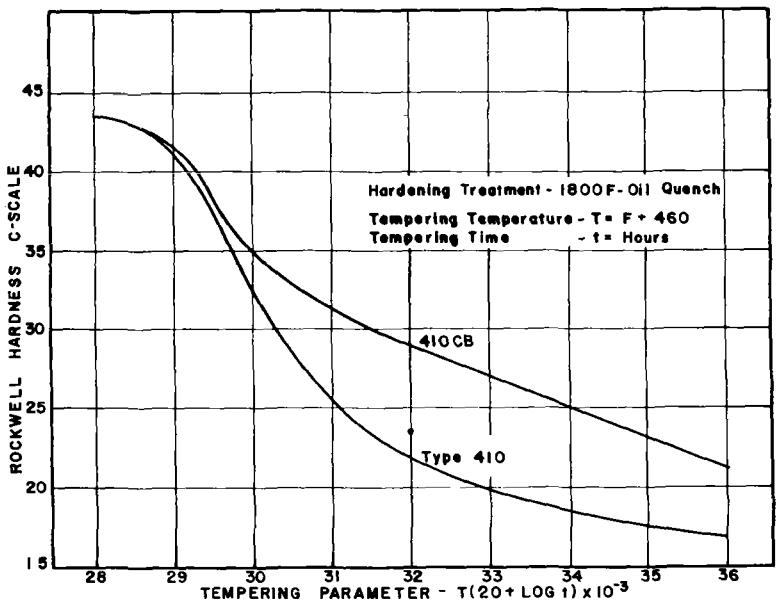


FIG. 1—Master Tempering Curves for Types 410 and 410 Cb Stainless Steels.

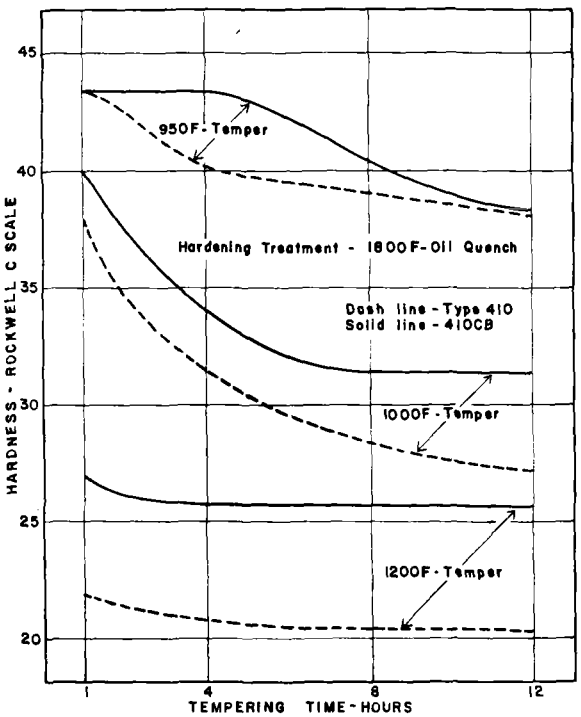


FIG. 2—Tempering Characteristics of Types 410 and 410 Cb Stainless Steels.

show that a slight drop in hardness from the as-hardened level occurs on reheating up to 700 F.

Tempering of the regular Type 410 in the range 700 to 1000 F produces a change from the M_3C-type carbide to the M_7C_3-type and $M_{23}C_6$-type carbides by a process of assimilation of the M_3C carbide into the matrix and the formation of new M_7C_3 and $M_{23}C_6$ carbides. This stage of tempering in regular Type 410 is accompanied by a modest degree of secondary hardening, a notable loss of notch-impact toughness, and an increase in chemical corrosion rates. The appearance of the M_7C_3 carbide is accompanied by an increase in the chromium content of the carbide and, thereby, results in some local chromium depletion.

With tempering treatments higher than 1000 F, a progressive decrease in the proportion of M_7C_3 carbide and an accompanying increase in the $M_{23}C_6$ carbide are developed. Gradual agglomeration of carbides occurs along with rapid loss of hardness as the tempering temperature approaches the annealing range at 1400 F. The role of columbium in altering the tempering characteristics of Type 410 is considered to result, principally, from an effect on nucleation of the alloy carbide, $M_{23}C_6$, and on restraining the growth or coalescence of the alloy carbide. To a minor degree, the columbium can occur as a separate columbium-rich carbide. On the assumption that the secondary hardening cited for regular Type 410 is linked to the presence of a coherent carbide precipitate, then columbium atoms in solid solution with the precipitate could intensify the coherency stress (9). Such an effect would be expected to shift the temperature or time or both for the occurrence of the peak in secondary hardening. Once the secondary hardening reaction is passed, the tempering characteristics of regular Type 410 are affected by the rate of coarsening of the $M_{23}C_6$ carbide. In this regard, the columbium can reduce the coalescence of the alloy carbide and, by maintaining a dispersion of carbides, can lower the rate of softening of Type 410. Finally, some support for the occurrence of a separate columbium-rich carbide in Type 410 Cb stainless steel is offered later.

Grain Size:

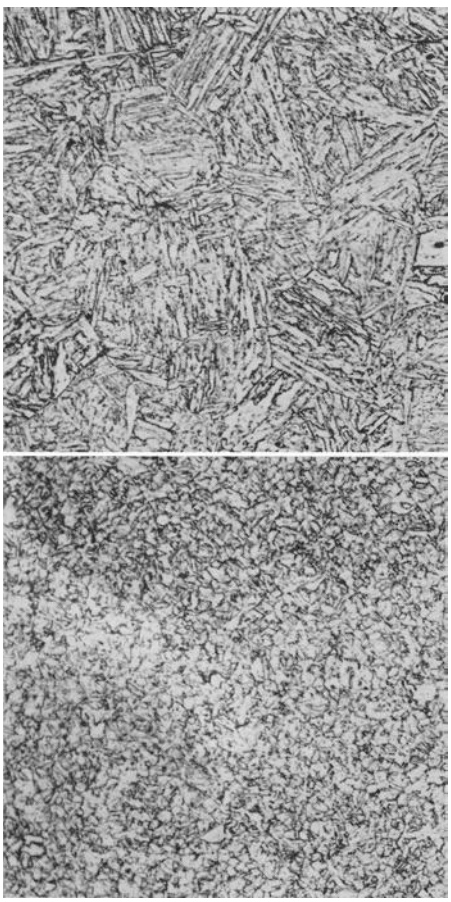
A small addition of columbium to Type 410 produces a marked refinement in its grain structure. This effect is evident in

TABLE 2—VARIATION IN GRAIN SIZE WITH TEMPERATURE OF HEATING.

Material	Chemical Composition, per cent[a] [b]							
	C	Mn	P	S	Si	Cr	Ni	Cb
410	0.11	0.40	0.013	0.017	0.29	11.89	0.21	<0.005
410	0.12	0.45	0.014	0.018	0.23	11.97	0.20	<0.005
410 Cb	0.13	0.43	0.011	0.019	0.20	11.67	0.16	0.10
410 Cb	0.12	0.50	0.015	0.015	0.30	12.08	0.23	0.15

Heating Temperature, deg F[c]	ASTM Grain Size Class (100 ×)	
	410	410 Cb
1700	6	8 to 9
1800	5	8
1900	4 to 5	8
2000	4	7 to 8

[a] Bar section: 1½ in. round.
[b] Delta ferrite: none.
[c] Time at heating temperature: 1 hr.



(*top*) Type 410—Hardened, 1800 F, oil quenched; tempered, 1400 F, 4 hr, air cooled; etchant, hydrochloric acid, picric acid in ethyl alcohol.

(*bottom*) Type 410 Cb—Hardened, 1800 F, oil quenched; tempered, 1400 F 4 hr, air cooled; etchant, hydrochloric acid, picric acid in ethyl alcohol.

FIG. 3—Structures and Grain Size for Types 410 and 410 Cb Stainless Steels (×250).

the grain size measurements presented in Table 2.

Regular Type 410 exhibited ASTM grain size from Class 6 when heated at 1700 F and to a Class 4 after heating at 2000 F. With similar heat treatments, Type 410 Cb exhibited grain sizes from Class 8.5 to Class 7.5, respectively. The comparative grain structures for Type 410, with and without a minor addition of columbium, are illustrated in Fig. 3. The microstructures are representative of the hardened and tempered conditions. The photomicrographs show that the comparatively smaller grain size, inherent for Type 410 Cb in the as-hardened condition, is retained after tempering treatments at temperatures up to 1400 F. As indicated heretofore, a minor addition of columbium to Type 410 is considered to produce a small proportion of a columbium-rich carbide. The grain refinement exhibited by Type 410 Cb results, most likely, from the effects of dispersion of columbium-rich carbides which constitute a mechanical barrier to grain growth after recrystallization. This obstructive quality of the columbium-rich carbides is developed from their relative insolubility in a Type 410 matrix.

ROOM-TEMPERATURE MECHANICAL PROPERTIES

The several aspects of Type 410 Cb considered above have some bearing on the strength and toughness of this material. Results of room-temperature tension, hardness, and Charpy V-notch impact tests are reported in Table 3 for sections hardened from 1850 F and, thereafter, tempered at temperatures ranging from 500 to 1400 F. Some of these data are charted in Fig. 4. The tensile properties of regular Type 410 and Type 410 Cb, after stress-relieving treat-

TABLE 3—ROOM-TEMPERATURE MECHANICAL PROPERTIES.

Material	Chemical Composition, per cent							
	C	Mn	P	S	Si	Cr	Ni	Cb
410	0.12	0.45	0.014	0.018	0.23	11.97	0.20	<0.005
410	0.13	0.56	0.010	0.016	0.40	12.20	0.16	<0.005
410	0.12	0.48	0.015	0.016	0.20	11.82	0.27	<0.005
410 Cb	0.12	0.51	0.012	0.020	0.31	12.01	0.19	0.14
410 Cb	0.12	0.56	0.008	0.017	0.31	11.95	0.15	0.15
410 Cb	0.13	0.43	0.011	0.019	0.20	11.67	0.16	0.10

Stress Relief or Temper, deg F[b] [c]	Material	Ultimate Tensile Strength, 1000 psi	0.2% Yield Strength, 1000 psi	Elongation in 2 in., %	Reduction of Area, %	Rockwell Hardness	Charpy Impact V-Notch, ft-lb
500	410 Cb	195	161	16	61	C 43	50
	410	190	155	16	60	C 43	40
700	410 Cb	194	162	16	61	C 43	55
	410	185	152	16	61	C 41	45
900	410 Cb	199	156	18	60	C 43	30
	410	189	148	17	59	C 42	15
1000	410 Cb	157	138	18	64	C 34	37
	410	146	131	18	61	C 28	20
1100	410 Cb	137	121	19	64	C 28	68
	410	122	104	19	63	C 24	45
1200	410 Cb	125	109	20	65	C 25	95
	410	109	90	21	65	C 20	90
1300	410 Cb	114	94	22	69	C 22	110
	410	100	81	24	69	B 97	110
1400	410 Cb	101	79	26	72	B 99	110
	410	90	64	27	73	B 92	110

[a] Bar section: 1 in. round.
[b] Hardening treatment: 1850 F, oil quenched.
[c] Stress-relief or tempering treatment: 4 hr, air cooled.
NOTE—Values for mechanical properties are averages for specimens from three heats of each material.

ments at 500 and 700 F are similar. With comparable tempering treatments from 900 to 1400 F, Type 410 Cb exhibits consistently higher ultimate tensile strengths, 0.2 per cent yield strengths, and hardness levels than the regular Type 410. This relationship is consistent with the greater resistance to softening, under tempering treatments, cited for the Type 410 Cb.

The tensile properties of Type 410 and Type 410 Cb after various tempering treatments are compared in Table 3. For any given tempering temperature within the range 1000 to 1300 F, Type 410 Cb developed ultimate tensile strengths which ranged from about 10,000 to 15,000 psi greater than for the regular Type 410. Similarly, the differentials in 0.2 per cent yield strength ranged from 7000 to 15,000 psi, Type 410 Cb exhibiting the higher strengths. With a further comparison of the information in Table 3, a specified ultimate tensile strength is obtained in Type 410 Cb with a tempering treatment which ranges from about 50 to 135 F higher than that applicable to regular Type 410.

In a prior section of this presentation reference was made to a measurable loss of notch-impact toughness in regular Type 410 on tempering within the range 800 to 1000 F. The Charpy V-notch impact test data listed in Table 3 and plotted in Fig. 4 indicate the extent of this embrittlement in regular and modified Type 410. The data curves in Fig. 4 indicate that the Charpy V-notch impact strengths are not affected adversely with reheating up to 700 F. Tempering treatments at 900 to 1000 F produce a trough pattern for the impact strength values. With tempering treatments higher than 1000 F, the recovery of toughness in Type 410 Cb precedes that in regular Type 410.

The temper brittleness indicated for regular and modified Type 410 has its counterpart in plain carbon steels and in low alloy steels (15). The metallographic examination of temper-embrittled Type 410 impact test specimens has indicated an abnormal susceptibility of the grain boundaries to attack by chemical etchants, particularly a hydrochloric acid-picric acid-ethyl alcohol solution. No discrete intergranular precipitates were detected. The theory that temper embrittlement is associated with segregation of certain elements to the grain boundaries of alloy steels (16) appears to explain the observation noted in this work. The Charpy V-notch impact contours in Fig. 4 indicate that Type 410 Cb exhibits a higher level of notch-impact strength in the trough region and a more rapid rate of recovery of toughness, with tempering temperatures above 900 F, than the regular Type 410. These characteristics are associated with the comparatively small grain size of Type 410 Cb whereby, in consideration of the MacLean-Northcutt theory, segregation of a given content of elements is accommodated on a greater grain boundary area than for Type 410. Thus, in Type 410 Cb a specific total volume of segregate should be "thinned out." Metallographic observations of hardened and tempered sections disclose that, after tempering within the range 900 to 1100 F, Type 410 Cb, after chemical etching, exhibits a short, discontinuous grain boundary chemical attack. Actually, in Type 410 Cb sections reheated at 900 F to develop temper embrittlement a preferential grain boundary attack was not resolved clearly. Test sections tempered at 1000 and 1100 F with substantial recovery of toughness exhibited the localized chemical attack. With similar treatments, the regular Type 410 displayed more of a continuous grain boundary chemical attack after tempering at 1000 or 1100 F.

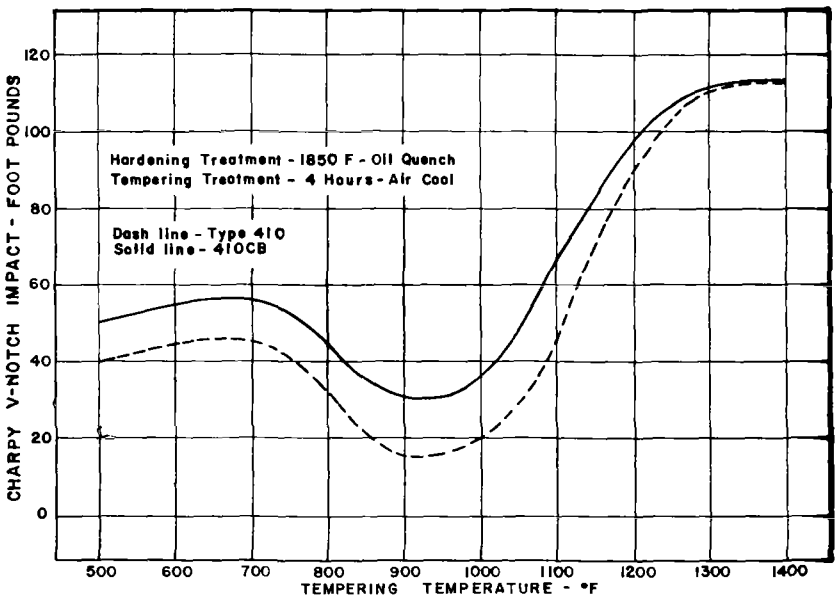


FIG. 4—Notch Impact Strengths of Types 410 and 410 Cb Stainless Steels.

CORROSION RESISTANCE

The corrosion resistance of Type 410 Cb in a variety of media was examined by routine laboratory tests and atmospheric exposure tests. Immersion test specimens were machined to 0.750-in. round by 0.750-in. long sections. Salt fog specimens were of a standard cone section. Prior to testing, all specimens were cleaned in trichloroethylene and passivated in 20 per cent nitric acid and 2 per cent sodium dichromate for 20 min at 120 F. All boiling temperature, 80 and 35 C tests were carried out with one specimen per flask and with 500 ml of solution. Immersion tests were divided into five 48-hr test periods. With excessively high corrosion rates, the tests were terminated after one or two periods. Conversely, with very low corrosion rates, the final three periods were carried out with purposeful activation. A number of corrosion tests produced active and passive periods. For this condition, only the active corrosion rates were considered. Specimen blanks were hardened from 1800 F and stress-relieved or tempered within the range 500 to 1200 F.

Corrosion tests for 60-day periods in running tap water or in 100 per cent relative humidity atmosphere at 120 F produced no visible discoloration of regular or modified Type 410. Outdoor exposure in an industrial atmosphere for a nine-month period produced no notable deterioration. Tests in a number of solutions of sulphuric acid and hydrochloric acid produced high corrosion rates of an extent to preclude delineation of any trends. In phosphoric acid and formic acid solutions, corrosion rates were very erratic, being developed with active and passive periods, and, again, no distinctive trends were obtained. Exposure to 5 per cent salt fog for 24 hr disclosed that the two steels were of equal resistance and indicated, also, that tempering treat-

ments from 1000 to 1200 F furthered a modest increase in weight losses compared to those obtained for similar specimens tempered within the range 500 to 900 F.

In nitric acid and acetic acid solutions, the two steels exhibited similar corrosion rates in which a marked increase was noted for test specimens tempered within the range 1000 to 1200 F. This variation of corrosion rates with tempering temperature in the 12 per cent chromium stainless steel is related to depletion of some chromium from the matrix by formation of stable chromium carbides (4). Strict evaluation of materials on the basis of laboratory corrosion tests, involving some accelerated form of testing, is understandably difficult. However, for the subject material, the results of laboratory tests and some varied service performance indicate that a minor addition of columbium is neutral insofar as affecting the general corrosion resistance of Type 410 stainless steel.

TABLE 4—EFFECT OF HEAT TREATMENT ON STRESS-CORROSION RESISTANCE OF TYPES 410 AND 410 Cb.

Material	C	Mn	P	S	Si	Cr	Ni	Cb
	Chemical Composition, per cent[a]							
410	0.12	0.46	0.016	0.016	0.24	12.02	0.24	<0.005
410 Cb	0.13	0.43	0.011	0.019	0.20	11.67	0.16	0.10

Material	Tempering Temperature, deg F	Applied Tensile Stress, 1000 psi	Time for Fracture, hr: 6% Sodium Chloride, ½% Acetic Acid, Hydrogen Sulphide	Time for Fracture, hr: Boiling 42% Magnesium Chloride
410	300	101	0.8 - 0.6 - 1.1 - 1.0	...
410 Cb	300	102	1.7 - 2.5 - 2.3 - 2.2	...
410	600	89	2.0 - 3.4 - 3.6 - 2.1	451.2 - 227.5
410 Cb	600	99	1.0 - 2.4 - 2.4 - 1.9	N.B.[b]
410	800	98	0.6 - 1.5 - 1.0 - 1.1	241.4 - 100.6
410 Cb	800	103	1.7 - 4.7 - 2.0 - 2.0	829.5 - 96.3
410	850	110	0.9 - 0.9 - 1.2 - 0.9	23.6
410 Cb	850	110	2.0 - 2.4 - 1.4 - 2.4	39.8
410	875	108	0.4 - 0.9 - 0.6 - 0.4	13.9
410 Cb	875	110	0.8 - 1.6 - 1.3 - 1.3	53.5
410	900	92	0.8 - 0.4 - 0.9 - 1.3	21.8
410 Cb	900	97	2.2 - 1.5 - 4.4 - 1.8	48.5
410	925	102	1.5 - 0.9 - 0.75 - 1.4	83.9
410 Cb	925	102	2.6 - 3.0 - 2.6 - 2.6	137.4
410	950	98	1.9 - 1.6 - 1.2 - 1.1	74.2
410 Cb	950	102	2.4 - 2.4 - 2.8 - 2.6	421.4
410	975	94	0.4 - 0.8 - 0.3 - 0.9	N.B.
410 Cb	975	98	1.5 - 1.8 - 2.7	929.8
410	1000	84	1.9 - 1.1 - 1.3 - 1.0	297.8
410 Cb	1000	92	1.1 - 1.3 - 1.4 - 1.1	225.2
410	1025	84	2.6 - 1.7 - 2.3 - 2.1	N.B.
410 Cb	1025	92	2.0 - 2.9 - 2.0 - 1.9	N.B.
410	1050	76	2.8 - 5.5 - 3.4 - 21.9	466.6 - 857.2
410 Cb	1050	86	3.7 - 7.2 - 7.1 - 34.7	N.B.
410	1100	69	11.7 - 16.3 - 6.4 - 23.2	...
410 Cb	1100	81	...	...
410	1125	65	...	...
410 Cb	1125	80	27.5 - 17.0 - 7.5 - 8.5	...

[a] Bar section: ⅜ in. round.
[b] N.B. = no break at 1000 hr, test discontinued.

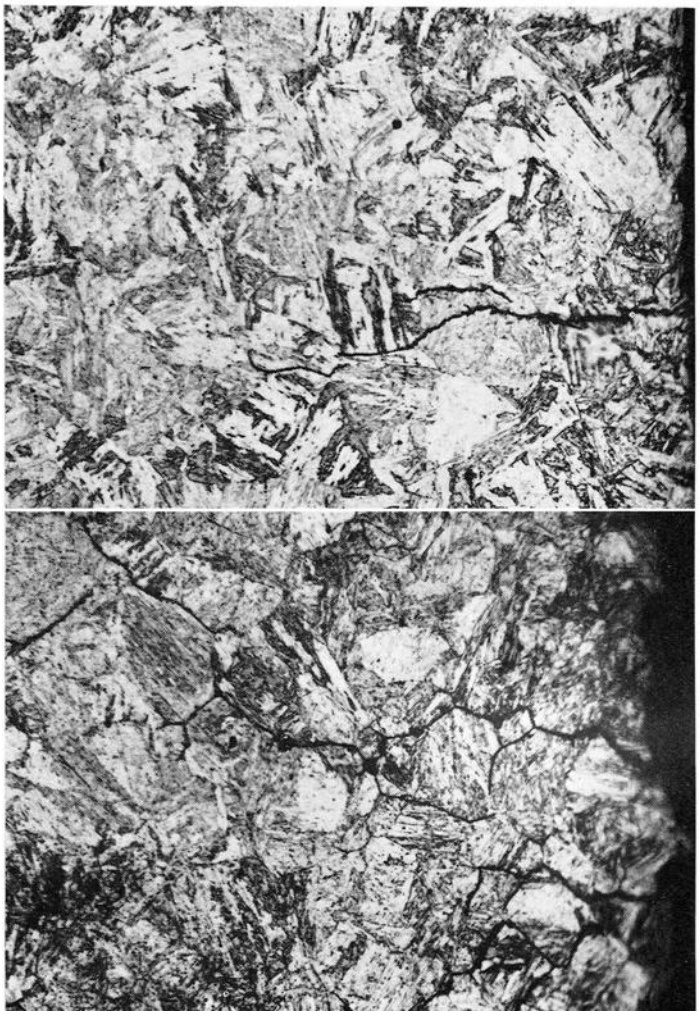
Stress-Corrosion Cracking

Along with other metal systems, the 12 per cent chromium stainless steel is subject to stress-corrosion cracking, the result of a combined action of tensile stress and corrosion effects (17). The occurrence of stress-corrosion cracking in components of industrial equipment is a limiting factor, often, to full and proper utilization of the potential utility of the materials of construction. In applications of the 12 per cent chromium stainless steels, resistance to stress-corrosion cracking is reported to be improved significantly with heat treatments which produce a hardness level of Rc 30 or lower. In the present work, stress corrosion tests on Types 410 and 410 Cb were carried out with equipment wherein a direct tensile stress is applied to a test specimen by dead-weight loading through a simple lever system (18).

The stress level for each specimen was established at two-thirds of the 0.2 per cent tensile yield strength determined for each condition of heat treatment. After hardening from 1800 F, test specimens were tempered within the range 300 to 1125 F for 4 hr periods.

Stress-corrosion tests were completed in a 6 per cent sodium chloride and ½ per cent acetic acid solution, saturated with hydrogen sulphide at 80 F, and in a 42 per cent magnesium chloride solution at 309 F. The results of stress corrosion tests are shown in Table 4. The times for fracture in the 6 per cent sodium chloride, ½ per cent acetic acid, hydrogen sulphide solution ranged under 3 hr for regular and modified Type 410 specimens tempered from 300 to 1025 F. The average values for times to fracture, in the 300 to 1025 F temper range, ranged moderately higher for the modified material as compared to the respective values for the regular Type 410. A notably sharp increase in time for fracture in both materials developed with specimens tempered at 1050 F and higher, there being a four to sixfold increase in time to fracture. These results provide a pattern, similar to that described elsewhere, in which a strong susceptibility to stress-corrosion cracking exhibited by hardened Type 410, is reversed as tempering temperature is increased to produce a hardness level under Rc 32 (17,19).

The stress-corrosion tests carried out in boiling 42 per cent magnesium chloride solution produced a test pattern which differed from that described for tests in the 6 per cent sodium chloride, ½ per cent acetic acid, hydrogen sulphide solution. The results of tests in the boiling 42 per cent magnesium chloride solution could be divided into three zones. Specimens tempered at 600 and 800 F withstood fracture for time periods ranging from 96 to more than 1000 hr. Following this series of tests, the specimens of both materials, tempered at 850, 875, and 900 F, exhibited time periods of 14 to 54 hr for fracture. Finally, with temper

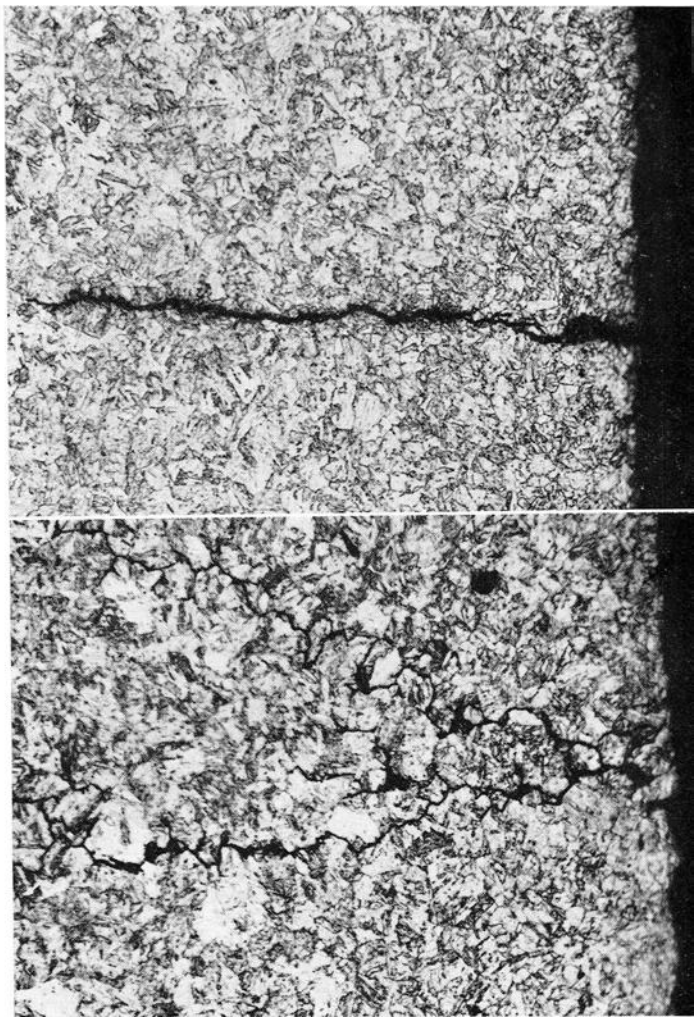


(*top*) Six per cent salt, one half per cent acetic acid, plus hydrogen ulfide.

(*bottom*) Forty-two per cent boiling magnesium chloride.

NOTE—Heat treatment, 1800 F, oil quenched plus 900 F, 4 hr, air ooled; etchant, hydrochloric acid, picric acid in ethyl alcohol.

FIG. 5—Typical Appearances of Stress-Corrosion Cracks in Type 410 tainless Steel (×250).



(*top*) Six per cent salt, one half per cent acetic acid, plus hydrogen sulfide.

(*bottom*) Forty-two per cent boiling magnesium chloride.

NOTE—Heat treatment, 1800 F, oil quenched, plus 900 F, 4 hr, air cooled; etchant, hydrochloric acid, picric acid in ethyl alcohol.

FIG. 6—Typical Appearances of Stress Corrosion Cracking in Type 410 Cb Stainless Steel (×250).

treatments within the range 950 to 1050 F, the time periods required for fractures were increased again within the range of 100 to more than 1000 hr.

The modes of failure for the two steels are illustrated in the photomicrographs of Figs. 5 and 6. For the tests in 6 per cent sodium chloride, ½ per cent acetic acid, hydrogen sulphide solution, the fractures were predominantly transgranular. In the tests with the boiling 42 per cent magnesium chloride solution, the fractures proceeded, for both materials, through grain boundaries.

The mechanisms which operate to produce stress-corrosion cracking in heat treated 12 per cent chromium stainless steel and other materials have not been resolved clearly. The role of hydrogen, diffusing into the Type 410 during corrosion, initiating or propagating internal fissures or cracks is a point in question. Metallographic examination of the specimens after fracture in the 6 per cent sodium chloride, ½ per cent acetic acid, hydrogen sulphide solution disclosed the presence of very short cracks normal to the direction of applied tensile stress. Occasionally, linking of several microcracks to form a single, longer crack was noted. These cracks were found in specimens for all heat treated conditions. The appearance of the fracture areas varied with the tempering treatment and hardness of each specimen. For specimens tempered at 300 to 1000 F, the fracture surfaces exhibited a cleavage-type separation with no visible deformation of grains. For specimens tempered at 1025 to 1125 F, the areas of fracture included a considerable degree of grain flow or deformation. In fact, the transverse microcracks were reoriented, in several observations, to become parallel to the direction of applied tensile stress. These observations suggest that microcracks are developed by pressure effects of hydrogen. At a hardness level of Rc 35 or higher, the heat treated steels, on incurring such microcracks, do not have a proper capacity for plastic strain and, eventually, a cleavage-type fracture is developed. For the specimens tempered at 1025 to 1125 F, internal pressure build-up and occurrence of microcracks from hydrogen can be countered by local plastic deformation of the metal to prolong time for fracture.

The nature of the cracking in the 42 per cent magnesium chloride solution suggests that this aggressive solution promotes failures through selective grain boundary corrosion.

The effect of a small addition of colum-

bium to Type 410, on its performance in the accelerated stress-corrosion cracking tests described herein, can be considered to be mild in a positive sense. Basically, no apparent damaging effect resulted from the added columbium and, in fact, some trend for improved resistance to stress-corrosion cracking is indicated.

peratures ranging up to 900 F. Commonly, Type 410 is used in an annealed or normalized condition.

Short-time tension tests were carried out on regular and modified Type 410 in two different conditions of heat treatment at temperatures from 75 to 1100 F. Test specimens were hardened from 1850 F and tempered at 1200 or 1400 F. Standard ASTM procedures for short-time elevated temperature tension testing were employed.

TABLE 5—SHORT-TIME ELEVATED-TEMPERATURE TENSION TESTS.

CHEMICAL COMPOSITION, PER CENT[a]

Material	C	Mn	P	S	Si	Cr	Ni	Cb
410 Cb	0.12	0.48	0.015	0.008	0.36	11.90	0.43	0.19
410 Cb	0.11	0.49	0.012	0.021	0.35	12.08	0.25	0.15
410	0.12	0.49	0.013	0.019	0.33	12.07	0.20	<0.005
410	0.14	0.30	0.015	0.014	0.32	12.77	0.20	<0.005

Material	Tempering Temperature, deg F	Test Temperature, deg F					
		75	500	700	900	1000	1100
ULTIMATE TENSILE STRENGTH, 1000 PSI							
410	1200	106	90	85	73	64	51
410	1200	107	91	85	74	63	52
410 Cb	1200	122	106	101	93	83	71
410 Cb	1200	122	107	102	93	83	69
410	1400	90	77	71	61	53	42
410	1400	90	77	71	61	51	41
410 Cb	1400	99	85	80	68	57	46
410 Cb	1400	102	86	80	70	61	49
0.2% TENSILE YIELD STRENGTH, 1000 PSI							
410	1200	87	78	74	67	60	47
410	1200	84	76	74	65	59	48
410 Cb	1200	107	97	91	80	74	62
410 Cb	1200	108	98	91	81	76	63
410	1400	64	57	55	49	46	40
410	1400	62	55	50	48	44	37
410 Cb	1400	78	66	63	57	51	43
410 Cb	1400	80	69	67	60	55	47
ELONGATION IN 2 IN., %							
410	1200	22	20	17	20	24	28
410	1200	21	19	17	20	25	28
410 Cb	1200	21	20	18	19	21	22
410 Cb	1200	21	21	18	20	21	22
410	1400	26	23	25	25	31	33
410	1400	26	24	22	25	27	34
410 Cb	1400	25	23	20	21	26	31
410 Cb	1400	24	23	22	22	25	27

[a] Bar section: 1 in. round.
[b] Hardening treatment: 1850 F, oil quenched.
[c] Tempering treatment: 4 hr, air cooled.

MECHANICAL PROPERTIES AT ELEVATED TEMPERATURES

The 12 per cent chromium stainless steel is used in industrial equipment which operates at temperatures up to about 1300 F. The limited mechanical strength of this material restricts its usage, in stressed apparatus, to temperatures under 1000 F. One of the extensive applications of Type 410 stainless steel is in steam turbine blading and associated components subject to ambient tem-

Results of the tension tests are listed in Table 5. For the series of specimens tempered at 1200 F, Type 410 Cb exhibited an advantage of 14,000 psi in ultimate tensile strength at room temperature, and this advantage was maintained throughout the temperature range of testing up to 1100 F. Similarly, Type 410 Cb displayed a 0.2 per cent yield strength advantage of 20,000 psi at room temperature over that for regular Type 410, and most of this difference was retained at temperatures up to 1100 F.

For the 1400 F temper series, Type 410 Cb exhibited modest advantages over regular Type 410 in ultimate tensile strength and 0.2 per cent yield strength. The differences noted between the materials in the 1400 F temper group were reduced considerably over those noted above for the 1200 F temper series. An teresting comparison can be made to indicate that the mechanical strength of Type 410 Cb tempered at 1400 F is quite similar to the strength of the regular Type 410 tempered at 1200 F for the testing range of 75 to 1100 F.

The tensile ductilities of the two steels as indicated by elongation and reduction of area for 1200 and 1400 F temper were comparable.

SUMMARY

1. A minor addition of columbium is without effect on the quenched hardness or general corrosion resistance of a heat-hardenable 12 per cent chromium stainless steel (Type 410).

2. A controlled amount of columbium produces a marked degree of grain refinement, a reduced susceptibility to temper embrittlement, a mild improvement in resistance to stress-corrosion cracking, improved control of tempered hardness, and greater short-time, elevated temperature tensile strength in a 12 per cent chromium stainless steel.

CONCLUSIONS

The addition of a controlled, minor amount of columbium to a heat-hardenable 12 per cent chromium stainless steel (Type 410) facilitates commercial processing of this material and enhances some of the properties which promoted its extensive industrial usage. These advantages are developed without loss of the basic characteristics of the 12 per cent chromium stainless steel.

Acknowledgments:

The author expresses his appreciation to numerous associates who assisted in this work. Special recognition is due G. C. Pierpont for determination of mechanical properties, E. E. Denhard, Jr., for corrosion and stress-corrosion tests, and R. H. Mackenzie and W. J. Lanning for metallographic and photographic work. The author thanks G. N. Goller, supervising research metallurgist and F. K.

Bloom, manager, both of the Baltimore Research and Technology Laboratory of Armco Steel Corp., for review of this paper.

REFERENCES

(1) C. A. Zapffe, *Stainless Steels*, Am. Soc. Metals, Cleveland, Ohio, 1949, pp. 16–20.

(2) *Elevated Temperature Properties of Chromium Steels, ASTM STP 228*, Am. Soc. Testing Mats., 1958.

(3) J. H. G. Monypenny, "Stainless Steel With Particular Reference to the Milder Varieties (Stainless Iron)," *Transactions*, Am. Institute Mining, Metallurgical, and Petroleum Engrs., Vol. 70, 1924, pp. 47–72.

(4) F. K. Bloom, "Effect of Heat Treatment and Related Factors on Straight Chromium Stainless Steels," *Corrosion*, Vol. 9, 1953, pp. 56–65.

(5) F. M. Beckett and R. Franks, "Titanium and Columbium in Plain High Chromium Steels," *Transactions*, Am. Institute Mining, Metallurgical, and Petroleum Engrs., Vol. 113, 1934, pp. 136–142.

(6) D. L. Newhouse, B. R. Seguin, and E. M. Lape, "Some 12 Per Cent Chromium Alloys for 1000 F to 1200 F Operation," *Transactions*, Am. Soc. Mechanical Engrs., Vol. 76, 1954, pp. 1107–1122.

(7) J. H. Holloman and L. D. Jaffe, "Time-Temperature Relations in Tempering Steel," *Transactions*, Am. Institute Mining, Metallurgical, and Petroleum Engrs., Vol. 162, 1954, pp. 223–249.

(8) W. Tofaute, A. Sponheuer, and H. Bennek, "The Transformation, Hardening and Tempering Characteristics of Steels Containing Up to 12 per cent Chromium and 1 per cent Carbon," *Archiv Eisenhuttenwesen*, Vol. 8, No. 11, May, 1935, pp. 499–506.

(9) R. W. Ballufi, M. Cohen, and B. L. Averbach, "The Tempering of Chromium Steels," *Transactions*, Am. Soc. Metals, Vol. 43, 1951, pp. 497–525.

(10) R. L. Rickett, W. F. White, and C. S. Walton, "Isothermal Transformation, Hardening and Tempering of 12 per cent Chromium Steel," *Transactions*, Am. Soc. Metals, Vol. 44, 1952, pp. 138–175.

(11) K. Kuo, "Carbides in Chromium, Molybdenum and Tungsten Steels," *Journal*, Iron and Steel Inst., Vol. 173, 1953, pp. 363–375.

(12) K. J. Irvine, D. J. Crowe, and F. B. Pickering, "Physical Metallurgy of 12 per cent Cr Steels," *Journal*, Iron and Steel Inst., Vol. 195, Part 4, August, 1960, pp. 386–405.

(13) K. C. Mills, B. B. Argent, and A. G. Quarrell, "The Carbide Constitution and Tempering Behavior of Chromium-Vanadium-Niobium Steels at 700 C," *Journal*, Iron and Steel Inst., Vol. 197, Part 1, January, 1961, pp. 9–21.

(14) J. J. Hauser, J. M. Capenos, and B. R. Banerjee, "Submicroscopic Structures in Tempering Type 410 Stainless Steel," *Transactions Quarterly*, Am. Soc. Metals, Vol. 54, No. 3, September, 1961, pp. 514–525.

(15) B. C. Woodfine, "Temper Brittleness: A Critical Review of the Literature," *Journal*, Iron and Steel Inst., Vol. 173, 1953, pp. 229–240.

(16) D. MacLean and L. Northcutt, "Micro-Examination and Electrode Potential Measurements of Temper-Brittle Steels," *Journal*, Iron and Steel Inst., Vol. 158, 1948, pp. 169–177.

(17) F. K. Bloom, "Stress-Corrosion Cracking of Hardenable Stainless Steels," *Corrosion*, Vol. 11, No. 8, August, 1955, pp. 351t–361t.

(18) E. E. Denhard, Jr., "Effect of Composition and Heat Treatment on the Stress-Corrosion Cracking of Austenitic Stainless Steels," *Corrosion*, Vol. 16, July, 1960, pp. 359t–369t.

(19) R. E. Lochen and E. R. Miller, "Stress-Corrosion of 12 per cent Chromium Stainless Steel," *Industrial and Engineering Chemistry*, Vol. 51, No. 6, June, 1959, pp. 763–764.

DISCUSSION

G. D. GARDNER[1]—The data you have presented on this modified 12 per cent chromium alloy is of considerable interest especially at strength levels attained by tempering at 1100 F. Has any work been done to determine the weldability of the columbium stabilized alloy at this strength level? Of particular interest would be weldability of a relatively heavy section.

H. TANCZYN (*author*)—Welding of Type 410 Cb stainless steel calls for the procedures established in welding regular Type 410 of comparable carbon content. Preheating of the weld components to 500 F is important to preclude cracking in the weld and weld heat-affected regions. Type 410 Cb welds, in the post-weld stress-relieved or normalized and tempered conditions, exhibit specific advantages over similar welds of the regular Type 410. These advantages correspond to those cited for wrought products of Type 410 Cb over those of regular Type 410.

[1] U. S. Industrial Chemicals Co., Tuscola, Ill.

A HIGH-STRENGTH WELDABLE STAINLESS STEEL FOR ELEVATED-TEMPERATURE SERVICE

By F. C. Hull,[1] Personal Member, ASTM

Synopsis

Based on considerations of hot cracking, tensile, rupture, and creep strength, high-temperature stability, and oxidation resistance, a chromium-nickel-manganese-molybdenum stainless steel strengthened with boron, zirconium, vanadium, and nitrogen was developed. Although rupture and creep strength reached maxima at a level of about 0.17 per cent nitrogen, yield and tensile strength increased linearly with nitrogen to considerably higher levels. Working temperature and reductions and heat treating temperaturs had major effects on the properties. Tungsten-inert-gas welding has been used to join fabricated plate of this alloy into tubing and elbows used for steam-turbine reheat pipe. The nominal composition of this alloy, called Kromarc[2] 58 steel, is 16 per cent chromium, 20 per cent nickel, 10 per cent manganese, 2.25 per cent molybdenum, 0.2 per cent vanadium, 0.25 per cent silicon, 0.01 per cent boron, 0.01 per cent zirconium, 0.04 per cent carbon, 0.17 per cent nitrogen, and balance iron.

The alloy described herein was developed primarily for use as a steam-turbine piping material. The principal improvements needed for this application were a high degree of weldability combined with increased tensile, rupture, and creep strength, with the usual demanding requirements placed on impact strength, stability in long-time high-temperature service, oxidation and corrosion resistance, ease of fabrication, and reasonable cost. This paper includes an explanation of the factors that determined the composition of Kromarc 58 steel, an investigation of fabrication and heat treatment variables, and a summary of the properties of base metal and welds.

Bases of Selection of Alloy Composition

Hot Cracking:

The initial screening of alloys for susceptibility to hot tearing or hot cracking was by means of the cast-pin-tear (CPT) test. This test method indicated that manganese, molybdenum, tungsten, chromium, and nitrogen should decrease the susceptibility of stainless steels to microfissuring in welding (1).[3]

Because the resistance to hot cracking was improved by moderate levels of manganese in the first survey, it was decided to investigate the effects of still higher contents of manganese on hot cracking of iron-chromium-nickel alloys. The data along the abscissa in Fig. 1 showed that the greatest resistance to hot cracking was obtained in this alloy system with a manganese content of about 14 weight per cent.

Molybdenum was another element that reduced susceptibility to hot cracking, and, since it was also a desirable addition from the standpoint of increasing creep strength, the combined effects of manganese and molybdenum were investigated. The CPT test data are summarized in Fig. 1 in which the contour lines indicate compositions of equal cracking susceptibility. The nickel content was high enough that no delta ferrite formed to complicate the interpretation of the results. The alloy with the greatest resistance to hot cracking by this test procedure, that is, having the smallest mold number, contained about 1.5 per cent molybdenum and 12 per cent manganese.

For high temperature applications, the strength can be increased with only a slight reduction in resistance to hot cracking by using an alloy containing 16 per cent chromium, 20 per cent nickel, 10 per cent manganese, 2.25 per cent molybdenum, and balance iron. This alloy, called Kromarc 55 stainless steel, has been used as cast nozzle chambers for a steam turbine, and as welding electrodes for joining Type 316 and Kromarc steels. It was chosen as the material for a liquid-hydrogen bubble chamber (3) because of the complete stability of the austenite at temperatures approaching absolute zero.

Strength:

Elements which have been used in the past to strengthen stainless steels and other high-temperature alloys are molybdenum, tungsten, vanadium, columbium, titanium, copper, silicon, carbon, nitrogen, boron, and zirconium. Of these columbium, titanium, copper, and silicon were considered unsuitable as alloying additions for the present application because of their adverse effect on weldability. Carbon in excess of about 0.06 per cent is objectionable both from the standpoint of hot cracking and because of the formation of sheets of carbides at the grain boundaries in service at high temperatures.

The effects of molybdenum on rupture strength of several chromium-nickel-manganese steels are illustrated in Fig. 2, and the compositions of these steels are listed in Table 1. Individual test results are given in Table 2.[4] Both rupture and creep strength increased linearly from 0 up to 8 per cent molybdenum with accompanying rupture elongations of about 40 to 80 per cent. Heats 7427 and XMM 1990, both of which contained about 0.08 per cent carbon, had poor rupture ductilities compared to heats of lower carbon content. In spite of its favorable effect on strength, the molybdenum content must be limited to avoid undesirable side effects on hot cracking, oxidation resistance, and impact strength after prolonged aging.

Tungsten was also an attractive strengthening addition from the standpoint of reducing hot cracking, but in the present base composition, it was found that the tensile and creep properties of steels containing tungsten were not significantly better than those containing only molybdenum. Since tungsten is more expensive than molybdenum and about twice as much is needed to produce

[1] Advisory metallurgist, Westinghouse Research and Development Center, Pittsburgh, Pa.

[2] Kromarc is a trademark of the Westinghouse Electric Corp.

[3] The boldface numbers in parentheses refer to the list of references appended to this paper.

[4] Data for steels 7430, 7431, 7454, and XMM 2054 are presented in Table 4 of Ref. (2).

Copyright© 1965 by ASTM International

www.astm.org

an equivalent effect, it was decided to use molybdenum alone in the present alloys.

The effect of vanadium on strength was relatively small, if carbon and nitrogen contents were low. However, vanadium in the presence of about 0.1 per cent nitrogen produced a marked increase in creep strength (2).

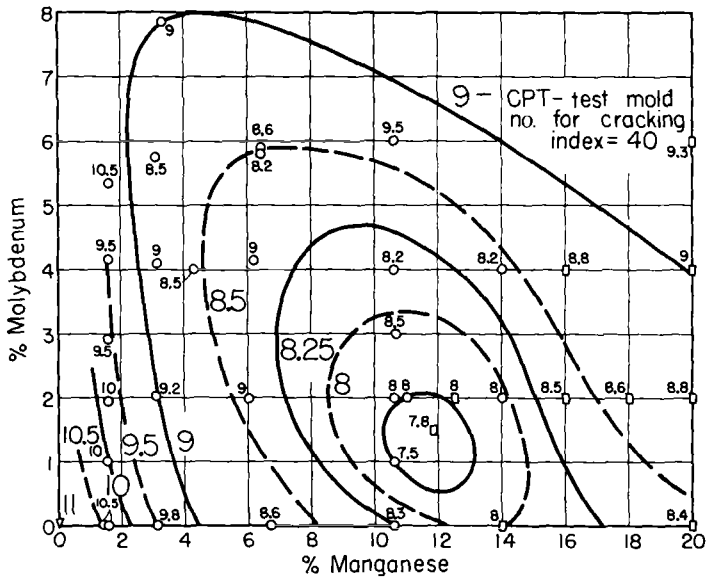


FIG. 1—Effect of Manganese and Molybdenum on Hot Cracking of Stainless Steels Containing 16 Per Cent Chromium and 13 to 20 Per Cent Nickel.

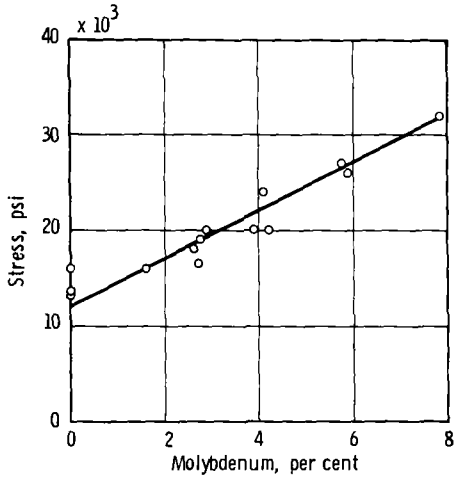


FIG. 2—Effect of Molybdenum on the 1000 hr Rupture Strength at 1200 F of Fe-Cr-Ni-Mn Steels.

Small amounts of boron and zirconium have been shown in the literature to have pronounced beneficial effects on strength and rupture ductility of nickel-base alloys. Even though the hot cracking study (1) had confirmed previous reports of the detrimental effects of these elements on weldability, the effects of small amounts of boron and zirconium on the properties of iron-chromium-nickel-manganese-molybdenum alloys were investigated (2). By keeping the boron and zirconium contents within the approximate limits shown for the alloys in Table 1, it was possible to achieve substantial strength increases while still maintaining sufficient resistance to hot cracking to permit welding of turbine piping.

Nitrogen is one of the most potent elements for increasing yield and tensile strength (4); in combination with boron, zirconium, and vanadium it increases creep and rupture strength (2) and decreases susceptibility to hot cracking.

Oxidation Resistance:

At the level of 16 per cent chromium, the alloys oxidized catastrophically (5) at elevated temperatures if molybdenum or vanadium contents or both were above certain limits. At 1200 F, in times up to 10,000 hr, no difficulty was encountered, but if the molybdenum content approached or exceeded about 4 per cent, or if the vanadium content exceeded about 0.5 per cent in combination with 2.5 per cent molybdenum, severe oxidation occurred in 10,000 hr at 1350 F, in 1000 hr at 1500 F, or in several hours at 2100 F.

Impact Strength:

In addition to carbide precipitation at grain boundaries during high-temperature service, certain stainless steels form sigma or chi which can lead to additional loss of impact strength. As a guide to selecting the composition of the present alloy, a study was made of the effects of several elements on embrittlement during 1000 hr aging at 1500 F of small chill-cast pin samples containing very low carbon and nitrogen. The property measured was the notched-impact bend angle at fracture. The results can be summarized by an equation which reduces the composition of an alloy to a single variable $\phi(c)$ which is related to the impact properties after aging:

$$\phi(c) = 0.55\ (\%\text{Cr-16}) + 0.25\ (\%\text{Mn-10}) + 0.6\%\ \text{Si} + \%\text{Mo} + \%\text{V} - 0.11\ (\%\text{Ni-20})$$

The larger the value of $\phi(c)$, the more precipitate was found in the structure after aging and the smaller was the limiting bend angle. A level of 3 for $\phi(c)$, corresponding approximately to a fracture angle of 45 deg, should not be exceeded if impact strength is an important requirement for a given application.

Delta Ferrite and Martensite:

In most stainless steel welding, the compositions of the electrodes are chosen so that the weld deposits contain about 2 to 10 per cent delta ferrite to prevent microfissuring. Kromarc steels, however, because of the beneficial effect of the high level of manganese and molybdenum, are sufficiently resistant to hot cracking that the deposits can be fully austenitic. An advantage of this characteristic is the elimination of the need for solution treating of welds. A further advantage results from the fact that the nickel content can be high enough to limit sigma and chi formation. Kromarc 58 does not transform to martensite even if it is cooled to, or deformed at, temperatures approaching absolute zero.

EXPERIMENTAL RESULTS

Preparation of Alloys:

All of the heats used in this investigation were prepared by induction melting. The 25-lb laboratory air melts were designated by a heat number in the series 7xxx. Larger heats, ranging from 100 to 5000 lb, were produced at the Westinghouse Materials Manufacturing Div., Blairsville, Pa., and were identified with the prefix KV or XMM.

In order to control the level of impurities in some heats used for welding wire, a few laboratory vacuum induction melts (VM) were made. However, manganese and manganese-nitrogen were added under a partial pressure of nitrogen to minimize losses.

Ingots were broken down by forging in several steps from 2100 F. Bars for tension and creep tests were forged at 1900 F in several steps from $1\frac{1}{4}$ in. square to $\frac{11}{16}$ and $\frac{13}{16}$ in. diameter, respectively, unless otherwise specified.

TABLE 1.—CHEMICAL COMPOSITION OF STEELS, WEIGHT PER CENT.[a]

Heat No.	Cr	Ni	Mn	Si	C	N	Mo	W	V	B	Zr	Ti[c]	O	P	S
7453	(16)[b]	(14)	5.94	(0.15)	0.0039	0.019	...	...	...	...	...	...	...	...	...
7055	16.5	17.1	6.47	0.39	0.025	0.029	...	...	...	...	...	...	...	...	...
7379	16.4	14.9	10.6	0.15	0.013	0.018	0.002	...	...	...	...	...	...	...	...
7392	16.3	14.0	12.0	0.15	0.0062	0.016	1.58	...	...	...	...	...	...	...	...
7430	(16)	(20)	7.08	(0.15)	0.0036	0.018	2.62	...	...	...	...	...	...	...	...
7431	(16)	(20)	10.6	(0.15)	0.0044	0.019	2.69	...	...	...	...	...	...	...	...
XMM 2054	17.1	16.0	10.5	0.26	0.032	0.040	2.74	...	...	...	...	...	...	...	...
7454	16.3	17.0	9.43	0.21	0.039	0.041	2.91	...	...	...	...	...	...	...	...
7427	(16)	(22)	8.93	(0.15)	0.078	0.017	3.88	...	...	...	...	...	...	...	...
7377	16.1	20.0	4.24	0.18	0.012	0.015	4.04	...	...	...	...	...	...	...	...
XMM 1990	16.4	19.7	9.5	0.24	0.080	0.024	4.18	...	...	...	...	...	...	...	...
7376	16.2	20.3	3.13	0.17	0.011	0.012	5.75	...	...	...	...	...	...	...	...
7374	16.4	19.9	6.40	0.16	0.010	0.011	5.91	...	...	...	...	...	...	...	...
7380	16.2	19.8	3.25	0.14	0.011	0.016	7.84	...	...	...	...	...	...	...	...
7440	(16)	(25)	10.7	(0.15)	0.0060	0.016	...	4.60	...	...	...	...	...	...	...
7441	(16)	(25)	11.7	(0.15)	0.0035	0.021	...	...	3.21	...	...	...	...	...	...
7488	(16.6)	(20.7)	(11.5)	(0.1)	(0.03)	0.13	(2.25)	...	(0.3)	(0.006)	0.0086	(0.05)	...	...	...
7489	(16)	(20)	8.62	(0.15)	0.044	0.12	2.00	...	0.31	0.0051	0.017	(0.05)	...	...	...
7530	(16)	(20)	8.53	(0.15)	0.035	0.019	2.12	...	0.29	0.010	0.016	(0.05)	...	...	...
7531	(16)	(20)	9.54	(0.25)	0.030	0.040	1.91	0.65	0.29	0.0060	0.049	(0.10)	...	...	...
7532	(16)	(20)	9.32	(0.25)	0.035	0.044	2.18	...	0.29	0.0071	0.005	(0.10)	...	...	...
7533	(16)	(20)	9.91	(0.25)	0.031	0.053	...	1.72	0.29	0.0083	0.003	(0.10)	...	...	...
7534	15.8	19.3	9.67	0.29	0.026	0.052	2.24	...	0.29	0.016	0.044	<0.01	...	...	...
7535	(16)	(20)	9.45	(0.25)	0.028	0.045	2.24	...	0.25	0.011	0.062	...	...	...	...
7571	15.0	19.7	10.4	0.12	0.038	0.19	2.25	...	0.26	0.0057	0.012	(0.10)	...	...	...
7572	(16)	(20)	10.6	(0.15)	0.030	0.23	2.23	...	0.25	0.0095	0.013	(0.05)	...	...	...
7577	15.0	19.5	8.17	0.096	0.034	0.19	2.40	...	0.24	0.012	0.017	(0.05)	...	...	...
VM 544	16.2	19.5	12.8	<0.02	0.016	0.20	2.63	...	0.25	0.018	0.026	...	...	...	...
VM 545	16.7	20.0	12.6	<0.02	0.017	0.15	2.61	...	0.23	0.025	0.012	...	0.0064	...	...
VM 548	15.6	22.0	9.88	0.03	0.0090	0.16	2.33	...	0.26	0.011	0.028	...	0.0065	0.0018	0.0035
VM 549	(15)	(22)	(10)	(0.03)	0.060	0.17	(2.25)	...	(0.25)	0.013	0.014	...	0.0062	...	...
VM 550	(15)	(22)	(10)	(0.03)	0.011	0.17	(2.25)	...	(0.25)	0.013	0.030	...	0.0092	...	...
VM 551	(15)	(22)	(10)	0.50	0.019	0.19	(2.25)	...	(0.25)	0.011	0.025	...	0.0021	...	...
VM 575	15.1	22.1	10.7	(0.05)	0.019	0.21	2.25	...	0.26	0.0077	0.008	...	0.0134	...	...
VM 579	15.3	22.0	10.8	0.05	0.025	0.21	2.23	...	0.28	0.0079	0.008	0.028	0.0105	...	...
KV 101	15.7	20.0	10.3	0.48	0.025	0.13	2.32	...	0.28	0.006	0.008	...	...	...	...
XMM 2232	16.0	20.4	9.03	0.37	0.031	0.10	2.24	...	0.26	0.007	0.025	...	...	...	...
XMM 2239	16.0	19.5	8.97	0.31	0.038	0.071	2.16	...	0.26	0.004	0.004	...	...	...	...
XMM 2240	15.9	19.4	9.02	0.31	0.034	0.094	2.11	...	0.26	0.005	0.009	...	...	...	...
XMM 2265	15.7	19.8	10.6	0.36	0.026	0.16	2.22	...	0.26	0.008	0.036	0.06	...	...	...
XMM 2284	15.9	20.1	11.0	0.20	0.021	0.17	2.27	...	0.25	0.007	0.020	0.06	...	...	...
XMM 2296	15.9	20.3	11.2	0.22	0.034	0.18	2.26	...	0.17	0.026	0.0058	(0.05)	0.0094	...	0.010
XMM 2336	15.5	23.2	10.6	0.13	0.020	0.21	2.12	...	0.24	0.0052	0.009	0.02	0.0063	0.003	0.007
XMM 7117	15.4	20.2	12.25	0.12	0.014	0.19	2.28	...	0.24	0.0025	0.0062	...	0.0062	...	0.014
XMM 7133	15.3	21.9	10.4	0.08	0.020	0.21	2.15	...	0.20	0.006	<0.002	...	...	...	0.014

[a] Balance iron.
[b] ( ) = nominal.
[c] (Ti) = amount charged.

Tensile Properties:

The strength and ductility of a typical heat of Kromarc 58 steel as a function of test temperature from −320 to +2000 F are shown in Fig. 3. Tensile properties for the temperature region of interest in steam-turbine design, room temperature to 1200 F, are given in Table 3.

The effect of nitrogen on the tensile properties of these steels was investigated with a series of heats that contained 0.019 to 0.30 per cent nitrogen. These steels were hot rolled to $\frac{5}{8}$ in. diameter with a 40 to 50 per cent final reduction of area, after holding for 15 min at 2000 F, and were heat treated for 1 hr at 1700 F and water quenched. Yield and tensile strengths at room temperature are shown to be linear functions of the nitrogen content in Fig. 4. A linear relationship was also found at 1025 F. Curves similar to these, but displaced to lower strengths, were obtained with heat treatments at temperatures from 1750 to 2200 F.

Dr. Roland Stickler of the Westinghouse Research and Development Center examined extraction replicas of two specimens from heat No. 7571 by X-ray and electron diffraction and identified the following phases:

Specimen	Heat Treatment, deg F	Room Temperature Strength, psi		Phases			
		0.2% Yield	Ultimate	$CrMoN_x$	Cr_2N	M_6C	Mn_4N
7571-3	1 hr 1700	77 200	108 600	...	XD	ED	ED
7571-5	20 hr 1500 + 1 hr 1800	50 100	100 600	XD	XD	ED	...

The large spheroidized particles in Fig. 5(*a*) and (*c*) are Cr_2N, the amount of which increases the higher the nitrogen content. Some of the larger particles in Fig. 5(*c*) may be $CrMoN_x$. In specimen 7571-5, $CrMoN_x$ would be expected (2) to precipitate during aging at 1500 F, and it may not have been dissolved by holding 1 hr at 1800 F. Smaller particles of M_6C were detected by electron diffraction in both samples. The most significant difference discovered was a fine intragranular precipitate of plates of Mn_4N which are believed to be the main reason for the higher strength of specimen 7571-3 (Fig. 5(*b*)). At 1800 F there was considerably less Cr_2N, there was no Mn_4N, and the grain size had increased; at 1900 F there was very little precipitate and the grains were much larger.

In other cases too, depending on the

prior working history, the strength of a steel after a 1700 F treatment was higher than would be expected from an extrapolation of tests with higher solution temperatures. Table 3 shows that initial working temperatures of 2000 and 2100 F led to higher strengths than working temperatures from 1900 F down to room temperature. These bars were all reduced 40 to 50 per cent in area without reheating and then heat treated 1 hr at 1700 F. With an optical microscope the difference appeared to be mainly because of incomplete recrystallization on heating 1 hr at 1700 F, in the case of the steels with the higher working temperatures. Two of these specimens were selected for more detailed study. Electron microscope pictures of carbon extraction replicas revealed the large spheroidized grain-boundary precipitate of Cr_2N in samples worked from 1800 F as well as from 2000 F, but the fine intragranular precipitate of Mn_4N (similar to Fig. 5(*b*)) was found only in the specimen rolled from 2000 F.

If the nitrogen content of an alloy is low and the work hardening is sufficiently severe, during heat treatment recrystallization occurs before general precipitation can proceed to an appreciable extent. The rate of precipitation from this recrystallized matrix is greatly reduced and, since the remaining nucleation sites are primarily at grain boundaries, the distribution of precipitate is poor from the standpoint of increasing strength. On the other hand, if precipitation can be induced in the worked structure, the rate of precipitation is greater and a favorable dispersion of particles results. This precipitate structure may then impede grain-boundary migration, and the relief of internal stress takes place by recovery and subboundary formation instead of recrystallization.

The factors which favor the formation of a fine dispersed precipitate, which can be used to increase tensile properties are the following: (1) a coarse grain size prior to the final working, (2) a high-working temperature, (3) a moderate amount of deformation, (4) a low heat-treatment temperature, and (5) a high-nitrogen content.

TABLE 2.—CREEP-RUPTURE TESTS AT 1200 F OF Cr-Ni-Mn STAINLESS STEELS CONTAINING Mo, W, OR V.

Heat No.	Heat Treatment, deg F, 1 hr	Stress, psi	Rupture Time, hr	Rupture Strain, %	Reduction of Area, %	Minimum Creep Rate, %/hr
7055	1800	27 000	6	40.7	40.2	3.38
	1800	21 000	48	36.0	35.2	0.51
	1800	16 000	366	23.3	26.5	0.043
	1800	11 000	2796	10.7	20.0	0.0035
7379	1800	28 000	25	32.7	33.3	0.69
	1800	24 000	91	35.8	36.2	0.19
	1800	20 000	325	24.8	35.9	0.039
	1800	15 000	1434	23.3	27.1	0.0098
7453	1900	25 000	4	30.0	29.5	3.29
	1900	20 000	36	35.4	35.3	0.63
	1900	18 000	78	41.7	40.7	0.35
	1900	14 000	486	44.7	44.6	0.062
	1800	25 000	4	29.0	25.8	4.17
	1800	13 000	403	48.3	45.1	0.054
7392	1800	30 000	2.9	50.3	54.1	10.7
	1800	25 000	33	64.0	62.0	1.05
	1800	22 000	113	62.7	65.5	0.23
	1800	18 000	394	58.1	57.0	0.045
7427	2100	35 000	36	27.3	26.1	0.23
	2100	30 000	118	20.3	26.0	0.078
	2100	24 000	369	16.5	18.3	0.023
	2100	20 000	637	11.0	15.4	0.012
	2100	20 000	893	12.0	15.2	0.0088
XMM 1990	2050	39 000	9	31.3	36.3	1.13
	2050	35 000	25	29.0	29.0	0.254
	2050	28 000	134	17.0	21.9	0.071
	2050	23 000	438	13.0	12.3	0.019
	2050	18 000	1528	8.0	9.0	0.0017
7377	2100	35 000	47	65.2	66.2	0.59
	2100	30 000	203	65.5	65.0	0.087
	2100	26 000	594	85.5	71.9	0.050
	2100	22 000	1835	82.3	72.3	0.013
7376	2000	42 000	21	55.3	56.7	1.14
	2000	34 000	190	62.7	59.0	0.112
	2000	30 000	433	61.3	69.8	0.052
	2000	26 000	1278	60.3	70.7	0.016
7374	2000	45 000	9.5	54.0	65.8	1.6
	2000	36 000	71	60.7	67.0	0.31
	2000	30 000	395	44.7	59.2	0.039
	2000	25 000	1296	59.0	64.0	0.019
7380	2100	50 000	12	41.7	43.6	0.78
	2100	42 000	68	52.0	48.3	0.46
	2100	38 000	170	51.0	48.6	0.10
	2100	30 000	1784	66.0	60.0	0.017
7440	1900	30 000	14.5	29.6	28.9	...
	1900	23 000	92	16.9	28.5	...
	1900	19 000	234	26.9	27.4	...
	1900	15 000	1102	23.1	22.0	...
7441	1850	45 000	0.3	22.5	26.8	...
	1850	30 000	28.5	14.0	19.2	0.14
	1850	26 000	64	14.9	20.6	...
	1850	20 000	170	27.6	26.3	...
	1850	16 000	279	7.3	22.0	...
	1850	13 000	2740	4.3	7.2	0.00045

Creep-Rupture Properties:

Rupture-test results for the steels investigated are listed in Table 4. (Data for heats 7488, 7489, 7530, 7532, and 7571 were given in Ref. (2).) The nitrogen content was one of the most important factors determining rupture and creep strength. However, rupture strength, Fig. 6, and creep strength reached maxima at about 0.17 per cent nitrogen, whereas yield and tensile strength continued to increase up to 0.3 per cent nitrogen.

The rupture and creep data for steels containing 0.12 per cent nitrogen or higher were plotted in Figs. 7 and 8 using the Larson-Miller parameter. The Type 316 stainless steel data presented for comparison are results for turbine piping obtained at the Westinghouse Steam Div. The rupture data (6) for Type 316 steel modified with 0.18 per cent nitrogen lie above the band for the standard composition but below that of Kromarc 58.

In the preceding section it was shown that a fine dispersion of precipitates increased yield and tensile strength. Bar stock from heat XMM 2336 was held for 1 hr at temperature, rolled from 2000 F, and heat treated at 1700, 1800, 1900, and 2000 F for 1 hr. The results of stress-rupture tests at 1200 F and 45,000 psi are shown in Table 3. At this stress level, the longest rupture time, the largest rupture ductility, and the smallest creep rate were all obtained with the 1700 F heat treatment. The 1700 F precipitates

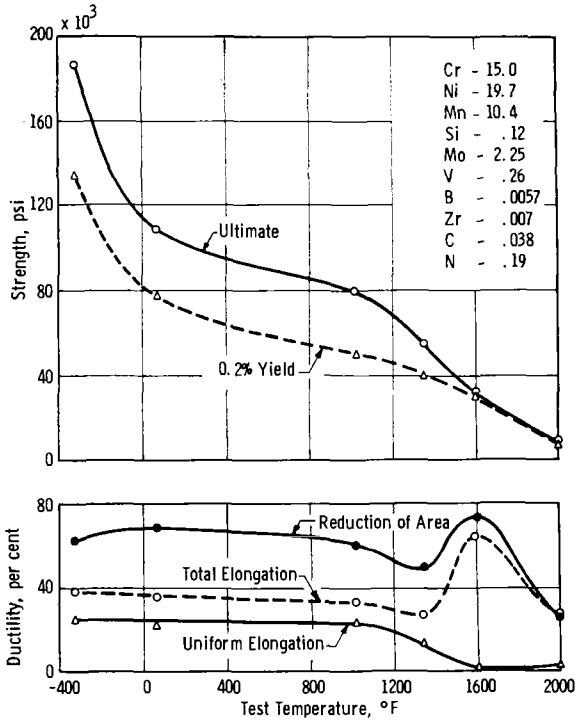


FIG. 3—Tensile Properties of Kromarc 58 Heat 7571, $\frac{5}{8}$ in. Diameter Bars Solution Treated 1 hr at 1700 F.

TABLE 3.—EFFECT OF ROLLING AND HEAT TREATING TEMPERATURES ON THE TENSILE AND CREEP-RUPTURE PROPERTIES OF KROMARC 58 HEAT NO. XMM2336.

Rolling Temperature, deg F,[a] 40 to 50% reduction of area	Heat Treatment Temperature, deg F, 1 hr	Tensile Properties					Creep-Rupture Properties, 1200 F and 45,000 psi			
		Test Temperature, deg F	0.2% Yield, psi	Ultimate Strength, psi	Elongation, %	Reduction of Area, %	Rupture Time, hr	Rupture Strain, %	Reduction of Area, %	Minimum Creep Rate, %/hr
2000	1700	RT	83 900	118 000	32.7	65.9	...	...	...	...
2100	1700	200	69 500	107 900	33.2	62.7	...	...	...	...
2100	1700	400	53 000	96 100	35.7	63.6	...	...	...	...
2100	1700	600	54 200	93 700	33.2	62.2	...	...	...	...
2100	1700	800	50 100	90 900	31.2	59.0	...	...	...	...
2100	1700	1000	56 100	88 900	27.3	57.7	...	...	...	...
2100	1700	1100	46 100	81 700	31.4	54.4	...	...	...	...
2100	1700	1200	47 600	74 200	31.1	50.3	...	...	...	...
RT[b]	1700	RT	56 100	109 700	40.0	69.6	62	22.0	38.7	0.11
1700	1700	RT	55 900	109 600	40.0	70.6	66	23.3	43.5	0.12
1800	1700	RT	53 900	107 400	40.4	70.0	63	21.7	42.6	0.13
1900	1700	RT	55 900	109 800	39.7	70.3	94	34.3	42.0	0.081
2000	1700	RT	83 900	118 000	32.7	65.9	373	18.2	60.5	0.0073
2100	1700	RT	85 700	120 400	28.5	62.2	472	10.6	32.9	0.0024
RT[b]	1700	1025	35 000	82 900	37.7	62.9	...	...	...	...
1700	1700	1025	35 500	83 100	37.1	62.9	...	...	...	...
1900	1700	1025	35 900	81 700	35.8	61.7	...	...	...	...
2000	1700	1025	48 900	85 400	29.1	55.2	...	...	...	...
2100	1700	1025	57 900	85 900	25.2	49.7	...	...	...	...
2000	1700	RT	83 900	118 000	32.7	65.9	373	18.2	60.5	0.0073
2000	1800	RT	51 300	104 700	43.3	70.1	93	14.3	31.0	0.038
2000	1900	RT	49 500	102 700	46.3	72.6	56	8.8	11.5	0.055
2000	2000	RT	45 100	99 600	50.7	73.6	42	11.3	18.1	0.078

[a] Held 1 hr at temperature before rolling.
[b] Annealed 1 hr at 1900 F before cold rolling.

of Mn_4N and M_6C, though fine, were still coarse compared to the VN_x particles formed during creep. The 1700 F precipitates, even so, reduced plastic strain on loading to high stresses, reduced primary creep, and apparently did not interfere with other precipitation reactions occurring during the tests.

The effects of initial rolling temperature on creep-rupture properties of heat XMM 2336 were similar to the effects on yield and tensile strength. Table 3 shows that rupture time increased abruptly by a factor of about six, and the minimum creep rate decreased simultaneously by more than a factor of ten as the working temperature was raised above 1900 F.

Welding:

Kromarc 58 steel has been welded with covered electrodes, consumable wire with argon shielding (MIG), and tungsten-inert-gas (TIG) with and without cold-wire feed. The composition of the weld metal is similar to the base metal, but preferably of lower carbon, silicon, and sulfur contents.

The properties reported here are for all-weld-metal specimens deposited in unrestrained 1-in.-thick grooved plates of Kromarc 58 steel. The deposits were radiographed to check for porosity, and $\frac{1}{4}$-in.-thick slices cut across the weld were bent to reveal microfissures if any were present.

The yield and tensile strengths and ductility were good for welds made with stick electrodes covered with conventional stainless steel fluxes, but the rupture strength and rupture ductility were much lower than those of TIG welds. The properties of MIG welds were intermediate. Until these deficiencies can be overcome, it is recommended that only TIG welding be used in the joining of this steel for high-temperature applications.

The tensile properties of a few welds are given in Table 5. For as-deposited weld metal there was also a linear relationship between strength and nitrogen content. In general, the yield strengths of the deposits were higher and the tensile strengths were lower than those of wrought bars of equivalent nitrogen content. Heat treatment of the weld should usually be avoided because it lowers the yield and tensile strengths.

The data for stress-rupture tests of some TIG deposits are listed in Table 6 and the results are summarized in Larson-Miller parameter curves in Figs 9 and 10. The creep-rupture strengths of these welds exceeded the average values for wrought bars.

BOILER CODE CONSIDERATIONS

The application of ASME boiler code criteria for determining allowable stresses is illustrated in Fig. 11. For Type 316 stainless steel, 62.5 per cent of the yield strength is controlling up to about 1035 F. Above this temperature, 60 per cent of the average stress to produce rup

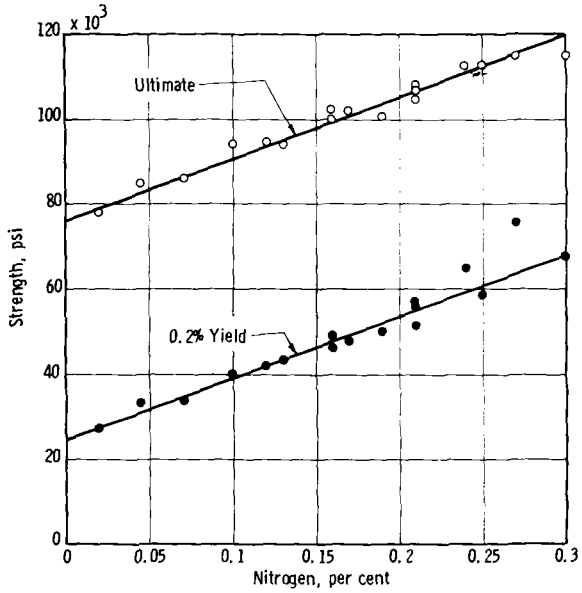
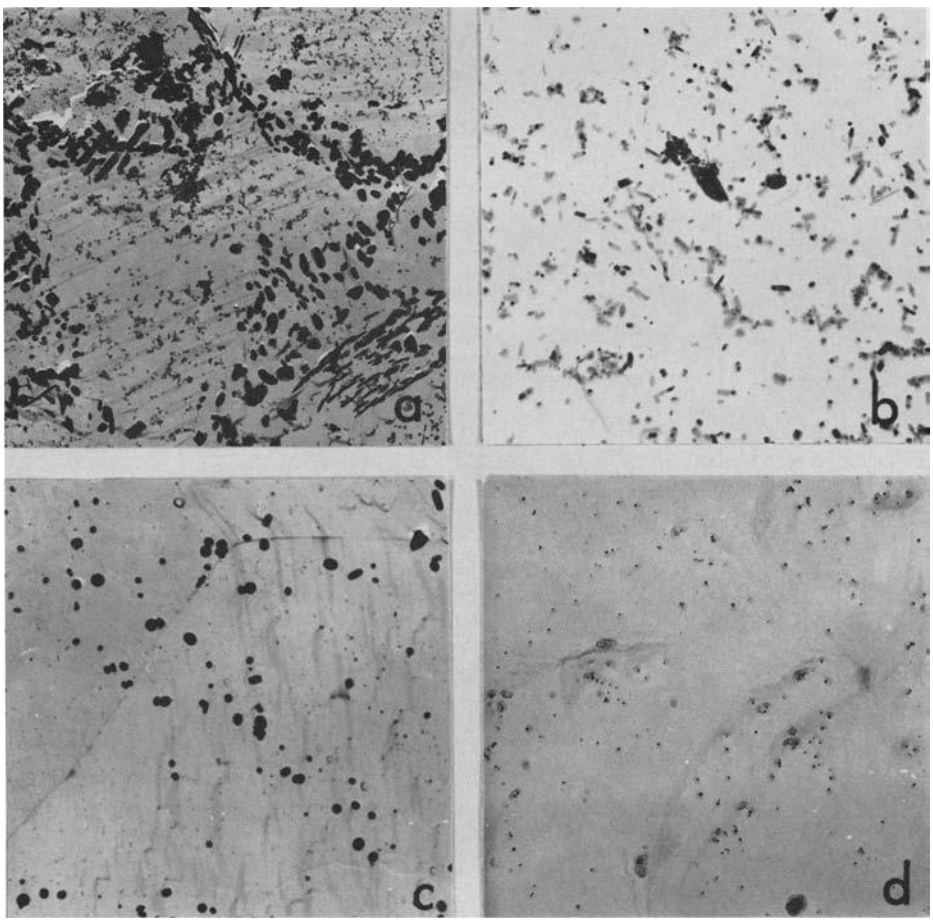


FIG. 4—Effect of Nitrogen on the Room-Temperature Tensile Properties of Kromarc 58 Stainless Steel Heat Treated 1 hr at 1700 F.



(*a*) Specimen 3; 1 hr at 1700 F; coarse spheroidized grain boundary precipitate, Cr_2N; fine intragranular precipitate, Mn_4N and M_6C (×4000).
(*b*) Specimen 3; 1 hr at 1700 F; fine intragranular precipitate, Mn_4N and M_6C (×12,000).
(*c*) Specimen 5; 20 hr at 1500 F and 1 hr at 1800 F; spheroidized precipitate from former boundaries, Cr_2N and $CrMoN_x$; fine intragranular precipitate, M_6C (×4000).
(*d*) Specimen 1; 1 hr at 1900 F; last remnants of intragranular precipitate (×15,000).
FIG. 5—Electron Micrographs of Carbon Extraction Replicas, Heat 7571 $\frac{5}{8}$ in. Diameter Bars Forged at 1900 F and Heat Treated as Indicated.

TABLE 4.—CREEP-RUPTURE TESTS OF KROMARC 58 WROUGHT STEELS.

Heat No.	Heat Treatment				Test Temperature, deg F	Stress, psi	Rupture Time, hr	Rupture Strain, %	Reduction of Area, %	Minimum Creep Rate, %/hr
	Time, hr	Temperature, deg F	Time, hr	Temperature, deg F						
7531	20	1500	1	1800	1200	45 000	1	38.8	51.5	15.4
					1200	35 000	37.5	33.5	24.0	0.27
					1200	30 000	242	10.3	28.6	0.025
					1200	25 000	851	40.7	68.6	0.0074
7533	20	1500	1	1800	1200	40 000	11.5	17.3	21.7	0.55
					1200	35 000	64	13.6	16.3	0.066
					1200	30 000	161	13.0	20.2	0.028
					1200	25 000	873	28.0	41.0	0.0027
7534	20	1500	1	1800	1200	45 000	7	28.5	33.4	2.0
					1200	40 000	87	21.0	27.7	0.08
					1200	35 000	136	21.0	29.2	0.039
					1200	30 000	708	36.0	62.3	0.0042
7535	20	1500	1	1800	1200	40 000	6	33.7	53.6	2.9
					1200	35 000	12	40.8	53.6	1.5
					1200	30 000	124	48.0	66.6	0.12
					1200	25 000	474	44.3	67.5	0.033
7577	...	...	1	1700	1200	45 000	176	17.0	33.7	0.039
					1200	35 000	1262	26.3	67.7	0.002
7572	...	...	1	1700	1200	50 000	112	13.3	27.2	0.048
					1200	45 000	292	21.3	42.8	0.020
					1200	40 000	495	31.6	66.5	0.0054
					1200	35 000	881	33.3	69.3	0.0022
VM 544	...	...	1	1700	1200	40 000	455	31.3	72.1	0.0075
VM 545	...	...	1	1700	1200	50 000	150	35.6	49.0	0.040
					1200	45 000	274	59.3	69.2	0.018
					1200	40 000	768	41.3	68.2	0.0034
					1200	35 000	1748	35.4	67.2	0.00095
VM 545	...	...	1	1700	1100	45 000	14234	31.0	51.7	0.0003
					1350	20 000	223	74.0	83.5	0.032
					1500	10 000	118	61.0	83.2	0.11
VM 548	...	...	1	1700	1200	50 000	111	26.0	51.8	0.033
					1200	42 500	361	42.3	69.8	0.0095
					1200	37 500	1459	41.0	75.8	0.0017
					1400	15 000	200	50.7	88.3	0.051
VM 549	...	...	1	1700	1200	50 000	81	14.7	49.8	0.055
					1200	45 000	226	14.7	52.9	0.015
					1200	42 500	535	26.7	64.0	0.0046
					1200	37 500	638	43.3	75.0	0.006
VM 550	...	...	1	1700	1200	50 000	120	33.3	47.8	0.075
					1200	42 500	698	46.0	73.4	0.0085
					1200	37 500	961	42.7	72.2	0.0040
					1100	60 000	48	22.0	23.7	0.10
VM 551	...	...	1	1700	1200	50 000	88	10.7	26.8	0.057
					1200	35 000	980	31.3	73.5	0.0027
					1300	27 500	274	48.0	82.0	0.0096
XMM 2239	...	...	1	2000	1200	45 000	4.2	37.1	38.0	4.0
					1200	40 000	25.8	22.7	24.4	0.23
					1200	35 000	88.6	20.8	21.5	0.068
	20	1500	1	1800	1200	35 000	158	15.7	26.4	0.036
					1200	30 000	423	25.0	40.0	0.0077
XMM 2240	...	...	1	2000	1200	45 000	9.5	28.1	28.1	0.36
					1200	40 000	46.8	19.3	19.9	0.045
					1200	35 000	115	15.7	14.5	0.014
	20	1500	1	1800	1200	35 000	193	19.0	26.9	0.013
XMM 2232	...	...	1	2000	1200	45 000	25.2	20.4	21.9	0.051
					1200	40 000	93	15.4	19.2	0.015
					1200	35 000	304	13.9	16.9	0.005
	20	1500	1	1800	1200	40 000	159	9.3	17.0	0.030
					1200	30 000	700+[a]			
	20	1500	1	1800	1200	40 000	51.5	4.5	17.1	0.020
					1200	35 000	197	3.3	16.2	0.0091
					1200	30 000	1245	8.0	40.3	0.00085
					1500	10 000	178	19.3	65.7	0.040

TABLE 4.—*Continued.*

Heat No.	Heat Treatment				Test Temperature, deg F	Stress, psi	Rupture Time, hr	Rupture Strain, %	Reduction of Area, %	Minimum Creep Rate, %/hr
	Time, hr	Temperature, deg F	Time, hr	Temperature, deg F						
KV 101.....	20	1500	1	1800	1200	45 000	112	33.8	36.0	0.031
					1200	40 000	288	41.5	54.9	0.0065
					1200	35 000	370	37.5	59.0	0.0067
	1	1800	20	1500	1200	45 000	36.7	53.3	54.6	0.42
					1200	40 000	80	46.2	64.0	0.133
					1200	35 000	277	46.7	72.9	0.071
XMM 2265[b].....	...	...	1	1700	1200	45 000	50.4	16.2	19.1	0.104
					1200	40 000	118	21.2	23.6	0.054
					1200	35 000	195	24.7	36.0	0.056
					1200	35 000	334	48.0	50.7	0.010
XMM 2284[c].....	...	...	1	1700	1200	45 000	61	5.3	15.7	0.012
					1200	45 000	58	5.3	18.0	0.012
					1200	35 000	661	8.7	28.3	0.0023
					1200	35 000	662	6.7	24.2	0.0020

[a] Overheated.
[b] Transverse base metal test on plate.
[c] Transverse weld test, broke in base metal (transverse direction).

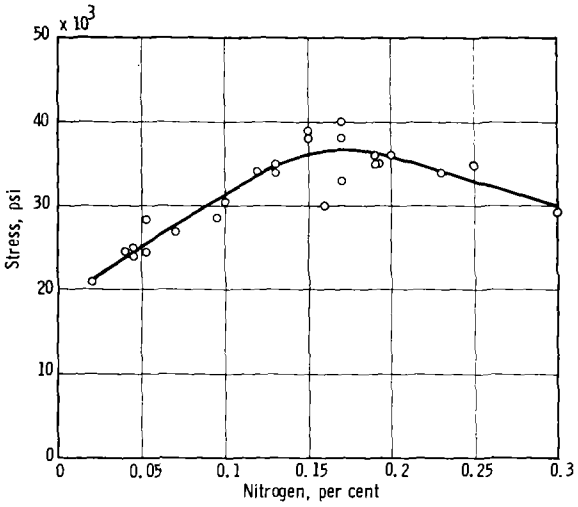


FIG. 6—Effect of Nitrogen on Stress for Rupture in 1000 hr at 1200 F for Kromarc 58 Steels.

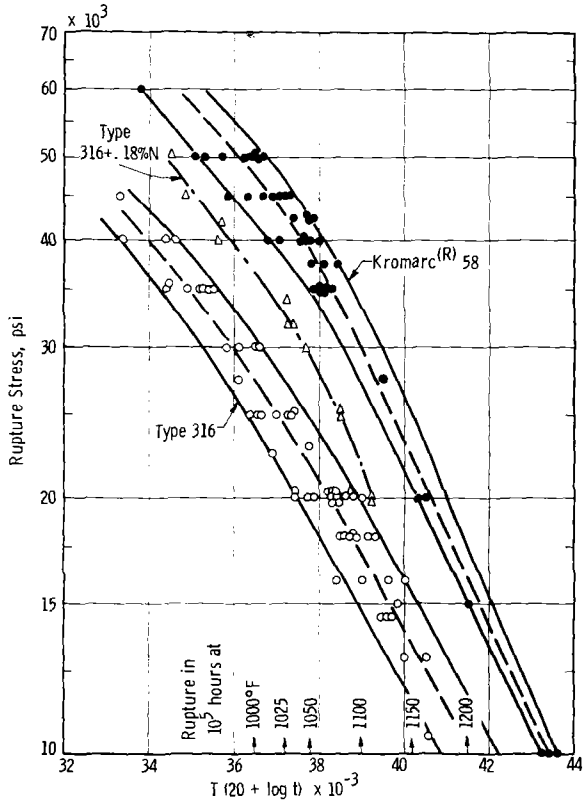


FIG. 7—Rupture Strength of Type 316 and Kromarc 58 Wrought Steels.

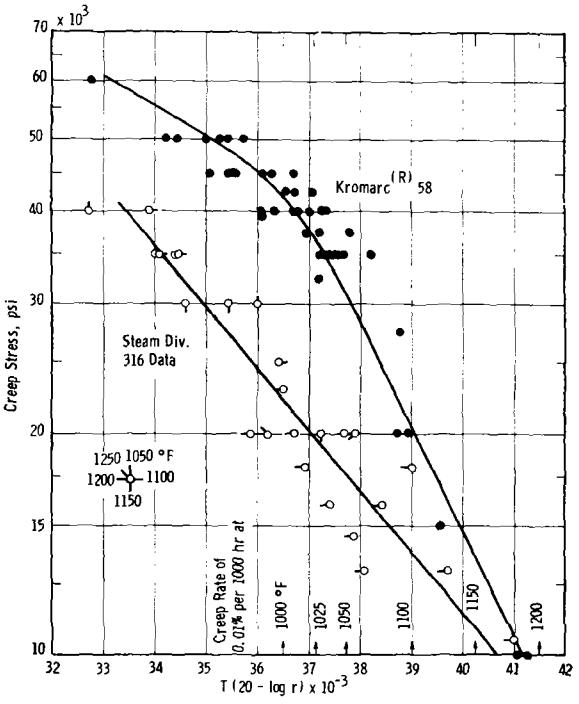


FIG. 8—Creep Strength of Type 316 and Kromarc 58 Wrought Steels.

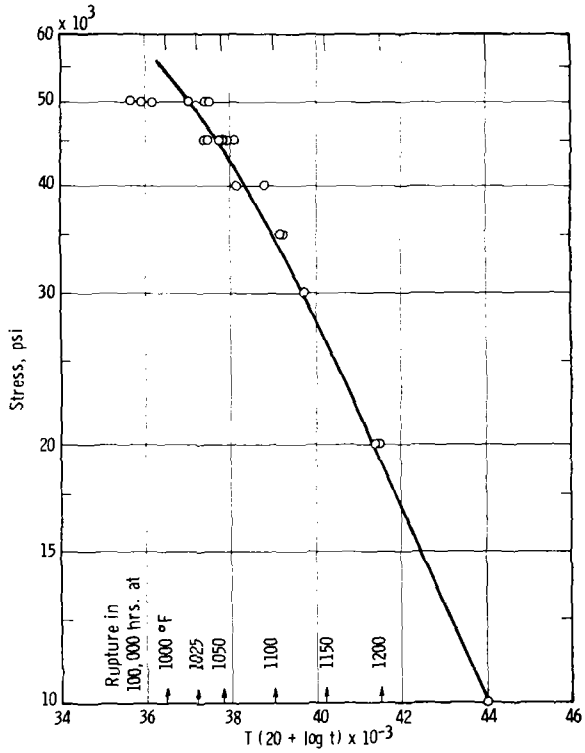


FIG. 9—Rupture Strength of Kromarc 58 Steel Tungsten Inert Gas Welds.

TABLE 5.—TENSILE PROPERTIES OF AS-DEPOSITED, ALL WELD METAL SPECIMENS OF KROMARC 58 STEEL.

Electrode Heat No.	Process	Test Temperature, deg F	0.2% Yield Strength, psi	Ultimate Strength, psi	Elongation, %	Reduction of Area %
XMM 2232	covered electrode	RT	67 200	94 000	39.3	58.7
		1025	40 500	63 300	31.0	36.0
XMM 2232[a]	covered electrode	RT	45 700	85 800	41.5	44.5
		1025	25 000	61 400	38.1	39.7
VM 545	TIG	RT	63 600	93 600	38.4	61.2
		1025	36 800	61 300	36.6	61.2
VM 548	TIG	RT	65 900	94 600	33.6	50.0
		1000	39 100	62 700	32.3	50.0
VM 550	TIG	RT	69 200	98 500	36.8	54.2
		1000	41 800	63 800	26.2	41.8
XMM 7133	TIG	RT	71 100	102 600	37.5	60.5
		600	52 700	76 400	32.0	47.1
		1025	50 400	71 900	31.0	45.2

[a] Weld heat treated 20 hr at 1500 F, 1 hr at 1800 F.

TABLE 6.—CREEP-RUPTURE TESTS OF AS-DEPOSITED TUNGSTEN INERT GAS WELDS OF KROMARC 58 STEELS.

Filler Wire Heat No.	Test Temperature, deg F	Stress, psi	Rupture Time, hr	Rupture Strain, %	Reduction of Area, %	Minimum Creep Rate, %/hr
VM 544	1200	45 000	873	10.0	20.0	0.0015
	1200	35 000	4680	19.0	53.8	0.00015
	1300	30 000	380	34.6	58.6	0.00033
VM 545	1200	45 000	574	22.7	42.0	0.0017
	1200	40 000	992	19.3	45.0	0.0008
	1200	35 000	665+ [a]	...	...	0.00025
	1200	50 000	49	30.7	59.3	0.227
	1200	35 000	4178	27.0	49.0	0.00014
	1350	20 000	742	43.3	69.5	0.0008
	1500	10 000	284	17.3	51.7	0.00038
XMM 2296	1200	50 000	66	16.7	6.0	0.0019
	1200	45 000	693	14.0	27.2	0.0008
	1200	40 000	2492	14.7	26.8	0.00008
VM 548	1200	50 000	398	24.0	50.0	0.0033
	1200	45 000	759	22.7	56.7	0.0012
	1400	20 000	207	20.6	56.1	0.0042
VM 575	1200	50 000	347	12.7	21.0	0.00096
VM 579	1200	50 000	213	7.3	23.2	0.00085
	1200	45 000	397	6.0	21.0	0.0019
XMM 7117	1200	50 000	34	4	13.6	...
	1200	45 000	377	4	13.6	...

[a] Stress raised to 50,000 psi after 665 hr.

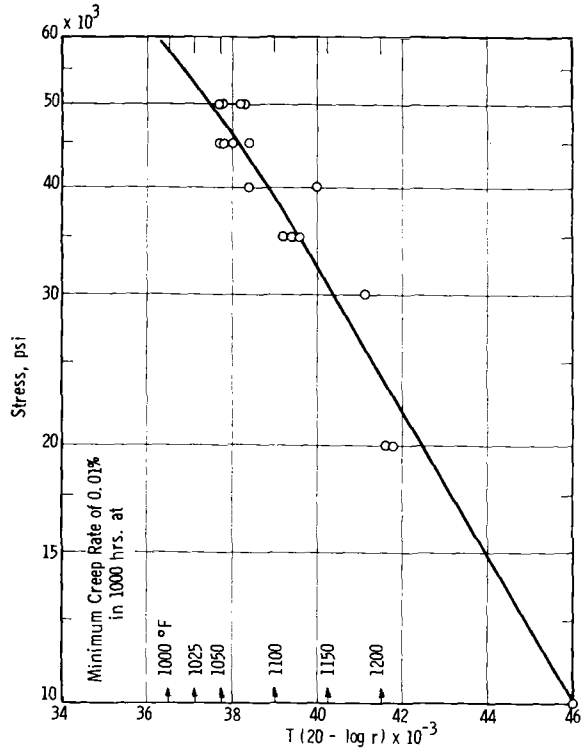


FIG. 10—Creep Strength of Kromarc 58 Steel Tungsten Inert Gas Welds.

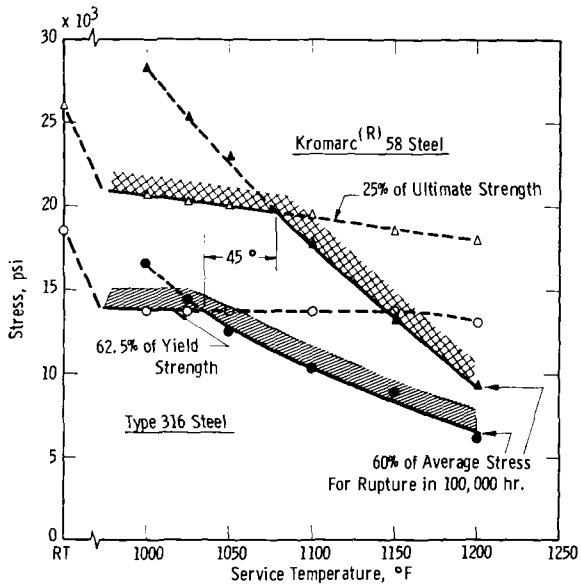


FIG. 11—Factors Determining Code Allowable Stresses for Type 316 and Kromarc 58 Steels.

ture in 100,000 hr is limiting. In the case of Kromarc 58 steel, 25 per cent of the ultimate strength controls up to about 1080 F, and then average rupture strength limits. The net effect of the increases in both tensile and creep-rupture properties of Kromarc 58 steel is to raise both the allowable stress and the useful service-temperature range before allowable stresses start dropping rapidly.

PRODUCTION EXPERIENCE

Approximately 150,000 lb of Kromarc 58 have been produced for steam-turbine applications. Induction melting was used initially to produce ingots weighing 5000 and 7500 lb. More recently, a 20,000-lb electric-arc furnace heat was made by commercial melting practices. This material also had acceptable properties and is being applied. Ingots were converted into billets for subsequent forging, rolling into plate, or piercing by press or hammer forging.

Tubing $10\frac{3}{4}$ and 14 in. in diameter and with a 0.35-in. wall has been produced from plate by TIG welding the longitudinal seam. Formed and welded 90-deg elbows, forged flanges, and the tubing have been assembled into a reheat steam line for a commercial turbine. Seamless tubing 5 in. in diameter with a 0.5 in. wall has been made by hot piercing and cold working. Pipe bends were easily made and matching seamless elbows and flanges have been produced. These components are being assembled into a steam inlet system for the same turbine.

CONCLUSION

A development program, aimed specifically at finding a weldable, high strength, wrought alloy for steam-turbine piping and a compatible fully austenitic welding wire, resulted in a new alloy, called Kromarc 58 steel. The starting point of the investigation was a study of the effects of alloying elements on weldability; later, other factors, such as strength, oxidation resistance, and impact strength, were considered in arriving at the following alloy composition: 16 per cent chromium, 20 per cent nickel, 10 per cent manganese, 2.25 per cent molybdenum, 0.2 per cent vanadium, 0.25 per cent silicon, 0.01 per cent boron, 0.01 per cent zirconium, 0.04 per cent carbon, 0.17 per cent nitrogen, and balance iron. This alloy has been produced by commercial processes as seamless or welded tubing, elbows, flanges, and wires; and these components have been fabricated by TIG welding into steam-turbine inlet and reheat pipe lines.

REFERENCES

(1) F. C. Hull, "Effects of Alloying Additions on Hot Cracking of Austenitic Chromium-Nickel Stainless Steels," *Proceedings*, Am. Soc. Testing Mats., Vol. 60, 1960, pp. 667–690.

(2) F. C. Hull and R. Stickler, "Effects of Nitrogen, Boron, Zirconium and Vanadium on the Microstructure, Tensile and Creep-Rupture Properties of a Chromium-Nickel-Manganese-Molybdenum Stainless Steel," Joint International Conference on Creep, New York, N.Y., Aug. 25–29, 1963.

(3) "Brookhaven's Big Bubble Bath," *The Esco Ladle*, Vol. 25 (9), 1962, pp. 4–7.

(4) K. J. Irvine, D. T. Llewellyn, and F. B. Pickering, "High-Strength Austenitic Stainless Steel," *Journal*, Iron and Steel Inst., Vol. 199, 1961, p. 193.

(5) E. A. Sticka, "Structural Stability of Commercial Wrought Austentic Steels for Power Plant Piping to 1450 F," *Proceedings*, Am. Power Conference, Vol. XXII, Illinois Institute of Technology, Chicago, Ill., 1960, pp. 288–301.

(6) W. F. Simmons and H. C. Cross, "Report on the Elevated-Temperature Properties of Stainless Steels," *Elevated-Temperature Properties of Stainless Steel, ASTM STP 124*, Am. Soc. Testing Mats., 1952, pp. 87–88.

DISCUSSION

G. D. GARDNER[1]—This interesting chrome-nickel stainless steel which you have developed for elevated temperature service would appear to be useful in corrosive environments. Has the corrosion resistance been studied in such environments as sulfuric and phosphoric acid?

F. C. HULL (*author*)—Kromarc 58 steel was developed specifically for service in power plants and turbines as piping and allied components for carrying high-temperature steam. As a result, we have not had the occasion to evaluate its corrosion resistance in the environments mentioned.

[1] U. S. Industrial Chemicals Co., Tuscola, Ill.

CREEP-RUPTURE PROPERTIES OF STAINLESS STEELS AT 1600, 1800, AND 2000 F

By K. G. Brickner,[1] G. A. Ratz,[2] and R. F. Domagala[3]

Synopsis

In recent years, there has been a trend toward the use of increasingly higher operating temperatures in many industrial processes to obtain greater operating efficiencies. This trend has created many design- and material-selection problems. As is now widely recognized, the difference between the behavior of metals at elevated temperatures and at room temperature necessitates an approach to the problem of design for elevated-temperature service different from that for room-temperature service. The occurrence of creep during elevated-temperature service, as well as the need for preventing actual rupture (the end result of creep), requires knowledge of the stresses and temperatures which materials must withstand without producing excessive creep or rupture. However, the designer is often faced with very limited engineering information of this type. For example, little information is available on the creep and creep-rupture properties of stainless steels at temperatures above 1500 F. To provide a basis for the selection of stainless steels for service between 1600 and 2000 F, creep and creep-rupture tests and metallographic and X-ray diffraction studies were conducted on sheet product of AISI Types 302, 309S, 310S, 314, and 316, and Type 310 Cb stainless steels at 1600, 1800, and 2000 F, and on sheet product of AISI Type 446 stainless steel at 1600 and 1800 F.

A program was initiated to determine the creep and creep-rupture properties of stainless steels between 1600 and 2000 F. This paper (1) summarizes the creep and creep-rupture properties determined in this program on sheet product of AISI Types 302, 309S, 310S, 314, and 316, and Type 310 Cb stainless steels tested in air at 1600, 1800, and 2000 F, and on sheet product of AISI Type 446 stainless steel tested in air at 1600 and 1800 F, and (2) rates these steels according to their creep-rupture strength at these temperatures. In addition, the results of metallographic studies and hardness measurements that were made on each steel before testing (in the annealed condition) and after long-time creep-rupture testing are included. Also given are the results of X-ray diffraction studies made on the specimens of each steel that failed after the longest times at each test temperature to determine the phases precipitated during testing.

Materials and Experimental Work

The steels used in this investigation were from commercial electric-furnace heats that were processed to sheet product between 0.050 and 0.070 in. thick. The compositions of these steels are shown in Table 1(*a*), and the composition limits as specified by the AISI are shown in Table 1(*b*). Note that, except for Type 310 Cb steel, which is not a recognized AISI grade, the compositions of all the steels used in this investigation were within the specification limits established by the AISI.

The samples of Type 302 steel were obtained from a cold-reduced coil that had been continuously annealed at 1975 F and then roller leveled, whereas the samples of the other austenitic steels were obtained from cold-reduced hand-mill sheets that had been annealed in a sheet-annealing furnace at 1990 F and then stretcher leveled. The samples of Type 446 steel were obtained from cold-reduced hand-mill sheets that had been annealed in a sheet-annealing furnace at 1975 F.

Creep-rupture specimens, of the design shown in Fig. 1, were machined from sheets of each steel. After being machined, the creep-rupture specimens were tested in air at 1600, 1800, and 2000 F in direct-load creep-rupture machines. (Unfortunately, sufficient data to permit the determination of the creep-rupture properties at 2000 F were not obtained on Type 446 stainless steel.) The minimum-creep-rate data were obtained by using a sensitive dial gage that was actuated by movement of the lower pull rod in the test assembly. These data were automatically recorded on film for the first 24 hr of testing, after which the dial gage was read periodically and the data were recorded manually.

In addition to the creep-rupture tests, Vickers hardness measurements and metallographic studies were conducted on each steel before and after long-time creep-rupture testing. X-ray diffraction studies were also made on residues that were extracted from creep-rupture specimens (of each steel) which failed after the longest test times at 1600, 1800, and 2000 F to determine the phases that had formed during testing. These residues were obtained from the specimens by extracting them electrolytically in a 5 per cent hydrochloric acid solution.

Results and Discussion

Creep-Rupture Tests:

The results of the creep-rupture tests are summarized in Table 2 and are presented graphically in Figs. 2–13.

The data in Table 2 indicate that at 1600 F the austenitic stainless steels investigated had 1000-hr creep-rupture strengths about 3 to 6 times higher than the creep-rupture strength of the ferritic Type 446 stainless steel. At 1800 F, however, the 1000-hr creep-rupture strengths of the austenitic stainless steels were only about 2 to 4 times higher than the strength of the ferritic steel. The superiority of the austenitic stainless steels is to be expected, for it is well known that the austenitic steels have better elevated-temperature strength than do the ferritic stainless steels.

The creep-rupture-strength data in Table 2 also indicate that Type 310S steel was markedly stronger (as much as 35 per cent) at 1600 and 1800 F than the next strongest steel tested. However, at 2000 F, Type 314 steel was slightly stronger than Type 310S steel.

The importance of oxidation resistance at these temperatures is indicated by the relatively low creep-rupture strength of the Type 316 steel at 1800 and 2000 F. Type 316 steel is the strongest standard stainless steel at 1500 F (1),[4] but above

[1] Research engineer, stainless steel products, Applied Research Laboratory, U. S. Steel Corp., Monroeville, Pa.

[2] Senior technologist, Applied Research Laboratory, U. S. Steel Corp., Monroeville, Pa.

[3] Manager, Metallurgical Processes, IIT Research Inst., Chicago, Ill.

[4] The boldface numbers in parentheses refer to the list of references appended to this paper.

Copyright© 1965 by ASTM International

www.astm.org

TABLE 1(*a*)—CHEMICAL COMPOSITION OF THE STEELS INVESTIGATED, PER CENT.
(CHECK ANALYSIS)

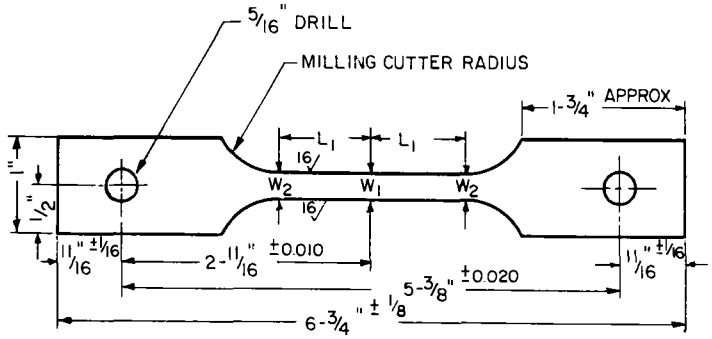
Steel	C	Mn	P	S	Si	Ni	Cr	Mo	N	Cb
AISI Type 302	0.05	1.35	0.031	0.006	0.72	8.5	17.2	...[a]	0.058	...[a]
AISI Type 309S	0.05	1.32	0.024	0.021	0.51	14.8	22.5	...[a]	0.023	...[a]
AISI Type 310S	0.07	1.50	0.028	0.007	0.61	20.5	24.6	...[a]	0.064	...[a]
Type 310 Cb	0.057	1.70	0.021	0.008	0.68	20.9	24.9	...[a]	0.063	0.92
AISI Type 314	0.04	1.48	0.019	0.008	2.15	20.7	24.1	...[a]	0.055	...[a]
AISI Type 316	0.05	1.40	0.033	0.025	0.41	13.5	17.6	2.20	0.029	...[a]
AISI Type 446	0.12	0.73	0.024	0.011	0.36	0.26	24.9	...[a]	0.17	...[a]

[a] Not determined because element was not intentionally added and was present only as a residual

TABLE 1(*b*)—AISI COMPOSITION LIMITS FOR THE STEELS INVESTIGATED, PER CENT.

AISI Type	C	Mn	P	S	Si	Ni	Cr	Mo	Cb
302	0.15 max	2.00 max	0.045 max	0.030 max	1.00 max	8.00 / 10.00	17.00 / 19.00	...[a]	...[a]
309S	0.08 max	2.00 max	0.045 max	0.030 max	1.00 max	12.00 / 15.00	22.00 / 24.00	...[a]	...[a]
310S	0.08 max	2.00 max	0.045 max	0.030 max	1.50 max	19.00 / 22.00	24.00 / 26.00	...[a]	...[a]
314	0.25 max	2.00 max	0.045 max	0.030 max	1.50 / 3.00	19.00 / 22.00	23.00 / 26.00	...[a]	...[a]
316	0.08 max	2.00 max	0.045 max	0.030 max	1.00 max	10.00 / 14.00	16.00 / 18.00	2.00 / 3.00	...
446[b]	0.20 max	1.50 max	0.040 max	0.030 max	1.00 max	...[a]	23.00 / 27.00	...[a]	...[a]

[a] Not specified.
[b] A maximum nitrogen content of 0.25 per cent is also specified for this grade.



$L_1 = 1\text{-}1/8 + 1/16, -0$
$W_1 = 0.250 \pm 0.003$
$W_2 = W_1 + 0.003$ to 0.005

FIG. 1—Sheet-Type Creep-Rupture Test Specimen Used in the Investigation.

about 1600 F, it is subject to rapid oxidation (2). This rapid oxidation of Type 316 steel during creep-rupture testing decreases the effective cross-sectional area of the test specimen and results in an apparent lower creep-rupture strength.

A comparison of the relative strengths of the steels studied in this investigation is very difficult because of the high test temperatures. These high temperatures accelerate microstructural changes that can greatly affect the strength of the steels depending on the time interval selected. Because in most engineering applications it is desirable to design a structure to last the longest possible time, it would appear logical to compare these steels according to their extrapolated creep-rupture strength at 10,000 hr. However, because of the expected variations in strength for each composition range and the error inherent in extrapolating data, relatively large variations between the creep-rupture strengths of these steels may not be statistically significant.

It is of interest to note that Type 310 Cb steel was substantially weaker than Type 310S steel, even though the two steels have about the same composition except for the columbium content of Type 310 Cb steel. The reason for this behavior is not definitely known, but it is believed to be associated with a softening of Type 310 Cb steel owing to the combining of columbium with the carbon and nitrogen in the steel. Smith and coworkers have shown that additions of carbon and nitrogen significantly increase the strength of stainless steels at elevated temperatures (3,4). Further confirmation that the low strength of Type 310 Cb steel is associated with the softening of its matrix is obtained by comparing the elongation at rupture of Type 310 Cb steel with that of Type 310S steel. Type 310 Cb steel had elongations between 22 and 150 per cent, whereas Type 310S steel had elongations between 18 and 51 per cent.

On the basis of limited minimum-creep-rate data (0.01 per cent/hr), Table 2, the steels exhibited the same trend in creep strength that they exhibited in creep-rupture strength. That is, the austenitic stainless steels were more resistant to creep than was the ferritic Type 446 stainless steel, Type 310S steel had the lowest creep rate at 1600 and 1800 F, and Type 314 steel had a creep rate at 2000 F slightly lower than that of Type 310S steel. It should be recognized that at these temperatures the second (minimum) stage of creep is relatively short, and, therefore, indiscriminate extrapolation of these data to times and stresses not tested should be avoided. Also, these data should not be converted to give the stress to produce a specific amount of creep in a particular length of time—for example, 1 per cent in 1000 hr. Expressing creep-rate data in this manner can give the impression that for the given stress, only 1 per cent creep will occur in 1000 hr. That is not true; much more creep—depending on the strain during primary creep and the time for the onset of tertiary creep—could occur.

Because elongation at rupture generally decreases with increasing time to rupture, it is very important for the designer to know the expected elongation at rupture of a steel after long-time testing. However, the relationship between elongation at rupture and time to rupture, in general, does not follow a consist-

TABLE 2—CREEP-RUPTURE-TEST RESULTS FOR THE STEELS INVESTIGATED.

Steel Type	Test Temperature, deg F	Stress, psi				Extrapolated Elongation at Rupture in 10,000 hr, %
		Rupture, hr			Creep Rate, 0.01%/hr	
		100	1000	10 000[a]		
302	1600	4700	2800	1750	2500	150
	1800	2450	1550	960	1300	30
	2000	1300	760	460	620	18
309S	1600	5800	3200	...[b]	3500	...[b]
	1800	2600	1650	1000	1000	105
	2000	1400	830	480	760	42
310S	1600	6600	4000	2500	4000	30
	1800	3200	2100	1350	1750	60
	2000	1500	1100	760	800	60
310 Cb	1600	5000	2500	1300	2400	60
	1800	2200	1200	660	460	100
	2000	1050	700	420	170	340
314	1600	4700	3000	1950	2300	110
	1800	2600	1700	1100	1000	120
	2000	1500	1120	850	900	82
316	1600	5000	2700	1400	2600	30
	1800	2650	1250	600	1200	35
	2000	1120	360	...[b]	400	...[b]
446	1600	1100	720	...[b]	800	...[b]
	1800	700	500	...[b]	420	...[b]

[a] Extrapolated data.
[b] Rupture times not long enough to determine accurate values.

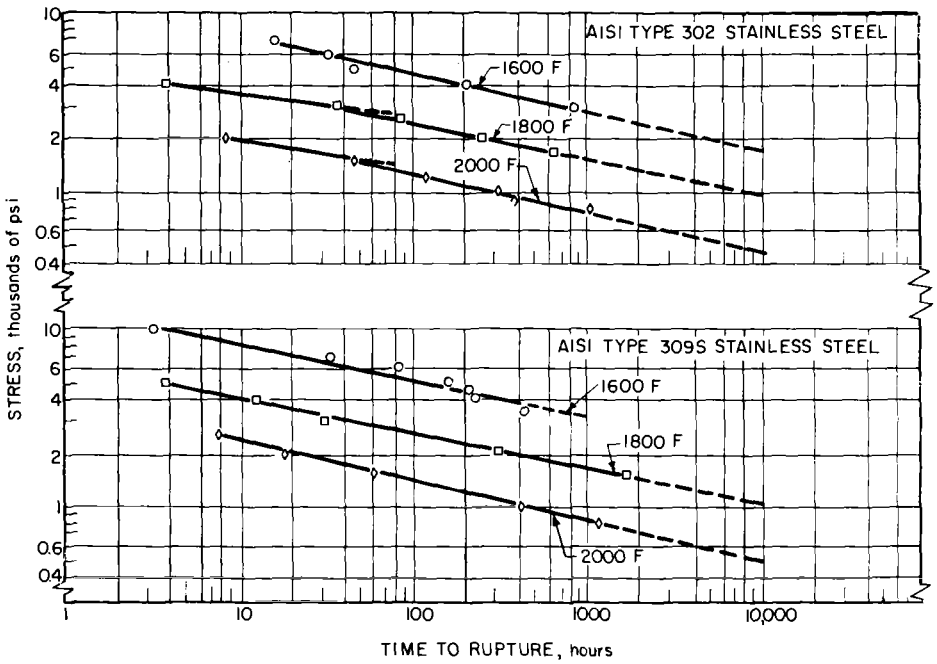


FIG. 2—Relation Between Stress and Time to Rupture for AISI Types 302 and 309S Stainless Steels.

ent pattern, and is not suited to extrapolation to rupture times beyond those tested. Therefore, to obtain an estimate of elongation at rupture after long-time testing, it is necessary to handle the data by the method developed by Smith and co-workers (5). Their method is based on the discovery that a straight line is obtained by plotting the logarithm of the stress originally applied against the logarithm of the ratio of the elongation at rupture to the time to rupture. Actually, this ratio is an average creep rate. The elongation at rupture data obtained after creep-rupture testing is presented graphically in this manner in Figs. 4, 7, 10, and 13. In addition, the elongations of the steels studied that may be expected after rupture in 10,000 hr are summarized in Table 2. Note that unlike the results obtained at lower test temperatures, there does not appear to be a tendency for the elongation to decrease to very low values with increasing time to rupture. Apparently at these temperatures, the grain boundaries do not restrict elongation. The high rupture elongations of the stainless steels at these temperatures could be advantageous under certain conditions because impending failures would be noticed more readily and equipment could be replaced before actual failure occurred in the steel.

A rough approximation of the oxidation resistance of the steels was obtained by visual examination of the broken creep-rupture specimens. This examination indicated that Types 310S, 314, and 446 steels had the best resistance to oxidation in air in the range 1600 to 2000 F and that the oxidation resistance of these steels was about the same. (However, relatively slight differences in oxidation resistance that cannot be distinguished visually probably exist.) This examination also indicated that the oxidation resistance of Types 310 Cb, 309S, 302, and 316 steels was less than that of the above steels and that the oxidation resistance decreased in the order listed. The oxidation of Type 316 steel at 1800 and 2000 F, and of Type 302 steel at 2000 F was considered to be so severe, however, that their usefulness as structural materials in an oxidizing environment at these higher temperatures would be limited.

These creep-rupture and relative oxidation-resistance results indicate that these stainless steels can be considered for many applications involving service between 1600 and 2000 F.

Metallographic and X-Ray Diffraction Studies:

The representative microstructures of the steels, in the annealed condition and after long-time creep-rupture testing at 1600, 1800, and 2000 F are shown in Figs. 14–16. With the exception of Type 446 steel, the microstructures of the steels in the annealed condition consisted of austenite and some undissolved carbides or nitrides or both. The microstructure of Type 446 steel in the annealed condition consisted of ferrite and some undissolved carbides or nitrides or both, Fig. 16(*a*).

The microstructure of Type 302 steel after long-time creep-rupture testing at 1600 and 1800 F, which is similar to that shown in Figs. 14(*c*) and (*d*), respectively, showed a considerable increase in the amount of phases precipitated compared with the microstructure of the annealed

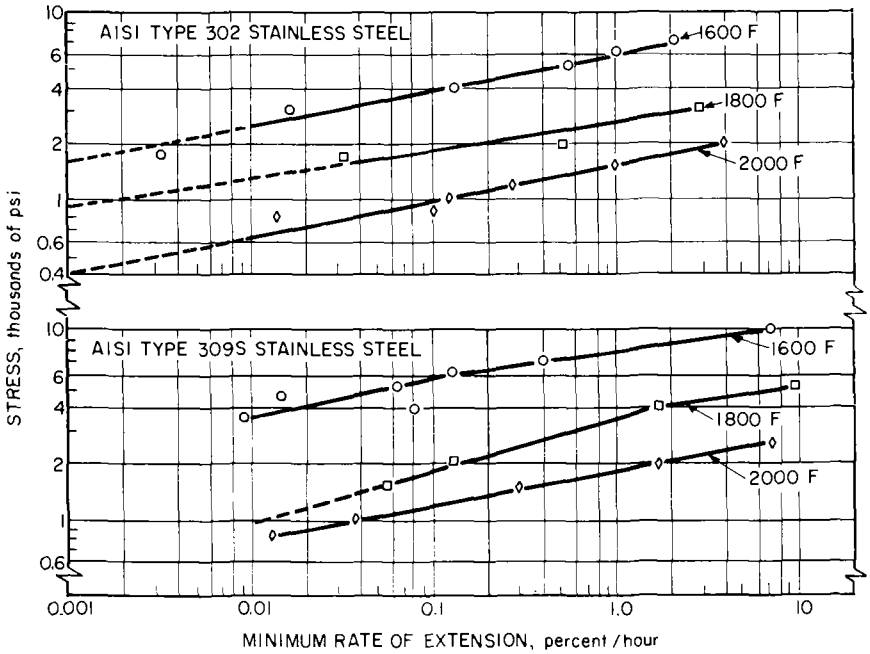


FIG. 3—Relation Between Stress and Minimum Rate Extension for AISI Types 302 and 309S Stainless Steels.

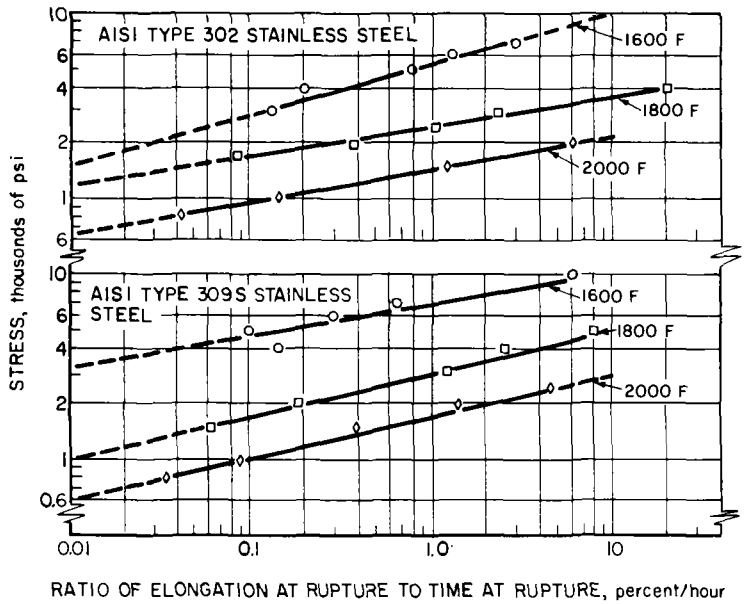


FIG. 4—Relation Between Stress and Ratio of Elongation at Rupture to Time at Rupture for AISI Types 302 and 309S Stainless Steels.

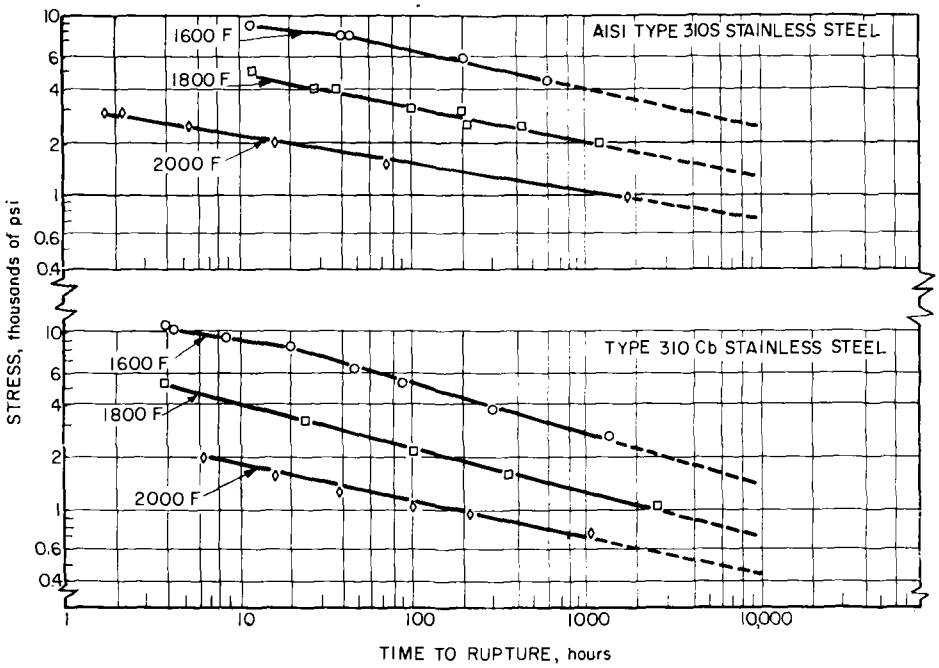


FIG. 5—Relation Between Stress and Time to Rupture for AISI Type 310S and Type 310 Cb Stainless Steels.

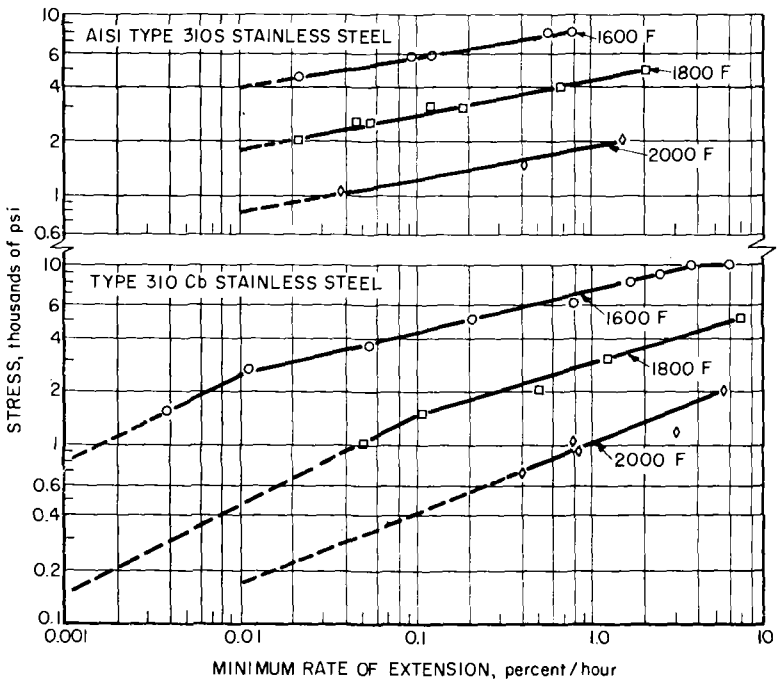


FIG. 6—Relation Between Stress and Minimum Rate of Extension for AISI Type 310S and Type 310 Cb Stainless Steels.

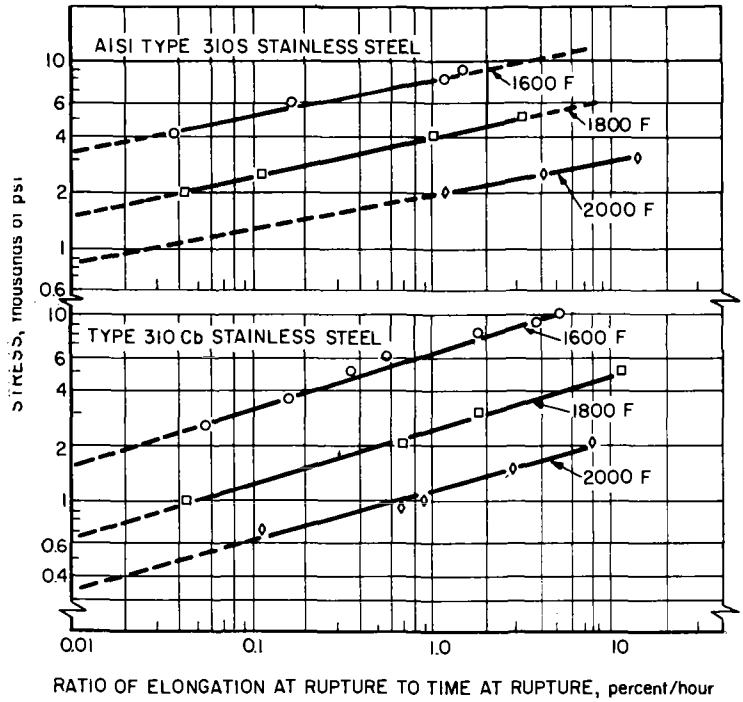


FIG. 7—Relation Between Stress and Ratio of Elongation at Rupture to Time at Rupture for AISI Type 310S and Type 310 Cb Stainless Steels.

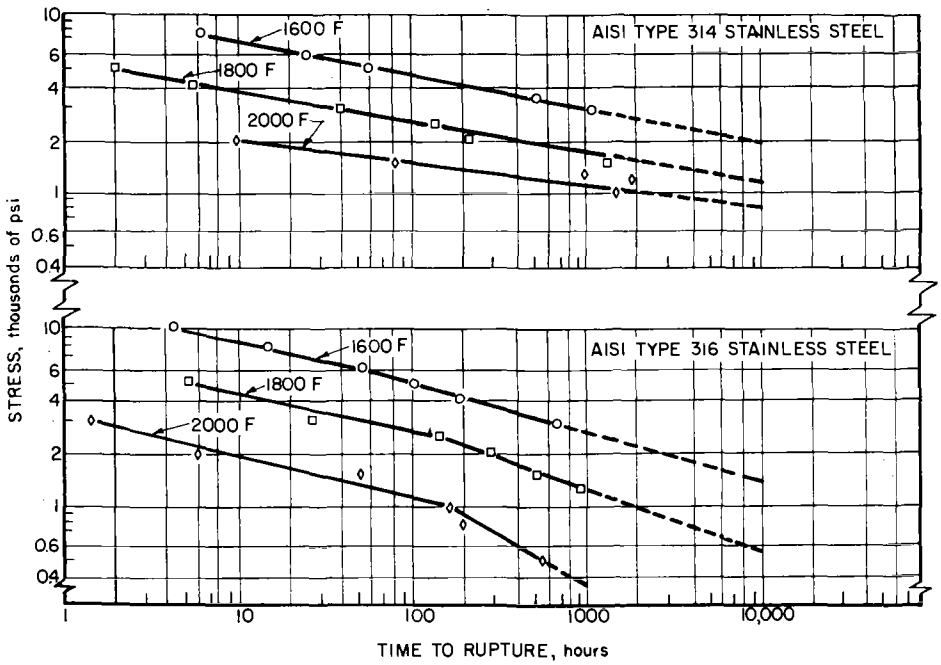


FIG. 8—Relation Between Stress and Time to Rupture for AISI Types 314 and 316 Stainless Steels.

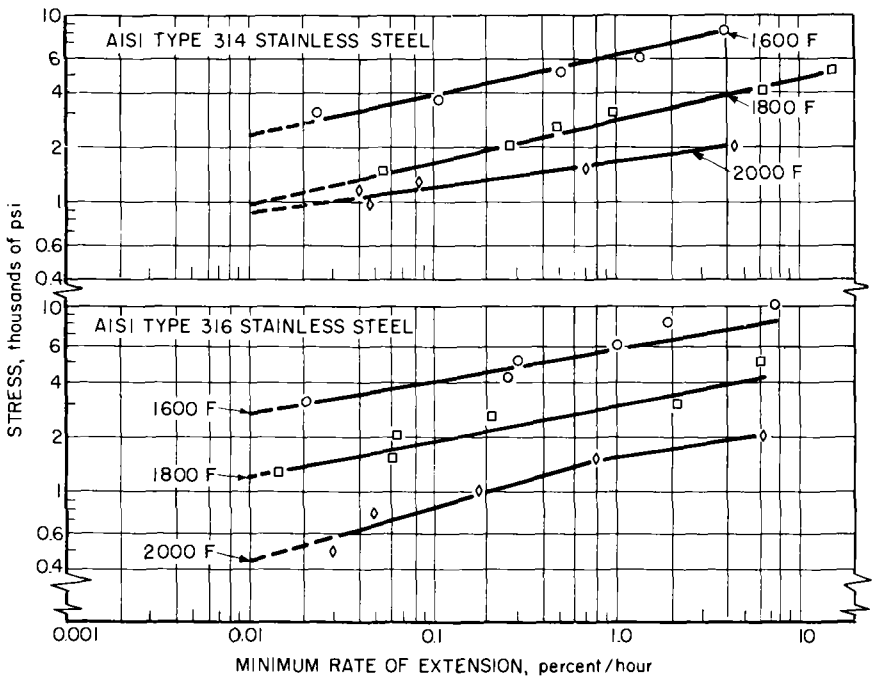


FIG. 9—Relation Between Stress and Minimum Rate of Extension for AISI Types 314 and 316 Stainless Steels.

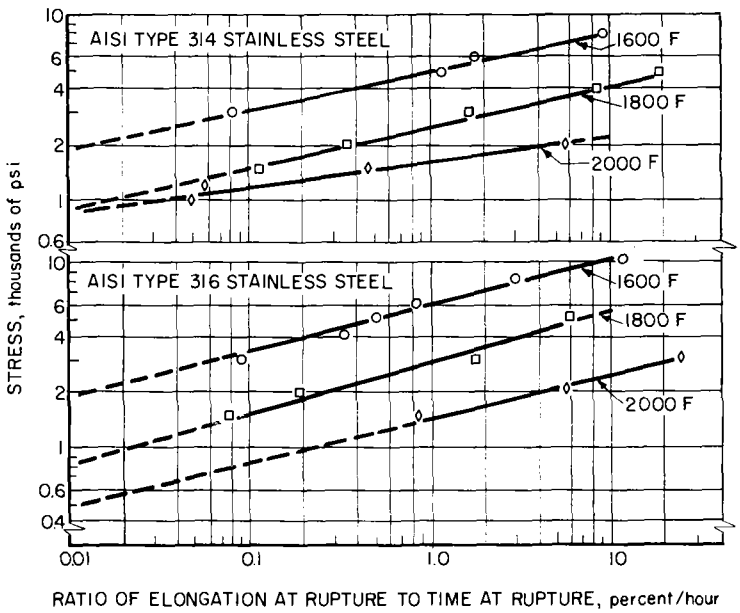


FIG. 10—Relation Between Stress and Ratio of Elongation at Rupture to Time at Rupture for AISI Types 314 and 316 Stainless Steels.

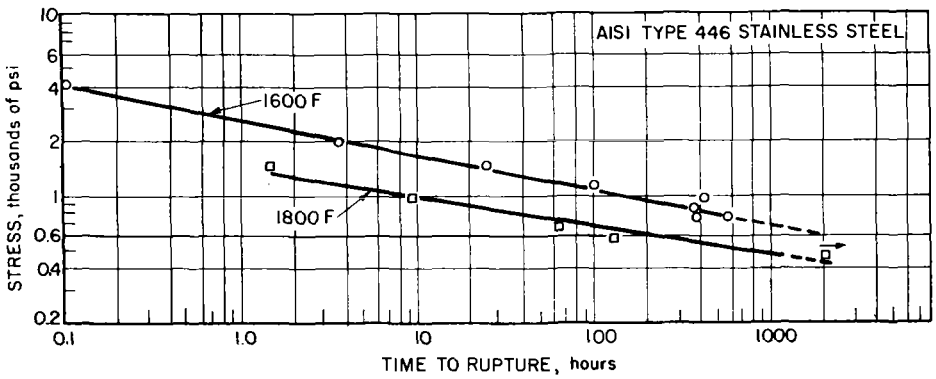


FIG. 11—Relation Between Stress and Time to Rupture for AISI Type 446 Stainless Steel.

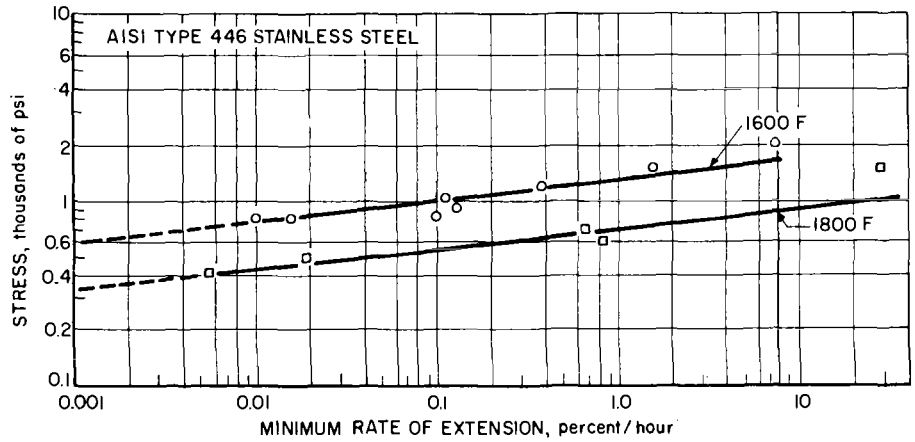


FIG. 12—Relation Between Stress and Minimum Rate of Extension for AISI Type 446 Stainless Steel.

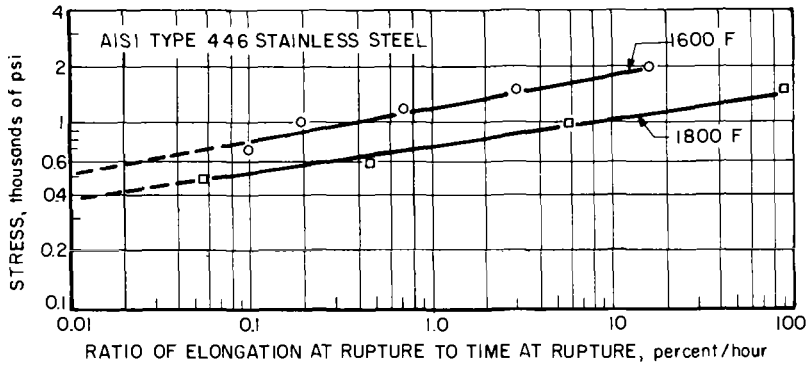
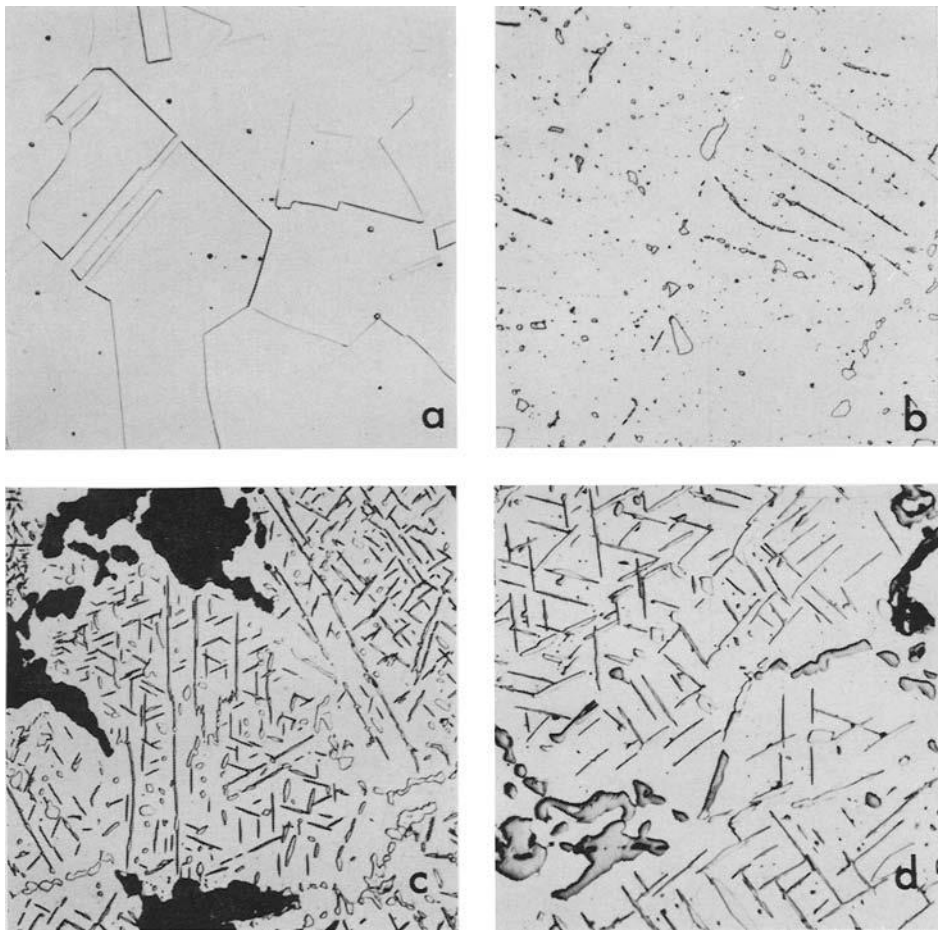


FIG. 13—Relation Between Stress and Ratio of Elongation at Rupture to Time at Rupture for AISI Type 446 Stainless Steel.



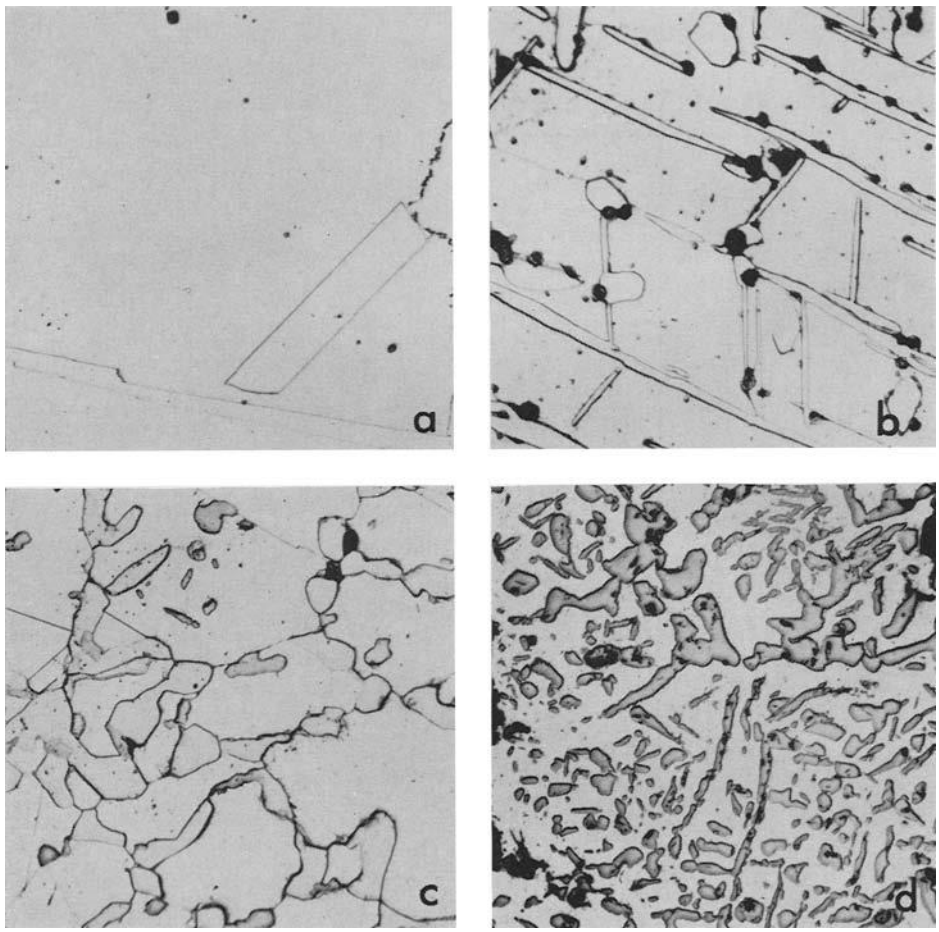
(*a*) Typical annealed structure of the austenitic stainless steels prior to exposure, Etched in Glyceregia.

(*b*) Typical structure of AISI Types 309S, 310S, and 316 stainless steels after creep-rupture testing at 1600 F.

(*c*) Typical structure of AISI Types 302, 304, and 310 stainless steels after creep-rupture testing at 1600 F.

(*d*) Typical structure of AISI Types 302, 309S, 310S, 314, and 316 stainless steels after creep-rupture testing at 1800 F.

FIG. 14—Representative Microstructure of Austenitic Stainless Steels After Annealing and After Long-Time Creep-Rupture Testing. Etched in Vilella's Reagent Except Where Noted (×500).



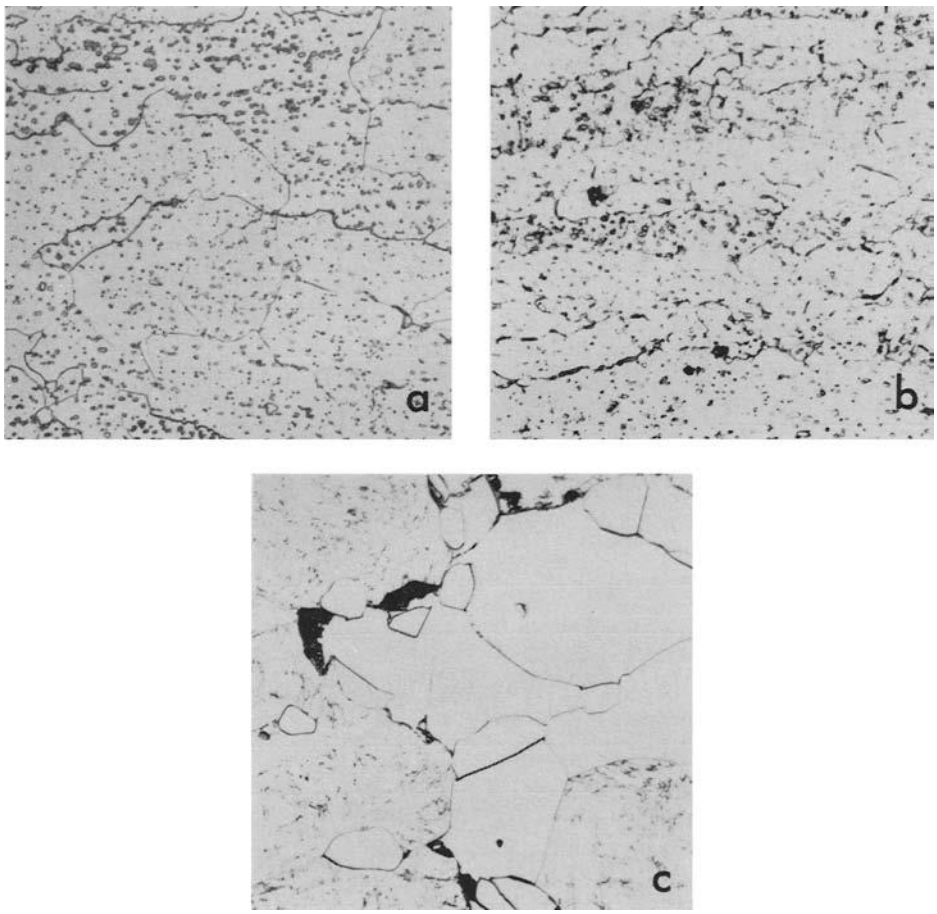
(*a*) Typical structure of AISI Types 302 and 316 stainless steels after creep-rupture testing at 2000 F.

(*b*) Typical structure of AISI Types 309S, 310S, and 314 stainless steels after creep-rupture testing at 2000 F.

(*c*) Typical structure of Type 310 Cb stainless steel after creep-rupture testing at 2000 F.

(*d*) Subscale oxides formed at the immediate surfaces of the specimens and contiguous to the fissures during long-time creep-rupture testing.

FIG. 15—Representative Microstructures of Austenitic Stainless Steels After Long-Time Creep-Rupture Testing. Etched in Vilella's Reagent (×500).



(*a*) Annealed structure prior to exposure.
(*b*) After creep-rupture testing for 582 hr at 1600 F.
(*c*) After creep-rupture testing for 2081 hr at 1800 F.

FIG. 16—Microstructure of AISI Type 446 Stainless Steel After Annealing and After Long-Time Creep-Rupture Testing. Etched in Vilella's Reagent (×500).

sample, which is similar to that shown in Fig. 14(*a*). The precipitated phases were believed to be carbides and chromium nitrides. X-ray diffraction studies of the extracted phases confirmed the presence of carbides of the $M_{23}C_6$ type, but did not indicate the presence of chromium nitrides probably because of the extraction technique used. Studies by other investigators (5,6) have shown that nitrogen is absorbed during creep-rupture testing in air and is precipitated as chromium nitrides in a Widmänstatten- or pearlitic-type structure. Chemical analyses of the long-time creep-rupture specimens of Type 302 steel indicate the absorption of nitrogen (in amounts ranging from 0.30 to 0.53 per cent nitrogen after testing as compared with 0.058 per cent nitrogen before testing). Thus, the precipitate in the Widmänstatten pattern is undoubtedly a chromium nitride. (Chemical analyses of the other steels after long-time creep-rupture testing also showed an increase in the amount of nitrogen.) After long-time creep-rupture testing at 2000 F, however, only a small amount of a precipitate (probably carbides), similar to that shown in Fig. 15(*a*), was observed at the grain boundaries. It is believed these precipitates formed in the specimen upon cooling from the test temperature. Except for this precipitate, and a larger grain size, the microstructure after testing at 2000 F was similar to the annealed microstructure.

Similarly, the microstructures of Types 309S, 310S, 310 Cb, 314, and 316 steels, in comparison with their annealed microstructures, all exhibited a considerable increase in the amount of precipitated carbides (which were identified by X-ray diffraction as the $M_{23}C_6$ type) at 1600 and 1800 F. However, after the steels were tested at 1600 F, the microstructures of Types 309S, 310S, and 316 steels did not show the pronounced Widmänstatten-type chromium nitride precipitate noted in Type 302 steel tested at 1600 F, whereas Types 310 Cb and 314 steels did show this precipitate (Fig. 14(*b*)). Further, Types 309S, 310S, and 314 steels, in contrast to Type 302 steel, also had chromium nitrides precipitated in a typical Widmänstatten pattern at 2000 F. Figure 15(*b*) shows a microstructure typical of Types 309S, 310S, and 314 steels, whereas Fig. 15(*a*) shows a microstructure typical of Type 302 steel. Type 316 steel after testing at 1800 and 2000 F had microstructures similar to the microstructure of Type 302 steel tested at 1800 and 2000 F. Type 310 Cb steel after testing at 1800 and 2000 F had precipitated phases that were more massive than those precipitated in the other steels, and the typical Widmänstatten pattern was not observed. The microstructure typical of Type 310 Cb steel after long-time testing at 2000 F is shown in Fig. 15(*c*). The samples of Type 446 steel after long-time creep-rupture testing at 1600 and 1800 F, Figs. 16(*b*) and 16(*c*), consisted of a matrix of ferrite with carbides and chromium nitrides. "Nitrogen pearlite" was present in some of the grains of this steel after testing at 1800 F; this phase can be seen as the dark etching areas at the grain boundaries in Fig. 16(*c*).

Also, at the 1600 F test temperature, sigma phase was detected in Types 309S, 310S, 310 Cb, 314, and 316 steels. No sigma phase was detected in the long-time creep-rupture specimens of Types 302 and 446 steels after the specimens were tested at 1600 F, nor was sigma phase detected in any steel at the higher test temperatures. These results are consistent with results presented in literature (7) which show that (1) austenitic stainless steels containing lesser amounts of ferrite-forming elements (such as chromium, molybdenum, silicon, and columbium) are less susceptible to the precipitation of sigma phase than are the austenitic stainless steels containing larger amounts of these elements, and (2) nickel raises the upper limit of the temperature range for the precipitation of sigma phase.

In addition, "subscale oxides" (spinels) were observed in all the steel specimens, particularly near the internal fissures formed in the specimens because of the stress and long-time exposure at elevated temperatures. The amount of these oxides increased proportionately with the increase in the amount of fissuring. Figure 15(*d*) shows the subscale oxide (gray etching constituents) observed contiguous to the fissures formed during testing. All steels, however, had somewhat similar amounts of these oxides at the immediate surfaces of the specimens at comparable time periods and testing temperatures.

These microstructural and X-ray diffraction studies indicate that microstructural changes, which can affect the mechanical properties of steels, can be expected to occur during service. An example of the effect of such microstructural changes would be the reduction in notch toughness in steels that contain a continuous carbide precipitate around the grain boundaries. The magnitude of such changes under service conditions cannot be accurately predicted, but designers should be aware that these changes do occur and make allowances for these changes in their designs.

TABLE 3—HARDNESS-TEST RESULTS FOR THE STEELS INVESTIGATED BEFORE AND AFTER LONG-TIME CREEP-RUPTURE TESTING.

	Steel Type						
	302	309S	310S	310 Cb	314	316	446
Annealed Condition Prior to Testing							
Diamond pyramid hardness	189	169	153	164	166	150	173
Rockwell B hardness[a]	91	86	81	85	86	80	87
Exposed at 1600 F for Indicated Time							
Exposure time, hr	844	439	607	1428	1037	668	582
Diamond pyramid hardness	208	134	156	161	176	132	180
Rockwell B hardness[a]	94.5	74	82	84	88	73	89
Exposed at 1800 F for Indicated Time							
Exposure time, hr	685	1677	1217	2652	1304	925	2081
Diamond pyramid hardness	409	198	193	181	134	220	174
Rockwell B hardness[a]	41.5[b]	92.5	91.5	89	74	96.5	87.5
Exposed at 2000 F for Indicated Time							
Exposure time, hr	1018	1174	1701	1119	1868	192	
Diamond pyramid hardness	201	234	225	164	172	182	
Rockwell B hardness[a]	93	99	97.5	85	87	89.5	

[a] The Rockwell hardness values were converted from diamond-pyramid-hardness values.
[b] Rockwell C hardness.

Hardness Tests:

The results of hardness tests made on the steels in the annealed condition and after long-time creep-rupture testing at 1600, 1800, and 2000 F are shown in Table 3. These data indicate that, except for the Type 302 steel after long-time testing at 1800 F, the steels exhibited relatively small changes in hardness after long-time exposure as compared with the hardness of the steels in the annealed condition. These small changes in hardness can be explained by the precipitation of some sigma and $M_{23}C_6$ type carbides, the absorption of nitrogen, and the formation of some chromium nitrides. Type 302 steel, however, exhibited a very large increase in hardness over that obtained on annealed specimens (409 DPH versus 189 DPH). This large increase in hardness probably was because of the transformation of austenite to ferrite (martensite) when the specimen was cooled from the testing temperature. X-ray diffraction studies performed on Type 302 steel long-time creep-rupture test specimen showed that appreciable quantities of ferrite were present in the specimens although ferrite was difficult to observe microscopically. The formation of ferrite, after long-time exposure of austenitic stainless steels at elevated temperatures, has been observed by other investigators (**8,9**). It has been postulated that the formation of the ferrite in these instances is the result of carbide precipitation that produces chromium and carbon depletion in the areas surrounding the carbides. The lean austenite formed by this alloy depletion can then transform to ferrite (martensite) on cooling.

SUMMARY

The present investigation was made to determine the creep and creep-rupture strengths of Types 302, 309S, 310S, 310 Cb, 314, and 316 stainless-steel sheet tested in air at 1600, 1800, and 2000 F, and of Type 446 stainless-steel sheet tested in air at 1600 and 1800 F. The results are summarized as follows:

1. The austenitic stainless steels are, in general stronger than the ferritic Type 446 stainless steel, although the difference in their strengths becomes less as the temperature is increased from 1600 to 1800 F.

2. Type 310S stainless steel has the highest creep and creep-rupture strengths at 1600 and 1800 F, whereas Type 314 stainless steel has the highest strengths at 2000 F.

3. Metallographic and X-ray diffraction studies on the long-time creep-rupture specimens tested at 1600, 1800, and 2000 F indicate that $M_{23}C_6$ type carbides were precipitated in the steels. Also, in Types 309S, 310S, 310 Cb, 314, and 316 steels, sigma phase was precipitated during long-time creep-rupture testing at 1600 F. In addition, subscale oxides (spinels) were found in the steels after long-time testing at 1600, 1800, and 2000 F. Nitrogen was absorbed during testing and was precipitated as chromium nitrides in a Widmänstatten pattern.

These results indicate that stainless steels can be considered for many applications involving service between 1600 and 2000 F.

REFERENCES

(1) W. F. Simmons and H. C. Cross, "Report on the Elevated-Temperature Properties of Stainless Steel," *Elevated Temperature Properties of Stainless Steel, ASTM STP 124*, Am. Soc. Testing Mats., 1952.

(2) J. H. G. Monypenny, "Stainless Steels in Industry," Vol. I, *Stainless Iron and Steel*, 3d edition, revised, Chapman & Hall, Ltd., London, 1951.

(3) G. V. Smith, F. Garofalo, and L. Zwell, "Influence of C and N on Creep and Creep-Rupture Properties and Structure of 18 Cr-8 Ni and 18 Cr-8 Ni-Mo Steels," presented at the AIME meeting on *The Relation of Structure to High-Temperature Properties*, Chicago, Ill., Nov. 4, 1957.

(4) G. V. Smith, F. Garofalo, R. W. Whitmore, and R. R. Burt, "Creep-Rupture Strength of Austenitic Cr-Ni-Mo Steels in Sheet and Bar Form," *Transactions*, Am. Soc. Mechanical Engrs., Vol. 81, December, 1959, p. 610.

(5) G. V. Smith, E. J. Dulis, and E. G. Houston, "Creep and Rupture of Several Chromium-Nickel Austenitic Stainless Steels," *Transactions*, Am. Soc. Metals, Vol. 42, 1950, pp. 935–977.

(6) E. J. Dulis, G. V. Smith, and E. G. Houston, "Creep and Rupture of Chromium-Nickel Austenitic Stainless Steels," *Transactions*, Am. Soc. Metals, Vol. 45, 1953, pp. 42–76.

(7) C. A. Zapffe, *Stainless Steels*, Am. Soc. Metals, Cleveland, Ohio, 1949.

(8) E. J. Dulis and G. V. Smith, "Ferrite Formation Associated with Carbide Precipitation in 18 Cr-8 Ni Austenitic Stainless Steel," *Transactions*, Am. Soc. Metals, Vol. 44, 1952, pp. 621–642.

(9) L. Zwell, E. J. Fasiska, and F. von Gemmingen, "X-Ray Identification of Phases in Type 316 Austenitic Stainless Steels Subjected to Creep Rupture," *Transactions*, Am. Institute Mining, Metallurgical, and Petroleum Engrs., Vol. 224, February, 1962, pp. 198–200.

THE EFFECTS OF NEUTRON EXPOSURE AND REACTOR ENVIRONMENTS ON STAINLESS STEELS

By S. H. Bush[1] and J. C. Tobin[2]

Synopsis

Stainless steels represent one of the major groups of structural and fuel cladding materials used in nuclear reactors. These steels have been used extensively in civilian power reactors. This paper reviews the performance of ferritic, martensitic, austenitic, and precipitation hardening stainless steels when exposed to neutrons, and the effects of reactor environment, whether water, gas, or liquid metal.

The effects of neutron irradiation on the mechanical properties of stainless steels are examined. Generally, exposure to neutron flux increases the yield strength substantially more than it does the ultimate tensile strength. This is accompanied by marked decreases in ductility. Uniform elongation becomes extremely small after exposures in the range 10^{20} to 10^{21} nvt.

The dynamic properties of the stainless steels such as creep, stress rupture, and low cycle fatigue are reviewed, based on the limited data available. The effects of stress application to stainless steels while exposed to neutrons are also discussed.

Specific consideration is given to surface corrosion, oxidation, and stress corrosion where the neutron induced heat flux plays a major role. Potential limitations to the use of these steels by such reactions are considered, as are possible solutions to the problems.

Certain indirect effects of a neutron environment such as thermal cycling due to varying gamma flux during reactor startup and shutdown and the deleterious effects of such cycling are considered in structural components and in fuel cladding. Other indirect effects unique to nuclear reactors such as the interaction of fuel with stainless cladding are discussed briefly.

The stainless steels, including austenitic, ferritic, martensitic, and precipitation hardening grades, have found extensive use in nuclear reactors as structural components and fuel cladding. Insofar as breadth of application is concerned, these alloys find more general application than any other family of metals. They have been used in water, steam, gases, liquid metals, organic coolants, and in uranyl sulfate solutions.

When one considers the penalty paid in excess enrichment because of their undesirably high-neutron capture cross sections, it is obvious that the stainless steels are selected for thermal reactors because no alternates exist in many cases. This establishes the obvious difference in that the stainless steels have superior mechanical properties and resistance to corrosive environments compared to such alternates as aluminum, magnesium, beryllium, and zirconium alloys under certain types of operating conditions. In some instances, stainless steels were the final alternate used after other structural materials with much lower neutron absorption cross sections had failed to meet minimum requirements of strength, corrosion resistance, or fabricability.

Rather surprisingly no comprehensive reviews covering the aforementioned parameters appear to be available for the various stainless steels. Work of Leeser et al (1–4)[3] has been published a number of times as has that of Wilson et al (5,6). Results from the USSR (7–10) are of particular interest. Irradiations at the Materials Testing Reactor and the Engineering Testing Reactor represent the highest levels of integrated neutron flux achieved at this time (11–16). The work of Joseph and Schreiber of Savannah River (17,18) is of importance in establishing the performance of stainless steels when irradiated in the stressed condition at low temperatures. Similar results are available at higher temperatures both in-reactor (19–21) and as post-irradiation stress-rupture tests (22).

Two survey articles worthy of note are Porter's (23) and Schreiber's (24). Porter (23) deals rather briefly with the stainless steels as a minor portion of a major review predominantly concerned with carbon and low-alloy steels. Schreiber (24) has compiled a concise condensation of data dealing with the stainless steels. This deals with both classified and unclassified documents, and represents the sole unclassified source for much of the data.

This paper reviews the in-reactor performance of the stainless steels when exposed to a variety of coolants. The variation of such parameters as composition, fabrication history, irradiation temperature, instantaneous and integrated flux, and environment are considered when data are available. The effects of neutron irradiation are considered in terms of basic damage mechanisms. A section of this review is devoted to changes in physical properties and to structural effects, such as diffusion, phase reversion, or variations in microstructure. The chemical reactions with stainless steels in various environments are also surveyed. Both those effects directly attributable to neutron flux and those effects indirectly caused by the heat or fission flux are considered in bulk corrosion and selective attack as seen in stress corrosion.

Finally, those mechanical properties of major concern to the designer are considered. Included are irradiation-induced changes in tensile, hardness, impact, creep, stress-rupture, and fatigue properties.

Irradiation Damage Mechanisms

Several mechanisms have been proposed to explain the effects of neutron irradiation on solids (25–29). A late review (30) presents an excellent summary of these various mechanisms. One can include displacement spikes (29), thermal spikes (25,28), and later somewhat more sophisticated models (26–30), as attempts to explain the mode of defect generation resulting in what we define as irradiation damage. Unfortunately, all models proposed to date are based on a number of

[1] Consulting metallurgist, Hanford Laboratories, Hanford Atomic Products Operation, Richland, Wash.

[2] Manager, Reactor Metals Research, Hanford Laboratories, Hanford Atomic Products Operation, Richland, Wash.

[3] The boldface numbers in parentheses refer to the list of references appended to this paper.

Copyright© 1965 by ASTM International

www.astm.org

assumptions, some of which are of doubtful validity. Limited success has accompanied attempts to predict damage in the mechanical properties of engineering significance. Another complication is the relative complexity of the composition of an engineering material such as an austenitic stainless steel. The metastability, phase changes, and possible maldistribution of constituents, to say nothing of changes in grain size or fabrication practice, limits one to a macroscopic evaluation of the effects of neutron flux on the alloys. The problem is further complicated by transmutation effects which are markedly responsive to the reactor neutron flux energy spectrum and to the effects of gamma heating which can generate thermal gradients with concomitant strains.

Because of these factors the information presented will be analyzed on the basis of its engineering significance insofar as reactor operation is concerned, and conclusions or extrapolations will be based on engineering rather than fundamental considerations.

Reactions With Reactor Environments

Under most circumstances the additional effect of a superposed neutron flux on the reaction of a stainless steel with its environment is quite nominal. In many instances the in-reactor changes are so limited as to be statistically meaningless. This is particularly true for the austenitic stainless steels where the rates of corrosion are insignificant in or out of the reactor.

A few fundamental experiments have been conducted to establish the effects of irradiation on the electrochemical behavior of stainless steels (31,32). Gerasimov and Aleksandrova (31) measured the anodic and cathodic polarization of a 1Khl8N9T steel in-reactor at 80 to 90 C (175 to 195 F) in 0.01N sodium sulfate and 0.01N sodium chloride. There appeared to be no apparent effect because of irradiation in the kinetics of the anode process in either solution; however, an increase in the rate of the cathode process was observed which was attributed to short-lived radiolytic products. One could infer that such a reaction could lead to an increase in the corrosion process. Comparable tests have been carried out on Types 304 and 410 stainless steels in the Belgian BR-1 reactor (32) utilizing an 0.1M bicarbonate solution. A substantial lack of reproducibility in the tests tended to mask any changes; however, there appeared to be a greater degree of passivation in the in-reactor specimens during the initial few days of irradiation compared to unirradiated results. Deterioration of cell components and the preliminary nature of the results renders no definite suspected conclusions. One can infer that a great deal more work must be done before it is possible to quantitatively predict a chemical behavior in-reactor.

A problem of potential concern in reactor components operating at lower temperatures is the enhanced permeation of hydrogen into these components. The introduction of hydrogen would be of graver concern in the ferritic or martensitic steels than in the austenitic stainless steels because of the impact energy transition-temperature shift caused by hydrogen in the body-centered-cubic metals. The effects of irradiation at higher temperatures, for example, 300 to 400 C (570 to 750 F), on hydrogen permeation appear minimal. Ashbridge and Sumerling (33) investigated hydrogen diffusion in an 18 chromium, 8 nickel, 1 columbium steel at 350 C (660 F); the only differences between in-reactor and ex-reactor tests were within the experimental error. At these higher temperatures this is not too surprising since the thermal effect should be markedly greater than the irradiation effect. This coupled with the extremely rapid diffusion rate of hydrogen leads one to the conclusion that any hydrogen introduced would diffuse very rapidly through the material. Howe (34) mentions tests at Chalk River where hydrogen pickup and embrittlement occurred in Type 410 stainless steel end fittings. In such a steel operated at lower temperatures, an enhanced pickup of hydrogen is potentially hazardous because of the gross loss in impact ductility.

Experimental results are available on the behavior of annealed and sensitized Type 304 and annealed Type 410 stainless steels in an organic coolant Santowax OM(18 per cent diphenyl, 47 per cent o-terphenyl, 30 per cent m-terphenyl, 5 per cent p-terphenyl) irradiated for several months at 600 to 700 F (315 to 370 C) (35). The radiolytic effects in the coolant resulted in a thick carbonaceous deposit on the specimens in both the ex-reactor and in-reactor portions of the loop. This deposit, believed to form on cooling, was readily removable. Actual corrosion weight gains were quite nominal; Type 304 stainless steel gained 0.01 mg/sq cm while Type 410 steel gained 0.85 mg/sq cm compared to no gain out of reactor for Type 304 and 0.1 mg/sq cm loss in Type 410. These differences could be because of the cleaning operation. The general conclusion was that corrosion of austenitic or martensitic stainless steels in the organic environment was quite limited, and that irradiation did not enhance the weight gain appreciably.

Prislinger (36) reported the corrosion behavior of Types 304-L, 309 Cb, and 347 stainless steels in acidified uranyl sulfate solution used in the Homogeneous Reactor Experiment-2. Exposures for several hundred hours at temperatures of 100 to 300 C (210 to 570 F) resulted in very limited corrosion. Any effect resulting from the fissioning event was obscured by the variations in temperature and solution composition.

Investigations have been made of the effect of irradiation on the corrosion of stainless steels in high-temperature water, steam, gases, and liquid metals. In most instances reported, the corrosion ascribable directly to temperature represents the significant and possibly the entire weight gain. There is a dearth of carefully controlled experiments in these environments, and no definite conclusions can be drawn at this time on the exact effect of neutron irradiation on corrosion rate. This is generally true whether we are considering carbon pickup from a molten metal or oxygen or nitrogen pickup from the other coolants or both.

It is possible that irradiation indirectly influences the interaction observed between uranium carbide fuel and stainless-steel cladding, and the cladding and carbon present as a contaminant in the liquid metal coolant. A fuel such as uranium carbide is often hyperstoichiometric, and reactions have been observed at 1000 F (540 C) with this excess carbon from the fuel diffusing through the sodium bond to the austenitic stainless steel cladding, resulting in extensive carbon penetration (37). The controlling step in this reaction is the rate of solution of carbon from UC_2 going to UC at the UC_2-Na interface because carbon diffuses so rapidly in stainless steel at 1000 F (540 C). A hyperstoichiometry of 0.06 per cent will increase carbon levels from 0.08 per cent to about 2.0 per cent in the steel. The hypostoichiometric uranium carbide does not react, but it is more subject to swelling on

irradiation. There has been evidence that the sodium coolant is a source of carbon (38); however, the quantity of carbon in the sodium is sufficiently low so that the observed effects are very limited because of the low concentration of carbon after it has diffused throughout the cladding. A long term possibility is decarburization of ferritic steel piping and carbon transport through the sodium followed by carburization of the stainless steel cladding (39).

Another phenomenon where irradiation plays a vital indirect role is in the stress-corrosion cracking of an austenitic stainless steel fuel-element cladding in superheated steam (40). Limited quantities of entrained moisture in the steam contained sufficient chlorides to cause drastic stress corrosion cracking of the stainless steel cladding. The high heat fluxes in the fuel element served as a concentrator of the chlorides so that initial levels of fractional parts per million ultimately reached several thousands of parts per million. These levels in conjunction with the thermally induced stresses resulted in cladding failures in short periods of time. Possible solutions to this problem would be the removal of all entrained liquid, reduction of chlorides to parts per billion, or minimization of stresses in the cladding. All are laden with difficulties so the current solution is to substitute alloys that are not susceptible to stress-corrosion cracking.

Another form of stress corrosion has been observed in Type 17-4 PH stainless steel given an H900 (480 C) stress relief. The levels of residual stress are sufficient to cause severe cracking in high purity water in a reactor (41,42). A careful analysis of the available data, including the absence of stress-corrosion in-reactor in Type 17-4 PH after an H1100 heat treatment, leads to the opinion that irradiation plays a secondary role in the stress corrosion of Type 17-4 PH. Conceivably radiolytic formation of hydrogen may play some part, but this is only one possiblity. Certainly Type 17-4 PH should not be used in the 900H condition in a reactor.

Neutron irradiation does not appear to play a major role in the chemical reactions between stainless steels and their surrounding environments at the temperatures these materials usually experience. Future experiments may reveal that an effect exists, but it appears safe to conjecture that it will not be a major one. These statements apply to bulk corrosion, not to localized or preferential corrosion.

Effects on Physical Properties

The physical properties of the stainless steels appear to be relatively unaffected by irradiation. Included in this category are such properties as density, dimensional changes, electrical resistivity, and elastic moduli.

Charlesby et al (43) conducted a clever experiment to determine the effect of irradiation on the elastic modulus of Elinar, a 50 per cent iron-40 per cent nickel-10 per cent chromium austenitic steel. This alloy was fabricated into a clock spring, and the in-reactor change in counting rate equated to a change in modulus. The average change noted was an increase of 0.1 per cent at 70 C (160 F). This would appear to be within the possible error owing to temperature fluctuations or other factors.

Very minor dimensional changes have been reported in austenitic stainless steels. In most instances the changes could be within the allowable error in measurements. In some instances the change could be the result of the formation of ferrite. This will be discussed under structural effects.

Changes in density can be equated to dimensional changes too. A limited number of measurements have been made. All data reported were collected in the early 1950's. Reported changes vary from -0.07 to $+0.63$ per cent for Type 347 stainless steel (44,45) to -0.06 per cent for 316 and -0.04 per cent for Type 348 stainless steel. Similar decreases of -0.05, -0.10, and -0.10 per cent were noted in Types 410, 410 malcomized, and 440C hardened stainless steels (45). One suspects that errors of measurement on the post-irradiation examination might account for most of the differences noted.

The influence of irradiation on the electrical resistivity of several austenitic stainless steels has been determined by various investigators (9,44–47). Specimens irradiated at higher temperatures (300 to 600 C) (570 to 1100 F) revealed no changes (47). The general effect appeared to be an increase in electrical resistivity of 0 to 2.5 per cent (9,44–46). This was true for annealed (9,44–46) and cold-worked (46) steels. It was also true over a range of compositions, Types 347 (44–46), 304, 309, and 316 (45), and special 18 chromium, 12 nickel, 2 manganese, titanium, and 18 chromium, 17 nickel steels (9).

A reasonable conclusion is that changes in physical properties are so nominal as to have little engineering significance.

Irradiation-Enhanced Structural Changes

The term "irradiation-enhanced structural changes in stainless steels" refers to such effects as variations in microstructure, changes heralding ferrite, formation in an austenitic stainless steel, observable changes in diffusion rates, or core-cladding interactions.

Extensive post-irradiation examinations of the microstructures of austenitic and martensitic stainless steels using optical and electron microscopy have not revealed changes in structure that can be attributed directly to irradiation. Specimens of Type 347 stainless steel irradiated to 1.2×10^{22} nvt (>1 Mev) in 120 F (50 C) water displayed no changes in microstructure (16).

The dislocation behavior in an irradiated austenitic stainless steel has been investigated utilizing transmission electron microscopy (48). No discernible diffraction effects were noted. It was postulated that a strong supersaturation of point defects exists, possibly in the form of a three-dimensional aggregate without an associated stress field. These defects tend to anchor the old dislocations while leading to the climb of some new dislocations. This is inference in part based on the absence of coalesced defects.

Howe (34) reports similar transmission electron microscopy studies on irradiated Type 410 stainless steel. The defects responsible for the change in mechanical properties in the steel were too small to be observed. These results appear to agree with Mogford and Hull's (49) postulate that conditions are not favorable in the ferritic steels for the growth of clusters of interstitials or vacancies to the point where they can be observed in the electron microscope.

Magnetic susceptibility, K, and magnetic permeability, μ, have been measured to determine the effect of irradiation on these values (1,7,50). Leeser and Murphy (1) measured the magnetic susceptibility of a large number of steels (Types 304, 309, 316, 329, 347, 431, 442, 446, 17-4 PH, USS-W) by the Guoy and Magne-Gage methods. The austenitic stainless steels displayed increases on

irradiation of 100 to 700 per cent, in the best readings, indicating the formation of ferrite. The changes in the other steels were much less, ranging from −18 per cent for the hardened Type 446 to a maximum of 30 per cent for Type 17-4 PH.

TABLE 1—REPRESENTATIVE COMPOSITIONS OF STAINLESS STEELS USED IN VARIOUS IRRADIATION PROGRAMS.

Material Designation	Country	Nominal Composition, Per Cent					
		C	Cr	Ni	Mo	Ti	Others
Austenitic:[a]							
AISI 301	US	0.08 to 0.20	17	7	...	...	...
AISI 302	US	0.08 to 0.20	18	9	...	...	...
AISI 302-B	US	0.08 to 0.20	18	9	...	...	2.5 Si
AISI 304	US	0.08	19	10	...	...	...
AISI 304-L	US	0.03	19	10	...	...	...
AISI 305	US	0.12	18	12	...	...	...
AISI 308	US	0.08	20	11	...	...	...
AISI 309	US	0.20	23	14	...	...	...
AISI 310	US	0.25	25	20.5	...	...	...
AISI 316	US	0.10	17	12	2.5	...	...
AISI 321	US	0.08	18	10	...	5 × C min	...
AISI 347	US	0.08	18	10	...	...	10 × C min (Nb + Ta)
Kh18N9[b]	USSR	...	...	...	...	...	...
1Kh18N9T[c]	USSR	0.10	18	9	...	0.5	...
Kh18N9T[c]	USSR	...	...	...	...	...	...
Kh18N12Mn2T	USSR	0.10	18	12	...	0.5	2 Mn
Kh14N14Mo3Nb	USSR	~0.10	14	14	3	...	0.5 Nb
Kh18N12	USSR	~0.10	18	12	...	...	...
Kh20N40 4(W + Nb)	USSR	~0.10	20	40	...	...	4(W + Nb)
Kh18N17	USSR	"	18	17	...	...	...
Kh17N5 2MO	USSR	"	17	5	2	...	...
Kh20N14S2	USSR	"	20	14	...	...	2 Si
Kh18N22V2T2	USSR	"	18	22	...	2	2 V
Kh18N9	USSR	0.06	18	9	...	...	...
Martensitic:							
410	US	0.15 max	12.5	...	...	...	...
414	US	0.15 max	12.5	2	...	...	...
420	US	0.15 min	13	...	...	...	...
440	US	0.75	17	...	0.75	...	...
X-13	USSR	0.12	13	...	0.5	...	7.5 Nb
Ferritic:							
446	US	0.2 max	25	...	...	...	0.25 N
Precipitation Hardening:[d]							
A-286	US	0.04	15	25	1.25	2	0.2 Al; 0.25 V; 0.25 Co; 0.004 B
AM-350	US	0.10	16.5	4.25	2.75	...	0.10 N
17-4 PH	US	0.04	16.5	4.25	...	...	0.25 Nb; 3.60 Cu
Stainless W	US	0.07	16.5	6.75	...	0.80	0.20 Al

[a] Generally these steels contain 2 per cent maximum Mn, 1 per cent max Si.
[b] Corresponds to AISI 302.
[c] Corresponds to AISI 321.
[d] These steels may contain as high as 1 per cent max Mn and Si.

The work of Reynolds et al (50) is much more quantitative. The authors measured the changes in permeability of Type 347 stainless steel in cold worked states of 0, 10, 19.8, 20, 32.5, 38.8, and 50.2 per cent. These specimens were irradiated in the Hanford reactors or at the Materials Testing Reactor. The per cent of ferrite caused by irradiation was determined with a low-permeability permeameter. The increase in ferrite, defined in terms of per cent increase in volume of the specimens, varied from 0.002 at zero cold work to about 0.025 at 50 per cent cold work. The authors believed that irradiation enhanced the growth of existing ferrite nuclei rather than causing the appearance of new ferrite nuclei. For example, at 50 per cent cold work a 17-fold increase in neutron exposure caused no more than a two- to three-fold increase in ferromagnetic induction. This indicates that the available supply of ferrite nuclei becomes exhausted and is accompanied by a diminution in the irradiation effect. The temperature of irradiation, less than 100 C (212 F), was believed to be too low to cause the observed changes.

The mechanism proposed by Reynolds et al (50) appears to be confirmed by Konobeevsky et al (7) who measured the magnetic permeability of an irradiated Kh18N9T steel. No ferromagnetism was observed if care was taken to prevent plastic deformation. Existing ferrite nuclei produced by cold work may grow, but there is little or no tendency to nucleate such nuclei exclusively by irradiation.

There appears to be no direct measurements of the effect of irradiation on the diffusion rates in the stainless steels. One would suspect that no changes would be observed much above room temperature. At lower temperatures an effect might well be observed. Indirect indications are seen in the recovery of damage in steels (9,34). Howe (34) reported an activation energy of 2.4 ev (55,500 cal/mol) for the recovery of Type 410 stainless steel. Assuming that the self-diffusion of iron in stainless steel is comparable to that in pure iron then Howe's value is virtually equivalent to that of self-diffusion. This suggests that the annihilation of defects during post-irradiation annealing is due to the formation and migration of new vacancies rather than the migration of those vacancies produced by irradiation.

Ibragimov et al (9) report two competing mechanisms in the recovery of damage in iron. The first has an activation energy of 16,500 cal/mol which seems to correspond to the diffusionless recovery observed in 95 per cent cold-worked iron where the activation energy (unirradiated) was 15,000 cal/mol. A second process had an activation energy of 28,200 cal/mol about one half that of self-diffusion. This too was believed to be diffusionless. There appears to be some discrepancy as yet unexplained in these and Howe's results. Of greater interest are the data on recovery reported by the authors (9) for several austenitic stainless steels and for nickel. All of these materials displayed comparable recovery behaviors, indicating that composition did not play a role in the recovery process.

One other area of concern is the possibility of an interaction between the fuel and the cladding. This is particularly important in a metallic fuel because of the low-melting eutectics formed between the steels and metallic uranium or plutonium. Once diffusion begins it will accelerate rapidly if the

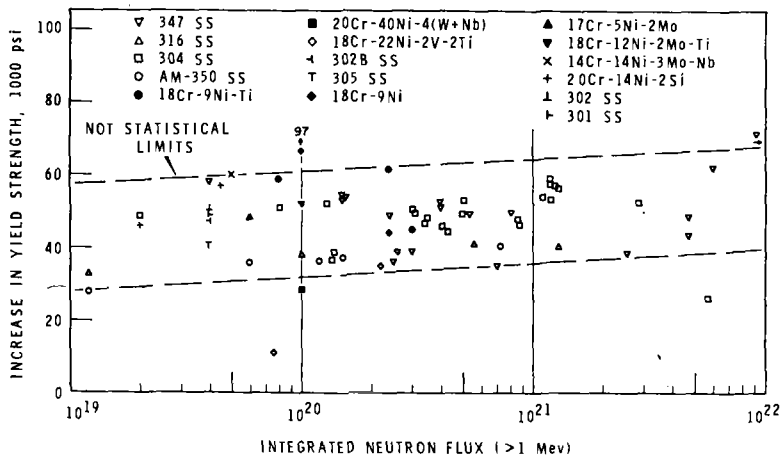


FIG. 1—The Effect of Neutron Irradiation on the Room-Temperature Yield Strength of Austenitic Stainless Steels. All Irradiations Below 200 C.

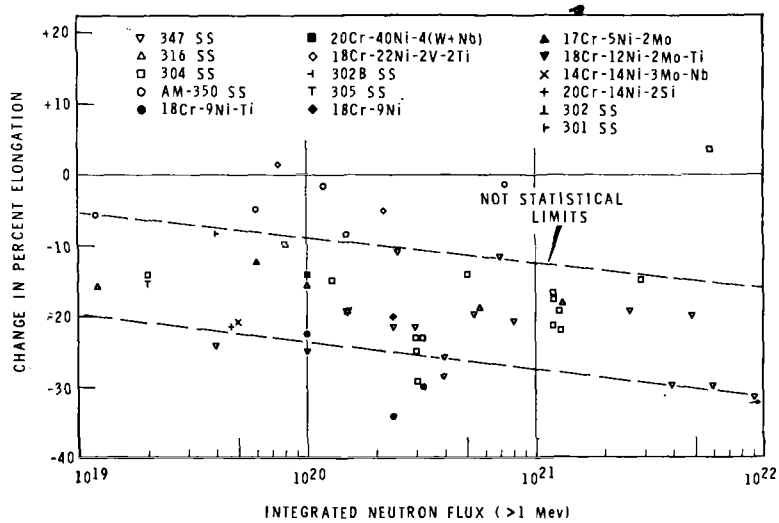


FIG. 2—The Effect of Neutron Irradiation on the Room-Temperature Tensile Elongations of Austenitic Stainless Steels. All Irradiations Below 200 C.

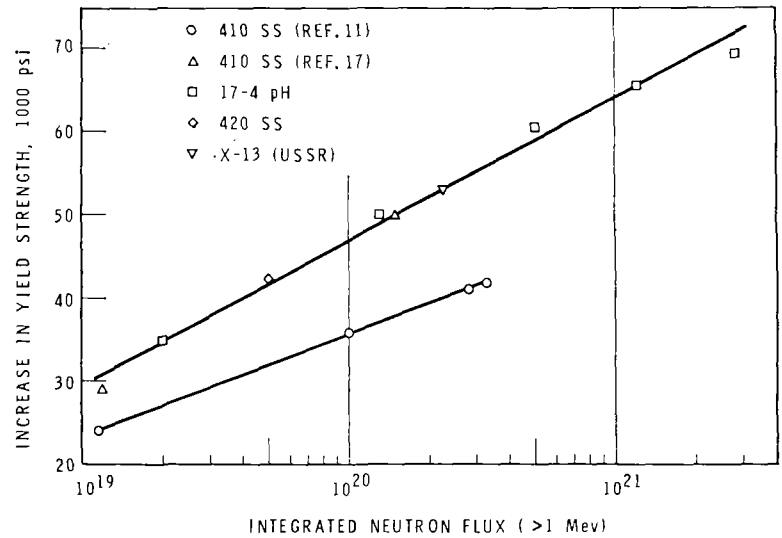


FIG. 3—The Effect of Neutron Irradiation on the Yield Strength of Ferritic, Martenistic, and Precipitation Hardenable Stainless Steels.

temperatures are sufficiently high. This effect does not occur with the fissile oxides, but it may still be a problem in the compounds such as plutonium carbide where the carbide decomposes to form plutonium and the dicarbide. In this case the metallic plutonium would alloy rapidly with the cladding forming a low melting eutectic. These effects are attributable only indirectly to irradiation in that the fission event produces the heat necessary for the reactions.

Generally, it can be said that direct changes are not observed in the microstructure, but several changes do occur such as ferrite formation, recovery, and core-cladding interactions.

MECHANICAL PROPERTIES

Tensile Properties—Austenitic Stainless Steels:

The widespread interest in the austenitic stainless steels for reactor structural components and fuel cladding is indicated by the substantial number of irradiation testing programs dealing with these materials during the past 15 years. Much of the work has been limited to pre- and post-irradiation tensile properties. These data are reviewed in the remaining paragraphs of this section; however, before considering the test results, it was felt that the alloys tested and representative compositions should be reviewed. These data are presented in Table 1.

If one plots changes between such post-irradiation and pre-irradiation properties as ultimate tensile strength, yield strength, elongation, and reduction in area as functions of integrated neutron flux normalized to greater than 1 Mev, a number of generalized conclusions can be drawn. Not too surprisingly such plots tend to yield "shotgun" patterns. Even so, it is possible to investigate the effects of such parameters as: (1) integrated neutron flux, (2) irradiation temperature, (3) differences in alloy composition, (4) post-irradiation annealing, (5) testing temperature, and (6) level of cold work.

A collection of most of the relevant data pertaining to the tensile properties of austenitic stainless steels is given in the first eight tables of the Appendix. An analysis of the data presented in these tables permits us to draw rather specific conclusions. These are:

1. Post-irradiation annealing (Table A-1) above 500 C (930 F) for a few hours removes essentially all irradiation induced changes in tensile properties; recovery is very limited at or near 300 C (570 F).

2. Limited recovery is observed in irradiated steels tension tested at or below 300 C (570 F); however, substantial recovery of damage occurs at 350 C (660 F). See Table A-2.

3. Irradiation at and above 250 C

(480 F) to low integrated fluxes appears to yield little or no damage, possibly because of recovery. There appears to be very limited or no residual damage in specimens irradiated at and above 450 C (840 F); however, irradiation at 250 C (480 F) followed by a short time as high as 500 C (930 F) does not remove the damage. See Table A-3.

4. It is difficult to assess the effects of cold work on the relative levels of damage occurring during irradiation. Very limited data leads to tentative conclusions that cold work reduces the loss in elongation and decreases the magnitude of increase in the yield strength. More tests are required to establish the effects of cold work. See Table A-4.

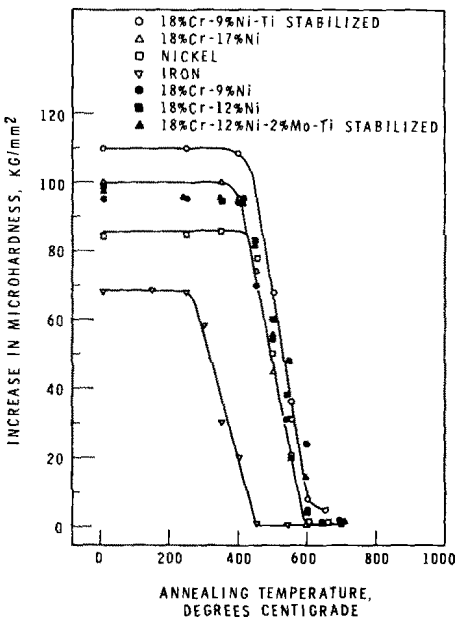


FIG. 4—Recovery of the Increase in Microhardness of Irradiated Nickel, Iron, and Austenitic Stainless Steels as a Function of Temperature of Annealing (Ref. 9).

5. An analysis of Table A-5 and Fig. 1 where flux and composition are varied but irradiation temperatures are low and all testing is done at room temperature, leads one to conclude that there is a continuing increase in yield strength with integrated flux, and that composition plays a minor role. Of course this ignores differences in neutron energy spectra, errors in measurement, and differences in specimen history and geometry, to cite a few factors. Type 316 stainless steel does appear to damage less than Types 304 or 347.

6. A semiaustenitic precipitation hardening steel such as Type AM-350 displays a much lower yield strength shift than the austenitic stainless steels over a range of integrated flux. See Table A-5 and Fig. 1.

7. Type 347 stainless steels can be divided into two categories, those with unirradiated yield strengths greater than 60,000 psi and those with yield strengths below 50,000 psi. It appears that more damage occurs in the steels with lower initial yield strengths. The higher strength group tends to duplicate the values observed with Type 316 stainless steel and Type AM-350.

8. One tensile value in Type 304 stainless steels is definitely out of line. The yield strength of a specimen irradiated to 5.7×10^{20} nvt > 1 Mev drops drastically while the elongation increases equally sharply. This behavior parallels that expected in a specimen operating at a higher temperature or given a post-irradiation anneal; however, this is the highest level to which Type 304 stainless steel has been irradiated so it is remotely conceivable that recovery is occurring.

9. Macrostructural changes such as occur in weldments or in heat-affected zones may change the base properties in the unirradiated state, but irradiation induced changes are remarkably similar. The weld (Type 308 stainless steel) itself, with higher initial yield strength and lower ductility, is somewhat less affected than the base metal (Type 304 stainless steel) or the heat-affected metal. See Table A-6.

10. Specimen geometries for tension testing range over a wide spectrum of sizes and shapes. In the few instances where a comparison is possible on the basis of the same material used and the same irradiation conditions, one can conclude that specimen size is a nominal effect insofar as irradiation-induced changes in tensile properties are concerned. See Table A-7.

11. Decreases in tensile elongation tend to become more marked with increased integrated neutron flux as seen in Fig. 2, but the remaining elongation is still quite adequate. This applies to over-all elongation and is not necessarily true for uniform elongation.

12. Both Types 301 and 310 stainless steels as extra full hard sheet have been irradiated and tested under cryogenic conditions (53). Integrated neutron fluxes were nominal, ranging from 4.5 to 10^{16} to 2×10^{17} nvt > 0.33 Mev. Irradiation induced changes were more pronounced in Type 301 stainless steel than Type 310 stainless steel. Generally, limited increases or little change was noted in yield and tensile strengths and nominal decreases in elongation in specimens irradiated at 475 F (250 C) or at −346 F (−210 C) and tested at 85 F (30 C). Decreases in yield strength, tensile strength, and elongation were noted in most instances when the specimens were irradiated at either −416 F (−250 C) or −346 F (−210 C) and tested at −393 F (−235 C) or −423 F (−255 C). Relevant data are given in Table A-8 of the Appendix.

Tensile Properties—Ferritic and Martensitic Stainless Steels:

The available information pertaining to ferritic or martensitic stainless steels or to martensitic precipitation hardening stainless steels is much more limited than is the case with the austenitic materials. Figure 3 presents the effect of irradiation on the change in yield strength and Table A-9 in the Appendix summarizes available information.

It appears from Fig. 3 that there are two distinct statistical universes. The points clustered at $4 - 9 \times 10^{19}$ nvt in Table A-9 should be shifted about one cycle because flux was cited as 200 ev and a fair estimate of the portion of the flux > 1 Mev would be one tenth. This would account for the data from Ref. (34). In the case of the Reactor Handbook data (45), the flux values are doubtful. Ignoring these points one sees two distinct regression lines, both continuing to increase with integrated flux. The increases are sufficiently large to raise a question concerning the extended use of these steels in a reactor, particularly Type 410 stainless steel where the elongation is continuing to drop.

Hardness Changes in Stainless Steels:

Changes in hardness due to irradiation tend to parallel similar changes in the yield strength. Unfortunately much of the potential value of the hardness data is lost because of the variety of hardness tests used and the errors inherent in transferring from one form of hardness measurement to another. As one would anticipate hardness measurements can be used to follow the effects of various levels of integrated flux, irradiation temperature, post-irradiation annealing, or certain irradiation induced structural changes.

An excellent example of the use of a hardness test is in following the recovery of damage in austenitic stainless steels during post-irradiation annealing. The

simplicity and accuracy of a microhardness test make it an obvious choice.

A Russian study (9) of recovery may have fundamental significance in understanding the joint mechanisms of damage and recovery during neutron irradiation. The results of Ibragimov et al (9) are presented in Fig. 4 for changes in the increase of microhardness of different austenitic stainless steels and pure nickel as a function of annealing temperature. One recovery curve applies to all the materials with a very nominal scatter indicating that the defect or defects causing the damage tend to recover independently of composition or melting point within the range studied. The curve for iron is shown because it does indicate that crystallographic structure may play a role.

Creep and Relaxation:

Creep rates of stainless steels under actual reactor operating conditions have been measured by a number of investigators. Coffin (19) measured creep rates of Type 347 stainless steel at 600 C (1110 F). As did others who worked in this field, he used a very ingenious method of determining the plastic deformation in a hydrostatically loaded tubular specimen held at constant temperature within an operating reactor. At stress levels of 18,000 and 24,000 psi, he found creep rates of 0.069 and 0.070 per cent/1000 hr, respectively, in-reactor. Corresponding ex-reactor rates were 1.17 and 3.52 per cent/1000 hr. He concluded that creep rates were markedly reduced by neutron irradiation. He also concluded that there was less effect of temperature on creep rate in the temperature range near 600 C (1110 F) than was found ex-reactor.

Work performed at Oak Ridge on the same material using a cantilever beam-type specimen was more extensive (20). However, tests were of a considerably shorter duration averaging around 250 hr as compared to 2000 hr tests performed by Coffin. Flux levels were also very low in this series of tests, about 4×10^{10} nvt. At 1500 F (815 C) under stress of 1500 psi, in-reactor strains were lower than ex-reactor strains during the first 100 hr of test. Deformation continued at a more constant and greater rate in-reactor thereafter. Rates were observed to diminish during reactor shutdown periods. After 250 hr the creep rate in-reactor was found to be 1.4 times the ex-reactor rate. During multitemperature operation of a single test at a stress of 8000 psi, a greater temperature dependence was observed for in-reactor creep than for a similar ex-reactor test in the temperature range 1200 to 1400 F (650 to 760 C). At 1200 F (650 C), the in-reactor rate was about one half of the ex-reactor rate. This ratio approached unity near 1400 F (760 C). These investigators concluded that a temperature existed in the normal recovery range for a given material below which in-reactor rates were lower. Above this temperature the in-reactor rates might be higher than ex-reactor measurements. This conclusion is in quantitative agreement with Coffin's observations. It was also observed that the effects of irradiation tend to be greater at higher rates of creep. It is rather remarkable that the Oak Ridge investigators found an effect in such a low-flux environment.

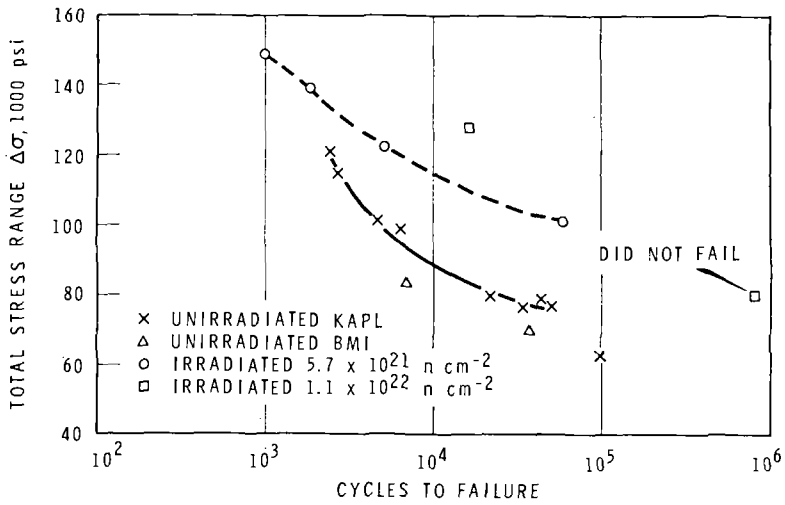


FIG. 5—The Effect of Stress Range on the Fatigue Properties of Irradiated AISI 347 Stainless Steel (Ref. 16).

Later work on stress relaxation measurements in Type 304 stainless steel has been performed by J. W. Joseph (17) and R. E. Schreiber (18). Joseph found that stainless steel stressed in the range 20,000 to 39,000 psi at a temperature less than 100 C (210 F) suffered as much as a 50 per cent stress relaxation during exposure to 9×10^{20} nvt. The 50 per cent reduction was observed for specimens stressed to 20,000 psi after an exposure of only 4×10^{20} nvt. No further effect was noted in continuing the irradiation to higher levels. A 39,000 psi stress suffered a reduction to about 32,000 psi after 9×10^{20} nvt. Data indicate that further reduction would have occurred had the exposure been continued. Tension stress relaxation specimens were used in Joseph's investigation. Schreiber supplemented this study with an investigation of torsion-type specimens. His conclusion was in qualitative agreement with that of Joseph in that marked relaxation occurred owing to low temperature exposure. For example, specimens stressed to 22,000 psi recovered to 14,500 psi after 10^{21} nvt at a temperature less than 100 C (210 F). Below applied stresses of 5000 psi relaxation was too small to measure. Apparently the relaxation was a continuous function of exposure. These relaxation experiments have been criticized as containing considerable measurement errors. Even if errors do exist, these two studies have well established the trend. The occurrence of this much relaxation at such a low temperature in-reactor must be considered as a manifestation of an accelerated creep process during irradiation. Some early experiments with Types 302 and 347 stainless steel springs reported relaxation in the surface fibers ranging from 2 to 20 per cent (45). These data tend to confirm the results of Joseph (17).

Fatigue:

Shober and Murr (16) have investigated the effect of neutron irradiation on the fatigue properties of Type 347 stainless steel. These were tension-compression push-pull tests with the total strain adjustable to any level. On the basis of pre- and post-irradiation tests, little or no difference was noted in the number of cycles to failure for the unirradiated and irradiated steel if the cyclic strain levels

remained between 0.6 and 1.3 per cent. At higher strains the stainless steel was less fatigue resistant after exposures of 5.7×10^{21} nvt and 1.1×10^{22} nvt. If the strain levels were below 0.6 per cent, the irradiated steel appeared to have an improved resistance to fatigue, and higher stresses were always required to cause failure in the irradiated stainless steel at a given number of cycles, as can be seen in Fig. 5.

An earlier investigation of fatigue in irradiated Type 304 stainless steel showed no effect on the fatigue life after an exposure of 10^{19} nvt (56). A plate-bending fatigue test was used in this instance on specimens after irradiation, and the S-N curves were identical for the irradiated steel and the unirradiated controls.

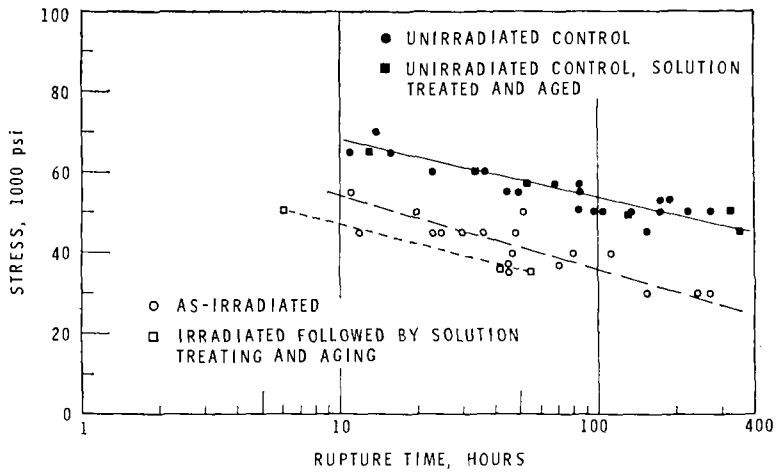


FIG. 6—Stress-Rupture Strength of A-286 Stainless Steel Irradiated Then Tested at 650 C (1200 F) (Ref. 55).

Late stress cycling work conducted in-reactor on Type 304 stainless steel specimens at 1300 F (700 C) revealed some effect of irradiation.[4] Thin tubular sections of the stainless steel were alternately expanded and compressed a fixed amount with helium while at temperature. Based on a limited number of in-reactor tests, the irradiated material fails in fewer cycles for a given total strain range than does the unirradiated controls. For example, the irradiated steel failed in 8 cycles versus 20 for the unirradiated at 0.04 total strain.

Stress Rupture:

An alarming decrease in the stress-to-rupture properties in a high-strength stainless steel, Type A-286, has been observed after irradiation (22,55). Some variation in this reduction was observed on a heat-to-heat basis. Typically, the stress to cause rupture in 1000 hr at 650 C (1200 F) was reduced from 41,000 psi in the unirradiated controlled material to 22,000 psi in material unirradiated to 10^{19} or 10^{20} nvt as seen in Fig. 6. This reduction in stress approaching 50 per cent is even more striking when the post-irradiation rupture life at a given stress is considered. A stress of 40,000 psi causes failure in about 1300 hr for the control material. The same stress causes failure in around 70 hr for this alloy after irradiation to 5×10^{19} or 1×10^{20} nvt. Reheat treatment of the alloy after irradiation did not appreciably change the post-irradiation properties. If any effect was noted, it consisted of a slight decrease in rupture time at a given stress because of post-irradiation, solution treatment, and aging. This result is quite similar to findings on age hardenable nickel-base alloys. The implications may be extremely serious when strength is a limiting parameter of an in-core stainless structural component.

Stress-rupture tests have been carried out in-reactor on Type 304 stainless steel tubular specimens (21). There appears to be a variation from heat-to-heat on the basis of these data. One heat of Type 304 stainless steel appears to be insensitive to irradiation at 1300, 1500, and 1600 F (700, 815, 870 C) while the other heat of steel is definitely affected by neutrons. There is a decrease in the stress required for rupture in-reactor analogous to the behavior of Type A-286.

Impact Strengths and Transition Temperatures:

The resistance to shock loading of the austenitic stainless steels as measured by impact testing is not drastically affected by neutron irradiation. Charpy V-notch tests performed at Battelle Memorial Institute (16) on Type 347 stainless steel before and after irradiation showed some small evidence of the existence of transition behavior. The fracture energy absorbed at liquid nitrogen temperature was observed to be 83 ft-lb for the unirradiated material as compared to 120 ft-lb at room temperature. Exposure to 5.7×10^{21} nvt caused a reduction to 65 ft-lb in the room-temperature impact strength. The impact for materials in this same irradiated condition was 19-ft-lb. The fracture surfaces of both the room-temperature and liquid-nitrogen-temperature specimens still displayed some evidence of plastic deformation prior to fracture. Other investigators (15,57) have found similar reductions in room-temperature impact strength of a number of other austenitic stainless steels.

The ferritic stainless steels have also been examined for the response of ductile-brittle transition temperature to neutron irradiation. Type 410 stainless steel (15) after oil quenching from 1800 F (1000 C) and drawing at 1000 F (540 C) was found to have a transition temperature close to 100 F (40 C). This determination was made with subsize Izod specimens and cannot be correlated directly with normal Charpy data. Irradiation to 1.3×10^{19} nvt caused very little obvious change in the transition temperature or the shape of the impact energy versus testing temperature curve. After irradiation of the same material to 1.6×10^{20} nvt, a slight increase in transition temperature was noted. This was accompanied by a lowering of the amount of energy absorbed on fracture above the ductile-brittle transition range. A very similar behavior was observed for Type 414 stainless steel; the condition of this steel prior to irradiation was unknown.

An expression relating to variation of transition temperature of ferritic stainless steels with neutron exposure is proposed by R. E. Schreiber (24). This expression is as follows:

$$T_t = A + B(1 - \exp[-E])^{1/2} \pm 15$$

In this expression T_t is the transition temperature in degrees centigrade, E is the exposure of the fast neutrons in units of 10^{20} nvt. Although it might be expected that these ferritic steels would

[4] C. N. Spalaris, private communication.

suffer a considerable damage in ductile-brittle transition behavior by neutron irradiation, the results quoted are not particularly alarming although they do not necessarily represent as complete a set of data as one might desire for design purposes. A 16 per cent chromium-15 per cent nickel iron-base alloy irradiated in the annealed condition did not behave as satisfactorily as the 400 series stainlesses. In the unirradiated state this alloy had a transition temperature near zero Fahrenheit (−20 C). Progressive increases in transition temperature were noted with increased exposure until 2.6×10^{20} nvt had shifted the transition temperature to about 200 F (100 C). This observation is in agreement with those made on ferrous alloys with lower alloy contents; that is, marked increases in ductile-brittle transition behavior have been measured for structural steels. Since this composition is not markedly different from the 400 series stainless steels which contain about 12 to 13 per cent chromium, it is possible that the condition of heat treatment prior to irradiation may have had a pronounced effect on the observed results.

CONCLUSIONS

The current state of knowledge dealing with the effects of neutron irradiation on the properties of austenitic, ferritic, martensitic, and precipitation hardening stainless steels has been reviewed. Several general conclusions are possible:

1. Neutron irradiation does not appear to play a major role in chemical reactions between stainless steels and their environments in the range of temperatures of interest. This applies to bulk corrosion, not to localized corrosion.

2. Neutron irradiation has a nominal effect on the physical properties of stainless steels; there appear to be no changes of engineering significance.

3. Irradiation can directly influence certain transformations such as ferrite formation and recovery of cold work. Even so the major effects tend to be indirect resulting from induced temperatures such as are seen at core-cladding interfaces.

4. The tensile properties of the austenitic, ferritic, and martensitic stainless steels are affected by neutron irradiation. Marked increases in the yield strength occur accompanied by less pronounced increases in the ultimate tensile strength. There are decreases in elongation and reduction of area. Both post-irradiation annealing, and testing at or above 350 C (660 F), and irradiation above 250 C (480 F) reduce these effects markedly.

5. The austenitic stainless steels appear to undergo a recovery of irradiation induced damage over a relatively narrow range of temperature between 400 to 600 C (750 to 1110 F); this recovery appears to be essentially independent of composition.

6. Irradiation accelerates the low-temperature relaxation in austenitic stainless steels. Results are uncertain insofar as creep is concerned, but it is possible that creep rates are reduced by irradiation.

7. The effect of irradiation on fatigue resistance is still uncertain. Post-irradiation results indicate there is a strain dependence with irradiated stainless steels less resistant at higher strains, but more resistant at lower strains compared to unirradiated controls. In-reactor strain cycling tests reveal a loss in fatigue resistance in biaxially loaded specimens compared to unirradiated controls.

8. The stress-to-rupture life of a precipitation hardenable stainless steel, Type A-286, is grossly reduced after irradiation when tested at 540 C (1010 F) and 650 C (1200 F). Type 304 stainless steel tubular stress-to-rupture specimens appear to have a reduced life during irradiation in some heats while there is no observable effect in other heats when compared to the unirradiated controls.

9. Irradiation has a nominal effect on the impact strength and transition temperatures of austenitic stainless steels. In ferritic stainless steels the effects range from nominal to marked, possibly owing to structural or compositional variations.

REFERENCES

(1) D. O. Leeser and W. F. Murphy, "Engineering Studies on Radiation Damage to Structural Materials," *USAEC Report CF-53-3-276*, Part 2, 1953, pp. 327–357.

(2) C. R. Sutton and D. O. Leeser, "Radiation Effects on Structural Materials," *Nuclear Engineering*, Am. Institute Chemical Engrs., 1954, pp. 208–221.

(3) C. R. Sutton and D. O. Leeser, "How Radiation Affects Structural Materials," *Iron Age*, Vol. 174, No. 8, August 19, 1954, pp. 128–131 and Vol. 174, No. 9, August 26, 1954, pp. 97–100.

(4) D. O. Leeser, "How Nuclear Radiation Affects Engineering Materials," *Materials and Methods*, Vol. 40, August, 1954, pp. 109–120.

(5) J. C. Wilson and R. G. Berggren, "Effects of Neutron Irradiation in Steel," *Proceedings*, Am. Soc. Testing Mats., Vol. 55, 1955, pp. 689–707.

(6) J. C. Wilson, "Radiation Effects on Metals," *Mechanical Properties of Metals*, Pennsylvania State University, University Park, Pa., 1958, pp. 263–275.

(7) S. T. Konobeevsky, N. F. Pravdyuk, and V. I. Kutaitsev, "The Effect of Irradiation on the Structure and Properties of Structural Materials," International Conference on the Peaceful Uses of Atomic Energy, United Nations, Aug. 8–20, 1955, *USSSR P/680*, Vol. 7, pp. 479–483.

(8) N. F. Pravdyuk, S. T. Konobeevsky, A. D. Armarev, and Y. I. Pokrovsky, "The Effect of Neutron Irradiation on the Mechanical Properties of Structural Materials," Second United Nations International Conference on the Peaceful Uses of Atomic Energy, Geneva, September, 1958, *P/2052*, Vol. 5, pp. 457–465.

(9) S. S. Ibragimov, V. S. Lyashenko, and A. I. Zavyalov, "An Investigation of the Structure and Properties of Several Steels and Other Metals After Irradiation With Fast Neutrons," *Reactor Science and Technology Journal Nuclear Energy*, Parts A and B, Vol. 16, January, 1962, pp. 45–49.

(10) N. F. Pravdyuk, A. D. Amaev, P. A. Platonov, V. N. Kuznetsov, and V. M. Golyanov, "The Effect of Neutron Irradiation on the Properties of Structural Materials," *Properties of Reactor Materials and the Effects of Radiation Damage*, D. J. Littler, editor, Butterworths, London, 1962, pp. 343–358.

(11) M. H. Bartz, "Performance of Metals During Six Years Service in the Materials Testing Reactor," Second United Nations International Conference on the Peaceful Uses of Atomic Energy, Geneva, September, 1958, *P/1878*, Vol. 5, pp. 466–474.

(12) M. J. Graber and J. H. Ronsick, "ETR Radiation Damage Surveillance Programs, Progress Report I," *USAEC IDO-16628*, Jan. 27, 1961.

(13) M. S. Robinson, "Radiation Damage Studies Program—ETR Loop Materials Progress Report," *USAEC Report IDO-16637*, April 19, 1957.

(14) M. S. Robinson, "Radiation Damage Studies Program—ETR Loop Materials Progress Report," *USAEC Report IDO-16409*, Sept. 16, 1957.

(15) H. T. Watanabe, "Radiation Damage Studies Program—ETR Loop Materials Progress Report," *USAEC Report IDO-16475*, Sept. 15, 1958.

(16) F. R. Shober and W. E. Murr, "Radiation-Induced Property Changes in AISI Type 347 Stainless Steel," *Preprint*, Am. Soc. Testing Mats., Los Angeles, Calif., Oct. 1, 1962.

(17) J. W. Joseph, Jr., "Stress Relaxation in Stainless Steel During Irradiation," *USAEC Report DP-369*, June, 1959.

(18) R. E. Schreiber, "Relaxation of Torsional Stresses in Stainless Steel During Irradiation," *USAEC Report DP-669*.

(19) L. F. Coffin, Jr., "Radiation Effects on Creep of Stainless Steel," *USAEC Report CF-53-3-276*, Part 2, 1953, pp. 258–267.

(20) J. C. Wilson, J. C. Zukas, and W. W. Davis, "Creep of Inconel and Stainless Steel Under Irradiation," *USAEC Report CF-53-3-276*, Part 2, 1953, pp. 258–267.

(21) W. E. Brundage et al, "Type 304 Stainless Steel Tube-Burst Tests," *USAEC Report ORNL-3364*, 1962, pp. 141–144.

(22) C. G. Collins, G. L. Hammons, F. C. Robertshaw, and W. A. Couts, "Radiation Effects on the Stress Rupture Properties of Inconel X and A-286," *USAEC Report APEX-676*, December, 1961.

(23) L. F. Porter, "Radiation Effects in Steel," *Materials in Nuclear Applications, ASTM STP 276*, Am. Soc. Testing Mats., 1959, pp. 147–195.

(24) R. E. Schreiber, "Mechanical Properties of Irradiated Stainless Steels," *USAEC Report DP-579*, September, 1961.

(25) F. Seitz and J. S. Koehler, "Displacement of Atoms During Irradiation," *Solid State Physics*, F. Seitz and D. Turnbull, editors, Academic Press, New York, N. Y., 1956.

(26) D. S. Billington and J. H. Crawford, Jr., *Radiation Damage in Solids*, Princeton University Press, Princeton, N. J., 1961.

(27) D. K. Holmes, "The Ranges of Energetic Atoms in Solids," *Radiation Damage in Solids*, Vol. 1, Vienna International Atomic Energy Agency, 1962, pp. 3–42.

(28) H. Brooks, "The Thermal Spike Picture of Radiation Damage," *USAEC Report KAPL-360*, Aug. 4, 1950.

(29) J. A. Brinkman, "On the Nature of Radiation Damage in Metals," *Journal Applied Physics*, Vol. 25, August, 1954, pp. 961–970.

(30) A. M. Goland, "Atomic Displacements in Solids by Nuclear Reaction," *ASTIA Report AD 278458*, May, 1962.

(31) V. V. Gerasimov and V. N. Aleksandrova, "The Effect of Radiation on the Electrochemical Behavior of 1Kh18N9T Steel," *Soviet Journal Atomic Energy*, Vol. 10, February, 1961, pp. 161–166.

(32) "Corrosion of Nuclear Materials" abstracted from "The Joint Research and Development Program Quarterly Digest—Euratom U.S. Agreement for Cooperation," *EURAEC-285*, Jan. 1 to March 31, 1962, Vol. 2 No. 1, pp. 30–33.

(33) J. Ashbridge and R. Sumerling, "The Effect of Irradiation on Permeation of Hydrogen through Stainless Steel," *United Kingdom Report IGR-TN/W-720*, November, 1957.

(34) L. M. Howe, "Radiation Damage in Zirconium, Zircaloy-2, and 410 Stainless Steel," *Canadian Report AECL-1484*, April, 1962.

(35) N. J. Gioseffi and H. E. Kline, "Behavior of Structural Materials Exposed to an Organic Moderated Reactor Environment," *USAEC Report NAA-SR-2570*, Oct. 1, 1959.

(36) J. J. Prislinger, "Results of Tensile Tests Performed on Materials Exposed in the Homogeneous Reactor Experiment No. 2 Blanket and Low-Flux Core Region," *USAEC Report ORNL-TM-337*, Oct. 2, 1962.

(37) B. A. Webb, "Compatibility of Uranium Carbides with 304 Stainless Steel in Sodium," *Am. Nuclear Soc. Transactions*, Vol. 4, 1961, p. 349.

(38) W. J. Anderson and G. V. Sneesby, "Carburization of Austenitic Stainless Steel in Liquid Sodium," *NAA-SR-5282*, Sept. 1, 1960.

(39) W. C. Hayes and O. C. Shepard, "Corrosion and Decarburization of the Ferritic Chromium-Molybdenum Steels in Sodium Coolant Systems," *NAA-SR-2973*, Dec. 1, 1958.

(40) C. N. Spalaris, "Materials for Superheat Reactors," *Nuclear Metallurgy Vol. VIII—A Symposium on Materials for Gas-and Water-Cooled Reactors, AIME IMD Special Report No. 11*, Vol. 208, 1962, pp. 191–211.

(41) "Dresden Shut Down: Control-Rod Drives" *Nucleonics*, Vol. 19, No. 1, January, 1961, p. 25.

(42) S. H. Bush, "Trip Report—Status of 17-4 PH and Other Precipitation Hardening Stainless Steels," *USAEC Report HW-68608*, Feb. 9, 1961.

(43) A. Charlesby, N. H. Hancock, and H. C. Sansom, "Effect of Atomic Pile Radiation on the Elastic Modulus of an Austenitic Steel," *United Kingdom Report AERE-MR-1434*, May 7, 1954.

(44) S. H. Paine, W. F. Murphy, and D. W. Hackett, "A Study of Irradiation Effects in Type A Nickel and Type 347 Stainless Steel Tensile Specimens," *USAEC Report ANL-6102*, July, 1960.

(45) Karl F. Smith, "Stainless Steels," Chapter 23, *Reactor Handbook Vol. 1 Materials*, C. R. Tipton, Jr., editor, Interscience Publishers, Inc. New York, N. Y., 1960, pp. 563–589.

(46) C. A. Bruch, W. E. McHugh, and R. W. Hockenbury, "Variations in Radiation Damage to Metals," *Transactions*, Am. Institute Mining and Metallurgical Engrs., Vol. 206, October, 1956, pp. 1348–1353.

(47) R. E. Bailey and M. A. Silliman, "Effects of Irradiation on the Type 347 Stainless Steel Flow Separator in the EBR-1 Core," *Radiation Effects on Materials, ASTM STP 233*, Am. Soc. Testing Mats., 1958, pp. 84–101.

(48) H. G. F. Wilsdorf and D. Kuhlmann-Wilsdorf, "Dislocation Behavior in Quenched and in Neutron Irradiated Stainless Steel," *Journal Nuclear Materials*, Vol. 5, No. 2, February, 1962, pp. 178–192.

(49) D. Hull and I. L. Mogford, "Precipitation and Irradiation Hardening Iron," *Philosophical Magazine*, Vol. 6, No. 64, April, 1961, pp. 535–546.

(50) M. B. Reynolds, J. R. Low, Jr., and L. O. Sullivan, "Study of the Radiation Stability of Austenitic Type 347 Stainless Steel," *Transactions*, Am. Institute Mining and Metallurgical Engrs., Vol. 203, April, 1955, pp. 555–559.

(51) E. E. Baldwin, "Programs on the Effects of Neutron Irradiation Upon the Mechanical Properties of Structural Materials," *USAEC Report TID-7588*, Oct. 15–16, 1959, pp. 189–204.

(52) J. W. Joseph, Jr., "Mechanical Properties of Irradiated Welds in Stainless Steel," *USAEC Report DP-534*, December, 1960.

(53) J. F. Watson, J. L. Christian, and J. W. Allen, "A Study of the Effects of Nuclear Radiation on High-Strength Aerospace Vehicle Materials at the Boiling Point of Hydrogen (−423 F)," *ERR-AN-085*, General Dynamics, Sept. 27, 1961.

(54) R. G. Berggren, W. E. Brundage, W. W. Davis, N. E. Hinkle, and J. C. Zukas, "Tensile and Stress Rupture Properties of Irradiated Stainless Steels and Inconel," *USAEC Report TID-7588*, 1959, pp. 205–217.

(55) F. C. Robertshaw, J. Moteff, F. D. Kingsbury, and M. A. Pugacz, "Neutron Irradiation Effects in A-286, Hastelloy-X and Rene' 41," *Radiation Effects in Metals and Neutron Dosimetry, ASTM STP 341*, Am. Soc. Testing Mats., 1963.

(56) D. O. Leeser and J. E. Kemme, "Fatigue Tests on Irradiated and Control Specimens of Type 304 Stainless Steel, Zirconium and a Tin-Zirconium Alloy," *USAEC Report CF-53-3-276*, Part 2, 1953, pp. 302–313.

(57) "Reactor Engineering Division Quarterly Report for December 1, 1953 through March 30, 1959," *USAEC Report ANL-5260*.

APPENDIX

TABLE A-1—THE EFFECT OF POST-IRRADIATION ANNEALING ON THE TENSILE PROPERTIES OF AUSTENITIC STAINLESS STEELS.

Material	Test No.	Nvt > 1 Mev	Irradiation Temperature	Post-Irradiation Anneal Yield Strength					Tensile Strength			Per Cent Elongation			Ref.
				Temperature	Time, hr	Unirradiated	Irradiated	Δ	Unirradiated	Irradiated	Δ	Unirradiated	Irradiated	Δ	
304	5G	$5.7–10^{21}$	?	335 C	5	77	104	27	108	114	6	46	54	8	(12)
304	5H	$5.7–10^{21}$	?	335 C	22	77	101	24	108	112	4	46	50	4	...
347	5P	$4.7–10^{21}$	?	335 C	4	67	107	40	96	117	21	56	34	−22	...
347	8A	$2.0–10^{21}$	250 to 500 C	400 C	89	56	90	34	93	108	15	92.5	29	−13.5	(47)
347	8B	$6.0–10^{20}$	250 to 500 C	400 C	89	56	64	8	93	95.5	2.5	42.5	31	−11.5	...
347	8C	$2.0–10^{21}$	250 to 500 C	500 C	79	58	59	1	91.5	92.5	1	37	38	1	...
347	8D	$6.0–10^{20}$	250 to 500 C	500 C	79	58	58.3	0.3	91.5	93	1.5	37	34	−3	...
347	8E	$2.0–10^{21}$	250 to 500 C	500 C	7	58	67.5	9.5	91.5	96.5	5	37	34	−3	...
347	8F	$6.0–10^{20}$	250 to 500 C	500 C	7	58	57.5	−8.5	91.5	91.5	0	37	37	0	...
347	8M	$2.0–10^{21}$	250 to 500 C	740 C	0.5	49.5	49.5	0	89	88.5	−0.5	37.5	39	1.5	...
347	8N	$6.0–10^{20}$	250 to 500 C	740 C	0.5	49.5	50	0.5	89	90.5	+1.5	37.5	43	5.5	...
347	10C	$5.7–10^{21}$	50 C	980 C	1	35	33	−2	89	86.5	−2.5	63	55.5	−7.5	(16)
347	10D	$1.2–10^{22}$	50 C	980 C	1	35	34	−1	89	87	−2	63	61	−2	(16)

TABLE A-2—THE EFFECT OF ELEVATED TEMPERATURE TESTING ON THE TENSILE PROPERTIES OF IRRADIATED AUSTENITIC STAINLESS STEELS.

Material	Test No.	Nvt > 1 Mev	Irradiated Temperature	Test Temperature	Yield Strength			Tensile Strength			Per Cent Elongation			Ref.
					Unirradiated	Irradiated	Δ	Unirradiated	Irradiated	Δ	Unirradiated	Irradiated	Δ	
347	10E	$5.7–10^{21}$	50	315 C	28	81	53	68.5	83.5	15	35.5	15.5	−20	(16)
347	10F	$1.2–10^{22}$	50	315 C	28	86	58	68.5	88	19.5	35.5	12.5	−23	...
347	10A	$5.7–10^{21}$	50	RT	35	98	63	89	112	23	63	33.5	−29.5	...
347	10B	$1.2–10^{22}$	50	RT	35	106.5	71.5	89	112.5	23.5	63	31	−32	...
376	14A	...	650	RT	30	27	−3	81	78	−3	62	56	−6	[a]
376	14B	...	650	700	13	25	12	36	67	37	48	46	−2	...
347	14C	...	650	RT	53	52	−1	100	95	−5	44	39	−5	...
347	14D	...	650	700	33	39	6	43	62	25	34	27	−7	...
Kh17N5M2	17A	$6.0–10^{19}$	80	RT	51.7	100	48.3	138	160	22	32	18.9	−13	(10)
Kh17N5M2	17D	$6.0–10^{19}$	80	350	41.1	60	19	71.5	86.5	15	22	14.7	−7	...
Kh17N5M2	17B	$6.0–10^{19}$	180	RT	51.7	88	36.3	138	152	14	32	24	−8	...
Kh17N5M2	17E	$6.0–10^{19}$	180	350	41.1	55.6	14.5	71.5	82	10.5	22	14.7	−7	...
A-286	19C	$7.0–10^{20}$	90	650	102.5	91	−11.5	109.5	111.0	2.5	+6	2.5	−3.5	(22)

[a] H. J. Pessl, private communication.

TABLE A-3—THE EFFECT OF IRRADIATION AT ELEVATED TEMPERATURES (>200 C) ON THE ROOM TEMPERATURE TENSILE PROPERTIES OF AUSTENITIC STAINLESS STEELS.

Material	Test No.	Nvt > 1 Mev	Irradiated Temperature	Yield Strength			Tensile Strength			Per Cent Elongation			Ref.
				Unirradiated	Irradiated	Δ	Unirradiated	Irradiated	Δ	Unirradiated	Irradiated	Δ	
304	1A	$3.0–10^{18}$	215 to 260 C	44.5	48.5	4	92.5	93.5	1	70.8	50	−11	(1)
309	1B	$3.0–10^{18}$	215 to 260 C	38.5	43.5	5	95	99	4	54	51	−3	...
316	1C	$3.0–10^{18}$	215 to 260 C	35	36.5	1.5	89.5	90	0.5	70	66.5	−3.5	...
347	1D	$3.0–10^{18}$	215 to 260 C	37.5	42.5	5	99	103	4	56.5	54.5	−2	...
Kh18N9T	3A	$1.4–10^{18}$	80 C	34	62.5	28.5	92.5	105	12.5	65	55	−10	(8)
	3B	$2.4–10^{18}$	300 C	37	59.5	22.5	101	104	3	64	50	−14	...
	3E	$4.4–10^{18}$	600 C	45.5	38.5	−7	108	108	0	62	70	8	...
Kh18N12M2T	3F	$1.0–10^{20}$	80 C	42.5	95	52.5	95	121	26	70	45	−25	...
	3G	$7.0–10^{18}$	300 C	49.5	51	1.5	98	112	14	60	57	−3	...
	3I	$1.1–10^{19}$	600 C	47	40	−7	108	101	−7	38	51	3	...
Kh18N14M3Nb	3J	$5.0–10^{19}$	80 C	35.5	95	59.5	95	127	32	50	29	−21	...
	3K	$3.7–10^{18}$	300 C	35.5	41	5.5	98	120	23	56	52	−4	...
Kh20N404(W + Nb)	3L	$1.0–10^{20}$	80 C	61	89.5	28.5	108	135	27	39	25	−14	...
	3M	$2.5–10^{18}$	300 C	59.5	71	11.5	117	122	5	39	28	−11	...
	3N	$3.5–10^{18}$	470	54	57	3	115	122	7	38	36	−2	...
	3-O	$4.4–10^{18}$	600	62.5	71	8.5	114	124	10	39	35	−4	...
347	8-O	$2.0–10^{21}$	250 to 500 C	56	99	43	90	104	14	39.5	19	−20.5	(47)
	8P	$6.0–10^{20}$	250 to 500 C	56	76	20	90	101.5	11.5	39.5	29	−10.5	...
347	13A	$2.6–10^{20}$	230 to 290 C	38.9	73.5	34.6	88.8	104.5	15.7	56.8	45.3	−11.5	(51)
316	14A	$2.6–10^{20}$	650 C	30	27	−3	81	78	−3	62	56	−6	[a]
347	14C	$2.6–10^{20}$	650 C	53	52	−1	100	95	−5	44	39	−5	...
Kh17N5M2	17A	$6.0–10^{19}$	80 C	51.7	100	48.3	138	160	22	32	18.9	−13	(10)
	17B	$6.0–10^{19}$	180 C	51.7	88	36.3	138	152	14	32	24	−8	...
	17C	$6.0–10^{19}$	340 C	51.7	83.5	31.8	138	155	17	32	27.6	−4	...
1Kh18N9T	17G	$7.0–10^{19}$	100 C	86.5	116.5	30	124	142	18	15	11	−4	...
	17H	$7.4–10^{19}$	300 C	68.5	104	17.5	124	136	12	15	16	1	...
	17I	$7.4–10^{19}$	500 C	86.5	82	4.5	124	117	−7	15	26	11	...
Kh18N12M2T	17M	$1.0–10^{20}$	80 C	43	95	52	95	121	26	70	45	−25	...
	17-O	$7.0–10^{18}$	300 C	43	51	8	95	112	17	70	57	−13	...
	17P	$1.0–10^{19}$	470 C	43	43	0	95	100	5	70	55	−15	...
	17Q	$1.1–10^{19}$	600 C	43	40	−3	95	101	6	70	51	−19	...
Kh18N22V2T2	17R	$7.4–10^{19}$	100 C	81	92	11	131	122	−9	29	31	2	...
	17T	$7.0–10^{19}$	300 C	81	78	−3	131	122	−9	29	26	−3	...
304	21A	$2.5–10^{20}$	315 to 370 C	42	45	3	85	86	1	70	66	−4	(35)
	21B	$2.5–10^{20}$		41	50	9	85.8	86.5	0.7	68	60	−8	...
347	22A	$8.0–10^{15}$	100 to 300 C	45	43.3	−1.7	90.8	87.7	−3	81.8	82.1	0	(36)
	22B	$2.6–10^{18}$	100 to 300 C	45	47.7	2.7	90.8	97	6	81.8	74.4	−7.4	...
	22C	$8.0–10^{15}$	100 to 300 C	53.9	56.8	3	96.9	97.3	0.5	55.8	56	0	...
	22D	$2.6–10^{18}$	100 to 300 C	53.9	62.4	8.5	96.9	100.2	4	55.8	52.6	−3.2	...
304	22E	$8.0–10^{15}$	100 to 300 C	64.3	62.8	−1.5	93.5	91.8	−1.5	67.6	63.7	−4	...
304 L	22F	$2.6–10^{18}$	100 to 300 C	64.9	67.7	3	94.5	96.2	1.5	70.9	61.6	−9.3	...
309 SCb	22G	$2.6–10^{18}$	100 to 300 C	58.4	59.5	1	96.1	99.8	3.7	59.1	49.9	−9.2	...

[a] H. J. Pessl, private communication.

TABLE A-4—EFFECT OF COLD WORK ON THE TENSILE PROPERTIES OF IRRADIATED AUSTENITIC STAINLESS STEEL.

Material	Test No.	Irradiated Nvt	Irradiated Temperature	Per Cent Cold Work	Test Temperature	Yield Strength			Tensile Strength			Per Cent Elongation			Ref.
						Unirradiated	Irradiated	Δ	Unirradiated	Irradiated	Δ	Unirradiated	Irradiated	Δ	
347	6A	$1–2–10^{20}$	90 C	0	RT	48.7	102.8	54.1	97.7	113.1	15.4	53.4	34.3	−19.1	(46)
	6B	$1–2–10^{20}$	90 C	30 to 40	RT	149.7	192.5	42.8	164.6	198.8	34.2	17.5	11.3	−6.2	...
1Kh18N9T	17F	$1.0–10^{20}$	80 C	0	RT	34[a]	131	97	92	142	50	66	43	−23	(10)
	17G	$7.0–10^{19}$	100 C	25	RT	86.5	116.5	30	124	142	18	15	11	−4	...

[a] Yield point.

TABLE A-5—THE EFFECT OF COMPOSITION ON THE ROOM TEMPERATURE TENSILE PROPERTIES OF AUSTENITIC STAINLESS STEELS IRRADIATED BELOW 200 C.

Material	Test No.	Nvt > 1 Mev	Yield Strength			Tensile Strength			Per Cent Elongation			Ref.
			Unirradiated	Irradiated	Δ	Unirradiated	Irradiated	Δ	Unirradiated	Irradiated	Δ	
Kh18N9T	2A	$2.4\text{-}10^{20}$	31.8	93.5	62	89	114	25	71	37	−34	(7)
	2B	$3.2\text{-}10^{20}$	38.5	83.5	45.9	91.5	100.5	9	66.5	36.5	−30	...
Kh18N9	2C	$2.4\text{-}10^{20}$	29.5	73.5	44	94	95	1	76	56	−20	...
Kh20N14S2	2D	$3.2\text{-}10^{20}$	40	79	39	86	101	15	60.5	38.5	−22	...
Kh18N9T	3A	$1.4\text{-}10^{18}$	34	62.5	28.5	92.5	105	12.5	65	55	−10	(8)
Kh18N12M2T	3F	$1.0\text{-}10^{20}$	42.5	95	52.5	95	121	26	70	45	−25	...
Kh14N14M3Nb	3J	$5.0\text{-}10^{19}$	35.5	95	59.5	95	127	32	50	29	−21	...
20Cr/40Ni/4(W + Nb)	3L	$1.0\text{-}10^{20}$	61	89.5	28.5	108	135	27	39	25	−14	...
Kh18N9T[a]	3P	$3.0\text{-}10^{17}$	34	52.5	18.5	92.5	102.5	10	66	65	−1	...
	3Q	$1.0\text{-}10^{20}$	34	131	96	92.5	142.5	50	66	43	−23	
347	4A	$2.4\text{-}10^{20}$	62	98	36	97	109	13	63	52	−11	(11)
	4B	$7.2\text{-}10^{20}$	62	97	35	96	110	14	63	51	−12	...
	4C	$2.6\text{-}10^{21}$	62	101	39	96	107	11	63	44	−19	...
	4D	$3.8\text{-}10^{21}$	63	107	44	96	115	19	63	32	−31	...
304	5A	$2.0\text{-}10^{19}$	77	126	49	108	127	19	46	32	−14	(12)
	5B	$1.3\text{-}10^{20}$	77	129	52	108	130	22	46	31	−15	...
	5C	$5.1\text{-}10^{20}$	77	130	53	108	131	23	46	32	−14	...
	5D	$1.2\text{-}10^{21}$	77	130	53	108	131	23	46	33	−13	...
	5E	$2.9\text{-}10^{21}$	77	129	52	108	129	21	46	31	−15	...
	9B	$1.5\text{-}10^{20}$	162.4	199	37	195.4	222	26.5	23	15	−8	...
347	10A	$5.7\text{-}10^{21}$	35	98	63	89	112	23	63	33.5	−29.5	(16)
	10B	$1.2\text{-}10^{22}$	35	106.5	71.5	89	172.5	23.5	63	31	−32	...
304	11M[b]	$2.9\text{-}10^{20c}$	34	79.8	46	83.5	98.9	15.5	65	36	−29	...
	11N	$3.0\text{-}10^{20c}$	34	80.6	47	83.5	99.4	16	65	42	−23	...
	11O	$1.2\text{-}10^{21c}$	34	92.7	59	83.5	104.2	20.5	65	46	−19	...
	11P	$1.2\text{-}10^{21c}$	34	91.5	58	83.5	104.4	21	65	42	−23	...
	11Q[d]	$2.9\text{-}10^{20c}$	34.1	83.9	50	83.2	99.8	16.5	64	42	−22	...
	11R	$3.0\text{-}10^{20c}$	34.1	83.7	50	83.2	99.3	16	64	39	−25	...
	11S	$1.2\text{-}10^{21c}$	34.1	90.9	57	83.2	104.9	21.5	64	42	−22	...
	11T	$1.2\text{-}10^{21c}$	34.1	91.2	57	83.2	104.6	21.5	64	15	−49	...
347	15A	$2.4\text{-}10^{20}$	33.2	72.8	39.5	85	102.9	18	55	34	−21	(44)
	15B	$4.0\text{-}10^{20}$	33.2	86.9	52.7	85	106.9	22	55	29	−26	...
	15C	$2.4\text{-}10^{20}$	33.0	82.5	49.5	86.4	105.8	19.4	64	37	−27	...
	15D	$4.0\text{-}10^{20}$	33.0	83.8	50.8	86.4	104.0	17.6	64	36	−28	...
Kh17N5M2	17A	$6.0\text{-}10^{19}$	51.7	100.0	48.3	138.0	160.0	22.0	32	18.9	−13	(10)
Kh20N14S2	17J	$2.5\text{-}10^{17}$	49	54.0	5.0	106.0	112.0	6.0	62	66	4	...
	17K	$1.2\text{-}10^{18}$	49	71.0	22.0	106.0	117.0	11.0	62	65	3	...
	17L	$2.0\text{-}10^{19}$	49	95.0	46.0	106.0	...	...	62	47	−15	...
	17M	$4.4\text{-}10^{19}$	49	106.0	57.0	106.0	127	21.0	62	40	−22	...
	5F	$5.7\text{-}10^{21}$	77	103	26	108	114	6	46	50	+4	(12)
316	5I	$1.2\text{-}10^{19}$	67	101	34	91	105	14	66	44	−16	...
	5J	$9.9\text{-}10^{19}$	67	105	38	91	108	17	60	44	−16	...
	5K	$5.6\text{-}10^{20}$	67	108	41	91	109	18	60	42	−18	...
	5L	$1.3\text{-}10^{21}$	67	107	40	91	111	20	60	42	−18	...
347	5M	$5.2\text{-}10^{20}$	67	116	49	96	117	21	56	36	−20	...
	5N	$8.0\text{-}10^{20}$	67	117	50	96	117	21	56	35	−21	...
	5-O	$4.7\text{-}10^{21}$	67	116	49	96	116	20	56	36	−20	...
AM-350	5Q	$5.9\text{-}10^{19}$	156	192	36	195	217	22	18	13	−5	...
	5R	$1.2\text{-}10^{20}$	156	192	36	195	220	25	18	16	−2	...
	5S	$7.3\text{-}10^{20}$	156	207	51	195	227	32	18	16	−2	...
347	6	$1.2\text{-}10^{20}$	48.7	102.8	54.1	97.7	113.1	15.4	53.4	34.3	−19.1	(46)
301	7A	$3.9\text{-}10^{19}$	38.4	87	48.5	98.7	113.2	14.5	56	48	−8	(5)
302	7B	$3.9\text{-}10^{19}$	33.8	84	50	95.5	111.3	16.0	...	...	...	...
302B	7C	$3.9\text{-}10^{19}$	33.5	81.5	48	107.8	125	17.0	...	...	...	...
304L	7D	$7.8\text{-}10^{19}$	24.4	75.5	51	86.3	103.8	17.5	63	58	−5	...
305	7E	$3.9\text{-}10^{19}$	32.1	71.4	39	98	103.6	5.5	...	...	...	...
321	7F	$7.8\text{-}10^{19}$	31.2	90.6	59.5	84.8	105.8	21	...	...	...	...
347	7G	$3.9\text{-}10^{19}$	37	96.5	59.5	97.6	114.8	17	49	25	−24	...
AM-350	9A	$1.2\text{-}10^{19}$	162.4	190	28	195.4	215	19.5	23	17	−6	(15)
Kh18N22V2T2	17R	$7.4\text{-}10^{19}$	81	92	11	131	122	−9	29	31	2	...
	17S	$2.2\text{-}10^{20}$	81	116	35	131	120	−11	29	24	−5	...
A-286	19A	$7.0\text{-}10^{20}$	113	140	27	164	148	−16	24	6	−18	(22)
304	24A[e]	$1.4\text{-}10^{20b}$	50	89	39	90	104	14	...	...	...	(17)
	24B	$4.1\text{-}10^{20b}$	50	94	44	90	105	15	...	...	...	...
	24C	$8.6\text{-}10^{20b}$	50	98	48	90	109	19	...	...	...	...
	24D[f]	$1.4\text{-}10^{26b}$	39	76	37	81	94	13	...	...	...	...
	24E	$4.1\text{-}10^{20b}$	39	83	44	81	96	15	...	...	...	...
	24F	$8.6\text{-}10^{20b}$	39	86	47	81	99	18	...	...	...	...
304	25A[g]	$2.7\text{-}10^{20b}$	46	92	46	...	...	...	...	...	...	(18)
	25B	$5.1\text{-}10^{20b}$	46	95	49	...	...	...	...	...	...	...
	25C	$1.0\text{-}10^{21b}$	46	100	51	...	...	...	...	...	...	...

[a] Yield point believed in error.
[b] Longitudinal.
[c] $->0.1$ Mev.
[d] Transverse.
[e] 0.125 in. diameter.
[f] 0.500 in. diameter.
[g] Torsion specimen 0.2 in. OD by 0.125 in. ID by 4 in. gage.

TABLE A-6—THE EFFECT OF MACROSTRUCTURE ON THE TENSILE PROPERTIES OF AN IRRADIATED AUSTENITIC STAINLESS STEEL.[a]

Material	Test No.	Nvt > 0.1 Mev	Yield Strength			Tensile Strength			Per Cent Elongation			Ref.
			Unirradiated	Irradiated	Δ	Unirradiated	Irradiated	Δ	Unirradiated	Irradiated	Δ	
304 Base	11A[b]	$2.5–10^{20}$	57.7	97.5	40	86.1	103.2	17	35.5	28	−7	(52)
308 Filler Weld	11B	$3.0–10^{20}$	57.7	97.7	40	86.1	103.1	17	35.5	28	−7.5	...
	11C	$1.0–10^{21}$	57.7	101.3	43.5	86.1	106.1	20	35.5	15	−20.5	...
	11D	$1.2–10^{21}$	57.7	96.6	39	86.1	102.3	16	35.5	19	−16.5	...
	11E[c]	$2.7–10^{20}$	45.0	87.3	42	85.4	101.5	16.5	50.5	39	−11.5	...
	11F	$3.0–10^{20}$	45.0	92.5	47.5	85.4	102.3	17	50.5	25	−25.5	...
	11G	$1.1–10^{21}$	45.0	94.8	50	85.4	105.3	20	50.5	31	−19.5	...
	11H	$1.2–10^{21}$	45.0	96.6	51.5	85.4	107.2	22	50.5	33	−17.5	...
	11-I[c]	$2.8–10^{20}$	39.1	85.1	46	83.8	100.7	17	63.5	42	−21.5	...
	11J	$1.1–10^{21}$	39.1	93.8	55	83.8	105.5	22	63.5	39	−24.5	...
	11K[e]	$2.9–10^{20}$	39.1	82.9	44	84.1	100.4	16	52	31	−21	...
	11L	$1.1–10^{21}$	39.1	93.8	55	84.1	104.6	20.5	52	33	−19	...
	11M[f]	$2.9–10^{20}$	34.0	79.8	46	83.5	98.9	15.5	65	36	−29	...
	11N	$3.0–10^{20}$	34.0	80.6	47	83.5	99.4	16	65	42	−23	...
	11-O	$1.2–10^{21}$	34.0	92.7	59	83.5	104.2	20.5	65	46	−19	...
	11-P	$1.2–10^{21}$	34.0	91.5	58	83.5	104.4	21.0	65	42	−23	...
	11Q[g]	$2.9–10^{20}$	34.1	83.9	50	83.2	99.8	16.5	64	42	−22	...
	11R	$3.0–10^{20}$	34.1	83.7	50	83.2	99.3	16	64	39	−25	...
308 Filler Weld	11S	$1.2–10^{21}$	34.1	90.9	57	83.2	104.9	21.5	64	42	−22	...
	11T	$1.2–10^{21}$	34.1	91.2	57	83.2	104.6	21.5	64	15	−49	...

[a] Irradiation temperature <100 C.
[b] Weld metal longitudinally along weld.
[c] Weld metal transverse.
[d] Heat affected zone longitudinal.
[e] Heat affected zone transverse.
[f] Plate longitudinal.
[g] Plate transverse.

TABLE A-7—THE EFFECT OF SPECIMEN SIZE ON THE TENSILE PROPERTIES OF IRRADIATED AUSTENITIC STAINLESS STEELS.

Material	Test No.	Nvt > 1 Mev	Yield Strength			Tensile Strength			Per Cent Elongation			Ref.
			Unirradiated	Irradiated	Δ	Unirradiated	Irradiated	Δ	Unirradiated	Irradiated	Δ	
347	15A[a]	$2.4–10^{20}$	33.2	72.8	39.5	85	102.9	18	55	34	−21	(44)
	15B	$4.0–10^{20}$	33.2	86.9	52.7	85	106.9	22	55	29	−26	...
	15C[b]	$2.4–10^{20}$	33.0	82.5	49.5	86.4	105.8	19.4	64	37	−27	...
	15D	$4.0–10^{20}$	33.0	83.8	50.8	86.4	104.0	17.6	64	36	−28	...
304	24A[c]	$1.4–10^{20}$	50	89	39	90	104.0	14	...	...	...	(17)
	24B	$4.1–10^{20}$	50	94	44	90	105.0	15	...	...	...	...
	24C	$8.6–10^{20}$	50	98	48	90	109.0	19	...	...	...	...
	24D[d]	$1.4–10^{20}$	39	76	37	81	94.0	13	...	...	...	...
	24E	$4.1–10^{20}$	39	83	44	81	96.0	15	...	...	...	...
	24F	$8.6–10^{20}$	39	86	47	81	99.0	18	...	...	...	...
301	25A[e]	$2.7–10^{20}$	46	92	46	...	...	...	...	...	...	(18)
	25B	$5.1–10^{20}$	46	95	49	...	...	...	...	...	...	...
	25C	$1.0–10^{21}$	46	100	54	...	...	...	...	...	...	...

[a] 0.075 by 0.075 by 1 in. gage.
[b] 0.020 by 0.250 by 1 in. gage.
[c] 0.125 in. diameter 2 in. gage.
[d] 0.500 in. diameter 2 in. gage.
[e] 0.200 in. OD by 0.125 in. ID by 4 in. gage.

TABLE A-8—THE EFFECT OF IRRADIATION AND TESTING AT CRYOGENIC TEMPERATURES ON THE TENSILE PROPERTIES OF AUSTENITIC STAINLESS STEELS (REF. 54).

Material	Nvt > 0.33 Mev	Irradiated Temperature, deg F	Test Temperature	Yield Strength			Tensile Strength			Per Cent Elongation		
				Unirradiated	Irradiated	Δ	Unirradiated	Irradiated	Δ	Unirradiated	Irradiated	Δ
301 SS extra-full-hard temper	$6.0–10^{16}$	475	85	201	221	20	213	221	8	...	...	...
	$2.0–10^{17}$	−416	−423	302	284	−18	391	284	−107	13	8	−5
	$4.6–10^{16}$	−346	85	201	180	−21	213	225	12	10	20	10
	$4.6–10^{16}$	−346	−393	302	250	−52	391	250	−141	13	6	−7
310 SS extra-full-hard temper	$6.0–10^{16}$	475	85	158	184	26	180	184	4	1	1	0
	$2.0–10^{17}$	−416	−423	246	254	8	297	267	−20	6	1	−5
	$4.6–10^{16}$	−346	85	158	158	0	180	178	−2	1	1	0
	$4.6–10^{16}$	−346	−393	246	235	−11	297	252	−45	6	2	−4

TABLE A-9—EFFECTS OF IRRADIATION ON THE ROOM-TEMPERATURE TENSILE PROPERTIES OF FERRITIC AND MARTENISTIC STAINLESS STEELS.

Material[a]	Test No.	Nvt > 1 Mev	Irradiated Temperature	Yield Strength			Tensile Strength			Per Cent Elongation			Ref.
				Unirradiated	Irradiated	Δ	Unirradiated	Irradiated	Δ	Unirradiated	Irradiated	Δ	
410 SS	1A	$1.2–10^{20}$[b]	'50 C	38	89	51	59.5	92	32.5	32.5	15.3	−17.2	(34)
	1B	$6.0–10^{19}$[b]	265 C	38	56.5	18.5	59.5	85.5	26	32.5	23.9	−8.6	...
	1C	$4.2–10^{19}$[b]	265 C	38	56	18	59.5	77.5	18	32.5	27.7	−4.8	...
	1D	$4.9–10^{19}$[b]	265 C	38	57	19	59.5	78	18.5	32.5	26.2	−6.3	...
	1E	$5.6–10^{19}$[b]	265 C	38	59	21	59.5	78	18.5	32.5	25.0	−7.5	...
	1F	$7.2–10^{19}$[b]	265 C	38	60	22	59.5	80.5	21	32.5	26.6	−5.9	...
	1G	$8.3–10^{19}$[b]	265 C	38	61	23	59.5	80	20.5	32.5	26.0	−6.5	...
X-13	2A	$2.4–10^{20}$	80 C	45	98	53	68	98	30	36.5	1.2	−35.5	(7)
410 SS	3A	$1.1–10^{19}$	35 C	147.7	171.2	23.5	177	194	17	20	17	−3	(11)
	3B	$1.0–10^{20}$	35 C	147.7	182.8	35	177	201	24	20	15	−5	...
	3C	$2.9–10^{20}$	35 C	147.7	188.9	41	177	204.7	27.7	20	14	−6	...
	3D	$3.3–10^{20}$	35 C	147.7	189.3	41.5	177	204.4	27.4	20	14	−6	...
410 SS	4A	$1.2–10^{19}$	35 C	147.7	175.5	28	177	225	48	20	17	−3	(15)
	4B	$1.5–10^{20}$	35 C	147.7	198	50	177	233	56	20	11	−9	...
414 SS	4C	$6.4–10^{19}$	35 C	...	206	...	...	240	...	...	15	...	...
17-4 PH	5A	$2.0–10^{19}$	35 C	144.7	179.4	34.7	148.5	181	32.5	16	13	−3	(12)
	5B	$1.3–10^{20}$	35 C	144.7	194.5	49.8	148.5	197	48.5	16	12	−4	...
	5C	$5.1–10^{20}$	35 C	144.7	205.5	60.8	148.5	206.4	58	16	11	−5	...
	5D	$1.2–10^{21}$	35 C	144.7	209.5	64.8	148.5	209.9	61.5	16	10	−6	...
17-4PH	5E	$2.9–10^{21}$	35 C	144.7	214.3	69.7	148.5	214.4	66	16	9	−7	(12)
446 SS	6A	$3.0–10^{19}$	>100 C	43.6	68.8	25.2	72.6	78.2	56	...	...	...	(54)
	6B	$5.0–10^{19}$	365 C	43.6	107	53.4	72.6	107.8	35.2	...	...	...	...
410 SS	7A	$3.0–10^{20}$	315 to 370 C	70	86	16	92.3	102.8	10.5	32	21	−11	(35)
410 SS (malcomized)	8A	$7.0–10^{19}$	<100 C	47	62	15	69	70	1	...	...	...	(45)
	8B	$7.0–10^{19}$	<100 C	44	61	17	70	75	5	...	...	...	...
440 SS (hardened)	8C	$7.0–10^{19}$	<100 C	185	205	20	199	240	41	...	...	...	...
	8D	$7.0–10^{19}$	<100 C	185	200	15	211	240	29	...	...	...	...
420 SS	9A	$5.0–10^{19}$	<100 C	47	90	43	83	95	12	19	10	−9	(24)
Stainless W	9B	$5.0–10^{20}$	<100 C	...	...	...	113	134	21	...	...	...	...

[a] All exhibited yield points.
[b] −>500 ev.

EVALUATION AND APPLICATION OF STAINLESS STEELS IN CRYOGENIC ENVIRONMENTS

By A. Hurlich[1] and W. G. Scheck[2]

Synopsis

Cold-rolled stainless steel sheet possesses combinations of properties and characteristics which make it suitable for use as cyrogenic propellant tankage for large missiles and spacecraft. While extra cold-rolled Type 301 is used in both the Atlas and Centaur vehicles, other alloys including Types 304 L and 310 have also been evaluated for these applications by screening tests including tension, notched-tension, crack propagation, cross-tension, and shear tests on resistance spot welded joints, and static tension and cyclic fatigue tests of large complex weld joint specimens. Data are presented on the properties of the three alloys in base metal and weld joint configurations.

Type 301 stainless steel can be cold rolled to the highest tensile strength of the three alloys because of its lowest austenite stability, resulting in considerable transformation to martensite upon cold rolling. This factor is also responsible for embrittlement which is particularly manifested in reduced strength and fatigue resistance of welded joints tested at liquid hydrogen temperature. Use of more highly alloyed and more stable stainless steel such as Type 310 eliminates low-temperature embrittlement but at sacrifice in payload potential because of reduced strength.

Low-temperature embrittlement of cold-rolled Type 301 was overcome by incorporating sheet of nickel foil between two sheets of stainless steel to be resistance welded. The nickel alloys into the weld nugget and produces completely stable austenitic nuggets which are tough and ductile at −423 F. Both the strength and fatigue resistance of missile weld joints are markedly increased by the nickel foil, permitting reliable use of Type 301 in cryogenic tankage down to −423 F. Nickel also greatly increases the ability of radiography to detect weld defects in nickel enriched spot welds and has resulted in improvement in welding procedures and quality control.

Austenitic stainless steels long have been employed for the construction of storage vessels, trailer tanks, transfer lines, and other equipment involved in the manufacture, transportation, and storage of liquified gases such as nitrogen, oxygen, methane, hydrogen, and others. Virtually all the stainless steels of the 300 series ranging from Types 302 to 347 have been used for these applications and have generally been used in the fully annealed condition, approximately 35,000 psi yield and 90,000 psi ultimate strength.

The development of missiles propelled by liquid oxygen and liquid hydrogen has necessitated the use of considerably higher strength materials for the fabrication of large, lightweight propellant tanks. Missile constructional materials must have yield strength-to-weight ratios at least 4 to 5 times as high as those of the annealed stainless steels and tensile strength-to-weight ratios at least two to two and a half times as high in order to meet reasonable performance requirements. Heat treatable and cold worked to strength aluminum alloys and severely cold-rolled stainless steels have proved to be the most successfully and widely used materials for the design and manufacture of cryogenic propellant tankage for missiles.

The highest strength-to-weight ratio material currently being employed for cryogenic propellant tankage is the 60 per cent cold rolled Type 301 stainless steel sheet used in the Atlas and Centaur missiles manufactured by General Dynamics/Astronautics. Both of these missiles incorporate similar design features in that the tanks are pressure stabilized monocoque structures with no internal stiffening or supporting members. The tanks are fabricated from cold-rolled sheet stock approximately one yard in width and from 0.010 to 0.030 in. in thickness, and are built up from overlapping ring segments capped by bulkheads made from stretch-formed gore sections. All joining is by means of fusion butt welding, overlap roll seam welding, and resistance spot welding. Doublers are resistance spot welded over the fusion butt weld joints to maintain essentially 100 per cent tensile efficiency in the vertical splice joints. Details of the design and fabrication of the Atlas have been previously described and will not be elaborated herein (1).[3] The general appearance of the Atlas tankage is shown in Fig. 1.

Cold-rolled Type 301 stainless steel of various tempers was chosen for the tank sidewalls and bulkheads as well as for propellant ducting since this alloy possessed satisfactory combinations of strength, resistance to brittle fracture at liquid oxygen temperature, corrosion resistance, weldability, and formability and was commercially available at reasonable cost. Other candidate materials were also evaluated for missile tankage and a number of tests were selected or devised for determining the characteristics and the relative merits of the various materials. These tests included standard tension tests of base metal, fusion butt weld, and overlapping roll seam weld joints, shear and cross-tension tests of individual resistance spot welds (see Fig. 2); and static-tension and cyclic-fatigue tests of large specimens incorporating actual missile weld joints (see Fig. 3). The tests were performed at various temperatures down to the lowest anticipated service temperature. In addition, various types of notched-tension tests were also performed to evaluate the notch sensitivity of the alloys. Finally, stress corrosion tests of both base metal and weld joint specimens were conducted in salt spray chambers, at seacoast exposure sites, and in contact with various chemical cleaning and processing formulations. The results of many such tests have been previously reported in the literature (2–5).

Base Metal and Weld Properties of Cold-Rolled Stainless Steels

A summary of the comparative base metal properties of cold-rolled Types 301,

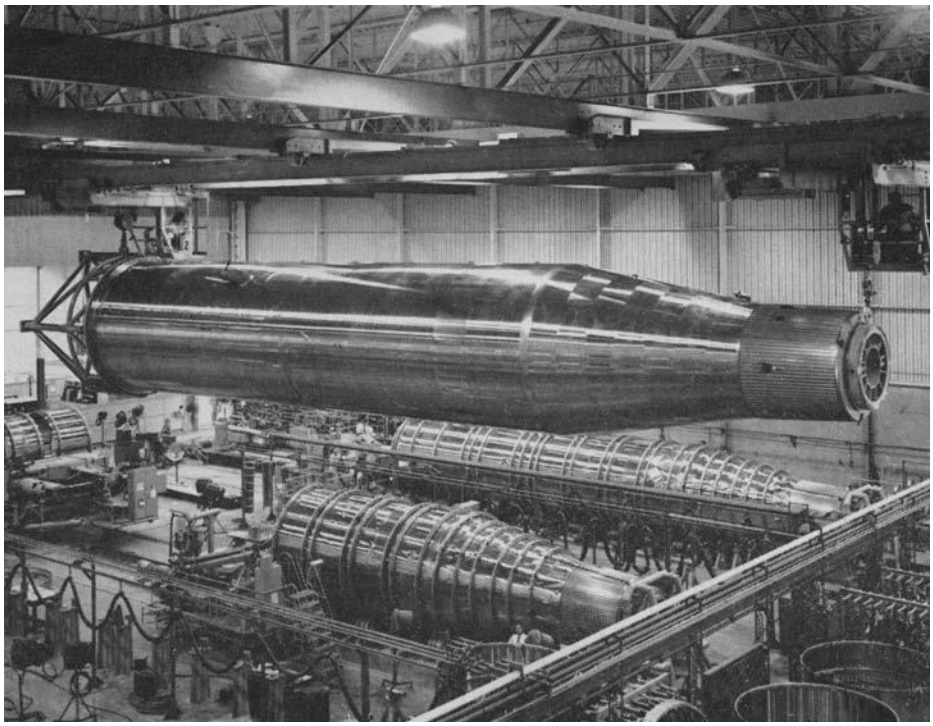
[1] Manager, Materials and Processes, General Dynamics/Astronautics, San Diego, Calif.

[2] Formerly research engineer, General Dynamics/Astronautics, San Diego, Calif., now with Narmco Research and Development Div., Whittaker Corp., San Diego, Calif.

[3] The boldface numbers in parentheses refer to the list of references appended to this paper.

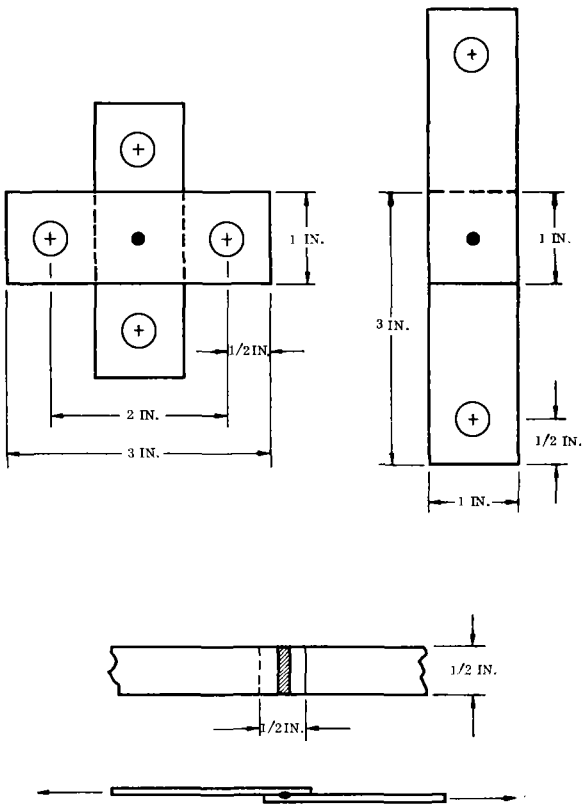
Copyright© 1965 by ASTM International

www.astm.org



NOTE—Corrugated front section is adapter structure. Tank has internal bulkhead separating fue and oxidizer tanks and is pressurized with dry nitrogen gas to maintain structural rigidity.

FIG. 1—Completed Atlas Tank Being Carried by Overhead Crane.



(*upper left*) Cross-tension test specimen for resistance spot welds.
(*upper right*) Shear test specimen for resistance spot welds.
(*bottom*) Overlap resistance roll seam weld test specimen.

FIG. 2—Evaluation of Test Specimens.

304 L, and 310 stainless steel sheet is presented in Table 1. The data includes smooth- and notched-tensile properties, elongation, and notched/unnotched strength ratios, both longitudinal and transverse, at room temperature, −100, −320, and −423 F. It is apparent that the 60 per cent cold-rolled Type 301 is stronger at all testing temperatures than either the 50 per cent cold-rolled Type 304 L or the 75 per cent cold-rolled Type 310 stainless steel sheet. The second significant factor is that the notched-tensile strength of Type 301 steel increases at a less rapid rate than that of the other alloys, with a consequent decrease in the notched/unnotched strength ratio with decreasing temperatures. The notched/unnotched strength ratios of both Types 304 L and 310 steels remain substantially constant over the temperature range of 75 to −423 F, using a side notched specimen having a stress-concentration factor of 6.3, while that of Type 301 steel decreases continuously with decreasing temperature, falling to a value of 0.90 in the longitudinal direction at a temperature of −423 F.

Table 2 covers the shear and cross-tension strength properties of individual resistance spot welds in the same three cold-rolled stainless steels, except that the thicknesses tested are now within the range of 0.010 to 0.012 in. Note that while both the shear and cross-tension strengths of spot welds in Types 304 L and 310 steels increase continuously with decreasing temperature from room to −423 F, the strengths of spot welds in Type 301 are lower at −423 F than at room temperature, with the cross-tension strength being considerably reduced. The tension/shear ratio is maintained relatively constant at approximately 0.5 at all temperatures in Types 304 L and 310 steels while it drops to a low of 0.15 for Type 301 at sub-zero temperatures.

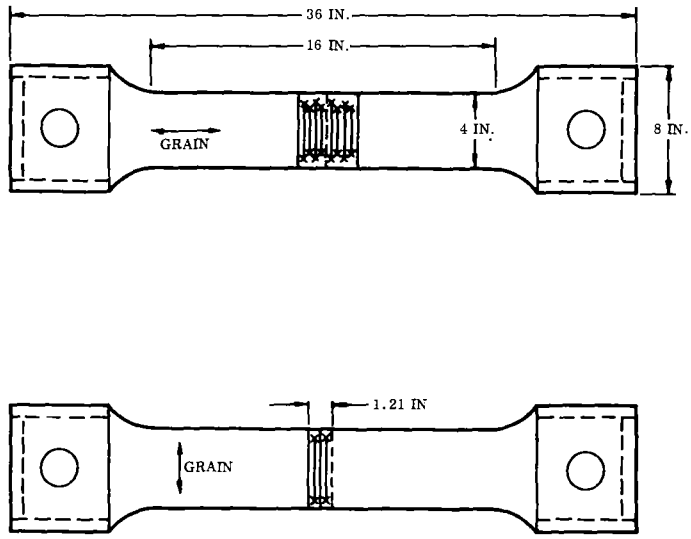
Table 3 presents yet a third comparison of the properties of Types 301, 304 L, and 310 cold-rolled stainless steels, this time in the form of static tensile strengths at 75, −320, and −423 F of complex weld joints simulating the vertical splice and circumferential welds used in both the Atlas and Centaur propellant tanks. The details of the weld joint designs are listed at the bottom of Table 3. Note that at room temperature, all weld joints have tensile efficiencies, based upon original base metal strengths, in the range of approximately 93 to 100 per cent. At both −320 and −423 F the tensile effi-

ciencies of weld joints in Types 304 L and 310 steels lie substantially within this same range, while the tensile efficiency of weld joints in Type 301 steel falls 73 to 80 per cent at −320 F and 67 to 72 per cent at −423 F. Thus, while the weld joints in Type 301 steel are approximately 10 per cent higher in strength than those of, for example, Type 310 steel at room temperature, weld joints in Type 310 are approximatly 25 per cent stronger than similar welds in Type 301 at the temperature of liquid hydrogen. At −320 F, both alloys show roughly equivalent strengths in both the longitudinal and transverse weld joints.

The above behavior is reflected also in the high stress-low cycle fatigue properties of weld joints in these alloys. Figure 4 includes a series of S-N curves covering the results of fatigue tests conducted at +75, −320, and −423 F on longitudinal weld joints (see Table 3 for details of the design of this joint) in Types 301 and 310 cold-rolled stainless steels. At +75 F, the fatigue life of Type 301 weld joints is superior (800 cycles of life in the stress range of 0 to 150 ksi as compared to 300 cycles for Type 310 over the same stress range), while at −320 F both alloys show approximately the same fatigue life. Reference to Table 3 shows that the longitudinal weld joints in both materials have approximately equal tensile strengths at −320 F; these tensile strengths are considerably higher than those at 75 F, thus accounting for the higher fatigue life as compared to the room-temperature behavior.

At −423 F, the fatigue life of weld joints in Type 301 steel is sharply reduced to levels considerably lower than the room-temperature values—for example, a life of 300 cycles results from stressing in the range of 0 to 150 ksi. The fatigue life of weld joints in Type 310 steel, on the other hand, continues to increase with decreasing temperature to −423 F, which is consistent with the increase in static tensile strength of the weld joints at this temperature.

The picture that emerges from these data is that cold rolled Type 301 stainless steel, while reliable in over-all performance at sub-zero temperatures down to −320 F, becomes excessively embrittled at −423 F as manifested by increased notch sensitivity, reduction in shear and cross-tension strengths of resistance spot welds, and reduced static tensile strength and impaired fatigue life of complex missile weld joints. There is a sound metallurgical explanation for this behavior. Type 301 steel contains 17 per cent chromium and 7 per cent nickel and is thus of a metastable composition. While completely austenitic in the quenched condition, this alloy undergoes transformation to martensite when cold rolled at ambient temperature; 60 per cent cold rolling produces a composite microstructure that is approximately 60 per cent martensitic and 40 per cent austenitic (6).



(*top*) Longitudinal.
(*bottom*) Transverse.
FIG. 3—Missile Weld Joints.

TABLE 1—MECHANICAL PROPERTIES OF COLD-ROLLED STAINLESS STEEL SHEET ALLOYS (LONGITUDINAL TESTS).[a]

Alloy	Test Temperature, deg F	0.2% Yield Strength, ksi	Tensile Strength, ksi	Elongation, %	Notched Tensile, ksi[b]	Notched/Unnotched Strength Ratio
60% cold-rolled Type 301, 0.025 in.	+75	200	224	10.8	240	1.07
	−100	237	253	14.7	248	0.98
	−320	254	323	19.5	298	0.92
	−423	308	335	3.5	302	0.90
50% cold-rolled Type 304 L, 0.012 in.	+75	158	180	2.5	199	1.11
	−100	179	200	4.5	219	1.10
	−320	195	242	26.5	267	1.10
	−423	234	275	1.5	310	1.13
75% cold-rolled Type 310, 0.020 in.	+75	156	180	2.5	198	1.10
	−100	185	203	5.0	224	1.10
	−320	228	253	8.7	279	1.10
	−423	261	291	8.4	328	1.13

[a] All data represent averages of five replicate tests.
[b] $K_t = 6.3$.

TABLE 2—MECHANICAL PROPERTIES OF RESISTANCE SPOT WELDS IN STAINLESS STEEL SHEET ALLOYS.[a]

Alloy	Test Temperature, deg F	Shear Strength, lb/spot	Cross-Tension Strength, lb/spot	Tension/Shear Ratio
60% cold-rolled Type 301 0.011 in. thick	+75	390	213	0.55
	−320	470	70	0.15
	−423	379	65	0.17
50% cold-rolled Type 304 L 0.012 in. thick	+75	409	256	0.63
	−320	634	265	0.42
	−423	666	306	0.46
75% cold-rolled Type 310 0.010 in. thick	+75	293	168	0.57
	−320	422	202	0.48
	−423	464	232	0.50

[a] All data represent averages of 20 to 100 replicate tests.

The resulting low carbon martensite is reasonably tough at temperatures down to −320 F, but exhibits brittle behavior at liquid hydrogen temperature. Furthermore, the degree of embrittlement manifested by this steel may be quite erratic at −423 F, with some heats being satisfactorily tough while others may be severely embrittled. This variation in fracture behavior has been found to be attributable to relatively minor variations in chemistry, principally carbon, nickel, and manganese, within the allowable range for Type 301 steel, to variations in the amount of cold rolling, and to the temperature of the steel when cold working is accomplished. It is also found that straining the 60 per cent cold-rolled alloy to fracture at −423 F results in essentially 100 per cent transformation to martensite, and that martensite formed at these extreme sub-zero temperatures is more brittle than martensite developed at room or moderately elevated temperatures in the range of +200 to +400 F (7).

TABLE 3—COMPARISON OF STRENGTHS OF MISSILE WELD JOINTS IN EXTRA HARD COLD-ROLLED STAINLESS STEELS.

Test Temperature, deg F	Weld Joint Type[a]	Average of 9 Type 301 Production Lots		Type 304 L		Type 310	
		Strength, ftu, ksi	Efficiency, %[b]	Strength, ftu, ksi	Efficiency, %	Strength, ftu, ksi	Efficiency, %
+75	Longitudinal	211	93.5	182	100	187	100
+75	Transverse	126	100	179	92.5	194	97
−320	Longitudinal	262	80.5	235	97	259	100
−320	Transverse	240	73.5	252	99	269	99
−423	Longitudinal	234	72.5	251	91.3	286	89.4
−423	Transverse	213	66.9	269	91.1	288	91.8

[a] Longitudinal joint—heliarc fusion butt weld roll planished, reinforced with spot-welded doubler with four rows of spots on each side of butt weld; transverse joint—overlapping roll seal weld with one row of spot welds on each side of seam weld.
[b] Efficiency relative to base metal strength at same temperature.

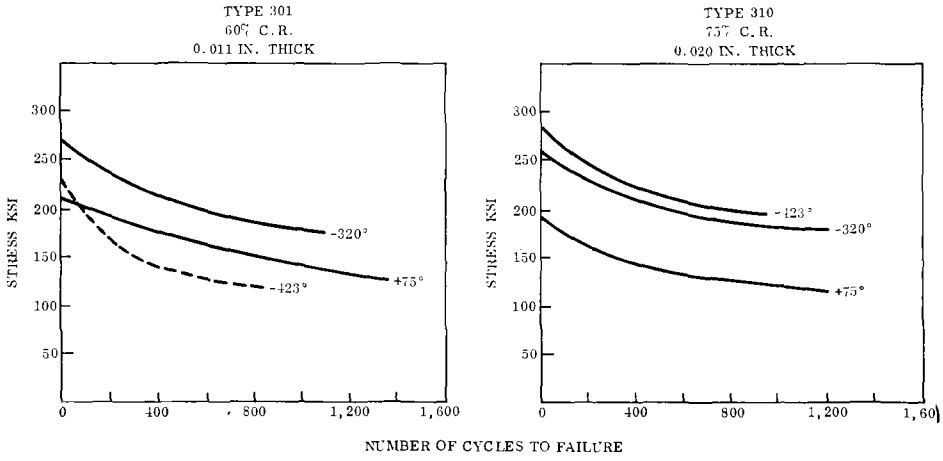


FIG. 4—Fatigue Behavior of Complex Weld Joints in Cold-Rolled Stainless Steels.

TABLE 4—EFFECT OF NICKEL FOIL ON SHEAR AND CROSS-TENSION STRENGTHS OF RESISTANCE SPOT WELDS IN TYPE 301 FULL HARD STAINLESS STEELS.[a]

Thickness	Test Temperature, deg F	Standard Welds No Nickel Reinforcement		Welds Reinforced With 0.003-in.-Nickel Foil Between Sheet	
		Shear Strength, lb/spot	Cross-Tension Strength, lb/spot	Shear Strength, lb/spot	Cross-Tension Strength, lb/spot
0.011 in.	+75	390	213	371	209
	−320	470	70	487	197
	−423	379	65	615	131
0.016 in.	+75	652	354	547	361
	−320	637	96	818	259
	−423	487	78	865	149
0.020 in.	+75	978	508	754	558
	−320	1054	169	1139	296
	−423	801	166	1168	268

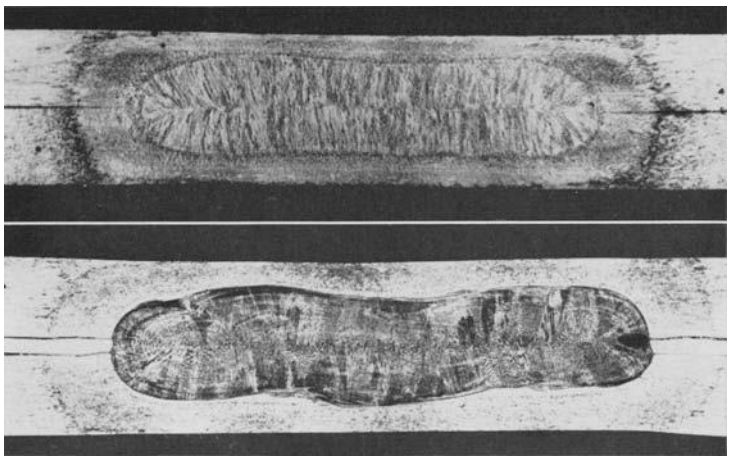
[a] All data represent averages of 10 replicate tests.

The data contained in Tables 1–3 and in Fig. 4 clearly demonstrate that the 60 per cent cold-rolled Type 301 stainless steel could be hazardous to use for liquid hydrogen applications. Early in the Centaur program the practice was established to test each heat of Type 301 steel for suitability for use at −423 F by fabricating weld joint specimens and subjecting them to cyclic fatigue tests at liquid hydrogen temperature and weeding out those lots of material which showed poor fatigue life.

While changing to Types 304 L or 310 stainless steels would improve both the uniformity and the reliability of the liquid hydrogen tankage material, the 10 per cent weight penalty involved was considered unacceptable. It was early recognized that the advantage possessed by these steels resulted from their greater austenite stability traceable to increased nickel contents as compared to Type 301 steel, Type 304 containing 10 per cent and Type 310 20 per cent nickel as compared to 7 per cent nickel in Type 301. Tests have shown that 75 per cent cold-rolled Type 310, even when strained to fracture at a temperature of −423 F is completely austenitic without the slightest trace of martensite formation (6). While increased nickel results in enhanced resistance to brittle fracture through retention of the austenitic crystal structure, it also reduces the work hardening or strengthening ability for the same reason since much of the strengthening of cold-worked metastable austenitic stainless steels is because of the transformation to the harder and stronger martensite.

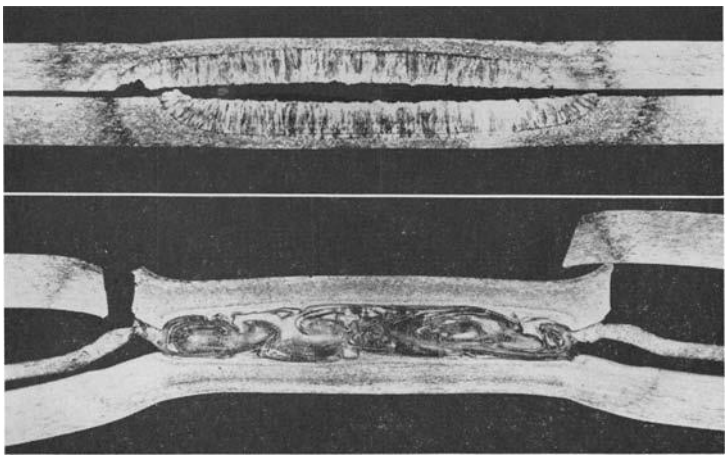
INCREASING STRENGTH OF RESISTANCE WELDS IN COLD-ROLLED TYPE 301

An attempt was made accordingly to increase the strength of resistance welds in Type 301 stainless steels at −423 F since it was observed that fractures both in static shear and cross tension and in fatigue tests on complex weld joints always initiated in or near the heat affected weld zones. Initially, an attempt was made to reduce the stress concentration effect of the spot weld nuggets by increasing the size of the weld nuggets, but this resulted in a decrease in strength owing to the increased size of the annealed areas. A second attempt conceived by one of the metallurgists of the materials research group involved the



(*top*) Cross section of resistance spot weld showing weld nugget, heat affected zone and base metal. (*bottom*) Cross section of 0.003-in. nickel foil reinforced resistance spot weld; nickel has melted and alloyed into weld nugget.

FIG. 5—Microstructures of Weld Nuggets in Nickel-Free and Nickel-Reinforced Resistance Spot Welds in 0.016-in. Type 301 Cold-Rolled Stainless Steel (×50). Reduced One Half for Reproduction.



(*top*) Nickel-free weld. Brittle fracture through weld nugget. Average cross-tension strength. 65 lb per spot. (*bottom*) Nickel reinforced weld. Plug pulled out of top sheet with ductile shear fracture. Average cross-tension strength, 131 lb per spot.

FIG. 6—Microstructures of Weld Nuggets in Nickel-Free and Nickel-Reinforced Resistance Spot Weld in 0.011-in. Type 301 Cold-Rolled Stainless Steel Fractured in Cross Tension at −423 F (×50). Reduced One Half for Reproduction.

TABLE 5—EFFECT OF NICKEL FOIL ON TENSILE STRENGTHS OF OVERLAP ROLL SEAM WELDS IN TYPE 301 FULL HARD STAINLESS STEEL.[a]

Thickness	Test Temperature, deg F	Base Metal Tensile Strength, psi	Tensile Strength of Joint, psi, Based on Cross-Sectional Area of Base Metal	
			Standard Weld No Nickel Reinforcement	Weld Reinforced With 0.003-in.-Nickel Foil Between Sheet
0.011 in.	+75	206 000	166 000	173 000
	−320	295 000	265 000	289 000
	−423	328 000	190 000	298 000
0.016 in.	+75	...	175 000	169 000
	−320	...	166 000	231 000
	−423	...	139 000	236 000

[a] All data represent averages of 10 replicate tests.

insertion of a thin foil of silver braze between two sheets of Type 301 stainless steel to be resistance spot welded. The heat of welding caused melting of the braze alloy and the development of a ring of braze joint around the weld nugget without increasing the extent of annealing and softening of the cold-worked stainless steel. The silver braze which was melted in the weld nugget alloyed with the steel and did not result in embrittlement even when tested at −423 F. This technique did produce positive results in increasing the static tensile and fatigue strength both of individual spot welds and complex weld joints, but was not considered satisfactory because of galvanic corrosion difficulties introduced by dissimilar metals in contact within faying surfaces capable of moisture entrapment and because of concern about introducing foreign alloying elements such as silver, copper, and others, into stainless steel weld joints.

The above tests were integrated with previous experience with superior low-temperature toughness of the higher nickel stainless steels (Types 304 L and 310), and it was decided to employ nickel foil inserted between the sheets of cold-rolled Type 301 stainless steel in order to increase the nickel content and hence the austenite stability of the weld nuggets. The first attempt at this was immediately successful and led to an extensive investigation of this procedure. At about the same time, experiments were also being conducted on thin skinned electroformed nickel shapes which were welded to cold-rolled Type 301 stainless steel sheet, and it was found that fusion welds and resistance spot welds between these two materials showed superior strength and resistance to brittle fracture at −423 F as compared to similar welds between two pieces of Type 301 stainless steel.

The initial evaluation tests with nickel foil reinforced welds consisted of extensive shear and cross-tension testing performed at 75, −320, and −423 F on single resistance spot welds. It was found that only minor variations in weld schedules were required to make acceptable welds in nickel-reinforced joints as compared to welds in steel-to-steel joints. The comparison in spot weld strength properties between nickel-free and nickel-reinforced joints in 0.011, 0.016, and 0.020-in.-thick cold-rolled Type 301 stainless steel is shown in Table 4.

Note that in regular 301-301 joints, the spot weld shear strength at −423 F is always somewhat but not significantly lower at −423 F than at 75 F, but the cross-tension strength drops at −423 F to approximately one fourth the room-temperature value, while at −320 F it is only slightly better than at −423 F. With 0.003-in.-thick nickel reinforcement, the shear strength increases consistently with decreasing test tempera-

TABLE 6—EFFECT OF NICKEL FOIL ON MECHANICAL PROPERTIES OF COMPLEX WELD JOINTS IN THE TYPE 301 FULL HARD STAINLESS STEEL.[a]

Thickness	Test Temperature, deg F	Nickel Foil in Joint	Tensile Strength of Complex Weld Joint, psi	Stress Range, ksi	Fatigue Properties	
					Number of Cycles to First Leak	Number of Cycles to Fracture
0.011 in.....	+75	No	207 000	0 to 145	462	945
	+75	No	207 000	0 to 180	196	319
	+75	Yes	210 000	0 to 140	459	1531
	+75	Yes	210 000	0 to 186	362	496
	−320	No	269 000	0 to 140	>2000	+2000
	−320	No	269 000	0 to 214	350	389
	−320	Yes	288 000	0 to 140	>2000	>2000
	−320	Yes	288 000	0 to 214	>2000	>2000
	−423	No	236 000	0 to 140	275	736
	−423	No	236 000	0 to 170	100	200
	−423	Yes	307 000	0 to 140	>4000	>4000
	−423	Yes	307 000	0 to 170	>900	1225

[a] All data represent averages of two or three replicate tests.

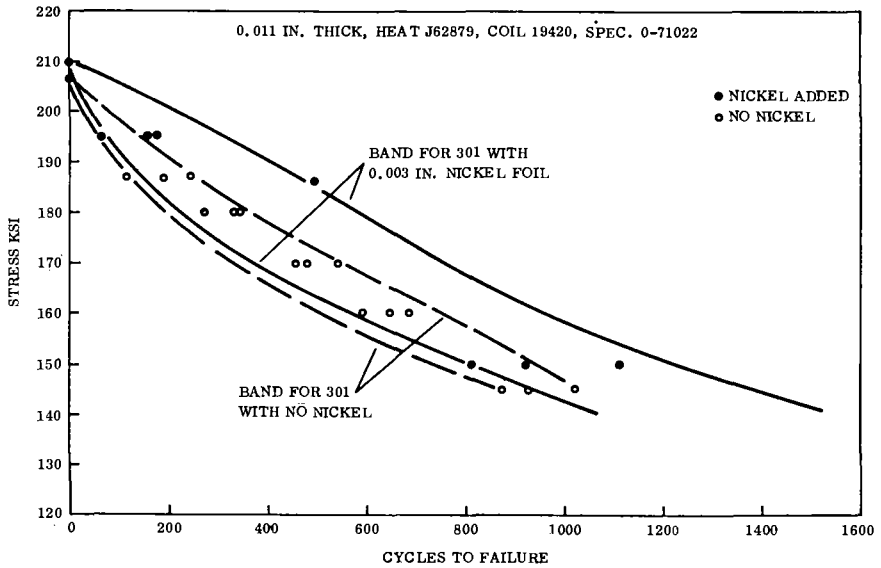


FIG. 7—Fatigue Strength of Longitudinal Weld Joint at Room Temperature.

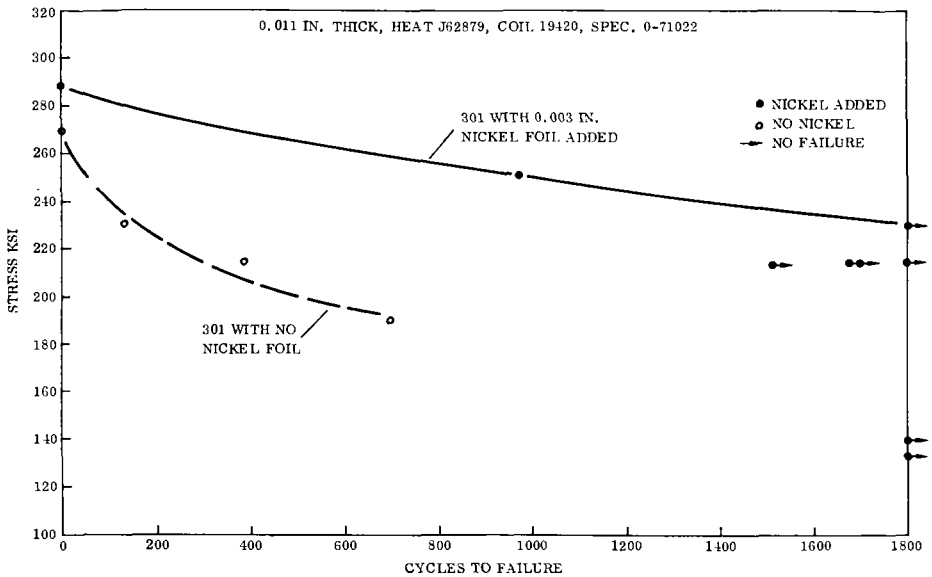


FIG. 8—Fatigue Strength of Transverse Weld Joint at −320 F.

ture while the −423 F cross-tension strength decreases to only one half the room-temperature value, or approximately double the cross-tension strength of the nickel-free welds.

Tests were performed with various thicknesses of nickel foil sandwiched between the stainless steel sheet, and it was found that, for thin gauges of steel in the range of approximately 0.010 to 0.020 in. thick, the use of 0.003-in.-thick nickel foil gave reasonably optimal results.

The microstructures of weld nuggets in nickel-free and nickel-reinforced resistance spot welds are shown in Fig. 5. The upper photograph shows a cross section of a typical weld nugget in a 301-301 resistance spot weld at a magnification of ×50. Note the normal nugget which had been molten during welding and which had resolidified in a columnar fashion, with a heat affected zone surrounding the nugget area. The lower photomicrograph shows a nickel-reinforced weld nugget in the same material. Note the rather heterogeneous microstructure which resulted from the fact that melting took place so rapidly and for so short a time that completely homogeneous alloying of the nickel into the stainless steel could not occur. In fact, microchemical analysis of such nuggets show nickel variations from spot to spot, with nickel ranging from 15 per cent to approximately 40 per cent in various areas. In any case, the nickel content of the weld nugget is increased to the level where complete austenite stability is achieved. Micromagnetic and hardness tests show the weld nuggets to remain completely untransformed even when they are tested to fracture at liquid hydrogen temperature. The nickel does not melt and achieve a braze joint between itself and the steel immediately outside the area of the weld nugget.

The explanation for the higher low-temperature strengths of nickel-reinforced spot weld nuggets lies in the change in the mechanism of fracture when they are tested in either shear or cross tension. Figure 6 shows typical cross sections of both types of welds which had been tested in cross tension at −423 F. These photomicrographs, also at a magnification of ×50, show the brittle fracture across the middle of the spot weld nugget of a nickel-free weld (top photo), and the ductile shear failure and nugget pull-out characteristic of a nickel-reinforced weld (bottom photo). Note particularly the extensive deforma-

tion and sheet thinning which preceded the fracture of the nickel reinforced nugget and also the heterogeneous structure of this weld nugget.

Nickel reinforcement results in similar behavior of overlap roll seam weld joints such as are employed in the circumferential weld joints in the Atlas and Centaur tanks, see Table 5. This table contains data on the tensile strengths of base metal, nickel-free overlap seam welds, and nickel-reinforced overlap seam welds in 0.011 and 0.016-in.-thick Type 301 steel tested at 75, −320, and −423 F. While the base metal tensile strength increases from approximately 200,000 psi at 75 F to over 325,000 psi at −423 F, the nickel-free overlap seam weld joint has a tensile strength at −423 F of only 140,000 to 190,000 psi and is lower at this temperature than its strength at −320 F. The nickel-reinforced overlap seam weld, on the other hand, increases in strength with decreasing temperature and, in the case of the 0.011-in.-thick material, approaches a strength of 300,000 psi at −423 F. The room-temperature strength of overlap seam or fusion butt weld joints is, of course, considerably lower than that of the base metal since the weld zone is annealed and softened from the originally severely cold-worked condition.

Both static tension and cyclic fatigue tests in the range of high stress-low cycle fatigue were also performed on the complex missile weld joints shown in Fig. 3. Typical test data are shown in Table 6 and Figs. 7–10. As can be seen in Table 6, neither the room-temperature static tensile strength nor the fatigue resistance of the longitudinal weld joint are significantly affected by placing 0.003-in.-thick nickel foil under the 4-in.-wide doubler sheet which is spot welded across the fusion butt joint. This weld joint, see Fig. 3, contains four staggered rows of resistance spot welds on each side of the fusion butt weld and develops essentially 95 to 100 per cent weld efficiency at room temperature. When tested at −320 F, however, and especially at −423 F, both the static tensile strength and fatigue resistance of the nickel-reinforced joints are markedly higher than those of the nickel-free joints. As a matter of fact, nickel-reinforced weld joints in the 0.011-in.-thick material listed in Table 6 had a tensile strength at −423 F approximately 70,000 psi higher than the nickel-free joint of the same basic design, and had a fatigue life of 1225 cycles when stressed from 0 to 170 ksi as compared to 200 cycles for the nickel-free joint.

Curves of the high stress-low cycle fatigue behavior of the longitudinal missile weld joint when tested at 75, −320, and −423 F are shown in Figs. 7–9. At room temperature the fatigue resistance of nickel-free and nickel-reinforced joints overlap as shown by the bands plotted in Fig. 7, although there is a tendency for the nickel-reinforced joints to show a somewhat higher fatigue life. At −320 F, however, there is a marked superiority of the nickel-reinforced weld joint, see Fig. 8. Specimens without nickel foil showed a fatigue life of approximately 400 cycles when stressed to the range of 0 to 215 ksi, while nickel-reinforced specimens did not fail when cycled up to 1800 times over the same stress range.

Comparative fatigue data on weld joints tested at −423 F are shown in Fig. 9 which shows cycles to failure for both nickel-free and nickel-reinforced weld joints. The fatigue bands shown in Fig. 9 indicate an approximately 10-fold increase in fatigue life at many stress levels for the nickel-reinforced joint. Figure 10 shows plots of the same tests covered by Fig. 9, except that the number of cycles to the development of the first crack rather than the number of cycles to complete fracture of the specimens is plotted against the stress level. The first crack is detected by

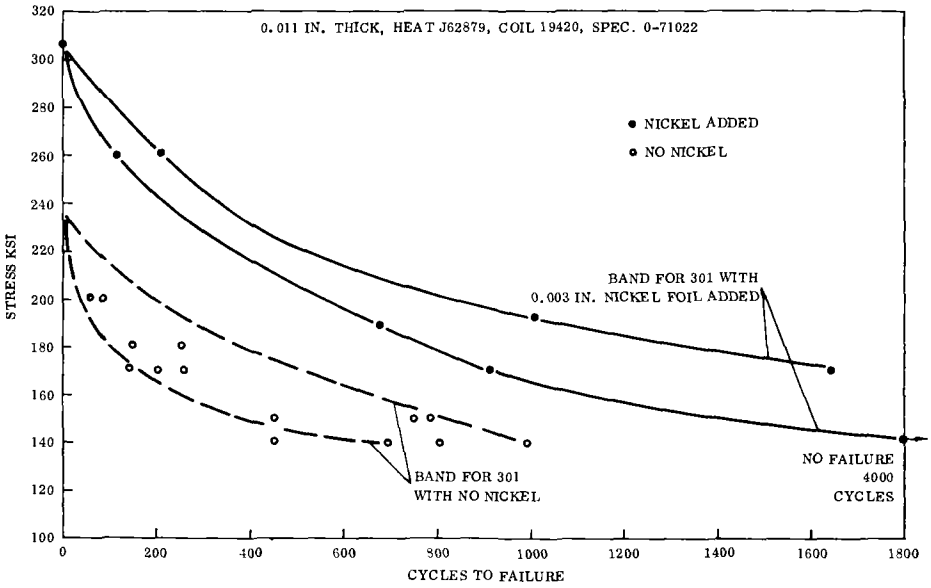


FIG. 9—Fatigue Strength of Longitudinal Weld Joint at −423 F. (Cycles to failure).

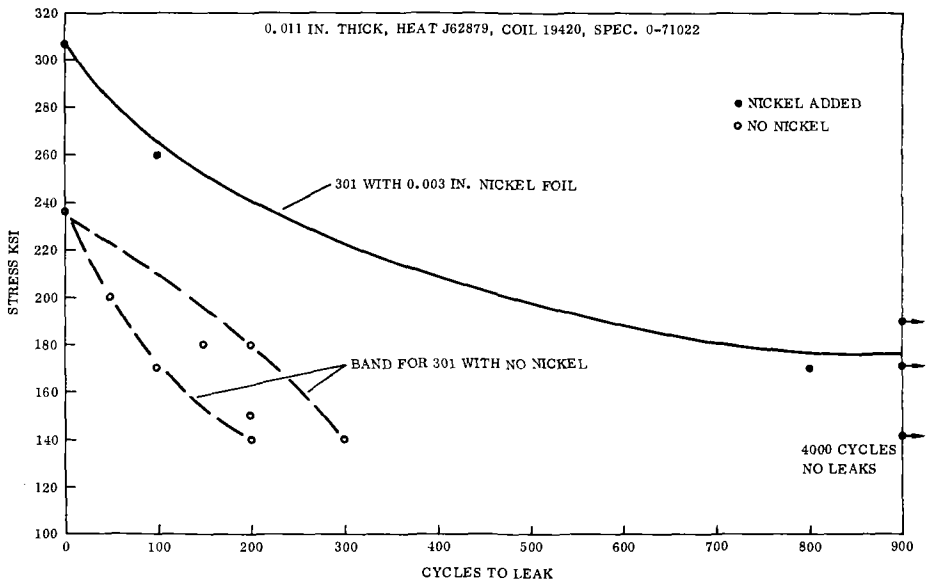
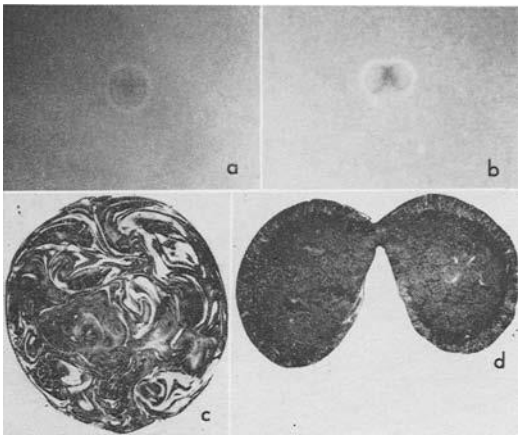


FIG. 10—Additional Plots Showing Fatigue Strength of Longitudinal Weld Joint at −423 F (Cycles to first leak).

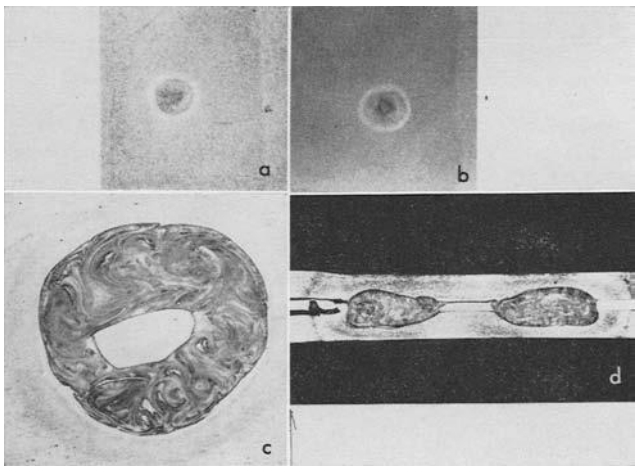
means of dye penetrant checks which are conducted every 25 cycles of test after removal of the specimens from the liquid hydrogen test chamber. These curves show a 5 to 10-fold increase in life to initial crack formation.

The above data demonstrate that nickel reinforcement permits the safe use of severely cold-rolled Type 301 stainless steel for liquid hydrogen applications in that the material now behaves similar to the completely austenitic Type 310 steel. The tough weld nuggets act as springs, permitting local deformation without crack or fracture initiation, resulting in redistribution of stresses and lowering of peak stress concentration levels around individual spot welds. There is a very negligible weight penalty involved in the insertion of nickel foil under doublers, between overlap welds, and under bracketry resistance spot welded to steel propellant tankage. This weight penalty is significantly less than the 10 per cent increase in weight which would result if a changeover were made to 75 per cent cold-rolled Type 310 steel; 75 per cent cold rolling representing the maximum practicable degree of cold working which is currently commercially feasible.



(*a*) Well formed circular weld nugget (×5).
(*b*) Incompletely formed weld nugget (×5).
(*c*) Oxalic acid etched plan view of (*a*) showing "marble cake" structure (×30).
(*d*) Oxalic acid etched plan view of (*b*) (×30).

FIG. 11—X-ray Images of Nickel-Reinforced Resistance Spot Welds. Reduced One Half for Reproduction.



(*a*) Toroidal "doughnut" weld (×5).
(*b*) Another toroidal "doughnut" weld (×5).
(*c*) Plan view of (*a*) (×30).
(*d*) Cross section of (*b*), etched in oxalic acid, showing unfused midsection of nugget and typical "doughnut" configuration (×30).

FIG. 12—Additional Views of X-ray Images of Nickel-Reinforced Resistance Spot Welds. Reduced One Half for Reproduction.

IMPROVED RADIOGRAPHY THROUGH USE OF NICKEL FOIL

An unexpected but nevertheless significant additional benefit results from the use of nickel foil reinforced weld joints incorporating resistance spot welds. Because of the difference in radiopacity between nickel and stainless steel, subtle weld defects are now sharply revealed in nickel reinforced welds which were hitherto completely masked in even the most sensitive X-rays taken of resistance spot welds in thin steel-to-steel joints. On the upper left of Fig. 11 is shown an X-ray image, magnified ×5, through a resistance spot weld in 0.016-in.-thick stainless steel. Below this is shown a plan view of a polished and etched surface through the spot weld which is completely circular in shape. The X-ray image also shows this circular form. Note the mottled "marble cake" structure of the weld nugget resulting from the nonhomogeneous admixture of nickel in the composite nickel-steel weld nugget. The upper right of Fig. 11 shows a weld nugget in the shape of a bent figure 8, while the lower right photomicrograph shows a polished and etched view of this same nugget at a magnification of ×30. The photomicrograph is an exact duplicate of the X-ray image and demonstrates the sensitivity of X-ray examination in showing weld irregularities in nickel-reinforced resistance spot welds.

Up to this time, X-ray examination of resistance spot welds in thin gauge steel sheet failed to disclose weld irregularities caused by malformed nuggets. The sensitivity of X-rays in revealing weld defects in nickel-reinforced spot welds is even more clearly shown in Fig. 12. The torus or so-called "doughnut" spot welds shown in the X-ray images and photomicrographs of Fig. 12 may be caused by dirty or improperly shaped electrodes or by current or voltage fluctuations during welding and can be a common occurrence if careful controls over welding are not exercised. Previously, this type of weld defect could be detected only by destructive testing—for example, sectioning welds, polishing and etching them, and observing them under hand glasses or microscopes. X-rays of steel-to-steel welds had been found previously to be incapable of revealing this defect condition which can now be detected 100 per cent of the time in nickel-reinforced joints.

Thus, the introduction of nickel-reinforced weld joints permitted reliable 100 per cent radiographic inspection of weld quality and also resulted in notable improvements in production welding

practices since corrective measures were immediately developed and applied.

Tests are now underway at General Dynamics/Astronautics to evaluate and apply the basic principles of foil reinforcement of resistance spot welds to increase the strength and toughness, especially at cryogenic temperatures, of joints in many metals. Preliminary promising results have been obtained by using vanadium foil to improve the strength of resistance spot welds in titanium and titanium base alloys, and in welding titanium to steel by using somewhat thicker vanadium sheet between the titanium and the steel. The vanadium on one side alloys with the titanium and on the other with the steel. Patent applications have been entered for the reinforcement of resistance spot welds both by the technique of a braze joint around the resistance weld nuggets and by the technique of modifying the alloy content of weld nuggets to develop desired mechanical properties.

A final advantage appears to be developing for the nickel reinforcement of spot welds in stainless steels. The nickel becomes sacrificial to the stainless steel upon exposure to corrosive environments reducing the tendency towards weld decay and also reducing the tendency for the cold-rolled stainless steel to undergo stress-corrosion cracking.

Acknowledgment:

Appreciation is expressed to General Dynamics/Astronautics for permission to present and publish this paper. Special thanks are extended to C. J. Kropp, materials research group, for his excellent work on correlation of radiographic images of defects in nickel-reinforced resistance spot welds with actual defects observed in metallographically prepared cross-sectional specimens.

REFERENCES

(1) A. Hurlich, "Metals and Fabrication Methods Used for the Atlas," *Metal Progress*, Vol. 76, No. 5, November, 1959.

(2) J. F. Watson and J. L. Christian, "Mechanical Properties of High Strength 301 Stainless Steel Sheet at 70, −320, and −423 F in the Base Metal and Welded Joint Configurations," *Low-Temperature Properties of High-Strength Aircraft and Missile Materials, ASTM STP 287*, 1960.

(3) J. F. Watson and J. L. Christian, "Low-Temperature Properties of Cold-Rolled AISI Types 301, 302, 304 ELC, and 310 Stainless Steel Sheet," *Low-Temperature Properties of High-Strength Aircraft and Missile Materials, ASTM STP 287*, 1960.

(4) A. Hurlich and J. F. Watson, "Selection of Materials for Use at Cryogenic Temperatures," *Metal Progress*, Vol. 79, No. 4, April, 1961.

(5) J. F. Watson, J. L. Christian, T. T. Tanalski, and A. Hurlich, "Correlation of Notched:Unnotched Tensile Ratios With Tensile Fatigue Properties of Complex Welded Joints in High Strength 300 Series Stainless Steels at Cryogenic Temperatures," *Evaluation of Metallic Materials in Design for Low-Temperature Service, ASTM STP 302*, 1962.

(6) J. F. Watson and J. L. Christian, "A Study of Austenite Decomposition at Cryogenic Temperatures," *Transactions*, Am. Institute of Mining, Metallurgical and Petroleum Engrs., October, 1962.

(7) E. B. Mikus, "The Influence of Rolling Temperature on the Cryogenic Properties of Type 300 Series Stainless Steels," *Report No. MRG-244*, General Dynamics/Astronautics, February, 1962.

(8) C. J. Kropp, "Interpretation of Radiographic Images of Nickel Foil Reinforced Resistance Spot Welds in Type 301 Stainless Steel," *Report No. AR-592-1-434*, General Dynamics/Astronautics, April, 1963.

EXPERIENCE WITH STAINLESS STEELS IN UTILITY POWER PLANTS

By G. E. Lien[1]

Synopsis

Utilities have pushed steam temperatures to 1050 F and above during the past 15 years with the result that more stainless steel has been used in superheaters, main steam piping, and turbine parts. Recently, this trend has been reversed, and temperatures have dropped back to 1000 F leaving stainless steel in a very competitive fight for its right to again lead the assault on higher temperatures and efficiencies. Stainless Types 347, 321, and 316 have been used extensively. Type 304 and nickel alloys IN 102 and Inconel alloy 800 are going to be factors in the future.

Utility power plants are an amazing complex of metallurgical, mechanical, and electrical technology. They are ever changing as new methods and materials are developed, tested, and used, and as the materials in service react to their environment. Stainless steel is part of this changing picture and this paper will briefly cover its role from the standpoint of the American Electric Power Co. system (AEP system).

Nuclear power plant applications for stainless alloys will be left to others with the hope that at some time the important roles played by these materials in the changing efficiency and cost comparisons of nuclear and fossil fuel plants can be evaluated.

In 1962, the utility industry in the United States represented an investment of 56 billion dollars. This provided an installed capacity of 191 million kw which generated power sales of 774 billion kw-hr. The AEP system, with 2.6 per cent of the investment and 3.5 per cent of the capacity, produced 4.5 per cent of the power. The industry capacity will double in the next ten years as it has in each of the past decades. Thermal efficiency is improving steadily in the industry, and the AEP system has been a dynamic force in this effort. Over the past 15 years, efficiency has been synonymous with stainless steel tubes and piping in high temperature steam applications.

The 25 boilers installed on the AEP system since 1949 have utilized stainless steel tubing in the boiler superheat and reheat sections. This is representative of a number of the large utility companies that have operated with steam temperatures of 1050 F and higher. Stainless turbine leads or main steam piping are used in 27 units of which 8 are in the AEP system, and 13 belong to Public Service Electric and Gas Co. of New Jersey. AEP has had 6 stainless turbine shells. With this as a vantage point let us review the stainless experience and its place in the next generation of units.

Stainless in Superheaters

Twin Branch Unit 5 went into service in July 1949. It followed Public Service's Sewaren Unit 1 by a few months as the second unit utilizing 1050 F steam at 2000 psi. Six similar units followed on the AEP system in the following three years. The superheaters in each of these units contain a total of 3600 ft of Type 347 stainless (19 chromium, 9 nickel, columbium) tubing, 2.5-in. outside diameter by 0.520-in. wall forming two 30-ft long parallel banks in each of 60 rows across the superheater. Figure 1 shows the location of the tubes in the boiler. At both ends of each of these tube banks dissimilar butt welds join the stainless to 2.25 chromium, 1 molybdenum ferritic (ASTM Specification A 213[2]) tubes. The same ferritic material is used for main steam piping to the turbine stop valves where a dissimilar weld again converts to austenitic Type 347 for the valves, turbine leads, and turbine inner shell. No stainless was used in the 1000 F reheaters of these units.

Type 347 superheater tubing installed during the period 1949 to 1951 has given good service. In common with other alloys it has suffered from failures attributed to welded support attachments. These attachments, usually a cast stainless material, must withstand temperatures over 100 deg higher than the tube metal, and rupture of the tube at the attachment weld has been a serious problem. Butt welds have been successful although dissimilar butt welds made with Type 347 and lower alloy electrodes have been susceptible to cracking, and many have been replaced or repaired. Recent welding techniques using alloy 600 (Inconel) electrodes have effectively eliminated dissimilar weld failures.

The Korean War, and later economics, dictated a change to stainless Type 321 (19 chromium, 9 nickel, titanium) for superheater and some piping applications. In 1956 after five years of serivice, low-creep strength in some tubes became apparent. This strength problem was studied in the SP-6 research program (1,2)[3] under the ASTM-ASME Joint Committee's Steam Power Panel. The program resulted in the recommendation of the "H grade" specifications which, through restricted carbon-titanium ratios and heat treatment above 2000 F for Type 321, assured specified long-time high-temperature strength. Boilers with pre "H grade" type tubes are being carefully watched for tube swelling. In many of these boilers replacement tubing has been required, while in some, the original tubing has been given the high-temperature heat treatment to increase its strength.

By 1957 several generations of boilers operating with main and reheat superheater outlet temperatures of 1050 F and pressures in the 2000 psi range were in service on the AEP system. Boilers, for 225 Mw units, contained 21,000 ft of 2-in.-outside diameter by 0.260 and 0.280-in. wall tubes in the superheater, 2500 ft of 2.5-in.-outside diameter by 0.110-in. wall in the intermediate reheater, and 1100 ft of 2.5-in.-outside diameter by 0.150 to 0.210-in. wall in the reheater outlet. Figure 2 shows a typical boiler.

Supercritical Steam Generators

In 1956, in a major technological step,

[1] Head, Piping and Metallurgy Section, Mechanical Engineering Div., American Electric Power Service Corp., New York, N. Y.

[2] Specification for Seamless Ferritic and Austenitic Alloy-Steel Boiler, Superheater, and Heat Exchanger Tubes (A 213), *1964 Book of ASTM Standards*, Part 1, a.

[3] The boldface numbers in parentheses refer to the list of references appended to this paper.

Copyright© 1965 by ASTM International

Philo Unit 6 combined the first commercial supercritical steam generator with a new high in steam pressure of 4500 psi, steam temperature of 1150 F, and with two stages of reheat at 1050 F and 1000 F (3–5). This 120-Mw prototype unit utilized increased percentages of Type 321 stainless tubes in a superheater size range of 1.31-in.-outside diameter by 0.335-in. wall. The smaller outside diameter heavy wall was a characteristic of this and following supercritical units. In 1959, steam temperatures and pressures hit their current peak of 1200 F at 5000 psi in Philadelphia Electric Company's Eddystone Unit 1 (6). In this steam generator 17 chromium-14 nickel, copper molybdenum tubing was used in the final portions of the superheater.

Expanding on the Philo experience, two 500-Mw-supercritical pressure units utilizing steam at 3500 psi, 1050 F with two stages of reheat at 1050 F were placed in service in 1960. These units at Breed and Sporn plants were the last of the present AEP system series of units utilizing main steam temperatures of 1050 F and represented the peak in use of austenitic tubing for superheater and reheater service. The boilers contained 35,000 ft of 2 in. by 0.295 to 0.415 in. Type 321 H material in the superheater and 2,000 ft of 3 in. by 0.210 to 0.255 in. Type 321 H in the reheaters.

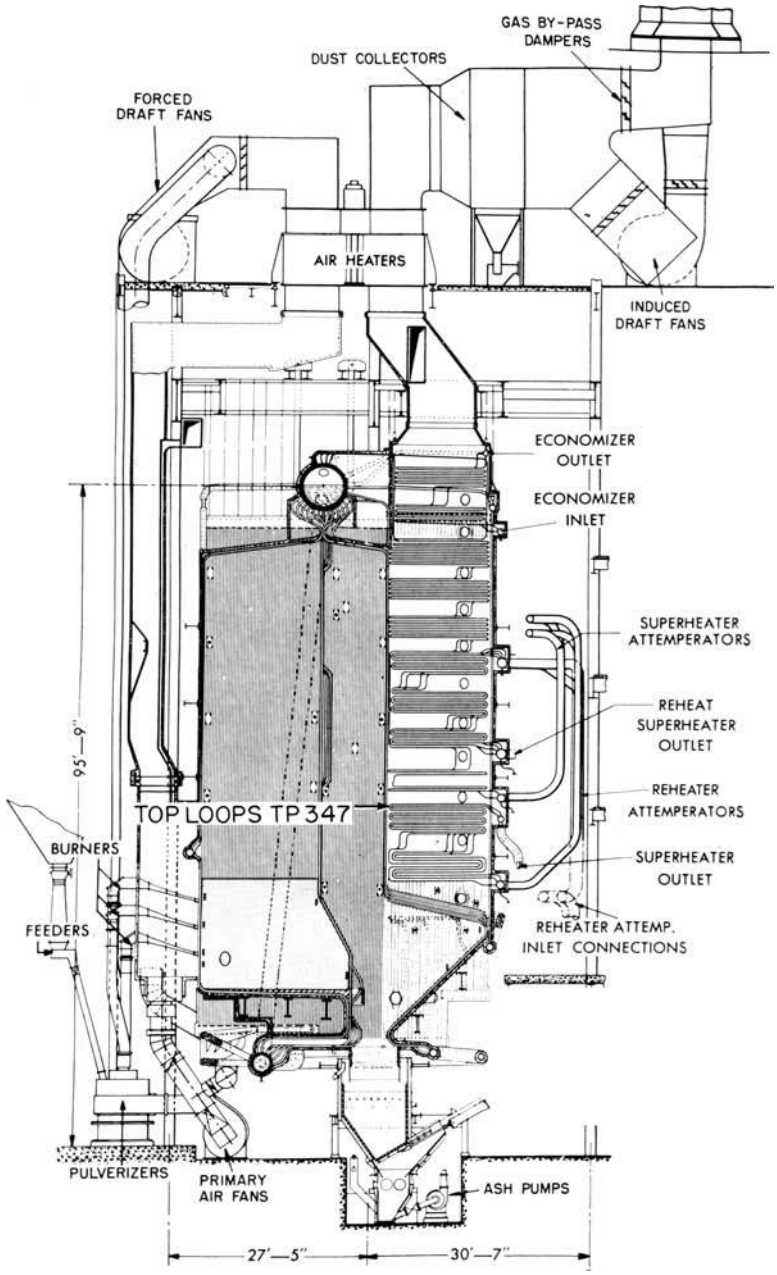


FIG. 1—150-Mw-Unit Boiler (1949), 1050 F, 2100-psi Main Steam, 1000 F, 500-psi Reheat, TP 347 Stainless in Final Loops of Superheater.

Tanners Creek Plant Unit 4 is now under construction and represents the newest AEP design. It is a 600-Mw unit of 3500 psi 1000 F main steam design with two stages of reheat at 1025 and 1050 F. Stainless is not required in the reheater and only 17,000 ft of 2-in.-outside diameter by 0.320-in. wall Type 321 H and 2000 ft of 1.75-in.-outside diameter by 0.340-in. wall Type 304 H is used in the superheater as shown in Fig. 3. The support lugs that have given difficulty have been eliminated by literally wrapping tubes around the pendant sections and forming particular tubes into supports. The highest temperature tubes have also been buried in the pendant section to avoid contact with the highest temperature gases and possible liquid phase corrosion.

CORROSION OF SUPERHEATER TUBES

Superheaters are the proving ground for high-temperature alloys. They operate at highest steam pressures in the system and at metal temperatures approximately 100 F higher than the steam they carry. These temperatures vary across the boiler as gas temperatures, up to 2300 F, assume different flow patterns. In addition, the tubes must withstand the attacks of corrosive gases and ash deposits.

In 1955 and 1956, a number of utilities experienced serious corrosion from deposits of ash from vanadium-bearing residual fuel oils. Many fuel additives were tried but the solution, in general, was to use a better and more costly grade of fuel with controlled sulfur and vanadium contents. While the AEP system did not experience this type of corrosion because only coal was burned, liquid phase coal ash corrosion started developing soon afterward in some boilers with superheaters in the 1100 to 1300 F metal temperature range (7,8). This corrosion acts quickly and severely to pit the tube and reduce its wall thickness to the point where failure occurs. Fortunately, not all superheaters are subject to this corrosion which attacks both ferritic and austenitic tubes. High alkali-high sulfur coals in combination with high metal and gas temperatures provide the environment for the attack. Corrosion is most severe on those surfaces of the tubes that are swept by flue gases such as the lead tubes in a bank. The

long term solution appears to be to remove the hot tubes from the high gas temperature area. This is being done on Tanners Creek Unit 4. Coatings for tubes in service are being tried, but the application is difficult and depends on materials that will in themselves resist this attack.

NEW ALLOYS FOR SUPERHEATERS

While we are on the subject of superheaters, let us start on our forward look and high temperature units. This is possibly because of both high relative material costs and the responsibilities they must face in guaranteeing performance of the expensive materials. This is reflected, for example, in the quantity

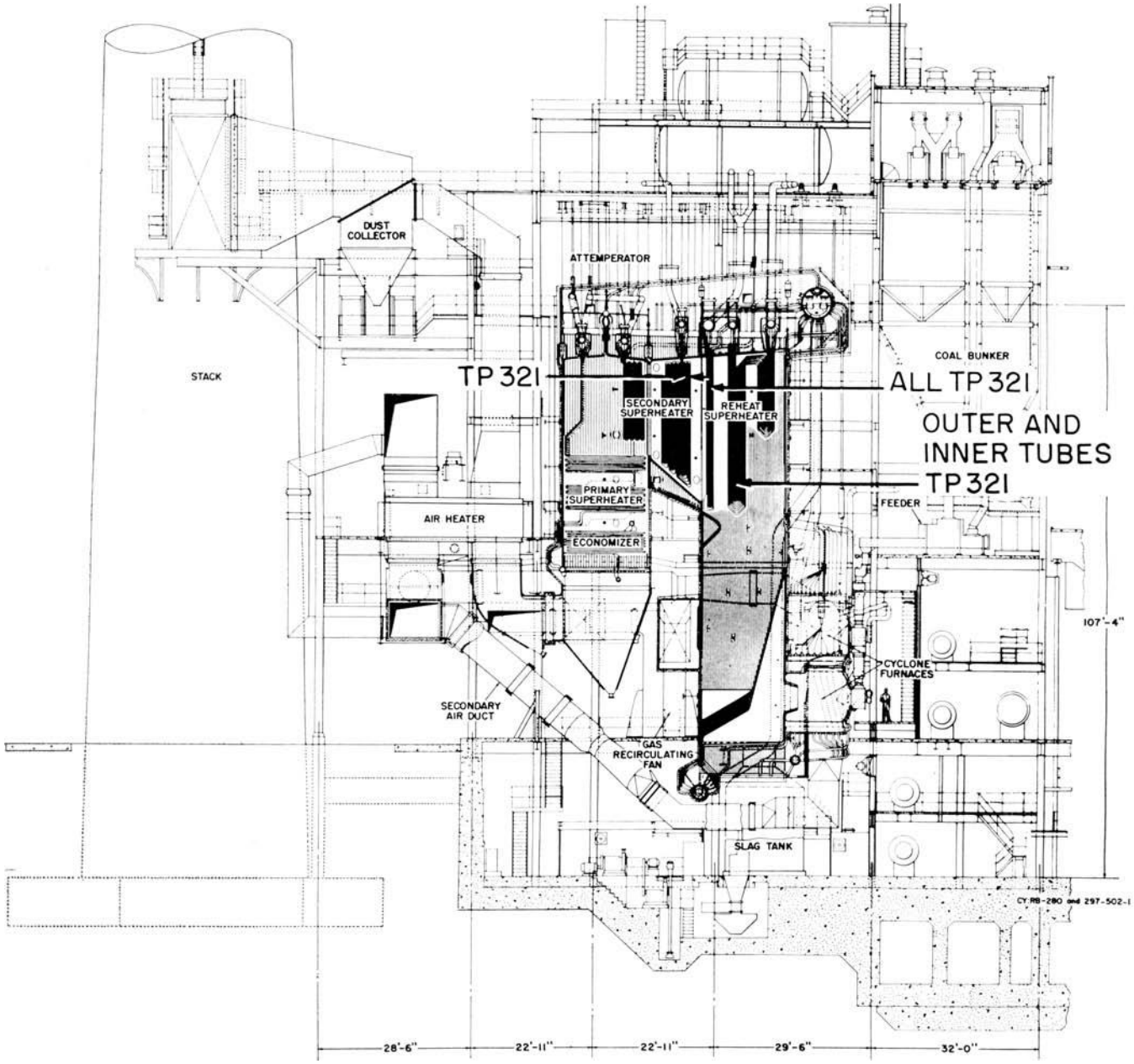


FIG. 2—225-Mw-Unit Boiler (1957), 1050 F, 2100-psi Main Steam, 1050 F, 500-psi Reheat, Type 321 Stainless in Superheater and Reheater.

complete coverage. Thin metal shields have been successful but are costly.

These shields are strapped or spot-welded to the tube in the area of the attack, and, since they are poorly cooled by the tube, their metal temperature is above the thermal stability of the ash; thus, corrosion does not take place. The study of different shield materials may eventually contribute information on into what is needed to allow the utility industry to move again into higher temperatures and therefore better thermal efficiency. Making the statement in this manner acknowledges the economic factors that have brought about the retreat from 1050, 1100, and 1200 F steam temperatures back to 1000 F. Boiler and turbine manufacturers seem to place higher premiums on stainless materials of stainless used in the aforementioned 1000 F 600-Mw unit.

This economic squeeze must be countered by advances in high-temperature metallurgy, manufacturing methods, design, and engineering evaluations of existing and new materials. As new alloys are developed, and laboratory screening tests indicate that their properties are attractive, many tests must be made to

provide information for establishing high temperature long time properties. However, before assigning working stresses, code groups prefer that a material has been proven to some extent in actual operation. Such service was provided by the Babcock & Wilcox Co. experimental role of prototype, has also provided an operating base for 15-15N tubes and recently for tubes of Type 304, IN 102, and alloy 800. Service test programs like these must be set up throughout industry to cover the broad base of operating conditions required for material evaluation. Testing that will substantiate new code rules and formulas to utilize high temperature materials more effectively with higher allowable stresses will also have major economic importance.

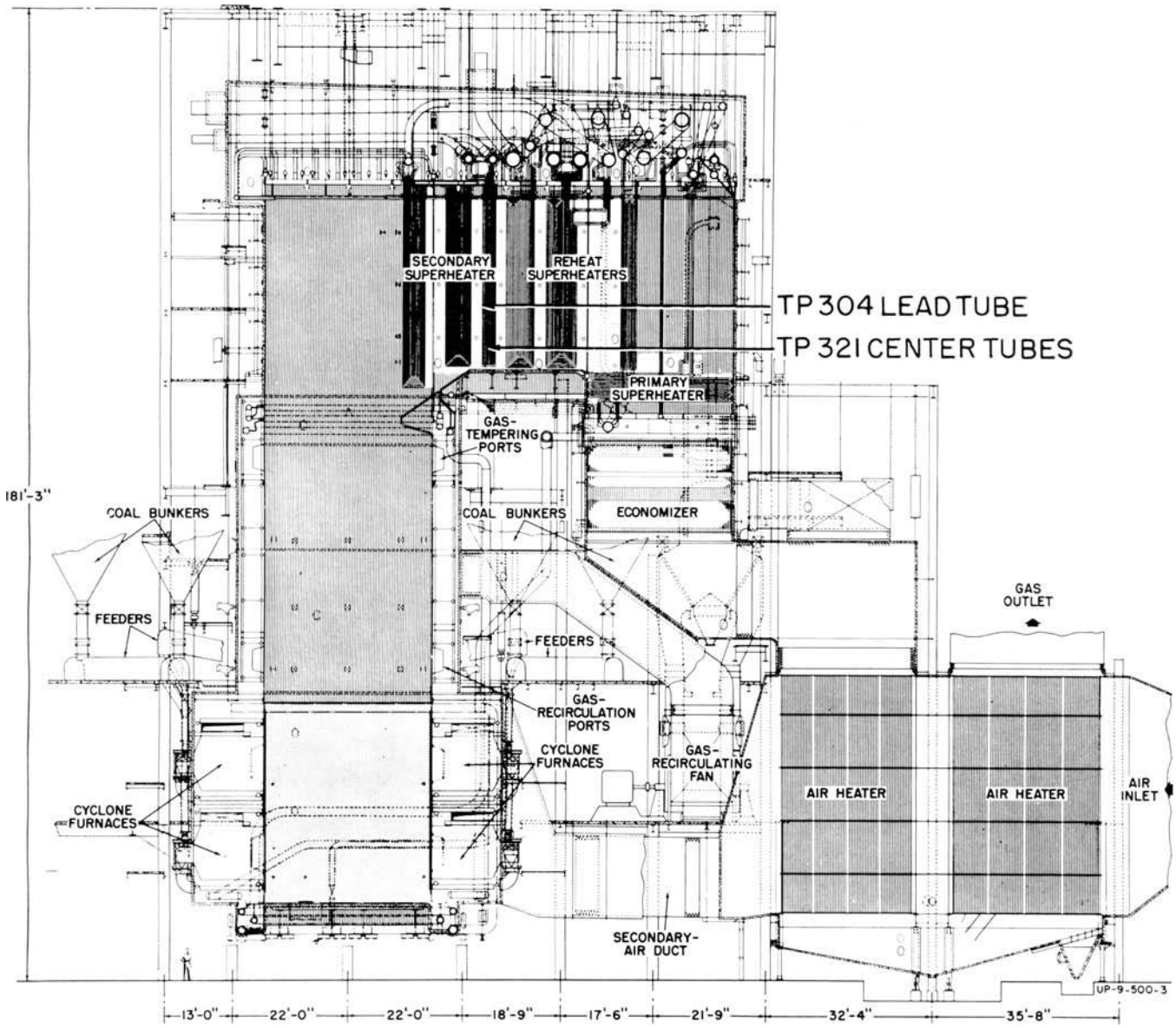


FIG. 3—600-Mw-Unit Steam Generator (1964), 1000 F, 3600-psi Main Steam, 1025 F, 1000 psi First Reheat, 1050 F, 400-psi Second Reheat, Type 321 H Stainless in Secondary Superheater.

superheater at our Twin Branch Plant which gave valuable data on superheater alloys at 1250 F (9). The test program of the ASME Research Committee on High Temperature Steam Generation at Philip Sporn Plant has also made significant contributions in the tests of ferritic materials at 1100 and 1200 F and austenitic alloys at 1200, 1350, and 1500 F (10,11). Likewise the Philo boiler, in its

PIPING

Turbine Piping:

The Twin Branch series of seven units had low alloy main steam piping which joined to stainless stubs on the stainless turbine stop valves. The 6-in.-outside diameter 1-in. wall pipes from the valves to the turbine shell were Type 347 on five units and Type 321 on two units. Some cracks developed in the heat affected zone of butt welds in this turbine piping but not of a magnitude suffered by other utilities where major valve and pipe sections had to be replaced by other stainless materials or, in some instances, by low-alloy ferritic materials (12–14). Development of the 16 chromium, 8 nickel, 2 molybdenum welding electrode in 1955 alleviated this condition by making successful repair

welding possible. This electrode has adequate ductility to permit a weld to cool and yield without cracking the base material.

Several of the 14 in. outside diameter by 3-in. wall dissimilar welds between the austentic and low alloy ferritic pipe developed cracks after ten years of service. Others have been removed to permit repairing the adjoining Type 347 welds at the stop valve body which developed cracks after ten years of service.

Main Steam Piping:

The performance of Type 347 stainless piping was considered so satisfactory that this alloy was chosen in 1954 for the main steam and turbine lead piping for Philo Unit 6. Welding electrodes of 16-8-2 composition were used on all welds. Those on the turbine leads were heat treated at 1950 F while those in the main steam pipes were left as welded. To date, performance of the butt welds subjected to both treatments has been excellent so that any advantages of the heat treatment have not been apparent.

The welds at the small pipe and temperature well connections on the main pipes were left rough in the as-welded condition. Cracks were found around many of these connections in contrast to very minor cracking at similar connections on turbine piping that had been ground to a smooth contour with the pipe. Repairs included careful grinding.

Major cracks, however, were found in the wall of the pipe at each of the 64 heavy hanger attachment lug welds. The cracks appeared after two years service and are attributed to severe expansion stresses engendered by the design of the lugs. These lugs were removed, and pipe clamps and small welded holding lugs were substituted. The new lug welds were carefully ground to a smooth contour with the pipe. Subsequent inspections of the main steam pipe welds have shown only minor new or recurring cracks.

The general Type 347 weld cracking problem was explored in depth in the recent ASTM-ASME Joint Committee, Steam Power Panel, SP-5 research program (1,15). The mechanism of cracking was traced, but elimination of the cause through specification modification was not accomplished. As a result the SP-5 report contains a cautionary statement that the use of A1S1 Type 347 steel as presently specified should be avoided for heavy section pressure parts for high-temperature piping.

Public Service is using Type 347 in the main steam piping of three units which pioneered 1100 F at 2350 psi in 1953 to 1955 (17, 18). They have since had satisfactory service from Type 316 main steam piping on seven units operating at these same steam conditions. Type 316 main steam piping at Eddystone has also shown good service after operating at 1150 and 1200 F (8).

Stainless main steam piping is now needed at steam temperatures above 1060 F because of the low allowable stress and the corrosion rate of low alloy ferritic 2.25 chromium molybdenum. Between 1000 and 1050 F stainless is in the economic picture if a new plant layout is arranged so that short stainless pipes produce permissible forces and moments at the boiler and turbine terminal connections while longer loops of the heavier wall ferritic pipes would be required for comparable flexibility. Where route lengths are justifiably long and flexibility with ferritic heavy wall pipe is inherent, the use of austenitic alloy at present prices does not appear to be justified, even when taking into account the savings on supports, insulation, and erection labor.

TABLE 1—CODE ALLOWABLE STRESSES AND WALL THICKNESSES REQUIRED FOR 10-IN.-ID PIPES, 3500 PSI DESIGN.

Material	Stress at 1000 F	Wall	Stress at 1100 F, psi	Wall	Stress at 1200 F, psi	Wall
P22(2¼ Cr,1 Mo)	7 800	2.59	...	...	...	...
Type 304	8 800	2.43	7 500	3.04	4 500	5.08
Type 304 (proposed for pipe)	9 450	2.23	8 500	2.59	6 000	3.53
Type 321	13 500	1.47	10 300	2.05	5 000	4.43
Type 316	14 000	1.41	10 400	2.03	6 800	3.05
IN 102[a]	30 500	0.60	29 000	0.65	18 500	1.00

[a] IN 102 estimated stresses are calculated using test data and present ASME boiler code rules.

Main Steam Pipe Tests:

The use of stainless for utility piping has been accompanied by an increase in the number and complexity of tests on the material. While adding to the reliability of the material it has also added appreciably to its cost. More of this reliability is needed in the uniformity of the alloy itself as it is produced and processed to ASTM specifications. Some efforts have been made to broaden specifications to reduce cost. This often leads to an inferior product from which acceptable pieces must be selected through testing and elimination. ASTM Specification A 430[4] for high-temperature materials and a number of inspection procedures now use hot ductility tests to evaluate weldability (16). This is a very important technique that examines the material physically, in the actual welding temperature range, and gives it a performance rating. This method still needs additional work to correlate the results with actual welding experience, and it is hoped that the knowledge gained will answer some of the questions of welding variables between heats of stainless. With this knowledge the test itself might be in turn abbreviated or eliminated. At present it adds a considerable cost to the finished product and cannot be performed until heavy investments in semifinished products have already been made. Proof tests for high temperature properties are being developed and will be most valuable.

The need for exact specifications and reliable acceptance tests is very apparent to the utility engineer. His material evaluations must be based on a 30-year material life with reliable trouble-free performance. A shorter life is not going to be economical regardless of price. We know steel producing methods are being changed continuously, and we must provide a base of information that will evaluate these changes in a quick analysis. Type 304, for example, has become stronger in recent years as produced commercially. Is this trend likely to follow in other alloys or could the long time properties drop off without this being apparent or understood in time to correct it? The elements added in the scrap may be what is needed for long-time strength, but will we miss a crucial one for a critical heat unless it is specifically called for in the specification?

Stronger Pipe Materials:

The higher allowable stresses proposed for Type 304 will change the competitive picture toward more stainless steam pipes, but a sizeable advance in material strength into the IN 102 (nickel balance, with 15 chromium, 7 iron, 3 colum-

[4] Specification for Austenitic Steel Forged and Bored Pipe for High-Temperature Service (A 430), *1964 Book of ASTM Standards*, Part 1, a.

bium, 3 molybdenum, 3 tungsten) range is needed. Larger units require larger pipes, and in the critical fight to keep end reactions within reason only thinner walls are going to make an economical arrangement possible.

ASME boiler code allowable stresses for some previously mentioned materials are shown in Table 1. Comparable wall thicknesses for 10-in.-inside diameter pipes of the material, for 3500 psi design, are also shown to illustrate the advantages of stronger materials.

TURBINE SHELLS

Austenitic high-pressure turbine inner shell castings were used on six of the seven Twin Branch series of units. These were very large pieces weighing many tons and were joined together in halves with very heavy bolted flanges. Thicknesses varied between flange, shell, and nozzle areas. Unfortunately, stresses set up by temperature differentials across the heavy sections caused warping and cracking. This could not be repaired and replacement with low-alloy ferritic material became necessary. A low-alloy inner shell was used on the 1150 F Philo Unit 6. The turbine design, however, used shields of Type 347 steel and cooling steam at 1000 F between the shield and the shell.

CONDENSERS AND CONDENSATE SYSTEMS

Welded stainless Type 304 condenser tubes are now under consideration for a new 600-Mw unit. They have been successful on other utility systems where corrosion resistance to certain river waters has made stainless attractive and, in some instances, mandatory. The small fouling build up on stainless compared with copper alloys has offset some of its thermal conductivity disadvantages. Condenser design is presently based on the conductivity of clean tubes and comparative studies of conductivity after a period of service are needed to evaluate the comparative effects of fouling on conductivity and its effect on condenser design. In supercritical units the need for eliminating sources of possible copper pickup in the condensate and feed water cycles has also led to serious consideration of stainless condenser and feed-water heater tubes. The condenser under consideration will require 44,000, 35 ft, $\frac{3}{4}$-in.-outside diameter, 0.0299-wall weldrawn Type 304 tubes. Tube quality and a reliable tube-to-tube-sheep joint will be absolutely essential where such a large number of tubes are involved.

Schedule 10S Type 304 pipe has been used for condensate pipe from the 500,-000-gal clean condensate storage tanks. Here water purity in the low parts per billion range must be maintained and stainless can assure this.

CONTINUED USE OF STAINLESS

As we have seen, stainless has been an important factor in the advancement of utility power plants over the past 15 years. Temperatures have been raised and efficiencies improved. The recent reversal of this trend has been mainly the result of the cost of using stainless. Perhaps an influencing factor has been the engineering advances which have produced economies of construction which have compensated temporarily for lower efficiencies. Higher temperatures, higher efficiencies and improved reliability of units still are sought after very much, but they will be attained only as stainless can price itself back into the economic picture. To do this requires a more effective utilization of a material through a better understanding of its capability to perform in a particular service. This understanding will provide the basis for higher allowable stresses and revisions of code rules. Improved manufacturing processes will also be needed to minimize the required inspections and yet assure specified quality. Concurrent with these improvements, and benefiting from them, will be the development of new alloys and their qualifications by testing under actual service conditions. We can speed this by continued study of the improvements made possible through the actual service experience with stainless steels and by aggressive work on operating problems that have hampered its effective use.

REFERENCES

(1) H. M. Soldan, "The SP-5 and SP-6 Projects" *Transactions*, Am. Soc. Mechanical Engrs., Vol. 85, 1963, p. 147.

(2) J. E. White and J. W. Freeman, "Metallurgical Principles Governing the Creep-Rupture Strength of Type 321 (18-8+Ti) Austenitic Steel Super-Heater Tubing With Limited Extension to Type 304 (18-8) and Type 316 (18-8+Mo) Austenitic Steels," *Transactions*, Am. Soc. Mechanical Engrs., Vol. 85, 1963, p. 119.

(3) Philip Sporn, "A New Power Generation Milestone," *Electrical World*, June 29, 1953, pp. 72–76.

(4) S. N. Fiala, "First Commercial Supercritical Pressure Steam-Electric Generating Unit for Philo Plant," *Transactions*, Am. Soc. Mechanical Engrs., Vol. 79, 1957, pp. 389–407.

(5) W. H. Rowand and A. M. Frendberg, "First Commercial Supercritical Pressure Steam Generator For Philo Plant," *Transactions*, Am. Soc. Mechanical Engrs., Vol. 79, 1957, pp. 409–418.

(6) J. H. Harlow, "Engineering The Eddystone Plant for 5000 Psi, 1200F Steam," *Transactions*, Am. Soc. Mechanical Engrs., Vol. 79, 1957, p. 1410.

(7) P. Sedor, E. K. Diehl, and D. H. Barnhart," External Corrosion of Superheaters in Boilers Firing High-Alkali Coals," *Transactions*, ASME Journal of Engineering for Power, July, 1960, pp. 181–193.

(8) J. H. Harlow, "Observations Regarding Eddystone No. 1 After Inspection Following First Year of Operation 5000 Psi 1150F," presented at the ASME-AIEE Power Conference, Septemebr, 1961.

(9) J. Hoke and F. Eberle, "Experimental Superheater For Steam at 2000 Psi and 1250 F-Report After 14,281 Hours of Operation," *Transactions*, Am. Soc. Mechanical Engrs., Vol. 79, 1957, p. 307.

(10) C. L. Clark, J. J. B. Rutherford, A. B. Wilder, and M. A. Cordovi, "Metallurgical Evaluation of Superheater Tube Alloys After 12 and 18 Months' Exposure to Steam at 1200, 1350, and 1500 F," *Transactions*, Am. Soc. Mechanical Engrs., Vol. 84, 1962, p. 258.

(11) F. Eberle and C. H. Anderson, "Scaling Behavior of Superheater Tube Alloys in ASME High Temperature Steam Research Tests at 1100–1500 F," *Transactions*, Am. Soc. Mechanical Engrs., Vol. 84, 1962, p. 223.

(12) R. M. Curran and A. W. Rankin, "Austenitic Steels In High Temperature Steam Piping," *Transactions*, Am. Soc. Mechanical Engrs., Vol. 79, 1957, p. 1398.

(13) G. E. Lien, F. Eberle, and R. O. Wylie, "Results of Service Test Program on Transition Welds Between Austenitic and Ferritic Steels at the Philip Sporn and Twin Branch Plants," *Transactions*, Am. Soc. Mechanical Engrs., Vol. 76, 1954, p. 7075.

(14) T. T. Frankenberg, A. G. Lloyd, and E. B. Morris, "Operating Experience with the First Commercial Supercritical Pressure Steam-Electric Generating Unit at the Philo Plant," *Proceedings*, Am. Power Conference, 1958.

(15) T. M. Cullen and J. W. Freeman, "Metallurgical Factors Influencing Hot Ductility of Austenitic Steel Steam Piping at Heat-Affected Zone Temperatures During Welding. *Transactions*, Am. Soc. Mechanical Engrs., Vol. 85, 1963, p. 151.

(16) H. M. Soldan and Charles R. Mayne, "Ductility Related to Service Performance of Heavy-Wall Austenitic Pipe Welds," *Welding Journal Research Supplement*, March, 1957.

(17) F. P. Fairchild, "Eight Years of Experience With Austenitic-Steel Piping Materials at Elevated Steam Conditions," *Transactions*, Am. Soc. Mechanical Engrs., Vol. 79, 1957, p. 1371.

(18) R. A. Baker and H. M. Soldan, "Service Experiences at 1050 F and 1100 F of Piping of Austenitic Steels," *Paper 71*, Joint International Conference on Creep, 1963.

DISCUSSION

H. S. AVERY[1]—G. E. Lien has provided an excellent review and analysis of the alloy problems of utility power plants. A trend toward greater efficiency at higher temperatures and pressures was interrupted and reversed by the cost of austenitic alloys but hope was expressed that better understanding of stainless steels and improved manufacturing methods would again permit progress toward higher efficiency

This discussion will emphasize various features of castings that have been neglected. It is noteworthy that only wrought grades of the austenitic corrosion resistant alloys have been evaluated by extensive steam plant service, and yet cast tubing has certain advantages that may solve some of the problems.

The production of centrifugally cast alloy tubing in permanent molds has been a major manufacturing development of the past ten years. Large tonnages have been used by the petrochemical industry where, though pressures are lower, temperatures are much higher and operating conditions are generally more severe than in steam power service. One new plant is using a design temperature of 2100 F, and various installations operate in the 1500 to 1900 F range.

The wrought grades, because carbon adds hot strength and makes the higher carbon alloys more difficult to hot work, are characteristically made with low carbon, such as 0.04 to 0.10 per cent, and seldom exceed 0.20 per cent. The cast alloys do not have this carbon limitation and can be freely specified at whatever carbon level is most desirable. Moreover, because their carbide distribution and habit are not disturbed by the process of hot working, they have a superior uniformity. Their status "as cast" is much like the wrought material after a carefully selected and applied solution heat-treatment. (They are not entirely comparable because the cast alloy has a carbon concentration gradient that cannot be attained after hot working).

The end result is that the cast alloys can and usually are put into service with no heat treatment. At the low carbon levels their creep-rupture properties may match those of the wrought grades, but with higher carbon they are superior. Compare the cast HK40 alloy with the Type 310 stainless steels in ASTM STP 124.[2] This 0.35 to 0.45 per cent carbon 26 per cent chromium: 20 per cent nickel alloy provides extrapolated 100,000 hr rupture stresses of 6400 psi at 1400 F, 2900 psi at 1600 F, and 1270 psi at 1800 F. The wrought Type 310 stainless steel gives midrange properties of about 2640, 1290, and 650 psi. The HK40 is not only about twice as strong at red heat, but it provides these properties with a ±20 per cent range as established by more lots than ASTM STP 124 lists for creep-rupture tested Type 310.

It is thus understandable why the petrochemical industry has adopted HK40 instead of Type 310 for many of the tubular assemblies that operate above 1500 F, even though there are no codes that guide design. The experience of this industry with such tubes now extends to something like ten years. Long units are made regularly from centrifugal castings joined together with arc welded butt joints. These tube assemblies are in effect reaction vessels, fired externally and containing inflammable hydrocarbon gases under pressure inside. The internal gas pressure causes hoop stresses, while the dead weight of the tubing and the catalyst contained therein imposes longitudinal stress; and thermal gradients add their stress complications.

For steam plants the HK and Type 310 alloys (26 chromium-20 nickel) just described are needlessly high in alloy content. They are useful to above 2000 F. For a maximum temperature of 1600 F the HF grades are more appropriate. The CF (cast) and 304 (wrought) types are related stainless steels, but it is well to recognize that their low carbon contents, necessary for resistance to intergranular attack by corrosive liquid chemicals, limit their creep strength at red heat. The HF alloys are specifically intended for heat resisting service at 1200 F and above, and they exploit the strengthening effect of carbon.

The general characteristics of the HF alloys were described in 1951.[3] Recently there have been added long term creep-rupture tests that validate log-log plots of rupture times and creep rates out to 13,000 hr. These indicate for an HF33 alloy (0.33 per cent carbon, 19.9 per cent chromium, 9.6 per cent nickel) the 100,000 hr rupture strengths are about 10,700 psi at 1200 F., 6700 psi at 1300 F, 4200 psi at 1400 F, 2600 psi at 1500 F, and 1650 psi at 1600 F.[4] This grade, when coupled with the adaptability of the centrifugal casting process to producing large tubes with thick walls, may solve some of the steam plant problems.

[1] Metallurgical Dept., American Brake Shoe Co., Mahwah, N. J.

[2] *Elevated Temperature Properties of Stainless Steel, ASTM STP 124*, Am. Soc. Testing Mats., 1952.

[3] H. S. Avery, C. R. Wilks, and J. A. Fellows, "Cast Heat Resistant Alloys of the 21%Cr; 9%Ni Type," *Transactions*, Am. Soc. Metals, Vol. 44, 1952, pp. 57–80.

[4] Alloy Casting Inst. sponsored work that is pending publication.

MODIFIED TYPE 316 STAINLESS STEEL WITH LOW TENDENCY TO FORM SIGMA

By C. E. Spaeder, Jr.[1] and K. G. Brickner[2]

Synopsis

A study was made to determine whether decreasing the chromium or the chromium and molybdenum contents of AISI Type 316 stainless steels would decrease the tendency for sigma-phase formation without impairing the elevated-temperature strength of the steel.

The results of this study showed that in comparison with AISI Type 316, a modified Type 316 steel with about 14 per cent chromium instead of the normal 16 to 18 per cent chromium had about the same coefficient of thermal expansion, similar room- and elevated-temperature tensile properties, similar creep and creep-rupture strengths, and slightly better hot workability. Moreover, the impact strength of modified Type 316 steel after exposure for 6000 hr at 1100, 1300, and 1500 F was markedly superior to that of AISI Type 316 steel. The results of X-ray and metallographic studies indicated that the superior impact strength of the modified Type 316 was the result of lesser amounts of sigma formed in the new steel.

Because AISI Type 316 stainless steel has excellent elevated-temperature tensile properties and creep and creep-rupture strengths, it is used for elevated-temperature service in the range 1100 to 1500 F, the most frequent applications being in the range 1100 to 1300 F. However, during long-time service in the 1100 to 1500 F range, Type 316 steel undergoes microstructural changes that greatly decrease its impact strength, particularly upon cooling to room temperature after long-time service at elevated temperatures. This decrease in impact strength is primarily associated with the precipitation of $M_{23}C_6$ type carbides and sigma phase (1)[3] although other precipitates, such as Cr_7C_3, Mo_2C, and chi phase (Fe_3CrMo) have been detected in Type 316 steel after long-time exposure at elevated temperatures (2) and may also contribute to the decrease in toughness of this steel. As would be expected, this decrease in toughness is of concern to designers because of the increased likelihood that elevated-temperature equipment made of this steel will be damaged as a result of maintenance performed after the equipment is shut down and cooled to room temperature. In fact, concern regarding this decrease in toughness often results in the selection of an alternative material of lower strength for some applications. Thus, the development of a Type 316 stainless steel having improved toughness after elevated-temperature exposure was highly desirable. Such a steel should be particularly useful in the steam-power industry for applications in which long-time service between 1100 and 1300 F is encountered.

The best approach to developing such a steel is to minimize the formation of sigma phase, which is a hard, brittle phase with a complicated body-centered lattice structure (3). It generally forms in austenitic stainless steels between 925 and 1775 F and forms at a maximum rate between 1375 and 1650 F (4). The formation of sigma is enhanced by such additions as chromium, molybdenum, and silicon (3). Sigma forms relatively rapidly from a ferritic matrix but relatively slowly from an austenitic matrix (5). It is apparent, therefore, that the formation of sigma phase in Type 316 steel may be minimized by lowering the amounts of ferrite-stabilizing elements, which would lead to a Type 316 steel with greater austenite stability

Although it was known that lowering the content of chromium or molybdenum or both would decrease the amount of sigma formed in the steel, the effect of these composition changes on the elevated-temperature properties of Type 316 steel was not known. Therefore, the creep-rupture properties of a low-chromium Type 316 steel with 1 to 3 per cent molybdenum were determined. The first phase of this investigation indicated that a modified Type 316 steel with about 14 per cent chromium and a normal molybdenum content (2.00 to 3.00 per cent) would have tensile properties from room temperature to 1500 F similar to AISI Type 316 steel and would have microstructure stability such that only small amounts of sigma would form in the range 1100 to 1500 F.

Accordingly, this steel was selected for additional studies to obtain creep data, additional elevated-temperature tensile properties, impact strength after long-time exposure, thermal-expansion data, and hot-workability data. This paper summarizes the studies that led to the development of the modified Type 316 steel and compares its properties with those obtained on a laboratory induction-furnace heat of regular AISI Type 316 steel.

Materials and Experimental Work

As the first phase of this investigation, three 100-lb induction-furnace heats (Steels A, B, and C in Table 1) of a low-chromium-content (14 per cent) Type 316 stainless steel were melted with three levels of molybdenum content, nominally 1.0, 2.0, and 3.0 per cent. As will be discussed later in the paper, Steel C appeared to meet the objective of this investigation and accordingly, Steels D and E, which are similar in composition to Steel C, were melted to supply additional material for testing. In addition, Steel F, which was melted for comparison, is regular AISI Type 316 steel. The composition limits of the Type 316 steel as specified by the AISI are shown in Table 1. The experimental steels contain about 14 per cent chromium, whereas the AISI specification requires 16.0 to 18.0 per cent. The carbon contents of Steels B and E are slightly above the maximum check-analysis limit (0.09 per cent) specified by the AISI, but these slight differences are not expected to affect significantly the results of the study.

The laboratory heats were forged into $\frac{3}{4}$-in.-square bars at about 2050 F, air-

[1] Research engineer, Stainless Steel Products, Applied Research Laboratory, U. S. Steel Corp., Monroeville, Pa.

[2] Technologist, Applied Research Laboratory, U. S. Steel Corp., Monroeville, Pa.

[3] The boldface numbers in parentheses refer to the list of references appended to this paper.

Copyright© 1965 by ASTM International

cooled, and then annealed by reheating for ½ hr at 1975 F and water quenching to room temperature. These annealed bars were machined into standard 0.505-in.-diameter longitudinal tension specimens and 0.250-in.-diameter longitudinal creep-rupture specimens. The tension specimens were tested at room temperature, whereas the creep-rupture tests were conducted at 1100, 1300, and 1500 F.

Also, annealed bars from Steels D and F were machined into standard 0.158-in.-diameter dilatometric specimens and 0.252-in.-diameter longitudinal elevated-temperature tension specimens. The dilatometer measurements were made from room temperature to 1500 F at heating and cooling rates of 250 F/hr. The tension tests were conducted at 900, 1100, 1300, and 1500 F. Annealed bars from these two heats were exposed for 100, 500, 1000, 3000, and 6000 hr at temperatures of 1100, 1300, and 1500 F.

TABLE 1—COMPOSITIONS OF THE STEELS INVESTIGATED, PER CENT (CHECK ANALYSES).

Steel	Heat No.	C	Mn	P	S	Si	Ni	Cr	Mo	N
					Modified Type 316 Stainless Steel					
A	H3144-1[a]	0.09	1.99	0.007	0.028	0.65	11.79	13.96	0.99	0.034
B	H3145-1[a]	0.10	2.03	0.009	0.028	0.67	11.87	14.04	1.95	0.034
C	H3146-1[a]	0.09	1.99	0.008	0.029	0.65	11.91	14.05	2.89	0.033
D	M6126-1[a]	0.067	1.60	0.005	0.006	0.70	12.20	14.4	2.58	0.023
E	K4409-2[a]	0.10	1.87	0.006	0.011	0.61	12.10	13.70	2.75	0.028
					AISI Type 316 Stainless Steel					
F	M6127-1[a]	0.065	1.60	0.006	0.009	0.75	12.3	17.4	2.63	0.019
Specification limits for AISI Type 316 stainless steel		0.08 max	2.00 max	0.045 max	0.030 amx	1.00 max	10.00 — 14.00	16.00 — 18.00	2.00 — 3.00	[b]

[a] Laboratory 100-lb induction-furnace heats.
[b] Not specified.

TABLE 2—CREEP-RUPTURE TEST RESULTS FOR MODIFIED TYPE 316 STAINLESS STEELS AND FOR AISI TYPE 316 STAINLESS STEEL.

Steel	Alloy Modification, % Cr	Alloy Modification, % Mo	Test Temperature, deg F	Stress Rupture, psi 100 hr	Stress Rupture, psi 1000 hr	Stress Rupture, psi 10 000 hr	Stress Creep Rate, psi 0.001 %/hr	Stress Creep Rate, psi 0.0001%/hr
				Modified Type 316				
A	14	1	1100	37 000	29 000	23 000	[a]	[a]
			1300	18 000	12 000	8 100	[a]	[a]
			1500	8,100	5,100	3 400	[a]	[a]
B	14	2	1100	43 000	33 000	27 000	[a]	[a]
			1300	19 000	14 000	10 000	...	...
			1500	9 700	6 800	4 600	...	...
C	14	3	1100	48 000	37 000	29 000	[a]	[a]
			1300	22 000	16 000	12 000	[a]	[a]
			1500	10 500	8 000	6 000	[a]	[a]
D	14	2½	1100	40 000	28 000	20 000	21 000	15 000
			1300	19 000	13 000	9 000	8 800	6 200
			1500	9 500	6 400	4 400	3 700	2 500
				AISI Type 316				
F	17	2½	1100	39 000	28 000	20 000	22 000	16 000
			1300	19 000	13 000	8 500	8 500	6 000
			1500	10 000	6 100	3 800	3 800	2 500

[a] Not determined.

Standard Charpy V-notch impact specimens were then machined from these exposed bars and from unexposed annealed bars and tested at room temperature.

Metallographic studies were made on the creep-rupture specimens before and after creep-rupture testing at 1100, 1300, and 1500 F, and on the impact specimens after long-time exposure. In addition, X-ray diffraction studies were conducted on the creep-rupture specimens after testing and on the impact specimens after exposure. X-ray diffraction-patterns were made on residues obtained by etching a sample for long periods of time (24 to 48 hr) in Vilella's reagent. The residue was removed from the specimen surface several times during the etching cycle by rinsing the surface with alcohol. It was washed and decanted several times with distilled water to remove impurities picked up from the etching reagent.

The X-ray diffraction results could not reveal quantitative information on the precipitates formed; accordingly, a metallographic technique was used to obtain such information. Impact specimens of Steels D and F that had been exposed at 1500 F for 6000 hr were etched by using a special technique developed by Dulis and Smith (1) to distinguish between the carbide phase, and the sigma or chi or both phases formed. This differential etching technique consisted of etching the samples in Vilella's reagent to reveal sigma or chi or both phases and the carbides present. These specimens were photographed and then repolished and etched in cold ferricyanide reagent to delineate the carbide phase only, and again photographed. Point-count techniques similar to the method described by Howard and Cohen (6) were used to measure the amount of carbide phase and sigma or chi or both phases in the samples etched with Vilella's reagent. The same techniques were used to measure the amount of carbide phase in the samples etched with the cold ferricyanide reagent. The difference between these two measurements is approximately the amount of sigma or chi or both phases present.

In addition, Magne-Gage measurements (to determine the amount of ferrite or other magnetic constituents present) and Vickers hardness measurements were made on the steels before and after the long-time creep-rupture testing and after long-time exposure at elevated temperatures.

An additional heat, Steel E, was melted and processed to ⅝-in.-diameter stock for hot-twist tests, which are used to evaluate the hot workability of steels, by twisting bar-type specimens to failure at the desired temperatures. In the present study, ⅝-in.-diameter by 24-in.-long specimens of this steel were heated for ½ hr at different temperatures in the range 1950 to 2450 F and tested at a

TABLE 3—ROOM- AND ELEVATED-TEMPERATURE TENSILE PROPERTIES OF MODIFIED TYPE 316 STEELS AND OF AISI TYPE 316 STEEL.[a]

Steel	Alloy Modification, % Cr	Alloy Modification, % Mo	Test Temperature, deg F	Yield Strength, 0.2% Offset, psi	Tensile Strength, psi	Elongation in 2 in., %	Reduction of Area, %
MODIFIED TYPE 316 STEEL							
A	14	1	75	34 100	80 700	67.0	77.0
B	14	2	75	35 600	81 500	61.0	76.0
C	14	3	75	36 500	83 000	61.0	76.0
D	14	2½	75	34 000	82 900	62.0	76.0
			900	19 900	67 100	44.0	67.0
			1100	16 300	60 800	43.0	68.0
			1300	16 700	44 900	49.0	65.0
			1500	15 000	30 000	62.0	74.0
AISI TYPE 316 STEEL							
F	17	2½	75	35 800	85 700	64.0	75.0
			900	18 500	66 700	44.0	70.0
			1100	17 700	61 600	44.0	68.0
			1300	15 600	46 200	49.0	64.0
			1500	14 800	36 600	54.0	78.0

[a] Note—The values are the averages of results obtained on duplicate specimens.

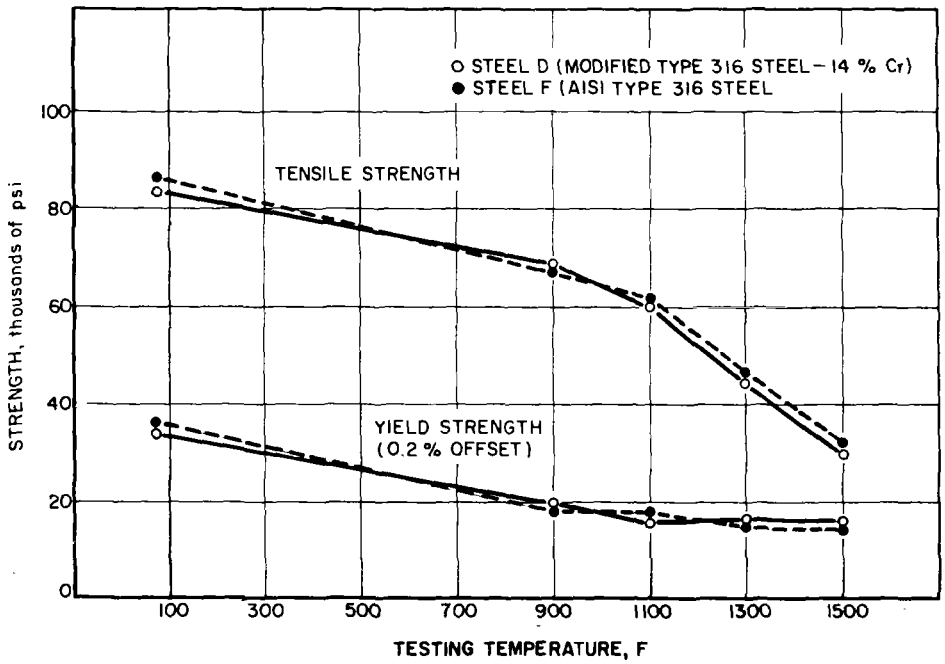


FIG. 1—Effect of Testing Temperature on the Yield and Tensile Strengths of Modified Type 316 and AISI Type 316 Stainless Steels.

speed of 128 rpm. An electric counter recorded the number of twists sustained by the specimens before failure occurred.

RESULTS AND DISCUSSION

Creep-Rupture and Tension-Test Results:

The creep and creep-rupture data for Steels A, B, C, D, and F are summarized in Table 2. A comparison of the 1000-hr rupture strength of Steels A, B, and C indicates that the creep-rupture strength increased as the molybdenum content of the steels increased from 0.99 to 2.89 per cent. Note that the creep-rupture strength of Steel A is near the low side of the statistically determined range (7) for commercial AISI Type 316 steel, whereas Steel B is in the middle of the range, and Steel C is near the high side of this range. (The statistically determined ranges for the 1000-hr creep-rupture strengths of Type 316 steel were 27,600 to 34,000 psi at 1100 F, 11,500 to 16,800 psi at 1300 F, and 4800 to 7300 psi at 1500 F.)

Because the results of an X-ray study indicated that only traces of sigma were present in Steels A, B, and C, the most promising of these steels, Steel C, was selected for additional studies. At this point in the investigation, it appeared that a lower chromium modification of Type 316 steel would fulfill the objective of this investigation. Accordingly, Steels D (modified Type 316 steel) and F (regular AISI Type 316 steel) were melted to provide material for extensive testing. As will be discussed later, Steel E was melted to supply material for hot-workability studies.

A comparison of the creep and creep-rupture data, Table 2, for Steels D and F shows that the creep and creep-rupture strength of the modified and regular Type 316 stainless steels do not differ significantly at 1100, 1300, and 1500 F. Note that the rupture strength of these two laboratory-melted steels is on the low side of the previously mentioned statistically (7) determined ranges for commercially melted steels. It is believed that this lower strength of Steels D and F is because of the relatively low nitrogen content of these steels.

The results of tension tests at room temperature on Steels A, B, C, D, and F are shown in Table 3 along with the results of elevated-temperature tension tests for Steels D and F. The data for Steels D and F are shown graphically in Fig. 1. Figure 1 shows, as would be expected, that as the testing temperature increased, the yield and tensile strengths of both steels decreased, the greatest decrease occurring in the tensile strength.

TABLE 4—RESULTS[a] OF ROOM-TEMPERATURE CHARPY V-NOTCH IMPACT[b] AND VICKERS HARDNESS TESTS ON MODIFIED TYPE 316 AND AISI TYPE 316 STAINLESS STEELS BEFORE AND AFTER LONG-TIME EXPOSURE AT ELEVATED TEMPERATURES.[c]

Exposure Temperature, deg F	Exposure Time, hr	Steel D (Modified Type 316 Steel, 14% Cr) Impact Strength, ft-lb	Steel D (Modified Type 316 Steel, 14% Cr) Hardness, DPH	Steel F (AISI Type 316 Steel) Impact Strength, ft-lb	Steel F (AISI Type 316 Steel) Hardness, DPH
Prior to exposure		240	133	240	131
1100	100	179	150	223	140
	500	167	137	143	149
	1000	135	152	132	144
	3000	120	162	118	159
	6000	108	173	100	179
1300	100	142	137	124	143
	500	90	142	79	143
	1000	68	146	66	150
	3000	68	147	53	149
	6000	42	160	33	172
1500	100	86	138	87	139
	500	61	139	60	140
	1000	50	145	36	136
	3000	47	151	18	166
	6000	40	153	15	168

[a] Each value shown is the average of the results of duplicate tests.

[b] Impact tests were conducted at 80 F.

[c] Note—The steels were annealed at 1975 F for ½ hr and water-quenched before exposure.

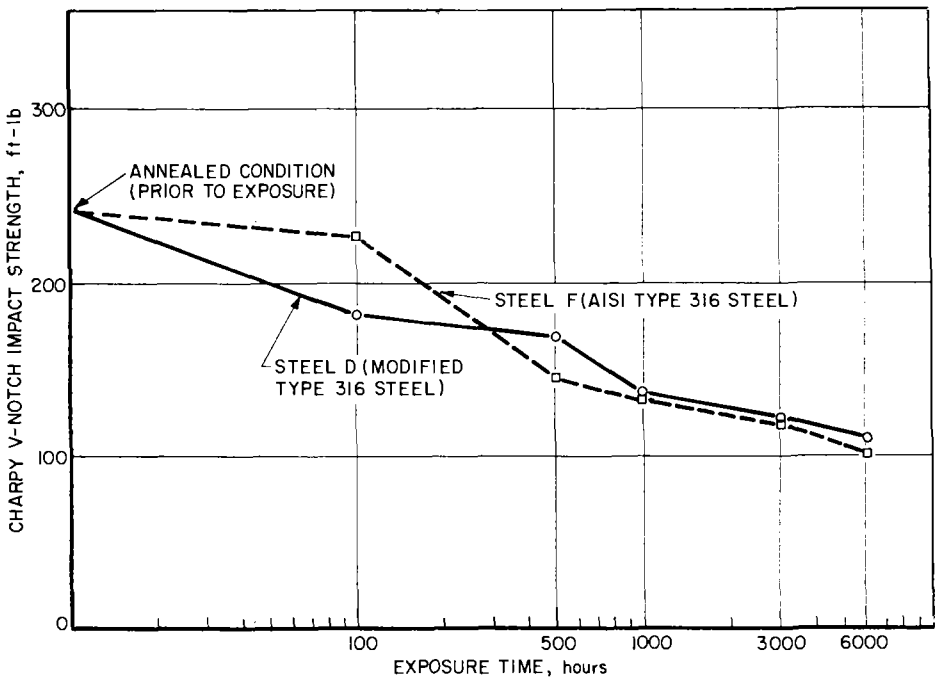


FIG. 2—Effect of Long-Time Exposure at 1100 F on the Room-Temperature Impact Strength of Modified Type 316 and AISI Type 316 Stainless Steels.

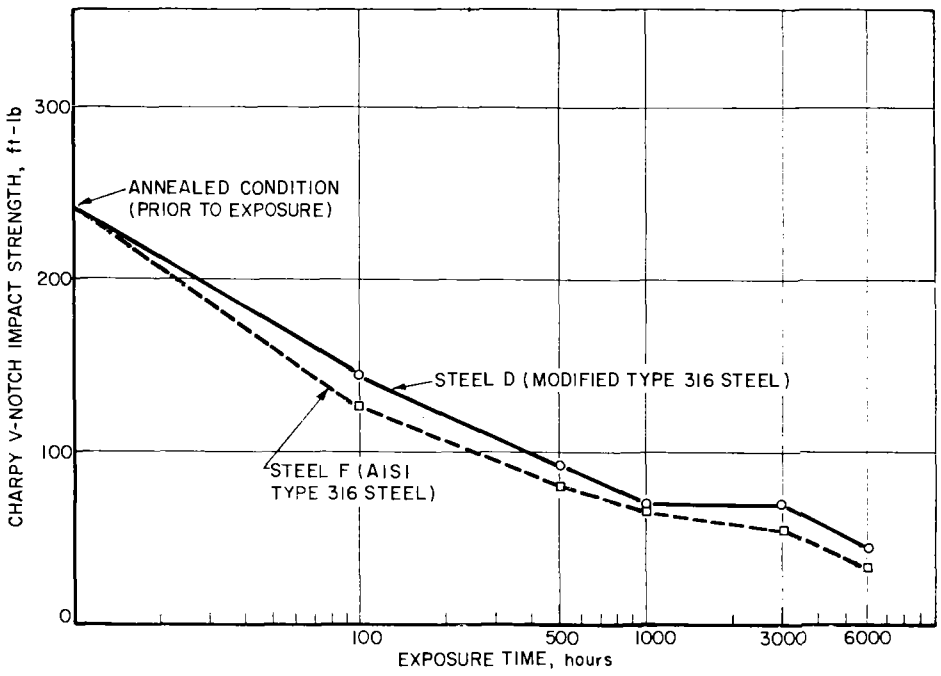


FIG. 3—Effect of Long-Time Exposure at 1300 F on the Room-Temperature Impact Strength of Modified Type 316 and AISI Type 316 Stainless Steels.

A comparison of the yield and tensile strength and the elongation and reduction of area, Table 3, shows that these values were about the same for both steels over the temperature range investigated.

Impact-Test Results:

The results of room-temperature impact tests on the modified and regular Type 316 steels before and after long-time exposure at 1100, 1300, and 1500 F are listed in Table 4, and are presented graphically in Figs. 2–4. These results show that the impact strength of both steels after exposure decreased with both increasing time and increasing temperature in the 1100 to 1500 F range. A comparison of the impact strength of the two steels after long-time exposure shows that the modified Type 316 steel (Steel D) was superior to the regular Type 316 steel (Steel F), the superiority being most pronounced after long-time exposure at the highest temperature, 1500 F. For example, the impact strength of the modified Type 316 steel after 6000 hr exposure at 1100, 1300, and 1500 F was 108, 42, and 40 ft-lb, respectively, as compared with 100, 33, and 15 ft-lb, respectively, for the regular Type 316 steel.

After short exposure times (about 500 hr and less), the impact strength of the two steels did not differ significantly, even at 1500 F. However, this was to be expected because other investigations (1) have shown that during exposure at temperatures at which both sigma and carbides may form, the carbide precipitation occurs first and is completed in a relatively short time, whereas sigma phase does not precipitate until most of the carbide precipitation has been completed. Therefore, it appears that the initial loss of impact strength of both steels is probably because of carbide precipitation ($M_{23}C_6$), whereas the decrease in impact strength that occurs during the latter stages of exposure is probably because of the precipitation of sigma or chi or both phases. Therefore, on the basis of the metallographic and X-ray results discussed later in the paper, it is concluded that the superior impact strength (particularly after exposure at 1500 F) of the modified Type 316 steel is because of the smaller quantities of intermetallic precipitates (such as sigma or chi or both phases) formed in this steel.

Although oxidation studies were not included in this investigation, a comparison of the amount of scale formed in the modified Type 316 and regular AISI Type 316 steel during exposure at 1500 F for 6000 hr indicates that the oxidation resistance of the two steels was about the same in still air. However, additional studies will be conducted to obtain quantitative information on the oxidation and corrosion resistance of the modified Type 316 steel.

Hardness-Test Results:

The results of hardness tests on these impact specimens are also listed in Table 4. The results show that the hardness of both steels generally increased with increasing exposure time and that the hardness was slightly higher after exposure at 1100 F than at 1300 and 1500 F. For example, the modified Type 316 steel before exposure exhibited a DPH hardness of 133, whereas during 6000 hr exposure at 1100, 1300, and 1500 F, the hardness increased to 173, 160, and 153,

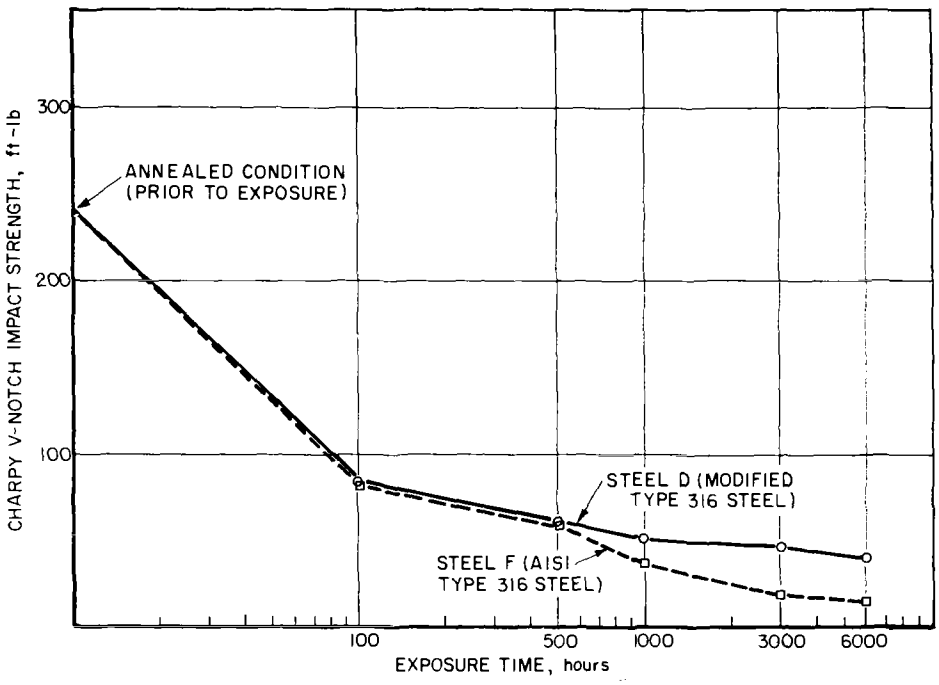
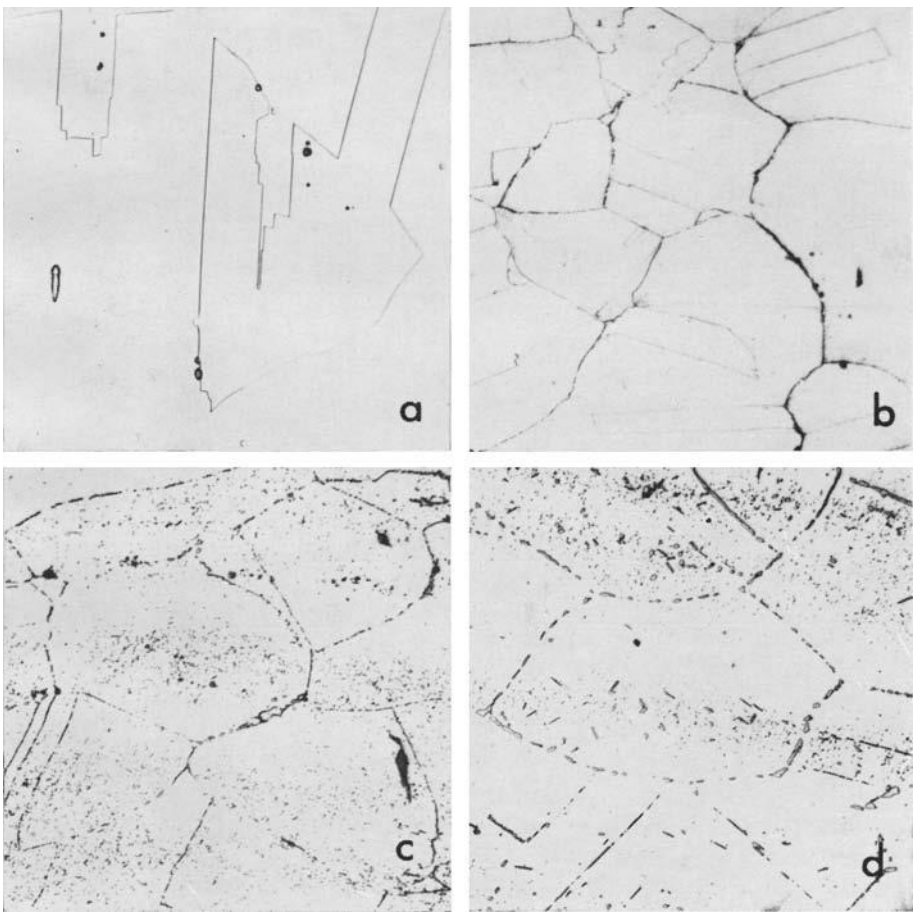


FIG. 4—Effect of Long-Time Exposure at 1500 F on the Room-Temperature Impact Strength o Modified Type 316 and AISI Type 316 Stainless Steels.



(*a*) Prior to exposure. Annealed for ½ hr at 1975 F and water-quenched. Hardness of 133 DPH (67 R_B).

(*b*) After creep-rupture testing for 1632 hr at 1100 F at a stress of 26,000 psi. Hardness of 191 DPH (88 R_B).

(*c*) After creep-rupture testing for 1291 hr at 1300 F at a stress of 13,000 psi. Hardness of 160 DPH (79 R_B).

(*d*) After creep-rupture testing for 1615 hr at 1500 F at a stress of 6000 psi. Hardness of 141 DPH (71 R_B).

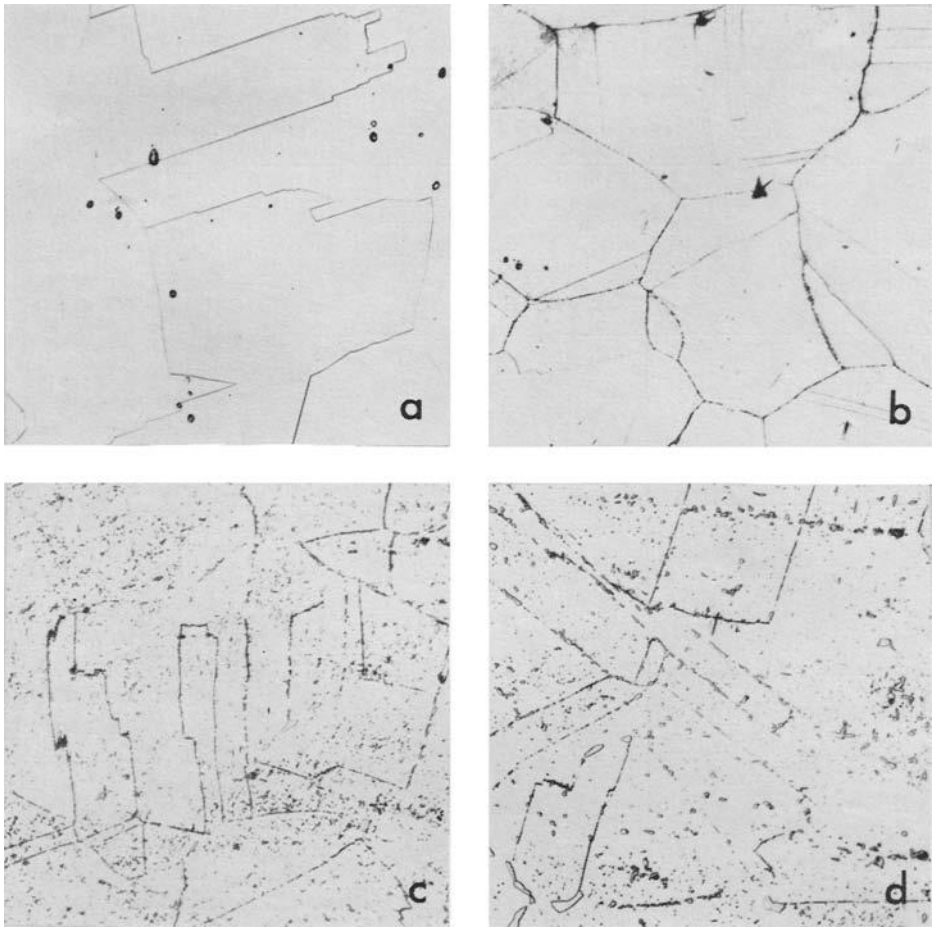
FIG. 5—Microstructure of Modified Type 316 Stainless Steel Before and After Long-Time Creep-Rupture Testing at 1100, 1300, and 1500 F. Etched in Vilella's Reagent (×500).

respectively. The regular Type 316 steel before exposure exhibited a DPH hardness of 131, whereas during 6000 hr exposure at 1100, 1300, and 1500 F, the hardness increased to 179, 172, and 168, respectively. The increase in hardness that occurred in both steels during all conditions of exposure is primarily because of the precipitation of carbides rather than to the formation of sigma or chi or both, inasmuch as the metallographic and X-ray diffraction studies, which are discussed later in the paper, showed that carbide precipitation occurred in both steels during all exposures whereas sigma or chi or both formed only during some exposures. The slightly lower hardness of the samples exposed for 6000 hr at 1300 and 1500 F compared with that of the samples exposed for 6000 hr at 1100 F is attributed to an agglomeration of the carbides at the higher temperatures, which is also discussed later in the paper.

A comparison of the hardness of the two steels shows that the modified Type 316 steel, except at 1100 F, was generally softer than the regular Type 316 steel after the same exposure time at a particular temperature. For similar exposures, the greatest difference in the hardness of the two steels was observed for the specimens exposed at 1500 F for 3000 and 6000 hr. At 1100 F there was no consistent difference in the hardness of the two steels.

Metallographic and X-ray Diffraction Studies:

The microstructures of the two steels, before and after long-time creep-rupture testing at 1100, 1300, and 1500 F, are shown in Figs. 5 and 6. The microstructures of the modified Type 316 steel and regular Type 316 steel in the annealed condition were similar and consisted of austenite and a few undissolved carbides, Figs. 5(*a*) and 6(*a*), respectively. Long-time creep-rupture testing at 1100 F resulted in an increase in the amount of carbides, Figs. 5(*b*) and 6(*b*). Similarly, after long-time testing at 1300 F, the amount of precipitated carbides increased, Figs. 5(*c*) and 6(*c*). (Because the longest time for the creep-rupture tests at 1300 F was 1291 hr, the quantities of sigma present are probably too small to be observed in these photomicrographs.) Long-time creep-rupture testing at 1500 F resulted in agglomeration of the carbides, Figs. 5(*d*) and 6(*d*). Also, it is possible that the prominent angular particles shown in these figures, particu-



(*a*) Prior to exposure. Annealed for ½ hr at 1975 F and water-quenched. Hardness of 131 DPH (66 R_B).

(*b*) After creep-rupture testing for 2079 hr at 1100 F at a stress of 26,000 psi. Hardness of 202 DPH (90 R_B).

(*c*) After creep-rupture testing for 973 hr at 1300 F at a stress of 13,000 psi. Hardness of 185 DPH (86 R_B).

(*d*) After creep-rupture testing for 1974 hr at 1500 F at a stress of 6000 psi. Hardness of 155 DPH (77 R_B).

FIG. 6—Microstructure of AISI Type 316 Stainless Steel Before and After Long-Time Creep-Rupture Testing at 1100, 1300, and 1500 F. Etched in Vilella's Reagent (×500).

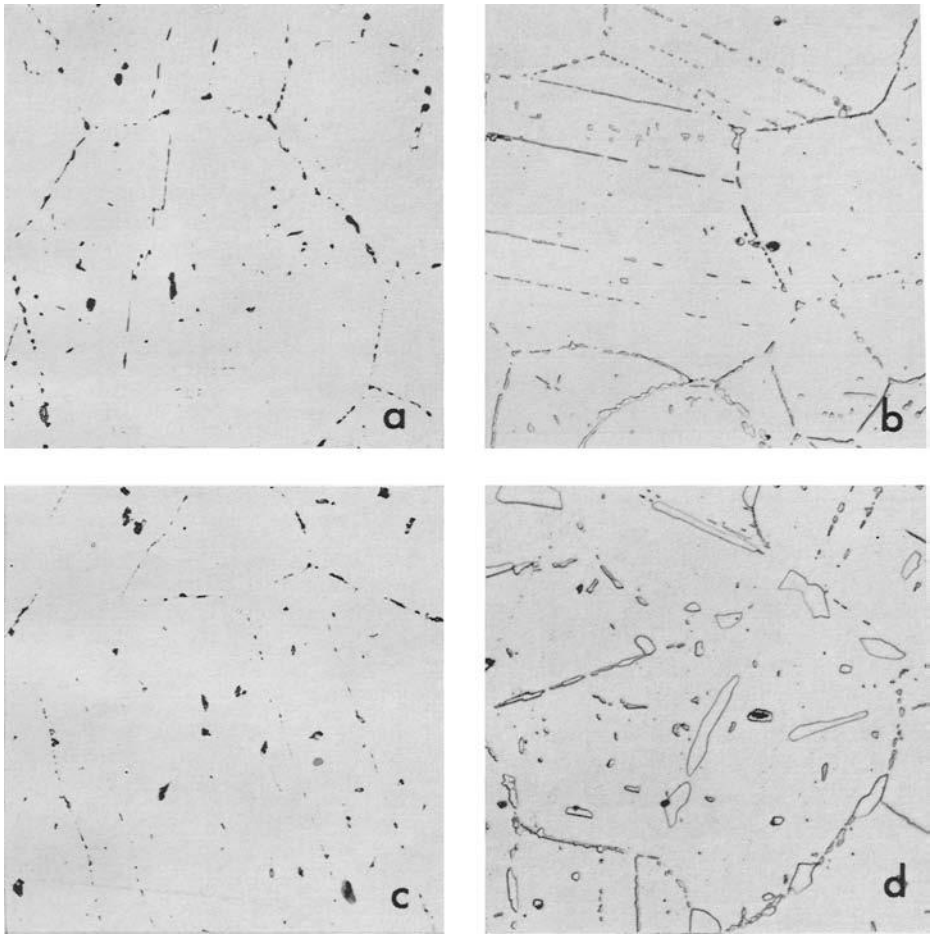
TABLE 5—RESULTS OF X-RAY DETERMINATIONS MADE ON RESIDUES EXTRACTED FROM CREEP-RUPTURE AND IMPACT SPECIMENS OF MODIFIED TYPE 316 AND AISI TYPE 316 STAINLESS STEELS BEFORE AND AFTER EXPOSURE AT ELEVATED TEMPERATURES.[a]

Test Temperature, deg F	Specimen Type	Steel D (Modified Type 316 Steel—14% Cr)		Steel F (AISI Type 316 Steel)	
		Exposure Time, hr	Phases Detected	Exposure Time, hr	Phases Detected
1100	Creep rupture	39	$M_{23}C_6$	35	$M_{23}C_6$
	Creep rupture	136	$M_{23}C_6$	112	$M_{23}C_6$
	Creep rupture	399	$M_{23}C_6$	714	$M_{23}C_6 + \sigma^b$
	Creep rupture	1632	$M_{23}C_6$	2079	$M_{23}C_6 + \sigma^b$
	Impact	3000	$M_{23}C_6$	3000	$M_{23}C_6$
	Impact	6000	$M_{23}C_6$	6000	$M_{23}C_6$
1300	Creep rupture	66	$M_{23}C_6$	72	$M_{23}C_6$
	Creep rupture	280	$M_{23}C_6$	337	$M_{23}C_6 + \sigma^b$
	Creep rupture	584	$M_{23}C_6 + \sigma^{bd}$	550	$M_{23}C_6 + \sigma^b$
	Creep rupture	1291	$M_{23}C_6 + \sigma^{bd} + \chi^{cd}$	973	$M_{23}C_6 + \sigma^b$
	Impact	3000	$M_{23}C_6 + \sigma^b + \chi^{cd}$	3000	$M_{23}C_6$[e]
	Impact	6000	$M_{23}C_6 + \sigma^b + \chi^{cd}$	6000	$M_{23}C_6 + \sigma^b + \chi^c$
1500	Creep rupture	75	$M_{23}C_6 + \sigma^{bd} + \chi^{cd}$	98	$M_{23}C_6 + \sigma^b + \chi^{cd}$
	Creep rupture	275	$M_{23}C_6 + \sigma^{bd}$	251	$M_{23}C_6 + \sigma^b$
	Creep rupture	511	$M_{23}C_6$[e]	520	$M_{23}C_6 + \sigma^b$
	Creep rupture	1615	$M_{23}C_6 + \sigma^{bd}$	1070	$M_{23}C_6 + \sigma^b + \chi^{cd}$
	Impact	3000	$M_{23}C_6 + \sigma^b$	3000	$M_{23}C_6 + \sigma^b + \chi^c$
	Impact	6000	$M_{23}C_6 + \sigma^b$	6000	$M_{23}C_6 + \sigma^b + \chi^c$

[a] Note—The material from which the impact specimens were machined was exposed at the indicated temperatures without stress. [b] σ = Sigma phase. [c] χ = Chi phase. [d] Trace amounts. [e] Light pattern; only carbides could be distinguished.

larly in Fig. 6(*d*), are sigma or chi or both particles.

The results of the analysis of the X-ray diffraction patterns, obtained on the residues extracted from the broken creep-rupture and impact specimens, are presented in Table 5. A comparison of the results obtained on the two steels shows that sigma phase formed in the 316 steel exposed at 1100 F, note that sigma phase was observed in as few as 714 hr in the creep-rupture specimens, whereas it was not observed in as long as 600 hr in the impact specimens. The earlier presence of sigma in the creep-rupture specimens of the regular Type 316 steel at 1100 F is the result of the increase in the nucleation rate of sigma



(*a*) Steel D etched with cold ferricyanide to show carbides.
(*b*) Steel D etched with Vilella's reagent to show carbides and sigma phase.
(*c*) Steel F etched with cold ferricyanide to show carbides.
(*d*) Steel D etched with Vilella's reagent to show carbides and sigma phase.

FIG. 7—Comparison of Microstructures of Impact Test Specimens of Steel D (Modified Type 316 Steel, 14 Per Cent Chromium, Hardness of 153 DPH (76 R_B)) and Steel F (AISI Type 316 Steel, Hardness of 168 DPH (84 R_B)) After 6000-hr Exposure at 1500 F (×500).

regular Type 316 steel at a lower temperature and in shorter times than it did in the modified Type 316 steel. Moreover, in many of the specimens of the modified Type 316 steel in which sigma phase was observed, it was present only in trace amounts. At 1100 F, sigma phase was not observed in the creep-rupture specimens of the modified Type 316 steel after 1632 hr, nor in the impact specimens after 6000 hr. In the regular Type 316 steel, sigma phase was observed in the impact specimens after 600 hr at 1100 F. Sigma phase was not observed in the creep-rupture specimens of the regular Type 316 steel after 1632 hr, nor in the impact specimens after 6000 hr at 1100 F.

Because X-ray diffraction techniques do not reveal quantitative information of the phases present, the impact test specimens of Steels D and F that had been exposed for 600 hr at 1100, 1300, or 1500 F were examined by the special metallographic techniques discussed earlier in the paper. Of the specimens examined, only the samples exposed at 1500 F had measurable amounts of sigma or chi or both phases. The amount of sigma or chi or both phases formed was determined by measuring the total amount of sigma, chi, and carbide phases in the samples etched in Vilella's reagent, Figs. 7(*b*) and (*d*), and then measuring the amount of carbides in the samples etched in cold ferricyanide reagent, Figs. 7(*a*) and (*c*). The difference between these two measurements is an approximation of the sigma or chi or both phases present in the sample. The results of these measurements indicate that the amount of sigma or chi or both phases in modified Type 316 steel was between 0.5 and 1 per cent, whereas the amount present in the regular Type 316 steel was between 2 and 3 per cent.

TABLE 6—LINEAR THERMAL-EXPANSION CHARACTERISTICS OF MODIFIED TYPE 316 AND AISI TYPE 316 STAINLESS STEELS.[a]

Temperature Range, deg F	Coefficient of Linear Expansion,[b] in./in./deg F × 10^{-6}
STEEL D (MODIFIED TYPE 316 STEEL—14% CR)	
80 to 600	9.8
80 to 1000	10.1
80 to 1200	10.3
80 to 1500	10.6
STEEL F (AISI TYPE 316 STEEL)	
80 to 600	9.6
80 to 1000	9.9
80 to 1200	10.1
80 to 1500	10.3

[a] Note—The steels were annealed at 1975 F for ½ hr and water-quenched prior to testing.
[b] The results shown were obtained on single specimens, and the measurements were made at a heating and cooling rate of 250 F per hr.

Magne-Gage measurements made on both the steels, in the annealed condition and after long-time exposure at elevated temperatures, showed that these steels did not contain a magnetic phase in measurable amounts, that is, in amounts greater than 0.5 per cent.

Thermal Expansion and Hot-Twist Test Results:

The results of dilatometric measurements made from room temperature to 1500 F, which are summarized in Table 6, show that the linear coefficient of expansion of the modified Type 316 steel was slightly higher than that of the regular Type 316 stainless steel. However, the difference may not be statistically significant.

The results of the hot-twist tests conducted on Steel E are shown graphically

in Fig. 8 along with the band of test values exhibited by 14 commercial heats of AISI Type 316 stainless steel. These results indicate that the hot workability of the 14 per cent chromium-modified Type 316 steel, as determined by the number of twists to failure and the shape of the hot-twist curve, is slightly better than that of AISI Type 316 steel.

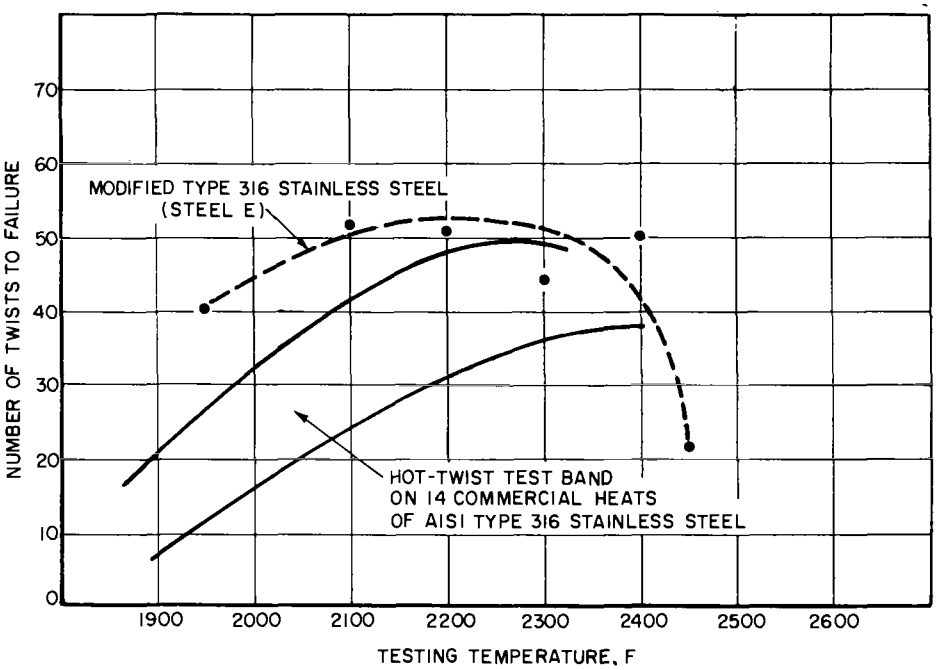


FIG. 8—Effect of Testing Temperature on the Hot Workability of Modified Type 316 Steel and AISI Type 316 Steel as Determined by the Number of Twists to Failure.

SUMMARY

The present investigation was conducted to develop a modified Type 316 steel that would have the strength of AISI Type 316 steel but greater toughness after long-time exposure at elevated-temperatures. A steel of this type would be suitable for such applications as super-heater tubes that require 20-year service at 1200 F. In the present study, the effect of lowering the chromium or chromium and molybdenum content of AISI Type 316 steel was determined. The results are summarized as follows:

1. A modified Type 316 stainless steel with about 14 per cent chromium has room- and elevated-temperature mechanical properties similar to those of AISI Type 316 steel.

2. The room-temperature impact strength of the modified Type 316 steel after long-time elevated-temperature exposure was superior to that of Type 316 stainless steel.

3. The results of X-ray diffraction and metallographic studies indicated that the modified steel is more resistant to sigma formation than is Type 316 steel.

4. The linear coefficient of expansion of the modified Type 316 steel was slightly greater than that of Type 316 steel, although the difference may not be statistically significant.

5. The results of hot-twist tests indicate that the hot workability of the low-chromium Type 316 steel is slightly better than that of AISI Type 316 steel.

Acknowledgment:

The authors are indebted to their associates at U. S. Steel and in particular to D. E. Hickman, who conducted the elevated-temperature tests, P. H. Stoll, who conducted the X-ray studies, and J. M. Heffernan, who conducted the metallographic studies.

REFERENCES

(1) E. J. Dulis and G. V. Smith, "Identification and Mode of Formation and Re-Solution of Sigma Phase in Austenitic Chromium-Nickel Steels," *The Nature, Occurrence, and Effects of Sigma Phase, ASTM STP 110,* Am. Soc. Testing Mats., 1950, p. 3.

(2) L. Zwell, E. J. Fasiska, and F. von Gemmingen, "X-Ray Identification of Phases on Type 316 Austenitic Stainless Steels Subjected to Creep Rupture," *Transactions of Metallurgical Soc.*, Am. Institute Mining, Metallurgical, and Petroleum Engrs., Vol. 224, February, 1962, pp. 198–200.

(3) F. B. Foley, "The Sigma Phase," *Alloy Casting Bulletin No. 5,* July, 1945.

(4) C. A. Zapffe, *Stainless Steels,* Am. Soc. Metals, Cleveland, Ohio, 1949, pp. 231–233.

(5) G. V. Smith, *Properties of Metals at Elevated Temperatures,* McGraw-Hill Book Co., Inc., New York, N. Y., 1950, pp. 335–336.

(6) R. T. Howard and M. Cohen, "Quantitative Metallography by Point Counting and Linear Analysis," *Transactions,* Am. Institute Mining, Metallurgical, and Petroleum Engrs., Vol. 172, 1947, pp. 413–426.

(7) G. V. Smith, F. Garofalo, R. W. Whitmore, and R. R. Burt, "Creep-Rupture Strength of Austenitic Cr-Ni-Mo Steels in Sheet and Bar Form," *Transactions,* Am. Soc. of Mechanical Engrs., Vol. 81, December, 1959, pp. 610–616.

EFFECT OF COMPOSITION AND SECTION SIZE ON MECHANICAL PROPERTIES OF SOME PRECIPITATION HARDENING STAINLESS STEELS

By W. C. Clarke, Jr.[1] and H. W. Garvin[2]

Synopsis

Applications have developed in which the high-strength properties associated with precipitation hardening stainless steel alloys are of considerable interest in large and medium section sizes. In a number of instances, transverse loading is involved. In common with other high strength materials, ductility in the transverse direction is lower than in the longitudinal direction. This paper presents transverse tension data obtained on a number of these alloys which serve to define this characteristic in a variety of shapes and sizes. The alloys discussed are 17-7 PH, PH 15-7 Mo, PH 13-8 Mo, 17-4 PH, and 15-5 PH. It is demonstrated that structural characteristics, particularly delta ferrite and certain precipitates, markedly influence transverse ductility and, in large sections of 17-7 PH and PH 15-7 Mo, longitudinal ductility. Vacuum remelting does not help the directional ductility characteristics in compositions in which delta ferrite is a major controlling factor. Alloys in which composition changes have been incorporated to vary these structural factors have been developed. One of these is PH 13-8 Mo which is a composition employing aluminum as a hardening agent in which the analysis is adjusted to eliminate delta ferrite. This steel has excellent transverse ductility, especially in products made from double vacuum melted ingots. Another new material which has been called 15-5 PH contains copper as a hardening agent and is free of delta ferrite. In this modified composition the transverse ductility across the dead center of large sections is somewhat inferior to the transverse ductility obtainable at intermediate and surface locations in products made from air-melted ingots. Consumable electrode vacuum remelting eliminates the lower dead center transverse ductility in delta ferrite free products, such as 15-5 PH, by minimizing gross segregation, and excellent transverse ductility is obtained in any location.

Some discussion is presented on the effects of varying heat treatments on transverse ductility of several of these steels.

In recent years a class of alloys known broadly as the precipitation hardening stainless steels has become of increasing importance in a variety of applications because of having certain attractive characteristics. In general, the most important of these are ease of fabricability, attainment of high strengths with relatively good ductility by simple heat treating procedures applied after fabrication, and excellent corrosion resistance. For the purpose of this presentation, the term precipitation hardening stainless steels refers to Group I and Group II alloys according to a previously published method of classification.[3] Group I alloys are martensitic as solution treated and are hardened by a simple low temperature precipitation hardening treatment. Alloys of this type are: Stainless W, 17-4 PH, PH 13-8 Mo, and 15-5 PH. Group II alloys are essentially austenitic as solution treated. They become martensitic after an intermediate treatment and are then hardened by a simple low-temperature precipitation-hardening treatment. Alloys of this type are 17-7 PH, PH 15-7 Mo, AM 350, AM 355, and the new PH 14-8 Mo.

In common with most high-strength materials, these alloys do not have the same mechanical properties transverse to the principal direction of rolling or forging as they do longitudinally. Primarily there may be a substantial difference in ductility as measured in a tension test with other properties such as tensile or yield strength often little affected. This paper presents work which has been done to study this problem in some of these materials and presents data on alloys designed to be better in this regard.

Of the alloys discussed in this paper, the Group II alloys, 17-7 PH and PH 15-7 Mo, are poorest with respect to transverse ductility in large sections and in through thickness ductility in flat rolled products. In spite of this characteristic tons of these materials have been used successfully in a myriad of critical applications. This has been particularly true in thin flat rolled products where through thickness loading is rarely of any significance. In addition, ductility in any direction in which a stress is normally applied in thin section extrusions has been shown to be perfectly adequate for safe use. In many instances forgings of these materials have been applied successfully and safely where forging configuration has permitted directional flow to be developed sufficiently in the direction of load application.

The alloys studied in some detail by the authors on which data are presented are 17-7 PH, PH 15-7 Mo, PH 13-8 Mo, 17-4 PH, and 15-5 PH.

The tension tests described in this report were carried out in accordance with ASTM Method E 8.[4]

17-7 PH and PH 15-7 Mo

These two compositions are discussed together because they have essentially the same transverse ductility characteristics. Typical analyses of them, as well as of the other grades referred to in this paper, are shown in Table 1.

PH 15-7 Mo is a modification of 17-7 PH in which molybdenum has been substituted in part for chromium to obtain higher mechanical properties and improved elevated temperature properties.

Group II alloys must have closely controlled chemistry so that they will remain austenitic as solution annealed but be unstable sufficiently so that transformation to martensite will occur when either one of two types of intermediate heat treatments is applied. At the chromium levels involved, necessary composition balances result in a second-

[1] Senior research engineer, Research and Technology, Armco Steel Corp., Baltimore, Md.

[2] Research engineer, Research and Technology, Armco Steel Corp., Baltimore, Md.

[3] L. F. Weitzenkorn, "Classifying the Precipitation Hardening Stainless Steels," Regional Technical Meetings of AISI, 1958, pp. 423–431.

[4] Methods of Tension Testing of Metallic Materials (E 8), *1964 Book of ASTM Standards*, Part 30.

Copyright© 1965 by ASTM International

www.astm.org

ary structural phase which consists of fairly substantial amounts of delta ferrite. This phase may constitute as much as 12 to 30 per cent of the structure in these two alloys. Delta ferrite has been observed to detract from transverse ductility in other martensitic stainless steels,[5] and it does so in these alloys. It has been found that the size and shape which the delta ferrite pools develop as the product is hot worked from the ingot has a controlling effect on ductility in any given direction. In Table 2 are illustrations of this difference in directionality in various hot worked configurations of both 17-7 PH and PH 15-7 Mo. It will be noted that even longitudinal ductility may be quite poor in sections 6 by 6 in. and larger. This is because the original delta ferrite in the ingot has not been elongated much and still presents a large area in terms of individual pools normal to the direction of the tension test.

As illustrated by the data in this table, when an item such as the flat rolled plate has been given sufficient reduction so that very thin rather than broad ferrite pool faces exist normal to the direction of tension testing, the long transverse ductility is quite satisfactory.

Such items when tested through the thickness which is in a direction in which broad areas of individual ferrite pools exist normal to the tension specimen exhibit virtually nil ductility. Figures 1–5 illustrate in three dimensional perspective the ferrite configurations in some typical sections of items in Table 2. It can be theorized on the basis of the structures shown and the levels of ductility associated with them in the various directions that there is a critical length/width ratio for individual pools of ferrite normal to the tension testing direction above which cracks of a critical size are readily generated at the ferrite martensite interfaces. The easy propagation of these cracks results in low or nil ductility. When these steels are given conditioning treatments which raise the martensite transformation (M_s) temperature so that a martensitic transformation occurs either above room temperature or at −100 F, a carbide precipitation occurs principally at the ferrite austenite interfaces. During these treatments in addition to the carbide precipitation, the ferrite pool appears to shrink and a rim of what seems to be a brittle martensite results within the rim of carbides. Numerous metallographic studies indicate that fracture of the tension specimen preferentially follows this rim. In Fig. 6 a typical cross section of a fractured face of a transverse tension specimen made on a large

TABLE 1—TYPICAL COMPOSITIONS OF ALLOYS DISCUSSED.

Alloy	C	Mn	Si	Cr	Ni	Mo	Al	Cu	Cb + Ta
17-7 PH	0.07	0.50	0.30	17.00	7.10	...	1.17	...	...
PH 15-7 Mo	0.07	0.50	0.30	15.10	7.10	2.25	1.17	...	...
PH 13-8 Mo	0.04	0.40	0.30	12.75	8.10	2.15	1.05	...	...
17-4 PH	0.04	0.28	0.60	16.00	4.25	...	...	3.30	0.23
15-5 PH	0.04	0.25	0.40	15.00	4.60	...	...	3.30	0.23

TABLE 2—TYPICAL MECHANICAL PROPERTIES OF AIR MELTED AND VACUUM REMELTED 17-7 PH AND PH 15-7 MO IN VARYING SECTION SIZES.

Grade	Melting Method	Condition[a]	Section Size, in.	Direction[b]	Location[c]	Ultimate Tensile Strength, psi	Yield Strength, 0.2 % Offset, psi	Elongation in 4 × D, %	Reduction of Area, %
17-7 PH	arc air	TH 1050	12 by 12	L	I	180 000	...	BOG	nil ductility
				T	I	155 000	...	1.0	0.0
17-7 PH	vacuum remelted	TH 1050	12 by 12	L	I	194 000	178 000	6.0	5.0
				T	I	155 000	...	0.0	1.0
PH 15-7 Mo	arc air	TH 1050	9½ by 9½	T	I	167 000	161 000	1.5	1.0
17-7 PH	arc air	TH 1050	6 by 6	L	I	169 000	...	2.0	2.0
				T	I	140 000	...	0.0	0.0
17-7 PH	vacuum remelted	TH 1050	6 by 6	L	I	179 000	...	8.0	14.0
				T	I	150 000	...	1.0	0.0
PH 15-7 Mo	arc air	TH 1050	4 by 4	L	I	206 000	189 000	9.0	40.0
				T	I	198 000	...	2.0	0.0
17-7 PH	arc air	RH 950	3⅜ϕ	L	I	205 000	181 000	3.0	6.0
				T	C	185 000	...	1.0	0.0
17-7 PH	vacuum remelted	RH 950	3⅜ϕ	L	I	216 000	198 000	7.0	11.0
				T		188 000	...	3.0	2.0
17-7 PH	arc air	TH 1050	2¼ by 2½	L	I	196 000	191 000	11.0	40.0
				LT	I	192 000	...	0.0	0.0
17-7 PH	arc air	TH 1050	4-in. plate	L	...	195 000	...	10.0	25.0
				LT	...	186 000	...	1.0	0.5
				ST	...	112 000	...	broke in threads	
17-7 PH	arc air	TH 1050	2¼-in. plate	L	...	179 000	156 000	12.0	31.0
				LT	...	178 000	154 000	10.0	26.0
				ST	...	113 000	...	0.0	0.0
PH 15-7 Mo	arc air	RH 1050	1⅛-in. plate	L[d]	...	203 000	...	11.0	45.0
				LT[d]	...	199 000	...	10.0	46.0
				ST[d]	...	150 000	...	0.0	0.0
17-7 PH	arc air	TH 1050	0.050 sheet	L	...	193 000	182 000	10.0	...
				T	...	193 000	182 000	10.0	...

[a] Condition: TH 1050—1900 F for 1 hr air cooled plus 1400 F for 1½ hr air cooled plus 1050 F for 1 hr air cooled.
RH 950—1900 F for 1 hr air cooled plus 1750 F for ½ hr air cooled to 55 F within 1 hr plus −100 F for 8 hr plus 950 F for 1 hr air cooled.
RH 1050—same as RH 950 except final age 1050 F for 1 hr air cooled.
[b] Direction: L = longitudinal; T = transverse; LT = long transverse; ST = short transverse.
[c] Location: I = intermediate; C = center.
[d] Miniature tensile specimens 1⅛-in. long. Data courtesy of North American Aviation, Inc., Los Angeles, Calif.

[5] G. E. Dieter, "Effect of Microstructure and Heat Treatment on the Mechanical Properties of AISI Type 431 Stainless Steel," *Transactions*, Am. Soc. Metals, 1958, Vol. 50, pp. 722–737.

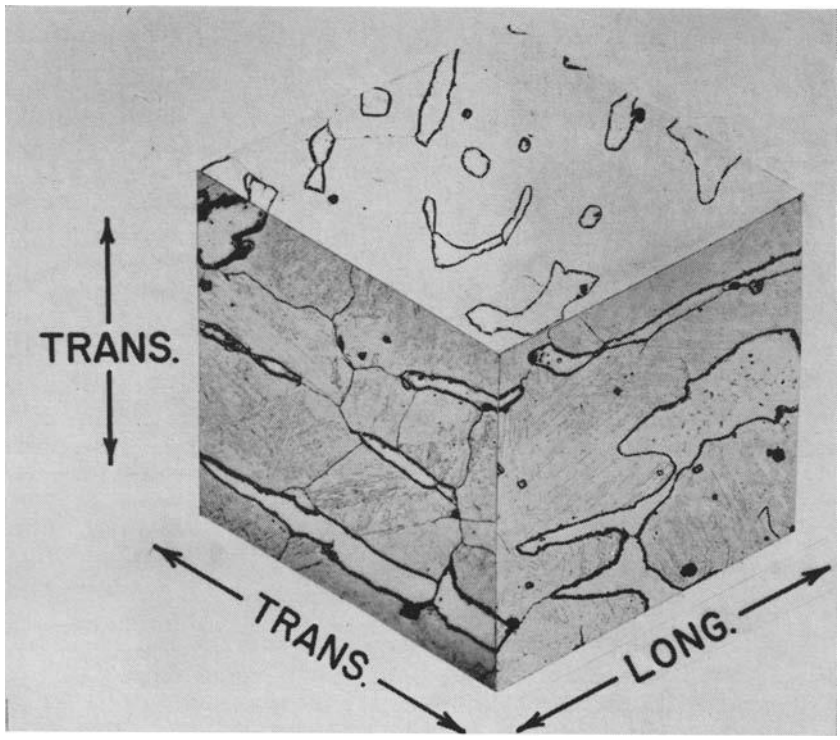


FIG. 1—Synthetic Three-Dimensional Portrayal of Ferrite Distribution in a 12 by 12 in. Section of 17-7 PH. Condition TH1050. Etchant: Picric-Hydrochloric Acid by Immersion (×150).

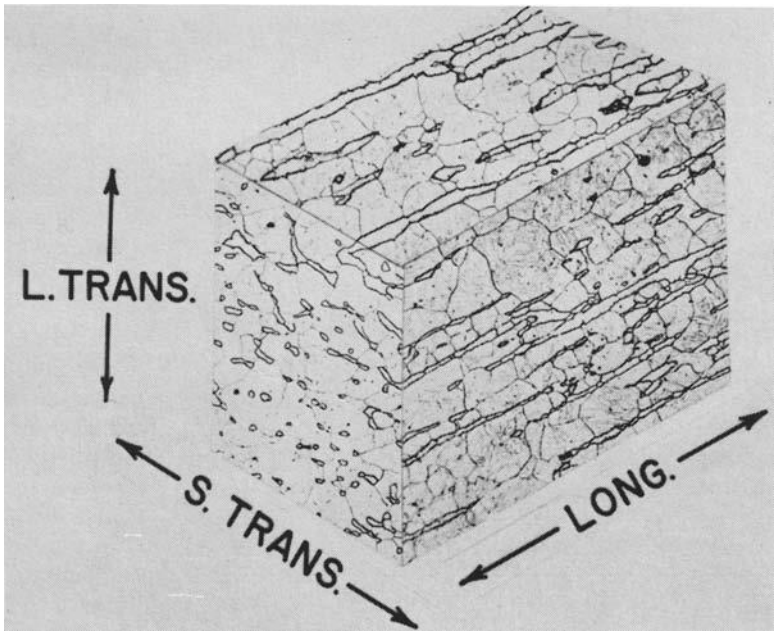


FIG. 2—Synthetic Three-Dimensional Portrayal of Ferrite Distribution in a $2\frac{1}{4}$ by $2\frac{1}{2}$ in. Section of 17-7 PH. Condition TH1050. Etchant: Picric-Hydrochloric Acid by Immersion (×150).

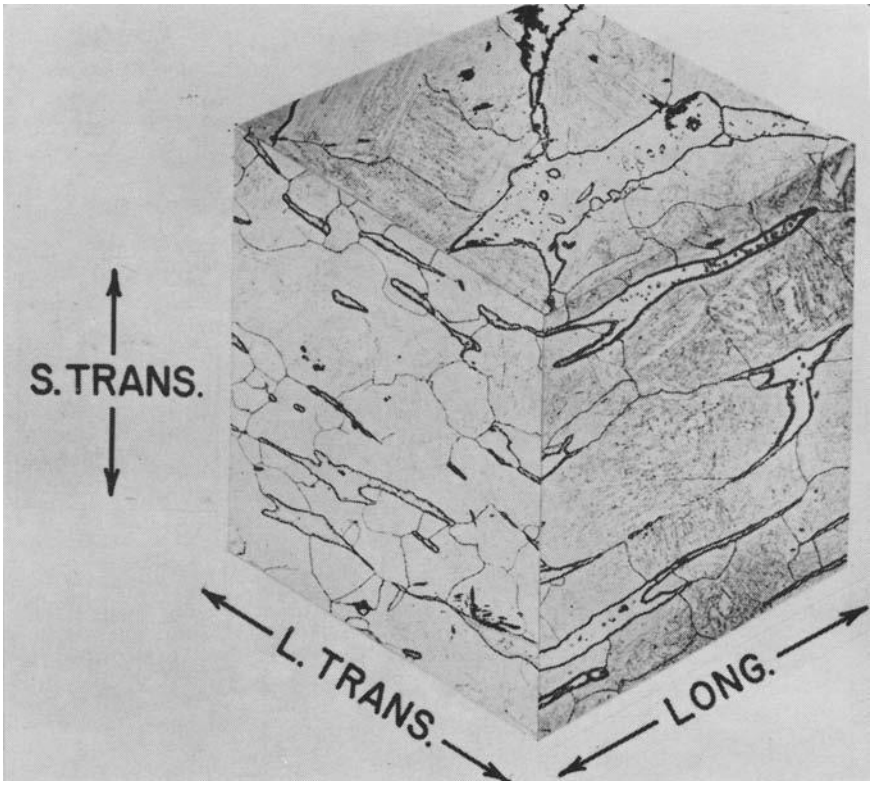


FIG. 3—Synthetic Three-Dimensional Portrayal of Ferrite Distribution in a 4-in.-Thick Plate of 17-7 PH. Condition TH1050. Etchant: Picric-Hydrochloric Acid by Immersion (×150).

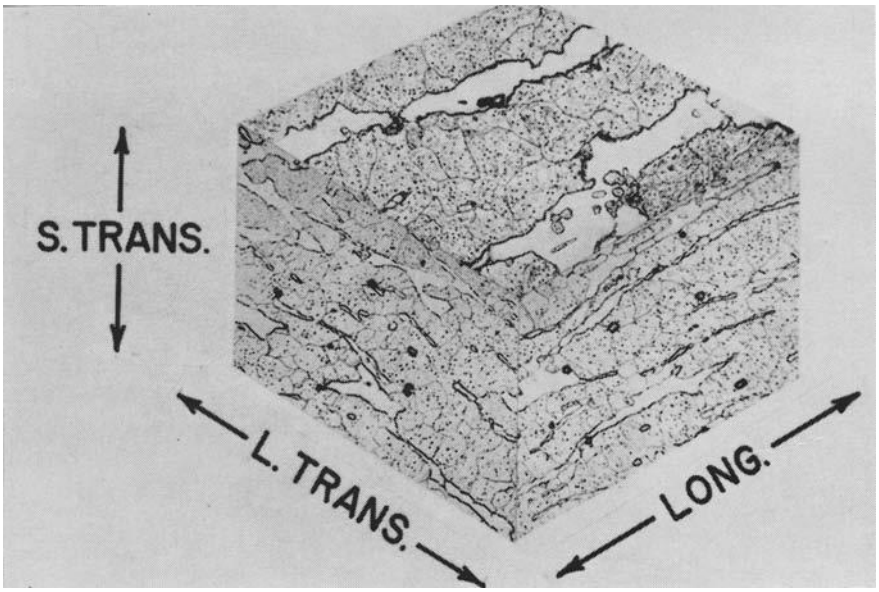


FIG. 4—Synthetic Three-Dimensional Portrayal of Ferrite Distribution in a 2¼-in.-Thick Plate of 17-7 PH. Condition TH1050. Etchant: Picric-Hydrochloric Acid by Immersion (×150).

sized item of 17-7 PH may be seen. It illustrates clearly the part which the delta ferrite and the boundary precipitate play in the path of the fracture. A more enlarged view of the nature of the rim formation is shown in Fig. 7.

In instances where low ductility is as delta ferrite controlled as it is in 17-7 PH and PH 15-7 Mo, vacuum remelting is ineffective in improving this characteristic. This is illustrated by data on vacuum remelted items compared with similar sized items arc air melted made from the same heat of material which are shown adjacent to each other in Table 2.

The effect of a great number of heat treating cycles was investigated in an attempt to find one that would improve the transverse ductility of these grades without a considerable loss in strength. Overaging even at 1150 F did not produce any improvement in this regard. In addition, the effect of prehomogenizing treatments at various times at temperatures up to 2250 F produced no improvement. Variations of solution treating times and temperatures and conditioning treatment times and temperatures were totally ineffectual. One treatment did produce a very slight improvement in ductility in material treated to TH 1050 properties. This consisted of the following sequence applied to A condition treated material —1400 F, 1½ hr air cooled plus 1700 F for 1 hr air cooled plus 1400 F, 1½ hr air cooled plus 1050 F, 1 hr air cooled. This treatment raised the long transverse ductility of the 2¼ by 2½-in. bar item in Table 2 from nil ductility to 4 per cent elongation in 4 × D and 16 per cent reduction of area. This treatment has also been effectively used in improving longitudinal ductility in certain forgings of these grades which were of such shapes that longitudinal ductility was borderline.

As a result of the transverse ductility characteristics of these alloys, there have been areas of application where they have not been usable. Because such areas are important we have studied other high strength precipitation hardening stainless steels designed to have much better transverse properties. One of the directions pursued has led to the development of PH 13-8 Mo.

PH 13-8 Mo

Research work was undertaken to develop an alloy free of delta ferrite in which aluminum was used as the hardening agent which would develop similar strength properties to those of 17-7 PH or PH 15-7 Mo when heat treated through the same cycles. Table 3 illustrates briefly the transition from PH 15-7 Mo to PH 13-8 Mo. As indicated in this table, a marked improvement in transverse ductility is immediately achieved upon elimination of the ferrite. The second heat shown in the series was ferrite free by virtue of its carbon content in combination with the lowered chromium. It was indicated in the course of this research, however, that following certain types of heat treatment undesirable carbide precipitation does develop in the austenitic grain

boundaries which can decrease transverse ductility. Furthermore, carbon aggravates segregation and can lead to problems with transverse ductility caused by retention of austenite. For these reasons, the type of analysis represented in the last two heats of this group was found to be superior. These compositions were low in carbon and were also free of delta ferrite. The alloy so developed is actually a Group I type in that it is martensitic as cooled from solution treatment, and it can be directly hardened with a simple low temperature precipitation hardening treatment. It is, however, compatible in response when given the heat treating cycles normally applied to 17-7 PH and PH 15-7 Mo. This is illustrated by the properties shown in Table 3 which were obtained by using the RH 950 heat treatment.

At the present time a new Group II alloy which has been named PH 14-8 Mo is under active development.[6] It is being evaluated as a possible skin material for the Mach 3 transport for which materials are now under study by NASA. Two of the prime advantages of PH 14-8 Mo which make it superior to prior precipitation hardening stainless steels are greatly increased crack propagation resistance and increased resistance to embrittlement at temperatures of 600 to 800 F.

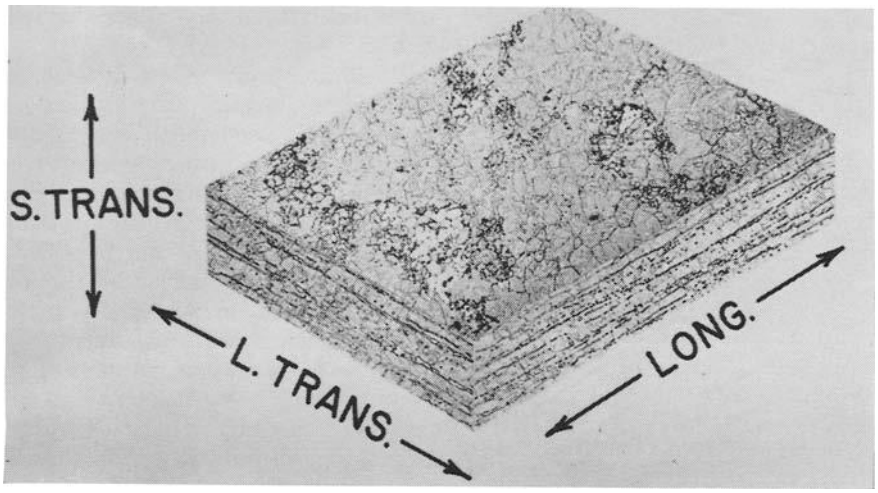


FIG. 5—Synthetic Three-Dimensional Portrayal of Ferrite Distribution in a 0.146-in. Sheet of 17-7 PH. Condition TH1050. Etchant: Picric-Hydrochloric Acid by Immersion (×150).

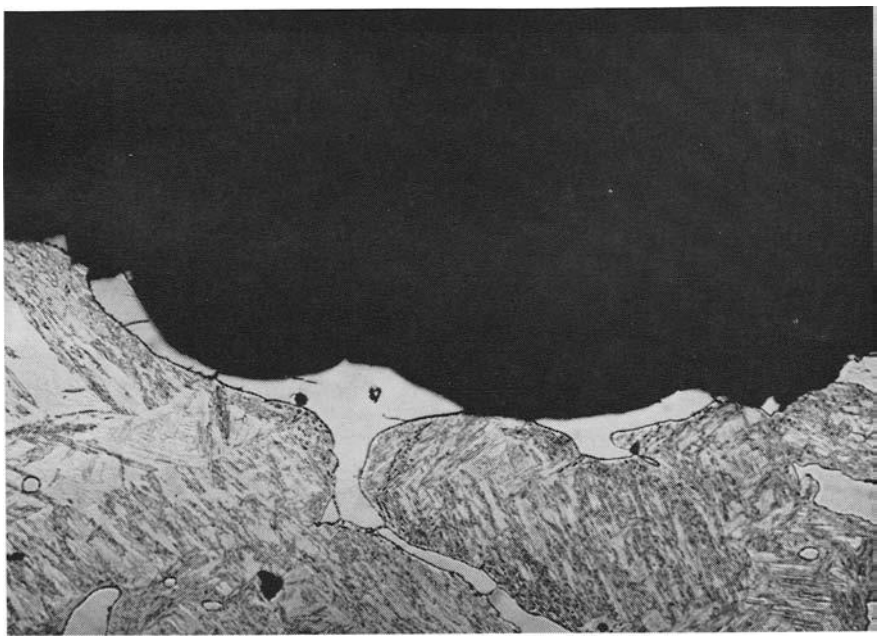


FIG. 6—Preferential Fracture Path Along Ferrite Boundary in Transverse Tension Specimen of 17-7 PH. Condition TH1050. Etchant: Picric-Hydrochloric Acid by Immersion (×250).

PH 13-8 Mo is currently being evaluated as a material for heavy structural members in the proposed Mach 3 transport. Certain advantages have been found in the properties of such materials when the elements manganese, phosphorus, sulfur, silicon, and nitrogen are maintained at low levels. The best levels can only be obtained practically by vacuum induction melting.

PH 13-8 Mo has been made by vacuum induction melting, and the product has then been vacuum remelted to minimize any tendency towards central segregation. Some mechanical properties on this material are shown in Table 4. These data indicate that this product exhibits superlative transverse ductility even through the dead center of configurations where this characteristic is normally most difficult to obtain.

17-4 PH AND 15-5 PH

17-4 PH is a Group I type of alloy and as such has predominantly a martensitic type structure in the solution treated condition. A wide variety of properties can be obtained by applying treatments of from 900 F for 1 hr up to 1150 F for 4 hr. The transverse ductility characteristics of this alloy are much superior to those of 17-7 PH and PH 15-7 Mo. This factor, however, can be variable within the composition limits considered normal.[7] Part of this variability is because of the presence of delta ferrite, and part of it appears to be because of gross segregation effects. Delta ferrite in this alloy normally varies from 0 to about 8 per cent although it can at times be higher in sections 10 in. square or larger, particularly in the central area. Some typical examples of mechanical properties of 17-4 PH in varying section sizes are shown in Table 5. As will be noted in this table, the short transverse ductility through the center of two rectangular sections is quite low. In most cases, however, a respectable level of transverse ductility is obtained. Where delta ferrite is the major controlling factor in terms of transverse ductility, vacuum remelting

[6] D. C. Perry, H. Tanczyn, and W. C. Clarke, Jr., "Developmental PH 14-8 Mo-A Tough High Strength Stainless Steel," *Metal Progress*, June, 1963.

[7] L. P. Spalding, "Precipitation Hardening Stainless Steels in Supersonic Aircraft," *ASM Metals Engineering Quarterly*, Vol. 2, No. 4, November, 1962, pp. 14–20.

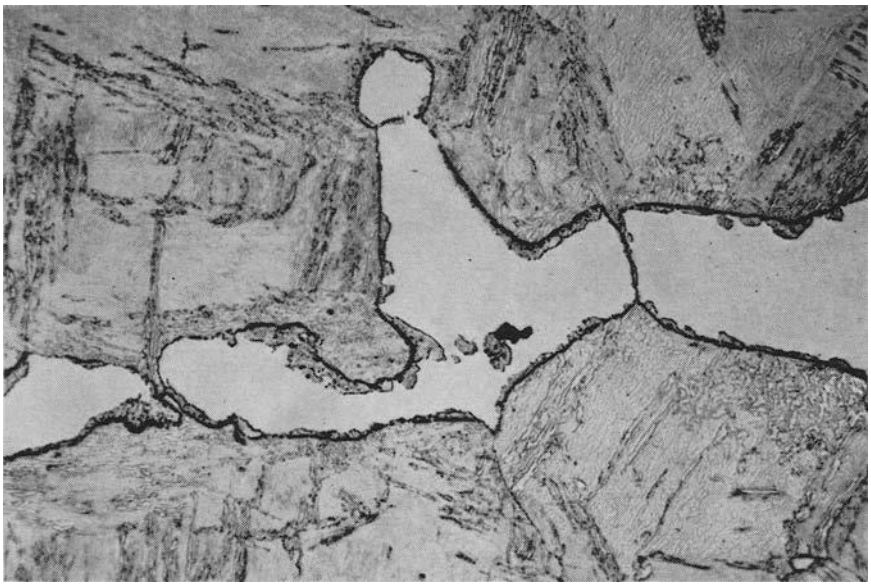


FIG.7— Ferrite Pools in 17-7 PH Showing Rim of Martensitic Phase Inside Precipitated Carbide Boundary. Condition TH1050. Etchant: Sodium Cyanide Electrolytic (×500).

TABLE 3—MECHANICAL PROPERTIES OF SEVERAL VARIATIONS OF ALUMINUM HARDENED PRECIPITATION HARDENING STAINLESS STEELS, CONDITION RH 950.[a]

Composition							Section Size, in.	Direction and Location[b]	Ultimate Tensile Strength, psi	Yield Strength, 0.2% Offset, psi	Elongation in 4 × D, %	Reduction of Area, %
C	Mn	Si	Cr	Ni	Mo	Al						
0.078	0.64	0.39	15.10	7.31	2.19	1.22	1 by 4	LTC	229 000	196 000	3.0	2.0
							½ by 4	LTC	226 000	196 000	2.0	3.0
0.071	0.47	0.30	14.60	7.36	2.21	1.12	1 by 4	LTC	227 000	199 000	9.0	31.0
							½ by 4	LTC	232 000	202 000	10.0	30.0
0.034	0.35	0.35	12.74	7.83	2.20	0.92	4 by 4	TI	226 000	202 000	4.5	15.0
							1 by 4	LTC	222 000	201 000	9.0	37.0
							½ by 4	LTC	224 000	201 000	11.0	38.0
0.025	0.38	0.43	13.08	8.61	2.17	1.02	4 by 4	TI	226 000	204 000	5.8	13.5
							1 by 4	LTC	222 000	205 000	9.0	29.0
							½ by 4	LTC	224 000	202 000	10.0	36.0

[a] 1750 F for ½ hr air cooled plus −100 F for 8 hr plus 950 F for 1 hr air cooled.
[b] LTC = long transverse center; TI = transverse intermediate.

TABLE 4—MECHANICAL PROPERTIES OF DOUBLE VACUUM MELTED PH 13-8 MO.

Section Size, in.	Condition[a]	Direction and Location[b]	Ultimate Tensile Strength, psi	Yield Strength, 0.2 % Offset, psi	Elongation in 4 × D, %	Reduction of Area, %	Charpy V-Notch, ft-lb
9 by 9.....	A 950	LI	218 000	196 000	14.0	37.0	...
		TI	220 000	201 000	13.0	31.0	...
		TC	213 000	190 000	14.0	33.0	...
3 by 8.....	A 950	LI	214 000	188 000	16.0	66.0	18
		LTC	220 000	198 000	14.0	63.0	...
		STC	218 000	193 000	14.0	53.0	...
3 by 8.....	A 1000	LI	217 000	188 000	16.0	66.0	50
	A 1050	LI	195 000	187 000	15.0	69.0	111
	A 1100	LI	173 000	162 000	18.0	72.0	149
3 by 8.....	O RH 950	LI	225 000	204 000	14.0	66.0	28
		STC	223 000	200 000	13.0	61.0	...

[a] A 950—1825 F for ½ hr air cooled plus 950 F for 1 hr air cooled.
A 1000—1825 F for ½ hr air cooled plus 1000 F for 1 hr air cooled.
A 1050—1825 F for ½ hr air cooled plus 1050 F for 1 hr air cooled.
A 1100—1825 F for ½ hr air cooled plus 1100 F for 1 hr air cooled.
O RH 950—1150 F for 4 hrs air cooled plus 1700 F for 1 hr air cooled plus −100 F for 8 hr plus 950 F for 1 hr air cooled.
[b] LI = longitudinal intermediate; TC = transverse center; STC = short transverse center.

does not change the level of ductility perceptably as is illustrated in this table. Most of the cases of low transverse ductility observed in this material are in products which are heat treated to maximum or near maximum obtainable strength levels. This does not apply frequently in sections of sizes 10 by 10 in. and larger where even overaged material may have a low level of transverse ductility across the dead center. Figure 8 is a photograph of a cross section of a fractured end of a transverse tensile, and it illustrates the way in which the fracture tends to develop along the ferrite pools.

Heat treatment does influence the transverse ductility of this grade as shown in Table 6 which illustrates the fact that in many instances use of higher aging temperatures markedly improves this property. Table 7 shows the effect of applying a homogenizing treatment of 2150 F for 1½ hr and cooling to room temperature followed by a normal solution treatment and subsequent aging. Such homogenization improves transverse ductility to some extent. This treatment appears to be most effective when applied to sections of intermediate size but is not always effective in larger sections. Because of the fact that there are applications where full strength properties are desired which require good short transverse ductility, and because there are applications for large sections, that is, 10 by 10 in. to 16 by 16 in. which are used overaged in which transverse ductility across the dead center is important, a modified composition of this alloy has been developed directed at these applications. This composition in which chromium has been lowered and nickel slightly raised is designed to be free of delta ferrite and is known as 15-5 PH.

Some typical mechanical properties of air melted and vacuum remelted 15-5 PH items in the H 900 condition are shown in Table 8. It will be noted that in the one air melted section shown in this table the dead center short transverse ductility is significantly lower than that obtainable in the same direction at the edge and intermediate. This difference is the result of the effect of gross segregation phenomenon which we are studying currently in an attempt to further improve properties in air melted material in this region. As can be seen in this table when 15-5 PH is vacuum remelted, an excellent level of transverse ductility is obtained across the dead center of a variety of shapes. It is evident that this material, particularly when vacuum remelted, has considerable merit.

TABLE 5—MECHANICAL PROPERTIES OF 17-4 PH IN VARYING SECTION SIZES.

Melting Method	Condition[a]	Section Size, in.	Direction[b]	Location[c]	Ultimate Tensile Strength, psi	Yield Strength, 0.2% Offset, psi	Elongation in 4 × D, %	Reduction of Area, %
Arc air	H 900	12 by 12	L	I	198 000	173 000	13.0	36.0
			T	I	193 000	171 000	7.0	12.0
Vacuum remelted	H 900	12 by 12	L	I	196 000	176 000	13.0	38.0
			T	I	197 000	176 000	4.0	7.0
Arc air	H 900	6 by 6	L	I	198 000	174 000	15.0	49.0
			T	I	199 000	176 000	11.0	29.0
Vacuum remelted	H 900	6 by 6	L	I	201 000	181 000	16.0	52.0
			T	I	199 000	178 000	10.0	30.0
Arc air	H 925	3½ by 3½	L	I	202 000	180 000	15.0	50.0
			T	I	203 000	177 000	11.0	31.0
Arc air	H 950	3 by 11½[d]	LT	C	192 000	174 000	13.0	42.0
			ST	C	185 000	171 000	3.0	5.0
Arc air	H 950	5 by 10[d]	L	I	197 000	178 000	12.0	35.0
			LT	C	197 000	172 000	11.0	23.0
			ST	C	192 000	171 000	2.0	3.0
Arc air	H 950	3 in. thick[d] plate cross rolled	L	...	195 000	168 000	14.0	47.0
			LT	...	195 000	175 000	17.0	52.0
			ST	...	194 000	175 000	12.0	31.0

[a] H 900—1900 F for 1 hr air cooled plus 900 F for 1 hr air cooled.
H 925—1900 F for 1 hr air cooled plus 925 F for 4 hr air cooled.
H 950—1900 F for 1 hr air cooled plus 950 F for 4 hr air cooled.
[b] L = longitudinal; T = transverse; LT = long transverse; ST = short transverse.
[c] I = intermediate; C = center.
[d] Data courtesy of North American Aviation, Inc., Los Angeles, Calif.

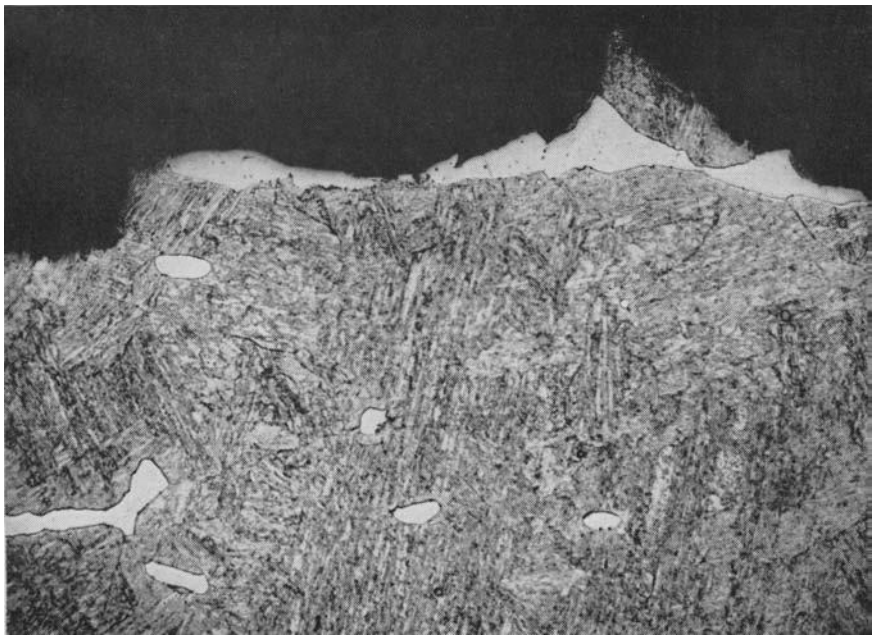


FIG. 8—Preferential Fracture Path Along Ferrite Boundary in Transverse Tension Specimen of 17-4 PH. Condition H900. Etchant: Picric-Hydrochloric Acid by Immersion (×250).

TABLE 6—EFFECT OF OVERAGING ON TRANSVERSE DUCTILITY OF 17-4 PH.

Plate Thickness, in.	Direction[a]	Condition[b]	Ultimate Tensile Strength, psi	Yield Strength, 0.2% Offset, psi	Elongation in 4 × D, %	Reduction of Area, %
4	L	H 925	183 000	177 000	16.0	55.0
	ST		184 000	...	5.5	3.2
4	L	H 1025	163 000	160 000	17.3	57.0
	ST		163 000	159 000	12.0	28.0
4	L	H 1075	155 000	147 000	17.5	61.0
	ST		154 000	148 000	10.0	21.0
4	L	H 1150	148 000	136 000	20.0	63.0
	ST		148 000	134 000	13.0	31.0

[a] L = longitudinal; T = transverse; ST = short transverse.
[b] H Conditions all 4 hr at temperature indicated; 1900 F for 1 hr air cooled, A condition precedes all H treatments.

SUMMARY OF CONCLUSIONS

It is concluded from the work presented that:

1. Alloys of the character of 17-7 PH and PH 15-7 Mo have inherently poor transverse ductility in larger sections and in the short transverse direction in thinner sections.

2. The presence of substantial amounts of delta ferrite and of precipitation at the rim of the delta ferrite pools is largely responsible for this characteristic.

3. The shape and size of the delta ferrite pools in terms of the individual pool length to width ratio normal to the direction of testing is important in effecting ductility. In sections 6 by 6 in. and larger, 17-7 PH and PH 15-7 Mo exhibit low longitudinal ductility because insufficient reduction has left unfavorably shaped delta ferrite pools normal to the longitudinal direction.

4. Heat treatments of any type were not significantly effective in improving the transverse ductility of 17-7 PH or PH 15-7 Mo.

5. Vacuum remelting does not improve transverse ductility in 17-7 PH and PH 15-7 Mo.

6. A new precipitation hardening stainless steel using aluminum as the hardening agent has been made which is free of delta ferrite and is compatible in heat treatment response with 17-7 PH and PH 15-7 Mo. This alloy designated as PH 13-8 Mo has good transverse ductility particularly when double vacuum melted by induction and remelt techniques.

7. 17-4 PH has relatively good transverse ductility characteristics, but they are variable largely because of variations in delta ferrite content.

8. Overaging will in many instances induce a marked improvement in transverse ductility in 17-4 PH but frequently will not improve center transverse ductility in sections 10 by 10 in. and larger. An homogenizing heat treatment of 2150 F applied prior to the normal solution treatment has been helpful in improving the transverse ductility of 17-4 PH particularly in products of smaller cross sections.

9. A modified copper containing precipitation hardening stainless steel designated as 15-5 PH is free of delta ferrite and has improved transverse ductility compared to 17-4 PH. Center transverse ductility is still lower than edge and

TABLE 7—EFFECT OF HOMOGENIZING HEAT TREATMENT ON TRANSVERSE DUCTILITY OF 17-4 PH.

Section Size, in.	Direction[a]	Location	Condition[c]	Ultimate Tensile Strength, psi	Elongation in 4 × D, %	Reduction of Area, %
4ϕ	T	C	H 925	187 000	2.8	7.3
			Ho + A + H 925	190 000	5.0	7.0
4-in.-thick plate	ST	I	H 925	184 000	5.6	3.1
			Ho + A + H 925	195 000	11.5	26.0
6-in.-thick plate	ST	I	H 925	191 000	1.0	14.3
			Ho + A + H 925	193 000	10.0	24.5

[a] L = longitudinal; T = transverse; ST = short transverse.
[b] C = center; I = intermediate.
[c] H conditions all 4 hr at temperature indicated; 1900 F for 1 hr air cooled, A condition precedes all H treatments. Ho 2150 F for 1½ hr air cooled.

TABLE 8—MECHANICAL PROPERTIES OF AIR MELTED AND VACUUM REMELTED 15-5 PH IN THE H 900[a] CONDITION.

Melting Method	Section Size, in.	Direction[b]	Location[c]	Ultimate Tensile Strength, psi	Yield Strength, 0.2 % Offset, psi	Elongation in 4 × D, %	Reduction of Area, %
Arc air	12 by 14	ST	E	188 000	172 000	11.0	36.0
		ST	I	188 000	172 000	11.0	32.0
		ST	C	186 000	176 000	4.0	9.0
Vacuum remelted	12 by 14	ST	E	186 000	172 000	11.0	34.0
		ST	I	186 000	174 000	11.0	35.0
		ST	C	186 000	170 000	11.0	32.0
Vacuum remelted	3 by 5½	L	I	188 000	187 000	15.0	54.0
		ST	C	189 000	...	14.0	46.0
Vacuum remelted	3½ by 12	L	I	187 000	185 000	15.0	50.0
		ST	C	190 000	...	14.0	48.0
Vacuum remelted	3½ by 15½	L	I	193 000	190 000	11.0	40.0
		ST	C	193 000	192 000	8.0	28.0
Vacuum remelted	4 by 24	L	I	194 000	189 000	12.0	40.0
		ST	C	194 000	189 000	12.0	36.0

[a] 1900 F for 1 hr air cooled plus 900 F for 1 hr air cooled.
[b] L = longitudinal; ST = short transverse.
[c] E = edge; I = intermediate; C = center.

intermediate in products made from air cast ingots. This is evidently the result of gross segregation. Vacuum remelting overcomes this problem and imparts excellent transverse ductility to this alloy in any location.

Acknowledgments:

The authors wish to acknowledge the assistance of many members of the staff of Research and Technology of the Armco Steel Corp. for invaluable assistance in carrying out the work presented. They wish to particularly acknowledge the work of R. H. Mackenzie, metallographer, for preparation of the photomicrographs and of M. Clogg, Jr., research engineer, for conducting much of the test work described. The authors wish also to thank F. K. Bloom, manager of the Baltimore Research Laboratories for his invaluable suggestions with respect to the manner of presentation.

NEW CAST HIGH-STRENGTH ALLOY GRADES BY STRUCTURE CONTROL

By F. H. Beck;[1] E. A. Schoefer,[2] Personal Member, ASTM; J. W. Flowers;[3] and M. G. Fontana[4]

Synopsis

As normally made commercially, the CF type cast alloys (19 per cent chromium, 9 per cent nickel) are austenitic, but may contain from 0 to 50 per cent ferrite depending on the balance among the constituent elements within the chemical ranges specified for the various grades. Statistical analysis of mechanical properties of many heats produced by a number of foundries has demonstrated that strength and ductility are functions of the ferrite content in these alloys. At room temperature, strength increases substantially but ductility decreases only slightly with increasing ferrite content. A series of alloys has been studied to determine the effect of ferrite content on their strength at elevated temperature (up to 1200 F) and on their susceptibility to form sigma phase after long exposure at elevated temperature. Results indicate that alloys containing 20 to 30 per cent ferrite have improved strength without detrimental loss of ductility or impact strength at temperatures of 800 F or below.

About ten years ago a considerable mass of data on mechanical properties of cast corrosion resistant alloys was assembled by the Alloy Casting Institute for the purpose of establishing the "representative" values for each alloy type as made commercially. Statistical analyses of the data showed that for most of the alloys the spread of properties was fairly consistent from producer to producer. In general, the ultimate tensile strengths, yield strengths, and elongations were found to be normally distributed and could be characterized by the usual statistics of "mean value" and "standard deviation." For several alloys, however, the mean values of the samples reported by the various producers showed significant differences and when grouped together the frequency distribution of the data departed from the normal error function curve. The CF-8 alloy type (nominal composition: 19 chromium, 9 nickel, 0.08 carbon max) and the related higher carbon CF-20 and molybdenum-containing CF-8M types, were notable in this respect. Because the representative property values for these grades were well above minimum specification requirements, they were published along with those of the other alloy types (1).[5] Subsequently, some producers when called on to make nonmagnetic castings in the CF-8 composition found that many of the heats would not meet minimum strength specifications.

The data were restudied by one of the authors (2) to determine whether the tensile properties showed significant correlation with the ferrite contents of the specimens. Although the CF-8 alloy has an essentially austenitic structure, it may contain from zero up to about 35 per cent ferrite depending on the balance of the constituent elements within the stated chemical ranges for the grade. Wholly austenitic alloys such as the CK-20 type (25 chromium, 20 nickel) have somewhat lower average tensile strength than CF-8, but values for the strongly ferritic type CE-30 (29 chromium, 9 nickel) are considerably higher than the CF-8 average. Thus, it was postulated that the wide range of properties observed for the CF-8 alloy was related to the variations in structure that might occur as the composition balance fell on one side or the other of the austenite boundary line.

Tensile properties of 298 compositions in the CF-8 range were analyzed. Of the eight companies that supplied data, five companies each gave results of 25 tests, one gave 26 tests, another 30 tests, and the last gave 117 tests. The distribution of the reported tensile strengths grouped in class intervals of two thousand psi is shown in Fig. 1. Except for the large 117 test group, the samples are distributed in approximately symmetrical fashion about their modal class. If such a distribution of strengths as shown for the entire 298 test array were truly representative of all CF-8 alloys, then such a spread between the modal classes as exhibited by Companies B and C, for example, would occur by chance less than once in several billion times. Accordingly, it may be inferred that these samples are significantly different.

Direct measurement of ferrite content was impossible for the specimens, but an estimate was made from the chemical composition of each heat by means of the constitution diagram developed by Schaeffler (3) in connection with the study of ferrite content in chromium-nickel alloy welds. This diagram requires the conversion of all ferrite-promoting elements into "chromium equivalents" and all austenite-promoting elements into "nickel equivalents" through the use of factors chosen to represent the ferritizing or austenitizing power of each element. The lines delineating constant ferrite contents on this diagram are not constant ratios of the chromium and nickel equivalents. To obtain such constant ratios it is necessary to shift the coordinates of the diagram so that the origin is at the intersection of the constant-ferrite-content lines. This is accomplished by subtracting 4.99 from the chromium equivalent and adding 2.77 to the nickel equivalent when using the following factors for the elements:

Ferritizing		
Chromium	1.0	
Silicon	1.5	
Molybdenum	1.0	
Columbium	1.0	
Austenitizing		
Nickel	1.0	
Manganese	0.5	
Carbon	30.0	
Nitrogen	26	(N > 0.02)

The factor of 26 for nitrogen is based on

[1] Professor, Department of Metallurgical Engineering, The Ohio State University, Columbus, Ohio.

[2] Executive vice president, Alloy Casting Inst., New York, N. Y.

[3] Army Materials Research Agency, Watertown Arsenal, Watertown, Mass.

[4] Professor and chairman, Department of Metallurgical Engineering, The Ohio State University, Columbus, Ohio.

[5] The boldface numbers in parentheses refer to the list of references appended to this paper.

Copyright© 1965 by ASTM International

www.astm.org

work by Binder, Brown, and Franks (4) and when applied to nitrogen present in excess of 0.02 per cent appears to compensate successfully for nitrogen variations in estimating the ferrite content of the CF-8 alloy.

A "composition ratio" of the chromium to the nickel equivalents (modified as described above) can be computed from the chemical composition of each heat, and facilitates considerably statistical analysis of the test data. This ratio is related to ferrite content as shown in Fig. 2 where the curve is derived from the Schaeffler diagram and the data points are from the present research and a previous study by Fontana (5).

From the correlations found between the composition ratio and the tensile properties of the 298 heats investigated, Schoefer (2) concluded that tensile and yield strengths of the CF-8 alloys were direct functions of ferrite content and that there was a significant but slight negative correlation of ferrite content and ductility. He indicated that by balancing the compositions to provide a controlled minimum ferrite content, a producer should be able to supply CF-8 type castings of higher minimum strength levels than set forth in current specifications such as ASTM Specifications A 296[6] or A 351.[7]

Further analyses of commercial heats have been made to corroborate the earlier investigation. Figures 3 and 4 show the regression lines for a sample of 277 heats of CF-8 and 62 heats of CF-8M produced by one foundry. The chemical compositions of all of these heats were determined spectrographically and the tension tests made under essentially identical conditions by the producer. In addition, ferrite determinations (by Magne-Gage) were made on 50 heats after solution annealing treatment. Because nitrogen contents were not obtained, the data were adjusted for nitrogen content in computing the composition ratio by a factor derived from the 50 heats for which ferrite content was known. The slope of the regression line in Fig. 3 is in agreement with the earlier work as is width of the scatter band. The outer lines representing ± two standard deviations indicate that about 95 per cent of all heats of CF-8 or CF-8M with a given composition ratio (or ferrite content) should have tensile strengths falling within these limits. The experimental heats used in the investigation at Ohio State University are plotted on this chart and are in reasonable agreement except for the 16 per cent ferrite heat P-CF8M-16 which seems a little on the strong side. On the other hand, in Fig. 4, most of the yield strengths for the experimental heats fall significantly above the band based on commercial heats. No explanation can be offered other than a possible difference in testing technique.

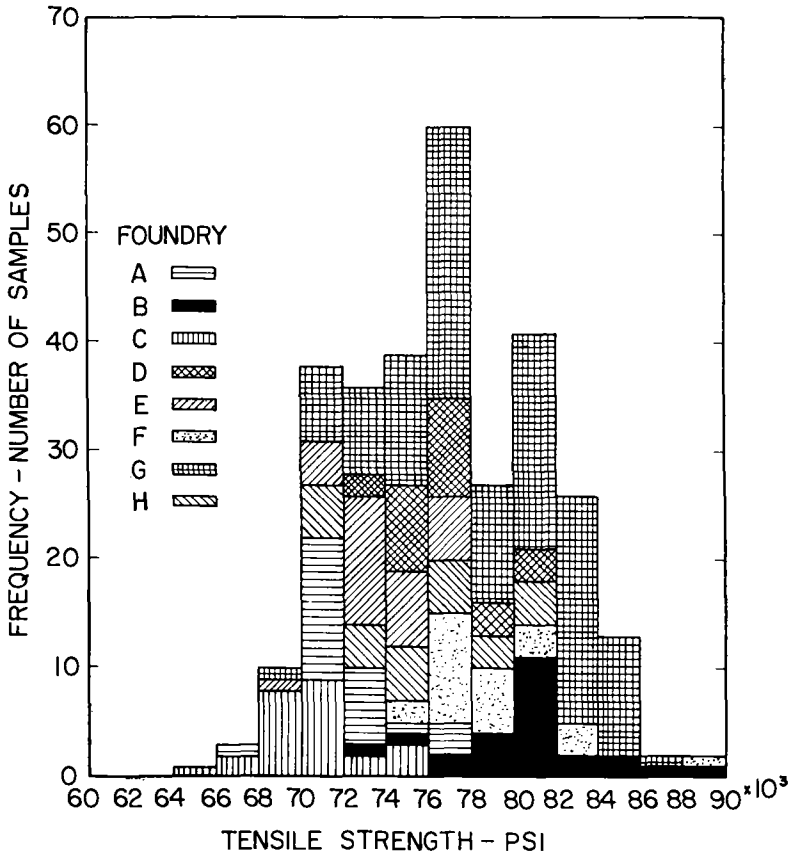


FIG. 1—CF-8 Type Alloy. Histogram Showing Frequency Distribution of 298 Specimens from Eight Foundries.

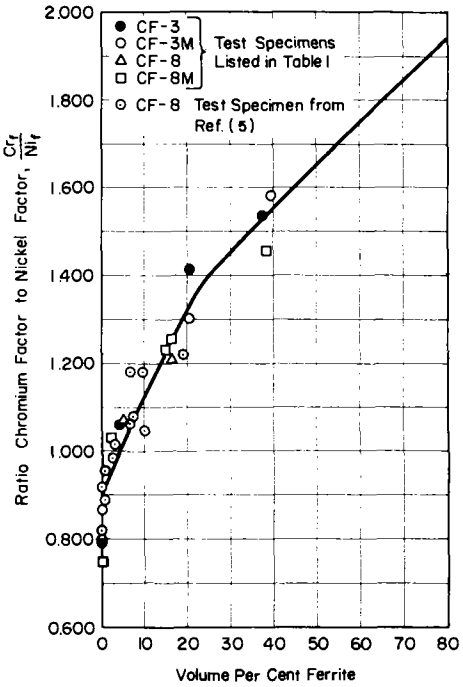


FIG. 2—Composition Ratio and Ferrite Content Relationship. (The curve is derived from the Schaeffler diagram, not from the data points which are added for comparison.)

Figures 5–8 show similar regression lines for 245 heats of CF-3 alloy from four producers tested at room temperature and for 175 of these heats tested at 670 F. These data were assembled in connection with the establishment of allowable stresses for this grade in nuclear service. At room temperature the experimental heats of both CF-3 and CF-3M fall within the expected values for tensile strength. The high ferrite CF-8M specimen is outside the range for yield strength, but the rest of the heats are within the indicated limits. The situation is quite different at 670 F. Here two values are shown for each experimental heat for tests at 600 and 800 F. Test

[6] Corrosion-Resistant Iron-Chromium and Iron-Chromium-Nickel Alloy Castings for General Application (A 296), *1963 Book of ASTM Standards*, Part 2.

[7] Ferritic and Austenitic Steel Castings for High-Temperature Service (A 351), *1964 Book of ASTM Standards*, Parts 1–2, a.

results for the CF-3 alloys are in satisfactory agreement with the scatter band, but the CF-3M alloys at the 20 and 39 per cent ferrite levels are significantly above the plus 3σ limit for both tensile and yield strengths. It may be inferred, therefore, that at such ferrite levels molybdenum has a significant strengthening influence on the low-carbon CF alloy.

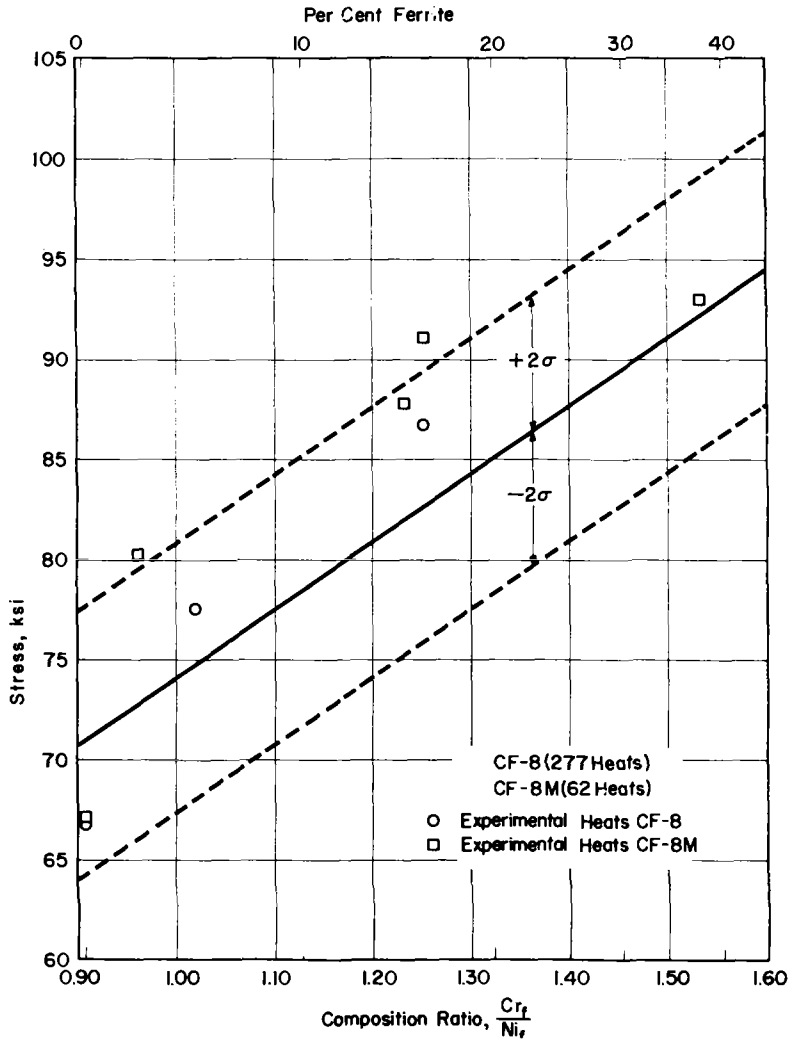


FIG. 3—Tensile Strength at Room Temperature as a Function of Composition Ratio for CF-8 and CF-8M Alloys.

Production of Controlled Ferrite Heats:

The present experimental study was undertaken to determine:

1. The feasibility of producing controlled-ferrite-content heats.
2. The effect of ferrite content on corrosion resistance of the CF-type alloys.
3. The effect of ferrite content on the mechanical properties of the alloy, and the influence of time and temperature on stability of the structure and properties.

Experimental heats for this study were produced by a commercial foundry in accordance with chemical composition specifications based on the composition ratio/ferrite relationship shown in Fig. 2. Aim points were specified for the individual elements, including nitrogen, to provide definite composition ratios and ferrite contents. The intended ratios and those actually obtained are shown in Table 1, together with the intended ferrite content and the actual amount as indicated by the composition ratio and as measured by Magne-Gage.

The success achieved in producing the experimental heats is assurance that control of ferrite content within reasonable limits should be practicable in commercial production. Questions immediately arise, however, as to the effect of substantial amounts of ferrite on the characteristics of the alloys. Will corrosion resistance be impaired? Will structural change occur with time or temperature that will adversely affect the mechanical properties?

EFFECT OF FERRITE CONTENT ON CORROSION RESISTANCE OF CF ALLOYS

The experimental alloys[8] used in this investigation were also the subject of another study (6) concerned with the effect of ferrite on the corrosion resistance of CF-type alloys. Results of the corrosion investigation show that the duplex structures promote improved corrosion resistance through anodic polarization of the ferrite phase. The materials of intermediate ferrite content provide the optimum combination of mechanical properties and corrosion resistance.

Resistance to stress corrosion cracking by chloride environments was of particular interest. Figure 9 is a summary of the stress corrosion data presented on these materials. In this figure data show the relative cracking tendencies of a large number of materials. Total bar length indicates the yield strength of the material. The transition zone indicates the stress level required to cause stress corrosion cracking for each material when exposed for 8 hr to the vapor condensation phase of an aqueous solution containing 875 ppm sodium chloride at 400 F. Ferrite improves the cracking resistance greatly. Compare the intermediate ferrite-containing alloys with the fully austenitic materials.

EXPERIMENTAL PROGRAM

Eighteen alloy compositions were prepared by induction melting from virgin material and cast into standard ACI tensile bar molds. Compositions were selected to provide a spread in analysis which would extend approximately over the composition ranges established for commercial alloys of the CF-3, CF-8, CF-3M, CF-8M, and CF-8C types, and to yield ferrite contents in the range of 0 to 44 volume per cent. Chemical compositions, alloy designations, ACI types, volume per cent ferrite contents, and room-temperature mechanical properties for all materials are listed in Table 2. Ferrite contents and mechanical properties are for specimens water quenched from a 2-hr solution heat treatment at 2050 F.

Mechanical tests, light and electron microscopy examinations, and X-ray determinations were used to study the effect of ferrite on the mechanical prop-

[8] See Table 2, p. 168

erties. Duplex (ferrite-austenite) structures were compared with the fully austenitic alloys after exposure of varying time intervals up to 400 hr in the temperature range 600 to 1550 F. Selected alloys of intermediate and high ferrite content were examined after exposure of 1000 to 4000 hr at 600 and 800 F. These temperatures and long exposure times result in microstructural and mechanical property changes. In addition to carbide formation, structural changes may involve the formation of sigma phase, chi phase, and a body centered cubic phase (885 F embrittlement) in stainless steels. All of these are adequately described in the literature; however, the latter three warrant a brief discussion here in order to provide sufficient background for interpretation of the data presented.

Sigma phase, a hard, brittle, intermediate phase having a complicated crystal structure with tetragonal symmetry and 30 atoms per unit cell, occurs in many binary and ternary systems of the transition metals. In stainless steels sigma phase is based on the compound iron-chromium, but its range of composition is quite extensive, and it may contain appreciable amounts of nickel and molybdenum. A schematic phase diagram for sigma in the iron-chromium system is described by Cook and Jones (7).

Sigma phase in fully austenitic alloys is formed in the approximate temperature range of 1100 to 1700 F. The rate of formation is usually slow and is maximum at about 1500 F. Ferritizers promote sigma formation while austenitizers suppress it. It is found to form primarily at the grain boundaries of the austenite with some discontinuous formation within the grains, and it is usually intimately associated with carbide precipitation. Although it is not known whether sigma can form directly from the austenitic matrix, some recent work indicates that a sequence of reactions may be followed: carbides precipitate first, fine ferrite particles form adjacent to the carbides, and the sigma eventually forms from the ferrite.

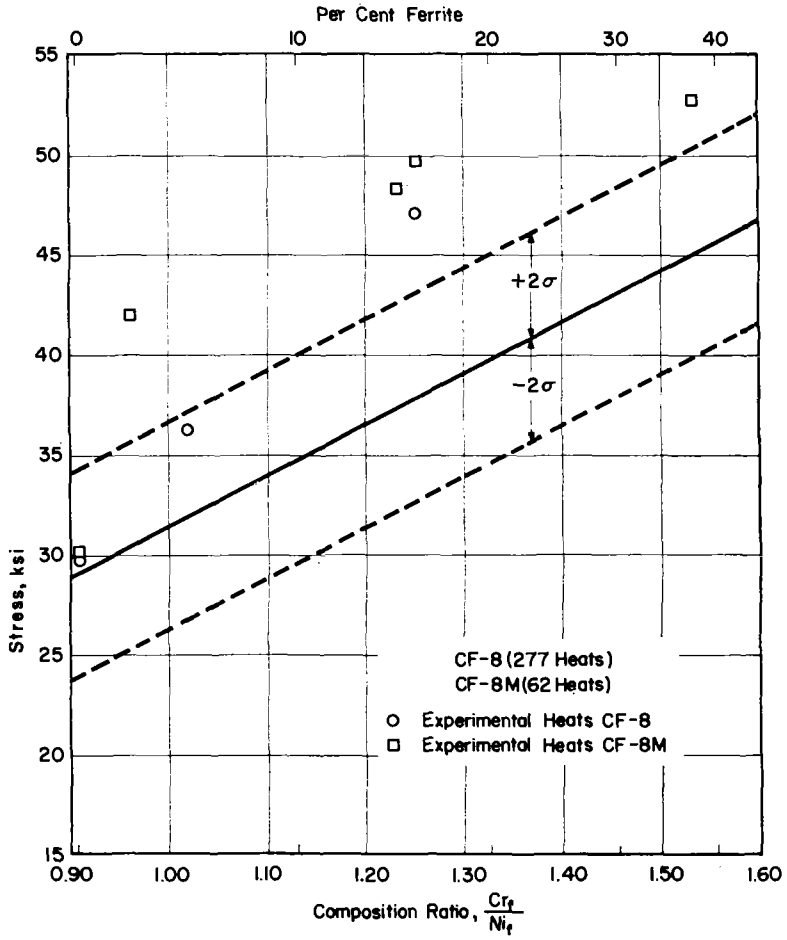


FIG. 4—Yield Strength (0.2% offset) at Room Temperature as a Function of Composition Ratio for CF-8 and CF-8M Alloys.

Ferrite in duplex (ferrite-austenite) alloys has been shown to increase the probability of sigma formation, particularly when the alloys contain a high concentration of chromium, molybdenum, and silicon. The temperature range of sigma formation is regarded as about 1100 to 1700 F. In alloys of the 18-8 type with 2 to 3 per cent molybdenum and retained delta ferrite, the maximum rate of formation occurs at about 1550 F with ferrite transforming entirely to sigma and austenite in less than $\frac{1}{2}$ hr.

In general, the solution annealed alloys display increases in room-temperature tensile strength, yield strength, and hardness with increasing ferrite content. Corresponding losses were generally observed for per cent elongation, reduction of area, and impact strength. The CF-8C alloy series displayed significantly lower values with respect to per cent reduction of area and to impact strength.

Short-time hot tension tests at 600 F showed that, except for C-CF3-37, which displayed a definite increase in tensile and yield strengths with a corresponding increase in hardness and loss in ductility and impact strength, no pronounced effects resulted from the 400-hr exposures at 600 F.

The results of elevated temperature tension tests are influenced by temperature, which tends to reduce the strength properties. Effects of microstructural changes with time at temperature are generally in the direction of increasing the strength properties at the expense of ductility. These effects become evident upon increasing the temperature of testing from 600 to 800 F. After 400 hr a marked increase in strength and hardness with corresponding losses in ductility and impact strength are observed for the alloys of high ferrite content, C-CF3-37, N-CF3M-39, O-CF8M-38, and S-CF8C-44. The effect is observed to a lesser extent for the alloys of intermediate ferrite content F-CF8-16, M-CF3M-20, J-CF8M-15, P-CF8M-16, and T-CF8C-13. These observations are readily made from Figs. 10 and 14 for tensile strength and impact strength, respectively. There is little or no change observed in the microstructure at these temperatures, and ferrite content is unaffected.

The effect of sigma on mechanical properties depends to a large extent on the amount, size, and distribution of the sigma particles. In general, sigma in-

creases the hardness, yield strength, and tensile strength, but decreases the impact resistance, both at room temperature and at elevated temperatures. Loss in ductility is particularly severe when the sigma phase forms a nearly continuous network around the austenite grains.

Chi phase, the ideal composition $Fe_{36}Cr_{12}M_{10}$, has a complicated crystal structure related to the sigma phase, has the approximate temperature range of existence close to that of the sigma phase, and can exist as an equilibrium phase along with sigma. It is found in small amounts in molybdenum-containing stainless steels, and has the same general effect on properties as sigma phase.

885 F Embrittlement is well known to occur in ferritic stainless steels with chromium contents greater than 13 per cent. These materials undergo a marked increase in hardness and decrease in room-temperature impact resistance when heated in the temperature range 750 to 1050 F, or when slowly cooled through this range. Recent work has established that this embrittlement, which is most severe at 885 F, is caused by the precipitation of a body-centered cubic phase with the approximate composition 80 per cent chromium, 20 per cent iron.

It has also been noted that austenitic alloys with retained ferrite can undergo an increase in hardness and decrease in ductility when heated in this range. The nature of this embrittlement has not been extensively studied in duplex alloys. It is found to be more severe in alloys containing molybdenum, but the mechanism of its formation is undetermined.

PROCEDURE

Heat Treatments:

Sigma forming tendencies of the alloys were determined by changes in microstructure, ferrite content, and Brinell hardness for specimens exposed at either 1550 F (for periods of 48, 100, and 150 hr) or at 1400 F (for periods of 25 or 400 hr), and by Charpy V-notch impact tests on specimens exposed for 48 hr at 1550 F or for 25 and 400 hr at 1400 F.

The effect of elevated temperature exposures on mechanical properties and microstructure was determined on specimens heated at 600, 800, 1000, and 1200 F for 25 and 400 hr. Specimens were in the form of rough-machined tensile bars and rectangular blocks which were subsequently machined into tension, impact, and metallographic specimens. Selected alloys were exposed for long times (1000, 2000, and 3000 hr at 600 F, and 1000, 2000, 3000, and 4000 hr at 800 F) to obtain additional data on the influence of exposure time on impact, hardness, ferrite content, and microstructure.

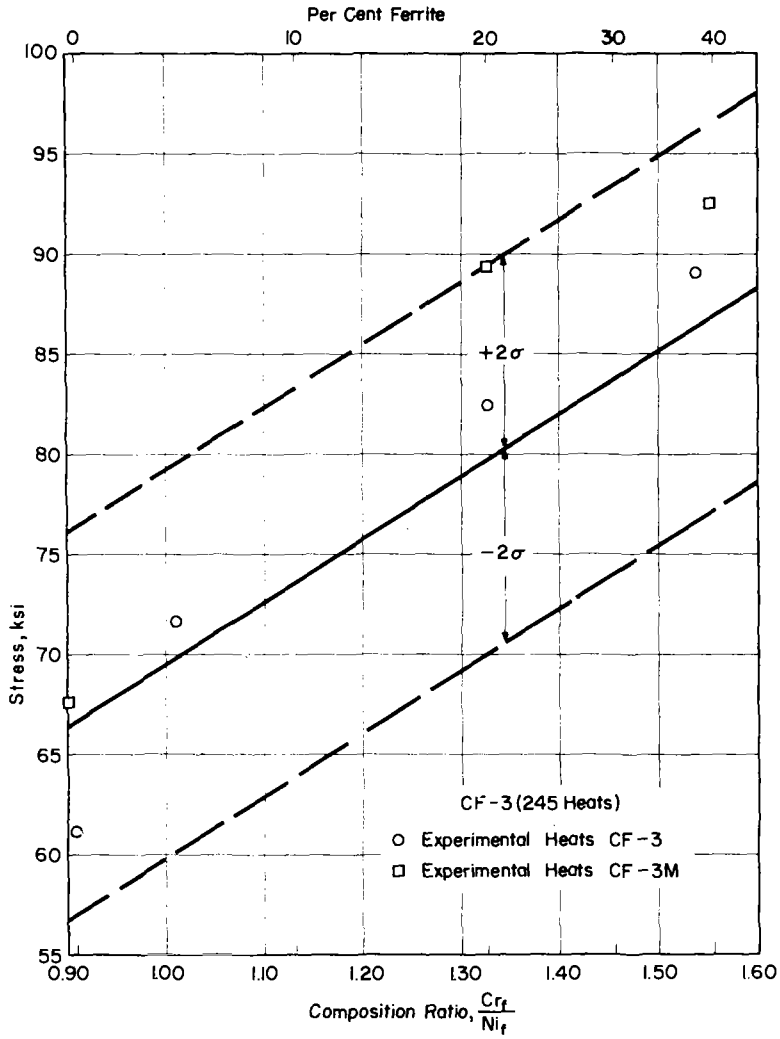


FIG. 5—Tensile Strength at Room Temperature as a Function of Composition Ratio for CF-3 and CF-3M Alloys.

Mechanical Testing:

One tension specimen was employed per alloy for each condition. All specimens were standard ASTM 0.505 tensile bars with 2-in.-gage lengths. Load-elongation curves were automatically plotted at a strain rate of 0.05 in./in./min. Yield strengths were determined by the 0.2 per cent offset method.

Specimens for elevated temperature tension testing (short-time hot tensile) were heated to the desired temperature (subsequent to initial exposures of 25, or 400 hr at 600, 800, 1000, and 1200 F) by means of a three-element chromel-wound resistance furnace which enclosed the tension specimen. The temperature was measured by means of a chromel-alumel thermocouple mounted adjacent to the center of the specimen. A 1-hr time period was maintained between the time the desired temperature was indicated and the time of the test to insure thermal equilibrium.

Impact tests were performed at room temperature on standard Charpy V-notch specimens (0.010-in.-notch radius). The average of three impact tests was reported as the impact value of each condition. Broken impact specimens were used for Magne-Gage ferrite determinations, Brinell hardness tests, and metallographic examinations.

Brinell hardness tests were made for

all alloys in all conditions using a 3000-kg load and 10-mm steel ball. The average of five values was reported for each specimen, except for the specimens of alloy J-CF8M-15 utilized for long-time aging at 800 and 900 F, for which the specimen size was such that only one impression could be made.

Ferrite Determination:

Volume per cent ferrite was estimated on all specimens by means of the Aminco-Brenner Magne-Gage according to the calibration established by Watts (8) and verified by Mancini (9). Twenty-five determinations were made on each specimen, and the average value reported.

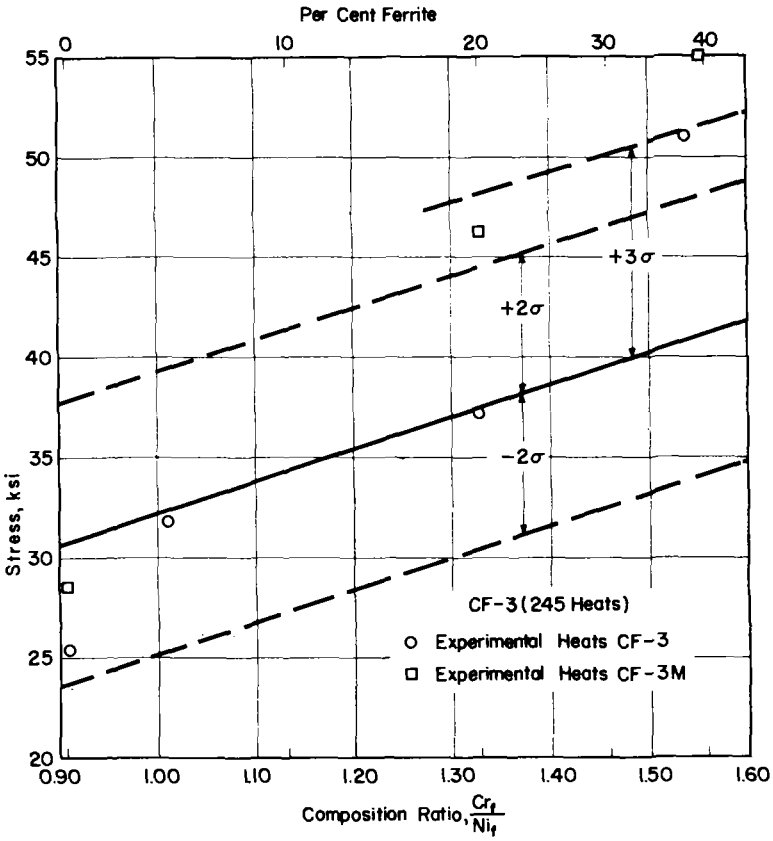


FIG. 6—Yield Strength (0.2% offset) at Room Temperature as a Function of Composition Ratio for CF-3 and CF-3M Alloys.

Metallography:

Conventional mechanical polishing was employed for most specimens. Electrolytic polishing with a bath containing two parts methyl alcohol to one part concentrated nitric acid was used to some advantage on several of the fully austenitic alloys.

Vilella's reagent (10-cm³ hydrochloric acid, 100-cm³ methyl alcohol, 1-g picric acid) was used to distinguish between the austenite and ferrite in solution-quenched alloys with duplex microstructures, and to outline the phases in transformed structures. Oxalic acid was equally suitable for solution-quenched duplex microstructures.

The differentiation between carbides and sigma, when these phases precipitate at the grain boundaries of fully austenitic alloys, cannot be made by etching procedures alone unless the phases are very well developed. Ten per cent oxalic acid was used to etch the austenitic alloys in this study. This reagent attacks carbide and sigma indiscriminantly but does serve to indicate grain boundary precipitation.

The presence of sigma phase in duplex microstructures was determined by an etching procedure developed by Gilman (10). As utilized in this study, the method consisted of immersing the specimen in Vilella's reagent for 2 or 3 sec to outline the general structure, and then etching electrolytically for a few seconds in 10 normal potassium hydroxide at a potential difference of about 4 to 6 v to develop the full structure. The electrolytic etching step causes films to be formed on the phases and thus permits a clear differentiation to be made. When the specimen is lightly washed, dried, and examined under the microscope without a filter, sigma phase appears dark reddish-brown, the austenite matrix appears light pink, and newly formed austenite in the ferrite pools usually appears white. Partially transformed ferrite usually appears light brown, but the colors are sometimes variable, perhaps as a result of compositional differences. Overvigorous washing or overetching causes cracks to appear in the films on the ferrite. The method was found to yield reproducible results over the range of compositions studied.

Etching of specimens of alloy J-CF8M-15 aged at 800 F and 900 F required slightly different procedures which will be discussed in conjunction with the results for aging.

Residue Extraction and X-Ray:

Positive evidence of sigma phase formation was obtained by X-ray studies of residues from alloy J-CF8M-15 subsequent to exposures at 1550 F for 48 hr and 900 F for 1300 hr. These residues were electrolytically extracted in 10 per cent ferric chloride using a J-CF8M-15 anode and a Type 304 stainless steel cathode. After a portion of the specimen was dissolved, the solution was decanted with distilled water and the residue was washed, dried, mixed with tragacanth gum, and formed into a wire-shaped specimen for use in a Debye-Scherrer X-ray powder camera. Chromium radiation was employed.

EFFECT OF TIME AND TEMPERATURE ON STRUCTURAL STABILITY AND MECHANICAL PROPERTIES

Tension Tests:

Room-temperature data for solution annealed material (water quenched subsequent to a 2-hr exposure at 2050 F) and short-time elevated temperature test data are plotted in Figs. 10–13 which are for tensile strength, yield strength, per cent elongation, and per cent reduction in area, respectively. These values are plotted as a function of *ferrite content* which is of primary interest.

Results of the 1 and 25-hr exposures at 1000 F show that alloys with ferrite in the original microstructure maintain higher hot tensile strengths up to this temperature. Although microstructural changes which accompany the property changes are slight at 800 F, there is definite evidence for precipitation within the ferrite at 1000 F after 25-hr ex-

posure. Upon increasing the time at temperature to 400 hr, the effects of these microstructural changes on tensile properties become more pronounced with high ferrite-containing alloys being most affected.

At 1200 and 1400 F sigma phase formation has a strengthening and embrittling effect on ferrite-containing alloys. High yield strengths up to 1200 F for short times of 25 hr are accompanied by reasonably good values of per cent elongation and per cent reduction of area. The high ferrite materials, C-CF3-37, N-CF3M-39, O-CF8M-38, and S-CF8C-44 display substantial increases in tensile strength, yield strength, and hardness with increased exposure times of 400 hr at 1200 F. Corresponding losses are observed in impact, ductility, and ferrite content. Changes in tensile and yield strengths for the intermediate ferrite contents are not so pronounced; however, elongation and reduction of area show that considerable microstructural changes had taken place after 400 hr of exposure for all alloys containing ferrite of intermediate levels. These reflections are also shown in losses of impact resistance and ferrite content for alloys F-CF8-16, M-CF3M-20, J-CF8M-15, and T-CF8C-13. Austenitic alloys, D-CF8-0 and G-CF8M-0 display substantial increases in yield strength and losses in ductility after 400 hr at 1200 F. Alloy H-CF8M-2 is included in this group. Impact strengths show a drop, but the values after 400 hr are still very high.

Effect of Prior Elevated Temperature Exposure on Room-Temperature Impact, Hardness, and Ferrite Content:

Room-temperature impact strength was determined for all materials in the solution annealed and heat treated conditions. These data are presented in Figs. 14 and 15 and corresponding hardness and ferrite data are given in Tables 3 and 4.

In general, impact resistance decreased with increasing ferrite content for all alloys. Exceptions to this were the high values obtained for the CF-3M and CF-8M alloys of intermediate ferrite content (15 to 20 per cent ferrite) and he low values for the CF-8C alloys of intermediate ferrite content in the solution annealed condition.

Although a slight loss in impact strength was observed in isolated cases subsequent to exposures at 600 F, the first consistent evidence of the effect of ferrite on reducing the impact resistance occurred after long-time exposures at 800 F. These data showed only a small loss in impact resistance for the alloys containing intermediate ferrite content (13 to 20 per cent) after exposures of 400 hr at 800 F. A more pronounced loss in impact, in excess of 50 per cent, was observed for the high ferrite containing alloys (37 to 44 per cent ferrite). Results of 3000 and 4000-hr exposures at 600 and 800 F are described below.

All of the ferrite-containing alloys displayed a loss in impact strength after 25 hr of exposure at 1000 F, with further reduction after 400 hr. This loss in impact strength was accompanied by precipitation within the ferrite. The effect of ferrite on impact strength was even more pronounced at 1200 F. At this temperature a loss in impact strength was also observed for the fully austenitic CF-8, CF-3M, and CF-8M alloys.

Effect of Long-Time Exposures at 600 and 800 F on Impact Strength, Hardness, and Ferrite Content:

Room-temperature impact, ferrite content, and hardness were determined for selected alloys of the intermediate- and high-ferrite contents after exposures of up to 3000 hr at 600 F and up to 4000 hr at 800 F, Fig. 15 and Tables 3 and 4.

Although some loss in impact resistance was observed with extended times at 600 F, values were high even after 3000 hr at temperature. The effect was greatest for alloy C-CF3-37, less for alloy K-CF3-20, and only slight for alloy F-CF8-16. Ferrite content and hardness were essentially unaffected by the extended times at this temperature.

Upon increasing the exposure temperature from 600 to 800 F, more complete and informative data were obtained. The effect of ferrite content became more pronounced and the superiority of the

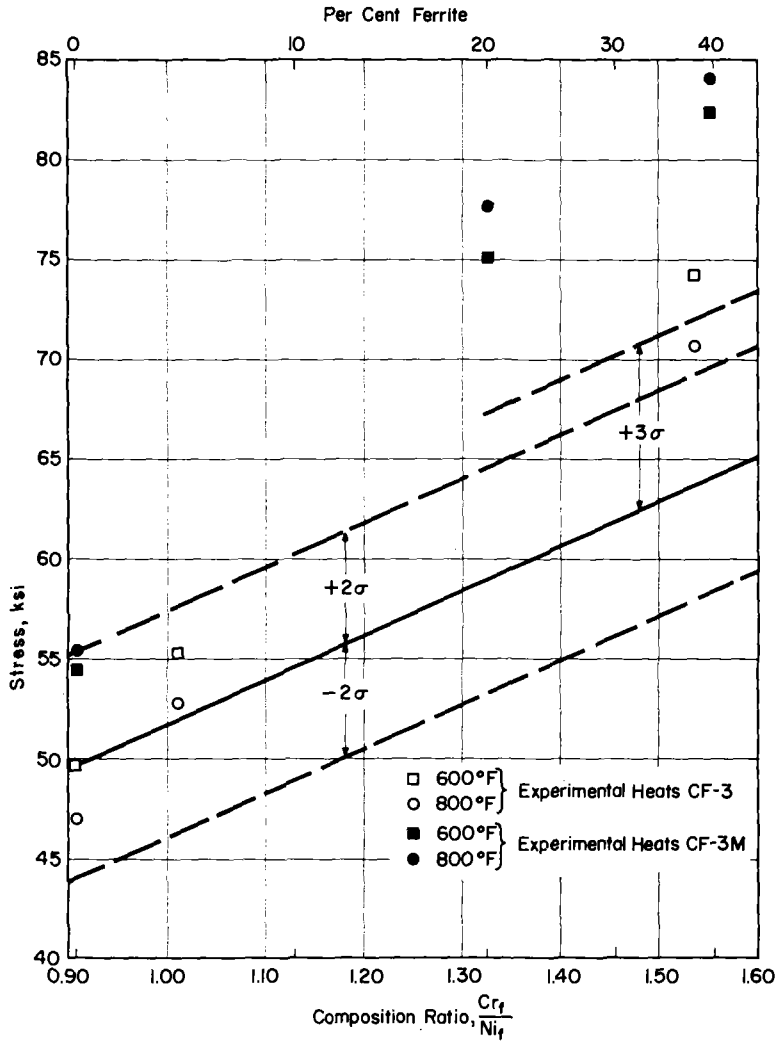


FIG. 7—Tensile Strength of Commercial Heats at 670 F and of Experimental Heats at 600 and 800 F for CF-3 Alloys. (Also at 600 and 800 F for experimental heats of CF-3M alloy.)

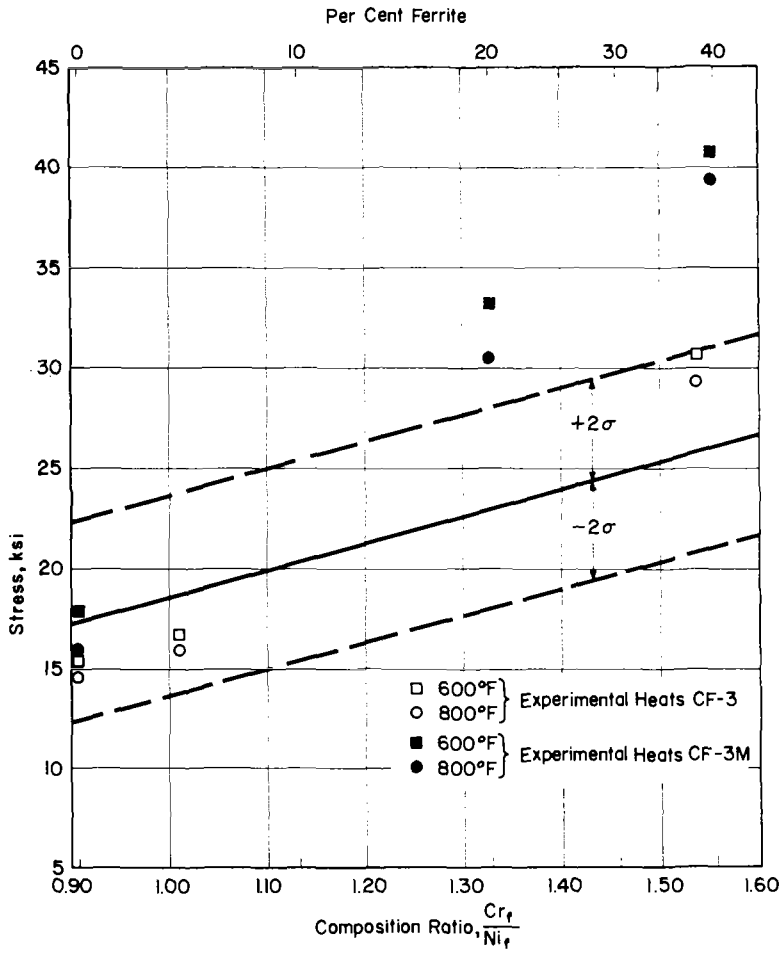


FIG. 8—Yield Strength (0.2% offset) of Commercial Heats at 670 F and of Experimental Heats at 600 and 800 F for CF-3 Alloys. (Also at 600 and 800 F for experimental heats of CF-3M alloy.)

TABLE 1—COMPOSITION RATIOS AND FERRITE CONTENTS OF EXPERIMENTAL HEATS.

Alloy Type	Composition Ratio		Ferrite Content		
	Intended	Actual	Intended	Actual	
				Indicated[a]	Magne-Gage
CF-3	0.814	0.793	0	0	0
	1.129	1.061	10	6	4
	1.251	1.417	16	27	20
	1.482	1.538	33	38	37
CF-3M	0.897	0.867	0	0	0
	1.263	1.306	16	19	20
	1.455	1.587	30	43	39
CF-8	0.862	0.806	0	0	0
	1.110	1.072	9	7	5
	1.348	1.210	21	14	16
CF-8M	0.809	0.751	0	0	0
	1.198	1.034	13	5	2
	1.429	1.232	28	15	15
	1.386	1.256	24	16	16
	1.459	1.412	31	27	38
CF-8C	0.892	0.826	0	0	0
	1.268	1.132	17	10	13
	1.268	1.404	17	26	44

[a] Indicated by actual composition ratio.

nonmolybdenum containing materials was indicated from impact results. Alloys of the intermediate ferrite level, except for alloy T-CF8C-13, displayed significant drops in impact strength upon increasing the time of exposure at 800 F from 400 to 1000 hr. Additional losses in impact strength were observed upon further increases in exposure times to 3000 and 4000 hr; however, the strengths after these long exposure periods were still high, in the range of 30 to 60 ft-lb.

Impact strengths of the high ferrite-containing alloys, which displayed large reductions after the 400-hr exposures, were not significantly altered upon increasing the times to 1000, 2000, 3000, and 4000 hr. Impact strengths of the molybdenum-containing alloys of this group and of alloy T-CF8C-13 were in the order of 12 to 15 ft-lb; alloy C-CF3-37, of the high ferrite group, maintained an impact strength of 20 to 25 ft-lb.

Effect of Exposures at 1400 and 1550 F on Room-Temperature Impact, Hardness, and Ferrite Content:

Of the alloys in the CF-3 group, only C-CF3-37 was affected by a substantial reduction in impact resistance from the 102 ft-lb solution-annealed value to 44 ft-lb after 48 hr at 1550 F. This loss in impact strength was accompanied by a drop in ferrite content. Increasing the time at 1550 F to 150 hr caused only slight increases in hardness for the same alloy.

CF-8 alloys displayed results similar to the CF-3 series. Alloy F-CF8-16, in which the impact resistance dropped from 100 to 77 ft-lb, is comparable to losses in impact strength observed for alloys D-CF8-0 (149 to 88 ft-lb) and E-CF8-5 (122 to 92 ft-lb) after 48-hr exposure at 1550 F. The ferrite-containing alloys of this series showed a decrease in ferrite after 24 hr at temperature. Hardness was unaffected after 150 hr of exposure; however, this series of alloys did not include a high ferrite containing alloy.

More pronounced effects were observed for the molybdenum bearing CF-3M and CF-8M alloys. CF-3M alloys and alloy O-CF8M-38 were exposed to 1400 F for periods of 25 or 400 hr. The remaining CF-8M specimens were exposed to 1550 F for 48 hr. Of the CF-3M materials, L-CF3M-0 dropped in impact strength from 155 to 73 and 37 ft-lb after 25 and 400-hr at 1400 F. Alloys M-CF3M-20 and N-CF3M-39, which possessed solution-annealed impact strengths of 128 and 78 ft-lb, respectively, both displayed impact strengths of approximately 5 ft-lb after both the 25 and 400-hr exposures at 1400 F. Increases in hardness, more pronounced with increasing ferrite content, were observed for all specimens with increasing time at temperature. Ferrite contents of

alloys M-CF3M-20 and N-CF3M-39 dropped from very low values after 25 hr exposure to zero per cent after 400 hr.

CF-8M specimens of G-CF8M-0 and J-CF8M-15 were exposed to 1550 F for 48 hr. Impact strengths dropped from 140 to 41 ft-lb and from 96 to 10 ft-lb for alloys G-CF8M-0 and J-CF8M-15, respectively. This was accompanied by increases in hardness for both alloys, and a complete loss of ferrite in alloy J-CF8M-15. Increasing the time at 1550 F to 150 hr caused no further change in hardness. Alloy O-CF8M-38 showed a drop in impact resistance from 100 to approximately 5 ft-lb upon being exposed at 1400 F for 25 or 400 hr. The ferrite content decreased to 1.5 per cent after 25 hr and to zero per cent after 400 hr. An increase in hardness was observed.

The CF-8C alloys, which displayed low impact values in comparison to the other solution annealed alloys described, showed losses in impact to values comparable to the CF-3M materials of similar ferrite levels after comparable exposures at 1400 F. The impact values for R-CF8C-0, T-CF8C-13, and S-CF8C-44 dropped from 51, 19, and 34 ft-lb to 41, 11, and 4 ft-lb after 25 hr and to 39, 5, and 5 ft-lb after 400 hr at 1400 F. Substantial amounts of ferrite exist in both ferrite-containing heats after the high-temperature exposures. The zero ferrite alloy showed a loss in hardness and the ferrite-containing alloys displayed an increase in hardness with increased exposure time.

The exceptionally low impact strength for alloy T-CF8C-13 in the solution annealed condition is related to the presence of columbium carbide in the microstructure. The lower value for T-CF8C-13 as compared to S-CF8C-44 probably results from the greater concentration of precipitate in the continuous but less massive ferrite stringers of the lower ferrite-bearing alloy.

Relation of Structure to Mechanical Properties:

600 to 1000 F—Although no significant changes were found in the ferrite contents or the microstructures of any of the alloys after the exposures at 600 and 800 F, some grain boundary precipitation was observed after 400 hr at 1000 F in the fully austenitic alloys. The low ferrite alloys dropped slightly in ferrite content after 400 hr at 1000 F, but the only microstructural change appeared to be carbide precipitation at or near the austenite-ferrite interface.

Visible precipitation was apparent in alloys of intermediate-ferrite content. In alloy F-CF8-16, the precipitation was heaviest at the austenite-ferrite interfaces as illustrated by comparing the solution annealed structure of Fig. 16 with that of the 400-hr, 1000 F structure of Fig. 17. The microstructure of alloy J-CF8M-15 showed a much heavier general precipitation within the ferrite pools. These two alloys displayed slight drops in ferrite content.

The high ferrite containing alloys showed somewhat more pronounced microstructural changes after 400 hr at 1000 F. Alloy C-CF3-37, when etched in oxalic acid, revealed precipitation within the ferrite pools and at boundaries within the ferrite. The changes in hardness, impact strength, and elevated temperature tensile properties of alloy C-CF3-37, when exposed in the 600 to 1000 F temperature range, indicate that the early stages of a precipitation hardening reaction also occurred in the ferrite of this alloy. Room-temperature impact strengths were particularly affected after 400 hr at 800 and 1000 F.

Metallographic examinations of the CF-8C alloys disclosed that a phase believed to be columbium carbide was present in these alloys in the annealed condition. The columbium carbides were present in an interdendritic form and persisted through all heat treatments used in this work.

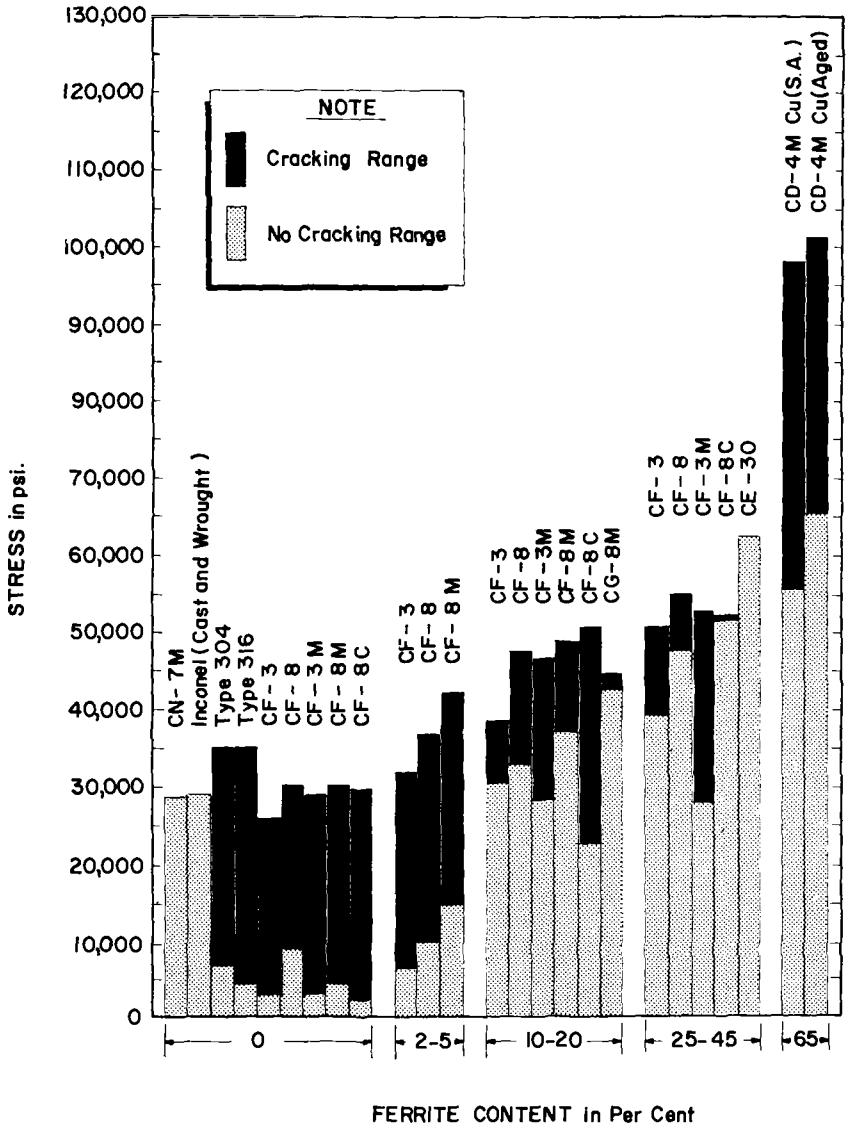


FIG. 9—Yield Strength of Various Alloys at Different Levels of Ferrite Content, and Stress above which Stress-Corrosion Cracking Occurs in a Chloride Environment.

1200 F—Microstructural changes of all the alloys were more pronounced at 1200 F. The fully austenitic alloys showed intergranular precipitation after 25 hr at 1200 F, and the precipitation was quite heavy after 400 hr at this tempera-

ture. The nature of the precipitate was not established, although carbides are undoubtedly present at the grain boundaries. It was not determined whether any sigma phase was formed; however, the severity of the effect of the precipitation on alloy G-CF8M-0 at high temperatures, coupled with the fact that the alloy contains molybdenum, would favor sigma phase formation in the molybdenum-containing alloys.

Ferrite contents of the duplex alloys dropped slightly after 25 hr at 1200 F. These decreases were apparently accounted for by growth of austenite into the ferrite. Some carbide precipitation was also apparent. After 400 hr the ferrite decreases were more pronounced in the low ferrite containing alloys, and sigma phase was formed in all except alloy E-CF8-5. A slight amount of sigma formed adjacent to the untransformed ferrite in alloy B-CF3-4 after 400 hr at 1200 F. The behavior of alloy H-CF8M-2 was more difficult to evaluate because of the presence of the unidentified dark etching microstructural constituents in the ferrite phase. It appears that this alloy is capable of forming sigma phase in ferrite pools and at austenite grain boundaries after 400 hr at 1200 F.

At 1200 F intermediate ferrite-containing alloys are subject to sigma phase formation by decomposition of the ferrite into austenite and sigma. Alloy F-CF8-16 formed the least amount of sigma after 400 hr at 1200 F, and the amount formed was detrimental only to the room-temperature impact resistance. The microstructure of alloy F-CF8-16 had some sigma particles formed around the untransformed ferrite in the original ferrite pools, Fig. 18. Alloy J-CF8M-15 had a partially transformed structure, consisting of sigma phase, new austenite, and untransformed ferrite in the original ferrite pools, Fig. 19. The solution annealed microstructure is similar to that of Fig. 16.

The high-ferrite alloys underwent the most pronounced variations in microstructure of the alloys investigated. The ferrite in alloy C-CF3-37, Fig. 20, had undergone varying degrees of transformation. Some ferrite pools were completely transformed into well-developed sigma phase and new austenite, while in others only austenite had formed within the ferrite pools and at the edge of the pools. The solution annealed structure of alloy C-CF3-37 is illustrated in Fig. 21 which is typical of solution annealed structures of high ferrite content. Even though the transformation of ferrite in molybdenum-free alloys was less than in the molybdenum bearing alloys after 400 hr, the effect of the sigma formed on the room-temperature impact strength and on elevated temperature properties was quite pronounced.

1400 F—All austenitic alloys showed evidence for grain boundary precipitation after 400 hr at 1400 F, but no definite identifications of the precipitate were made.

Sigma phase was formed in varying amounts in all ferrite-containing alloys. The original ferrite of the molybdenum bearing alloys was completely decomposed into new austenite and sigma phase in 400 hr. Transformation was not completed in the remaining ferrite-containing alloys, but large amounts of sigma were present in alloys C-CF3-37 and F-CF8-16 after 400 hr at 1400 F. The mode of formation of sigma in the ferrite-containing alloys was new austenite and very

TABLE 2—CHEMICAL COMPOSITION, FERRITE CONTENT AND MECHANICAL PROPERTIES OF ALLOYS.[a]

Alloy			Per Cent Composition							Room-Temperature Properties					
Designation	ACI Type	Volume Ferrite, %	C	Mn	Si	Cr	Ni	Mo	N[b]	Tensile Strength, ksi	Yield Strength, ksi, 0.2 % offset	Elongation, %	Reduction in Area, %	Charpy Impact V-Notch, ft-lb	Hardness, BHN
A	CF3	0	0.020	0.78	1.20	16.97	13.35	...	0.030	61.2	25.4	63	74	149	116
B	CF3	4	0.020	0.83	1.29	19.28	10.07	...	0.075	71.8	31.8	73	68	122	133
K	CF3	20	0.023	0.84	1.21	20.36	8.25	...	0.013	82.5	37.2	57	69	110	142
C	CF3	37	0.020	0.83	1.50	21.81	7.68	...	0.056	89.1	51.0	48	67	102	164
D	CF8	0	0.080	0.74	1.22	18.08	12.20	...	0.050	66.9	29.9	60	65	145	127
E	CF8	5	0.070	0.80	1.25	19.99	9.38	...	0.062	77.6	36.3	60	68	122	158
F	CF8	16	0.080	0.78	1.28	21.37	8.08	...	0.077	86.8	47.1	52	64	100	156
L	CF3M	0	0.026	1.28	0.90	17.16	13.46	2.48	0.051	67.6	28.6	70	73	155	116
M	CF3M	20	0.026	0.91	1.43	20.31	10.86	2.59	0.039	89.6	46.2	53	67	128	149
N	CF3M	39	0.021	0.77	1.14	21.59	9.50	2.78	0.015	92.5	55.0	43	65	78	172
G	CF8M	0	0.080	0.85	1.12	16.72	15.02	2.51	0.042	67.0	30.0	57	65	140	129
H	CF8M	2	0.070	0.61	1.30	18.99	11.36	2.60	0.074	80.2	42.0	60	58	88	160
J	CF8M	15	0.070	0.79	1.39	20.17	9.55	2.40	0.064	87.8	48.4	45	64	96	164
P	CF8M	16	0.070	0.58	0.95	21.76	8.86	2.35	0.110	91.2	49.8	47	70	119	174
O	CF8M	38	0.050	0.82	1.27	21.87	9.64	2.65 Cb	0.035	93.0	52.7	42	65	100	173
R	CF8C	0	0.080	1.43	0.79	18.34	11.17	0.56	0.054	72.0	29.2	52	41	51	128
T	CF8C	13	0.080	1.29	1.93	20.60	8.53	0.78	0.110	93.2	50.7	38	37	19	164
S	CF8C	44	0.070	1.04	1.54	22.35	8.34	0.80 Mo	0.042 Cu	89.4	52.0	38	42	34	168
	CD 4MCu(S.A.)	65	0.025	0.89	0.90	25.03	5.52	2.08	3.15	107.5	97.9	17	44	44	228
	CD 4MCu(Aged)	65	0.025	0.89	0.90	25.03	5.52	2.08	3.15	138.8	100.7	9	10	10	300
	CE30	28	0.250	0.54	1.80	28.16	9.64	...	...	100.2	62.5	11	18	...	190
	CG8M	17	0.056	1.12	1.06	20.17	10.40	3.52	...	86.8	44.6	42	59	...	156
	CN7M	0	0.040	0.70	0.88	20.22	29.78	2.75 Cb	3.50	65.0	28.3	45	69	...	140
	Inconel (Cb)	0	0.052	0.79	1.28	14.20	73.20	1.89	...	78.2	28.6	41	39	...	132

[a] Note—Except for alloy CD-4MCu, all specimens were water quenched from 2050 F.
Alloy CD-4MCu given modified solution anneal and modified solution anneal plus age.
S.A.: 2050 F, 2 hr, F.C. to 1750 F 0.5 hr and oil quenched, stress relieve 600 F 2 hr and air cooled.
S.A. and age: S.A. as above + 3 hr at 900 F.

[b] Nitrogen determination by vacuum fusion.

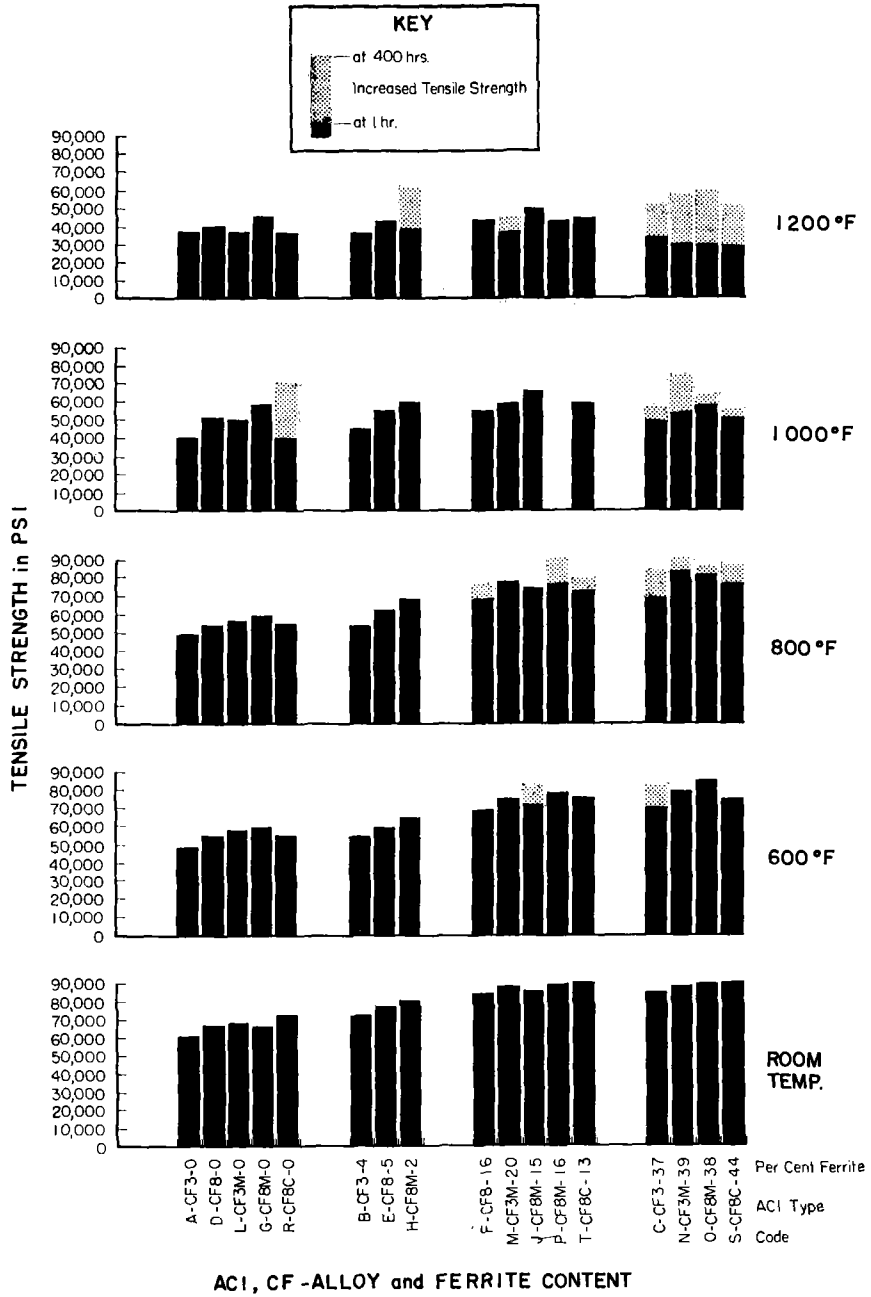


FIG. 10—Short-Time, Elevated-Temperature Tensile Strength after 1 and 400 hr at Temperatures Indicated. (Initially, all specimens water-quenched from 2050 F exposure of 2 hr.)

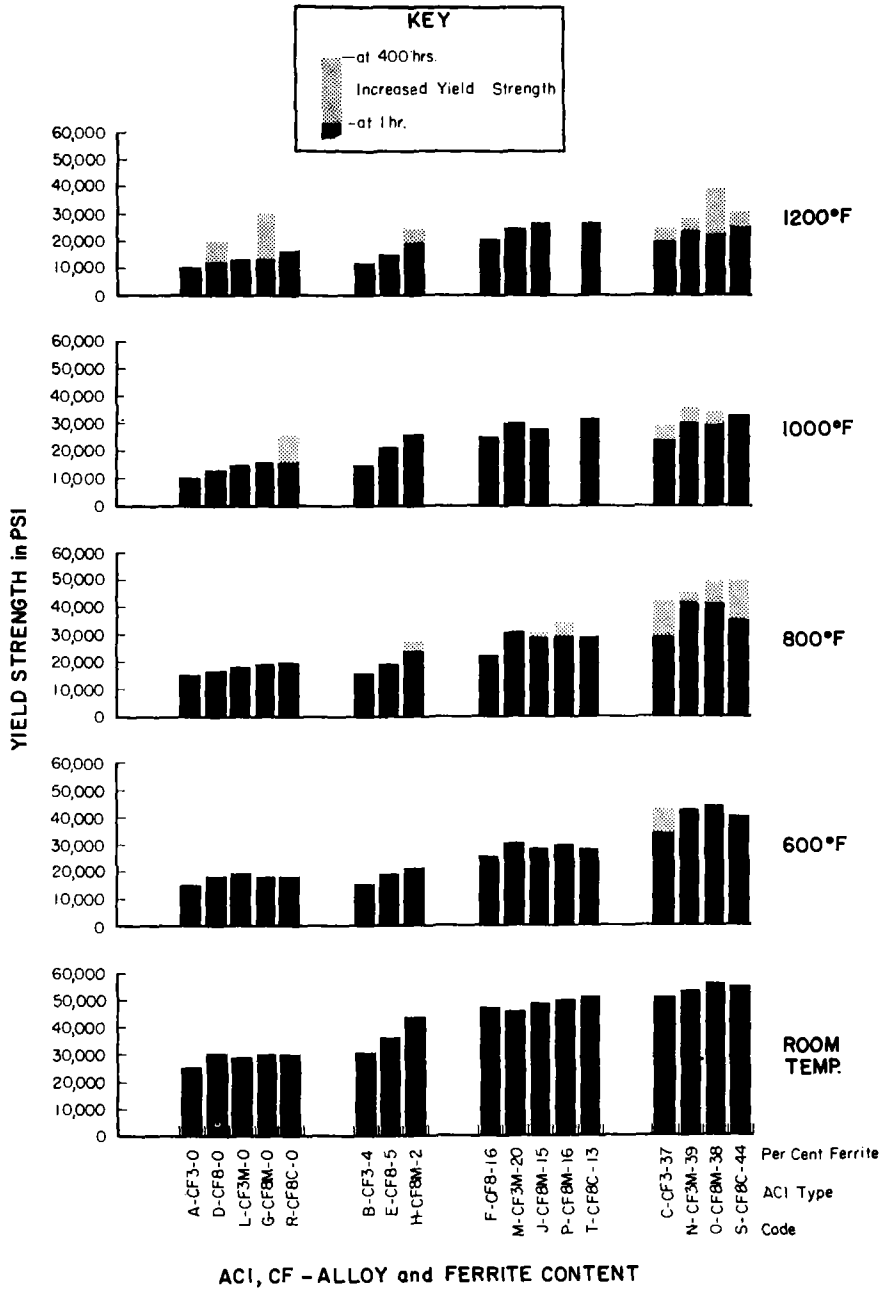


FIG. 11—Short-Time, Elevated-Temperature Yield Strength after 1 and 400 hr at Temperatures Indicated. (Initially, all specimens water-quenched from 2050 F exposure of 2 hr.)

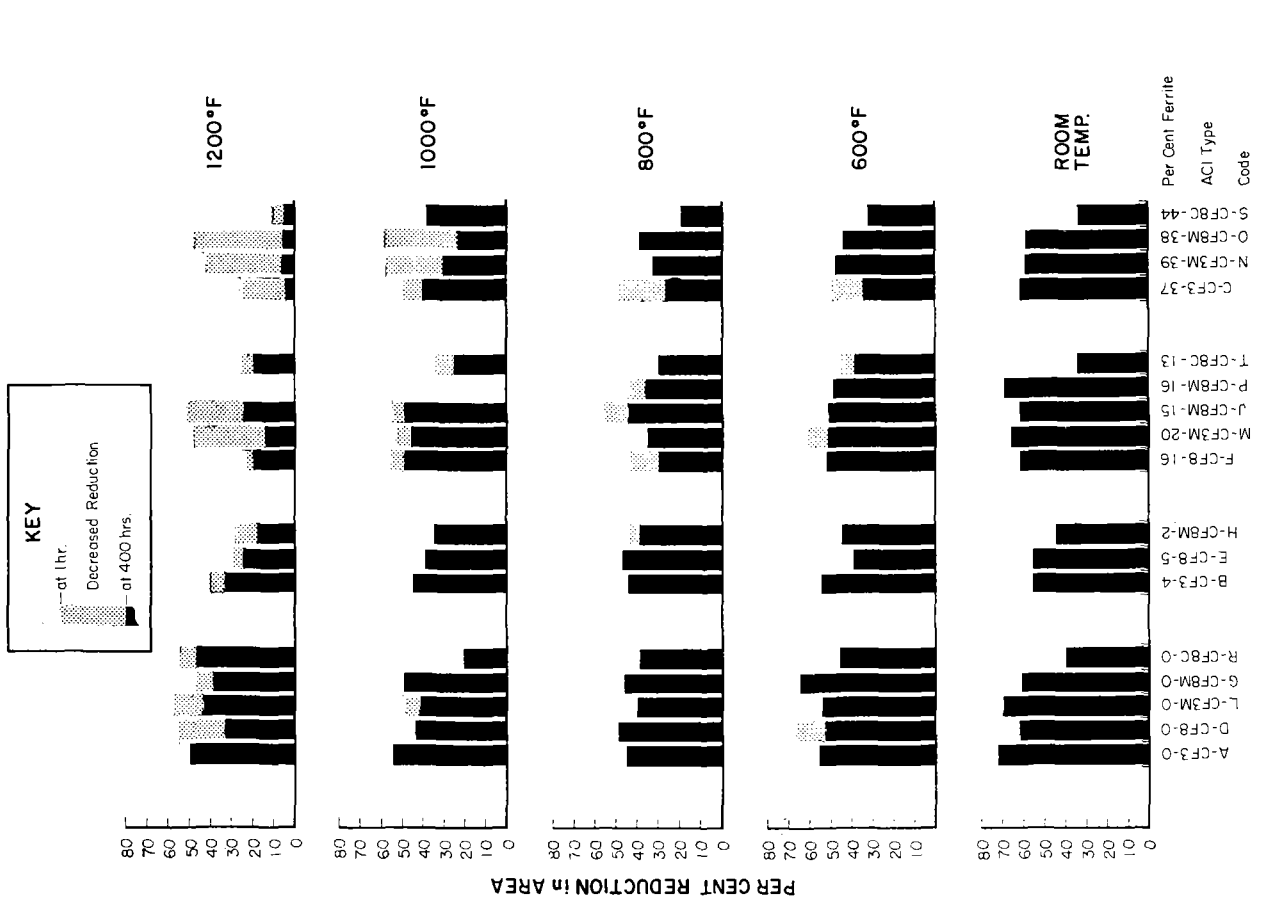


FIG. 12—Short-Time, Elevated-Temperature Elongation (% in 2 in.) after 1 and 400 hr at Temperatures Indicated. (Initially, all specimens water-quenched from 2050 F exposure of 2 hr.)

FIG. 13—Short-Time, Elevated-Temperature Reduction in Area (%) after 1 and 400 hr at Temperatures Indicated. (Initially, all specimens water-quenched from 2050 F exposure of 2 hr.)

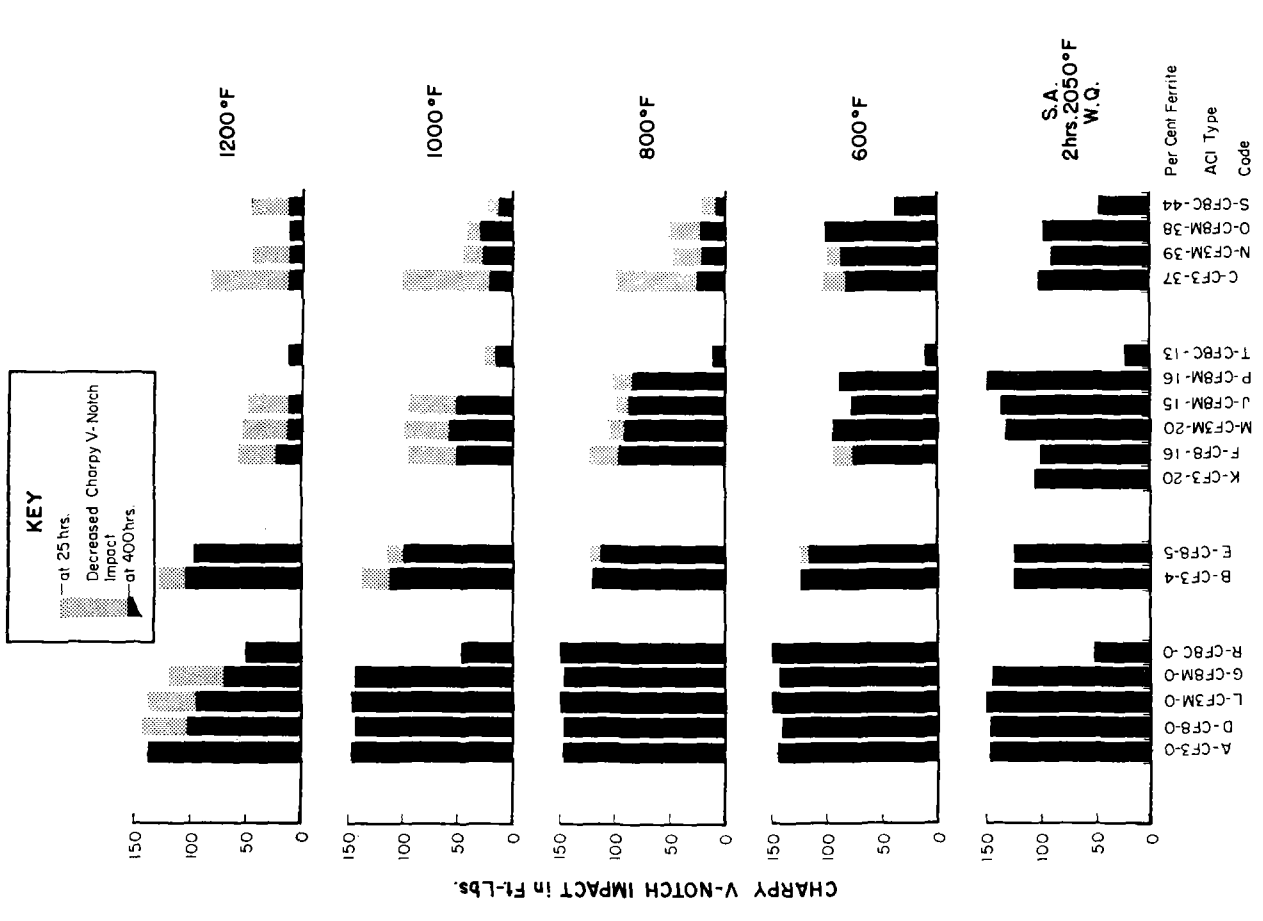


FIG. 14—Room-Temperature Charpy V-Notch Impact after 25 and 400 hr at Temperatures Indicated. (Initially, all specimens water-quenched from 2050 F exposure of 2 hr.)

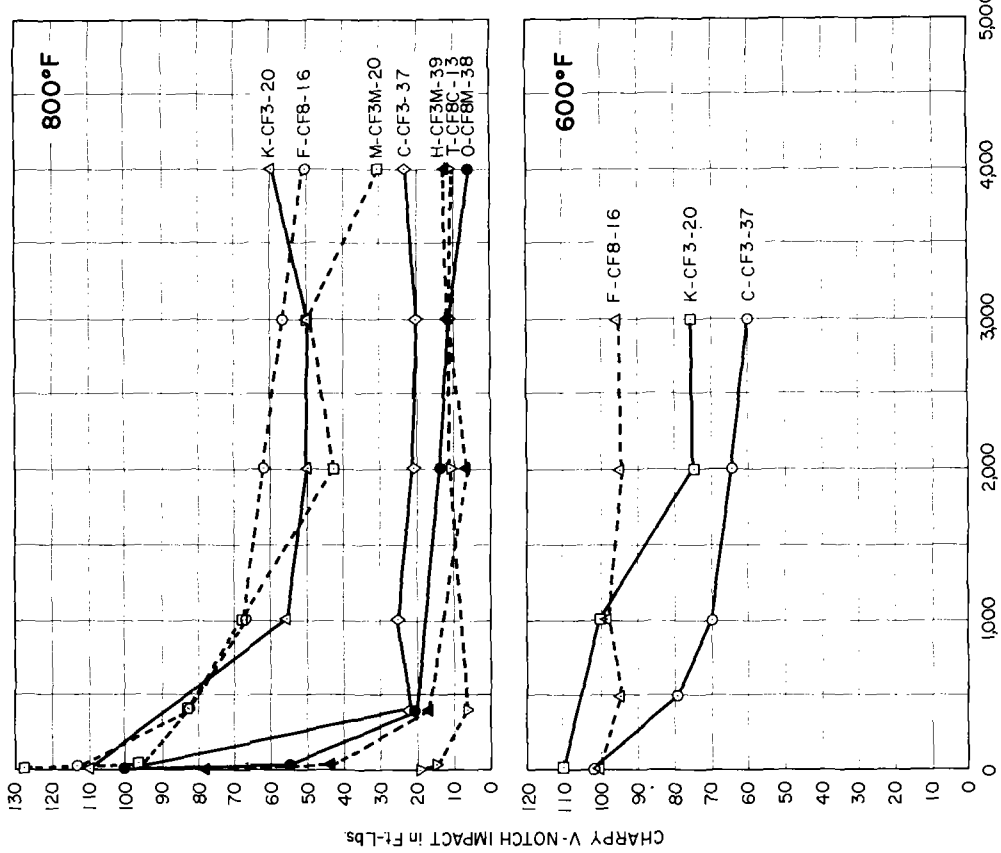


FIG. 15—Effect of Very-Long-Time Exposure at 600 and 800 F on Room-Temperature V-Notch Impact Strength.

TABLE 3—ROOM-TEMPERATURE BRINELL HARDNESS AFTER ELEVATED TEMPERATURE EXPOSURES.

(Solution annealed value for per cent ferrite indicated.)

Alloy Type		CF-3				CF-8			CF-3M			CF-8M					CF-8C		
Code		A	B	K	C	D	E	F	L	M	N	G	H	J	P	O	R	T	S
Ferrite, %		0	4	20	37	0	5	16	0	20	39	0	2	15	16	38	0	13	44
Exposure Temperature, deg F	Time, hr																		
600	25	116	126	...	174	125	154	151	122	163	175	126	162	166	174	181	133	171	179
	400	116	131	...	195	126	156	159	121	161	177	128	163	177	172	176	127	180	229
	1000	...	...	151	188	...	...	159	...	...	...	...	...	...	...	...	...	...	...
	2000	...	...	152	190	...	...	159	...	...	...	...	...	...	...	...	...	...	...
	3000	...	...	156	188	...	...	167	...	...	...	...	...	...	...	...	...	...	...
800	25	116	127	...	185	124	155	159	127	177	217	126	162	169	190	202	134	180	200
	400	118	124	...	203	126	156	170	126	189	239	131	163	192	194	227	129	165	248
	1000	...	...	165	207	...	...	167	...	...	...	...	...	...	...	...	...	...	...
	2000	...	...	170	207	...	...	174	...	196	...	...	...	...	...	254	...	196	...
				170	201			167											
	3000	...	...	152	209	...	...	158	...	189	246	...	...	...	...	258	...	202	...
				175				172											
	4000	...	...	184	205	...	...	176	...	202	250	...	...	...	...	...	...	197	...
1000	25	116	127	...	173	121	157	153	125	168	184	131	164	167	...	194	133	176	196
	400	121	133	...	205	129	160	173	127	170	200	131	170	192	...	202	136	189	200
1200	25	116	131	...	174	121	156	154	118	162	179	131	162	167	...	184	137	176	204
	400	120	134	...	192	128	160	166	122	174	218	149	170	175	...	220	129	186	241
1400	25	...	...	...	...	...	...	...	121	184	229	...	...	...	...	229	153	184	209
	400	...	...	...	...	...	...	...	125	197	246	...	...	...	...	239	133	198	223
1550	48	116	133	...	164	130	158	160	...	...	...	141	165	185	...	...	...	...	...
	100	116	133	...	169	130	158	161	...	...	...	141	170	185	...	...	...	...	...
	150	116	133	...	174	130	158	161	...	...	...	142	170	183	...	...	...	...	...
Solution annealed		116	133	142	164	127	158	156	116	149	172	129	160	164	174	173	128	164	168

TABLE 4—PER CENT FERRITE AFTER ELEVATED TEMPERATURE EXPOSURES.

(Solution annealed value for per cent ferrite used as reference.)

Alloy Type		CF-3				CF-8			CF-3M			CF-8M					CF-8C		
Code		A	B	K	C	D	E	F	L	M	N	G	H	J	P	O	R	T	S
Ferrite, %		0	4	20	37	0	5	16	0	20	39	0	2	15	16	38	0	13	44
Exposure Temperature, deg F	Time, hr																		
600	25	0.0	3.4	...	37.2	0.0	4.8	15.5	0.0	21.0	41.7	0.0	2.4	15.3	16.0	38.1	0.0	13.0	41.7
	400	0.0	3.5	...	36.4	0.0	4.8	15.2	0.0	21.0	40.5	0.0	2.4	15.0	18.0	38.7	0.0	12.4	44.7
	1000	...	...	22.1	37.8	...	...	15.4	...	...	...	...	...	...	...	...	...	...	...
	2000	...	...	22.1	37.2	...	...	13.6	...	...	...	...	...	...	...	...	...	...	...
	3000	...	...	22.0	36.6	...	...	15.0	...	...	...	...	...	...	...	...	...	...	...
800	25	0.0	3.4	...	38.9	0.0	5.0	15.0	0.0	21.0	40.5	0.0	2.0	15.4	16.5	36.6	0.0	11.8	42.9
	400	0.0	3.2	...	36.0	0.0	4.4	15.0	0.0	19.2	34.8	0.0	2.6	15.2	16.2	36.6	0.0	12.4	43.2
	1000	...	...	22.0	37.0	...	...	16.0	...	...	...	...	...	...	...	...	...	...	...
	2000	...	...	22.0	36.0	...	...	16.5	...	18.0	...	...	...	...	...	36.0	...	12.0	...
				21.0	32.0			15.0											
	3000	...	...	22.0	29.0	...	...	14.4	...	19.0	40.0	...	...	...	...	37.0	...	13.0	...
				22.0				15.0											
	4000	...	...	18.0	28.0	...	...	16.0	...	19.0	38.0	...	...	...	...	...	...	11.0	...
1000	25	0.0	3.3	...	36.9	0.0	5.0	14.8	0.0	18.6	39.8	0.0	2.0	15.4	...	37.5	0.0	12.0	40.8
	400	0.0	2.4	...	36.0	0.0	4.0	14.0	0.0	17.0	35.7	0.0	2.0	13.8	...	36.2	0.0	12.6	39.6
1200	25	0.0	2.4	...	33.6	0.0	4.6	13.6	0.0	13.8	29.4	0.0	1.6	13.8	...	28.2	0.0	10.0	22.8
	400	0.0	2.0	...	21.0	0.0	3.6	10.2	0.0	4.4	8.0	0.0	2.0	7.0	...	7.8	0.0	7.8	10.6
1400	25	...	...	...	...	...	...	...	0.0	0.8	3.0	...	...	...	...	1.5	0.0	6.4	12.4
	400	...	...	...	...	...	...	...	0.0	0.0	0.0	...	...	...	...	0.0	0.0	2.4	7.8
1550	48	0.0	2.0	...	30.0	0.0	2.4	11.0	...	...	...	0.0	0.0	0.0	...	...	...	...	...
	100	0.0	2.0	...	30.0	0.0	2.4	11.0	...	...	...	0.0	0.0	0.0	...	...	...	...	...
	150	0.0	2.0	...	30.0	0.0	2.4	10.9	...	...	...	0.0	0.0	0.0	...	...	...	...	...

fine carbides formed at the original austenite-ferrite interface; the remaining ferrite then transformed into sigma and new austenite. Formation of large amounts of sigma phase was accompanied by a marked decrease in the Charpy V-notch impact strength and increases in Brinell hardness.

1550 F—The only change in microstructure observed for alloys D-CF3-4, E-CF8-5, and F-CF8-16 was a growth of the austenite into the ferrite pools and some apparent carbide precipitation. The change in microstructure for alloy F-CF8-16 after 150 hr is shown in Fig. 22.

A slight amount of sigma phase was detected in former ferrite pools of alloy C-CF3-37 after 100 and 150-hr exposures at 1550 F. The principal reason for the drop in ferrite content in this alloy was the formation of new austenite. The microstructure of this alloy after 150 hr is illustrated in Fig. 23.

It is concluded that the alloys with the higher ferrite contents are particularly susceptible to embrittlement by sigma phase formation in the temperature range 1200 to 1500 F. The lower ferrite alloys and fully austenitic alloys are generally embrittled to a lesser degree, at least for the time periods investigated. Metallographic examinations and ferrite determinations showed that the decomposition of the ferrite in alloys M-CF3M-20, N-CF3M-39, and O-CF8M-38 was almost complete after a 25-hr exposure at 1400 F, while the ferrite in alloy S-CF8C-44 was almost 75 per cent transformed.

Impact strength at room temperature dropped appreciably for alloys C-CF3-37, D-CF8-0, G-CF8M-0, and J-CF8M-15, after a 48-hr exposure at 1550 F. The ferrite contents of the alloys with an initial duplex microstructure decreased during the first 48 hr of heating, and remained essentially constant afterwards. Alloy J-CF8M-15 contained no ferrite after 48 hr at temperature.

The ferrite pools in alloy J-CF8M-15 transformed completely to sigma phase and new austenite. Specimens exposed for time periods shorter than 48 hr showed that austenite formed first in the ferrite pools, and the remaining ferrite transformed to sigma and austenite. The reaction was essentially complete after 8 hr, and further time at temperature produced only a coalescence of the sigma particles. An X-ray powder pattern obtained from a residue extracted from this alloy aged for 1300 hr at 900 F gave a

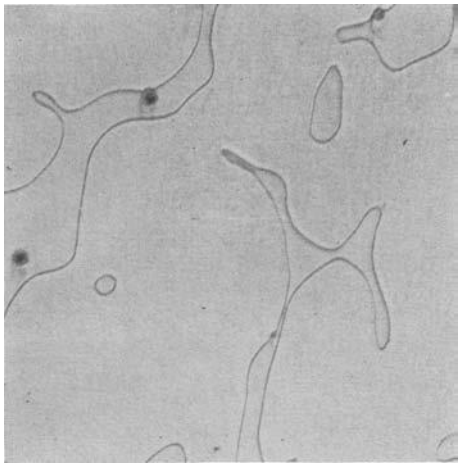


FIG. 16—Alloy F-CF8-16 Solution Annealed Structure Showing Ferrite Pools in Austenite Matrix. Etched Vilella's Reagent (×500).

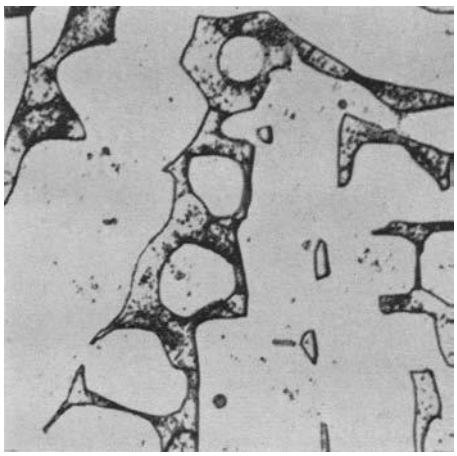


FIG. 17—Alloy F-CF8-16 after 400 hr at 1000 F Precipitation in Ferrite. Etched Oxalic Acid, Electrolytic (×500).

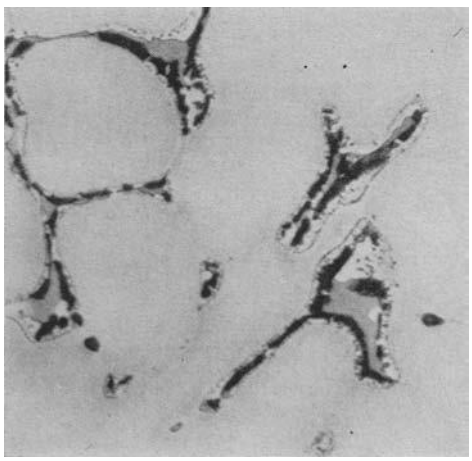


FIG. 18—Alloy F-CF8-16 after 400 hr at 1200 F Austenite White, Ferrite Gray, Sigma Black. Etched Vilella's Reagent; 10N KOH (×500).

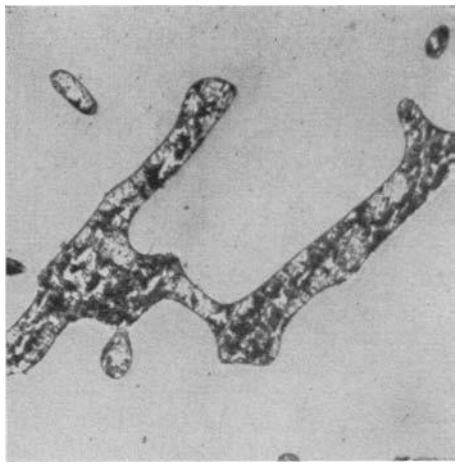


FIG. 19—Alloy J-CF8M-15 after 400 hr at 1200 F. Austenite White, Ferrite Gray, Sigma Black. Etched Vilella's Reagent; 10N KOH (×500).

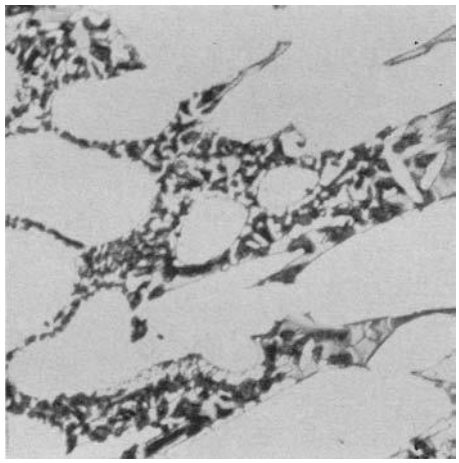


FIG. 20—Alloy C-CF3-37 after 400 hr at 1200 F. Austenite White, Ferrite Gray, Sigma Black. Etched Vilella's Reagent; 10N KOH (×500).

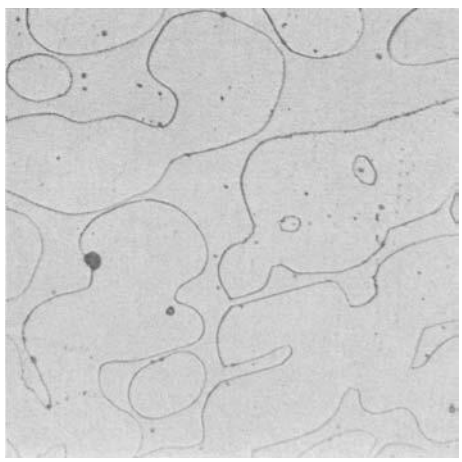


FIG. 21—Alloy C-CF3-37 Solution Annealed Structure. Etched Oxalic Acid, Electrolytic (×500).

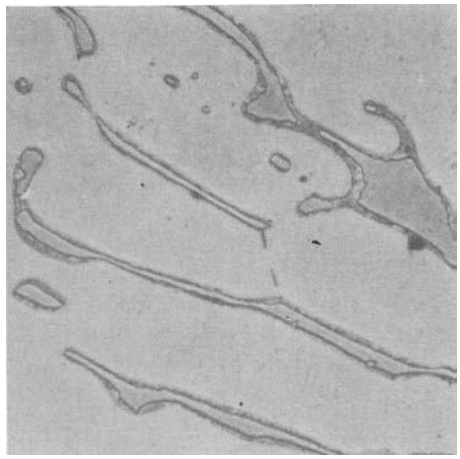


FIG. 22—Alloy F-CF8-16 after 150 hr at 1550 F. Austenite and Ferrite. Etched Vilella's Reagent; 10N KOH (×500).

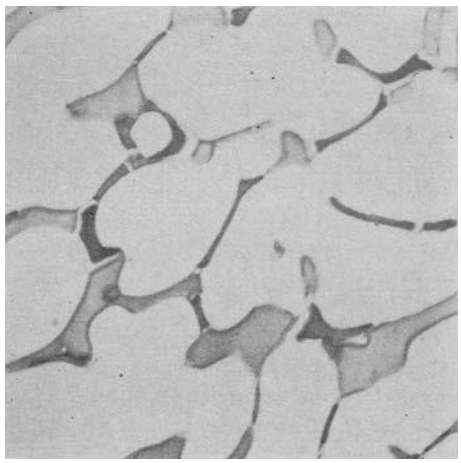


FIG. 23—Alloy C-CF3-37 after 150 hr at 1550 F. Austenite White, Ferrite Gray, Sigma Black. Etched Vilella's Reagent; 10N KOH (×500).

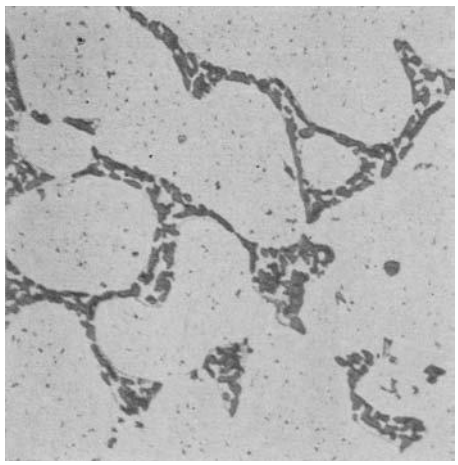


FIG. 24—Alloy J-CF8M-15 after 150 hr at 1550 F. Austenite White, Sigma Black. Etched Vilella's Reagent; 10N KOH (×500).

powder pattern from which the interplanar spacings were calculated. These values were compared with values from the literature (11,12). The powder pattern demonstrated the presence of sigma phase in the overaged microstructure. It was not certain whether the sigma phase formed directly as the age-hardening precipitate or whether it formed concurrently with an age-hardening process. The general precipitation visible in the microstructure of alloy J-CF8M-15 heated at 1000 F for 400 hr indicated that overaging was considerably faster at 1000 F than at 900 F. The microstructure after 150 hr exposure at 1550 F for this alloy is shown in Fig. 24.

Effect of Nitrogen:

The effect of nitrogen level on the properties of two CF-8M alloys with similar analyses and ferrite contents was observed for P-CF8M-16 and J-CF8M-15. Alloy P-CF8M-16, with the higher nitrogen, generally maintained a strength advantage over alloy J-CF8M-15 at 600 and 800 F, but the data for exposures at 800 F seem to indicate a greater embrittling tendency for alloy P-CF8M-16. Microstructural differences were not pronounced.

CONCLUSIONS

1. Cast alloys of the CF-3, CF-8, CF-3M, and CF-8M types are regularly made commercially within the chemical ranges stated in ASTM Specifications A 296 and A 351 with ferrite content percentages varying from very low (0 to 5 per cent) to very high (35 to 40 per cent) and the wide range of mechanical properties observed can be attributed to the wide range of ferrite contents possible within the permissible chemistry.

2. Mechanical properties of these alloys are functions of ferrite content at both room and elevated temperatures; tensile and yield strengths being directly, and ductility and impact strength being inversely related to ferrite content.

3. Ferrite content can be controlled by proper balancing of the major and minor chemical constituents of the alloys, and commercial production of controlled ferrite alloys is feasible.

4. At temperatures of 800 F and below, alloys containing up to 35 per cent ferrite show no deleterious effects from microstructural changes resulting from temperature of exposure.

5. Change in mechanical properties is dependent on time of exposure to elevated temperature, but values tend to stabilize at acceptable levels with increasing time at temperature below 800 F.

6. Minimum mechanical properties now set forth in ASTM specifications reflect the possibility of obtaining such low values if the composition balances tend toward wholly austenitic structures.

7. Substantially higher minimum mechanical property values could be set for higher strength grades for service up to 800 F, and these could be met in commercial practice by production of alloys with controlled ferrite contents without danger of loss of ductility after prolonged exposure.

Acknowledgments:

The authors are indebted to the Alloy Casting Institute for its interest and support of the research and to the Esco Corp., Portland, Ore. for providing the experimental material used in this program.

Measurements of ferrite contents and tensile properties of the 339-heat sample of CF-8 and CF-8M alloys were obtained by C. D. Robinson of The Bonney-Floyd Co., Columbus, Ohio. Other data on commercial heats were supplied by the following producers:

Cooper Alloy Corp., Hillside, N. J.
The Duraloy Co., Scottdale, Pa.
The Duriron Co., Inc., Dayton, Ohio
Empire Steel Castings, Inc., Reading, Pa.
Esco Corp., Portland, Ore.
General Alloys Co., Boston, Mass.
Lebanon Steel Foundry, Lebanon, Pa.
The Midvale Co., Philadelphia, Pa.
The Ohio Steel Foundry Co., Springfield, Ohio
Sandusky Foundry & Machine Co., Sandusky, Ohio
U. S. Pipe & Foundry Co., Burlington, N. J.

REFERENCES

(1) E. A. Schoefer, *ACI Data Sheets*, Alloy Casting Inst., Mineola, N. Y., 1954.
(2) E. A. Schoefer, "Influence of Composition on Properties of Fe-Cr-Ni Alloys," Master's thesis, Polytechnic Institute of Brooklyn, 1957.
(3) A. L. Schaeffler, "Welding Dissimilar Metals," *Iron Age*, Vol. 162, No. 1, July, 1948, pp. 72–9.
(4) W. O. Binder, C. M. Brown, and Russell Franks, "Resistance to Sensitization of Austenitic Chromium-Nickel Steels of 0.03% Max. Carbon Content," *Transactions*, Am. Soc. Metals, Vol. 41, 1949, pp. 1301–1371.
(5) M. G. Fontana, "Progress Report No. 18a to Alloy Casting Institute," The Ohio State University Research Foundation, January, 1954.
(6) J. W. Flowers, F. H. Beck, and M. G. Fontana, "Corrosion and Age Hardening Studies of Some Cast Stainless Alloys Containing Ferrite," *Corrosion*, NACE Journal of Science and Engineering, May, 1963.
(7) A. J. Cook and F. W. Jones, "The Brittle Constituent of the Iron-Chromium System (Sigma Phase)," *Journal*, Iron and Steel Inst., Vol. 148, 1943, p. 217.
(8) A. A. Watts, "The Roles of Ferrite and Titanium in the Stabilization of 18 Cr-8 Ni Cast Stainless Alloys," Doctoral dissertation, The Ohio State University, 1952; also *ACI Report No. 15*, 1952.
(9) G. A. Mancini, "The Effect of Ferrite on the Corrosion of CF-8 Type Alloys by Various Media," Master's thesis, The Ohio State University, 1958; also *ACI Report No. 350-II*, 1958.
(10) J. J. Gilman, "Electrolytic Etching—The Sigma Phase Steels," *Transactions*, Am. Soc. Metals, Vol. 44, 1952, p. 566.
(11) H. C. Vacher and C. J. Bechtoldt, "Delta Ferrite-Austenite Reactions and the Formation of Carbide, Sigma, and Chi Phases in 18 Chromium-8 Nickel-3.5 Molybdenum Steels," *Journal of Research*, National Bureau of Standards, Vol. 83, 1954, p. 67.
(12) J. F. Brown, W. D. Clark, and A. Parker, "Extraction of Minor Phases from Austenitic Steels," *Metallurgia*, Vol. 56, 1957, p. 215.

THE EFFECT OF SMALL COLUMBIUM ADDITIONS TO TYPE 304 STAINLESS STEEL

By R. B. G. Yeo[1] and T. E. Scott[2]

Synopsis

The present investigation was undertaken to evaluate the potentiality of grain refinement as a strengthening mechanism in wrought austentic stainless steels. Attention was focused on additions of columbium to Type 304 stainless steel base compositions.

The results show that small additions of columbium retard recrystallization and grain growth during annealing following cold working. For example, the addition of about 0.2 per cent columbium to a Type 304 L base composition is capable of increasing its yield strength by about 50 per cent to about 40,000 psi. This same addition to a Type 304 base, coupled with the elimination of the process anneal after hot-working, produces a yield strength increase of about 100 per cent, that is, up to 50,000 to 60,000 psi. This effect is observed even when the hot-finishing temperature is sufficiently high to give a recrystallized structure before cold working and final annealing.

Cold working is used widely to strengthen austenitic stainless steels, and yield strengths up to about 150,000 psi normally are achieved. Strengths up to about 240,000 psi, coupled with good toughness, have been attained in some compositions through sub-zero rolling followed by aging at 800 F.[3]

Cold-worked Type 18-8 stainless steel is usually annealed in the range 1950 to 2050 F, although recrystallization occurs at lower temperatures. The higher annealing temperatures are used commercially to ensure the rapid and complete solution of chromium carbides.

In an attempt to raise the recrystallization temperature to the normal annealing range, the effect of small additions of columbium to Type 18-8 stainless steels were evaluated in the present investigation.

The investigation had two essential parts directed towards the following objectives:

1. Determination of the composition that most effectively prevented loss of strength and hardness as the annealing temperature was raised.
2. A study of the effects on strength and hardness of some processing variables.

Materials

All alloys were induction melted in magnesia crucibles using Armco iron, electrolytic nickel, and ferrochromium melting stock. Deoxidation was accomplished with silicon-manganese. Final additions were made following slag removal and temperature adjustment.

The ingots were forged and hot rolled at either 2000 or 2300 F after soaking at these temperatures. The hot-rolled product was either in the form of $\frac{3}{4}$-in. round bars or $2\frac{1}{2}$ by $\frac{3}{8}$-in. plate. Further processing details will be given where they are pertinent to the discussion.

Test Results

Effects of Columbium:

The effect of columbium was determined in a series of heats containing about 0.07 per cent carbon, representative of Type 304 stainless steel. These heats were both forged and rolled using a soaking temperature of 2300 F in order to dissolve most of the columbium carbides.

The hot-rolled bar stock was given a shaping pass in the cold mill and was solution treated for 2 hr at 2300 F to ensure a uniform starting condition. The bars were cold reduced about 45 per cent in area, and specimens were annealed for 1 hr at temperatures between 1100 and 2300 F. Hardness and metallographic examination were used to assess the annealing characteristics. The steels were etched electrolytically for 20 sec at 0.2 v in concentrated nitric acid to reveal the grain size clearly.

Raising the annealing temperature above 1100 F had little effect until the steels began to soften at temperatures above 1300 F. Annealing above this temperature caused the room-temperature hardness of the columbium steels to fall less rapidly than that of the columbium-free steels. A double inflection was evident when hardness was plotted against annealing temperature, Fig. 1. As the columbium content increased the double inflection became more pronounced. The first inflection corresponded with the completion of recrystallization while the second indicated the onset of grain growth. This is illustrated by the micrographs shown in Fig. 1. The hardness of all the steels lay within the range 65 to 70 Rockwell B after annealing at 2300 F. It is evident that columbium additions of less than 0.5 per cent exert a significant effect within an important practical annealing temperature range.

An isothermal representation of the data from the annealing study shows that hardness increased linearly with columbium content up to a limiting value which depended on the annealing temperature, Fig. 2. Columbium contents above this sharp inflection offered no apparent advantage. The inflection point of the isotherms moved from about 0.18 per cent to about 0.35 per cent columbium as the temperature was increased from 1800 to 2200 F. At 2300 F no effect of columbium was noted up to 0.46 per cent, which was the highest level examined in this series. The curves also suggest that recrystallization was incomplete at annealing temperatures below about 1800 F.

The locus of the limiting columbium contents lies very close to data published for the solubility of columbium carbide,[4,5] Fig. 3. This suggests that the grain growth is restricted by the presence

[1] Formerly supervisor, Steel Section, Research Laboratory, The International Nickel Co., Inc., Bayonne, N. J., now with Development Operations Office, Richard Thomas and Baldwins, Ltd., Newport, Monmouthshire, England.

[2] Formerly research metallurgist, Steel Section, Research Laboratory, The International Nickel Co., Inc., Bayonne, N. J., now with Ames Laboratory, University of Iowa, Ames, Iowa.

[3] See p. 17.

[4] K. Bungardt and G. Lennartz, "Precipitation Reactions and Intercrystalline Corrosion in a Chromium-Nickel Austenitic Stainless Steel Containing Columbium," *Archiv für das Eisenhuttenwesen*, Vol. 29, 1958, p. 359.

[5] K. J. Irvine, J. D. Murray, and F. B. Pickering, "Structural Aspects of Creep Resisting Steel," *Special Report No. 70*, Indian Standards Inst., 1961, p. 252.

Copyright© 1965 by ASTM International

www.astm.org

of columbium carbide. Once this carbide dissolves, coarsening occurs in the normal manner.

The effects of carbon and columbium were then studied in greater detail to reveal the benefits of columbium additions.

The hardening effects of carbon and columbium were similar in the range 0.02 to 0.08 per cent, Fig. 4. The greater

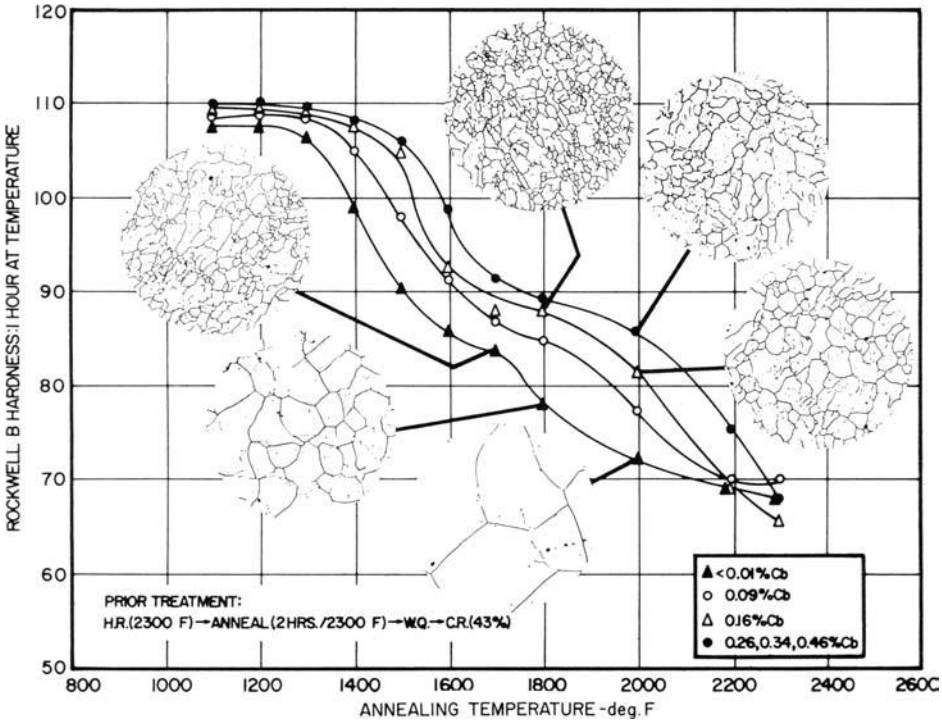


FIG. 1—Effect of Columbium Content and Annealing Temperature on Hardness and Microstructure. Etchant: Electrolytic Nitric Acid (×250). Reduced One Half for Reproduction.

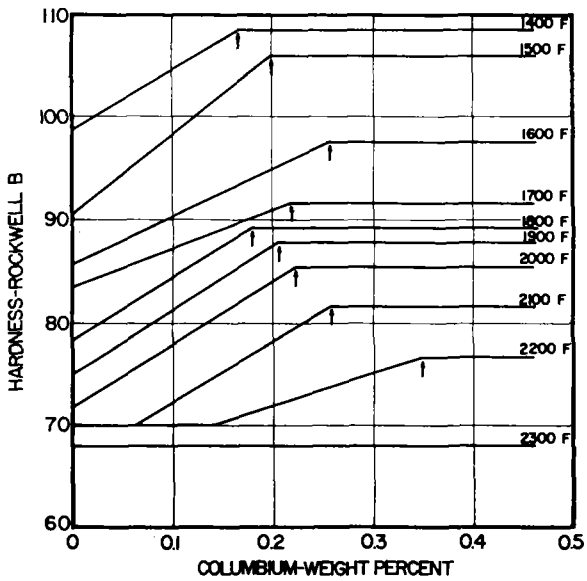


FIG. 2—Effect on Hardness of Columbium Content at Different Annealing Temperatures.

determine their optimum levels. Chemical composition was correlated with grain size, hardness, and yield strength for a fixed annealing temperature of 1800 F following 50 per cent cold reduction. This temperature was chosen because the previous results summarized in Fig. 1 indicated that it would clearly tolerance of these alloys for columbium permitted its hardening effectiveness to be extended above this range. Thus the addition of 0.2 per cent columbium caused the hardness of the steels to be raised from about 135 to 185 DPH.

The interrelation between columbium, carbon, hardness, and grain size is shown in Fig. 5. Carbon additions alone caused no grain refinement while the hardness was raised slightly. Columbium additions up to at least 0.2 per cent both hardened and refined the grain size of the stainless steel. The correlation between grain size and the sum (Cb + C) is indicated in Fig. 6. The hardness of the different alloys is also shown.

Figure 7 shows the effect of columbium plus carbon on the 0.2 per cent offset yield strength of alloys annealed for 1 hr at 1800 F. The sharp increase in yield strength was independent of carbon content which varied from 0.015 to 0.11 per cent in this series. These steels contained from 0.02 to 0.04 per cent nitrogen. Up to about 0.2 per cent (Cb + C) the yield strength obeyed the following equation:

$$\text{yield strength, ksi} = 109\ (\text{Cb} + \text{C}) + 22.3$$

The columbium level at which further strengthening ceased abruptly was in reasonable agreement with that shown in Fig. 2. The yield strengths of alloys containing more than about 0.2 per cent columbium lay in a band between about 40,000 and 44,000 psi, the higher carbon alloys being the stronger. The ductility of the steels was consistently high, their elongations varying from 60 to 75 per cent and their reductions of area from 70 to 80 per cent.

The significant feature of these data is that steels containing 0.02 per cent carbon could be treated with about 0.2 per cent columbium, obtaining a yield strength as high as 40,000 psi after annealing for 1 hr at 1800 F.

The Evaluation of Processing Variables:

The effect of final annealing temperature was an integral part of the study of the effects of columbium. Attempts were made also to evaluate variations in prior processing. The normal procedure for producing rolled stainless steel products is to hot roll, process anneal, cold roll, and final anneal. Particular attention was paid to the effects of process-annealing temperature because it affects the level and distribution of columbium in solution.

Hot-rolled bar stock of a columbium-containing series which had a hardness of about 109 Rockwell B was process annealed for 1 hr at temperatures between 2000 and 2400 F. It was subjected to 45 per cent cold reduction with and without these prior process annealing treatments. A final annealing treatment of 1 hr at 1800 F was given.

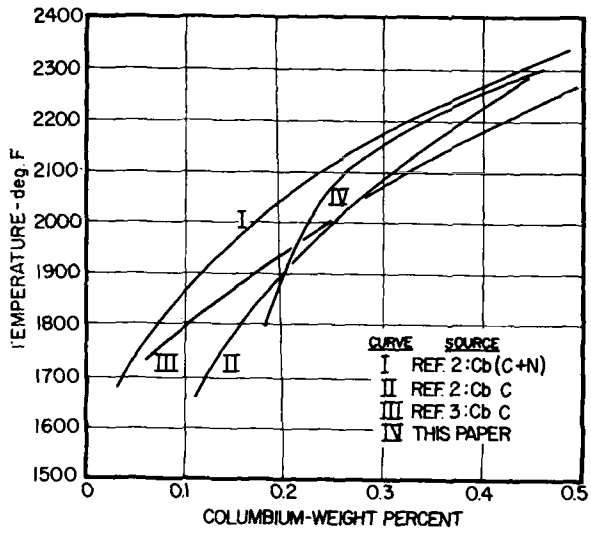


FIG. 3—Relation Between Locus of Inflection Points from Fig. 2 and Solubility Limit of Columbium Carbide.

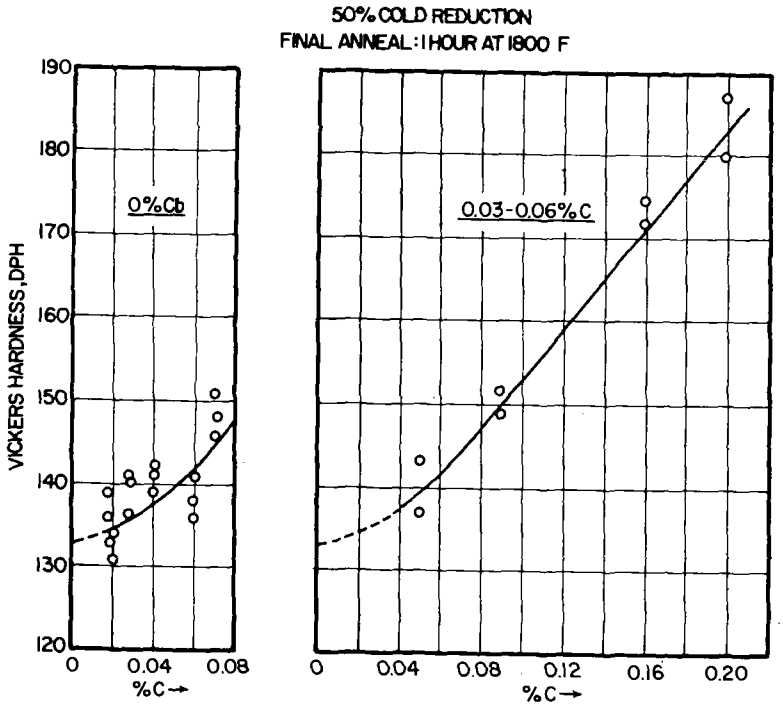


FIG. 4—Effect on Hardness of Carbon Alone and of Columbium at Carbon Levels Between 0.03 and 0.06 Per Cent.

Figure 8 shows the effect of columbium content on yield strength for several process annealing treatments. Although the degree of cold working and the final annealing temperature were maintained constant, it was found that yield strength increased with columbium content up to different levels which were dependent on the process annealing treatment. Raising the process annealing temperature from 2000 to 2400 F had little effect on the yield strength of the columbium-free steels, and it caused an increase of about 5000 psi in the columbium-containing steels.

Elimination of Process Annealing:

When it was found that the steels were responsive to changes in treatment before cold rolling, the effect of eliminating the process anneal was studied. Lengths of the bar stock, which had been finished at about 1700 F and had a hardness of about 109 Rockwell B, were cold rolled and then annealed at 1800 F. The results plotted in Fig. 8 show that eliminating the process anneal resulted in a significant strengthening effect, although the steels were given the final annealing treatment at 1800 F. At about 0.3 per cent columbium, the steel treated in this way had a yield strength of almost 56,000 psi. It was also noted that the columbium-free steel showed only a very slight increase in strength when the process anneal was eliminated.

To check whether residual cold work was the cause of the higher strength in the steels which had not been process annealed, another steel was tested. A plate of Type 304 stainless steel which contained 0.17 per cent columbium was hot rolled to strip in two passes starting at 2300 F and finishing at about 2000 F. The hot-rolled structure was fully recrystallized with a Rockwell B hardness of 75 to 80. (Process annealing in the temperature range 1450 to 2050 F

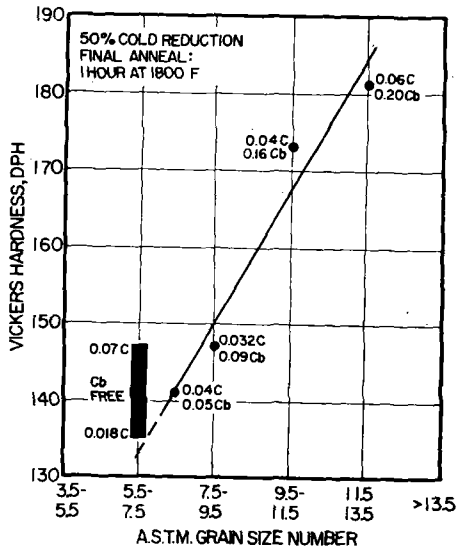


FIG. 5—Effect of Carbon and Columbium on Grain Size and Hardness.

raised this hardness, not lowered it. For instance, annealing at 1750 F raised the hardness by 10 points over that of the hot-rolled stock.) Specimens of the steel were then cold reduced 45 per cent without a prior process anneal and were given a final annealing treatment at 1800 F. The steel had a 0.2 per cent offset yield strength of 50,500 psi, which is in close agreement with that shown in Fig. 8 for a steel containing 0.17 per cent columbium. Therefore, the columbium-containing steels exhibited higher yield strengths in the annealed condition if the process annealing treatment was eliminated. This higher strength cannot be attributed to cold work remaining after hot working, in view of the low hot-rolled hardness of 75 to 80 Rockwell B. Furthermore, the final anneal at 1800 F was above the recrystallization temperature, and the columbium-free

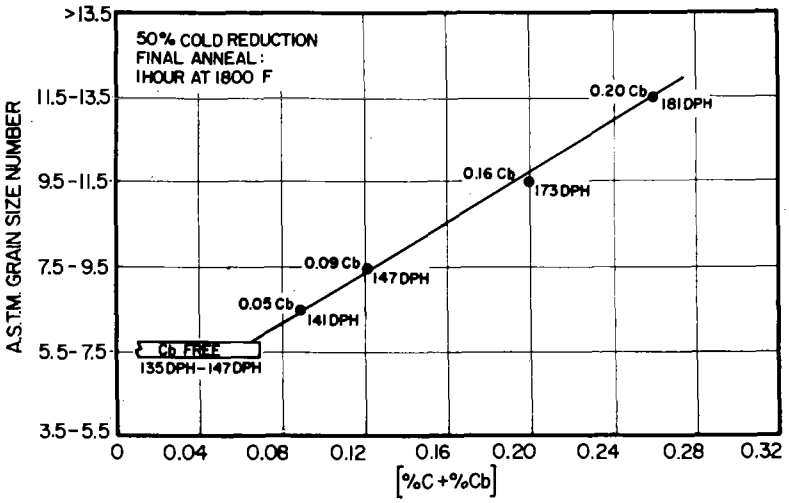


FIG. 6—Correlation of Grain Size with Columbium-Plus-Carbon Combinations.

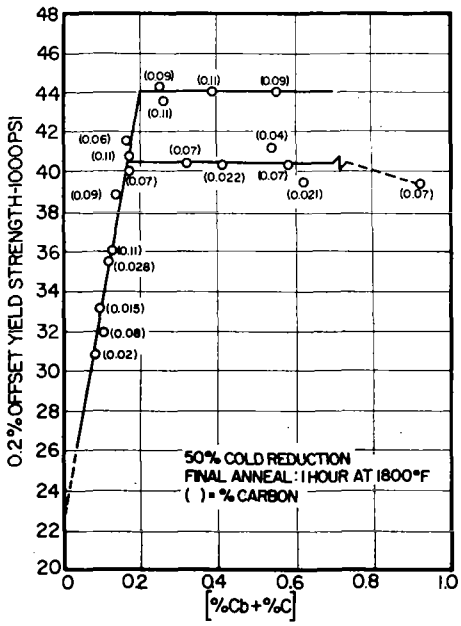


FIG. 7—Effect of (% Cb + % C) on 0.2 Per Cent Offset Yield Strength.

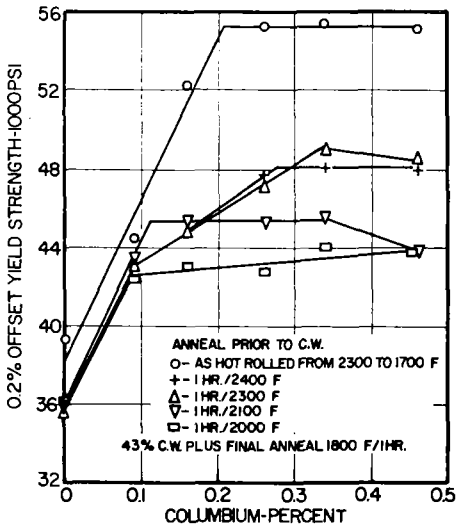


FIG. 8—Effect of Process Annealing Temperature Prior to Cold Work and Final Anneal at 1800 F on Yield Strength of Type 304 Base Alloy with 0.07 Per Cent Carbon.

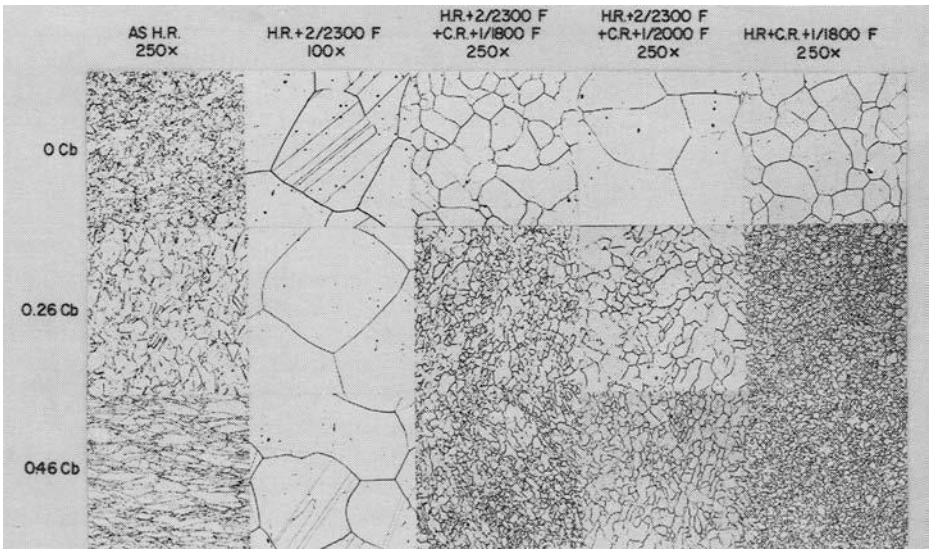


FIG. 9—Effect of Columbium Content and Several Processing Steps on Grain Size of a Type 304 Stainless Steel Composition Containing 0.07 Per Cent Carbon. Reduced One Half for Reproduction.

steels did not show a strengthening response.

The effects of processing on the microstructure of three steels containing 0, 0.26, and 0.46 per cent columbium are shown in Fig. 9. The first column shows the structure of the hot-rolled alloys which were finished at about 1700 F. A process annealing treatment at 2300 F eliminated all apparent effects of columbium, as seen by the micrographs of the second column. The effect of columbium in restricting grain growth during final annealing of cold-rolled stock is illustrated in Columns 3 and 4. Finally, the microstructures in Column 5 clearly demonstrate the remarkably fine grain structure obtained in the columbium-containing steels by omitting the process anneal between hot and cold rolling.

CONCLUSIONS

1. Additions of columbium raised both the recrystallization and the grain-coarsening temperatures of cold-rolled Type 18-8 stainless steel.

2. After annealing at 1800 F, columbium raised the 0.2 per cent offset yield strength to between 40,000 and 45,000 psi depending on the carbon content in the range 0.015 to 0.11 per cent.

3. The yield strength of annealed, columbium treated, Type 18-8 stainless steel could be raised to over 50,000 psi by eliminating the process anneal prior to cold work and final annealing.

Acknowledgments:

The authors wish to acknowledge R. A. Bulwith and F. J. Macolino for assistance with experimental and metallographic work, respectively.

DISCUSSION

K. E. PINNOW[1]—In view of the reported effects of aluminum on the grain size of austenitic stainless steels,[2] I would like to ask the authors if the addition of aluminum to the alloys studied had any effect on grain size and mechanical properties.

R. B. G. YEO AND T. E. SCOTI (*authors*)—Although Mr. Pinnow notes that Thielsch stated that aluminium acts as a grain refiner and thought a level of about 0.03 per cent to be most effective, no proof was given. The table reproduced by Thielsch from the work of Vialle shows results similar to those we obtained from aluminium additions. We examined several potential grain refiners including aluminium but found only columbium to be significantly affective.

[1] Crucible Steel Co. of Am., Pittsburgh, Pa.
[2] H. Thielsch, "Physical Metallurgy of Austenitic Stainless Steels," *The Welding Journal*, December, 1950, p. 604-S.

Stress Corrosion and Evaluation Tests for Stainless Steels

Effect of Heat Treatment and Welding on Corrosion Resistance of Austenitic Stainless Steels

By J. R. Auld*

Abstract

The thermal effects of annealing, sensitization and welding on the resistance to corrosion by plant process solutions were determined for nine stainless steel alloys. Field corrosion information from exposure of 1200 test coupons is recorded and correlated with the 240-hour boiling 65 percent nitric acid test. The results show (1) general corrosion and pitting as well as intergranular corrosion can be accelerated in certain solutions by improper heat treatment and welding; many solutions do not cause accelerated corrosion of improperly heat treated stainless steels; (2) the boiling 65 percent nitric acid test is a satisfactory quality test for Types 302, 304, 304L, 347, 316 and 317 stainless steels, but is not a satisfactory quality test for Types 321, 316L and 318 stainless steels; and (3) single-pass welds on 1/8-inch thick material will cause severe intergranular corrosion in only a very few instances.

Introduction

Selection of stainless steels for use in corrosive services is based on their resistance to general corrosion when the alloys are in the annealed condition. Improper annealing and welding of austenitic stainless steels can cause structural changes in the alloys. These changes will, in certain media, increase the corrosion rate a thousandfold that of the alloy in the properly annealed condition. The accelerated corrosion, which takes place primarily at the grain boundaries, is called intergranular corrosion. The grain boundaries are made susceptible to accelerated corrosion by formation of precipitates in the grain boundary zones. The precipitates formed by thermal treatments in the 900 to 1400 F (480 - 750 C) range are usually chromium-rich carbides. In certain alloys sigma phase is the precipitate.

The materials engineer has the choice of selecting stainless steels purchased to specifications which do or do not require evaluation tests. Evaluation tests are accelerated laboratory tests which determine if the stainless steel material has been properly annealed. We have many installations where unevaluated stainless steels have performed satisfactorily, but we have had a number that did not. This study was made to determine how adversely the performance of stainless steel in the industrial environments would be affected by thermal treatments known to adversely affect the performance of these alloys in the 65 percent HNO_3 evaluation test. As the specific corrosive environments of the laboratory evaluation test rarely represent the conditions encountered in the chemical processes, our program was planned to establish the environments which do or do not produce intergranular corrosion on improperly annealed material and to establish a basis for relaxation or insistance on adherence to the acceptance test specification.

The data on which this paper is based were obtained from tests on approximately 1200 specimens, representing nine austenitic stainless steel alloys, in various heat treated and welded conditions, and exposed in about 45 plant locations within the Du Pont Company.

* Consultant, Materials Engineering Service Division, Engineering Department E. I. du Pont de Nemours & Co., Wilmington, Delaware.

Composition of Materials

The chemical analyses of the alloys used in this study are shown in Table 1. The alloys represent commercial heats of 1/8 in. sheet purchased from three producers.

The chemical analyses of the weld wires and weld metal pads are shown in Table 2. The Type 308 rod was used for the Types 302 and 304 welded corrosion samples. Type 347 rod was used to make the Types 321 and 347 welded corrosion samples.

Test Specimens and Exposures

The corrosion samples, 2-3/4 in. square x 1/8 in., were heat treated and welded to provide various degrees of sensitization, or susceptibility to intergranular corrosion. Sensitization occurs when the austenitic alloy is heated between 900 F (480 C) and 1400 F (850 C). In the welded specimens sensitization is localized in a narrow strip of base metal, near the weld, which has been subjected to 900-1400 F (480-850 C) range by the heat developed during welding.

The boiling 65 percent nitric acid test was used as a reference for determining the degree of sensitization caused by each thermal treatment. The standard treatments were (1) mill anneal (1 hour 1950-2050 F (1065-1120 C), water quench), (2) severely sensitized (1 hour 1250 F (680 C), water quench) and (3) as welded (diamond pattern 110-ampere and 90-ampere single beads) applied

Copyright© 1965 by ASTM International

www.astm.org

to one surface of the specimen. Many special heat treatments were given to specific alloys and are shown in Table 27.

The treated samples were installed in racks containing approximately 25 specimens, and were exposed in chemical plant operating equipment and storage tanks.

TABLE 1 - MATERIALS FOR CORROSION SAMPLES

AISI Type	Analysis % by Weight									
	C	Mn	Si	P	S	Cr	Ni	Cb	Ti	Mo
302	0.09	1.38	0.54	0.029	0.016	18.16	8.78	--	--	--
304	0.07	0.95	0.32	0.022	0.014	19.64	9.15	--	--	--
304L	0.032	1.17	0.39	0.025	0.009	18.96	10.30	--	--	--
321	0.04	1.53	0.47	0.020	0.009	17.48	10.32	--	0.38	--
347	0.06	1.84	0.46	0.023	0.007	17.72	10.97	0.80	--	--
316	0.06	1.74	0.53	0.023	0.017	17.78	12.79	--	--	2.20
316L	0.032	1.79	0.48	0.025	0.010	17.20	13.35	--	--	2.49
317	0.067	1.80	0.57	0.020	0.019	18.49	13.64	--	--	3.18
318	0.07	0.99	0.68	--	--	18.31	14.11	0.91	--	2.43

Results and Discussion

The results are presented in tables showing comparative corrosion rates and corrosion appearances of samples exposed to process solutions and the boiling 65 percent HNO_3 test.

Reference tables shown in the appendix record all results. Summary tables which contain selected data from the reference tables are inserted in the text to assist in the discussion of significant trends with respect to types of exposures which do or do not cause accelerated corrosion of improperly heat treated stainless steels. The intergranular attack appearance was determined by examination under a low power microscope. The intergranular corrosion appearance nomenclature used in the tables is:

No Intergranular Corrosion - Equipment life can be estimated directly from the corrosion rate.

Mild Intergranular Corrosion - Equipment life can be estimated by multiplying the calculated corrosion rate by 2.

Severe Intergranular Corrosion - Equipment life can be estimated by multiplying the calculated corrosion rate by 3 to 1000.

Mild Weld Decay (WD) - Welded equipment life can be estimated by multiplying the corrosion rate in the zone adjacent to the weld by 2.

Severe Weld Decay (WD) - Welded equipment life can be estimated by multiplying the corrosion rate in the zone adjacent to the weld by 3 to 1000.

Before discussing the results, it is well to emphasize that the exposure conditions are process environments; only the primary chemicals were recorded. Most of the solutions also contained other ingredients which, to the best of our knowledge, had no effect on intergranular corrosion, and we have chosen not to complicate this presentation by their inclusion. The temperature and pressure conditions recorded must, it will be appreciated, represent average conditions. Over a 10,000-hour exposure, temperature fluctuation from batch operation, process upsets and plant shutdowns will be significant.

For these reasons, the actual corrosion rates cannot be accepted as reproducible in the sense that tests in the laboratory, under controlled conditions, are reproducible.

Our conclusions are based upon the analysis of these results as much from a trend aspect as from an absolute rate consideration. Our objective was to obtain significant demonstrations of the influence of the environment involved and its relationship to the acceptance test values. Consequently, the differences in corrosion rates and appearances caused by each thermal treatment are the important results.

TABLE 2 - WELD ROD FOR WELDED SAMPLES

Rod Type	Used With	Analysis % by Weight									Analysis of	
		C	Mn	Si	S	P	Cr	Ni	Mo	Cb	Core Wire	Undiluted Weld Pad
308	302, 304	0.06	1.89	0.38	0.019	0.022	21.14	10.13	--	--	X	
		0.060	1.80	0.472	0.010	0.018	19.98	10.12	--	--		X
308L	304L	0.025	1.52	0.28	0.009	0.008	20.67	10.33	--	--	X	
		0.026	0.81	0.185	0.020	0.009	18.98	9.75	--	--		X
347	321, 347	0.06	1.86	0.48	0.018	0.020	21.27	10.12	--	(a)	X	
		0.061	1.67	0.56	0.018	0.010	20.26	9.96	--	1.01		X
316	316	0.06	2.00	0.50	0.014	0.021	18.87	13.08	2.20	--	X	
		0.058	1.89	0.585	0.011	0.021	18.28	13.04	2.28	--		X
316L	316L	0.030	1.58	0.53	0.010	0.026	18.93	12.87	2.14	--	X	
		0.023	0.90	0.224	0.013	0.021	17.80	12.84	2.21	--		X
317	317	0.06	1.85	0.54	0.019	0.020	20.28	13.80	3.79	--	X	
		0.046	1.78	0.605	0.012	0.023	19.90	13.72	3.56	--		X
318	318	0.05	1.90	0.35	0.015	0.017	19.53	12.87	2.35	(b)	X	
		0.057	1.81	0.514	0.010	0.020	18.71	12.91	2.25	1.20		X

(a) Added in coating to yield 0.9% in undiluted weld metal. (b) Added in coating to yield 1.0% in undiluted weld metal.

TABLE 3 - TYPE 316 IN 3 TO 10% H_2SO_4 AT 50 C

Condition	Intergranular Attack, Appearance		Corrosion Rate, in/mo	
	65% HNO_3**	3-10% H_2SO_4	3-10% H_2SO_4 4752 hr	65% HNO_3** 240 hr
Mill Anneal	None	None	0.00072	0.00076
Severely Sensitized	Severe	Severe	0.00339*	0.100
Mildly Sensitized	Mild	Mild	0.00113	0.00600
As Welded	Severe WD	Mild WD	0.00105	--

* Specimen is rubberlike ** Boiling

TABLE 4 - TYPE 317 IN 30% H_2SO_4 AT 10 C

Condition	Intergranular Attack, Appearance		Corrosion Rate, in/mo	
	65 % HNO_3*	30% H_2SO_4	30% H_2SO_4 4752 hr	65% HNO_3* 240 hr
Mill Anneal	None	None	Nil	0.00114
Severely Sensitized	Severe	Severe (No General)	0.00017	0.090
Mildly Sensitized	Mild	None	0.00001	0.00250
As Welded	Severe WD	None	0.00001	--

* Boiling

TABLE 5 - TYPE 304 IN MIXED ACID (72% H_2SO_4 + 1.5% HNO_3) AT 60 C

Condition	Intergranular Attack Appearance		Corrosion Rate, in/mo	
	65% HNO_3*	72% H_2SO_4 + 1.5% HNO_3	72% H_2SO_4 + 1.5% HNO_3 10,039 hr	65% HNO_3* 240 hr
Mill Anneal	None	None	0.00025	0.00052
Severely Sensitized	Severe	Severe	0.00400	0.0300
Mildly Sensitized	Mild	Severe	0.00300	0.00550
As Welded	Mild WD	Severe WD	0.00036	--

* Boiling

Additional mixed acid (H_2SO_4 + HNO_3) information is shown in Reference Table 17.

Sulfuric Acid Exposure

The results of thermal treatments on Type 316 stainless steel exposed to 3 to 10 percent H_2SO_4 at 50 C are shown in Table 3. The reference HNO_3 attack appearances are shown in the left-hand column. Reading left to right, the H_2SO_4 attack appearances are in the next column; the H_2SO_4 corrosion rates in the next, and the reference HNO_3 corrosion rates in the right-hand column. The same format will be used in subsequent tables.

The severely sensitized specimen, 1 hour 1250 F (680 C), water quench, shows severe intergranular corrosion, in the nitric acid test and the H_2SO_4 process solution. The process specimen was rubber-like, indicating complete penetration of the grain boundaries of the 1/8-inch thickness in 4,752 hours. The mildly sensitized specimen (5 hours at 1090 F (590 C), water quenched) showed mild intergranular corrosion, as it did in the "HNO_3" test. Mild weld decay was also observed.

In a 10 C, 30 percent H_2SO_4 solution, Type 317 (Table 4) had nil corrosion in the annealed condition. The severely sensitized specimens, however, showed severe intergranular attack in sulfuric acid and nitric acid. The sulfuric acid attack was limited to corrosion in the grain boundaries, whereas the nitric acid attack was combined general corrosion and grain boundary corrosion. The mildly sensitized and as-welded conditions did not promote intergranular corrosion in this process solution.

The 3 to 10 percent (Table 3) and 30 percent (Table 4) sulfuric acid data are taken from the sulfuric acid exposure, Reference Table 16.

Other results showed that improper heat treatment caused:

1. Mild intergranular corrosion of the alloys in 40 percent H_2SO_4.
2. Increased general corrosion of the alloys in 60 percent H_2SO_4.
3. No intergranular or increased general corrosion of the alloys in 78 percent and 93 percent H_2SO_4.
4. No intergranular or increased general corrosion in wet H_2S (Table 26).

Mixed Acid Exposure

Mixed acid (H_2SO_4 + HNO_3) is apparently severe on improperly heat-treated stainless steels. In a 60 C, 72 percent H_2SO_4 + 1.5 percent HNO_3 mixture (Table 5) severe intergranular corrosion did occur to mildly and severely sensitized Type 304. The difference in corrosion rate and appearance between the mildly sensitized and severely sensitized specimens in the HNO_3 test was large. The process solution, however, made no significant distinction between these conditions. Note the severe weld decay on the as-welded specimen. This is one of the rare instances where severe weld decay was observed on the 1/8-in. thick, single-pass weld specimens exposed to process solutions. If these acids, 72 percent H_2SO_4 and 1.5 percent HNO_3 at 60 C were separated and samples run in each, experience has shown that intergranular corrosion would not occur in either solution, regardless of the heat treatment condition.

TABLE 6 - TYPE 321 IN 5% HNO_3 AT 150-225 C AND 250 PSI

Condition	Intergranular Attack Appearance		Corrosion Rate, in/mo	
	65% HNO_3*	5% HNO_3	5% HNO_3 1,186 hr.	65% HNO_3* 240 hr.
Mill Anneal	None	None	0.00070	0.00102
Severely Sensitized	Severe	Severe	0.00470	0.0250
As Welded	None	Mild WD	0.00085	--
Stabilized and Sensitized	None	Mild	0.00200	0.00250
Stabilized and Welded	None	Mild	0.00200	--

*Boiling

TABLE 7 - TYPE 316 IN 20% ORGANIC ACID MIXTURE AT 70 C

Condition	Intergranular Attack, Appearance		Corrosion Rate, in/mo	
	65% HNO_3*	20% Organic Acid Mixture	20% Organic Acid Mixture	65% HNO_3*
Mill Anneal	None	None	0.00020	0.00076
Severely Sensitized	Severe	None	0.00070	0.100
Mildly Sensitized	Mild	None	0.00050	0.00600
As Welded	Severe WD	None	0.00027	--

* Boiling

Nitric Acid Exposures

Five percent HNO_3 at 225 C and 250 psi (Table 6) caused intergranular corrosion of improperly heat treated Type 321. The corrosion rates for the process solution and the evaluation test solution were comparable for the severely sensitized condition. The resistance to sensitization in both solutions was improved by the stabilization treatments (4 hours at 1700 F (925 C), air cool).

However, comparing the process corrosion rates on the as welded specimen with those of the stabilized and welded specimen, some degree of sensitization was caused by the stabilizing treatment itself. The information obtained from this specific heat of steel confirms other published information that Type 321, due to the unpredictable effect of thermal treatment, is a questionable alloy for hot nitric acid services.

At ambient temperatures concentrations of HNO_3 up to 67 percent did not cause intergranular corrosion regardless of heat treatment or alloy. The presence of chlorides in the acid did not accelerate pitting or general corrosion of improperly heat treated stainless steels (Reference Table 18).

Organic Acid Exposure

Improper heat treatment of Type 316 stainless steel exposed to a 20 percent organic acid mixture at 70 C (Table 7) can cause accelerated corrosion. In this solution there was no evidence of intergranular attack. The general corrosion rate of the severely and mildly sensitized specimens, however, was significantly higher than that of the annealed and as-welded specimens.

Results of an exposure in 93 percent organic acid mixture at 120 C (Reference Table 19) show no effects of thermal treatment.

TABLE 8 - TYPE 302 IN pH 4 BRACKISH WATER CONTAINING 5000-10,000 PPM CHLORIDE ION AT AMBIENT TEMPERATURE

Condition	Intergranular Attack and Pitting Appearance			Weight Loss g/16.5 sq in	Corrosion Rate in/mo
	65% HNO_3**	4 pH Brackish Water		4 pH Brackish Water	65% HNO_3**
	Intergranular Attack	Intergranular Attack	Pitting	11,592 hr	240 hr
Mill Anneal	None	None	Mild	0.0378	0.00114
Severely Sensitized	Severe	Severe in pits	Severe	41.8056*	0.0920
Mildly Sensitized	Mild	None	Mild	0.3998	0.00190
As Welded	Severe WD	Mild WD in pits	Mild	0.1847	--

* 1/8 in. thickness pitted through. ** Boiling.

Water Exposure

Improper heat treatment of Type 302 exposed in pH 4 brackish water containing 5,000 - 10,000 ppm chloride ion at ambient temperature (Table 8) can cause an unusual effect. The corrosion rate has been changed to weight loss for this exposure. All specimens except the severely sensitized specimen have rates under 0.00001 inch/mo. Weight loss reflected the severe pitting resulting from severe sensitization. Severe intergranular attack was observed in the pits on the specimen which lost 30 percent of its weight during the exposure.

TABLE 9 - WATER + ORGANIC LIQUID AND 110 PPM NaCl AT 70 C - pH 7.5

Alloy*	Weight Loss g/16.5 sq in.	Pitting Appearance
302	0.0154	Mild
304	0.0332	Mild
304L	2.2284	Severe
321	0.4495	Severe
347	0.8227	Severe
316	0.0105	None
316L	0.0131	None
317	0.0191	None
318	0.0117	None

* Mill annealed condition.

Additional results in acidic and basic (pH range) water are shown in Reference Tables 22 and 26. The data indicate that thermal treatments:

1. Caused increased pitting of stainless steels in acidic water with 330 ppm NaCl and above.
2. Did not cause a significant increase in pitting in basic water containing 110 ppm NaCl.
3. Did not cause pitting in acidic water containing less than 50 ppm NaCl.

The data from basic water containing chlorides is controversial. We have indicated that heat treatment had no effect in basic or neutral solutions. The alloy, however, may be significant. No one wants to believe the data in Table 9 are correct; however, this exposure, water plus organic liquid and 110 ppm NaCl at 70 C and pH 7.5 says Type 304L has less resistance to pitting than any of the other alloys.

Dissolved Neutral or Basic (pH range) Salts Exposure

The results of exposures in metallic acetate, sodium bichromate, $ZnCl_2$ plus NH_4Cl, and ammonium sulfamate salt solutions are recorded in Reference Tables 23 and 25. Improper heat treatment and welding had no significant effect on the stainless steel alloys when they were exposed to these process solutions.

Anhydrous Halogen Exposure

Information from the exposure of thermally treated stainless steels exposed in process solutions involving anhydrous HF, HCl, metallic chlorides and chlorine are shown in Reference Tables 20 and 26. Thermal treatments were ineffective in increasing the corrosion rate of the alloys in anhydrous halogen environments.

Organic Liquid Exposures

Anhydrous organic liquids, solutions which are normally handled in stainless steel to prevent iron

contamination of the product, did not accelerate corrosion when the alloys were improperly heat treated or welded. The exposure conditions for these solutions are shown in Reference Table 24.

Chlorinated organic liquid containing trace amounts of H_2O and HCl also did not accelerate corrosion when the alloys were exposed to the solution in the various sensitized conditions. The results are shown in Table 25.

Strong Alkali Exposures

Solutions in this category of environment included sodium cyanide, ferricyanide and hydroxide. The corrosion results and exposure conditions in Reference Table 21 show no effect regardless of alloy or heat treatment condition.

Corrosion Effect Summary

By way of summary to this point, the results showed that intergranular, general and pitting corrosion of austenitic stainless steels were accelerated in certain process solutions by improper heat treatment and by welding.

The solutions in which this was so with an estimate of concentration limits are:

1. Boiling nitric acid up through 65 percent, the highest concentration tested.
2. Sulfuric acid up through 60 percent.
3. Mixed acid (H_2SO_4 + HNO_3) up through 80 percent, the highest total concentration tested.
4. A 20 percent organic acid mixture.
5. Acidic water containing NaCl, 330 ppm and above.

Solutions which did not cause accelerated pitting, intergranular or general corrosion due to improper heat treatment and welding were:

1. Dissolved neutral or basic (pH range) salts.
2. Anhydrous halogens.
3. Anhydrous organic liquids.
4. Chlorinated organic liquid with traces of H_2O and HCl.
5. Strong alkalies up through 50 percent, the highest concentration tested.
6. Cold nitric acid up through 67 percent, the highest concentration tested.
7. Sulfuric acid, 78 percent and above.
8. Wet hydrogen sulfide.
9. Basic (pH range) water containing chlorides.
10. Acidic (pH range) water containing less than 50 ppm NaCl.
11. A 93 percent organic acid mixture.

TABLE 10 - TYPE 321 IN MIXED ACID (60% H_2SO_4 + 20% HNO_3) AT 45 C

Condition	Intergranular Attack Appearance		Corrosion Rate (in/mo.)	
	65% HNO_3*	60% H_2SO_4 +20% HNO_3	60% H_2SO_4 + 20% HNO_3 9,096 hr.	65% HNO_3* 240 hr.
Mill Anneal	None	None	0.00005	0.00102
Severely Sensitized	Severe	Severe	0.00015	0.0250
As Welded	None	Mild WD	0.00007	--
Stabilized and Sensitized	None	Mild	0.00010	0.00250
Stabilized and Welded	None	Mild	0.00007	--

*Boiling

Suitability of the Nitric Acid Evaluation Test

Data discussed in the previous section indicated that the standard HNO_3 evaluation test is a good test for predicting effect of thermal treatments on Types 302, 304, 316 and 317 exposed to all process solutions. In the following section limitations of the HNO_3 test for predicting effect of thermal treatments on low carbon and stabilized alloys exposed to process solutions are discussed.

TABLE 11 - TYPES 304 VS 321 IN 4 pH BRACKISH WATER CONTAINING 5000 - 10,000 PPM Cl^- AT AMBIENT TEMPERATURE

Condition	Intergranular Attack and Pitting Appearance			Wt. Loss g/16.5 sq in Brackish Water 11,592 hr	Corrosion Rate in/mo 65% HNO_3* 240 hr
	65% HNO_3* Inter-granular	Brackish Water Inter-granular	Brackish Water Pitting		
Type 304					
Mill Anneal	None	None	Mild	0.0152	0.00052
Severely Sensitized	Severe	Severe in pits	Severe	11.4894	0.0300
Mildly Sensitized	Mild	Severe in crevice	Mild	0.3411	0.00300
As Welded	Mild WD	None	Mild	0.1455	---
Type 321					
Mill Anneal	None	None	Mild	0.0224	0.00102
Severely Sensitized	Severe	None	Mild	0.364	0.0250
As Welded	None	None	Mild	0.0215	---
Stabilized and Sensitized	None	None	Mild	0.0687	0.00250
Stabilized and Welded	None	None	Mild	0.0223	---

* Boiling

Type 321

The data from the exposure of Type 321 (Table 10) in the mixed acid (60 percent H_2SO_4 + 20 percent HNO_3) at 45 C show that the 65 percent HNO_3 test is capable of predicting the effect of thermal treatments on this alloy in this solution. The corrosion rates in the nitric acid test were a better indicator than the corrosion appearance. Except for the severely sensitized condition, it is difficult to detect visually intergranular corrosion of Type 321 in a 240-hour exposure. However, mild weld decay and mild intergranular corrosion were visually detected in the 9000-hour process exposure of the as-welded and stabilized samples

The results of the exposure of Types 304 and 321 in a pH 4 brackish water containing up to 10,000 ppm chloride ion are compared in Table 11. In the severely sensitized condition both alloys have high nitric acid corrosion rates. In this industrial solution, Type 304 weight losses agreed with the 65 percent HNO_3 test results. Even the mildly sensitized sample showed a weight loss comparable with this mildly sensitized nitric acid corrosion rate. The Type 321 samples, however, showed no significant difference regardless of thermal treatment in the aqueous chloride environment.

These results show that titanium stabilization eliminates heat treatment effects in acidic water containing chlorides. Exposures in sulfuric and organic acid solutions also indicate that thermal treatments had no significant effect on corrosion resistance of Type 321. The conclusion is, therefore, that the HNO_3 evaluation test can be used to indicate expected performance of Type 321 only when the alloy is to be used in hot nitric acid or mixed acid, (H_2SO_4 + HNO_3) environments.

TABLE 12 - TYPE 347 IN MIXED ACID (72% H_2SO_4 + 1.5% HNO_3) AT 60 C

Condition	Intergranular Attack Appearance		Corrosion Rate in/mo	
	65% HNO_3*	72% H_2SO_4 +1.5% HNO_3	72% H_2SO_4 + 1.5% HNO_3 10,039 hr	65% HNO_3* 240 hr
Mill Anneal	None	None	0.00030	0.00082
Severely Sensitized	None	None	0.00034	0.00185
As Welded	None	None	0.00054**	--
Spoiled & Sensitized***	Severe	Severe	0.00500	0.500
Stabilized & Sensitized	None	None	0.00046	0.00150
Stabilized & Welded	None	None	0.00070**	--

* Boiling

** General corrosion rate of weld metal higher than base metal

*** One hr 2400 F, WQ + 20 hr 1200 F furnace cool.

Type 347

Test results on Type 347 (Table 12) in mixed acid (72 percent H_2SO_4 + 1.5 percent HNO_3) were representative of those obtained in most process solutions where the HNO_3 test results accurately indicate (or predict) the corrosion performance of sensitized material. The correlation between the process solution and the nitric acid test, based both on intergranular appearance and corrosion rate, was excellent. One possible exception is when Type 347 is in the stabilized condition. The corrosion rate on the stabilized and sensitized samples in the mixed acid was slightly higher than on the severely sensitized sample. In the nitric acid test, the effect was reversed.

Another exposure in a weak mixed acid, 0.3 to 1 percent H_2SO_4 + HNO_3 at 100 C (Reference Table 17) showed the most pronounced example of the detrimental effect of stabilization of the Type 347 alloy. In 4,000 hours none of the nine alloys, regardless of heat treatment, lost more than 0.1 gram, except the stabilized and sensitized Type 347 which lost 12 grams. In this weak acid solution, the severely sensitized Type 302 which lost less than the 0.1 gram, and had no visible intergranular surface corrosion, showed severe intergranular cracking.

TABLE 13

TYPE 304L IN 5% HNO_3 AT 150-225 C - 250 PSI

Condition	Intergranular Attack Appearance		Corrosion Rate in/mo.	
	65% HNO_3*	5% HNO_3	5% HNO_3 1,186 hr	65% HNO_3* 240 hr
Mill Anneal	None	None	0.00040	0.00050
Severely (1 hr) Sensitized	Mild	Severe	0.00510	0.00180
As Welded	None	None	0.00041	--
Over (20 hr) Sensitized	Severe	Severe	0.00550	0.0600

* Boiling

Type 304L

The performance of Type 304L exposed to 5 percent HNO_3 at 225 C under pressure is compared to the nitric acid test in Table 13. The agreement between the process solution and the evaluation test is only fair.

Note the significant difference in the 65 percent HNO_3 corrosion rates on the samples sensitized for 1 hour and for 20 hours. In 5 percent HNO_3 exposure the samples sensitized for 1 hour and for 20 hours had the same corrosion rate. This process solution, which gave high general corrosion rates on Type 304L, did not recognize the degrees of sensitization predicted by the evaluation test. The absence of weld decay on the welded sample was predicted by the nitric acid test results.

In other process solutions where the general corrosion rates were low, the 65 percent nitric acid test accurately predicted the various degrees of sensitization for the Type 304L alloy.

TABLE 14 - TYPES 316 VS 316L IN WATER + 1275 PPM $NaClO_2$, pH 3 AT 65 C

Condition	Intergranular Attack and Pitting Appearance			Corrosion Rate (in/mo)	
	65% HNO_3* Intergranular Attack	$NaClO_2$, pH 3 Intergranular Attack	$NaClO_2$, pH 3 Pitting	$NaClO_2$, pH 3 1080 hr	65% HNO_3* 240 hr
316					
Mill Anneal	None	None	Mild	0.00003	0.00076
Severely Sensitized	Severe	Severe in pits	Severe	0.00055	0.100
As Welded	Severe WD	None	Mild	0.00005	--
316L					
Mill Anneal	None	None	Mild	0.00005	0.00097
Severely Sensitized	Severe	None	Mild	0.00010	0.0330
As Welded	None	None	Mild	0.00005	--
Stabilized and Sensitized	Severe	None	Severe	0.00019	0.00850

*Boiling

Type 316L

The data for Type 316L exposed to an aqueous, pH 3, 65 C sodium chlorite solution are shown in Table 14. Regular Type 316 was included for a direct comparison of the effects of thermal treatments. In the severely sensitized condition, both alloys showed severe intergranular corrosion in the nitric acid test. In the chlorite solution severely sensitized Type 316 showed severe pitting with intergranular corrosion in the pits. Accelerated pitting of the severely sensitized Type 316L sample did not occur. These results also show that a stabilization treatment improved resistance of Type 316L in nitric acid, but in the process solution, the stabilization treatment was detrimental. Our conclusions are that the nitric acid evaluation test is an acceptable test for Type 316, but is not an acceptable test for Type 316L.

TABLE 15 - TYPE 318 IN 3-10% H_2SO_4 AT 50 C

Condition	Intergranular Attack Appearance		Corrosion Rate (in/mo)	
	65% HNO_3*	3-10% H_2SO_4	3-10% H_2SO_4 4,752 hr	65% HNO_3* 240 hr
Mill Anneal	None	None	0.00090	0.00125
Severely Sensitized	Severe	None	0.00120	0.0170
As Welded	None	None	0.00141	--
Stabilized and Sensitized	Mild	None	0.00171	0.00235
Stabilized and Welded	None	None	0.00160	--
Reannealed, Stabilized and Sensitized	Mild	Mild	0.00149	0.00150

*Boiling

Type 318

Table 15 shows the results for Type 318 exposed in a 3 to 10 percent H_2SO_4 solution at 50 C. In both boiling nitric acid and 50 C sulfuric acid, the annealed samples had the same corrosion rate. The severely sensitized samples showed high rates in nitric acid but low rates in sulfuric acid. Stabilization heat treatments were required to improve the resistance to sensitization of Type 318 in the nitric test. In the process solution, the stabilization heat treatment had no significant effect. The reannealed, stabilized, and sensitized sample, however, showed a mild intergranular surface attack.

These results showed that the nitric acid evaluation test is not capable of predicting the performance of thermally treated Type 318 stainless steel in many process solutions.

Summary

We have reviewed information which shows:

1. Intergranular corrosion, general corrosion and pitting of austenitic stainless steels can be accelerated by thermal treatments in certain process solutions.
2. Many solutions do not cause accelerated corrosion of thermally treated stainless steels.
3. Short time thermal treatments as in the welding of 1/8-in. sheet will cause accelerated intergranular corrosion in only a few process services.

The boiling 65 percent nitric acid test is:

1. A satisfactory quality test for Types 302, 304, 347, 316 and 317 in process solutions.
2. Not a satisfactory quality test for Types 321, 316L and 318 in many process solutions.
3. Difficult to interpret for Type 304L in process solutions having high general corrosion rates.

DISCUSSION

Discussion by A. Moskowitz, Crucible Steel Company of America, Pittsburgh, Pa.:

So called "stabilizing" heat treatments at about 1600 F have been recommended in the past for both titanium- and columbium-containing stainless steels (Types 321 and 347). The purpose of the treatment is supposedly to insure that the carbon is combined with the titanium or columbium. Mr. Auld's paper indicated several instances where such a "stabilizing" treatment made for increased corrosion.

In a test program conducted by the Field Corrosion Subcommittee, High Alloys Committee, Welding Research Council, results have been obtained also indicating that a 1600 F treatment can be detrimental to Type 347 stainless steel. There were two environments in which material given a 4-hour, 1600 F "stabilizing" treatment before sensitizing at 1250 F (1 hour) showed intergranular corrosion, which was not shown for the same material given the sensitizing treatment alone. The environments were waste sulfuric acid (4 percent maximum, air-free, at 190 F), and nitric acid (12 percent maximum, at 155 F maximum, also 20 percent at 175 F, with metal nitrates present). There was no instance in which the 1600 F treatment was helpful in lessening intergranular attack or weld line attack.

Parallel data for Type 321 had been planned for, but unfortunately was not obtained. However, it is interesting to note that the 1600 F treatment prior to sensitization was detrimental rather than helpful to Type 321 in the Huey Test.

Also included in the program were exposures of Types 321, 347 and 318, both as-welded and welded, plus given a 1-hour treatment at 1600 F. Results were mixed, but in general the 1600 F treatment did not provide clear-cut assistance in reducing intergranular attack or weld line attack. In fact, corrosion rates were often higher for materials given the 1600 F treatment.

TABLE 16. EXPOSURE IN SULFURIC ACID[c]

Material and Condition		Laboratory Evaluation		Field Exposure Conditions and Results									
		65% HNO_3 Boiling, 240 Hr		78% & 93% H_2SO_4 20°C, 4,392 Hr		60% H_2SO_4 + .015 g/l Cu^{++} 35°C, 4,752 Hr		40% H_2SO_4 + .015 g/l Cu^{++} 50°C, 2,828 Hr		30% H_2SO_4 10°C, 4,752 Hr		3% to 10% H_2SO_4 50°C, 4,752 Hr	
AISI Type	Condition[a]	Corr. Rate in./mo.	Intergranular Attack Appearance	Wt. Loss[b] g/16.5 $in.^2$	Intergranular Attack	Corr. Rate in./mo.	Intergranular Attack	Corr. Rate in./mo.	Intergranular Attack	Corr. Rate in./mo.	Intergranular Attack	Corr. Rate in./mo.	Intergranular Attack
302	Mill Annealed	0.00114	None	-	-	-	-	-	-	0.00087	None	-	-
302	Severely Sensitized	0.0625-0.093	Severe	-	-	-	-	-	-	0.00344	Severe	-	-
302	Mildly Sensitized	0.00185-0.00221	Mild	-	-	-	-	-	-	0.00114	None	-	-
302	As Welded	-	Severe W. D.*	-	-	-	-	-	-	0.00121	None	-	-
304	Mill Annealed	0.00052	None	0.0795	None	0.00011	None	0.00084	None	Nil	None	0.00653	None
304	Severely Sensitized	0.0237-0.0394	Severe	-	-	-	-	-	-	0.00024	Severe	-	-
304	Mildly Sensitized	0.00282-0.00323	Mild	-	-	-	-	-	-	0.00084	Mild	-	-
304	As Welded	-	Severe W. D.*	-	-	-	-	-	-	0.00093	None	-	-
304L	Mill Annealed	0.00050	None	-	-	-	-	-	-	0.00001	None	-	-
304L	Severely Sensitized	0.00167-0.00188	Mild	-	-	-	-	-	-	0.00031	None	-	-
304L	As Welded	-	None	-	-	-	-	-	-	0.00049	None	-	-
304L	Over Sensitized (20 Hr)	0.0606-0.0822	Severe	-	-	-	-	-	-	0.00123	Severe	-	-
321	Mill Annealed	0.00102	None	-	-	-	-	-	-	0.00228	None	-	-
321	Severely Sensitized	0.0178-0.0252	Severe	-	-	-	-	-	-	0.00002	None	-	-
321	As Welded	-	None	-	-	-	-	-	-	0.00021	None	-	-
321	Stabilized & Sensitized	0.00167-0.00254	None	-	-	-	-	-	-	0.00013	None	-	-
321	Stabilized & Welded	-	None	-	-	-	-	-	-	0.00014	None	-	-
347	Mill Annealed	0.00082	None	-	-	-	-	-	-	0.00002	None	-	-
347	Severely Sensitized	0.00178-0.00214	None	-	-	-	-	-	-	0.00003	None	-	-
347	As Welded	-	None	-	-	-	-	-	-	0.00032	None	-	-
347	Spoiled & Sensitized	0.0645-0.934	Severe	-	-	-	-	-	-	0.00215	Severe	-	-
347	Stabilized & Sensitized	0.00110-0.00171	None	-	-	-	-	-	-	0.00020	None	-	-
347	Stabilized & Welded	-	None	-	-	-	-	-	-	0.00005	None	-	-
316	Mill Annealed	0.00076	None	0.0622	None	0.00036	None	0.00001	None	0.00001	None	0.00072	None
316	Severely Sensitized	0.0973-0.1058	Severe	0.0615	None	0.00162	None	0.00014	Mild	0.00032	Severe (NG*)	0.00339	Severe (R*)
316	Mildly Sensitized	0.00599-0.00639	Mild	0.0611	None	0.00024	None	0.00003	None	0.00001	None	0.00113	Mild
316	As Welded	-	Severe W. D.*	0.0641	None	0.00070	None	0.00001	None	0.00004	None	0.00105	Mild W. D.*
316L	Mill Annealed	0.00097	None	0.0605	None	0.00011	None	0.00001	None	0.00001	None	0.00094	None
316L	Severely Sensitized	0.0257-0.0401	Severe	0.0627	None	0.00051	None	0.00009	None	0.00001	None	0.00139	Mild
316L	As Welded	-	None	0.0696	None	0.00036	None	0.00015	None	0.00002	None	0.00156	None
316L	Stabilized & Sensitized	0.00626-0.0116	Severe	0.0912	None	0.00099	None	0.00024	None	0.00004	None	0.00174	Mild
316L	Stabilized & Welded	-	None	0.0737	None	0.00036	None	0.00003	None	0.00002	None	0.00182	Mild
316L	Reann. & Stab. & Sens.	0.00121-0.00165	Mild	1.0710	None	0.00109	None	0.00066	None	0.00007	Severe (NG*)	0.00158	Mild
317	Mill Annealed	0.00114	None	0.0487	None	0.00035	None	None	None	Nil	None	0.00040	None
317	Severely Sensitized	0.0777-0.102	Severe	0.0575	None	0.00054	None	0.00001	Mild	0.00017	Severe (NG*)	0.00305	Severe (R*)
317	Mildly Sensitized	0.00242-00.0253	Mild	0.0684	None	0.00040	None	0.00006	None	0.00001	None	0.00051	Mild
317	As Welded	-	Severe W. D.*	0.0545	None	0.00029	None	0.00008	None	0.00001	None	0.00084	Mild W. D.*
318	Mill Annealed	0.00125	None	0.0526	None	0.00023	None	0.00000	None	0.00001	None	0.00090	None
318	Severely Sensitized	0.0137-0.0214	Severe	0.0530	None	0.00037	None	0.00000	None	0.00001	None	0.00120	None
318	As Welded	-	None	0.0501	None	0.00082	None	0.00000	None	Nil	None	0.00141	None
318	Stabilized & Sensitized	0.00204-0.00271	Mild	0.0736	None	0.00116	None	0.00011	None	0.00003	None	0.00171	None
318	Stabilized & Welded	-	None	0.0501	None	0.00101	None	0.00010	None	Nil	None	0.00160	None
318	Reann. & Stab. & Sens.	0.00130-0.00275	Mild	0.0922	None	0.00056	None	0.00018	None	0.00002	None	0.00149	Mild

a. See Table 27 for Laboratory Heat Treatments.
b. Corrosion rate is less than 0.00001 in/mo on the annealed specimens, therefore weight loss (grams/16.5*2) was used to show differences.
c. For additional results see Table 25 .

*W. D. - Weld Decay
NG - No general corrosion - grain boundary attack only
R - Rubber-like, grain boundaries completely removed

TABLE 17. EXPOSURE IN MIXED ACID ($H_2SO_4 + HNO_3$)

Material and Condition		Laboratory Evaluation		Field Exposure Conditions and Results					
		65% HNO_3, Boiling, 240 Hr		72% H_2SO_4 + 1.5% HNO_3 60°C, 10,039 Hr		60% H_2SO_4 + 20% HNO_3 45°C, 9,096 Hr		0.3% to 1.12% Mixed Acid 100°C, 4,344 Hr	
AISI Type	Condition[a]	Corr. Rate in./mo.	Intergranular Attack Appearance	Corr. Rate in./mo.	Intergranular Attack	Corr. Rate in./mo.	Intergranular Attack	Wt. Loss[b] g/16.5 in.^{2}	Intergranular Attack
302	Mill Annealed	0.00114	None	0.00035	None	0.00005	None	0.0377	None
302	Severely Sensitized	0.091-0.093	Severe	Dissolved	Severe	0.00045	Severe	0.0560	Sev. Int. Crk.*
302	Mildly Sensitized	0.00171-0.00221	Mild	0.00040	None	0.00009	None	0.0371	None
302	As Welded	-	Severe W.D.*	0.00050	Severe W.D.*	0.00008	Severe W.D.*	0.0301	None
304	Mill Annealed	0.00052	None	0.00025	None	0.00004	None	0.0322	None
304	Severely Sensitized	0.0237-0.0321	Severe	0.00400	Severe	0.00044	Severe	0.0471	None
304	Mildly Sensitized	0.0035-0.0082	Mild	0.00300	Severe	0.00020	Severe	0.0480	None
304	As Welded	-	Mild W.D.*	0.00036	Severe W.D.*	0.00006	Severe W.D.*	0.0425	None
304L	Mill Annealed	0.00050	None	0.00020	None	0.00004	None	0.0276	None
304L	Severely Sensitized	0.00167-0.00188	Mild	0.00340	Severe	0.00007	Mild	0.1576	None M.P.*
304L	As Welded	-	None	0.00020	None	0.00004	None	0.0407	None
304L	Over Sensitized (20 Hr)	0.0606-0.0616	Severe	0.00310	Severe	0.00025	Severe	0.1629	None M.P.*
321	Mill Annealed	0.00102	None	0.00040	None	0.00005	None	0.0316	None
321	Severely Sensitized	0.0240-0.0250	Severe	0.00107	Severe	0.00015	Severe	0.0412	None
321	As Welded	-	None	0.00047 W.M.*	Mild W.D.*	0.00007 W.M.*	Mild W.D.*	0.0268	None
321	Stabilized & Sensitized	0.00167-0.00254	None	0.00060	Mild	0.00010	Mild	0.0622	None M.P.*
321	Stabilized & Welded	-	None	0.00055 W.M.*	Mild	0.00007 W.M.*	Mild	0.0480	None
347	Mill Annealed	0.00082	None	0.00030	None	0.00005	None	0.0387	None
347	Severely Sensitized	0.00178-0.00193	None	0.00034	None	0.00005	None	0.0363	None
347	As Welded	-	None	0.00054 W.M.&K.*	None	0.00005 W.M.*	None	0.0358	None
347	Spoiled & Sensitized	0.0878-0.934	Severe	0.00500	Severe	0.00025	Severe	0.0365	None
347	Stabilized & Sensitized	0.00122-0.00171	None	0.00046	None	0.00005	None	12.1088	None
347	Stabilized & Welded	-	None	0.00070 W.M.&K.*	None	0.00005 W.M.*	None	0.0389	None
316	Mill Annealed	0.00076	None	0.00037	None	0.00005	None	0.0389	None
316	Severely Sensitized	0.0973-0.1058	Severe	-	-	-	-	0.0470	None
316	Mildly Sensitized	0.00555-0.00639	Mild	-	-	-	-	0.0381	None
316	As Welded	-	Severe W.D.*	-	-	-	-	0.0340	None
316L	Mill Annealed	0.00097	None	-	-	-	-	0.0355	None
316L	Severely Sensitized	0.0361-0.0401	Severe	-	-	-	-	0.0405	None
316L	As Welded	-	None	-	-	-	-	0.0418	None
316L	Stabilized & Sensitized	0.00626-0.00775	Severe	-	-	-	-	0.0620	None
316L	Stabilized & Welded	-	None	-	-	-	-	0.0370	None
316L	Reann. & Stab., & Sens.	0.00121-0.00165	Mild	-	-	-	-	0.0360	None
317	Mill Annealed	0.00114	None	-	-	-	-	0.0257	None
317	Severely Sensitized	0.0777-0.102	Severe	-	-	-	-	0.0388	None
317	Mildly Sensitized	0.00242-0.00253	Mild	-	-	-	-	0.0260	None
317	As Welded	-	Severe W.D.*	-	-	-	-	0.0351	None
318	Mill Annealed	0.00125	None	-	-	-	-	0.0310	None
318	Severely Sensitized	0.0137	Severe	-	-	-	-	0.0270	None
318	As Welded	-	None	-	-	-	-	0.0345	None
318	Stabilized & Sensitized	0.00204-0.00233	Mild	-	-	-	-	0.0572	None
318	Stabilized & Welded	-	None	-	-	-	-	0.0353	None
318	Reann. & Stab., & Sens.	0.00130-0.00147	None	-	-	-	-	0.0371	None

a. See Table 27 for Laboratory Heat Treatments.

b. Corrosion rate is less than 0.00001 in./mo. on the annealed specimen, therefore, weight loss (grams/16.5 in.^{2}) was used to show differences.

* W.M. - Corrosion rate on weld metal is higher than on base metal.
K. - Knife line corrosion, narrow corrosion line immediately adjacent to weld metal.
Sev. Int. Crk. - Severe Intergranular Cracking
M.P. - Mild Pitting

TABLE 18. EXPOSURE IN NITRIC ACID

Material and Condition		Laboratory Evaluation		Field Exposure Conditions and Results							
		65% HNO_3 Boiling, 240 Hr		5% HNO_3 250 psi 150-225°C, 1,186 Hr		HNO_3-20% to pH 3.5 100°C, 7,368 Hr		67% HNO_3 Ambient Temp., 10,563 Hr		10% HNO_3 with 3000 ppm $MgCl_2$ Ambient Temp., 4,728 Hr	
AISI Type	Condition[a]	Corr. Rate in./mo.	Intergranular Attack Appearance	Corr. Rate in./mo.	Intergranular Attack	Corr. Rate in./mo.	Intergranular Attack	Wt. Loss[b] g/16.5 in.^{2}	Intergranular Attack	Wt. Loss[b] g/16.5 in.^{2}	Intergranular Attack
302	Mill Annealed	0.00114	None	0.00150	Mild	-	-	0.0780	None	0.0085	None
302	Severely Sensitized	0.0625-0.0930	Severe	0.01210	Severe	-	-	0.0851	None	0.0089	None
302	Mildly Sensitized	0.00171-0.00221	Mild	0.00120	Mild	E*	Mild	0.0755	None	0.0095	None
302	As Welded	-	Severe WD*	0.00260	Severe WD*	0.00010	Mild WD*	0.0776	None	0.0037	None
304	Mill Annealed	0.00052	None	0.00040	None	0.00006	None	0.0304	None	0.0040	None
304	Severely Sensitized	0.0313-0.0394	Severe	0.00220	Severe	0.00004	Mild	0.0602	None	0.0128	None
304	Mildly Sensitized	0.00282-0.00323	Mild	0.00180	Severe	0.00004	Mild	0.0389	None	0.0082	None
304	As Welded	-	Mild WD*	0.00046	Mild WD*	0.00004	Mild WD*	0.0425	None	0.0036	None
304L	Mill Annealed	0.00050	None	0.00040	None	0.00005	None	0.0406	None	0.0065	None
304L	Severely Sensitized	0.00167-0.00188	Mild	0.00510	Severe	0.00005	Mild	0.0438	None	0.0068	None
304L	As Welded	-	None	0.00041	None	E*	None	0.0464	None	0.0015	None
304L	Over Sensitized (20 Hr)	0.0780-0.0850	Severe	0.00550	Severe	0.00012	Mild	0.0401	None	0.0058	None
321	Mill Annealed	0.00102	None	0.00070	None	-	-	0.0640	None	0.0020	None
321	Severely Sensitized	0.0246-0.0252	Severe	0.00470	Severe	0.00006	Mild	0.0505	None	0.0053	None
321	As Welded	-	None	0.00085	Mild WD*	0.00004	None	0.0464	None	0.0047	None
321	Stabilized & Sensitized	0.00243-0.00254	None	0.00200	Mild	0.00007	Mild	0.0910	None	0.0003	None
321	Stabilized & Welded	-	None	0.00200	Mild	0.00005	None	0.0507	None	0.0017	None
347	Mill Annealed	0.00082	None	0.00100	None	0.00003	None	0.0573	None	0.0078	None
347	Severely Sensitized	0.00202-0.00214	None	0.00200	Mild	0.00005	None	0.0464	None	0.0023	None
347	As Welded	-	None	0.00110	None	0.00008	None	0.0534	None	0.0032	None
347	Spoiled & Sensitized	0.0645-0.130	Severe	0.01500	Severe	0.00008	Severe	0.0668	None	0.0011	None
347	Stabilized & Sensitized	0.00110-0.00154	None	0.00170	Mild	0.00009	None	0.0904	None	0.0077	None
347	Stabilized & Welded	-	None	0.00190	Mild	0.00014	None	0.0579	None	0.0033	None
316	Mill Annealed	0.00076	None	0.00100	None	0.00004	None	0.0810	None	0.0111	None

a. See Table 27 for Laboratory Heat Treatments.

b. Corrosion rate is less than 0.00001 in./mo. on all specimens.

*WD - Weld Decay

E -- Erosion of edges caused excessive weight loss, these samples fell to bottom of tank.

TABLE 19. EXPOSURE IN ORGANIC ACIDS

Material and Condition		Laboratory Evaluation		Field Exposure Conditions and Results			
		65% HNO_3 Boiling, 240 Hr		93% Organic Acid Mixture 120°C, 1,939 Hr		20% Organic Acid Mixture 70°C, 1,824 Hr	
AISI Type	Condition[a]	Corrosion Rate in./mo.	Intergranular Attack Appearance	Corrosion Rate in./mo.	Intergranular Attack	Corrosion Rate in./mo.	Intergranular Attack
302	Mill Annealed	0.00114	None	-	-	0.00058	None
302	Severely Sensitized	0.0625-0.093	Severe	-	-	0.00154	None
302	Mildly Sensitized	0.00171-0.00197	Mild	-	-	0.00110	None
302	As Welded	-	Severe W. D.*	-	-	0.00070	None
304	Mill Annealed	0.00052	None	0.01120	None	0.00014	None
304	Severely Sensitized	0.0237-0.0394	Severe	-	-	0.00080	None
304	Mildly Sensitized	0.00282-0.00323	Mild	-	-	0.00140	None
304	As Welded	-	Mild W. D.*	-	-	0.00130	None
304L	Mill Annealed	0.00050	None	-	-	0.00140	None
304L	Severely Sensitized	0.00167-0.00188	Mild	-	-	0.00140	None
304L	As Welded	-	None	-	-	0.00200	None
304L	Over Sensitized (20 Hr)	0.0606-0.0822	Severe	-	-	0.00140	None
321	Mill Annealed	0.00102	None	-	-	0.00070	None
321	Severely Sensitized	0.0240-0.0252	Severe	-	-	0.00140	None
321	As Welded	-	None	-	-	0.00200	None
321	Stabilized and Sensitized	0.00243-0.00254	None	-	-	0.00120	None
321	Stabilized and Welded	-	None	-	-	0.00150	None
347	Mill Annealed	0.00082	None	-	-	0.00030	None
347	Severely Sensitized	0.00202-0.00214	None	-	-	0.00100	None
347	As Welded	-	None	-	-	0.00100	None
347	Spoiled & Sensitized	0.0645-0.0708	Severe	-	-	0.00110	None
347	Stabilized and Sensitized	0.00110-0.00154	None	-	-	0.00100	None
347	Stabilized and Welded	-	None	-	-	0.00100	None
316	Mill Annealed	0.00076	None	0.00090	None	0.00020	None
316	Severely Sensitized	0.104-0.105	Severe	0.00120	None	0.00070	None
316	Mildly Sensitized	0.00555-0.00639	Mild	0.00110	None	0.00050	None
316	As Welded	-	Severe W. D.*	0.00100	None	0.00027	None
316L	Mill Annealed	0.00097	None	0.00100	None	0.00020	None
316L	Severely Sensitized	0.0257-0.0312	Severe	0.00100	None	0.00030	None
316L	As Welded	-	None	0.00100	None	0.00020	None
316L	Stabilized and Sensitized	0.00626-0.00755	Severe	0.00100	None	0.00070	None
316L	Stabilized and Welded	-	None	0.00100	None	0.00024	None
316L	Reann., Stab., & Sens.	0.00125-0.00165	Mild	0.00100	None	0.00070	None
317	Mill Annealed	0.00114	None	0.00100	None	0.00008	None
317	Severely Sensitized	0.0777-0.102	Severe	0.00110	None	0.00040	None
317	Mildly Sensitized	0.00242-0.00253	Mild	0.00100	None	0.00007	None
317	As Welded	-	Severe W. D.*	0.00100	None	0.00005	None
318	Mill Annealed	0.00125	None	0.00100	None	0.00030	None
318	Severely Sensitized	0.0137	Severe	0.00100	None	0.00030	None
318	As Welded	-	None	0.00100	None	0.00030	None
318	Stabilized and Sensitized	0.00204-0.00233	Mild	0.00100	None	0.00070	None
318	Stabilized and Welded	-	None	0.00100	None	0.00030	None
318	Reann., Stab., & Sens.	0.00130-0.00147	Mild	0.00100	None	0.00080	None

a. See Table 27 for Laboratory Heat Treatments

*W. D. - Weld Decay

TABLE 20. EXPOSURE IN ANHYDROUS HALOGENS[c]

Material and Condition		Laboratory Evaluation		Field Exposure Conditions and Results							
		65% HNO_3 Boiling, 240 Hr		HF, HCl, Metallic Chloride Liquid Mixture 100° - 160°C, 1,440 Hr				Metallic Chloride (Liquid) 40°C, 27,324 Hr	SCl_x, 20°C, 6,120 Hr		
AISI Type	Condition[a]	Corr. Rate in./mo.	Intergranular Attack Appearance	Corr. Rate in./mo.	Intergranular Attack	Intergranular Attack in Crevices	Stress Corrosion Cracks	Intergranular[b] Attack	Corr. Rate in./mo.	Intergranular Attack	Pit Depth, in.
302	Mill Annealed	0.00114	None	0.00126	None	Mild	None	None	0.00004	None	0.002
302	Severely Sensitized	0.0625-0.093	Severe	0.00124	None	Mild	None	None	0.00004	None	0.002
302	Mildly Sensitized	0.00171-0.00410	Mild	0.00105	None	Mild	None	None	0.00003	None	0.002
302	As Welded	-	Severe WD*	0.00123	None	Mild	Cracked	None	0.00002	None	0.002
304	Mill Annealed	0.00052	None	0.00080	None	Mild	None	None	0.00003	None	0.002
304	Severely Sensitized	0.0237-0.0394	Severe	0.00074	None	Mild	None	None	0.00003	None	0.002
304	Mildly Sensitized	0.00282-0.00820	Mild	0.00084	None	Mild	None	None	0.00003	None	0.002
304	As Welded	-	Mild WD*	0.00131	None	Mild	Cracked	None	0.00004	None	0.002
304L	Mill Annealed	0.00050	None	0.00328	None	Mild	None	None	0.00003	None	0.002
304L	Severely Sensitized	0.00110-0.00188	Mild	0.00189	Loc. Sev.*	Mild	None	None	0.00003	None	0.002
304L	As Welded	-	None	0.00132	Loc. Sev.*	Severe	None	None	0.00004	None	0.002
304L	Over Sensitized (20 Hr)	0.0606-0.0822	Severe	0.00133	None	Mild	None	None	0.00006	None	0.002
321	Mill Annealed	0.00102	None	0.00139	None	Mild	None	None	0.00006	None	0.005
321	Severely Sensitized	0.0178-0.0252	Severe	0.00148	None	Mild	None	None	0.00006	None	0.005
321	As Welded	-	None	0.00138	None	Mild	Cracked	None	0.00006	None	0.005
321	Stabilized & Sensitized	0.00167-0.00254	None	0.00188	None	Mild	None	None	0.00006	None	0.005
321	Stabilized & Welded	-	None	0.00222	None	Mild	None	None	0.00006	None	0.005
347	Mill Annealed	0.00082	None	0.00196	None	Mild	None	None	0.00006	None	0.005
347	Severely Sensitized	0.00178-0.00214	None	0.00174	None	Mild	None	None	0.00006	None	0.005
347	As Welded	-	None	0.00147	None	Mild	Cracked	None	0.00007	None	0.005
347	Spoiled & Sensitized	0.0645-0.934	Severe	0.00134	Loc. Sev.*	Severe	None	None	0.00006	Mild	0.005
347	Stabilized & Sensitized	0.00110-0.00171	None	0.00152	None	None	Cracked	None	0.00007	None	0.005
347	Stabilized & Welded	-	None	0.00254	None	None	Cracked	None	0.00005	None	0.005
316	Mill Annealed	0.00076	None	0.00254	None	None	None	None	0.00003	None	None
316	Severely Sensitized	0.0973-0.1058	Severe	0.00230	None	None	None	Loc. Mild*	-	-	-
316	Mildly Sensitized	0.00119-0.00639	Mild	0.00210	None	None	None	None	-	-	-
316	As Welded	-	Severe WD*	0.00220	None	None	None	Int. Surf. Crks.*	-	-	-
316L	Mill Annealed	0.00097	None	0.00320	None	None	None	None	-	-	-
316L	Severely Sensitized	0.0257-0.0401	Severe	0.00350	None	None	None	Mild	-	-	-
316L	As Welded	-	None	0.00400	None	None	None	None	-	-	-
316L	Stabilized & Sensitized	0.00626-0.0116	Severe	0.00450	None	None	None	Mild	-	-	-
316L	Stabilized & Welded	-	None	0.00500	None	None	None	None	-	-	-
316L	Reann. & Stab. & Sens.	0.00121-0.00165	None	0.00410	None	None	None	None	-	-	-
317	Mill Annealed	0.00114	None	0.00210	None	None	None	None	-	-	-
317	Severely Sensitized	0.0777-0.102	Severe	0.00300	None	None	None	None	-	-	-
317	Mildly Sensitized	0.00242-0.00253	Mild	0.00300	None	None	None	None	-	-	-
317	As Welded	-	Severe WD*	0.00220	None	None	None	None	-	-	-
318	Mill Annealed	0.00125	None	0.00340	None	None	None	None	-	-	-
318	Severely Sensitized	0.0137-0.0214	Severe	0.00340	None	None	None	None	-	-	-
318	As Welded	-	None	0.00300	None	None	None	None	-	-	-
318	Stabilized & Sensitized	0.00204-0.00271	Mild	0.00330	None	None	None	None	-	-	-
318	Stabilized & Welded	-	None	0.00310	None	None	None	None	-	-	-
318	Reann. & Stab. & Sens.	0.00130-0.00275	Mild	0.00400	None	None	None	None	-	-	-

a. See Table 27 for Laboratory Heat Treatments

b. Corrosion rate less than 0.00001 in./mo.; all samples were pitted to a depth of 0.01 in.

c. See Table 26 for additional results.

* WD - Weld Decay
Loc. Sev. - Localized Severe
Loc. Mild - Localized Mild
Int. Surf. Crks. - Intergranular Surface Cracks

TABLE 21

EXPOSURE IN ALKALINE SOLUTIONS

Field Exposure Conditions	Alloys Tested	Results
1. 26% NaCN + 6% NaOH, 40 C; 17,016 hr	302, 304, 304L 321, 347, 316*	Corrosion rates on all alloys in all heat treated conditions[a] were less than 0.00001 in/mo. No intergranular corrosion[b] or pitting was observed.
2. 20% Sodium Ferricyanide 45 C; 16,320 hr	302, 304, 304L 321, 347, 316*	Corrosion rates on all alloys in all heat treated conditions[a] were less than 0.00001 in/mo. No intergranular corrosion[b] or pitting was observed.
3. 50% NaOH, 50 C; 24,300 hr	302, 304, 304L 321, 347, 316*	Corrosion rates on all alloys in all heat treated conditions[a] were less than 0.00001 in/mo. No intergranular corrosion[b] or pitting was observed.

* Mill annealed only. [a] See Table 27 for laboratory heat treatments.

[b] See Table 18 for laboratory evaluation test results.

TABLE 23

EXPOSURE IN NEUTRAL SALTS[c]

Field Exposure Conditions	Alloys Tested	Results
1. 12% Metallic Acetate, pH 8.5 25 C; 18,024 hr	302, 304, 304L 321, 347, 316*	Corrosion rates on all alloys in all heat treated conditions[a] were less than 0.00001 in/mo. No intergranular corrosion[b] or pitting was observed.
2. 69% Sodium Bichromate, pH 4, Ambient Temp; 16,968 hr	302, 304, 304L 321, 347, 316*	Corrosion rates on all alloys in all heat treated conditions[a] were less than 0.00001 in/mo. No intergranular corrosion[b] or pitting was observed.
3. Saturated Ammonium Sulfamate 60 C; 5,376 hr	All nine	Corrosion rates on all alloys in all heat treated conditions[a] were less than 0.00001 in/mo. No intergranular corrosion[b] or pitting was observed.

* Mill annealed only. [a] See Table 27 for laboratory heat treatments.

[b] See Table 22 for laboratory evaluation test results. [c] See Table 25 for additional results.

TABLE 22. EXPOSURE IN WATER CONTAINING CHLORIDES[c]

Material and Condition		Laboratory Evaluation		Field Exposure Conditions and Results											
		65% HNO_3 Boiling, 240 Hr		H_2O + Organic Liquid + 110 ppm NaCl, pH 7.5, 70°C 4,872 Hr			H_2O + 1275 ppm. $NaClO_2$, pH 3 65°C, 1,080 Hr			Brackish Water, 5,000-10,000 ppm Cl⁻ pH 4, Ambient Temp., 11,592 Hr			H_2O + 330 ppm NaCl pH 1.5, 80°C, 5352 Hr		
AISI Type	Condition[a]	Corr. Rate in./mo.	Intergranular Attack Appearance	Wt. Loss[b] g/16.5 $in.^2$	Intergranular Attack	Pitting	Corr. Rate in./mo.	Intergranular Attack	Pitting	Wt. Loss[b] g/16.5 $in.^2$	Intergranular Attack	Pitting	Corr. Rate in./mo.	Intergranular Attack	Pitting
302	Mill Annealed	0.00114	None	0.0154	None	Mild				0.0378	None	Mild			
302	Severely Sensitized	0.091-0.093	Severe	0.0414	None	Mild				41.8056	SIP*	Severe			
302	Mildly Sensitized	0.00171-0.00221	Mild	0.0220	None	Mild				0.3998	None	Mild			
302	As welded		Severe WD*	0.0064	None	Mild				0.1847	SI WD*	Mild			
304	Mill Annealed	0.00052	None	0.0322	None	Mild	0.00047	None	Severe	0.0152	None	Mild	0.00020	None	Severe
304	Severely Sensitized	0.0237-0.0394	Severe	0.2648	None	Severe				11.4894	SIP*	Severe			
304	Mildly Sensitized	0.00282-0.0082	Mild	0.0815	None	Mild				0.3411	SIC*	Mild			
304	As Welded		Mild WD*	0.0330	None	Mild				0.1455	None	Mild			
304L	Mill Annealed	0.00050	None	2.2284	None	Severe				0.0287	None	Mild			
304L	Severely Sensitized	0.00167-0.00188	Mild	3.0647	None	Severe				0.1573	SIC*	Mild			
304L	As Welded		None	2.8352		Severe				0.0847	None	Mild			
304L	Over Sensitized (20Hr)	0.0606-0.0822	Severe	2.4139	None	Severe				2.8045	SIC*	Severe			
321	Mill Annealed	0.00102	None	0.4495	None	Severe				0.0224	None	Mild			
321	Severely Sensitized	0.0178-0.0252	Severe	0.9969	None	Severe				0.0364	None	Mild			
321	As Welded		None	0.5222	None	Severe				0.0215	None	Mild			
321	Stabilized & Sensitized	0.00167-0.00254	None	1.5185	None	Severe				0.0687	None	Mild			
321	Stabilized & Welded		None	0.1464	None	Severe				0.0223	None	Mild			
347	Mill Annealed	0.00082	None	0.8227	None	Severe				0.0245	None	Mild			
347	Severely Sensitized	0.00178-0.00214	None	0.2480	None	Severe				0.0577	None	Mild			
347	As Welded		None	0.4947	None	Severe				0.0275	None	Mild			
347	Spoiled & Sensitized	0.0645-0.934	Severe	0.8959	None	Severe				43.1655	SIP*	Severe			
347	Stabilized & Sensitized	0.00110-0.00171	None	0.7696	None	Severe				0.0748	None	Mild			
347	Stabilized & Welded		None	0.0942	None	Severe				0.0570	None	Mild			
316	Mill Annealed	0.00076	None	0.0105	None	None	0.00003	None	Mild	0.0180	None	Light	0.00001	None	None
316	Severely Sensitized	0.0973-0.1058	Severe	0.0174	None	None	0.00055	SIP*	Severe	2.7258	SIP*	Severe	0.00073	Severe	Severe
316	Mildly Sensitized	0.00119-0.00639	Mild	0.0206	None	None	0.00015	None	Mild	0.0203	None	Light	0.00004	None	None
316	As Welded		Severe WD*	0.0154	None	None	0.00005	None	Mild	0.0220	None	Light	0.00002	None	None
316L	Mill Annealed	0.00097	None	0.0131	None	None	0.00005	None	Mild	0.0185	None	Light	0.00001	None	None
316L	Severely Sensitized	0.0257-0.0401	Severe	0.0117	None	None	0.00010	None	Mild	0.0174	None	Light	0.00001	None	None
316L	As Welded		None	0.0202	None	None	0.00005	None	Mild	0.0187	None	Light	0.00001	None	None
316L	Stabilized & Sensitized	0.00626-0.0116	Severe	0.0224	None	None	0.00019	None	Severe	0.0180	None	Light	0.00003	None	None
316L	Stabilized & Welded		None	0.0193	None	None	0.00016	None	Mild	0.0687	None	Light	0.00003	None	None
316L	Reann. & Stab. & Sens.	0.00121-0.00165	Mild	0.0275	None	None	0.00025	None	Mild	0.0256	SIC*	Light	0.00013	Mild	None
317	Mill Annealed	0.00114	None	0.0191	None	None	0.00004	None	Mild	0.0113	None	Light	0.00001	None	None
317	Severely Sensitized	0.0777-0.102	Severe	0.0190	None	None	0.00049	SIP*	Severe	0.1110	Mild	Mild	0.00154	Severe	Severe
317	Mildly Sensitized	0.00242-0.00253	Mild	0.0228	None	None	0.00010	None	Mild	0.0128	None	Light	0.00002	SIC*	Mild
317	As Welded		Severe WD*	0.0215	None	None	0.00002	None	Mild	0.0155	None	Light	0.00002	None	None
318	Mill Annealed	0.00125	None	0.0117	None	None	0.00003	None	Mild	0.0085	None	Light	0.00003	None	None
318	Severely Sensitized	0.0137-0.0214	Severe	0.0165	None	None	0.00008	None	Mild	0.0197	None	Light	0.00006	None	None
318	As Welded		None	0.0117	None	None	0.00005	None	Mild	0.0148	None	Light	0.00001	None	None
318	Stabilized & Sensitized	0.00208-0.00271	Mild	0.0150	None	None	0.00011	None	Mild	0.0165	None	Light	0.00005	None	None
318	Stabilized & Welded		None	0.0163	None	None	0.00006	None	Mild	0.0133	None	Light	0.00002	None	None
318	Reann. & Stab. & Sens.	0.00130-0.00275	Mild	0.0216	None	None	0.00014	None	Mild	0.0185	None	Light	0.00003	None	None

a. See Table 27 for Laboratory Heat Treatments.

b. Corrosion rate is less than 0.00001 in/mo. on the annealed specimen, therefore, weight loss (grams/16.5 in^2) was used to show differences.

c. For additional results see Table 26.

* W.D. - Weld Decay
S.I.P. - Severe Intergranular Attack in Pits
S.I.C. - Severe Intergranular Attack in Crevice
S.I.W.D.- Severe Intergranular Attack in Weld Decay Zone

TABLE 24

EXPOSURE IN ANHYDROUS ORGANIC LIQUIDS[c]

Field Exposure Conditions	Alloys Tested	Results
1. Hydrogenated Compound 30 and 190 C; 18,000 hr	All nine	Corrosion rates on all alloys in all heat treatment conditions[a] were less than 0.00001 in/mo. No intergranular corrosion[b] or pitting was observed
2. Cyanogenated Compound 35 C; 19,000 hr	304*, 316, 316L 317, 318	Corrosion rates on all alloys in all heat treatment conditions[a] were less than 0.00001 in/mo. No intergranular corrosion[b] or pitting was observed.
3. Chlorinated Compound 40 C; 15,000 hr	304*, 316, 316L 317, 318	Corrosion rates on all alloys in all heat treatment conditions[a] were less than 0.00001 in/mo. No intergranular corrosion[b] or pitting was observed.

* Mill annealed only. [a] See Table 27 for laboratory heat treatments.

[b] See Table 22 for laboratory evaluation test results. [c] See Table 15 for additional results.

TABLE 26

MISCELLANEOUS EXPOSURES WHICH DO NOT ACCELERATE CORROSION

Exposure	Field Exposure Conditions	Results
1. Sulfuric Acid (Use with Table 16)	Wet H_2S - 105 C 10,752 hr	No intergranular, general or pitting corrosion of any of the nine alloys in any heat treatment condition.
2. Anhydrous Halogenous (Use with Table 20)	Chlorine - 10 C 25,304 hr	No intergranular, general or pitting corrosion of any of the nine alloys in any heat treatment condition
3. H_2O Containing Chlorides (Use with Table 22)	1.4 pH H_2O containing less than 50 ppm NaCl-40 C; 12,948 hr	No intergranular, general or pitting corrosion of any of the nine alloys in any heat treatment condition.

TABLE 25. EXPOSURE IN NEUTRAL SALTS[c] AND CHLORINATED LIQUID[d] WITH TRACES OF H_2O AND HCL

Material and Condition		Laboratory Evaluation		Field Exposure Conditions and Results				
		65% HNO_3, Boiling, 240 Hr		Chlorinated Organic, Traces of H_2O and HCl, 90°C, Air Free, 812 Hr		40% $ZnCl_2$ + NH_4Cl, pH7, 100°C, 1640 Hr		
AISI Type	Condition[a]	Corr. Rate in./mo.	Intergranular Attack Appearance	Corr. Rate in./mo.	Intergranular Attack	Wt. Loss[b] g/16.5 in.^{2}	Intergranular Attack	Other Surface Conditions
302	Mill Annealed	0.00114	None	0.00096	None	0.9724	None	Stress Corrosion Cracking & Pittir
302	Severely Sensitized	0.0625-0.093	Severe	0.00098	None	1.6860	None	Stress Corrosion Cracking & Pittir
302	Mildly Sensitized	0.00171-0.00221	Mild	0.00094	None	1.6775	None	Stress Corrosion Cracking & Pittir
302	As Welded	-	Severe WD*	0.00086	None	1.0925	None	Stress Corrosion Cracking & Pittir
304	Mill Annealed	0.00052	None	0.00084	None	0.6305	None	Stress Corrosion Cracking & Pittin
304	Severely Sensitized	0.0313-0.0394	Severe	0.00074	None	1.1848	None	Stress Corrosion Cracking & Pittin
304	Mildly Sensitized	0.00282-0.00323	Mild	0.00077	None	1.1053	None	Stress Corrosion Cracking & Pittin
304	As Welded	-	Mild WD*	0.00078	None	1.4090	None	Stress Corrosion Cracking & Pittin
304L	Mill Annealed	0.00050	None	0.00061	None	2.3443	None	Stress Corrosion Cracking & Pittin
304L	Severely Sensitized	0.00167-0.00188	Mild	0.00064	None	1.3267	None	Stress Corrosion Cracking & Pittin
304L	As Welded	-	None	0.00057	None	1.7331	None	Stress Corrosion Cracking & Pittin
304L	Over Sensitized (20 Hr)	0.0780-0.0850	Severe	0.00063	None	2.2802	None	Stress Corrosion Cracking & Pittin
321	Mill Annealed	0.00102	None	0.00058	None	2.3000	None	Stress Corrosion Cracking & Pittin
321	Severely Sensitized	0.0240-0.0252	Severe	0.00058	None	1.4000	None	Stress Corrosion Cracking & Pittin
321	As Welded	-	None	0.00058	None	2.1000	None	Stress Corrosion Cracking & Pittin
321	Stabilized and Sensitized	0.00243-0.00254	None	0.00056	None	1.9000	None	Stress Corrosion Cracking & Pittin
321	Stabilized and Welded	-	None	0.00057	None	1.5000	None	Stress Corrosion Cracking & Pittin
347	Mill Annealed	0.00082	None	0.00050	None	0.0410	None	Stress Corrosion Cracking & Pittin
347	Severely Sensitized	0.00202-0.00214	None	0.00047	None	4.4000 (2 pcs.)*	None	Stress Corrosion Cracking & Pittin
347	As Welded	-	None	0.00049	None	1.6000	None	Stress Corrosion Cracking & Pittin
347	Spoiled & Sensitized	0.0645-0.130	Severe	0.00046	None	2.8000	None	Stress Corrosion Cracking & Pittin
347	Stabilized and Sensitized	0.00110-0.00154	None	0.00048	None	12.0000 (2 pcs.)*	None	Stress Corrosion Cracking & Pittin
347	Stabilized and Welded	-	None	0.00047	None	2.0000	None	Stress Corrosion Cracking & Pittin
316	Mill Annealed	0.00076	None	0.00021	None	2.1000	None	Stress Corrosion Cracking & Pittin
316	Severely Sensitized	0.104-0.105	Severe	0.00013	None	Not Weighed	None	Stress Corrosion Cracking & Pittin
316	Mildly Sensitized	0.00555-0.00639	Mild	0.00013	None	Not Weighed	None	Stress Corrosion Cracking & Pittin
316	As Welded	-	Severe WD*	0.00014	None	Not Weighed	None	Stress Corrosion Cracking & Pittin
316L	Mill Annealed	0.00097	None	0.00012	None	Not Weighed	None	Stress Corrosion Cracking & Pittin
316L	Severely Sensitized	0.0257-0.0312	Severe	0.00013	None	Not Weighed	None	Stress Corrosion Cracking & Pittin
316L	As Welded	-	None	0.00013	None	Not Weighed	None	Stress Corrosion Cracking & Pittin
316L	Stabilized and Sensitized	0.00626-0.00755	Severe	0.00020	None	Not Weighed	None	Stress Corrosion Cracking & Pittin
316L	Stabilized and Welded	-	None	0.00013	None	Not Weighed	None	Stress Corrosion Cracking & Pittin
316L	Reann., Stab., & Sens.	0.00125-0.00165	Mild	0.00020	None	Not Weighed	None	Stress Corrosion Cracking & Pittin
317	Mill Annealed	0.00114	None	0.00011	None	Not Weighed	None	Stress Corrosion Cracking & Pittin
317	Severely Sensitized	0.0841-0.0970	Severe	0.00011	None	Not Weighed	None	Stress Corrosion Cracking & Pittin
317	Mildly Sensitized	0.00242-0.00253	Mild	0.00011	None	Not Weighed	None	Stress Corrosion Cracking & Pittin
317	As Welded	-	Severe WD*	0.00010	None	Not Weighed	None	Stress Corrosion Cracking & Pittin
318	Mill Annealed	0.00125	None	0.00013	None	Not Weighed	None	Stress Corrosion Cracking & Pittin
318	Severely Sensitized	0.0137	Severe	0.00013	None	Not Weighed	None	Stress Corrosion Cracking & Pittin
318	As Welded	-	None	0.00013	None	Not Weighed	None	Stress Corrosion Cracking & Pittin
318	Stabilized and Sensitized	0.00204-0.00233	Mild	0.00014	None	Not Weighed	None	Stress Corrosion Cracking & Pittin
318	Stabilized and Welded	-	None	0.00014	None	Not Weighed	None	Stress Corrosion Cracking & Pittin
318	Reann., Stab., & Sens.	0.00130-0.00147	Mild	0.00020	None	Not Weighed	None	Stress Corrosion Cracking & Pittin

a. See Table 27 for Laboratory Heat Treatments.

b. Weight loss (grams/16.5 in.^{2}) was used to show differences with respect to pitting.

c. See Table 23 for Additional Results in Neutral Salts.

d. See Table 24 for Additional Results in Organic Liquids

* W.D. - Weld Decay
(2 pcs) - Cracked in two pieces

TABLE 27 - LABORATORY HEAT TREATMENTS

AISI Type	Laboratory Heat Treatment	Condition
302		Mill Annealed
302	1 hr 1250 F WQ	Severely Sensitized
302	1 hr 1010 F WQ	Mildly Sensitized
302		As Welded
304		Mill Annealed
304	1 hr 1250 F WQ	Severely Sensitized
304	4 hr 1010 F WQ	Mildly Sensitized
304		As Welded
304L		Mill Annealed
304L	1 hr 1250 F WQ	Severely Sensitized
304L		As Welded
304L	2 hr 1200 F FC	Over Sensitized
321		Mill Annealed
321	1 hr 1250 F WQ	Severely Sensitized
321		As Welded
321	4 hr 1700 F AC + 1 hr 1250 F WQ	Stabilized and Sensitized
321	4 hr 1700 F AC	Stabilized and Sensitized
347		Mill Annealed
347	1 hr 1250 F WQ	Severely Sensitized
347		As Welded
347	1 hr 2400 F WQ + 20 hr 1200 F FC	Spoiled and Sensitized
347	4 hr 1600 F AC + 1 hr 1250 F WQ	Stabilized and Sensitized
347	4 hr 1600 F AC	Stabilized and Welded
316		Mill Annealed
316	1 hr 1250 F WQ	Severely Sensitized
316	5 hr 1090 F WQ	Mildly Sensitized
316		As Welded
316L		Mill Annealed
316L	1 hr 1250 F WQ	Severely Sensitized
316L		As Welded
316L	4 hr 1600 F WQ + 1 hr 1250 F WQ	Stabilized and Sensitized
316L	4 hr 1600 F AC	Stabilized and Sensitized
316L	1 hr 2000 F WQ + 4 hr 1600 F AC + 1 hr 1250 F WQ	Reann., Stab., and Sens.
317		Mill Annealed
317	1 hr 1250 F WQ	Severely Sensitized
317	4 hr 1090 F WQ	Mildly Sensitized
317		As Welded
318		Mill Annealed
318	1 hr 1250 F WQ	Severely Sensitized
318		As Welded
318	4 hr 1600 F AC + 1 hr 1250 F WQ	Stabilized and Sensitized
318	4 hr 1600 F AC	Stabilized and Welded
318	1 hr 2100 F WQ + 4 hr 1600 F AC + 1 hr 1250 F WQ	Reann., Stab., and Sens.

WQ - Water Quench AC - Air Cool FC - Furnace Cool

An Appraisal of Evaluation Tests for Stainless Steel Automotive Trim

By J. F. Bates* and E. H. Phelps*

Abstract

Within the past few years the automotive industry and the steel producers have been experimenting with a variety of stainless steels for automotive trim exposed to corrosion by road-deicing salts. Several new laboratory tests have been developed to evaluate the corrosion resistance of these steels. In the present study the results of six evaluation tests are tested statistically for significant correlation with the results of service tests conducted on automobiles.

The Dip-and-Dry Test and the Thermographic Test each showed a significant correlation with service-test results. The CASS Test and Spot Test are believed to be effective in detecting surface depletion of chromium, a condition causing poor corrosion resistance. The CASS Test did not, however, predict service performance where there was no surface depletion of chromium. The Ferric Chloride Immersion Test did not have a significant correlation with service. It was, however, extremely sensitive to different surface-finishing operations and may have some merit as a quality control test for a finishing operation. The Corrodkote Test showed no merit for predicting service performance of stainless steel automotive trim.

The absence of any really good correlations with service should lend a note of caution against the extensive use of these evaluation tests. It points to the need for more reliable tests for the evaluation of stainless steel for automotive trim.

Introduction

Within the past few years the automotive industry and its suppliers, the steel producers, have been experimenting with several new and improved stainless-steel compositions and finishes for exterior automotive trim. Because the automotive market for stainless steel is very large, the development and evaluation of these materials has constituted a major effort on the part of both producers and consumers.

The most widespread and most damaging corrosive condition encountered by exterior trim is the winter exposure in northern areas to road splash containing the road-deicing salts, sodium chloride and calcium chloride. Where cinders and open-hearth or blast furnace slag are also used, to increase traction, soluble sulfur compounds leached from these are believed to have a strong synergistic effect on the corrosive action of the chloride salts. Other commonly encountered corrodents are the calcium chloride used to settle dust on unpaved roads and sea-water spray in coastal areas.

These corrosive conditions cause attack of chromium-plated carbon steel components, chromium-plated die castings, and anodized aluminum trim as well as stainless steel trim. Work is in progress at other laboratories to establish the optimum processing conditions for these other trim finishes. The present paper is concerned only with the performance of stainless steel trim.

Evaluation tests for stainless steels have been used in the past primarily as acceptance tests by the auto industry and as quality control tests by the steel producers. Continuing modification in steels and finishes, however, has introduced such tests into research and development because the seasonal nature of service testing does not afford continuous opportunity to test new concepts.

An evaluation test, ideally, is one which will cause corrosion identical in nature and intensity with that encountered in service, but in much less time. Common methods of increasing the rate of corrosion are to increase the temperature, to increase the degree and/or frequency of wetting, to increase the concentration of the corrodents, and to substitute more active corrodents for those encountered in service. An example of the last method is the common use of ferric and cupric salts as more active oxidants than oxygen. Past experience in corrosion studies has shown that such measures rarely if ever achieve their complete aim. The form and characteristics of the attack are usually changed somewhat from those seen in service and the attack is often much more intense than that encountered in service. The most common aim, therefore, is that an evaluation test shall have a good correlation with service, separate good material from poor, and reliably rank materials with varying degrees of merit.

It is the purpose of this paper to examine six tests commonly used to evaluate the corrosion performance of stainless steel for automotive trim, and to describe various methods which have been

* Applied Research Laboratory, United States Steel Corporation, Monroeville, Pennsylvania.

Copyright© 1965 by ASTM International

www.astm.org

used to interpret the results of each. The measure of value placed on each test is its correlation with service tests conducted during the winters of 1960-1961 and 1961-1962.

Table 1

Typical Results of Service Test

Type and Nominal Composition, percent	Finish*	Ratings as Washed: Visual Mean	Visual Std Dev	% RG Mean	% RG Std Dev
18 Cr Type 430	BA	1.6	0.84	88.1	8.5
18 Cr Type 430	BA, B	1.6	0.92	84.4	16.5
17 Cr, 1 Mo	BA	0.9	0.33	96.3	1.9
17 Cr, 1 Mo	BA, B	1.1	0.39	95.3	2.0
17 Cr, 1 Mo, 0.5 Cb	BA	1.0	0.00	95.2	2.3
17 Cr, 1 Mo, 0.5 Cb	BA, B	0.8	0.45	97.1	1.6
Type 301	BA	0.1	0.33	98.4	0.7
Type 201	P&B	0.3	0.46	97.9	1.8

* BA - bright annealed; B - buffed; P&B - polished and buffed.

The comparisons between the service and evaluation tests are shown in typical plots of one with the other for each evaluation test. Each evaluation was examined statistically as follows:

1. The linear correlation coefficient between the service test result and the evaluation test result was calculated. This coefficient is a measure of the closeness of fit to a straight line.
2. The critical value of the correlation coefficient was determined at the 0.05 level for each comparison. This value was the correlation coefficient for which there was a 5 percent statistical probability of error.
3. The calculated correlation coefficient was tested for statistical significance by comparison with the critical value. A value equal to or greater than the critical coefficient was significant.
4. In the few instances in which the points fit a quadratic curve significantly better than a straight line, the values of the quadratic correlation coefficients are also given.

The values used in the plots and calculations of correlation coefficients are the mean of about 8 values for the service ratings and of from 2 to 6 values for the evaluation tests. Typical examples of the service-test data and the spread inherent therein are given in Table 1. The correlation coefficients calculated using the means would be expected to be a little higher than those calculated using the individual data. It is not felt, however, that the data justified a more refined calculation, because such calculation would probably not change any of the conclusions in the present paper.

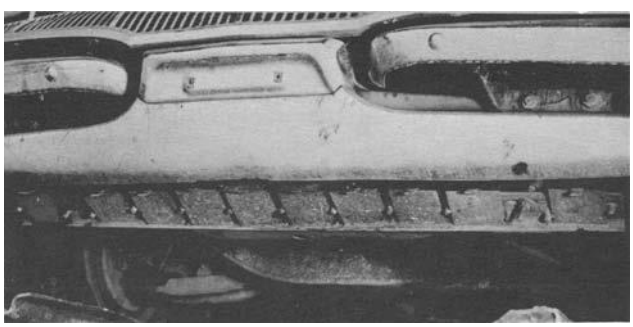


Figure 1 - Typical installation of test rack with corrosion test specimens behind front bumper of automobile (approximately 0.12 actual size.)

The Tests

Service Tests

The 14 steels exposed during the 1960-1961 winter included specimens from several heats of AISI Type 430 stainless steels with the bright No. 2 strip finish commonly used at that time for automotive trim. Specimens from a group of austenitic steels were exposed in the dull 2B finish because a high-gloss finish was not then available. The sheared specimens, 4 inches by 3-7/8 inches, were deburred by grinding the edges, identified, washed with detergent, rinsed with acetone, and air dried.

The specimens were randomly arranged and mounted on test racks that were fastened beneath and behind the front bumpers of automobiles, as recently described by G. F. Bush.[1] Each rack held 10 specimens. A typical rack installation is shown in Figure 1. The test racks are constructed of carbon steel covered with a baked plastic coating (Plastisol) to protect the racks from corrosion and to prevent galvanic contact between the specimens and the racks. From 6 to 12 specimens of each steel were tested. The specimens were exposed for about 2-1/2 months in early 1961 in the Pittsburgh area, where chloride deicing salts and sulfur-containing gritty aggregates are used on the roads. The specimens were rinsed with tap water to remove road dirt but no corrosion product prior to evaluation

The second exposure, during the 1961-1962 winter, was expanded to include 57 variations of steel composition and finish. The materials were exposed in the Chicago, Cleveland and Pittsburgh areas for approximately 4 months in early 1962. The second exposure was patterned after the first with some slight modification. Ten specimens of each material were exposed, with the bottom one-third of each specimen covered with a pressure-sensitive tape to preserve its original appearance. The specimens were cleaned by scrubbing with a brush after a brief soak in a detergent solution; loose corrosion product as well as road dirt was removed.

Specimens from both exposures were given an integral visual rating by comparison with the standards shown in Figure 2. The rating "O" was used for the second exposure only. This new rating was made necessary because the materials in the second exposure were cleaned more thoroughly after exposure than those in the first exposure; also, because the materials tested in the second exposure were generally more corrosion resistant.

A second, instrumental method of rating was used for the steels in the 1961-1962 exposure. Each specimen was rated with a Gardner 45-degree glossmeter. The meter was set using a mirror as

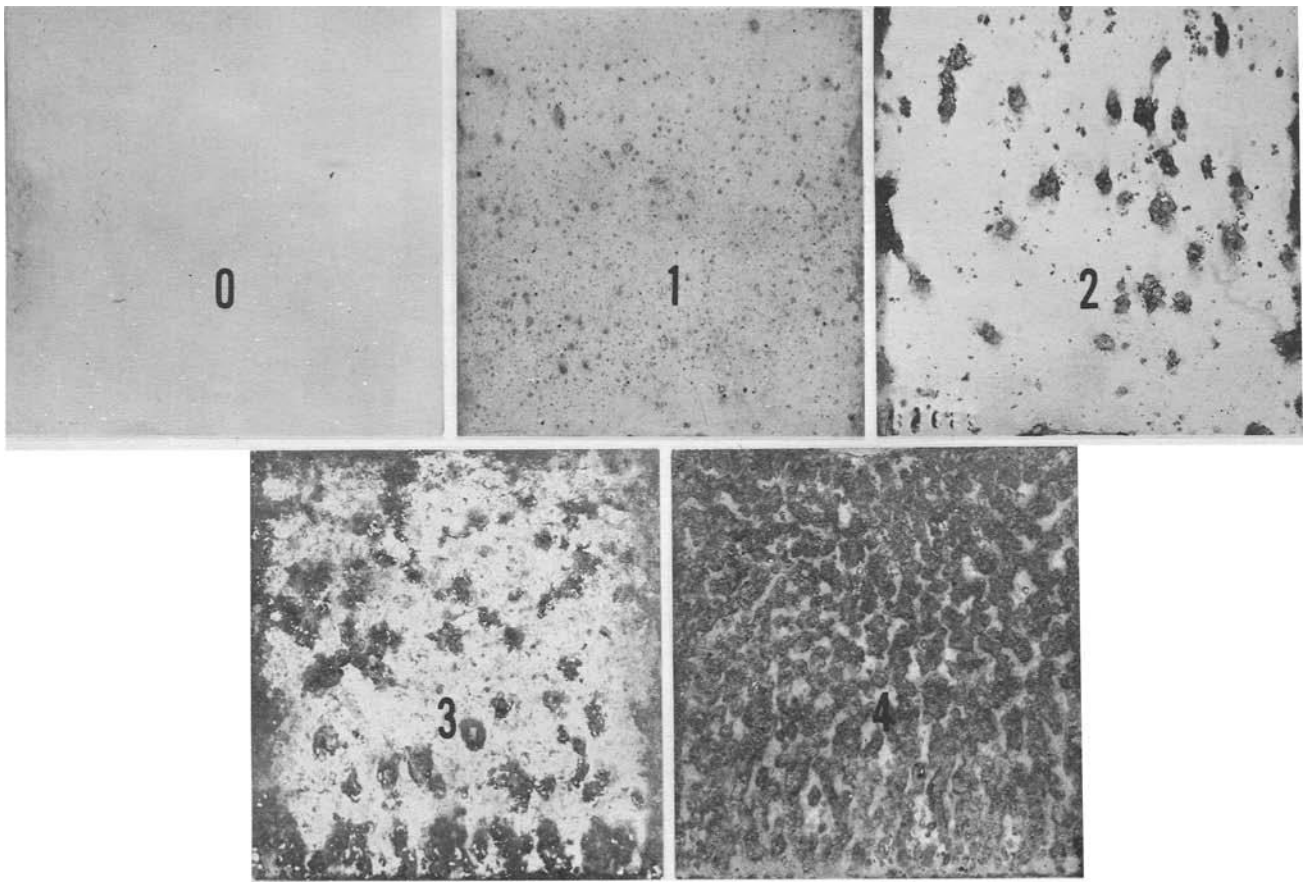


Figure 2 - Visual rating standards. Approximately 0.7 actual size. (0) essentially no corrosion; (1) light flecks; (2) isolated blotches; (3) blotches and spreading; (4) almost covered.

100 percent gloss. Three readings were then made on the uncorroded portion of the specimen and 6 readings on the corroded portion. The following formula was used to calculate the percent retained gloss (% RG) rating:

$$\frac{\text{Av. reading on corroded portion of spec.}}{\text{Av. reading on uncorroded portion of spec.}} \times 100\% = \% \text{ RG rating}$$

Typical specimen ratings are shown in Figure 3. This glossmeter rating method was developed at the Applied Research Laboratory and has not been previously reported in the literature, so it will be examined briefly. Because the % RG rating is a ratio of two readings, the absolute values of the readings do not affect the rating so long as the calibration of the instrument did not change during the time of the readings. An optical instrument is usually most sensitive in the mid-range of its calibration and it is presumed that this applies to the glossmeter also. Thus a mirror was a useful calibration standard because the high-gloss steel finishes had a rating of about 70 percent the gloss of a mirror. Further, the method is most sensitive where the difference in gloss between the corrosion product and the uncorroded surface is the greatest; it is quite insensitive on a dull or matte finish. Because various cleaning operations can appreciably alter the gloss of a finish, it is important that any cleaning operation on the corroded metal be precisely duplicated on the uncorroded metal. Within these limitations, however, the method is regarded as a simple and useful way to describe the effect of corrosion on the surface of automotive trim materials.

The quadratic correlation coefficient for the two rating methods was 0.907, a significant correlation.

The essential results from the 1961-1962 service exposure are summarized in Table 1. The most corrosion-resistant materials were the austenitic AISI Types 201 and 301 stainless steels. The next most resistant were the ferritic steels with 1 percent molybdenum (Type 430 Mo) and 1 percent molybdenum with 0.5 percent columbium (Type 430 MoCb). The least corrosion-resistant were the ferritic stainless steels without molybdenum (Type 430). It was further noted that buffing did not significantly improve the corrosion performance of a bright-annealed surface.

Spot Test

The Spot Test consists of exposing the steel for 5 minutes to a solution made by dissolving 10 grams of ferric chloride ($FeCl_3 \cdot 6H_2O$), 5 grams of sodium chloride, and 2.5 milliliters of concentrated hydrochloric acid in 200 milliliters of distilled water. The attack was rated as heavy etch (HE), medium etch (ME), light etch (LE), very light etch (VLE), and no attack. An etched surface was

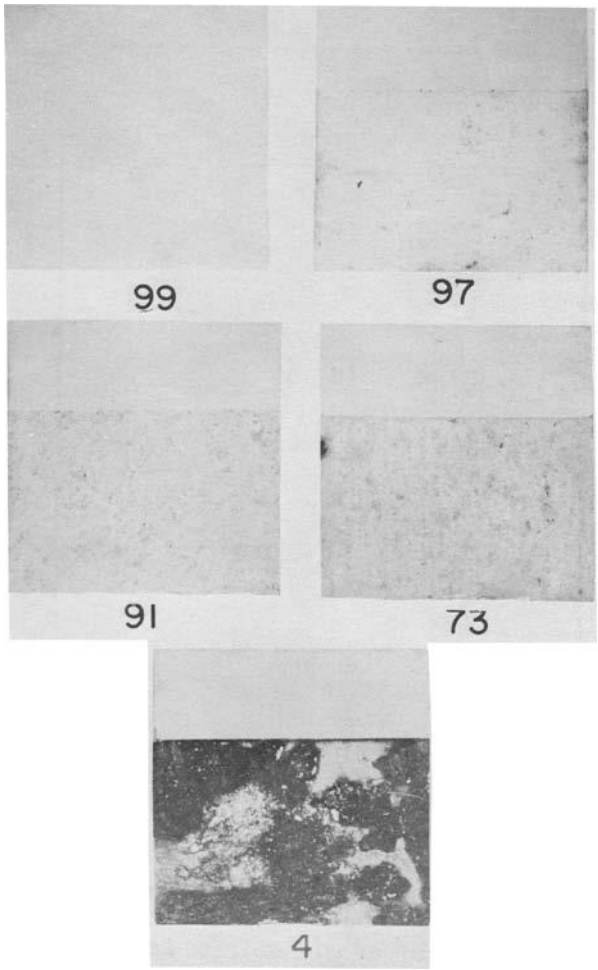


Figure 3 - The appearance of corrosion test specimens with the captioned percent retained gloss (approximately 1/2 actual size).

reported by Trax and Holzwarth[2] to indicate that the surface has been depleted in chromium during processing; a similar etch, called "frosting," will sometimes appear on such material during service. Only the steels from the first exposure were exposed to this test.

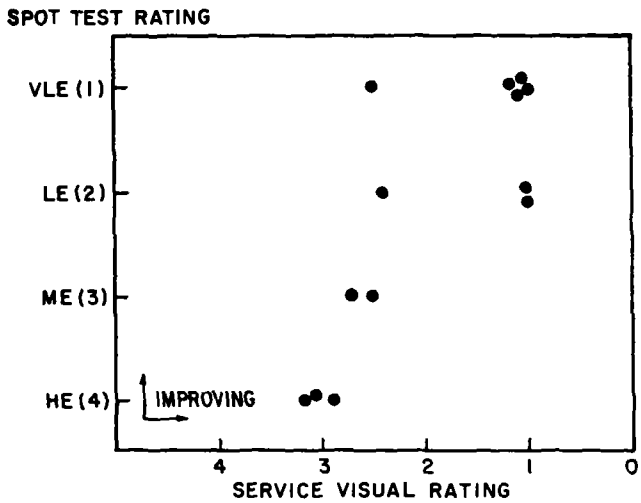


Figure 4 - Correlation of Spot and Service Tests. VLE = very light etch; LE = light etch; ME= medium etch; HE = heavy etch.

Figure 4 shows the correlation between the service visual rating and the rating in the Spot Test. For purpose of statistical treatment the HE, ME, LE, and VLE ratings were equated to 4, 3, 2 and 1, respectively. The linear correlation coefficient was 0.807 and the quadratic coefficient was 0.892. The critical linear correlation coefficient was 0.553. It can be seen that those steels which were poor in the Spot Test were also poor in the service test; however, there were some steels which performed poorly in service even though they had a good Spot Test rating. Even though the latter steels were apparently not depleted in chromium, the service exposure was sufficiently severe to cause some pitting and corrosion attack.

CASS Test

In the CASS Test, specimens are exposed for 16 hours at 120 F in a salt-spray cabinet to a fog from a solution containing 0.26 gram of cupric chloride ($CuCl_2 \cdot 2H_2O$) and 50 grams of sodium chloride per liter of solution, and acidified with acetic acid to a pH of 3.2 in the collected solution. The specimens are rated by means of a transparent grid marked off into 100 one-quarter-inch squares. The percentage of frosting plus pitting is determined by placing the grid on the specimen and counting the grid units containing frosting or pitting corrosion visible with the unaided eye. The rating was assigned from the following standards.

Percent Frosting Plus Percent Pitting	Rating
0	1
<5	2
5 - 15	3
15 - 25	4
25 - 35	5
>35	6

This test was initially developed for chromium-plated trim materials.[3]

The CASS Test results are compared with service results for the 1960-1961 exposure in Figure 5, and for the 1961-1962 exposure in Figure 6. It is noteworthy that whereas there was some semblance of correlation with service for the first exposure, there was none at all for the second. This is explained as follows.

The linear correlation coefficient for the 1960-1961 exposure (Figure 5) was 0.678, with a quadratic coefficient of 0.951; the critical linear coefficient was 0.553. For the 1961-1962 exposure (Figure 6) the linear coefficient was 0.437 for the service visual rating and 0.100 for the service % RG rating; the critical linear coefficient was 0.532--the correlation was not significant.

The difference in the results between the two years is remarkable. If the exposures were assumed to be essentially similar, the difference must lie in the materials. The first exposure, in which the correlation with service was significant, included several annealed-and-pickled steels which the Spot Test had indicated were depleted in chromium at the surface. The only steels from the second exposure which were exposed in the CASS Test were a group which had been polished and buffed, removing about 1 mil from the surface, and which

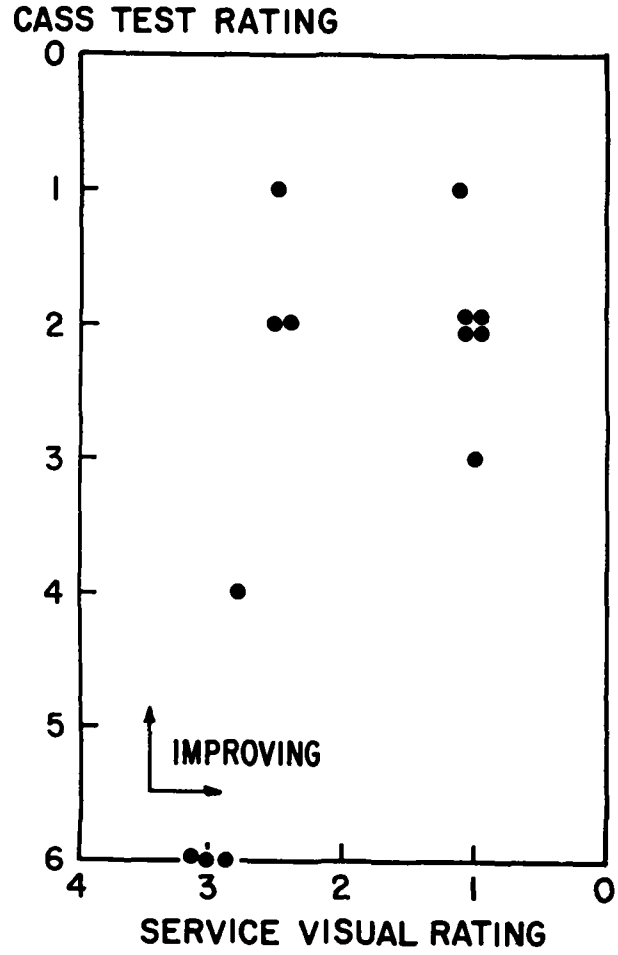


Figure 5 - Correlation of CASS and Service Tests, 1960-1961.

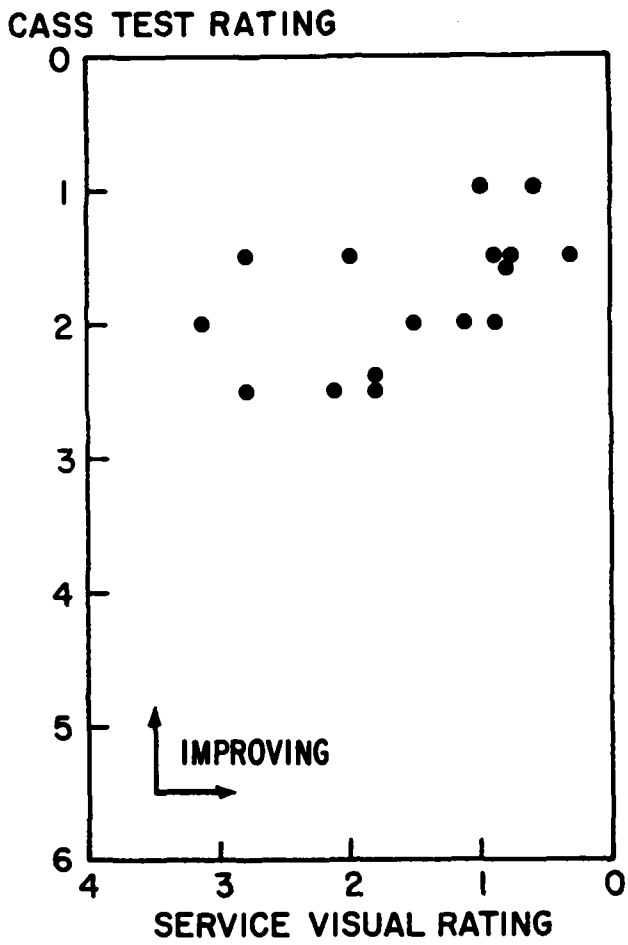


Figure 6 - Correlation of CASS and Service Tests, 1961-1962.

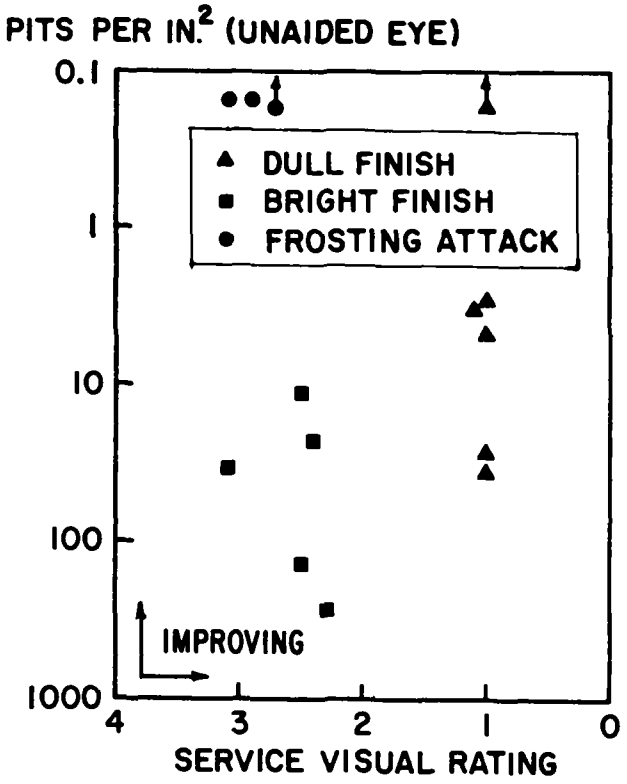


Figure 7 - Correlation of $FeCl_3$ and Service Tests, 1960-1961.

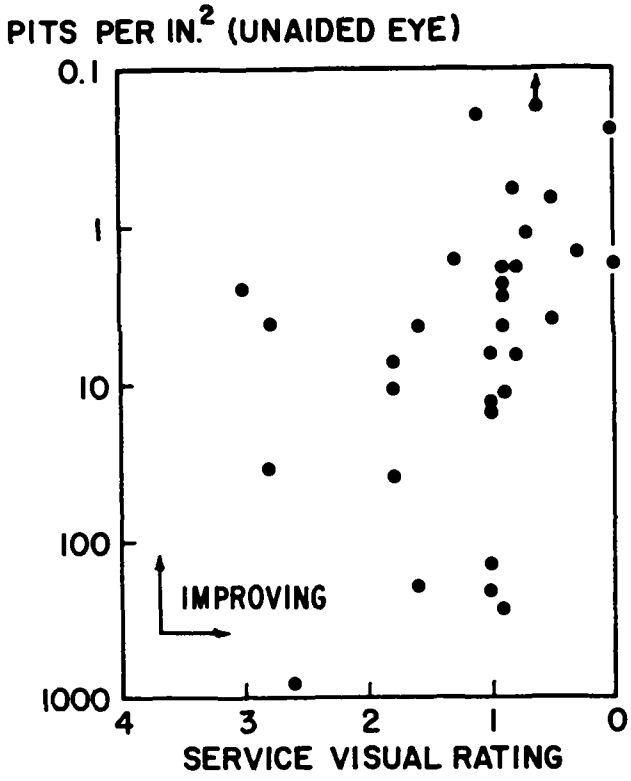


Figure 8 - Correlation of $FeCl_3$ and Service Tests, 1961-1962.

should not have had a chromium-depleted surface. Thus, it seems probable that the CASS Test is valid only where chromium depletion of the metal surface is a factor in the corrosive attack.

Ferric Chloride Test

In the Ferric Chloride Test, specimens are immersed for 2 hours at 95 F in a solution containing 4-1/2 milliliters of concentrated hydrochloric acid and 108 grams of ferric chloride ($FeCl_3 \cdot 6H_2O$) per liter of solution. The principal method of evaluation is to count the pits visible with the unaided eye and express the rating as pit density.

The comparison for the first exposure is shown in Figure 7. The data are seen to lie in three groups, each too small to warrant statistical treatment. One group, six austenitic stainless steels with a dull, 2B finish, had a service rating of close to 1, but had a variation in pit density of about 3 orders of magnitude. One group of three lots of Type 430 stainless had a visual service rating of 3, but pit densities of less than 1 per square inch. However, these steels etched in the Ferric Chloride Test as they had in the Spot Test, indicating that a low pit count alone is not necessarily a complete description of the performance of a steel in this test. The remaining five points show no semblance of a correlation with service. In summary, the Ferric Chloride Test showed no promise in the 1960-1961 exposure.

This test was evaluated on a larger scale when its results were compared with those of the 1961-1962 service exposure. For the pit density as measured with the unaided eye, the correlation coefficient was 0.307 for the service visual rating (Figure 8) and 0.152 for the service % RG rating; the critical correlation coefficient was 0.355. Because the pits varied greatly in size and the pit density measurement gave such a poor correlation, weight losses were determined. The correlation coefficient of these was 0.109 for the service visual rating and 0.011 for the service % RG rating; the critical correlation coefficient was 0.405. The percent area corroded by pitting was estimated. The correlation coefficient of this rating was 0.050 for the service visual rating and 0.044 for the service % RG rating; the critical correlation coefficient was 0.553. Examination of the surfaces of many specimens with a microscope at 100X revealed a myriad of tiny pits not visible to the unaided eye. The correlation coefficient for pit density at 100X was 0.211 for the service visual rating and 0.325 for the service % RG rating; the critical correlation coefficient was 0.533. Thus, of all the methods used to evaluate the results of this test, none had a significant correlation with either of the service ratings, indicating that the test, when used with a variety of steel compositions and finishes, will not predict service performance.

In spite of this poor correlation with service the Ferric Chloride Test is in some ways the most interesting of the accelerated tests because it is very sensitive to small changes in surface condition. The bright-annealed surfaces usually had very high pit densities, although they performed well in service. Buffing of the bright-annealed surface invariably reduced the pit density, as measured with the unaided eye, by one or more orders of magnitude, but as indicated in Table 1, buffing did not improve the service performance of the bright-annealed steels.

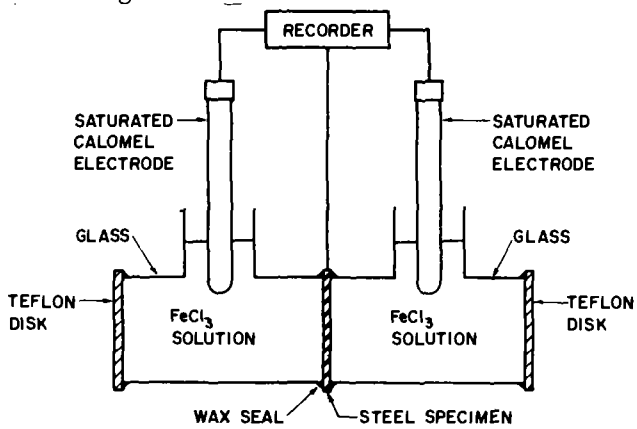


Figure 9 - Cell for potentiometric studies.

It has been postulated that residual stearic acid from the buffing operation improved the performance in the Ferric Chloride Test. Attempts to verify this, however, have been inconclusive:

1. When a buffed specimen was boiled for 1/2 hour in a detergent solution, a treatment which should remove stearic acid, its pit density in a subsequent Ferric Chloride Test was increased by a factor of 100.
2. Treatment of a buffed specimen for 16 hours at 140 F in a detergent solution, another treatment which should remove stearic acid, decreased the pit density in a subsequent Ferric Chloride Test by a factor of 5.
3. Anodic passivation of bright-annealed steels in several of the common acids (no treatment with stearic acid) decreased the pit density to a very low figure.
4. Boiling a passivated specimen for 1/2 hour in a detergent solution, even when there cannot be any stearic acid present, caused it to pit in a subsequent Ferric Chloride Test at about the same rate as the original bright-annealed materials.

Thus, the performance of a steel in the Ferric Chloride Test is not per se related to the presence or absence of stearic acid on the surface. All of the above changes in sensitivity to the Ferric Chloride Test were effected without any visible change in the appearance of the specimen.

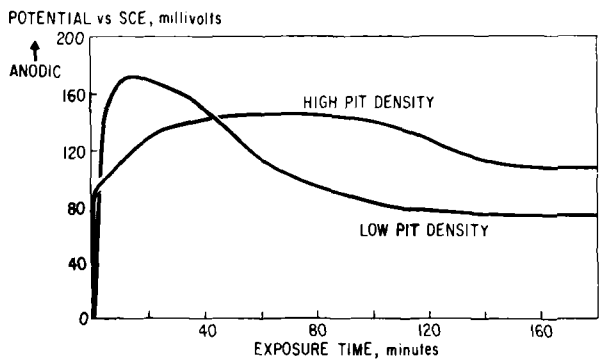


Figure 10 - Typical time-potential curves in $FeCl_3$ Test.

Specimens which had been buffed on one side only had pit densities on the two sides which varied by factors of about 100. To separate the effect on the two sides, the steel specimen was mounted in the split cell shown in Figure 9, in which the variation in potential was recorded with time as pitting proceeded. Typical time-potential curves are shown in Figure 10. The curve representing surfaces with a low pit density frequently exhibited an anodic peak, whereas the second curve is more typical of those surfaces with a high pit density. These data indicate that the test responds to differences in the electrochemical nature of the surface. Such curves, however, did not have a significant correlation with service.

In one series of experiments the pit density was noted at 100X after time exposure times ranging from 2.5 minutes to four hours. After 5 minutes no new pits had formed, but those which had formed continued to grow. This raises the interesting possibility that the two-hour test period could be shortened to 5 minutes if the pits were counted with a microscope.

But of what value would even a short-time test be that did not correlate with service? The extreme sensitivity of the Ferric Chloride Test to surface condition suggests that it could be used as a quality control test for some surface treatment operation such as buffing, anodic passivation, or perhaps even an operation unrelated to corrosion resistance.

Dip-and-Dry Test

The solution used in this test consisted of

1. Distilled water	2100	ml
2. Sodium chloride	105.0	g
3. Calcium chloride ($CaCl_2 \cdot 2H_2O$)	105.0	g
4. Sodium sulfate (Na_2SO_4)	1.0	g
5. Sodium sulfite (Na_2SO_3)	0.5	g
6. Sodium thiosulfate ($Na_2S_2O_3$)	0.2	g

The solution was made by dissolving the ingredients in the order listed above. The solution was repeatedly vacuum-filtered, using a No. Y2 Whatman filter paper, until clear. Before using, the solution pH was adjusted to 9.3 with dilute solutions of hydrochloric acid or sodium hydroxide. The solution was used within 48 hours after preparation.

Specimens (1 by 6 inches) were sheared from sheet material, immersed for 15 minutes in a detergent, rinsed in distilled water, and attached to an elevator mechanism activated by an electrical timer arrangement. The cylinder rhythmically raised and lowered the cross-piece, thus periodically immersing the specimens into beakers containing the test solution. The cycle consisted of a 1- to 2-second immersion period and a 98- to 100-second drying period. The specimens were dried with 250-watt infrared heat lamps. The specimen and solution temperature was controlled by a set of shutters and individual powerstats on the heat lamps. The specimen temperature was held at 110 to 130 F and the solution temperature at 90 to 110 F. During the drying cycle the specimens came to complete dryness except for a 1/2-inch length at the bottom. The total test duration was 8 hours (about 290 cycles). After completion of the test, the specimens were rinsed in running hot water, dipped in acetone, and dried in a stream of hot air.

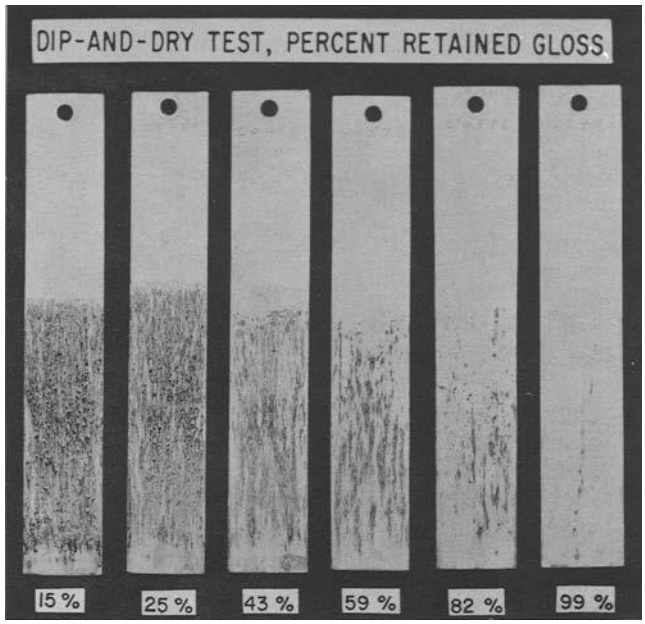


Figure 11 - Dip-and-Dry Test. Approximately 0.6 actual size.

The % RG for the specimens was measured in the following three conditions: (a) as corroded and washed in the above manner; (b) washed in tap water after measurement (a) by lightly rubbing with a soft-bristle brush; (c) scoured with non-abrasive scouring powder after measurement (b). Figure 11 shows typical specimens, each labeled with its respective rating.

The correlation coefficients with the service visual rating were 0.738 for the as-corroded condition (see Figure 12), 0.637 for the as-washed condition, and 0.522 for the as-scoured condition; the correlation coefficients with the service % RG rating were 0.551 for the as-corroded condition, 0.616 for the as-washed condition, and 0.558 for the as-scoured condition. The critical correlation coefficient was 0.290, showing that all readings are significant and that the Dip-and-Dry Test can, in some measure, predict service performance of the stainless steels. For example, in Figure 12, if a Dip-and-Dry rating of 40% RG or higher and a service rating of 1 or lower are considered good, approximately 90 percent of all poor material would be rejected and 96 percent of all good material would be accepted. Figure 12 shows such a degree of data spread, however, that a chance shifting of points could easily change these favorable ratios.

Thermographic Test

The Thermographic Test is an interesting modification of the older Ferroxyl Test.[4] In the Thermographic Test the solution used is the same as that for the Dip-and-Dry Test. Photographic print paper was washed free of silver and dried. It was cut 1/4 inch smaller than the specimens and soaked in the test solution for at least 15 minutes. The wet paper was rolled on the test surface with a

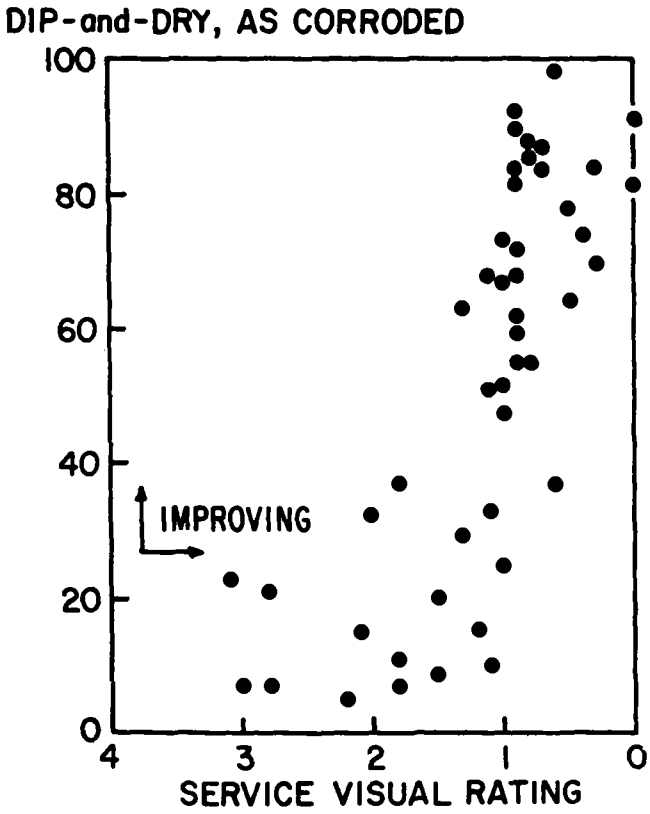


Figure 12 - Correlation of Dip-and-Dry and Service Tests.

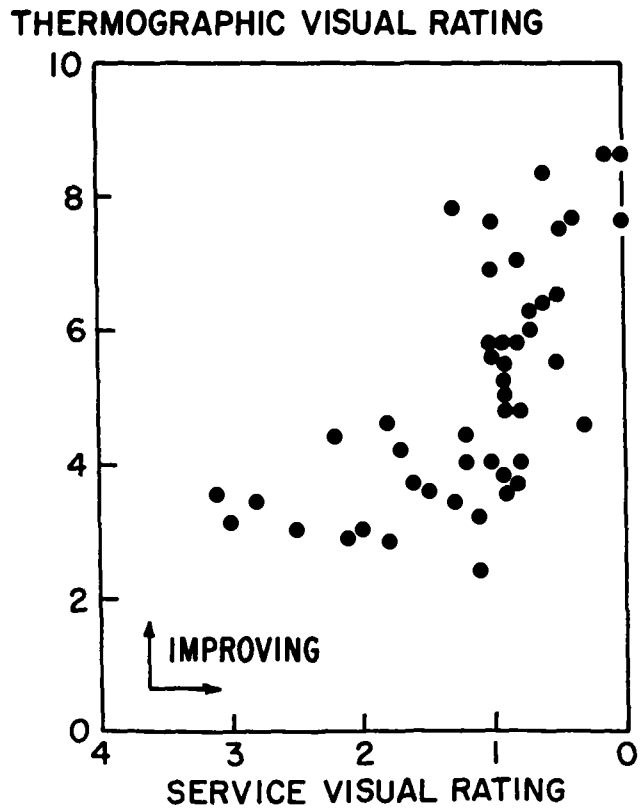


Figure 13 - Correlation of Thermographic and Service Tests.

print roller, the gelatin side next to the metal surface. The specimen and paper were enclosed in a polyethylene bag which was folded over several times, and a rubber band was placed around the package. The package was placed in an oven at 110 C for ten minutes, after which the print paper was removed promptly. At this point the results were evaluated by two different methods:

1. Some of the test papers were analyzed for iron. It was assumed that all constituents in the steel were dissolved equally and that, knowing the percent iron in the steel, the total weight of corrosion product could be calculated. 2. Other papers were dipped into a solution of potassium ferricyanide to develop the pitted areas as blue spots on the paper. The papers were evaluated then according to Table 2.

Table 2
Conversion of Percent Area Corroded to Rating Number

Rating No.	Percent Area Corroded
10.0	0.0
9.0	0.01 - 0.1
8.0	0.1 - 0.25
7.0	0.25 - 0.5
6.0	0.5 - 1.0
5.0	1.0 - 2.5
4.0	2.5 - 5
3.0	5 - 10
2.0	10 - 25
1.0	25 - 50
0.0	100

The visual Thermographic rating had a linear correlation coefficient of 0.680 and a quadratic coefficient of 0.743 with the service visual rating, and a linear coefficient of 0.393 with the service % RG rating. The weight of corrosion product had a linear correlation coefficient of 0.724 with the service visual rating and a coefficient of 0.439 with the service % RG rating. For all comparisons the critical correlation coefficient was 0.290; thus, all comparisons are significant.

It appears that this test has some merit in predicting performance, although as with the Dip-and-Dry Test the data spread shown in Figure 13 is undesirably large. If, for example, a service rating of 1 or lower was considered good, approximately 95 percent of the material accepted would be good, but approximately 33 percent of the material rejected would also be good. The latter is an undesirably high rejection rate.

Corrodkote Test

The Corrodkote Test is one which was developed to evaluate chromium-plated auto trim.[3] In this test a slurry of 120 grams of kaolin, 4.0 grams of ammonium chloride, 0.66 gram of ferric chloride ($FeCl_3 \cdot 6H_2O$), 0.14 gram of cupric nitrate ($CuNO_3 \cdot H_2O$), and 200 milliliters of distilled water was applied to the panels and allowed to dry. The panels were placed in a humidity cabinet at 100 F and 95 percent relative humidity for 3 hours. The specimens were then cleaned and rated. They were subsequently coated, exposed, cleaned, and rated two more times, for a total of three 3-hour exposures for each panel. They were rated by

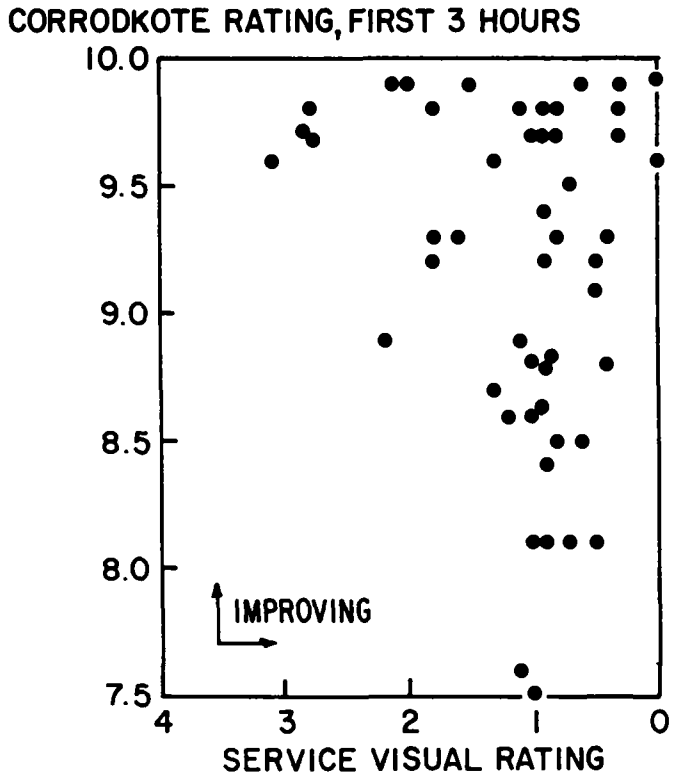


Figure 14 - Correlation of Corrodkote and Service Tests.

comparison with a series of dot charts, which are summarized in Table 2.

The correlation coefficients for the relationship between the service visual rating and Corrodkote rating after the first, second, and third exposures were 0.159, 0.108, and 0.111, respectively. One comparison is shown in Figure 14. The correlation coefficients for the relationship between the service % RG and the Corrodkote rating after the first, second, and third exposures were 0.141, 0.037 and 0.071, respectively. The critical correlation coefficient was 0.282, verifying that the test had no merit for predicting service (Figure 15).

Summary and Conclusions

The calculated correlation coefficients for all evaluation tests are shown in Table 3. The Dip-and-Dry Test and the Thermographic Test are considered best. It is noteworthy that these two tests with the best correlation with service both use the same solution, and that the solution is the only one which simulates road slush containing deicing salts and sulfur compounds. Further, these two tests are the only ones which, in the absence of surface deficiencies, distinguish between different chemical compositions of the metal.

It is believed that both the Spot and CASS Tests are suitable for detecting a chromium-depleted surface, but the relative simplicity of the Spot Test commends it in preference to the elaborate, time-consuming CASS Test. The CASS Test is apparently not suitable if there is no chromium depletion.

Table 3

Correlation Coefficients

Evaluation Tests	Service Tests: Visual	Service Tests: % RG	n**	Critical Coefficient for Linear Correlation
Spot Test 1960-1961	0.803 0.892*		13	0.553
CASS Test 1960-1961	0.678 0.951*		13	0.553
CASS Test 1961-1962	0.437	0.100	14	0.532
Ferric Chloride Test 1960-1961 (Pit density with unaided eye)	Insufficient data but no apparent correlation			
Ferric Chloride Test 1961-1962				
Pit density with unaided eye	0.307	0.152	31	0.355
Pit density at 100X	0.211	0.325	13	0.553
Percent area corroded	0.050	0.044	13	0.553
Weight loss	0.109	0.011	24	0.404
Corrodkote Test				
First 3 hours	0.159	0.141	49	0.282
Second 3 hours	0.108	0.037	49	0.282
Third 3 hours	0.111	0.071	49	0.282
Dip-and-Dry Test				
As corroded	0.738	0.414	46	0.290
As washed	0.637	0.616	46	0.290
As scoured	0.522	0.558	46	0.290
Thermographic				
Visual Rating	0.680 0.743*	0.393	46	0.290
Weight of corrosion product	0.724	0.439	46	0.290
Service % RG	0.907*		57	0.261

Values underlined are significant.
** n is the number of comparisons.
* These values are for correlation to a quadratic curve; they are given only where they are significantly greater than the linear coefficients.

The Ferric Chloride Test is not good as a screening test to predict service. It may at times serve as a quality control test for some finishing operation such as buffing or passivation.

The Corrodkote Test shows no merit for predicting service performance of stainless steel automotive trim.

The absence of any really good correlations with service, however, should lend a note of caution against extensive use of the presently available evaluation tests. It further points to the need for more reliable tests for use in acceptance and quality control tests, and for research use.

Acknowledgments

The authors wish to acknowledge the aid of D. C. Vreeland, H. J. Bhatt, L. J. Kotnik, A. W. Loginow and B. K. Stewart in conducting and evaluating these tests.

References

1. G. F. Bush. Iron Age, pp 91-94, December 20, 1962.
2. R. V. Trax and J. C. Holzwarth. Corrosion, 16, 271t-274t, (1960) June.
3. W. L. Pinner. 48th Annual Technical Proceedings, American Electroplaters Society, pp 27-31 (1961).
4. American Metal Market, January 17, 1963.

Accelerated Tests As a Method of Predicting Service Corrosion of Exterior Automotive Trim

By G. F. Bush*, W. J. Garwood*, and B. E. Tiffany*

A wide variety of accelerated, or short term, tests are conducted daily upon a host of different materials in an attempt to predict the behavior of the material in service or to evaluate the relative merits of material modifications or changes. They are also used for control purposes to insure product quality as well as for identification. It would be extremely time consuming and unprofitable to attempt to list them all or even those which might be considered as major tests. The American Society for Testing and Materials alone publishes 11 large volumes on test methods. Other national societies, government agencies and private industry publish still others.

This is said in an attempt to establish the relative importance of accelerated tests to material and product engineers and ultimately to the consumer. Without any attempt to minimize the value of existing tests, it is apparent that a great many of them were originated in laboratories to evaluate given properties or characteristics in the test environment, as opposed to actual service.

The 20 percent, and more recently, the 5 percent neutral salt spray has been used for a great many years to evaluate the corrosion resistance of metals. As it is so widely specified and used, the test has been carried on for decades. Too few workers have paused to consider the significance of this and other accelerated tests. Too few have asked, "Does this test reflect the type of failures encountered in service?" "What is the relationship between a given time in this test and some unit of time in actual service?" "Can it guarantee that parts which pass the test requirements will also be good in service?"

Essentially, these were the questions asked by Mr. John Dykstra, President, Ford Motor Company, on July 14, 1959, regarding the corrosion resistance of exterior decorative trim used on Company products.

At that time the 5 percent neutral salt spray was used to measure the corrosion resistance of anodized aluminum, augmented by such tests as dye staining (anthraquinone violet RN) coating thickness (metallurgical microscope) and coating weight and density (analytical balance).

The neutral salt spray test was used also to test all varieties of stainless steel used for trim. A drop test, using a solution of ferric chloride, was used to a more limited degree.

A relatively new test known as Corrodkote, was used to evaluate electroplated steel and nonferrous metals such as zinc base die castings and brass. Other automotive manufacturers and suppliers were using an equally new test, known as CASS, for these same materials. Both tests were augmented by thickness measurements (metallurgical microscope and chemical) as well as adhesion tests (grinding wheel and others).

"Were these tests any good?" was the question to be answered. As casual observation revealed numerous instances of failure on cars in service, the obvious answer would be that they were not. However, the same casual observation revealed that a great number of similar parts, sometimes on the same vehicle as the failed parts, had not corroded. Did this mean that the tests were good?

Because there was no way of correlating service observations with specific accelerated test data, no conclusive judgement could be made on the merits of the various tests. It should be noted also that casual observation of service corrosion may be an extremely unreliable basis for a judgment, unless spread over a sufficient number of cars to be statistically significant.

It was obvious the only way to truly evaluate the tests would be to have identical parts and expose some of them in service, while conducting accelerated tests on the remainder. Then, by a comparison of service results with test results, each of the accelerated tests could be rated.

Accordingly an exterior decorative trim corrosion program was instituted in the summer of 1959 to:

1. Evaluate existing accelerated tests on each exterior trim material.
2. Evaluate the influence of material and process variables on corrosion resistance.
3. Develop new and accelerated tests as required.

This paper is restricted to the evaluation of existing accelerated tests on stainless steel only.

In an attempt to guard against haphazard or accidental correlation of the laboratory tests with service, it was decided to include materials or processes which should give either better or worse corrosion resistance than the standard systems being investigated. As a result, the 1959 program consisted of 7,618 specimens reflecting a total of 135 variables. Since then a total of 28,105 specimens have been exposed to service or accelerated tests and rated for corrosion.

* Ford Motor Company, Detroit, Michigan.

Copyright© 1965 by ASTM International

www.astm.org

The service exposure involved two types of specimens, flat panels measuring 4 in. x 4 in. and regular hub caps. These latter were used to evaluate electroplating systems and variables on steel. The panels were used for anodized aluminum, stainless steel and electroplated zinc die castings and other nonferrous metals. A total of 24 specimens was service exposed for each variable being investigated. They were exposed on cars operating in three distinct areas: Detroit and suburbs, representing typical exposure in a location using salt for snow and ice removal; Buffalo, representing more severe winter exposure than Detroit, also using sodium chloride; and finally, the Rouge area of Ford Motor Company, representing exposure to an industrial atmosphere as well as to normal Detroit salt and snow. The panels were exposed in special racks suspended below and behind the front bumper. (Figure 1). The hub caps were mounted on the wheels of the test vehicles. In this fashion the test pieces were exposed to service for the winter months, essentially November 15 to April 15 of the following year. The reasoning behind the selection of the size, shape and location of the test panels has been explained in detail previously.[1]



Figure 1 - A test car showing the panels mounted on a rack, below and behind the front bumper.

After removal from the test vehicles, the panels and hub caps are soaked in warm water containing a mild detergent and are scrubbed with a soft bristle brush or sponge to remove road dirt. One half of each specimen is then cleaned with a suspension of a fine abrasive to permit the corrosion rater to determine the type and amount of base metal corrosion actually present. Thus, each specimen receives two ratings: "washed" and "cleaned". (Figure 2). The "washed" rating represents what an average car owner might see. The "cleaned" rating represents what a "care-taker" owner might see.

With the aid of dot charts (Figure 3), the percent area defective for each of three major defects (blistering, pitting and etching) is estimated. These are then weighted by a factor intended to reflect the seriousness of each defect and are then added together to obtain a "Total Weighted Area Defective". This is converted to a Rating Number, called "Protection", by means of a graph. (Figure 4). A second number, called "Appearance" and representing the extent and degree of staining, is derived from the "Protection" value by subtracting from it the sum of the stained areas, each area multiplied by a factor for three degrees of staining. Details of the rating method and its derivation have also been published previously.[2]

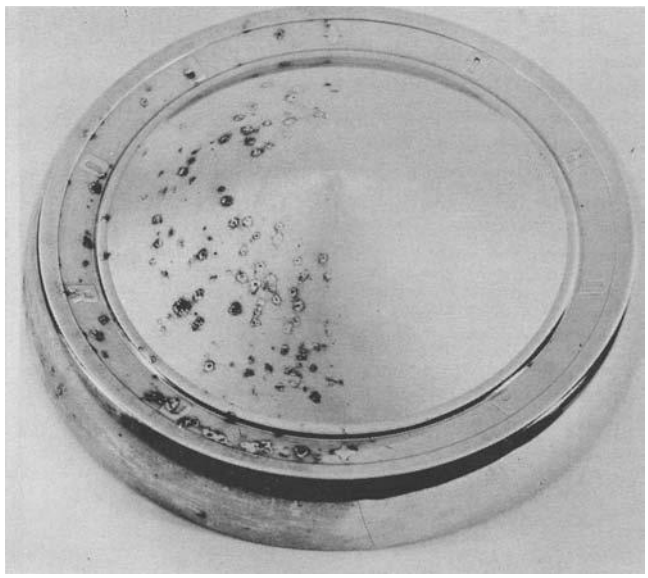


Figure 2 - A test hub cap, illustrating the "washed" (left) and "cleaned" conditions used for rating.

The accelerated tests are carried on concurrently with service exposure and wherever possible are rated by the same method. Where not feasible, the accelerated tests are rated by the best of the known methods. In this program the accelerated tests included:

Ferricyanide spot
Corrodkote
Cass
Ferric chloride spot
Ferric chloride immersion
Salt slag immersion (dip-dry)
Thermographic

Prior to analyzing the results of the initial program, it was anticipated that the correlation of the various accelerated tests with service could be determined by simple inspection. (Figure 5). Unfortunately, this proved impossible. Reversals in service between the "washed" and "cleaned" ratings are found frequently. Which of these should the accelerated test match? In other instances, accelerated tests such as CASS and Corrodkote, which were conducted for more than one cycle, also showed reversals from one cycle to another. (Figure 6). Again, cycles were selected in some instances which were so severe that no difference between series could be observed, while actual service caused some greater or lesser difference in corrosion on the identical series. Would a less severe exposure in the accelerated test have found the same difference? To answer this, it was necessary to wait for the next program simply because of the sheer volume of work entailed.

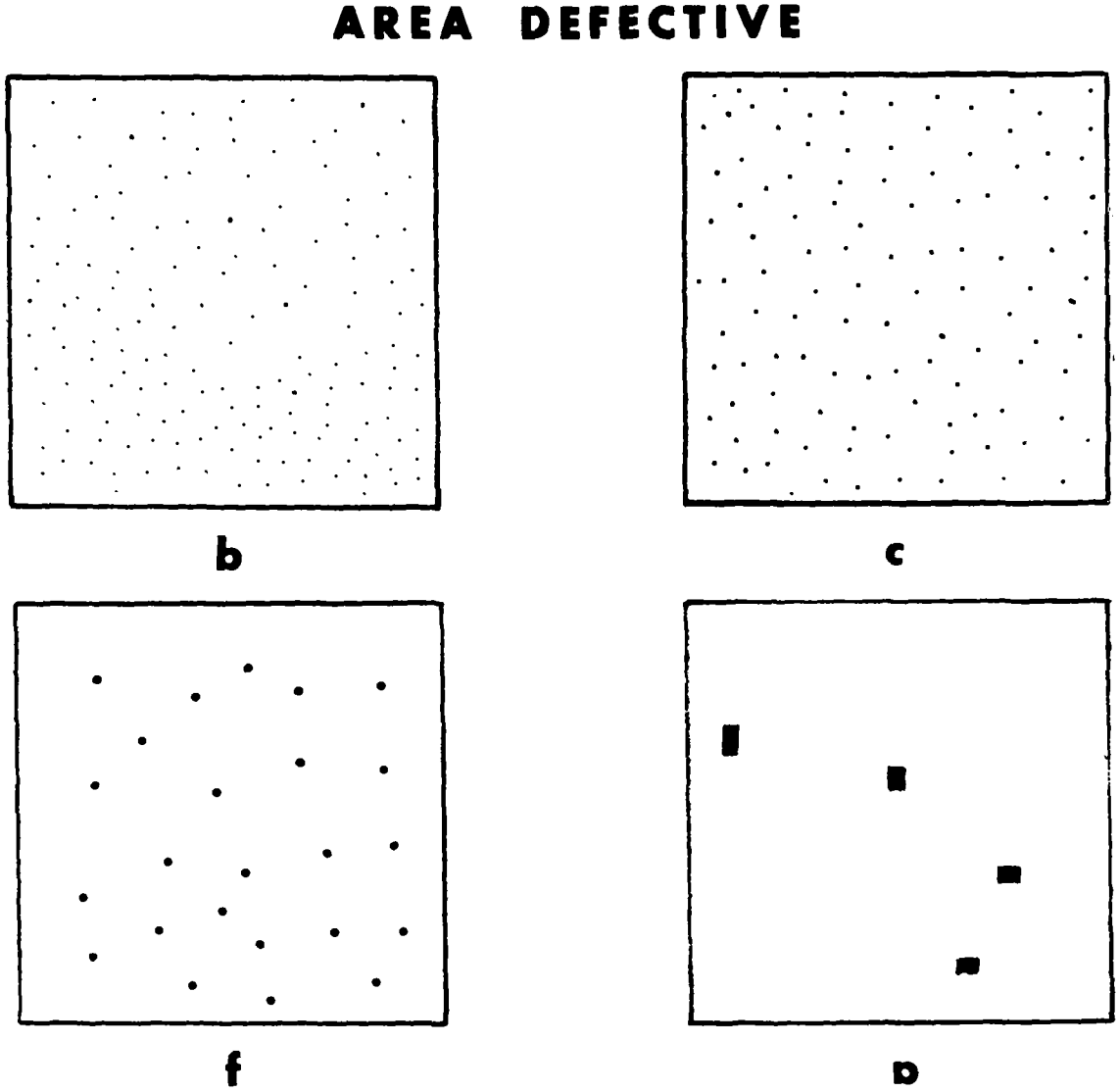


Figure 3 - A typical dot chart used to estimate the percent area defective for each of three recognized major defects. In this chart, four variations of a defective area of 1 percent are shown. (Courtesy of Chrysler Corporation)

Another factor which has caused some difficulty is that the method of rating corrosion, previously described, was developed only after the accelerated tests for the 1959 program had been finished. Thus, some of the accelerated test data from the first year are reduced in value.

When it was found that simple inspection could not be used, a technique was employed as follows: If series A, B and C exposed in service were rated as A best, B second and C poorest, then it was rationalized that a good accelerated test would establish an identical order of merit. If any other order of merit were found, the test was declared to be a failure for this specific comparison.

This technique seemed unfair in the instances where the tests correctly predicted that A was superior to B, but then erred and found C possibly equivalent to one of the others. Was the test a complete failure, in such an instance, or was it right insofar as it predicted the correct order of merit for two of the three series involved?

After considerable debate among ourselves, we decided that the latter approach was more nearly correct and by counting the number of times a given test agreed with service, arrived at a percentage correlation figure.

This proved to be quite laborious as reversals were found between washed and cleaned service, as previously noted,and also from one year's service to another. Add to these the reversals found from one cycle of an accelerated test to another and it will be realized that we had considerable uncertainty as to the significance of our correlation values.

During the third year of this program, some limited work was done with two dimensional graphs in which results from a specific accelerated test were plotted against the results from service. If there had been perfect correlation, the points on

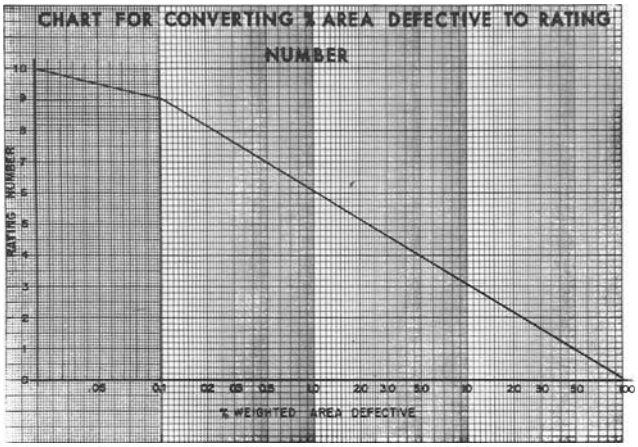


Figure 4 - The graph used to convert the total percent weighted area defective to a rating number called "Protection". Note that it is an arithmetic graph for values 0 to 0.1 percent area defective to reflect our interest in superior materials.

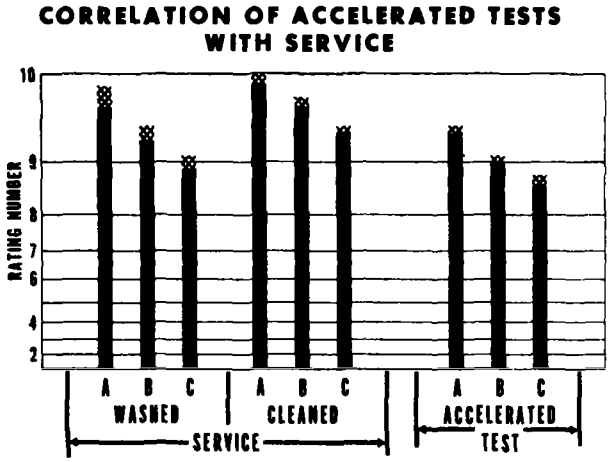


Figure 5 - A hypothetical comparison showing obvious correlation of "washed" service with "cleaned" service. Both were predicted, at least in order of merit, by the Accelerated Test.

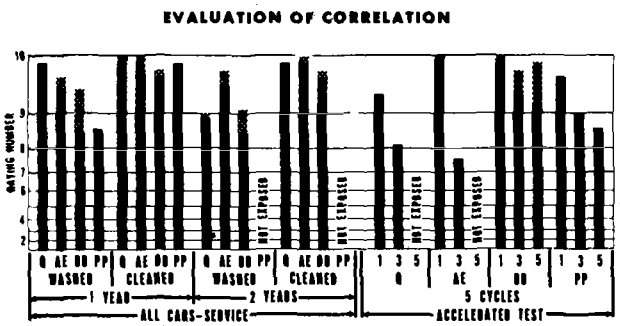


Figure 6 - Actual data from the Corrosion Program illustrating reversals both in Service and in the Accelerated Test.

the graph would have fallen in a straight line. As may be imagined, the points did not fall in a straight line, but rather in a scatter diagram. (Figure 7). This suggested that the Simple Correlation Coefficient (SCC) "r", used by statisticians be employed.

This can be developed from the equation

$$r = \frac{n\Sigma xy - \Sigma x \Sigma y}{\left[(n\Sigma x^2 - (\Sigma x)^2)\,(n\Sigma y^2 - (\Sigma y)^2) \right]} \; 1/2$$

where

n = number of items per variable

Σx = sum of the values of variable x

Σy = sum of the values of variable y

$(\Sigma x)^2$ = square of the sum of the values of x

$(\Sigma y)^2$ = square of the sum of the values of y

Σx^2 = sum of the squares of the values of x

Σy^2 = sum of the squares of the values of y

Σxy = sum of the products of x and y

As an example

$n = 4$

	x	x^2	y	y^2	xy
	1	1	3	9	3
	2	4	3	9	6
	2	4	5	25	10
	4	16	6	36	24
sum	9	25	17	79	43

Substituting these values in the formula

$$r = \frac{4 \times 43 - 153}{\left[(4 \times 25 - 81)\,(4 \times 79 - 289) \right]} \; 1/2 = +.83$$

This indicates that as x increases, y increases (+) and that y is correlated to x to the extent that 68 percent (.83) of the variables have been accounted for.

Accordingly, it was decided to use this method to determine the correlation between service and the various accelerated tests. Furthermore, it was decided to use a confidence level of 95 percent in an attempt to be sure that our conclusions were reasonably correct. The average ratings of all series for all materials from three years of testing was fed into an IBM 704 computer, but this paper will be limited to our evaluation of accelerated tests versus service, for stainless steel only.

Ferricyanide Spot Test

In this procedure a piece of dye transfer paper is soaked in a ferricyanide solution. Then it is placed in contact with the specimen being tested and dried in position under a heat lamp. Next the paper is removed from the specimen and the amount of blue on the paper and the part is evaluated. We found the test to be so erratic that it was abandoned after preliminary evaluation. It merits no consideration whatever in our opinion.

Corrodkote

The composition of the paste, the test conditions and procedure used were essentially in conformity

EVALUATION OF CORRELATION

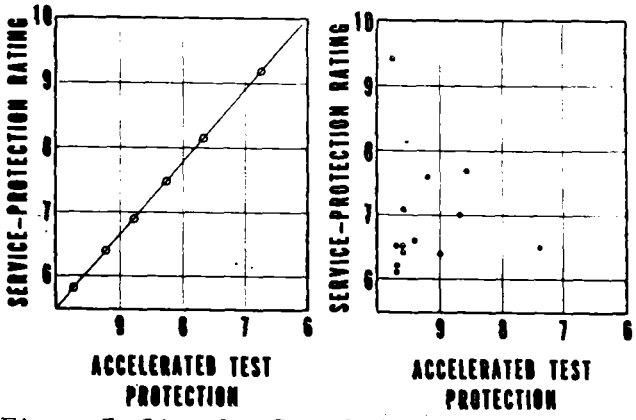


Figure 7 - Simple Correlation Coefficient. The graph on the left shows perfect correlation (r = 1.0). The one on the right is a typical scatter diagram coefficient of which is to be determined (and is obviously less than r = 1.0).

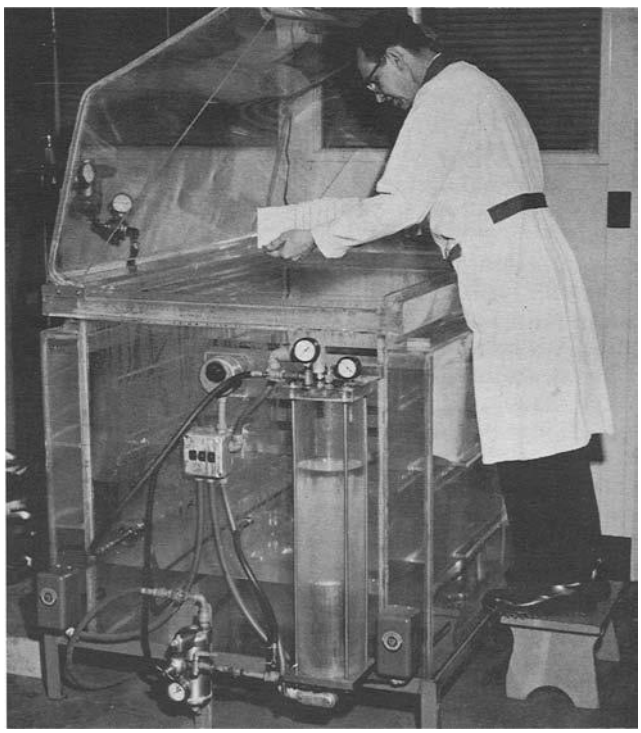


Figure 8 - Specimens of stainless steel covered with the Corrodkote paste being placed in the test box.

with ASTM B 380. However, since the test had never been used on stainless steel, so far as is known, we did not know how long an exposure time should be used. Accordingly, single panels were exposed for 6 and 16-hour cycles respectively. After inspection of these results, it was arbitrarily decided to use a basic cycle of 16 hours and multiples thereof for the set of 5 panels used for each series. Only one panel from each series was exposed in a given 16-hour cycle so as to obtain an "average" condition over the 5 panels involved and to avoid losing entire series in the event of a test malfunction. (See Figure 8.)

TABLE 1

Corrodkote - 6 hour cycle * vs Service

Service	Number of Series	Minimum SCC @ 95%	"r"
1st year Washed	4	.95	.14
Cleaned	4	.95	.35
2nd year Washed	4	.95	-.32
Cleaned	4	.95	.25
3rd year Washed	4	.95	-.53
Cleaned	4	.95	.35

*Data represents one panel only from each series.

Considering first the 6-hour cycle on one panel, versus average service results for one, two and three winters' exposure, both washed and cleaned, the simple correlation coefficients shown in Table 1 were derived.

TABLE 2

Corrodkote - 16 hour cycle * vs Service

Service	Number of Series	Minimum SCC @ 95%	"r"
1st year Washed	5	.88	-.19
Cleaned	5	.88	-.22
2nd year Washed	5	.88	.21
Cleaned	5	.88	.00
3rd year Washed	5	.88	-.10
Cleaned	5	.88	.41

*Data represents one panel only from each series.

While this data shows that there is no correlation between this test and service, it is of interest that the correlation coefficient is increasing with increasing service exposure. However, the two negative numbers are disconcerting in that they may indicate an inverse trend, i.e., the worse in Corrodkote the better in service.

The one 16-hour cycle on one panel of each series provided the data shown in Table 2. This again shows no correlation between the test and service.

TABLE 3

Corrodkote - 2 x 16 hour cycles vs Service

Service	Number of Series	Minimum SCC @ 95%	"r"
1st year Washed	11	.60	-.08
Cleaned	11	.60	-.40
2nd year Washed	11	.60	.81
Cleaned	11	.60	.01
3rd year Washed	11	.60	.77
Cleaned	11	.60	-.35

Note. Underlined data is significant at the 95% level of confidence.

TABLE 4

Service	Number of Series	Minimum SCC @ 95%	"r" 6 hours	"r" 12 hours
1st year Washed	36	.32	.55	.61
Cleaned	36	.32	.55	.57
2nd year Washed	36	.32	.39	.36
Cleaned	36	.32	.27	.42

Note, Underlined data is significant at the 95% level of confidence.

The two 16-hour cycles, run on 5 panels of each series versus the service averages provided the correlation coefficients shown in Table 3.

TABLE 5

Service	Number of Series	Minimum SCC @ 95%	Buffed 6-hour	Buffed 12-hour	Unbuffed 6-hour	Unbuffed 12-hour
1st year Washed	12	.58	.42	.63	.57	.53
Cleaned	12	.58	.30	.50	.63	.48
2nd year Washed	12	.58	.39	.58	.28	.23
Cleaned	12	.58	.57	.74	.48	.29

Note: Underlined data is significant at the 95% level of confidence.

Reversing the previous data, at least for the second and third winter's "washed" rating, there does appear to be a reasonably good relationship between 32 hours in this test and extended service.

In the new series of stainless steel for the 1960-61 program, it was decided to use a basic 6-hour cycle for the Corrodkote test. Our S.C.C. for all series versus one and two winters in service is shown in Table 4.

This shows that there is a correlation of a relatively low order between both the 6-hour cycle and the 2 x 6 hour cycle and service. The more prolonged test, i.e., 12 hours, did not show any significant increase in correlation. Neither was there any improvement in correlation of the tests with increased service exposure.

It may be of interest to examine these results in somewhat greater detail to see wherein the accelerated tests succeeded and wherein they failed.

Of the total 36 series exposed, we can pick out subgroups for consideration as entities. For example 12 series were buffed on one half of the surface as part of their processing and the other half was not buffed. How did the Corrodkote test fare regarding this specific group? It should be noted that buffing should be the sole variable involved. See Table 5.

For the buffed series, correlation did increase with increasing time in the test and some agreement with service is evident. This is not true for the unbuffed series where the 6-hour test did show some very limited correlation on one occasion, whereas the 12-hour test did not.

TABLE 6

Service	Number of Series	Minimum SCC @ 95%	"r" 6-hour	"r" 12-hour
1st year Washed	6	.81	.32	.31
Cleaned	6	.81	.32	.00
2nd year Washed	6	.81	.13	.11
Cleaned	6	.81	-.21	-.27

TABLE 7

	Number of Series	Minimum SCC @ 95%	"r" Washed	"r" Cleaned
Corrodkote				
1 cycle (3 hours)	60	.25	.51	.63
3 cycles (9 hours)	58	.26	.21	.40
5 cycles (18 hours)*	52	.27	.39	.30

* 4 cycles of 3 hours each plus one of 6 hours.

Significantly, this test was completely ineffective in predicting service for the series which had been chromium-flashed, as shown in Table 6. The longer test cycle was not helpful.

In the third year of the program, it was decided to use the minimum Corrodkote cycle. For our specific equipment, a series of preliminary tests indicated that the minimum cycle time was 3 hours.

TABLE 8

Type 430

	Number of Series	Minimum SCC @ 95%	"r" Washed	"r" Cleaned
Corrodkote				
1 cycle (3 hours)	16	.50	.55	.43
3 cycles (9 hours)	16	.50	.39	.24
5 cycles (18 hours)	16	.50	.42	.24

Type 433

Corrodkote				
1 cycle (3)	5	.88	.13	-.17
3 cycles (9)	5	.88	.87	.68
5 cycles (18)	5	.88	.46	.29

This was used for the 1961-1962 stainless series, with multiples thereof and yielded the data in Table 7 for all of the series exposed versus one year's service.

This again tends to show that the test can predict service to some degree. It tends to show better correlation with "cleaned" service and with the minimum test cycle.

In attempting to determine wherein the test succeeded or failed, certain subgroups such as types 430, 433 and 434 can be examined, versus one year's service. See Table 8.

Obviously the test was not particularly successful and disagreed with the all-panel results in agreeing once with "washed" service and not at all with "cleaned" service.

After 3 cycles, for the "washed" service rating, there is a strong correlation, though at a confidence level of slightly less than 95 percent.

Similarly, for Type 434 the data fail to show any consistent correlation with one year of service, either "washed" or "cleaned" ratings.

In recapitulation of the Corrodkote test, the best correlation for each of the three major test conditions evaluated are shown in Table 9.

This tends to show that the more severe test condition, i.e., 2 x 16 hours, was the best of those evaluated. We are somewhat surprised by this as this test appeared to be far too severe and we suspected it was masking differences which actually existed. These data tend to show that we were in error, pending a more complete analysis of all of the data from the first year of the test.

Copper Modified Acetic Acid Salt Spray (CASS)

The CASS test (Figure 9) was run during the first year of the program only and was abandoned because of lack of promise. This was also conducted in accordance with ASTM Method B 368 and preliminary screening tests run. Because of the relative lack of attack, a basic cycle of 16 hours' exposure was chosen. The correlation coefficients in Table 10 represent 5 such cycles, or a total of 80 hours' exposure in the CASS test; versus service. This data shows no correlation with service exposure, either "washed" or "cleaned", confirming our original premise that it was an unsatisfactory test for stainless steel. The negative coefficients indicate an inverse relationship, that is, the worse the corrosion resistance in the test, the better in service and vice versa.

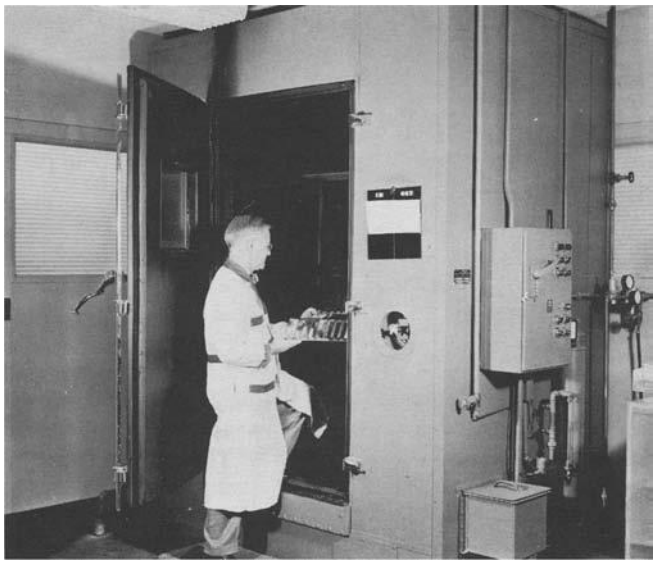


Figure 9 - Specimens of stainless steel in a slotted plastic holder being placed in a walk-in box for "CASS" testing.

Ferric Chloride Spot Test

This particular test involves placing a few drops of an acidic ferric chloride solution upon the surface of the part for a specific time. After washing with water, the part is rated for the degree of etching.

The solution is made up as follows:

10 gms ferric chloride ($FeCl_3$-$6H_2O$)
5 gms sodium chloride (Na Cl)
2.5 ml hydrochloric acid (37%)
Dilute to 200 ml with water.

The procedure is as follows: Clean specimen with water and acetone. Place a drop or two of the test solution on specimen. Start a stopwatch and determine when the bubbling action commences.(1) After that time, allow the solution to remain on the part for 5 minutes. Rinse off solution, dry and rate for etch.

These specimens were rated by comparison with standards as follows:

4-no etching
3-light etch
2-medium etch
1-heavy etch

On series from the 1959-1960 program, exposed in service for three years, the S.C.C. for this test was as shown in Table 11.

From the very low correlation coefficients it can be seen that it is not an acceptable test. The negative factor again indicates an inverse relationship.

The rating method was modified in the next year's program, to take into account the dark pit frequently found in the center of the test spot. On all series from the 1960-1961 program, the results were as shown in Table 12. This correlation was even worse than for the 1959-1960 program and on this basis the test was discontinued.

(1) Because of the difficulty in determining accurately when the bubbling action began, an arbitrary total time of 5 minutes was used.

TABLE 9

Corrodkote Cycles	Service	Number of Series	Minimum SCC @ 95%	"r"
2 x 16 hours	2 year Washed	11	.60	.81
2 x 6 hours	1 year Washed	36	.32	.61
1 x 3 hours	1 year Cleaned	60	.25	.69

TABLE 10

Service	Number of Series	Minimum SCC @ 95%	"r"
1st year Washed	11	.60	-.19
Cleaned	11	.60	-.22
2nd year Washed	11	.60	-.21
Cleaned	11	.60	.00
3rd year Washed	11	.60	-.10
Cleaned	11	.60	.41

TABLE 11

Service	Number of Series	Minimum SCC @ 95%	"r"
1st year Washed	11	.60	-.31
Cleaned	11	.60	-.16
2nd year Washed	11	.60	.34
Cleaned	11	.60	-.32
3rd year Washed	11	.60	.47
Cleaned	11	.60	-.52

TABLE 12

Service	Number of Series	Minimum SCC @ 95%	"r"
1st year Washed	36	.32	.18
Cleaned	36	.32	.03
2nd year Washed	36	.32	-.04
Cleaned	36	.32	-.06

Ferric Chloride Immersion Test

This test was suggested by Crucible Steel Company and was first used for the 1960-61 program. It consists of immersing the specimen of stainless steel in a solution containing 108 grams of Fe $Cl_3$6H_2O and 4.5 ml of concentrated hydrochloric acid per liter for four hours at a temperature of 30 C. The resistance to pitting has been evaluated by methods such as the "percent weight loss" as well as by the number of "pits per square inch". Rating numbers based on the "dot charts" have also been used. The data for all series in the 1960-61 program are shown in Table 13.

TABLE 13

Service	Number of Series	Minimum SCC @ 95%	"r" Percent Wt. Loss	"r" Pit Rating
1st year Washed	36	.32	.32	.03
Cleaned	36	.32	.25	.03
2nd year Washed	36	.32	.25	-.11
Cleaned	36	.32	.23	-.07

It is rather surprising that the Percent Weight Loss showed better (though unacceptable) correlation than the Pit Rating. Other investigators felt that rating by weight loss was completely unacceptable because of the attack in the raw edges of the specimens.

On the basis of the foregoing data, the test would appear to be relatively useless. However, when examined by subgroups, somewhat better correlation can be seen. For example, taking the 12 series which had half of each panel buffed, the test results were as shown in Table 14.

TABLE 14

Service	Number of Series	Minimum SCC @ 95%	"r" Buffed Wt. Loss	Buffed Pit Rate	Unbuffed Wt. Loss	Unbuffed Pit Rate
1st year Washed	12	.58	.67	-.66	.57	.16
Cleaned	12	.58	.54	-.52	.43	-.09
2nd year Washed	12	.58	.53	-.56	.29	.40
Cleaned	12	.58	.67	-.62	.29	-.03

Considering the buffed condition only, the SCC for both methods of rating were quite similar and were above or near the minimum for 95 percent confidence. Note, however, that the pit rating is said to be an inverse function, contrary to weight loss and to the intent of the test.

Peculiarly, the correlation for the unbuffed condition was much less. Again the percent weight loss showed better correlation (though again unacceptable) than the pit rating.

While this test would normally have been abandoned at this stage, it was continued for the 1961-1962 program because other investigators were not convinced that the test had little merit.

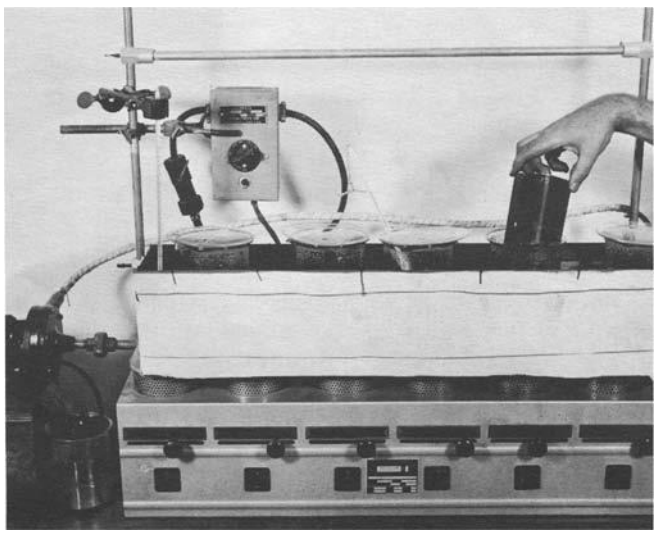


Figure 10 - Ferric chloride immersion test showing a bent 4 in. x 4 in. panel being inserted into a beaker of solution in a constant temperature bath.

In order to accommodate as many beakers as possible in the constant temperature bath, a size was chosen which would accept a standard 4 in. x 4 in. panel only if it were slightly bent (Figure 10). It was observed that the pitting on these specimens appeared to be concentrated in the area of maximum curvature. This is probably the location of high residual tensile stresses, according to other limited tests. For this reason a second set of panels measuring 4 in. x 3 in. was tested, without any prior forming or bending. Consequently, two sets of data are available. The number of pits per square inch was actually counted, so as to conform more exactly with other investigators.

The results for all series included in the 1961-62 program versus one year's service are shown in Table 15.

Considering both methods of rating, at least versus washed service, the 4 in. x 3 in. panels were slightly more consistent than the 4 in. x 4 in., possibly proving that the bending of the larger panels in a nonuniform manner caused erroneous results. The negative correlation again indicates an inverse function, i.e., the better in service the worse in the test, or vice versa.

While other data on subgroups are available, they tend to confirm the all-series results that the test can reliably forecast service for less than 25 percent (.49) of the variables.

TABLE 15

	Number of Series	Minimum SCC @ 95%	"r" Washed	"r" Cleaned
(4" x 4")% Wt. Loss	58	.26	-.40	-.08
Pits/in.^{2}	57	.26	-.13	-.01
(4" x 3")% Wt. Loss	60	.25	-.31	-.07
Pits/in.^{2}	60	.25	-.49	-.12

Dip-Dry or Salt Slag Immersion Test

Certain areas of the United States use a mixture of slag from steel-making operations plus salt for snow and ice control on roads. It has been observed that corrosion of stainless steel, as well as other metals, is quite severe where this salt slag mixture is used. Accordingly, a test has been devised for stainless steel to simulate this exposure which is known variously as the Dip-Dry or the Salt Slag Immersion Test.

Briefly, the procedure consists of dipping the specimen in the corrosive solution, withdrawing and heating (drying) it under specified conditions for 100 seconds, then dipping and drying alternately for a total of 8 hours.

The test solution is made up as follows:

Distilled Water	1050 ml
Sodium Sulfate (Reagent Grade)	0.50 g
Sodium Sulfite (Reagent Grade)	0.25 g
Sodium Thiosulfate (Reagent Grade)	0.10 g
Sodium Chloride (C.P.)	52.50 g
Calcium Chloride (Reagent Grade)	52.50 g

Our experience with the test is limited because of the limited number of specimens which can be tested at one time, the inherent difficulties of maintaining standard test conditions and the length of the test. In the latter respect, some tests are now being conducted for 100 cycles or approximately 3 hours, rather than 8, but we still have reservations concerning the test method.

The results obtained on representative series selected from our 1961-62 program are shown versus one year's service, in Table 16.

While we are running this test on samples from this winter's program, the limited data fail to confirm the enthusiastic claims of other investigators. It does not appear to be a test.

TABLE 17

	Number of Series	Minimum SCC @ 95%	"r" Washed	"r" Cleaned
Panel	59	.25	.52	.36
Paper	59	.25	.51	.26

Thermographic Test

A modification of the dip-dry test has been developed by Union Carbide Metals Company which has the appeal of a quick test and very simple equipment. In essence, it consists of soaking a piece of photographic print paper, from which the silver was removed by "fixing", in the dip-dry corrosive solution. This is placed face down on the test specimen, rolled to insure intimate contact, placed in a Saran Wrap envelope and heated to 100 C for 10 minutes. The photographic print is then developed by immersion in a 1 percent potassium ferricyanide solution (Figure 11). Both the print and the panel can be rated. The results on series from our 1961-62 program versus one year's service are shown in Table 17.

TABLE 17

	Number of Series	Minimum SCC @ 95%	"r" Washed	"r" Cleaned
Panel	59	.25	.52	.36
Paper	59	.25	.51	.26

This indicates that there is some relationship between the test and the "washed" service rating particularly, for both the panel and the paper. However, the correlation is still poor.

Considering only the Type 430 stainless steel series, the test shows improved correlation, versus one winter's service, as shown in Table 18.

TABLE 18

	Number of Series	Minimum SCC @ 95%	"r" Washed	"r" Cleaned
Panel	16	.50	.73	.67
Paper	16	.50	.83	.73

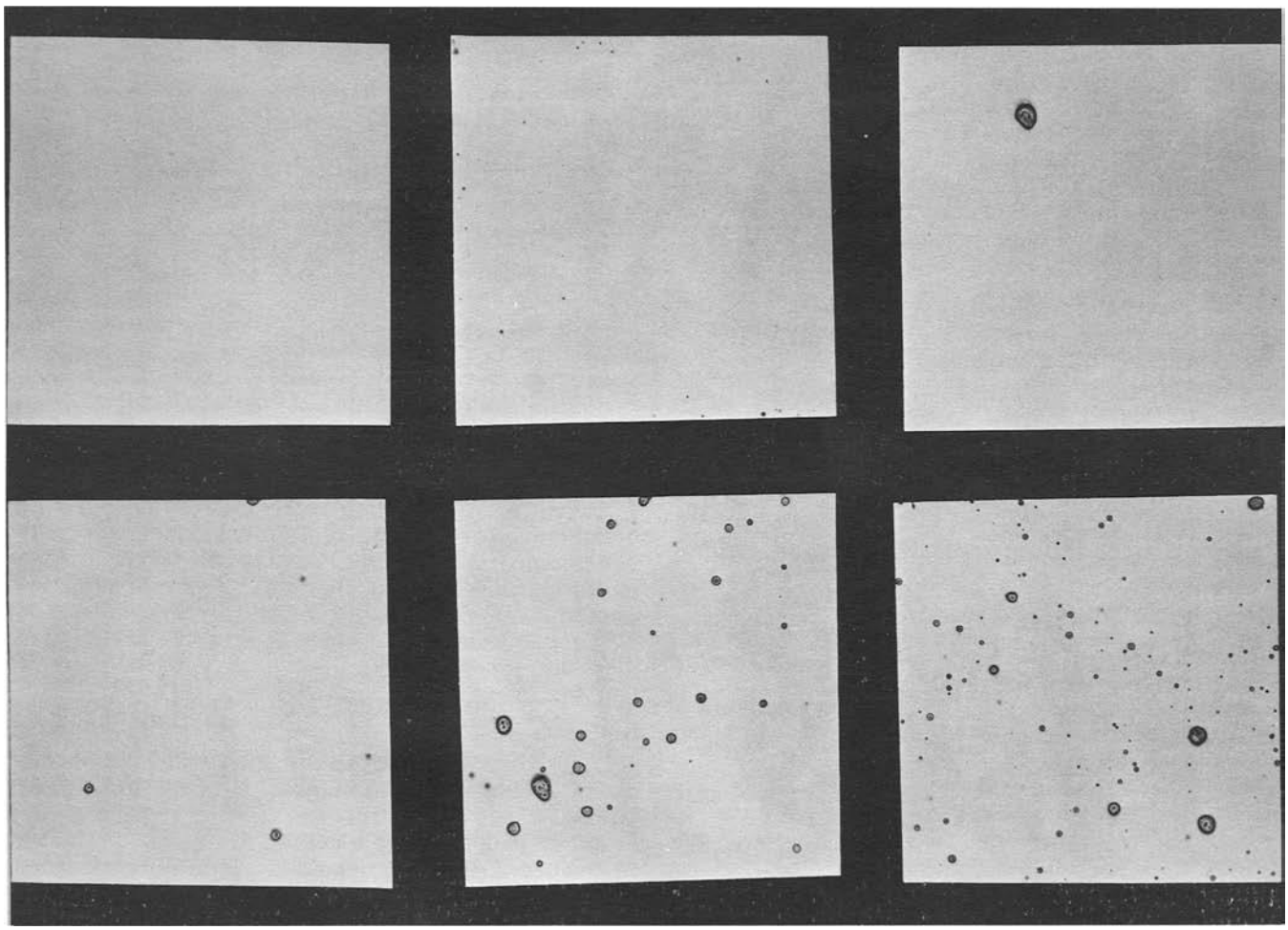


Figure 11 - Thermographic prints of six different stainless steels ranging from very good (upper left) to very bad (lower right).

These coefficients, particularly for the paper versus "washed" service, are beginning to approach values which could be useful in predicting corrosion resistance in service.

It may be of interest that it was not quite as successful on Type 434 and that it was a complete failure on all series which had been flash chromium-plated.

In summary, seven accelerated tests have been evaluated versus service and the best correlation found under any conditions are as shown in Table 19. Only Corrodkote, using 2 cycles of 16 hours each, and a very special case of the Thermographic test are approaching a useable degree of correlation with service.

TABLE 19

Test	Service	"r"	Minimum SCC @ 95%
Ferricyanide Spot	-	none	-
Corrodkote (2 x 16 hrs.)	Two Year Washed	.81	.60
Cass (5 x 16 hrs.)	Three Year Cleaned	.41	.60
Ferric Chloride Spot	Three Year Cleaned	-.52	.60
Ferric Chloride Immersion	One Year Washed	-.49	.25
Salt Slag Immersion	One Year Washed	.42	.63
Thermographic	(430) One Year Washed	.83	.50

In conclusion, we have not found any accelerated test which will reliably predict the corrosion resistance of decorative stainless steel in automotive service(2). To do this, we believe that the test we are seeking must have a Simple Correlation Coefficient of approximately .95 at a confidence level of at least 95 percent. This would mean that we would be confident 19 times out of 20 that the test would accurately predict service 9 times out of 10. You will appreciate that this still leaves considerable room for error, but that it would be distinctly superior to our present tests.

References

1. G. F. Bush. Corrosion of Exterior Automotive Trim. SAE Preprint 650A, January, 1963.
2. J. Nasea, Jr., B. E. Tiffany and G. F. Bush. Research Method of Rating Corrosion of Automotive Exterior Trim. Plating, Vol. 49, p 989 (1962).

(2) Major findings on the influence of material and process variables on the corrosion resistance of stainless steel in service have been published in Iron Age, December 20, 1962, pp 91-94. G. F. Bush. "How to Ward Off Corrosion in Stainless Steel Trim".

DISCUSSIONS

Discussion by H. L. Black, Universal-Cyclops Steel Corp., Bridgeville, Pa.:

The excellent study on corrosion resistance of bright trim for automobiles which has been under way in Mr. Bush's laboratory for the past several years has been continually showing its value. It has prompted Universal-Cyclops Steel to undertake its own program aimed at improving the corrosion resistance of stainless steel trim molding.

TABLE I

ATMOSPHERIC AND ACCELERATED CORROSION TESTING PROGRAM (1961–1962)

ALLOYS

	NOMINAL COMPOSITION								
TYPE	C	Mn	Si	Cr	Ni	Mo	Cb	N	Fe
430	0.065	0.50	0.40	17.25	---	---	---	---	Balance
434	"	"	"	"	---	1.00	---	---	"
435	"	"	"	"	---	---	0.45	---	"
436	"	"	"	"	---	1.00	0.45	---	"
201	0.10	6.50	"	"	4.50	---	---	---	"
301	0.10	1.00	"	"	7.00	---	---	---	"

SURFACE CONDITIONS

Annealed and Pickled	Unibrite
Belt Ground	Bright Annealed
Temper Passed	Chromium Flashed Plus Buffed

During the winter of 1961-62, we initiated a project similar to that being conducted by Mr. Bush aimed at (1) determining the relative corrosion resistance of various grades of stainless steel with several surface finishes and (2) evaluating the accelerated tests which were then being used as acceptance tests in the automotive industry or tests which were proposed for use. The alloys and surface conditions tested are shown in Table 1. We conducted tests on a total of thirty-nine alloy and surface variations. Table 2 lists the in-service and the accelerated tests which were conducted. The number after each test indicates the number of duplicate samples tested in that environment.

Figure 1 illustrates the manner in which panels were attached to automobiles. In order to provide an even more severe in-service exposure we attached panels to the left side of trucks, as shown in Figure 2. These trucks were in almost constant use between our plant in Pittsburgh and our plant in Titusville, in northwestern Pennsylvania. These panels were exposed to very severe salt, slag and ash conditions. On the basis of corrosion ratings, we estimate this exposure to be two or three times more severe than the automobile exposure.

TABLE 2

Atmospheric and Accelerated Corrosion Testing Program (1961-1962)

SERVICE EXPOSURE

- Automobile Panels (5)
- Truck Panels (8)

ACCELERATED CORROSION TESTS

- Cass Test (2)
- Corrodkote Test (2)
- Dip-Dry Test (2)
- Ferric Chloride Immersion Test (2)
- Ferric Chloride Drop Test (2)
- Collectate Test (2)
- Thermographic Test (2)

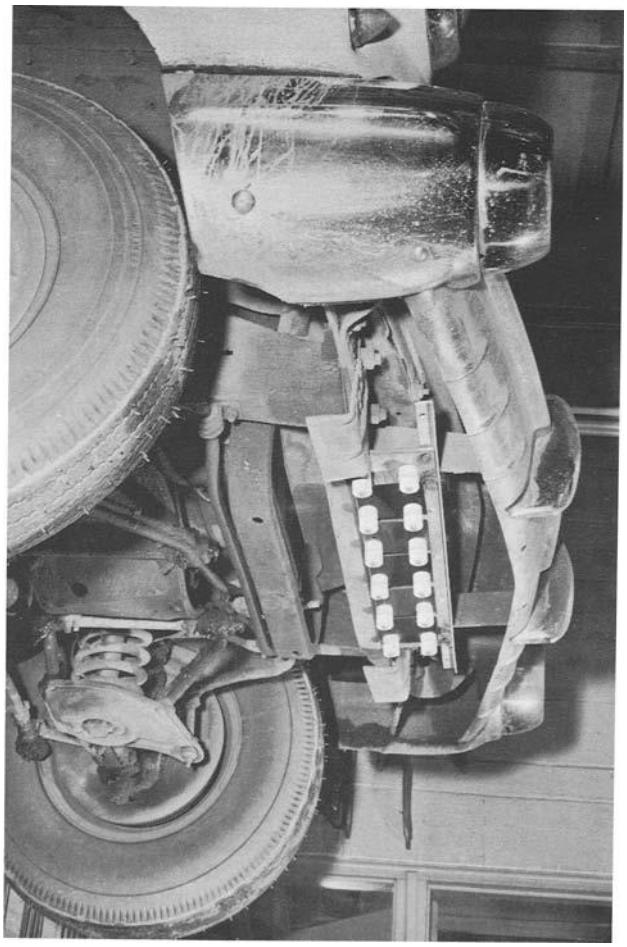


Figure 1 - Installed automobile corrosion rack.

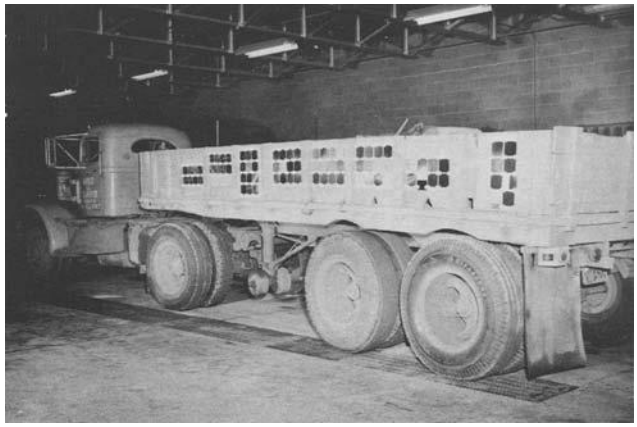


Figure 2 - Installed truck corrosion racks.

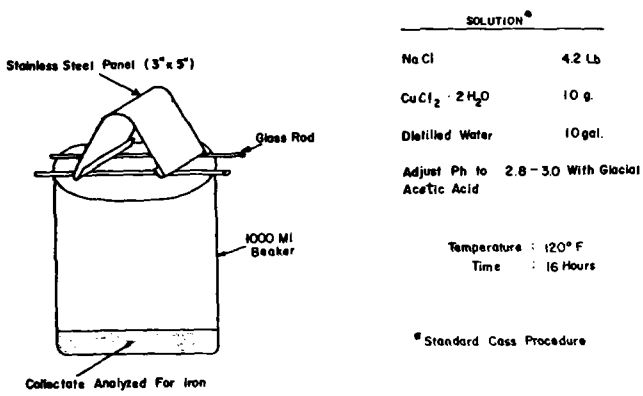


Figure 3 - Collectate test.

Mr. Bush has already discussed the accelerated tests; however, we conducted one additional test which should be briefly described. This is the "collectate" test (Figure 3). A "tent"-shaped panel is suspended over a beaker and is exposed to a standard CASS test cycle. The "collectate" which runs off the panel is then analyzed for iron content as a measure of corrosion resistance. This test was developed by Mr. Bush and Dr. Tiffany.

We used Mr. Bush's Manufacturing Development Laboratory corrosion rating method for all tests with the exception of the ferric chloride immersion test (rated by pits per square inch) and the "collectate" test (rated by grams of iron per liter of collectate). Protection number ratings are given for panels in the "cleaned" condition.

Table 3 is a tabulation of the simple correlation coefficients (SCC) which were calculated for truck exposure versus the accelerated tests. In general, our results agree with the results presented by Mr. Bush. In no case is the SCC high enough to be considered "good". The ferric chloride test and the thermographic test (panels and film ratings both) showed no correlation with in-service results. The only major point of disagreement in results is in

TABLE 3

CORRELATION OF TRUCK EXPOSURE WITH ACCELERATED TESTS

Accelerated Test	Number in Series	Minimum SCC at 95%	Calculated SCC
Cass	39	0.320	0.588
Corrodkote	39	0.320	0.426
Dip-Dry	39	0.320	0.623
Ferric Chloride Immersion	39	0.320	0.173
Collectote	39	0.320	0.530
Thermographic Panels	31	0.355	0.167
Thermographic Films	31	0.355	.0.138

the thermographic test where Mr. Bush found fair correlation. This disagreement could at least partially be caused by the difficulties in determining the corrosion ratings for this test.

TABLE 4

CORRELATION OF IN-SERVICE EXPOSURES

In-Service Test	Number in Series	Minimum SCC at 95%	Calculated SCC
Truck No.1 Set No.1 vs. Set No. 2	39	0.320	0.716
Truck No. 2 Set No.1 vs. Set No. 2	39	0.320	0.560
Truck No.1 vs. Truck No. 2	39	0.320	0.710

Unfortunately, perhaps we cannot attain too much better correlation than this. Actual in-service test correlation, as shown in Table 4, is not much better than the best accelerated test correlation. For example, the correlation between two trucks, each with two identical sets of samples, is only 0.710.

Since no test, with the exception of the two which showed no correlation, seemed to be significantly superior to any other in respect to correlation, we decided to try other evaluation procedures to further determine the strong and weak points of each test.

Figure 4 shows a plot of the average of the auto exposure protection number ratings versus the average of the truck exposure ratings. This type plot clearly illustrates the relative severity of the two environments and shows the truck exposure to be much more severe than the auto. In fact, we estimate the truck exposure to be equal to two or three years of normal automobile exposure. This plot will also give some idea of correlation between the tests. Perfect correlation (SCC = 1) and equal severity of tests would be shown by all points lying on a straight line with a slope of 45°. Figures 5 and 6 show similar plots for the accelerated tests versus both automobile and truck exposure. These plots give good visual indication of both test severity and amount of scatter in results.

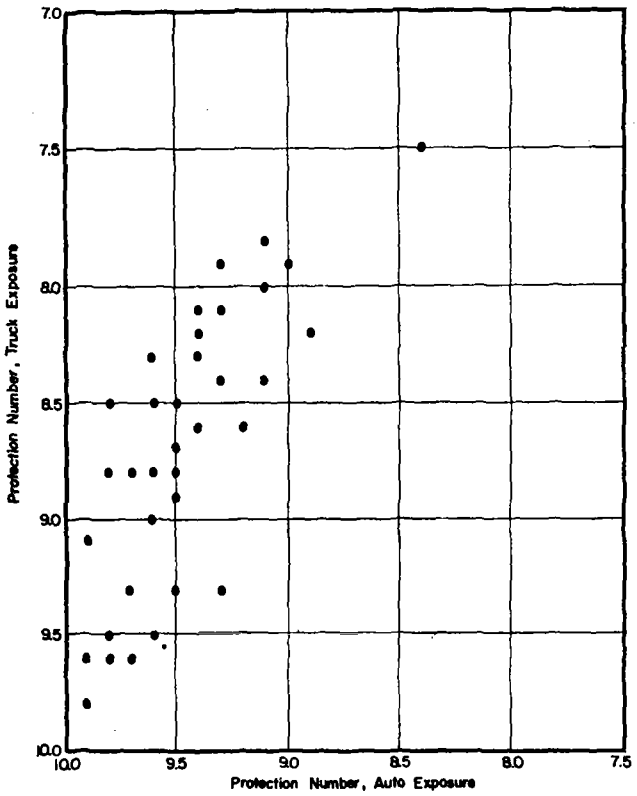


Figure 4 - Service exposure comparison, auto vs truck.

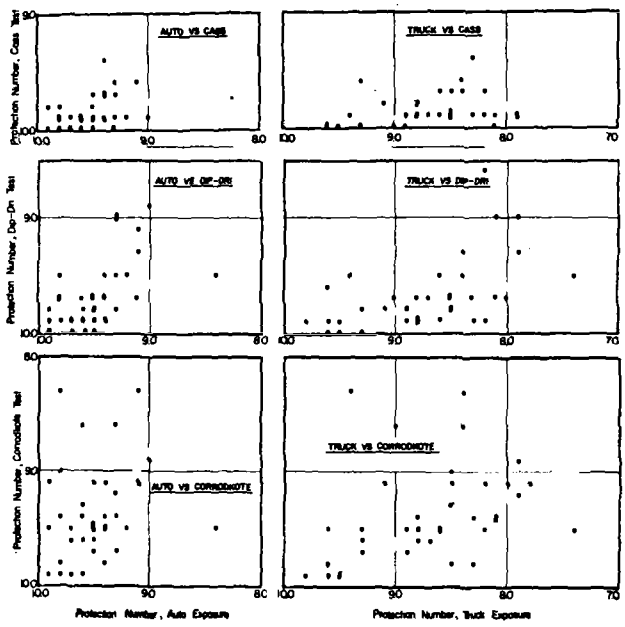


Figure 5 - Service exposure vs CASS, Dip-Dri and Corrodkote tests.

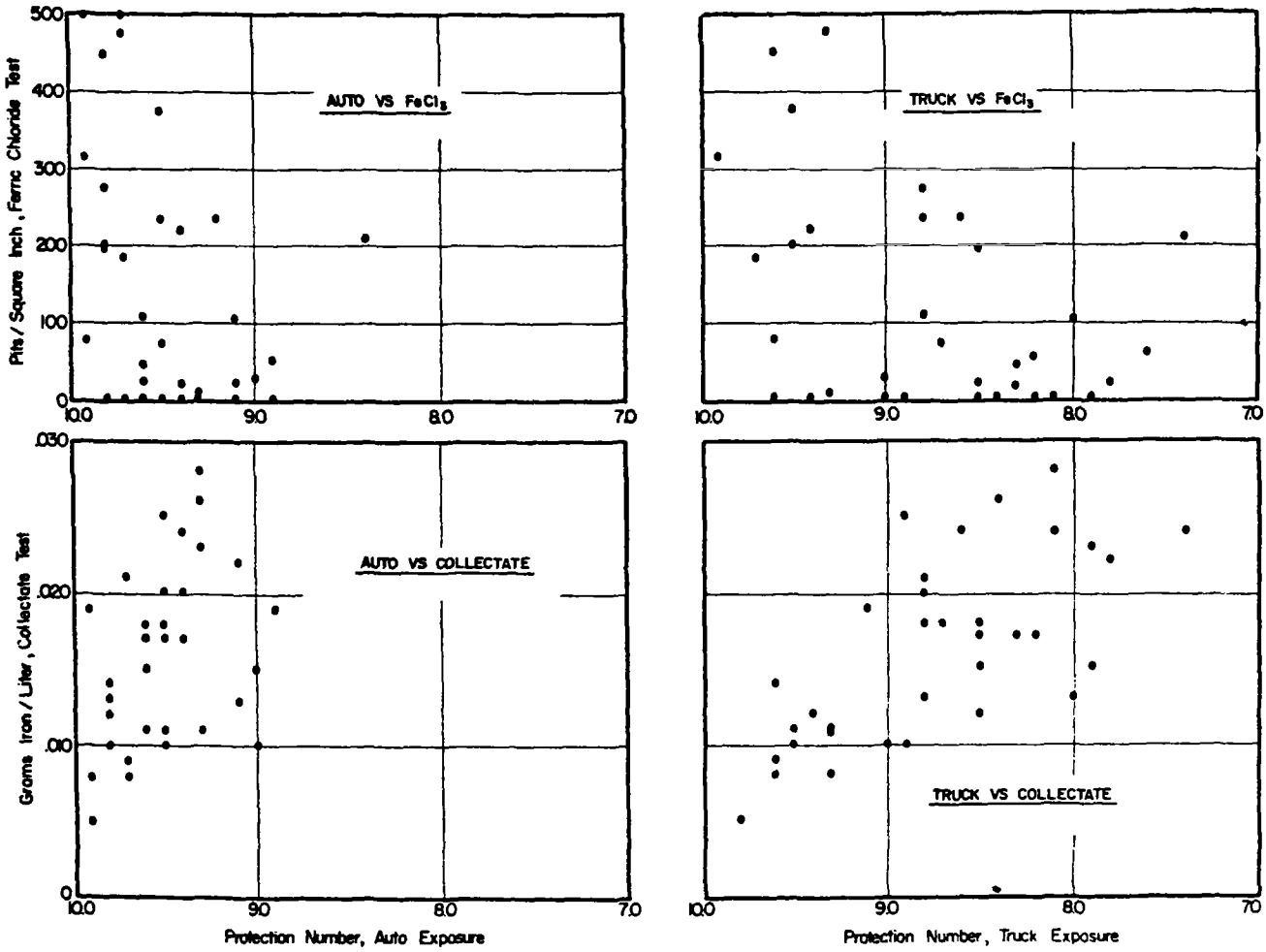


Figure 6 - Service exposure vs ferric chloride and collectate tests.

Figure 7 is a bar graph showing the average protection number ratings of three surface conditions (Unibrite[1], bright anneal and temper pass) for Types 434, 436, 201 and 301. According to protection number ratings of the in-service truck exposure panels, the corrosion resistance of the grades in order of worst to best is Type 434, 436, 201 and 301. The alloys are arranged in the same relative order in the remaining bar graphs.

A summary of all of the preceding data would lead to the following brief conclusions concerning each accelerated corrosion test:

CASS - Not severe enough; does not indicate superior corrosion resistance of the austenitic alloys; does not show enough spread in results among grades.

Dip-Dry - Not enough spread in results among grades and not quite as severe as would be desired for for maximum usefulness; does not indicate the superiority of the austenitic grades.

Corrodkote - Reverses the relative superiority of the grades.

Collectate - Indicates the improved corrosion resistance of the austenitics with substantial spread in results among grades, but the test requires chemical analysis for rating.

(1) Unibrite refers to a proprietary production buff finish developed by Universal-Cyclops Steel Corporation.

Ferric Chloride - No correlation with in-service exposure.

Thermographic - No correlation with in-service exposure.

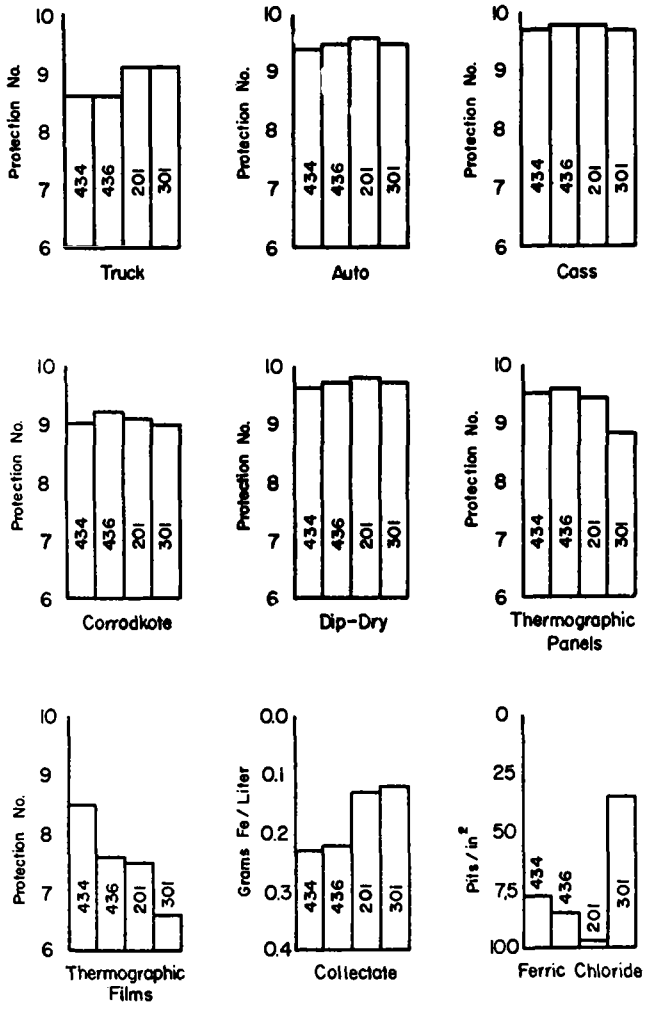


Figure 7 - Comparison of truck exposure relative ratings with accelerated tests. (Average of Unibrite, bright anneal and temper pass surfaces).

All of the data presented here definitely point out the inadvisability of using any accelerated test to predict in-service performance of an alloy or of a particular surface condition. Not only may these tests not correlate with in-service conditions very well, but as shown in several tests, the results may actually be reversed from the in-service results.

We are continuing our work on this study, and currently have another series of panels and specimens in test. We are also experimenting with modifications on existing accelerated tests in hopes of developing one which will better agree with in-service results.

A Laboratory Test for Determining Susceptibility of Nickel-Molybdenum and Nickel-Molybdenum-Chromium Alloys to Intercrystalline Corrosion and Its Use in Development of Resistant Alloys

By H. Grafen*

Nickel-base alloys containing molybdenum and chromium frequently have been employed in chemical industry as particularly corrosion resistant materials where the resistance of the known austenitic chromium-nickel steels failed to be adequate. In the light of their high strength at elevated temperatures they are suited for reaction apparatus operating under high pressures and at high temperature. Frequently they find application as cladding material.

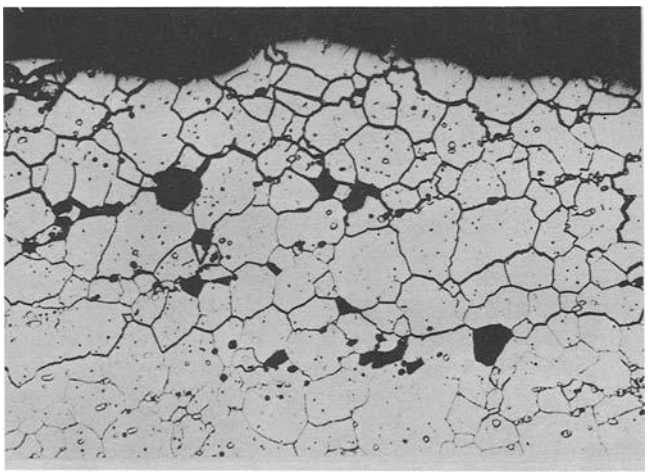


Figure 1 - Grain-boundary attack.

Different failures of these alloys in operation show, however, that intercrystalline corrosion can occur here in case of specific microstructures and certain corrosion agents. This corrosion can have different appearances depending on the external conditions. Figure 1 shows a defect in a heat-affected zone of a weld. Here intercrystalline corrosion attack penetrates the material uniformly. Figure 2 presents a defect having the character of a crack occurring due to external tensional stresses. In both cases, however, the cause of corrosion is the susceptibility of the grain boundaries. The intercrystalline attack follows clearly the precipitation along the grain boundaries. The precipitation behavior of these alloys is definitely associated with the corrosion susceptibility of the grain boundaries.

* Materials Testing Laboratory of the Badische Anilin-und-Sodafabrik, Ludwigshafen a/R, Germany.

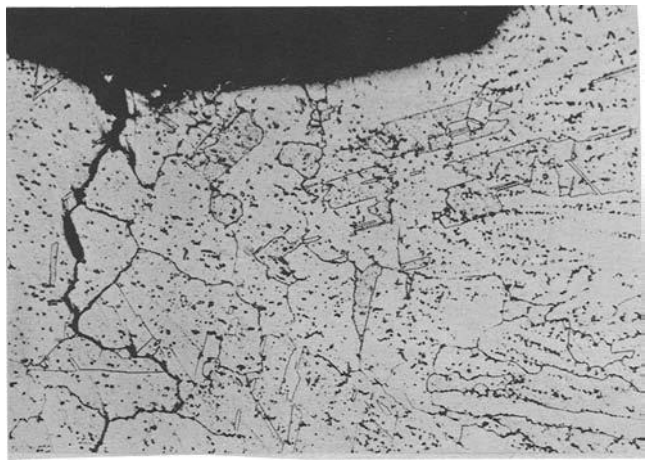


Figure 2 - Intercrystalline corrosion-crack by stresses.

STP369-EB/Apr. 1965

According to the constitutional diagram of the Ni-Mo[1] or Ni-Mo-Cr system[2] commercial alloys, for example Hastelloy B and Hastelloy C (they are registered trade marks of the Union Carbide Corporation) are heterogenous at room temperature. A nickel-molybdenum alloy with 25 to 30 percent molybdenum becomes homogenous only above 900 C; a nickel-molybdenum-chromium alloy with about 60 percent nickel, 15 percent molybdenum and 15 percent chromium remains heterogenous below 1150 C. A homogenous structure and optimum corrosion resistance associated with it can be achieved only by solution annealing at 1150-1200 C for nickel-molybdenum alloys and at 1200-1240 C for nickel-molybdenum-chromium alloys, followed by water quenching.

One has to assume that precipitations known in complex systems play a part in intercrystalline corrosion. In order to be able to investigate this, one has to develop, first, a laboratory test which can show intercrystalline corrosion comparatively rapidly and unequivocally of correspondingly heat treated samples.

Determination of Intercrystalline Corrosion

A number of testing methods and testing solutions are known for austenitic steels. It is important to distinguish between two test methods. While in Germany the tests are generally conducted on the basis of optical examination, that is, by observing the failure of the grain boundaries on bending after subjecting specimens to treatments in the test solutions, in the United States it is more common

Copyright© 1965 by ASTM International

www.astm.org

to determine the loss of weight after a single or several boiling treatments. Both methods have advantages and disadvantages. The determination of the depth of penetration and severity of the attack by optical methods varies to some extent from operator to operator, while the loss-of-weight method reflects corrosion effects not based on intercrystalline attack. In scientific work, preference should be given to optical evaluations. Loss of weight methods is more useful for technical acceptance tests.

In order to develop a laboratory test suitable for the above nickel alloys, several known testing solutions were examined for their suitability. As test pieces for all these tests were employed welded or heat treated thermally precipitated specimens of Hastelloy C or Hastelloy B. From all these investigations a rapid testing method was evolved, equally suitable for Ni-Mo and Ni-Mo-Cr alloys. In this test, strips or bars (for example 10 x 50 x 2 mm or 6 x 6 x 50 mm) are placed for 24 hours in boiling 10 percent hydrochloric acid and then bent over a mandrel. Corrosion of grain boundaries after the hydrochloric acid treatment becomes evident by tearing in the area of grain boundaries on bending. Occasionally deterioration of the specimen surfaces (grain drop-out) is observed before bending. An optical evaluation of these processes is done preferably at a magnification of 10 to 20 diameters. In the following, this method will be called "hydrochloric acid test". Figure 3 shows the appearance of bent specimens of Hastelloy C, after the hydrochloric acid test, as a function of different heat treatments.

corrosion attack is sufficiently differentiated, i.e., it corrodes grain boundary areas in which the concentration of different elements has been changed by the precipitation processes, at a substantially faster rate than their surroundings. In the present case a marked attack on the grain boundaries in hydrochloric acid is caused by the molybdenum depletion of the grain boundaries, because this directly explains the behavior of these alloys in hydrochloric acid. This point will be elaborated upon later in connection with the studies of precipitates.

Another point must be elucidated a bit further. Previously it has been frequently held that in intercrystalline corrosion the grain boundaries act as an active anode, and the passive grain surface as cathode. This concept was derived from chromium-nickel austenitic steels, where precipitation of chromium carbides at the grain boundaries lead to the chromium depletion of the surrounding areas. Chromium content, however, controls the tendency towards passivation of iron alloys. It was thought that this chromium depletion caused activation of these zones, and thus the intercrystalline attack could be conceived as the formation of an active-passive element.[4]

Recent investigations demonstrate that this conception does not apply generally, and the intercrystalline corrosion is not necessarily associated with the passive state. Even in solutions, in which passivation cannot occur, intercrystalline corrosion is possible. The electrochemical processes can be conceived in the simplest way as processes on a mixed electrode. The depletion

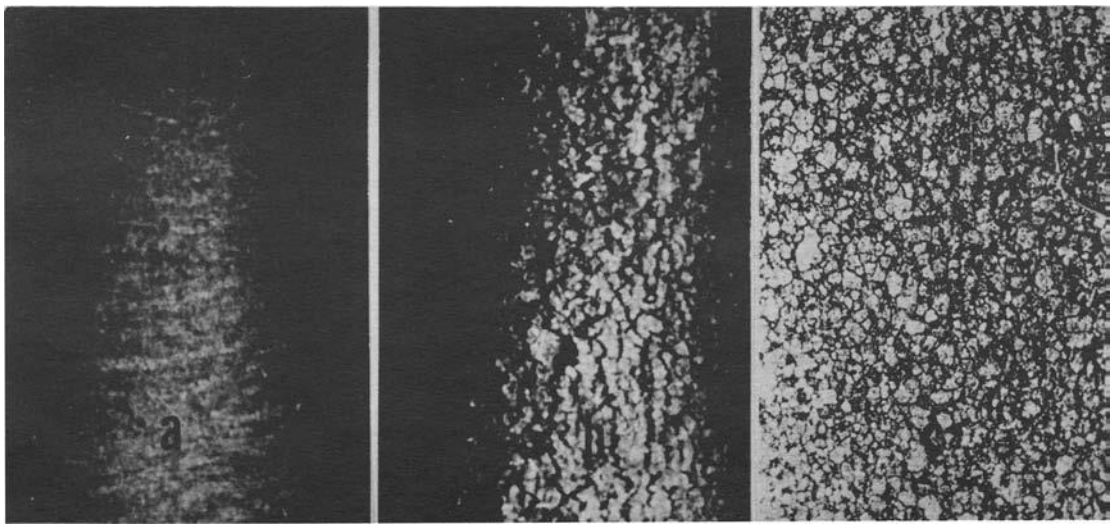
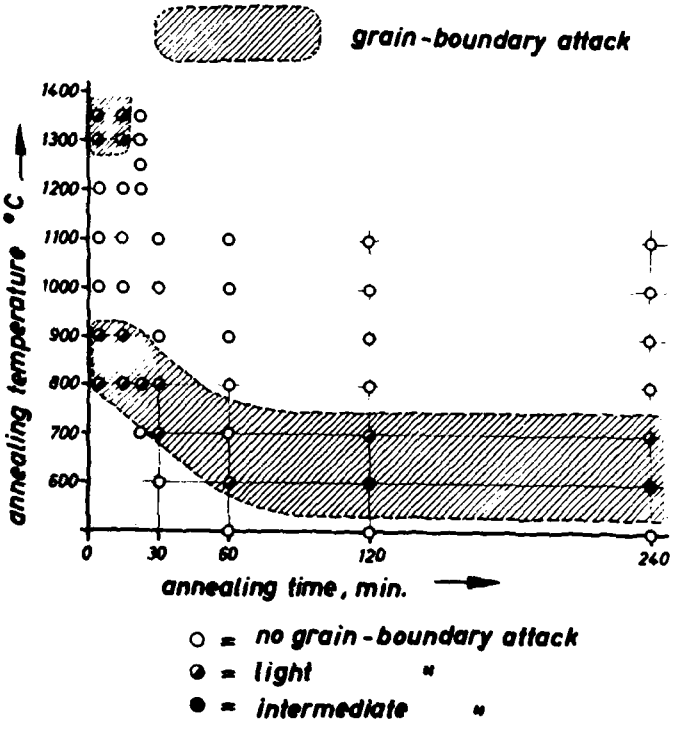


Figure 3 - Hydrochloric acid test. Heat treatment: (a) 1220 C/1h/H_2O; (b) 800C/1h/H_2O; (c) 1100C/1h/H_2O. (b) and (c) showed intercrystalline corrosion; (a) showed no intercrystalline corrosion.

One could object that hydrochloric acid is a proper test solution for Hastelloy B, but that Hastelloy C has very low resistance to boiling hydrochloric acid. This is correct. Important for the suitability of a solution for testing intercrystalline corrosion is, however, the fact that its

of the grain boundary areas in alloying elements, caused by precipitation, changes the electrochemical requirements for the solution of grains and grain boundaries. A nobler potential is established on the surface of a grain than at its boundary. The conditions are about the same as when a noble



Analysis	Ni	Cr	Mo	Fe	W	Si	Mn	V	Co	S	C
	67,0	0,2	26,9	4,9	0,18	0,31	0,26	0,21	-	0,07	0,02

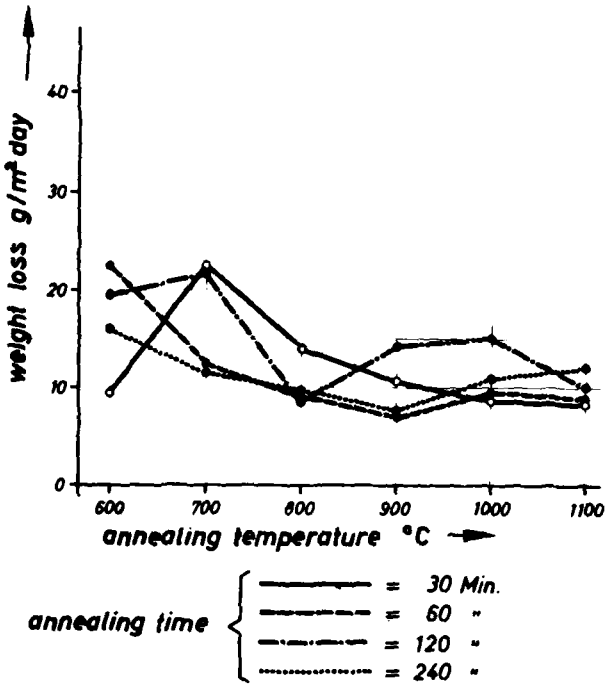


Figure 4 - Diagram of the intercrystalline corrosion and embrittlement from Hastelloy B.

and a less noble metal are in contact in an electrolyte. Under such conditions, the less noble metal dissolves faster. The greater the difference in potentials between noble and less noble areas the faster the dissolution will occur. Here a pronounced effect is exerted also by the surface ratios. When the less noble area (grain boundary) is small as compared with the noble area (grain surface) the dissolution is further intensified.

Plotting Intercrystalline Corrosion Diagrams[3]

The intercrystalline corrosion based on the hydrochloric acid test of different alloys as a function of thermal treatment has been plotted in a few diagrams.

Figure 4 presents the results obtained for Hastelloy B; on the left half of the figure are given, in addition, the weight losses. The alloy is resistant to intercrystalline corrosion outside of the shaded areas. Above 1250 C a small unstable field is shown. In the 800-900 C range the intercrystalline susceptibility disappears with increasing tempering time. At these apparently comparatively high temperatures the depleted grain boundary zones are replenished in time by diffusion.

The two ranges of grain boundary susceptibility seen in the diagram occur in practice mostly in parts welded by argon arc or heliarc, since in these methods a brief heating of the seam edges to a high temperature takes place. Therefore the high temperature susceptibility range occurs as knifelike corrosion, Figure 5, while the 600-900 C range occurs at a certain distance from it, Figure 6.

A susceptibility diagram for Hastelloy C is shown in Figure 7. The range of a marked embrittlement, determined by a bending test in which only

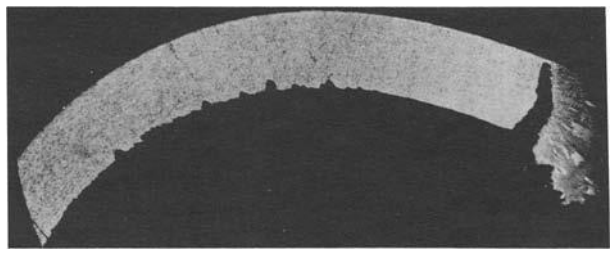


Figure 5 - Intercrystalline corrosion directly beside the welding seam.

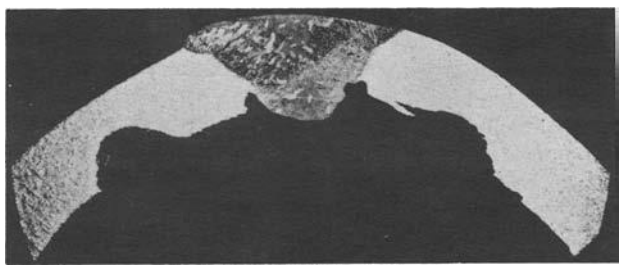


Figure 6 - Intercrystalline corrosion some millimeters beside the welding seam.

a 90° bend was achieved, is also shown. The weight loss curves presented on the left of Figure 7 show an enormous rise at the appearance of the grain boundary susceptibility. The weight loss then decreases at higher temperatures with the coagulation of the precipitate. On annealing in the temperature range of 800-1000 C precipitation within the grains occurs after a certain time in addition to the original precipitation at the grain boundaries.

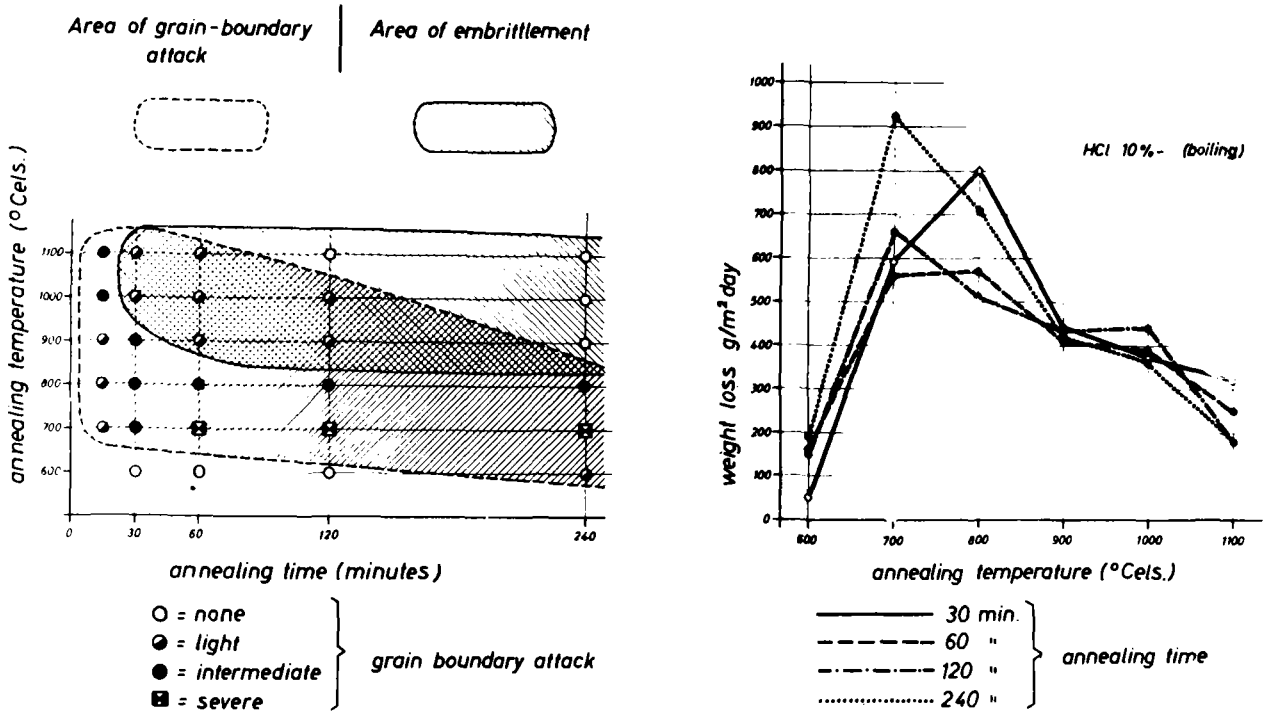


Figure 7 - Diagram of the intercrystalline corrosion and embrittlement from Hastelloy C.

This results in a less pronounced intercrystalline susceptibility and an increase of surface attack in the hydrochloric acid test.

Figure 8 shows three different forms of precipitation and the effect on the type of corrosion and embrittlement. It can be seen in the diagram that nickel-molybdenum-chromium alloys have a very wide susceptibility range. Therefore, in practice intercrystalline corrosion occurs both in the heat affected zones of welds and in hot worked area.

Precipitation Leading To Intercrystalline Corrosion

For the general understanding of the corrosion mechanism it is important to know which new phases are formed at the grain boundaries.

Therefore samples treated in the same way as when determining the diagram for intercrystalline corrosion, were used to extract electrolytically the phases present which were then identified by X-ray film structure methods.

In the susceptible Hastelloy B were observed, in addition to carbides of the Me_6C type and Mo_2C in the 550-900 C range, certain intermetallic Ni-Mo phases, at lower temperatures predominantly Ni_4Mo with a tetragonal structure and above 850 C predominantly the hexagonal Ni_3Mo. These phases were expected based on the binary Ni-Mo diagram. In the 1300 C susceptibility field one finds a higher molybdenum content in Me_6C and an increasing proportion of Mo_2C; in addition one can observe a sigma phase composed of iron and molybdenum. This phase increases with an increasing iron content of the alloy and appears, according to the Fe-Mo constitutional diagram,[5] above 1250 C with an average molybdenum content of about 60 percent.

In all these cases one deals with the formation of molybdenum-rich phases. It can be safely assumed, therefore, that the intercrystalline susceptibility of Ni-Mo alloys is caused by the molybdenum depletion of grain boundary zones since all these phases precipitate preferably at grain boundaries.

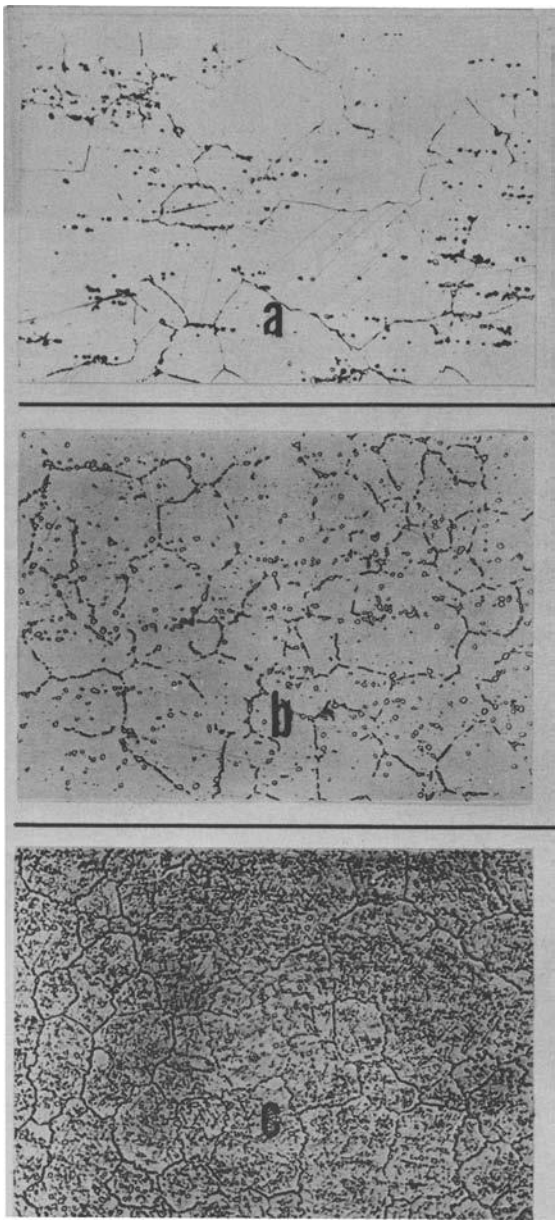
The extracted matter from susceptible samples of Hastelloy C contain, in addition to small amounts of carbides of the Me_6C type and traces of $Cr_{23}C_6$, mostly a tetragonal sigma phase, as has been already found in Ni-Mo-Cr alloys by Proetzl.[8] The elements predominant in the sigma phase are nickel, molybdenum and chromium, as has been shown by microanalysis of the isolate. Depending on the composition of the alloys it can also contain some iron.(1) According to Bloom and Grant[9] the compositional limits lay between 23-32 percent Ni, 18-54 percent Cr and 15-58 percent Mo.

One can see that the sum of chromium and molybdenum in the sigma phase is substantially higher than in the matrix. In addition, it can be shown that chromium and molybdenum are interchangeable within wide limits.

The intercrystalline corrosion susceptibility of Hastelloy C can be interpreted, therefore, as being associated with the depletion of grain boundary areas in chromium and molybdenum as a result of sigma precipitation at the grain boundaries. The precipitation temperature is very important. Figure 9 shows the behavior for two different precipitation temperatures.

---

(1) For the identification of sigma phase were used, for (σ -FeCrNiMo) space lattice parameter, data of Allten[6] and for (σ CrNiMo) those of Bechtoldt and Vaher.[7]



Analysis	Ni	Cr	Mo	Fe	W	Si	Mn	V	Co	S	C
	56,0	15,0	15,8	5,4	3,8	0,44	0,36	0,23	2,0	0,01	0,04

	Heat Treatment	Susceptibility to Intercryst. Corrosion	Embrittlement
a	700 C/1h/H_2O	yes	no
b	1100 C/3h/H_2O	no	yes
c	950 C/3h/H_2O	less (increase of general corrosion)	yes

Figure 8 - Influence of temperature on σ -phases form of precipitation in Hastelloy C.

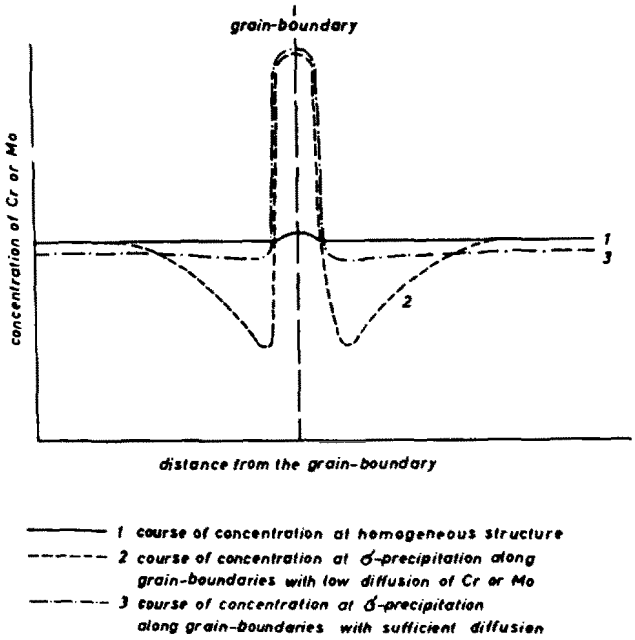


Figure 9 - Course of concentration from Cr and Mo at the grain-boundary.

Even in a homogeneous alloy there is a slight concentration difference between the grain boundaries and grain bodies due to a short passage through the critical temperature range during quenching (Curve 1). Curve 2 shows concentration changes following sigma precipitation for the case when the diffusion velocity of chromium or molybdenum is too slow for the equalization of the concentration gradient in the matrix. Curve 3 presents finally the conditions encountered when a complete concentration equalization in the grains is achieved. Curve 2 represents a state in which the material is particularly susceptible to intercrystalline corrosion. The difference in potential between the precipitate and the matrix is here at its maximum. The susceptibility to corrosion is correspondingly the highest at low precipitation temperatures regardless of the small amount of precipitate, since the diffusion velocity required for equalization of concentration gradients in the grains is too low. With a rising precipitation temperature one approaches the state characterized by Curve 3. The intercrystalline attack becomes weaker. In Hastelloy C, the sigma phase should contain about 35 percent chromium and molybdenum, because the supply of chromium or molybdenum in the matrix is just about the same. These contents, however, may shift because of different diffusion coefficients of these elements at different precipitation temperatures.

The hydrochloric acid test shows only molybdenum depletion. Since, in Hastelloy C, as a rule, a certain depletion in chromium also occurs testing solutions for chromium must also show an intercrystalline corrosion susceptibility. Such is the case. Figure 10 shows a bent specimen which has been treated for 24 hours with boiling 60 percent nitric acid.

Testing with the solution proposed by Streicher[10] for austenitic steels (sulfuric acid and ferric sulfate) is also possible. Figure 11 presents some samples tested by this method. Figure 12 depicts weight losses as a function of heat treatment. The weight loss curve obtained under the same conditions in a 10 percent HCl is shown for the purpose of comparison. The curves differ somewhat from each other. At lower precipitation temperatures, for example at 700 C, hydrochloric acid presents clearer results. This can be associated with the above-mentioned fact that the proportion of chromium and molybdenum in the sigma phase at different precipitation temperatures differs somewhat, so that in one case molybdenum depletion and in another chromium depletion is more predominant.

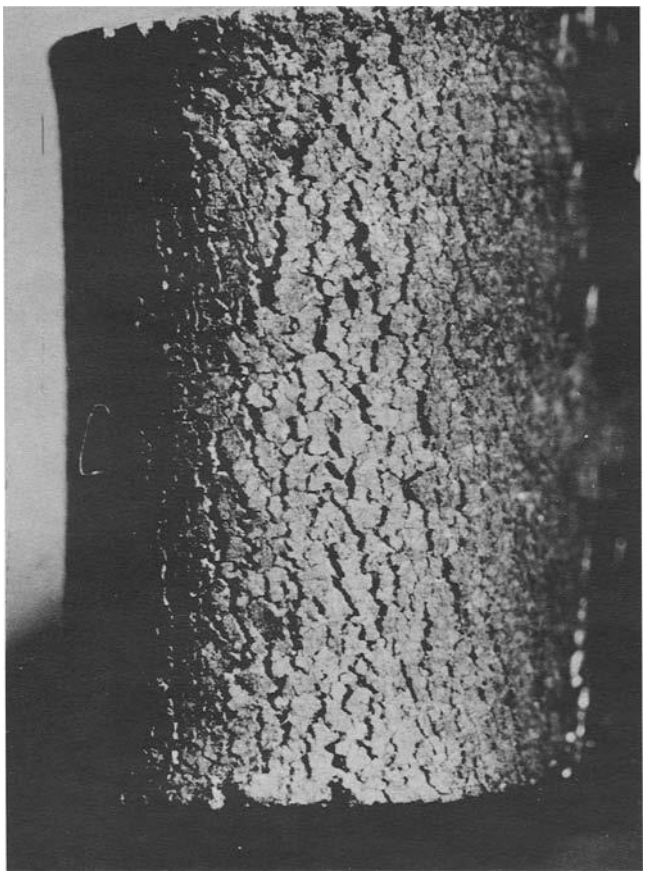


Figure 10 - Grain-boundary attack by nitric acid.

After the processes leading to intercrystalline corrosion have been clarified to some degree, the possibilities of changing the tendency towards precipitation, therefore susceptibility, by varying the composition of the alloys have been investigated. Since nickel-molybdenum alloys do not present any serious difficulties from the standpoint of intercrystalline corrosion if a good solution annealing treatment precedes fabrication and if an appropriate welding method is used and since from the standpoint of alloy technology only a lowering of the iron content is desirable, the investigations described in the following deal with the improvement of Hastelloy C.

Ternary System Ni-Cr-Mo and the Effect of C, Fe, Mn and Si On Precipitation Behavior

A technological improvement of alloys presupposes the knowledge of the constitution diagram of their main constituent elements. Since the Ni-Cr-Mo alloys became industrially important, the ternary system of these elements has been investigated in its isothermal sections, at 1250 C by Bloom and Grant[9] and at 1200 C by Manly, Kamen, Lement and Beck.[11] Both groups of investigators found the same equilibria, as well as the existence of both ternary crystals, sigma and P. However, such large quantitative differences of concentration were recorded that they become important for industrial alloys. Thus, for example, an alloy with 20 percent Cr and 20 percent Mo is found at 1200 C, according to Rideout and coworkers, still in the homogenous gamma field (when we designate a homogenous cubic face-centered solid solution as gamma), whereas, according to Bloom and Grant, it is in the heterogenous two-phase gamma-P field at 1250 C, though a higher solubility of the gamma solid solution should be expected at 1250 C. In order to permit separation and to study the effect of time at different temperatures on the equilibria, three isothermal sections at 1200, 1000 and 800 C were newly determined using 48 alloys melted in a high-frequency furnace under 10^{-4} mm mercury absolute pressure. The alloys were either forged or diffusion annealed and held for 30 hours at the experimental temperature following a two-hour homogenization annealing. In this way the state of equilibrium was substantially reached. The phases so produced were investigated microscopically and roentgenographically. The investigations were limited to alloys with a high nickel content. No alloys with less than 40 percent nickel were melted, since they cannot be used commercially.

A part of the results are presented in Figure 13 which contains, in addition, the compositions of the alloys investigated. (Original metals were 99.99 to 99.95 percent pure).

Both ternary crystals, sigma and P, were found, in agreement with the previous investigations. The results of Rideout and coworkers were substantially confirmed. Of the two phases, sigma and P, the sigma phase is the more important according to the former investigations of commercial alloys, in which the P phase is essentially absent. The establishment of a constitutional diagram facilitates the determination of the optimum homogenization temperature and provides indications of the suitable composition. The basic composition limits can be considered as 60 and 65 percent nickel, 20 and 25 percent chromium and 15 percent molybdenum, alloys with a higher nickel content being more sluggish to form precipitates. It was notable that the pure ternary alloys were very sluggish to form precipitates and several hours of annealing was required before any precipitation of sigma phase could be seen at the grain boundaries. In commercial alloys only a few seconds elapses before precipitates can be seen.

Samples containing sigma phase were as susceptible in the hydrochloric acid test as were the commercial alloys.

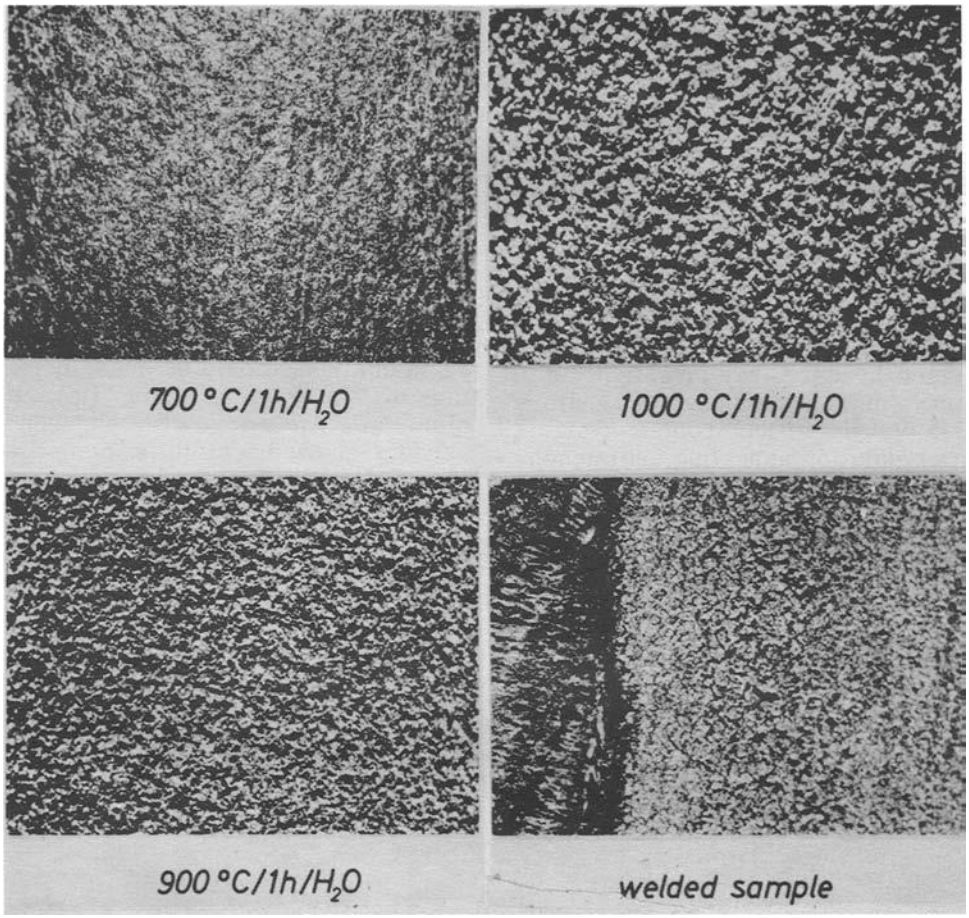


Figure 11 - Testing of intercrystalline corrosion in H_2SO_4 with $Fe_2(SO_4)_3$. Concentration: 400 ml H_2O, 236 ml concentrated +25g H_2SO_4 $Fe_2(SO_4)_3$.

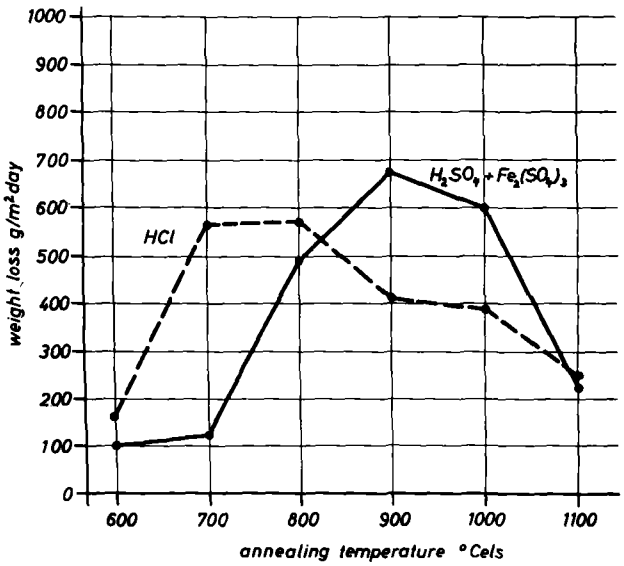


Figure 12 - Comparison between HCl test and $H_2SO_4 + Fe_2(SO_4)_3$ test. Time of annealing: 1 hour.

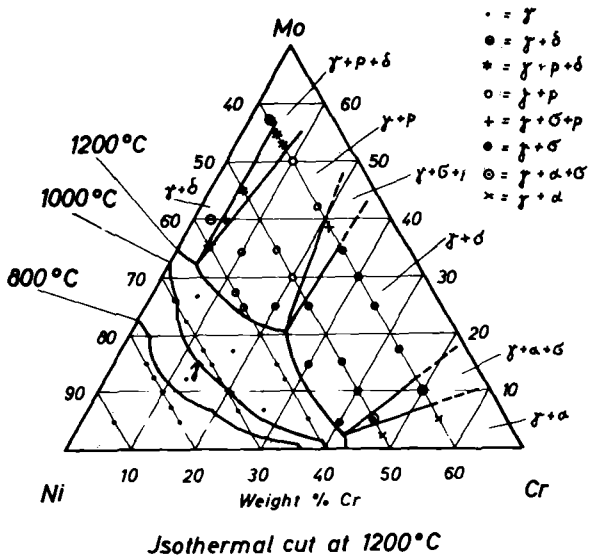
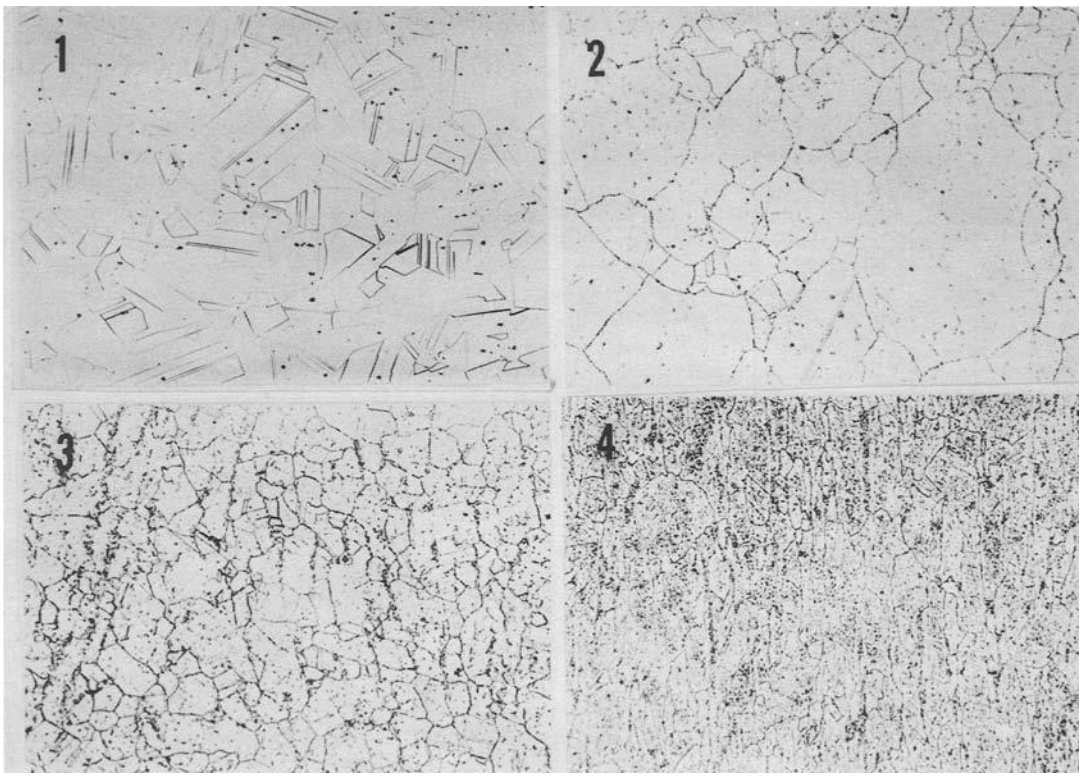


Figure 13 - Ternary system of Ni-Cr-Mo.

The very slow precipitation rate in the ternary systems, as compared with Hastelloy C, suggests that addition of other elements to the basic composition changes the saturation surface of nickel solid solution which exerts a marked influence on the precipitation rate of the sigma phase. Effect of addition of carbon up to 0.1 percent, and of iron, manganese and silicon up to several percent was investigated.

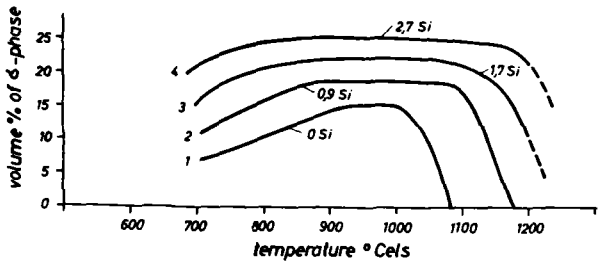
The above elements were added to a basic heat containing 60 percent nickel, 25 percent chromium and 15 percent molybdenum. The precipitation behavior was evaluated both by microscopic study of the structure and by an X-ray investigation in a high-temperature, high-vacuum camera. Alloys with more than 1.5 percent silicon contained sigma phase directly after solution annealing and quenching. Alloys with silicon content of 0.8 to 0.9 percent became heterogenous after annealing for 1 hour at 1150 C and subsequent water quenching. Precipitation in silicon-containing alloys can be seen particularly clearly after 1-hour annealing at 1100 C and water quenching, as shown in Figure 14. Silicon-free alloys remain homogenous under the same conditions. In a pure ternary alloy with 60 percent nickel, 25 percent chromium and 15 percent molybdenum, precipitation occurs first below 1090 C, but in an alloy with 0.9 percent silicon already below 1180 C. Structure determination with X-rays was extended over the range of 700 to 1200 C. Exposures were made in steps of 100 C. While in case of the basic alloy (60 percent nickel, 25 percent chromium and 15 percent molybdenum) the diffraction pattern of the P phase was weak, in the remaining 14 alloys only the lines of sigma phase could be seen, indicating a broadening of the gamma-sigma field by the alloying elements. An alloy with an iron content of 3.1 percent showed a slightly intensified precipitation of the sigma phase without causing a perceptible shifting in regard to the phase boundaries of the gamma solid solution. Higher iron contents than those presently investigated are thus not recommended for commercial alloys, since iron belongs



Alloy-No.	Ni	Cr	Mo	Si
1	59,8	25,1	15,1	-
2	59,5	24,8	14,9	0,9
3	58,9	24,6	14,7	1,7
4	58,4	24,3	14,6	2,7

Figure 14 - Influence of Si on the behavior of precipitation. Heat treatment: 1100 C/1h/H_2O.

to sigma-phase formers and would exert assuredly a less favorable effect at higher concentrations. Manganese additions above 1.5 percent, however, cause a slight reduction of sigma precipitation which is connected with the broadening of the gamma solid solution range to somewhat lower temperatures. No carbon effect was found.



Alloy-No.	Ni	Cr	Mo	Si
1	59,8	25,1	15,1	-
2	59,5	24,8	14,9	0,9
3	58,9	24,6	14,7	1,7
4	58,4	24,3	14,6	2,7

Figure 15 - Influence of Si on the behavior of precipitation.

Addition of silicon increased sigma formation very markedly, as shown in Figure 15. Curves for temperatures above about 900 C should present approximate equilibria. At lower temperatures the equilibrium is not reached, since with lower temperatures a steady increase of the sigma phase is to be expected. Reduction of the precipitation rate here requires too long a time for reaching equilibria.

The volume percentage of sigma phase was estimated through the intensity of the X-ray interference lines.

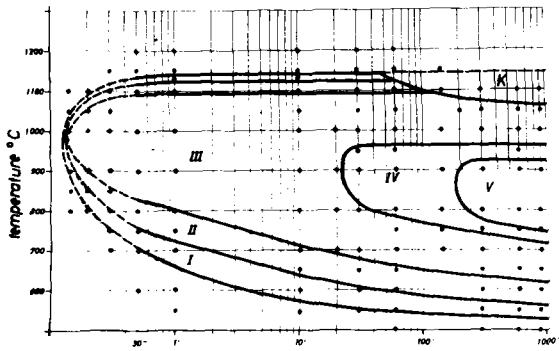
The results show that an alloy with lowest possible tendency toward intercrystalline corrosion should be practically free of silicon.

Effect of Alloy Improvement with Respect to Use in Chemical Apparatus

It is naturally interesting to see how far the improvements described in the above studies can be successfully applied in practice. Thus, several experimental heats have been made, in which the possibilities of replacing silicon with other deoxidizing elements have been checked. Magnesium appeared to be the most suitable and is used as such in nickel-magnesium alloy.

Figures 16 and 17 show two time-temperature-precipitation diagrams, one for Hastelloy C with 0.61 percent silicon and another for a new alloy with 0.01 percent silicon. Fields I in the diagrams show the range, in which the first recognizable indications of precipitation can be seen. In Fields II grain boundaries are partially surrounded with the precipitate; Fields III cover areas, in which precipitate forms a continuous film at the grain boundaries. In Fields IV begins the precipitation within grains, while in Fields V heavy precipitates are present both at the boundaries and within the grains. At higher temperatures, Fields K are also shown. In these fields originally laminarily-connected precipitates coagulate first in a string of small spheres and then into larger globules.

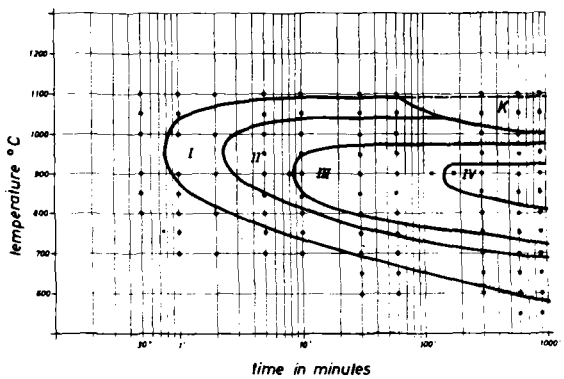
The boundary between Field I and the field of the homogenous state gives an indication of the time required for the beginning of sigma precipitation. At the saturation temperature this time is infinite. With decreasing temperature the effect of the increase in supersaturation is superimposed on decreasing atomic mobility, so that with decreasing temperature the induction time first rapidly decreases, passes a minimum, and then increases.



Analysis	Ni	Cr	Mo	Fe	W	Mn	Co	C	Si	Ti	Mg
HastelloyC	56,3	15,1	13,3	5,3	3,9	0,36	2,1	0,05	0,61	-	-

Figure 16 - Time-temperature diagram of precipitation from Hastelloy C.

In the commercial alloy with 0.61 percent silicon the required time at 980 C amounts to about 3 seconds, Figure 16; in a practically silicon-free alloy it becomes 45 seconds at 950 C, Figure 17. However, both Fields I and Fields II have but little importance to intercrystalline corrosion, which is not the case for Fields III, in which connected precipitates are present at grain boundaries. The minimum time in which these fields can be reached is 3 seconds for the alloy with 0.61 percent silicon and for an alloy practically free from silicon it is 500 seconds. Heat treating required for obtaining a homogenous structure is facilitated in the same proportion as this time increases.



Analysis	Ni	Cr	Mo	Fe	W	Mn	Co	C	Si	Ti	Mg
Heat B	60,3	22,6	14,0	2,26	-	0,84	-	0,042	0,01	-	<0,01

Figure 17 - Time-temperature diagram of precipitation from an alloy without Si.

Table 1

Analysis										
Alloy	Ni	Cr	Mo	Co	Fe	W	Mn	Si	C	Mg
Hastelloy C	56,3	15,1	15,3	2,1	5,3	3,9	0,36	0,61	0,05	-
Heat F	59,3	22,0	16,5	-	1,1	-	0,30	0,23	0,05	0,17
Heat G	59,4	24,1	14,1	-	1,4	-	0,85	0,04	0,03	0,11

Table 1 presents compositions of the two new alloys and of Hastelloy C. These alloys were compared from the standpoint of technological behavior and of corrosion properties. Mechanical strength figures differ very little, so that they do not need to be examined here more closely. Heat G is practically silicon-free, while Heat F has a low silicon content of 0.23 percent. Both experimental heats can be homogenized at 1150 C after forging. When cooled in air, no precipitation occurred in 6 mm thick plate made of Heat F, while a 10 mm thick plate made of Heat G remained homogeneous. In Hastelloy C however definite grain boundary precipitates were observed after oil quenching from 1220 C (in this case 1150 C does not suffice for solution annealing). On weld testing it has been found that Heat F can be welded up to 3 mm thickness, without any critical precipitation in the heat-affected zone, while Hastelloy C having the same thickness showed a marked grain boundary precipitate, Figure 18. Heat G up to 6 mm thickness could be welded without appreciably affecting the heat-affected zone. There is a possibility of welding without difficulties even substantially thicker parts, which can be done, for example, by following welding with a water spray. All welded samples were tested in the hydrochloric acid test and behaved well. If it happens that a heat treatment becomes necessary, for example, after hot working, the alloy can be heat treated at 1150 C using air cooling, or air blast in case of heavier sections. The soaking time needed is about 1/2 to 1 hour.

Figure 19 demonstrates the efficiency of homogenizing annealing at 1150 C followed by air cooling. Heavy grain boundary precipitates obtained in alloy G by annealing at 900 C were eliminated by this type of solution annealing.

Induction annealing is also basically possible.

One of the most efficient methods for determination of sigma precipitation is impact testing, because even a small content of this hard and very brittle phase sharply reduces impact strength of alloys.[12,13,14] At the same time hardness is raised. In Table 2 are given impact strength characteristics of Hastelloy C and of the new alloy G (averages of three determinations) as a function of critical heat treatment. Determinations were conducted on the small (4 x 3 x 27 mm) sharp notched DIN 50119 impact specimens. While with the commercial alloy a marked drop in impact strength occurs after 1 hour at 700 C, partically no reduction in impact strength can be observed in Heat G. After other annealing treatments decreases in impact strength of the experimental alloy G is substantially smaller than of Hastelloy C. The reduced precipitation tendency shows itself also in the smaller increase of hardness.

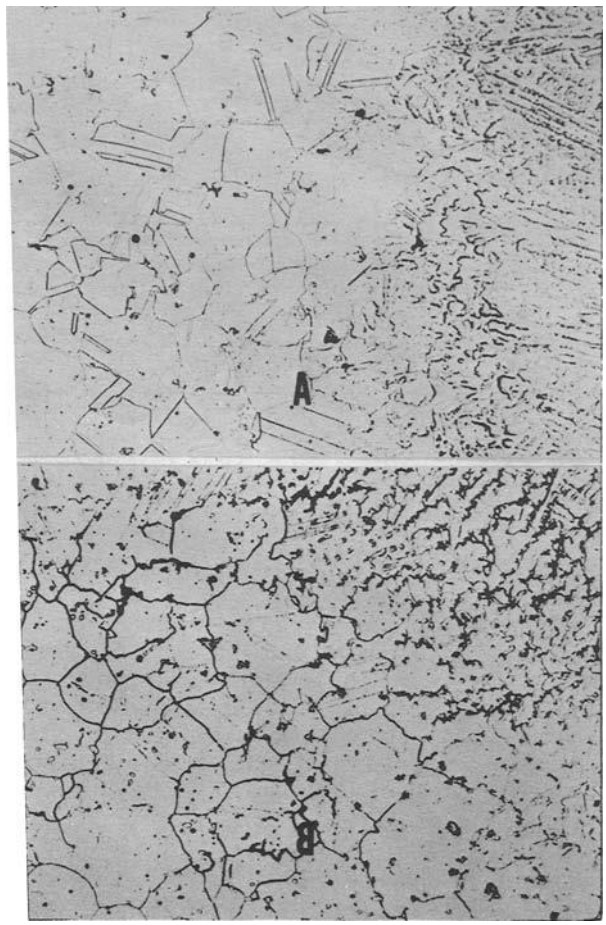
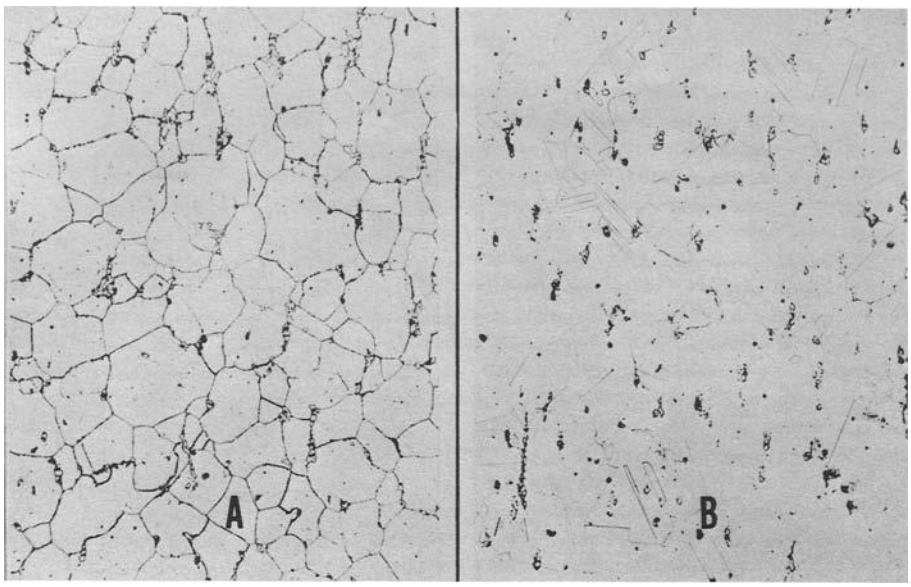


Figure 18 - Influence of welding heat. (A) Heat F, heat-affected zone without precipitation. (B) Hastelloy C, heat-affected zone with precipitation.

Table 2
Hardness and impact strength relating to heat treatment

	Hastelloy C		Heat G	
Heat treatment	impact strength mkg/cm²	hardness HV10 kg/mm²	impact strength mkg/cm²	hardness HV10 kg/mm²
solution annealing	9,5	234	11,2	242
700 °C/1h	3,6	268	10,4	248
900 °C/20h	0,7	315	1,8	265
1000 °C/30h	1,2	269	3,5	254

Figure 20 shows two welded samples after hydrochloric acid testing. The thinner bend test (sheet 2.5 mm thick) was made of Hastelloy C alloy as given in Table 1, the thicker sample (sheet 8 mm thick) was made of the new alloy G.



Analysis	Ni	Cr	Mo	Co	Fe	W	Mn	Si	C	Mg
Heat G	59,4	24,1	14,1	-	1,4	-	0,85	0,04	0,03	0,11

Figure 19 - Effect of solution annealing at 1150 C followed by air cooling. Heat treatment: (A) 1200C/1h/H_2O, 900C/1h/H_2O. (B) 1200C/1h/H_2O, 900C/1h/H_2O + 1150C/1h/air.

After solution annealing both strips were arc welded with matching alloy electrodes. While the Hastelloy C sample shows severe intergranular corrosion near the welded seam, the substantially thicker sample of the new alloy behaves well, even though it contains (as has been shown by structure study) some precipitate which was produced by very slow cooling. Although sigma precipitates at grain boundaries of alloy G, the depletion in chromium and molybdenum is lower, because the chromium content of the matrix is appreciably higher than in the previous commercial alloys. An increased chromium content is thus advantageous.

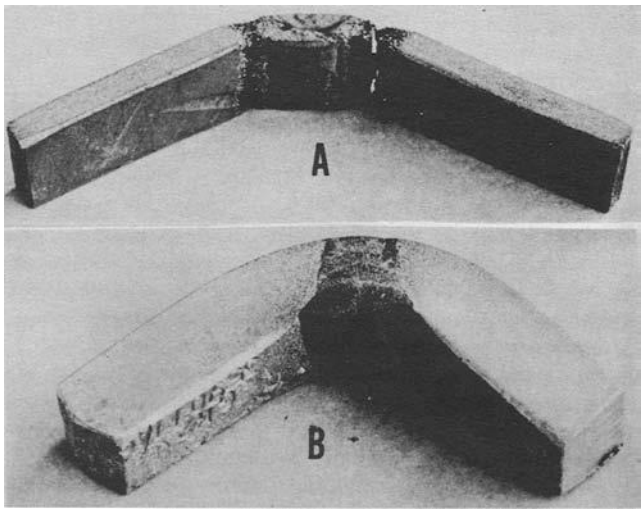


Figure 20 - Welded samples after hydrochloric acid test. (A) Hastelloy C, thickness, 2.5 mm(0.1 in.). (B) Heat G, thickness 8 mm (0.31 in.).

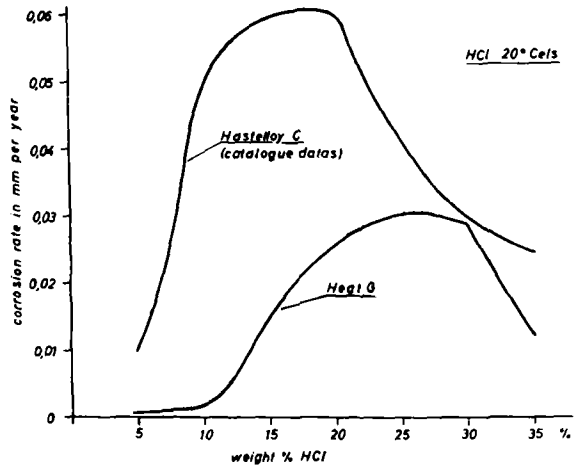


Figure 21 - Corrosion resistance in hydrochloric acid.

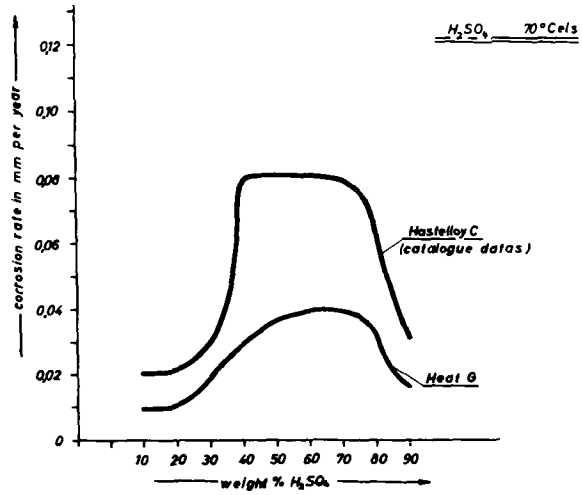


Figure 22 - Corrosion resistance in sulfuric acid.

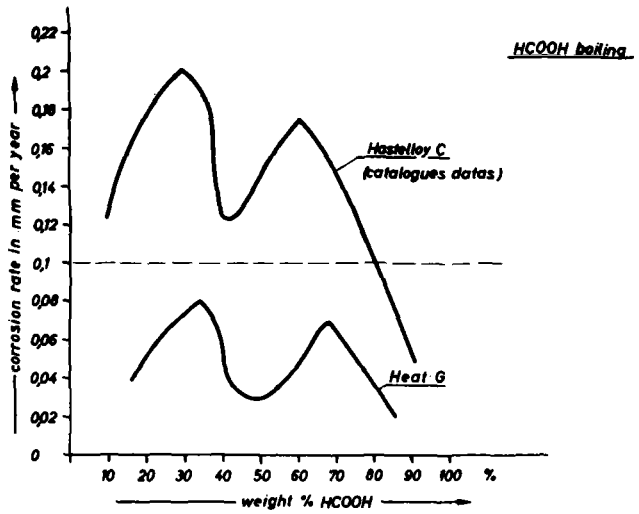


Figure 23 - Corrosion resistance in formic acid.

The resistance of the new alloys to general corrosion was checked on forged and homogenized samples of Heat G. Homogenization consisted of heating at 1150 C with subsequent air cooling. Samples were exposed to hydrochloric, sulfuric and formic acids of different concentrations for 4 weeks, loss of weight determined and from it the linear reduction of thickness, in millimeters per year, was calculated. Figures 21,22 and 23 show the reduction of thickness curves. For comparison, corresponding values for Hastelloy C, taken from a catalog of the Haynes Stellite Company,[15] are included. The new alloys in all cases show a definitely lower thickness reduction than the commercial alloy as a result of a higher chromium content. Particularly good corrosion resistance towards organic acids can be expected since formic acid is the most corrosive of all aliphatic acids.

References

1. M. Hansen. Constitution of Binary Alloys, p 968, McGraw-Hill Company, Inc., New York (1958).
2. S. P. Rideout and P. A. Beck. NACA Tech. Note 2683 (1952) April
3. H. Grafen and Gg. Bohm. Z. Metallkde, 51, 245 (1960).
4. H. J. Rocha. Stahl u Eisen, 70, 608 (1950).
5. M. Hansen. Constitution of Binary Alloys, p 669, McGraw-Hill Company, Inc., New York (1958).
6. A. G. Allten. J. Metals, 6 904 (1954).
7. C. J. Bechtoldt and H. C. Vacher. Journ. Research of the N.B.S., Vol. 58, p 7 (1957).
8. M. Protzl. Arch. Eisenhuttenwes., 29 p 745 (1958).
9. P. S. Bloom and N. J. Grant. Trans. AIME Journ. of Metals, p 261 (1954).
10. M. A. Streicher. Journ. Electrochem. Soc., Vol. 106 p 161 (1959).
11. S. Rideout, W. P. Manly, E. L. Kamen, B. S. Lement and P. A. Beck. Trans. AIME Journ. of Metals, p 872 (1951).
12. E. Baerlecken and W. Hirsch. Stahl u. Eisen, 75, p 570 (1955).
13. G. N. Emmanuel. ASTM publ. No. 110, p 146 (1950).
14. Anonym. Proc. ASTM, 53 p 143, p 177 (1953).
15. Corrosion Resistance of Haynes Alloys. Haynes Stellite Company, Division of Union Carbide Corporation, USA (1958) November.

An Evaluation of Accelerated Strauss Testing

By L. R. Scharfstein* and C. M. Eisenbrown*

Introduction

As a stainless steel producer, we are often requested by customers to perform ASTM Test Designation: A 393-55T on materials prior to shipment. This test, commonly known as the Strauss Test, is officially entitled "Conducting Acidified Copper Sulfate Test for Intergranular Attack in Austenitic Stainless Steel". The purpose of conducting the test is to ascertain whether or not the finished product will be prone to suffer intergranular attack in service due to the presence of a chromium-rich carbide grain boundary precipitate. Stabilized and low carbon grades of austenitic stainless steels are also tested to verify the correct composition. These steels are tested in the "sensitized" condition. A sensitizing heat treatment of 1 hour at 1250 F in air followed by an air cool is suggested in A 393. All other materials are tested in the "as-received" condition. In the A 393 test the test specimen is exposed for a period of 72 hours to a boiling aqueous solution containing approximately 16 percent H_2SO_4 and 6 percent $CuSO_4$ by weight. After exposure to boiling acid, the specimen is bent through 180 degrees and the surface is examined at 5X to 15X for the presence of fissures. Fissuring is an indication of intergranular attack.

It has been common knowledge for many years that the A 393 test is very mild and does not readily reveal susceptibility to intergranular attack in service, since many samples with a grain boundary precipitate do pass this test. The addition of copper to the Strauss solution is known to accelerate grain boundary attack.[1] Our object was to evaluate the effectiveness of the copper modification to A 393. Before this work could be meaningful it was necessary to establish quantitative limits on the ability of the standard A 393 test to detect a grain boundary chromium-rich carbide precipitate.

TABLE 1

CHEMICAL ANALYSES OF TYPE 304 HEATS TESTED

AISI Type	Heat Number	C	Mn	Si	P	S	Cr	Ni	Mo	Cu	Co
304	801257	.068	.90	.60	.022	.015	18.48	9.43	.20	.23	.07
304	X42653	.051	.82	.69	.022	.012	18.10	8.68	.31	.24	.07

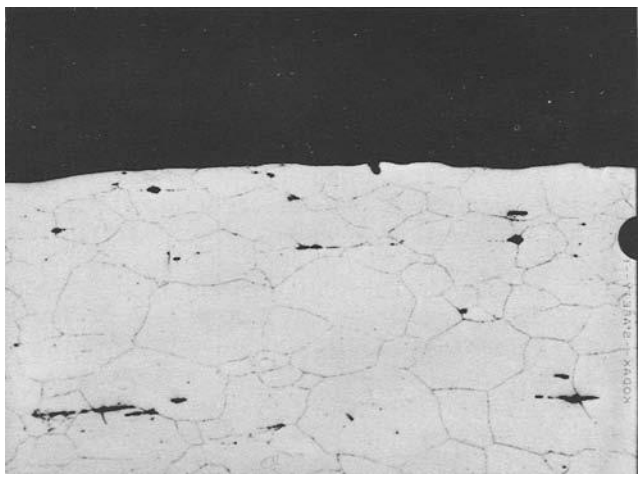


Figure 1 - Cross section through bend in 0.051 percent C, Type 304 specimen after sensitizing at 1250 F for 5 hours and testing under A 393 procedure. Magnification 175X. Etched.
STP369-EB/Apr. 1965

Effect of Varying Time of Sensitization

Standard A 393 Test

Two commercial heats of AISI Type 304 stainless steel at two levels of carbon, 0.051 percent and 0.068 percent, were selected for intensive study. See Table 1 for the analyses. Suitable specimens 3 in. x 3/4 in. x 0.100 in. were prepared from each heat after sensitization at 1250 F in air for 1, 2, 3, 4 and 5 hours, respectively, followed by air cooling. The ASTM A 393 standard test was then made with each specimen. Although it is well known that one hour at 1250 F would be sufficient to precipitate a damaging grain boundary precipitate in these steels,[2] the A 393 test procedure did not detect a failure in any specimens of the 0.051 percent carbon material regardless of time at 1250 F. All the specimens of 0.068 percent carbon material sensitized up to and including 4 hours also passed this test. One specimen of 0.068 percent C material sensitized for 5 hours was borderline and one specimen representing 5 hours of sensitization was a definite failure. Figure 1 shows the microstructure and lack of intergranular penetration in the bend region of the 0.051 percent C material which previously had been sensitized for 5 hours and exposed to the standard A 393 solution for 72 hours.

*Corrosion Research, The Carpenter Steel Company, Reading, Pennsylvania.

Copyright© 1965 by ASTM International

www.astm.org

Copper Modified Strauss Test

The addition of copper to the Strauss test solution to accelerate corrosion was first described by H. J. Rocha in a discussion to a paper by Brauns and Pier.[1] Subsequent to this, some test results and explanations of mechanisms were published by Streicher[3] and Cihal and Prazak.[4] The addition of copper to the standard A 393 solution shifts the redox potential in the more active direction. If the specimen is in contact with copper in the solution, the potential of the specimen is shifted slightly more active since copper behaves as the anode and austenitic stainless steel as the cathode in this medium. Electrical resistance and weight-loss measurements made by Streicher show an acceleration in intergranular attack of 3 to 100 times when copper is employed.

We investigated the use of copper in aiding the detection of a grain-boundary precipitate in the heats of Type 304 containing 0.051 and 0.068 percent carbon. Here again, we sensitized these heats at 1250 F in air for periods of 1, 2, 3, 4 and 5 hours, respectively, followed by air cooling.

Copper in Solution

No Contact with Specimen

Copper shot of electrolytic quality, purchased from a laboratory supply house, was added to the standard A 393 test solution. Since some copper dissolves during the test, two levels of copper were tested, namely, 3 g and 5 g, respectively. The sensitized specimens were tested either separately or in pairs in Erlenmeyer flasks with cold finger condensers. The specimens were held in vented glass cradles which insulated them from making galvanic contact with the copper in the bulk solution. Boiling tests were run for 24- and 48-hour periods, respectively. Failures were observed in the bend for tests conducted for 48 hours on material sensitized for 2 or more hours. No failures were found for specimens from either heat representing only 1 hour of sensitization. No difference was observed between the high and low levels of copper but 48 hours of boiling was much more effective than 24 hours in indicating failure in the bend.

Copper in Contact with Specimen

Figure 2 shows three different methods used to place the specimen in contact with copper in the boiling standard A 393 solution. Again the same two heats of AISI Type 304 stainless steel (0.051 and 0.068 percent carbon, respectively) were tested after sensitization at 1250 F. The specimens, in contact with copper, were exposed for 24 hours to the boiling solution. For the first time in this experimental program, all the sensitized specimens failed. Thus, after 24 hours of exposure time, even the 1-hour sensitized specimen failed after bending (see Figure 3).

Of the three methods used to make contact with the specimen, we prefer those using shot or turnings in a glass cradle. The failures in these cases were much more apparent, possibly by assuring that a large area of copper is making good contact with the specimen. The confining dimensions of a glass cradle insure a tight fit between the specimen and the copper particles.

Figures 4 and 5 schematically summarize the zones of "pass" and "fail" in the various tests described above using the 0.051 and 0.068 percent carbon 18-8 stainless steels. The standard A 393 test refers to 72 hours of exposure; the copper - no contact test refers to copper in solution without contacting the specimen, the 48-hour test; the copper in contact with the specimen, refers to a 24-hour test wherein copper plate, shot or turnings were in intimate contact with the specimen in the Strauss test solution.

Production Testing

From the previous testing, it appeared that a copper-contact test performed with the Strauss test solution would be suitable for production testing. One more major point remained to be clarified. Would the test be too severe and therefore show "fail" for properly heat-treated material? In order to gain experience on this point we ran the copper-contact accelerated Strauss test on production heats of AISI Types 304, 304L, 316, 316L, 321 and 347, and on Carpenter No. 20-Cb. The low carbon and stabilized grades were tested in the "as received + sensitized condition" (1 hour at 1250 F and air cooled). The other materials were tested in the "as-received" condition. A total of 47 production heats were thus exposed to the accelerated test in the Strauss solution and all passed the test. Further proof of the safety of the test was supplied by submitting 18 heats of Type 304 in the as-received condition to the accelerated test for 48 hours instead of 24 hours. All 18 heats passed. Beside the two heats of Type 304 deliberately sensitized, 8 heats of Type 316 were deliberately sensitized. All eight heats failed (Table 2). Figure 6 shows the very apparent fissuring in the bend of one of these specimens. On the basis of the tests performed with production heats of austenitic stainless steels, it is concluded that the 24-hour, copper-contact Strauss test is an accurate and safe test for testing mill products.

Discussion

As was mentioned previously, the explanation of the influence of copper on accelerating grain-boundary attack in boiling $CuSO_4$-H_2SO_4 was very satisfactorily discussed by Streicher[3] and Cihal and Prazak.[4] It is therefore the purpose of this discussion to emphasize those aspects of the work performed by these investigators that clarify our results and tend to emphasize the reliability of the accelerated Strauss test.

Streicher observed that the potential of a stainless steel specimen is initially +0.34 v (vs saturated calomel electrode) in the A 393 solution. Addition of copper to the solution, not in contact with the specimen, rapidly alters the potential of the stainless steel in the active direction to +0.13 v. When the stainless steel specimen is in contact with copper, the potential of the steel is further

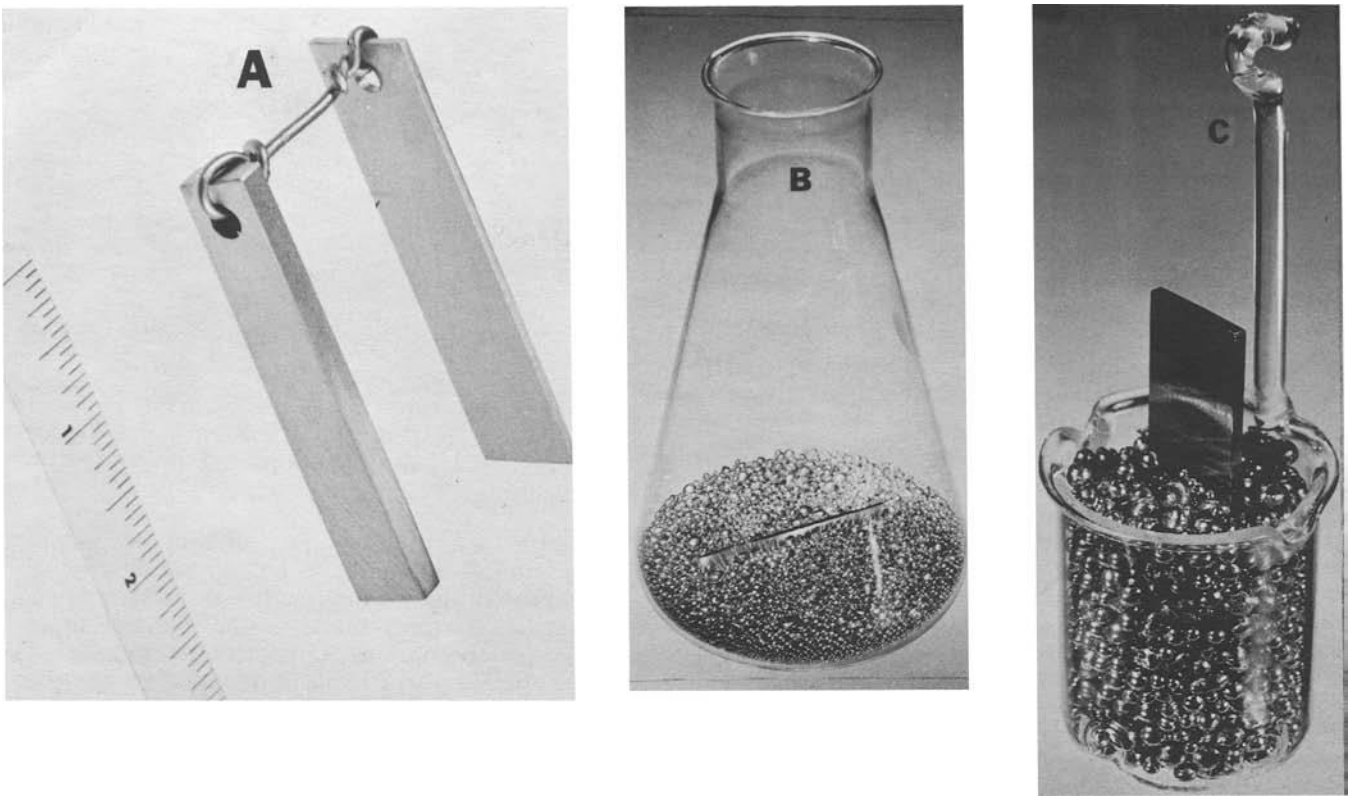


Figure 2 - Three methods of placing specimen in contact with copper. (A) Copper bus bar material electrically coupled to specimen through copper wire. (B) Specimen embedded in copper shot in the test flask. (C) Specimen embedded in shot in vented glass cradle.



Figure 3 - Cross section through bend in 0.068 percent C, Type 304 specimen after sensitizing at 1250 F for 1 hour and testing under A 393 procedure. Magnification 175X. Etched.

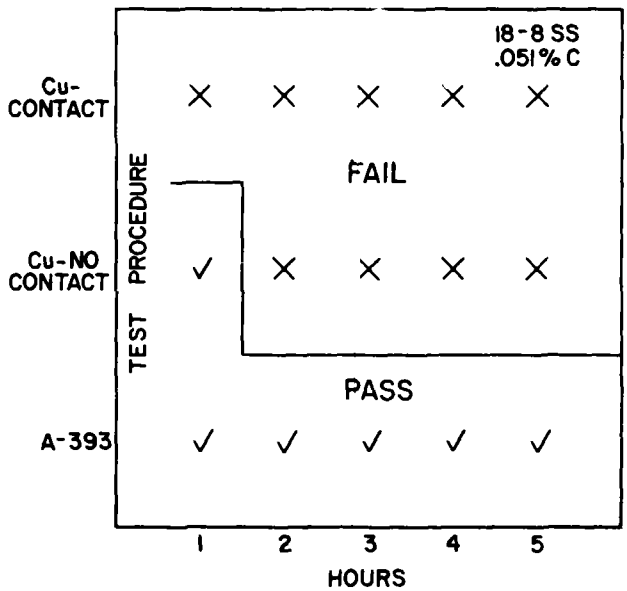


Figure 4 - Schematic diagram showing effect of hours of sensitization at 1250 F on ability of 0.051 C, 18-8 stainless steel to pass the standard A 393 test (72-hour), Cu-no contact (48-hour) test and Cu-contact (24-hour) test.

TABLE 2

COPPER-CONTACT ACCELERATED STRAUSS TESTING RESULTS OF PRODUCTION HEATS (24 Hr. Exposure)

Material	No. Heats Tested	No. Heats Failed	No. Heats Pass	Remarks
Type 304	18	0	18	Mill Annealed-48 Hr. Test
Type 304	7	0	7	Mill Annealed
Type 304L	3	0	3	Mill Annealed + Lab. Sens.
Type 316	8	0	8	Mill Annealed
Type 316L	5	0	5	Mill Annealed + Lab. Sens.
Type 347	3	0	3	Mill Annealed + Lab. Sens.
Type 321	2	0	2	Mill Annealed + Lab. Sens.
Carpenter No. 20-Cb	1	0	1	Mill Annealed + Lab. Sens.
Type 304	2	2	0	Mill Annealed + Lab. Sens.
Type 316	8	8	0	Mill Annealed + Lab. Sens.

Note: Lab. Sens. = Laboratory sensitized by heating for 1 hour at 1250°F in air followed by air cool.

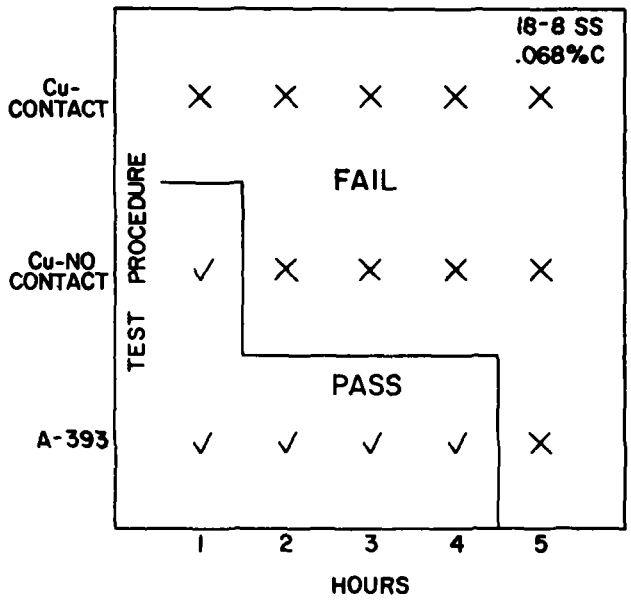


Figure 5 - Schematic diagram showing effect of hours of sensitization at 1250 F on ability of 0.068 percent C, 18-8 stainless steel to pass the standard A 393 (72-hour) test, Cu-no contact (48-hour) test and Cu-contact (24-hour) test.

activated to +0.06 v, the potential of the copper in this solution. The copper contact produces dissolution of the stainless steel at a constant potential. The dissolution of stainless steel in a Strauss solution not initially containing copper will cause a gradual drift in potential to a more active potential as the Cu^{2+} ions are reduced to Cu^{1+} and copper at the local cathodes. Here, then, is an obvious deficiency in the ASTM A 393 test. The actual redox potential of the test solution varies with time depending upon the amount of corrosion, size of specimen and number of specimens in the same flask. The copper contact test maintains constant conditions from start to finish from test-to-test regardless of rate of specimen attack, size or number.

It was also shown by Streicher that the copper-accelerated tests do not alter the character of the attack. The attack as measured by electrical resistance change was in a constant relationship

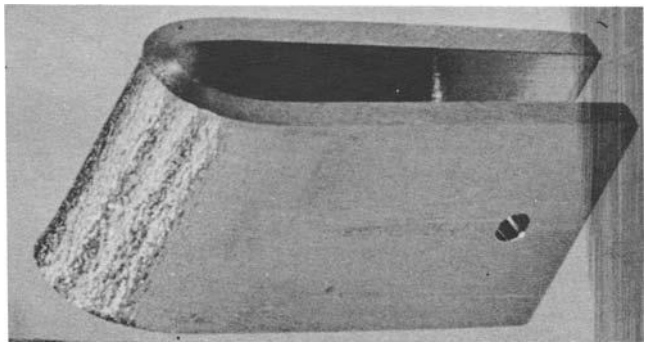


Figure 6 - Bend test conducted on AISI Type 316 after 1250 F; 1-hour sensitization and exposure to Strauss test solution embedded in copper for 24 hours. Note fissures in bend.

with weight loss, regardless of test procedure, i.e., standard A 393, copper-no contact or copper-in-contact with the specimen. It was further shown that the Strauss test leads to the deepest intergranular penetration as a function of weight loss of either the Huey or Ferric Sulfate tests, two other common tests for detecting susceptibility to intergranular attack in austenitic stainless steels. The explanation for this phenomenon is that the rate of attack in $CuSO_4$-H_2SO_4 does not lead to grain dropping - the most likely contributor to high weight loss.

Conclusions

1. The ASTM A 393 test for intergranular attack in austenitic stainless steels (Strauss Test) was evaluated for ability to detect a sensitizing heat treatment in AISI Type 304 at two levels of carbon. It was concluded that this test requires over 4 hours of heating at 1250 F of 0.100 in. thick material in order to fail. For most practical purposes this test is therefore not adequate or accurate.

2. The addition of metallic copper to the A 393 solution either in contact or not in contact with the stainless test specimen accelerates the intergranular attack. A satisfactory test consists of embedding the specimen in copper shot or turnings for 24 hours of exposure in boiling A 393 solution. Type 304 with 0.051 percent carbon, sensitized for 1 hour at 1250 F, failed when tested in this manner. Results obtained with specimens not in contact with copper in the boiling solution would indicate that 72 hours of exposure would be required to fail the 0.051 percent carbon material after only 1 hour of sensitization.

3. The 24-hour copper-contact accelerated Strauss test is accurate in not failing properly heat treated or balanced compositions manufactured under steel mill conditions. Production heats of AISI Types 304L, 304, 316L, 316, 321 and 347 and Carpenter No. 20-Cb all passed the test when properly melted and heat treated in the mill.

Acknowledgments

The authors wish to thank Arnold R. Klein, Technician, for his excellent and efficient effort in

preparing, testing and evaluating approximately 200 test specimens and to thank The Carpenter Steel Company for permission to publish this paper.

References

1. E. Brauns and G. Pier. Stahl w Eisen, 75, 579-586 (1955). See Discussion by H. J. Rocha.
2. W. O. Binder, C. M. Brown and R. Franks. Resistance to Sensitization of Austenitic Chromium-Nickel Steels of 0.03 percent Max. Carbon Content. Trans ASM, Vol. 41, 1301-1370 (1949).
3. M. A. Streicher. General and Intergranular Corrosion of Austenitic Stainless Steels in Acids. J. Electrochem, Soc., 106, 161-180 (1959).
4. V. Cihal and M. Prazak. A Contribution to the Explanation of Intergranular Corrosion of Chromium-Nickel Steel. Corrosion, 16, 530t-532t (1960) October.

DISCUSSIONS

Discussion by W. Schwenk, Mannesman-Forschungsinstitut, 41 Duisburg-Wanheim, West Germany:

I do agree with the authors' opinion that the Strauss solution (110 g $CuSO_4 \cdot 5\ H_2O$ + 100 ml concentrated H_2SO_4/liter) with addition of metallic copper behaves as well as a potentiostat. The figure shows the cathodic polarization curve of the Cu^{2+} reduction process in boiling Strauss solution. The reaction is unpolarized. At 10 ma/sq cm current density the overvoltage amounts only to about 10 mv.

Without metallic copper addition the redox potential of the Strauss solution is not defined. In pure solutions it amounts about 0.5 v vs S.C.E. With addition of metallic copper or other metals, which react with the Strauss solution by producing copper, an equilibrium potential of about 0.11 v will be observed (compare figure). The time until reaching the equilibrium state may last up to 3 hours, as to the behavior of copper addition.

All electrodes consisting of stainless steel or noble metals (e.g., Pt, Cu) have the same redox potential, about 0.11 v in Strauss solution being in equilibrium with metallic copper. This effect is regardless of whether there is metallic contact between stainless steel samples and copper or not. Consequently, concerning intergraunlar corrosion, any influence of a galvanic coupling of the samples between each other or with copper is not be to expected. The corrosion controlling potential will be kept constant, because the cathodic reaction is unpolarized (compare figure). I've never observed any influence of metallic contact with copper in experiments.

Boiling Strauss solution with metallic copper addition has been the usual solution for testing intergranular corrosion susceptibility in Germany for nearly 10 years.[1,2] The time for testing lasts 15 hours only, and the standard test is registered in Stahl-Eisen-Prufblatt (VDEh) 1875-61 since 1961. To my experience the Strauss test with metallic copper addition is sufficiently sensitive to intergranular corrosion susceptibility caused by chromium carbide precipitation.[3]

References

1. E. Brauns and G. Pier. Stahl und Eisen, 75, 579 (1955).
2. H. J. Rocha. Discussion to (1), p 586.
3. H. J. Schuller, P. Schwaab and W. Schwenk. Archiv Eisenhuttenwesen, 33, 853 (1962).

Reply by L. R. Scharfstein:

1. We agree with Dr. Schwenk that without metallic copper the redox potential is undefined. That is the reason for our statement that "The actual redox potential of the solution (without copper) varies with time, etc....." appearing in our "Discussion" in the text of the paper.

2. We agree with Dr. Schwenk that stainless steel or noble metal electrodes all have the same redox potential in Strauss solution but do not agree that copper is as noble as platinum or stainless steel in this medium. We refer him to the paper by M. A. Streicher (Reference 3 in our paper). Streicher observed an emf of +0.13 v with both stainless steel and platinum in the standard Strauss solution. The potential of copper, however, was constant at +0.06 v. The footnote on page 175 of Streicher's paper describes an experiment which beautifully demonstrates that there is a galvanic current flowing between copper and stainless steel in this medium. We quote: "Specimens of copper and stainless steel, connected through a microammeter, were partially immersed in boiling sulfuric acid without cupric sulfate. The stainless steel dissolved with vigorous evolution of hydrogen and was the anode of the couple. When the couple was immersed in a second solution of sulfuric acid of the same concentration containing cupric sulfate, evolution of hydrogen on the stainless steel was suppressed. There was a reversal and a large decrease of the current between the specimens. The stainless steel became the cathode and the copper became the anode of the galvanic couple." This galvanic couple thereby reduces the anodic polarization, primarily, at the more susceptible grain boundaries. Streicher observed this increase in corrosion rate by making quantitative measurements of weight loss and electrical resistance increase. (See his Figures 21 and 22). We observed this effect by observing bend fissures in specimens when in contact with copper and not observing fissuring in similar specimens uncoupled to copper, although the time of test uncoupled was twice as long. (See our Figures 4 and 5).

3. We are familiar with the work of H. J. Rocha (see our Reference 1) but only became aware of Stahl-Eisen-Prufblatt 1875-61 after our paper was written. We believe that for the same reasons the standard Strauss Test is inadequate, a 15-hour test is also inadequate since we have recently observed that one is unable in that time period to detect fissures in bends of similarly sensitized 18-8 stainless steel when carbon content is approximately 0.040 percent.

Relationship of Heat Treatment and Microstructure to Corrosion Resistance in Wrought Ni-Cr-Mo Alloys

By M. A. Streicher*

Abstract

In an investigation of the effect of heat treatment on microstructure and corrosion resistance, seven heats of wrought Ni-Cr-Mo alloy were heated in the range of 800 F to 2375 F. Corrosion was studied in reducing and in oxidizing acids. Oxalic acid etch structures produced by various precipitates were classified and correlated with corrosion rates. Two maxima in corrosion rates were found: one on specimens heated near 1400 F and the other on specimens heated near 1900 F. In hydrochloric acid, only the maximum at 1400 F is revealed, while in chromic acid, only the maximum at 1900 F is detected. Both maxima are revealed by exposure to nitric acid, pure sulfuric acid and ferric sulfate-sulfuric acid solution.

Studies of the microstructures and analysis of residues from dissolution in bromine-methanol solution show that sigma phase, in microscopic or submicroscopic form, is mainly responsible for changes in corrosion resistance produced by heat treatments. carbides of the M_6C type containing molybdenum and tungsten as major elements are also present but have a minor effect on corrosion. No chromium carbide, $Cr_{23}C_6$, was found.

Incompletely dissolved precipitates in the form of submicroscopic phases have a deleterious influence on corrosion. Multiple solution-annealing treatments at 2250 F, rather than length of time at temperature, were found most effective in completely dissolving this phase.

Corrosion in reducing acids is under cathodic control. Intergranular attack and the corrosion potentials are a function of the anions of the acid. In oxidizing solutions, corrosion is governed by anodic polarization. The cathodic process consists of reduction of metallic cations. Both grain face and grain boundary zones are passive. Anodic polarization is governed by the presence of such cations as ferric ions and hexavalent chromium ions.

On the basis of data presented, a simple, rapid method for evaluating Ni-Cr-Mo alloys for susceptibility to intergranular attack is proposed. It consists of electrolytic etching in oxalic acid to detect the presence of incipient fusion resulting from overheating during annealing, and a 24-hour test in boiling solution of ferric sulfate-50 percent sulfuric acid. Material free of all kinds of damaging precipitates has a low rate of corrosion in this test.

Introduction

Alloys of 58 percent Ni-15 percent Cr-17 percent Mo with 5 percent Fe and 5 percent W(1) are frequently used in severely corrosive environments for which the corrosion resistance of the austenitic stainless steels has proven inadequate. As in the case of stainless steels, it is known that the corrosion resistance of the Ni-Cr-Mo alloys may be adversely affected by improper heat treatments. However, there has been no rapid and reliable test method for detecting such damage in the Ni-Cr-Mo alloys, and there has been no detailed investigation of the relation of microstructure to corrosion. In a search for a rapid, quantitative evaluation method, tests were made on heat-treated specimens of a Ni-Cr-Mo alloy in a recently developed test solution now being used to detect susceptibility to rapid intergranular attack in austenitic stainless steels.[1] It was found that corrosion of the Ni-Cr-Mo alloy in boiling 50 percent sulfuric acid containing ferric sulfate as a passivating inhibitor varies in a reproducible manner with the temperature of heat treatment. A test period of only 24 hours was found ample to separate properly heat-treated from improperly heat-treated specimens on the basis of their corrosion rates determined from measurements of weight loss.

The present investigation was then undertaken to determine, in detail, the effect of heat treatment and microstructure on corrosion resistance in the ferric sulfate-sulfuric acid solution and in several other acids. From the data obtained, a rapid, quantitative evaluation method for detecting susceptibility to intergranular corrosion in wrought Ni-Cr-Mo alloys was developed. By means of this test, solution-annealing temperatures and procedures essential for optimum corrosion resistance in this alloy were determined.

* Engineering Materials Laboratory, E. I. du Pont de Nemours & Co., Inc., Wilmington 98, Delaware.

(1) Hastelloy C, product of Union Carbide Corporation.

Copyright© 1965 by ASTM International

www.astm.org

TABLE 1—Analyses of Alloys*

Heat	Content, Percent Weight											
	Cr	Mo	W	Fe	V	Co	Mn	C**	Si**	P	S	Ni
A	15.56	15.88	3.47	5.10	0.22	1.12	0.56	0.060	0.55	0.010	0.011	Bal.
B	16.36	15.52	4.14	5.08	0.31	0.85	0.59	0.065	0.74	0.007	0.006	Bal.
C	15.81	15.73	3.69	5.55	0.24	0.90	0.57	0.045	0.70	0.007	0.008	Bal.
D	15.85	16.17	3.91	5.32	0.24	0.96	0.53	0.050	0.75	0.009	0.009	Bal.
E	14.88	15.80	3.88	5.68	0.25	1.55	0.80	0.045	0.53	0.010	0.007	Bal.
F	15.83	15.98	3.69	5.22	0.22	0.88	0.54	0.053	0.61	0.006	0.006	Bal.
H	15.44	15.77	3.79	5.83	0.26	1.27	0.58	0.055	0.80	0.009	0.006	Bal.

* Hastelloy C samples supplied in form of ⅛-inch sheet.
** Separate determinations of C and Si were made on corrosion test specimens.

Experimental Plan and Methods

Material from seven commercial heats of Ni-Cr-Mo alloy was selected for this investigation (analyses in Table 1). Significant variations in the effect of heat treatment on corrosion resistance were observed in these heats, even though their analyses were very similar. Specimens were heat treated in the range of 800 F to 2375 F. The microstructures produced were studied in the light microscope by means of several etching methods and in the electron microscope by the removal of carbon extraction replicas. Residues isolated by dissolution of heat-treated alloy specimens in bromine-methanol solution were analyzed spectroscopically and by x-ray diffraction.

Corrosion rates were measured in boiling 50 percent sulfuric acid with ferric sulfate inhibitor and, for comparison, in boiling 10 percent hydrochloric acid and in boiling 10 percent chromic acid (CrO_3). The hydrochloric acid solution has been used previously on Ni-Cr-Mo alloys,[2,3,4] and the use of chromic acid was proposed by Schley.[5] Less detailed tests were also made in several other corrosive solutions to explore the extent of applicability of the results obtained in the ferric sulfate-sulfuric acid solution. Electrode potential measurements were made to provide data on the mechanism of corrosion.

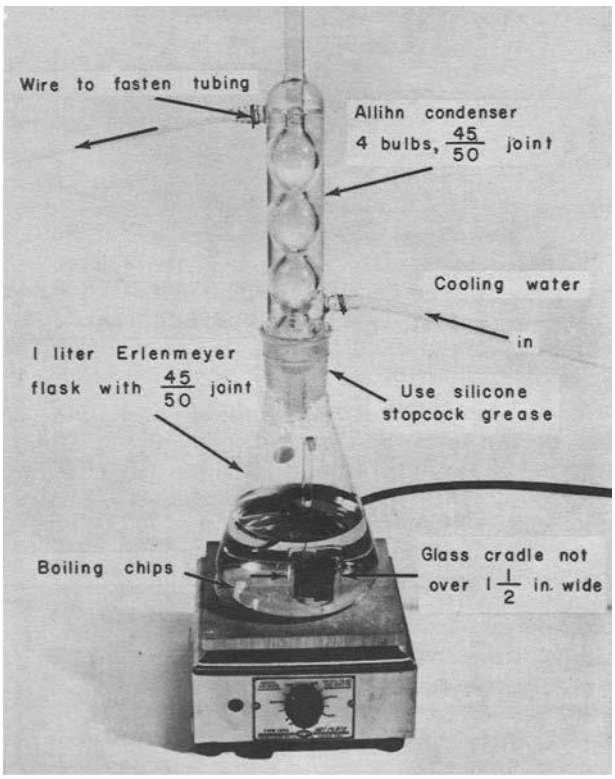


Figure 1 - Apparatus used for corrosion tests.

Specimens, 1 inch x 3/4 inch, were cut from mill-annealed sheets, 1/8 inch thick, of Ni-Cr-Mo alloys. For heat treatments, electric furnaces and an argon atmosphere were used. All treatments were for 1 hour unless otherwise indicated. Water quenching was used on all specimens. Before testing, the specimens were ground to an 80-grit finish, washed, measured and weighed.

Corrosion tests were made in the apparatus shown in Figure 1. All parts, except the glass cradle, are standard laboratory equipment. A ground glass-joint is essential to prevent loss of vapor and consequent concentration of boiling sulfuric acid. The specimen is held in a glass cradle with several holes to permit circulation of solution. One specimen was tested in each flask containing 600 ml of solution. Because reproducibility of the corrosion tests depends on the concentrations of the test solutions, details are given below for the preparation of these solutions.

Ferric Sulfate-Sulfuric Acid Solution

Measure 400.0 ml of distilled water in a 500-ml graduate and pour into the wide-mouth Erlenmeyer flask. Then measure 236.0 ml of reagent-grade sulfuric acid, whose concentration must be in the range of 95.0 to 98.0 percent by weight, into a 250-ml graduate. Add the acid slowly to the water to prevent boiling by the heat evolved.*

Weigh (trip balance) 25 g of reagent-grade ferric sulfate [containing about 75 percent $Fe_2(SO_4)_3$] and add to the sulfuric acid solution. Drop boiling chips into the flask; put condenser in place; boil the solution until all ferric sulfate is dissolved. The specimen is then immersed in the solution for 24 hours.

Hydrochloric Acid Solution

Measure 338.0 ml of water into the 1-liter Erlenmeyer flask and add 109.7 ml of reagent-grade hydrochloric acid, 36.5 to 38.0 percent by weight, using graduates and taking precautions as described above. An exposure period of 24 hours in boiling solution is generally used.

* Caution: Use eye protection and rubber gloves for handling acid. Use hood for test flask.

Chromic Acid Solution

Weigh 67 g CrO_3 and add to 600 ml of distilled water. Because of the low rate of corrosion, exposure periods of 48 to 96 hours in boiling solution are required to reveal the effect of heat treatments.

Metallographic Examination

Several series of specimens, heat treated at 100 F intervals from 800 F to 2000 F and at more frequent intervals above this temperature, were examined metallographically by light electrolytic etching in 10 percent oxalic acid solution at room temperature. Results on heat H primarily are used to illustrate the following summary.

Solution-annealed alloys of the compositions of Table 1 are essentially single-phase, austenitic, solid solutions. The only other phase visible in the microstructure (Figures 2 and 9) consists of circular islands which remain throughout the entire range of heat treatments. In agreement with previous investigators,[7,8] these islands were found to be an M_6C carbide. Spectroscopic analysis gave molybdenum, tungsten and silicon as major constituents of the residue. There were no changes in microstructure in the range of 800 F to 1150 F or 1200 F.

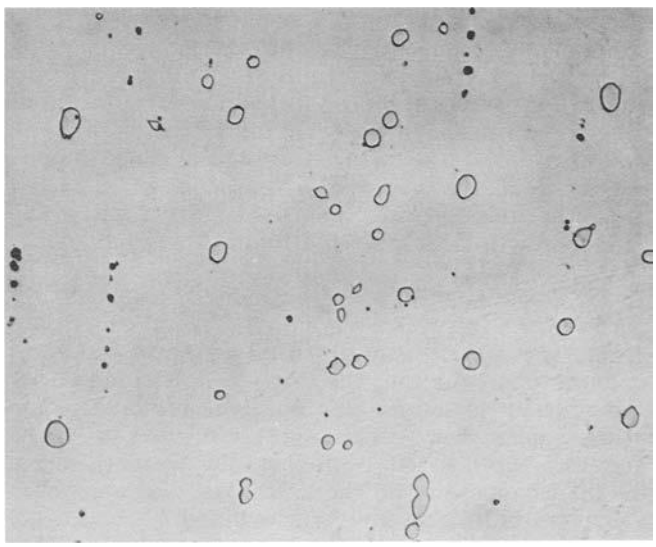


Figure 2 - Microstructure of heat H heated 1 hour at 1100 F. Electrolytically etched in oxalic acid. Solution-annealed structure containing some M_6C carbides. 650X.

Above 1200 F etching readily outlines grain boundaries (Figure 3). This structure was also examined by electron microscopy. Surfaces were coated with a film of carbon by evaporation.[9] The film was then separated from the surface by dissolving the metal in a bromine-methanol solution which dissolved all metallic phases. Some nonmetallic inclusions adhered to the carbon film and were examined in the electron microscope. A typical structure (Figure 4) for a specimen heated at 1300 F shows some tiny precipitates at the grain boundaries. Analysis of bromine-methanol residues gave an M_6C carbide, $a_c = 11.02$ Å, and molybdenum, tungsten and silicon as major constituents. No chromium carbide, $Cr_{23}C_6$, was detected in this or any of the other residues. Sigma-phase precipitates, if present, are not detected by this carbon replica technique because they are dissolved in the bromine-methanol solution. Furthermore, there is a possibility that sigma phase may be present in a submicroscopic, pre-precipitation form. This type of sigma phase has been clearly shown to occur in 18 Cr-8 Ni-Mo stainless steels and is one of the causes of rapid intergranular attack on these steels in nitric acid.[1,6,11]

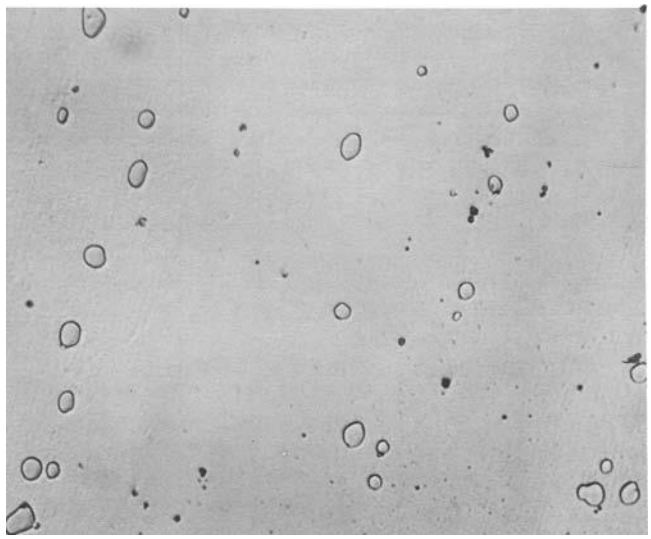


Figure 9 - Microstructure of heat H heated 1 hour at 2250 F. Electrolytically etched in oxalic acid. Solution-annealed structure containing islands of M_6C carbides. 650X.

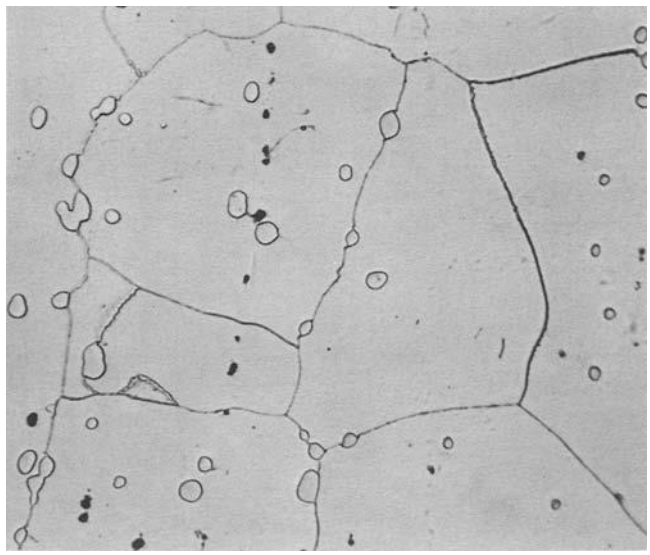


Figure 3 - Microstructure of heat H treated 1 hour at 1400 F. Electrolytically etched in oxalic acid. Etching at island carbides and at grain boundaries only. 625X.

Beginning at about 1600 F there is profuse precipitation within the grains and at twin bounda-

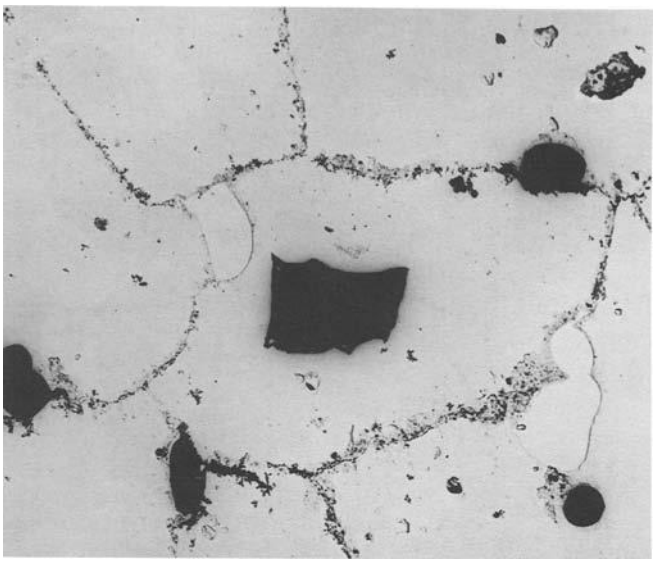


Figure 4 - Electron photomicrograph of heat H heated 1 hour at 1300 F. Carbon extraction replica indicates that tiny nonmetallics are precipitated at grain boundaries. Large carbides are probably M_6C present at all temperatures. 2,500X.

ries. The needle-like precipitate formed in the range of 1600 F to 1700 F is less readily etched than the grain boundaries at 1300 F. Increasing the temperature to 1800 F or 1900 F increases the amount of this precipitate, which is now etched more readily (Figure 5). (Because corrosion of heat H was not as pronounced when heated at these temperatures as on other heats of this investigation, a specimen from heat D was used to illustrate precipitates at 1900 F in Figure 5.) Prötzl[7] and Class, Gräfen, and Scheil[10] have identified precipitates formed at these and at higher temperatures as sigma phase, and Schley,[5] by electrolytic extraction with sulfuric acid in alcohol, as $Ni_7 Mo_6$. The analysis of residues from dissolution in bromine-methanol gave the same results as described for the heat treatment at 1400 F. In addition, an unidentified constituent having a lattice parameter of $a_c = 4.74$ Å was found. Schley[5] suggested that this may be zirconium carbide. An electron photomicrograph of precipitates formed at 1800 F is shown in Figure 6.

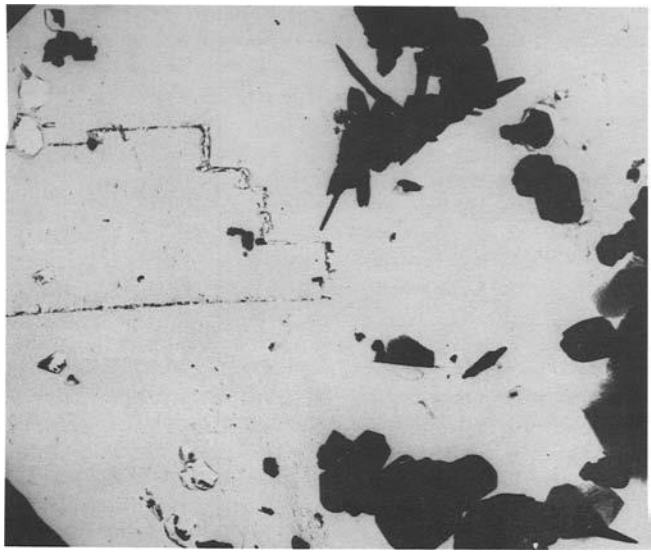


Figure 6 - Electron photomicrograph of heat H heated 1 hour at 1800 F. Carbon extraction replica of same type of structure as Figure 5. 3,000X.

Above 1900 F less precipitate is formed than below this temperature, and it is confined primarily to grain boundaries. Chains of islands surround the grains (Figure 7). These appear to be a more etch-resistant phase surrounded by carbides (Figure 8).

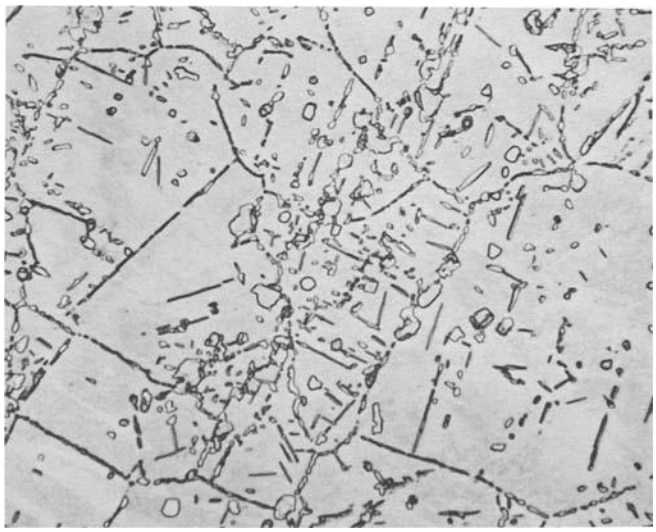


Figure 5 - Microstructure of heat D heated 1 hour at 1900 F. Electrolytically etched in oxalic acid. Precipitate forms at twin boundaries and within grains in the form of needles. 650X.



Figure 7 - Microstructure of heat H heated 1 hour at 2150 F. Electrolytically etched in oxalic acid. Precipitate is largely confined to grain and twin boundaries in the form of islands. 650X.

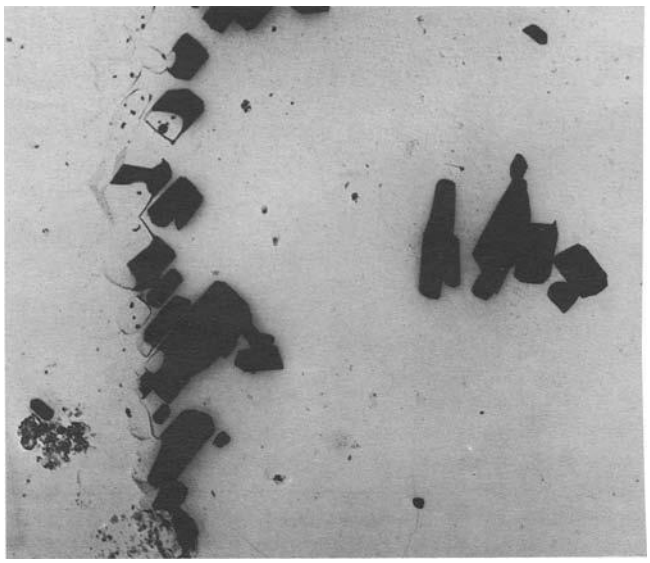


Figure 8 - Electron photomicrograph of heat H heated 1 hour at 2150 F. Carbon extraction replica of the same type of structure as Figure 7. 8,550X.

In the narrow range of 2200 F to 2275 F no precipitates are formed. The only phase present is that in the circular islands found at all temperatures and consisting of M_6C (Figure 9).

At higher temperatures, from 2275 F to 2350 F, depending on the alloy, a new precipitate is formed, probably as a result of incipient melting. This appears both at grain boundaries and at isolated points in the grains (Figure 10). The dendritic structures observed in electron photomicrographs suggest that nonmetallics, probably the low-melting M_6C carbides, are involved in this process (Figures 11 and 12). Again, X-ray analysis gave an M_6C carbide, $a_c = 11.01$ Å, and the major constituents of the residue were molybdenum, tungsten and silicon.

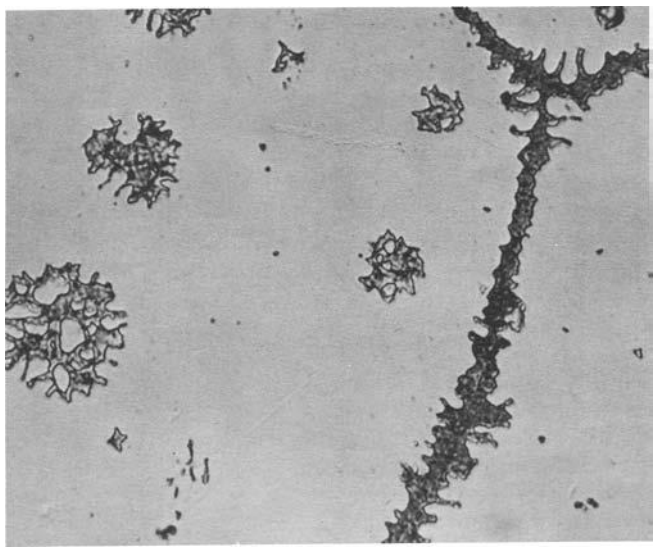


Figure 10 - Microstructure of heat H heated 1 hour at 2375 F. Electrolytically etched in oxalic acid. Structure formed during incipient fusion at boundaries of large grains and at points within grains. 650X.



Figure 11 - Electron photomicrograph of heat H heated 1 hour at 2375 F. Carbon extraction replica showing dendritic nonmetallic formed during incipient fusion. 5,200X.

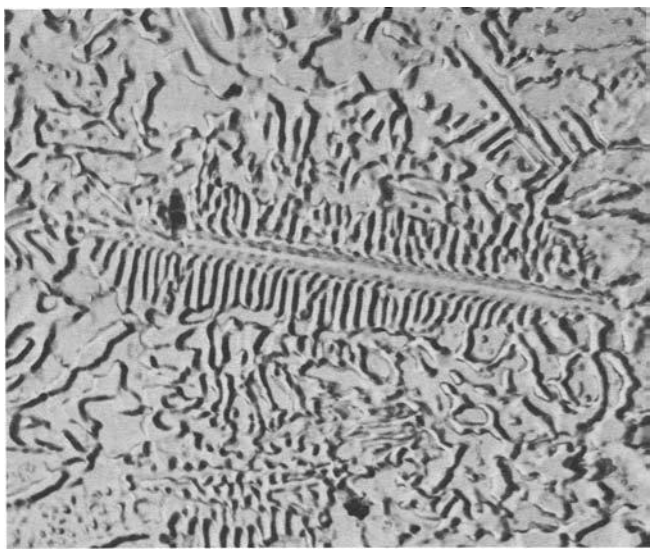


Figure 12 - Electron photomicrograph of heat H heated 1 hour at 2375 F. Carbon extraction replica of surface showing structure formed by incipient fusion. 13,500X.

Classification of Etch Structures

In addition to the light etching described above, the specimens were also deliberately over-etched electrolytically in oxalic acid for 10 to 20 seconds at 1 ampere per sq cm, in an effort to obtain characteristic etch structures that could be readily classified. When all constituents except the large circular carbides are dissolved in the austenitic matrix, steps are formed between the grains and at twin boundaries as a result of the slightly different rates of dissolution of variously oriented

grains (step structure, Figure 13). Above about 1200 F the precipitates at the boundaries cause grooves which remain relatively shallow even after prolonged etching (groove structure, Figure 14). Above 1400 F a new type of precipitate is formed which causes rapid and deep etching at grain boundaries and at twin boundaries (ditch structure). A mild form of this is shown in Figure 15. In the following discussion, a classification of step structure signifies that there is no evidence of grooves or ditches. Groove structure indicates pure grooving without any ditches. When there is some ditch structure in addition to grooves, the structure is rated as "ditch." Incipient fusion (Figure 16) is classified as high-temperature structure. Schematic cross sections of the first three structures are given in Figure 17.

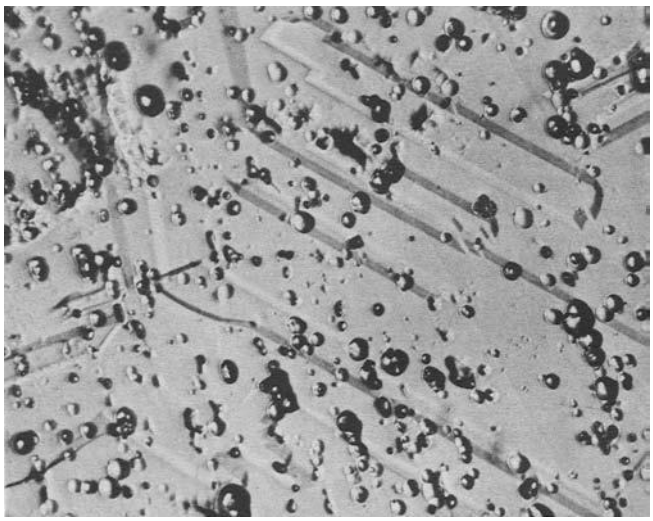


Figure 13 - Step structure, formed by over-etching in oxalic acid, 20 seconds at 1 ampere per sq cm. It is formed on solution-annealed specimens similar to those of Figures 2 and 9. 210X.

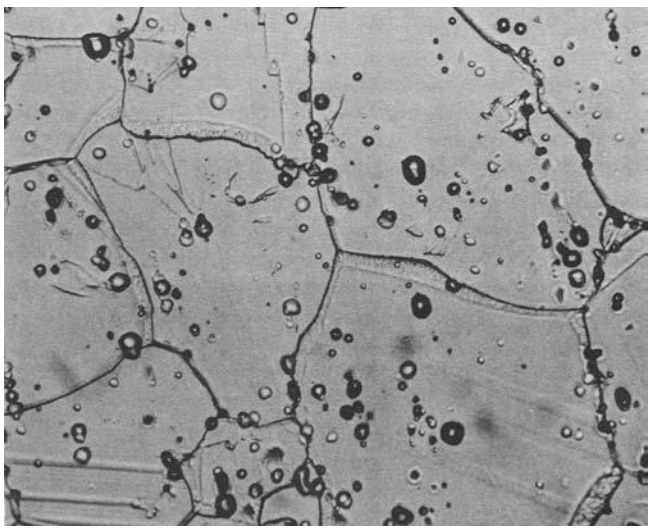


Figure 14 - Groove structure, formed by over-etching in oxalic acid, 20 seconds at 1 ampere per sq cm. This structure is formed in the range of 1200 F to 1400 F and is shown, lightly etched, in Figure 3. 425X.

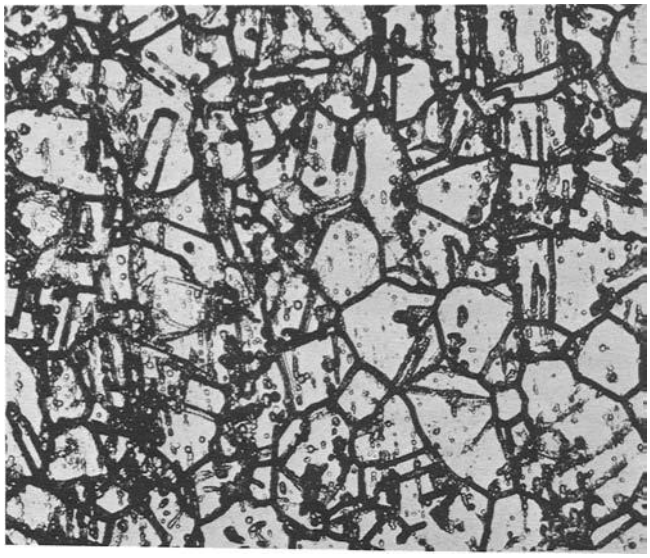


Figure 15 - Ditch structure, formed by over-etching in oxalic acid, 20 seconds at 1 ampere per sq cm. This structure is formed in the range of 1400 F to 2200 F and is shown, lightly etched, in Figure 5. 210X.

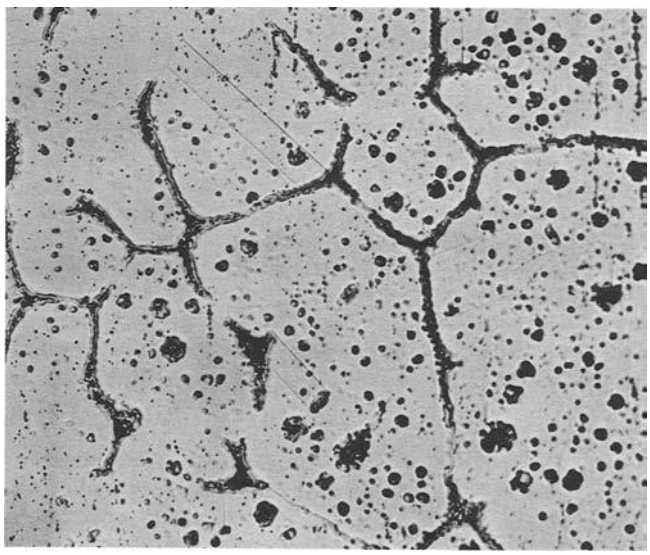


Figure 16 - High-temperature structure, formed by over-etching in oxalic acid, 20 seconds at 1 ampere per sq cm. This structure is the result of incipient fusion and is shown, lightly etched, in Figure 10. 125X.

Corrosion Tests

Weight-loss data obtained on heat B in the ferric sulfate-sulfuric acid solution and in hydrochloric acid are plotted and correlated with oxalic acid etch-structure classifications in Figure 18 as a function of heat-treating temperature. Up to about 1100 F there is no effect on corrosion rate in these solutions. As soon as the higher heat-treating temperatures produce a groove structure, the corrosion rate in both solutions increases rapidly. A maximum is reached in hydrochloric acid at about 1400 F. Above this temperature, ditch

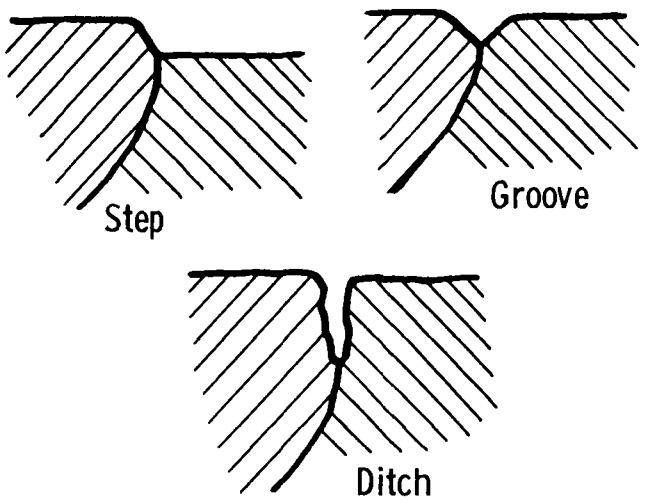


Figure 17—Cross sections of oxalic acid etch structures.

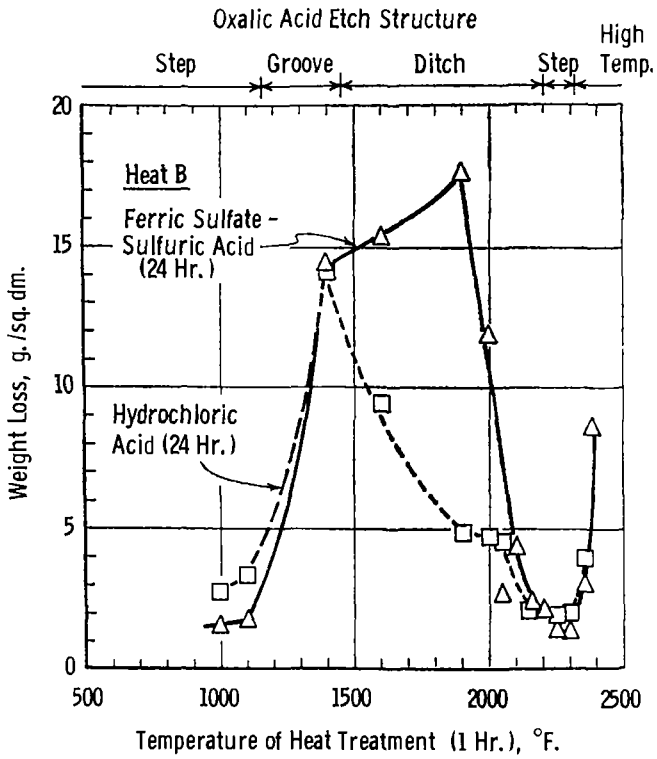


Figure 18—Effect of heat treatment on corrosion and etch structures of heat B. Solutions: boiling 50 percent sulfuric acid with 42 g/l ferric sulfate; boiling 10 percent hydrochloric acid.

structures appear and there is a rapid decrease in corrosion in this solution, but attack in ferric sulfate-sulfuric acid increases further until 1900 F. At 2150 F corrosion rates in both solutions are low, even though there is still a small amount of precipitate in the microstructure. In the narrow range of 2200 F to 2300 F, corrosion rates are as low as on the as-received material. Above this temperature the rate in both solutions again increases as a result of precipitates formed by incipient fusion.

These phenomena and several additional effects are shown in Figure 19 on heat D. Again, there is a low-temperature maximum at about 1300 F in both ferric sulfate-sulfuric acid and hydrochloric acid solutions. Above this temperature, corrosion in both solutions decreases. However, in the ferric sulfate-sulfuric acid solution this decrease is reversed, and a new maximum is reached at about 1900 F. At higher temperatures this rate decreases to a minimum value at 2200 F. Surprisingly, the rate in both solutions between 2200 F and 2300 F (step structure) is less than one-half of the rate observed on as-received specimens and those heated in the range 900 F to 1100 F, all of which had step structures. This phenomenon is discussed further in the section below on "Multiple Solution-Annealing Treatments."

Results of 48-hour tests in chromic acid on heat D are also plotted in Figure 19. Corrosion in this solution increases on specimens heated above 1100 F, but the increase is gradual and does not reach a maximum until about 1900 F, which is near the second maximum in the ferric sulfate-sulfuric acid solution. Above 1900 F there is a rapid decrease to the same low rate observed on specimens heated below 1100 F. This is in contrast to the behavior in the other two solutions in which the rate at 2200 F to 2300 F is only one-half of the as-received rate.

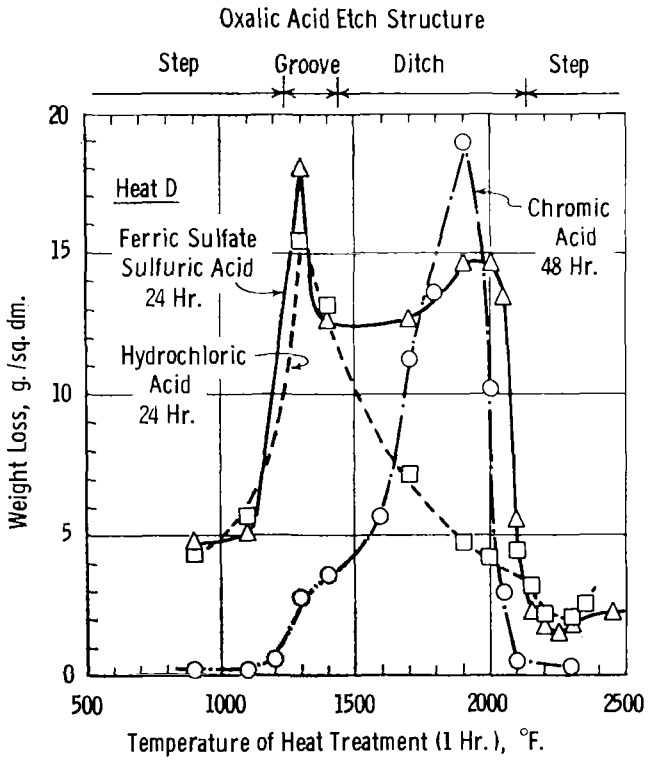


Figure 19—Effect of heat treatment on corrosion and etch structure of heat D. Solutions: boiling 50 percent sulfuric acid with 42 g/l ferric sulfate; boiling 10 percent hydrochloric acid; boiling 10 percent chromic acid (CrO_3).

In all three solutions rapid corrosion is a result of intergranular attack. This is illustrated in Figures 20 to 22. On specimens heated in the range of 1200 F to 1400 F (groove structure), preferential attack is confined largely to grain boundaries. In the range of 1500 F to 2100 F (ditch structure), precipitation also takes place on twin boundaries and elsewhere. As a result, the grains are subdivided into very small particles which are readily undermined and dislodged.

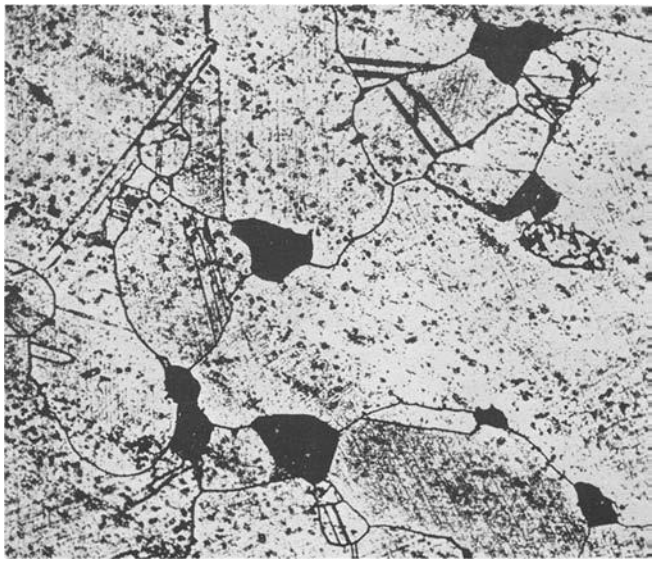


Figure 20 - Intergranular attack in ferric sulfate-sulfuric acid solution. Heat H heated 1 hour at 1400 F and immersed 3 hours in boiling solution of 50 percent sulfuric acid with 42 g/l ferric sulfate. 130X.

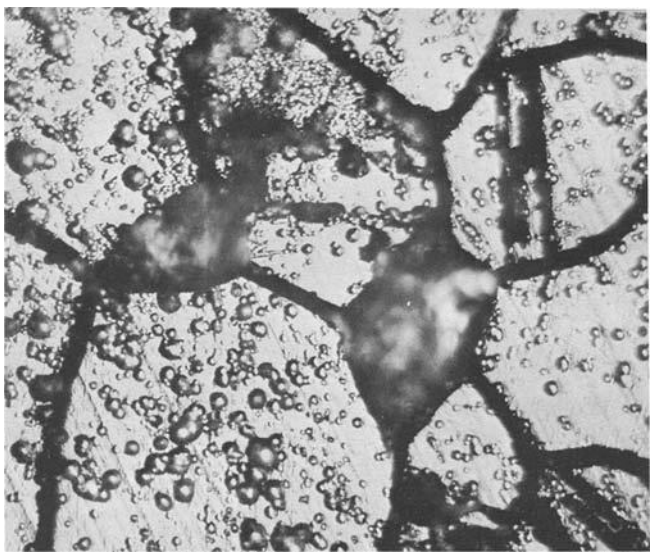


Figure 21 - Intergranular attack in hydrochloric acid solution. Heat H heated 1 hour at 1500 F and immersed 6 hours in boiling 10 percent solution. 425X.

A third type of response is shown by heat H (Figure 23), which was tested in all three solutions. Maximum corrosion rates in ferric sulfate-sulfuric acid and in hydrochloric acid occur at about 1400 F; in chromic acid, at 1900 F. However, the maximum at 1900 F is weak, an exposure of 96 hours in chromic acid being required to reveal it clearly. In ferric sulfate-sulfuric acid solution there is no maximum rate, merely an arrest. As in Figure 18, the range of low corrosion rates is very narrow: 2200 F to 2300 F for heat H.

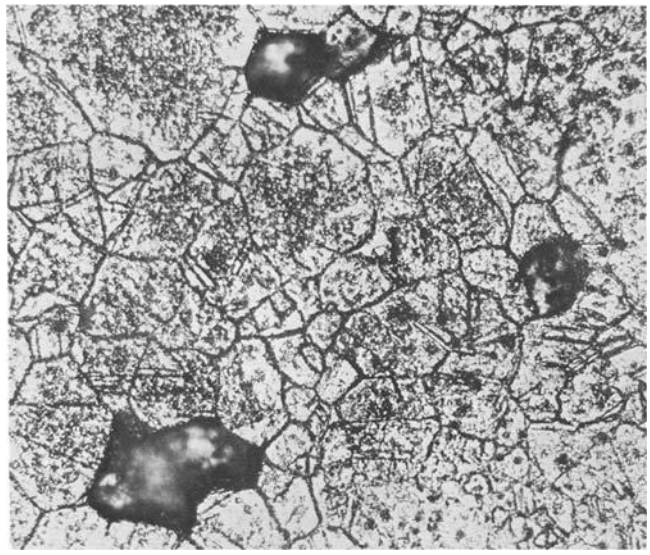


Figure 22 - Intergranular attack in chromic acid. Heat C heated 1 hour at 1900 F and immersed 26 hours in boiling 10 percent CrO_3. 210X.

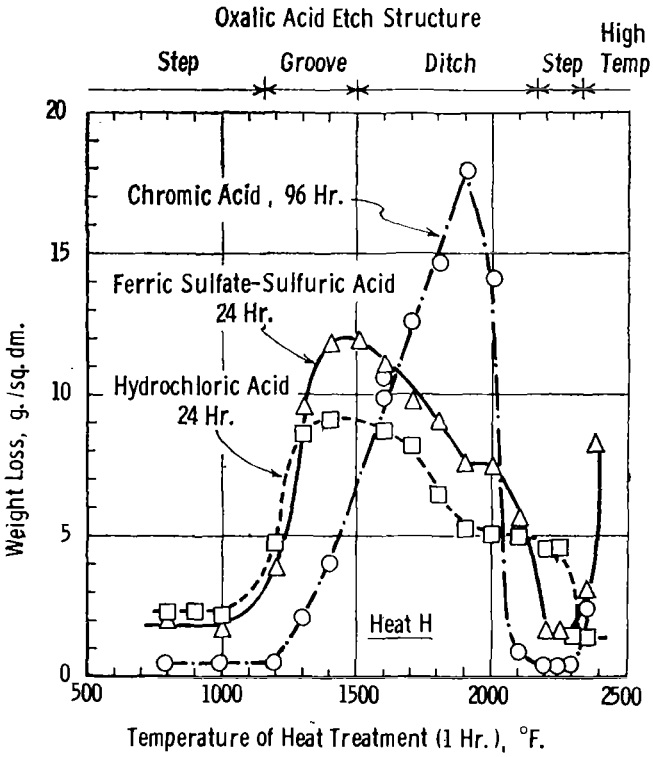


Figure 23—Effect of heat treatment on corrosion and etch structures of heat H. Solutions: boiling 50 percent sulfuric acid with 42 g/l ferric sulfate; boiling 10 percent hydrochloric acid; boiling 10 percent chromic acid (CrO_3).

Tests in Other Media

To determine whether heat treatment affects corrosion in media other than the three acids discussed above, tests were made in nitric and sulfuric acids and in ferric and magnesium chloride solutions. Detailed data on heat H in boiling 25 percent sulfuric acid and in boiling 30 percent nitric acid are plotted in Figure 24, along with the data obtained in ferric sulfate-sulfuric acid solu-

tion. It is apparent that the same heat treatments which increase corrosion in the latter solution also accelerate attack in sulfuric and in nitric acids. Pitting corrosion in ferric chloride (10 percent at 50 C) and in boiling 42 percent magnesium chloride was greatly increased on specimens of heat H heated at 1400 F and, to a lesser extent, on specimens heated at 1900 F.

Multiple Solution-Annealing Treatments

In tests on heat D (Figure 19) it was found that heating mill-annealed, as-received specimens at 2250 F, i.e., re-annealing, reduced corrosion in ferric sulfate-sulfuric acid and in hydrochloric acid from 4.5 to about 2.0 g/sq dm. Both the as-received and the re-annealed specimens had step structures, therefore were free of visible precipitates.

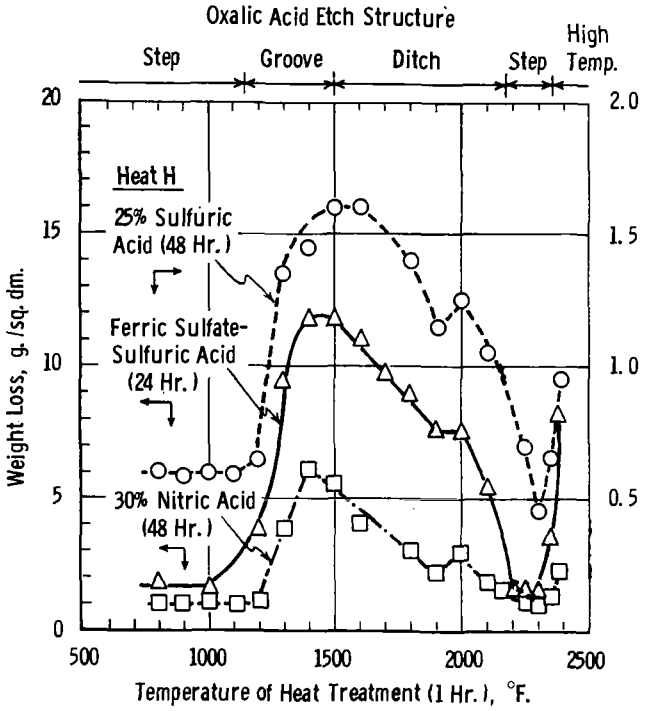


Figure 24—Effect of heat treatment on corrosion of heat H. Solutions: boiling 25 percent sulfuric acid; boiling 30 percent nitric acid; boiling 50 percent sulfuric acid with 42 g/l ferric sulfate.

Pertinent data on re-annealing for all heats are listed in Table 2. Corrosion in the ferric sulfate-sulfuric acid and the hydrochloric acid solutions on all re-annealed specimens was lower than on as-received specimens. The differences in rates are small for heats B, E, F and H, but are appreciable for heats A, C and D. In chromic acid, however, re-annealing had no effect on any of the heats.

To determine whether time at temperature or the number of annealing cycles is the determining factor, tests were made on one heat, A, which showed the re-annealing effect and one heat, H, in which there was almost no such effect. A group of specimens from each heat was first heated for 1 hour at 1900 F to form large quantities of precipitates. One specimen from each heat was then annealed at 2250 F for 4, 9, 14, 24, 34 and 64 minutes. Since 4 minutes was required to reach the annealing temperature, the length of time at temperature is found by subtracting 4 minutes from each of these values. The corrosion rates obtained on these specimens in the ferric sulfate-sulfuric acid solution are plotted in Figure 25 along with the rate obtained on specimens heated only at 1900 F. All specimens heated to 2250 F, even the 4-minute specimens, had step structures; i.e., they did not contain any visible precipitate. Length of time at temperature had no effect on the corrosion rate.

Two of the tested specimens of heat A, which had been heated for 24 minutes and 64 minutes, were then re-annealed for the same length of time as the first treatment at 2250 F. Thus, one specimen had two annealing treatments for 24 minutes each at 2250 F and the other had them for 64 minutes. The specimens were then refinished by grinding and were retested. After the double annealing treatments, the rates of these two specimens of heat A were as low as those of heat H, which had had only one solution-annealing treatment. Again, the results were independent of time at temperature. There was no difference between the 24-minute and the 64-minute specimens. Other tests on specimens as much as 1 inch thick verified that not length of time at temperature but rather the number of annealing cycles is the main factor in dissolving precipitates, i.e., in solution-annealing this alloy.

TABLE 2—Effect of Re-annealing Treatments on Corrosion

Heat[a]	Corrosion, g/sq dm								
	Ferric Sulfate-Sulfuric Acid[b]			Hydrochloric Acid[c]			Chromic Acid[d]		
	As-Rec.[e]	2250 F[f]	ΔW[g]	As-Rec.	2250 F	ΔW	As-Rec.	2250 F	ΔW
A	4.5	1.9	2.6	3.2	1.7	1.5	..	..	.....
B	1.6	1.4	0.2	2.7	1.9	0.8	..	..	.....
C	4.6	1.8	2.8	4.4	1.8	2.6	0.3	0.3	0.0 (48 hr)
D	4.7	1.4	3.3	4.3	2.1	2.2	0.2	0.3	0.0 (48 hr)
E	2.0	1.8	0.2	..	..	..	0.4	0.3	0.1 (72 hr)
F	3.2	3.2	0.0	2.6	1.8	0.8	0.3	0.3	0.0 (48 hr)
H	1.8	1.6	0.2	2.3	1.8	0.5	0.4	0.4	0.0 (96 hr)

[a] Analyses in Table 1.
[b] Boiling 50 percent sulfuric acid with ferric sulfate, 24-hour test.
[c] Boiling 10 percent hydrochloric acid, 24-hour test.
[d] 10 percent CrO_3 by wt, boiling, length of time as shown.
[e] As-Rec. = Weight loss of as-received, mill-annealed specimen or specimen heat treated below 1100 F.
[f] 2250 F = Weight loss of specimen heated 1 hour at 2250 F, water quenched.
[g] ΔW = Rate of as-received specimen minus rate of specimen heated 1 hour at 2250 F.

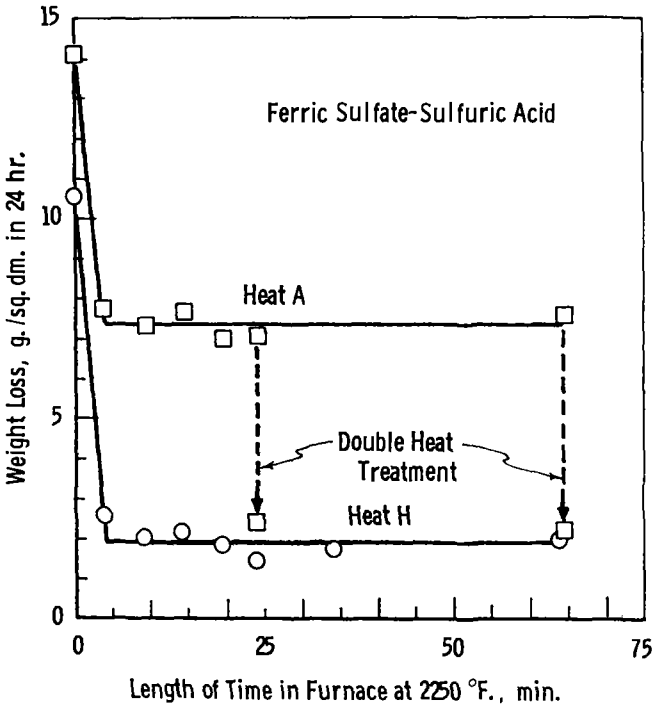


Figure 25—Effect of double solution-annealing treatment on corrosion. (Time required to heat specimen to 2250 F: 4 minutes; solution: boiling 50 percent sulfuric acid with 42 g/l ferric sulfate).

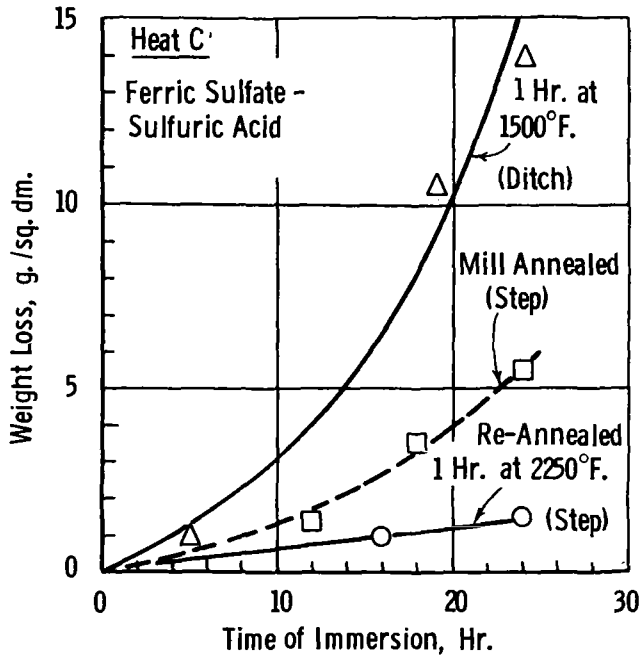


Figure 26—Effect of length of time of immersion in ferric sulfate-sulfuric acid solution. Solution: boiling 50 percent sulfuric acid with 42 g/l ferric sulfate. Mill-annealed specimen contains submicroscopic precipitate.

These results on multiple annealing treatments indicate that in some heats of Ni-Cr-Mo alloy there is incomplete solution of precipitates. They are left in a submicroscopic form. To obtain data on this, corrosion on two metallographically polished specimens was observed. Precipitates were first formed in both specimens at 1900 F, then one specimen was heated once for 1 hour at 2250 F and the other was given this solution-anneal twice. The initial stages of corrosion on the specimen given a single annealing treatment clearly outlined grains by preferential attack. No such preferential attack was observed on the specimen which had been given two annealing treatments. Weight-loss versus immersion-time curves for these specimens also showed this effect; i.e., the specimen given the single annealing treatment had a weight-loss curve similar to that observed on an intergranularly corroding specimen (Figure 26).

It was not possible to relate the effect of double-annealing on appearance to variations in composition of the seven heats investigated.

Mechanism of Corrosion

To obtain data on the mechanism of corrosion in the different types of acid solutions used in this investigation, electrode-potential measurements were made in boiling solutions with 600 ml of solution and specimens measuring 1 inch by 2 inches. The apparatus was the same as previously described.[6] A platinized platinum electrode was immersed to determine the oxidation-reduction potential of the solutions, and the steady-state corrosion potentials were measured on variously heat-treated alloy specimens. Table 3 contains a summary of these measurements.

The acids fall into two groups: those in which there is hydrogen evolution (hydrochloric and pure sulfuric acids) and those in which the cathodic process consists of the reduction of other cations, i.e., ferric ions in ferric sulfate-sulfuric acid and hexavalent chromium ions in chromic acid solution. Heat treatment of the Ni-Cr-Mo alloys does not affect their steady-state corrosion potentials in either type of solution.

Neither the corrosion potential of the alloy nor the oxidation-reduction potential of the solution (Pt electrode) indicates which of the two corrosion maxima is exhibited, or whether both are revealed, by a given solution. To obtain additional data on this problem, tests were made on heat C in oxalic acid solution for 230 hours (Table 3). The corrosion potential of the alloy in this acid (-0.21 v) is even more negative than in hydrochloric acid

TABLE 3—Electrode Potential Measurements in Boiling Solutions

Solution	Potential vs Saturated Calomel Electrode, v				Corrosion Maxima	
		Heat H[a]				
	Pt (Platinized)	Annealed	1 Hr at 1400 F	1 Hr at 1900 F	1400 F	1900 F
Oxalic Acid (10%)	+0.15[d]	−0.21	−0.21	−0.21	Yes	Yes
Hydrochloric Acid (10%)	+0.32[d]	−0.20	−0.20	−0.20	Yes	No
Sulfuric Acid (25%)	+0.35[d]	−0.16	−0.17	−0.17	Yes	Yes
Ferric Sulfate-Sulfuric Acid[b]	+0.58	+0.56	+0.56	+0.56	Yes	Yes
Nitric Acid (30%)	+1.00	+0.55	+0.62	+0.54	Yes	Yes
Chromic Acid[c] (10% CrO_3)	+1.02	+0.84	+0.85	+0.85	No	Yes

[a] Analysis in Table 1.
[b] 50 percent sulfuric acid containing 5.5 g/l Fe^{+3} + 1.15 g/l Fe^{+2}.
[c] Potentials were unaffected by addition of 5 g/600 ml of Cr $(OH)_3$.
[d] These potentials indicate the presence of some oxygen.

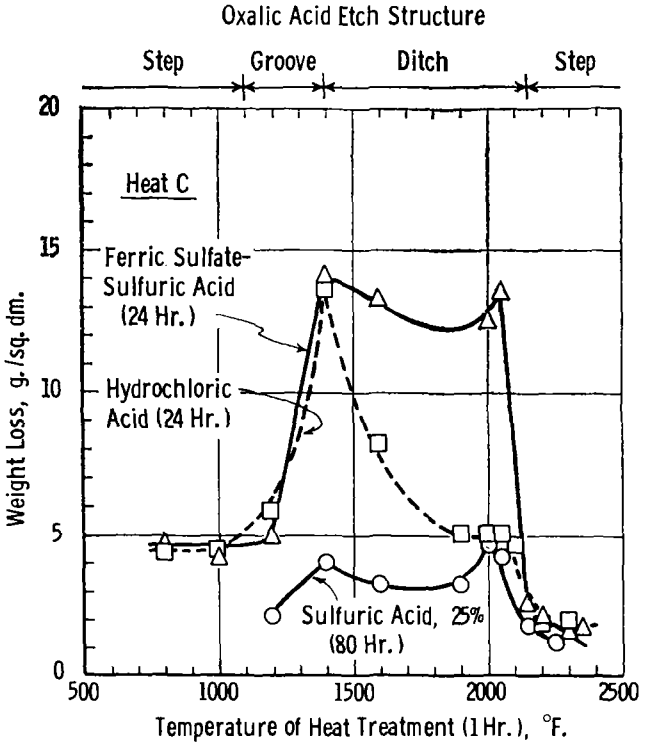


Figure 27—Effect of heat treatment on oxalic acid etch structure and corrosion of heat C. Solutions: boiling 50 percent sulfuric acid with 42 g/l ferric sulfate; boiling 10 percent hydrochloric acid; boiling 25 percent sulfuric acid. (Solution changed at 16-hour intervals.)

(-0.20 v). Heat C has pronounced corrosion maxima at both 1400 F and 1900 F and shows the multiple heat-treatment effect in ferric sulfate-sulfuric acid solution (Figure 27). Even though the corrosion potentials are very similar in these two acids, hydrochloric acid reveals primarily the maximum near 1400 F. (Figure 27 for heat C and Figures 18, 19 and 23 for other heats), and oxalic acid reveals both maxima at 1400 F and at 1900 F. Data obtained on heat C in pure (25 percent) sulfuric acid give further support to the view that the corrosion potential does not determine which maxima are detected in a given solution. The corrosion potential in sulfuric acid is -0.16 v. This is near that in hydrochloric acid (-0.20 v), yet both maxima are also revealed in sulfuric acid (Figure 27). Thus, the anion of the acid, rather than the corrosion potential, determines which maximum is revealed.

In oxidizing solutions both maxima are revealed in ferric sulfate-sulfuric acid and in nitric acid, and only the 1900 F maximum in chromic acid.

In hydrochloric, oxalic and pure sulfuric acids the corrosion potentials are near that of a hydrogen electrode, indicating that the dissolution process is governed by the cathodic reaction, the evolution of hydrogen gas. This is supported by results of other tests in 10 percent hydrochloric acid, with and without a platinized platinum gauze in contact with the Ni-Cr-Mo specimen. Contacting the specimen with the gauze increases its rate of dissolution by a factor of 8. Thus, increasing the surface area on which hydrogen can be evolved increases the rate of dissolution.

The increase in rate of corrosion caused by heat treatments that form precipitates may be the result of the increased number of sites where hydrogen is readily evolved and/or of changes in alloy composition immediately adjacent to the precipitates. The difference in behavior of the Ni-Cr-Mo alloy in hydrochloric and in pure sulfuric acid suggests that the latter factor is the more important. For a given rate of hydrogen evolution, the anodic reaction on annealed specimens is distributed more or less uniformly over the surface. In contrast, when zones adjacent to precipitates are depleted in alloy content, in heat-treated (sensitized) specimens, most of the anodic reaction, electrochemically equivalent to the given rate of hydrogen evolution, is concentrated at these zones. The result is rapid, preferential attack leading to intergranular penetration, undermining, and dislodgement of grains.

In ferric sulfate-sulfuric acid and in chromic acid solutions, the corrosion potentials are identical to, or near, the potentials of the Fe^{+3}/Fe^{+2} and Cr^{+6}/Cr^{+3} reactions on the platinum electrode. There is no hydrogen evolution, and the corrosion process is controlled by polarization of anodic areas; i.e., there is anodic control. The alloy surfaces are passivated. This passive state is a dynamic condition in which there are continual dissolution and reformation of a protective, passive film by a reaction between the dissolving metal and the corroding solution. Even in specimens containing precipitates, both the grain faces and the boundaries are passive. However, at the boundaries, the corrosion current (metal dissolution) required to keep the film in repair, thereby polarizing the boundaries to the same potential as the grain faces, is much greater. The reason for this is that the precipitates deplete the adjacent metal of alloying elements. Again, the result is preferential attack at the boundaries leading to dislodgement of grains.

Application of these concepts to the differences in action of the reducing and oxidizing solutions in revealing the 1400 F and 1900 F corrosion maxima leads to the following conclusions. In reducing acids, alloy corrosion is a function of the anion of the acid, chloride vs sulfate. Chloride ions affect the rate primarily when depletions of alloying elements are of the type produced by precipitates formed during heat treatments in the range of 1200 F to 1400 F (groove structure). Sulfate ions affect corrosion on depleted zones of this type and on depleted zones associated with ditch structure (the high-temperature corrosion maxima at 1700 F to 2050 F).

In oxidizing acids, anodic polarization, therefore the presence or absence of intergranular attack, is affected by the cations in the solution, ferric or hexavalent chromium ions. Thus, low-temperature depletion (groove structure) leads to large differences in grain-boundary and grain-face polarization only in ferric sulfate-sulfuric acid solution. The high-temperature type of depletion

(ditch structure) leads to differences in anodic polarization between grain boundaries and grain faces in both chromic acid and ferric sulfate-sulfuric acid solution.

Corrosion of the Ni-Cr-Mo alloy in oxidizing solutions is similar to intergranular attack on austenitic stainless steels in such solutions.[6] However, intergranular attack on Ni-Cr-Mo alloys in reducing acids, boiling hydrochloric and sulfuric acid solutions, is in marked contrast to the behavior of stainless steels. There is no intergranular attack on sensitized 18 Cr-8Ni stainless steels in these acids.[12] This is probably related to the fact that relatively large variations in the chromium content of stainless steels have little or no effect on their corrosion rate in reducing acids. For example, increasing the chromium content from 15 to 25 percent in iron-chromium alloys is without effect on their corrosion rates in sulfuric acid.[13] As a result, the corrosion rate of chromium-depleted zones adjacent to chromium carbide precipitates in stainless steels is the same as that of undepleted grain faces, and there is no preferential intergranular attack.

In contrast, variations in chromium content of Ni-Cr-Mo alloys does affect their corrosion in hydrochloric acid.[10] Therefore, depleted zones adjacent to precipitates do corrode more rapidly than grain faces.

Summary and Conclusions

Typical effects of heat treatments on Ni-Cr-Mo alloys observed in this investigation have been summarized in the schematic diagram of Figure 28.

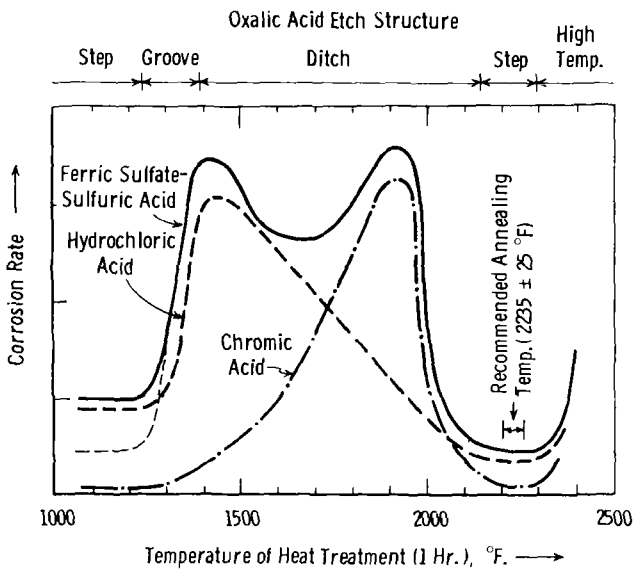


Figure 28—Schematic summary of relationship of heat treatment, etch structures and corrosion of wrought Ni-Cr-Mo alloys.

1. Heating for 1 hour up to 1100 F or 1200 F: no effect on microstructure (step structure, Figure 13) or on corrosion in any of the solutions used in this investigation.

2. Range 1200 F to 1400 F: formation of a precipitate, primarily at grain boundaries, leading to pure groove structure (Figure 14). A large increase in rate of corrosion in hydrochloric acid, ferric sulfate-sulfuric acid, pure sulfuric acid and nitric acid. A small increase of corrosion in chromic acid.

3. Range 1300 F to 1500 F: low-temperature maximum occurs in all solutions tested except chromic acid, which does not reveal this maximum.

4. Range 1400 F to 2200 F: etch structures contain some ditch structure along with other structures, or consist of pure ditch structure (Figure 15). Precipitation takes place not only at grain boundaries in this range but also at twin boundaries and throughout the grains. In the range of 2050 F to 2150 F the amount of this precipitate is relatively small and does not greatly affect the corrosion rate.

5. Range 1500 F to 1700 F: decrease in corrosion rate in hydrochloric acid and increase in corrosion rate in chromic acid.

6. Range 1700 F to 2050 F: high-temperature maximum occurs in all but hydrochloric acid, which does not detect this maximum. Rate in hydrochloric acid gradually decreases in this range.

7. Range 2050 F to 2200 F: corrosion in all solutions decreases to low rate. The small amount of ditch structure formed in this range does not have a large effect on corrosion.

8. Range 2200 F to 2275 F: all precipitates, except large island carbides, are in solid solution (step structure, Figure 13). Corrosion rates in all solutions are low.

9. Range 2235 ± 25 F: recommended for commercial annealing practice to dissolve precipitates and prevent incipient fusion by overheating.

10. Above 2275 F: incipient fusion leading to formation of precipitate (high-temperature structure, Figure 16). Presence of this precipitate reduces mechanical properties.[14] Large quantities greatly increase corrosion in all solutions used in this investigation.

Even though the high-temperature maximum is not detected in hydrochloric acid nor the low-temperature maximum in chromic acid, there is some effect of heat treatment in these ranges on corrosion in the two acids.

Positive identification of the phases that precipitate in this alloy is difficult and is complicated by the possibility that submicroscopic phases may be involved, especially in the temperature range in which groove structure is found, 1200 F to 1400 F. A submicroscopic form of sigma phase has been

found to cause intergranular attack of 18 Cr-8 Ni-Mo stainless steels in nitric acid.[1,6,11] Precipitates formed in the range of 1600 F to 2100 F have been identified as sigma phase[7,10] and $Ni_7 Mo_6$[5] by previous investigators. This phase in microscopic or submicroscopic form is primarily responsible for the effect of heat treatment on corrosion resistance in these alloys. Isolation and analysis of nonmetallic residues from bromine-methanol solution showed only an M_6C carbide with molybdenum, tungsten and silicon as the major constituents. This was the same for specimens heated at 1300 F, 1800 F, 2250 F and 2375 F. Only the quantity of residue varied. It was greatest for the specimens heated at 1300 F and at 1800 F. Chromium carbide, $C_{23}C_6$, was not found.

In some heats of Ni-Cr-Mo alloy, multiple solution-annealing cycles are more effective in dissolving precipitates than is length of time at annealing (2250 F) temperature. Incomplete dissolution in the matrix of a submicroscopic precipitate appears to be responsible for the relatively high corrosion rate of some heats of alloy which have had only one solution-annealing treatment.

Both in reducing and in oxidizing acids, preferential attack adjacent to precipitates appears to be a result of depletion of alloying constituents in these zones. In reducing acids corrosion is controlled by the rate of hydrogen evolution. A large part of the corresponding anodic corrosion current is concentrated in the depleted zones because of their lower corrosion resistance. In oxidizing acids, corrosion is governed by anodic polarization (anodic control). No hydrogen is evolved and the cathodic reaction consists of the reduction of ferric, hexavalent chromium or other ions. There is preferential attack at depleted zones because the corrosion current required to polarize them to the passive potential is greater than that required to polarize undepleted grain-face surfaces to the same passive potential.

The corrosion potential of Ni-Cr-Mo alloys in reducing and in oxidizing solutions is unaffected by the presence of precipitates formed by heat treatments.

Considerable variation in response to heat treatments has been observed among the seven heats studied in this investigation. It has not been possible to relate these differences in behavior to the small variations in the compositions given in Table 1. For example, data on corrosion maxima, summarized in Table 4, are independent of the relatively small variations in carbon and silicon contents of seven heats. In a study on heats containing from zero to 2.7 percent silicon, Class, Gräfen and Scheil[10] concluded that silicon promotes the formation of sigma phase.

On the basis of the results and conclusions described above, an evaluation method has been formulated for routine detection of susceptibility to intergranular attack in Ni-Cr-Mo alloys. The 24-hour test described in the following section is used primarily to determine the effectiveness of solution-annealing treatments. To be successful, these treatments must be made under carefully controlled conditions, 2235 ± 25F, and must be followed by a rapid quench.

The conclusions described in this section are applicable only to wrought Ni-Cr-Mo alloys. An investigation of three heats of cast Ni-Cr-Mo alloys has shown that their response to heat treatment and their behavior in acid solutions differ markedly from that described in this article for wrought alloys.

TABLE 4—Corrosion Maxima: Rates and Temperatures*

Heat	Low-Temperature Maximum				High-Temperature Maximum			
	Ferric Sulfate-Sulfuric Acid		Hydrochloric Acid		Ferric Sulfate-Sulfuric Acid		Chromic Acid	
	Rate g/sq dm/24 hr	Temp., F	Rate g/sq dm/24 hr	Temp., F	Rate, g/sq dm/24 hr	Temp., F	Rate, g/sq dm/48 hr	Temp., F
A	11.8	1400 (arrest)	9.8	1400	14.7	1900	....	....
B	14.0	1400	14.5	1400	17.5	1900	....	....
C	14.0	1400	13.5	1400	13.5	2050	19.0	1900
D	18.0	1300	15.5	1300	14.7	1950	16.0	1900
E	17.4	1500	....	....	None	None	7.7	1700
F	13.8	1350	9.8	1400	9.5	1900 (arrest)	18.4	1900
H	12.0	1450	9.2	1450	7.5	1950 (arrest)	7.6	1900

* Temperature of heat treatment, 1 hour in argon atmosphere, water quenched.
Corrosion tests in: boiling 50 percent sulfuric acid with 42 g/l ferric sulfate; boiling 10 percent hydrochloric acid; boiling 10 percent chromic acid.

Formulation of an Evaluation Method

Previous experience with evaluation tests for stainless steels has shown that acceptance and rejection tests that are to be used in commercial practice by persons with diverse interests and experience should have the following characteristics:

1. If possible, rejection of material should be based on a quantitative test resulting in a numerical value, such as a corrosion rate.

2. Laboratory techniques must be highly standardized and so elementary that laboratory personnel not specifically trained in these techniques can readily perform and interpret the tests.

3. The evaluation method should be based, as much as possible, on a scientific understanding of the properties of the material rather than on empirically established practices.

Three different methods of evaluation were considered in formulating the recommended procedure:

Use of Oxalid Acid Etch Only. Accept material having step structure and reject all material having other etch structures.

This would be the simplest and most rapid method. However, rejection would be based on evaluation of microstructures rather than on a quantitative corrosion rate. Furthermore, in certain heats the incompletely dissolved, but invisible, form of precipitate (which does affect the rate of corrosion) would not be detected because such material also has a step structure.

Ferric Sulfate-Sulfuric Acid Test Only. Accept all material having a corrosion rate below a certain maximum permissible value.

This procedure detects the effect on corrosion of visible and invisible precipitates but does not reveal the presence of small amounts of incipient fusion, which are undesirable because of their deleterious effect on mechanical properties.[14] For this reason a combination of two tests is recommended.

Combined Use of Oxalic Acid Etch and Ferric Sulfate-Sulfuric Acid Test. Etch first, examine structure microscopically, and reject only those specimens which have evidence of incipient fusion (high-temperature structure, Figure 16). All other specimens are tested for 24 hours in the boiling ferric sulfate-50 percent sulfuric acid solution (apparatus in Figure 1). Examination of data on weight loss in ferric sulfate-sulfuric acid solution (Table 2) shows that specimens of all heats annealed at 2250 F and water-quenched have weight losses less than 3.8 g/sq dm in 24 hours, or a rate less than 0.050 inch/month.*

This evaluation method detects incipient fusion and the effects of visible and invisible precipitates. As the appearance of incipient fusion (overheating) is rare in commercial practice, almost all rejections will be on the basis of quantitative corrosion rates. Those exceeding 0.050 inch/month can be reduced by one or more additional annealing treatments at 2235 ± 25 F.

Acknowledgment

The writer wishes to thank S. J. Kucharsey for his skillful assistance with metallographic work and corrosion tests, E. D. Nicholson for the electron micrographs, R. P. Jackson for assistance with corrosion tests, and Dr. G. Teufer for X-ray data.

Alloys tested and heat analyses were supplied by the Haynes Stellite Co., Kokomo, Indiana.

References

1. M. A. Streicher. A.S.T.M. Bulletin No. 229, p 77 (1958) April.
2. E. Brauns and G. Pier. Mannesmann Research Laboratory, Duisburg-Huckingen, Germany. Private communication.
3. H. J. Rocha as reported by K. Bungardt and H. H. Weigand. Z. Metallkunde, 50, 11-18 (1959).
4. H. Gräfen and G. Böhm. Z. Metallkunde, 51, 245 (1960).
5. J. R. Schley. Haynes Stellite Company, Kokomo, Indiana. Private communication (1959) and letter of May 27, 1963.
6. M. A. Streicher. J. Electrochem. Soc., 106, 161 (1959).
7. M. Prötzl. Arch. Eisenhüttenw., 29, 745-56 (1958).
8. E. D. Weisert. Corrosion, 13, 659t-671t (1957) October.
9. D. E. Bradley. J. Inst. Met., 83, 35 (1954).
10. I. Class, H. Grafen and E. Scheil. Z. Metallkunde 53, 283-93 (1962).
11. W. O. Binder and C. M. Brown. A.S.T.M. Special Tech. Publ. No. 93, Symposium on Evaluation Tests for Stainless Steels, p 146 (1949).
12. M. A. Streicher. A Testing System for Detecting Susceptibility to Rapid Intergranular Attack in Various Grades of Austenitic Stainless Steels. To be published.

---

* Inches/month = $\frac{31.7 \times \Delta W}{A \times t}$, where t = time of exposure in hours.

A = area of specimen in sq cm, and ΔW = weight loss in g.

13. M. A. Streicher. Corrosion, 14, 59t-70t (1958) February.

14. Literature on Hastelloy C. Haynes Stellite Company, Kokomo, Indiana.

A Testing System for Detecting Susceptibility to Rapid Intergranular Attack in Various Grades of Austenitic Stainless Steels

By M. A. Streicher

Summary(1)

Most of the problems in this field were sharply delineated[1] in the "Symposium on Evaluation Tests for Stainless Steels," held in 1949 by the American Society for Testing and Materials. Investigations on intergranular corrosion undertaken since then have resulted in information and new, rapid testing methods which have largely fulfilled the future needs as defined in the papers and discussions at that time. The purpose of the present paper is to outline a rational testing sequence for evaluating the susceptibility of various grades of stainless steels to rapid intergranular attack by means of a description of the essential characteristics and fields of application of presently available test methods in the light of recent research on intergranular corrosion.

TABLE 1 - **APPLICATION OF EVALUATION TESTS FOR DETECTING SUSCEPTIBILITY TO INTERGRANULAR ATTACK IN AUSTENITIC STAINLESS STEELS**

The Oxalic Acid Etch Test may be applied to the grades of stainless steels listed in the rectangles when used in connection with the test indicated by the arrow.

OXALIC ACID ETCH TEST

AISI: 304, 304L ACI: CF-3, CF-8	AISI: 304, 304L, 316, 316L, 317, 317L ACI: CF-3, CF-8, CF-3M, CF-8M	AISI: 316, 316L, 317, 317L
↓	↓	↓
NITRIC ACID TEST* (240 hr. in boiling solution)	**FERRIC SULFATE-SULFURIC ACID TEST** (120 hr. in boiling solution)	**NITRIC-HYDROFLUORIC ACID TEST** (4 hr. at 70°C.)
Chromium carbide in: 304, 304L, CF-3, CF-8 Chromium carbide and sigma phase in (a): 316, 316L, 317, 317L, 321, 347, CF-3M, CF-8M End-grain in: all grades	Chromium carbide in: 304, 304L, 316, 316L, 317, 317L, CF-3, CF-8 Chromium carbide and sigma phase in: 321, CF-3M, CF-8M (b)	Chromium carbide in: 316, 316L, 317, 317L

AISI: American Iron and Steel Institute Designations for austenitic stainless steels.
ACI: Alloy Casting Institute Designations.
(a) Must be tested in Nitric Acid Test when destined for service in nitric acid.
(b) To date, no data have been published on the effect of sigma phase on corrosion of AISI 347 in this test.

NOTE: For each corrosion test, the types of susceptibility to intergranular attack detected are given along with the grades of stainless steels in which they may be found. These lists may contain grades of steels in addition to those given in the rectangles. In such cases, the acid corrosion test is applicable, but not the Oxalic Acid Etch Test.

* The Nitric Acid Test is also applied to AISI 309, 310, 348, and AISI 410, 430, 446, and ACI CN-7M

(1) Only this Summary was submitted by the author. It is taken from the section on austenitic stainless steels in "Theory and Application of Evaluation Tests for Detecting Susceptibility to Intergranular Attack in Corrosion Resistant Alloys," which is to be published elsewhere.

Metallurgical factors in stainless steels which affect corrosion in solutions used for evaluation tests include precipitates of chromium carbides, sigma phases in molybdenum-bearing and in stabilized grades of stainless steels, nonmetallic inclusions and grain size. The testing sequence

Copyright© 1965 by ASTM International

www.astm.org

described below is based on the following tests: Oxalic Acid Etch,[2] Ferric Sulfate-Sulfuric Acid,[3] Nitric Acid,[4] and Nitric-Hydrofluoric Acid.[5] This sequence (Table 1) is based on the fact that sigma phase in Cr-Ni-Mo steels, which may or may not be visible in the microstructure, may lead to high corrosion rates only in nitric acid, and that sigma phase in stabilized alloys, which also may or may not be visible in the microstructure, may lead to high corrosion rates in both the nitric acid and ferric sulfate-sulfuric acid solutions.

Only those grades of stainless steels are listed for which data on their performance in various evaluation tests have been furnished. Other grades may be added as new data are made available. The choice of the corrosion evaluation test and the applicability of the etch test for screening are governed by the metallurgical factors leading to rapid intergranular corrosion and by the type of environment to which the steel is to be exposed in service; i.e., whether or not it will be exposed to nitric acid.

The oxalic acid etch test is a rapid method for identifying, by simple etching, those specimens of certain grades of steel which are essentially free of chromium carbide precipitate. These specimens will have low corrosion rates in certain corrosion tests and can, therefore, be eliminated (screened) from testing as "acceptable." In most cases, the 120-hour ferric sulfate-sulfuric acid test in combination with the oxalic acid etch tests provides the required information in the shortest time. All grades of stainless steels listed in Table 1 may be evaluated in this test except those specimens of molybdenum-bearing grades (e.g., Types 316, 316L, 317 and 317L) which represent steel intended for service in nitric acid, which is rare in commercial practice. And of all the grades which are listed for testing in the ferric sulfate-sulfuric acid solution, only Types 321 and 347 cannot be screened by etching in oxalic acid.

On AISI Types 316, 316L, 317 and 317L only, the 4-hour nitric-hydrofluoric acid test may be used in place of the ferric sulfate-sulfuric acid test to provide test results in 4 hours rather than in 120 hours.

The 240-hour nitric acid test must be applied to stabilized steels and to the few molybdenum-bearing grades intended for service in nitric acid and to all grades of steel which might be subject to end-grain corrosion in nitric acid service.

References

1. F. L. LaQue. A.S.T.M. STP No. 93, "Symposium on Evaluation Tests for Stainless Steels," pp 1-40 (1949).
2. M. A. Streicher. A.S.T.M. Bulletin No. 188, p 35 (February, 1953).
3. M. A. Streicher. A.S.T.M. Bulletin No. 229, pp 77-86 (April, 1958).
4. A.S.T.M. Designation A262-55T, "Recommended Practice for Boiling Nitric Acid Test for Corrosion Resisting Steels," A.S.T.M. Book of Standards, 1961, Part 3, p 382, American Society for Testing and Materials, Philadelphia, Pennsylvania.
5. D. Warren. A.S.T.M. Bulletin No. 230, pp 45-56 (May, 1958).

Effect of Heat Treatment, Composition and Microstructure on Corrosion of 18 Cr-8Ni-Ti Stainless Steels in Acids

By M. A. Streicher*

Abstract

Titanium additions to 18Cr-8Ni steels can effectively eliminate susceptibility to intergranular attack associated with the precipitation of chromium carbides. However, these additions also drastically reduce the grain size of these steels and promote the formation of sigma phase. Both of these factors modify the behavior of titanium-stabilized steels in corrosive environments. A detailed investigation of the influence of heat treatment and microstructure on the corrosion resistance of four titanium-stabilized, AISI 321, heats is described.

Incomplete stabilization of carbon by titanium leads to precipitation of chromium carbides on heating in the range of 800 F to 1600 F. This type of susceptibility is readily detected in the oxalic acid etch test, the nitric-hydrofluoric acid test, the copper sulfate-sulfuric acid test, the ferric sulfate-sulfuric acid test, and in the nitric acid test.

A second type of susceptibility to intergranular attack is associated with the formation of sigma phase, which may precipitate in a submicroscopic form during heating in the range of 1150 to 1550 F. It is detected only in the nitric acid test and, to a lesser extent, in the ferric sulfate-sulfuric acid test.

The action of various acid solutions on titanium-stabilized stainless steels are compared by means of metallographic studies of microstructures and of progressive corrosion, and by measurements of weight loss and change in electrical resistance of corroding specimens. The data obtained are used to explain the action of acids on these steels and to recommend procedures for evaluation testing.

Titanium is used in 18Cr-8Ni steels to prevent the precipitation of chromium carbides during exposure to temperatures in the range of 800 F to 1700 F, for example during welding. Precipitation of chromium carbides at grain boundaries may cause rapid intergranular attack in a large number of acid media. However, in addition to preventing the formation of chromium carbides by combining with carbon, titanium additions drastically reduce the grain size of these steels and promote the formation of sigma phase. Both of these factors, in turn, modify the behavior of these steels in corrosive environments. The present investigation was undertaken to determine the effect of heat treatment, composition and microstructure of titanium-stabilized steels (AISI 321) on their performance in solutions used for evaluation tests. This information provides criteria for the selection of evaluation methods which may be applied to these steels to detect susceptibility to rapid intergranular attack.

Metallography of Titanium-Stabilized Stainless Steel

Nonmetallic Inclusions

The microstructure of titanium-stabilized 18Cr-8Ni stainless steels has been studied extensively by Simpkinson.[1] It consists of a matrix of austenite in which are distributed carbide and carbonitride phases, and some ferrite. These steels are readily recognized in the "as-polished" condition by characteristic nonmetallic inclusions. One type is cube-shaped and has been identified as a nitrogen-rich solid solution of TiN and TiC. Another type of inclusion consists of TiC with perhaps some TiN in solid solution and appears as irregularly shaped particles located at grain boundaries. In addition, titanium sulfide, Ti_2S, is found in residues derived from dissolved steels.[2,3] By electrolytic extraction methods,[4,5] other inclusions have been separated from annealed Type 321 steel, SiO_2, FeO, Cr_2O_3, TiO_2 and Al_2O_3. The source of the aluminum oxide is aluminum added during the steel-making process. Aluminum is employed to deoxidize the molten steel prior to the addition of low-carbon ferrotitanium. This deoxidation is considered necessary to obtain optimum recovery of titanium.[6]

Titanium Carbide

Titanium combines more readily with carbon in these steels than does chromium. However, to be effective, the amount of titanium added must be sufficient to combine with all the carbon which may precipitate at the temperature of the lowest solubility, about 1200 F, and there must be an opportunity for titanium to react with carbon. The

* Engineering Materials Laboratory, Engineering Department, E. I. du Pont de Nemours & Co. Wilmington, Delaware.

Copyright© 1965 by ASTM International

www.astm.org

carbide formed is TiC,[1] and, because the atomic weights of Ti and C are 48 and 12, the theoretical minimum amount of titanium is four times the carbon content, neglecting the amount of carbon which is soluble at 1200 F. The solubility of carbon varies from about 0.007 percent to 0.02 percent, depending on the length of time of heating.[7,8] In actual practice, the amount of titanium required to prevent the formation of chromium carbide is more than four times the carbon content. The reasons for this are that, as mentioned above, some titanium oxide is formed and that nitrogen and sulfur also combine readily with titanium. Furthermore, excess titanium is required to offset any fluctuations in the concentration of carbon or titanium in the steel and to compensate for any titanium that is soluble.

For the formation of titanium carbide, the steel must be exposed to a temperature in the range of about 1600-1750 F.[1,4,9] At higher temperatures, titanium carbide dissolves in austenite, and below this range its formation is very slow. Thus, no titanium carbide is formed in 2 hours at 1230 F.[9] Titanium carbide precipitates randomly throughout the austenitic structure as fine particles, which have been called "dot carbides."[1]

Chromium Carbide

Any carbon in excess of solubility (about 0.02 percent for heat treatments of 1 to 2 hours at 1250 F) which is not in combination with titanium may form chromium carbide, $Cr_{23}C_6$, during exposure in the range of 800 F to 1600 F. As in the case of other 18Cr-8Ni steels, this carbide precipitates preferentially at grain boundaries and may lead to accelerated intergranular attack in many corrosive environments. It is dissolved by heat treatments at temperatures greater than about 1700 F and remains in solution if the steel is cooled rapidly.

Ferrite and Sigma Phase

Additions of titanium to the metastable solid solution of austenite in stainless steel promote the formation of ferrite. This action is enhanced by the combination of titanium with carbon and nitrogen and their consequent removal from the austenitic solid solution. Both of these elements, especially nitrogen, promote the formation and stability of austenite. As a result, Type 321 steels frequently contain some ferrite, especially in the cast or welded condition. Also, in this type of steel, some of the austenite (nonmagnetic) may be transformed to ferrite (magnetic) by cold work more readily than in the other grades.

Heating the steel in the range 1150-1550 F transforms some ferrite to austenite and some to nonmagnetic chromium-rich sigma phase.[1,10] Steward and Urban[6] found that titanium and aluminum in ferrite promote this transformation, but Simpkinson[1] has not found such an effect for aluminum.

Bungardt and Lennartz[4] have suggested that dissolution of chromium carbides by heating above 1700 F forms chromium-rich points which serve as nuclei for the formation of sigma phase. Because chromium carbides precipitate primarily at grain boundaries, the sigma phase formed at these points would also be at the grain boundaries.

In contrast to the action of ferrite, sigma phase is known to cause accelerated intergranular attack in nitric acid.[11] For example, accelerated intergranular attack in boiling 65 percent nitric acid has been observed on 18Cr-8Ni-Mo steel containing a pre-precipitation form of sigma phase; i.e., the sigma phase could not be detected in the microstructure.[12,13,14] Thus, there is a possibility that in AISI-321 steel, heat treatments in the range of 1150-1550 F may also form this type of sigma phase, which is not detectable in the microstructure, along with a quantity which is readily visible but is insufficient to account for a large effect on corrosion.

Grain Size

Titanium additions to steel have a marked grain-refining effect.[15] In the case of stainless steels, this is illustrated in Figure 1. The grain size of the 18Cr-8Ni-Mo steel (Figure 1-A) is typical for the regular carbon grades. Reduction of the carbon content (ELC grades) is accompanied by an appreciable increase in grain size (Figure 1-B). However, addition of titanium, 0.53 percent, as shown in Figure 1-C, results in a marked reduction of grain size. The large-grained, low-carbon grades are frequently used for the same purpose as the stabilized grades, i.e., for equipment which is to be welded without subsequent annealing treatments. Therefore, any comparison of the behavior of these two grades of stainless steel must include the effect of grain size on intergranular corrosion.

It is commonly accepted in the literature that the severity of intergranular attack increases with increasing grain size.[9,16-20] This concept has been developed from data obtained on intergranular corrosion produced in copper sulfate-sulfuric acid solutions. Intergranular corrosion was measured by determining the change in electrical resistance of corroding specimens. It was assumed that the cause of the greater severity of intergranular attack observed on large-grained steel was that the amount of carbon available per unit area of grain-boundary surface was much greater in large- than in small-grained steel. The greater grain-boundary surface of small-grained steel was thought to result in a less continuous precipitation of chromium carbide, and, therefore, less severe intergranular attack. Apparent support for this view was found in the observation that the larger grained Type 321 steels were most likely to suffer intergranular attack.[9]

In a more recent investigation[12] it was shown that the influence of grain size depends on the solution used for producing intergranular attack and on the method of measurement, i.e., weight loss or change in electrical resistance. Such factors as length of time required to undermine and dislodge grains and the length of the path of grain boundaries through the cross section of a resistance-measurement specimen largely determine the effect of grain size. From metallographic

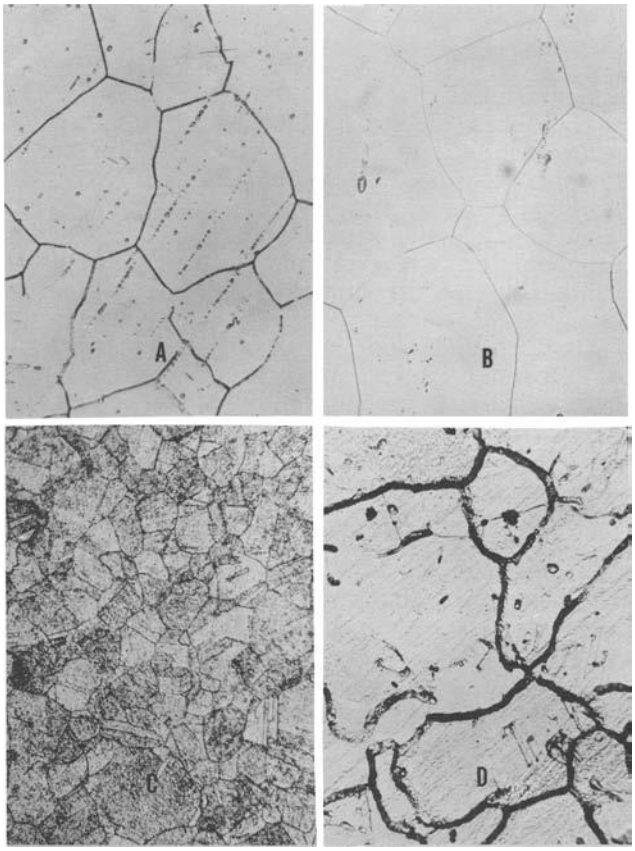


Figure 1 - Grain size in stainless steels (500X). (A) AISI-316 steel (M316) heated 1 hour at 1250 F and etched electrolytically in oxalic acid. (B) AISI-316L steel (FI-4) exposed 5 hours to ferric sulfate-sulfuric acid solution. (C) AISI-321 (GR-9) electrolytically etched in nitric acid at room temperature. (D) AISI-321 (FF-7) heated 1 hour at 1250 F and etched electrolytically in oxalic acid. Ditch structure indicates precipitation of chromium carbide because of insufficient amount of titanium.

observations of chromium carbides in stainless steel surfaces (when these carbides are isolated by the bromine-methanol method[22]), it is apparent that the width of the zone of metal affected by precipitation is relatively narrow. Therefore, other things being equal, there is probably little difference between the amount of chromium carbide formed per unit area of grain boundary for large- and for small-grained steels. Only when the grain diameter is so small that it is equal to the width of this zone will the amount of precipitate be a function of the total grain-boundary surface, i.e., the grain size.

The relationship of grain size and severity of intergranular attack in AISI-321 steel, mentioned above, is readily explained by the grain-refining and carbide-stabilizing properties of titanium. Intergranularly precipitated chromium carbides have been observed on larger-grained AISI-321 steels. This suggests that the amount of titanium added was insufficient to combine with all carbon or to produce the grain-refining effect. As a result, chromium carbides were formed at the boundaries of relatively large grains.

An example of this type was observed in the present investigation. Figure 1-D shows the relatively large grain size of an imcompletely stabilized steel. The Ti/C ratio is only 4.0, and, as might be expected, after a heat treatment of 1 hour at 1250 F, the oxalic acid etch reveals chromium carbides at the grain boundaries.

In addition to these effects of grain size on intergranular attack in steels containing grain-boundary precipitates, there is also an influence of grain size on corrosion of annealed steels in nitric acid solution. This is described below.

Experimental Plan

To determine the effect of microstructure on corrosion of AISI-321 steels, the results of various heat treatments on specimens of four heats were studied in five different corrosion tests. As the characteristics of these tests have been described elsewhere, only the most essential details involved in their use are given below.

Steels and Heat Treatments

Four commercial heats of titanium-stabilized steel were selected for detailed investigation of the effect of composition, heat treatment, and, to some extent, welding, on their behavior in the five tests described below. High-spot tests were also made on several other heats, and on a larger group of specimens representing about 15 different heats. All the supplementary tests confirmed the observations made on the original four heats; i.e., their performance was representative of the behavior of all of the AISI-321 steels. Analyses of the steels are given in Table 1.

Another series of specimens was heat treated before welding to provide specimens for a study of weld decay. Two types of welds were made: (a) cross welds made with consumable AISI-347 electrodes and (b) butt welds. Welded specimens were air-cooled.

TABLE 1—Analyses of Stainless Steels

Steel		Weight Percent											
AISI Type	Code	Cr	Ni	Mo	C	Ti	Ti/C	Al	Si	P	S	Cu	N
316	316M	17.7	12.6	2.45	0.046	...	..	....	0.61	....	....	....	....
316L	FI-4	16.2	13.2	2.2	0.020	...	..	....	0.47	....	....	....	....
321	GQ-7	17.1	9.5	...	0.067	0.62	9.3	0.076	0.58	0.032	0.017	0.19	0.015
321	GQ-8	17.5	9.4	...	0.056	0.53	9.5	0.069	0.58	0.031	0.016	0.34	0.010
321	GR-1	18.1	10.1	...	0.060	0.55	9.1	0.077	0.58	0.010	0.006	0.21	0.032
321	FF-7	17.8	9.2	...	0.070	0.28	4.0	0.041	0.79	0.028	0.023	....	0.026
321	GR-9	17.0	10.3	...	0.065	0.53	9.7	..	0.59	0.022	0.029	....	....

Unless otherwise indicated, welded specimens were 1 in. x 2 in.; all others, 1 in. x 1 in. Thicknesses were 1/4 in. for GQ-7, GQ-8, 1/8 in. for GR-1, and 1/16 in. for FF-7.

The heat treatments are listed in Table 2 (and subsequent tables). An as-received mill-annealed specimen was tested to obtain a base rate for comparison with the results of the other heat treatments. From the previous discussion of the microstructure of AISI-321 steels it is apparent that the heat treatments at 1250 F will result in chromium carbide precipitate in incompletely stabilized steels, either because the amount of titanium is insufficient to combine with all carbon, or because there has not been a previous opportunity for the titanium to react completely with carbon. The heat treatment at 1250 F will also transform some austenite and ferrite to sigma phase. If observations made on Type 316 steels are valid on AISI-321 steel, this transformation may not be detectable by microscopic examination.

Heat treatment at 1650 F forms TiC and, if enough titanium is present, should prevent formation of any chromium carbide during subsequent heat treatments at 1250 F. Heat treatments at 1700 F and 1800 F, before sensitization, were made to determine the maximum temperature which may be used for stabilization of carbon by titanium. If the steel is heated in the range where titanium carbide dissolves, subsequent heating at 1250 F will result in carbide precipitation.

An attempt was made to detect the formation of magnetic ferrite and its conversion to nonmagnetic austenite and sigma phase with a Magne Gage. Ferrite formed by cold work (stamping of numbers on the specimens) was readily detected, but the changes in the Magne Gage readings produced by heat treatments were not large enough to permit definite conclusions. All the welds contained ferrite, which was readily detectable with an ordinary magnet.

TABLE 2—Oxalic Acid Etch Test

Heat Treatment	Oxalic Acid Etch Structure			
	GQ-7	GQ-8	GR-1	FF-7
As-Received	S	S	S	S
1 hr at 1250 F	S	S	S	D
2 hr at 1250 F	S	S	S	D
4 hr at 1650 F	S	S	S	S
4 hr at 1650 F + 1 hr at 1250 F	S	S	S	D
4 hr at 1700 F + 1 hr at 1250 F	S	S	S	D
½ hr at 1800 F + 1 hr at 1250 F	S	S	S	D
Heat Treatment Before Welding	**Oxalic Acid Etch Structure of Weld-Affected Zone***			
Cross Welds				
As-Received	F	F	F	..
4 hr at 1650 F	S	S	S	..
4 hr at 1700 F	F	S	S	..
½ hr at 1800 F	S	F	F	..
Butt Welds				
As-Received	F	F	F	..
4 hr at 1650 F	S	S	S	..
4 hr at 1700 F	F	F	S	..

Specimens: welded—1 in. x 2 in.; Others—1 in. x 1 in.
F —Ferrite in weld-affected zone.
S —Step structure.
D —Ditch structure.
*Ferrite in all weld structures and step structure on all unaffected base plates.

Testing Methods

Oxalic Acid Etch. The specimen to be tested is polished and etched electrolytically in 10 percent oxalic acid. In the standard test,[24,25] a current of 1 amp/sq cm is used for 1.5 minutes. However, it was found that because of the action of inclusions, titanium carbides, and the very small grain size, a lighter etch was required, and this was used throughout the investigation. Because of the small grain size, etch structures must be examined at about 500X. The presence of any chromium carbides at grain boundaries is readily detected by a characteristic "ditch" structure (Figure 1-D). In the absence of chromium carbides, steps are formed between the grains, "step" structure. (See Figures 2-A and 12.) When none of the grains are completely encircled by ditches the designation is "dual" structure. On some AISI-321 steel slight grooving was also observed in a few specimens which had "step" structures (Figure 2-B). The oxalic acid etch does not reveal a submicroscopic type of sigma phase which leads to rapid corrosion in some acid solutions.

The oxalic acid etch test[24] is used as a rapid method for screening stainless steels from other evaluation tests which require from 4- to 240-hour exposures. When applicable,[23] specimens having "step" or "dual" structures may be eliminated from testing in other solutions because they are known to have low rates of corrosion. Specimens having a "ditch" structure must be tested in solutions which provide quantitative results to determine whether their corrosion rates are smaller or greater than the maximum permissible rate. Because the oxalic acid etch is confined to the detection of chromium carbides it may be used to screen only those grades of stainless steels in which sigma phase (which leads to rapid corrosion in the given test) does not occur.

Nitric Acid Test. For this test the standard recommended practice[26] of five 48-hour periods of exposure in 65 percent boiling nitric acid was used. Weight-loss measurements were converted to inches per month. Tests were made in 1-liter Erlenmeyer flasks with a "cold finger" condenser. The specimens were held in glass cradles, immersed in 600 ml of solution which was changed at least once every 48 hours.

Both chromium carbide and sigma phase precipitates in 18Cr-8Ni-Mo steels are detected by this solution.

Nitric-Hydrofluoric Acid Test. For the present investigation a 10 percent nitric acid-3 percent hydrofluoric acid solution at 65 C was used for three 30-minute periods with 200 ml of freshly made solution for each period.(1) The solution was held in a plastic, cylindrical container which was heated by immersion in a water bath. Specimens were held in plastic cups suspended in the solution. Weight-loss measurements were converted to

(1) This solution was made by adding 550 ml of 65 percent nitric acid and 312 g of 48 percent hydrofluoric acid to 4,000 ml of water.

inches penetration per month. In tests on 18Cr-8Ni-Mo stainless steel, this solution revealed the presence only of chromium carbide and not of sigma phase precipitates.[12,27,28]

Copper Sulfate-Sulfuric Acid Test. The solution used for most tests was the same as that given in the ASTM Recommended Practice:[29] a boiling solution of 15.7 percent H_2SO_4 and 5.7 percent $CuSO_4$. This was prepared by adding 100 g $CuSO_4 \cdot 5H_2O$ and 100 ml of H_2SO_4 (sp gr = 1.84) to 840 ml of water. Apparatus was the same as that used for the nitric acid test. To avoid accumulation of corrosion products the solutions were changed at least every 100 hours. The progress of intergranular attack was followed by measurement of electrical resistance with a precision Kelvin bridge, the most sensitive quantitative method available for this test. Specimens were machined and ground to a cross section of 0.6 x 0.15 cm and a length of 3 to 6 cm. Any heat treatments required were made before machining. For standard tests, exposures of 72 hours are frequently used. In the present investigation exposures were extended in some cases to 2,000 hours. Resistance measurements and weight-loss determinations were made on the same specimen. On Types 304 and 316 steels this solution leads to intergranular attack only when there are chromium carbides at the grain boundaries.[12]

Rocha[30] and others[12,31] have recently shown that the rate of intergranular attack (in this solution) can be greatly accelerated by simultaneous immersion of metallic copper (in the form of turnings or chips) in this solution. An additional increase in the rate of corrosion is obtained by putting the stainless steel in contact with the metallic copper. The total increase in rate of this latter test over the test without metallic copper is by a factor of about 100.[12]

In the present investigation an even more rapidly acting solution was used by adding metallic copper, but not in contact with the stainless steel specimen, to a copper sulfate solution in 50 percent sulfuric acid.

Ferric Sulfate-Sulfuric Acid Test. This solution has recently been developed to provide a rapid quantitative testing method in which corrosion products do not affect the corrosion process.[12,32,33] Susceptibility to intergranular attack associated with chromium carbides is readily detected in this solution in all grades of stainless steels. Sigma phase in 18Cr-8Ni-Mo steels, which leads to rapid intergranular attack only in nitric acid, does not cause rapid intergranular attack in this solution. A boiling 50 percent solution of sulfuric acid containing 25 g/600 ml of ferric sulfate is used in a 1-liter Erlenmeyer flask equipped with a 13-in.-long Allihn condenser. Connection between the condenser and the flask is by a ground glass joing.[33] Intergranular attack in this solution is more rapid than in the nitric acid test and the normal testing period is only 120 hours. Corrosion is determined from weight losses, which are converted to inches per month. For some of these tests the same type of long, flat specimens as described above under "Copper Sulfate-Sulfuric Acid Test" were also used to obtain data on change in resistance.

Experimental Results

Oxalic Acid Etch. The results of oxalic acid etching are given in Table 2 and are illustrated in Figures 1-D, 2, 3 and 4. On GQ-7, GQ-8 and GR-1 steels, none of the heat treatments produced any intergranular chromium carbide precipitate. A typical step structure is shown in Figure 2-A. The characteristic grooving shown in Figure 2-B may be associated with a tendency to intergranular formation of ferrite. Figures 2-C and 2-D show cubic nonmetallic inclusions (solid solution of TiN and TiC). Figure 2-D also illustrates the formation of "dot" titanium carbides at 1650 F Other results on heat GR-9, shown in Figures 2-C and 2-D, are discussed under "Comparison of Tests."

The FF-7 heat, which does not contain enough titanium for complete stabilization (Ti/C ratio of 4.0) and has a "normal" grain size, responds like an unstabilized steel. All heat treatments at 1250 F result in chromium carbide precipitate, regardless of any prior stabilizing heat treatments

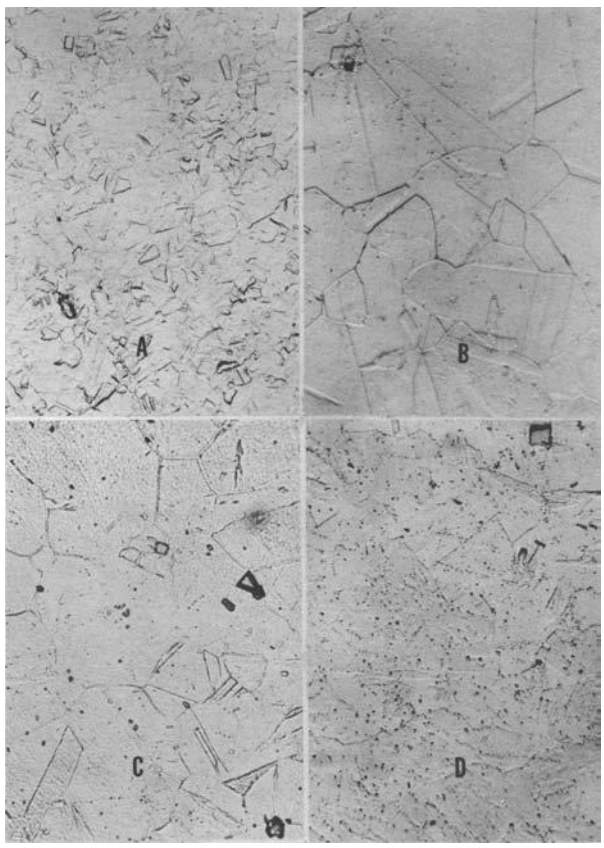


Figure 2 - Oxalic acid etch structures on AISI-321 steels. (A) GR-1 steel, as-received (annealed). Typical step structure (500X). (B) GQ-7 steel, heated 1 hour at 1250 F. Step structure and characteristic grooving (1000X). (C) GR-9 steel, heated 1 hour at 1250 F. Step structure and some grooving (1000X). (D) GR-9 steel, heated 4 hours at 1650 F and 1 hour at 1250 F. Step structure, "dot" titanium carbides and a cube of nitrogen-rich solid solution of TiN and TiC (1000X).

(Figure 1-D). Treatment at 1650 F without subsequent heating at 1250 F results in step structure because this temperature is too high to precipitate chromium carbide.

Examination of the welds and the weld-affected zone revealed ferrite in the cast structure of all welds (Figure 3). Immediately adjacent to the welds there was considerable grain growth and ferrite formation in stringers and at grain boundaries. The only exception was on material which had been heated 4 hours at 1650 F before welding. This treatment insures a more complete combination and precipitation of titanium carbide. As a result, most of the titanium is removed from solid solution and the ferrite-forming tendency of the austenite is reduced.

Nitric Acid Test. Corrosion on stainless steels is largely concentrated at grain boundaries, even on annealed steels. Grooves are formed, which account for a large part of the weight loss. On annealed steels of "normal" grain size this grooving does not lead to undermining and dislodgment of grains. However, the small-grained AISI-321 steels have more grain boundaries per unit of surface area, and grooving may lead to undermining and dislodgment of grains (Figure 5-A). This effect of grain size is illustrated in a comparison of corrosion rates on annealed specimens of titanium-stabilized steels. Heat FF-7, because of its low titanium content, has a larger grain size than any of the other heats (Figures 1-D and 2-A, B, C; note differences in magnification of photomicrographs). The nitric acid corrosion rate of this heat is lower than that of the others.

Microscopic examination of polished and corroded surfaces also shows that grain-face corrosion in nitric acid is greater on titanium-stabilized steels than on unstabilized steels of the same chromium and nickel content. This is probably caused by the removal of nonmetallic inclusions.

The increases in corrosion rates by these two factors are magnified by the action of corrosion products in the nitric acid solution. One of these corrosion products, chromium, accelerates corrosion.[34] As the steel dissolves, divalent chromium enters the solution. This is rapidly oxidized to the trivalent state, which, in turn, is oxidized more gradually to hexavalent chromium. The latter ion is readily reduced on the stainless steel surface; it also appears to depolarize the anodic reaction, thereby causing accelerated intergranular attack on both annealed and on sensitized steel.[12]

This effect of dissolved chromium on the corrosion of AISI-321 steel is illustrated in Figures 5-B and 6. In this test, trivalent chromium was added. Enough of this is converted to the hexavalent state in 18 hours to cause appreciable grain-dropping and an 18-fold increase in the corrosion rate of an annealed specimen.

In various depressions on the metal surface, such as grooves at grain boundaries and small pits formed when nonmetallic inclusions are undermined or dissolved, corrosion products including chromium ions are concentrated and result in an increase in the rate of corrosion at these points. To obtain reproducible results on titanium-stabilized steels, it is especially important to control the concentration of corrosion products by regular replacement of the nitric acid test solution. Furthermore, it is essential to use the same type of condenser and test apparatus for all tests. Allihn condensers, which leave the test solution open, or multisample test equipment, in which there is continuous removal of corrosion products,

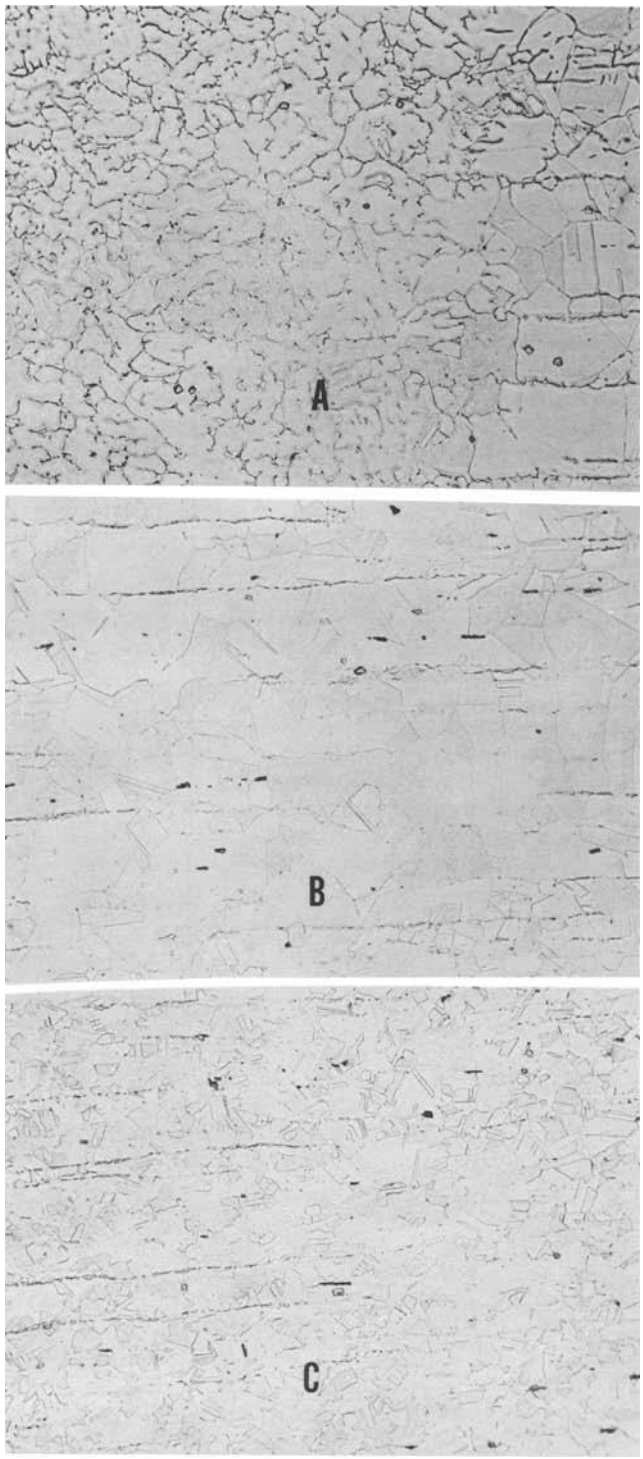


Figure 3 - Oxalic acid etch of welded specimen (210X). Butt weld on "as-received" GQ-8 steel. (A) Weld metal and juncture with base plate. (B) Heat affected zone with ferrite stringers and grain growth. (C) Base plate with ferrite produced by welding, 0.1 inch from weld.

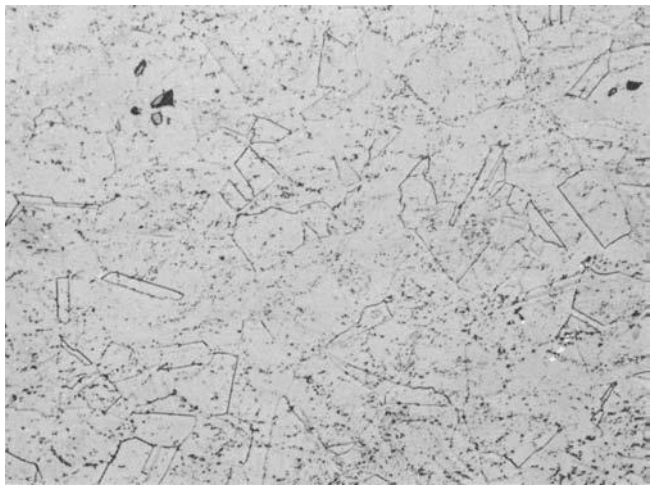


Figure 4 - Oxalic acid etch of GQ-7 heat (440X). Heat treatment: 1/2 hour at 1800 F + 1 hour at 1250 F.

affect the concentration of hexavalent chromium and thereby the results of corrosion tests, even on annealed specimens.[23,35]

Thus, the combined effect of smaller grain size and larger quantities of nonmetallic inclusions magnified by the action of the hexavalent chromium-ion corrosion produce results in a nitric acid corrosion rate on annealed, stainless steels which is higher (0.0010 to 0.002 in/mo) than that (0.007 in/mo) observed on stabilized steels having the same chromium and nickel content.

Data showing the effect of heat treatment (and welding) on corrosion in the nitric acid test are given in Tables 3 and 4, and Figures 7 and 8. The corrosion rates obtained with heat FF-7 illustrate the effect of chromium carbides which form in this steel because of an insufficient amount of titanium. Heating at 1250 F results in accelerated intergranular attack, which increases with length of time of heating. Grain-dropping results in the characteristic curvature of the weight-loss versus time curves (Figure 7). Stabilizing heat treatments at 1650, 1700, and 1800 F before sensitization reduce somewhat the rate of intergranular attack but do not eliminate it; nor does heating for periods up to 6 hours at 1650 F before sensitization eliminate the susceptibility to accelerated corrosion (Table 4).

Heat GQ-8 is a completely stabilized steel whose rate is unchanged by heating at 1250 F, even for 2 hours. As expected, further stabilizing treatments at 1650 F and 1700 F are without appreciable effect on the nitric acid corrosion rate. Heating at 1800 F somewhat increases the corrosion rate.

Sensitization (1 or 2 hours at 1250 F) without prior stabilization, of heat GR-1, and especially heat GQ-7, resulted in a marked increase in the nitric acid corrosion rate (Figure 8). Stabilizing heat treatments at 1650 F and 1700 F promote the formation of TiC and thereby increase the stability of austenite. Subsequent heating at 1250 F did not increase the nitric acid corrosion rate over the rate for the as-received specimen. Prolonged heating at 1650 F reduced the rate even below that of the as-received material (Tables 3 and 4). At 1800 F in GQ-7 some of the TiC dissolved and predisposed the steel to ferrite and sigma formation during subsequent heating at 1250 F. There was no intergranular ditching in the oxalic acid etch structure of this specimen (Figure 4).

The nitric acid corrosion rates of welded specimens are somewhat higher than those of unwelded specimens because of preferential attack on weld metal and, in some cases, because of localized corrosion at and near the fusion zone. The high temperatures involved in welding dissolve the TiC in the base plate and cause considerable grain growth (Figure 3-B). Ferrite forms in the base plate and in the weld metal. In nitric acid this leads to preferential attack along the weld as

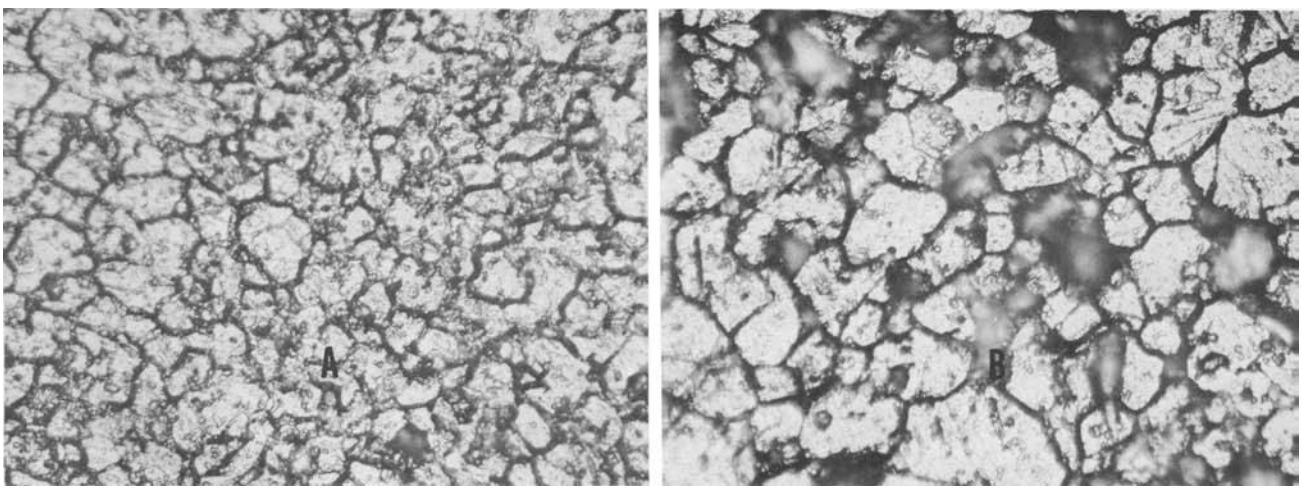


Figure 5 - Nitric acid corrosion on annealed AISI-321 steel (440X). (A) Heat GQ-8; annealed (as-received) after 68 hours' exposure to boiling 65 percent nitric acid. (B) Heat GQ-7, annealed (as-received). Corrosion in boiling 65 percent nitric acid with 1.26 g $Cr(NO_3)_3 \cdot 9H_2O$/600 ml (0.005 mol/l Cr^{+3}). Exposure: 18 hours.

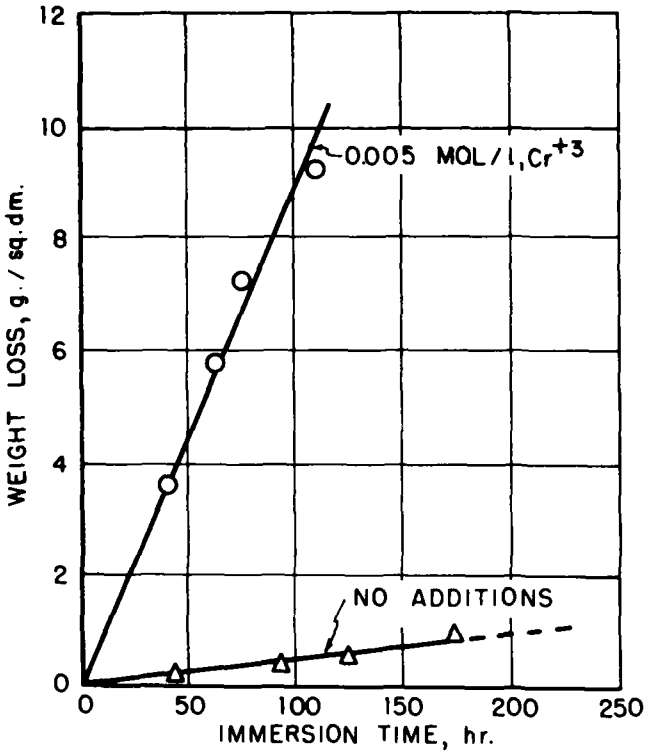


Figure 6—Effect of dissolved chromium on corrosion of annealed AISI-321 steel in boiling nitric acid. Steel: GQ-7, annealed. Solution: 65 percent boiling nitric acid, chromium added as $Cr(NO_3)_3 \cdot 9H_2O$, 1.26 g/600 ml.

TABLE 3—240-Hr. Nitric Acid Test

Heat Treatment	Corrosion Rate, in./mo			
	GQ-7	GQ-8	GR-1	FF-7
As-Received	0.00194	0.00118	0.00129	0.00093
1 hr at 1250 F	0.00837	0.00115	0.00262	0.0124
2 hr at 1250 F	0.00646	0.00139	0.00246	0.0264
4 hr at 1650 F	0.00189	0.00098	0.00082	0.00123
4 hr at 1650 F + 1 hr at 1250 F	0.00180	0.00097	0.00092	0.00363
4 hr at 1700 F + 1 hr at 1250 F	0.00178	0.00105	0.00094	0.00417
½ hr at 1800 F + 1 hr at 1250 F	0.00907	0.00212	0.00094	0.00644
Heat Treatment Before Welding				
Cross-Welds				
As-Received	0.00175	0.00154	0.00112	.....
4 hr at 1650 F	0.00211	0.00127	0.00092	.....
4 hr at 1700 F	0.00172	0.00118	0.00092	.....
½ hr at 1800 F	0.00178	0.00136	0.00106	.....
Butt Welds				
As-Received	0.00175	0.00263	0.00253	.....
4 hr at 1650 F	0.00215	0.00119	0.00113	.....
4 hr at 1700 F	0.00214	0.00119	0.00092	.....

Specimens: Welded—1 in. x 2 in., Others—1 in. x 1 in.
Welds: GQ-7 —Slight attack at ferrite-containing zone.
GQ-8 —Pitting at fusion zone.
GR-1 —No preferential attack.

Calculations: inches per month $= \frac{287 \times \triangle W}{A \times t \times d}$

t = time of exposure in hr
A = area in sq cm
$\triangle W$ = weight loss in grams
d = density in g/cu cm = 7.92
inches per month x 8350 x density = milligrams per sq dm per day

shown in Table 3. (There is no weld decay. This occurs in a zone parallel, not adjacent, but at some distance from the weld. In this zone the thermal cycle associated with welding results in precipitation of chromium carbides in unstabilized, high carbon stainless steels.)

Even though the attack adjacent to the weld, "fissure" corrosion,[37] looks like "knife-line" corrosion,[36] its cause is not the same as that usually held responsible for the latter type of localized corrosion in AISI-321 or -347 steels.[37] The cause of "knife-line" attack is attributed to chromium carbides. During welding, the base plate adjacent to the weld is heated to temperatures over 1900 F, and titanium carbides are dissolved. Subsequent heating at about 1250 F will then cause

TABLE 4—Effect of Stabilizing Heat Treatment (1650 F) And Sensitization (1250 F) on Corrosion in The Nitric Acid Test

Heat Treatment	Corrosion Rate, in./mo	
	FF-7	GQ-7
1 hr at 1250 F	0.0124	0.0083
1 hr at 1650 F + 1 hr at 1250 F	0.0101	0.0022
2 hr at 1650 F + 1 hr at 1250 F	0.0092	0.0016
3 hr at 1650 F + 1 hr at 1250 F	0.0077	0.0017
4 hr at 1650 F + 1 hr at 1250 F	0.0036	0.0018
5 hr at 1650 F + 1 hr at 1250 F	0.0077	0.0014
6 hr at 1650 F + 1 hr at 1250 F	0.0049	0.0015

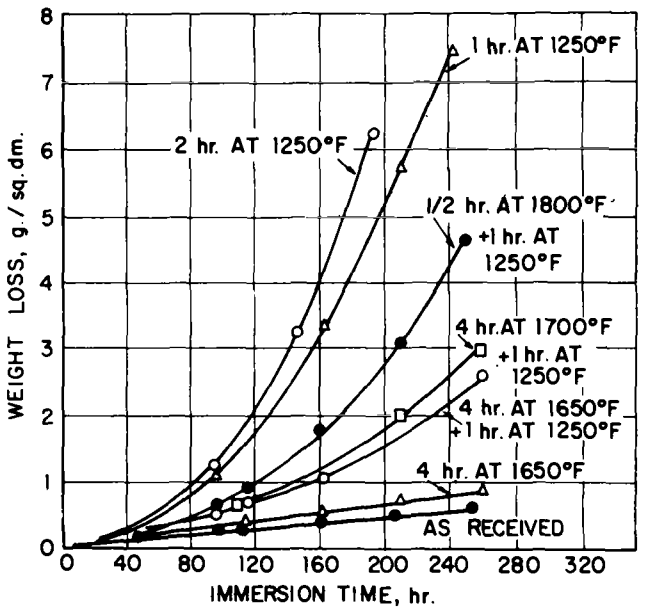


Figure 7—Effect of heat treatment on corrosion of heat FF-7 in nitric acid test.

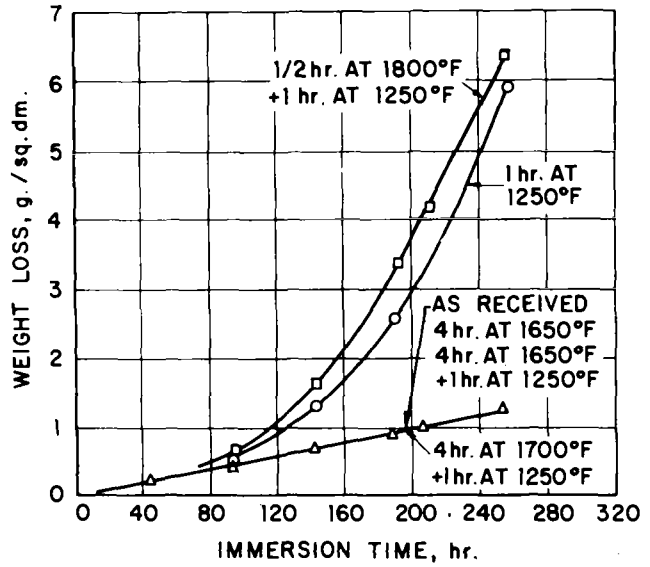


Figure 8—Effect of heat treatment on corrosion of heat GQ-7 in nitric acid.

chromium carbide precipitation and intergranular attack adjacent to the weld.

The localized attack adjacent to welds, as observed in this investigation of nitric acid attack, is caused not by chromium carbides (the steels were not heated at 1250 F after welding) but by ferrite and transformation products from ferrite and austenite. Further evidence for this is given by the results of tests in nitric-hydrofluoric acid solution (Table 5). There was no localized attack in this solution, which readily detects susceptibility to intergranular attack associated with chromium carbides.

A weld made on an as-received specimen of FF-7 steel and tested in nitric acid did not show weld decay. Therefore, the tendency toward carbide precipitation in this steel, as shown in Table 3, is not great enough to cause weld decay in a 1/16-inch sheet.

Nitric-Hydrofluoric Acid Test. Corrosion rates obtained in this solution are given in Table 5. Except on Heat FF-7, these rates are independent of the heat treatment of the specimen. The rates on FF-7 reflect the presence of intergranularly precipitated chromium carbides, which form in this steel after heating at 1250 F because of incomplete stabilization by titanium.

Welding did not affect the over-all corrosion rate, nor was there any evidence of localized attack on the base plate adjacent to the welds. These results, together with the absence of any effect of heat treatment on heats GQ-7 and GQ-8, indicate that ferrite, its transformation products, or unstable austenite, do not lead to accelerated corrosion in the nitric-hydrofluoric acid test.

TABLE 5—Nitric-Hydrofluoric Acid Test

Heat Treatment	Corrosion Rate, in./mo*			
	GQ-7	GQ-8	GR-1	FF-1
As-Received	0.650	0.374	0.495	0.994
1 hr at 1250 F	0.553	0.432	0.567	6.883
2 hr at 1250 F	0.662	0.445	0.551	5.525
4 hr at 1650 F	0.435	0.439	0.308	0.604
4 hr at 1650 F + 1 hr at 1250 F	0.435	0.554	0.503	1.081
4 hr at 1700 F + 1 hr at 1250 F	0.527	0.351	0.325	1.181
½ hr at 1800 F + 1 hr at 1250 F	0.513	0.463	0.425	2.223
Heat Treatment Before Welding				
Cross Welds				
As-Received	0.571	0.458	0.410	....
4 hr at 1650 F	0.412	0.458	0.308	....
4 hr at 1700 F	0.482	0.444	0.442	....
½ hr at 1800 F	0.428	0.445	0.546	....
Butt Welds				
As-Received	0.842	0.446	0.425	....
4 hr at 1650 F	0.457	0.438	0.425	....
4 hr at 1700 F	0.308	0.400	0.363	....

*Average rate of three 30-minute periods at 65 C in 10 percent HNO_3-3 percent HF

Welds: No preferential attack at weld-affected zone.

Specimens: Welded—1 in. x 2 in.; all others—1 in. x 1 in.

Copper Sulfate-Sulfuric Acid Test. The results of electrical resistance measurements and weight-loss determinations on specimens exposed up to 2,000 hours in the standard solution (15.7 percent sulfuric acid) are given in Table 6. The variation in the resistance determinations is about 1.5 percent on the specimens used. Only on the FF-7 heat, which contains intergranularly precipitated chromium carbides, is there any effect of heat treatment on intergranular attack in this solution. The weight-loss determinations are in agreement with the resistance measurements. Of the various tests investigated, the copper sulfate-sulfuric acid test in this form is the least sensitive in detecting susceptibility to intergranular attack.

In this standard test there was no sigma-phase effect on sensitized specimens of heats GQ-7 and GR-9 (Tables 3 and 9) which have high nitric acid corrosion rates, even though free of intergranularly precipitated chromium carbides. To determine whether this is a result of the low rate of corrosion in this solution, or whether this solution does not attack sigma phase, tests were made in 50 percent sulfuric acid solution containing copper sulfate and metallic copper. The results are also given in Table 6; they indicate that there is a very small effect on heat GQ-7, which shows a larger effect than heat GR-9 in nitric acid and in ferric sulfate-sulfuric acid solution. The smaller sigma-phase effect in heat GR-9 is not revealed in this rapid test, even though the testing time was doubled (to 140 hours).

TABLE 6—Copper Sulfate-Sulfuric Acid Test; 2,000-Hour Exposures

Heat Treatments	Percent Change in Electrical Resistance*			
	GQ-7	GQ-8	GR-1	FF-7
As-Received	0.7	0.9	1.4	1.6
1 hr at 1250 F	1.3	0.9	0.9	18.0
4 hr at 1650 F	0.9	0.9	1.0	1.7
4 hr at 1650 F + 1 hr at 1250 F	1.0	0.7	0.8	7.8
4 hr at 1700 F + 1 hr at 1250 F	1.0	0.7	1.0	1.4
½ hr at 1800 F + 1 hr at 1250 F	1.1	0.8	0.4	1.3
	Weight Loss, g/sq dm*			
As-Received	0.23	0.23	0.19	0.29
1 hr at 1250 F	0.31	0.23	0.21	1.6
4 hr at 1650 F	0.32	0.23	0.23	0.35
4 hr at 1650 F + 1 hr at 1250 F	0.38	0.22	0.23	0.80
4 hr at 1700 F + 1 hr at 1250 F	0.37	0.22	0.23	0.35
½ hr at 1800 F + 1 hr at 1250 F	0.38	0.23	0.20	0.30
	Weight Loss, g/sq dm**			
	GQ-7 (70 hr)		GR-9 (140 hr)	
As-Received	1.435		4.937	
1 hr at 1250 F	1.833 (R = 1.3)		5.146 (R = 1.0)	
4 hr at 1650 F + 1 hr at 1250 F	1.307		4.992	

*Testing Conditions: 15.7% sulfuric acid, 5.7% copper sulfate, no metallic copper. Specimens: 0.6 x 0.15 cm, 6 cm long. Changes of less than 1.5% are within experimental error.

**Testing Conditions: 50% sulfuric acid, 71.4 g/600 ml $CuSO_4 \cdot 5H_2O$, metallic copper immersed simultaneously but not in contact with stainless steel specimen. R = ratio of rate of "sensitized" specimen to rate of "as-received" specimen.

Ferric Sulfate-Sulfuric Acid Test. Data obtained in this solution are given in Table 7 and Figures 9, 10 and 11. The recommended length of testing time is 120 hours. To magnify small effects of heat treatments on corrosion the testing time was extended to 240 hours in this investigation.

As in all other tests, incomplete stabilization on heat FF-7 is readily detected in this test (Figures 9 and 10-A). Heating for 1 hour at 1250 F is essentially without effect on heat GQ-8. There is no preferential attack at grain boundaries (Figure 10-B), only a general roughening of the surface.

Heats GR-1, GQ-7 and GR-9 respond in varying degrees to heating of as-received material for 1 hour at 1250 F. Weight-loss data for heat GR-9 have been plotted in Figure 11-A. The slope of the

TABLE 8—Summary of Tests

Heat Treatment	Oxalic Acid Etch Structure				HNO_3-HF Test, Ratio[a]				$Fe_2(SO_4)_3$-50% H_2SO_4, Ratio[c]			
	GQ-7	GQ-8	GR-1	FF-7	GQ-7	GQ-8	GR-1	FF-7	GQ-7	GQ-8	GR-1	FF-7
As-Received	step	step	step	step	....	....	....	....	....	....	....	....
1 Hr at 1250 F	step	step	step	ditch	0.9	1.1	1.1	7.3	2.4	1.1	1.4	6.8
2 Hr at 1250 F	step	step	step	ditch	1.0	1.2	1.1	5.9	....	....	....	....
4 Hr at 1650 F	step	step	step	step	0.7	1.2	0.6	0.6	....	....	....	....
4 Hr at 1650 F + 1 Hr at 1250 F	step	step	step	ditch	0.7	1.5	1.0	1.1	....	....	....	....
4 Hr at 1700 F + 1 Hr at 1250 F	step	step	step	ditch	0.8	1.0	0.7	1.3	....	....	....	....
½ Hr at 1800 F + 1 Hr at 1250 F	step	step	step	ditch	0.8	1.2	0.9	2.4	....	....	....	....
	HNO_3 Test, Ratio[a]				$CuSO_4$-H_2SO_4 Test, Ratio[b]				$Fe_2(SO_4)_3$-50% H_2SO_4, % ΔR[d]			
As-Received	....	....	....	....	....	....	....	....	....	....	....	....
1 Hr at 1250 F	4.3	1.0	2.0	13.5	1.9	1.0	1.0	11.2	8	2	3	37
2 Hr at 1250 F	3.3	1.2	1.9	28.4	....	....	....	....	....	....	....	....
4 Hr at 1650 F	1.0	0.8	0.6	1.3	1.3	1.0	1.0	1.0	....	....	....	....
4 Hr at 1650 F + 1 Hr at 1250 F	0.9	0.8	0.7	3.9	1.4	0.8	1.0	4.9	....	....	....	....
4 Hr at 1700 F + 1 Hr at 1250 F	0.9	0.9	0.7	4.5	1.4	0.8	1.0	0.9	....	....	....	....
½ Hr at 1800 F + 1 Hr at 1250 F	4.7	1.8	0.7	7.0	1.6	0.9	1.0	0.8	....	....	....	....

[a] Ratio of corrosion rates of "heat-treated" over "as-received" specimen. Ratios of less than 1.5 are within experimental error.
[b] Ratio of percent change in resistance of "heat-treated" over "as-received" specimens after 2000-hr exposure. Ratios of less than 2 are within experimental error.
[c] Ratio of corrosion rates after 120 hr.
[d] Percent change in resistance after 120 Hr.

TABLE 7—Ferric Sulfate-Sulfuric Acid Test

Heat	Heat Treatment	Corrosion Rate, in./mo 120 Hr (R)*	240 Hr (R)*
GQ-7	As-Received	0.00269 ——	0.00279 ——
	1 hr at 1250 F	0.0068 (2.4)	0.00726 (2.6)
GQ-8	As-Received	0.00188 ——	0.00191 ——
	1 hr at 1250 F	0.00212 (1.1)	0.00232 (1.1)
GR-1	As-Received	0.00188 ——	0.00203 ——
	1 hr at 1250 F	0.00260 (1.4)	0.00346 (1.7)
FF-7	As-Received	0.00209 ——	0.00212 ——
	1 hr at 1250 F	0.0141 (6.8)	0.0237 (11.2)
GR-9	As-Received	0.00305 ——	0.00298 ——
	1 hr at 1250 F	0.00850 (2.8)	0.0084 (3.0)
	4 hr at 1650 F + 1 hr at 1250 F	0.0033 (1.1)	0.00328 (1.1)

* Ratio of corrosion rate of heat-treated to that of as-received specimen. Specimens: 1 in. x 1 in.

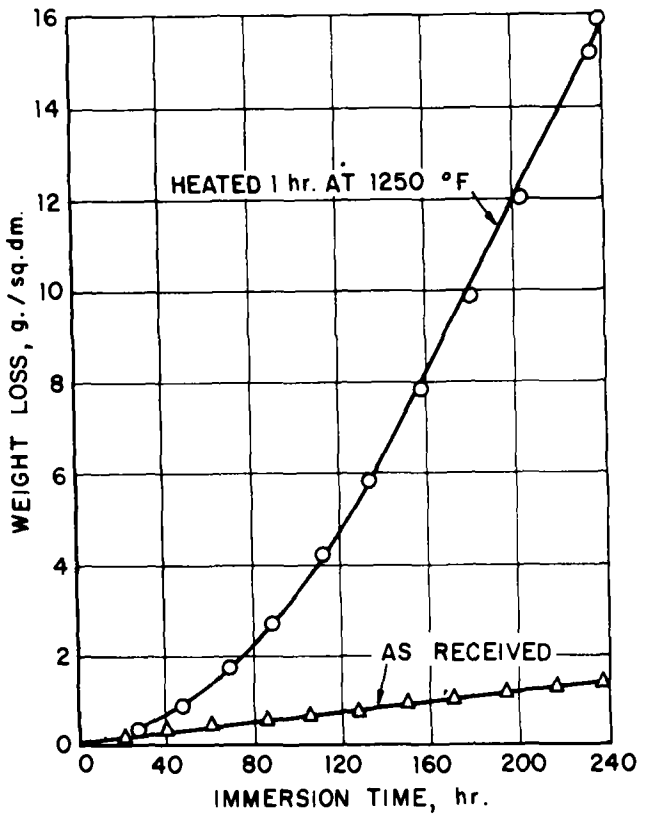


Figure 9—Corrosion of heat FF-7 in sulfuric acid-ferric sulfate test.

line of the specimen heated 1 hour at 1250 F increases with immersion time. Figures 10-C and D show this form of corrosion on heat GQ-7. This behavior in ferric sulfate-sulfuric acid solution is similar to that in nitric acid, except that the increase in corrosion rate of the sensitized steel over that of the annealed steel is less than in nitric acid. This form of corrosion is avoided by heating 4 hours at 1650 F before the 1-hour treatment at 1250 F. Because the treatment at 1650 F increases the stability of austenite by

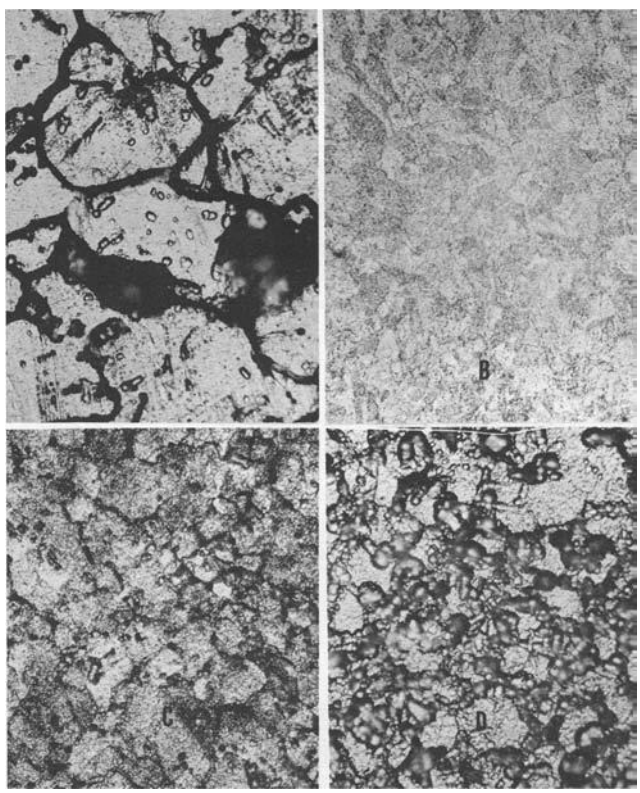


Figure 10-Attack of ferric sulfate-sulfuric acid solution on AISI-321 steels heated 1 hour at 1250 F. (500X). (A) Heat FF-7 after 47 hours' exposure. (B) Heat GQ-8 after 5 hours' exposure. (C) Heat GQ-7 after 20 hours' exposure. (D) Heat GQ-7 after 84 hours' exposure.

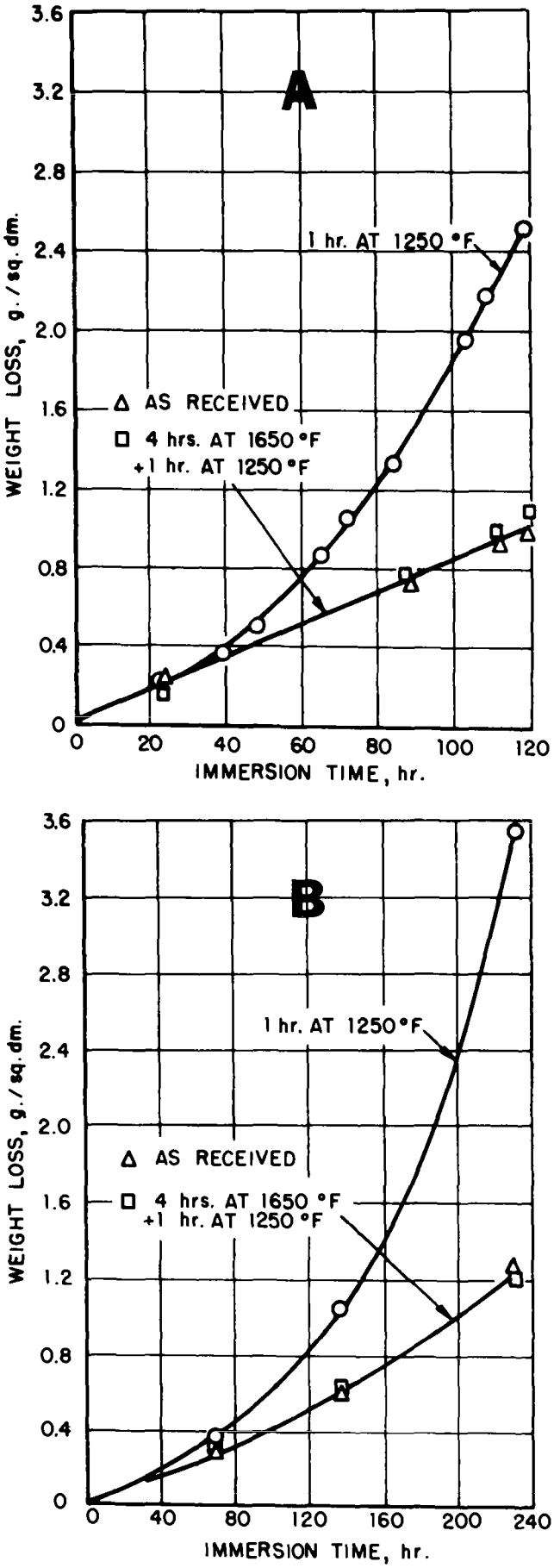


Figure 11—Effect of heat treatment on corrosion of heat GR-9 in ferric sulfate-sulfuric acid and in nitric acid solution. (A) Ferric sulfate-50 percent sulfuric acid. (B) 65 percent nitric acid.

precipitating TiC, and there is no evidence of chromium carbides in the oxalic acid etch structures of these specimens, the higher corrosion rates of specimens heated 1 hour at 1250 F are probably associated with an invisible transformation product from austenite. This problem is discussed further in the following section.

There is more grain-face or general corrosion on titanium-stabilized than on unstabilized steels in this solution. This leads to a roughening of the surface (cf. Figures 10-B and 13-A) but not to an appreciable increase in the corrosion rate. Corrosion products do not accelerate corrosion in this solution as is the case in nitric acid in which pits formed by the removal of nonmetallic inclusions serve to concentrate hexavalent chromium ions.

Comparison of Tests

The data on corrosion in the five tests used in this investigation have been summarized in Table 8 for a comparison of the effects of heat treatment and microstructure. Corrosion rates have been converted to ratios of rate of heat-treated to rate of as-received specimen. The ratio of rates is a sensitive measure of the ability of a solution to detect changes produced by heat treatments, i.e., of the resolving power of the test.

Additional data on the effect on corrosion of transformation products from austenite are given in Tables 9 and 10. For comparison, similar data on AISI-316 and -316L steels are also given in Table 9 and some photomicrographs in Figures 12 and 13.

The following is a summary of the effect of microstructure and the changes produced by heat treatments on the corrosion of AISI-321 steels in the five tests used in this investigation.

Grain Size

On as-received, annealed steels, nitric acid corrosion rates are greater for titanium-stabilized heats, which have very small grains, than on other

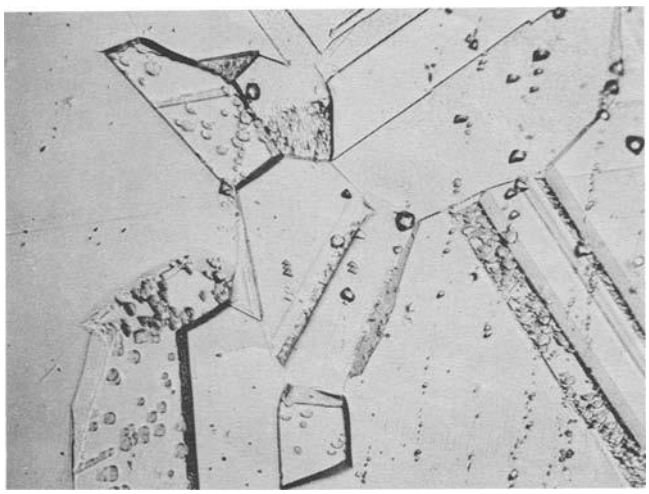


Figure 12 - Electrolytic etch of AISI-316 steel in 10 percent oxalic acid (425X). Steel: FI-4 (0.020 percent C, 16.2 percent Cr), heated 1 hour at 1250 F. Etch: 1 amp/sq cm for 1.5 minutes.

TABLE 9—Comparison of Tests: Effect of Transformation Products in AISI-321 and -316 Steels

Steel		Heat Treatment	Oxalic Acid Etch Structure	Corrosion Rate						Copper Sulfate-Sulfuric Acid
				Nitric Acid		Nitric-Hydrofluoric Acid		Ferric Sulfate-Sulfuric Acid		
				in./mo	(R)*	in./mo	(R)*	in./mo	(R)*	% Change in Resistance in 2000 Hr
AISI-321	GR-9	As-Received	Step	0.00192	——	0.83	——	0.00305	——	....
		1 Hr at 1250 F	Step**	0.00554	(2.9)	0.87	(1.1)	0.0085	(2.8)	....
		4 Hr at 1650 F + 1 Hr at 1250 F	Step**	0.00190	(1.0)	0.79	(1.0)	0.0033	(1.1)	....
	GQ-7	As-Received	Step	0.00194	——	0.650	——	0.00269	——	(X)
		1 Hr at 1250 F	Step	0.00837	(4.3)	0.553	(0.9)	0.00658	(2.4)	(X)
		4 Hr at 1650 F + 1 Hr at 1250 F	Step	0.00189	(0.9)	0.435	(0.7)	0.00387	(1.4)	(X)
AISI-316	M316	As-Received	Step	0.00077	——	0.16	——	0.00164	——	(X)
		1 Hr at 1250 F	Ditch	0.015	(19.0)	0.87	(5.6)	0.013	(7.8)	235
	FI-4 (316 L)	As-Received	Step	0.00111	——	0.50	——	0.00173	——	(X)
		1 Hr at 1250 F	Step***	0.039	(35.6)	0.51	(1.0)	0.00236	(1.4)	(X)

* (R)—Ratio of measurement on heat-treated specimen divided by measurement on as-received specimen.
** See Figure 2-C and D.
*** See Figure 12.
(X) Changes in resistance are within experimental error.

TABLE 10—Effect of Heat Treatment on Corrosion of AISI 321 Steels

Heat No. Steel	Ti/C Ratio	Oxalic Acid Etch Structure**	Corrosion Rate								
			Nitric Acid Test—240-Hr, in./mo[a]					Ferric Sulfate-Sulfuric Acid Test—120 Hr, in./mo[b]				
			As-Received	1 Hr at 1250 F		4 Hr at 1650 F + 1 Hr at 1250 F		As-Received	1 Hr at 1250 F		4 Hr at 1650 F + 1 Hr at 1250 F	
					(R)*		(R)*			(R)*		(R)*
1	5.7	Ditch	0.00094	0.018	(19)	0.0044	(5)	.....	.....	....	.....	....
4	5.3	Ditch	0.00066	0.025	(38)	0.0082	(12)	.....	.....	....	.....	....
6	3.9	Ditch	0.00099	0.0056	(6)	0.0015	(2)	.....	.....	....	.....	....
12	6.0	Ditch	0.00081	0.026	(32)	0.0020	(2)	.....	.....	....	.....	....
15	5.2	Ditch	0.00228	0.0062	(3)	0.0026	(1)	.....	.....	....	.....	....
5	6.0	Dual	0.00096	0.022	(23)	0.0019	(2)	.....	.....	....	.....	....
10	5.8	Dual	0.00063	0.020	(32)	0.00083	(1)	.....	.....	....	.....	....
17	5.8	Dual	0.00058	0.020	(35)	0.00079	(1)	.....	.....	....	.....	....
2	7.7	Step	0.00169	0.028	(17)	0.00214	(1)	0.00247	0.0100	(4)	0.00275	(1)
3	6.8	Step	0.00099	0.0066	(7)	0.00145	(1)	.....	.....	....	.....	....
8	6.0	Step	0.00061	0.016	(26)	0.00070	(1)	0.00177	0.00482	(3)	0.00188	(1)
16	7.3	Step	0.00075	0.013	(17)	0.00089	(1)	0.00211	0.00705	(3)	0.00245	(1)
18	7.7	Step	0.0010	0.0048	(5)	0.00118	....	.....	.....	....	.....	....
19[c]	5.8	Dual	0.00062	0.016	(26)	0.00078	(1)	0.00156	0.00816	(5)	0.00216	(1)
20	7.4	Dual	0.00092	0.026	(28)	0.00179	(2)	.....	.....	....	.....	....
24	7.7	Step	0.00091	0.015	(16)	0.00120	(1)	.....	.....	....	.....	....

* Ratio of corrosion rate of heat-treated to that of "as-received" specimen.
** Specimen heated 1 hr at 1250 F.
[a] Nitric acid corrosion rates were determined in multi-sample tester.[34] In this apparatus the effect of dissolved chromium is largely eliminated and, as a result, the rates are lower than those obtained in tests made with flasks (48-hr periods).
[b] Tests made on the same specimens as used for nitric acid tests.
[c] In a nitric-hydrofluoric acid test the ratios of specimens of this heat were unity for both the sensitized, and the stabilized and sensitized specimens.

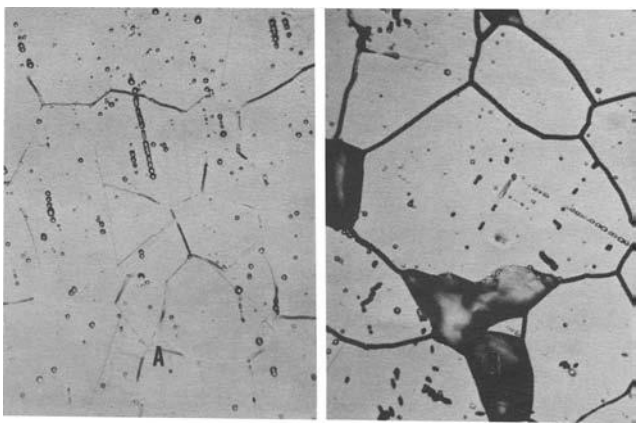


Figure 13 - Corrosion of AISI-316 steel in ferric sulfate-sulfuric acid test (500X). Steel: M 316. (A) Annealed; exposure 40 hours. (B) Heated 1 hour at 1250 F; exposure, 27 hours.

grades of stainless steels whose grains are considerably larger, because in this solution a large part of the weight-loss on such specimens is a result of grooving at grain boundaries. In ferric sulfate-sulfuric acid solution (also in the nitric-hydrofluoric acid and the copper sulfate-sulfuric acid solutions) there is relatively little intergranular grooving on annealed steels (Figure 13-A); consequently, corrosion rates of titanium-stabilized steels are about the same as those of other 18Cr-8Ni grades.

On steels of normal grain size, which are susceptible to intergranular attack, penetration along grain boundaries extends to several layers of grains ahead of the outer layers from which there is grain-dropping. In contrast, on titanium-stabilized heats the small grains are readily undermined and rapidly dislodged when there is rapid attack in nitric acid and ferric sulfate-sulfuric acid solutions associated with sigma phase. As a result, there is continuous removal of layers of grains without appreciable intergranular penetration beyond the surface of the

metal. There is little "sugaring," i.e., dropping of grains from corroded specimens after removal from the solution, and it is sometimes difficult to establish whether accelerated corrosion is caused by intergranular attack.

Chromium Carbide

Susceptibility to intergranular corrosion associated with the precipitation of chromium carbides is readily detected by all five tests used in this investigation (Table 8, heat FF-7). Heating of this incompletely stabilized steel at 1250 F produced a ditch structure in the oxalic acid etch and an increase in corrosion rate in all acid tests.

Titanium Carbide

Heating at 1650 F increases the amount of TiC precipitate in those heats in which this reaction has not been carried to completion. If all the carbon has been reacted with titanium, subsequent heating at 1250 F does not produce any chromium carbides and is without effect on the TiC reaction. The stabilizing heat treatment at 1650 F was without appreciable effect on the corrosion rate in any of the tests (Tables 8 and 9). Heating at 1650 F increased the amount of TiC precipitate in heat GR-9 (Figures 2-C and D) without increasing further the relatively high rate of the as-received specimen (0.00192 in/mo). In nitric acid the removal of titanium carbides and other nonmetallic inclusions causes roughening of the surface and contributes to an increase in grain-face corrosion by concentrating corrosion products which include hexavalent chromium ions.

Sigma Phase

In heats GQ-7, GR-1 and GR-9, heating as-received material at 1250 F does not precipitate chromium carbides (step structure in oxalic acid etch and ratio of one in HNO_3-HF test), but the rates in the nitric acid test and, to a lesser extent, in the ferric sulfate-sulfuric acid test are increased. Heat treatment at 1650 F before heating at 1250 F prevents this increase in corrosion rate in these two tests (Tables 8, 9 and 10). Thus, exposure at 1250 F may form sigma phase (at grain boundaries) which is not detectable in the microstructure but which may greatly affect the corrosion rate.

This phenomenon has previously been observed in AISI-316 steels.[12,13,14,32] Some results illustrating the effects of this invisible phase are given in Table 9. After heating at 1250 F, the 0.046 percent C, AISI-316 (M316) steel corrodes intergranularly (Figure 13) in the four tests listed in Table 9. As shown by the oxalic acid etch structure, this is largely a result of precipitation of chromium carbides. However, after heating 1 hour at 1250 F, the extra-low-carbon (0.020 percent C) steel, FI-4, has a step structure in the oxalic acid etch (Figure 12), a ratio of about one in the nitric-hydrofluoric acid and the ferric sulfate-sulfuric acid tests, but a ratio of 35.6 in the nitric acid test. In AISI-316L steels, this type of intergranular corrosion can be prevented in most cases by a heat-treatment at 1500-1600 F, before exposure at 1250 F.[11]

Similarly, heating of AISI-321 steels at 1650 F before exposure to 1250 F prevents the formation of the sigma-phase type of susceptibility to intergranular attack. This is shown in Tables 8 and 9, and especially in Table 10, which contains data on additional tests made to investigate this second type of susceptibility to intergranular corrosion in AISI-321 steels. From the data in Table 10, it is apparent that the increase in corrosion rates in the ferric sulfate-sulfuric acid test resulting from this type of susceptibility is only about 25 percent of that found in the nitric acid test (cf. ratios of steels heated 1 hour at 1250 F in the two tests).

There is an important difference in the behavior of sigma phase in AISI-321 and -316L steels. In the 18Cr-8Ni-Mo steels, sigma-phase susceptibility is revealed only in nitric acid, while in the 18Cr-8Ni-Ti steels both the nitric acid and, to a lesser extent, the ferric sulfate-sulfuric acid tests detect this type of susceptibility.

The reactions at 1650 F which prevent accelerated corrosion associated with sigma phase upon heating at 1250 F are not known with certainty because the changes in microstructure are on a submicroscopic scale. However, it is known that heating at 1650 F precipitates TiC and therefore removes titanium from the austenite, promotes austenite stability, and may prevent its transformation to sigma phase upon heating at 1250 F.

Mechanism of Corrosion

Electrode potential measurements[12,13] on stainless steels on which there is intergranular attack show that in nitric acid and in sulfuric acid solutions inhibited with ferric or cupric sulfate both the grain faces and the grain boundaries are passive. This passive state is a dynamic condition in which there is continual dissolution and reformation of a protective, passive film by a reaction between the dissolving metal and the corroding solution. For example, the weight of stainless steel dissolved in sulfuric acid-ferric sulfate solutions is electrochemically equivalent to the weight of ferric ions reduced. There is no evolution of hydrogen gas, even on rapidly corroding boundaries. However, at these boundaries the corrosion current (metal dissolution) required to keep the film in repair, and thereby to polarize the boundaries to the same potential as the grain faces, is much greater (Figure 14). The reason for this is that precipitation of chromium carbides ($Cr_{23}C_6$) or chromium-rich sigma phase greatly depletes adjacent metal in chromium.

The results of measurements of electrode potential on stainless steels immersed in the four hot acid solutions employed for evaluation tests are given in Table 11. These are the potentials to which both grain faces and grain boundaries are polarized. In all solutions listed, chromium depletion caused by the formation of chromium carbides is readily detected. However, the ability to detect changes in composition associated with the formation of sigma

TABLE 11—Potentials of Stainless Steels in Solutions Used For Evaluation Tests

Test Solution	Electrode Potential[a] Volts	Phases Detected		
		Chromium Carbide	Sigma	
		AISI 304, 316, 321	AISI 321	AISI 316
Nitric Acid[b]	+0.75 to +0.95	yes	yes	yes
Ferric Sulfate-Sulfuric Acid[c]	+0.60	yes	yes	no
Copper Sulfate-Sulfuric Acid[d]	+0.1 to +0.34	yes	no	no
Nitric-Hydrofluoric Acid[e]	+0.3 to −0.1	yes	no	no
Hydrochloric Acid[f]	−0.4	no	no	no

[a] Potential of stainless steel vs saturated potassium chloride calomel electrode.
[b] Boiling 65% acid solution.
[c] Boiling 50% sulfuric acid containing 5.5 g/l Fe^{+3} and 1.15 g/l Fe^{+2}.
[d] Boiling 15.7% acid containing copper sulfate. Without metallic copper potential is +0.35 v; with metallic copper, +0.10 v.
[e] A 10% nitric acid, 3% hydrofluoric acid at 65 C was used. Potential oscillates.
[f] 10% boiling hydrochloric acid.

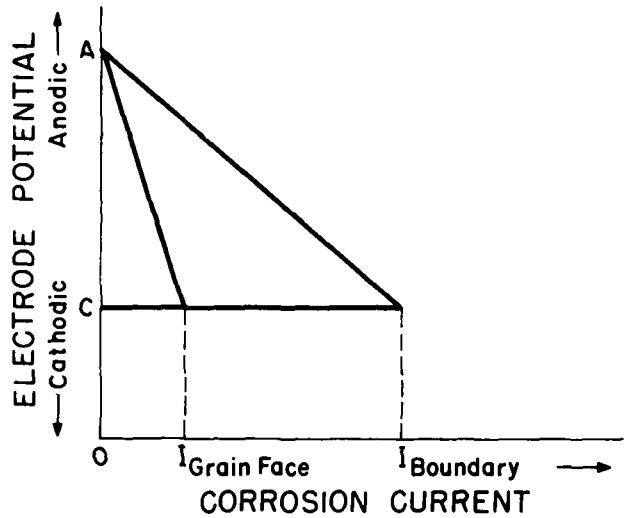


Figure 14—Local cell polarization on grain faces and boundaries of corroding stainless steel. In ferric sulfate-sulfuric acid solutions grain faces and grain boundaries are both polarized to the oxidation-reduction potential of the solution. The corrosion current of corroding boundaries is greater than that on grain faces.

phase appears to decrease with changes in corrosion potential towards the potential observed on nonpassive stainless steel, i.e., in hydrochloric acid. However, the corrosion potential is only one of the factors which determine the ability of the solution to detect susceptibility to intergranular attack associated with sigma phase. This is shown by polarization measurements on sensitized low-carbon 18Cr-8Ni-Mo (FI-4) steel. Specimens of this composition which contain sigma phase in a submicroscopic form, corrode intergranularly in nitric acid but not in ferric sulfate-sulfuric acid or copper sulfate-sulfuric acid solution. Potentiostatic polarization of this steel in sulfuric acid (without ferric or cupric salts) to the potential, 0.7 to 0.95 v, which it has in nitric acid, does not result in intergranular attack in this solution. Therefore, the ability of an evaluation test solution to detect sigma phase depends not only on the potential to which it polarizes the steel but also on the anodic polarization characteristics of grain faces and depleted zones which, in turn, depend on the composition of the corroding solutions.

Conclusions

The conclusions given below are derived from data obtained in the present investigation and from an evaluation of information given in the literature.

1. Incomplete stabilization of carbon in AISI-321 steels by titanium, which results in precipitation of chromium carbides at grain boundaries when the steel is heated in the range 800-1600 F, is readily detected by all five evaluation tests used in this investigation: oxalic acid etch, nitric acid, nitric-hydrofluoric acid, copper sulfate-sulfuric acid and ferric sulfate-sulfuric acid tests.

2. A second type of susceptibility to rapid intergranular attack on titanium-stabilized stainless steels is associated with the formation of sigma phase which may be present in submicroscopic form. This second type of susceptibility is formed by heating in the range 1150-1550 F.[1,10] It is detectable only in the nitric acid and, to a lesser extent, in the ferric sulfate-sulfuric acid tests and is not apparent in the oxalic acid etch test, nor is it revealed by testing in nitric-hydrofluoric or copper sulfate-sulfuric acid solutions. (This is in contrast to the action of sigma phase in 18Cr-8Ni-Mo steels, Table 9.)

3. Both the intergranular precipitation of chromium carbides and the formation of sigma phase may be prevented in steels containing adequate amounts of titanium by heating at 1600-1750 F for 1 to 4 hours.[6,37] This so-called "stabilizing treatment" precipitates TiC, which ties up carbon and removes titanium from austenite. As a result, during subsequent heating at 1250 F, there is no carbon available for formation of chromium carbide, and, because removal of titanium from austenite increases its stability, there is less possibility for transformation of austenite to sigma phase. Therefore, stabilizing heat treatments are frequently essential to insure optimum corrosion resistance in these steels.

If the steel is heated above 1800 F, titanium carbides dissolve to an increasing extent as the temperature is increased. Subsequent heating in the range 800-1600 F then causes precipitation of chromium carbides and high rates on intergranular corrosion.[37,38]

4. Welding of AISI-321 steels results in ferrite in the cast structure of the weld and, frequently, also in the zone adjacent to the weld.[44] There may be partial transformation of this ferrite during air cooling.

These phases cause accelerated localized attack adjacent to the weld in nitric acid, "fissure" corrosion,[37,39] but not in nitric-hydrofluoric acid solution. Although similar in appearance to "knife-line" corrosion, this localized attack in nitric acid is not associated with chromium carbides, which are usually considered to be the cause of "knife-line" attack.[36]

5. The relatively high corrosion rates of annealed titanium-stabilized steels in the nitric acid test are caused by the small grain size of these steels, by nonmetallic inclusions, and by the accelerating

effect of the chromium-ion product. In nitric acid most of the corrosion is at the grain boundaries, even on annealed steels. Because the grain size of AISI-321 steels is much smaller than that of unstabilized steels, the weight loss on AISI-321 specimens is greater. Corrosion products, including chromium ions which are converted to the hexavalent state in the nitric acid test, accumulate in the grain boundary grooves and in pits formed by the removal of nonmetallic inclusions. This action of corrosion products greatly magnifies the effects of grain boundaries and nonmetallic inclusions.

6. Carbon contents in excess of about 0.06 percent are undesirable because of the relatively large amounts of titanium required for stabilization and because it has been found that carbon increases the corrosion rate of these steels regardless of the heat treatment, i.e., even in the annealed condition.[21,37,39,40]

According to theory, the required minimum ratio of titanium to carbon is 4. However, to provide for titanium nitride and sulfide formation and other contingencies, ratios of 6 to 8 have been recommended.[39,41,42,43] The data of Table 10 also suggest a minimum ratio of 6. This range of Ti/C ratios should not be exceeded appreciably because any excess of titanium remains dissolved in austenite and promotes the formation of ferrite and the transformation to sigma phase, which accelerates corrosion in nitric acid and in ferric sulfate-sulfuric acid.

7. On the basis of these conclusions, the following evaluation methods are recommended for titanium-stabilized stainless steels:

a. Steels intended for service in nitric acid environments should be evaluated in the nitric acid test.[26]

b. If susceptibility to rapid intergranular attack associated with precipitates of chromium carbides and of sigma phase is to be detected, the nitric acid test[26] or the ferric sulfate-sulfuric acid test[33] may be used.

c. If susceptibility associated only with the presence of chromium carbide precipitate is to be detected, the oxalic acid etch test may be applied to screen specimens from either the nitric-hydrofluoric acid or the copper sulfate-sulfuric acid tests.(2) All specimens having "step" or "dual" structures have low rates of corrosion in these two tests. Those having a "ditch" structure in the oxalic acid etch must be tested in the nitric-hydrofluoric and the copper sulfate-sulfuric acid solutions to determine whether or not their rates are within the maximum permissible limits.[23]

Acknowledgment

The writer wishes to thank S. J. Kucharsey, technician, Engineering Research Laboratory, E. I. du Pont de Nemours & Co., Inc., Wilmington, Delaware, for his able assistance with the experimental work.

(2) If this test is selected for evaluation, metallic copper and 50 percent sulfuric acid should be used with copper sulfate to increase the rate of attack.

References

1. T. V. Simpkinson. Trans. ASM, 49, 721-44 (1957).
2. J. F. Brown, W. D. Clark and A. Parker. Metallurgia, 56, 215 (1957).
3. K. Wetzlar and G. Lennartz. DEW Technische Berichte, 1, 15 (1961).
4. K. Bungardt and G. Lennartz. Arch. f. Eisenhüttenwesen, 27, 127-133 (1956).
5. E. E. Cheburkova. Zavodskaya Laboratoriya, 15, 275-277 (1949).
6. R. S. Stewart and S. F. Urban. Symposium on on the Nature, Occurrence and Effects of Sigma Phase. ASTM STP No. 110, 128-144 (1950).
7. J. J. Heger and J. L. Hamilton. Corrosion, 11, 6t-10t (1955) January.
8. S. J. Rosenberg and C. R. Irish. J. Research NBS, 48, 40-8 (1952).
9. F. J. Phillips. Trans. ASM, 39, 891-914 (1947).
10. W. Goedecke. Werkstoffe u. Korrosion, 5, 488-496 (1954).
11. D. Warren. Corrosion, 15, 221t-232t (1959) May.
12. M. A. Streicher. J. Electrochem. Soc., 106, 161 (1959).
13. W. O. Binder and C. M. Brown. Symposium of Evaluation Tests for Stainless Steels. ASTM STP No. 93, 146 (1949).
14. D. C. Buck and J. J. Heger; F. F. Philips and B. R. Queneau. Symposium of Evaluation Tests for Stainless Steels. ASTM STP No. 93, 56 (1949).
15. G. F. Comstock. Titanium in Iron and Steel, pp 73 and 215. John Wiley & Sons, Inc., New York (1955).
16. E. C. Bain, R. H. Aborn and J. J. B. Rutherford. Trans. Amer. Soc. for Steel Treating, 21, 481-509 (1933).
17. J. J. B. Rutherford and R. H. Aborn. Inst. Mining Met. Engrs., 100, 293 (1932).
18. A. Ferri. Metallurgia Italiana, 43, 432-434 (1951).
19. H. D. Newell. Trans. Am. Soc. Steel Treating, 19, 673-732 (1932).
20. J. J. B. Rutherford and R. H. Aborn. Trans. AIMME, 100, 293-305 (1932).
21. H. T. Shirley and J. E. Truman. J. Iron Steel Inst., 172, 377-380 (1952).
22. E. M. Mahla and N. A. Nielsen. Trans. ASM, 43, 290-322 (1951).
23. M. A. Streicher. Intergranular Corrosion of Austenitic Stainless Steels, a Testing System for Detecting Susceptibility to Rapid Intergranular Attack. Second International Congress on Metallic Corrosion, New York (1963).
24. ASTM Book of Standards, "Tests for Detecting Susceptibility to Intergranular Attack in Stainless Steels: (A) Oxalic Acid Etch Test for Classification of Etch Structures of Stainless Steels." In press.
25. M. A. Streicher. ASTM Bulletin No. 188, p 35 (1953) February; also Werkstoffe u. Korrosion, 5, 363 (1954).
26. ASTM Book of Standards, "Tests for Detecting Susceptibility to Intergranular Attack in Stainless Steels: (C) Nitric Acid Test for Detecting

Susceptibility to Intergranular Attack in Stainless Steels." In press.
27. M. H. Brown, W. B. DeLong and W. R. Myers. Symposium on Evaluation Tests for Stainless Steels. ASTM, STP No. 93, 103-120(1949).
28. D. Warren. ASTM Bulletin No. 230, p 45 (1958) May.
29. ASTM Book of Standards, 1961, Part 3, p 393, A383-55T, "Recommended Practice for Conducting the Acidified Copper Sulfate Test for Intergranular Attack in Austenitic Stainless Steels." ASTM. Philadelphia.
30. H. J. Rocha: Discussion to Stahl u. Eisen, 75, 579-86 (1955).
31. E. Brauns and G. Pier. Stahl u. Eisen, 75, 579-86 (1955).
32. M. A. Streicher. ASTM Bulletin No. 229, p 77 (1958) April.
33. ASTM Book of Standards, "Tests for Detecting Susceptibility to Intergranular Attack in Stainless Steels: (B) Ferric Sulfate-Sulfuric Acid Test for Detecting Susceptibility to Intergranular Attack in Stainless Steels." In press.
34. W. B. DeLong. Symposium on Evaluation Tests for Stainless Steels ASTM, STP No. 93, 211-214 (1949).
35. H. T. Shirley and J. E. Truman. J. Iron Steel Inst., 171, 354 (1952).
36. M. G. Fontana. Ind. Eng. Chem., 42, 99A (1950); 44, 87A (1952); and 45, 91A (1953).
37. E. J. Heeley and A. T. Little. J. Iron Steel Inst., 182, 241-55 (1956).
38. E. A. Kachik and D. H. Desy. Unpublished results, Engineering Research Laboratory, E. I. du Pont de Nemours & Co., Inc., Wilmington, Delaware.
39. H. T. Shirley and C. G. Nicholson. J. Iron and Steel Inst., 170, 111 (1952).
40. R. S. Stewart. Metal Progress, 971-3 (1947) December.
41. E. I. Astrov and V. N. Biryukova. Vestnik Mashinostroeniya, 33, 61-65 (1953).
42. S. J. Rosenberg and J. H. Darr. Trans. ASM. 41, 1261-1287 (1949).
43. A. V. Shreider. Zhurnal Prikladnoi Khimii, 28, 608-15 (1955).
44. R. M. Holt and O. P. Nicholson. J. Iron and Steel Inst., 200, 715 (1962).

Recent Advances in the Metallurgy of Stainless Steels

TIME-TEMPERATURE-SENSITIZATION (TTS) DIAGRAMS FOR TYPES 347, 304L, AND 316L STAINLESS STEELS

By H. F. Ebling[1] and M. A. Scheil[2]

Synopsis

Time-temperature-sensitization diagrams were developed for two heats of sheet materials of Types 347, 304L, and 316L stainless steels. Curves were derived from corrosion data obtained by the boiling nitric acid test of specimens heated to temperatures between 700 and 1500 F for times up to 35,000 hr. The results of these tests indicate that these types of stainless steels can become badly sensitized (susceptible to intergranular attack). In addition, these steels can recover from sensitization if held sufficiently long at some temperatures. These effects were studied with the material in the full annealed condition and in a stabilized condition (stabilized by heat treatment). The stabilized condition appears to benefit only the Type 347 material.

Austenitic stainless steels of the 18 Cr-8 Ni class with its modifications are the most commonly used alloys to combat severe corrosion problems. These stainless alloys are susceptible to a number of different types of corrosive attack depending upon the environment to which they are exposed. Among the most common types of attack are pitting, stress corrosion, and intergranular. Of these, the susceptibility to intergranular attack is the only type which is entirely influenced by the heat treatments given to the alloy. If an alloy is susceptible to intergranular attack, it is referred to as being sensitized. Thus, an alloy failing by intergranular corrosion can be traced back to a sensitizing heat treatment by the fabricator or an improper anneal by the metal producer.

The generally accepted explanation as to the cause of sensitization of an 18-8 alloy is as follows: The preferred sites for the precipitation of carbides resulting from the rejection of carbon from austenite is on the grain boundaries and twin boundaries. The formation of chromium carbides (about 94 per cent by weight chromium) effectively lowers the chromium content of the adjacent metal, thus lowering its corrosion resistance. The formation of sigma phase (about 45 per cent by weight chromium) resulting from unstable austenite similarly occurs at the grain boundaries and can cause sensitization but to a lesser degree than carbides.

[1] Metallurgist, Metallurgical Research Dept., A. O. Smith Corp., Milwaukee, Wis.

[2] Director, Metallurgical Research Dept., A. O. Smith Corp., Milwaukee, Wis.

Laboratory Corrosion Testing

There are several laboratory tests designed to reveal whether or not an 18-8 alloy is sensitized or susceptible to intergranular attack. These tests are the acidified copper sulfate test (ASTM Method A 393),[3] boiling nitric acid test (ASTM Method A 262),[4] nitric-hydrofluoric acid test,[5] electrolytic oxalic acid etch test (ASTM Method A 262),[4] and the ferric sulfate-sulfuric acid test.[6] The acidified copper sulfate test or Strauss test was the first qualitative laboratory test used to detect sensitized 18-8 alloys.

The boiling nitric acid or Huey test, which was developed shortly afterwards, is a quantitative test and is extensively used as a standard test for 18-8 stainless steels. There have been many controversies concerning the results of the boiling nitric acid test when compared to results of other tests. Many believe that this test is too severe and does not represent conditions which may be found in any particular process. However, the fact is that these laboratory tests are not performed to justify the use of the material for a particular process. What these tests do reveal is a poor annealing procedure or some change in metal structure because of fabricating heat treatments which upsets the original corrosion characteristics of the material. With this in mind, the use of the boiling nitric acid test is justified.

It is claimed that the acidified copper sulfate test and the ferric sulfate-sulfuric acid test reveals sensitization of metal only by chromium carbide precipitation on the grain boundaries. The boiling nitric acid test, on the other hand, reveals sensitization of metal when chromium carbide or the sigma phase or both are precipitated at the grain boundaries. Thus, this test shows grain boundary weakness regardless of cause. This is important because some chemical processes can attack metal which is sensitized by the suspected precipitation of sigma phase. If this were not the case, Type 316L material would practically never fail in service by intergranular corrosion. From our laboratory experience in testing Type 316L, no sensitized material resulting from normal fabricating heat treatments was found by using the acidified copper sulfate test. However, some of the same heat treatments produced badly sensitized material when using the boiling nitric acid test. Since it is known that Type 316L can fail by intergranular corrosion in service, it has to be concluded that the boiling nitric acid test is the proper test to reveal susceptibility to intergranular attack.

[3] Recommended Practice for Conducting Acidified Copper Sulfate Test for Intergranular Attack in Austenitic Stainless Steel (A 393), *1964 Book of ASTM Standards*, Part 3.

[4] Recommended Practice for Boiling Nitric Acid Test for Corrosion-Resisting Steels (A 262), *1964 Book of ASTM Standards*, Part 3.

[5] F. K. Bloom and M. E. Carruthers, "Accelerated Corrosion Testing of Chromium-Nickel Stainless Steel Weldments," *Evaluation Tests for Stainless Steels, ASTM STP 93*, Am. Soc. Testing Mats., 1949, pp. 87–100.

[6] M. A. Streicher, "Intergranular Corrosion Resistance of Austenitic Stainless Steels," *ASTM Bulletin No. 229*, Am. Soc. Testing Mats., April, 1958, pp. 77–86.

Experimental Procedure

The 18-8 types of stainless steels are unstable in the mill annealed condition principally because the austenite is super-saturated with carbon; however, it is in this condition that the susceptibility to intergranular corrosion is at the minimum.

Unfortunately, this condition is easily upset by fabricating procedures such as welding, hot forming, and stress relieving. To overcome this deficiency, carbon stabilizer additions such as columbium or titanium were made to

Copyright© 1965 by ASTM International

www.astm.org

effect a more stable structure. Columbium and titanium form more stable carbides than chromium. The preference of precipitating carbon as columbium or titanium carbide lessens the opportunity for the formation of the undesired chromium carbides. A second method to accomplish this was to lower the carbon content to 0.03 per cent max. With these improvements in 18-8 stainless steels, it was believed that it would be possible to fabricate articles easily without upsetting the material's original corrosion resistance. However, these alloys are also being used in service at moderately high temperatures. The effect of time and temperature on the corrosion resistance of these alloys has not been explored too well. It is the purpose of this paper to show the effect of these conditions on a few heats of Types 347, 304L, and 316L stainless steels.

TABLE 1—NITRIC ACID CORROSION DATA OF TYPE 347 STAINLESS STEEL HEAT A, COMMERCIAL ANNEALED STOCK.[a]

Time, hr	Temperature, deg F								
	700	800	900	1000	1100	1200	1300	1400	1500
0	0.008	0.008	0.008	0.008	0.008	0.008	0.008	0.008	0.008
1	...	...	...	...	...	0.015	0.023	0.019	0.011
3.5	...	...	...	...	0.009	0.027	0 034	0.019	0.010
10	...	...	...	0.008	0.026	0.054	0.039	0.018	0.009
35	...	...	...	0.022	0.112	0.085	0.027	0.014	0.012
100	0.011	0.008	0.008	0.055	0.181	0.062	0.026	0.012	0.008
350	...	...	0.010	0.218	0.290	0.058	0.025	0.023	...
1 000	...	...	0.042	0.495	0.391	0.037	0.017	0.017	...
3 500	0.007	0.008	0.335	0.516	...	...	...	...	...
10 000	0.006	0.010	1.14[2]	0.097	...	...	...	...	...
35 000	0.012	0.042	1.48[2]	0.053	...	...	...	...	...

TABLE 2—CHEMICAL ANALYSIS OF HEATS.

Element	Heat					
	A	B	C	D	E	F
	Type					
	347	347	304L	304L	316L	316L
C	0.07	0.08	0.022	0.026	0.024	0.023
Mn	1.50	1.28	1.04	0.72	1.54	1.40
P	0.031	0.020	0.021	0.020	0.018	0.018
S	0.008	0.022	0.018	0.020	0.018	0.013
Si	0.38	0.41	0.34	0.34	0.30	0.32
Cr	18.41	18.30	19.31	18.38	18.14	18.42
Ni	11.75	10.72	9.39	9.41	13.43	12.62
Mo	...	...	...	...	2.50	3.00
Cb	0.81	0.77	...	...	...	...
N_2	0.050	0.030	0.053	0.013	0.030	0.020

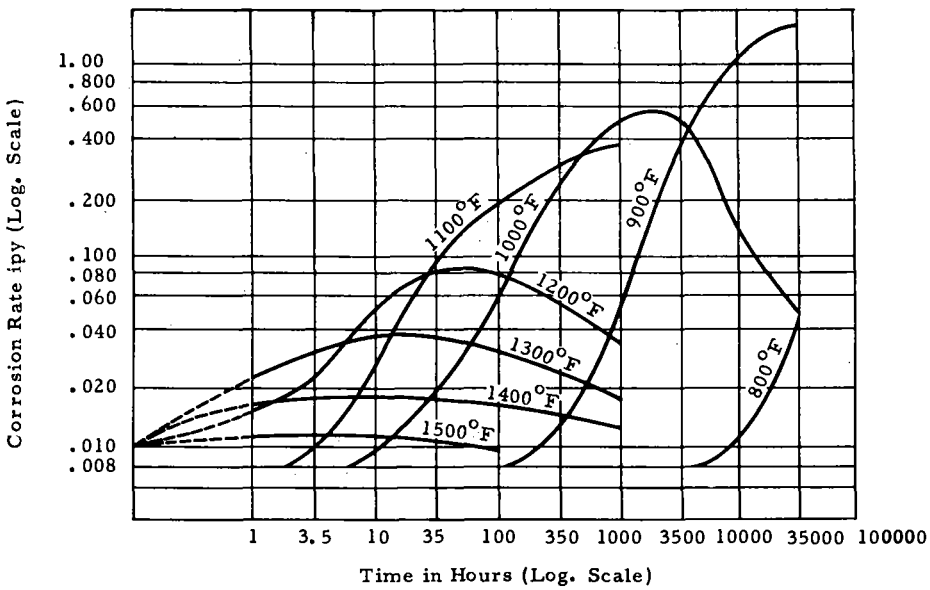


FIG. 1—Temperature Contour Graph, Effect of Time on Corrosion Rate, Data from Type 347 Steel Heat A.

All the heats involved in these tests were commercial heats received in the mill annealed condition. The material was in sheet form rolled to 12 gage (0.109 in.) thickness. Coupons approximately 2 in. by 3 in. were cut and used for each test condition. Corrosion specimens were 1 in. by 2 in. The remainder of the coupon was saved for a duplicate specimen, if deemed necessary, or microstudy and other tests which might be suggested later. All the corrosion specimens were prepared and tested in accordance with ASTM A 262 standards. Specimens were tested for five 48-hr periods, except when corrosion rates exceeded one inch penetration per year (ipy). Tests on these specimens were discontinued. At the lower temperatures corrosion tests were not made at each short time interval because sensitization was not expected to occur.

TYPE 347 STAINLESS STEEL

About 30 years ago the first heats of Type 347 stainless steel were made commercially. This 18 Cr-8 Ni alloy had a columbium addition which supposedly stabilized the carbon, thus preventing intergranular susceptibility of the alloy. The amount of columbium necessary to do this was in the range of 8 to 10 times the carbon content. Laboratory tests, particularly the acidified copper sulfate test, indicated that this stabilized austenitic stainless steel was practically immuned to intergranular attack regardless of the heat treatment. This viewpoint is still held by many metallurgists.

Experimental Procedure and Results:

The investigation of Type 347 stainless steel was made using two selected heats, each from a different producer and both being a commercial 12 gage sheet product, mill annealed, pickled, and furnished with a 2D finish. The results of corrosion tests made on one of these two heats are listed in Table 1. The figures listed are the averages of the five periods used in the test. When a superscript is used, it indicates that the test was discontinued at the numbered period, and the corrosion rate given is the rate obtained from the last period tested. All corrosion rates are expressed in inches penetration per year (ipy). The analyses of the heats are shown in Table 2.

Originally it was planned to explore temperatures only from 700 to 1000 F;

however, it was necessary to extend the temperature range to 1500 F in order to show the over-all effect. Even though the tests at the higher temperatures could not be completed for the longer time periods, the effect of the time-temperature relationships do show definite trends. It is to be noted that Type 347 develops high corrosion rates after 1000 hr at 900 F and after 100 hr at 1000 F. It is also noted that the corrosion rate shows a decrease between 3500 and 35,000 hr at 1000 F. Plotting this data, making temperature contour curves, a family of curves is obtained as shown in Fig. 1. From this it can be seen that the highest corrosion rates are obtained by the lower temperatures, although the time involved is much longer. If the data is replotted making time contour curves, a family of curves is obtained as shown in Fig. 2. This gives a different picture of the effect of time and temperature on the corrosion rate. In addition, the effect of intermediate temperatures can be interpolated to some extent. By taking the time-temperature relationship at any particular corrosion rate level, graphs showing the contours of various corrosion levels as a function of time and temperature can be made. These are shown in Figs. 3 and 4. The data are now in a form which can easily show the limitations of time and temperature for a particular corrosion level.

These graphs are, in effect, the same as the familiar time-temperature-transformation (TTT) diagrams. Thus these graphs could be called time-temperature-sensitization (TTS) diagrams for wrought Type 347 stainless steels. From these diagrams the corrosion rate resulting from any simple heat treatment can be predicted. The time indicated on the graphs discussed in this paper is the accumulative time at the given temperature. The condition of 1000 F for 1000 hr does not necessarily mean that the 1000 hr is one continuous heat treatment, but could be ten 100-hr heat treatments.

Discussion of Results:

By looking over the magnitude of the corrosion rates obtained in some of these conditions, one questions the stability of Type 347 alloy. However, Type 347 wrought material, under certain conditions, is one of the most resistant of the 18-8 austenitic materials as far as intergranular attack is concerned. The corrosion resistance of Type 347 can be greatly increased, at least for the two heats involved in these tests, by giving the material an intermediate heat treatment of 1650 F for two hr. The specimens were cooled at a rate equivalent to a $\frac{3}{4}$-in. thick plate. This treatment is sometimes referred to as a stabilization heat treatment, and it certainly proves to be of value. Corrosion rates were obtained on specimens of Heats A and B given this stabilization heat treatment prior to the intermediate temperatures. The TTS diagrams for these heats are shown in Figs. 5 and 6. As far as the tests have been completed, the corrosion rates are reduced in some cases to one tenth the rates obtained on the sensitized conditions of the annealed material.

It is noted that there is a similarity in the TTS diagrams of these two heats. However, the curves for Heat B are

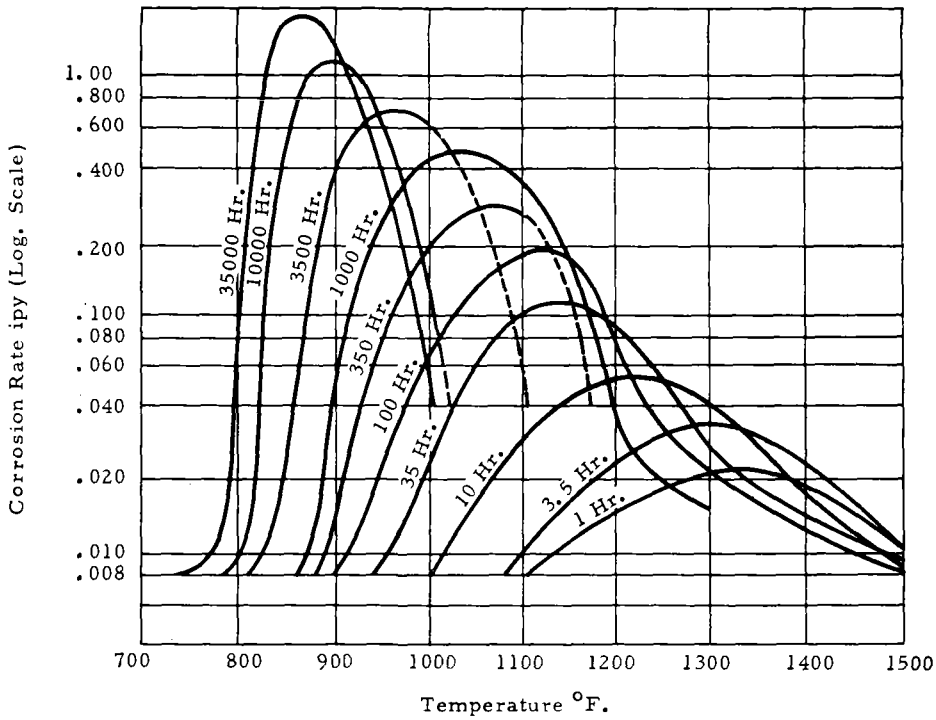
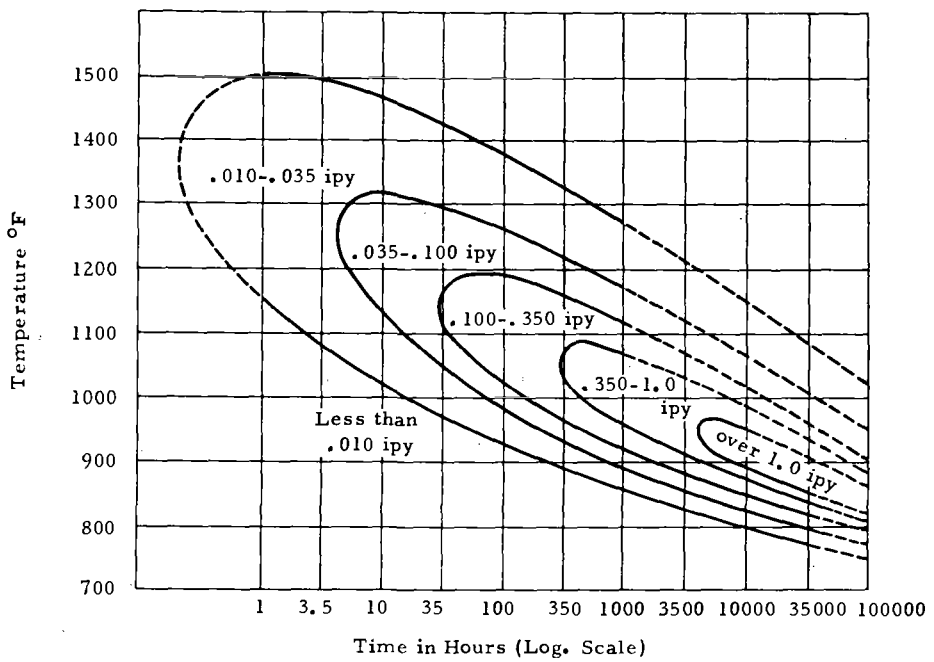
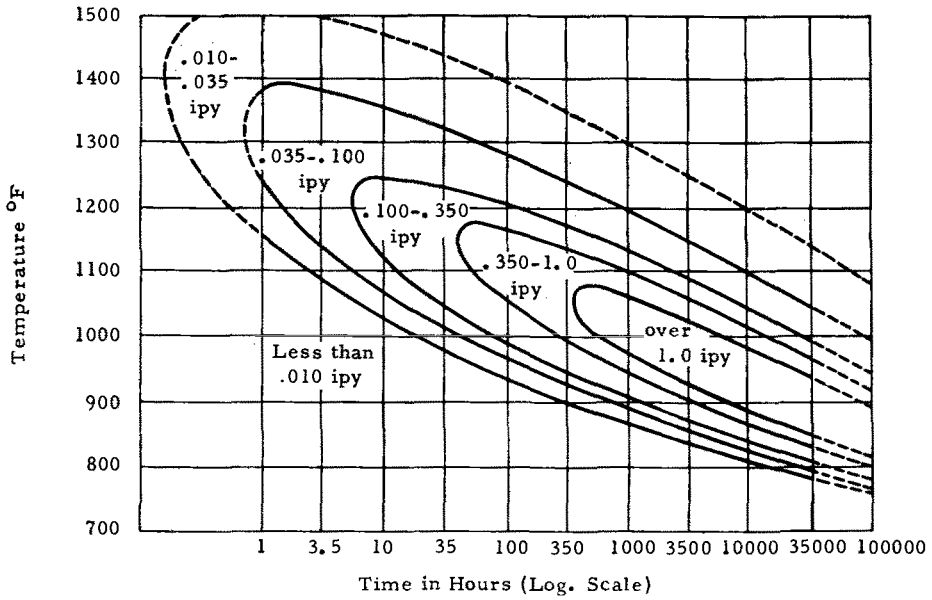


FIG. 2—Time Contour Graph, Effect of Temperature on Corrosion Rate, Data from Type 347 Steel Heat A.

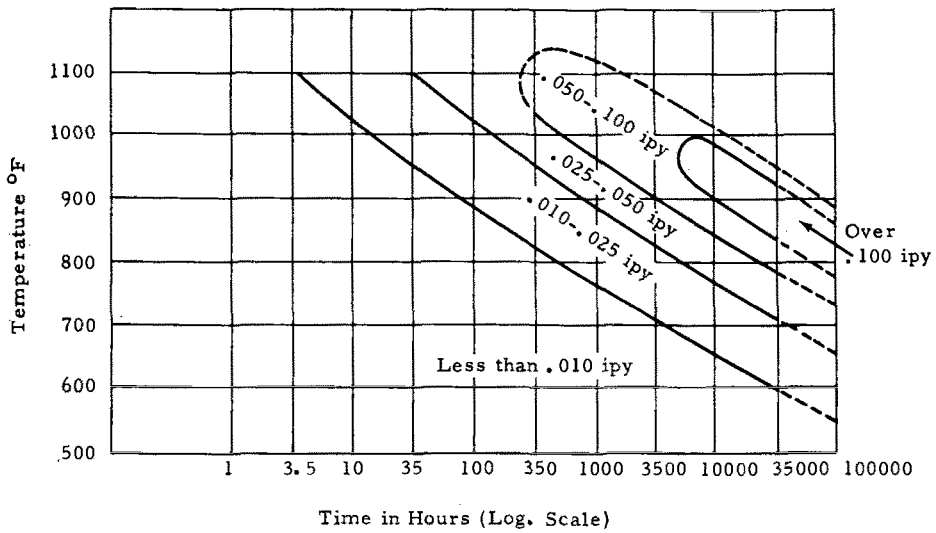


NOTE—Sensitization as determined by the boiling nitric acid test.

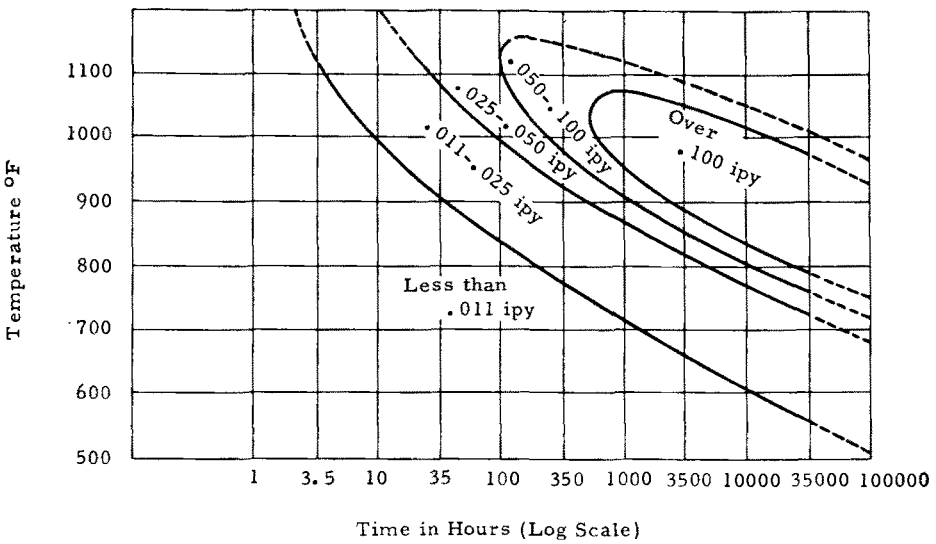
FIG. 3—Time-Temperature-Sensitization Diagram of Type 347 Steel Heat A.



NOTE—Sensitization as determined by the boiling nitric acid test.
FIG. 4—Time-Temperature-Sensitization Diagram of Type 347 Steel Heat B.



NOTE—Sensitization as determined by the boiling nitric acid test.
FIG. 5—Time-Temperature-Sensitization Diagram of Type 347 Steel Heat A, Stabilized at 1650 F, 2 hr, Heated and Cooled Between ½ in. and ¼ in. Stainless Plates.



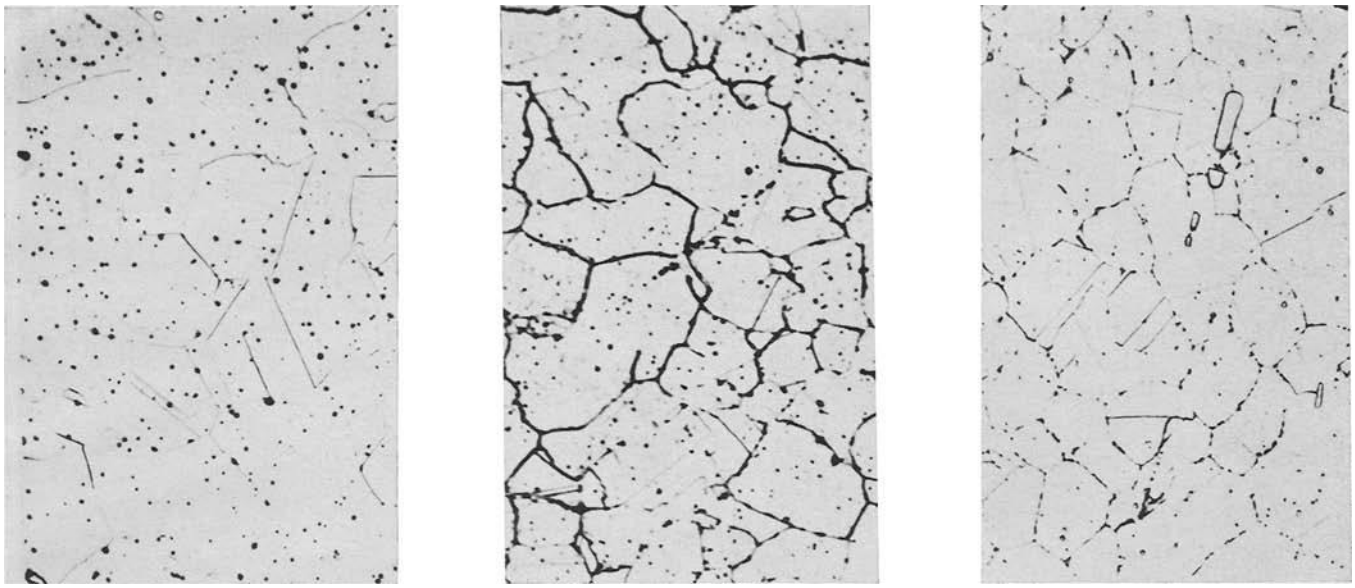
NOTE—Sensitization as determined by the boiling nitric acid test.
FIG. 6—Time-Temperature-Sensitization Diagram of Type 347 Steel Heat B, Stabilized at 1650 F, 2 hr, Heated and Cooled Between ½ in. and ¼ in. Stainless Plates.

pushed to the left and somewhat downward indicating a higher level of susceptibility for intergranular attack. If all Type 347 wrought materials were found to have this similarity, perhaps a sensitivity factor could be obtained from the chemistry of the heat which would serve as a bench mark to construct the TTS diagram for a particular material. If a sensitivity factor cannot be obtained by the chemistry, two or three corrosion tests could be made and the results of these tests would serve as bench marks to construct such a diagram. At present we do not have enough data to predict that a general pattern could be established.

Microscopic Examination:

Microscopic examinations were made on selected specimens from these two Type 347 heats. This examination revealed no apparent differences between the annealed stock and the stabilized stock. Figure 7 shows the microstructures of Heat A developed by etching with aqua regia and cupric chloride and photographed originally at a magnification of ×1000. The first micrograph represents the stabilized (1650 F—2 hr) condition. It is noted that the grain boundaries are not too well delineated by the etch. The corrosion rate obtained on this structure is less than 0.010 ipy. The second micrograph represents the heat treated condition of 1000 F for 3500 hr. Here a heavily attacked grain boundary is noted which is typical of sensitized material. The corrosion rate obtained on this structure is over 0.5 ipy. The third micrograph represents the heat treated condition of 1000 F for 35,000 hr. Here it is noted that the grain boundaries are delineated but are not badly attacked. The corrosion rate obtained on this structure is 0.053 ipy.

The reason for the intergranular weakness, as shown by the corrosion rates, and the microstructure is primarily the result of carbide precipitation. However, there has been a feeling that this is not the only cause, but this carbide precipitation can be accompanied by sigma formation which also competes for chromium from the adjacent areas. The recovery of corrosion resistance may be attributed to the fact that all the supersaturated carbon has been precipitated and, through diffusion, the chromium is being replenished in the badly depleted areas. If this occurs in all heats, this development of a self-healing process may eventually effect a true stabilization of the material.



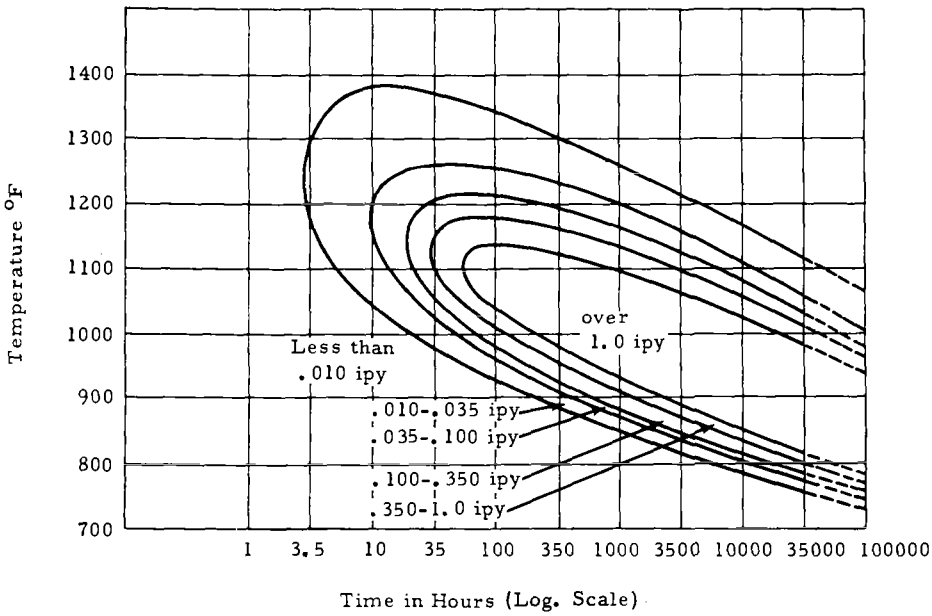
(*left*) Stabilized condition, corrosion rate 0.009 ipy.
(*center*) Heated at 1000 F for 3500 hr, corrosion rate 0.516 ipy.
(*right*) Heated at 1000 F for 35,000 hr, corrosion rate 0.053 ipy.
FIG. 7—Microstructure of Type 347 Steel Heat A. Developed by Aqua Regia-Cupric Chloride Etch (×1000).

Conclusions:

It has been shown that in spite of the intended stabilization by the columbium addition, sensitization will eventually occur in the annealed material. At temperatures above 900 F (and possibly below) the material will reach a maximum in sensitization. After this peak is reached, the material will proceed through a self-healing stage, and true stabilization can occur. It has been shown that a prior stabilization heat treatment of 1650 F for 2 hr at heat greatly reduces the maximum sensitization stage which occurs in the commercially annealed material. The stabilizing heat treatment at 1650 F effectively lowers the quantity of supersaturated carbon by allowing the formation of columbium carbides at a more favorable temperature than the annealing temperature. The solubility of carbon in austenite is considerably lower at the 1550 to 1650 F stabilizing temperature range than at the annealing temperature of above 2000 F.

TYPE 304L STAINLESS STEEL

The first commercial heats of Type 304L were produced shortly after World War II. However, it was not until the acute shortage of columbium which occurred after the Korean conflict that Type 304L was recognized as material competitive to Type 347. It was not very long before metallurgists preferred Type 304L over Type 347 because it was less difficult to weld. At this time there was some concern about a particular type of attack, referred to as "knife line" attack, in welded Type 347 material.



NOTE—Sensitization as determined by the boiling nitric acid test.
FIG. 8—Time-Temperature-Sensitization Diagram of Type 304L Steel Heat C.

Experimental Procedure and Results:

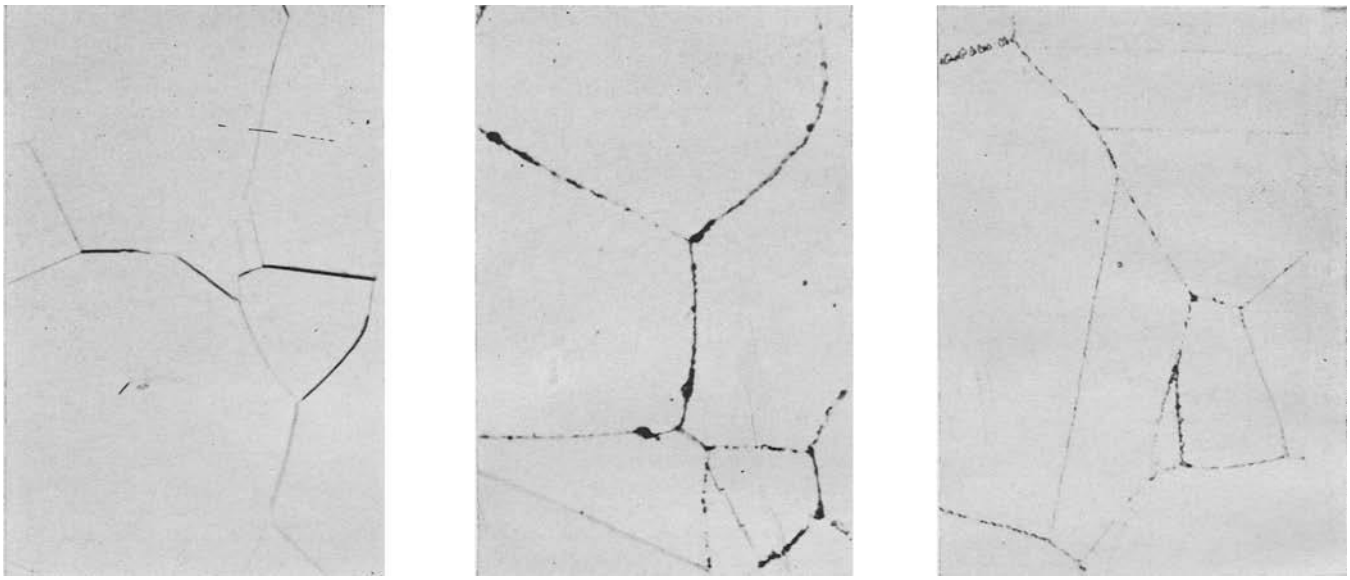
The two heats of Type 304L used in these experiments were chosen at random from heats supplied by different producers. The material used was commercially annealed 12 gage sheet supplied with a 2D finish. The heat treatments and the corrosion tests were carried out similarly, in fact, simultaneously with the Type 347 specimens. From this data it was noted that at 700 and 800 F there was no sensitization occurring up to 10,000 hr. At 800 F there was a large increase in the corrosion rate of the 35,000 hr specimen. At 900 F sensitization occurred between 350 and 1000 hr, and at 1000 F between 35 and 100 hr. At the 1100 F temperature, sensitization began after 10 hr and reached a maximum at about 1000 hr. Continued exposure at this temperature desensitized the alloy. At 1300, 1400, and 1500 F corrosion rates were of a low order for the times tested.

Only slight differences in the corrosion rates between the two heats were noted. The data from Heat C were used in constructing a TTS diagram. This is shown in Fig. 8.

This diagram shows the increase in intergranular corrosion resistance for the short time exposures. That is, the curves are shifted to the right. However, it is noted that the curves are more closely packed, which indicates that sensitization in Type 304L material, once initiated, occurs much more rapidly than in the Type 347 material. As far as this heat is concerned, heat treatments at 1400 F and above did not show any great loss of corrosion resistance. Treatments at 1300 F showed only a slight loss in corrosion resistance, and even at 1200 F it requires about 7 hr in order to exceed a corrosion rate of 0.025 ipy and about 25 hr to exceed a corrosion rate of 0.050 ipy. If one arbitrarily chose 1200 F for 1 or 2 hr as a sensitization heat treatment to characterize the corrosion resistance of Type 304L heats, this alloy would look very good compared to Type 347.

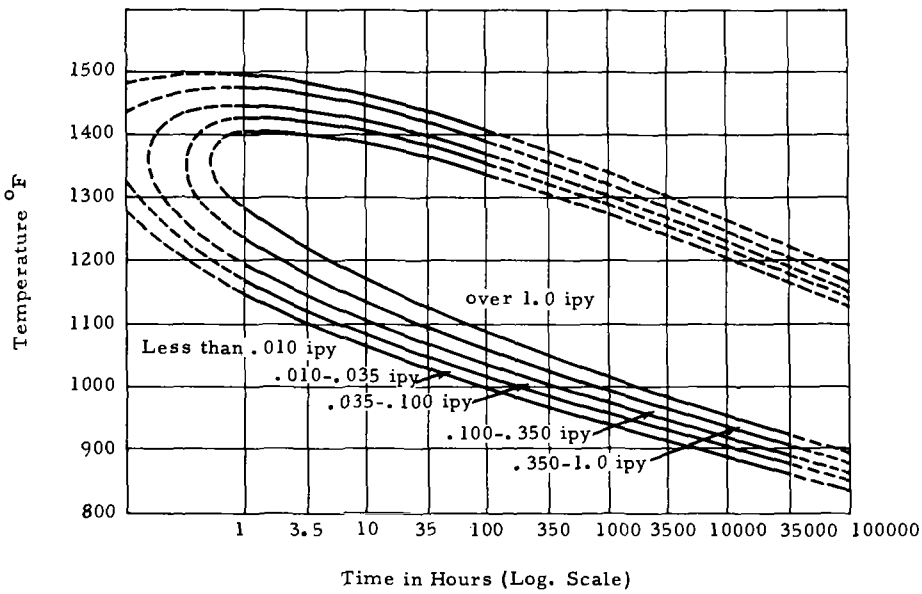
However, it is a mistake to assume that the corrosion resistance of Type 304L will be better than Type 347 at lower temperatures if held for long times. As an example, in Heat C a sensitization heat treatment of 1200 F for 3.5 hr will result in a corrosion rate of 0.012 ipy compared to 0.070 ipy for Type 347 Heat B in the same condition. At 900 F, a time of 1000 hr increases the corrosion rate to 0.267 ipy, whereas under the same conditions Type 347 Heat B would have a rate of 0.057 ipy. Again, if this corrosion pattern is found to be characteristic for all heats of Type 304L, it may be possible to construct a diagram for a particular heat by a calculation from the chemistry or by a few corrosion tests of well chosen time-temperature relationships which will serve as bench marks for a complete diagram.

Using a stabilization heat treatment of 1650 F, 2 hr, does not accomplish any beneficial effect on Type 304L. As a matter of fact, with the stabilization heat treatment Heat D showed the effect of initiating sensitization earlier at temperatures below 1100 F. In the annealed stock results, the 10,000 hr exposure at 700 F was 0.007 ipy compared to the 0.044 ipy for the stabilized condition; 10,000 hr at 800 F was 0.010 ipy in the annealed condition compared to 0.064 ipy in the stabilized condition. From the few tests made, it appears that it is not very likely that a simple stabi-



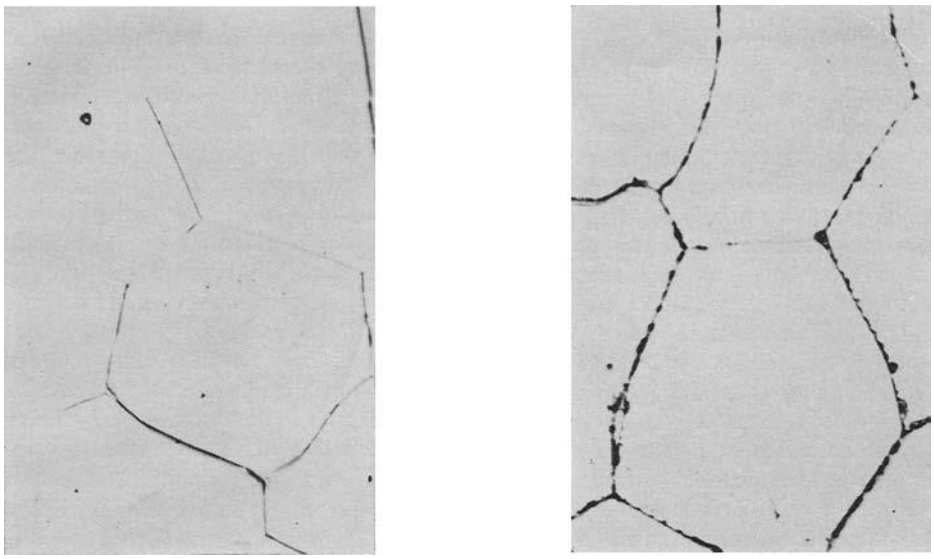
(*left*) Annealed condition, corrosion rate 0.006 ipy.
(*center*) Heated at 1000 F for 10,000 hr, corrosion rate 2.05 ipy.
(*right*) Heated at 1100 F for 10,000 hr, corrosion rate 0.042 ipy.

FIG. 9—Microstructure of Type 304L Steel Heat C. Developed by Aqua Regia-Cupric Chloride Etch (×1000).



NOTE—Sensitization as determined by the boiling nitric acid test.

FIG. 10—Time-Temperature-Sensitization Diagram of Type 316L Steel Heat F.



(*left*) Heat F, annealed condition, corrosion rate 0.005 ipy.
(*right*) Heat E, heated at 1000 F for 10,000 hr, corrosion rate 2.29 ipy.
FIG. 11—Microstructure of Type 316L Steel. Developed by Aqua Regia-Cupric Chloride Etch (×1000).

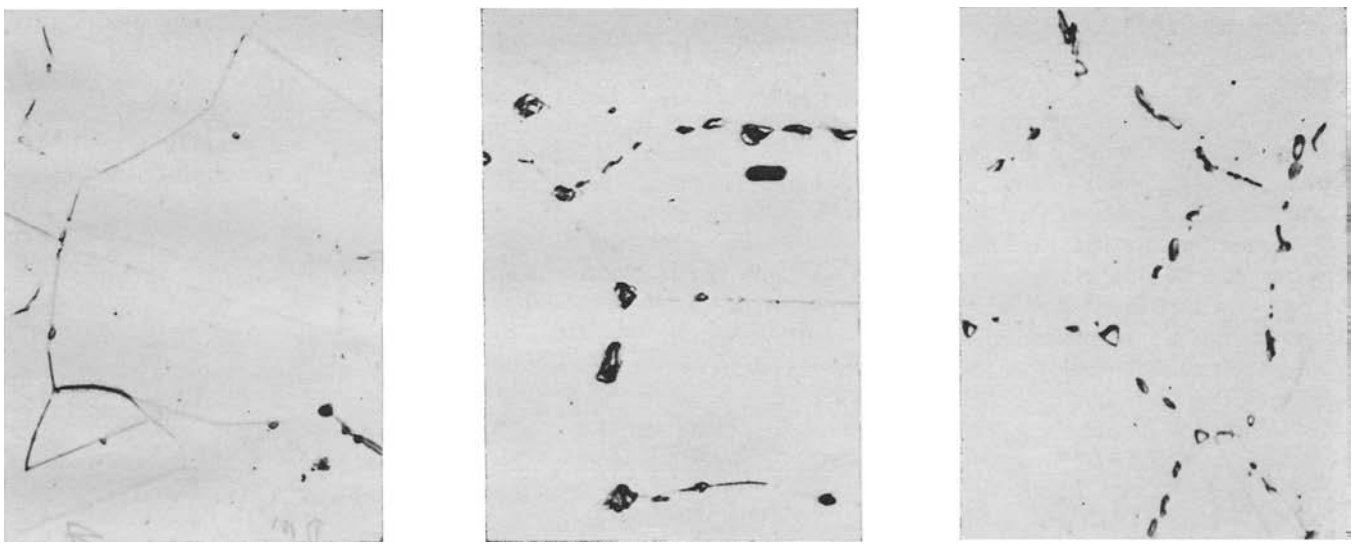
by heat treatment. On the other hand, Type 347 is not much better than Type 304L if used in the commercial annealed condition.

TYPE 316L STAINLESS STEEL

Commercial low carbon heats of Type 316 were also made shortly after World War II. Type 316L is considered to have the best service corrosion resistance of all the 18-8 types of materials. The 2 to 3 per cent molybdenum addition increases the corrosion resistance toward pitting, sulfuric and sulfurous acids, and neutral chloride solutions. However, it is not immune to intergranular attack as far as the nitric acid test is concerned.

Experimental Procedure and Results:

The two heats of Type 316L material used in this investigation were from the same producer. Both heats were commercial 12 gage sheet product, annealed, pickled, and furnished with a 2D finish.



(*left*) Heat E, stabilized condition, corrosion rate 0.007 ipy.
(*center*) Heat F, stabilized condition, corrosion rate 0.006 ipy.
(*right*) Heat E, heated at 1400 F for 100 hr, corrosion rate 0.012 ipy.
FIG. 12—Microstructure of Type 316L Steel. Developed by Aqua Regia-Cupric Chloride Etch (×1000).

lizing heat treatment given to this alloy will be very effective.

Microscopic Examination:

The microstructure of Type 304L is shown in Fig. 9. The first micrograph is the annealed stock showing no visible grain boundary constituents. This structure is also typical of the material given the stabilizing heat treatment. The second micrograph is the sensitized structure showing the badly attacked grain boundaries from etching. This structure represents the specimen heated at 1000 F for 10,000 hr. The third micrograph is the structure of the desensitized material as represented by the specimen exposed at 1100 F for 10,000 hr. Although carbides are present along grain boundaries and twin lines, the corrosion rate had been reduced to 0.042 ipy.

Conclusions:

From what is seen of the intergranular corrosion resistance of Type 304L, it is apparent that this material will successfully resist sensitization from the normal short time fabricating heat treatments. Beyond this, there is no further advantage. As much as is known at present, Type 304L should not be substituted for Type 347 since it cannot be stabilized

The heat treating and the corrosion tests were carried out in the same manner as the previous materials. It was noted that these heats were quite corrosion resistant to exposures up to 10,000 hr at 900 F and up to 350 hr at 1000 F. The corrosion rates were quite high in the 1200 and 1300 F temperature range. In the data for Heat F, a large degree of desensitization took place at 1400 F where after 1 hr a corrosion rate of over 2 ipy was obtained, and this was reduced to 0.015 ipy after the time was extended to 35 hr.

A time-temperature-sensitization dia-

gram was made for Heat F and is shown in Fig. 10. Comparing this to the previous diagrams, it is noticed immediately that the curves lie about 100 F above the Type 304L and 347 materials. Noted also was that the curves are packed closely, and they lie much further to the left. This then extends the area where corrosion rates over 1 ipy will occur in less than 1 hr at temperatures between 1300 and 1400 F. Even at 1200 F corrosion rates would be in range of 0.1 ipy after 1 to 2 hr. While this temperature would be ideal to establish bench marks for constructing similar diagrams, it is not a good temperature to use arbitrarily for some corrosion specification. It is this area which precipitates all the controversies over the use of the boiling nitric acid test. The 1200 F sensitization temperature used for the characterizing of corrosion resistance of all 18-8 alloys, and in particular Type 316L, has no reasonable explanation in light of the information presented in this paper.

In order to determine the effect of a stabilizing heat treatment on Type 316L, additional tests were made on material which was heated to 1650 F, held for 2 hr, and cooled equivalent to a $\frac{3}{4}$-in.-thick section. This material was then given the intermediate heat treatments and corrosion tested. It was noted that there was very little difference between these results and those obtained on the original commercially annealed material. At present, it appears doubtful that a prior stabilizing heat treatment would have a beneficial effect on Type 316L.

Microscopic Examination:

Microstructures of Type 316L are shown in Fig. 11. The first micrograph represents the typical structure of the commercially annealed material showing no apparent grain boundary constituents. In the sensitized condition, the second micrograph, a grain boundary precipitate is seen. Whether or not this precipitate is carbide or sigma still remains unresolved. However, after the 1650 F, 2-hr stabilizing heat treatment, a difference was noted between the two heats. This is shown in Fig. 12. The first micrograph, Heat E, has very little grain boundary constituent. Heat F, shown in the second micrograph, developed a considerable amount of grain boundary constituent after the same heat treatment. This precipitate is presumably sigma and in this form does not affect the intergranular corrosion resistance of the material. The reason for this is that the sigma phase is in the form of fairly large particles, and these do not form a continuous network. Furthermore, the temperature at which this phase was formed is high enough to allow the chromium to diffuse rapidly into the depleted area adjacent to the new phase. The third micrograph is Heat E after being heated at 1400 F for 100 hr. This heat now also shows large particles of the presumed sigma phase at the grain boundary. The corrosion resistance of this structure is almost as good as the material given only the stabilizing heat treatment.

SUMMARY

In this investigation an attempt was made to present an over-all picture of the corrosion resistance to intergranular attack for three types of 18-8 stainless steels. A time-temperature-sensitization diagram for each of these materials was constructed. From these diagrams the effect of time and temperature on the corrosion rate can be observed. It was noted that the diagrams were distinctly different for each type of material. If upon further work involving many more heats of each material it is found that these patterns persist, each type of stainless steel could be characterized by such diagrams. It has also been shown that a single test at an arbitrary temperature and time cannot establish or reveal the character of a material in respect to its susceptibility to intergranular corrosion. The lack of having a general knowledge and a complete picture of the intergranular corrosion resistance of stainless steels caused many problems concerning the use of these materials and test methods for evaluating these materials.

It is hoped that the information presented in this paper will clarify this situation and establish a better understanding of the nature of intergranular corrosion in stainless steels.

Acknowledgment:

The authors are grateful to the management of A. O. Smith Corp. for supporting this research project and for permission to publish these results. We also acknowledge the assistance of E. D. Ralph in conducting the corrosion work.

DISCUSSION

F. C. HULL[1]—What is the morphology of carbides as a function of time? In recent publications, by using the technique of electron micrographs of carbon extraction replicas, several authors have shown how the morphology of the carbide precipitation in stainless steels varies with time and temperature of exposure. The severity of corrosion depends very markedly on whether the carbide forms continuous or connected paths through the alloy. Have the authors analyzed their data from this viewpoint?

H. F. EBLING AND M. A. SCHEIL (*authors*)—Your question is a good one. We have not made extraction of the grain boundaries and analysis of this material to know whether it could be carbides or possibly sigma, as we suspect.

We have a good deal of work to do to make an identification of the grain boundary material, and your question would be one which we would like to see answered.

C. H. SAMANS[2]—We have considerable data on nitric acid tests on 13 stainless steels, some of which differ only in carbon content, which are now being correlated. Some of the results differ significantly from those reported here. In particular, we have found for many of these steels a failure zone for holding times exceeding, roughly, 50 hr between 850 and 1150 F. As a first approximation at least the extent of this failure zone seems to be affected very little by the carbon content.

L. W. LHERBIER[3]—In respect to the stabilizing treatment, have you studied the effects of time at 1650 F or the effect at higher temperatures?

MESSRS. EBLING AND SCHEIL—We have not done much work exploring time and temperature relationships for the stabilization heat treatment. Theoretically, stabilization is accomplished by precipitating carbon in excess of its solubility at a particular temperature. If the excess carbon precipitated as chromium carbides, enough time must be allowed to diffuse chromium to the depleted area surrounding the chromium carbide. When this is accomplished, the amount of free carbon (soluble) is reduced in the material, and the carbides already formed are harmless as far as intergranular corrosion is concerned. If this explanation is correct, it would be better to use lower stabilizing temperatures and longer times at heat to effect the best conditions.

Stabilization heat treatments are used with some success in materials having a carbon content of 0.04 to 0.10 per cent. In materials of 0.03 per cent carbon max (about 0.03 per cent carbon soluble in austenite) there will be no benefit from this treatment; however, this treatment is sometimes used as for stress relieving or a substitute for full annealing.

R. DEFUSCO[4]—What method is used to determine corrosion penetration in nitric acid?

MESSRS. EBLING AND SCHEIL—The corrosion penetration was measured from calculations involving the weight loss. This standard procedure is described in ASTM A 262. It is conceded that the penetration calculated from the weight loss is not a good method but is recognized as a standard procedure. Penetration as revealed by change in electrical resistance would be a better method, but this has not been used to any great extent as yet.

MR. DEFUSCO—Do you have corrosion data in other media such as lithium hydroxide?

MESSRS. EBLING AND SCHEIL—We have not used any other test media. The boiling nitric acid test is a recognized standard test for determining intergranular susceptibility in stainless steels.

J. J. HEGER[5]—What is the minimum cooling rate that can be tolerated without danger of intergranular corrosion for Type 304L after a stress relief at 1400 to 1500 F?

MESSRS. EBLING AND SCHEIL—The curves presented are developed from isothermal data. It is doubtful that one could determine the effect of continuous cooling on these curves. In the case of standard TTT diagrams where gross transformations take place, one can estimate with some confidence the effect of continuous cooling on the curves developed by isothermal data. However, the TTS curves are not based on a major transformation; they are based on minor but very important formations of precipitates at the grain boundaries and the effect of this on the nitric-acid corrosion resistance of the material. Technically, TTS curves are based on diffusion rather than on transformation phenomena.

We have only one test made on Type 304L which was heated to 1400 F, held for 15 hr and furnace cooled at a rate of 20 F/hr. This treatment resulted in a corrosion rate of over 1 in. per year. Until data are accumulated from many heats of Type 304L in which the effect of cooling rate on the corrosion resistance is explored, there is little hope in giving a general answer to your question.

E. J. DULIS[6]—What would you estimate to be the effect of various amounts of delta ferrite on the TTS curves of the type of steels studied?

MESSRS. EBLING AND SCHEIL—It is our belief that the amount of delta ferrite is not important, but the location, distribution, and temperature at which it was formed are the factors which could influence the nitric acid corrosion resistance of material containing it. Delta ferrite formed along grain boundaries and subjected to temperatures below 1400 to 1500 F for short times can be partially or wholly converted to the sigma phase. The effect of sigma phase formed at the lower temperatures on the nitric acid resistance of the material is similar to that of carbide precipitation, and their effects are additive. This in effect would shift the TTS curves to the left. The TTS curve shown for Type 316L illustrates this. The carbon levels of the Type 316L and 304L are very close, yet the Type 316L curves are shifted considerably to the left of Type 304L. It is our belief that the increased susceptibility to intergranular attack

[1] Advisory metallurgist, Research and Development Center, Westinghouse Electric Corp., Pittsburgh, Pa.

[2] American Oil Co., Whiting, Ind.

[3] Universal-Cyclops Steel Corp., Bridgeville, Pa.

[4] Knolls Atomic Power Laboratory, Schenectady, N. Y.

[5] U. S. Steel Corp., Pittsburgh, Pa.

[6] Crucible Steel Company of America, Pittsburgh, Pa.

in Type 316L is the result of the formation of the sigma phase on the grain boundaries.

A. MOSKOWITZ[7]—The 1600 F "stabilizing" treatment for Type 347 stainless steel was mentioned in this paper. Results indicating that such a treatment can be detrimental to Type 347 have been obtained in a test program conducted by the Welding Research Council. There were two environments in which material given a 4 hr 1600 F treatment before sensitization at 1250 F (1 hr) showed intergranular attack, which was not shown by the same material given only the sensitizing treatment. There was no instance in which the 1600 F treatment was helpful in lessening intergranular attack or weld line attack.

A paper presented by J. R. Auld in March, 1963, at the Second International Congress on Metallic Corrosion, "Effect of Heat Treatment and Welding on Corrosion Resistance of Austenitic Stainless Steel," also indicated several instances where a 1600 F treatment made for increased corrosion.

[7] Central Research Laboratory, Crucible Steel Company of America, Pittsburgh, Pa.

ALLOYING PRECIPITATION HARDENING STAINLESS STEELS FOR STRENGTH AND STABILITY

By D. C. Perry[1] and M. W. Marshall[2]

Synopsis

Stainless steels 17-7 PH and PH 15-7 Mo could not be used in their highest /strength conditions because they lacked toughness. Overaging was employed to obtain good fracture strengths but with a considerable sacrifice in useful tensile properties. Even in the overaged condition, these steels become embrittled after long-time exposure at temperatures of 600 to 700 F.

This paper described alloy development studies that have resulted in a new precipitation hardening steel, PH 14-8 Mo. This stainless steel has exceptionally high net fracture strengths in excess of 225,000 psi. Long time exposure studies at temperatures of 400 to 750 F show marked resistance to embrittlement.

This breakthrough in toughness and stability is attributed to close control of chemical composition, especially carbon, phosphorus, sulfur, and nitrogen. The merits of air and vacuum melting processes in obtaining the desired results are also discussed.

During the past 10 to 15 years, the precipitation hardening stainless steels have been used in many military and civilian applications. Their unique combination of fabricability, strength, and corrosion resistance have made them useful engineering materials.

As with most materials, compromises in hardening treatment were necessary for the best combination of strength and toughness, depending on the end use. For example, 17-7 PH and PH 15-7 Mo are not normally used in their highest strength conditions because of low toughness. Lowering the strength level by overaging improved toughness to a useful level, and, in this condition, thousands of tons have been used. Even in this condition, however, these steels lost toughness and became embrittled after long-time exposure at temperatures of 600 to 700 F.

This paper describes studies that have led to a new semi-austenitic precipitation hardening stainless steel, PH 14-8 Mo, which overcomes many of the shortcomings of the previously mentioned steels.

PH 14-8 Mo was specifically developed for use in the supersonic commercial transport airplane. Material requirements for this airplane are very demanding. In addition to having high strength, corrosion and stress corrosion cracking resistance, weldability, fabricability, and so on, high fracture toughness and stability at elevated temperatures are required.

We are concerned here primarily with three of these requirements, namely, strength, toughness, and stability. *Strength* to enable the designer to design efficient airframe components to perform at temperatures ranging from about −100 to 650 F; *toughness* to resist the propagation of a crack until it can be detected by normal inspection procedures and repaired; and *stability* to retain toughness from −100 to 650 F over the life of the aircraft which may be as long as 30,000 to 50,000 hr of flight time (10 to 15 years).

Stability, and here we mean metallurgical stability, has at least two meanings. To some, stability means no change or degradation of properties after 30,000 to 50,000 hr exposure at temperatures up to 650 F. Others, and we subscribe to this view, recognize that some change of properties does occur, but at such a rate that useful and often excellent engineering properties remain even after a severe elevated temperature exposure.

Toughness Tests

The same tests are used to measure toughness and stability. The change in toughness because of a given exposure and the toughness level itself, are measures of stability.

At the Armco Research Center we have used a number of toughness tests, namely:

1. Center notch fatigue cracked (1).[3]
2. National Aeronautics and Space Administration (NASA) edge notch (1).
3. Allison bend test (instrumented bend test) (2).
4. Precracked sheet charpy (3).

The Allison bend test has proved to be an excellent test, being both inexpensive and discriminating. As we were able to improve toughness, the Allison bend test proved to be incapable of separating very tough materials, and we switched to the precracked charpy which has proved to be another inexpensive reliable toughness test.

The center notch fatigue cracked specimen and the NASA edge notch specimen have been included to present toughness data in terms with which more engineers are familiar.

Metallurgy of the Semiaustenitic PH Stainless Steels

The chemistry of the semiaustenitic precipitation hardenable stainless steels is so balanced that they are austenitic in the annealed or solution treated condition, and can be transformed to "martensite" by suitable thermal sequences and subsequently further strengthened by an aging treatment. This heat treating sequence can be combined with a brazing operation as in the manufacture of brazed honeycomb panels when the flow-point of the brazing alloy is compatible with the conditioning temperaure of the steel.

The chemical compositions of two of the standard semiaustenitic stainless steels are given in Table 1. The only difference between these two steels is that we have substituted 2 per cent molybdenum for 2 per cent chromium in going from 17-7 PH to PH 15-7 Mo. Both steels have identical microstructures. In Condition A (annealed) they have 10 to 20 per cent delta ferrite (Fig. 1).

Heating at temperatures of 1300 to 1800 F (called the conditioning temperature) results in the precipitation of carbon as $Cr_{23}C_6$ (4) in the ferrite austenite

[1] Senior research engineer, Armco Research Center, Armco Steel Corp., Middletown, Ohio.
[2] Supervising research metallurgist, Armco Research Center, Armco Steel Corp., Middletown, Ohio.

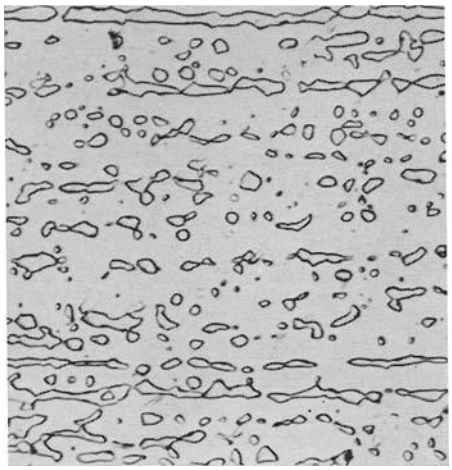
[3] The boldface numbers in parentheses refer to the list of references appended to this paper.

Copyright© 1965 by ASTM International

www.astm.org

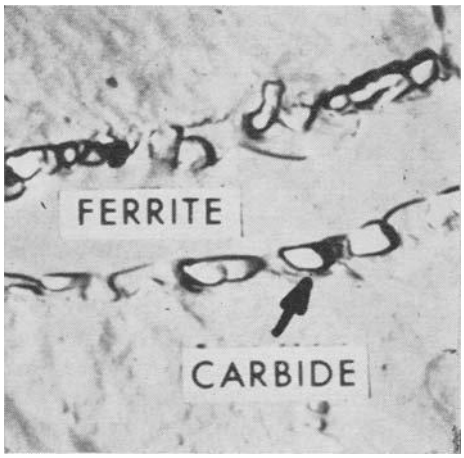
TABLE 1—CHEMICAL COMPOSITION.

	C	Mn	P	S	Si	Gr	Ni	Mo	Al
17-7 PH.....	0.07	0.60	0.02	0.015	0.45	17.1	7.1	...	1.2
PH 15-7 Mo.....	0.07	0.60	0.02	0.015	0.45	15.2	7.1	2.2	1.2



NOTE—Structure showing 10 to 20 per cent delta ferrite in matrix of austenite.

FIG. 1—PH 15-7 Mo Condition A, NaCN Etch (×1000).



NOTE—Structure showing chromium carbides ($Cr_{23}C_6$) in delta ferrite martensite interface.

FIG. 2—PH 15-7 Mo Condition RH 1050 Vilella etch (×18,000).

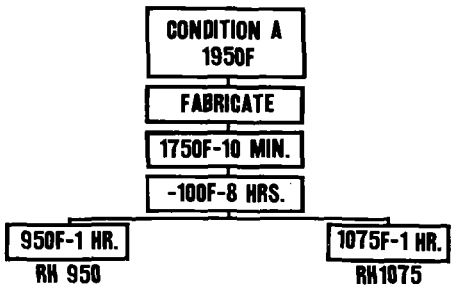


FIG. 3—Recommended Heat Treating Sequence for 17-7 PH and PH 15-7 Mo Stainless Steels.

interface. This precipitation results in a decrease in the stability of the austenite so that on cooling to the martensite transformation (Ms) temperature, the austenite transforms to martensite. We then have the situation pictured in Fig. 2, namely, carbides at the ferrite-martensite interface. Finally, precipitation hardening at a temperature of 900 to 1100 F completes the heat treatment.

It has been observed that cracks, almost without exception, follow the ferrite-martensite interface. Since carbides are generally hard and brittle, it was not surprising that failure would occur in this location.

It was reasoned that if these carbides could be eliminated from the ferrite-martensite interface, toughness could be improved. The problem here was to adjust the rest of the analysis so that carbon could be lowered but still retain the semiaustenitic qualities of 17-7 PH and PH 15-7 Mo. In addition, the heat treatment time had to be kept reasonably short to be compatible with users' heat treatments and processing schedules.

But before this lower carbon PH steel (PH 14-8 Mo) is described, strength, stability and toughness of other semi-austenitic PH steels should be stated.

The data given in this paper are on sheet or strip produced from commercial ingots by hot and cold rolling on continuous mills unless otherwise noted. Test data are on specimens taken transverse to the direction of rolling.

PROPERTIES OF PH 15-7 Mo

The heat treating sequences to develop Conditions RH 950 (high strength) and RH 1075 (overaged for toughness) are given in Fig. 3.

As stated above, PH 15-7 Mo is not normally used in its highest strength condition because of its low fracture toughness. Overaging at a temperature of 1050 to 1075 F lowers strength but improves toughness to a usable level. Table 2 lists typical strengths and toughness of PH 15-7 Mo in the RH 950 and RH 1075 conditions. Note the increase in notch strength/yield strength (NS/YS) ratio of from 0.47 for Condition RH 950 to 0.65 for Condition RH 1075, corresponding with a reduction in the tensile strength of about 235,000 psi to about 210,000 psi. At this toughness level, PH 15-7 Mo has found many applications such as in brazed honeycomb panels in the RS 70.

All steels of this type tend to gain strength and lose toughness when exposed to temperatures of 500 to 800 F for long periods of time, and PH 15-7 Mo is no exception.

One of the screening tests for measuring the toughness and stability of materials for the supersonic transport airplane (SST) is exposure for 1000 hr at 650 F under 50,000 psi load using the NASA edge notch specimen (0.0007-in.-max root radius) (5). Table 3 presents data developed at the University of Syracuse on PH 15-7 Mo Condition RH 1050.[4] Note the relatively low notch strengths and NS/YS ratios. From these data, PH 15-7 Mo is obviously not a good candidate for extended use at temperatures of 650 F.

Another way of measuring stability is long time exposures at elevated temperature under no load. PH 15-7 Mo Condition RH 1075 was exposed at 400, 550, and 700 F for times up to 7500 hr with no load. Figure 4 gives the results of these tests. Here the Allison bend test is used as the toughness test. Note that at 400 and 550 F the strength and toughness are essentially unchanged after 7500 hr exposure. (The small increase in toughness is a result of the 400 F stress relief.) Exposure at 700 F, however, shows a rapid initial gain in strength, and then a continued gain but at a lesser rate. The Allison parameter, initially 0.05, drops to 0.0 within the first 1000 hr exposure at 700 F. Comments as to the theorized mechanism of this continued gain in strength will be given later.

Electron micrographs before and after exposure at 700 F for 7500 hr reveal little difference in structure.

PROPERTIES OF PH 14-8 Mo

Effect of Carbon on Toughness:

It was stated earlier that it was reasoned that if carbides could be eliminated from the ferrite-martensite interface, toughness would be improved. Table 4 shows the effect of carbon on the toughness of four 30-lb laboratory induction heats. Note the improvement in toughness from 0.10 (0.077 per cent C) to 0.53 (0.032 per cent C). In these heats the analysis was kept constant except for changes in nickel to compensate for the planned change in carbon. Heat A is representative of PH 15-7 Mo while heats C and D are more representative of the early PH 14-8 Mo heats.

[4] NASA Contract NASR-43, Syracuse University.

Effects of Minor Elements on Toughness:

It is well known that imperfections in the crystal lattice tend to reduce ductility and toughness in pure metal whiskers. Thus it was logical to determine if elements such as phosphorus, sulfur, and nitrogen had such an effect on PH 14-8 Mo. Phosphorus and sulfur can be controlled by melting practice or raw material selection or both. Nitrogen is always present in the air-melted aluminum bearing PH steels in the amounts of about 0.025 to 0.05 per cent. It cannot be substantially lowered in consumable electrode vacuum arc remelting but can be essentially excluded by the vacuum induction melting process.

Phosphorus and Sulfur:

Table 5 compares the toughness of two 30-lb air induction heats, Heat E with normal phosphorus and sulfur, and Heat F with low phosphorus and sulfur. The beneficial effect over and above that of the low carbon is obvious.

The effect of nitrogen was studied using 30-lb laboratory vacuum induction heats. These data are given in Table 6 using the precracked sheet charpy test as the measure of toughness. This change in testing procedure was made because the toughness of steels like Heat G became so great that a finite Allison parameter could not be determined. The work per unit of area (W/A) of 820 obtained on Heat H is approximately equal to an Allison parameter of about 0.60. The W/A of 1682 obtained on Heat G is extremely high and is indicative of the very potent effect of low nitrogen on toughness.

The effects of manganese and silicon on toughness of PH 14-8 Mo were also studied on 30-lb vacuum induction heats. Data given in Table 7 show a relatively small effect of manganese and silicon on toughness, with the higher purity Heat K having higher toughness.

Summary of Effect of Minor Elements:

From these data it is obvious that good toughness is obtained in air melted PH 14-8 Mo with low phosphorus and sulfur contents. Even higher toughness is obtained, when, in addition, the nitrogen content is reduced to very low levels, levels obtainable on a tonnage basis only by vacuum induction melting. Elimination of manganese and silicon, possible by vacuum induction melting, gives an additional increase in toughness.

TABLE 2—MECHANICAL PROPERTIES OF PH 15-7 Mo (TRANSVERSE DIRECTION).

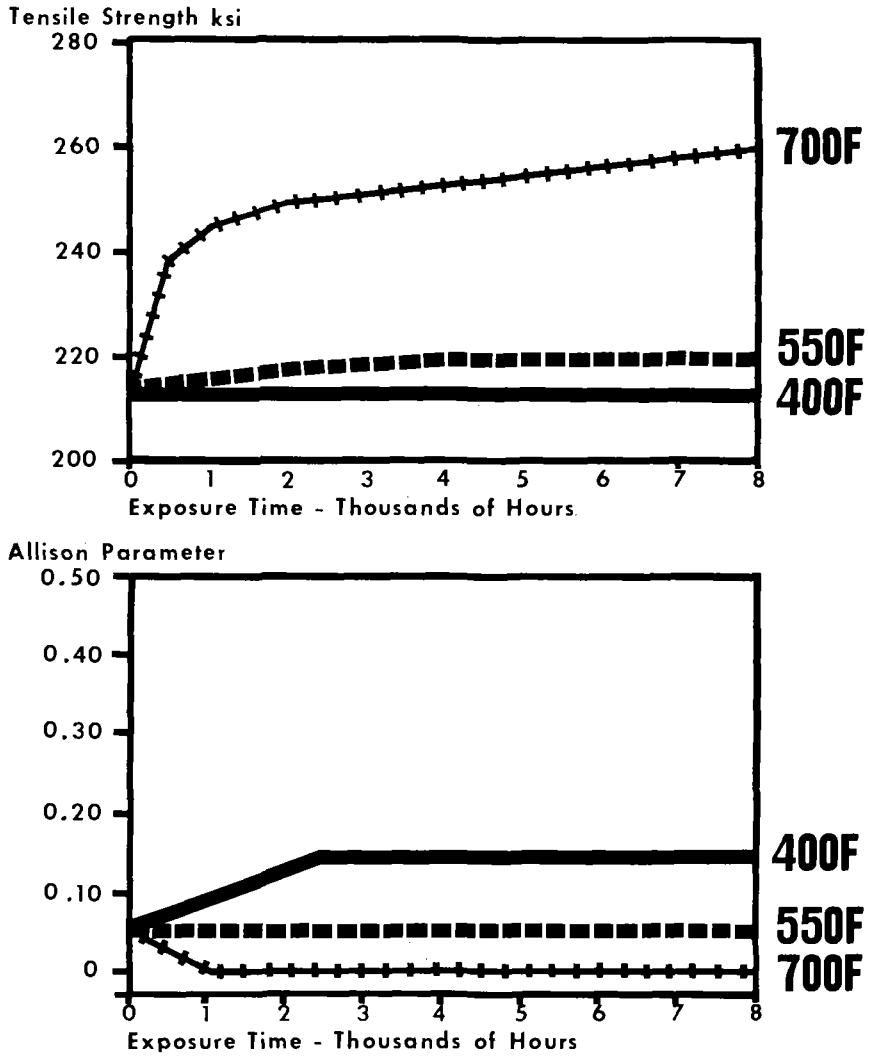
Condition	Ultimate Tensile Strength, ksi	0.2% Offset Yield Strength, ksi	Allison Bend	Notch Strength[a]	NS/YS
RH 950, no exposure	235	220	0.02	105	0.47
RH 1075, no exposure	212	207	0.10	135	0.65

[a] Center notch strength, 0.050-in.-thick sheet, 2-in.-wide specimen, fatigue cracked.

TABLE 3—PH 15-7 Mo EDGE NOTCH[a] VERSUS TENSILE STRENGTH.
(Exposed at 650 F, 1000 hr, 50 ksi load, transverse direction)

	Test Temperature, deg F	Tensile Strength, ksi	0.2% Offset Yield Strength, ksi	Notch Strength, ksi	NS/YS
Condition RH 1050	−100	230	215	99	0.44
	75	214	200	120	0.57
	650	177	168	113	0.65

[a] NASA Specimen, Syracuse University, NASA Contract NASR-43.



(*top*) Effect of exposure time on strength.
(*bottom*) Effect of exposure time on toughness.

FIG. 4—PH 15-7 Mo Condition RH 1075: Effect of Long Time Exposure at Elevated Temperatures on Strength and Toughness.

PROPERTIES OF PH 14-8 Mo

The heat treatment (Fig. 5) of PH 14-8 Mo is similar to that of 17-7 PH and PH 15-7 Mo. Because of its lower carbon content, it is more sluggish than 17-7 PH or PH 15-7 Mo and requires a longer austenite conditioning time (6). However, it still is compatible with brazing cycle heat treatments used in brazed honeycomb panels.

TABLE 4—EFFECT OF CARBON CONTENT ON TOUGHNESS OF PH 14-8 Mo.

Heat	C	Cr	Ni	Ultimate Tensile Strength, ksi	Allison
A	0.077	14.53	7.35	225	0.10
B	0.048	14.43	7.94	231	0.22
C	0.039	14.47	8.09	224	0.39
D	0.032	14.54	8.12	236	0.53

	Mn	P	S	Si	Mo	Al
All Heats	0.40	0.02	0.02	0.40	2.2	1.2

TABLE 5—EFFECT OF PHOSPHORUS AND SULFUR ON TOUGHNESS OF PH 14-8 Mo.

Heat	P	S	Ultimate Tensile Strength	Allison
E	0.019	0.023	225	0.39
F	0.002	0.004	226	0.63

	C	Mn	Cr	Ni	Mo	Al
Both heats	0.04	0.55	14.5	8.1	2.2	1.2

TABLE 6—EFFECT OF NITROGEN ON TOUGHNESS OF PH 14-8 Mo.

Heat	N	Ultimate Tensile Strength, ksi	Precrack Charpy,[a] W/A
G	0.0017	226	1682
H	0.028	225	820

	C	Mn	P	S	Si	Cr	Ni	Mo	Al
Both heats	0.03	Nil	0.001	0.002	Nil	14.4	8.4	2.3	1.2

[a] 0.050-in.-thick sheet.

TABLE 7—EFFECT OF MANGANESE AND SILICON ON TOUGHNESS OF PH 14-8 Mo.

Heat	Mn	Si	Ultimate Tensile Strength, ksi	Precrack Charpy,[a] W/A
J	0.34	0.34	218	1254
K	0.01	0.006	220	1605

	C	P	S	Cr	Ni	Mo	Al
Both heats	0.03	0.002	0.004	15.0	8.3	2.2	1.2

[a] 0.050-in.-thick sheet.

A comparison of the strength, toughness, and stability of air melted PH 14-8 Mo, air melted PH 15-7 Mo, and vacuum induction melted PH 14-8 Mo is given in Table 8. The conventional mechanical properties of all three steels are identical. The toughness of air melted PH 14-8 Mo even after the severe exposure of 1000 hr at 750 F is greater than air melted PH 15-7 Mo after no exposure. Further note that the toughness of vacuum induction melted PH 14-8 Mo after exposure at 750 F for 1000 hr is greater than that of air melted PH 14-8 Mo with no exposure.

The stability of air melted PH 14-8 Mo Condition SRH 950 (235,000 psi ultimate tensile strength) was studied in the same manner as PH 15-7 Mo, that is, exposed at 400, 550, and 700 F with no load for times up to 7500 hr. These data are presented in Fig. 6. A comparison with Fig. 4 shows that, like PH 15-7 Mo, the strength of PH 14-8 Mo is essentially unchanged after exposure at 400 and 550 F. Unlike PH 15-7 Mo Condition RH 1075 which continues to gain strength with exposure at 700 F, air melted PH 14-8 Mo Condition SRH 950 stops gaining strength after about 3000 hr exposure.

The toughness of PH 14-8 Mo is unchanged after 7500 hr at 400 F and is reduced slightly by exposure at 550 F. At 700 F, toughness drops for about the first 1000 hr exposure, then is unchanged up to the present limit of our data. (These tests are continuing and will not be completed until December, 1965). Here the air melted PH 14-8 Mo Condition SRH 950, at an initial strength of 245,000 psi, has higher toughness left after 7500 hr at 700 F than PH 15-7 Mo Condition RH 1075 at an initial strength level of 215,000 psi with no exposure.

The chemical composition of air melted PH 14-8 Mo and PH 15-7 Mo is essentially the same except for the carbon, phosphorus, and sulphur contents (see Table 9). It had been theorized previously, that the continued strengthening of 17-7 PH and PH 15-7 Mo on long time exposure at elevated temperatures was a continuation of the nickel-aluminum precipitation reaction. Since the strengthening of PH 14-8 Mo apparently ceases after about 3000 hr at 700 F and the aluminum and nickel contents are essentially the same as in PH 15-7 Mo which continues to strengthen under identical exposure conditions, it is apparent that the strengthening mechanism is a complex one, involving perhaps, in addition to the nickel-aluminum precipitation, carbon, phosphorus, or sulfur, or a combination thereof. Studies are under way in an attempt to understand this behavior.

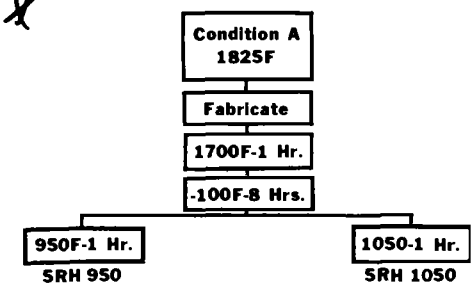


FIG. 5—Recommended Heat Treating Sequence for PH 14-8 Mo Stainless Steel.

Another comparison of PH 15-7 Mo and air and vacuum induction melted PH 14-8 Mo is shown in Table 10.[5] Here the three steels are tested at −100, 75, and 650 F before and after an exposure of 1000 hr at 650 F under 40,000 psi load. Comparison is made on the basis of notch strength and NS/YS ratio using the sharp edge notch NASA specimen. Note the superiority of air melted PH 14-8 Mo over air melted PH 15-7 Mo and vacuum induction melted PH 14-8 Mo over air melted PH 14-8 Mo.

Notch strength is much more indicative of the usefulness of a material than the NS/YS ratio since it has a strength level connotation. When a change in ratio is reported because of elevated temperature exposure, this change may be because of an increase in yield strength, not a loss in notch strength. Hence an examination of the change in notch strength itself, not the ratio, is a better indication of stability.

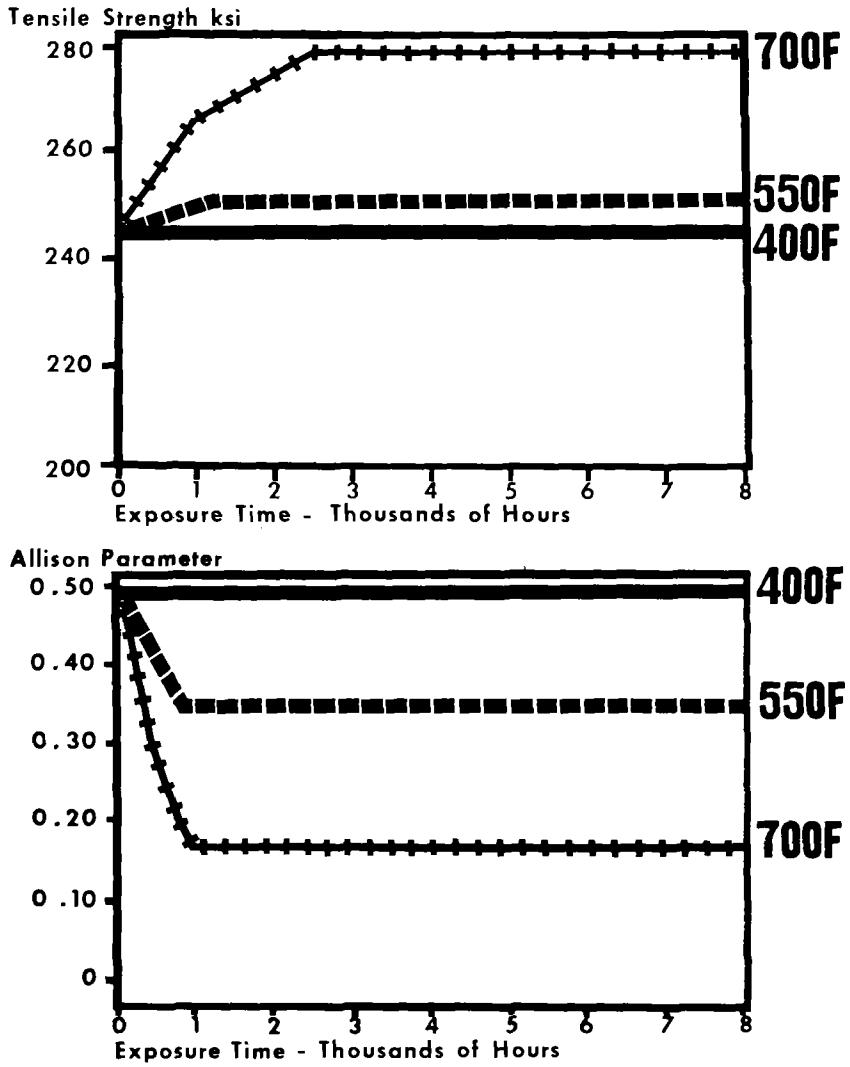
[5] G. B. Espey, private communication.

TRANSITION TEMPERATURE

The transition temperature of the three steels being discussed was determined at a tensile strength level of 235,000 psi using the precracked sheet charpy. These data are presented in Fig. 7. Note that at −300 F, the transition temperatures of the two PH 14-8 Mo steels have not been reached. Also note that at −300 F the impact strength of the vacuum induction melted steels is equal to the room-temperature impact strength of the air melted PH 14-8 Mo. In turn, the impact strength of air melted PH 14-8 Mo at −300 F is much greater than PH 15-7 Mo at any test temperature.

TABLE 8—MECHANICAL PROPERTIES OF PH 14-8 Mo VERSUS PH 15-7 Mo (TRANSVERSE DIRECTION).

	Tensile Strength, ksi	Yield Strength, ksi	Elongation, % in 2 in.	Allison Bend	
				No Exposure	750 F 1000 hr
PH 15-7 Mo, air arc, RH 950.....	235	220	5	0.02	0.0
PH 14-8 Mo, air arc, SRH 950.....	235	220	5	0.45	0.15
PH 14-8 Mo, vacuum induction SRH 950.....	235	220	5	>2.0	0.77



(*top*) Effect of exposure time on strength.
(*bottom*) Effect of exposure time on toughness.

FIG. 6—PH 14-8 Mo Condition SRH 950: Effect of Long Time Exposure at Elevated Temperatures on Strength and Toughness of Air Melted PH 14-8 Mo.

CONCLUSIONS

Data have been presented showing the beneficial effects of low carbon, phosphorus, sulfur, silicon, manganese, and nitrogen on the toughness and stability of a high-strength semiaustenitic precipitation hardening stainless steel, PH 14-8 Mo.

Excellent toughness and stability were obtained on air melted PH 14-8 Mo. In fact, while the previous semiaustenitic precipitation hardening stainless steels continue to strengthen and embrittle with increasing exposure at temperatures up to 700 F, PH 14-8 Mo does not. After approximately 2500 hr exposure at 700 F, no further changes in properties occurred. Excellent toughness was retained even after exposures at 700 F.

Still greater toughness, with like stability, is obtained in vacuum induction melted PH 14-8 Mo.

These levels of properties make PH 14-8 Mo useful wherever toughness and stability at elevated temperatures are required, or whenever high toughness in light-weight structures is needed at cryogenic temperatures.

Acknowledgments:

The authors wish to thank G. E. Selby, supervisor, Mechanical Testing Laboratory and his staff for performing the many tests required, J. C. Wilkins and R. E. Pence for the electron micrographs, C. R. Taylor and E. D. Scherrer for the vacuum induction heats, R. J. Bendure and his staff of chemists for the many chemical analyses required, Louis Davis for his careful preparation and heat treating of the many specimens, and other members of the Armco Research Center who aided in various phases of the work leading to the publication of this paper.

TABLE 9—CHEMICAL COMPOSITION AND MECHANICAL PROPERTIES OF PH 15-7 Mo AND PH 14-8 Mo.

	C	Mn	P	S	Si	Cr	Ni	Mo	Al	N	Ultimate Tensile Strength, ksi	0.2% Yield Strength, ksi	Allison
PH 15-7 Mo, air.....	0.07	0.60	0.020	0.015	0.40	15.2	7.1	2.2	1.2	0.03	235	220	0.05
PH 14-8 Mo, air.....	0.035	0.30	0.005	0.005	0.40	14.5	8.1	2.2	1.2	0.03	235	220	0.50
PH 14-8 Mo, vacuum induction.....	0.035	<0.05	0.002	0.002	<0.05	15.1	8.5	2.2	1.2	0.001	235	220	>2.0

TABLE 10—EFFECT OF EXPOSURE AT 650 F FOR 1000 HR UNDER 40 KSI LOAD ON NOTCH STRENGTH AND NS/YS RATIO, TRANSVERSE DIRECTION.[a,b]

Grade	Condition	Type[c] Melt	Exposure[d]	Test Temperature					
				−100 F		75 F		650 F	
				Notch Strength, ksi	NS/YS	Notch Strength, ksi	NS/YS	Notch Strength, ksi	NS/YS
PH 15-7 Mo	RH 1050	air	None						
			Yes	99.0	0.44	120	0.57	113	0.65
PH 14-8 Mo	SRH 950	air	None	202.3	0.83	194.7	0.92	128.5	0.76
			Yes	185.8	0.72	179.8	0.76	118.4	0.65
PH 14-8 Mo	SRH 950	vacuum	None	246.1	0.99	224.7	1.01	164.5	0.97
			Yes	221.2	0.84	201.8	0.84	152.1	0.84
PH 14-8 Mo	SRH 1050	vacuum	None	247.5	1.09	230.9	1.10	154.4	1.02
			Yes	243.5	1.00	217.9	0.97	166.7	0.94

[a] NASA edge notch specimen: 0.025 thick, 0.0007 max root radius.
[b] Data: Courtesy Lewis Labs, NASA.
[c] Air = air arc furnace; vacuum = vacuum induction.
[d] Exposure: 1000 hr at 650 F under 40 ksi load.

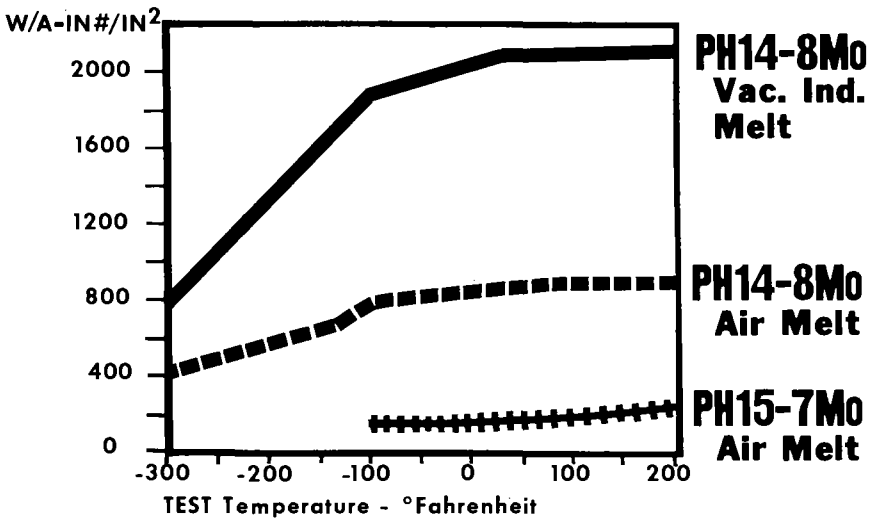


FIG. 7—Transition Temperature Curves of Several Precipitation Hardening Stainless Steels. All Heat Treated to a Tensile Strength of 235,000 psi.

REFERENCES

(1) "Fracture Testing of High Strength Sheet Material," *ASTM Bulletin*, Am. Soc. Testing Mats., January, 1960, pp. 30-39.
(2) "Fracture Testing of High Strength Sheet Material," *ASTM Bulletin*, Am. Soc. Testing Mats., February, 1960, pp. 18-28.
(3) G. M. Orner and C. E. Hartbower, "Sheet Fracture Toughness Evaluated by Charpy Impact and Slow Bend," *Welding Research Supplement*, September, 1961, pp. 405S to 416S.
(4) J. C. Wilkins, R. E. Pence, and D. C. Perry, "Aging Mechanism in Precipitation Hardening Stainless Steel," presented at AIME symposium on *Recent Advances in the Metallurgy of Stainless Steels*, Cleveland, Ohio, Oct. 24, 1963.
(5) G. B. Espey, R. T. Bubsey, and W. F. Brown, Jr., "A Preliminary Report on NASA Sheet Alloy Screening Program for Mach 3 Transport Skins," presented at 65th Annual Meeting of ASTM, June, 1962.
(6) D. C. Perry, H. Tanczyn, and W. C. Clarke, Jr., "New PH Steel Matches Strength and Toughness," *Metal Progress*, June, 1963, pp. 101-105.

DISCUSSION

E. J. DULIS[1]—What is considered to be the effect of vacuum melting PH 14-8 Mo in improving toughness; that is, if carbon, phosphorus, sulfur, and nitrogen could be lowered by air melting, what would be the influence of vacuum melting?

D. C. PERRY AND M. W. MARSHALL (*authors*)—Carbon, phosphorus, and sulfur can be adjusted to the desired levels in PH 14-8 Mo by air melting practices using proper scrap selection and proper melting practices. If it were possible to get the desired nitrogen levels by air melting, there would be no need to employ vacuum melting. The melting practice, that is, air or vacuum, is unimportant if the desired chemistry is obtained.

MR. DULIS—Is the 8 hr hold at −100 F required or could shorter times be employed?

MESSRS. PERRY AND MARSHALL—With some heats, a time shorter than 8 hr at −100 F can be employed. However, the 8 hr are necessary to insure that all heats transform properly. Refrigeration at −150 F may enable the time at refrigeration temperature to be reduced. Refer to June 1963 issue of *Metal Progress*, pp. 101-105 for charts on the effect of refrigeration temperature and time on mechanical properties of PH 14-8 Mo.

K. G. BRICKNER[2]—What is the effect of section thickness on notch toughness of PH 14-8 Mo?

MESSRS. PERRY AND MARSHALL—PH 14-8 Mo has been developed as a sheet and strip material and is not recommended for use in plates or heavy sections, especially where high short transverse properties are required. Limited data have suggested that the toughness is not as good in plate thicknesses as it is in sheet thicknesses.

[1] Director of research, Crucible Steel Co. of America, Pittsburgh, Pa.

[2] Research engineer, Applied Research Laboratory, U. S. Steel Corp., Monroeville, Pa.

FINE STRUCTURE AND PROPERTIES OF A 12-Cr MoWV MARTENSITIC STAINLESS STEEL

By B. R. Banerjee,[1] J. J. Hauser,[2] and J. M. Capenos[3]

Synopsis

A comprehensive characterizing of fine structures in Type 422 stainless steel has effectively related structural parameters to smooth- and notch-tensile properties and to corrosion and stress-corrosion resistance. By a departure from conventional heat treatment for this steel, fracture toughness can be increased nearly fourfold at the same yield strength, and corrosion properties can be substantially improved. These marked improvements in properties are explained in terms of dislocation rearrangements and precipitation strengthening effects.

Although the strength and temperature resistance of Type 422 stainless steel has been utilized commercially for a number of years, no comprehensive study of its fine structural characteristics has been reported to date. Therefore, this study (1)[4] was undertaken to characterize Type 422 structurally in terms of its tempering behavior and to relate these fine-structural characteristics to strength and fracture properties.

Material and Methods

A commercial-grade Type 422 stainless steel was hot forged and rolled to 0.120-in.-thick sheets. Table 1 gives the composition of the steel.

The hot-rolled sheets were annealed by slow cooling from 1600 to 1300 F, held at 1300 F, and furnace cooled to room temperature. Slightly oversized tension specimens for the determination of both smooth and notch properties were sheared, heat treated, and finish ground all over to final dimensions. For smooth tensile properties, specimens of 2 in. gage length, 0.35 in. width, and 0.067 in. thickness were tested; for notch tensile properties, center-notched (2) fatigue-cracked specimens 0.067 by 2 by 7.5 in. were tested. The pinholes were reamed, and the center notch was spark-discharge machined. Fatigue cracks, measuring 0.3 to 0.4 in., were introduced by tension-tension. Austenitizing was done at 1900 F for 1 hr, in an argon atmosphere, to avoid delta-ferrite in the structure. The specimens were oil quenched from the austenitizing temperature, refrigerated in liquid nitrogen, and then tempered in air for 2 hr. Austenitizing, refrigerating, and tempering were done in rapid succession.

Quantitative X-ray diffraction showed that there was 1 to 3 per cent retained austenite both before and after the refrigerating treatment. Tempering at 1000 F was needed to transform this austenite; however, the amount of austenite is too small to affect appreciably secondary hardening in this material.

For transmission electron microscopy, sheet specimens were cold rolled to about 0.001-in. thickness, sealed under argon in vycor tubes, and heat treated. A modified Heidenreich technique (3) using a 10 per cent chromic acid in glacial acetic acid electrolyte was found to be satisfactory. For extraction replicas, the specimens were double etched in Vilella's reagent (4 + 4 min) with rinse-dry steps after each etching. Plastic strip replication gave satisfactory results. For electron fractography, a two-stage cellulose-acetate carbon replica technique, described elsewhere (4), was used.

Mechanical Properties

Figure 1 shows hardness and smooth-tensile properties of Type 422 stainless steel as a function of tempering temperature.

The quenched material possesses the maximum tensile strength. Tensile and yield strengths show minima of about 230,000 and 160,000 psi, respectively, at about 500 to 600 F. The yield strength then increases up to about 900 F, and subsequently declines. But the tensile strength and hardness do not reach their inflection points until 1000 F. Elongation increases with tempering temperatures to about 700 F, then decreases to about 1000 F—suggesting temper embrittlement. Upon tempering at higher temperatures, elongation again begins to increase.

Figure 2 shows the net-fracture stress (σ_n), fracture toughness (K_{c3}), crack propagation resistance (R),

$$R = \frac{\sigma_n}{\sigma_y}$$

and the per cent shear characteristic as a function of tempering temperature.

The fracture properties of Type 422 stainless steel change radically with tempering temperature. A pronounced peak or high toughness occurs in the 400 to 600 F region. This peak is followed by a temper-brittle region which reaches minimum toughness at about 950 F. Above 1000 F, fracture toughness is regained but at increasing penalty to yield and tensile strength.

Tempering in the secondary hardening region, at 980 to 1000 F, gives smooth-tensile strengths of 226,000 to 238,000 psi and yield strengths of 161,000 to 165,000 psi. But these strength properties are associated with fracture toughness (K_{c3}) of 50,000 to 64,000 psi $\sqrt{\text{in.}}$ and crack-propagation resistance of 0.32 to 0.42. This observed trend of declining toughness in the secondary hardening temper region is in general agreement with previous data (5). Thus for high-strength sheet applications this heat treatment, though now used for commercial applications (6), would not be suitable from the viewpoint of fracture mechanics.

A much better combination of strength and toughness parameters may be obtained, as Fig. 2 shows, by radically departing from the accepted method of tempering in the secondary hardening region. For example, tensile strengths of 231,000 to 233,000 psi, and yield strengths of 163,000 to 165,000 psi, combined with fracture toughness (K_{c3}) of 235,000 to 242,000 psi $\sqrt{\text{in.}}$, can be obtained by tempering at 500 to 600 F.

[1] Manager, Applied Physics and Basic Research, Research Div., Crucible Steel Company of Am., Pittsburgh, Pa.

[2] Staff metallurgist, Research Div., Crucible Steel Company of Am., Pittsburgh, Pa.

[3] Staff microscopist, Research Div., Crucible Steel Company of Am., Pittsburgh, Pa.

[4] The boldface numbers in parentheses refer to the list of references appended to this paper.

Copyright© 1965 by ASTM International

www.astm.org

TABLE 1—COMPOSITION OF TYPE 422 STAINLESS STEEL.

C	Mn	P	S	Si	Ni	Cr	V	W	Mo	N	O	H, ppm
0.20	0.74	0.014	0.018	0.24	0.81	12.22	0.23	1.05	1.01	0.017	0.0072	0.4

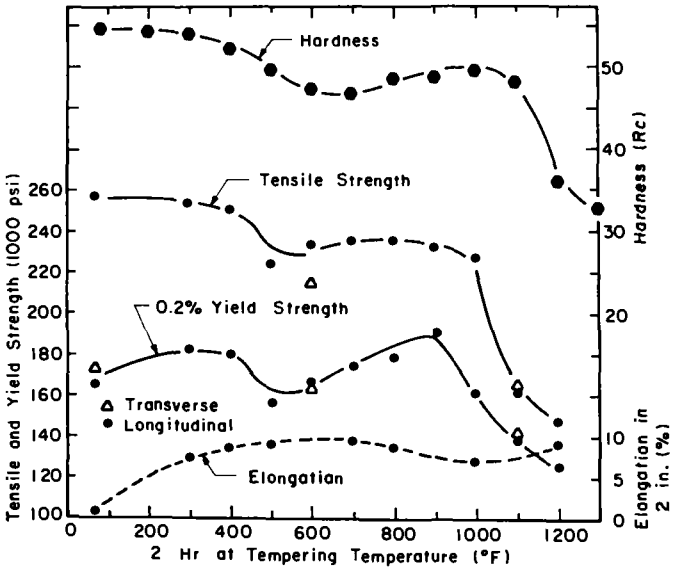


FIG. 1—Hardness and Smooth Tensile Properties of Type 422.

This substantial toughness peak has been previously overlooked, and Type 422 continues to be conventionally heat treated by tempering at 980 F for maximum strength, or at 1200 F or higher for high-temperature applications.

Thus, high strength and high toughness can be combined in Type 422 stainless steel by deliberately avoiding the secondary hardening region and tempering instead at 500 to 600 F. Admittedly, higher tempering temperatures of 1200 F or above, with substantial compromise in strength, may be favored for elevated-temperature applications because of increased temperature stability. But for high-strength applications at temperatures from below room temperature to the tempering temperature (500 to 600 F), this deliberate departure from conventional heat treating concepts offers significant advantages for many aerospace applications, although a limitation may occur in those applications where shape and section size demand a higher stress relief temperature.

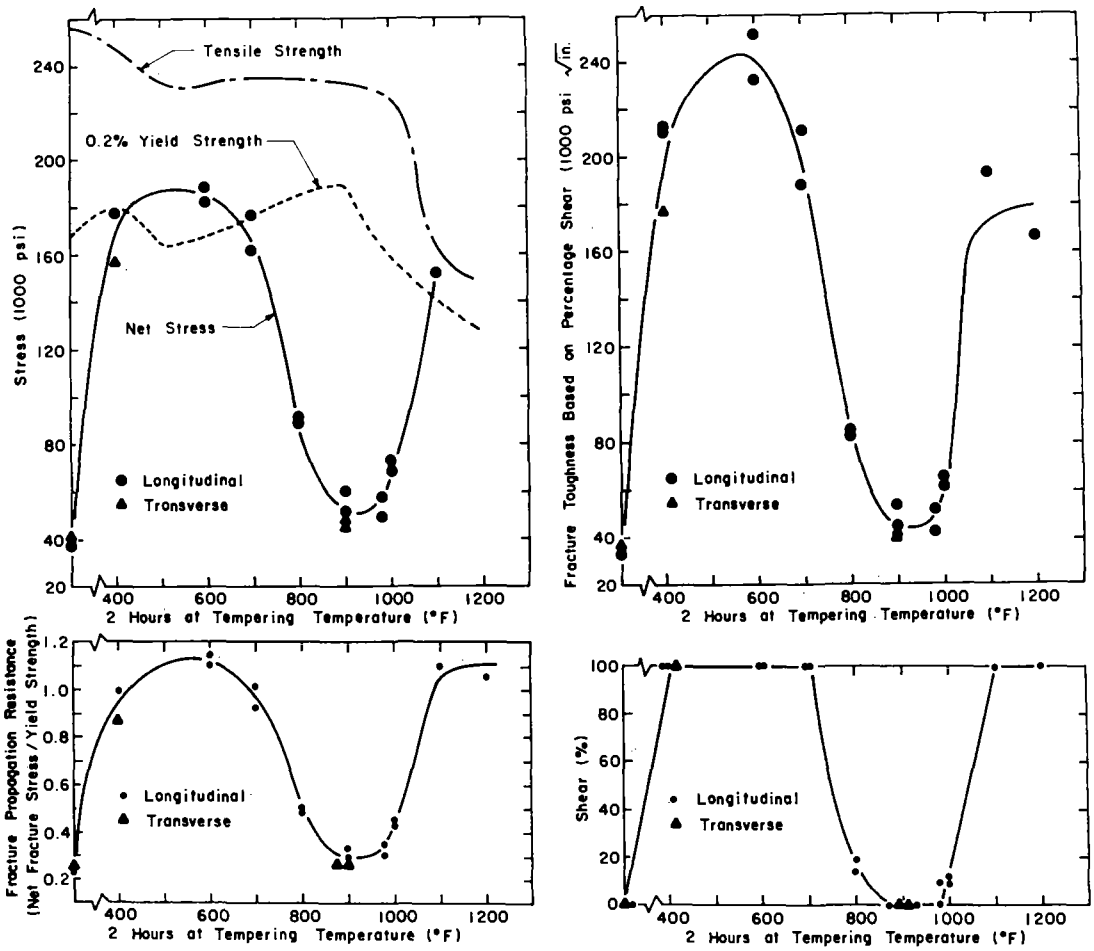


FIG. 2—Fracture Properties of Type 422.

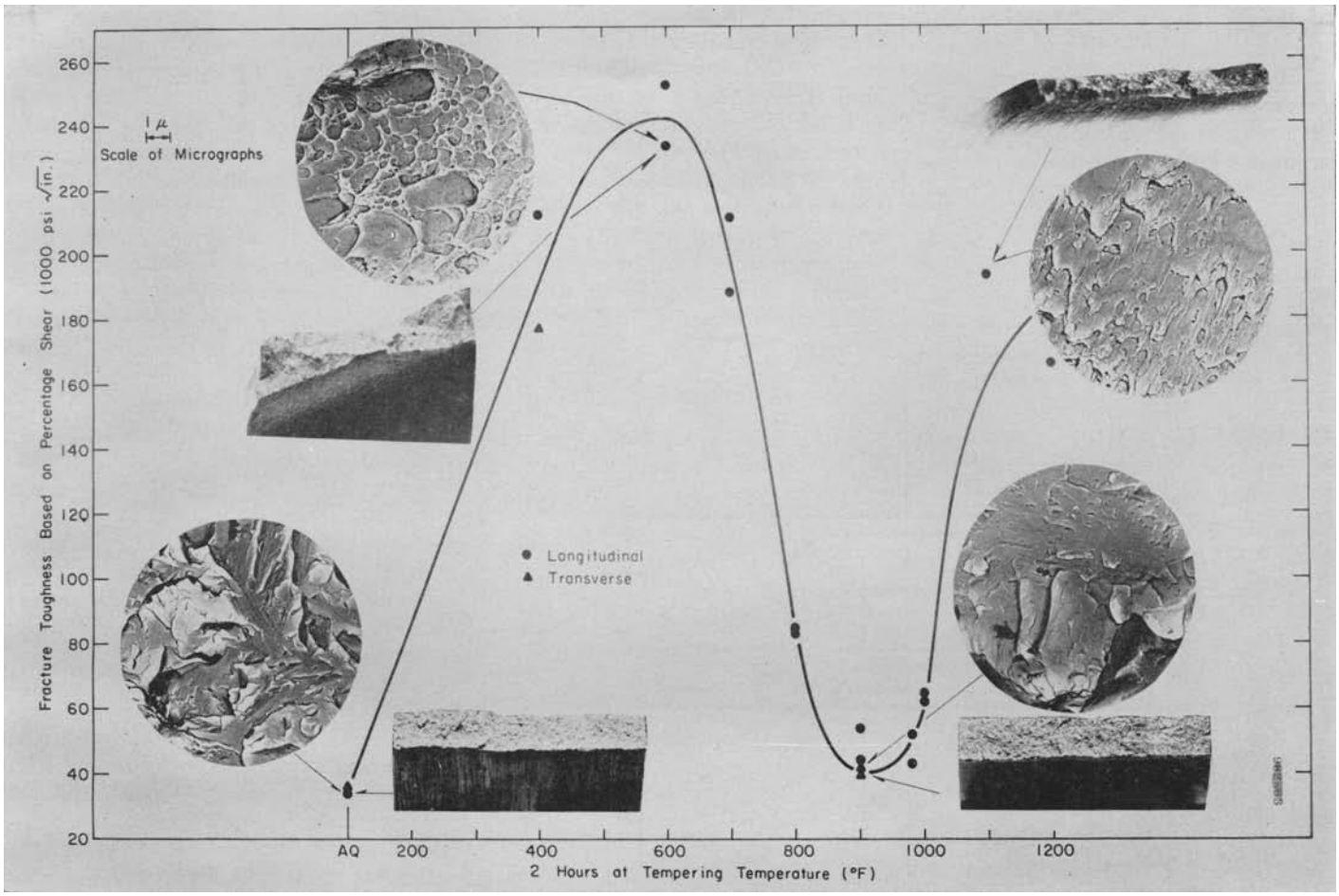


FIG. 3—Toughness, Macroscopic and Submicroscopic Fracture Appearance of Type 422, Tempered as Shown.

FRACTURE APPEARANCE

The radical changes in fracture appearance (Fig. 3) correspond to the changes observed in fracture properties. The changes in macroscopic appearance, as well as the submicroscopic fracture facets in the electron fractographs of smooth tensile specimens, tend to confirm the inflection points on the fracture-toughness curve (Fig. 3).

The fractures of the quenched specimen and the 900 F tempered specimen have the appearance of a flat-transverse fracture. These fractures correspond to the valleys in the fracture-toughness tempering curve. Electron fractographs show that the fracture facets are mainly cleavage steps. The large cleavage facets have river markings and secondary cleavage tongues which are typical of brittle fracture. Some regions of quasi-cleavage contain evidence of plastic deformation.

On the contrary, the fracture in the 600 F tempered specimen with a fracture toughness of 240,000 psi $\sqrt{\text{in.}}$ is a full-shear type—with a small central transverse region. The corresponding electron fractograph shows equiaxed dimples and evidence of plastic tearing (elongated tear dimples)—characteristic of extensive plastic shear.

The 1100 F tempered specimen has a trough-and-ridge shear fracture, and the electron fractograph shows extensively elongated dimples. But the yield stength is relatively low at this tempering temperature, and therefore the high toughness is less useful from an engineering applications viewpoint.

Thus, both the macroscopic fracture appearance and the detailed electron fractography support the fact that the 500 to 600 F tempering region provides a means of obtaining substantially improved toughness combined with high strength in this stainless steel.

TABLE 2—PROPERTIES OF TYPE 422 STAINLESS STEEL.[a]

Tempering Temperature, deg F	Tensile Strength,[b] 1000 psi	0.2% Yield Strength,[b] 1000 psi	K_{c3} Fracture Toughness,[b] 1000 psi$\sqrt{\text{in.}}$	Charpy V-Notch Impact,[c] ft-lb	Stress Corrosion Susceptibility,[c, d] Days to Failure	Corrosion Attack,[c, e] in 2 days
500	233	163	235	...	no failure (550 F)	none
600	231	165	242	...	...	...
700	234	176	200	9	no failure	none
800	235	184	84	7	...	...
900	232	188	49	5	...	slight
980	238	165	50	6	2.2 (950 F)	...
1000	226	161	64	...	2.2 to 4.4	heavy
1050	188	140	115	...	2.7 to 4.3	...
1100	165	138	193	...	21 to 32	slight
1200	150	126	166	15	no failure	slight

[a] Specimens were austenitized at 1900 F for 1 hr, oil quenched, refrigerated in liquid nitrogen, and tempered 2 hr at the indicated temperature.
[b] B. R. Banerjee and J. J. Hauser, ASD-TDR-62-1034 (1).
[c] Data for a different heat of Type 422 stainless steel.
[d] Data from tests with 100,000 psi stress, 4 to 5 per cent salt spray, and a 60-day test period.
[e] Data from tests with 10 per cent HNO_3 at 125 F.

CHEMICAL AND STRESS CORROSION PROPENSITY

The increased chemical and stress corrosion propensity of Type 422 when tempered in the secondary hardening region has been accepted as a material limitation over which there is no metallurgical control.

Table 2 shows data for stress corrosion and chemical attack of Type 422 stainless steel with various tempering treatments. These properties are vastly improved when the material is tempered in the 500 to 700 F region. Similar improvements in laboratory stress corrosion tests have been reported, though the improvement under a marine environment was somewhat less (7). In fact, using this data (7), Brown (8) concluded: "This may suggest that metallurgical conditions producing high notch sensitivity may also possess relatively poor corrosion resistance." Thus, adopting the lower temperature tempering treatments would not only combine high strength with high ductility but would also remove the undesirable stress and chemical attack susceptibility encountered with tempering in the secondary hardening region.

CARBIDE ANALYSIS

To identify the carbide structures in Type 422 stainless steel, electrolytically extracted residues were analyzed by X-ray diffraction, and extraction replicas were analyzed by electron diffraction. Austenitizing this steel at 1900 F does not dissolve all of the $M_{23}C_6$ carbide, and, upon subsequent tempering, two precipitated carbides appear: M_3C and $M_{23}C_6$. Figure 4 shows the relative intensity of electron diffraction lines from these precipitated carbides (rated as weak, medium, and strong) as a function of tempering temperature. The M_3C carbide was first detected by electron diffraction after 400 F tempering. The carbide diffraction pattern became more distinct and persisted upon tempering at 500 through 900 F. Upon tempering above 900 F, the M_3C pattern became weaker and was replaced by the alloy carbide $M_{23}C_6$. The decrease in intensity of the M_3C pattern suggests a resolution of this carbide. The $M_{23}C_6$ diffraction became stronger and sharper above 1000 F.

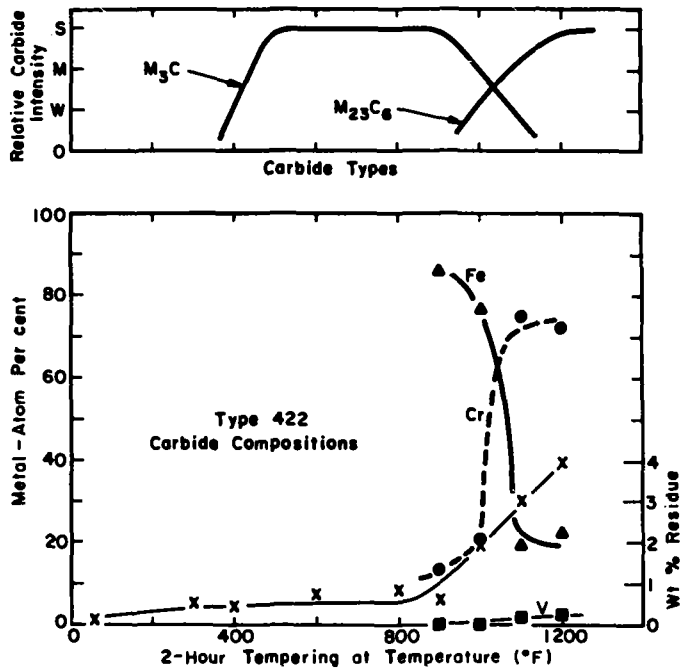
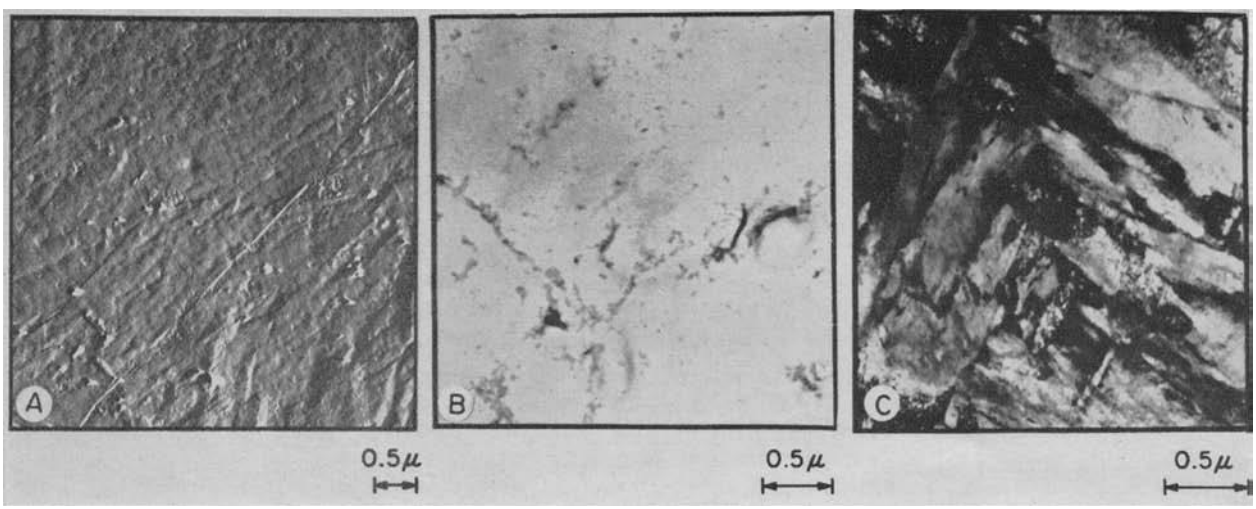


FIG. 4—Carbide Types and Compositions in Type 422, Tempered as Shown.

Figure 4 also gives the weight per cent of extracted residues obtained from quenched and tempered specimens. The weight percentages were determined by anodically dissolving specimens in a 1 per cent hydrochloric acid-alcohol solution and collecting and weighing the residues. The quenched specimen contained about 0.2 per cent residue, consisting mostly of residual $M_{23}C_6$. Upon tempering to about 500 F, the residue increases to about 0.7 to 0.9 weight per cent. This would account for only a small portion of carbon in the steel; thus, most of the carbon in the steel (0.2 per cent) must be still dissolved in the martensite in this tempering region. When $M_{23}C_6$ precipitates above 900 F, how-



(*a*) Surface replica
(*b*) Extraction replica
(*c*) Transmission

FIG. 5—Appearance of Type 422 Oil Quenched from 1900 F.

ever, more carbon enters the carbide, and the weight per cent residue curve rises rapidly to about 3 to 4 per cent.

The metal atom concentration in the carbides is illustrated in Fig. 4, in terms of the metal atom percentage. The iron atom per cent declines rapidly at about 900 F, while the chromium atom percentage correspondingly increases. Vanadium is also detected in the carbide at 900 F and above. The metal atom percentages for molybdenum and tungsten are not shown in Fig. 4, because their values were very low. At 1100 and 1200 F the percentage of molybdenum was about 2.0 while that of tungsten at 1200 F was only 1.0.

FINE STRUCTURES

The quenched structure as seen by surface replication (Fig. 5(*a*)) has a relatively smooth surface with some grooving of the prior austenite boundaries. The individual martensite laths, however, are not clearly delineated. The extraction replica (Fig. 5(*b*)) shows only some filmy carbide precipitate mostly at prior austenite boundaries. Since no epsilon carbide was identified in this alloy upon tempering, the prior austenite boundary precipitate may represent early M_3C. The transmission micrograph shows some dislocation networks in a matrix of high dislocation density (Fig. 5(*c*)).

Upon tempering at 300 F, despite some increased surface roughening of the martensite matrix in the surface replica micrograph (Fig. 6(*a*)), the extraction replica (Fig. 6(*d*)) shows no increase in carbide precipitation. Reduced dislocation density and some dislocation network growth suggest partial recovery, in the absence of rapid carbide precipitation (Fig. 6(g)).

Upon tempering at 400 F, the surface replica micrograph (Fig. 6(*b*)) shows pronounced delineation of martensite lath boundaries and prior austenite boundaries. The extraction replica (Fig. 6(*e*)) suggests general carbide precipitation in a filmy morphology; this carbide was identified by electron diffraction as

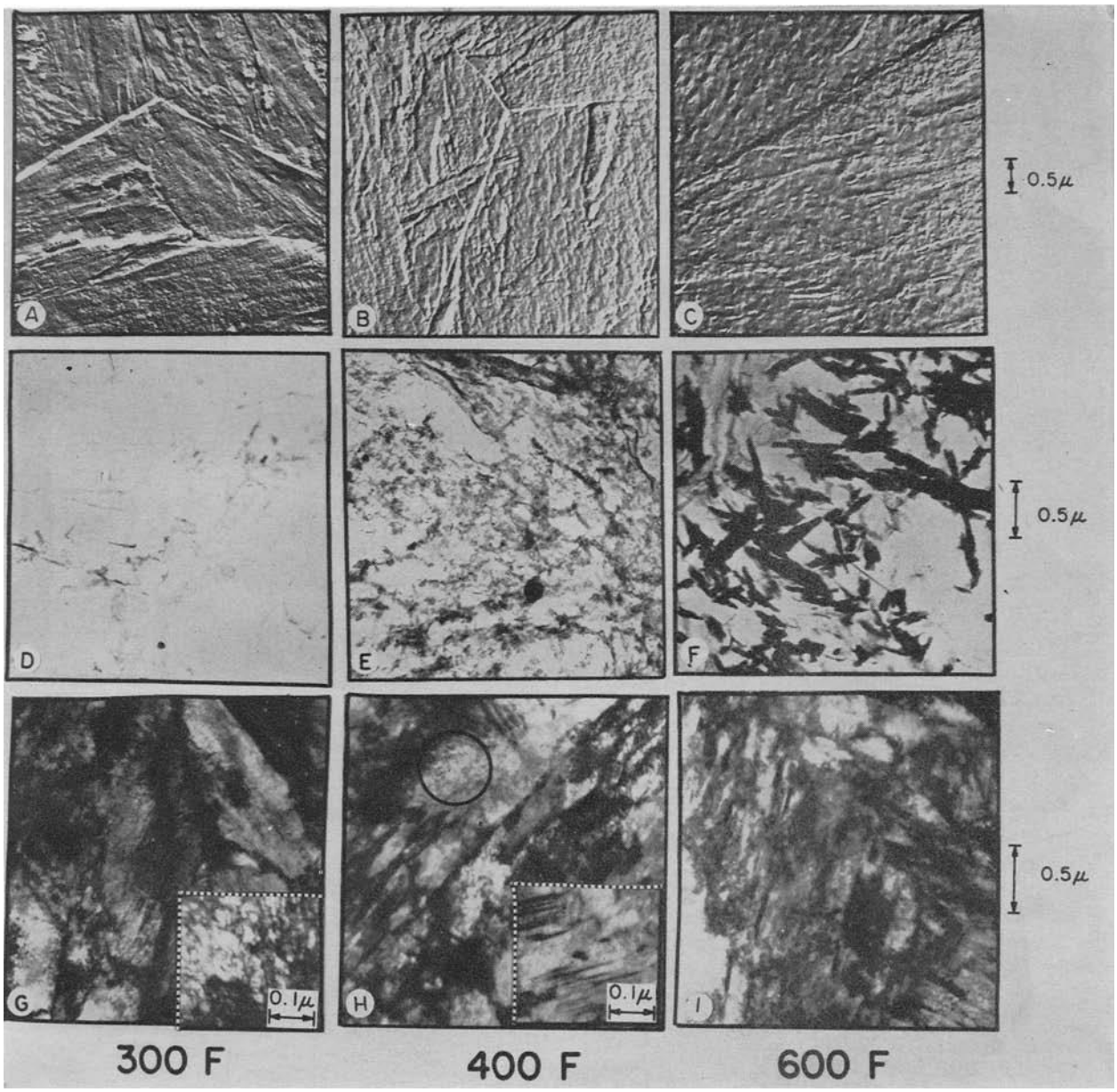


FIG. 6—Surface Replicas (*top*), Extraction Replicas (*center*), and Transmission Micrographs (*bottom*) of Type 422, Tempered as Shown.

essentially two-dimensional M_3C. The transmission micrograph (Fig. 6(*h*)) shows some carbide precipitates superimposed on a partially recovered dislocation structure.

The 600 F tempered surface replica (Fig. 6(*c*)) shows distinctly discernible tion, the fracture properties increase to a maximum at around 500 to 600 F tempering.

At 700 F, the surface replica (Fig. 7(*a*)) shows a reversed trend—suggesting increased surface roughening and decreased size of the carbide precipitate. locked dislocation nodes are seen in the high magnification insert in Fig. 7(*h*). The increased surface roughening of the surface replica, the reduced size of M_3C in the extraction replica, and the increased dislocation locking with precipitation of the $M_{23}C_6$ alloy carbide at dis-

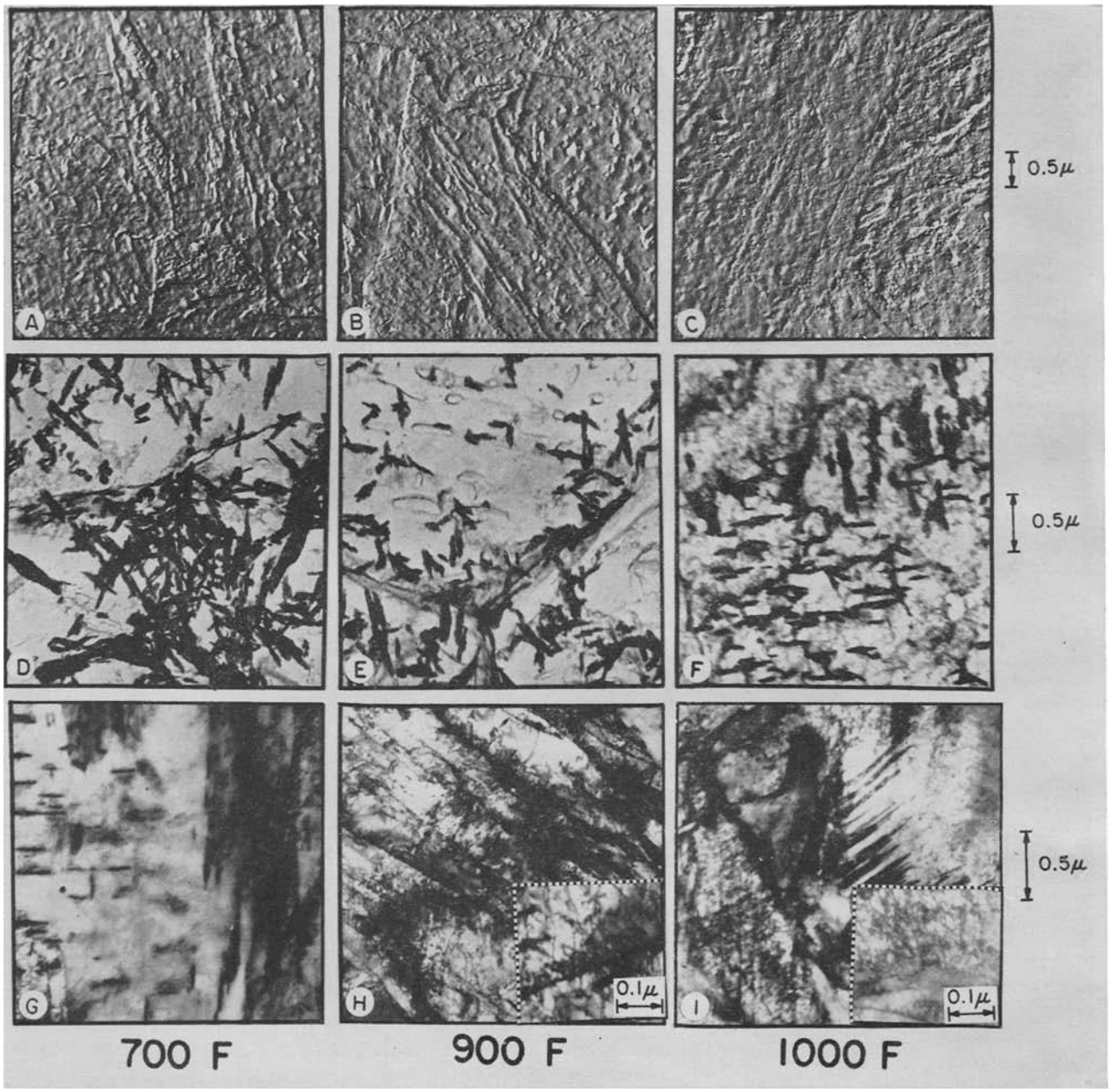


FIG. 7—Surface Replicas (*top*), Extraction Replicas (*center*), and Transmission Micrographs (*bottom*) of Type 422, Tempered as Shown.

M_3C carbide plates upon a somewhat less roughened martensite matrix. The extraction replica (Fig. 6(*f*)) also shows M_3C carbide with a platy morphology. The transmission micrograph (Fig. 6(*i*)) suggests further recovery in terms of reduced dislocation density and network growth. During these stages of partial recovery in terms of dislocation structures and accompanying M_3C precipita-

Both the surface replica and the extraction replica (Fig. 7(*d*)) suggest a new finely dispersed precipitate in addition to the M_3C plates. The transmission micrograph (Fig. 7(*g*)) also suggests a new finely dispersed precipitate appearing at dislocation intersections.

The above trends are more pronounced at 900 F tempering (Figs. 7(*b*), (*e*), and (*h*)); a preponderance of precipitate-

location jogs and intersections in the transmission micrograph are clearly apparent. At 1000 F tempering, further general roughening of the martensite surface (Fig. 7(*c*)) increased general cloudy precipitation of the finely dispersed $M_{23}C_6$ alloy carbide (Fig. 7(*f*)), and pronounced dislocation locking and increased dislocation density (Fig. 7(*i*)) characterize the fine structural aspects.

During these stages of M_3C carbide dissolution and simultaneous alloy carbide precipitation at dislocation jogs and intersections, the fracture properties rapidly decline reaching a minimum at 900 to 1000 F tempering.

Upon tempering at 1100 F, dislocation-climb processes are activated to mark the beginning of a cell structure (Fig. 8(*g*)), which effectively reduces dislocation density within the cells. The general reduction in dislocation density and the growth of the alloy-carbide precipitate (Fig. 8(*d*)) produce a smoother martensitic surface replica structure (Fig. 8(*a*)).

At 1200 and 1300 F tempering, there is further acceleration of the climb-induced cell structure formation, which eventually produces complete recrystallization and replacement of the martensite lath structure (Fig. 8). Along with these basic structural changes in the matrix, rapid growth of the spheroidal alloy-carbide precipitate particles further contributes to a general reduction in strength with accompanying increase in ductility.

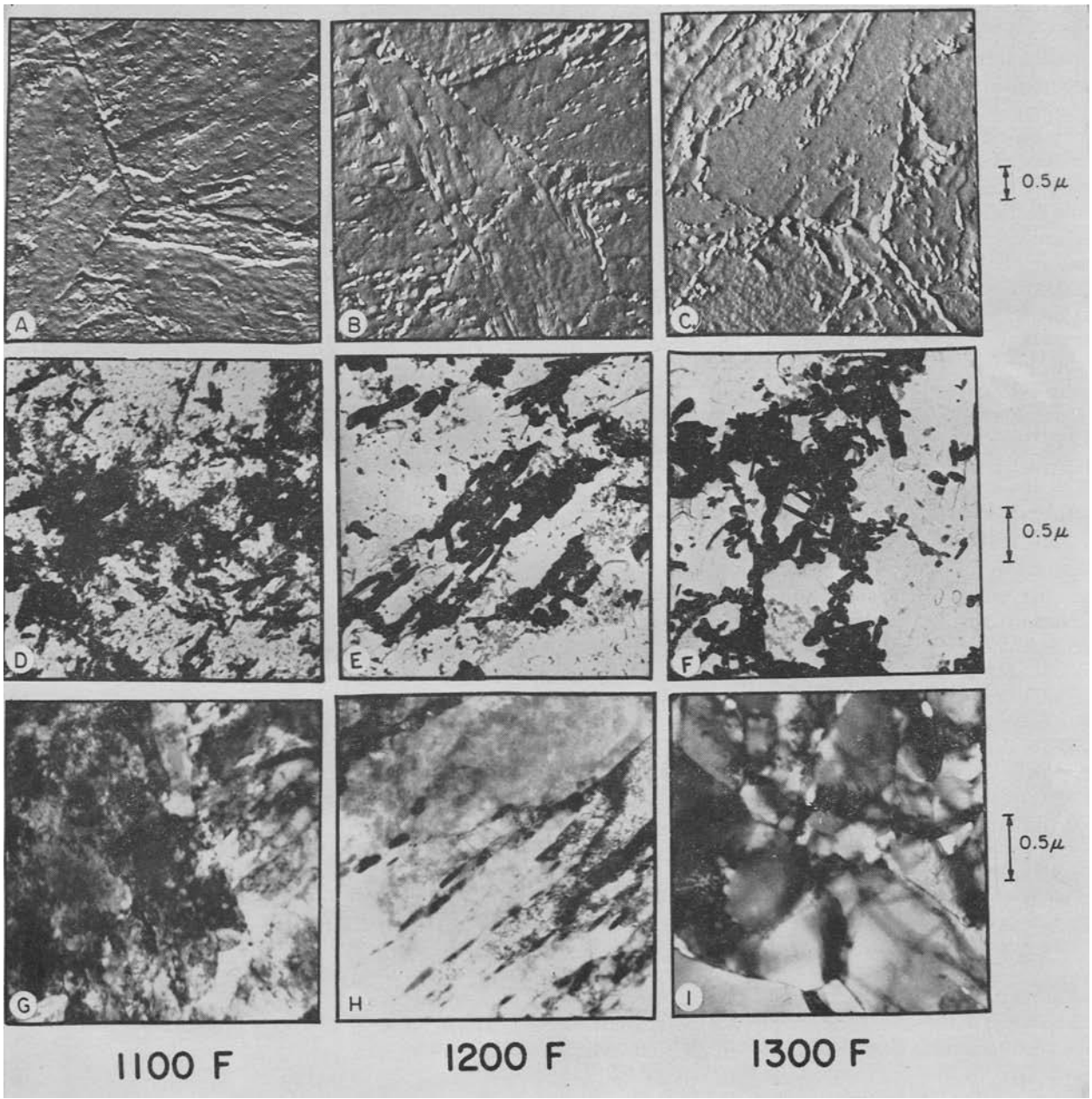


FIG. 8.—Surface Replicas (*top*), Extraction Replicas (*center*), and Transmission Micrographs (*bottom*) of Type 422, Tempered as Shown

DISCUSSION

In Type 422 stainless steel no substantial amount of general carbide precipitation occurs until 400 F tempering, although some filmy M_3C possibly precipitates at an accelerated rate at prior austenite boundaries during the quench and upon tempering up to 300 F. Thus, upon tempering at these lower temperatures, glide-based recovery processes (9) and annealing out of quenched-in vacancies may lead to somewhat reduced dislocation density and improved fracture toughness. In fact, these recovery processes—probably the result of the temperature-dependent reduction in resistance to dislocation movement—continue up to 600 F as the M_3C carbide morphology shifts to the platy form. Indeed, near 600 F, Type 422 exhibits a maximum in fracture toughness and an optimum combination of yield strength, fracture toughness, and corrosion and stress-

corrosion resistance. This is contrary to the conventional practice of tempering Type 422 stainless steel near or slightly beyond the secondary hardening region (6).

At higher tempering temperatures, the M_3C becomes unstable and redissolves, and this process is simultaneously accompanied by precipitation of the $M_{23}C_6$ alloy carbide. Under the conditions of local carbon supersaturation (10) because of the dissolution of the M_3C carbide, the alloy carbide tends to precipitate preferentially at dislocation jogs and intersections. Also increased dislocation arrays may be produced to accommodate the severe martensite lattice distortion created by the M_3C carbide dissolution (10). Upon tempering in the 900 to 1000 F region, transmission microscopy did indeed demonstrate increased dislocation density with numerous dislocation networks locked with precipitation at jogs and intersections, and temper brittleness is simultaneously encountered.

Thus in Type 422 stainless steel the marked property improvements in yield strength, fracture toughness, corrosion and stress-corrosion resistance, when tempered in the 500 to 600 F region, are explained in terms of recovery of dislocation structures, along with a precipitation strengthened matrix. The temper brittleness phenomenon in the 900 to 1000 F region is understood (10) in terms of an increased dislocation locking by precipitation at dislocation jogs and intersections, which raises the dislocation unpinning stress, and an increased dislocation density, which permits crack formation without plastic deformation—thus reducing the effective surface energy. Both of these factors would conduce to embrittlement, according to Cottrell's (11) brittle fracture model.

SUMMARY

Type 422 stainless steel was structurally characterized, and its fine structures were related to tempering response. The secondary-hardening tempering region was shown to be not necessarily the desirable tempering region for all applications. For optimally combining toughness, strength, and corrosion properties, Type 422 stainless steel may be tempered at 500 to 600 F for applications where operating temperature and section size or complexity do not preclude its use.

Tempering in the secondary hardening region (980 to 1000 F) gave tensile strength of 226,000 to 238,000 psi, yield strength of 161,000 to 165,000 psi and fracture toughness (K_{c3}) of 50,000 to 64,000 psi $\sqrt{\text{in.}}$ By tempering at 500 to 600 F, however, tensile strengths of 231,000 to 233,000 psi and yield strengths of 163,000 to 165,000 psi, combined with fracture toughness (K_{c3}) of 235,000 to 242,000 psi $\sqrt{\text{in.}}$, were obtained. Corrosion and stress corrosion resistance are also improved by tempering at the lower temperatures.

These marked improvements in properties in Type 422 stainless steel are explained in terms of dislocation rearrangements, along with a precipitation strengthened matrix. The temper brittleness in the 900 to 1000 F region is understood in terms of an increased dislocation locking by precipitation at dislocation jogs and intersections, which increased the dislocation unpinning stress, and an increased dislocation density, which permits crack formation without plastic deformation. Both factors produce the observed embrittlement.

Acknowledgments:

The authors would like to express their appreciation to F. S. Snyder, G. S. Felbaum, and other Crucible Research staff members who have assisted in this program.

The support of Materials Central, Directorate of Advanced Systems Technology, Aeronautical Systems Division, Wright-Patterson Air Force Base—through contracts AF33(616)-8156, and AF33(657)-10337—is also gratefully acknowledged.

REFERENCES

(1) B. R. Banerjee and J. J. Hauser, "Processing Variables on Crack Propagation of High Strength Steels and Titanium," *ASD-TDR 62-1034*, Part I, April, 1963; "A New Heat Treatment for High-Alloy High Strength Martensitic Steels," *ASD Contract No. AF33(657)-10337*, First. Quarterly Report, April 30, 1963.

(2) "Fracture Testing of High Strength Materials," *ASTM Bulletin*, Am. Soc. Testing Mats., Vol. 4, 1960, p. 29; Vol. 5, 1961, p. 389.

(3) J. M. Capenos, J. J. Hauser, and B. R. Banerjee, "Transmission Electron Microscopy of Type 410 Stainless Steel," *Advances in Electron Metallography and Electron Probe Microanalysis, ASTM STP 317*, 1962, p. 26.

(4) B. R. Banerjee, J. J. Hauser, and J. M. Capenos, "Etch-Shadow Extraction Replica in Fracture Studies," *Review Scientific Instruments*, Vol. 34, 1963, p. 477.

(5) G. B. Espey, M. H. Jones, and W. F. Brown, Jr., "The Sharp Edge Notch Tensile Strength of Several High Strength Steel Sheet Alloys," *Proceedings*, Am. Soc. Testing Mats., Vol. 59, 1959, p. 837.

(6) R. J. Fiorentino, D. B. Roach, and A. M. Hall, "Heat Treatment of High Strength Steels for Airframe Applications," *DMIC Report No. 119*, Battelle Memorial Institute, Columbus, Ohio, Nov. 27, 1959.

(7) E. H. Phelps and A. W. Loginow, "Stress Corrosion of Steels for Aircraft and Missiles," *Corrosion*, Vol. 16, July, 1960, p. 97.

(8) W. F. Brown, Jr., G. B. Espey, and M. H. Jones, "Considerations In Selection of Wing and Fuselage Sheet Materials for Trisonic Transports," *SAE Transactions*, Vol. 70, 1962, p. 583.

(9) W. R. Hibbard and C. G. Dunn, "A Study of ⟨112⟩ Edge Dislocations in Bent Si-Fe Single Crystals," *Acta Metallurgica*, Vol. 4, 1956, p. 306.

(10) B. R. Banerjee, "Fracture Micromechanics in High-Strength Steels," *Structure and Properties of Ultra High-Strength Steels, ASTM STP 370*, Am. Soc. Testing Mats., February, 1965.

(11) A. H. Cottrell, "Theory of Brittle Fracture in Steel and Similar Metals," *Transactions*, Am. Institute of Mining, Metallurgical, and Petroleum Engrs., Vol. 212, 1958, p. 192.

FURTHER STUDIES ON THE FORMATION OF SIGMA IN 12 TO 16 PER CENT CHROMIUM STEELS

By D. C. Ludwigson[1] and H. S. Link[2]

Synopsis

Sigma, a hard intermetallic phase in the iron-chromium system, has a complex tetragonal structure and was formerly thought to be the cause of 885 F embrittlement. Although previous investigators have found that sigma can form in ferritic stainless steels at chromium contents as low as 13 per cent and at temperatures as high as about 1500 F, the alpha – alpha plus sigma boundary of this system was not known with certainty at low chromium concentrations where equilibrium is established very slowly. The present study concerns the effects of exposures at 900, 1050, and 1200 F for durations up to 76,000 hr on annealed specimens and on cold-reduced specimens from a series of laboratory heats of simulated commercial purity steels containing nominally 12, 13, 14, 15, and 16 per cent chromium.

In the cold-reduced condition, all the steels developed sigma during exposure at 900 F, all but the 12 per cent chromium steel developed sigma at 1050 F, and none of the steels developed sigma at 1200 F. In the annealed specimens, sigma had formed within the time studied only in the 14, 15, and 16 per cent chromium steel specimens exposed at 1050 F.

As would be expected, the cold reduced specimens softened during exposure. However, precipitation hardening (885 F embrittlement) occurred in the annealed specimens containing 15 and 16 per cent chromium during exposure at 900 F. The 16 per cent chromium steel, and to a lesser extent the 15 per cent chromium steel, overaged after prolonged exposure at this temperature.

These results show that the alpha – alpha plus sigma boundary for commercial purity chromium steels is located at a lower chromium concentration than was heretofore reported. In addition, the observation—for what is believed to be the first time—of the reversal of 885 F embrittlement by overaging substantiates the prediction made by other investigators.

Sigma, a hard intermetallic phase in the iron-chromium system, has a complex tetragonal structure (1)[3] and is capable of embrittling iron-chromium alloys subjected to elevated temperatures for extended periods of time. Sigma formation has been studied by a number of investigators and the alpha – alpha plus sigma solvus is fairly well established at high temperatures. However, at low temperatures and at low chromium contents it is not known with certainty because sigma forms very slowly at lower temperatures.

Trietschke and Tammann (2), apparently the first to suggest the formation of sigma, in 1908 observed a thermal arrest in certain cooling curves during their experiments with iron-chromium alloys. They interpreted the thermal arrest to be the result of the formation of a compound. It was not until 1927, however, that the first observation of sigma in the microstructure of iron-chromium alloys was reported. In that year, Bain and Griffiths (3) published photomicrographs of a "B-constituent" in iron-chromium alloys that they found to be "corundum hard." In discussing the Bain and Griffiths paper, McDowell (4) suggested that the "B-constituent" was the intermetallic compound FeCr.

Despite the observations of Bain and Griffiths, there was considerable doubt at that time whether sigma could exist in iron-chromium alloys. Jänecke (5), in 1917, and Murakami (6), in 1918, had not observed an iron-chromium compound in the alloys that they studied. Likewise, Kruetzer (7) and Westgren, Phragmen, and Negresco (8), in 1928, noted an absence of compounds in their iron-chromium alloys. In addition, Adcock (9), in his classic work on the iron-chromium constitution diagram in 1931, failed to observe an iron-chromium compound in any of his high-purity binary alloys. Other investigators, however, notably Chevenard (10), in 1927, and Wever and Jellinghaus (11), in 1931, did find evidence of sigma as an intermetallic compound (FeCr) by X-ray methods. By 1934, when Eriksson (12) had confirmed the work of Wever and Jellinghaus, the existence of sigma had been generally accepted, and today there is no doubt about the existence of this phase. Although the apparent contradictory observations of the early investigators were perplexing at that time, today the differences in these observations are attributed to variations in the purity or thermal-mechanical history of the alloys studied or both. The impurities, such as manganese, phosphorus, sulfur, and silicon, present in commercial chromium stainless steels but absent in binary iron-chromium alloys, are thought to hasten sigma formation. In addition, strain apparently hastens sigma formation.

Once the existence of sigma in iron-chromium alloys was established, efforts were made to define the range of composition and temperature over which sigma could form. Since the early thirties investigators have found sigma at progressively lower chromium concentrations and, correspondingly, lower temperatures as they came to recognize the role of long exposure times and strain in establishing equilibrium. Wever and Jellinghaus (11), in modifying Oberhoffer and Esser's (13) original iron-chromium phase diagram, were the first to show the sigma region on a constitution diagram. This diagram, shown in Fig. 1, indicates that sigma can form in iron-chromium alloys containing 38 to 59 per cent chromium and at temperatures as high as 930 C (1705 F). Kinzel and Crafts (14), in their 1937 summary of previous work, offered a constitution diagram, Fig. 2, showing sigma at somewhat lower concentrations of chromium. In 1943, Cook and Jones (15) published a diagram, Fig. 3, showing sigma at 25 per cent chromium. In 1950, Heger (16) found sigma in a commercial-purity 17 per cent chromium steel aged for 5000 hr at 1050 F. Heger used severe cold work (95 per cent reduction) to hasten sigma formation. In 1951, Shortsleeve

[1] Technologist, Applied Research Laboratory, U.S. Steel Corp., Monroeville, Pa.

[2] Chief research engineer, high strength steels, Applied Research Laboratory, U.S. Steel Corp., Monroeville, Pa.

[3] The boldface numbers in parentheses refer to the list of references appended to this paper.

Copyright© 1965 by ASTM International

www.astm.org

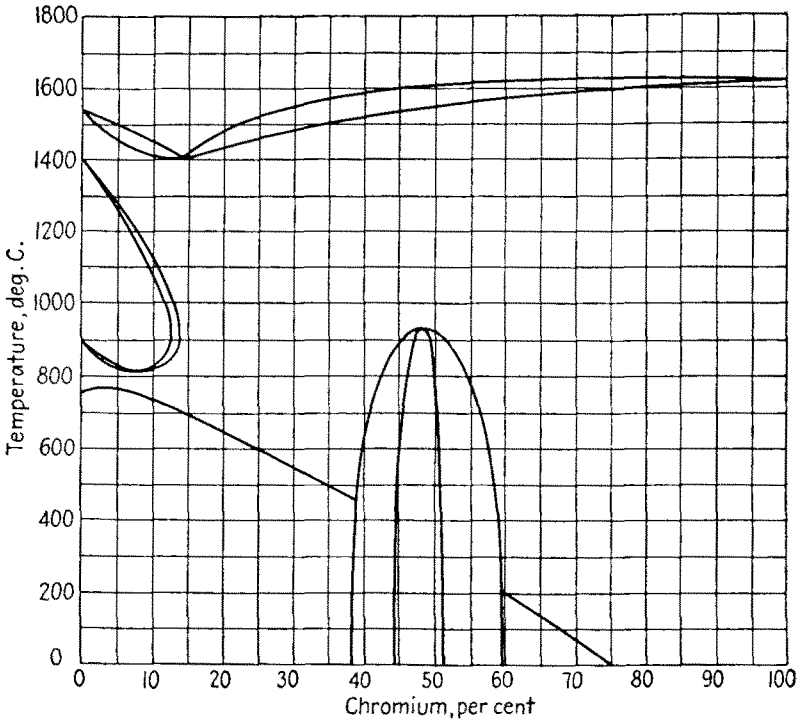


FIG. 1—The Iron-Chromium Constitution Diagram of Oberhoffer and Esser as Modified by Wever and Jellinghaus (1931).

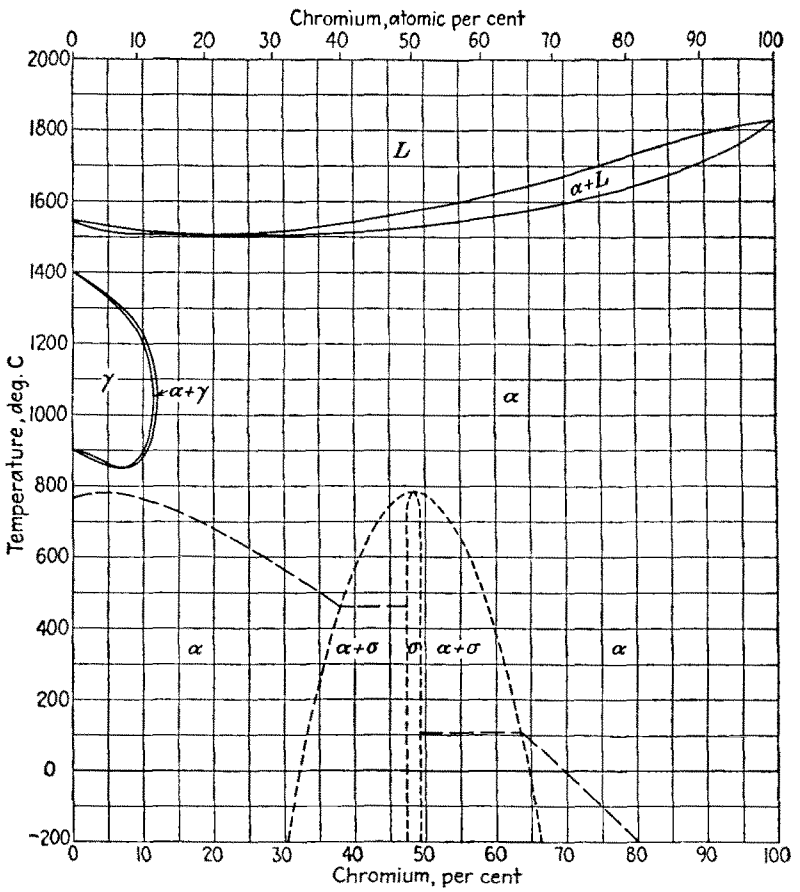


FIG. 2—The Iron-Chromium Constitution Diagram of Kinzel and Crafts (1937).

and Nicholson (17), in a study of iron-rich iron-chromium alloys, proposed the alpha – alpha plus sigma boundary shown in Fig. 4. Shortsleeve and Nicholson found sigma in a chromium steel of simulated commercial purity containing 18.29 per cent chromium. In 1952, Link and Marshall (18) found sigma in steels containing as little as 13 per cent chromium that were aged for 10,000 hr at 900 F and proposed the alpha – alpha plus sigma boundary shown in Fig. 5. As Heger had done, Link and Marshall used severe cold work to hasten sigma formation. More recently (1958), a summarization of work on the iron-chromium diagram was published by Hansen (19), Fig. 6. Hansen's diagram indicates that sigma may be at equilibrium at temperatures up to about 815 C (1500 F), but the diagram is indefinite for the composition limits of sigma at temperatures lower than about 700 C (1290 F).

Prior to 1951, the hardening that occurred in chromium steels subjected to temperatures in the range 700 to 1000 F, usually termed "885 F embrittlement" (20), was attributed to sigma formation. In that year, however, Heger (21) emphasized the suggestion of Bandel and Tofaute (22) that embrittlement was caused by a precipitation-hardening process that was an early stage in the formation of sigma. Heger suggested that the transition phase was nucleated and grown from the alpha matrix, and subsequently dissolved in favor of the equilibrium precipitate, sigma. He theorized that the transition phase was coherent with the matrix and that the resulting coherency strains were responsible for 885 F embrittlement. He further theorized that when the equilibrium phase (sigma) formed at the expense of the nonequilibrium transition phase, overaging would be observed.

In 1953, Fisher, Dulis, and Carroll (23) extracted the "transition phase" and identified it as a body-centered cubic constituent (a = 2.878 A) containing about 85 per cent chromium and about 15 per cent iron. A year later Heger (24) and Fisher, Dulis, and Carroll (25) clarified the relationship between sigma and the chromium-rich ferrite precipitate. They suggested that the chromium-rich precipitate is the first to form during aging. This precipitate, however, is metastable and dissolves, and thus supplies chromium atoms for the formation of the equilibrium precipitate, sigma.

Williams and Paxton (26), in 1957, published a partial phase diagram of the iron-chromium system showing the miscibility gap implied by Fisher and his co-workers (23). This diagram, as revised by Williams (27) a year later is shown in Fig. 7. The position of the miscibility gap in this diagram varied with the experimental method (hardness,

resistivity, and chemical) used to determine it. However, the gap always closed at about 560 C (1040 F). Williams and Paxton found that the chromium-rich precipitate particles are very small, 25 to 250 A, and apparently always remain completely coherent with the matrix.

The investigation described herein is a continuation of the work begun by Link and Marshall (18). These investigators examined, in the annealed and in the cold-reduced conditions, a series of 12 to 16 per cent chromium steels of simulated commercial purity that had been exposed at 900, 1050, and 1200 F for 5000 and 10,000 hr. Because sigma forms slowly in these low-chromium ferritic stainless steels, the Link and Marshall steels were given additional exposures. Metallographic examination of these steels after exposures of 43,000 and 76,000 hr and hardness tests after the same exposures form the basis of this paper.

Materials and Experimental Work

For the investigation, the steels studied earlier by Link and Marshall (18) were used. These steels consisted of five 26-lb experimental heats of simulated commercial purity containing approximately 12, 13, 14, 15, and 16 per cent chromium that were melted, cast into ingots and forged into $\frac{3}{4}$ by $\frac{1}{2}$-in. bars. The results of the chemical analyses of these heats are given in Table 1. The forged bars were annealed at 1550 F. A part of each bar was then cold-reduced about 95 per cent. Specimens of each annealed bar and of each cold-reduced bar were exposed at 900, 1050, and 1200 F. Specimens from each of the 30 specimens being aged had been examined by Link and Marshall (18) after exposures of 5000 and 10,000 hr. For the present work, separate sets of specimens were removed from the furnace and examined after exposures of 43,000 and 76,000 hr.

Each specimen was mounted, polished, etched in Vilella's reagent (hydrochloric and picric acids in alcohol), and examined metallographically. Although Vilella's reagent outlines both sigma and carbides, sigma could be distinguished from carbide in most specimens by its characteristic shape, distribution, size, and clarity. In specimens where the distinction between sigma and carbide was questionable, however, the specimen was repolished and etched in glyceregia (mixed acids in glycerol). This reagent attacks sigma but only outlines carbides.

Through quantitative metallography

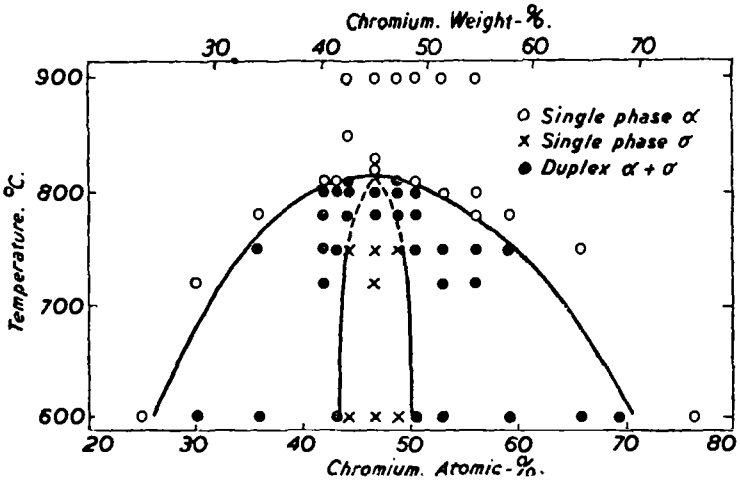


FIG. 3—The Iron-Chromium Constitution Diagram of Cook and Jones (1943).

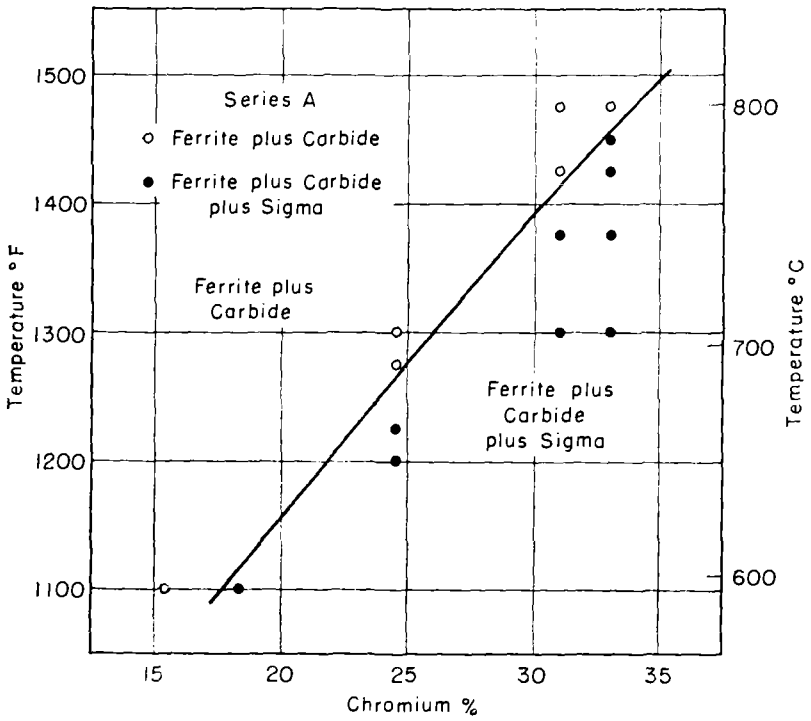


FIG. 4—The Alpha-Alpha plus Sigma Boundary of Shortsleeve and Nicholson (1951).

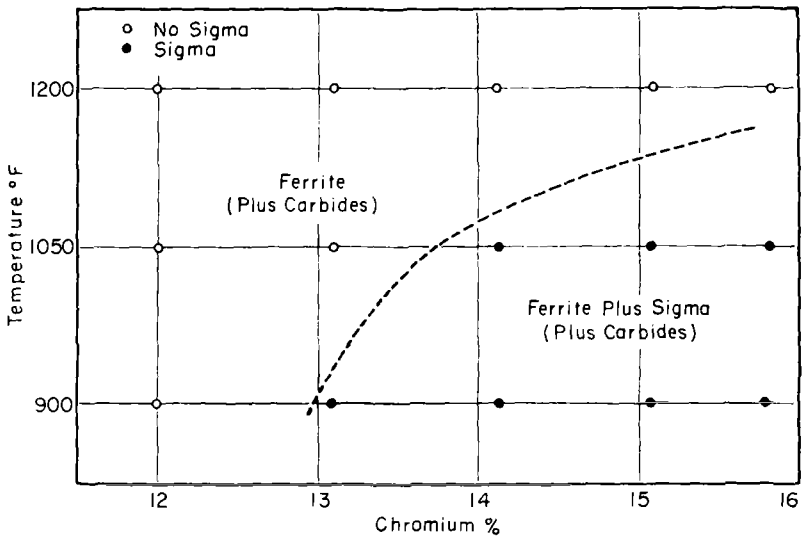


FIG. 5—Results of Metallographic and X-ray Diffraction Studies on 0.08 Per Cent Carbon, 12 to 16 Per Cent Steels That Had Been Heated for 10,000 hr at the Indicated Temperatures. (Steels were cold-reduced about 95 per cent prior to heating.) Link and Marshall (1952).

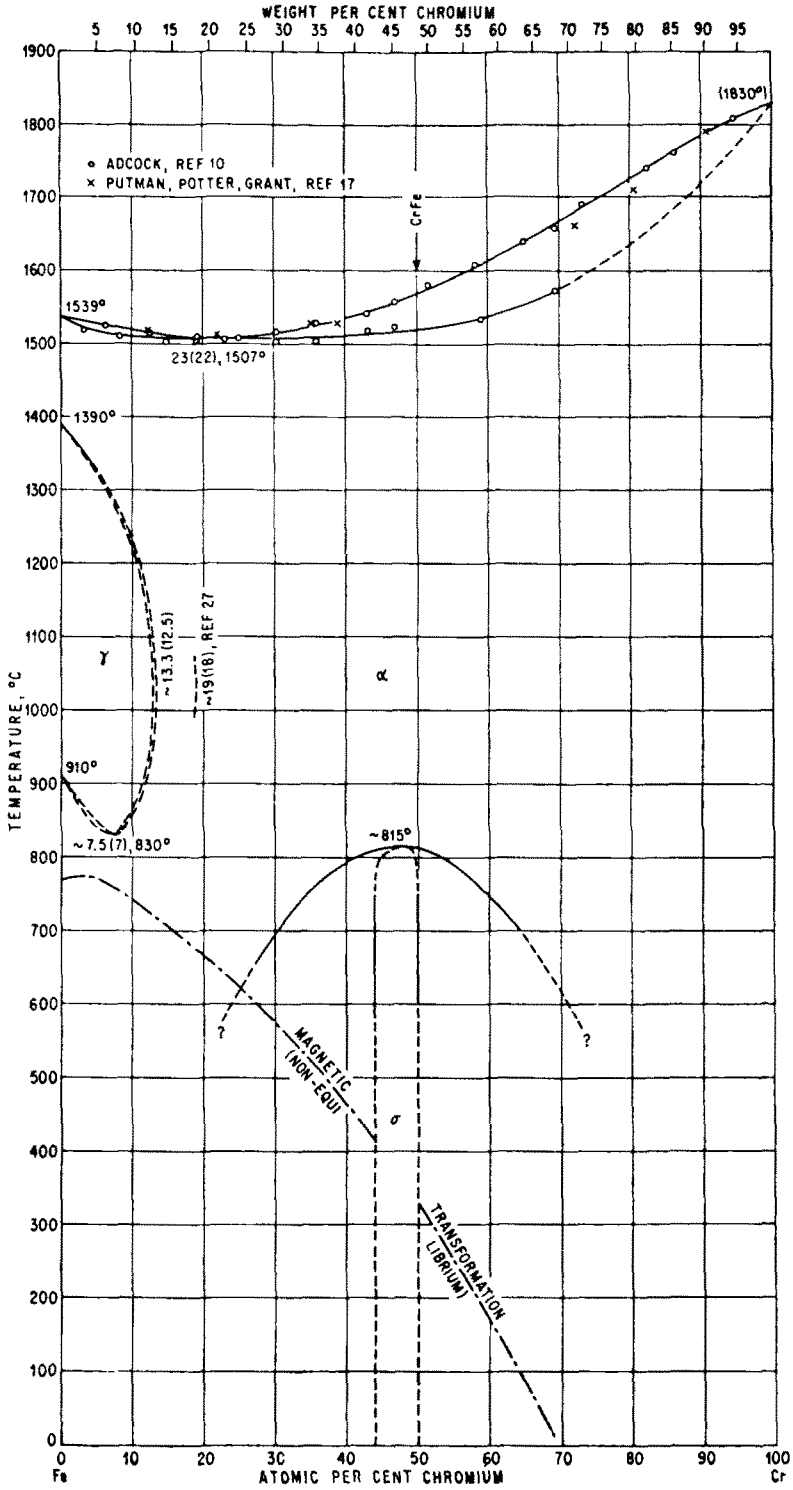


FIG. 6—The Iron-Chromium Constitution Diagram of Hansen (1958).

an estimate was made of the volume fraction of sigma in the specimens exhibiting this phase by a point-counting technique. In some cases, the image of the prepared specimen was projected on a transparent grid of random points; in other cases this grid was placed over one or more photomicrographs of the specimen.

The alpha – alpha plus sigma solvus was drawn on the basis of the observed sigma contents. In drawing this solvus it was assumed that the logarithm of the atom fraction of chromium at the solvus is a linear function of the reciprocal of the absolute temperature. From the solvus thus drawn and from the knowledge that the microstructure would be 100 per cent sigma at about 42 per cent chromium (19), the volume fraction of sigma at equilibrium in each of the experimental steels was calculated by the lever rule.

The minimum heat of solution of sigma in ferrite was calculated from the slope of the solvus line according to the equation[20]

$$\Delta H_{sol} = \frac{2.3RT_1T_2\Delta \log_{10} A}{\Delta T} \quad \ldots\ldots(1)$$

where:

ΔH_{sol} = the heat of solution;
$\Delta \log_{10} A$ = the difference in the logarithms of the atomic per cent chromium at two absolute temperatures, T_1 and T_2, on the solvus;
R = the gas constant; and
ΔT = the difference between T_1 and T_2.

The use of atomic per cent chromium in this equation rather than the activity of chromium represents an assumption of unit activity coefficients. This assumption, although necessary if the calculation is to be made, may introduce some error in the value of ΔH_{sol}.

The hardnesses of all the specimens were measured with a Vickers hardness tester (2.5-kg load).

RESULTS AND DISCUSSION

Metallographic Examination:

As shown in Table 2, metallographic examination revealed that sigma formed in all the cold-reduced steels aged for 76,000 hr at 900 F, in cold-reduced steels containing 13 per cent chromium or more and aged for 76,000 hr at 1050 F, and in annealed steels containing 14 per cent chromium or more and aged for 76,000 hr at 1050 F. But, sigma was absent from some steels when they were aged for shorter periods of time. No sigma formed in any specimens aged at 1200 F nor in annealed specimens aged at 900 F. The quantitative metallography data, given in Table 3, show that the largest amounts of sigma formed in the five annealed and cold-reduced steels aged at 900 F. Somewhat smaller amounts of sigma formed in four of the five annealed and cold-reduced steels aged at 1050 F. The least amounts of sigma formed in three of the five annealed steels aged at 1050 F.

In general, the amount of sigma found in a group of specimens increased as chromium content increased. However, the concentration of sigma in the 15 per cent chromium steel was always equal to or greater than the concentration of sigma in the 16 per cent chromium steel. The reason for this anomalous behavior is not known, but it may be the result of

low silicon and high nitrogen content of the 16 per cent chromium steel.

The data in Table 3, together with the photomicrographs in Figs. 8, 9, and 10, illustrate the changes in structure that occur in the sigma-containing specimens during aging. Of the group of cold-reduced steels aged at 900 F, sigma content generally increased with increasing exposure time, and apparently equilibrium was not achieved after 76,000 hr. In addition, the size of the individual sigma particles increased, through growth and agglomeration, during aging. This latter change is illustrated, for the 15 per cent chromium steel, by the photomicrographs in Fig. 8.

When the cold-reduced steels were aged at 1050 F, larger amounts of sigma formed as aging time was increased. After an initial exposure period of 10,000 hr, however, the amount of sigma did not increase in the 15 and 16 per cent chromium steels as the aging time was extended. It is likely that the equilibrium concentration of sigma has been formed in these steels. As illustrated in Fig. 9, the size of the individual sigma particles in the 15 per cent chromium steel increased by growth and agglomeration with longer aging time.

Among the annealed steels aged at 1050 F there appeared to be a tendency toward increased amounts of sigma with extended aging times up to 43,000 hr. In addition, there was an increase in particle size with increasing aging time. This change in particle size is illustrated for the 15 per cent chromium steel in Fig. 10.

The structures of the annealed and of the annealed and cold-reduced steels, after 76,000 hr exposure at 900, 1050, and 1200 F, are illustrated in Figs. 11 and 12, respectively. It is apparent that cold work prior to aging hastened the formation of sigma. No structural changes, other than the appearance of sigma in some specimens, could be attributed to a change in chromium content. However, an agglomeration of carbides accompanied the increase in aging temperature. In addition, the sigma particles of the annealed and cold-reduced steels were larger in specimens aged at 1050 F than in specimens aged at 900 F.

Of particular interest is the detection, for what is believed to be the first time, of sigma in a 12 per cent chromium steel. Figure 13 shows the appearance of sigma in the 12 per cent chromium steel that was cold-reduced and then exposed for 76,000 hr at 900 F. The sigma can be seen in this figure as discrete, irregularly shaped particles rather uniform in both size and distribution.

The alpha – alpha plus sigma solvus in commercial-purity, 12 to 16 per cent chromium steels, at temperatures from 900 to 1200 F, is shown in Fig. 14. This figure is based on the microstructures of cold-reduced steels exposed for 76,000 hr at 900, 1050, and 1200 F. At 900 F the alpha – alpha plus sigma solvus lies at a chromium content less than 12.00 per cent; at 1050 F the solvus lies between 12.00 and 13.07 per cent chromium; and at 1200 F the boundary lies at a chromium content greater than 15.80 per cent. A minimum heat of solution, 4200 cal/mole, was derived from the solvus drawn in Fig. 14 by using Eq 1.

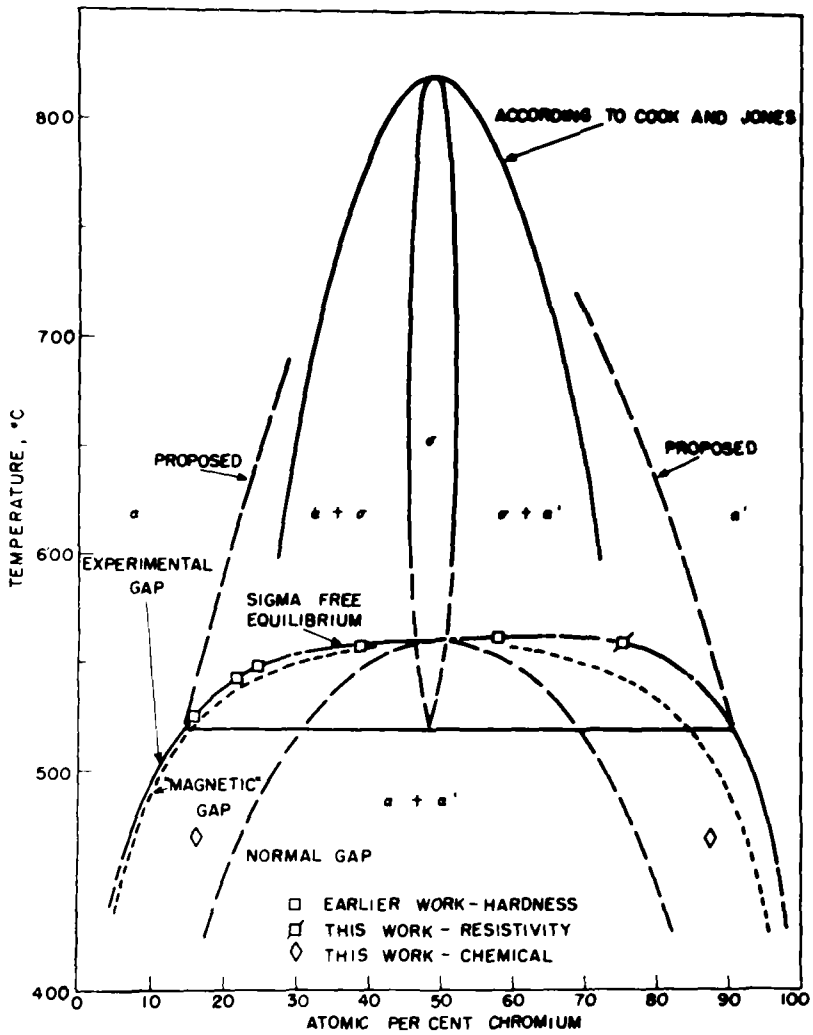


FIG. 7—Revised Low-Temperature Iron-Chromium Phase Diagram of Williams (1958).

TABLE 1—LADLE ANALYSES OF STEELS INVESTIGATED, PER CENT.

NOTE.—The steels consisted of 26-lb experimental heats of simulated commercial purity.

Nominal Chromium Content	C	Mn	P	S	Si	Ni	Cr	N[a]
12.....	0.07	0.55	0.010	0.024	0.54	0.11	12.00	0.034
13.....	0.08	0.53	0.012	0.024	0.50	0.12	13.07	0.041
14.....	0.08	0.55	0.010	0.024	0.56	0.12	14.14	0.044
15.....	0.08	0.55	0.009	0.022	0.64	0.11	15.05	0.036
16.....	0.08	0.55	0.008	0.027	0.43	0.16	15.80	0.065

[a] Nitrogen analyses were made on samples aged at 900 F for 5000 hr.

The solvus shown in Fig. 14 indicates that about 12.6 per cent chromium is soluble in commercial-purity iron at 1050 F, and that about 9.5 per cent chromium is soluble at 900 F. As shown in Table 4, this finding predicts equilibrium sigma contents at 1050 F in fair agreement with the observed sigma contents and confirms the contention that equilibrium was achieved at this tem-

TABLE 2—MICROSTRUCTURE OF AGED CHROMIUM STEELS.

Nominal Chromium Content, per cent	Aging Temperature, deg F	Microstructure[a] of Annealed and Aged Steels				
		As-Annealed	Aging Time, hr			
			5000[b]	10,000[b]	43,000	76,000
12	900	F + C	F + C	F + C	F + C	F + C
	1050	F + C	F + C	F + C	F + C	F + C
	1200	F + C	F + C	F + C	F + C	F + C
13	900	F + C	F + C	F + C	F + C	F + C
	1050	F + C	F + C	F + C	F + C	F + C
	1200	F + C	F + C	F + C	F + C	F + C
14	900	F + C	F + C	F + C	F + C	F + C
	1050	F + C	F + C	F + C + S	F + C + S	F + C + S
	1200	F + C	F + C	F + C	F + C	F + C
15	900	F + C	F + C	F + C	F + C	F + C
	1050	F + C	F + C	F + C + S	F + C + S	F + C + S
	1200	F + C	F + C	F + C	F + C	F + C
16	900	F + C	F + C	F + C	F + C	F + C
	1050	F + C	F + C	F + C + S	F + C + S	F + C + S
	1200	F + C	F + C	F + C	F + C	F + C
		Microstructure[a] of Cold-Reduced and Aged Steels				
		As Cold-Reduced	Aging Time, hr			
			5000[b]	10,000[b]	43,000	76,000
12	900	F + C	F + C	F + C	F + C + S	F + C + S
	1050	F + C	F + C	F + C	F + C	F + C
	1200	F + C	F + C	F + C	F + C	F + C
13	900	F + C	F + C	F + C + S	F + C + S	F + C + S
	1050	F + C	F + C	F + C	F + C	F + C + S
	1200	F + C	F + C	F + C	F + C	F + C
14	900	F + C	F + C + S	F + C + S	F + C + S	F + C + S
	1050	F + C	F + C + S	F + C + S	F + C + S	F + C + S
	1200	F + C	F + C	F + C	F + C	F + C
15	900	F + C	F + C + S	F + C + S	F + C + S	F + C + S
	1050	F + C	F + C + S	F + C + S	F + C + S	F + C + S
	1200	F + C	F + C	F + C	F + C	F + C
16	900	F + C	F + C + S	F + C + S	F + C + S	F + C + S
	1050	F + C	F + C + S	F + C + S	F + C + S	F + C + S
	1200	F + C	F + C	F + C	F + C	F + C

[a] F = ferrite; C = carbide; and S = sigma.
[b] Data previously reported by Link and Marshall, Ref. (**18**).

perature. Predicted equilibrium sigma contents at 900 F that are greater than those observed, Table 4, confirm the contention that equilibrium has not been achieved after 76,000 hr at 900 F.

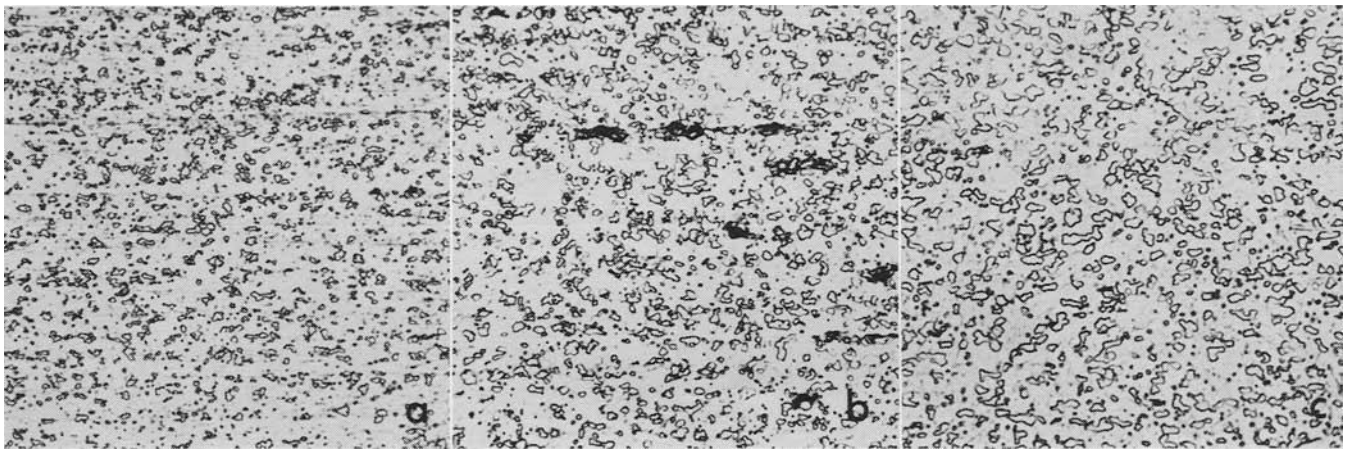
TABLE 3—VOLUME PER CENT SIGMA IN 12 TO 16 PER CENT CHROMIUM STEELS.

Nominal Chromium Content, per cent	Annealed and Cold-Reduced Steels Aged at 900 F for the Indicated Time, hr			
	5000	10,000	43,000	76,000
12	ND[a]	ND	<1	3
13	ND	<1	3	4
14	<1	8	7	8
15	8	11	12	14
16	5	11	12	14
	Annealed and Cold-Reduced Steels Aged at 1050 F for the Indicated Time, hr			
	5000[b]	10,000[b]	43,000	76,000
13	ND	ND	ND	<1
14	<1	2	4	5
15	3	10	10	9
16	2	9	7	9
	Annealed Steels Aged at 1050 F for the Indicated Time, hr			
	5000	10,000	43,000	76,000
14	ND	<1	<1	<1
15	ND	<1	3	3
16	ND	<1	3	3

[a] ND = none detected.
[b] Measurements previously reported by Link and Marshall, Ref. (**18**).

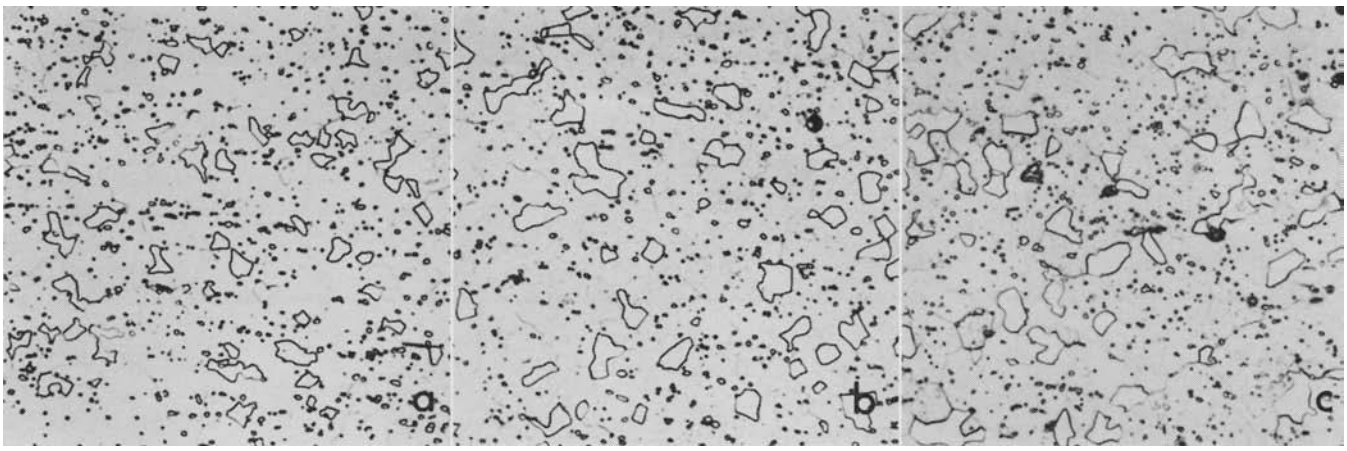
Hardness Studies:

The results of hardness measurements made on the annealed and aged steels are given in Table 5 and illustrated in Figs. 15-17. The 15 and 16 per cent chromium steels exhibited precipitation



(*a*) 5,000 hr (*b*) 43,000 hr (*c*) 76,000 hr

FIG. 8—Microstructures of a Cold-Reduced 15 Per Cent Chromium Steel Aged at 900 F for the Indicated Times. Etched in Vilella's Reagent (×1000). (The clear etching phase is sigma; carbides also appear in each microstructure.)



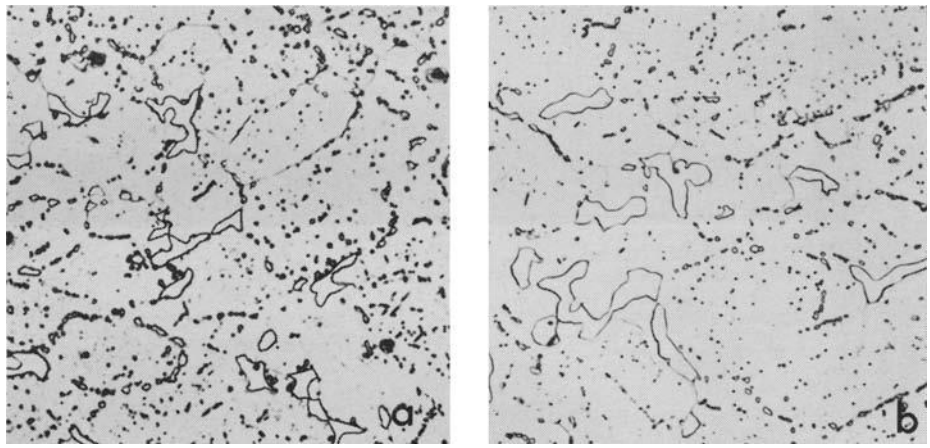
(*a*) 5,000 hr (*b*) 43,000 hr (*c*) 76,000 hr

FIG. 9—Microstructures of a Cold-Reduced 15 Per Cent Chromium Steel Aged at 1050 F for the Indicated Times. Etched in Vilella's Reagent (×1000). (The clear phase is sigma; carbides also appear in each microstructure).

hardening, and the 16 per cent chromium steel, and to a lesser extent the 15 per cent chromium steel, overaged when exposed at 900 F. The hardness changes that occurred in the 12, 13, and 14 per cent chromium steels exposed at 900 F are not of sufficient magnitude to permit any conclusions about precipitation hardening and overaging. Likewise, because the changes that occurred in the annealed steels during exposure at 1050 and 1200 F are relatively small, no conclusions can be drawn about precipitation hardening in these steels.

The hardness measurements discussed in the preceding paragraph tend to confirm the results of studies by Fisher, Dulis, and Carroll (23), Williams and Paxton (26), and Williams (27). Fisher and his co-workers found a coherent chromium-rich ferrite precipitate in several chromium stainless steels including two of the steels in this program: the cold-reduced 15 and 16 per cent chromium steels aged for 10,000 hr at 900 F. They pointed out that this precipitate was responsible for 885 F embrittlement. In addition, these investigators and Heger (21) predicted the overaging observed, for what is believed to be the first time, during this investigation. Williams proposed that the miscibility gap, Fig. 7, has a maximum at about 1040 F. On the basis of this diagram, precipitation hardening would be expected below 1040 F but not above 1040 F. The present study appears to confirm this expectation.

Fisher[4] recently explained that the observed overaging is caused by the re-solution of the embrittling chromium-rich precipitate in favor of sigma formation. In support of this reasoning he has exhibited an electron micrograph, Fig. 18, showing the chromium-rich precipitate. This precipitate was found only at great distances, on the diffusion scale, from any sigma particles. Apparently, sigma "feeds" on the chromium atoms supplied by the dissolving chromium-rich precipitate.



(*a*) 43,000 hr (*b*) 76,000 hr

FIG. 10—Microstructures of an Annealed 15 Per Cent Chromium Steel Aged at 1050 F for the Indicated Times. Etched in Vilella's Reagent (×1000). (The clear etching phase is sigma; carbides also appear in each microstructure).

The results of hardness measurements made on the cold-reduced and aged steels are given in Table 5 and illustrated in Figs. 19, 20, and 21. All specimens softened during the first 5000 hr exposure. As might be expected, the specimens aged at 900 F softened the least, and generally, the specimens aged at 1200 F softened the most. In general, the specimens aged at 1050 and 1200 F reached minimum hardness values after being exposed 5000 hr, but most of the specimens aged at 900 F continued to soften throughout the entire 76,000-hr exposure. Metallographic examination revealed that the softening of the specimens aged at 1050 and 1200 F was the result of recrystallization. However, metallographic examination of the specimens aged at 900 F revealed that recrystallization was complete only after an exposure of at least 43,000 hr. Therefore, the softening observed in the specimens aged at 900 F for 5000 and 10,000 hr is believed to be the result of recovery and, possibly, partial recrystallization.

SUMMARY

The salient conclusions reached as a result of this investigation are listed below:

1. At 1200 F the alpha – alpha plus sigma boundary in commercial-purity chromium steels lies at a chromium content greater than 15.80 per cent.

2. At 1050 F the alpha – alpha plus sigma boundary in commercial-purity chromium steels lies at a chromium content between 12.00 and 13.07 per

[4] R. M. Fisher, private communication.

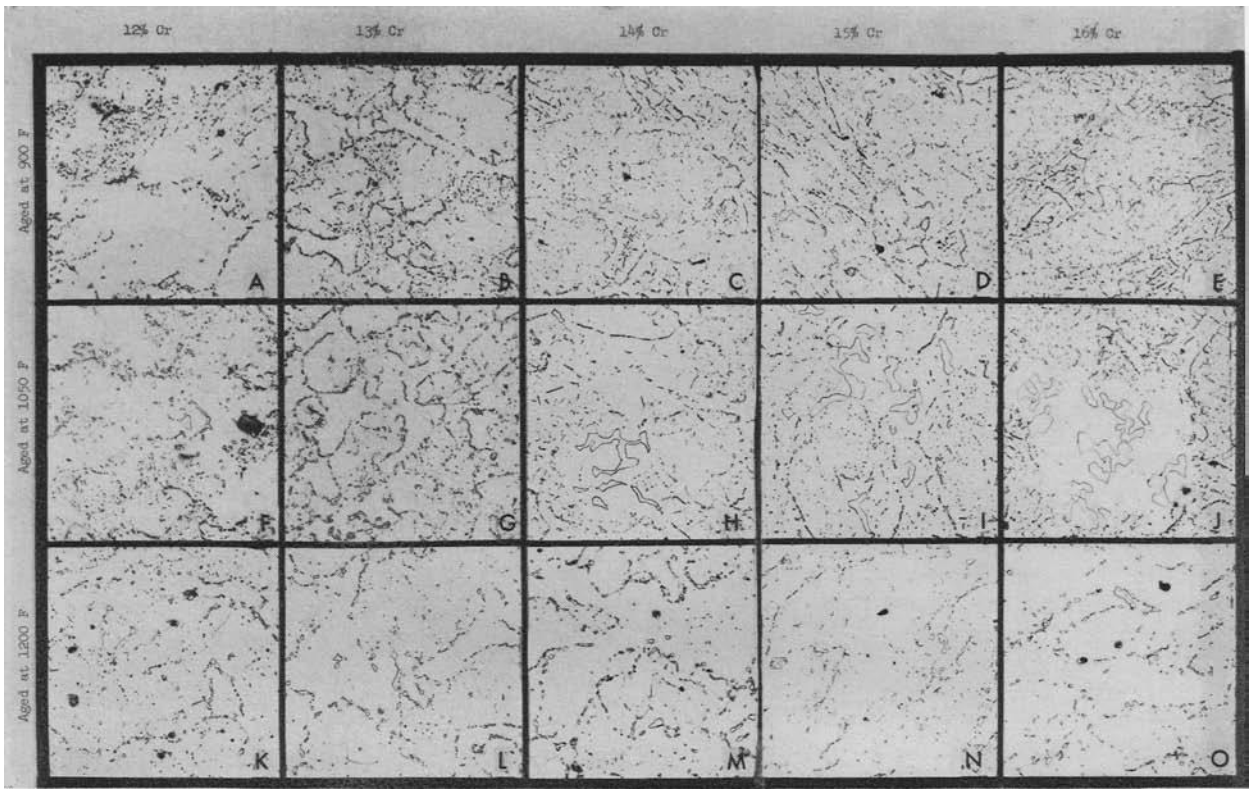


FIG. 11—Microstructures of Annealed Chromium Steels Aged for 76,000 hr. Etched in Vilella's Reagent (×1000). (The clear etching phase in Plates H, I, and J is sigma; carbides also appear in each microstructure). Reduced one half for reproduction.

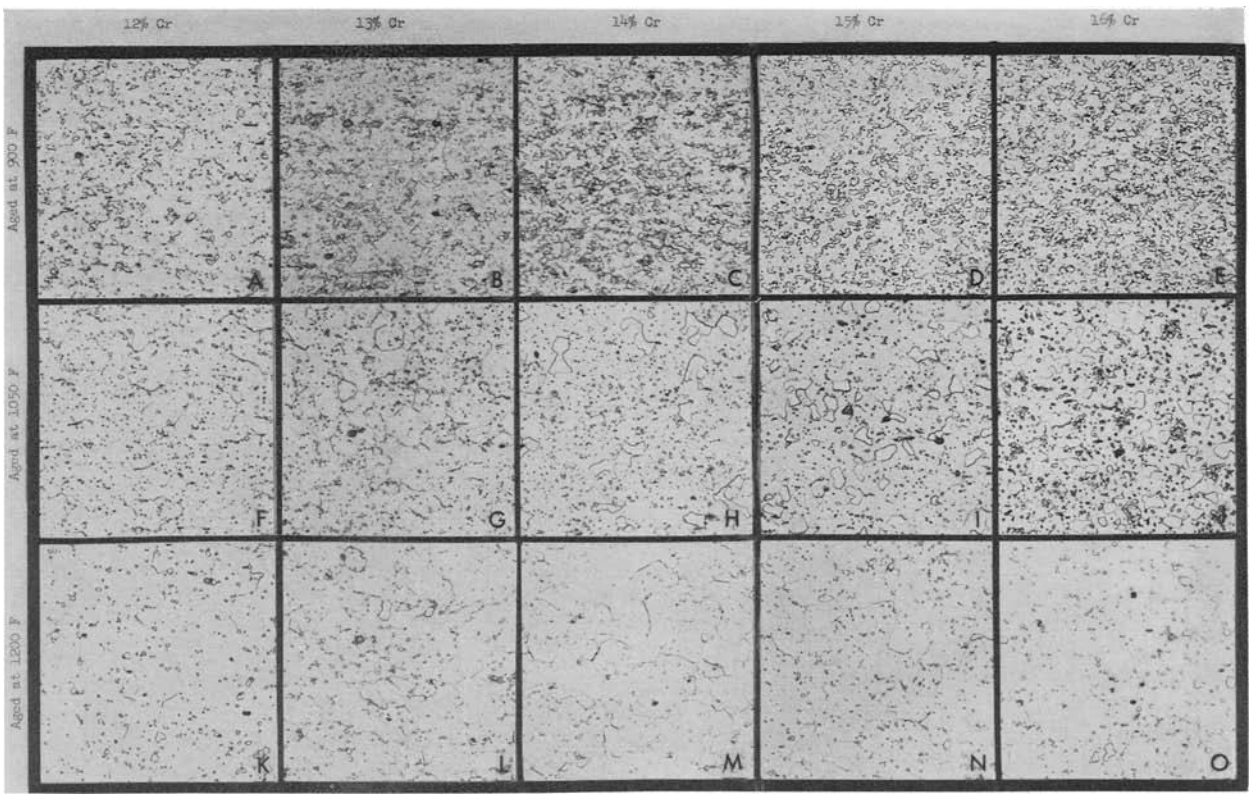


FIG. 12—Microstructure of Annealed and Cold-Reduced Chromium Steels Aged for 76,000 hr. Etched in Vilella's Reagent (×1000). (The clear etching phase in Plates A, B, C, D, E, H, I, and J is sigma. Carbides also appear in each microstructure. Although some sigma could be found in the 13 per cent chromium steel aged at 1050 F, the structure illustrated in Plate G is more representative than fields containing sigma.) Reduced one half for reproduction.

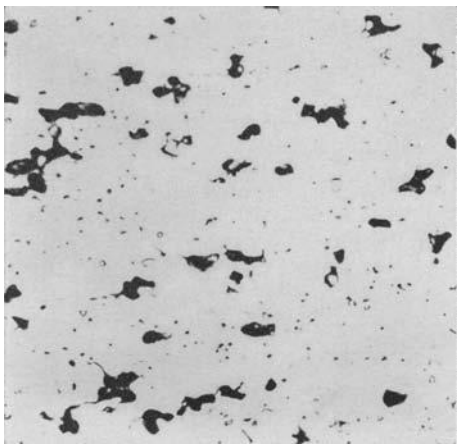


FIG. 13—Microstructure of Cold-Reduced 12 Per Cent Chromium Steel Aged at 900 F for 76,000 hr. Etched in Glyceregia (×1500). (The dark etching phase is sigma).

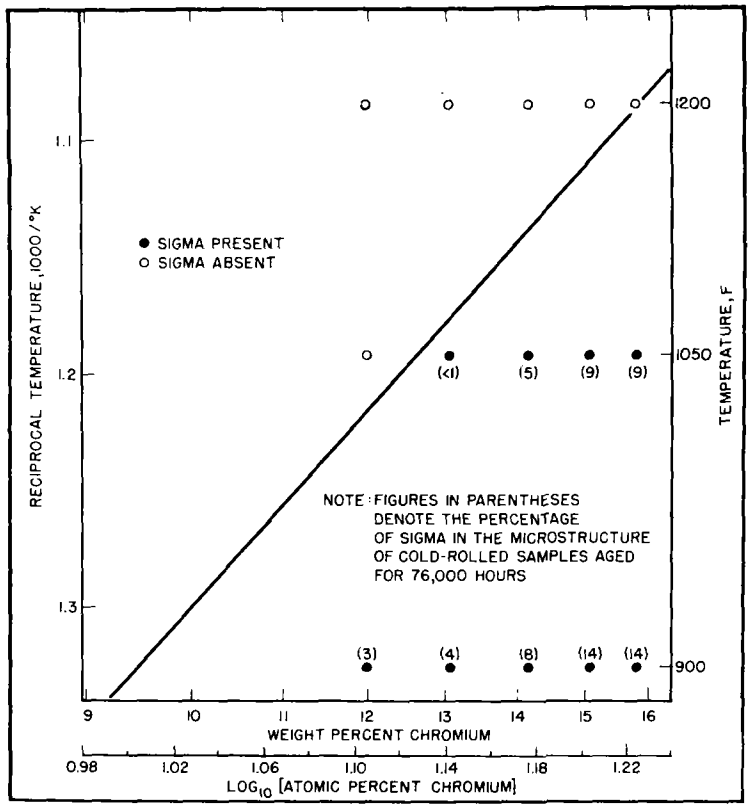


FIG. 14—The Effect of Temperature on the Solubility of Sigma in 12 to 16 Per Cent Chromium Commercial-Purity Steels.

TABLE 4—A COMPARISON OF THE OBSERVED AND THE ESTIMATED EQUILIBRIUM SIGMA CONTENTS IN COLD-ROLLED CHROMIUM STEELS AGED FOR 76,000 HR.

NOTE—Equilibrium sigma contents were calculated by using the lever law, the solvus line drawn in Fig. 14, and a sigma–alpha plus sigma boundary at 42 per cent chromium.

Nominal Chromium Content, per cent	Aged at 900 F		Aged at 1050 F	
	Observed Sigma Content, per cent	Equilibrium Sigma Content, per cent	Observed Sigma Content, per cent	Equilibrium Sigma Content, per cent
12	3	7.7	0	0
13	4	11.0	<1	1.6
14	8	14.3	5	5.2
15	14	17.1	9	8.3
16	14	19.4	9	10.9

TABLE 5—HARDNESS OF AGED CHROMIUM STEELS.

Nominal Chromium Content, per cent	Aging Temperature, deg F	Diamond Pyramid Hardness[a] of Annealed and Aged Steel					Nominal Chromium Content, per cent	Aging Temperature, deg F	Diamond Pyramid Hardness[a] of Cold-Reduced and Aged Steels				
		As-Annealed[b]	Aging Time, hr						As Cold-Reduced	Aging Time, hr			
			5000[b]	10,000[b]	43,000	76,000				5000[b]	10,000[b]	43,000	76,000
12	900	142	137	136	148	138	12	900	333	247	203	159	200
	1050	142	150	146	140	144		1050	333	153	175	222	167
	1200	142	143	142	148	138		1200	333	145	150	171	200
13	900	150	153	160	169	159	13	900	350	258	227	213	222
	1050	150	166	164	167	154		1050	350	170	175	141	194
	1200	150	166	153	155	149		1200	350	153	172	163	195
14	900	153	157	164	172	171	14	900	350	270	262	224	219
	1050	153	170	166	168	163		1050	350	179	166	200	209
	1200	153	164	160	172	154		1200	350	155	177	161	159
15	900	151	170	191	196	186	15	900	356	276	258	232	229
	1050	151	162	159	183	166		1050	356	196	193	189	198
	1200	151	162	155	150	148		1200	356	159	168	179	193
16	900	170	227	251	225	211	16	900	363	283	287	246	227
	1050	170	177	176	181	178		1050	363	193	183	203	199
	1200	170	159	175	171	155		1200	363	162	160	170	205

[a] Average of three measurements made with a 2.5-kg load on the indenter.
[b] Data previously reported by Link and Marshall, Ref. (**18**).

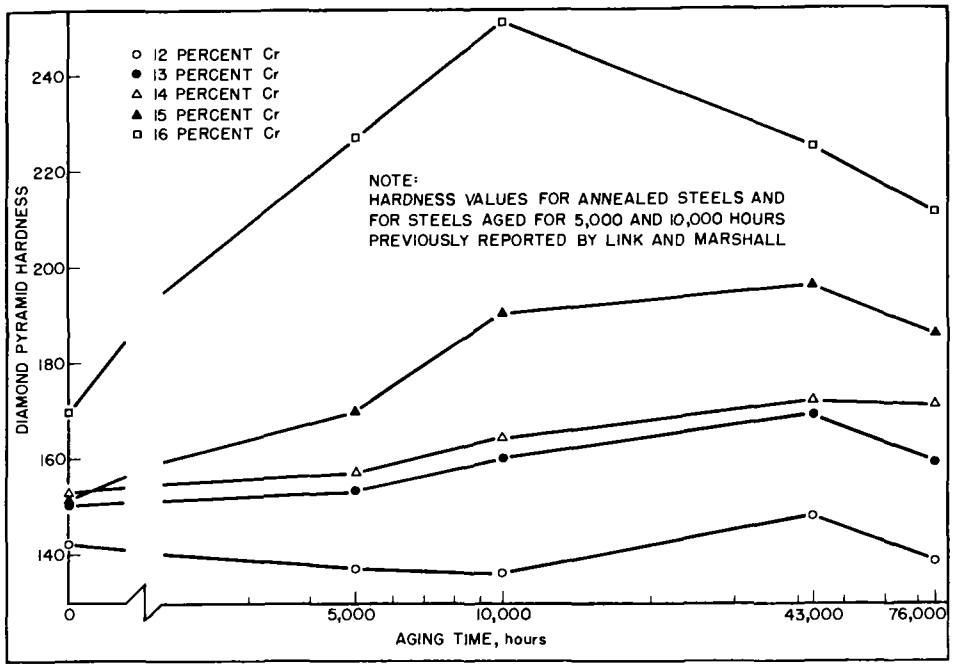


FIG. 15—Diamond Pyramid Hardness of Annealed Chromium Steels Aged for Various Times at 900 F.

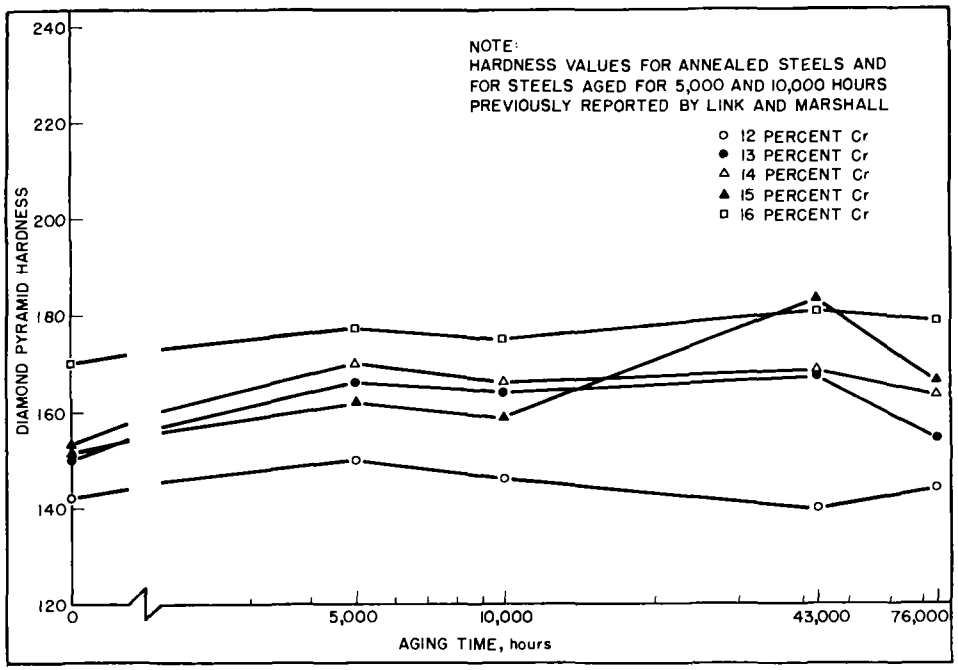


FIG. 16—Diamond Pyramid Hardness of Annealed Chromium Steels Aged for Various Times at

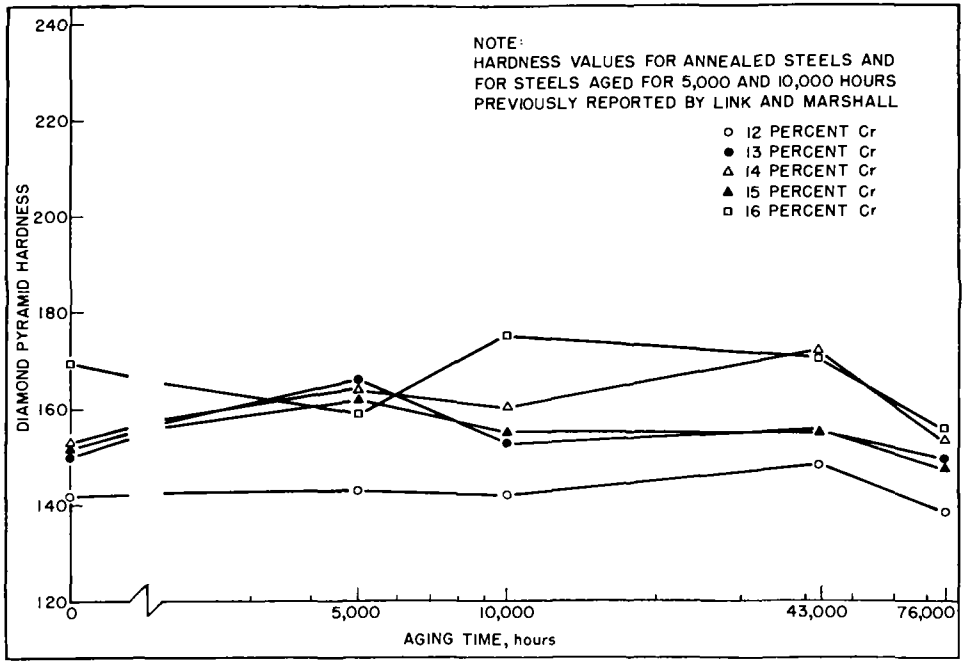


FIG. 17—Diamond Pyramid Hardness of Annealed Chromium Steels Aged for Various Times at 1200 F.

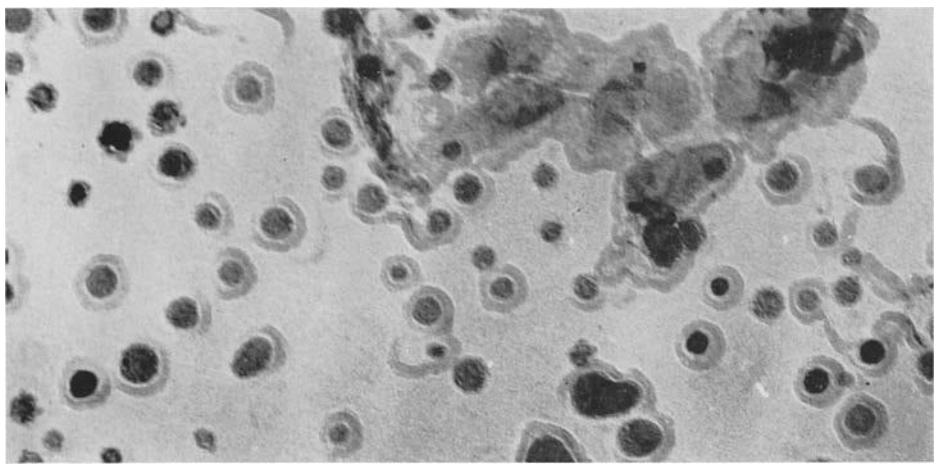


FIG. 18—Electron Micrograph of 16 Per Cent Chromium Steel Cold-Reduced 95 Per Cent and Aged at 900 F for 76,000 hr (×144,000). (The dark particles are the body-centered cubic precipitate; the halo around these particles is a replicating effect. The precipitate was found only at great distances, on the diffusion scale, from sigma particles, according to R. M. Fisher.)

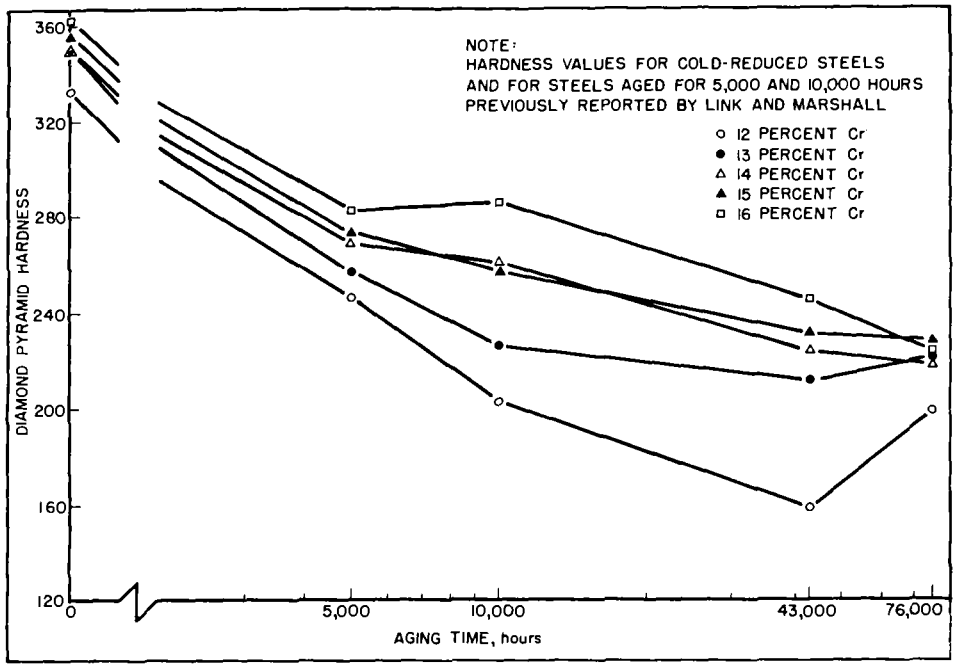


FIG. 19—Diamond Pyramid Hardness of Cold-Reduced Chromium Steels Aged for Varinus Times at 900 F.

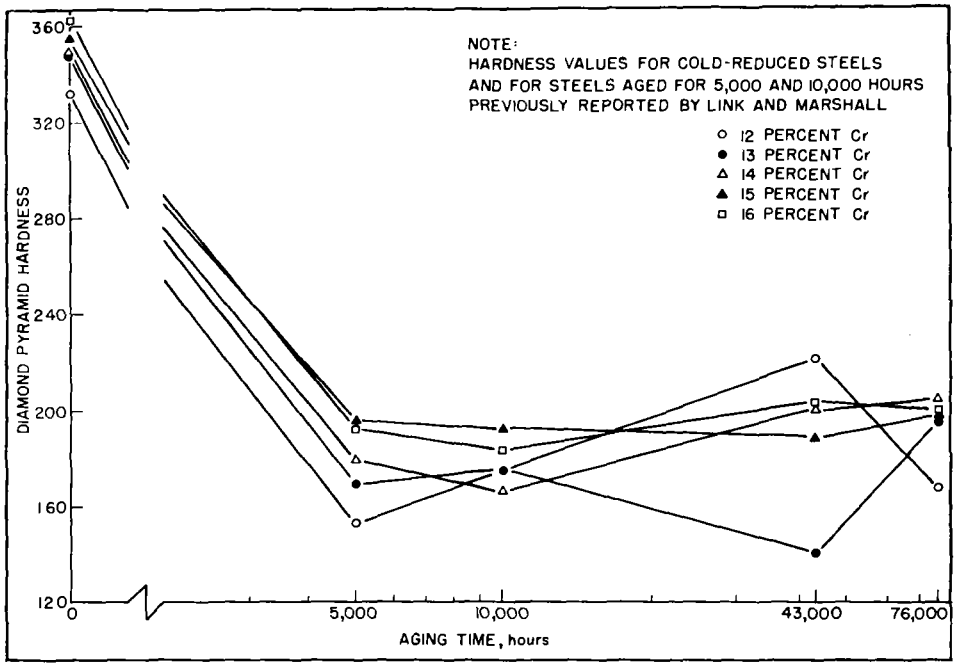


FIG. 20—Diamond Pyramid Hardness of Cold-Reduced Chromium Steels Aged for Various Times at 1050 F.

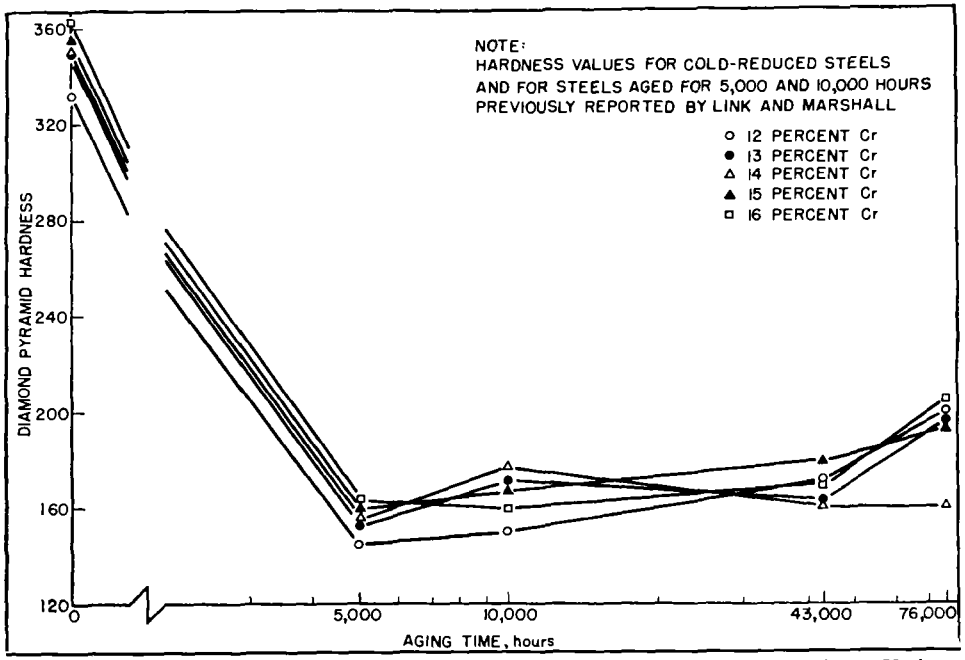


FIG. 21—Diamond Pyramid Hardness of Cold-Reduced Chromium Steels Aged for Various Times at 1200 F.

cent, and most probably at about 12.6 per cent chromium.

3. At 900 F the alpha – alpha plus sigma boundary in commercial-purity chromium steels lies at a chromium content less than 12 per cent and most probably at about 9.5 per cent chromium. This is believed to be the first time sigma has been observed in a stainless steel with a chromium content as low as 12 per cent.

4. The heat of solution of sigma in commercial-purity chromium steels is at least 4200 cal/mole.

5. Commercial-purity steels containing about 15 per cent or more chromium undergo hardening because of the coherent precipitation of a chromium-rich ferrite at 900 F.

6. A commercial-purity steel containing 15.80 per cent chromium overages during exposure at 900 F for more than 10,000 hr. This is the first reported observation of the reversal of 885 F embrittlement by overaging.

Acknowledgment:

The authors with to thank R. M. Fisher for his counsel during the preparation of this paper and for supplying the electron micrograph shown in Fig. 18. The encouragement and support of this program by J. J. Heger, who originally conceived it, is also greatly appreciated. The cooperation of J. M. Heffernan, who prepared the photomicrographs that constitute an important segment of this paper, is also acknowledged.

REFERENCES

(1) G. J. Dickins, A. M. B. Douglas, and W. H. Taylor, "Sigma-Phase in the Co-Cr and Fe-Cr Systems," *Journal of the Iron and Steel Inst.*, Vol. 167, 1951, p. 27.

(2) W. Trietschke and G. Tammann, "The Alloys of Iron and Chromium," *Z. anorg. Chemie*, Vol. 55, 1907, pp. 402–411.

(3) E. C. Bain and W. E. Griffiths, "An Introduction to the Iron-Chromium-Nickel Alloys," *Transactions*, Am. Institute of Mining, Metallurgical, and Petroleum Engrs., Vol. 75, 1927, pp. 166–210.

(4) R. L. McDowell, "Discussion," *Transactions*, Am. Institute of Mining, Metallurgical, and Petroleum Engrs., Vol. 75, 1927, p. 213.

(5) E. Jänecke, "The Constitution of Iron-Chromium Alloys," *Z. Electrochem.*, Vol. 23, 1917, pp. 49–55, and *The Metallurgist*, Vol. 7, September 25, 1931, pp. 139–140.

(6) T. Murakami, "On the Structure of Iron-Carbon-Chromium Alloys," *Science Reports*, Sendai, Series 1, Vol. 7, 1918, pp. 217–276, and *The Metallurgist*, Vol. 7, September 25, 1931, pp. 139–140.

(7) C Kruetzer, "X-ray Diffraction Measurements in the Systems Iron-Chromium and Iron-Phosphorus," *Z. Phys.*, Vol. 48, 1928, pp. 556–566, and *Chemical Abstracts*, Vol. 22, 1928, p. 3126.

(8) A. Westgren, G. Phragmen, and F. Negresco, "On the Structure of the Iron-Chromium-Carbon System," *Journal of the Iron and Steel Inst.*, Vol. 117, 1928, pp. 383–400.

(9) F. Adcock, "The Chromium-Iron Constitutional Diagram," *Journal of the Iron and Steel Inst.*, Vol. 124, No. II, 1931, pp. 99–149.

(10) P. Chevenard, "Experimental Investigations of Iron, Nickel, and Chromium Alloys," *Trav. Mem., Bur. Int. Poids et Mesures*, Vol. 17, 1927, p. 90, and *The Metallurgist*, Vol. 7, September 25, 1931, pp. 139–140.

(11) F. Wever and W. Jellinghaus, "The Two-Component System: Iron-Chromium," *Mitt. Kaiser-Wilhelm Inst.*, Vol. XIII, 1931, p. 143–147, and *Chemical Abstracts*, Vol. 25, 1931, p. 5655.

(12) S. Eriksson, "X-ray Investigation of the Iron-Chromium-Nitrogen System," *Jernkontorets Annaler*, N.S. 89, 1934, pp. 530–543.

(13) P. Oberhoffer and H. Esser, "The Iron-Chromium Diagram," *Stahl und Eisen*, Vol. 47, 1927, pp. 2021–2031.

(14) A. B. Kinzel and W. Crafts, *The Alloys of Iron and Chromium: Vol. I—Low-Chromium Alloys*, McGraw-Hill Book Co., New York, N.Y., 1937.

(15) A. J. Cook and F. W. Jones, "The Brittle Constituent of the Iron-Chromium System," *Journal of the Iron and Steel Inst.*, Vol. 148, No. II, 1943, pp. 217–226.

(16) J. J. Heger, "The Formation of Sigma Phase in a 17 Per Cent Chromium Steel," *The Nature, Occurrence, and Effects of Sigma Phase, ASTM STP 110*, Am. Soc. Testing Mats., 1950, pp. 75–78.

(17) F. J. Shortsleeve and M. E. Nicholson, "Transformation in Ferritic Chromium Steels Between 1100 and 1500 F," *Transactions*, Am. Soc. Metals, Vol. 43, 1951, pp. 142–156.

(18) H. S. Link and P. W. Marshall, "The Formation of Sigma Phase in 13 to 16 Per Cent Chromium Steels," *Transactions*, Am. Soc. Metals, Vol. 44, 1952, pp. 549–559.

(19) M. Hansen, *Constitution of Binary Alloys*, McGraw-Hill Book Co., New York, N.Y., 1958.

(20) H. D. Newell, "Properties and Characteristics of 27 Per cent Chromium-Iron," *Metal Progress*, Vol. 49, May, 1946, pp. 997–1006, 1016–1028.

(21) J. J. Heger, "885 F Embrittlement of the Ferritic Chromium-Iron Alloys," *Metal Progress*, August, 1951, pp. 55–61.

(22) G. Bandel and W. Tofaute, "Brittleness of Chromium-Rich Steels at Temperatures Around 930 F," *Archiv fur das Eisenhüttenwesen*, Vol. 15, No. 7, 1942, pp. 307–319, Brutcher Translation No. 1893.

(23) R. M. Fisher, E. J. Dulis, and K. G. Carroll, "Identification of the Precipitate Accompanying 885 F Embrittlement in Chromium Steels," *Journal of Metals Supplement*, May, 1953, pp. 1–6.

(24) J. J. Heger, discussion of above paper, "Identification of the Precipitate Accompanying 885 F Embrittlement in Chromium Steels," *Journal of Metals*, May, 1954, p. 663.

(25) R. M. Fisher, E. J. Dulis, and K. G. Carroll, authors' reply to Heger's discussion, *Journal of Metals*, May, 1954, pp. 663–664.

(26) R. O. Williams and H. W. Paxton, "Nature of Aging of Binary Iron-Chromium Alloys Around 500 C," *Journal of the Iron and Steel Inst.*, Vol. 185, March, 1957, pp. 358–374.

(27) R. O. Williams, "Further Studies of the Iron-Chromium System," *Transactions*, Am. Inst. Mining, Metallurgical, and Petroleum Engrs., August, 1958, pp. 497–502.

DISCUSSION

C. H. SAMANS[1]—Some 12 per cent chromium steels definitely embrittle in refining service. If this is not 885 F or sigma, there must be some other hardening mechanism. Any suggestions? If sigma forms, must the alloy be reheated to redissolve it?

D. C. LUDWIGSON AND H. S. LINK (*authors*)—We do not believe that the possibility of sigma formation or 885 F embrittlement in a 12 per cent chromium steel should be ruled out. Our data showed that sigma did form in our 12 per cent chromium steel at 900 F. Although we did not detect 885 F embrittlement in this simulated-commercial-purity steel after exposure for 76,000 hr at 900 F, it is possible that such embrittlement might develop upon longer exposure. Furthermore, moderate variations in residual elements in commercial 12 per cent chromium steels or the presence of small amounts of strain, such as might be introduced during fabrication, could favor susceptibility to embrittlement. If Mr. Samans has made observations that would suggest some other mechanism to be responsible for the loss of ductility in 12 per cent chromium steel, we would be interested in learning of his findings.

Because we conducted no experiments on the resolution of sigma in our steels, we cannot answer Mr. Samans query on this subject. However, the phase rule indicates that it is necessary to alter temperature, pressure, or composition to cause the disappearance of an equilibrium phase.

P. A. JENNINGS[2]—In this paper, the authors have described the results of their latest work which pertains to the presence or absence of sigma phase in wrought 12, 13, 14, 15 and 16 per cent chromium steels where specimens, either annealed or cold reduced (95 per cent), were exposed at 900, 1050 and 1200 F for periods of 43,000 and 76,000 hr.

As everyone knows, the environment parameters conducive to the formation of sigma phase are stress, temperature, and time. Of these three, I would like to place special emphasis on the importance of stress.

To be truly rigorous, it should be realized that commercial products when specified "annealed" actually must be furnished with some degree of cold work present because of the necessity for straightening or flattening operations. For example, bars and tubing must be straightened after annealing and sheet material must be temper rolled, or may be roller or stretcher leveled. To accomplish the necessary straightening, the yield point of the material must be exceeded for the particular product being processed.

Now, in Table 2 of this paper the authors show that for annealed material, only 14, 15 and 16 per cent chromium steels developed sigma phase after exposure at 1050 F for 10,000, 43,000 and 76,000 hr. However, since all commercial products in the annealed condition contain some amount of stress because of the straightening operation, it is reasonable to suppose that the propensity to form sigma phase in these steels may occur at lower temperatures, or at shorter time periods, or both.

[1] American Oil Co., Whiting, Ind.

[2] Senior research engineer, research and technology, Armco Steel Corp., Middletown, Ohio.

DEVELOPMENT OF A MODIFIED ALLOY 20 STAINLESS STEEL

By H. L. Black[1] and L. W. Lherbier[2]

Synopsis

Alloy 20 is a low carbon, 20 per cent chromium, 30 per cent nickel austenitic stainless steel that contains molybdenum, copper, and columbium as primary alloying elements. The alloy is especially resistant to corrosive attack in sulfuric acid. Although satisfactory for a majority of sulfuric acid applications, there are some areas where its corrosion resistance is somewhat deficient. Another deficiency, of more interest to the producer than the user, is its poor hot workability. This study was designed to develop a modified Alloy 20 with improved corrosion resistance that would have higher product yields through improved workability.

The results of tests on a series of experimental heats indicate that the hot workability of Alloy 20 can be significantly improved by additions of titanium and to a lesser degree by increasing carbon, columbium, and boron and decreasing chromium and molybdenum. The effect of nickel is variable. Copper variations and calcium additions have no effect on workability.

In respect to corrosion resistance in sulfuric acid, all increases in alloying elements produced either no significant effect or a reduction of corrosion resistance, with the exception of nickel. A significant increase in sulfuric acid corrosion resistance was observed with increasing nickel content. A significant detrimental effect on corrosion was observed with increasing amounts of chromium. All other elements studied, including titanium, had no significant effect on corrosion resistance in sulfuric acid.

Alloy 20 is not new from the standpoint of composition since the current chemical analysis range is very similar to that of Durimet 20, originally developed some time ago as a casting alloy (1).[3] Recently, the alloy has been made in wrought form commercially by several steel companies through the use of rare earth additions or special deoxidation methods in the melting operations. Alloy 20 is basically a low carbon austenitic stainless steel containing nickel, chromium, molybdenum, and copper as the main alloying elements. Columbium has been added to the composition for improved resistance to intergranular corrosion in welded products. The current nominal chemical analysis of this alloy is as follows:

C	Cr	Ni	Mo	Cu	Cb + Ta	Fe + Residuals
0.05	20.0	30.0	2.50	3.50	0.75	balance

The alloy was primarily designed for resistance to sulfuric acid attack but can also be used in many other corrosive environments. Alloy 20 is greatly superior in corrosion resistance to the standard 18 per cent chromium-8 per cent nickel stainless steels, especially in sulfuric acid, hot acetic acid, and phosphoric acid solutions (2). Many uses involve applications where the 18-8 grades would be unsatisfactory because of high temperatures or contaminants that accelerate attack or both.

From the steel producers' standpoint, Alloy 20 is classified as one of the difficult-to-work, high alloy, corrosion resistant steels. Hot working difficulties are not surprising considering that the alloy was originally designed as a casting alloy. Common problems in producing wrought product include cracks (Fig. 1), tears, scabs, and similar hot workability defects. Consequently, processing of this alloy generally results in low and variable product yields. This hot workability problem, coupled with the need for an alloy with improved corrosion resistance, prompted the initiation of the present investigation. The goal of the work was to develop a modified Alloy 20 composition having improved hot workability and superior corrosion resistance in sulfuric acid.

Background

Workability:

The term hot workability is misleading unless the word is restricted to a specific set of conditions for a given composition. For example, the hot workability of an alloy may be good or poor, depending on whether the process involves working a billet to a bar or an ingot to a billet. Generally speaking, the hot working of an ingot to a billet presents more difficulty. This work concerned the problem of converting a heterogeneous ingot structure to homogeneous billet, bar, or plate product.

Many factors are important for successful hot workability of difficult-to-work alloys. Such factors, all of which have been applied to the Alloy 20 composition, include (3):

1. Careful selection of raw materials for melting.
2. Optimum melting practices, techniques, or methods, including deoxidation practice.
3. Good ingot surface quality and optimum ingot size.
4. Control of ingot heating practices, including gradual heating and thorough soaking, avoiding direct impingement of the flame, avoiding high sulfur fuels, turning the material in the furnace to avoid cold sides, and the use of a neutral or slightly oxidizing atmosphere.
5. Control of the ingot hot working process by working the material as soon as the ingot is withdrawn from the furnace, using light reductions on the initial passes, and keeping square ingots square until the as-cast structure is sufficiently broken down.
6. Removal of cracks and tears by grinding to avoid their propagation.

Corrosion:

The development of an alloy with better resistance to sulfuric acid attack is important. Sulfuric acid is perhaps the most widely used compound in the chemical and allied process industries. This acid has frequently been referred to as the foundation of the chemical industry and enjoys a wide diversity of applications. Thus, a material with

[1] Group metallurgist, Stainless Steel Section, Technology and Development Laboratory, Universal-Cyclops Steel Corp., Bridgeville, Pa.

[2] Section metallurgist, Product Development, Technology and Development Laboratory, Universal-Cyclops Steel Corp., Bridgeville, Pa.

[3] The boldface numbers in parentheses refer to the list of references appended to this paper.

Copyright© 1965 by ASTM International

improved corrosion resistance to sulfuric acid would be important economically to the chemical industry.

PROCEDURE

Material:

Laboratory heats were melted to study the limits of forging temperature and the effect of variations in alloying elements on the hot workability of Alloy 20. The experimental heats were air melted in a 35-lb induction furnace. A total of 45 ingots was cast with variations in carbon, chromium, nickel, molybdenum, copper, titanium, columbium, and boron. Calcium additions were also studied. The nominal analysis of Alloy 20, along with the elemental ranges studied, is listed in Table 1.

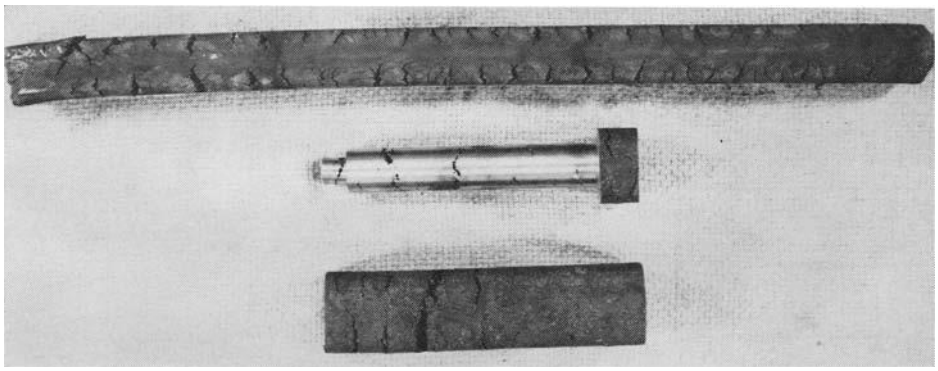


FIG. 1—Illustration of Cracking Problem Frequently Encountered in Processing Alloy 20.

Workability Tests:

Hot workability may be measured by several methods, including the upset, hot tension, tensile impact, hot twist, and hot bend tests (3). The fact that so many tests exist indicates how elusive workability is to measure. For this study we chose the hot tension test, primarily because of some previous measure of success in determining the hot workability range of various high temperature alloys.

All of the experimental heats were cast into $2\frac{1}{8}$-in. square ingots, stripped hot, and were allowed to air cool. After the hot tops were removed tensile blanks were cut from the top half of each ingot for high-strain-rate tension tests. The specimens were machined from the mid-radius position and were tested at 1825, 1950, 2075, and 2200 F. The tensile machine was operated at a head travel speed of 8-in./min. Data obtained included ultimate strength, elongation, and reduction of area.

The high-strain-rate tensile data were supplemented with edge crack ratings obtained on round cornered square product processed on a two-high rolling mill. The bottom half of each ingot was rolled to $1\frac{1}{8}$-in. bar. All ingots were thoroughly heated and rolled at a starting temperature of 2100 F. The percentage reduction per pass was kept low and was of equal magnitude on all ingots. The rolled product obtained from each experimental heat was visually inspected and put into five broad relative rating categories, according to the amount and severity of edge cracks. These rating categories were very severe, severe, poor, fair, and good.

Corrosion Tests:

Unlike the high-strain-rate tension specimens which were taken from the cast product, the specimens for corrosion testing were obtained from the $1\frac{1}{8}$-in. wrought bar rolled from each heat. All bars were annealed at 1950 F and water quenched. Cylindrical weight loss specimens $\frac{1}{2}$ in. diameter by 1 in. long were machined from each bar. Specimens were lapped to a 150 grit finish to insure an identical surface on all corrosion test pieces. Prior to testing, all specimens were thoroughly cleaned by ultrasonic degreasing followed by an alcohol rinse.

Tests were conducted in boiling 10 and 20 per cent nonaerated sulfuric acid for one period of 72 hr. Upon completion of the testing, the specimens were cleaned, dried, and weighed. From the calculated weight loss, the corrosion rate in inches penetration per year (IPY) was computed. Duplicate and sometimes triplicate specimens from each heat were tested in each environment.

RESULTS

Workability:

The general effect of the alloying variations on hot strength and ductility, as determined by the high-strain-rate tension test, is shown in Table 2. Increases in carbon, nickel, chromium, molybdenum, and columbium caused slight increases in hot strength. These increases, however, were quite small in all instances and are probably of little significance. To illustrate the point, a curve plotting strength versus per cent nickel, the alloying element that showed the greatest variation, is shown in Fig. 2. No effect on the hot strength of this alloy system was observed for the copper, titanium, and boron variations or for the calcium additions.

As is normally the case, the strength of any given composition decreased with increasing test temperature. However, the observed strength decrease for Alloy 20 was relatively small. To illustrate, Fig. 3 shows the comparative effect of temperature on the strength of Alloy 20 and René 41, one of the current nickel-base high-temperature alloys (4). The difference in magnitude of the strength change for the two alloys is readily evident. Consequently, one might be reluctant to comment on the significance of strength changes with temperature as affecting the workability of this alloy system.

TABLE 1—NOMINAL CHEMICAL ANALYSIS OF ALLOY 20 WITH CHEMICAL RANGES STUDIED.

Element	Alloy 20 Composition, %	Variations, %
C	0.05	0.01 to 0.11
Cr	20.0	15.0 to 22.0
Ni	30.0	20.0 to 50.0
Cu	3.5	1.5 to 4.0
Mo	2.5	2.0 to 6.0
Cb	0.75	0 to 1.50
Ti	...	0 to 1.50
B	...	0.0009 to 0.005
Ca	...	add 0.05

The ductility measurements of high-strain-rate tension tests usually provide a better indication of hot workability. However, as the data in Table 2 show, only carbon and nickel produced any significant effects. Increasing carbon results in an increase in ductility and theoretically better workability. The effect of nickel is variable and is shown in Fig. 4. Ductility is a maximum at about 30 per cent nickel. Other than the effects of carbon and nickel, we could determine no optimum working temperature between 1825 and 2200 F; that is, ductility values for any composition were essentially uniform throughout this temperature range.

The effect of alloying variations on the

TABLE 2—EFFECT OF ALLOYING VARIATIONS ON HIGH-TEMPERATURE STRENGTH AND DUCTILITY OF ALLOY 20 AT HIGH-STRAIN RATES.

Element	Variation, %	Effect on Strength	Effect on Ductility
C	0.01 to 0.11	slight	positive
Ni	20 to 50	slight	variable
Cr	15 to 22	slight	none
Mo	2 to 6	slight	none
Cu	1.5 to 4	none	none
Cb	0 to 1.5	slight	none
Ti	0 to 1.5	none	none
B	0.0009 to 0.005	none	none
Ca	add 0.05	none	none

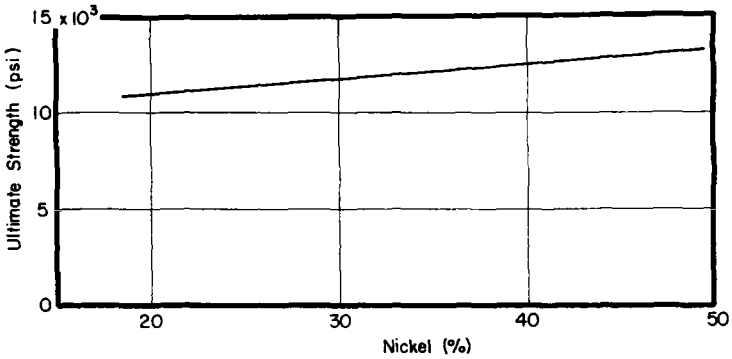


FIG. 2—Variation in High-Temperature Strength with Nickel Content (2075 F).

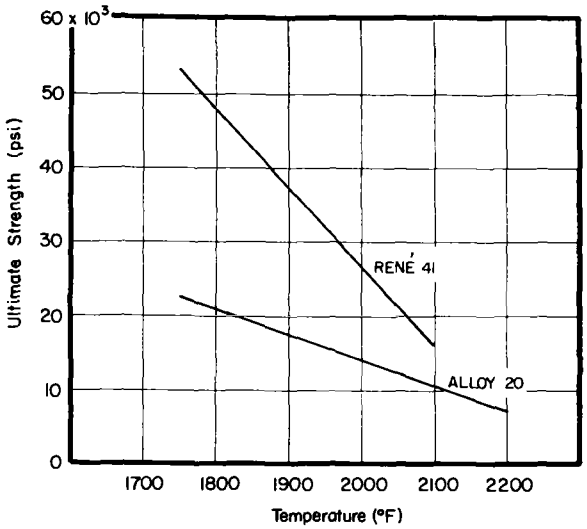


FIG. 3—Variation in Strength with Test Temperature for Alloy 20 in Comparison with Nickel-Base-High Temperature Alloy.

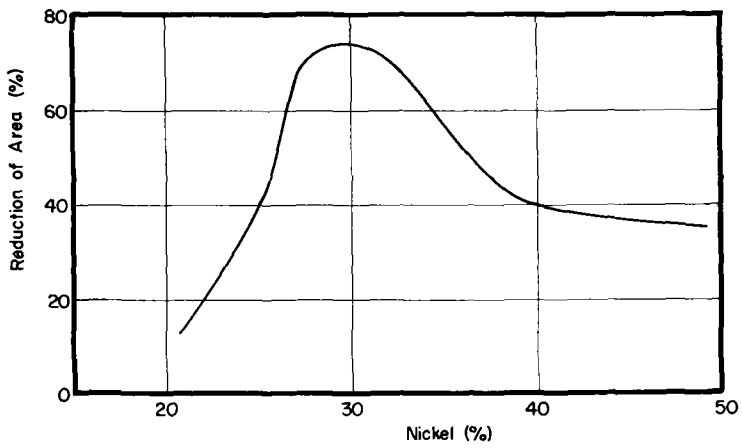


FIG. 4—Effect of Nickel Content on the High-Strain Rate Ductility of Alloy 20.

edge-crack ratings of rolled bars is shown in Table 3. Perhaps the largest effect was the improvement in workability with increasing amounts of titanium. The ratings vary from severe edge cracking at the 0 per cent titanium level to edge-crack ratings of very good at 1.5 per cent titanium. This improvement is illustrated in Fig. 5.

Increasing carbon content improves workability. This effect of carbon is in agreement with the ductility values obtained with the high-strain-rate tension tests. A somewhat smaller increase in workability is observed also when increasing amounts of columbium and boron are added to the Alloy 20 composition. The effect of nickel on edge-crack ratings agrees with the ductility values obtained with the high-strain-rate tension tests. Edge-crack ratings for

TABLE 3—EFFECT OF ALLOYING VARIATIONS ON EDGE-CRACK RATINGS ON 1⅛-IN. RCS ALLOY 20 BAR.

Element	Variation, %	Edge-Crack Rating
Ti	0 to 1.5	severe to very good
C	0.01 to 0.11	severe to good
Cb	0 to 1.5	severe to fair
B	0.0009 to 0.005	poor to good
Ni	20 to 50	very severe to fair to severe
Cu	1.5 to 4	poor to poor
Ca	add 0.05	poor to poor
Mo	2 to 6	poor to severe
Cr	15 to 22	good to poor

increasing nickel content range from very severe to fair and back to severe.

Increasing copper content and calcium additions produced no effect on workability. The edge crack ratings were poor in all cases. Two elements, chromium and molybdenum, showed decreasing workability with an increase in alloy content. The low chromium variation exhibited a rating of good while at the high level of chromium an edge-crack rating of poor was obtained. Molybdenum ratings were poor to severe with increasing amounts of this element.

Corrosion:

The effect of variations in alloying elements on the corrosion resistance of Alloy 20 in 10 and 20 per cent sulfuric acid solutions is shown in Table 4. Within the alloying ranges studied, no effect on corrosion rate was observed for variations in carbon, copper, molybdenum, titanium, boron, or calcium. Note that titanium additions do not adversely affect the corrosion rate. Titanium, therefore, could be added to the Alloy 20

composition for improved workability without affecting the corrosion rate in sulfuric acid.

Increasing nickel contents reduce the rate of corrosion in sulfuric acid significantly. As nickel is increased from 20 per cent to between 30 and 35 per cent the corrosion rate is rapidly decreased in sulfuric acid solutions: see Fig. 6 for the results of tests in a 10 per cent sulfuric acid solution. Reasonably low rates of corrosion can be obtained at the 30 to 33 per cent nickel level, the upper end of the current specification ranges for this grade. This particular nickel level would also give maximum hot workability as predicted by both the high-strain-rate tension test and the edge-crack ratings on rolled-bar products.

The effect of columbium has been termed negative in the sense that the corrosion rate increases with increasing columbium content in the 10 per cent acid solution. The effect, as shown in Fig. 7, is relatively minor when compared with the previous effect observed for nickel. Furthermore, essentially no difference in corrosion rate is observed in a 20 per cent acid solution. The other negative effect observed, that due to chromium, is much more significant. Figure 8 shows a plot of the data in the 10 per cent acid solution. The corrosion rate increases significantly with increasing chromium content. Similar test data were obtained in a 20 per cent acid solution. This relationship, while opposite from that normally expected in most environments, is not unusual in boiling sulfuric acid and has been reported in the literature (5). Thus, we see that decreased chromium content not only tends to improve the hot workability but also tends to improve the corrosion resistance of this material in sulfuric acid solutions.

DISCUSSION

The results of the workability studies show the insensitivity of the high-strain-rate tension test in determining the hot workability of Alloy 20 for most of the alloying variations studied. The fact that rolling of cast product showed significant effects of alloy variations indicates that the main reason for the failure of the hot tension test was the lack of a similar stress-strain relationship between the test and the rolling conditions.

Explaining why we obtained such a drastic change in workability with titanium additions is difficult. Little fundamental work has been done to determine factors responsible for the hot ductility of pure metals, let alone complex alloys such as Alloy 20. Current information indicates that the ductility at high temperatures is controlled by one or combinations of the following factors (6):

1. Ease of dislocation movement.
2. Number of ways dislocations can move.
3. Ease of twinning.
4. Ease of grain boundary shearing and moving.
5. Rate of atomic mobility.
6. Ease of recrystallization.

As a preliminary step to determine the effect of titanium, a microstructural study was conducted on specimens obtained from cast product that exhibited widely different hot workability as determined by edge-crack ratings. Figure 9 shows an electron microscope photograph of material with no titanium and very poor workability at a magnification of ×40,000. The distinguishing feature of this material is clean grain boundaries with very few carbides. In contrast to the material with no titanium, material with an appreciable titanium content did not reveal this condition. Rather, the high titanium materials with good workability exhibited numerous discontinuous particles at the grain boundaries. An electron microscope photograph of this condition is shown in Fig. 10.

With this information, one might look at the possible advantageous aspects of numerous discontinuous carbides precipitated at grain boundaries. Cracks arise from a combination of grain boundary sliding and slipping across the boundary. The presence of numerous particles, probably titanium carbides, can restrict cracks to inter-carbide spaces which, because of the good fit across the carbide/grain interface, prevents the cracks from spreading.

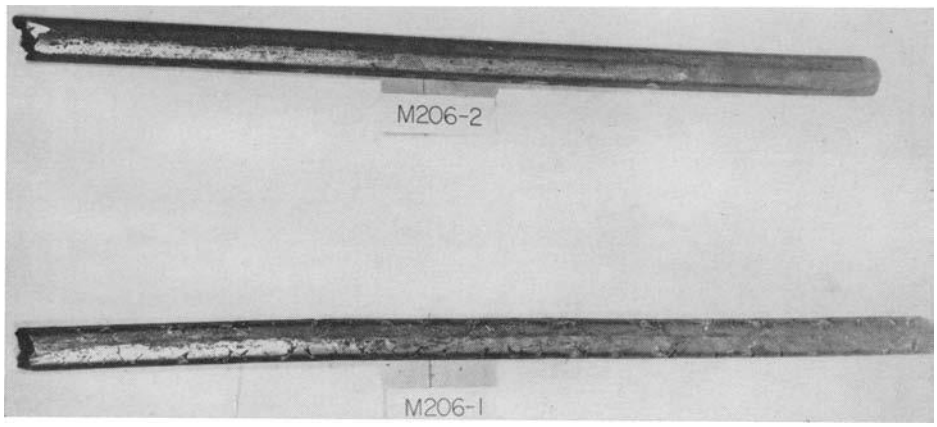


FIG. 5—Surface Cracking in Alloy 20 with Titanium Addition (*top*) and Without Titanium (*bottom*).

TABLE 4—EFFECT OF ALLOYING VARIATIONS ON THE CORROSION RATE OF ALLOY 20 IN 10 AND 20 PER CENT SULFURIC ACID SOLUTIONS.

Element	Variation, %	Effect on Corrosion Rate
Ni	20 to 50	decreases
C	0.01 to 0.11	none
Cu	1.5 to 4	none
Mo	2 to 6	none
Ti	0 to 1.5	none
B	0.0009 to 0.005	none
Ca	add 0.05	none
Cb	0 to 1.5	increases
Cr	15 to 22	increases

Good ductility could then be obtained provided that other modes of plastic flow are available (6). Such a situation is certainly possible since moving dislocations can surmount obstacles such as precipitates or other stationary dislocations by dislocation climb, a process controlled by the mobility of atoms. Certainly more work is needed to predict the exact cause of the differences noted in workability.

The results obtained on the experimental heats indicate that the hot workability of Alloy 20 can be significantly improved by additions of titanium. A substantial increase in workability can also be obtained at high carbon levels. Further increases in workability of a much smaller degree can be obtained by increasing columbium and boron and decreasing chromium.

Of the above mentioned elements, only columbium seriously reduces corrosion resistance in sulfuric acid. However, high carbon contents would be detrimental from the standpoint of intergranular corrosion in welded structures,

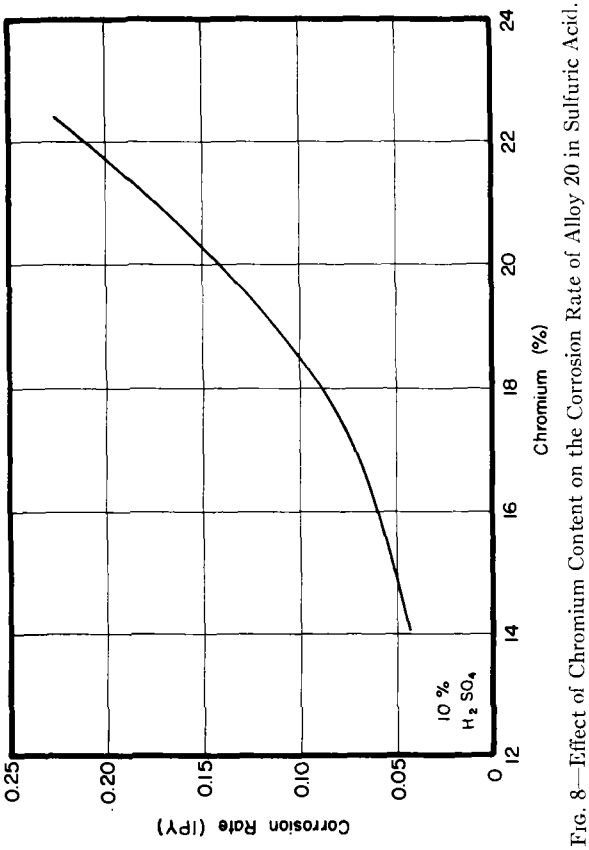


FIG. 8—Effect of Chromium Content on the Corrosion Rate of Alloy 20 in Sulfuric Acid.



FIG. 9—Electron Micrograph of Grain Boundary Structure in Alloy 20 with No Titanium (×40,000). Reduced one third for reproduction.

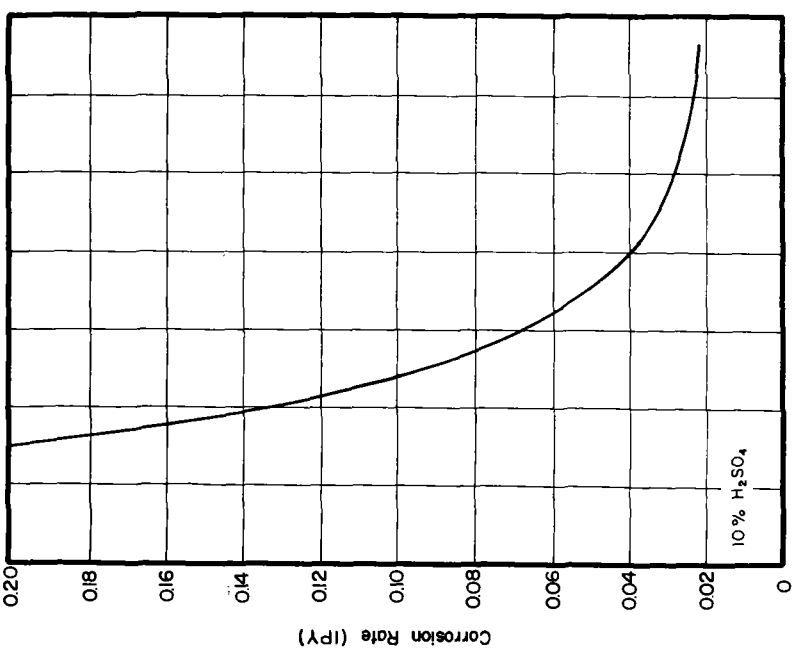


FIG. 6—Effect of Nickel Content on the Corrosion Rate of Alloy 20 in Sulfuric Acid.

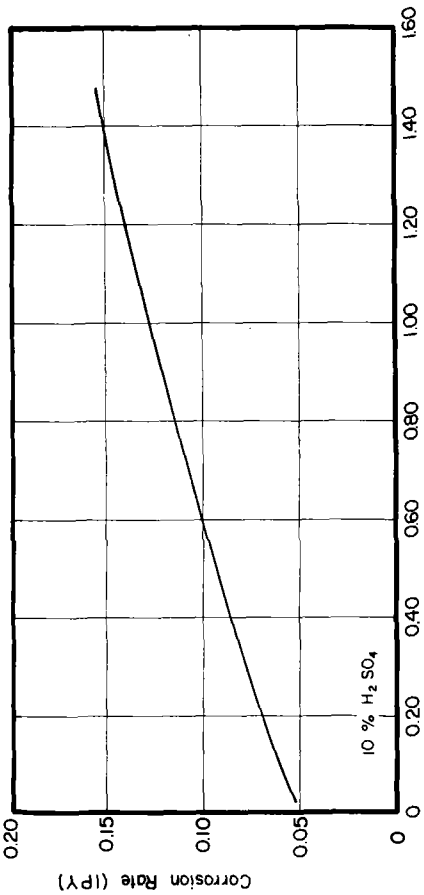


FIG. 7—Effect of Columbium Content on the Corrosion Rate of Alloy 20 in Sulfuric Acid.

and low chromium would be detrimental to the general corrosion resistance of a material in oxidizing solutions such as nitric acid. Consequently, the recommended modified composition of Alloy 20 for corrosive environments of all types would be the standard analysis with a titanium addition. For sulfuric acid environments only, the recommended composition would consist of the standard Alloy 20 analysis with low chromium and a titanium addition.

CONCLUSIONS

The experimental heats of Alloy 20 show the following effects of composition on hot workability:

1. A large increase in workability with increasing titanium content.
2. A substantial improvement in workability with increasing carbon content.
3. A variable effect because of nickel with maximum hot workability at 30 per cent.
4. Slight increase in workability with increasing amounts of columbium and boron.
5. Slight decrease in workability with increasing amounts of chromium and molybdenum.
6. No effect or copper or calcium.

The experimental heats of Alloy 20 show the following effects of composition on corrosion resistance in sulfuric acid:

1. A significant beneficial effect with increasing nickel content up to 30 to 35 per cent and a leveling off from there on.
2. A very slight detrimental effect with increasing columbium content.
3. A significant detrimental effect with increasing chromium content.
4. No effect of carbon, copper, molybdenum, titanium, boron, or calcium.

PRODUCTION EXPERIENCE

Confirmation of the beneficial effect of titanium on the hot workability of Alloy 20 has been obtained on large commercial heats. Titanium has been added to 13 ton electric arc furnace heats and has proved successful. The average product yield has increased significantly with an average titanium content of 0.60 per cent. Of particular significance is the fact that the titanium containing ingots were rolled satisfactorily to blooms without prior ingot conditioning and with no edge cracking. In addition, no detrimental effect, as illustrated in Fig. 11, is observed on the corrosion resistance of this material in sulfuric acid solutions ranging from 5 to 40 per cent. The production of heats with low chromium content and a titanium addition currently is being considered.



FIG. 10—Electron Micrograph of Grain Boundary Structure in Alloy 20 with Titanium (×40,000). Reduced one third for reproduction.

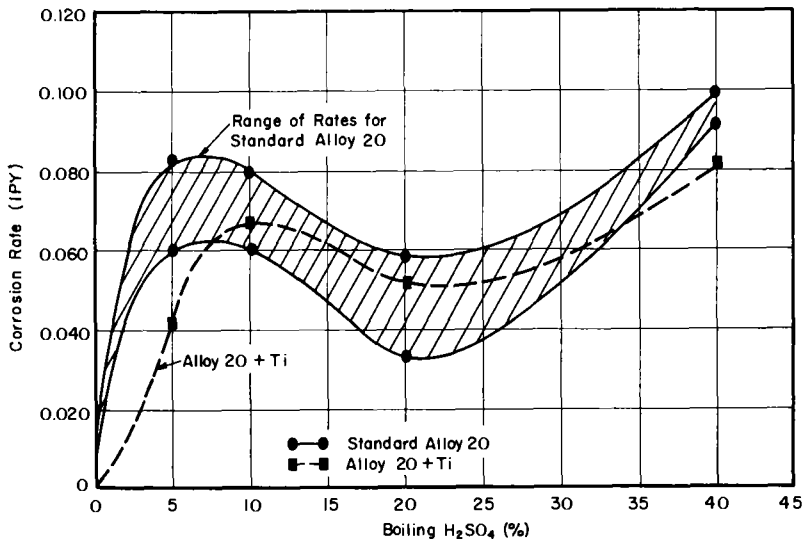


FIG. 11—Corrosion Rate of Commercial Size Heats of Alloy 20 in Various Concentrations of Sulfuric Acid.

REFERENCES

(1) M. G. Fontana, *Corrosion: A Compilation*, Hollenback Press, Columbus, Ohio, 1957.
(2) *Working Data—Stainless and Heat Resisting Steels*, Carpenter Steel Co., Reading, Pa., 1960.
(3) H. Freeman and T. N. Kelley, "Hot Working of Super Duty Alloys," *AIME Metallurgical Society Conference on Quality Requirements of Super Duty Steels*, Pittsburgh, Pa., May 5–6, 1958.
(4) R. J. France, *Experimental Forgeability Results on René 41*, Universal-Cyclops Steel Corp., Bridgeville, Pa., Jan. 21, 1958.
(5) *The Role of Molybdenum and Copper in Corrosion Resistant Steel and Alloys*, Climax Molybdenum Co., New York, N. Y., 1961.
(6) O. D. Sherby, "Limitations in Forming and Shaping," *ASM Metal Engineering Quarterly*, Am. Soc. Metals, May, 1962.

DISCUSSION

K. J. GODA[1]—In your earliest work, I recall you were using aluminum for improving the hot workability of Uniloy 20. How does this element fit in with the recent studies you have made on other elements?

H. L. BLACK AND L. W. LHERBIER (*authors*)—In the past, Universal-Cyclops carried out an extensive program on production heats to investigate the effect of aluminum and boron additions, deoxidation practice, and other methods believed to aid workability in an effort to improve the hot workability of Uniloy 20. A notable improvement in workability was attained by several changes in practice, but we felt that we had reached the optimum workability which could be achieved by these methods. The program which we have presented represents an attempt to further improve the workability of this difficult alloy by a major change in chemistry, while at the same time retaining, or improving, corrosion resistance.

[1] Carpenter Steel Co., Reading, Pa.

H. F. EBLING[2]—Is the type of attack from sulfuric acid general or intergranular?

MESSRS. BLACK AND LHERBIER—In all concentrations of boiling sulfuric acid used in our study, the corrosion attack was general. We saw no evidence of any intergranular attack.

MR. EBLING—Have you made corrosion tests in nitric acid?

MESSRS. BLACK AND LHERBIER—We conducted the standard 65 per cent boiling nitric acid test (Huey test—ASTM Specification A 434[3]) on all experimental compositions and on the titanium modified production size heats. The corrosion rate of titanium bearing Uniloy 20 was less than 0.006 IPY. We found no intergranular attack in any composition in the solution annealed condition (1950 F—water quench). Specimens in the "sensitized" condition did suffer intergranular corrosion if they did *not* contain columbium or titanium.

[2] A. O. Smith Corp., Milwaukee, Wis.

[3] Specification for Quenched and Tempered Alloy Steel Bars, Hot-Rolled or Cold-Finished (A 434), *1964 Book of ASTM Standards*, Part 3.

B. R. BANERJEE[4]—Have you attempted to identify the continuous and discontinuous grain-boundary phases?

MESSRS. BLACK AND LHERBIER—We are presently conducting an investigation to identify these grain boundary phases, but we have no results to report thus far.

[4] Crucible Steel Company of America, Central Research Laboratory, Pittsburgh, Pa.

RELATIONSHIP BETWEEN METALLURGICAL STRUCTURE AND PROPERTIES OF A PRECIPITATION HARDENING STAINLESS STEEL

By G. N. Aggen[1] and R. H. Kaltenhauser[2]

Synopsis

The mechanical properties and corrosion resistance of AM-355, a precipitation-hardening stainless steel, were found to be highly dependent upon carbide morphology. Corrosive attack in salt spray could always be associated with carbide precipitation at matrix discontinuities such as austenite or delta-ferrite grain boundaries. Continuous carbide precipitation at austenite grain boundaries was found to promote stress-corrosion failures in salt spray and to adversely affect certain mechanical properties such as ductility and impact strength.

Heat treatments, based upon the transformation characteristics of the alloy, were developed which produced uniform carbide dispersions. This structure resulted in significant improvements in mechanical properties and resistance to rusting, pitting, and stress corrosion in salt spray.

Carbide morphology was studied by light and electron microscopy as affected by: (1) heat treatment variables such as solutioning temperatures and times, cooling rates, and precipitation temperatures and times; (2) prior history of the alloy; and (3) transformation characteristics of the alloy.

Users of the alloy have accepted the new heat treatment that was developed. This has led to new applications for the alloy in relatively severe marine environments.

Since about 1950 several wrought precipitation-hardening stainless alloys were developed that have attained commercial importance. A review of the major developments in this field has been published by Lena (1).[3] He describes the heat treatments and properties of this class of commercial alloys and their metallurgical background.

Some of these alloys possess a dual structure, that is, they are austenitic in the annealed condition and martensitic in the hardened condition. The terms "controlled-transformation" and "semi-austenitic" have been used to describe them. The first term, which is more descriptive of their nature, will be used here when referring to them. These alloys are useful in applications that require the cold-forming characteristics of austenite for fabrication purposes and also require high strengths, achievable only by a martensitic structure, after heat treatment. The good forming characteristic of austenite is also highly desirable in the manufacture of sheet and strip products from these alloys. Many applications, such as structural components of aircraft, require sheet and strip produced to gage and flatness tolerances that can be achieved only by cold rolling of continuous coils or strands.

The controlled-transformation stainless alloys require very close control of chemical composition in order to produce the desired characteristics in both the annealed and hardened conditions. The effects of two metallurgical phenomena must be controlled or balanced to achieve the desired results. These are:

1. The dependence upon chemical composition of the austenite stability as measured by the martensite transformation (Ms) temperature.

2. The precipitation of carbides and its effects upon changing the chemical composition of austenite and, thereby, its Ms temperature.

Austenite stability, as used here, is the stability of austenite against transformation to martensite. This may be measured by the Ms temperature of the austenite or by its Md temperature, that is, the maximum temperature at which a given amount of cold reduction will produce a measurable amount of martensite. All of the alloying elements commonly found in stainless steels increase the stability of the austenite, that is, decrease its Ms temperature. This is true whether they are ferrite formers or austenite formers. Equations relating austenite stability to composition have been developed for alloys close to stainless steels in composition by Post and Eberly (2), Eichelman and Hull (3), Monkman et al (4), and Irvine et al (5).

Among the alloying elements that have been studied, carbon and nitrogen have by far the most potent effects in depressing the Ms temperature. A 0.1 per cent increase in either alloying element depresses the Ms temperature by 260 to 300 F. Other alloying elements, with the exception of cobalt which is relatively neutral, depress the Ms about 50 to 110 F per cent addition. For equal weight per cent additions carbon and nitrogen are 25 to 60 times as effective in depressing Ms temperatures.

The solubility of carbon in stainless steels has been determined by Rosenberg and Irish (6), Krivobok and Grossman (7), Aborn and Bain (8), and Greene (9). Agreement between various investigators on the 18 per cent chromium, 8 per cent nickel composition is fairly good and appears to be in good accord with metallographic observations made on AM-355, the controlled-transformation steel examined in this investigation.

Assuming an initial carbon content of about 0.12 per cent and using the carbon-solubility data of Krivobok and Grossman (7) for 18 per cent chromium and 8 per cent nickel alloys, all carbides will be in solution at 1900 F and above. This corresponds to the high-temperature annealing treatment for controlled-transformation stainless steels, in which condition they are essentially austenitic. If equilibrium is attained during a reannealing treatment at about 1700 F, all but about 0.05 per cent carbon is rejected from solid solution as $M_{23}C_6$. This corresponds to the "low-temperature" or "trigger-annealing" or "conditioning" treatment applied to controlled-transformation steels. The rejection of 0.07 per cent carbon as $Cr_{23}C_6$ from AM-355, which nominally contains about 0.12 per cent carbon, will deplete the matrix of about 1.2 per cent chromium in addition to the

[1] Research associate, Research Laboratory, Allegheny Ludlum Steel Corp., Brackenridge, Pa.

[2] Project supervisor, Research Laboratory, Allegheny Ludlum Steel Corp., Brackenridge, Pa.

[3] The boldface numbers in parentheses refer to the list of references appended to this paper.

Copyright© 1965 by ASTM International

carbon. Using the equations relating Ms temperature depression to chemical composition the rejection (3,4) of these elements from solution raises the Ms temperature of the remaining austenite by 280 to 300 F.

This precipitation of the $M_{23}C_6$ carbides is the reaction upon which the controlled-transformation stainless steels are based. The chemical compositions of the alloys are adjusted such that when all elements are in solution the Ms temperature is below room temperature. Upon trigger annealing or precipitation of carbides in the temperature range of 1400 to 1750 F, the Ms temperature is raised to above room temperature. Frequently a refrigeration heat treatment at −100 F is used to further abet the transformation to martensite.

In order for this precipitation mechanism to operate satisfactorily, two requirements must be met during the trigger-annealing treatment. These are as follows:

1. The precipitation of carbides must occur fairly rapidly so that trigger-annealing times may be reasonably short.

2. The precipitation of carbides must occur uniformly, or reasonably so, throughout the matrix.

Precipitation of carbides at the austenite grain boundaries alone does not meet these requirements. Such precipitation leads to the well known "sensitization" phenomenon (10–13) in stainless steels with the attendant impairment of corrosion resistance. Also, if a material is coarse grained, depletion of carbon and chromium is not uniform throughout the grain but is concentrated only at the grain boundaries after short precipitation times. This is associated with the slow diffusion rates at these temperatures of elements such as chromium and molybdenum to the grain boundaries where they combine with carbon as $M_{23}C_6$. As a result any transformation to martensite which occurs is confined only to the grain-boundary regions. The mechanical properties obtainable from such a structure are also unsatisfactory.

Bendure et al (14) studied the effects of cold work and delta ferrite on the kinetics of carbide precipitation in austenitic stainless steels and in two controlled-transformation stainless steels. They showed quantitatively that cold work tremendously accelerated carbide precipitation in Type 301 stainless steel. Data presented in this investigation indicate, however, that the acceleration of precipitation is at least partially caused by the formation of martensite produced during cold working. They also showed that delta ferrite similarly accelerated carbide precipitation in stainless steels.

Bendure et al (14) observed similar effects of finely dispersed delta ferrite on carbide precipitation in two commercial controlled-transformation stainless steels. They also observed additional rejection of carbides during aging of the controlled-transformation steels (after transformation to martensite) at 950 F, whereas no carbides were precipitated in the austenitic condition below 1150 F. This observation, incidentally, indicates the influence that prior transformation to martensite may have upon carbide precipitation as did their experiments on cold rolled Type 301 stainless steel.

Irvine et al (5) show a time-temperature-transformation (TTT) curve for carbide precipitation in a controlled-transformation steel containing no delta ferrite. The curve was obtained for the alloy during reheating, presumably after quenching to room temperature from about 1920 F. The carbide-precipitation curve was C-shaped showing a nose for beginning of precipitation at about 1475 F and 1.1 min. The authors evaluated both ferrite-free and ferrite-containing controlled-transformation steels and recognized the importance of ferrite in obtaining rapid carbide precipitation during trigger annealing. They also noted that carbide precipitation was accelerated in areas that were formerly martensitic at room temperature but did not utilize this mechanism in heat treatment.

Based partly upon the preceding discussions the main requirements for controlled-transformation stainless steels are seen to be as follows:

1. They must contain sufficient chromium content to provide adequate corrosion and oxidation resistance. A minimum of about 12 per cent chromium is obligatory and for most applications amounts of 15 per cent or more are highly desirable.

2. Their carbon content must be sufficient such that a substantial increase in Ms temperature can be obtained through precipitation of carbides. That is, when all the carbides are dissolved the alloy must have an Ms temperature below room temperature and when carbides are precipitated the Ms temperature must be above room temperature.

3. Some means of precipitating carbides effectively during the trigger-annealing treatment is required. Usually this is achieved by introducing 10 to 20 per cent delta ferrite in a well-dispersed form throughout the microstructure. The fine dispersion of ferrite required can only be achieved at present by substantial hot or cold reduction. Cold reduction is particularly effective in dispersing delta-ferrite particles. This generally limits the available product forms of these alloys to those having small section sizes such as sheet, strip, wire, and small-diameter bars.

4. The martensite formed after trigger annealing must generally be strengthened by a precipitation-hardening mechanism to obtain the desired high mechanical properties.

TABLE 1—CHEMICAL COMPOSITION OF AM-355 ALLOY.

Alloy	C	Mn	Si	Cr	Ni	Mo	N	Fe
AM-355	0.13	0.75	0.50[a]	15.5	4.3	2.8	0.10	balance

[a] Maximum.

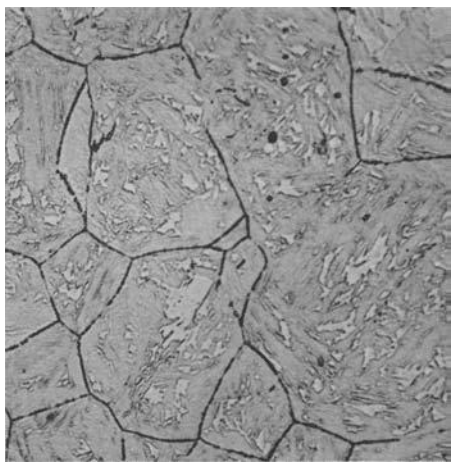


FIG. 1—AM-355 Sheet, 1950 F, Air Cooled Plus 1710 F, Air Cooled Plus Sub-Zero Cooled and Tempered (×500).

AM-355 ALLOY

AM-355 is a slight modification of AM-350, a controlled-transformation stainless steel containing about 10 per cent delta ferrite. AM-355 was designed specifically to produce improved properties in large-section products such as plate, billets, and large forgings. To accomplish this, the composition was

adjusted to reduce or eliminate delta ferrite, a constituent shown to affect deleteriously transverse mechanical properties (15), and to reduce the austenite stability. The resulting nominal composition is shown in Table 1. Amounts of delta ferrite up to about five per cent are often observed, but generally zero to trace amounts are present.

Early in the development of AM-355 two problems were noted. In large-section products, such as billets, center segregation was observed. The condition was readily apparent since it was typified by longitudinal bands of retained austenite that could not be readily removed by homogenizing heat treatments. This condition was corrected by remelting the alloy by the consumable-electrode process. The second problem concerned the difficulty in obtaining satisfactory mechanical properties using the heat treatments recommended for the AM-350 alloy, that is, high-temperature annealing at 1950 F followed by trigger annealing and tempering. This problem was traced to the nonuniform carbide precipitation that resulted from this series of heat treatments. During annealing at 1950 F a coarse-grained austenitic structure was obtained. Upon trigger annealing carbides precipitated only at the austenite grain boundaries. Upon subsequent cooling to room temperature (or −100 F) transformation occurred only in the depleted areas adjacent to the grain boundaries. An example of the microstructure obtained by these treatments is illustrated in Fig. 1. The light areas in the photomicrograph are retained austenite. The retained austenite comprises about 26 per cent of the matrix in this specimen as determined by X-ray measurements. Note that these areas are more highly concentrated at the centers of the austenite grains. This type of structure produced low proportional limits and yield strengths and, frequently, low-ductility values as well.

This problem was circumvented by eliminating the annealing operation at 1950 F altogether and prescribing a definite hot-working procedure, that is, finish hot working in the temperature range of 1700 to 1800 F with sizeable reductions in area. Since heavy-section products generally are machined instead of being formed, the austenite characteristic of the alloy (produced by annealing at 1950 F) was seldom required. By hot finishing in the temperature range of 1700 to 1800 F, a fine grain size is achieved and carbides are precipitated fairly uniformly during hot working.

AM-355 alloy was used successfully in several commercial applications, primarily as bars and forgings for jet-turbine and airframe components. Problems were occasionally encountered which, in most cases, could be related to improper hot-working or heat-treating practices.

Examples of such problems follow:

1. Low transverse ductility of bars. This problem was particularly prevalent in the short-transverse direction of large bars where the width to thickness ratio exceeded about two to one. The recommended hot-working practices could not be followed in producing these bars on mill equipment because of their size and shape. Low tensile-ductility values could often be attributed to delta-ferrite particles present as plates parallel to the fracture surface. In other cases, however, the bars contained no delta ferrite and low ductility values were caused by intergranular fractures at room temperature associated with heavy intergranular carbide precipitation.

2. Low tensile ductility and impact strength of small bars in the longitudinal direction. This was observed in only one instance. It was apparent from the microstructures, that is, coarse grain size with intergranular carbides, that the bars were finish rolled from a high temperature. Both the tensile and impact fractures at room temperature were wholly intergranular.

3. Inadequate corrosion and stress-corrosion resistance in salt water and salt spray. This behavior was frequently observed in sheet products, in bar products that had been joined by high-temperature brazing operations and in roll-formed compressor blades that were annealed at 1950 to 2000 F during fabrication. Poor corrosion resistance

TABLE 2—EFFECT OF PRELIMINARY HEAT TREATMENTS ON THE MECHANICAL PROPERTIES OF AM-355 SHEET.

Number	Preliminary Heat Treatment	0.2% Yield Strength, psi	Ultimate Tensile Strength, psi	Elongation in 2 in., %
1.....	none	156 800	204 600	17.5
2.....	1375 F, 3 hr	167 300	217 800	15.0
3.....	1710 F and sub-zero cool	183 300	222 200	13.5
4.....	sub-zero cool	184 200	222 900	13.5

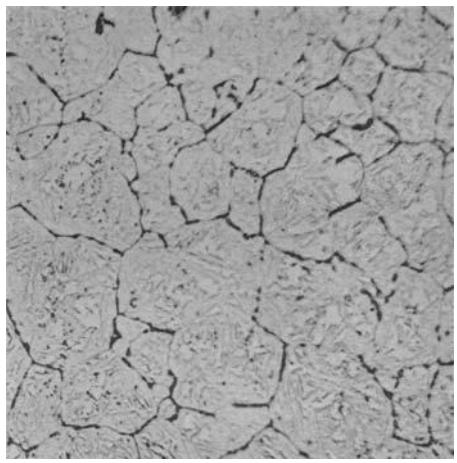


FIG. 2—AM-355 Sheet, 1950 F, Air Cooled Plus 1710 F, Air Cooled Plus Sub-Zero Cooled and Tempered (×500).

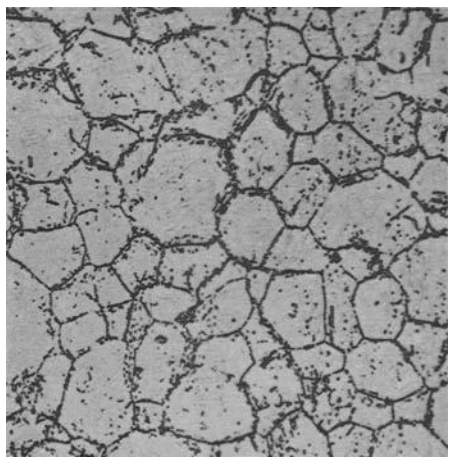


FIG. 3—AM-355 Sheet, 1950 F, Air Cooled Plus 1375 F, Air Cooled Plus 1710 F. Air Cooled Plus Sub-Zero Cooled and Tempered (×500).

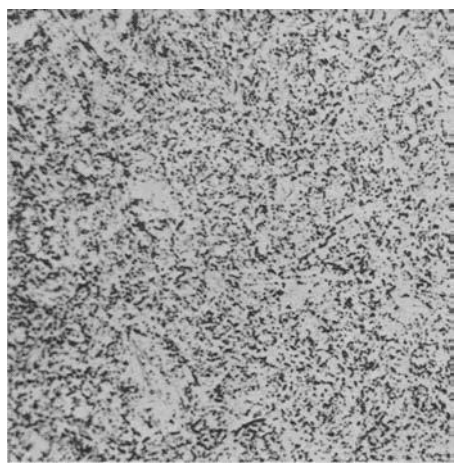


FIG. 4—AM-355 Sheet, 1950 F, Air Cooled Plus 1710 F, Air Cooled Plus Sub-Zero Cooled Plus 1710 F, Air Cooled Plus Sub-Zero Cooled and Tempered (×500).

could always be related to intergranular carbides (16).

In an effort to improve sheet, a product that required a preliminary high-temperature annealing treatment for fabrication, various preliminary heat treatments were applied to sheet that had been annealed at 1950 F (17). These included a preliminary heat treatment at 1375 to 1475 F developed for bar products, double heat treatments and a sub-zero cool at −100 F. The subsequent hardening heat treatments, in all cases, comprised trigger annealing or conditioning at 1710 F followed by cooling to −100 F, holding for 3 hr and aging 3 hr at 850 F. The mechanical properties obtained by use of the various preliminary treatments are shown in Table 2.

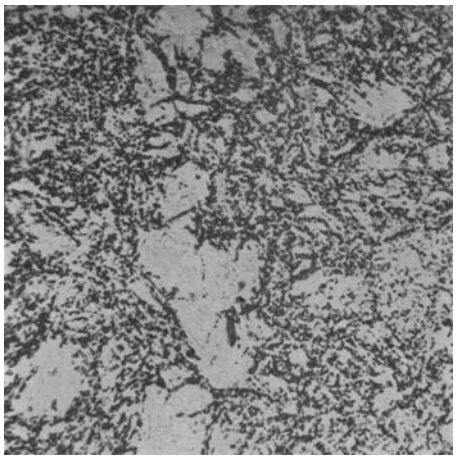


FIG. 5—AM-355 Sheet, 1950 F, Air Cooled Plus Sub-Zero Cooled Plus 1710 F, Air Cooled Plus Sub-Zero Cooled and Tempered (×500).

Both the double heat treatment (No. 3 in Table 2) and the preliminary refrigeration (No. 4 in Table 2) were found to be effective in producing satisfactory mechanical properties. These effects were reproduced in three heats selected to exhibit a wide range of Ms temperatures. The resulting microstructures from one heat are illustrated in Figs. 2–5. Upon cooling from 1950 F this heat had a completely austenitic structure at room temperature. If no preliminary heat treatment was used, reheating to 1710 F produced carbide precipitation solely at the austenite grain boundaries (Fig. 2). The smooth light areas are retained austenite which persisted throughout the subsequent sub-zero cooling and tempering operations.

A preliminary heat treatment at 1375 F (Fig. 3) precipitated sufficient carbides at the austenite grain boundaries to produce some martensite upon cooling to room temperature. The areas that transformed to martensite exhibited carbide precipitation upon reheating to 1710 F. These areas are shown in Fig. 3 as dark regions generally concentrated near the austenite grain boundaries. The treatment at 1375 F, however, was not particularly effective in reducing the severity or continuity of the grain-boundary precipitation. Areas of retained austenite are observed again within the grains, but these are much smaller than those observed in Fig. 2.

A preliminary treatment at 1710 F followed by sub-zero cooling was very effective in redistributing carbides (Fig. 4). In essence this structure is obtained by repeating the hardening heat treatment that produced the structure shown in Fig. 2. Wherever martensite was present after the first heat treatment (see Fig. 2), carbides are precipitated after the second heat treatment (see Fig. 4). Retained austenite, though present, is not readily observed in the microstructure.

A preliminary treatment, comprising only a sub-zero cool at −100 F, produces the structure shown in Fig. 5. The large areas free of carbides did not transform to martensite during the first sub-zero cool while the remaining areas did. Though the microstructure is not as uniform as that produced by the double treatment (Fig. 4), the mechanical properties at room temperature are equivalent (Table 2). Retained austenite, which persists during the remainder of the heat treatment, is observed in the large carbide-free areas. These preliminary heat treatments, though interesting, were not pursued further at the time because they seemed rather complicated for commercial adaptation.

Roll-formed compressor blades of AM-355, when used in a newly developed engine application involving exposures to marine atmospheres, were found to have inadequate corrosion resistance. An intensive heat-treatment program was initiated by the manufacturer of the engine in order to improve the corrosion resistance of the roll-formed blades. Bergman and Palty (16) were able to establish a definite relationship in the alloy between the presence of intergranular carbides and corrosive attack in salt environments. They developed a heat treatment involving a high-temperature anneal and refrigeration, which resulted in acceptable mechanical properties and corrosion resistance.

The success of the heat treatment depended upon several metallurgical characteristics of the alloy. First, the initial annealing temperature and time had to be adequate to dissolve the grain-boundary carbides. Second, the cooling rate from the annealing temperature needed to be sufficiently high to avoid intergranular carbide precipitation during cooling. Third, the refrigerating operation had to produce sufficient transformation to martensite such that subsequent conditioning treatments did not result in carbide precipitation at austenite grain boundaries. Since the Ms temperature also had to be fairly low to allow roll forming of the blades, a close control of Ms temperature was required. These and other metallurgical characteristics of the alloy, which were needed to specify heat treatments exactly, were not known.

SCOPE

Bergman and Palty (16) showed that corrosive attack of AM-355 in salt environments was highly dependent upon the carbide morphology. McCunn and Murray (17) first explored heat treatments which appeared capable of producing uniform carbide dispersions and excellent mechanical properties in the alloy. These were illustrated in Table 2 and Figs. 2–5. Bergman and Palty also developed a specific heat treatment which appeared to produce the best combination of strength and corrosion resistance for their application.

Based upon these investigations the following sequence of heat treatments appeared capable of improving the corrosion resistance and mechanical properties of AM-355:

1. Anneal at a temperature and time adequate to dissolve all carbides.
2. Cool at a rate sufficiently high to avoid precipitation of carbides at austenite grain boundaries.
3. Sub-zero cool at a temperature and time adequate to produce substantial transformation to martensite such that uniform carbide dispersions are achieved during following heat-treating operations.
4. Reheat to a conditioning temperature and time which will produce a uniform carbide dispersion. Enough carbides must be precipitated such that the Ms temperature is raised to values adequate to produce a nearly completely martensitic structure upon subsequent sub-zero cooling. Preferably, carbide precipitation at the former austenite

grain boundaries should be completely avoided.

5. Sub-zero cool.

6. Temper to the desired hardness or strength level.

Determination of the conditions of heat treatment which meet these various requirements constitute a major portion of this investigation.

The success of this heat-treatment sequence in producing satisfactory properties in AM-355 is highly dependent upon the amount of transformation to martensite produced during the first sub-zero cool (third step in the above sequence). In general, it is desirable to have an Ms temperature below room temperature upon quenching from high temperatures. The excellent forming characteristics of austenite can then be used to advantage, particularly in sheet and plate products. Upon sub-zero cooling enough transformation to martensite must occur and must be sufficiently uniform, such that uniform carbide dispersions are obtained upon reheating. If large areas of retained austenite are present (see Fig. 5) and encompass grain boundaries, subsequent precipitation treatments could produce heavy intergranular carbide networks in these regions. Under these conditions the heat treatment could result in more harm than benefit to the properties of the alloy.

Once a satisfactory heat treatment was devised, the effects of this heat treatment upon the corrosion and mechanical properties of AM-355 were evaluated. Parallel specimens, treated according to presently specified heat treatments for the alloy, were also evaluated for comparative purposes. This was believed necessary before revised heat treatments could be confidently recommended to users of the alloy.

RESULTS AND DISCUSSIONS

Solutioning of Grain-Boundary Carbides:

Solutioning of grain-boundary carbides was examined in twelve commercial heats of bar stock. Temperatures of 1825 to 1950 F and times up to 4 hr were investigated. Bars were generally examined in the as-rolled condition. Bars from two heats, however, were also furnace cooled at 100 F/hr from 1950 F in order to produce massive grain-boundary carbides prior to resolutioning treatments.

As-received bars were generally fine-grained and contained both intergranular and random carbides. In this initial condition 1 hr at 1875 F or 30 min at 1900 F completely dissolved all intergranular carbides. In a few heats some random carbides persisted even after holding for 2 hr at 1900 F. If massive intergranular carbides were present, by prior furnace cooling from 1950 F, 4 hr at 1875 or 1900 F were required to completely dissolve them. The heats examined differed noticeably in the rates or temperatures at which grain-boundary carbides were dissolved. The differences were not obviously related to the differences in reported chemical compositions.

In view of these data 1 to 3 hr at 1900 ± 25 F was believed adequate and has been specified for commercial use.

Isothermal Carbide Precipitation:

Bars from seven commercial heats were selected to determine the beginning of carbide precipitation, upon cooling from the solution temperature, as functions of time and precipitation temperature.

The major portion of the work was conducted on one heat after solution annealing at 1950 F for 30 min. This solution treatment is adequate to dissolve all carbides in AM-355. Bars from this heat were cut into approximately ½-in.-thick disks, solution annealed in salt baths and transferred as rapidly as possible into nearby salt baths at temperatures within the carbide-precipitation range. The disks were water quenched immediately upon removal from the second salt bath. The disks were sectioned longitudinally and examined metallographically at ×500 to ×2000 magnifications. Many of the specimens were later removed from the metallographic mounts and re-examined utilizing electron microscopy.

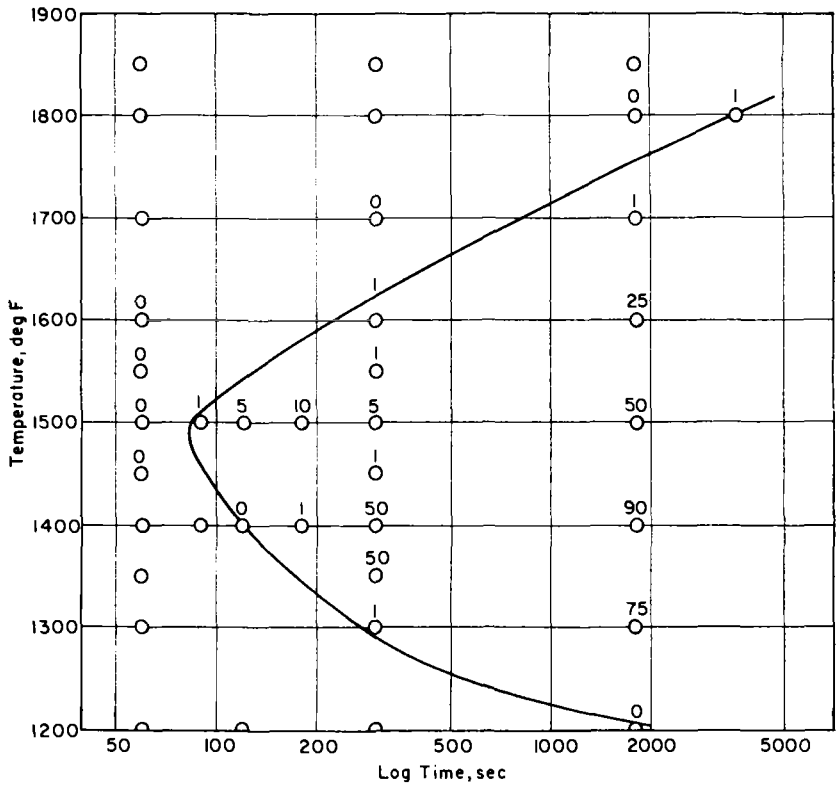


FIG. 6—Time-Temperature-Transformation (TTT) Curve for Carbide Precipitation in AM-355 Upon Cooling from 1950 F.

The results obtained upon cooling from 1950 F are shown in Fig. 6. The C-curve of Fig. 6 is based upon etching attack at the austenite to austenite (γ-γ) grain boundaries, presumably as a result of carbide precipitation. The numbers on Fig. 6 are estimates of the percentages of grain-boundary areas exhibiting attack. Where etching attack was not pronounced, it was generally present near delta-ferrite stringers or at junctions of three austenite grain boundaries.

The C-curve is typical of a reaction involving nucleation and growth of a new phase. The position of the curve agrees well in the 1400 to 1750 F range with the results reported by Irvine et al (5) on a 17 per cent chromium, 4 per cent nickel and 3 per cent manganese steel.

Both Irvine et al's and the present work resulted in C-curves which differ substantially from those reported for austenitic stainless steels. Stickler and Vinckier (13), as an example, obtained a nose at about 1650 F and 40 sec for carbide precipitation at austenite grain boundaries in Type 304 stainless steel.

Rather limited continuous-cooling tests were used to relate carbide precipitation during cooling to that obtained isothermally. A specimen from the same heat exhibited traces of intergranular carbide precipitation when cooled at about 300 F/min from 1950 to 1650 F and 100 F/min to 950 F. The method used to relate the two conditions was taken from a paper by Manning and Lorig (18). They proposed a method to relate continuous-cooling to isothermal treatments on the formation of pearlite and proeutectoid constituents in low-alloy steels. The method should apply equally well to carbide precipitation in stainless steels. Manning and Lorig's method predicted that the given cooling rate of about 145 F/min should produce small amounts of carbides while a cooling rate of 175 F/min was adequate to suppress precipitation. The agreement between calculations and observations appeared sufficiently good to assume that Manning and Lorig's method was valid for this purpose. Lowering the carbide-solution temperature from 1950 to 1900 F or below moved the nose of the curve to longer times, that is, from about 80 sec to 2 min or longer at 1500 F. The grain size, of course, also decreased with decreasing annealing temperature.

TABLE 3—Ms TEMPERATURES VERSUS ANNEALING TEMPERATURES.
Solutioning Time: 15 min at temperature.

Solution Temperature, deg F	Ms Temperature, deg F
1825	131
1850	97
1900	72

The results on six additional heats agreed reasonably well with those of the first heat at equivalent solution temperatures and again showed increasing precipitation rates with increasing solution temperatures.

Specimens held 5 or 30 min at temperatures of 1300, 1400, and 1500 F were also examined by electron microscopy at ×7500 magnification. Fewer grain-boundary carbides were observed in the replicas than would have been expected from the metallographic examinations. This indicates that etching attack is occurring prior to the precipitation of microscopically visible carbide particles.

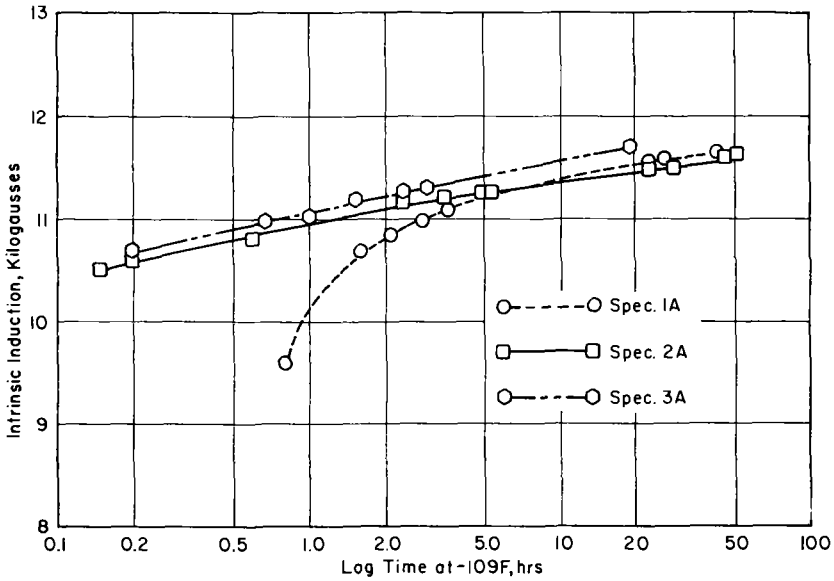
On the basis of these results a minimum cooling rate of 150 F/min from the solutioning temperature (1900 F) to 1200 F has been specified for commercial use. The C-curve of Fig. 6, since it involves a solution temperature of 1950 F, is expected to be representative of about the worst conditions encountered in practice.

Isothermal Transformation to Martensite:

Bar stock was selected from a heat for which Ms temperatures had been previously measured as a function of solutioning-annealing temperature. The Ms temperatures are given in Table 3. These had been determined dilatometrically after solution annealing 15 min, air cooling to room temperature, and quenching into liquid nitrogen.

The sub-zero cooling operation was evaluated only at a transformation temperature of about −110 F. Though this temperature might not produce maximum transformation to martensite, if an isothermal component was found, it is easily achieved by the use of solid carbon dioxide which sublimes at −109 F. This temperature is also used commercially in heat treating AM-355 and other controlled-transformation stainless steels. Sub-zero cooling, following the carbide-solution treatment, was studied as a function of holding time at −110 F. Transformation to martensite was followed by measuring the magnetic intrinsic induction of AM-355 at 1060 oersteds. Thermal-stabilization effects were explored by comparing annealed specimens that were cooled immediately to −110 F versus others that were held 7 to 27 days at temperatures above and below the Ms temperature before cooling to −110 F. Carbide-solution temperatures of 1850, 1875, and 1900 F were examined.

Upon completion of the heat treatments, the specimens were tempered 3 hr at 925 ± 10 F in an argon-atmosphere tube furnace. This was done to darken the martensite, by a tempering action, for subsequent metallographic examination. Longitudinal and transverse sections were cut from each bar and mounted for metallographic examination and retained-austenite measurements by X-rays. The retained-austenite measurements by X-ray were the same on both longitudinal and transverse sections, indicating the absence of preferred orientation in the specimens.



NOTE—Spec. 1A: held 27.2 days at 32 F.
Spec. 2A: directly cooled to −109 F.
Spec. 3A: held 21.1 days at 140 F.

FIG. 7—Isothermal Transformation of AM-355 at −109 F, 1850 F Anneal.

The martensite-transformation behavior of AM-355 at about −100 F is illustrated in Fig. 7. The curves, upon quenching from all three temperatures, show a continuous increase in intrinsic induction with holding time at temperature, caused by isothermal transformation to martensite. If the initial portions of the curve are ignored, the transformation reaction proceeds very nearly linearly on a semilogarithmic scale.

This is in agreement with a reaction-

path concept offered by Machlin and Cohen (19) to reconcile the athermal and isothermal modes of transformation. According to their theory, strain embryos activated during cooling lead to the conventional athermal transformation, and strain embryos activated by thermal fluctuations lead to isothermal transformation. With certain assumptions they derived an expression predicting that the percentage of isothermal transformation should increase linearly with the logarithm of time. The expression, however, applied only after a time interval required to activate one half of the embryos.

TABLE 4 — INTRINSIC - INDUCTION MEASUREMENTS VERSUS RETAINED-AUSTENITE MEASUREMENTS BY X-RAYS.

Specimen	Intrinsic Induction in Gausses		Retained Austenite by X-rays, %
	1060 Oersteds	4000 Oersteds	
1C.....	12 050	13 000	8.2
2C.....	12 050	13 000	12.0
3C.....	11 900	12 900	15.2

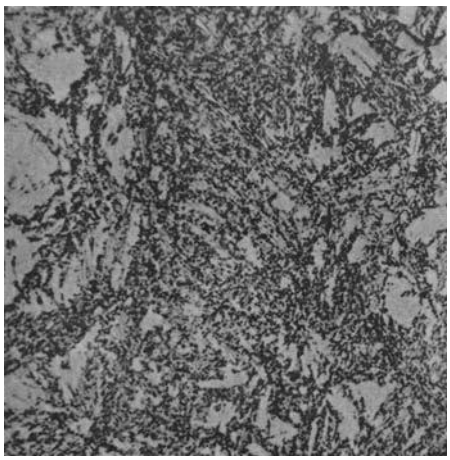


FIG. 8—Microstructure of AM-355, 1950 F Anneal, Water Quenched Plus Sub-Zero Cooled Plus 1425 F, 16 hr (×500).

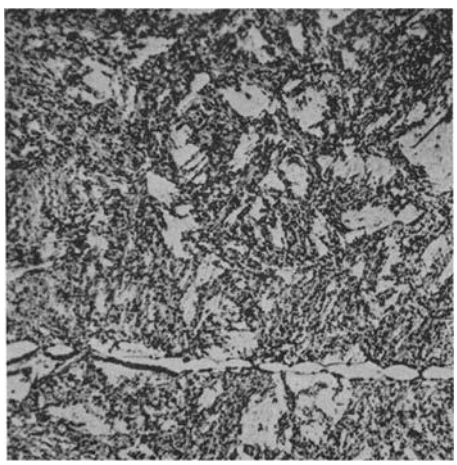


FIG. 9—Microstructure of AM-355, 1950 F Anneal, Water Quenched Plus Sub-Zero Cooled Plus 1750 F, 1 min (×500).

Figure 7, representing specimens quenched from 1850 F, shows that pronounced stabilization has resulted from holding a specimen at 32 F, a temperature below the Ms, prior to cooling to −110 F. No stabilization effects are observed upon holding a specimen above the Ms temperature. Similar stabilization effects, though less pronounced, are observed upon annealing from 1875 and 1900 F also. The stabilization, in all cases, disappeared after holding 3 to 5 hr at −110 F.

Assuming that the effects of alloying additions are additive and that a homogeneous solid solution is attained when annealing the alloy, calculations indicate that AM-355 should have a maximum intrinsic induction at saturation of about 15,300 gausses. The effects of individual alloying elements used in the calculations were obtained from Hoselitz (20). On this basis an intrinsic induction of 11,000 gausses is equivalent to 65 to 70 per cent martensite. The actual amount of martensite should be somewhat higher since 1060 oersteds is not sufficient to produce saturation in the alloy. Between about 3 and 50 hr at −110 F the intrinsic induction increases by about 500 gausses which is equivalent to about 5 per cent transformation. Since transformation to martensite at this stage of the heat treatment is important only in assuring a uniform carbide distribution upon reheating, 3 hr at −100 F appears adequate. If more pronounced stabilization effects are observed, either from a thermal origin or from strains produced by quenching, longer holding times at −100 F may be advisable.

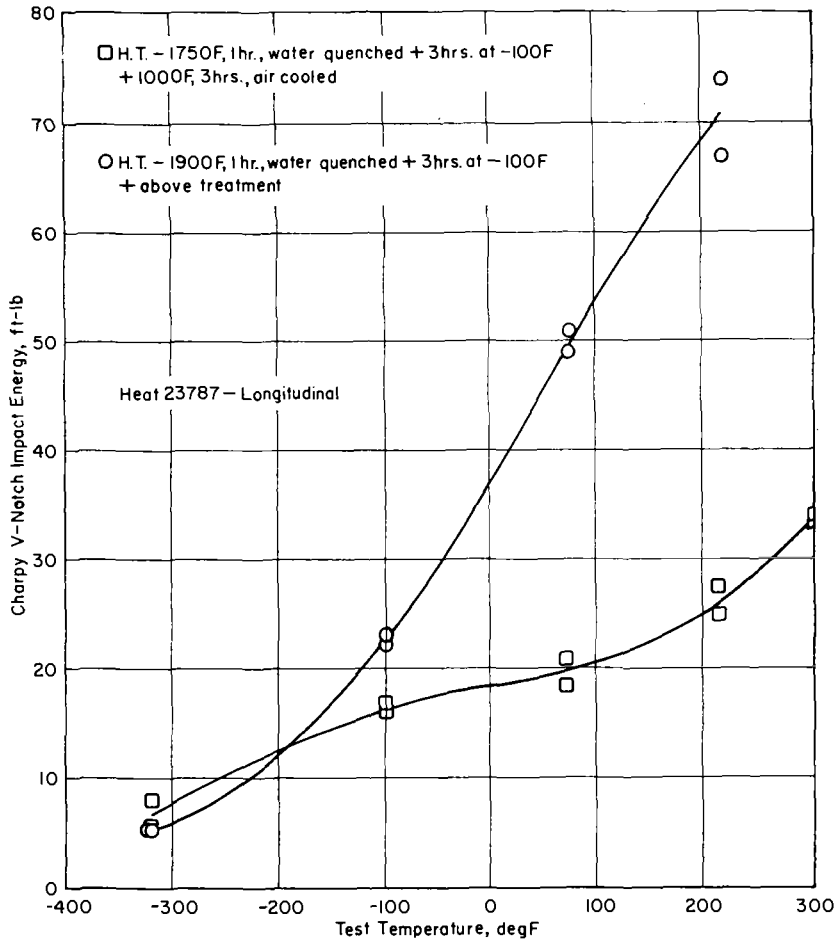


FIG. 10—Comparative Impact Energy Curves for Heat 23787, Longitudinal Direction.

The relationship between intrinsic-induction values and retained austenite, measured by X-rays, is shown in Table 4.

The retained-austenite values were obtained on specimens cut from the ends of the induction specimens using an X-ray method reported by Ogilvie (21). Retained austenite could also be observed metallographically at ×2000 magnification using a sodium-hydroxide etchant. Qualitatively, the amounts observed

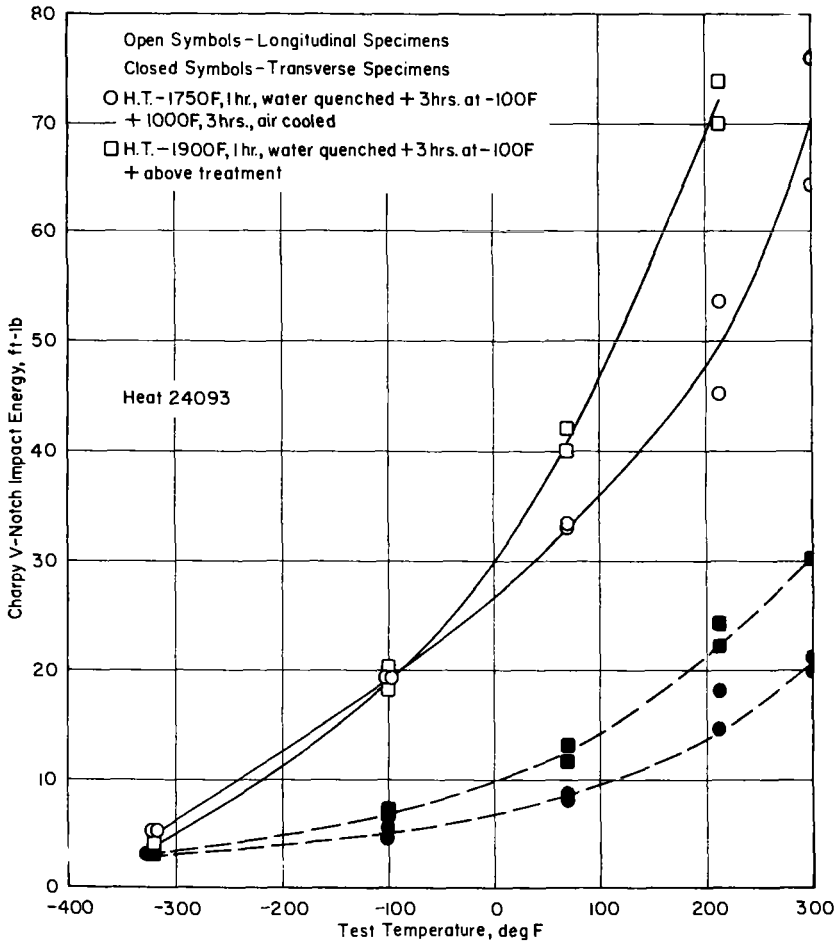


FIG. 11—Comparative Impact Energy Curves for Heat 24093.

TABLE 5—COMPARATIVE ROOM-TEMPERATURE TENSILE PROPERTIES OF AM-355.

Heat Treatments: A—1750 F, 1 hr, water quenched + 3 hr at −100 F + 1000 F, 3 hr, air cooled.
B—1900 F, 1 hr, water quenched + 3 hr at −100 F + above heat Treatment A.
C—Same as A except tempered 3 hr at 850 F instead of 1000 F.
D—Same as B except tempered 3 hr at 850 F instead of 1000 F.

Heat Number	Product	Test Direction[a]	Heat Treatment	0.02% Yield Strength, psi	0.2% Yield Strength, psi	Ultimate Tensile Strength, psi	Elongation in 4d, %	Reduction of Area, %
22191.....	4¼ in. square	L	A	149 400	163 600	172 100	16.0	56.4
		T	A	138 600	156 000	169 000	18.5	42.0
		L	B	149 200	167 200	176 400	17.5	62.4
		T	B	142 100	161 300	174 800	20.0	49.1
22310.....	5 in. dia	L	A	140 800	163 600	172 300	18.0	58.6
		T	A	144 000	160 900	171 700	13.0	37.7
		L	B	145 500	163 900	175 000	17.5	60.2
		T	B	144 000	163 200	173 300	13.5	39.1
23452.....	1⅛ in. dia	L	A	147 300	176 000	188 200	20.0	58.0
		L	B	158 300	176 400	190 400	20.0	61.0
23787.....	1¼ in. dia	L	A	152 800	177 500	192 600	19.5	54.8
		L	B	146 000	174 900	191 600	20.0	62.4
		L	C	128 800	181 000	220 200	15.0	52.0
		L	D	129 700	182 000	222 600	16.0	55.4
24093.....	2¼ in. dia	L	A	159 400	177 100	186 400	19.5	59.3
		L	B	154 400	175 500	186 500	19.5	63.1

[a] L = longitudinal; T = transverse.

metallographically agreed with the X-ray values. Upon photographing, however, the retained austenite was not sufficiently well defined for quantitative measurements. The correlation between induction values and retained austenite does not appear particularly good. The induction values, however, represent averages over a fairly large specimen, while the X-ray measurements and metallographic observations were confined to a much smaller portion of the specimen.

In view of these data 3-hr refrigeration at −100 F has been adopted for commercial use.

Effect of Conditioning Temperature on Microstructure:

Bars from two heats were solution annealed 1 hr at 1950 F and water quenched. The bars, while slightly, warm, were transferred to a refrigerator, held 16 to 20 hr at −100 F and air warmed to room temperature.

The refrigerated bars from both heats were cut into wafers and reheated in an argon-flushed tube furnace. Times from 1 min to 16 hr and temperatures of 1100 to 1800 F were investigated. The wafers were air cooled after heat treatment.

Metallographic specimens were prepared from longitudinal sections of each wafer and examined at ×500 to ×2000 magnifications. After metallographic examination and photography several specimens were selected and re-examined using electron microscopy. These included specimens condition heat treated various times at 1425, 1600, and 1750 F.

Figures 8 and 9 illustrate the structures observed when partial transformation to martensite preceded the conditioning treatments. In the temperature range of 1100 to 1600 F carbides are precipitated only in former martensitic areas or at delta-ferrite boundaries (Fig. 9). After 10 min at 1750 F minute traces of carbides appear to be present at the austenite grain boundaries. The effect becomes more apparent at longer times and at higher temperatures. At times of 10 min and longer at 1425 F the former retained austenite areas exhibit increasing amounts of martensite upon cooling to room temperature. One minute is adequate at 1600 F and higher to produce equivalent effects.

Discrete carbide particles were observed metallographically within 30 min at 1100 F and 1 min at 1250 F showing that the kinetics of carbide precipitation in former martensitic areas are greatly accelerated in comparison to that occurring at austenite grain boundaries (Fig. 6). Surface replicas examined at ×7500 magnification showed that the matrix carbides were remarkably uniform in size after conditioning at temperatures between 1425 to 1750 F. Some growth with time was observed at any one temperature, but the apparent equilibrium size at various

emperatures remained about the same about 0.1 to 0.3 μ).

Partial transformation of the alloy to martensite produced two pronounced changes in carbide precipitation. One effect was to accelerate the rate of carbide precipitation. This can be attributed to several factors. The martensite in this alloy forms as oriented laths in the parent austenite and does not completely revert to austenite until held for about 16 hr at 1750 F. The martensite, by forming noncoherent boundaries within the austenite, provides many more sites for carbide nucleation than does the parent austenite grain. These boundaries should also serve as good diffusion paths for molybdenum and chromium, since grain-boundary diffusion coefficients are generally much higher than bulk coefficients. Also, the diffusion coefficients of molybdenum (22) and carbon (23), and probably of chromium, are higher in ferrite than in austenite. Both effects should aid the growth of carbide particles since diffusion of molybdenum and chromium appears to control the rate of growth.

The other pronounced effect of partially transforming the structure to martensite is to improve the uniformity of carbide precipitation. The improved uniformity is operative over a very wide range of temperature and time combinations. The distribution is far more uniform than that achieved by fairly severe cold working of a stable austenitic stainless steel.

In view of these data, a conditioning treatment of 10 min to 1 hr at 1750 F has been adopted for commercial use. Traces of intergranular carbides were observed metallographically with this treatment, but data presented in the next section indicate that the amount present is not deleterious to mechanical properties or corrosion resistance except, perhaps, in severe environments. Lower temperature conditioning treatments may be used to suppress intergranular carbide precipitation completely but at some sacrifice to mechanical properties.

TABLE 6—COMPARATIVE ROOM-TEMPERATURE CHARPY V-NOTCH IMPACT PROPERTIES OF AM-355.

Heat Treatments: A—1750 F, 1 hr, water quenched + 3 hr at −100 F + 1000 F, 3 hr, air cooled
B—1900 F, 1 hr, water quenched + 3 hr at −100 F + above heat Treatment A
C—Same as A except tempered 3 hr at 850 F instead of 1000 F.
D—Same as B except tempered 3 hr at 850 F instead of 1000 F.

Heat Number	Product	Test Direction[a]	Heat Treatment	Charpy V-Notch Impact Energy, ft-lb
23452	1⅛ in. dia	L	A	23.0
		L	B	31.0
23607	1 in. dia	L	A	34.2
		L	B	41.5
23422	1 in. plate	T	A	15.2
		T	B	19.7
22191	4¼ in. square	T	A	5.0
		T	B	12.0
22310	5 in. dia	T	A	5.8
		T	B	7.8
23787	1¼ in. dia	L	A	19.8
		L	B	50.0
23787	1¼ in. dia	L	C	13.3
		L	D	17.8
24093	2¼ in. dia	L	A	33.3
		L	B	41.0
		T	A	8.3
		T	B	12.3

[a] L = longitudinal; T = transverse.

Evaluation of New Heat Treatments:

Concurrently with the metallographic work on the alloy, the mechanical properties of AM-355 were evaluated with the following heat treatment.

1900 to 2000 F, 1 to 3 hr, water quenched + 3 hr at −100 F + 1710 to 1750 F, 10 min to 1 hr, water quenched + 3 hr at −100 F + tempered 3 hr at 850 to 1000 F, air cooled.

The properties obtained with this heat treatment were compared with those obtained with the standard heat treatment previously specified for the wrought alloy. The only difference in the new heat treatment is the addition of the preliminary carbide-solution annealing treatment at 1900 to 2000 F and the sub-zero cool at −100 F to provide a more desirable carbide distribution. Heat treatments, where common to both conditions, were conducted on all specimens from a given heat in single furnace loads to eliminate temperature variations as a variable. In all cases, temperatures were controlled to within 10 F of those listed. Metallographic specimens from each lot were examined for comparison with the test results.

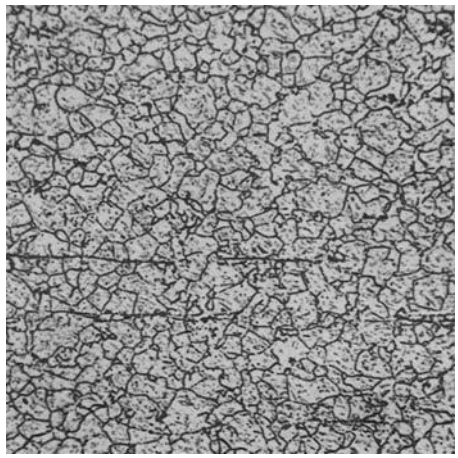


FIG. 12—Microstructure of Heat 23787, 1750 F, 1 hr, Water Quenched Plus Sub-Zero Cooled Plus 1000 F, 3 hr (×250).

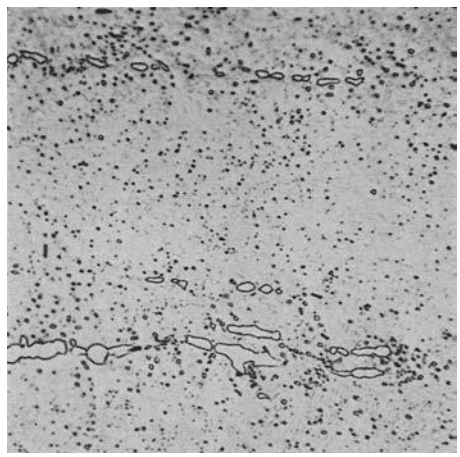


FIG. 13—Microstructure of Heat 23787, 1900 F, 1 hr, Water Quenched Plus Sub-Zero Cooled Plus 1750 F, 1 hr, Water Quenched Plus Sub-Zero Cooled Plus 1000 F, 3 hr (×250).

Comparative room-temperature tensile properties were obtained on specimens with both heat treatments. Both longitudinal and transverse specimens, where product sizes permitted, were evaluated. The listed values are generally average

results from duplicate specimens. Comparative Charpy V-notch impact properties were obtained from several heats at room temperature. Impact properties as a function of test temperature were obtained on two heats. The impact values were averages of two or three test results. Stress-rupture properties at 900 and 1000 F were obtained from the same two heats. Comparative room-temperature fatigue tests were obtained on one heat. These were conducted on R. R. Moore rotating-beam fatigue machines.

Stress-corrosion tests were conducted on many of the heats in longitudinal and transverse directions. Most of the tests were conducted in 5 per cent neutral salt fog, but a few earlier tests were made in a 20 per cent salt environment. The two concentrations are about equivalent in the severity of their effects. The specimens were machined to flats, generally about 0.050 in. thick by 0.5 in. wide, and stressed in bending as a two-point loaded beam. The desired stresses were obtained by applying SR-4 strain gages and loading the specimens to the equivalent strains. All specimens were finish machined after heat treatment by grinding. They were then passivated for 5 min in a 25 per cent nitric-acid solution at 125 F. The passivation treatment was used to remove traces of iron or scale contamination from the final grinding operation.

TABLE 7—COMPARATIVE STRESS-RUPTURE PROPERTIES OF AM-355 AT 900 F.
Heat Treatments: A—1750 F, 1 hr, water quenched + 3 hr at −100 F + 1000 F, 3 hrs, air cooled.
B—1900 F, 1 hr, water quenched + 3 hr at −100 F + above heat Treatment A.

Heat Number	Product	Heat Treatment	Test Temperature, deg F	Test Stress, psi	Rupture Life, hr	Elongation in 8d, %	Reduction of Area, %
23787.....	1¼ in. dia	A	900	110 000	96	17.1	44.9
		A	900	105 000	12	18.4	59.8
		A	900	100 000	396	11.0	31.2
		B	900	110 000	251	17.6	61.5
		B	900	105 000	443	22.0	50.6
		B	900	100 000	612	17.7	61.5
24093.....	2¼ in. dia	A	900	110 000	5	16.0	60.2
		A	900	105 000	7	17.3	59.2
		A	900	100 000	514	22.5	59.0
		B	900	110 000	10	17.7	65.1
		B	900	105 000	14	18.7	66.7
		B	900	100 000	630	18.8	64.3

TABLE 8—COMPARATIVE STRESS-CORROSION TESTS ON AM-355.
Heat Treatments: A—1710 to 1750 F, 1 hr, water quenched + 3 hr at −100 F + 1000, 3 hr, air cooled.
B—1900 to 2000 F, 1 hr, water quenched + 3 hr at −100 F + treatment A above.

Heat Number	Product	Test Direction[a]	Heat Treatment	Stress, psi	Duration of Test, days	Comments
21683.....	1 in. dia	L	A[b]	125 000	32	failed
		L	B	125 000	126	no cracks, discontinued
21870.....	1 in. dia	L	A[b]	125 000	39	failed
		L	B	125 000	126	no cracks, discontinued
22404.....	¾ in. dia	L	A[c]	125 000	206	no cracks, discontinued
		L	B	125 000	206	no cracks, discontinued
23295.....	1½ in. square	L	A[c]	125 000	206	no cracks, discontinued
		L	B	125 000	388	no cracks, discontinued
22191.....	4¼ in. square	T	A	125 000	313	no cracks, discontinued
		T	B	125 000	313	no cracks, discontinued
		T	B	150 000	313	no cracks, discontinued
		T	B	165 000	313	no cracks, discontinued
		L	B	165 000	313	no cracks, discontinued
22310.....	5 in. dia	T	A	125 000	313	no cracks, discontinued
		T	B	125 000	313	no cracks, discontinued
		T	B	150 000	313	no cracks, discontinued
		T	B	165 000	313	no cracks, discontinued
		L	B	165 000	313	no cracks, discontinued
23422.....	1 in. plate	T	B	125 000	360	no cracks, discontinued
		T	B	150 000	360	no cracks, discontinued

[a] L = longitudinal; T = transverse.
[b] Contained networks of grain boundary carbides.
[c] Well-dispersed carbides with no visible grain boundary carbides.

Room-temperature tensile properties and stress-corrosion tests in 5 per cent neutral salt fog were made on two heats of the AM-355 casting composition. The comparative heat treatments in this case were slightly different to agree with those used in practice.

Tables 5–9 and Figs. 10 and 11 illustrate the effects of improving the carbide distribution upon the mechanical properties and stress-corrosion resistance of AM-355 alloy. The improved carbide distribution is achieved by prefacing the standard heat treatment with a carbide solution anneal at 1900 to 2000 F and a sub-zero heat treatment at −100 F. It should be understood that the standard heat treatment produces a range of structures depending upon the product size and hot-working practice. In small section-size products, of 30 or more heats recently examined, approximately 30 per cent exhibit structures in which grain-boundary carbides cannot be seen metallographically. In the remaining 70 per cent grain-boundary carbides are observed to widely varying degrees. Because of this feature improvements in properties, if detected, should also vary depending upon the improvement in carbide dispersion that is achieved by the new heat treatment.

Table 5 shows comparative room-temperature tensile properties obtained on transverse and longitudinal specimens. The improved structural uniformity achieved by the new heat treatment produces a small, but consistent, improvement in tensile ductility. The yield and tensile strengths are generally improved slightly also.

Table 6 and Figs. 10 and 11 illustrate comparative impact properties. At room temperature the impact properties are consistently improved 25 per cent or more with the new heat treatment. As shown in Figs. 10 and 11, the improvement in impact properties is dependent upon the test temperature. At very low temperatures, such as −320 F, the impact strength is apparently controlled by the cleavage characteristics of the grains. Improving the structure at grain boundaries had no effect upon impact properties at this temperature. As the temperature increases and cleavage

fractures become less predominant, the improved structural uniformity becomes progressively more effective in increasing the impact strength. Directionality in impact properties is apparent from Table 6 and Fig. 11.

The differences in room-temperature impact properties between the two heat-treated conditions correlated very well with differences in microstructure. Figures 12 and 13 illustrate the microstructures obtained in Heat 23787 with the "old" and "new" heat treatments. The improved carbide distribution, as shown in Table 6 and Fig. 10, more than doubled the impact energy absorbed at room temperature in this case. Figure 12, however, represents an extreme case of intergranular carbide precipitation. Generally the old heat treatment produces

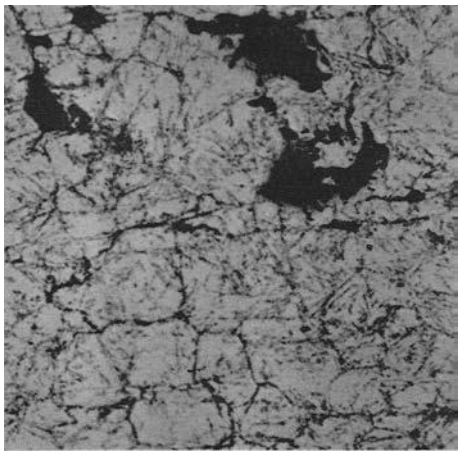


FIG. 14—AM-355 Bar, Exposed 40 Days at 110,000 psi in 5 Per Cent Salt Spray, Unetched (×250).

structures varying from that shown in Fig. 12 to one in which intergranular carbides cannot be seen metallographically.

The carbide distribution appeared to have no effect upon the room-temperature fatigue properties. The results from either heat treatment could be represented reasonably well by a single curve. Normally with a 1000 F temper the alloy exhibits a fatigue limit at room temperature of about 110,000 psi with which the present results agreed.

The stress-rupture test results at 900 F, shown in Table 7, show that the improved carbide distribution produces noticeable increases in both rupture strength and ductility. Since the ductility varies with the duration of the test, the ductility was compared at about equal rupture times for both heat treatments. At 1000 F the stress-rupture life was equivalent with either heat treatment. The reduction of area at fracture, however, was consistently higher with the new heat treatment.

Table 8 describes the results of comparative stress-corrosion tests made on AM-355. Stress corrosion and general rusting and pitting in salt spray took place along grain boundaries that contain precipitated carbides. Corrosive attack was found to occur at either austenite-to-austenite grain boundaries or at delta-ferrite grain boundaries in agreement with observations by Bergman and Palty (16). In the latter case, since delta ferrite is not a continuous phase, corrosive attack resulted in isolated pits at or near the exposed surfaces. Figure 14 shows several pits and intergranular stress corrosion cracks which developed in AM-355 after 400 days in salt spray under a stress of 110,000 psi. The structure has not been metallographically etched but was etched by the salt spray. Only a small area of the specimen surface became etched in this manner. Metallographic examinations of other sections revealed that this area contained more intergranular precipitated carbides than the remainder of the specimen.

Corrosive attack along grain boundary carbides by salt spray does not normally occur in stainless steels. May[4] has shown that even 2.9 years of marine atmosphere exposure did not significantly attack sensitized Type 302 stainless steel. Renshaw (24) studied the effects of salt spray exposure on the straight chromium stainless steels and found that salt spray attack did not proceed along networks of grain boundary carbides. In AM-355, however, the amount of grain boundary carbide precipitation correlates directly with corrosive attack in salt spray. This is seen from Table 8 by comparing the performance of Heats 21683 and 21870 with that of Heats 22404 and 23295. When hardened by the conventional heat treatment (Treatment A), Heats 21683 and 21870 contained a network of grain-boundary carbides and cracked after approximately 35 days in salt spray. Heats 22404 and 23295 contained well-dispersed carbides with only a few visible grain boundary carbides and did not crack after 206 days exposure. This variation in metallurgical structure can occur with the conventional heat treatment as a result of the various processing and heat-treatment factors previously discussed.

Upon removal of the grain-boundary carbides in Heats 21683 and 21870 (Treatment B), their stress corrosion performance was significantly improved as shown in Table 8. By applying the new heat treatment to obtain structures that are consistently free of grain boundary carbides, no stress corrosion failures have yet been observed in 5 per cent salt spray.

TABLE 9—COMPARATIVE PROPERTIES OF AM-355 CASTINGS.

Heat Treatments: A—2000 F, 1 hr, air cooled + 1425 F, 3 hr, air cooled + 1075 F, 3 hr, air cooled + 1750 F, 1 hr, water quenched + 3 hr at −100 F + 950 F, 3 hr, air cooled.
B—2000 F, 1 hr, air cooled + 3 hr at −100 F + 1425 F, 3 hr, air cooled + 1075 F, 3 hr, air cooled + 1750 F, 1 hr, water quenched + 3 hr at −100 F + 950 F, 3 hr air cooled.

Room-Temperature Mechanical Properties

Heat Number	Heat Treatment	0.02% Yield Strength, psi	0.2% Yield Strength, psi	Ultimate Tensile Strength, psi	Elongation in 4d, %	Reduction of Area, %
3350.....	A	131 900	165 200	190 700	12.5	30.8
	B	130 900	168 100	189 200	16.5	40.2
3376.....	A	120 300	160 400	194 200	11.0	25.2
	B	125 800	162 300	195 800	12.5	40.8

Stress-Corrosion Tests

Heat Number	Heat Treatment	Stress, psi	Duration of Test, days	Comments
3350.....	A	150 000	13	small cracks in 7 days, failed 13 days
	B	125 000	262	no cracks, discontinued
	B	150 000	262	no cracks, discontinued
3376.....	A	150 000	274	one specimen cracked in 127 days, but no extension of crack, discontinued
	B	125 000	328	no cracks, discontinued
	B	150 000	274	no cracks, discontinued

[4] T. P. May, private communication.

These include tests on various heats of bar, plate, and billet at stresses of 125,000 psi and higher with exposure times of 200 days to more than one year.

In addition to improved stress-corrosion resistance, the improved uniformity in structure also produces improved corrosion resistance in salt spray. In 20 or more corrosion specimens examined during the past year, the alloy appears fully equivalent to Types 302 and 304 and perhaps equivalent to Type 316 in salt fog. With the standard heat treatment the alloy exhibits erratic behavior but is generally definitely inferior to the standard austenitic stainless steels.

Table 9 describes comparative evaluations made on two AM-355 heats of the cast composition. The 2000 F heat treatment is used primarily to homogenize the castings. The "equalize and overtemper" operation (1425 + 1075 F) is used to prepare castings for machining operations. The 950 F tempering temperature is used instead of 1000 F because many heats of the cast composition will either overage or partially reaustenitize at 1000 F. In agreement with the test results on wrought products, an improved carbide distribution produces slight improvements in room-temperature tensile and impact strengths and improved stress-corrosion resistance. On both heats the tensile ductility, as measured by reduction of area values, was markedly improved.

SUMMARY

To summarize, a new heat treatment has been developed for AM-355 which produces a large improvement in uniformity of carbide distribution. The improved carbide distribution is shown to be of some benefit to certain mechanical properties such as tensile strength and ductility and stress-rupture strength and ductility. Significant improvements in impact properties over a wide temperature range are also obtained. In addition, general corrosion resistance and stress-corrosion resistance to salt spray are markedly increased.

REFERENCES

(1) A. J. Lena, *Precipitation from Solid Solution*, Am. Soc. Metals, Metals Park, Ohio, 1959, p. 278.

(2) C. B. Post and W. S. Eberly, "Stability of Austenite in Stainless Steels," *Transactions*, Am. Soc. Metals, Vol. 39, 1947, p. 868.

(3) G. H. Eichelman, Jr. and F. C. Hull, "The Effect of Composition on the Temperature of Spontaneous Transformation of Austenite to Martensite in 18-8 Type Stainless Steel," *Transactions*, Am. Soc. Metals, Vol. 45, 1953, p. 77.

(4) F. C. Monkman, F. B. Cuff, and N. J. Grant, "Computation of Ms for Stainless Steels," *Metal Progress*, Vol. 71, No. 4, 1957, p. 94.

(5) K. J. Irvine, D. T. Llewellyn, and F. B. Pickering, "Controlled-transformation Stainless Steels," *Journal*, Iron and Steel Inst., Vol. 192, 1959, p. 218.

(6) S. J. Rosenberg and C. R. Irish, "Solubility of Carbon in 18 Percent-Chromium-10 Percent-Nickel Austenite," *Journal of Research*, National Bureau of Standards, Vol. 48, 1952, p. 40.

(7) V. N. Krivobok and M. A. Grossman, "Influence of Nickel on the Chromium-Iron-Carbon Constitutional Diagram," *Transactions*, Am. Soc. for Steel Treating, Vol. 18, 1930, p. 808.

(8) R. H. Aborn and E. C. Bain, "Nature of the Nickel-Chromium Rustless Steels," *Transactions*, Am. Soc. for Steel Treating, Vol. 18, 1930, p. 837.

(9) O. V. Greene, "Discussion—Nature of the Nickel-Chromium Rustless Steels," *Transactions*, Am. Soc. for Steel Treating, Vol. 18, 1930, p. 877.

(10) E. C. Bain, R. H. Aborn, and J. J. B. Rutherford, "The Nature and Prevention of Intergranular Corrosion in Austenitic Stainless Steels," *Transactions*, Am. Soc. for Steel Treating, Vol. 21, 1933, p. 481.

(11) B. Strauss, H. Schottky, and J. Hinnueber, *Zeitschrift der Anorganischen Chemie*, Vol. 188, 1930, p. 309.

(12) E. M. Mahla and N. A. Nielsen, "Carbide Precipitation in Type 304 Stainless Steel—An Electron Microscope Study," *Transactions*, Am. Soc. Metals, Vol. 43, 1951, p. 290.

(13) R. Stickler and A. Vinckier, "Morphology of Grain-Boundary Carbides and Its Influence on Intergranular Corrosion of 304 Stainless Steel," *Transactions*, Am. Soc. Metals, Vol. 54, 1961, p. 362.

(14) R. J. Bendure, L. C. Ikenberry, and J. H. Waxweiler, "Quantity and Form of Carbides in Austenitic and Precipitation Hardening Stainless Steels," *Transactions*, Am. Institute of Mining, Metallurgical, and Petroleum Engrs., Vol. 221, 1961, p. 1032.

(15) H. J. Noble and W. H. Sharp, "Steels and Protective Treatments for Use Up to 1000 F," *Transactions*, Soc. Automotive Engrs., Vol. 64, 1956, p. 59.

(16) P. A. Bergman and A. E. Palty, "Development of Corrosion Resistance in AM-355," *Transactions*, Am. Soc. Metals, Vol. 56, No. 3, 1963, p. 728.

(17) T. H. McCunn and E. Murray, "Processing and Evaluation of Tensile Properties of AM-355 Sheet in the H Condition," *Report No. SS-402*, Allegheny Ludlum Steel Corp., Brackenridge, Pa., 1959.

(18) G. K. Manning and C. H. Lorig, "The Relationship Between Transformation at Constant Temperature and Transformation During Cooling," *Transactions*, Am. Institute of Mining, Metallurgical, and Petroleum Engrs., Vol. 167, 1946, p. 442.

(19) E. S. Machlin and M. Cohen, "Isothermal Mode of the Martensitic Transformation," *Transactions*, Am. Institute of Mining, Metallurgical, and Petroleum Engrs., Vol. 194, 1952, p. 489.

(20) K. Hoselitz, *Ferromagnetic Properties of Metals and Alloys*, Oxford University Press, New York, N. Y., 1952.

(21) R. E. Ogilvie, "Retained Austenite by X-Rays," *Norelco Reporter*, Vol. 6, No. 3, 1959, p. 60.

(22) J. L. Ham, "The Rate of Diffusion of Molybdenum in Austenite and in Ferrite," *Transactions*, Am. Soc. Metals, Vol. 35, 1945, p. 331.

(23) J. K. Stanley, "The Diffusion and Solubility of Carbon in Alpha Iron," *Transactions*, Am. Inst. of Mining, Metallurgical, and Petroleum Engrs., Vol. 185, 1949, p. 752.

(24) W. G. Renshaw, "Properties of Heliarc and Arc Welded Straight Chromium Steels," *Report No. 303*, Allegheny Ludlum Steel Corp., Brackenridge, Pa., 1952.

AGING MECHANISMS IN PRECIPITATION-HARDENING STAINLESS STEELS

By J. C. Wilkins,[1] R. E. Pence,[1] and D. C. Perry[1]

Synopsis

The mechanism of age hardening in the 17-7PH and PH15-7Mo stainless steels was studied by electron microscopy and "selected area" electron diffraction using direct-transmission thin-foil techniques and the extracted-particle carbon-replica techniques. The precipitates in the specimens aged from 6 to 24 hr at 1050 F were NiAl, and at 100 hr they were NiAl and Ni_3Al. The presence of these precipitates was indicated by moiré patterns, round disks, and strain areas.

In recent years the precipitation-hardening stainless steels have been the subject of several investigations on the mechanism of age hardening. The earlier phases of our work were previously reported in an ASTM symposium (1).[2] As background to the more recent studies, the earlier work is briefly reviewed. Further progress is reported in this present paper.

The materials studied are 17-7PH and PH15-7Mo stainless steel sheets, developed and produced by the Armco Steel Corp. The chemical composition ranges for these steels are given in Table 1.

The commercial treatments for hardening these types of stainless steels are recorded in Table 2. In addition to the commercial hardening treatments, specimens were overaged at 1050 F for 6, 12, 24, and 100 hr for investigation of the aging mechanism.

17-7PH and PH15-7Mo precipitation-hardening stainless steels annealed at 1950 F and air cooled (Condition A) contain stringers of ferrite (varying from 5 to 15 per cent) in a matrix of austenite (Figs. 1 and 2). The hardness in Condition A is approximately 88 R_B.

In order to age harden, these types must first be transformed from an austenitic to a martensitic structure (Fig. 3). This is accomplished by treating to Condition T (hardness: 30 R_C) or Condition R-100 (hardness: 38 R_C). (See Table 2). The mechanism of transformation to Condition T consists of removing carbon from solution in austenite during heating to and holding at 1400 F. Carbides ($M_{23}C_6$) first form at the stringer-matrix interfaces; and if the carbon content is on the high side of the specification, carbides will also form in the grain boundaries (Fig. 4). Removal of carbon and chromium from the austenite matrix results in the material becoming unstable with resultant transformation to martensite during cooling to room temperature (Figs. 4 and 5). In the process of heat treating to Condition R-100 for transformation, material is heated for a short time at 1750 F. Only a few carbides form during this treatment, and the austenite is more stable than after the 1400 F treatment, requiring several hours at −100 F to transform to martensite.

When transformed material is aged (Conditions TH1050 and RH950) considerable veining is observed throughout the matrix (Fig. 6). This is evidence of precipitation or composition changes in the martensitic areas or both, making them more susceptible to attack when etched for microscopic examination.

The hardness attained in Condition TH1050 is approximately 44 R_C, an increase of 14 points R_C over Condition T. In Condition RH950 the hardness is 48 R_C, an increase of 10 points R_C over Condition R-100. These increases in hardness are attributed to the age hardening characteristics of the PH grades.

The decrease in hardness as the time of aging is increased is the result of reversion from the harder martensitic matrix to a softer austenite (Table 3).

Thin foil sections and extraction techniques for direct transmission were used for identification of the precipitates by means of electron microscopy and "selected-area" electron diffraction.

Thin-Section Foils for Direct Transmission Studies

Specimens of 17-7PH and PH15-7Mo stainless steels were cold reduced to 0.001 to 0.002 in. thickness, bright annealed at 1950 F, and given various conditioning treatments. Thin-section foils were produced by electropolishing to a thickness of approximately 1500 A (0.000006 in.) by the Bollmann technique (2). This technique consists of electropolishing with pointed stainless steel cathodes mounted close to the center of the specimen and spaced approximately 1 mm away from each surface. When a hole appears in the foil, the electrodes are backed off to about 1 cm, and polishing is continued until small holes appear around the larger hole. The areas between the holes are thin enough for examination by transmission. The electrolyte was 60 per cent orthophosphoric acid and 40 per cent sulfuric acid. A current density of 1.5 amp/cm² at 9 v was used for polishing.

In Condition A, the foils contained twinned austenitic grains (Fig. 7). In the annealed condition the austenite grains are free from the type of dislocations associated with strained or transformed material.

In Condition T, the matrix structure had concentrations of dislocations induced by the transformation from austenite to martensite (Fig. 8). This structure is typical of a low-carbon martensite, which is needle-like (at lower magnifications), and relatively soft (3). Small ferrite patches were dispersed throughout the matrix. Very few dislocations were noted in the ferrite patches. These ferrite patches were small, since the larger stringers usually observed by optical microscopy were broken up during the cold reduction to the foil thicknesses of 0.001 to 0.002 in. prior to heat treatment and electrothinning. Carbides surrounded the ferrite pools. These carbides had a tendency to be oblong or pyramidal in shape.

The thin foil structure in Condition TH1050 (Fig. 9) was similar to the

[1] Senior metallurgist, metallurgist, and senior research engineer, respectively, Research and Technology, Armco Steel Corp., Middletown, Ohio.

[2] The boldface numbers in parentheses refer to the list of references appended to this paper.

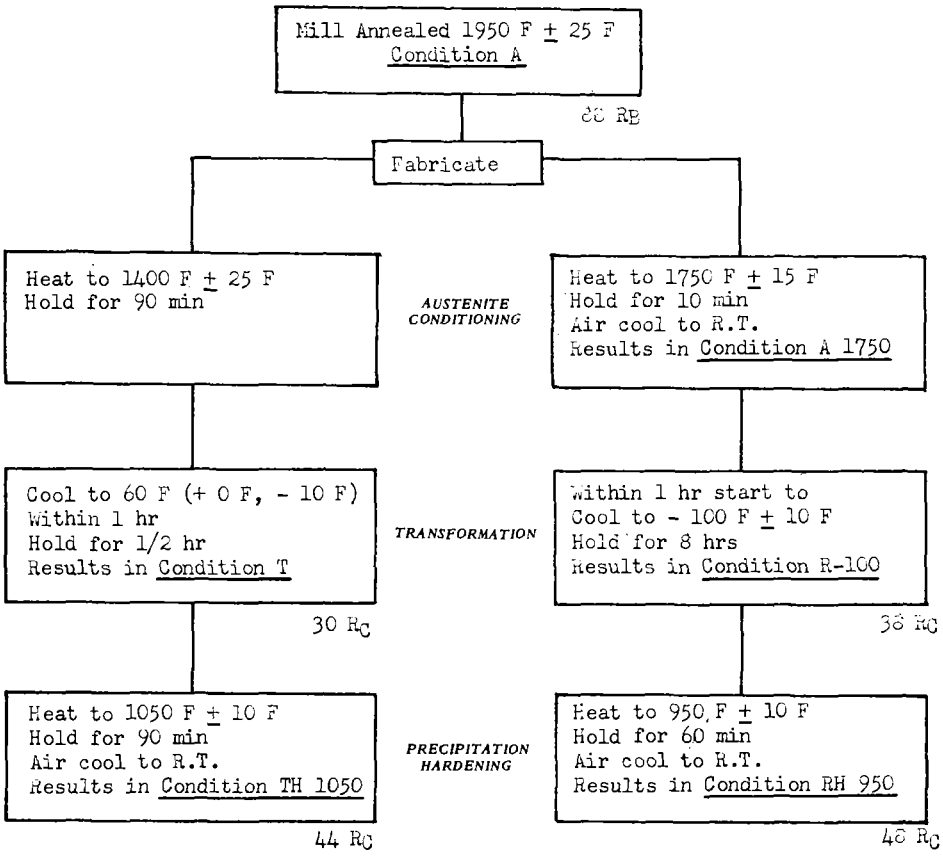
Copyright© 1965 by ASTM International

www.astm.org

TABLE 1—CHEMICAL COMPOSITION OF ARMCO 17-7PH AND PH15-7Mo STAINLESS STEELS, PER CENT.

Element	17-7PH	PH15-7Mo
Carbon	0.09 max	0.09 max
Manganese	1.00 max	1.00 max
Phosphorus	0.04 max	0.04 max
Sulfur	0.04 max	0.04 max
Silicon	1.00 max	1.00 max
Chromium	16.00 to 18.00	14.00 to 16.00
Nickel	6.50 to 7.75	6.50 to 7.75
Aluminum	0.75 to 1.50	0.75 to 1.50
Molybdenum	...	2.00 to 3.00

TABLE 2—HEAT TREATMENTS FOR ARMCO 17-7PH AND PH15-7Mo STAINLESS STEELS.



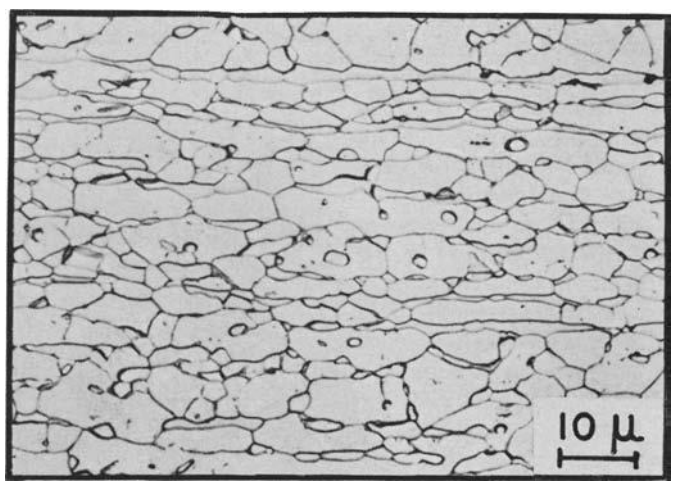


FIG. 1—Stringers of Ferrite in a Matrix of Austenite in PH15-7Mo Stainless Steel, Condition A (Annealed) (×1000). (Etch: nitric-acetic acid, followed by oxalic acid; electrolytic).

structure of Condition T. There was no evidence of precipitates in the thin sections after this aging treatment. After aging at 1050 F for 100 hr several changes were noted in the thin-section foils (Figs. 10 and 11). These electron micrographs have certain features which parallel the observations of Nicholson, Thomas, and Nutting (4) in the age hardening aluminum-copper alloys. This work cites the Guinier-Preston zone theory as a mechanism of age hardening.

In many areas of the thin-section foils moiré patterns between the precipitate and matrix were observed. (See Arrow 1 in Fig. 10). These parallel patterns result from the imaging of two unequal crystal gratings with the electron beam. In this case the patterns are produced from the precipitate and matrix lattices when the precipitate plates lie parallel to the surface of the foil. Arrow 2 indicates an example of many thin rounded disks noted throughout the matrix. It is difficult to establish whether these disks are actually the precipitates (full size) or are dislocation rings around much smaller precipitates. According to Nicholson et al (4), dislocation rings are produced when the strains near a precipitate become very large and are relieved by the formation of an extra plane of atoms parallel to the plane of the precipitate. This reaction produces a stable dislocation ring around the precipitate. Many of the disks observed in Fig. 10 appear to have small dark centers, which may give credence to these assumptions. Arrow 3 (Fig. 11) indicates an area similar to those which have been explained as regions where the strain fields become large as the precipitate grows and eventually extend from one precipitate to the other (4).

SELECTED-AREA DIFFRACTION THROUGH THIN SECTIONS

Selected-area electron diffraction studies were made through the thin sections in Conditions A (Fig. 12), T, TH1050, and 1050 F aged for 100 hr (Fig. 13). The interpretation of the diffraction patterns is recorded in Table 4. The interplanar spacing or d values of 2.84 and 2.54 for the 1050 F, 100 hr aged specimen indicated that NiAl and Ni_3Al precipitates were present. These interplanar spacing values are unique for the nickel-aluminum precipitates as compared with austenite, ferrite, and carbides in the matrix. However, the intensity of diffraction from the precipitate is relatively

faint because of dilution by the martensitic matrix material. All other *d* values are also associated with the matrix material. No precipitates of this type were found in the TH1050 (90 min) specimen.

The selected area diffraction patterns indicate that there is a slight reversion of the martensite to austenite (γ iron) in Condition TH1050. This reversion of martensite to austenite during aging at 1050 F has been noted previously during x-ray studies at the Armco Research Center and by other investigators (5).

Extraction Methods for Selected-Area Diffraction

In order to concentrate the amount of aging precipitate to be examined and thus improve the sensitivity of the selected-area electron diffraction method, extraction replicas were made of the aged specimens.

Prior work had indicated that for extracting particles in these steels, Vilella's (hydrochloric acid-picric acid) was the best etchant. The etched specimens were placed in a vacuum evaporator, and a medium thick film of carbon was deposited on them. This film was stripped off the specimen using an electrolyte consisting of 1 part perchloric acid and 20 parts glacial acetic acid (5), at 32 v and 1.2 amp.

This method enabled specimens to be prepared which contained carbides from the interface of the ferrite stringers and precipitated particles from the matrix (Fig. 14).

An area of precipitate is shown in Fig. 15. A selected-area diffraction pattern taken in such a region indicated the presence of NiAl and Ni_3Al (Fig. 16). The carbides at the interface of the ferrite stringers and at the grain boundaries are identified as $Cr_{23}C_6$ (Figs. 17 and 18).

The electron diffraction data for specimens aged for various times are recorded in Table 5. Strong evidence of NiAl and Ni_3Al was found in the specimens aged for 100 hr. There was evidence of NiAl in specimens aged for 6, 12, and 24 hr with the intensity increasing as the time of aging increases. No indications of an aging precipitate were found in specimens aged at 1050 F for $1\frac{1}{2}$ hr.

Carbides in PH Stainless Steels

During the course of this investigation the carbides formed during the condi-

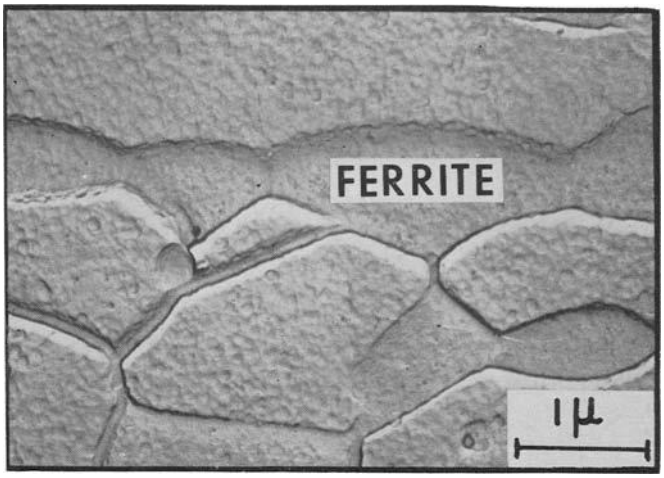


Fig. 2—Electron Micrograph (Plastic Replica) of PH15-7Mo Stainless Steel, Condition A (×18,000).

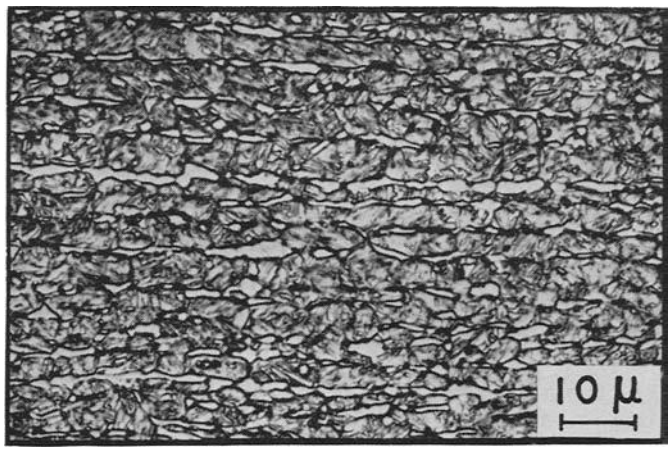


Fig. 3—The Transformed Structure of PH15-7Mo Stainless Steel in Conditions T, TH1050, or RH950 (×1000). (Ftch: same as in Fig. 1).

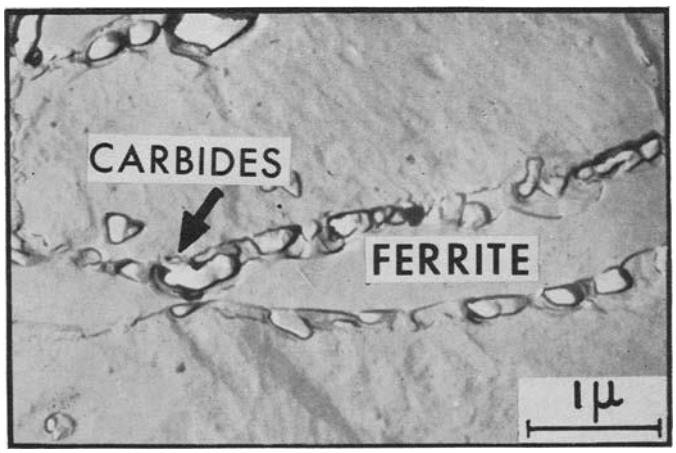


Fig. 4—Electron Micrograph (Plastic Replica) of PH15-7Mo Stainless Steel, Condition T (×18,000). (Note the carbides at the ferrite-martensite interface).

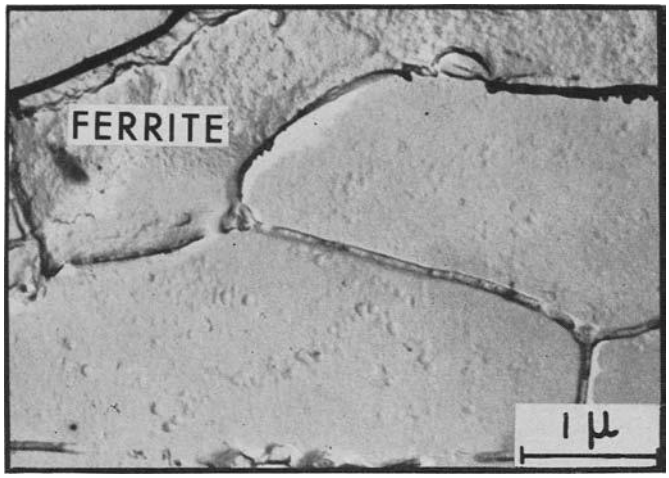


FIG. 5—Electron Micrograph (Plastic Replica) of PH15-7Mo Condition R-100 (×18,000). (There are fewer carbides in Condition R-100 than in Condition T).

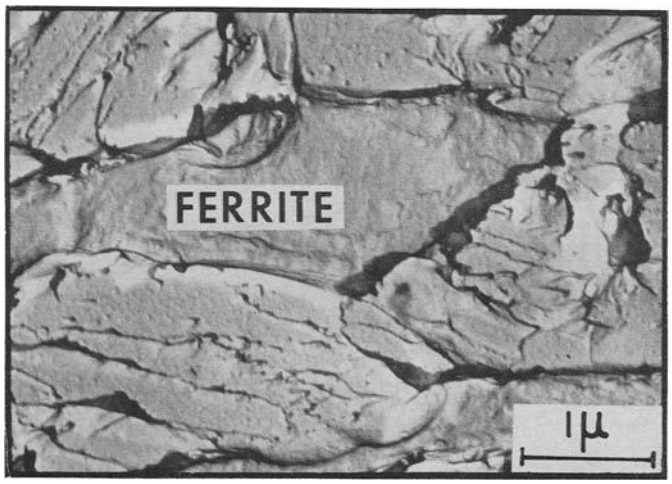


FIG. 6—The Transformed and Aged Conditions TH1050 and RH950 (×18,000). (Note the veining throughout the martensite).

TABLE 3—AUSTENITE IN TRANSFORMED AND AGED PH15-7Mo.

Time at 1050 F, hr	Austenite, %	Hardness, Rockwell C
0	3	30
1.5	5	44
6	8	41
24	10.5	40
100	12	37

tioning treatments (Condition T) were also studied. The carbides formed in both the 17-7PH and PH15-7Mo stainless steels were identified as $Cr_{23}C_6$ (Table 6). No difference in the carbides was detected as a result of the presence of molybdenum in PH15-7Mo. After aging for long periods of time (100 hr), the carbide areas contained small amounts of NiAl and Ni_3Al. These precipitates were probably in the matrix of the areas examined and not a part of the carbide particles.

DISCUSSION

Ordered-Disordered Structures in Precipitates:

The precipitate Ni_3Al belongs to the Cu_3Au (L12) type or face-centered cubic lattice structure. NiAl belongs to the C_sCl-L2 (B2) type or body-centered cubic lattice structure (6).

Burnett, Duff, and Vacher (5) refer to the precipitate NiAl as ordered ferrite (α' ferrite). This nomenclature was first used by Bradley (7) to designate the ordered phase found in the aluminum-iron-nickel system.

Internal stresses incident to the transformation to martensite in the heat treatment of the precipitation hardening steels result in lattice defects which became preferred sites for atomic diffusion during subsequent aging treatments.

During the first stages of aging the nickel-aluminum precipitates would be in a disordered state, making them indistinguishable from the ferrite and austenite lattices. However, as the time of treatment is increased, diffusion of aluminum and nickel atoms would occur so as to form the permanent ordered arrangements of the face-centered Ni_3Al and the body-centered NiAl structures. Diffraction lines characteristic of these ordered structures would permit their detection and identification.

The intensity of these superlattice lines is a direct measure of the perfection in the order attained by the structure.

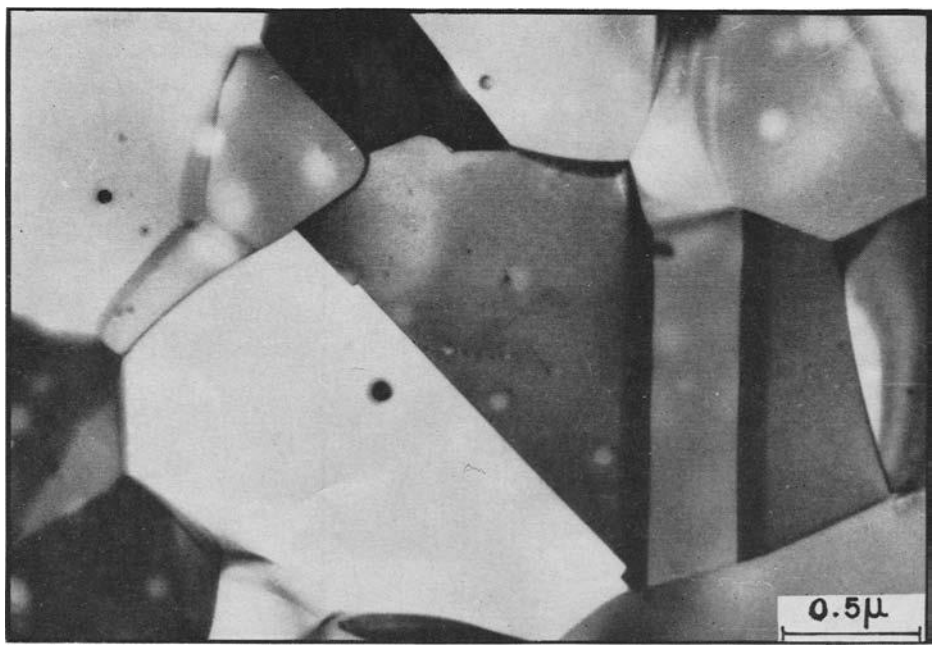


FIG. 7—Direct Transmission Through a Thin Foil of PH15-7Mo, Condition A (×50,000). (Structure is twinned austenite). Reduced One Third for Reproduction.

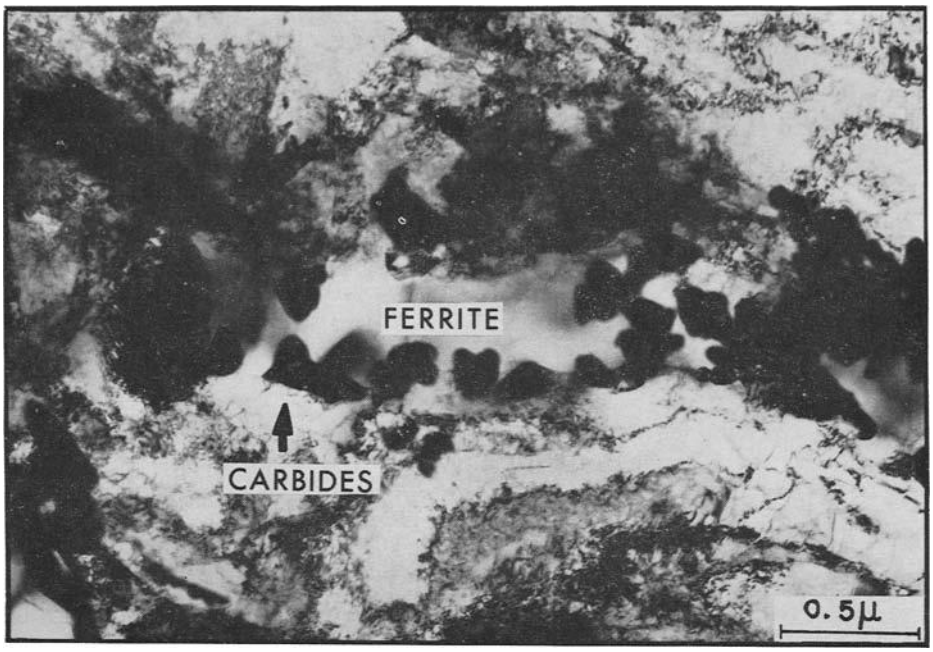


FIG. 8—Direct Transmission Through a Thin Foil of PH15-7Mo, Condition T (×50,000). (The dark particles are $Cr_{23}C_6$ at the martensite-ferrite interface). Reduced One Third for Reproduction.

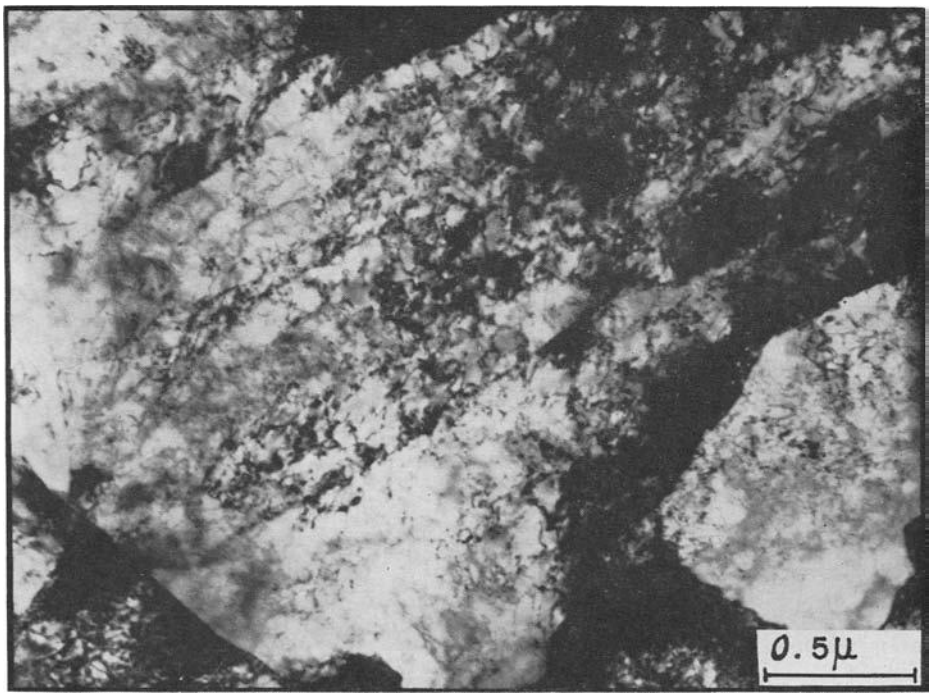
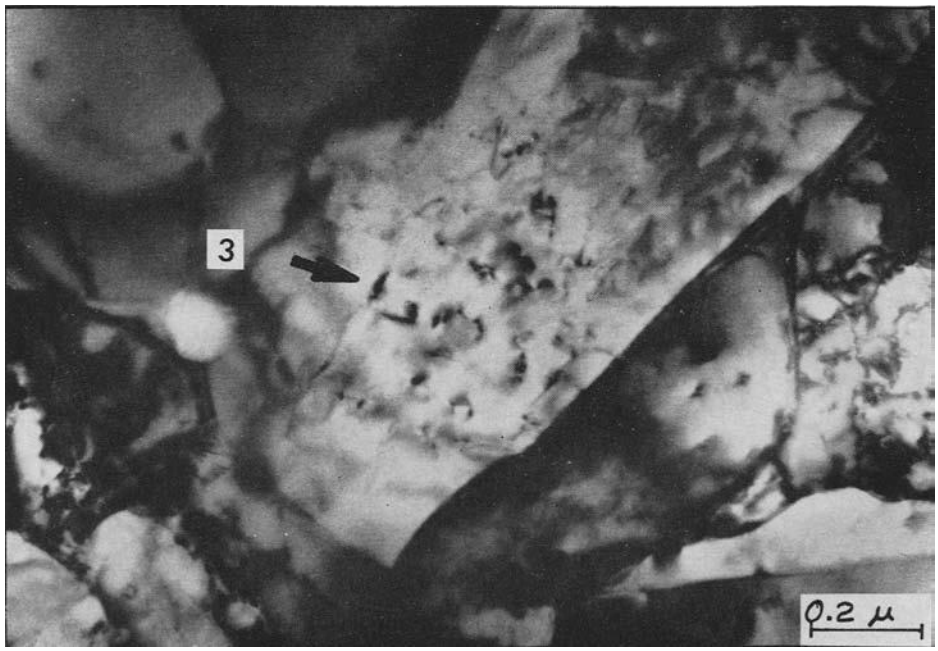
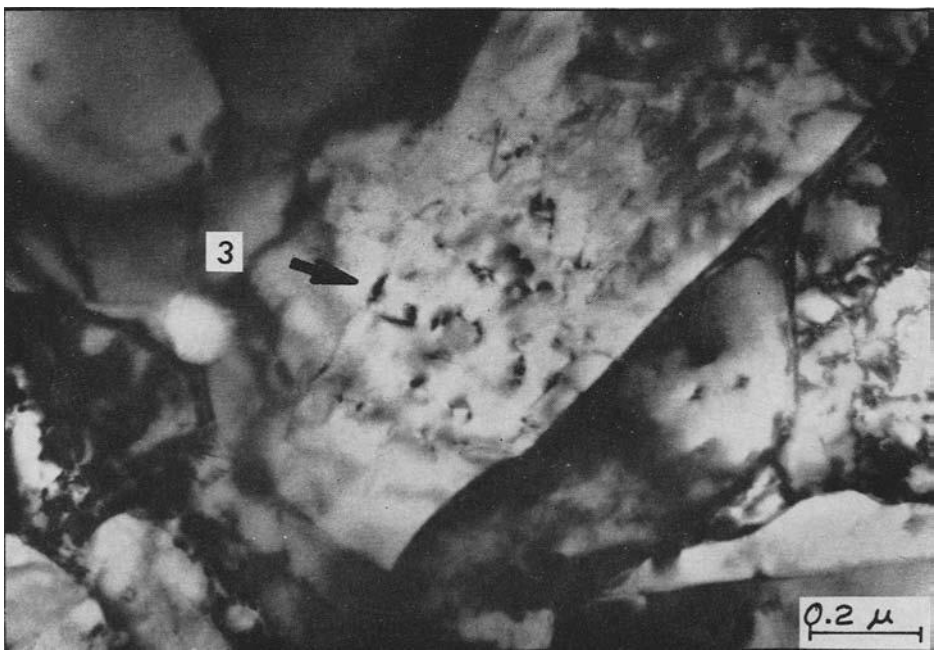


FIG. 9—Direct Transmission Through a Thin Foil of PH15-7Mo, Condition TH1050 (×50,000). Reduced One Third for Reproduction.



Arrow 1—moiré pattern.
Arrow 2—thin rounded discs.

FIG. 10—Direct Transmission Through a Thin Foil of PH15-7Mo, Transformed and Aged at 1050 F for 100 hr (×100,000). Reduced One Third for Reproduction.



Arrow 3—precipitates.

FIG. 11—Direct Transmission Through a Thin Foil of PH15-7Mo, Transformed and Aged at 1050 F for 100 hr (×100,000). Reduced One Third for Reproduction.

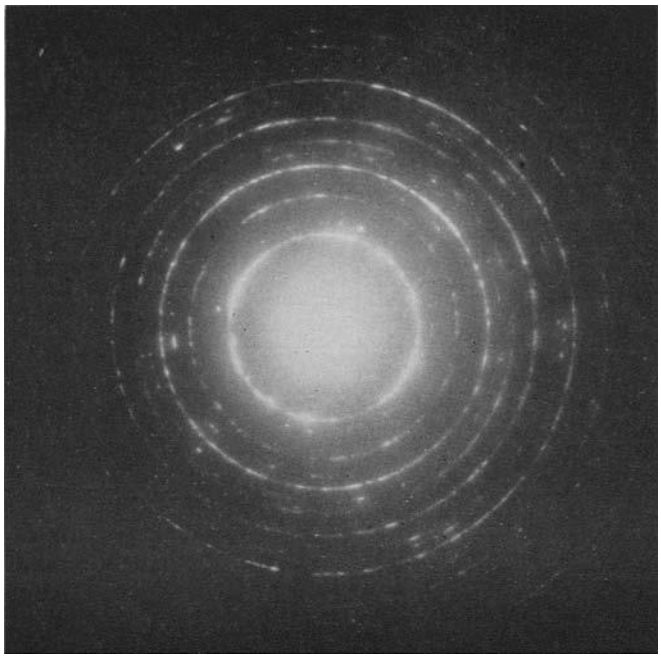


FIG. 12—Transmission Electron Diffraction Through a Thin Foil of PH15-7Mo, Condition A. (Pattern indicates austenite and ferrite).

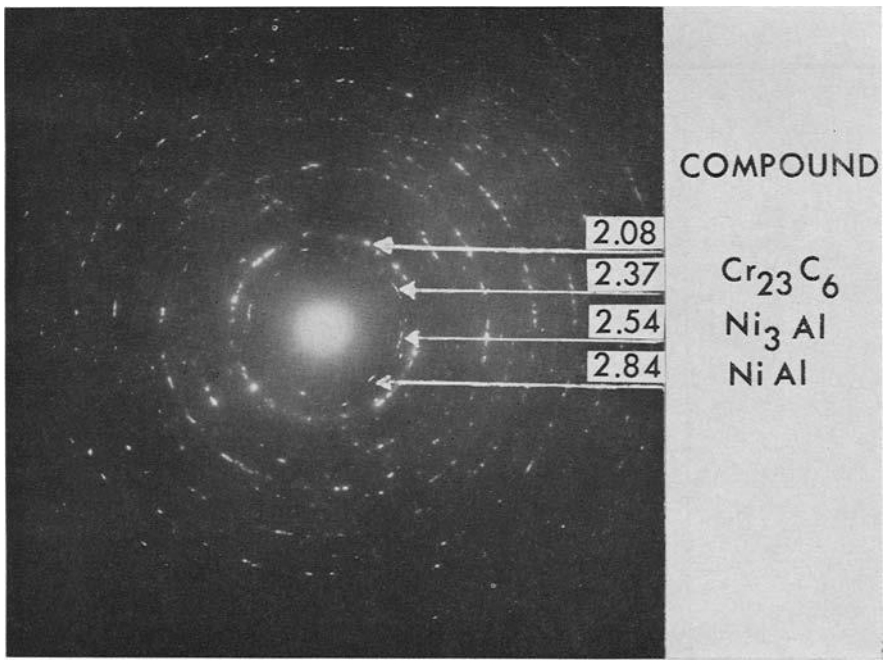


FIG. 13—Transmission Electron Diffraction Through a Thin Foil of PH15-7Mo, Transformed and Aged at 1050 F for 100 hr. (Pattern indicates presence of austenite, ferrite (martensite), $Cr_{23}C_6$, NiAl, and Ni_3Al).

TABLE 4—TRANSMISSION ELECTRON DIFFRACTION DATA THROUGH THIN FOILS OF PH15-7Mo.

CONDITION								X-RAY POWDER DATA FOR									
A		T		TH1050		1050 F 100 Hrs.		Ferrite		Austenite		$Cr_{23}C_6$		NiAl		Ni_3Al	
d	I/I_1	d	I/I_1	d	I/I_1	d	I/I_1	d	I/I_1	d	I/I_1	d	I/I_1	d	I/I_1	d	I/I_1
						2.84	W							2.87	40		
						2.54	MW									2.55	40
		2.35	VW	2.35	VW	2.37	W					2.38	100				
				2.17	VW	2.17	W					2.17	100				
2.08	S	2.08	S	2.08	S	2.08	S	2.03	100	2.08	100	2.05	100	2.02	100	2.07	100
1.82	MS	1.80	VVW	1.82	VW	1.82	W			1.80	80	1.80	100			1.80	70
1.45	M	1.45	M	1.45	M	1.45	MW	1.43	20					1.44	20	1.46	20
1.27	M			1.27	W	1.27	W			1.27	50	1.25	100	1.28	10	1.27	60
1.17	MS	1.17	MS	1.17	S	1.17	MS	1.17	30			1.17	75	1.17	70		
1.09	M			1.09	W	1.09	W			1.08	80					1.08	60

COMPOUNDS PRESENT			
Austenite + Ferrite	Ferrite (Martensite) + Trace $Cr_{23}C_6$	Austenite + Ferrite (Martensite) + Trace $Cr_{23}C_6$	Austenite + Ferrite (Martensite) + Trace $Cr_{23}C_6$ + Trace NiAl + Trace Ni_3Al

d = Interplanar Spacing Values

I/I_1 = Intensity

S = Strong
M = Medium
W = Weak
V = Very

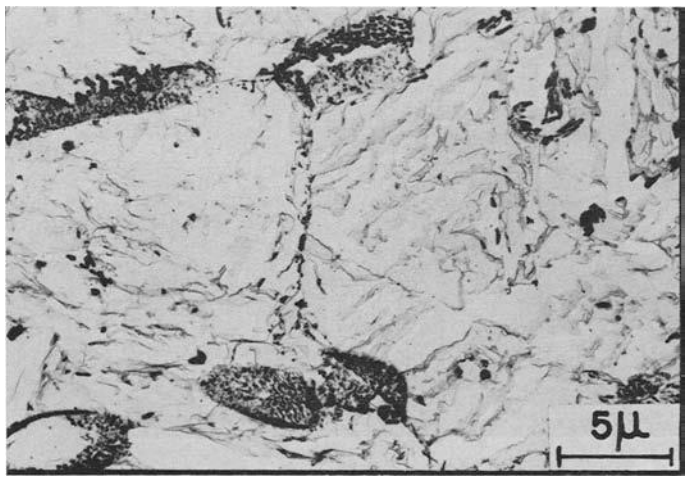


FIG. 14—Carbon Extraction Replica from a PH15-7Mo Specimen, Transformed and Aged at 1050 F for 100 hr (×3,000).

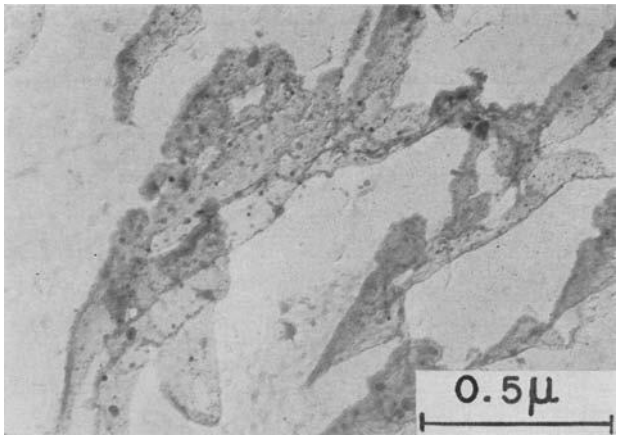


FIG. 15—Extraction Replica in the Area of the Precipitates (×50,000).

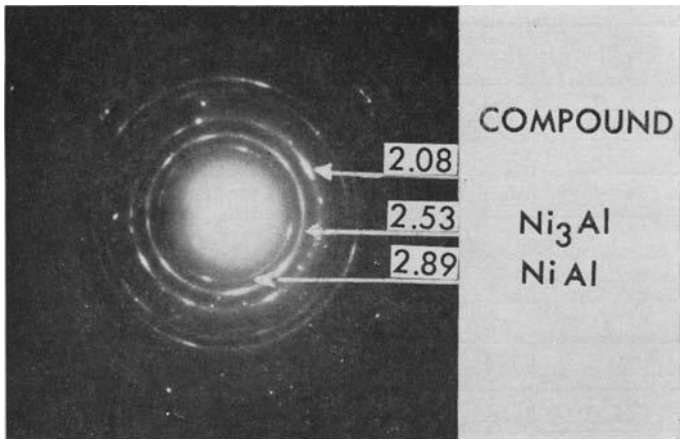


FIG. 16—Diffraction Pattern in the Precipitate Area. (Strong superlattice d values for NiAl and Ni_3Al are noted).

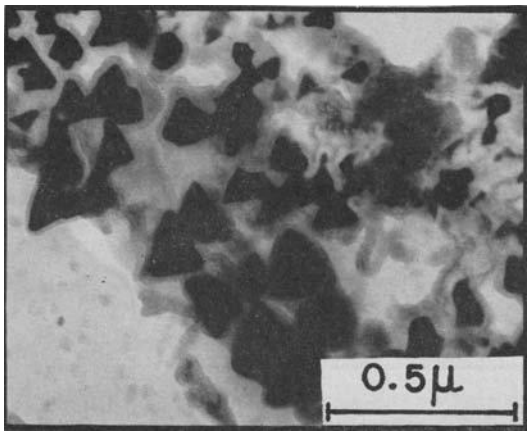


FIG. 17—Extraction Replica in an Area Containing Carbides (×50,000).

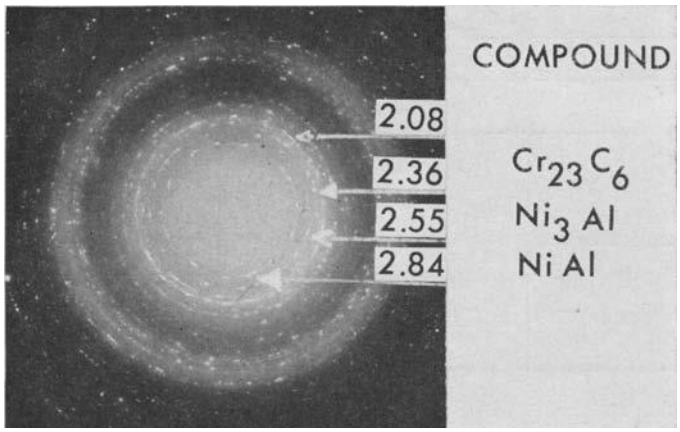


FIG. 18—Diffraction Pattern in the Carbide Area Indicate the Presence of $Cr_{23}C_6$, NiAl, and Ni_3Al.

Since the difference in the atomic scattering factors (based on atomic number) between nickel and aluminum is sufficiently large, relatively strong superlattice lines are obtained. This accounts for the strong superlattice d values of 2.88 for NiAl and 2.53 for Ni_3Al.

Since no superlattice indications were observed for the precipitation-hardening stainless steels after aging for short periods of time (1050 F for $1\frac{1}{2}$ hr), it is probable that the precipitates (if present) were still in the "disordered" arrangement and did not become "ordered" until after longer aging. Since the d values of 2.88 and 2.53 are the only interplanar spacing values which differentiate NiAl and Ni_3Al from ferrite (martensite), austenite, and $Cr_{23}C_6$, it would be difficult to identify the disordered precipitates by electron diffraction.

The stresses set up by the formation of precipitates of NiAl and Ni_3Al with disordered lattice structures in the dislocation zones, and the initial process of ordering could account for the marked increase in mechanical properties (strength and hardness) when material is aged to Condition TH1050. The gradual drop in these mechanical properties as the aging time is increased is perhaps not as much influenced by the process of ordering as by a gradual reversion of martensite to austenite.

Investigators (8) have indicated that the hardness increases as the particle size of precipitates increases until the particle reaches a critical size after which a drop in hardness will occur. Since the NiAl and Ni_3Al particles are very small, it is possible that many of these precipitates have not reached this critical size even at the 100-hr aging time, although the hardening effect of the precipitates is diminishing and the increase in hardness is more than counteracted by the softening effect of the martensitic matrix partially reverting to austenite.

Guinier-Preston Zone Theory:

Another theory of the mechanism of precipitation in alloys with a high degree of supersaturation follows the sequence of changes: super-saturated solid solution → Guinier-Preston zones → intermediate precipitate → equilibrium precipitate (4) and (6). By definition, a Guinier-Preston zone corresponds to a local change of composition without any change of phase. The more highly supersaturated the alloy, the more readily zones form. Although factors controlling their nucleation are not completely understood, it is probable that they form at vacancy clusters (3).

The vacancy clusters in this case are the imperfections introduced by the martensite transformation. Migration of nickel and aluminum into these defect regions would result in zone concentrations prior to precipitation.

The formation of Guinier-Preston zones is reported to lead to a marked increase in hardness. Probably the greatest increase occurs during the first formation of an intermediate phase. When this phase forms, its interface with the matrix usually remains co-

TABLE 5—ELECTRON DIFFRACTION DATA OF THE PRECIPITATE EXTRACTED FROM 17-7PH.

CONDITION																X-RAY POWDER DATA FOR											
TH 1050 (1-1/2 Hrs.)		1050 F 6 Hrs.		1050 F 12 Hrs.		1050 F 24 Hrs.		1050 F 100 Hrs.		Ferrite		Austenite		$Cr_{23}C_6$		NiAl		Ni_3Al	
d	I/I_1	d	I/I_1	d	I/I_1	d	I/I_1	d	I/I_1	d	I/I_1	d	I/I_1	d	I/I_1	d	I/I_1	d	I/I_1
		2.88	VW	2.88	M	2.89	MS	2.89	MS							2.87	40		
								2.53	S									2.55	40
														2.38	100				
														2.17	100				
2.05	MS	2.05	MS	2.05	MS	2.03	S	2.08	S	2.03	100	2.08	100	2.05	100	2.02	100	2.07	100
		1.80	MW	1.80	W	1.80	W	1.78	W			1.80	80	1.80	100			1.80	70
1.43	W	1.43	M			1.42	MW	1.43	MS	1.43	19			1.48	20	1.44	20	1.46	20
						1.27	MW	1.27	MW			1.27	50	1.25	100	1.28	10	1.27	60
1.18	W	1.20	W	1.20	W	1.17	MW	1.16	W	1.17	30			1.17	75	1.17	70		
								1.09	W			1.08	80					1.08	60
COMPOUNDS PRESENT																			
Ferrite (Martensite)		Austenite (Trace) + Ferrite (Martensite) + NiAl (Trace)		Austenite (Trace) + Ferrite (Martensite) + NiAl		Austenite (Trace) + Ferrite (Martensite) + NiAl		Austenite (Trace) + Ferrite (Martensite) + NiAl + Ni_3Al											

d = Interplanar Space Values

I/I_1 = Intensity

S = Strong
M = Medium
W = Weak
V = Very

TABLE 6—ELECTRON DIFFRACTION DATA OF THE CARBIDES EXTRACTED FROM 17-7PH AND PH15-7Mo.

17-7 PH Condition T		15-7 PH Condition T		17-7 PH 1050 F 100 Hrs.		X-RAY POWDER DATA FOR									
						Ferrite		Austenite		$Cr_{23}C_6$		NiAl		Ni_3Al	
d	I/I_1	d	I/I_1	d	I/I_1	d	I/I_1	d	I/I_1	d	I/I_1	d	I/I_1	d	I/I_1
				2.85	M							2.87	40		
				2.55	MW									2.55	40
2.36	MW	2.36	MW	2.36	M					2.38	100				
2.18	MW	2.18	M	2.15	M					2.17	100				
2.05	S	2.05	S	2.05	S	2.03	100	2.08	100	2.05	100	2.02	100	2.07	100
1.80	S	1.80	M	1.78	M			1.80	80	1.80	100			1.80	70
						1.43	19								
1.25	W	1.25	W	1.24	M			1.27	50	1.25	100			1.27	60
COMPOUNDS PRESENT															
$Cr_{23}C_6$		$Cr_{23}C_6$		$Cr_{23}C_6$ + NiAl + Ni_3Al (Trace)											

d = Interplanar Spacing Values

I/I_1 = Intensity

S = Strong
M = Medium
W = Weak
V = Very

herent, and as a result large strains develop, both in the precipitate and the surrounding matrix.

SUMMARY AND CONCLUSIONS

The mechanism of age hardening in the 17-7PH and PH15-7Mo stainless steels was studied by electron microscopy and "selected-area" electron diffraction using direct transmission thin foil techniques and the extracted-particle, carbon-replica techniques. Previous studies by optical microscopy and electron microscopy using replica techniques were briefly discussed.

Selected-area electron diffraction data indicated no precipitates in specimens in Condition TH1050 (aged 1½ hr at 1050 F). The precipitates in specimens aged 6, 12, and 24 hr at this temperature were NiAl, increasing in amount with increased aging time. The precipitates in specimens aged at 1050 F for 100 hr were NiAl and Ni_3Al.

Electron microscopy studies indicated the presence of precipitates at the longer aging times as evidenced by moiré patterns, and by circular areas which may be either the precipitated particles or smaller particles surrounded by dislocation rings.

The following theories were presented as the mechanism for precipitation:

1. The order-disorder theory in which the initial stages (including Condition TH1050) encompass the formation of a disordered lattice array. As the time of aging is increased, the atoms in the lattice tend to reassemble into a permanent or ordered arrangement. When this occurs the precipitates can be identified by electron diffraction as super-lattice structures of NiAl and Ni_3Al.

2. Another theory follows the sequence of changes: super-saturated solid solution → Guinier-Preston zones → intermediate precipitate → equilibrium precipitate. It is suggested that nickel and aluminum move into lattice defect areas causing zone concentrations to occur prior to precipitation. As time of aging increases intermediate precipitation occurs. Specimens in Condition TH1050 are believed to be at this stage of the precipitation sequence. When equilibrium precipitation is attained, NiAl and Ni_3Al precipitates can be identified.

Both the above theories offer reasonable explanations for the aging phenomena in these precipitation hardening stainless steels.

Acknowledgments:

The authors wish to thank J. A. Elias, R. H. Heyer, and M. W. Marshall for their assistance in the preparation of this paper.

REFERENCES

(1) J. C. Wilkins and R. E. Pence, "A Study of the Microstructure of Precipitation Hardening Stainless Steel Sheets," *Advances in Electron Metallography and Electron-Probe Microanalysis, ASTM STP 317*, Am. Soc. Testing Mat., 1962.

(2) P. M. Kelly and J. Nutting, "Techniques for the Direct Examination of Metal by Transmission in the Electron Microscope," *Journal of the Institute of Metals*, Vol. 87, pp. 385–391.

(3) J. Nutting, "Electron Transmission Metallography of Hardening Mechanism in Metal," *ASM 1960 Seminar on the Strengthening Mechanisms in Solids*, Am. Soc. Metals, pp. 93–99.

(4) R. B. Nicholson, G. Thomas, and J. Nutting, "Electron-Microscopic Studies of Precipitation in Aluminum Alloys," *Journal of the Institute of Metals*, Vol. 87, 1958–59, pp. 429–438.

(5) H. C. Burnett, R. H. Duff, and H. C. Vacher, "Identification of Metallurgical Reactions and Their Effect on the Mechanical Properties of 17-7PH Stainless Steel," *Journal of Research*, National Bureau of Standards, Vol. 66C, No. 2, April–June, 1962.

(6) A. Taylor, *X-Ray Metallography*, John Wiley and Sons, Inc., New York, N. Y., 1961.

(7) A. J. Bradley and A. Taylor, "An X-Ray Study of the Fe-Ni-Al Ternary Equilibrium Diagram," *Proceedings*, Royal Soc., London, Vol. 166, 1938, p. 353.

(8) R. W. Guard, "Mechanisms of Line Particle Strengthening," *ASM 1960 Seminar on the Strengthening Mechanism in Solids*, Am. Soc. Metals, pp. 262–264.

DISCUSSION

W. G. WILSON[1]—A previous paper by Perry indicates nitrogen is a potent factor in toughness. Does your work indicate any nitrogen precipitates?

J. C. WILKINS (*author*)—In the air-melted steels investigated, the nitrogen is combined as stable titanium or aluminum nitrides or both. There is no nitrogen available for the formation of precipitates during any of the thermal treatments.

K. J. GODA[2]—What role does molybdenum play in hardening and strengthening PH15-7Mo? I was surprised that no evidence of molybdenum was found in the $M_{23}C_6$-type carbide.

MR. WILKINS—Molybdenum is added to the PH stainless steels to improve room- and high-temperature properties for all conditions of heat treatment. This is apparently accomplished by a solid solution strengthening mechanism in these steels at this level of molybdenum.

MR. GODA—The Bureau of Standards hypothesized that ordered ferrite may be the strengthening mechanism of 17-7PH. What is your comment on this?

MR. WILKINS—Mr. Goda is referring to Ref. 5 of this paper, where the electron diffraction patterns indicated the presence of a (B_2)CsCl-type body centered cubic structure which was interpreted as ordered ferrite (α' ferrite), a designation given by Bradley in the aluminum-iron-nickel system. The ASTM X-Ray Powder Data File interprets the diffraction pattern to correspond to the NiAl precipitate. The electron diffraction patterns obtained by their work and by our work are the same. The only difference is the nomenclature used to express the identity of the precipitate. We prefer to refer to the precipitates as NiAl and Ni_3Al. This is pointed out in the paper, but was omitted in the oral presentation.

[1] Molybdenum Corporation of America, Pittsburgh, Pa.

[2] Carpenter Steel Co., Reading, Pa.

A STUDY OF INTERNAL-FRICTION PEAKS IN TYPE 304 STAINLESS STEEL CONTAINING NITROGEN

By J. F. Eckel[1] and C. R. Manning, Jr.[2]

Synopsis

Internal-friction studies were made on 304 austenitic stainless steel to determine if this is a valid method for measuring interstitial diffusion in face-centered metals and alloys. Both unnitrided and nitrided 304 stainless steel wires were tested in a torsional pendulum at frequencies from 0.33 to 1.1 cps. Internal-friction spectra were recorded and analyzed. The conclusions reached were that interstitial atoms can cause relaxation peaks to appear on the internal-friction spectra and that the observed peaks were much broader than nitrogen-induced peaks in body-centered cubic materials.

The occurrence of internal-friction peaks in body-centered cubic-type structures caused by interstitial atoms, such as nitrogen, has long been known. The mechanism to account for the internal-friction peaks in body-centered cubic-type structures has been described in detail by Snoek (1).[3] A parallel-type study of internal friction in face-centered cubic-type structures has not progressed to a position where the present theories can account completely for the observed phenomena. The first study of interstitial additions to face-centered cubic-type structures utilizing internal-friction measurements was by Rozin and Finkel'-shteyn (2) using 25 nickel-20 chromium steel in 1953. Other work has been carried on since then by scientists of the Academia Sinica on pure nickel and manganese steels. This work, as well as the work in Ref. (2) utilized only carbon as the interstitial atoms, but results from both studies pointed to the fact that the peaks were induced by diffusion of the interstitial atoms in the face-centered cubic lattice. In the paper presented here, the effect of nitrogen additions on the internal-friction behavior of 18-8 face-centered cubic austenitic stainless steel was studied by the use of a torsional pendulum.

Theoretical

There have been two theories postulated to explain the internal-friction peaks found in face-centered cubic metals associated with interstitial atoms. Both theories are based on the formation and rotation of an atomic pair causing anisotropic lattice distortion and stress-induced diffusion.

Atom Pair Rotation Theory of Cheng and Chang:

The first theory was proposed by Cheng and Chang (3) and is explained in detail by Wu and Wang (4). The theory can best be explained using Fig. 1 where a vacancy is shown at the $(\frac{1}{2}, \frac{1}{2}, 0)$ position. It postulates that an interstitial nitrogen atom may jump into this vacancy, thus forming a substitutional nitrogen atom. This would cause a dissipation of a certain amount of thermal energy and if another nitrogen atom should jump into the previously vacated interstitial position, more energy would be released and a stable nitrogen pair would be formed. This pair would consist of an interstitial nitrogen atom and a substitutional nitrogen atom. The nitrogen pair is formed at $(\frac{1}{2}, \frac{1}{2}, 0)$ and A_1 positions, and their axis is parallel to the A direction. Application of a compressive stress along the A-axis causes the interstitial nitrogen atom at Position A_1 to jump to Position B or a corresponding position in the C direction, thus providing some relief in the lattice strain. The nitrogen pair that was parallel to the A-axis or the load axis has rotated outward and is now normal to the A-axis. If a tensile load is applied along the A-axis through the nitrogen pair, a nitrogen atom that was in the B or C interstitial position will jump to the A_1 or A_2 position, corresponding to a rotation of the pair axis from a direction perpendicular to the tensile axis into a position parallel to it.

Cheng and Chang have stated that the stress relaxation resulting from the pair rotation induces the internal friction and that the mechanism for its generation is identical to that causing interstitial diffusion in α-iron. The only difference is the distance traveled by the atoms. In a body-centered cubic lattice, the interstitial atom moves $\frac{1}{2}\ a_o$ per jump along the $\langle 010 \rangle$, while in a face-centered cubic lattice, the movement is $\sqrt{2}a_o/2$ along $\langle 110 \rangle$ (where a_o is the lattice parameter).

They also postulated that because of the similarity of the diffusion peaks, the formula governing the peak magnitude for body-centered cubic lattices is applicable and that the effect of interstitial concentration on E_m (the unrelaxed modulus of elasticity) and E/N_r (the change in strain per unit volume caused by rotation of the axis to a direction parallel to the tensile axis) can be neglected in the face-centered cubic lattice giving

$$Q^{-1}_{\max} = \frac{CN_F}{T_1} \qquad (1)$$

where:

Q^{-1} = the peak height,
T_1 = the peak temperature,
N_F = the concentration of interstitial pairs, and
C = a constant.

Nitrogen pairs are formed by interaction between nitrogen atoms that have jumped into vacancies and their interstitial nitrogen neighbors. The number of pairs N_F under a fixed nitrogen concentration can be determined by: (1) the concentration of vacancies and (2) the state of the nitrogen distribution. Each of these is sensitive to temperature fluctuations and can be determined as follows: (The number of vacancies frozen in the crystal depends upon the cooling rate of the specimen.)

1. Wu and Wang (4) have investigated the number of lattice vacancies available in a face-centered cubic lattice. Their investigations with ferrous alloys were made by quenching wire specimens from 1200 C to below 350 C where the vacancies were assumed to be immobile. The

[1] Head, Department of Metals & Ceramic Engineering, Virginia Polytechnic Inst., Blacksburg, Va.

[2] Research metallurgist, National Aeronautical Space Administration, Langley Field, Va.

[3] The boldface numbers in parentheses refer to the list of references appended to this paper.

Copyright© 1965 by ASTM International

www.astm.org

cooling rate was estimated from the following equation:

$$\frac{\partial T}{\partial t} = \gamma\left(\frac{\partial^2 T}{\partial t^2} + \frac{1}{r}\frac{\partial T}{\partial r}\right) \quad \ldots\ldots(2)$$

where γ is thermal diffusivity and r is the radius of the wire. Their calculations indicated that a cooling time from 1200

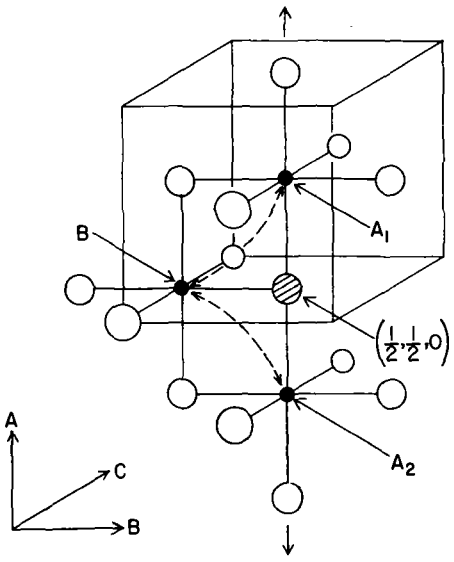


FIG. 1—Interstitial Atom Pair Diffusion in Cubic Lattices (according to Cheng and Chang, Ref. 3).

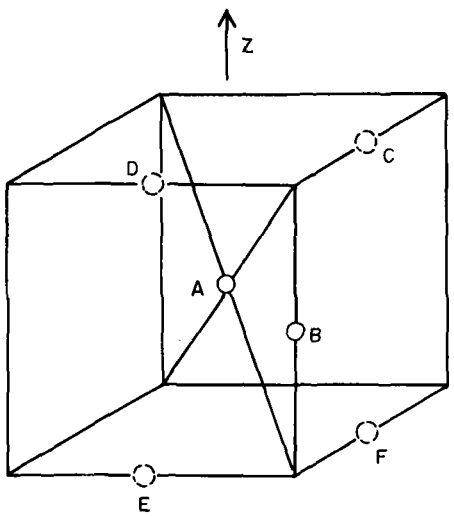


FIG. 2—Interstitial Atom Pair Diffusion in Cubic Lattices (according to Tsien, Ref. 5).

to 350 C of 0.04 sec was achieved. The majority of the supersaturated vacancies did not have a chance to move and were frozen in. Thus, at the temperature of most internal-friction measurements, the lifetime of the vacancies is probably that of several years.

2. The state of the nitrogen atoms or redistribution is a function of the activation energy, E_F, for vacancy formation. A specimen with constant vacancy concentration, such as being dealt with in internal-friction studies, should have an increasing nitrogen pair concentration with decreasing temperature if the atoms have enough mobility to attain thermal equilibrium at each temperature.

Their theory also states that the height of the internal-friction peaks varies parabolically with low nitrogen concentration and linearly with high nitrogen concentration.

Atom Pair Rotation Theory of Tsien:

The second theory put forward to explain internal-friction peaks in face-centered cubic lattices was recently published by Tsien (5). A second face-centered cube shown in Fig. 2 is used to describe their theory. The interstitial positions A and B are occupied by an atomic pair. The very presence of the interstitial pair can cause an anisotropic distortion in the lattice. In the A-B direction, the distortion of the cube is greater than in a direction normal to it. Applying a tensile stress in the Z direction will cause either Atom A or Atom B to become unstable and one will be forced to jump to either position D, D, E, or F to relieve the lattice strain. This will position the pair so that the angle between them and the direction of the stress is a minimum. This causes a maximum relaxation to be obtained, whence arises more anelastic deformation in the direction of the stress. It is the same nature as internal-friction peaks in body-centered cubic lattices caused by interstitial atoms. Tsien states that the activation energy of the internal-friction peaks is equivalent to the activation energy of the diffusion of interstitial atoms, and the peak height is proportional to the number of nitrogen pairs. Statistical theory indicated that the number of interstitial pairs is proportional to the square of the interstitial content.

TABLE 1—HEAT ANALYSIS OF TYPE 304 STAINLESS STEEL WIRE, PER CENT.

C	0.070
Mn	1.02
P	0.020
S	0.026
Si	0.51
Cr	18.46
Ni	10.28

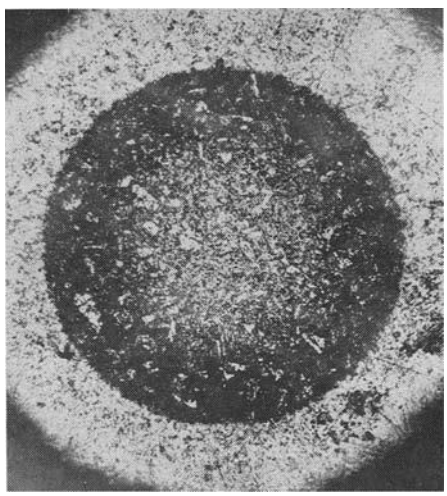


FIG. 3—Nitrided Case on Type 304 Stainless Steel Wire.

EXPERIMENTAL PROCEDURE

Torsional Pendulum:

The apparatus used to conduct the internal-friction tests consisted of a torsional pendulum which was fashioned after the equipment designed by Ke (6). The frequency of vibration covered a range of 0.33 to 1.1 cps.

Specimen Preparation:

All specimens were in the form of 0.025-in.-diameter AISI 304 austenitic stainless steel wire that had been cold drawn. The heat analysis of the wire is given in Table 1, and a nitrogen analysis by Allegheny-Ludlum Steel Corp. showed 0.05 per cent nitrogen. Andrews (7) stated that cold drawing causes some of the austenite to be transformed to α-iron. To make sure that the wire used in this investigation was fully austenitic, specimens were encapsulated in an evacuated Vycor tube and solution heat treated 48 hr at 1025 C and water quenched. Another set of wires from the same coil was nitrided by placing them in a furnace for 40 hr at 925 C and passing ammonia through the furnace. The ammonia dissociated and entered the lattice as monatomic nitrogen. The nitrogen was found to be driven well into the lattice of the wire as shown in Fig. 3 by the heavily nitrided case. These wires were then encapsulated and heat treated as stated before. The solution treatment was designed to drive nitrogen through the lattice and produce a homogeneous structure. All wires subjected to the solution treatment were placed in small ceramic tubes within the evacuated Vycor glass tube. This served as an effective method to remove camber and to provide straight specimens.

RESULTS AND DISCUSSION

The study was originally initiated to determine whether interstitial nitrogen

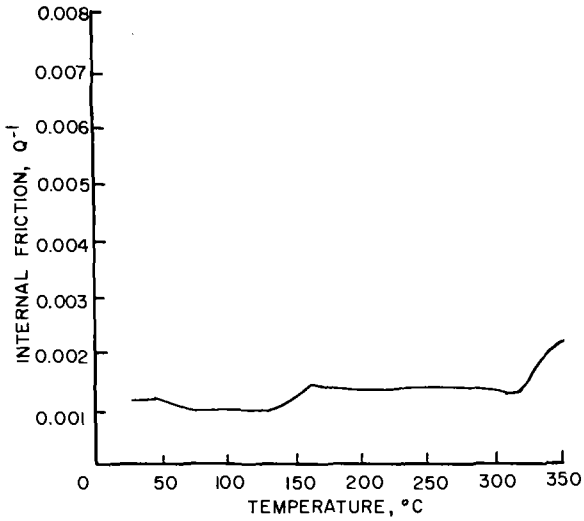


FIG. 4—Relaxation Spectrum at a Frequency of 1.05 cps for Unnitrided Type 304 Stainless Steel.

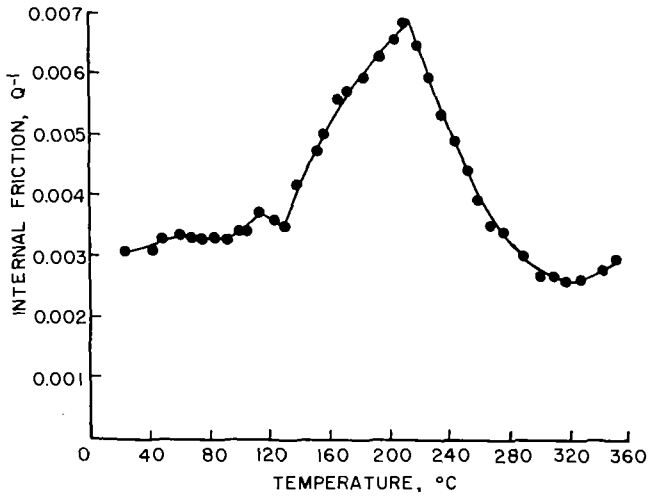


FIG. 5—Relaxation Spectrum of Type 304 Stainless Steel Containing Nitrogen at a Frequency of 1.09 cps.

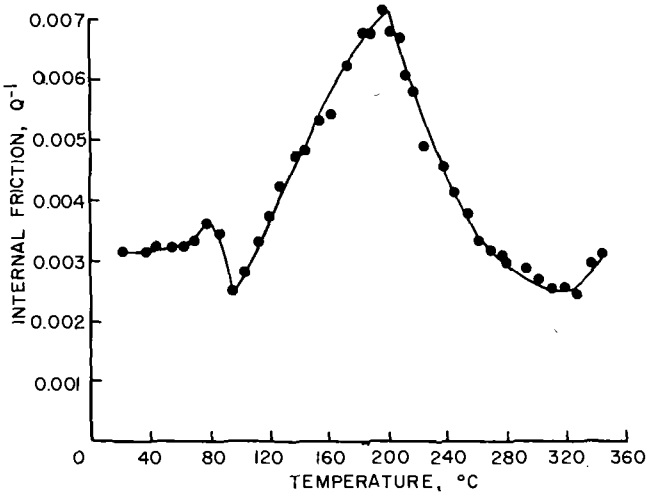


FIG. 6—Relaxation Spectrum for Type 304 Stainless Steel Containing Nitrogen at a Frequency of 0.57 cps.

could cause internal-friction peaks in austenitic stainless steel. If it did induce relaxation peaks in the austenite, it was also the purpose to determine both activation energy and the diffusion constants for nitrogen diffusion in austenite. The frequency of vibration was varied during the investigation to allow activation energy calculations from maximum peak shifts.

Relaxation Spectra:

Figure 4 shows the relaxation spectrum for the unnitrided 304 stainless steel wire which was solution heat treated 48 hr at 1025 C and water quenched to maintain the austenitic structure. It was then tested at 1.05 cps. No major peaks were recorded below 325 C, and the peak starting at 325 C is believed to be associated with stress-induced formation of ferrite or quasimartensite because the wires became slightly magnetic after testing. A metallographic examination before and after testing revealed no major structural changes and did not show ferrite.

The relaxation spectra for heavily nitrided and solution heat treated specimens are shown in Figs. 5–7. The frequency of vibration employed in Fig. 5 was 1.09 cps. A major peak was noted in the spectrum with a maximum amplitude at 210 C which is believed to be caused by nitrogen. This peak was noticeably absent in the spectra of the unnitrided wires. The spectrum shown in Fig. 6 is for a vibrational frequency of 0.57 cps, and a major peak was noted with a maximum at 200 C. The upper spectrum in Fig. 7 was obtained with a frequency of 0.33 cps, and the major peak shifted to a still lower temperature of 192 C. After making this run, it was decided to cool the same specimen without removal from the apparatus and make an additional run. This resulted in a new relaxation peak at a much higher temperature, 249 C, but with a much lower amplitude. The results of this run are shown in Fig. 7. Ke and Yang (8) have reported that the separation and precipitation of carbon or other interstitial atoms, such as nitrogen, from solid solution, not only has the effect of lowering the amplitude of the internal-friction peaks, but also shifts the peak towards a higher temperature as experienced here. It was felt that the nitriding and solution heat treatment drove an excessive amount of nitrogen into the interstitial positions of the lattice.

Thus, supersaturation is indicated prior to the first run in Fig. 7. Evidence to support this was found by X-ray diffraction measurements. The normal iron-face-centered cubic lattice parameter as reported by Dijkstra (9) is 3.54 A. The atomic radius of iron is 1.26 A. The 304 austenitic stainless steel contains 18 per cent chromium and 8 per cent nickel in solid solution as the major alloying elements. The atomic radii of these two are only 1.28 and 1.25 A,

respectively. Therefore, not much increase in the lattice parameter would be expected, and Ke and Wang (10) reported a value of 3.62 A. A Debye Sherrer pattern of the nitrided wire was made, and the lattice parameter was found to be 4.15 A. This indicated that the lattice was considerably expanded by nitrogen. Ke and Yang (8) have stated that the amplitude of the relaxation peak is a function of the amount of the interstitial atom in solution. A nitrogen analysis showed 2.20 per cent nitrogen in the alloy after nitriding and solution heat treating. The decrease in amplitude is interpreted as resulting from formation of additional nitrides and lowering of the amount of nitrogen in solid solution. The microstructure before and after testing indicated many more nitrides were formed as the result of testing. A third run was made on the same specimen which produced an almost identical relaxation spectrum with that of the second. The magnitudes of the internal-friction peaks were essentially equal, indicating the amount of free nitrogen in the interstitial positions of the lattice had been stabilized. A fourth run was made at a higher frequency (0.66 cps) to displace the peak and permit calculation of the activation energy from these peaks. The peak temperature was 264 C, and the amplitude of the peak is comparable to the amplitude of carbon peaks found by Ke and Wang (10) in 18-8 stainless steel.

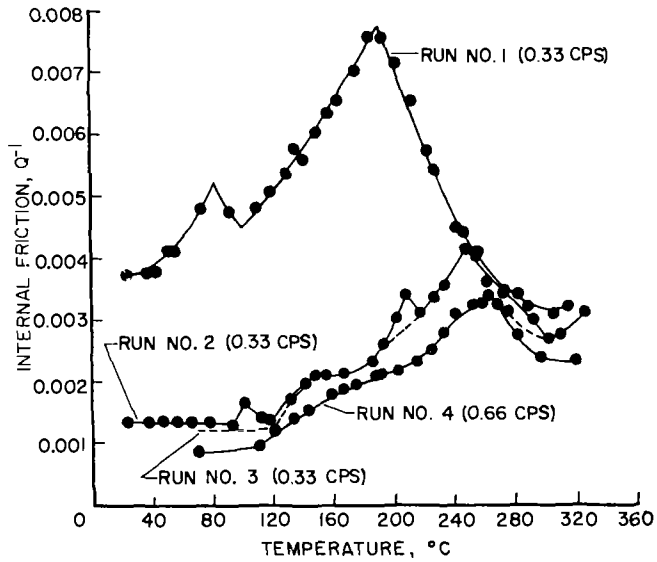


FIG. 7—Relaxation Spectra for Type 304 Stainless Steel Containing Nitrogen.

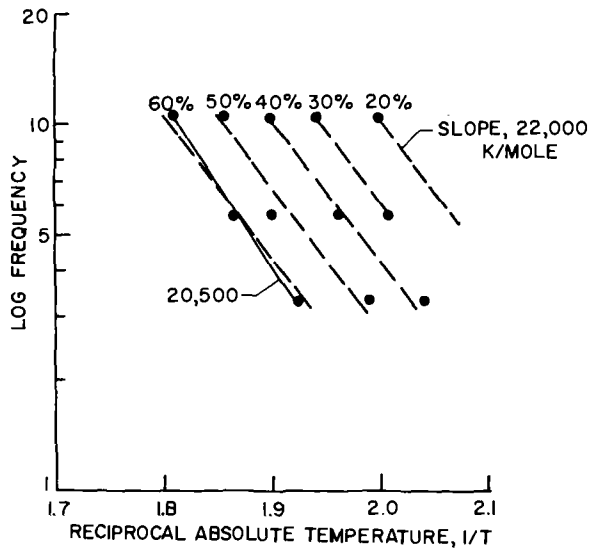


FIG. 8—Relationship Between Frequency and Absolute Temperature on the Lower Side of the Peak.

Activation Energy:

The use of various vibrational frequencies produced relaxation peaks at various temperatures which provided sufficient data to calculate the diffusion coefficient of nitrogen in austenite. These calculations were based on the assumption that the peaks being utilized were associated with a single relaxation time and that the process is diffusion controlled. The activation energy was obtained by calculation from data shown in Figs. 5–7 using the following equation:

$$\Delta H = 2.3R\left(\frac{\log f_1}{1/T_2} - \frac{\log f_2}{1/T_1}\right) \quad \ldots\ldots(3)$$

where f is the vibrational frequency in cycles per second, and T is the absolute temperature. It was found to be 28,700 cal/mole for the supersaturated solid solution and 25,800 cal/mole for the saturated solid solution. Values of activation energy for diffusion of carbon in α-iron reported by Wert (11) and in austenitic 18-8 stainless steel reported by Ke and Yang (8) were 20,000 and 30,000 cal/mole, respectively. Thus, the calculated values of 25,800 to 28,700 cal/mole found for activation energy of nitrogen diffusion in austenite seem to be very reasonable.

There appear to be some limitations to calculation of activation energy for the nitrogen diffusion in austenite by the above method. Calculation of the activation energy for nitrogen diffusion in austenite from half width measurements as suggested by Stephenson[4] gives values of 8,500 cal/mole which is much less than the expected value of 17,500 to 19,500 cal/mole. This is approximately two-thirds of the 25,800 to 28,700 cal/mole found by the frequency change measurements. The two-third value would be expected from measurements on body-centered cubic lattices. Cheng and Chang's theory considered interstitial atoms jumping into vacancies. If this were so, it would seem that the activation energy for stress-induced microdiffusion should be much lower than the activation energy found for macrodiffusion. Ke, Tsien, and Misek (12) found that the microdiffusion measurements for carbon atoms were slightly higher than the macrodiffusion measurements made by radioactive C^{14}. The theory of Tsien which does not depend on lattice vacancies and interstitial atoms jumping into substitutional positions would predict that the activation energy for microdiffusion would be equal to that of the macrodiffusion, and experimental discrepancies could give slightly higher values for either. Therefore, the theory of Tsien appears to be more plausible.

Ke and Yang (8) showed that internal friction induced by carbon in austenitic

[4] E. T. Stephenson, private communication.

stainless steels with a manganese content of 1.7 per cent was similar to pure nickel, and from this it was concluded that the internal-friction peak was caused by rotation of interstitial atomic pairs. For alloys containing large amounts of alloying elements the situation appears quite different, and these alloying elements may influence the interstitial atoms to a large degree. If one of the alloying elements shows a greater affinity for interstitial atoms than another, it may reduce the opportunity for the formation of the interstitial atomic pairs and may instead cause the formation of an alloying element interstitial pair. This would induce a number of relaxation times and complicate the interpretation.

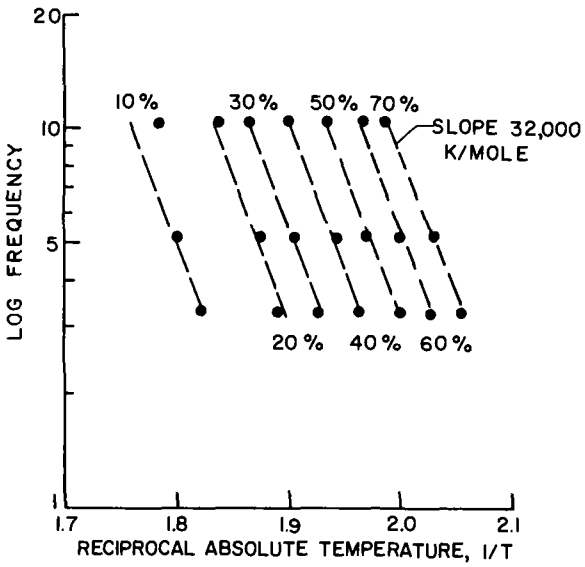


FIG. 9—Relationship Between Frequency and Absolute Temperature on Upper Side of Peak.

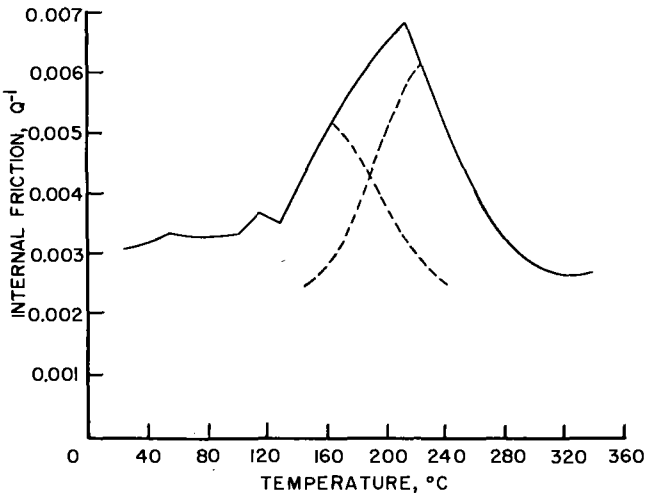


FIG. 10—Probable Form of Double Peak in Relaxation Spectrum.

Analysis of Relaxation Peaks:

Laxar, Frame, and Blickwede (13) have shown that a relaxation peak might be interpreted to have a single relaxation time but in reality may have multiple relaxation times. The activation energy can be calculated for a shift of any point on the relaxation peak as noted by Wert and Zener (14). This type analysis was applied to the curves in Figs. 5–7 for both the upper and lower side of the curve from 10 to 60 per cent of peak height on the low-temperature side and from 10 to 70 per cent of the peak height on the high-temperature side. The results are plotted in Figs. 8 and 9, and an average activation energy was calculated for each set of data. The value for the lower side activation energy was 22,000 cal/mole and for the upper side 32,000 cal/mole. The semi-log plots of frequency versus reciprocal of the absolute temperature, show the experimental points are connected by lines with activation energy values of 22,000 and 32,000 cal/mole. The results show very little scatter, although the results on the low-temperature side are not as consistent as on the high-temperature side. This consistency is a good indication that there are probably two separate relaxation times involved in this peak and in Fig. 10, the dotted line gives the probable breakdown of the involved peaks.

The question remains, what is causing the two relaxation peaks found in the austenite? One peak is probably caused by the rotation of the interstitial nitrogen pairs, and the other must be caused by an interaction between the nitrogen and an alloying element. It has been reported that when manganese is added to iron-carbon alloys, it may reduce the opportunity for formation of interstitial atom pairs. Thus, there may be a greater probability of formation of manganese-carbon atom pairs. In steels with a high manganese content, the internal-friction peak is caused by manganese-carbon atom pairs and not by carbon-carbon atom pairs. The amount of manganese in this alloy is not expected to interact in this way with the nitrogen nor is silicon, although silicon nitrides have been identified. The second peak is probably caused by an interaction with chromium. A nitrogen-chromium interaction has been reported by Dijkstra and Sladek (15). No evidence of nickel interaction with the nitrogen could be found in the literature. More work on face-centered cubic materials is needed to help identify the mechanism responsible for the broad relaxation peaks. It is believed that the first peak with an activation energy of 22,000 cal/mole represents nitrogen pair activity and that the second peak with an activation energy of 32,000 cal/mole is associated with the interaction between nitrogen and chromium. It is also felt strain aging may account for some of the internal friction.

CONCLUSIONS

The addition of nitrogen to 18-8 type austenitic stainless steels caused relaxation peaks to appear on the internal-friction spectra. These peaks appear to be much broader than nitrogen-induced peaks in body-centered cubic structures, and there is a strong indication that the peaks are not the results of a single activation process. A detailed analysis indicates the major peaks probably contained two smaller peaks with activation energies of 22,000 and 32,000 cal/mole. The lower temperature peak was probably caused by the rotation of the interstitial nitrogen pairs, while the other one was probably caused by the interaction of the atomic nitrogen with chromium

as a major alloying element.The amplitude of the peak also appears to be a function of the amount of nitrogen in solid solution.

Acknowledgments:

The authors would like to thank E. T. Stephenson of the Bethlehem Steel Co. and Adolph Lena of the Allegheny-Ludlum Steel Co. for their very helpful criticism of this paper. Also, thanks are expressed to R. A. Lincoln of the Allegheny-Ludlum Steel Co. for the nitrogen analysis and to the National Standard Co. who furnished the wire used in the investigation.

REFERENCES

(1) J. L. Snoek, *Physica*, Nederlandse Natuurekundige Vereniging, Netherlands, Vol. 6, 1939, p. 591; Vol. 8, 1941, p. 711; 1942, p. 862.

(2) K. M. Rozin and B. N. Finkel'shteyn, "Study of Phase Transformations by Internal Friction Method," *SSR* (Reports of the Academy of Science USSR), Vol. 91 (153), p. 811.

(3) K. C. Cheng and H. K. Chang, private communication to T. L. Wu and C. M. Wang, (see Ref. 4 below), Nanking University, 1957.

(4) T. L. Wu and C. M. Wang, "Mechanism of Carbon Diffusion Peak in F.C.C. Iron-Nickel Alloys," *Scientia Sinica*, Vol. 10, No. 5, 1958, pp. 1029–1053.

(5) C. T. Tsien, "On the Mechanism of Internal Friction Peak Induced by Diffusion of Interstitial Atoms in Face-Centered Cubic Crystals," *Scientia Sinica*, Vol. 10, No. 8, 1961, pp. 930–937.

(6) T. S. Ke, "Experimental Evidence of the Viscous Behavior of Grain Boundaries," *Physical Review*, Vol. 71, 1947, pp. 533–541.

(7) K. W. Andrews, "An X-ray Examination of Preferred Orientation and Transformation of Gamma to Alpha Iron in a Stainless Steel Wire," *Journal of Iron and Steel Inst.*, Vol. 184, 1956, pp. 274–286.

(8) T. S. Ke and P. W. Yang, "A Study of the Diffusion of Carbon in Gamma Iron by the Method of Internal Friction," *Scientia Sinica*, Vol. 6, No. 4, 1957, pp. 623–643.

(9) L. J. Dijkstra, "Elastic Relaxation and Some Other Properties of Solid Solution of Carbon and Nitrogen in Iron, "*Phillips Research Report*, Vol. 2, 1947, pp. 357–381.

(10) T. S. Ke and C. M. Wang, "Internal Friction Peaks Associated with Stress-Induced Diffusion of Carbon in Face-Centered Cubic Alloy Steels and Metals, *Scientia Sinica*, Vol. 4, No. 4, 1955, pp. 501–518.

(11) C. Wert, "The Metallurgical Use of Anelasticity," *Modern Research Techniques in Physical Metallurgy*, Am. Soc. Metals, 1953, pp. 225–250.

(12) T. S. Ke, C. H. Tsien, and C. Misek, "On the Internal Friction Peaks Associated with the Presence of Carbon in Nickel," *Scientia Sinica*, Vol. 4, No. 4, 1955, pp. 519–526.

(13) F. H. Laxar, J. W. Frame, and D. J. Blickwede, "The Effect of Aluminum on Strain Aging and Internal Friction in Low Carbon Steel," *Transactions*, Am. Soc. Metals, Vol. 53, 1961, pp. 683–696.

(14) C. Wert and C. Zener, "Interstitial Atomic Diffusion Coefficients," *Physical Review*, Series 2, Vol. 76, August, 1950, p. 601.

(15) L. J. Dijkstra and R. J. Sladek, "Effect of Alloying Elements on the Behavior of Nitrogen in Alpha Iron," *Transactions*, Am. Institute of Mining, Metallurgical, and Petroleum Engrs., Vol. 197, 1953, p. 69.

DISCUSSION

L. R. SCHARFSTEIN[1]—How was the nitrogen homogenized in the alloy after a case in NH_3 was accomplished?

C. R. MANNING, JR. (*author*)—The specimens were encapsulated in Vycor tubing under vacuum and homogenized at 1880 F for 40 hr and then water quenched to retain a completely austenitic structure.

MR. SCHARFSTEIN—Would it not be interesting to compare results with different methods of placing nitrogen in the alloy—such as during melting?

MR. MANNING—We feel that more work should be done such as changing the nitrogen level as well as introducing the nitrogen during melting, but if the nitrogen is homogenized properly after introduction by any method, very little difference in the results would be expected.

[1] Carpenter Steel Co., Reading, Pa.

ROPING AND INTERGRANULAR CORROSION OF 430 STAINLESS STEEL

By E. A. Parker[1]

Synopsis

Heat treating Type 430 stainless steel above 1650 prior to cold rolling in order to produce a lower roped steel results in sensitization of the steel on fast cooling. This sensitization causes rapid intergranular corrosion in hot nitric-hydrofluoric acid solutions unless the steel is desensitized prior to immersion. The time-temperature relationship for desensitization is given. In addition, a possible mechanism for sensitization-desensitization in ferritic stainless steels is presented.

During severe forming operations, thin gage 430 stainless steel strip tends to develop on its surface a series of ridges and valleys parallel to the cold-rolling direction. This surface phenomenon is called "roping" and is common to the ferritic stainless steels in about the 14 to 25 per cent chromium range. The reason roping occurs has not been determined, although carbide banding or preferred orientation have often been offered as possible causes.

Nevertheless, there apparently are two known methods of lowering the roping characteristics of these grades. One of these is by selective alloying; the other is by proper heat treatment of the hot band prior to cold rolling and final annealing.

Evans (1)[2] has indicated that columbium in the amount of 0.25 to 0.60 per cent minimizes the tendency to rope. Thompson and Lamont (2) confirmed the effect and also studied the effect of small additions of other elements. However, the production of low roped 430 stainless steel by the use of alloying elements is costly, and for this reason special heat treatments are often used to obtain a similar effect.

The heat treating characteristics of 430 stainless steel can be better understood with the help of the 17 per cent chromium-0.10 per cent carbon-iron phase diagram (Fig. 1). The important aspect of this diagram, exclusive of the carbide reactions, is that a two-phased $\alpha + \gamma$ region exists extending up to about 17 per cent chromium. In the commercial 430 alloy this range is moved to higher chromium contents because of the presence of austenitizers such as nitrogen and manganese, and the composition line falls in the two-phase field. The lower limit of this field is about 1610 F as reported by Nehrenberg and Lillys (3), and about 30 per cent austenite forms in this two phase field at temperatures such as those used during hot working. The austenite readily transforms to brittle martensite on air cooling. A hot-rolled coil, therefore, contains ferrite and martensite, as well as carbides which precipitate during cooling. In order to soften the material prior to cold rolling, the alloy is generally box annealed below the A_1, at about 1500 F. This treatment tempers the martensite and produces a recrystallized banded structure containing ferrite and carbides. The microstructures before and after annealing are shown in Fig. 2.

A lower roped material than normally obtained by conventional annealing also can be produced without changing the base composition, and it is made by heating the hot band above the A_1 temperature prior to cold rolling. However, when the alloy is heated above this temperature and cooled fairly rapidly, the alloy becomes sensitized and intergranular corrosion occurs during pickling in hot nitric-hydrofluoric acid solutions.

Examples of material that have and have not been attacked intergranularly are shown in Fig. 3. Specimens are shown at $\times 2$ and $\times 500$ magnification after being bent 180 deg after pickling. The attacked specimen at $\times 2$ magnification shows a crystalline surface, whereas the other specimen has a bright surface. At the higher magnification, the surface of the sensitized specimen shows intergranular attack to a depth of several grain diameters. The other specimen shows no intergranular corrosion.

The attack appears to vary according to the cooling rate from the annealing temperature, although the slowest cooling rate that provides immunity to attack has not been established. The material usually is cooled slowly enough to prevent transformation of austenite to martensite, but even with complete absence of martensite the attack can occur.

The attack is usually sufficiently detrimental so that cold rolling cannot be carried out unless the surface layers of the sheet are removed by an expensive grinding operation. The high-temperature treatment thus cannot be utilized because of the adverse effects of sensitization and intergranular corrosion.

In order to make use of the lower roping benefits obtained from a high-temperature treatment, work was undertaken to further study the phenomenon of intergranular corrosion of ferritic steels in nitric-hydrofluoric acid (HNO_3-HF) solutions. It was anticipated that a special thermal treatment could be devised whereby the lower roping tendency could be obtained without having the material susceptible to intergranular corrosion during pickling. The work in this report, therefore, covers the results obtained in trying to reach this objective.

Prior Work

A great deal of information has been published about intergranular corrosion of stainless steels. The majority of the published work deals mainly with the phenomenon as it occurs in austenitic types and not the ferritic types of stainless steels.

Austenitic stainless steels become sensitized by heating them in the temperature range of about 1000 to 1500 F. Carbide precipitation occurs at the grain boundaries, and the material is made susceptible to intergranular attack in various media. The susceptibility can be removed by reheating the alloy at temperatures above the sensitizing region to redissolve the carbides. This is

[1] Service metallurgist, Stainless and Strip Div., Jones & Laughlin Steel Corp., Louisville, Ohio.

[2] The boldface numbers in parentheses refer to the list of references appended to this paper.

Copyright© 1965 by ASTM International

www.astm.org

generally carried out at temperatures of 1800 F and higher, and carbide reprecipitation is prevented by means of a rapid cool.

In ferritic stainless steels the effects of temperature were originally thought to be completely opposite to those of the austenitic steels. Some of the first work indicated that sensitization occurred at high temperatures, as during welding, and desensitization occurred at the lower temperatures. Kiefer (5) observed that intergranular corrosion occurred closely adjacent to weld zones in specimens of 430 stainless steel that were tested in boiling 65 per cent nitric acid. The susceptibility to attack was removed on treating the welded specimens at 1300 F. Houdremont and Tofaute (6) showed that the ferritic stainless steel grades of 15 to 30 per cent chromium became sensitized on heating above 1560 F followed by rapid cooling. They ran corrosion tests in boiling copper sulfate-sulfuric acid solution (Krupp test)[3] and determined that additions of titanium of six times the carbon content increased the resistance to intergranular corrosion.

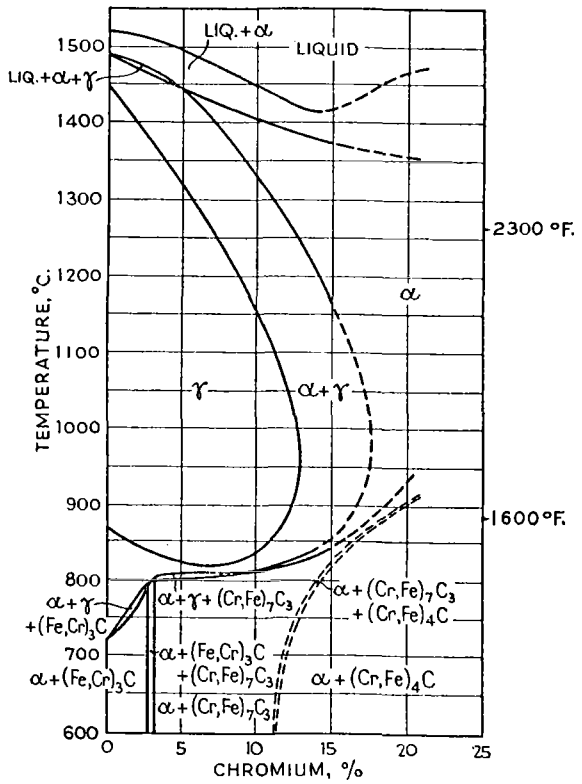
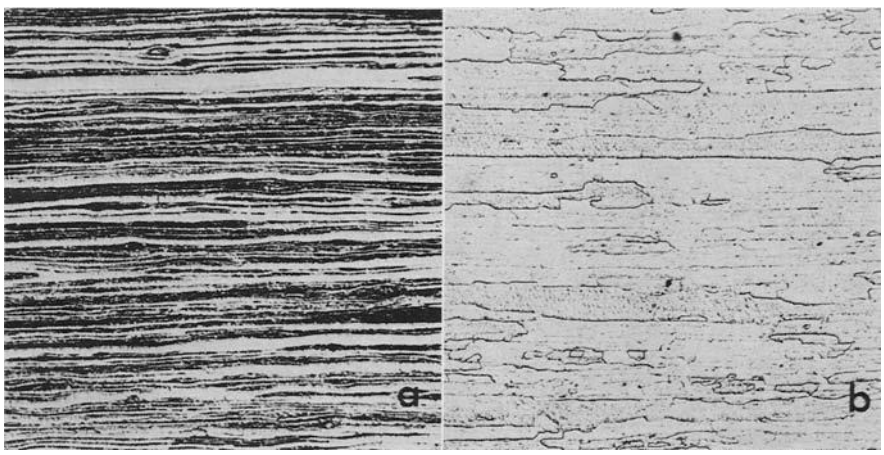


FIG. 1—Section Through the Fe-Cr-C Diagram at 0.1 Per Cent C (according to Tofaute et al (3)).



(*a*) Before annealing.
(*b*) After annealing.

FIG. 2—Microstructures of 430 Hot Band Before and After Annealing at 1500 F (×100).

Lula et al (7) investigated 16 to 28 per cent chromium steels and subjected welded specimens and individually heat treated specimens to Krupp and Huey tests.[4] Again sensitization occurred after heating at high temperatures followed by rapid cooling. However, they showed that sensitization actually took place during cooling and not while the material was at the higher temperatures. Freedom from sensitization was obtained by very rapid quenching of thin wires from the high temperatures. Therefore, in this respect the ferritic stainless steels were actually somewhat similar to the austenitic types. Both must be cooled rapidly from elevated temperatures in order to prevent sensitization, although the ferritic steels must be cooled much more rapidly. It is, therefore, incorrect to refer to sensitization of ferritic steels as occurring at the higher temperatures. It would perhaps be more proper to refer to "solutioning" at these higher temperatures.

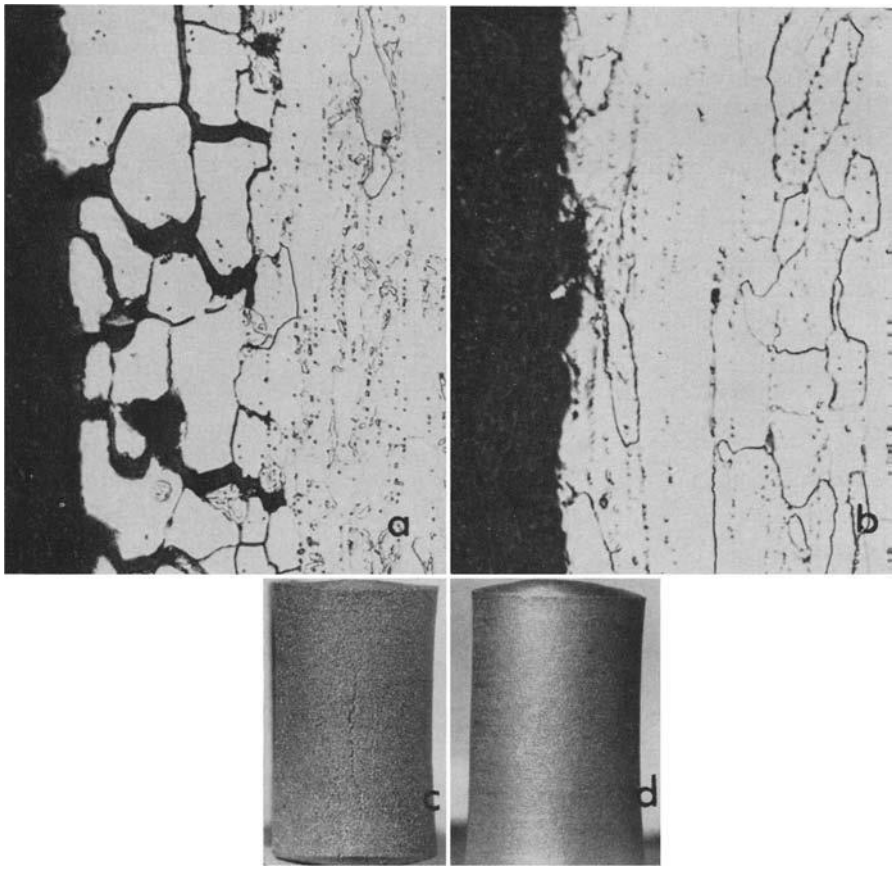
The work by Lula et al showed that sensitization would occur on cooling after specimens had been heated above 1700 F up to the melting point, although it was indicated the solution temperature might be time dependent. They further demonstrated that sensitized material could be desensitized on reheating in the temperature range of 1200 to 1500 F. This is the uppermost part of the range where the austenitic steels become sensitized. In this respect the ferritic stainless steels react opposite to the austenitic types.

Lula et al also indicated the susceptibility could be removed by furnace cooling from the solution temperature by passing through the sensitization range slowly. The susceptibility to attack was also found to vary with test solution, the Huey test being more severe than the Krupp test. Using the Huey test, they found that 430 stainless steel with a titanium to carbon ratio of 17.5 was not completely immune to intergranular corrosion.

The majority of the reported work has been carried out using either the copper sulfate-sulfuric acid solution or the Huey test. Both of these solutions are useful in studying the mechanism of attack. Little work has been done in using HNO_3-HF solutions as the test media, although Lincoln and Pruger (8)

[3] Similar to Strauss test.

[4] Sixty-five per cent boiling nitric acid test.



(*a*) Attacked (×500).
(*b*) Unattacked (×500).
(*c*) Attacked end view (×2).
(*d*) Unattacked end view (×2).

FIG. 3—Examples of Intergranular Attack in Sensitized 430 Stainless Steel (unattacked material is shown for comparison).

TABLE 1—CHEMICAL COMPOSITIONS OF MATERIALS USED IN THE INVESTIGATION.

Heat	C	Mn	P	S	Si	Cr	N	Ni	Mo	Cu
33503.....	0.07	0.37	0.018	0.010	0.39	16.90	0.027	0.38	0.09	0.11
32957.....	0.07	0.37	0.018	0.010	0.37	16.82	0.030	0.36	0.03	0.08
U430.....	0.07	0.41	0.023	0.010	0.35	17.00	0.027	0.11	0.05	0.05
58012.....	0.07	0.34	0.019	0.014	0.30	16.90	0.039	0.40	0.07	0.11
33205.....	0.035	0.48	0.035	0.030	0.12	17.84	0.055	0.37	0.06	0.05
32926.....	0.08	0.39	0.020	0.015	0.39	17.02	0.030	0.40	0.08	0.11
57556.....	0.08	0.39	0.022	0.011	0.33	16.90	0.029	0.19	0.03	0.20

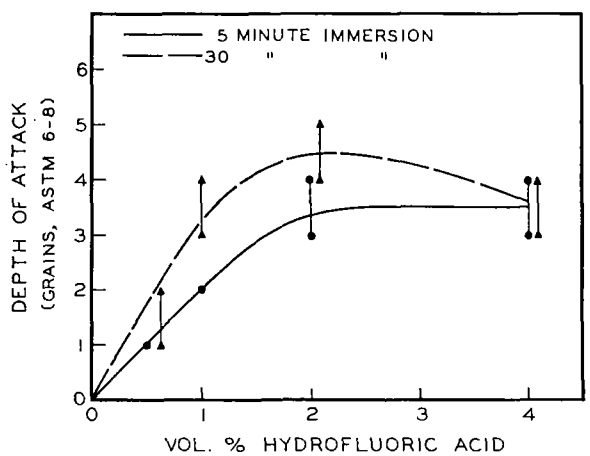


FIG. 4—Effect of HF Concentration in 15 Per Cent HNO_3 Solution at 150 F on the Depth of Intergranular Attack in 430 Stainless Steel Sensitized at 1650 F for 4 hr (heat 33503).

in 1953 showed that welds of 430 stainless steel were susceptible to intergranular corrosion in those media. Other than this work, no references were found on the effect of mill pickling solutions on the susceptibility of 430 stainless steel to intergranular attack.

In this work it was felt best to simulate as closely as possible the mill pickling cycle, since attack occurs very rapidly in sensitized material. Therefore, test solutions and procedures were used which were about the same as those used in the mill. Thus, the data in this paper were obtained almost completely from tests run in 15 per cent HNO_3-2 per cent HF pickling solution at 150 F. The time-temperature relationships for solutioning and desensitization were defined by isothermal and continuous cooling treatments for this type of test solution.

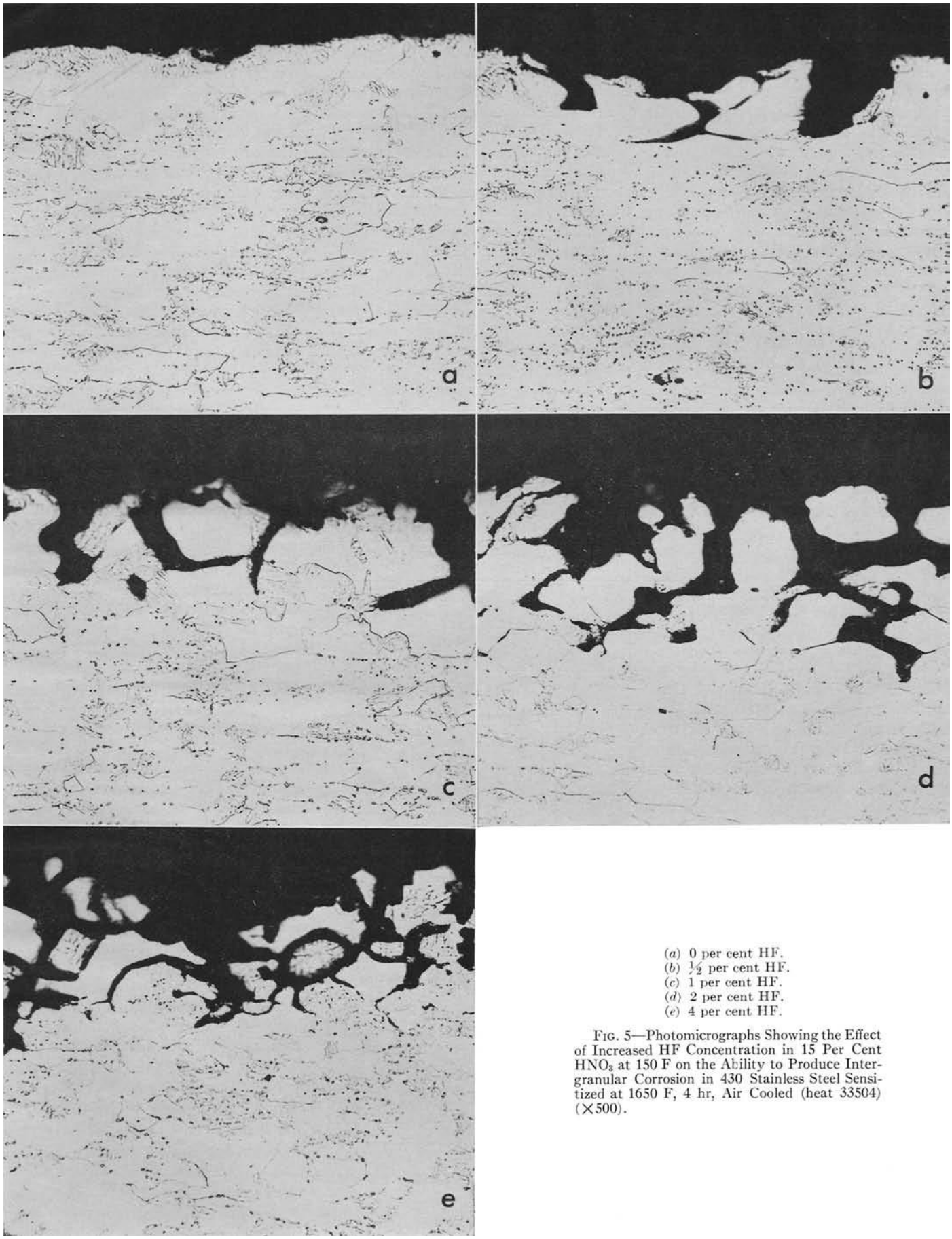
PROCEDURE

The material used in this investigation was commercial hot band from several heats of 430 stainless steel. The compositions of these heats are given in Table 1. One of the heats (32926) had previously been box annealed above the A_1 and had been pickled in the mill solutions, during which the surface corroded intergranularly. Therefore, prior to testing, material from this heat was surface ground to remove all evidence of intergranular attack. The other heats were used with the hot-rolled scale attached in order to better simulate mill conditions.

The usual procedure for preparing annealed hot band for cold rolling consists of several continuous steps. The material is first grit blasted to remove scale, immersed in about a 15 per cent sulfuric acid (H_2SO_4) solution at 170 F to dissolve any remaining scale, and finally pickled in a 10 to 15 per cent HNO_3-$\frac{1}{2}$ to 2 per cent HF solution at 150 F. Between each operation, the sheet is water rinsed.

Because of the different solutions used in the mill, the effects of various acids in producing intergranular corrosion on sensitized specimens (about 2 in. by $\frac{1}{2}$ in. by 0.12 in.) were first determined. Later, specimens were heat treated in various manners, and the solutioning and desensitization ranges were determined.

After each heat treatment test specimens were first grit blasted to remove all scale and were then immersed in the acid solutions generally for 5 or 30 min periods. Following washing, the speci-



(*a*) 0 per cent HF.
(*b*) ½ per cent HF.
(*c*) 1 per cent HF.
(*d*) 2 per cent HF.
(*e*) 4 per cent HF.

FIG. 5—Photomicrographs Showing the Effect of Increased HF Concentration in 15 Per Cent HNO_3 at 150 F on the Ability to Produce Intergranular Corrosion in 430 Stainless Steel Sensitized at 1650 F, 4 hr, Air Cooled (heat 33504) (×500).

mens were bent 180 deg, and the surfaces were examined both visually and microscopically for evidence of intergranular attack. The amount of attack was reported as the number of grains that were enveloped by intergranular attack. The attack generally varied up to several grain diameters. The widths of the grains were usually typical of an ASTM grain size of 6 to 8 after heat treating so that the specimens could be compared. The exception for this grain size occurred for hot-band specimens that were heat treated at 1400 F and below. These specimens all had grain widths finer than 8.

Results and Discussion

Hydrofluoric acid was assumed to be the substance most responsible for producing intergranular attack in sensitized Type 430 stainless steel. To substantiate this, specimens of 430 stainless steel in the sensitized[5] condition were immersed for 5 and 30 min periods in 15 per cent nitric acid solutions at 150 F containing various concentrations of hydrofluoric acid from 0 to 4 per cent by volume. Typical results of immersion tests on sensitized specimens after microscopic examination are shown in Figs. 4 and 5. No attack occurs unless hydrofluoric acid is present. The depth of attack varies with concentration, however, and the peak attack appears to level off at about 2 per cent. The total variation for a large number of specimens at 2 per cent HF indicates the range is broader than that shown in Fig. 4 and might extend from 1 to 4 grain diameters. The depth of attack on any particular specimen does not vary that much, however, and is usually 1 to 2 to 3 to 4 grain diameters.

Sensitized 430 stainless steel specimens were also immersed in solutions of 2 per cent HF with varying HNO_3 concentrations from 5 to 20 per cent. The depth of attack did not vary with HNO_3 concentration, and all subsequent tests were run in a 15 per cent HNO_3-2 per cent HF solution at 150 F.

[5] All specimens were sensitized at 1650 F for 4 hr except where indicated otherwise.

The effect of a 15 per cent sulfuric acid solution at 170 F in promoting intergranular attack was also checked. This solution by itself did not produce attack in sensitized specimens. The results of the 15 per cent H_2SO_4 immersion tests are given in Table 2.

It is concluded that the most important component of the mill pickling solutions in causing intergranular attack is hydrofluoric acid. Unfortunately without this acid, little if any pickling would be accomplished. This acid is strong in reducing power and is powerful in dissolving metal. The nitric acid on the other hand is strong in oxidizing power and tends to passivate the surface.

The solutioning range had been found by Lula et al (7) to extend from 1700 F to the melting point for holding times of $\frac{1}{2}$ hr. When specimens in this work were held at 1600 F for 4 hr or more, intergranular attack occurred in the 5 min 15 per cent HNO_3-2 per cent HF immersion tests. The solutioning range dropped to 1500 F when the immersion time increased to 30 min. Graphical representations of the solutioning time-temperature zones for the two immersion times are shown in Fig. 6.

TABLE 2—EFFECT OF H_2SO_4 ACID IN PRODUCING INTERGRANULAR ATTACK IN SENSITIZED SPECIMENS OF 430 STAINLESS STEEL, HEAT 33503.

Acid Immersion Treatment	Depth of Intergranular Attack After Bending 180 deg (× 200 to 500)
5 min in 15% HNO_3-2% HF at 150 F	1 to 2 grain diameter
30 min in 15% HNO_3-2% HF at 150 F	3 to 4 grain diameter
5 min in 15% H_2SO_4 at 170 F	no intergranular attack
30 min in 15% H_2SO_4 at 170 F	no intergranular attack

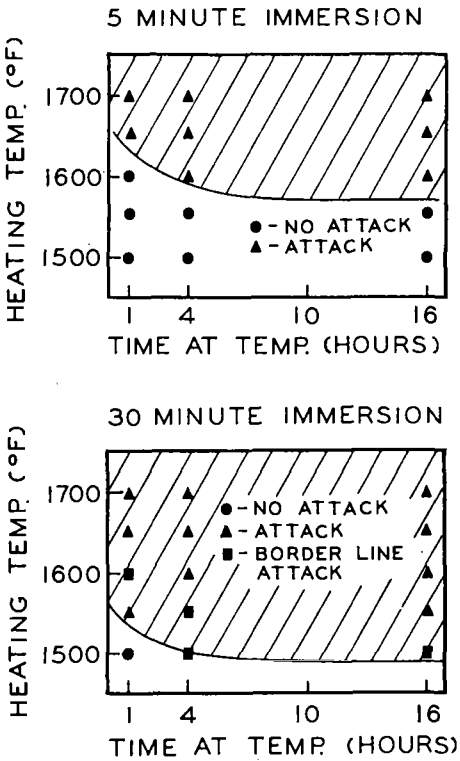


FIG. 6—Graphical Representation of the Solution Zones Which Result in Sensitization on Cooling, Shown for Two Different Immersion Times in 15 Per Cent HNO_3-2 per Cent HF at 150 F.

Solutioning of a particular phase or homogenization within the ferrite is probably occurring at these temperatures, and sensitization to varying degrees occurs on cooling. The longer, more severe test detects less sensitized material solutioned at the lower temperatures, whereas the shorter 5-min test reveals a greater degree of sensitization, typical of specimens solutioned at higher temperatures.

Very low cooling rates from the solutioning temperatures prevent susceptibility to attack. To determine the slowest critical cooling rate, specimens were solutioned at 1650 F and cooled at various constant rates to 1000 F and subjected to the 5 min 15 per cent HNO_3-2 per cent HF test at 150 F. Cooling at rates of approximately 40 F/hr or less prevents the material from being attacked intergranularly as shown in Fig. 7. Higher cooling rates cause attack although there is some scatter in results for different heats between 37 and 150 F/hr. At a cooling rate of 12 F/hr no intergranular attack occurs; however, the surface generally appears irregular and thus the range is broader as shown. The surface irregularity is thought to be the result of excessive oxidation which occurs during the very slow cool.

The fact that very low cooling rates remove the susceptibility to attack suggests that desensitization should be capable of being accomplished by isothermal treatments. A plot showing the desensitization range following isothermal treatments is shown in Fig. 8. In this case the specimens were cooled at 150 F/hr from the solution temperature, then held at the respective temperatures. The *C*-curve is fairly narrow and would require good temperature control for commercial utilization. The data in this figure were obtained from two heats of 430 stainless steel that previously had appeared to be attacked more severely than other heats.

There appears to be some variation in results from heat to heat. An additional curve on a less sensitive heat is shown in Fig. 9. The reason for the variation is uncertain in view of the similar chemical analyses.

Sensitized material may be desensitized by reheating in a particular time-temperature zone as shown in Fig. 10.

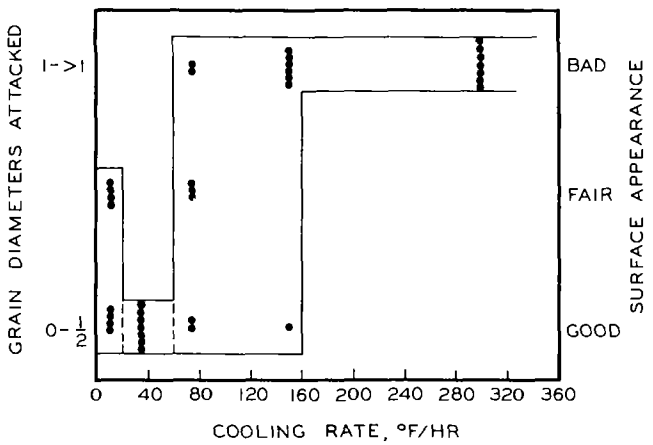


FIG. 7—Effect of Cooling Rate from 1650 F on the Susceptibility of 430 Stainless Steel Hot Band to Intergranular Attack in 15 Per Cent HNO_3-2 Per Cent HF at 150 F for an Immersion Time of 5 Min.

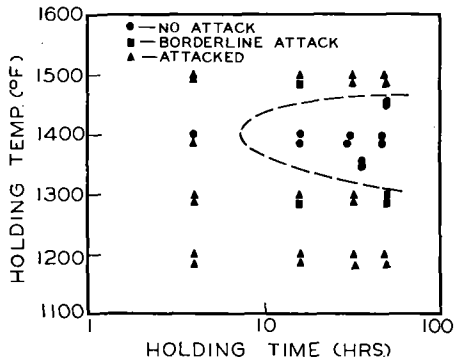


FIG .8—Desensitization *C*-Type Curve for 430 Stainless Steel Following Cooling at 150 F/hr from 1650 F and Isothermally Holding. Tested in 15 Per Cent HNO_3-2 Per Cent HF at 150 F (heats U430 and 32926).

material. During hot rolling, the 430 stainless steel is in the solution range, and during the final rolling passes and subsequent cooling becomes sensitized. The degree of sensitization for hot-rolled material does not appear to be as severe as that obtained in material only heated into the solution range and cooled. The fact that the hot band is in a severely hot-cold worked and distorted condition apparently tends to accelerate desensitization and to broaden the range.

The data above indicate the time-temperature zones where sensitized 430 stainless steel can be desensitized. The determination of these zones thus enables

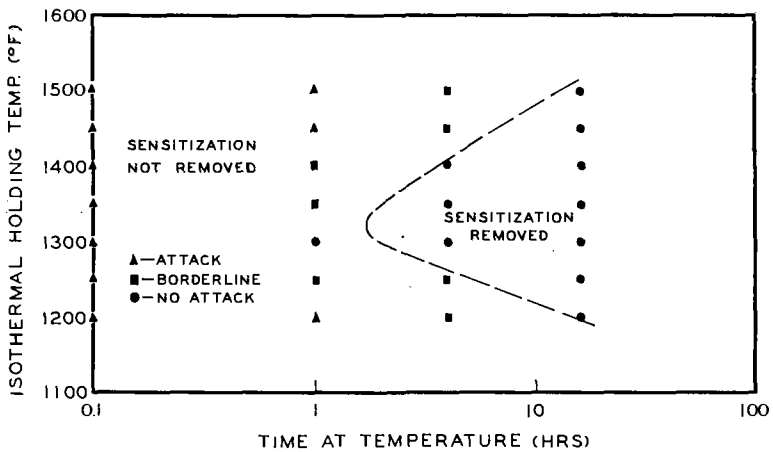


FIG. 9—Broader Desensitization *C*-Curve Obtained on Heat of 430 Stainless Steel Less Susceptible to Intergranular Attack Than Heats Shown in Fig. 8 (heat 33503).

Actually there appears to be two zones. One of these resembles the desensitization zone of the isothermally treated specimens in Figs. 8 and 9. This zone would typify the desensitization range for material that was initially solutioned at 1650 F for 4 hr and sensitized during air cooling. The much broader zone which extends up to the solution range, and includes the *C*-curve is typical of the desensitization zone for hot-rolled

one to select a suitable heat treatment than can be utilized in conjunction with the high temperature anneal (above the A_1). Thus a lower roped 430 stainless steel strip could be produced without intergranular corrosion occurring during processing. Probably the two best treatments would be: (1) controlled cooling at 37 F/hr from the solutioning temperature or (2) isothermally holding at 1400 F for 16 or more hours following solutioning and cooling.

MECHANISM OF INTERGRANULAR ATTACK

It is interesting to speculate on the various mechanisms that might be responsible for intergranular corrosion, now that the time-temperature relationships for solutioning and desensitization for a 15 per cent HNO_3-2 per cent HF solution have been determined.

Kiefer (5) originally thought that martensite formation at grain boundaries was responsible for intergranular attack in 430 stainless steel. He theorized that the susceptibility to attack was removed on reheating at 1300 F by tempering the martensite. Lula et al (7) showed that martensite formation was not necessary and attack occurred in completely ferritic 17 to 27 per cent chromium steels. They suggested that a nitride or carbide precipitated from the ferrite on cooling and strained the grain boundaries, making the alloy susceptible to attack. They showed that the susceptibility to attack was removed by reheating at 1200 to 1500 F for ½ hr, and suggested that these treatments relieved the stresses.

Houdremont and Tofaute (6) hypothesized that the attack was the result of the precipitation of an iron carbide. Freedom from attack obtained on reheating was believed to be caused by transformation of the iron rich carbide to a chromium-iron carbide which was not susceptible to attack.

Houdremont and Tofaute also presented data on 17 and 24 per cent chromium steels which suggested the attack was the result of the presence of nitrogen. Some of their data showing the effect of nitrogen content are given in Table 3. Complete freedom from attack was not obtained until the nitrogen content reached 0.005 per cent or less.

It has been hypothesized by some of the previous workers that sensitization is the result of the precipitation of a particular phase. However, it has not been possible to extract electrolytically any new phases or to identify new phases by other means. Although Lula et al (7) have reported the observation of a grain boundary precipitate in sensitized specimens, it has not been proved conclusively that the precipitate observed is the one responsible for intergranular corrosion. The material they examined contained considerable carbon in addition to nitrogen, and it is possible a grain boundary carbide may have precipitated. Since

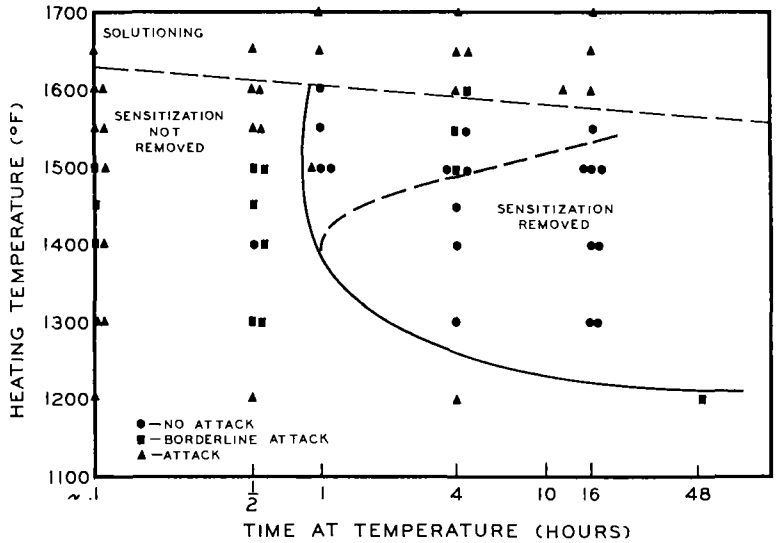


FIG. 10—Desensitization Ranges Obtained on Reheating 430 Stainless Steel. The *C*-Curve Contains the Desensitization Range for Material Solutioned and Air Cooled. The Broader Range Extending to Solution Range and Containing the *C* Curve Is for 430 Stainless Steel Hot Band that Had Been Hot Rolled in the Solution Range and Air Cooled.

TABLE 3—EFFECT OF NITROGEN CONTENT ON THE SUSCEPTIBILITY OF 17 AND 24% CHROMIUM STEELS TO INTERGRANULAR ATTACK IN A BOILING COPPER SULFATE-SULFURIC ACID SOLUTION (6).

Composition, per cent			Susceptibility to Attack
Cr	C	N	
17.3	0.02	0.016	attacked intergranularly
16.7	0.015	0.024	attacked intergranularly
18.1	0.012	0.025	attacked intergranularly
18.8	0.010	0.023	attacked intergranularly
18.6	0.010	0.010	attacked intergranularly
16.4	0.010[a]	0.005[a]	not attacked intergranularly
24.2	0.01 to 0.02	0.044	attacked intergranularly
24.2	0.03[a]	0.004[a]	not attacked intergranularly
24.0	0.01 to 0.02	0.058	attacked intergranularly
24.0	0.02[a]	0.003[a]	not attacked intergranularly
24.2	0.01 to 0.02	0.12	attacked intergranularly
24.2	0.02[a]	0.004[a]	not attacked intergranularly
24.2	0.01[a]	0.011[a]	attacked intergranularly
24.2	0.03[a]	0.004[a]	not attacked intergranularly
24.2	0.005	0.029	attacked intergranularly

NOTE—All other elements essentially the same except for variations in phosphorus from 0.009 to 0.28 in a few heats.

[a] After treating in dry H_2 at ~2400 F for 100 hr.

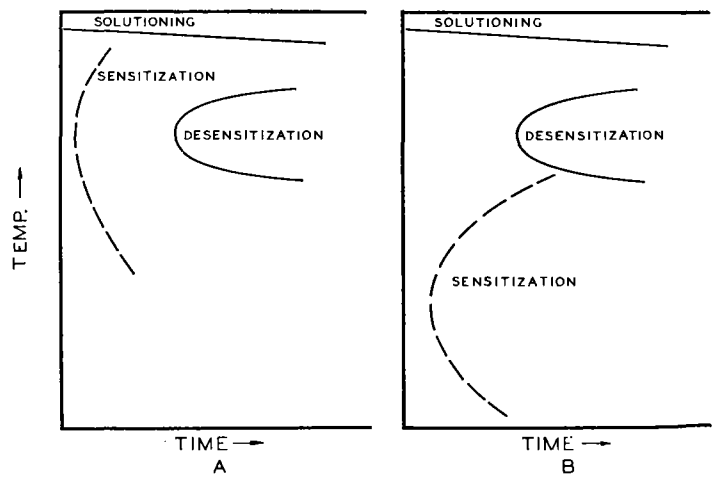


FIG. 11—Schematic Diagrams Representing Possible Reactions that May Occur During Sensitization and Desensitization of 17 Per Cent Ferritic Stainless Steels.

Houdremont and Tofaute have demonstrated that nitrogen appears to be responsible for the intergranular attack, the phase observed by Lula et al may have been a carbide not related to the mechanism. In our work no special carbide or nitride was observed or identified in sensitized specimens of 430 stainless steel by utilization of the electron microscope

Because no new phase has been identified there is the possibility another mechanism might be responsible for sensitization in ferritic steels. One mechanism might be that foreign atoms (nitrogen) may tend to segregate to grain boundaries during cooling from the solution temperature and supersaturate these areas without forming a precipitate. Therefore, because of the possible differences in composition, the electrochemical properties of the grain boundary areas may be different from those of the grains. Thus, in the proper electrolytes, intergranular corrosion would occur. Evans (9) cites examples where this type of mechanism may be the cause for intergranular corrosion. Perryman (10) and Lacombe and Wyon (11) have presented evidence on aluminum-iron alloys in support of this theory. There is also substantial evidence showing clustering of atoms around dislocations, and segregation at grain boundaries is not improbable. Chalmers and Thomas (12) have shown, by autoradiographic techniques, grain boundary segregation without precipitation in the lead-polonium system. Westbrook and Wood (13) have also showed that nitrogen and oxygen segregation can occur at grain boundaries in silver-magnesium intermetallic alloys.

On the basis of this hypothesis, desensitization can be rationalized as follows. Desensitization will occur if the grain boundary impurities diffuse away from the grain boundaries or precipitate as a new phase. Precipitation may also occur at the grain boundaries during desensitization; however, systemmatic examination should reveal this. It is speculated that most of the prior work has been concentrated on looking for precipitates in sensitized specimens, whereas it is possible they may exist in the desensitized materials.

It would be expected that the phase is a nitride (whether precipitation occurs during or after sensitization), and therefore any experimental work should be carried out using material as low as possible in carbon content. Carbon is

felt to be especially detrimental because carbides generally precipitate in the same temperature range that is of interest in studying sensitization and desensitization.

In conclusion, the sensitization and desensitization phenomena in ferritic stainless steels can be depicted schematically by either of the diagrams shown in Fig. 11. In the time-temperature-transformation (TTT) diagrams the sensitization curve is represented by a dashed line, since it is not known whether it represents the precipitation of a phase or the segregation of nonprecipitated impurities at the grain boundaries.

Two alternate diagrams are also shown, since it is not known whether sensitization occurs at the same temperature as desensitization or at lower temperatures. A significant difference between these diagrams and TTT diagrams for austenitic transformation is hat the desensitization curve does not appear to be appreciably altered when specimens are cooled to room temperature and reheated. This is because the reactions occur within and from the ferritic phase and not the austenitic phase.

REFERENCES

(1) C. T. Evans, "Columbium Curbs Wrinkling in Forming Stainless Steel Strip," *Iron Age*, Vol. 187, Feb. 23, 1961, pp. 96–97.

(2) J. Thompson and J. L. Lamont, "Non-Roping Ferritic Chromium Steels," *Electric Furnace Proceedings*, Am. Inst. Mining, Metallurgical, and Petroleum Engrs., Vol. 19, 1961, pp. 70–85.

(3) W. Tofaute, A. Sponheuer and H. Bennek, *Archiv fur das Eisenhuttenwesen*, Vol. VIII, 1935, p. 499.

(4) A. E. Nehrenberg and P. Lillys, "High Temperature Transformations in Ferritic Stainless Steels Containing 17 to 25% Chromium," *Transactions*, Am. Soc. Metals, Vol. 46, 1954, pp. 1176–1203.

(5) G. C. Kiefer, *Engineering Experiment Station News*, Ohio State University, Vol. 22, June, 1950, p. 21.

(6) E. Houdremont and W. Tofaute, "Resistance to Intergranular Corrosion of Ferritic and Martensitic Stainless Chromium Steels," *Stahl und Eisen*, Vol. 72, No. 10, 1952, pp. 539–545.

(7) R. A. Lula, A. J. Lena, and G. C. Kiefer, "Intergranular Corrosion of Ferritic Stainless Steels," *Transaction*, Am. Soc. Metals, Vol. 46, 1954, pp. 197–223.

(8) R. A. Lincoln and T. A. Pruger, "How and When to Use 430 Stainless," *Iron Age*, Vol. 171, Feb. 26, 1953, p. 127.

(9) U. R. Evans, *The Corrosion and Oxidation of Metals*, Chapter XVI, Edward Arnold Ltd., London, 1960.

(10) E. C. W. Perryman, "Grain Boundary Attack on Aluminum in Hydrochloric Acid and Sodium Hydroxide," *Journal Metals*, Vol. 5, 1953, p. 911.

(11) G. Wyon and P. Lacombe, Physical Society Conference on Defects in Crystalline Solids, 1954, p. 187.

(12) B. Chalmers and W. R. Thomas, "The Segregation of Impurities to Grain Boundaries," *Acta Metallurgical*, Vol. 3, 1955, p. 17.

(13) J. H. Westbrook and D. L. Wood, "A Source of Grain Boundary Embrittlement in Intermetallics," *Institute of Metals*, January, 1963, p. 174.

THIS PUBLICATION is one of many issued by the American Society for Testing and Materials in connection with its work of promoting knowledge of the properties of materials and developing standard specifications and tests for materials. Much of the data result from the voluntary contributions of many of the country's leading technical authorities from industry, scientific agencies, and government.

Over the years the Society has published many technical symposiums, reports, and special books. These may consist of a series of technical papers, reports by the ASTM technical committees, or compilations of data developed in special Society groups with many organizations cooperating. A list of ASTM publications and information on the work of the Society will be furnished on request.